Physics of the Dark Universe 49 (2025) 101965

Contents lists available at ScienceDirect

Physics of the Dark Universe

journal homepage: www.elsevier.com/locate/dark

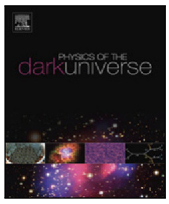

Review article

The CosmoVerse White Paper: Addressing observational tensions in cosmology with systematics and fundamental physics

Eleonora Di Valentino [1,*], Jackson Levi Said [2,3], Adam Riess [4,5], Agnieszka Pollo [6], Vivian Poulin [7], Adrià Gómez-Valent [8], Amanda Weltman [9], Antonella Palmese [10], Caroline D. Huang [11], Carsten van de Bruck [12], Chandra Shekhar Saraf [13], Cheng-Yu Kuo [14], Cora Uhlemann [15,16], Daniela Grandón [17], Dante Paz [18], Dominique Eckert [19], Elsa M. Teixeira [20], Emmanuel N. Saridakis [21,22,23], Eoin Ó Colgáin [24], Florian Beutler [25], Florian Niedermann [26], Francesco Bajardi [27,28], Gabriela Barenboim [29], Giulia Gubitosi [30,28], Ilaria Musella [31], Indranil Banik [32], Istvan Szapudi [33], Jack Singal [34], Jaume Haro Cases [35], Jens Chluba [36], Jesús Torrado [37], Jurgen Mifsud [38,39], Karsten Jedamzik [40], Khaled Said [41], Konstantinos Dialektopoulos [42,38], Laura Herold [4], Leandros Perivolaropoulos [43], Lei Zu [6], Lluís Galbany [44,45], Louise Breuval [46], Luca Visinelli [47,48], Luis A. Escamilla [49], Luis A. Anchordoqui [50], M.M. Sheikh-Jabbari [51], Margherita Lembo [52,53,54], Maria Giovanna Dainotti [55,56], Maria Vincenzi [57], Marika Asgari [16], Martina Gerbino [58], Matteo Forconi [59], Michele Cantiello [60], Michele Moresco [61,62], Micol Benetti [27,28], Nils Schöneberg [63,64], Özgür Akarsu [65], Rafael C. Nunes [66,67], Reginald Christian Bernardo [68], Ricardo Chávez [69,70], Richard I. Anderson [71], Richard Watkins [72], Salvatore Capozziello [30,27,28], Siyang Li [4], Sunny Vagnozzi [73,74], Supriya Pan [75], Tommaso Treu [76], Vid Irsic [77,78], Will Handley [79,80], William Giarè [49], Yukei Murakami [4], Abdolali Banihashemi [81], Adèle Poudou [82], Alan Heavens [83], Alan Kogut [84], Alba Domi [85], Aleksander Łukasz Lenart [86], Alessandro Melchiorri [87], Alessandro Vadalà [88,89,90], Alexandra Amon [91,92], Alexander Bonilla Rivera [93], Alexander Reeves [94], Alexander Zhuk [95,96,97], Alfio Bonanno [98], Ali Övgün [99], Alice Pisani [100,101], Alireza Talebian [102], Amare Abebe [103], Amin Aboubrahim [104], Ana Luisa González Morán [105], András Kovács [106,107], Andreas Lymperis [108], Andreas Papatriantafyllou [109], Andrew R. Liddle [110], Andronikos Paliathanasis [111,112,113], Andrzej Borowiec [114], Anil Kumar Yadav [115], Anita Yadav [116], Anjan Ananda Sen [117], Anjitha John William [118], Anne Christine Davis [119], Anowar J. Shajib [120,121,122], Anthony Walters [123,124,9], Anto Idicherian Lonappan [125], Anton Chudaykin [126], Antonio Capodagli [127], Antonio da Silva [110], Antonio De Felice [128], Antonio Racioppi [129], Araceli Soler Oficial [130], Ariadna Montiel [131], Arianna Favale [132,8], Armando Bernui [133], Arrianne Crystal Velasco [134,135], Asta Heinesen [136], Athanasios Bakopoulos [137,109], Athanasios Chatzistavrakidis [138], Bahman Khanpour [139], Bangalore S. Sathyaprakash [140], Bartek Zgirski [141], Benjamin L'Huillier [142], Benoit Famaey [143], Bhuvnesh Jain [144], Bing Zhang [145], Biswajit Karmakar [146], Branko Dragovich [147], Brooks Thomas [148], Carlos Correa [149], Carlos G. Boiza [150], Catarina Marques [151,152], Celia Escamilla-Rivera [153], Charalampos Tzerefos [154,155], Chi Zhang [156,157,158], Chiara De Leo [159], Christian Pfeifer [160],

* Corresponding author.
E-mail addresses: e.divalentino@sheffield.ac.uk (E. Di Valentino), jackson.said@um.edu.mt (J.L. Said).

https://doi.org/10.1016/j.dark.2025.101965
Received 13 May 2025; Accepted 15 May 2025
Available online 20 June 2025
2212-6864/© 2025 The Authors. Published by Elsevier B.V. This is an open access article under the CC BY license (http://creativecommons.org/licenses/by/4.0/).

Christine Lee [106], Christo Venter [161], Cláudio Gomes [162,163], Clecio Roque De bom [164], Cristian Moreno-Pulido [165], Damianos Iosifidis [166], Dan Grin [167], Daniel Blixt [27], Dan Scolnic [168], Daniele Oriti [169], Daria Dobrycheva [170], Dario Bettoni [171,172], David Benisty [173], David Fernández-Arenas [174], David L. Wiltshire [175], David Sanchez Cid [176,177], David Tamayo [178,152], David Valls-Gabaud [179], Davide Pedrotti [73], Deng Wang [180], Denitsa Staicova [181], Despoina Totolou [182], Diego Rubiera-Garcia [183], Dinko Milaković [184,185], Dominic W. Pesce [186,187], Dominique Sluse [188], Duško Borka [189], Ebrahim Yusofi [190,191], Elena Giusarma [192], Elena Terlevich [193,80], Elena Tomasetti [194,62], Elias C. Vagenas [195], Elisa Fazzari [196,197,198], Elisa G.M. Ferreira [199], Elvis Barakovic [200], Emanuela Dimastrogiovanni [201], Emil Brinch Holm [202], Emil Mottola [203], Emre Özülker [204], Enrico Specogna [204], Enzo Brocato [205,206], Erik Jensko [207], Erika Antonette Enriquez [134], Esha Bhatia [208], Fabio Bresolin [209], Felipe Avila [133], Filippo Bouchè [27,210], Flavio Bombacigno [211], Fotios K. Anagnostopoulos [212], Francesco Pace [213,214,215], Francesco Sorrenti [126], Francisco S.N. Lobo [110,216], Frédéric Courbin [217,218], Frode K. Hansen [219], Greg Sloan [5,220], Gabriel Farrugia [38,221], Gabriel Lynch [222], Gabriela Garcia-Arroyo [223], Gabriella Raimondo [60], Gaetano Lambiase [47,48], Gagandeep S. Anand [5], Gaspard Poulot [204], Genly Leon [224,225], Gerasimos Kouniatalis [226,155], Germano Nardini [227], Géza Csörnyei [228], Giacomo Galloni [229,230], Giada Bargiacchi [231], Giannis Papagiannopoulos [232], Giovanni Montani [233,234], Giovanni Otalora [235], Giulia De Somma [31,28], Giuliana Fiorentino [236], Giuseppe Fanizza [237], Giuseppe Gaetano Luciano [238], Giuseppe Sarracino [31], Gonzalo J. Olmo [211,239], Goran S. Djordjević [240], Guadalupe Cañas-Herrera [241], Hanyu Cheng [242,243,204], Harry Desmond [32], Hassan Abdalla [112], Houzun Chen [244], Hsu-Wen Chiang [245], Hume A. Feldman [246], Hussain Gohar [247], Ido Ben-Dayan [248], Ignacio Sevilla-Noarbe [176], Ignatios Antoniadis [249], Ilim Cimdiker [247], Inês S. Albuquerque [110], Ioannis D. Gialamas [129], Ippocratis Saltas [250], Iryna Vavilova [251], Isidro Gómez-Vargas [252], Ismael Ayuso [253], Ismailov Nariman Zeynalabdi [254], Ivan De Martino [172], Ivonne Zavala [255], J. Alberto Vázquez [153], Jacobo Asorey [256], Janusz Gluza [257], Javier Rubio [183], Jenny G. Sorce [258,259], Jenny Wagner [260,261,262], Jeremy Sakstein [263], Jessica Santiago [264], Jim Braatz [265], Joan Solà Peracaula [8], John Blakeslee [266], John Webb [80], Jose A.R. Cembranos [267], José Pedro Mimoso [110], Joseph Jensen [268], Juan García-Bellido [269], Judit Prat [270], Kathleen Sammut [38], Kay Lehnert [271], Keith R. Dienes [272,273], Kishan Deka [6], Konrad Kuijken [274], Krishna Naidoo [275], László Árpád Gergely [276,277], Laur Järv [278], Laura Mersini-Houghton [279], Leila L. Graef [280], Léo Vacher [281], Levon Pogosian [282], Lilia Anguelova [283], Lindita Hamolli [284], Lu Yin [285,286], Luca Caloni [229,230,287], Luca Izzo [288], Lucas Macri [289], Luis E. Padilla [290], Luz Ángela García [291], Maciej Bilicki [292], Mahdi Najafi [196,293], Manolis Plionis [21,294,295], Manuel Gonzalez-Espinoza [296,297], Manuel Hohmann [278], Marcel A. van der Westhuizen [103], Marcella Marconi [31], Marcin Postolak [298], Marco de Cesare [27,28], Marco Regis [299], Marek Biesiada [6], Maret Einasto [300], Margus Saal [301], Maria Caruana [38], Maria Petronikolou [302,155], Mariam Bouhmadi-López [303,304], Mariana Melo [151,152], Mariaveronica De Angelis [204], Marie-Noëlle Célérier [305], Marina Cortês [110], Mark Reid [186], Markus Michael Rau [16,306], Martin S. Sloth [307], Martti Raidal [129], Masahiro Takada [308], Masoume Reyhani [309,293], Massimiliano Romanello [310,311], Massimo Marengo [127], Mathias Garny [312], Matías Leizerovich [313,314], Matteo Martinelli [315,316], Matteo Tagliazucchi [317,62], Mehmet Demirci [318], Miguel A.S. Pinto [110,216], Miguel A. Sabogal [66], Miguel A. García-Aspeitia [319], Milan Milošević [320], Mina Ghodsi [321,106], Mustapha Ishak [322], Nelson J. Nunes [110], Nick Samaras [323], Nico Hamaus [324], Nico Schuster [100,324], Nicola Borghi [317,62,325], Nicola Deiosso [176], Nicola Tamanini [326], Nicolao Fornengo [327], Nihan Katırcı [328], Nikolaos E. Mavromatos [109,329], Nicholas Petropoulos [330], Nikolina Šarčević [331], Nils A. Nilsson [332,333], Nima Khosravi [334,335], Noemi Frusciante [30], Octavian Postavaru [336], Oem Trivedi [337,338], Oleksii Sokoliuk [339,340,341], Olga Mena [180], Paloma Morilla [342], Paolo Campeti [343,344], Paolo Salucci [281], Paula Boubel [345], Paweł Bielewicz [6], Pekka Heinämäki [346], Petar Suman [347], Petros Asimakis [348], Pierros Ntelis [100], Pran Nath [349], Predrag Jovanović [350], Purba Mukherjee [117,351], Radosław Wojtak [352], Rafaela Gsponer [353], Rafid H. Dejrah [354],

Rahul Shah [351], Rasmi Hajjar [180], Rebecca Briffa [38], Rebecca Habas [355], Reggie C. Pantig [356], Renier Mendoza [134,135], Riccardo Della Monica [172], Richard Stiskalek [357], Rishav Roshan [358], Rita B. Neves [49], Roberto Molinaro [31], Roberto Terlevich [359,80,360], Rocco D'Agostino [88,361], Rodrigo Sandoval-Orozco [362], Ronaldo C. Batista [363], Ruchika [172], Ruth Lazkoz [364], Saeed Rastgoo [365,366,367], Sahar Mohammadi [368], Salvatore Samuele Sirletti [369,370,371], Sandeep Haridasu [372,373], Sanjay Mandal [374], Saurya Das [375], Sebastian Bahamonde [376,377], Sebastian Grandis [378], Sebastian Trojanowski [6], Sergei D. Odintsov [379,380], Sergij Mazurenko [381], Shahab Joudaki [176,382], Sherry H. Suyu [383,384], Shouvik Roy Choudhury [385], Shruti Bhatporia [9], Shun-Sheng Li [386,387], Simeon Bird [388], Simon Birrer [389], Simone Paradiso [390], Simony Santos da Costa [391,392], Sofia Contarini [393], Sophie Henrot-Versillé [394], Spyros Basilakos [21,395,396], Stefano Casertano [5], Stefano Gariazzo [397], Stylianos A. Tsilioukas [398,21], Surajit Kalita [399,9], Suresh Kumar [400], Susana J. Landau [401], Sveva Castello [126], Swayamtrupta Panda [402,403], Tanja Petrushevska [404], Thanasis Karakasis [109], Thejs Brinckmann [405,406], Tiago B. Gonçalves [110,216], Tiziano Schiavone [407,408], Tom Abel [409], Tomi Koivisto [166,410], Torsten Bringmann [411], Umut Demirbozan [412], Utkarsh Kumar [413,414], Valerio Marra [415,184,185], Maurice H.P.M. van Putten [416,417], Vasileios Kalaitzidis [418], Vasiliki A. Mitsou [419], Vasilios Zarikas [420], Vedad Pasic [421], Venus Keus [422,423], Verónica Motta [424], Vesna Borka Jovanović [189], Víctor H. Cárdenas [424], Vincenzo Ripepi [31], Vincenzo Salzano [247], Violetta Impellizzeri [425], Vitor da Fonseca [110], Vittorio Ghirardini [426,427], Vladas Vansevičius [428], Weiqiang Yang [429], Wojciech Hellwing [292], Xin Ren [430,431], Yu-Min Hu [430,432], Yuejia Zhai [49], Abdul Malik Sultan [433], Abdurakhmon Nosirov [434], Adrienn Pataki [435], Alessandro Santoni [436,437], Aliya Batool [433], Amlan Chakraborty [438], Aneta Wojnar [439,440], Arman Tursunov [441,442], Avik De [443], Ayush Hazarika [444], Baojiu Li [445], Benjamin Bose [446,447], Bivudutta Mishra [448], Bobomurat Ahmedov [449,450], Claudia Scóccola [451], Crescenzo Tortora [31], D'Arcy Kenworthy [452], Daniel E. Holz [453], David F. Mota [454], David S. Pereira [110], Devon M. Williams [455], Dillon Brout [456], Dong Ha Lee [49], Eduardo Guendelman [457], Edward Olex [458], Emanuelly Silva [459], Emre Onur Kahya [460], Eva-Maria Mueller [461], Felipe Andrade-Oliveira [462], Feven Markos Hunde [292], F.R. Joaquim [463,464], Florian Pacaud [465], Francis-Yan Cyr-Racine [466], F. Pozo Nuñez [467], Gábor Rácz [468], Gene Carlo Belinario [469], Geraint F. Lewis [470], Gergely Dálya [471,472], Giorgio Laverda [473], Guido Risaliti [474,475], Guillermo Franco-Abellán [476], Hayden Zammit [38], Hayley Camilleri [38], Helene M. Courtois [477], Hooman Moradpour [478], Igor de Oliveira Cardoso Pedreira [479], Ilídio Lopes [480], István Csabai [481], James W. Rohlf [482], Jana Bogdanoska [483], Javier de Cruz Pérez [484], Joan Bachs-Esteban [473], Joseph Sultana [485], Julien Lesgourgues [486], Jun-Qian Jiang [487], Karem Peñaló Castillo [50], Kimet Jusufi [488], Lavinia Heisenberg [489], Laxmipriya Pati [166], Lón V.E. Koopmans [490], Lokesh kumar Duchaniya [491], Lucas Lombriser [492], María Pérez Garrote [172], Mariano Domínguez [493], Marine Samsonyan [494], Mark Pace [495,38], Martin Kršśák [496], Masroor C. Pookkillath [497], Matteo Peronaci [132], Matteo Piani [473], Matthildi Raftogianni [137], Meet J. Vyas [338], Melina Michalopoulou [137], Merab Gogberashvili [498], Michael Klasen [499], Michele Cicoli [500,501], Miguel Quartin [502,503], Miguel Zumalacárregui [504], Milan S. Dimitrijević [505], Milos Dordevic [506], Mindaugas Karčiauskas [507], Morgan Le Delliou [508,509,510], Nastassia Grimm [126], Nicolás Augusto Kozameh [493], Nicoleta Voicu [42], Nicolina Pop [511], Nikos Chatzifotis [109], Odil Yunusov [512], Oliver Fabio Piattella [513,514,515], Pedro da Silveira Ferreira [516], Péter Raffai [435,517], Peter Schupp [518], Pilar Ruiz-Lapuente [519], Pradyumn Kumar Sahoo [491], Roberto V. Maluf [520], Ruth Durrer [521], S.A. Kadam [522], Sabino Matarrese [523], Samuel Brieden [524], Santiago González-Gaitán [525], Santosh V. Lohakare [491], Scott Watson [526,527], Shao-Jiang Wang [528,529], Simão Marques Nunes [110], Soumya Chakrabarti [530], Subinoy Das [438], Suvodip Mukherjee [531], Tajron Jurić [532], Tessa Baker [533], Theodoros Nakas [332], Tiago Barreiro [110,534], Upala Mukhopadhyay [535], Veljko Vujčić [536], Violetta Sagun [537], Vladimir A. Srećković [538], Wangzheng Zhang [539], Yo Toda [540], Yun-Song Piao [487,541,542], Zahra Davari [543], for The CosmoVerse Network

[1] School of Mathematical and Physical Sciences, University of Sheffield, Hounsfield Road, Sheffield, S3 7RH, United Kingdom

[2] Institute of Space Sciences and Astronomy, University of Malta, Malta
[3] Department of Physics, University of Malta, Malta
[4] Department of Physics and Astronomy, Johns Hopkins University, Baltimore, MD, 21218, USA
[5] Space Telescope Science Institute, 3700 San Martin Drive, Baltimore, MD, 21218, USA
[6] National Centre for Nuclear Research, Pasteura 7, Warszawa, 02-093, Poland
[7] Laboratoire Univers & Particules de Montpellier (LUPM), CNRS & Université de Montpellier (UMR-5299), Place Eugène Bataillon, F-34095 Cedex 05, Montpellier, France
[8] Departament de Física Quàntica i Astrofísica and Institut de Ciències del Cosmos, Universitat de Barcelona, Av. Diagonal 647, Barcelona, E-08020, Spain
[9] High Energy Physics, Cosmology and Astrophysics Theory (HEPCAT) Group, Department of Mathematics and Applied Mathematics, University of Cape Town, Cape Town, 7700, South Africa
[10] McWilliams Center for Cosmology and Astrophysics, Department of Physics, Carnegie Mellon University, 5000 Forbes Avenue, Pittsburgh, PA, 15213, USA
[11] Harvard-Smithsonian Center for Astrophysics, 60 Garden St., Cambridge, MA, 02138, USA
[12] School of Mathematical and Physical Sciences, The University of Sheffield, Hounsfield Road, Sheffield, S3 7RH, United Kingdom
[13] Korea Astronomy and Space Science Institute, 776 Daedeok-daero, Yuseong-gu, Daejeon, Republic of Korea
[14] Physics Department, National Sun Yat-Sen University, No. 70, Lien-Hai Rd, Kaosiung City, 80424, Taiwan, ROC
[15] Fakultät für Physik, Universität Bielefeld, Postfach 100131, Bielefeld, 33501, Germany
[16] School of Mathematics, Statistics and Physics, Newcastle University, Herschel Building, Newcastle-upon-Tyne, NE1 7RU, UK
[17] Mathematical Institute, Leiden University, Gorlaeus Gebouw, Einsteinweg 55, Leiden, NL-2333 CC, The Netherlands
[18] Instituto de Astronomía Teórica y Experimental, UNC-Conicet, Laprida 854, Ciudad de Córdoba, Argentina
[19] Department of Astronomy, University of Geneva, Ch. d'Ecogia 16, Versoix, CH-1290, Switzerland
[20] Laboratoire Univers & Particules de Montpellier, CNRS & Université de Montpellier (UMR-5299), Montpellier, 34095, France
[21] National Observatory of Athens, Lofos Nymfon, Athens, 11852, Greece
[22] CAS Key Laboratory for Researches in Galaxies and Cosmology, School of Astronomy and Space Science, University of Science and Technology of China, Hefei, 230026, China
[23] Departamento de Matemáticas, Universidad Católica del Norte, Avda. Angamos 0610, Casilla 1280, Antofagasta, Chile
[24] Atlantic Technological University, Ash Lane, Sligo, Ireland
[25] Institute for Astronomy, University of Edinburgh Royal Observatory Edinburgh, Blackford Hill, Edinburgh, EH9 3HJ, UK
[26] Nordita, KTH Royal Institute of Technology and Stockholm University, Hannes Alfvéns väg 12, Stockholm, SE-106 91, Sweden
[27] Scuola Superiore Meridionale, Via Mezzocannone 4, Napoli, 80134, Italy
[28] Istituto Nazionale di Fisica Nucleare, Sezione di Napoli, Complesso Univ. Monte S. Angelo, Napoli, I-80126, Italy
[29] Departament de Física Teórica and IFIC, Universitat de València-CSIC, Burjassot, E-46100, Spain
[30] Dipartimento di Fisica Ettore Pancini, Universit'a di Napoli Federico II, Complesso Univ. Monte S. Angelo, Napoli, I-80126, Italy
[31] INAF-Osservatorio Astronomico di Capodimonte, Salita Moiariello 16, Napoli, 80131, Italy
[32] Institute of Cosmology & Gravitation, University of Portsmouth, Dennis Sciama Building, Burnaby Road, Portsmouth, PO1 3FX, UK
[33] Institute for Astronomy, University of Hawaii, 2680 Woodlawn Drive, Honolulu, HI, 96822, USA
[34] Physics Department, University of Richmond, Richmond, VA, 23173, USA
[35] Department of Mathematics, Universitat Politècnica de Catalunya, Carrer Colom 15, Terrassa, 08222, Spain
[36] Jodrell Bank Centre for Astrophysics, School of Physics and Astronomy, The University of Manchester, Manchester, M13 9PL, UK
[37] Instituto de Estructura de la Materia, CSIC, Serrano 121, Madrid, 28006, Spain
[38] Institute of Space Sciences and Astronomy, University of Malta, Malta
[39] Department of Physics, University of Malta, Malta
[40] University of Montpellier, France
[41] School of Mathematics and Physics, University of Queensland, 4072, Australia
[42] Department of Mathematics and Computer Science, Transilvania University of Brasov, Romania
[43] Department of Physics, University of Ioannina, Ioannina, 45110, Greece
[44] Institute of Space Sciences (ICE-CSIC), Campus UAB, Carrer de Can Magrans, s/n, Barcelona, E-08193, Spain
[45] Institut d'Estudis Espacials de Catalunya (IEEC), Castelldefels, Barcelona, 08860, Spain
[46] European Space Agency (ESA), ESA Office, Space Telescope Science Institute, 3700 San Martin Drive, Baltimore, MD, 21218, USA
[47] Dipartimento di Fisica "E.R. Caianiello", Università degli Studi di Salerno, Via G. Paolo II, Fisciano, SA, 84084, Italy
[48] INFN - Gruppo Collegato di Salerno, Via G.Paolo II, Fisciano, SA, 84084, Italy
[49] School of Mathematical and Physical Sciences, University of Sheffield, Hounsfield Road, Sheffield, S3 7RH, United Kingdom
[50] Department of Physics and Astronomy, Lehman College, City University of New York, New York, NY, 10468, USA
[51] School of Physics, Inst. for Research in Fundamental Science (IPM), P.O.Box: 19395-5531, Tehran, Iran
[52] Dipartimento di Fisica e Scienze della Terra, Università degli Studi di Ferrara, via Saragat 1, Ferrara, I-44122, Italy
[53] Istituto Nazionale di Fisica Nucleare, Sezione di Ferrara, Via G. Saragat 1, Ferrara, I-44122, Italy
[54] Sorbonne Université, CNRS, UMR 7095, Institut d'Astrophysique de Paris, 98 bis bd Arago, Paris, 75014, France
[55] National Astronomical Observatory of Japan, 2-21-1 Osawa, Mitaka, Tokyo, 181-8588, Japan
[56] Japan and Nevada Center for Astrophysics, University of Nevada, Las Vegas, 4505 Maryland Parkway, Las Vegas, 89154, USA
[57] Department of Physics, University of Oxford, Denys Wilkinson Building, Keble Road, Oxford, OX1 3RH, United Kingdom
[58] Istituto Nazionale di Fisica Nucleare, Sezione di Ferrara, Via Giuseppe Saragat, 1, Ferrara, 44122, Italy
[59] Physics Department and INFN sezione di Ferrara, Università degli Studi di Ferrara, via Saragat 1, Ferrara, I-44122, Italy
[60] INAF, Osservatorio Astronomico d'Abruzzo, Via Maggini snc, Teramo, I-64100, Italy
[61] Università di Bologna, Dipartimento di Fisica e Astronomia "Augusto Righi", via Piero Gobetti 93/2, Bologna, I-40129, Italy
[62] INAF - Osservatorio di Astrofisica e Scienza dello Spazio di Bologna, via Piero Gobetti 93/3, Bologna, I-40129, Italy
[63] University Observatory, Faculty of Physics, Ludwig-Maximilians-Universität, Scheinerstrasse 1, Munich, 81677, Germany
[64] Excellence Cluster ORIGINS, Boltzmannstr 2, Garching, 85748, Germany
[65] Department of Physics, Istanbul Technical University, Maslak, Istanbul, 34469, Türkiye
[66] Instituto de Física, Universidade Federal do Rio Grande do Sul, Porto Alegre, RS, 91501-970, Brazil
[67] Divisão de Astrofísica, Instituto Nacional de Pesquisas Espaciais, Avenida dos Astronautas 1758, São José dos Campos, São Paulo, 12227-010, Brazil
[68] Asia Pacific Center for Theoretical Physics, Pohang, 37673, Korea
[69] Universidad Nacional Autónoma de México, Instituto de Radioastronomía y Astrofísica, Morelia, Michoacán, 58090, México
[70] Secretaría de Ciencia, Humanidades, Tecnología e Innovación, Av. Insurgentes Sur 1582, Ciudad de México, 03940, México
[71] Institute of Physics, École Polytechnique Fédérale de Lausanne (EPFL), Observatoire de Sauverny, Versoix, 1290, Switzerland
[72] Department of Physics, Willamette University, Salem, OR, 97301, USA
[73] Department of Physics, University of Trento, Via Sommarive 14, Povo, TN, 38123, Italy
[74] Trento Institute for Fundamental Physics and Applications-INFN, Via Sommarive 14, Povo, TN, 38123, Italy
[75] Department of Mathematics, Presidency University, 86/1 College Street, Kolkata, 700073, India
[76] Department of Physics and Astronomy University of California, USA
[77] Kavli Institute for Cosmology (KICC), Madingley Road, Cambridge, CB3 0HA, United Kingdom

[78] Centre for Astrophysics Research, Department of Physics, Astronomy and Mathematics, University of Hertfordshire, College Lane, Hatfield, AL10 9AB, United Kingdom
[79] Kavli Institute for Cosmology (KICC), Madingley Road, Cambridge, CB3 0HA, UK
[80] Institute of Astronomy, University of Cambridge, Madingley Road, Cambridge, CB3 9AL, UK
[81] Institute of Theoretical Astrophysics, University of Oslo, P.O. Box 1029 Blindern, Oslo, 0315, Norway
[82] Laboratoire Univers et Particules de Montpellier (LUPM), CNRS et Université de Montpellier (UMR-5299), Place Eugène Bataillon, F-34095 Cedex 05, Montpellier, France
[83] Imperial Centre for Inference and Cosmology (ICIC), Department of Physics, Blackett Laboratory, Imperial College London, Prince Consort Road, London, SW7 2AZ, UK
[84] NASA Goddard Space Flight Center, 8800 Greenbelt Road, Greenbelt, MD, 20771, USA
[85] Erlangen Centre for Astroparticle Physics, Friedrich-Alexander-Universität Erlangen-Nürnberg, Department of Physics, Nikolaus-Fiebiger-Straße 2, Erlangen, 91058, Germany
[86] Astronomical Observatory, Jagiellonian University in Kraków, ul. Orla 171, Kraków, 30-244, Poland
[87] Dipartimento di Fisica "G. Marconi", Università di Roma Sapienza, Ple Aldo Moro 2, Rome, 00185, Italy
[88] INAF - Osservatorio Astronomico di Roma, Via Frascati 33, Monte Porzio Catone, 00078, Italy
[89] INFN - Sezione di Roma, Piazzale Aldo Moro, 2 - c/o Dipartimento di Fisica, Roma, 00185, Italy
[90] Dipartimento di Fisica, Università degli Studi di Roma Tor Vergata, via della Ricerca Scientifica 1, Rome, I-00133, Italy
[91] Department of Astrophysical Sciences, Princeton University, Peyton Hall, Princeton, NJ, 08544, USA
[92] Kavli Institute for Cosmology (KICC), University of Cambridge, Madingley Road, Cambridge, CB3 0HA, UK
[93] Instituto de Física, Universidade Federal Fluminense, Niterói, RJ, 24210-346, Brazil
[94] Institute for Particle Physics and Astrophysics, ETH Zürich, Wolfgang-Pauli-Strasse 27, Zürich, CH8093, Switzerland
[95] Astronomical Observatory, Odessa I.I. Mechnikov National University, Dvoryanskaya St. 2, Odessa, 65082, Ukraine
[96] Center for Advanced Systems Understanding, Untermarkt 20, Görlitz, 02826, Germany
[97] Helmholtz-Zentrum Dresden-Rossendorf, Bautzner Landstraße 400, Dresden, 01328, Germany
[98] INAF - Osservatorio Astrofisico di Catania, Via S.Sofia 78, I-95123 Catania, Italy, INFN, Sezione di Catania, Via. S.Sofia 64, Catania, I-95123, Italy
[99] Physics Department, Eastern Mediterranean University, Famagusta, Cyprus
[100] Aix-Marseille Université, CNRS/IN2P3, CPPM, Marseille, France
[101] Department of Astrophysical Sciences, Peyton Hall, Princeton University, Princeton, NJ, 08544, USA
[102] School of Astronomy, Institute for Research in Fundamental Sciences (IPM), P. O. Box 19395-5531, Tehran, Iran
[103] Centre for Space Research, North-West University, Potchefstroom, South Africa
[104] Department of Physics and Astronomy, Union College, 807 Union Street, Schenectady, NY, 12308, USA
[105] Instituto Nacional de Astrofísica, Óptica y Electrónica, Puebla, México
[106] MTA-CSFK Lendület Large-scale Structure Research Group, Konkoly Thege Miklós út 15-17, Budapest, H-1121, Hungary
[107] Konkoly Observatory, HUN-REN CSFK, MTA Centre of Excellence, Konkoly Thege Miklós út 15-17., Budapest, H-1121, Hungary
[108] Department of Physics, University of Patras, Patras, 26500, Greece
[109] National Technical University of Athens, School of Applied Mathematics and Physical Sciences, Physics Division, Athens, GR15780, Greece
[110] Instituto de Astrofísica e Ciências do Espaço, Faculdade de Ciências da Universidade de Lisboa, Edifício C8, Campo Grande, Lisbon, P-1749-016, Portugal
[111] School for Data Science and Computational Thinking and Department of Mathematical Sciences, Stellenbosch University, Stellenbosch, 7602, South Africa
[112] Centre for Space Research, North-West University, Potchefstroom, 2520, South Africa
[113] Departamento de Matemáticas, Universidad Católica del Norte, Avda. Angamos 0610, Casilla 1280, Antofagasta, Chile
[114] Institute of Theoretical Physics, University of Wroclaw, pl. M. Borna 9, Wroclaw, 50-204, Poland
[115] Department of Physics, United College of Engineering and Research, Greater Noida, 201310, India
[116] Department of Mathematics, Indira Gandhi University, Meerpur, Haryana, 122502, India
[117] Centre For Theoretical Physics, Jamia Millia Islamia, New Delhi, India
[118] Center for Theoretical Physics, Polish Academy of Sciences, al. Lotników 32/46, Warsaw, 02-668, Poland
[119] DAMTP, Centre for Mathematical Sciences, University of Cambridge, Cambridge, CB3 0WA, UK
[120] Department of Astronomy & Astrophysics, University of Chicago, Chicago, IL, 60637, USA
[121] Kavli Institute for Cosmological Physics, University of Chicago, Chicago, IL, 60637, USA
[122] Center for Astronomy, Space Science and Astrophysics, Independent University, Bangladesh, Dhaka, 1229, Bangladesh
[123] Astrophysics Research Centre, University of KwaZulu-Natal, Westville Campus, Durban, 4041, South Africa
[124] School of Mathematics, Statistics and Computer Science, University of KwaZulu-Natal, Westville Campus, Durban, 4041, South Africa
[125] Department of Physics, 9500 Gilman Drive, San Diego, CA, 92122, USA
[126] Département de Physique Théorique and Center for Astroparticle Physics, Université de Genève, 24 quai Ernest Ansermet, Genève, 1211 4, Switzerland
[127] Florida State University, Department of Physics, 77 Chieftain Way, Tallahassee, FL, 32306, USA
[128] Center for Gravitational Physics and Quantum Information, Yukawa Institute for Theoretical Physics, Kyoto University, Kyoto, 606-8502, Japan
[129] National Institute of Chemical Physics and Biophysics, Rävala 10, Tallinn, 10143, Estonia
[130] Department of Physics and EHU Quantum Center, University of the Basque Country UPV/EHU, Barrio Sarriena s/n, Leioa, 48940, Spain
[131] Physics Department, Centro de Investigación y de Estudios Avanzados del Instituto Politécnico Nacional (Cinvestav), PO. Box 14-740, Av. Instituto Politécnico Nacional 2508, Mexico City, Mexico
[132] Dipartimento di Fisica and INFN Sezione di Roma 2, Università di Roma Tor Vergata, via della Ricerca Scientifica 1, Rome, 00133, Italy
[133] Observatório Nacional, Rua General José Cristino 77, São Cristóvão, Rio de Janeiro, RJ, 20921-400, Brasil
[134] Institute of Mathematics, University of the Philippines Diliman, Quezon City, Metro Manila, Philippines
[135] Computational Science Research Center, University of the Philippines Diliman, Quezon City, Metro Manila, Philippines
[136] Niels Bohr Institute, Blegdamsvej 17, Copenhagen, DK-2100, Denmark
[137] Division of Applied Analysis, Department of Mathematics, University of Patras, Rio Patras, GR-26504, Greece
[138] Division of Theoretical Physics, Rudjer Bošković Institute, Bijenička 54, Zagreb, 10000, Croatia
[139] Department of Electrical Engineering, Mazandaran University of Science and Technology, Babol, Iran
[140] Institute for Gravitation and the Cosmos, Department of Physics and Department of Astronomy and Astrophysics, Pennsylvania State University, University Park, Pennsylvania, 16802, USA
[141] Universidad de Concepción, Departamento de Astronomía, Casilla 160-C, Concepción, Chile
[142] Department of Physics and Astronomy, Sejong University, Seoul, 05006, Korea
[143] Université de Strasbourg, CNRS UMR 7550, Observatoire astronomique de Strasbourg, 11 rue de l'Université, Strasbourg, 67000, France
[144] Center for Particle Cosmology, Department of Physics and Astronomy, University of Pennsylvania, Philadelphia, PA, 19104, USA
[145] Nevada Center for Astrophysics and Department of Physics and Astronomy, University of Nevada, Las Vegas, Las Vegas, NV, 89154, USA
[146] Institute of Physics, University of Silesia in Katowice, Poland
[147] Mathematical Institute of the Serbian Academy of Sciences and Arts, Kneza Mihaila 36, Belgrade, 11000, Serbia
[148] Department of Physics, Lafayette College, Easton, PA, 18042, USA
[149] Max Planck Institute for Extraterrestrial Physics, Garching, Germany
[150] Department of Physics, University of the Basque Country UPV/EHU, P.O. Box 644, Bilbao, 48080, Spain

[151] Faculdade de Ciências, Universidade do Porto, Rua do Campo Alegre, Porto, 4150-007, Portugal
[152] Instituto de Astrofísica e Ciências do Espaço, Universidade do Porto, Rua das Estrelas, Porto, 4150-762, Portugal
[153] Instituto de Ciencias Físicas, Universidad Nacional Autónoma de México, Cuernavaca, México
[154] Department of Physics, National & Kapodistrian University of Athens, Zografou Campus, Athens, GR 157 73, Greece
[155] National Observatory of Athens, Lofos Nymfon, Athens, 11852, Greece
[156] Key Laboratory of Dark Matter and Space Astronomy, Purple Mountain Observatory, Chines Academy of Sciences, Nanjing, 210023, People's Republic of China
[157] School of Astronomy and Space Science, University of Science and Technology of China, Hefei, 230026, People's Republic of China
[158] SISSA - International School for Advanced Studies, Via Bonomea 265, Trieste, 34136, Italy
[159] Sapienza University,Piazzale Aldo Moro, c/o Dipartimento di Fisica, Edificio E. Fermi, Roma, Italy
[160] Center of applied space technology and microgravity (ZARM), University of Bremen, Am Fallturm 2, Bremen, 28359, Germany
[161] Centre for Space Research, North-West University, Private Bag X6001, Potchefstroom, South Africa
[162] Centro de Física das Universidades do Minho e do Porto, Faculdade de Ciências da Universidade do Porto, Rua do Campo Alegre s/n, Porto, 4169-007,
[163] Universidade dos Açores Instituto de Investigação em Ciências do Mar - OKEANOS, Campus da Horta, Rua Professor Doutor Frederico Machado 4, Horta, 9900-140, Portugal
[164] Centro Brasileiro de Pesquisas Físicas, Rua Dr. Xavier Sigaud 150, Rio de Janeiro, RJ, CEP 22290-180, Brazil
[165] Departament d'Informàtica, Matemàtica Aplicada i Estadística, Universitat de Girona, Campus Montilivi, Girona, 17003, Spain
[166] Laboratory of Theoretical Physics, Institute of Physics, University of Tartu, W. Ostwaldi 1, Tartu, 50411, Estonia
[167] Department of Physics and Astronomy, Haverford College, Haverford, PA, 19041, USA
[168] Department of Physics, Duke University, Durham, NC, 27708, USA
[169] Depto. de Física Teórica, Facultad de Ciencias Físicas, Universidad Complutense de Madrid, Plaza de las Ciencias 1, Madrid, 28040, Spain
[170] Main Astronomical Observatory of National Academy of Sciences of Ukraine, 27 Akademik Zabolotnyi St., Kyiv, 03143, Ukraine
[171] Departamento de Matemáticas, Universidad de León, Campus de Vegazana, s/n, León, 24071, Spain
[172] Departamento de Física Fundamental and Instituto Universitario de Física Fundamental y Matemáticas (IUFFyM), Universidad de Salamanca, Plaza de la Merced, s/n, Salamanca, E-37008, Spain
[173] Leibniz-Institut für Astrophysik Potsdam (AIP), An der Sternwarte 16, Potsdam, 14482, Germany
[174] Canada-France-Hawaii Telescope, 65-1238 Mamalahoa Hwy, Waimea, HI, 96743, USA
[175] School of Physical and Chemical Sciences, University of Canterbury, Private Bag 4800, Christchurch, 8140, New Zealand
[176] Centro de Investigaciones Energéticas Medioambientales y Tecnológicas CIEMAT, Av Complutense 40, Madrid, 28040, Spain
[177] Physik-Institut, University of Zürich, Winterthurerstrasse 190, Zürich, CH-8057, Switzerland
[178] Instituto Tecnológico de Piedras Negras, Mexico
[179] LUX, CNRS, Observatoire de Paris, France
[180] Instituto de Física Corpuscular (IFIC), University of Valencia-CSIC, Parc Científic UV, c/ Catedrático José Beltrán 2, Paterna, E-46980, Spain
[181] Bulgarian Academy of Sciences, Institute for Nuclear Research and Nuclear Energy, 72 Tszarigradsko Chaussee, Sofia, 1784, Bulgaria
[182] Department of Physics, Aristotle University of Thessaloniki, A.U.Th. Campus, Thessaloniki, 54635, Greece
[183] Departamento de Física Teórica and IPARCOS, Universidad Complutense de Madrid, Madrid, E-28040, Spain
[184] INAF - Osservatorio Astronomico di Trieste, via Tiepolo 11, Trieste, 34131, Italy
[185] IFPU - Institute for Fundamental Physics of the Universe, via Beirut 2, Trieste, 34151, Italy
[186] Center for Astrophysics Harvard & Smithsonian, 60 Garden Street, Cambridge, MA, 02138, USA
[187] Black Hole Initiative, Harvard University, 20 Garden Street, Cambridge, MA, 02138, USA
[188] STAR Institute, University of Liège, Quartier Agora, Allée du six Août 19c, Liège, 4000, Belgium
[189] Department of Theoretical Physics and Condensed Matter Physics (020), Vinča Institute of Nuclear Sciences - National Institute of the Republic of Serbia, University of Belgrade, P.O. Box 522, Belgrade, 11001, Serbia
[190] School of Astronomy, Institute for Research in Fundamental Sciences (IPM), P.O. Box 19395-5531, Tehran, Iran
[191] Innovation and Management Research Center, Ayatollah Amoli Branch, Islamic Azad University, Amol, Mazandaran, Iran
[192] Physics Department, Michigan Technological University, 1400 Townsend Dr, Houghton, MI, 49931, USA
[193] Instituto Nacional de Astrofisica, Optica y Electronica, L.E.Erro N.1, Tonantzintla, Puebla, Mexico
[194] Dipartimento di Fisica e Astronomia "Augusto Righi" - Università di Bologna, via Piero Gobetti 93/2, Bologna, I-40129, Italy
[195] Department of Physics, College of Science, Kuwait University, Sabah Al Salem University City, P.O. Box 2544, Safat 1320, Kuwait
[196] Physics Department, Sapienza University of Rome, P.le A. Moro 5, Roma, 00185, Italy
[197] Istituto Nazionale di Fisica Nucleare (INFN), Sezione di Roma, P.le A. Moro 5, Roma, I-00185, Italy
[198] Physics Department, Tor Vergata University of Rome, Via della Ricerca Scientifica 1, Roma, 00133, Italy
[199] Kavli Institute for the Physics and Mathematics of the Universe (WPI), UTIAS, The University of Tokyo, Chiba, 277-8583, Japan
[200] Faculty of Natural Sciences and Mathematics, Department of Mathematics, University of Tuzla, Ul. Urfeta Vejzagića br. 4, Tuzla, 75000, Bosnia and Herzegovina
[201] Van Swinderen Institute for Particle Physics and Gravity, University of Groningen, Nijenborgh 3, Groningen, 9747 AG, The Netherlands
[202] Department of Physics and Astronomy, Aarhus University, Aarhus C, DK-8000, Denmark
[203] Department of Physics and Astronomy, University of New Mexico, Albuquerque, NM, 87131, USA
[204] School of Mathematical and Physical Sciences, University of Sheffield, Hounsfield Road, Sheffield, S3 7RH, UK
[205] INAF Osservatorio Astronomico dAbruzzo, via Mentore Maggini snc, Teramo, I-64100, Italy
[206] INAF - Osservatorio Astronomioco di Roma (OAR), via Frascati 33, Monte Porzio Catone, RM, 00078, Italy
[207] Department of Mathematics, University College London, Gower Street, London, WC1E 6BT, UK
[208] Department of Physics, Indian Institute of Technology, Guwahati, 781039, India
[209] Institute for Astronomy, University of Hawaii, 2680 Woodlawn Drive, Honolulu, HI, 96822, USA
[210] Istituto Nazionale di Fisica Nucleare, Sez. di Napoli, Via Cinthia 21, Napoli, 80126, Italy
[211] Departamento de Física Teórica and IFIC, Centro Mixto Universitat de València - CSIC. Universitat de València, Valencia, Burjassot-46100, Spain
[212] Department of Informatics and Telecommunications, University of Peloponnese, Karaiskaki 70, Tripoli, 22100, Greece
[213] Dipartimento di Fisica, Università degli Studi di Torino, Via P. Giuria 1, Torino, I-10125, Italy
[214] INFN - Sezione di Torino, Via P. Giuria 1, Torino, I-10125, Italy
[215] INAF - Istituto Nazionale di Astrofisica, Osservatorio Astrofisico di Torino, strada Osservatorio 20, Pino torinese, 10025, Italy
[216] Departamento de Física, Faculdade de Ciências da Universidade de Lisboa, Edifício C8, Campo Grande, Lisbon, P-1749-016, Portugal
[217] Institut de Ciències del Cosmos, Universitat de Barcelona, Martí i Franquès, 1, Barcelona, E-08028, Spain
[218] ICREA, Pg. Lluís Companys 23, Barcelona, E-08010, Spain
[219] Institute of Theoretical Astrophysics, University of Oslo, PO Box 1029 Blindern, Oslo, 0315, Norway
[220] Department of Physics and Astronomy, University of North Carolina, Chapel Hill, NC, 27599-3255, USA
[221] Department of Physics, University of Malta, Msida, Malta
[222] Department of Physics and Astronomy, University of California, Davis, CA, USA
[223] Instituto de Ciencias F´sicas, Universidad Nacional Autónoma de México, Cuernavaca, Morelos, 62210, México
[224] Departamento de Matemáticas, Universidad Católica del Norte, Avda. Angamos 0610, Casilla 1280, Antofagasta, Chile
[225] Institute of Systems Science, Durban University of Technology, PO Box 1334, Durban, 4000, South Africa

[226] Physics Department, National Technical University of Athens, 15780 Zografou Campus, Athens, Greece
[227] Faculty of Science and Technology, University of Stavanger, Stavanger, 4036, Norway
[228] European Southern Observatory, Karl-Schwarzschild str. 2., Garching, 85748, Germany
[229] Dipartimento di Fisica e Scienze della Terra, Università degli Studi di Ferrara, Via Giuseppe Saragat 1, Ferrara, I-44122, Italy
[230] Istituto Nazionale di Fisica Nucleare, Sezione di Ferrara, Via Giuseppe Saragat 1, Ferrara, I-44122, Italy
[231] INFN - Laboratori Nazionali di Frascati (LNF), Via E. Fermi 54, Frascati, Roma, 00044, Italy
[232] National & Kapodistrian University of Athens,Department of Physics, Zografou Campus, Athens, GR 157 73, Greece
[233] ENEA, Fusion and Nuclear Safety Department, C.R. Frascati, Via E. Fermi 45, Frascati, 00044, Italy
[234] Physics Department, "Sapienza" University of Rome, P.le Aldo Moro 5, Rome, 00185, Italy
[235] Departamento de Física, Facultad de Ciencias, Universidad de Tarapacá, Casilla 7-D, Arica, Chile
[236] INAF - Osservatorio Astronomico di Roma, Via Frascati 33, Monte Porzio Catone, Roma, I-00040, Italy
[237] Dipartimento di Ingegneria, Università LUM, S.S. 100 km 18, Casamassima, Bari, 70010, Italy
[238] Department of Chemistry, Physics and Environmental and Soil Sciences, Escola Politècnica Superior, Universidad de Lleida, Av. Jaume II, 69, Lleida, 25001, Spain
[239] Universidade Federal do Ceará (UFC), Departamento de Física, Campus do Pici, C.P. 6030, Fortaleza, CE, 60455-760, Brazil
[240] Department of Physics, University of Nis, Visegradska 33, Nis, Serbia, SEENET-MTP Centre, Nis, Serbia
[241] ESTEC - European Space Agency, Keplerlaan 1, Noordwijk, 2201 AZ, The Netherlands
[242] Tsung-Dao Lee Institute (TDLI), No. 1 Lisuo Road, Shanghai, 201210, China
[243] School of Physics and Astronomy, Shanghai Jiao Tong University, Dongchuan Road 800, Shanghai, 201240, China
[244] Institute for Astronomy, the School of Physics, Zhejiang University, Hangzhou, 310027, People's Republic of China
[245] Department of Physics, Southern University of Science and Technology, Shenzhen, 518055, China
[246] Department of Physics & Astronomy, University of Kansas, 1251 Wescoe Hall Drive, Lawrence, KS, 66045, USA
[247] Institute of Physics, University of Szczecin, Wielkopolska 15, Szczecin, 70-451, Poland
[248] Physics Department, Ariel University, Ariel,
[249] High Energy Physics Research Unit, Faculty of Science, Chulalongkorn University, Bangkok, 10330, Thailand
[250] CEICO, Institute of Physics, Czech Academy of Sciences, Na Slovance 2, Praha, 182 21, Czech Republic
[251] Main Astronomical Observatory of the National Academy of Sciences of Ukraine, Akademik Zabolotnyi 27, Kyiv, 03143, Ukraine
[252] Department of Astronomy of the University of Geneva, 51 chemin de Pegasi, Versoix, 1290, Switzerland
[253] Department of Theoretical Physics, University of the Basque Country UPV/EHU, P.O. Box 644, Bilbao, 48080, Spain
[254] Shamakhy Astrophysical Observatory, Shamakhy, 5626, Azerbaijan
[255] Physics Department, Swansea University, UK
[256] Departamento de Física Teórica, Centro de Astropartículas y Física de Altas Energías, Universidad de Zaragoza, Zaragoza, 50009, Spain
[257] Institute of Physics, University of Silesia, Katowice, Poland
[258] Univ. Lille, CNRS, Centrale Lille, UMR 9189 CRIStAL, Lille, F-59000, France
[259] Université Paris-Saclay, CNRS, Institut d'Astrophysique Spatiale, Orsay, 91405, France
[260] Helsinki Institute of Physics, P.O. Box 64, University of Helsinki, Helsinki, FI-00014, Finland
[261] Academia Sinica Institute of Astronomy and Astrophysics, 11F of AS/NTU Astronomy-Mathematics Building, Roosevelt Rd, Taipei, 106216, Taiwan, ROC
[262] Bahamas Advanced Study Institute and Conferences, 4A Ocean Heights, Hill View Circle, Stella Maris, Long Island, The Bahamas
[263] Department of Physics & Astronomy, University of Hawai'i at Manoa, Watanabe Hall, 2505 Correa Road, Honolulu, HI, 96822, USA
[264] Leung Center for Cosmology & Particle Astrophysics, National Taiwan University, Taipei, 10617, Taiwan
[265] National Radio Astronomy Observatory, 520 Edgemont Road, Charlottesville, VA, 22903, USA
[266] NSF NOIRLab, 950 N. Cherry Avenue, Tucson, AZ, 85719, USA
[267] Departamento de Física Teórica and IPARCOS, Facultad de Ciencias Físicas, Universidad Complutense de Madrid, Madrid, E-28040, Spain
[268] Utah Valley University, Orem, Utah, USA
[269] Instituto de Fisica Teórica UAM/CSIC, Universidad Autonoma de Madrid, Cantoblanco, Madrid, 28049, Spain
[270] Nordita, KTH Institute of Technology and Stockholm University, Stockholm, SE-106 91,
[271] Department of Physics, National University of Ireland, Maynooth, Ireland
[272] Department of Physics, University of Arizona, Tucson, AZ, 85721, USA
[273] Department of Physics, University of Maryland, College Park, MD, 20742, USA
[274] Leiden Observatory, Leiden University, P.O. Box 9513, Leiden, 2300 RA, The Netherlands
[275] Department of Physics and Astronomy, University College London, Gower Street, London, WC1E 6BT, UK
[276] Department of Theoretical Physics, University of Szeged, Tisza Lajos krt. 84-86, Szeged, H-6720, Hungary
[277] Department of Theoretical Physics, HUN-REN Wigner Research Centre for Physics, Konkoly-Thege Miklós út 29-33, Budapest, H-1121, Hungary
[278] Institute of Physics, University of Tartu, Estonia
[279] Department of Physics and Astronomy, UNC-Chapel Hill, USA
[280] Instituto de Física, Universidade Federal Fluminense, Niteroi, RJ, 24210-346, Brazil
[281] SISSA, Scuola Internazionale Superiore di Studi Avanzati, via Bonomea, 265, Trieste, 34136, Italy
[282] Department of Physics, Simon Fraser University, Burnaby, BC, V5A 1S6, Canada
[283] INRNE, Bulgarian Academy of Sciences, Sofia, 1784, Bulgaria
[284] Department of Physics, University of Tirana, Boulevard "Zogu I", Tirana, Albania
[285] Department of Physics, Shanghai University, Shanghai, 200444, China
[286] Asia Pacific Center for Theoretical Physics, Pohang, 37673, Korea
[287] CFisUC, Department of Physics, University of Coimbra, Coimbra, P-3004 - 516, Portugal
[288] INAF, Osservatorio Astronomico di Capodimonte, Salita Moiariello 16, I-80131 Napoli, Italy & DARK, Niels Bohr Institute, University of Copenhagen, Jagtvej 128, Copenhagen, 2200, Denmark
[289] NSF NOIRLab, 950 N Cherry Ave, Tucson, AZ, 85719, USA
[290] Astronomy Unit, Queen Mary University of London, Mile End Road, London, E1 4NS, UK
[291] Universidad ECCI, Cra. 19 No. 49-20, Bogotá, 111311, Colombia
[292] Center for Theoretical Physics, Polish Academy of Sciences, al. Lotników 32/46, Warsaw, 02-668, Poland
[293] PDAT Laboratory, Department of Physics, K.N. Toosi University of Technology, P.O. Box 15875-4416, Tehran, Iran
[294] Department of Physics, Aristotle University of Thessaloniki, Thessaloniki, 54124, Greece
[295] CERIDES- Excellence in Innovation and Technology, European University of Cyprus, Nicosia, 1516, Cyprus
[296] Laboratorio de investigación de Cómputo de Física, Facultad de Ciencias Naturales y Exactas, Universidad de Playa Ancha, Subida Leopoldo Carvallo 270, Valparaíso, Chile
[297] Laboratorio de Didáctica de la Física, Departamento de Matemática, Física y Computación, Facultad de Ciencias Naturales y Exactas, Universidad de Playa Ancha, Subida Leopoldo Carvallo 270, Valparaíso, Chile
[298] University of Wrocław, Institute of Theoretical Physics, pl. Maxa Borna 9, Wrocław, 50-206, Poland
[299] University of Torino and INFN, via P. Giuria 1, Torino, 10125, Italy
[300] Tartu Observatory, University of Tartu, Observatooriumi 1, Tõravere, 61602, Estonia

[301] Institute of Physics, University of Tartu, W. Ostwaldi 1, Tartu, 50411, Estonia
[302] Physics Department, School of Applied Mathematical and Physical Sciences, National Technical University of Athens, 15780 Zografou Campus, Athens, Greece
[303] IKERBASQUE, Basque Foundation for Science, Bilbao, 48011, Spain
[304] Department of Physics & EHU Quantum Center, University of the Basque Country UPV/EHU, P.O. Box 644, Bilbao, 48080, Spain
[305] Laboratoire d'étude de l'Univers et des phénomènes eXtrêmes, Observatoire de Paris, UMR 8262 CNRS, Sorbonne Université,
[306] High Energy Physics Division, Argonne National Laboratory, Lemont, IL, 60439, USA
[307] Universe-Origins, University of Southern Denmark, Campusvej 55, Odense M, 5230, Denmark
[308] Kavli Institute for the Physics and Mathematics of the Universe (WPI), The University of Tokyo Institutes for Advanced Study (UTIAS), The University of Tokyo, Chiba, 277-8583, Japan
[309] Department of Physics, K.N. Toosi University of Technology, P.O. Box 15875-4416, Tehran, Iran
[310] Dipartimento di Fisica e Astronomia "A. Righi" - Alma Mater Studiorum Università di Bologna, via Piero Gobetti 93/2, 40129 Bologna, Italy
[311] INAF - Osservatorio di Astrofisica e Scienza dello Spazio di Bologna, via Piero Gobetti 93/3, 40129, Bologna, Italy
[312] Technical University Munich, School of Natural Sciences, Physik Department T31, James-Franck Str. 1, Garching, 85748, Germany
[313] Universidad de Buenos Aires, Facultad de Ciencias Exactas y Naturales, Departamento de Física, Buenos Aires, Argentina
[314] CONICET - Universidad de Buenos Aires, Instituto de Física de Buenos Aires (IFIBA), Buenos Aires, Argentina
[315] INAF-Osservatorio Astronomico di Roma, Via Frascati 33, Monteporzio Catone, 00078, Italy
[316] INFN-Sezione di Roma, Piazzale Aldo Moro, 2 - c/o Dipartimento di Fisica, Edificio G. Marconi, Roma, 00185, Italy
[317] Dipartimento di Fisica e Astronomia Augusto Righi - Università di Bologna, via Piero Gobetti 93/2, Bologna, I-40129, Italy
[318] Department of Physics, Karadeniz Technical University, Trabzon, TR61080, Türkiye
[319] Depto. de Física y Matemáticas, Universidad Iberoamericana Ciudad de México, Prolongación Paseo de la Reforma 880, México D. F., 01219, Mexico
[320] Faculty of Sciences and Mathematics, University on Nis, Serbia
[321] Konkoly Observatory, HUN-REN Research Centre of Astronomy and Earth Sciences (CSFK), MTA Centre of Excellence, Konkoly Thege Miklós út 15-17., Budapest, H-1121, Hungary
[322] Department of Physics, The University of Texas at Dallas, Richardson, TX, 75080, USA
[323] Astronomical Institute, Faculty of Mathematics and Physics, Charles University, V Holešovičkách 2, Praha, CZ-180 00, Czech Republic
[324] Universitäts-Sternwarte München, Fakultät für Physik, Ludwig-Maximilians-Universität München, Scheinerstr. 1, München, D-81679, Germany
[325] INFN-Sezione di Bologna, Viale Berti Pichat 6/2, Bologna, 40127, Italy
[326] Laboratoire des 2 Infinis - Toulouse (L2IT-IN2P3), Université de Toulouse, CNRS, Toulouse Cedex 9, F-31062, France
[327] University of Torino and INFN/Torino, via P. Giuria 1, Torino, 10125, Italy
[328] Department of Electrical and Electronics Engineering Doğuş University, Umraniye, Istanbul, 34775, Türkiye
[329] Physics Department, King's College London, Strand, London, WC2R 2LS, UK
[330] Department of Physics, Faculty of Science, University of Thessaly, Thessaly, GR 35100, Greece
[331] Duke University, Durham, NC, 27708, USA
[332] Cosmology, Gravity and Astroparticle Physics Group, Center for Theoretical Physics of the Universe, Institute for Basic Science, Daejeon, 34126, Korea
[333] LTE, Observatoire de Paris, Université PSL, CNRS, LNE, Sorbonne Université, 61 avenue de lObservatoire, Paris, 75 014, France
[334] Department of Physics, Sharif University of Technology, Tehran, 11155-9161, Iran
[335] Department of Physics, Shahid Beheshti University, Tehran, 1983969411, Iran
[336] Center for Research and Training in Innovative Techniques of Applied Mathematics in Engineering, University Politehnica of Bucharest, Bucharest, 060042, Romania
[337] International Centre for Space and Cosmology, Ahmedabad University, Ahmedabad, 380009, India
[338] Department of Physics and Astronomy, Vanderbilt University, Nashville, TN, 37235, USA
[339] Main Astronomical Observatory of the National Academy of Sciences of Ukraine, 27 Akademik Zabolotny St., Kyiv, 03143, Ukraine
[340] Astronomical Observatory, Taras Shevchenko National University of Kyiv, 3 Observatorna St., Kyiv, 04053, Ukraine
[341] Department of Physics, University of Aberdeen, Aberdeen, AB24 3UE, UK
[342] Department of Physics, University of the Basque Country, Spain
[343] INFN Sezione di Ferrara, Via Saragat 1, Ferrara, 44122, Italy
[344] ICSC, Centro Nazionale "High Performance Computing, Big Data and Quantum Computing", Italy
[345] Research School of Astronomy and Astrophysics, The Australian National University, Mount Stromlo Observatory, Canberra, ACT, 2611, Australia
[346] Department of Physics and Astronomy, Vesilinnantie 5, University of Turku, Turku, 20014, Finland
[347] Centre for Theoretical Cosmology, Department of Applied Mathematics and Theoretical Physics, University of Cambridge, Wilberforce Road, Cambridge, CB3 0WA, UK
[348] Department of Physics, School of Applied Mathematical and Physical Sciences, National Technical University of Athens, 9 Iroon Polytechniou Str., Zografou Campus, Athens, GR 157 80, Greece
[349] Department of Physics, Northeastern University, Boston, MA, 02115, USA
[350] Astronomical Observatory, Volgina 7, P.O. Box 74, Belgrade, 11060, Serbia
[351] Physics and Applied Mathematics Unit, Indian Statistical Institute, 203 B.T. Road, Kolkata, 700 108, India
[352] DARK, Niels Bohr Institute, University of Copenhagen, Jagtvej 155, Copenhagen, 2200, Denmark
[353] Institute of Physics, Laboratory of Astrophysics, École Polytechnique Fédérale de Lausanne (EPFL), Observatoire de Sauverny, Versoix, CH-1290, Switzerland
[354] Department of Physics, Ankara University, Faculty of Sciences, Ankara, 06100, Turkiye
[355] INAF - Osservatorio Astronomico dAbruzzo, Via Maggini, Teramo, 64100, Italy
[356] Physics Department, Mapúa University, 658 Muralla St., Intramuros, Manila, 1002, Philippines
[357] Astrophysics, University of Oxford, Denys Wilkinson Building, Keble Road, Oxford, OX1 3RH, UK
[358] School of Physics and Astronomy, University of Southampton, Southampton, UK
[359] Instituto Nacional de Astrofísica, Óptica y Electrónica,Tonantzintla, Puebla, México
[360] Facultad de Astronomía y Geofísica, Universidad de La Plata, La Plata, Argentina
[361] INFN - Sezione di Roma 1, P.le Aldo Moro 2, Roma, 00185, Italy
[362] Instituto de Astronomía, Universidad Nacional Autónoma de México, Av. Universidad 3000, Col. Universidad Nacional Autónoma de México, Ciudad de México, C.P. 04510,
[363] Escola de Ciências e Tecnologia, Universidade Federal do Rio Grande do Norte, Campus Universitário Lagoa Nova, Natal, RN, 59078-970, Brazil
[364] Physics Department, University of the Basque Country UPV/EHU, 644 PO Box, Bilbao, 48080, Spain
[365] Department of Physics, University of Alberta, Edmonton, Alberta, T6G 2E1, Canada
[366] Department of Mathematical and Statistical Sciences, University of Alberta, Edmonton, Alberta, T6G 2G1, Canada
[367] Theoretical Physics Institute, University of Alberta, Edmonton, Alberta, T6G 2E1, Canada
[368] Islamic Azad University, Science and Research Branch, Tehran, Iran
[369] Dipartimento di Fisica e Scienze della Terra, Università degli Studi di Ferrara, Ferrara, 44122, Italy
[370] Dipartimento di Fisica, Università di Trento, Trento, 38123, Italy
[371] Department of Physics, Columbia University, New York, NY, USA
[372] SISSA, Via Bonomea 265, Trieste, 34136, Italy
[373] Institute for Fundamental Physics of the Universe (IFPU), Via Beirut 2, Trieste, 34014, Italy

[374] Faculty of Symbiotic Systems Science, Fukushima University, Fukushima, 960-1296, Japan
[375] Theoretical Physics Group and Quantum Alberta, Department of Physics and Astronomy, University of Lethbridge, 4401 University Drive, Lethbridge, Alberta, T1K 7Z2, Canada
[376] Kavli Institute for the Physics and Mathematics of the Universe (WPI), The University of Tokyo Institutes for Advanced Study (UTIAS), The University of Tokyo, Kashiwa, Chiba, 277-8583, Japan
[377] Cosmology, Gravity, and Astroparticle Physics Group, Center for Theoretical Physics of the Universe, Institute for Basic Science (IBS), Daejeon, 34126, Korea
[378] Universität Innsbruck, Institut für Astro- und Teilchenphysik, Technikerstrasse 25, Innsbruck, 6020, Austria
[379] Institute of Space Sciences (ICE, CSIC), C. Can Magrans s/n, Barcelona, 08193, Spain
[380] ICREA, Passeig Lluis Companys, 23, Barcelona, 08010, Spain
[381] Universität Bonn, Regina-Pacis-Weg 3, Bonn, 53113, Germany
[382] Institute of Cosmology & Gravitation, Dennis Sciama Building, University of Portsmouth, Portsmouth, PO1 3FX, UK
[383] Technical University of Munich, TUM School of Natural Sciences, Physics Department, James-Franck-Straße 1, Garching, 85748, Germany
[384] Max-Planck-Institut für Astrophysik, Karl-Schwarzschild Straße 1, Garching, 85748, Germany
[385] Institute of Astronomy and Astrophysics, Academia Sinica, No. 1, Section 4, Roosevelt Road, Taipei, 106319, Taiwan
[386] Ruhr University Bochum, Faculty of Physics and Astronomy, Astronomical Institute (AIRUB), German Centre for Cosmological Lensing, Bochum, 44780, Germany
[387] Leiden Observatory, Leiden University, Einsteinweg 55, Leiden, 2333 CC, The Netherlands
[388] University of California, Riverside, CA, 92507, USA
[389] Department of Physics and Astronomy, Stony Brook University, Stony Brook, NY, 11794, USA
[390] INAF - Osservatorio di astrofisica e scienza dello spazio, via Gobetti 93/3, Bologna, 40129, Italy
[391] Dipartimento di Fisica, Universit'a di Trento, Via Sommarive 14, Povo, Trento, 38123, Italy
[392] Trento Institute for Fundamental Physics and Applications (TIFPA), Via Sommarive 14, Povo, Trento, 38123, Italy
[393] Max Planck Institute for Extraterrestrial Physics, Giessenbachstrasse 1, Garching, 85748, Germany
[394] Universite Paris-Saclay, CNRS/IN2P3, IJCLab, Orsay, 91405, France
[395] Academy of Athens, Research Center for Astronomy and Applied Mathematics, Soranou Efesiou 4, Athens, 11527, Greece
[396] School of Sciences, European University Cyprus, Diogenes Street, Engomi, Nicosia, 1516, Cyprus
[397] Università di Torino, Physics department, via P. Giuria 1, Turin, 10125, Italy
[398] Department of Physics, University of Thessaly, Lamia, 35100, Greece
[399] Astronomical Observatory, University of Warsaw, Al. Ujazdowskie 4, Warszawa, PL-00478, Poland
[400] Data Science Institute, Plaksha University, Mohali, Punjab, 140306, India
[401] CONICET-Universidad de Buenos Aires-Instituto de Física de Buenos Aires, Av. Intendente Cantilo S/N, CABA, 1428, Argentina
[402] International Gemini Observatory, NSF NOIRLab, Casilla 603, La Serena, Chile
[403] Laboratorio Nacional de Astrofisica - MCTI, Itajuba, MG, 37504-364, Brazil
[404] Center for Astrophysics and Cosmology, University of Nova Gorica, Vipavska 11c, Ajdovščina, 5270, Slovenia
[405] Dipartimento di Fisica e Scienze della Terra, Università degli Studi di Ferrara, Via G. Saragat 1, Ferrara, I-44122, Italy
[406] Istituto Nazionale di Fisica Nucleare (INFN), Sezione di Ferrara, Via G. Saragat 1, Ferrara, I-44122, Italy
[407] Institute of Space Sciences (ICE,CSIC), C. Can Magrans s/n, Barcelona, 08193, Spain
[408] Galileo Galilei Institute for Theoretical Physics, Largo Enrico Fermi 2, Firenze, I-50125, Italy
[409] Department of Physics, Simon Fraser University, Burnaby, BC, V5A 1S6, Canada
[410] National Institute of Chemical Physics and Biophysics, Rävala pst. 10, Tallinn, 10143, Estonia
[411] Department of Physics, University of Oslo, Box 1048, Oslo, N-0316, Norway
[412] Institut de Física dAltes Energies (IFAE), The Barcelona Institute of Science and Technology, Campus UAB, Bellaterra (Barcelona), 08193, Spain
[413] Department of Physics, University of Ottawa, 75 Laurier Ave E, Ottawa, Canada
[414] Astrophysics Research Center of the Open University, The Open University of Israel, Raanana, Israel
[415] Departamento de Física, Universidade Federal do Espírito Santo, Vitória, ES, 29075-910, Brazil
[416] Department of Physics and Astronomy, Sejong Universe, Seoul, 05006, South Korea
[417] INAF-OAS, Bologna, via P. Gobetti 101, I-40129, Italy
[418] Scottish Universities Physics Alliance, University of Saint Andrews, North Haugh, Saint Andrews, Fife, KY16 9SS, UK
[419] Instituto de Física Corpuscular (IFIC), CSIC – Universitat de València, C/ Catedrático José Beltrán 2, Paterna (Valencia), 46980, Spain
[420] Department of Mathematics, University of Thessaly, GR-35100, Greece
[421] Department of Mathematics, Faculty of Natural and Mathematical Sciences, University of Tuzla, Urfeta Vejzagica 4, Tuzla, 75000, Bosnia and Herzegovina
[422] School of Theoretical Physics, Dublin Institute for Advanced Studies (DIAS), 10 Burlington Road, Dublin, D04 C932, Ireland
[423] Department of Physics and Helsinki Institute of Physics, Gustaf Hallstromin katu 2, University of Helsinki, Helsinki, FIN-00014, Finland
[424] Instituto de Física y Astronomía, Universidad de Valparaíso, Avda. Gran Bretaña 1111, Valparaíso, Chile
[425] Leiden Observatory, Leiden University, PO Box 9513, Leiden, 2300 RA, The Netherlands
[426] Max-Planck-Institut für extraterrestrische Physik, Gießenbachstraße 1, Garching, 85748, Germany
[427] INAF, Osservatorio di Astrofisica e Scienza dello Spazio, via Piero Gobetti 93/3, Bologna, 40129, Italy
[428] Center for Physical Sciences and Technology, Saulėtekio av. 3, Vilnius, 10257, Lithuania
[429] Department of Physics, Liaoning Normal University, Dalian, 116029, P. R. China
[430] Department of Astronomy, School of Physical Sciences, University of Science and Technology of China, Hefei, 230026, China
[431] Department of Physics, Institute of Science Tokyo, Tokyo, 152-8551, Japan
[432] CAS Key Laboratory for Research in Galaxies and Cosmology, School of Astronomy and Space Science, University of Science and Technology of China, Hefei, 230026, China
[433] Department of Mathematics, University of Okara, Okara, 56300, Pakistan
[434] Center for Astronomy and Astrophysics, Center for Field Theory and Particle Physics and Department of Physics, Fudan University, Shanghai, 200438, China
[435] Institute of Physics and Astronomy, ELTE Eötvös Loránd University, Budapest, 1117, Hungary
[436] Facultad de Física, Pontificia Universidad Católica de Chile, Vicuña Mackenna 4860, Santiago, Chile
[437] Institut für Theoretische Physik and Atominstitut, Technische Universität Wien, Wiedner Hauptstrasse 8–10, Vienna, A-1040, Austria
[438] Indian Institute of Astrophysics, Bengaluru, Karnataka, 560034, India
[439] University of Wroclaw, Poland
[440] Complutense University of Madrid,
[441] Max Planck Institute for Radio Astronomy, Auf dem Huegel 69, Bonn, D-53121, Germany
[442] Institute of Physics, Silesian University in Opava, Opava, CZ-74601, Czech Republic
[443] Universiti Malaya, Kuala Lumpur, Wilayah Persekutuan Kuala Lumpur, 50603,
[444] Department of Physics, Tezpur University, Napaam, Tezpur, Assam, 784028, India
[445] Institute for Computational Cosmology, Department of Physics, Durham University, South Road, Durham, DH1 3LE, UK
[446] Institute for Astronomy, University of Edinburgh, Royal Observatory, Blackford Hill, Edinburgh, EH9 3HJ, UK
[447] Higgs Centre for Theoretical Physics, School of Physics and Astronomy, Edinburgh, EH9 3FD, UK
[448] Department of Mathematics, BITS-Pilani Hyderabad Campus, India

[449] Institute for Advanced Studies, New Uzbekistan University, Movarounnahr str. 1, Tashkent, 100000, Uzbekistan
[450] Institute of Theoretical Physics, National University of Uzbekistan, Tashkent, 100174, Uzbekistan
[451] Departamento de Física, Facultad de Ciencias Físicas y Matemáticas, Universidad de Chile,
[452] The Oskar Klein Centre, Department of Physics, Stockholm University, Stockholm, SE - 106 91, Sweden
[453] Department of Physics, Department of Astronomy & Astrophysics, KICP, and EFI, University of Chicago, Chicago, IL, 60637, USA
[454] Institute of Theoretical Astrophysics, University of Oslo, Oslo, 0315, Norway
[455] Department of Physics and Astronomy, PAB, 430 Portola Plaza, Box 951547, Los Angeles, CA, 90095-1547, USA
[456] Departments of Astronomy and Physics, Boston University, Boston, MA, 02215, USA
[457] Ben Gurion University of the Negev, Beer Sheva, Israel
[458] Departamento de Física Teórica, Módulo 15, Facultad de Ciencias, Universidad Autónoma de Madrid, Madrid, 28049, Spain
[459] Instituto de Física, Universidade Federal do Rio Grande do Sul, Porto Alegre, RS, 91501-970, Brazil
[460] Department of Physics, Faculty of Arts and Sciences, Istanbul Technical University, Istanbul, Turkey
[461] Department of Physics and Astronomy, University of Sussex, Brighton, BN1 9QH, UK
[462] University of Zurich, Winterthurerstrasse 190, Zurich, 8057, Switzerland
[463] Instituto Superior Tecnico - IST, Universidade de Lisboa, Lisboa, 1049-001, Portugal
[464] Laboratorio de Instrumentaÿcao e Fsica Experimental de Partculas, 1649-003 Lisboa and 3004-516 Coimbra, Portugal
[465] Argelander-Institut für Astronomie, Universität Bonn, Auf dem Hügel 71, Bonn, 53121, Germany
[466] Department of Physics and Astronomy, University of New Mexico, Albuqerque, NM, 87106, USA
[467] Heidelberg Institute for Theoretical Studies (HITS), Schloss-Wolfsbrunnenweg 35, Heidelberg, 69118, Germany
[468] Department of Physics, University of Helsinki, Gustaf Hällströmin katu 2, Helsinki, FI-00014, Finland
[469] National Institute of Physics, University of the Philippines, Quezon City, Philippines
[470] Sydney Institute for Astronomy, School of Physics, A28, The University of Sydney, NSW, 2006, Australia
[471] L2IT, Laboratoire des 2 Infinis - Toulouse, CNRS/IN2P3, UPS, Toulouse Cedex 9, F-31062, France
[472] MTA-ELTE Astrophysics Research Group, Budapest, 1117, Hungary
[473] Centro de Astrofísica e Gravitação - CENTRA, Departamento de Física, Instituto Superior Técnico - IST, Universidade de Lisboa - UL, Av. Rovisco Pais 1, Lisboa, 1049-001, Portugal
[474] Dipartimento di Fisica e Astronomia, Università di Firenze, via G. Sansone 1, Sesto Fiorentino, Firenze, 50019, Italy
[475] INAF Osservatorio Astrofisico di Arcetri, Largo Enrico Fermi 5, Firenze, I-50125, Italy
[476] GRAPPA Institute, Institute for Theoretical Physics Amsterdam, University of Amsterdam, Science Park 904, Amsterdam, 1098 XH, The Netherlands
[477] Université Claude Bernard Lyon 1, IUF, IP2I Lyon, 4 rue Enrico Fermi, Villeurbanne, 69622, France
[478] Research Institute for Astronomy and Astrophysics of Maragha (RIAAM), P.O. Box 55134-441, Maragha, Iran
[479] Instituto de Física, Universidade Federal Fluminense, Avenida General Milton Tavares de Souza s/n, Gragoatá, Niteroi, Rio de Janeiro, 24210-346, Brazil
[480] Centro de Astrofísica e Gravitação - CENTRA, Departamento de Física, Instituto Superior Técnico - IST, Universidade de Lisboa - UL, Av. Rovisco Pais 1, 1049-001, Lisboa, Portugal
[481] Department of Physics of Complex Systems, ELTE Eötvös Loránd University, Budapest, 1117, Hungary
[482] Department of Physics, Boston University, Boston, Massachusetts, 02215, USA
[483] Institute of Physics, Ss Cyril and Methodius University in Skopje, North Macedonia
[484] Departamento de Física, Universidad de Córdoba, Córdoba, E-14071, Spain
[485] Department of Mathematics, Faculty of Science, University of Malta,
[486] Institute for Theoretical Particle Physics and Cosmology (TTK), RWTH Aachen University, Aachen, 52056, Germany
[487] School of Physical Sciences, University of Chinese Academy of Sciences, Beijing, 100049, China
[488] Physics Department, State University of Tetovo, Ilinden Street nn, Tetovo, 1200, North Macedonia
[489] Institute for Theoretical Physics, Universität Heidelberg, Philosophenweg 16, Heidelberg, 69120, Germany
[490] Kapteyn Astronomical Insitute, University of Groningen, P.O.Box 800, Groningen, 9700AV, The Netherlands
[491] Department of Mathematics, Birla Institute of Technology and Science-Pilani, Hyderabad Campus, Hyderabad, 500078, India
[492] Département de Physique Théorique, Université de Genève, 24 quai Ernest Ansermet, Genève, 1211 4, Switzerland
[493] IATE-OAC-UNC and CONICET, Laprida 854, Barrio Observatorio, Cordoba, 5000, Argentina
[494] Center for Cosmology and Astrophysics, Alikhanian National Laboratory and Yerevan State University, Yerevan, Armenia
[495] Institute of Applied Sciences, The Malta College of Arts, Science and Technology, Paola, Malta
[496] Department of Theoretical Physics, Faculty of Mathematics, Physics and Informatics, Comenius University in Bratislava, 84248, Slovak Republic
[497] Centre for Theoretical Physics and Natural Philosophy, Mahidol University, Nakhonsawan Campus, Phayuha Khiri, Nakhonsawan, 60130, Thailand
[498] Javakhishvili Tbilisi State University, 3 Chavchavadze Avenue, Tbilisi, 0179, Georgia
[499] Institut für Theoretische Physik, Universität Münster, Münster, 48149, Germany
[500] Dipartimento di Fisica e Astronomia, Università di Bologna, via Irnerio 46, Bologna, 40126, Italy
[501] INFN, Sezione di Bologna, viale Berti Pichat 6/2, Bologna, 40127, Italy
[502] Instituto de Física & Observatório do Valongo, Universidade Federal do Rio de Janeiro, Rio de Janeiro, RJ, Brazil
[503] PPG Cosmo, Universidade Federal do Espírito Santo, Vitória, ES, 29075-910, Brazil
[504] Max Planck Institute for Gravitational Physics (Albert Einstein Institute), Am Muhlenberg 1, Potsdam-Golm, D-14476, Germany
[505] Astronomical Observatory, Volgina 7, Belgrade, 11060, Serbia
[506] Vinca Institute of Nuclear Sciences - National Institute of the Republic of Serbia, University of Belgrade,
[507] Center for Physical Sciences and Technology, Sauletekio av. 3, Vilnius, 10257, Lithuania
[508] Institute of Theoretical Physics & Research Center of Gravitation; Key Laboratory of Quantum Theory and Applications of MoE; and Lanzhou Center for Theoretical Physics & Key Laboratory of Theoretical Physics of Gansu Province, Lanzhou University, Lanzhou, 730000, China
[509] Instituto de Astrofísica e Ciências do Espaço, Universidade de Lisboa, Faculdade de Ciências, Ed. C8, Campo Grande, Lisboa, 1769-016, Portugal
[510] Université de Paris-Cité, APC-Astroparticule et Cosmologie (UMR-CNRS 7164), Paris, F-75006, France
[511] Department of Physical Foundations of Engineering, Politehnica University of Timisoara, Timisoara, 300223, Romania
[512] National Research University TIIAME, Kori Niyoziy 39, Tashkent, 100000, Uzbekistan
[513] Dipartimento di Scienza e Alta Tecnologia (DiSAT), Università degli Studi dell'Insubria, via Valleggio 11, Como, 22100, Italy
[514] Istituto Nazionale di Fisica Nucleare (INFN), Sezione di MIlano, via Celoria 16, Milano, 20126, Italy
[515] Como Lake centre for AstroPhysics (CLAP), DiSAT, Università dellInsubria, via Valleggio 11, Como, 22100, Italy
[516] Centro Brasileiro de Pesquisas Físicas, Rua Dr. Xavier Sigaud 150, Rio de Janeiro, RJ, 22290-180, Brazil
[517] HUN-RENELTE Extragalactic Astrophysics Research Group, Budapest, 1117, Hungary
[518] School of Science, Constructor University, Bremen, 28759, Germany
[519] Instituto de Física Fundamental (CSIC), Serrano 123, 28006 Madrid, Spain and Institute of Cosmos Science (ICCUB), Martí i Franques 1, Barcelona, 08028, Spain
[520] Universidade Federal do Ceará (UFC), Departamento de Física, Campus do Pici, C.P. 6030, Fortaleza, CE, 60455-760, Brazil
[521] Département de Physique Thèorique, Université de Genève, Quai E. Ansemet 24, Geneve, 1211, Switzerland
[522] Department of Mathematics, School of Computer Science and Artificial Intellegence, S R Univrsity, Warangal, Telangana, 506371, India
[523] Dipartimento di Fisica e Astronomia G. Galilei, Università degli Studi di Padova, Padova, Italy

[524] Institute for Astronomy, University of Edinburgh, Royal Observatory Edinburgh, Blackford Hill, Edinburgh, EH9 3HJ, UK
[525] Instituto de Astrofísica e Ciências do Espaço, Faculdade de Ciências da Universidade de Lisboa, Campo Grande, Lisboa, PT1749-016, Portugal
[526] Department of Physics, Syracuse University, Syracuse, NY, 13244, USA
[527] Department of Physics and Astronomy, University of South Carolina, Columbia, SC, 29208, USA
[528] Institute of Theoretical Physics, Chinese Academy of Sciences, Beijing, 100190, China
[529] Asia Pacific Center for Theoretical Physics (APCTP), Pohang, 37673, Korea
[530] Department of Physics, School of Advanced Sciences, Vellore Institute of Technology, Vellore, Tiruvalam Rd, Katpadi, Tamil Nadu, 632014, India
[531] Department of Astronomy & Astrophysics, Tata Institute of Fundamental Research, 1, Homi Bhabha Road, Colaba, Mumbai, 400005, India
[532] Ruer Bokovi Institute, Zagreb, Croatia
[533] Institute of Cosmology and Gravitation, University of Portsmouth,
[534] ECEO, Universidade Lusófona, Campo Grande 376, Lisboa, 1749-024, Portugal
[535] Department of Physics and Materials Science, University of Luxembourg, Luxembourg City, L-1511, Luxembourg
[536] Astronomical Observatory Belgrade, Volgina 7, Belgrade, 11060, Serbia
[537] Mathematical Sciences and STAG Research Centre, University of Southampton, Southampton, SO17 1BJ, United Kingdom
[538] Institute of physics Belgrade, Belgrade University, Pregrevica 118, Belgrade, Serbia
[539] Department of Physics, the Chinese University of Hong Kong, Sha Tin, NT, Hong Kong,
[540] Department of Physics, Hokkaido University, Sapporo, 060-0810, Japan
[541] School of Fundamental Physics and Mathematical Sciences, Hangzhou Institute for Advanced Study, UCAS, Hangzhou, 310024, China
[542] International Center for Theoretical Physics Asia-Pacific, Beijing/Hangzhou, China
[543] School of Physics, Korea Institute for Advanced Study (KIAS), 85 Hoegiro, Dongdaemun-gu, Seoul, 02455, Korea

ABSTRACT

The standard model of cosmology has provided a good phenomenological description of a wide range of observations both at astrophysical and cosmological scales for several decades. This concordance model is constructed by a universal cosmological constant and supported by a matter sector described by the standard model of particle physics and a cold dark matter contribution, as well as very early-time inflationary physics, and underpinned by gravitation through general relativity. There have always been open questions about the soundness of the foundations of the standard model. However, recent years have shown that there may also be questions from the observational sector with the emergence of differences between certain cosmological probes. In this White Paper, we identify the key objectives that need to be addressed over the coming decade together with the core science projects that aim to meet these challenges. These discordances primarily rest on the divergence in the measurement of core cosmological parameters with varying levels of statistical confidence. These possible statistical tensions may be partially accounted for by systematics in various measurements or cosmological probes but there is also a growing indication of potential new physics beyond the standard model. After reviewing the principal probes used in the measurement of cosmological parameters, as well as potential systematics, we discuss the most promising array of potential new physics that may be observable in upcoming surveys. We also discuss the growing set of novel data analysis approaches that go beyond traditional methods to test physical models. These new methods will become increasingly important in the coming years as the volume of survey data continues to increase, and as the degeneracy between predictions of different physical models grows. There are several perspectives on the divergences between the values of cosmological parameters, such as the model-independent probes in the late Universe and model-dependent measurements in the early Universe, which we cover at length. The White Paper closes with a number of recommendations for the community to focus on for the upcoming decade of observational cosmology, statistical data analysis, and fundamental physics developments.

Executive summary

The CosmoVerse network is born out of the CosmoVerse COST Action (formally CA21136 - Addressing observational tensions in cosmology with systematics and fundamental physics [1,2]), which traces its origins to the SNOWMASS 2021 effort in the cosmic tensions sector [3–7]. This will be one of the key deliverables of the COST Action and one of its lasting legacies. The aim of this network is to establish synergy among researchers working across the disparate themes of observational cosmology, novel techniques of data analysis, and fundamental physics. This White Paper demonstrates how this effort has been successful, while also laying out a roadmap to sustain those efforts and expand the interdisciplinary nature of the topic across different areas of the community. Another core aspect of this effort is to harmonize approaches between the constituent subcommunities and to create a common language in which to discuss the topic of cosmic tensions.

In the White Paper, the accomplishment of these goals is demonstrated through the interwoven connections between the key communities of the network and the granular topics. This was achieved through a diverse set of actions, including the CosmoVerse Seminar

Series led by Eleonora Di Valentino [8], the CosmoVerse conferences and the discussions and presentations involved in these events [9], the CosmoVerse School held in Corfu in 2024 [10], the CosmoVerse Training Series, which involved a significant effort to bridge [11], as well as the CosmoVerse Journal Club, led by Enrico Specogna and Mahdi Najafi [12].

The CosmoVerse White Paper, edited by Jackson Levi Said and Eleonora Di Valentino, is a collective effort from the community to review the state of the art and identify opportunities to address tensions in cosmology over the coming years. This includes progress in observational cosmology and the exhaustive treatment of potential systematics, the development of new data analysis approaches for upcoming surveys and potential new physics models, as well as the construction of cosmological models that appropriately address the areas where the concordance model exhibits tensions. These topics are organized as follows:

- Section 1 - Introduction and state-of-the-art.
- Section 2 - Observational cosmology. *Coordinators: Adam Riess, Amanda Weltman, Antonella Palmese, Caroline D. Huang, Chandra Shekhar Saraf, Cheng-Yu Kuo, Cora Uhlemann, Dan Scolnic, Daniela Grandón, Dante Paz, Dominique Eckert, Florian Beutler, Gabriela Barenboim, Ilaria Musella, Istvan Szapudi, Jack Singal, Khaled Said, Leandros Perivolaropoulos, Lluís Galbany, Louise Breuval, Louise Breuval, Maria Giovanna Dainotti, Maria Vincenzi, Marika Asgari, Martina Gerbino, Margherita Lembo, Matteo Forconi, Michele Cantiello, Michele Moresco, Nils Schöneberg, Ricardo Chávez Murillo, Richard I. Anderson, Rick Watkins, Shahin Sheikh-Jabbari, Siyang Li, Tommaso Treu, Vid Iršič, Will Handley, William Giarè and Yukei Murakami*.
- Section 3 - Novel data analysis techniques. *Coordinators: Agnieszka Pollo, Adriá Gómez-Valent, Daniela Grandón, Jesus Torrado, Jurgen Mifsud, Lei Zu, Luis Escamilla, and Reginald Christian Bernardo*.
- Section 4 - Fundamental physics. *Coordinators: Vivian Poulin, Carsten van de Bruck, Elsa Teixeira, Emmanuel N. Saridakis, Eoin O Colgain, Florian Niedermann, Francesco Bajardi, Giulia Gubitosi, Indranil Banik, Jaime Haro Cases, Jens Chluba, Karsten Jedamzik, Konstantinos F. Dialektopoulos, Laura Herold, Leandros Perivolaropoulos, Luca Visinelli, Luis Anchordoqui, Micol Benetti, Özgür Akarsu, Rafael Nunes, Sunny Vagnozzi, Supriya Pan*.
- Section 5 - Discussion, White Paper recommendations, and future prospects.

In every section, the coordinators and contributing writers are identified at the beginning of each contribution. The preparation of the CosmoVerse White Paper involved a substantial number of people, with $\sim$ 65 coordinators, $\sim$ 350 contributing writers, and $\sim$ 130 endorsers. The project was reviewed by Alba Domi, Alexandra Amon, Anjitha John William Mini Latha, Anton Chudaykin, Bivudutta Mishra, Emil Mottola, Emmanuel N. Saridakis, Florian Pacaud, Germano Nardini, Marcin Postolak, Mariano Domínguez, Miguel A. García-Aspeitia, Nelson J. Nunes, Oem Trivedi, Oliver Fabio Piattella, Özgür Akarsu, Paolo Salucci, Pilar Ruiz-Lapuente, Rafid H. Dejrah, and Supriya Pan, and the bibliographic information was organized by Luca Visinelli. The notational conventions of the work are defined in Section 6. This is followed by a list of the glossary abbreviations in Section 7. The CosmoVerse Action and White Paper were aided by the administrative contributions of Hiba Wazaz.

1. Introduction

Cosmology has entered an era of unprecedented precision in and volume of observational measurements, with large-scale surveys providing high-quality data across multiple redshifts and cosmic epochs. This wealth of observational data allows for a deeper understanding of the Universe's composition, dynamics, and structure formation processes of the Universe. However, these advancements have also revealed significant tensions between early- and late-time cosmological measurements, challenging the standard cosmological model. These discrepancies not only question the consistency of this framework but also suggest the possibility of unrecognized systematic errors or the need for new physics beyond the standard model of cosmology.

The standard model of cosmology, or ΛCDM describes the Universe using a cosmological constant (Λ) and Cold Dark Matter (CDM), and gravity through Einstein's GR. It provides an excellent fit for a range of cosmological datasets, including the CMB and large-scale structure surveys. Nevertheless, the emergence of tensions in key cosmological parameters has become increasingly difficult to ignore. Among these, the most prominent include discrepancies in the measurements of the Hubble constant (H_0), the amplitude of matter fluctuations (S_8), and the sound horizon at the epoch of BAO.

These tensions raise profound questions about our understanding of the Universe's expansion history, structure formation, and the fundamental nature of DM and DE. If not due to systematic errors, such tensions may indicate the need for modifications of the standard model or additional components in the cosmic inventory. Addressing these issues requires a careful consideration of both observational and theoretical aspects, as well as a comprehensive approach that combines multiple cosmological probes.

1.1. State of the art status of cosmological tensions

The most statistically significant tension in cosmology is the H_0 tension, which refers to a significant and persistent discrepancy between measurements of the Hubble constant obtained from early- and late-time cosmological probes, challenging the completeness of the standard ΛCDM model and suggesting the possible need for new physics. Early Universe constraints, primarily from the *Planck* satellite (Section 2.1.18), which maps CMB anisotropies, provide a precise estimate of $H_0 = 67.4 \pm 0.5\,\mathrm{km\,s^{-1}Mpc^{-1}}$. This result relies on the angular scale of the acoustic peaks in the CMB power spectrum, under the assumptions of a flat ΛCDM model with standard radiation content. Consistency with Planck's result has also been demonstrated by ground-based experiments such as ACT and SPT, both of which measure the damping tail and lensing-induced smoothing of the CMB power spectrum with high precision, reinforcing the lower H_0 value.

BAO (see Section 2.1.19) provide an additional, independent probe of the expansion history by measuring the characteristic scale imprinted by sound waves in the early Universe, observable in the large-scale distribution of galaxies. This standard ruler, linked to the sound horizon at the epoch of baryon drag, enables precise distance measurements at various redshifts. Surveys such as BOSS, eBOSS, and DESI have reported H_0 values consistent with CMB constraints, further supporting the lower early Universe based estimate. Notably, DESI's latest BAO results, based on over six million galaxies across multiple redshift bins, when calibrated by the Planck + ΛCDM constraint on the sound horizon measured $H_0 = 68.5 \pm 0.6\,\mathrm{km\,s^{-1}Mpc^{-1}}$.

Late-time measurements of the Hubble constant H_0 using the distance ladder approach (Section 2.1.1) suggest a higher value than early Universe constraints, contributing to the persistent Hubble tension. The most precise distance ladder method involves three steps: (1) geometric distance measurements to calibrate the luminosities of Cepheid variables using Gaia parallaxes, detached eclipsing binaries, and water masers; (2) using these calibrated Cepheids to standardize SNIa observed with HST; and (3) measuring H_0 from SNIa distances in the Hubble flow, where cosmic expansion dominates.

Cepheid variables (Section 2.1.2) serve as primary standard candles due to their well-defined period–luminosity (P–L) relation, where the pulsation period correlates with intrinsic brightness. Systematic uncertainties, such as metallicity effects, crowding, and dust extinction, are mitigated through near-infrared photometry and consistent datasets from HST and JWST. The SH0ES collaboration recently measured $H_0 =$

$73.17 \pm 0.86\,\mathrm{km\,s^{-1}Mpc^{-1}}$ using this approach, indicating a $5-6\sigma$ tension with Planck. JWST's independent observations, particularly in Cepheid-rich fields, have validated and refined these results by reducing crowding biases and confirming the reliability of the Cepheid calibration, strengthening the significance of the Hubble tension.

SNIa (Section 2.1.7) serves as the most common, far-field rung of the distance ladder, extending measurements into the Hubble flow. The Pantheon+ dataset provides precise H_0 measurements consistent with local results but in tension with early Universe estimates.

While the above tools remain central to the Hubble tension, offering the strongest leverage, alternative standard candles such as the TRGB, Mira variables, J-region Asymptotic Giant Branch (JAGB) stars, SNII, SBF, and the BTFR provide valuable cross-checks. These independent methods, while varying in calibration techniques and stellar populations, consistently yield higher values of H_0 than early Universe constraints from the CMB, emphasizing the robustness of the tension and fueling interest in theoretical refinements.

The TRGB method (Section 2.1.4) measures distances using the sharp luminosity cutoff where Red Giant Branch (RGB) stars ignite helium as a standard candle. Calibrated with galaxies like the Magellanic Clouds and NGC 4258, TRGB provides precise distance estimates. For state-of-the-art measurements, it yields consistent distance measures to SNIa hosts as Cepheids. TRGB remains a valuable cross-check for the Hubble tension, with minimal sensitivity to metallicity (if measured in the I-band) and dust.

Mira variables (Section 2.1.6) are long-period pulsating stars used as standard candles for measuring H_0. Their period–luminosity relation, especially in the near-infrared, provides reliable distances. Calibrated using galaxies like the LMC and NGC 4258, Miras offer an independent cross-check on H_0 with minimal sensitivity to metallicity and crowding.

JAGB stars (Section 2.1.8) are standard candles used for measuring H_0 based on their narrow luminosity range in the near-infrared. They are carbon-rich Asymptotic Giant Branch (AGB) stars in an advanced stellar phase, providing distance estimates at long range. Calibrated using galaxies like NGC 4258, JAGB measurements offer a route to calibrate SNIa. Though newer and less tested than Cepheids or TRGB, they contribute to cross-validation efforts.

SNII (Section 2.1.9) measure H_0 using the correlation between their luminosity and decline rate during the plateau phase. They offer an alternative to SNIa, aiding cross-checks in the Hubble tension.

The SBF method (Section 2.1.5) measures H_0 using pixel-to-pixel luminosity variations in elliptical galaxies. Calibrated with nearby galaxies, SBF provides H_0 estimates which are independent of SNIa.

The BTFR (Section 2.1.11) estimates H_0 using the correlation between a galaxy's rotational velocity and baryonic mass. Recent calibrations, particularly addressing zero-point uncertainties between different standard candles like Cepheids and TRGB, have refined the measurement to $H_0 = 76.3 \pm 2.1(\mathrm{stat}) \pm 1.5(\mathrm{sys})\,\mathrm{km\,s^{-1}Mpc^{-1}}$, yielding another SNIa-independent measurement and further emphasizing the tension with early Universe estimates.

As an alternative to the distance ladder measurements, masers offer independent insights into the Hubble constant H_0. The maser technique (Section 2.1.3) uses 22 GHz H_2O maser emissions from rotating disks around supermassive black holes to directly measure distances. Each of 5 masers (leaving NGC 4258 aside as its often used to calibrate the distance ladder) yields a geometric distance and $H_0 = 73.9 \pm 3.0\ \mathrm{km\,s^{-1}Mpc^{-1}}$. The Megamaser Cosmology Project (MCP) has extended the precision of this method, producing results consistent with late-time measurements. Although rare, water masers provide a model-independent check, reinforcing the higher H_0 values obtained from local probes.

Strong gravitational lensing with time-delay measurements (Section 2.1.14) offers another independent method for estimating H_0. Multiple images of a background source, produced by a massive foreground lens, create time delays due to differences in the light paths. These delays depend on the lensing geometry and the Universe's expansion rate. Collaborations such as H0LiCOW and TDCOSMO have applied this technique, yielding $H_0 \approx 74.2 \pm 2.6\,\mathrm{km\,s^{-1}Mpc^{-1}}$, consistent with other late-time estimates.

Gravitational Wave (GW) events with electromagnetic counterparts, known as standard sirens (Section 2.1.17), provide an independent estimate of H_0 by measuring the luminosity distance from GWs emitted during compact object mergers. When an electromagnetic counterpart identifies the host galaxy, the redshift can be measured directly. Recent standard siren measurements yield $H_0 \approx 70.0 \pm 3.0\,\mathrm{km\,s^{-1}Mpc^{-1}}$, offering a model-independent constraint on cosmic expansion and contributing to the Hubble tension debate. However, this approach is still severely limited by the rarity of GW events with EM counterparts, with only a single event which is too close for a reliable measurement of H_0.

CC (Section 2.1.13) estimate H_0 using the differential ages of passively evolving galaxies. By dating stellar populations, this method infers the expansion rate without relying on standard candles. However, unlike the use of distances, this measure is not empirical, depending on astrophysical modeling of aging stellar populations, their metallicities, star formation histories, and initial mass functions, with an uncertainty dominated by the modeling effort. Recent measurements suggest $H_0 \approx 70.6 \pm 6.7\,\mathrm{km\,s^{-1}Mpc^{-1}}$, still consistent with both early and most late-time measurements. As a distance-ladder-independent probe, CC offer a different dimension of study of the Hubble tension.

HII galaxies (Section 2.1.10) measure H_0 using the correlation between their luminosity and emission line flux from ionized gas. The strong emission lines, primarily from young massive stars, allow for distance estimates based on the luminosity-size relation. Calibrated using nearby galaxies, HII galaxy measurements provide independent constraints on H_0 consistent with other local probes.

DESI has provided a novel avenue for measuring H_0 through the Fundamental Plane (FP) relation of early-type galaxies, with a calibration tied to the distance to the Coma cluster (Section 2.1.12). By leveraging DESI's extensive sample of over 4000 early-type galaxies, the FP relation was calibrated to provide precise distance estimates. For a distance to the Coma cluster of 98.5 ± 2.2 Mpc based on SNIa, DESI yields a local value of $H_0 = 76.5 \pm 2.2\,\mathrm{km\,s^{-1}Mpc^{-1}}$. This result is in significant tension with the value inferred from Planck measurements where ΛCDM is assumed, and which predicts a distance to Coma exceeding 110 Mpc. Historically, the distance to the Coma cluster has ranged from 90-100 Mpc, highlighting the discrepancy. By extending the Hubble diagram with FP-calibrated distances, DESI highlights a persistent conflict between local measurements and early Universe predictions.

Extended QSO cosmologies (Section 2.1.15) constrain H_0 using correlations between QSO luminosity and variability timescales. Their ability to probe higher redshifts than standard candles makes them valuable for testing cosmic expansion over extended epochs. Similarly, GRB observations (see Section 2.1.16) use correlations between their luminosity and spectral properties to estimate H_0, serving as additional high-redshift probes relevant to the Hubble tension.

Despite significant methodological diversity and substantial precision improvements, the tension between early- and late-time measurements of the Hubble constant H_0 persists at a statistically significant level, exceeding 5.9σ (Planck 2018 vs. SH0ES, alone, but higher when combining measures). This discrepancy challenges the completeness of the standard ΛCDM model and raises the possibility of new physics.

Related to the H_0 tension there is the sound horizon tension, which refers to a discrepancy in the inferred comoving sound horizon scale at the end of the baryon drag epoch, r_s^{drag}, derived from early- and late-time cosmological measurements. This standard ruler, crucial for calibrating cosmological distances, is determined by the physics of the early Universe, specifically the acoustic oscillations in the photon–baryon plasma before recombination. It is primarily constrained by measurements of the CMB power spectrum, where *Planck* data assuming ΛCDM suggest $r_s^{\mathrm{drag}} \approx 147.09 \pm 0.26$ Mpc. However, late-time

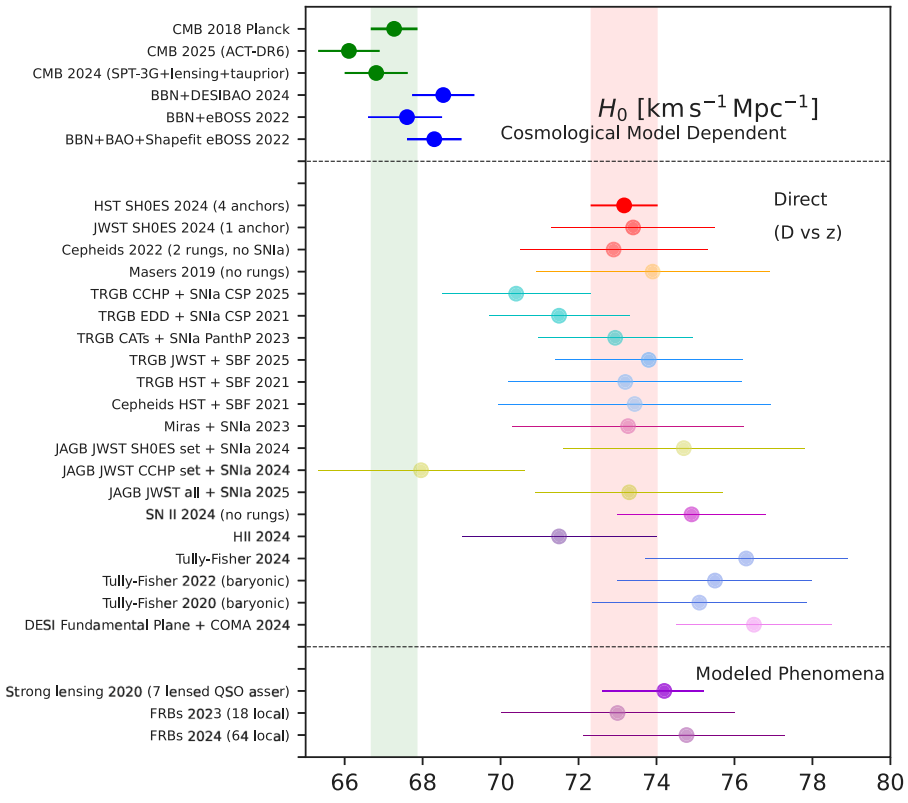

Fig. 1. Summary of H_0 estimates from different cosmological probes with error bars smaller than $3.5\,\mathrm{km\,s^{-1}Mpc^{-1}}$.

measurements, such as BAO data combined with local distance ladder determinations of H_0, suggest a lower sound horizon, with BAO-based estimates yielding approximately 137 Mpc, a difference of about 7% and a tension of 2.6σ significance.

This discrepancy arises because r_s^{drag} is directly connected to the expansion rate around recombination, meaning changes to the early Universe physics could shift its value. Solutions involving early-time modifications often require an enhanced expansion rate before recombination, which can reduce r_s^{drag}. Examples include models introducing additional relativistic species or EDE components. However, these scenarios face tight constraints from CMB observations, as the acoustic peak structure is highly sensitive to changes in photon diffusion and gravitational driving effects.

Late-time measurements rely on the BAO feature imprinted at the drag epoch, calibrated through local H_0 measurements, such as the SH0ES collaboration results. Since r_s^{drag} anchors the BAO scale, discrepancies in H_0 estimates propagate into inferred sound horizon measurements. This tension therefore highlights the need for consistent cross-calibration between early- and late-time probes and motivates further investigation into both systematics and extensions to the standard model of cosmology.

The combination of the estimates resulting from these, and other, approaches to estimating the value of H_0 points to a significant tension in the value of this parameter. This tension in the expansion rate of the Universe at current times is further detailed in Section 2.1, with the most prominent estimates shown in Fig. 1 (see also Fig. 2) and possible solutions in Fig. 3.

Another interesting tension is that related to S_8, which highlights a persistent discrepancy between measurements of the amplitude of matter fluctuations on cosmological scales inferred from early and late Universe observations. The parameter S_8, defined as $S_8 \equiv \sigma_8\sqrt{\Omega_m/0.3}$, combines the clustering amplitude σ_8 (the root-mean-square of matter fluctuations on scales of $8\,h^{-1}$ Mpc) with the present-day matter density parameter Ω_m. It provides a key measure of the growth of cosmic structures, making it a crucial probe of the standard cosmological model.

Current measurements from early-time data, such as the *Planck* 2018 results, which constrain the CMB temperature and polarization anisotropies (Section 2.1.18.6), yield a high precision estimate of $S_8 = 0.834 \pm 0.016$ assuming the ΛCDM model. However, late-time measurements derived from weak gravitational lensing (Section 2.2.1) and galaxy clustering surveys (Section 2.2.2), including KiDS, DES, and HSC, consistently report lower values of S_8. For example, DES Year 3 results obtained from combined galaxy clustering and WL measurements suggest $S_8 = 0.772 \pm 0.017$, while KiDS-1000 and HSC report similarly low values around $S_8 \approx 0.76$ with comparable uncertainties. This tension, at the $2-3\sigma$ level, persists across multiple independent data sets, indicating a possible systematic deviation between early and late-time probes of structure formation.

The origin of this tension remains under debate. On the one hand, it could be driven by systematic uncertainties in the analysis of WL data. These systematics include shear calibration biases, uncertainties in photometric redshift estimates, and baryonic feedback effects that suppress the small-scale power spectrum due to processes like Active Galactic Nucleus (AGN) feedback and gas ejection from galaxies. DES and KiDS collaborations have both extensively explored the role of such systematics, yet the tension persists even after conservative scale cuts and improved modeling of non-linear clustering.

On the other hand, the S_8 tension might hint at the need for extensions to the standard ΛCDM model. One potential modification involves evolving DE models, where a time-dependent equation of state parameter $w(z)$ could alter structure growth rates. Another possibility is modifications to the theory of gravity itself, such as $f(R)$ models or scalar-tensor theories, which could modify the relationship between the

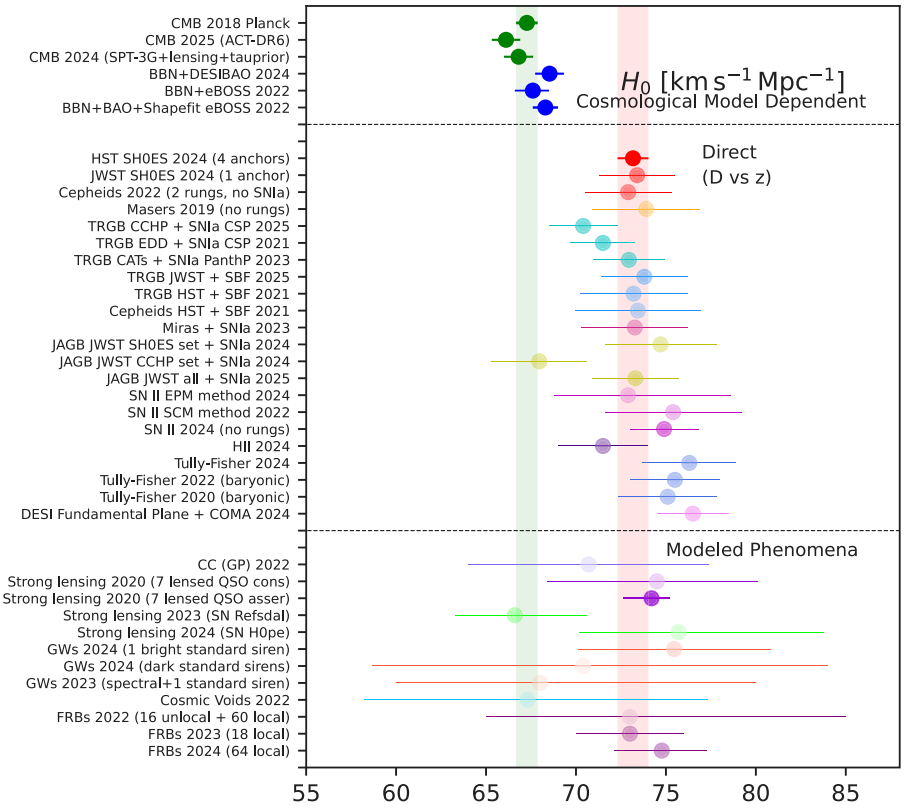

Fig. 2. Summary of H_0 estimates from all the cosmological probes in this White Paper following the order of the different sections.

matter distribution and lensing potential. Additionally, the presence of massive neutrinos, which suppress structure formation at late-times due to their free-streaming behavior, could also contribute to lowering the observed S_8 value if the neutrino mass is larger than currently assumed in the base ΛCDM model.

Notably, cross-correlation measurements between WL and other probes, such as CMB lensing (e.g., from Planck, ACT, and SPT) and galaxy clustering from BAO surveys, have shown consistency with both early and late-time datasets, complicating the overall picture. Furthermore, analyses that vary only the normalization of the power spectrum, such as the σ_8 parameter itself, have not fully resolved the tension, suggesting a more complex interplay between cosmic structure formation and expansion history.

The tension in the S_8 parameter may be milder but there is a growing effort to improve the constraints in observational estimates of the amplitude of matter fluctuations. These are detailed in Section 2.2, with the most prominent estimates also shown in Fig. 4, and possible solutions in Fig. 5.

1.2. Early vs local measurements and efforts for a solution

The persistence of the H_0 tension across independent datasets suggests either unresolved systematic errors or the need for extensions to the ΛCDM framework. Numerous theoretical solutions have been proposed, aiming to reconcile the observed discrepancy while preserving the success of the standard cosmological model in describing early and late-time observables. The most prominent of these efforts for a solution are shown in Fig. 6, which are also highlighted below, and detailed in Section 4:

- **Early Dark Energy (EDE)**: EDE models (Section 4.1.1) propose a transient DE component that briefly dominates the cosmic energy budget before recombination, reducing the size of the sound horizon and allowing for a higher inferred H_0 from CMB data. This mechanism involves a scalar field with a potential that activates temporarily and dilutes before significantly affecting late-time cosmology. Several variants of EDE have been explored in the literature. Oscillatory EDE models, often motivated by axion-like fields, involve a scalar field oscillating around the recombination epoch, injecting energy into the expansion rate. NEDE (see Section 4.1.2) refines this idea by introducing a phase transition where the scalar field rapidly decays, creating a sharper and more controlled impact on the expansion rate. Adiabatic Fluctuation EDE models, meanwhile, adjust the evolution of the scalar potential to balance early- and late-time cosmological constraints, though these often introduce parameter degeneracies. While EDE models have shown promise in alleviating the H_0 tension by increasing the inferred value from early-time data, they also introduce challenges. The models can exacerbate tensions in other cosmological parameters, particularly the amplitude of matter fluctuations S_8 and the matter density Ω_m. Depending on the specific data set, EDE can reduce the H_0 tension to $2-3\sigma$, however, recent CMB and LSS data sets show no evidence for this model and disfavor large fractions of EDE.
- **Late Dark Energy (LDE)**: Late Dark Energy (LDE) models (Section 4.2.1) attempt to address the Hubble tension by modifying the expansion history at low redshifts ($z \lesssim 1$). These models alter the equation of state parameter of DE, $w(z)$, away from the cosmological constant value $w = -1$. Some LDE scenarios involve a rapid transition in $w(z)$, where DE density evolves from a negative to a positive contribution, effectively accelerating the late-time expansion rate. Although LDE models can slightly raise H_0 without modifying the early Universe physics, they often face challenges in matching BAO and Type Ia supernova data simultaneously, as the shift in the expansion rate can introduce tension with large-scale structure constraints.
- **Rapid transitions in the late-Universe**: Rapid transitions in the DE from negative to positive values in the late Universe (Section 4.2.2) exhibit a sign-switching action in the vacuum energy

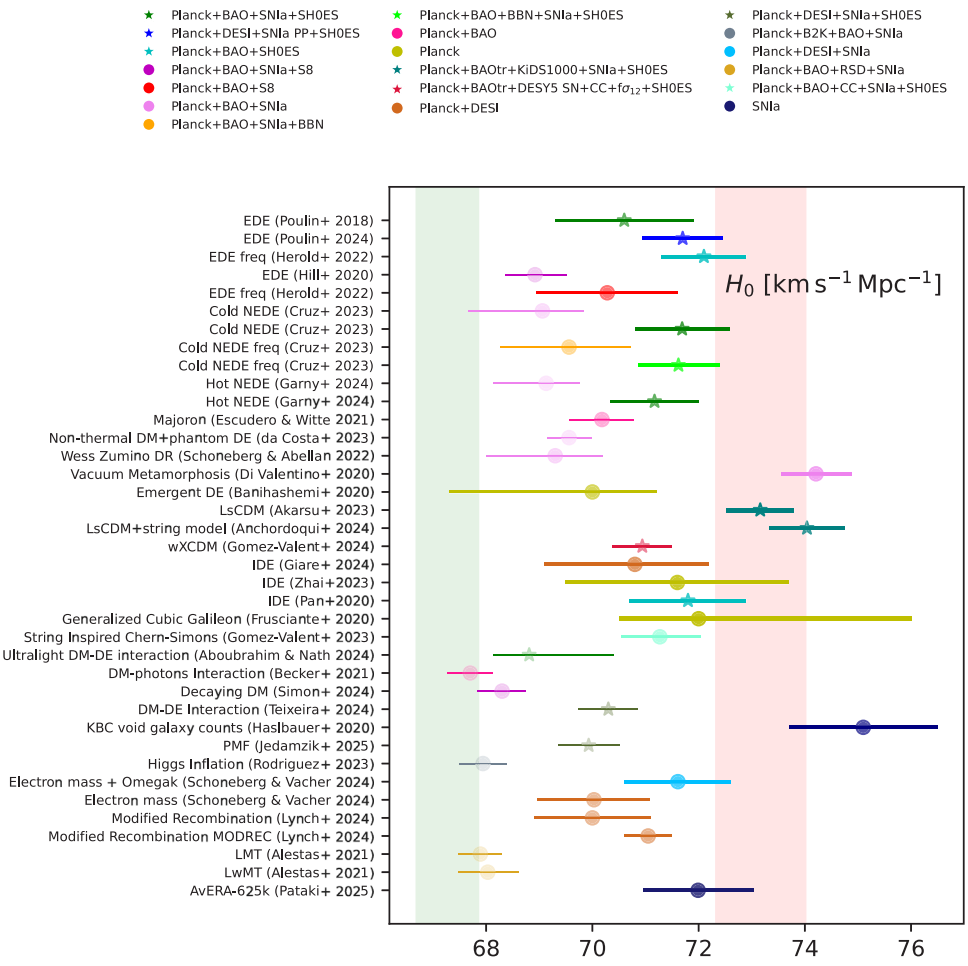

Fig. 3. Summary of models proposed to solve the H_0 tension in this White Paper following the order of the different sections.

while leaving the DE magnitude unchanged. These models allow for the possibility of simultaneously increasing the value of H_0 while also suppressing changes in S_8. The transition point is established primarily by BAO data sets, while also being supported by other contributions. Most models express an abrupt transition with a discontinuity in the vacuum energy density.

- **Interacting Dark Matter and Dark Energy (IDE) Models**: Interacting Dark Matter and Interacting Dark Energy (IDE) models (Section 4.2.3) propose a non-trivial energy exchange between DM and DE, modifying both the cosmic expansion rate and structure growth. This interaction, described by a coupling function Q, allows energy to transfer from one component to the other. Depending on the direction and strength of the coupling, IDE can either slow down or accelerate the expansion rate. IDE models can increase H_0 estimates while modifying the growth of structure, offering a way to reduce the S_8 tension simultaneously. However, strong constraints from CMB lensing and BAO measurements limit the parameter space of IDE models, and they often require fine-tuning to remain consistent with multiple datasets.
- **Modified Gravity Theories**: MG models (Sections 4.3.1 and 4.3.2) propose extensions to GR by altering the Einstein–Hilbert action, introducing additional scalar degrees of freedom, altering the underlying geometry itself, or changing the spacetime dimensionality, among other alternatives, which can affect both the cosmic expansion rate and the growth of large-scale structure. These modifications can impact the lensing potential and structure formation, leading to changes in the inferred values of H_0 and S_8. Several frameworks have been explored to address the Hubble tension within MG. $f(R)$ gravity, for example, generalizes GR by replacing the Ricci scalar with a nonlinear function of R, introducing an additional scalar mode that modifies both the background expansion and structure growth. Horndeski theories, which include non-minimally coupled scalar fields with derivative interactions, allow modifications to both the expansion history and lensing effects but often face constraints from CMB lensing and large-scale structure data. Other models, such as massive gravity and bimetric gravity, alter the graviton's properties, leading to modified cosmic acceleration and structure formation patterns. While some variants can reduce both the H_0 and S_8 tensions, they often require fine-tuning or introduce instabilities in the late Universe. Teleparallel gravity approaches, including $f(T)$ and $f(Q)$ theories, replace curvature with torsion or non-metricity as the primary geometrical property driving cosmic evolution. These models have been shown to affect the late-time expansion rate but remain under scrutiny for consistency with both early- and late-time datasets. Emerging curvature theories, such as AvERA [13,13,14] modify the late expansion history compared to the concordance model (Section 2.3.9) to solve the H_0 and ISW puzzles. While MG models offer a rich theoretical landscape to explore, many face difficulties in simultaneously resolving the H_0 and S_8 tensions while remaining consistent with solar system tests, CMB lensing, and BAO constraints.
- **Exotic Scenarios and Non-Standard Dark Matter Models**: Exotic scenarios (Sections 4.4.1, 4.4.2, and 4.4.3) explore extensions to the standard cosmological model involving non-standard physics in both the DM and DE sectors, which can influence the cosmic expansion history and structure formation. Among

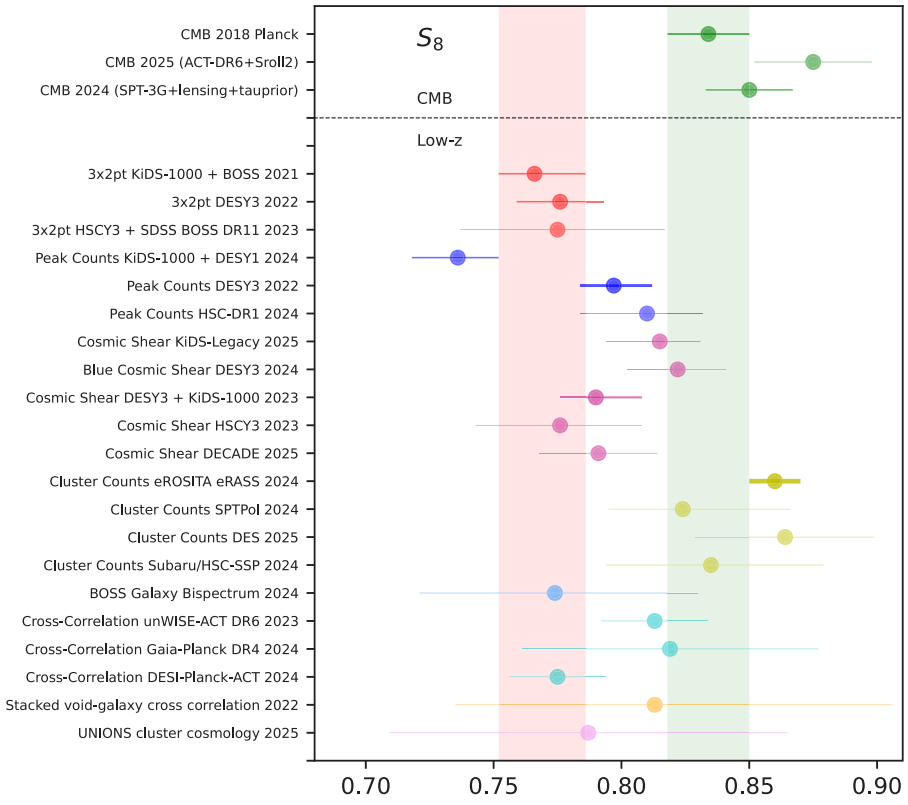

Fig. 4. Summary of S_8 estimates from different cosmological probes.

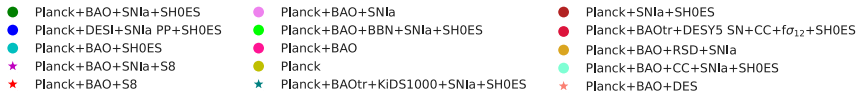

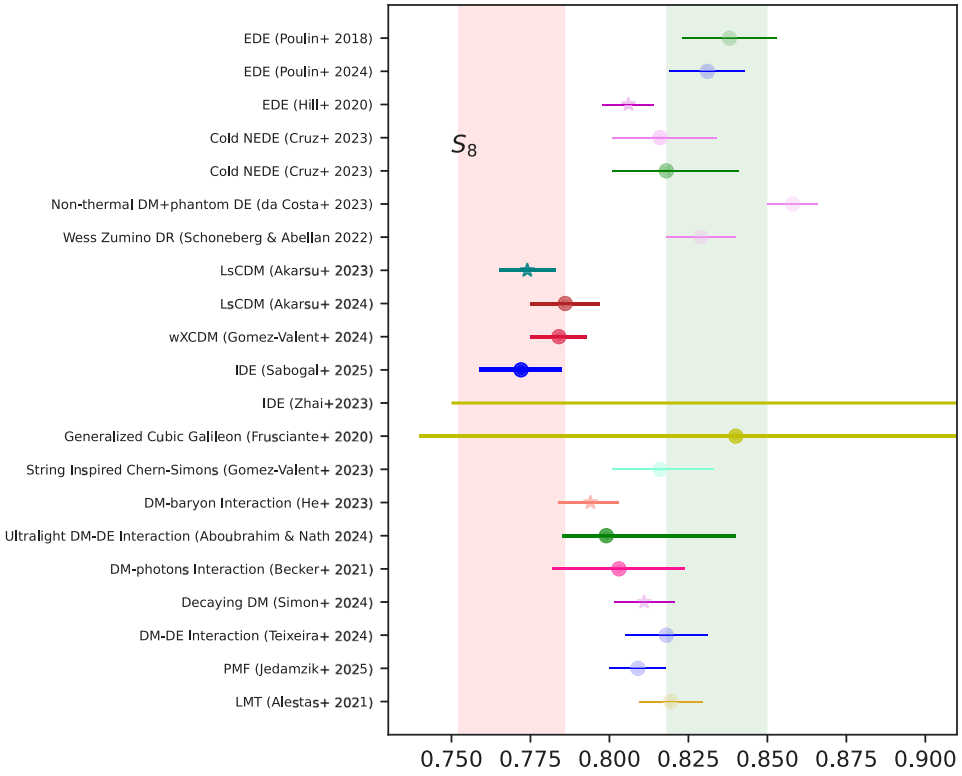

Fig. 5. Summary of models proposed to solve the S_8 tension in this White Paper following the order of the different sections.

these are decaying dark matter (DDM) models, where DM particles decay into lighter states. If this decay occurs before or during the recombination epoch, it can alter the expansion rate and reduce the sound horizon, leading to a higher inferred H_0. However, constraints from CMB lensing and large-scale structure limit the viability of DDM as a complete solution. Ultralight scalar fields, such as axion-like particles or fuzzy dark matter, have also been proposed. These fields can modify the standard expansion rate through their contributions to the cosmic energy density, potentially mimicking an additional relativistic species or altering structure formation on small scales. Nevertheless, precise measurements of the CMB power spectrum and the Lyman-alpha forest have placed stringent bounds on their properties. Primordial black holes and non-CDM models represent further exotic avenues, with the latter deviating from the standard cold, collisionless DM paradigm, often leading to a suppression of small-scale structure growth. While these models offer novel mechanisms to address cosmological tensions, most current models are tightly constrained by precision data from Planck, DESI, and the Pantheon+ supernova sample. However, they remain of theoretical interest, especially with upcoming data from CMB Stage-4 and JWST capable of probing extreme scenarios further.

- **Extra Relativistic Species and Neutrino Physics**: Extra relativistic species (Section 4.1.3) represent another class of proposed extensions aimed at resolving the Hubble tension. An increased number of relativistic degrees of freedom, commonly parameterized by $N_{\rm eff}$, leads to a higher early Universe expansion rate and a reduced sound horizon, potentially increasing the inferred H_0. This scenario can arise from new light particles, such as sterile neutrinos or dark radiation. Sterile neutrinos, in particular, can act as an additional relativistic species if they decouple before standard neutrinos while self-interacting or secret neutrino interactions can modify the thermal history of the Universe and delay neutrino decoupling, effectively altering $N_{\rm eff}$. However, current constraints from Planck, BAO, and CMB lensing data have limited viable deviations to $\Delta N_{\rm eff} \approx 0.2$. While insufficient to fully resolve the Hubble tension, such scenarios remain relevant in the context of early Universe physics and potential beyond-the-Standard-Model extensions.
- **Local Void Hypothesis:** The local void hypothesis (Section 4.5.1) posits that the Milky Way galaxy (MW) resides in a large, underdense region of the Universe, potentially biasing measurements of the Hubble constant due to a locally faster expansion rate compared to the cosmic average. The idea suggests that a void could lead to a larger measured H_0 locally while being lower on cosmological scales. However, the size and depth of such a void required to explain the entire Hubble tension would be inconsistent with current observations. Studies using CosmicFlows-4 and Pantheon+ supernova data, as well as analyses of bulk flows, have not identified an underdensity significant enough to fully explain the observed discrepancy assuming ΛCDM.
- **Primordial Magnetic Fields (PMFs):** PMF (Section 4.5.2) contributions are generated before recombination could influence the early Universe's expansion history and the formation of large-scale structures. PMF contributions can modify the photon–baryon plasma dynamics, alter the acoustic peaks in the CMB power spectrum, and shift the inferred sound horizon, all of which can affect the measurement of H_0. However, current constraints from the CMB, including non-detections of Faraday rotation and the damping tail suppression, limit the strength of PMFs, making it unlikely that they can fully account for the observed tension.
- **Inflationary Models:** Certain inflationary scenarios (Section 4.5.3.2) propose modifications to the early Universe's physics that could indirectly affect the H_0 measurement. Models involving non-standard reheating phases, features in the inflationary potential, or a modified primordial power spectrum have been investigated in this context. These scenarios can alter the early expansion history or the acoustic peak structure, impacting the inferred value of H_0 from CMB measurements. However, most inflationary modifications struggle to generate a significant enough shift in H_0 while remaining consistent with current CMB and large-scale structure data.
- **Varying Fundamental Constants:** The idea of varying fundamental constants (Section 4.8) explores the possibility that parameters such as the fine-structure constant α, the electron mass m_e, or the proton-to-electron mass ratio μ could change over cosmic time or with spatial position. If fundamental constants were to evolve, they could impact key cosmological observables, such as the sound horizon and the physics of recombination, altering the inferred values of H_0. Scalar fields coupled to the electromagnetic sector, as in models like varying-α theories, could drive such changes. However, stringent constraints from CMB, BBN, and QSO absorption spectra have significantly limited the variation of some of these constants and their ability to resolve the Hubble tension, while the others face issues of finding a coherent theoretical framework that can explain their variation.
- **Local Physics Solutions:** Local physics solutions (Section 4.9) suggest that the H_0 tension could arise from new physical effects specific to the local Universe rather than requiring modifications to the global cosmological model. One possibility is a local modification to the gravitational constant, $G_{\rm eff}$, which could alter the calibration of standard candles like Cepheid variables or SNIa, leading to a biased measurement of H_0. Another proposed local effect involves variations in the transparency of the Interstellar Medium (ISM) or modified extinction laws that could influence supernova observations. While some of these scenarios can explain a portion of the tension, they generally fail to provide a complete resolution and are often tightly constrained by measurements from cosmic bulk flows, galaxy clustering, and large-scale structure surveys.
- **Systematic Uncertainties and Calibration Issues**: A significant portion of the community continues to explore whether systematic errors could account for the observed tension. Potential sources include Cepheid calibration errors, host galaxy dust corrections, and selection effects in both early and late-time measurements. However, rigorous cross-calibrations between HST, JWST, and ground-based surveys like DESI and SH0ES have yet to identify a significant bias capable of resolving the tension completely.

1.3. Additional curiosities and anomalies

Other cosmological anomalies beyond the primary H_0 and S_8 tensions have emerged in recent years, revealing potential challenges to the standard ΛCDM model. These discrepancies span a wide range of physical scales and cosmological probes, motivating deeper investigations into both systematic effects and new physics. Key anomalies include:

- **The $A_{\rm lens}$ anomaly:** The $A_{\rm lens}$ parameter, introduced as a phenomenological extension to the standard CMB analysis, quantifies the amplitude of lensing-induced smoothing of acoustic peaks in the CMB power spectrum. Planck data suggest a value for $A_{\rm lens}$ slightly higher than expected under ΛCDM, with a significance of 2–3σ, potentially pointing to unmodeled effects in CMB lensing or physics beyond standard cosmology (Section 2.3.1).
- **Evidence for nonzero curvature:** While the standard model assumes a flat universe, Planck's CMB data, when analyzed without external priors, have shown mild evidence for a closed geometry with $\Omega_k < 0$. However, this claim remains controversial, as BAO and lensing measurements are consistent with a flat universe within 1σ (Section 2.3.2).

Fig. 6. Fundamental physics provides a number of potential solutions to address the challenge of tensions in cosmology.

- **CMB anisotropic anomalies:** Several statistically significant features have been identified in CMB data, including the hemispherical power asymmetry, alignments in low multipole moments, and the cold spot anomaly. While most of these could be attributed to cosmic variance, their persistence in multiple datasets (e.g., Planck, WMAP) raises the question of whether they hint at new physics or residual systematics (Section 2.3.3).
- **The w_0w_a tension:** Discrepancies have emerged in constraints on the DE equation of state parameters, w_0 and w_a, particularly when comparing results from CMB data with late-time probes such as SN and DESI BAO. Some results suggest a deviation from the cosmological constant value of $w_0 = -1$, which could indicate evolving DE or unresolved systematics (Section 2.3.4).
- **Neutrino Tension:** The sum of neutrino masses, $\sum m_\nu$, inferred from cosmological data, such as CMB and BAO observations, has shown tension with the lower bounds set by terrestrial neutrino oscillation experiments, which require $\sum m_\nu \gtrsim 0.06$ eV (normal ordering, NO) and $\sum m_\nu \gtrsim 0.1$ eV (inverted ordering, IO). Recent DESI BAO data combined with Planck and ACT CMB constraints yield tight upper limits, such as $\sum m_\nu < 0.05$ eV (2σ), challenging the inverted hierarchy and preferring the NO with a Bayes factor exceeding 46.5 in some datasets. Interestingly, some analyses allowing for extended models have reported a preference for *negative* neutrino masses, linked to enhanced CMB lensing signals in Planck and ACT data. This tension could stem from unaccounted systematics in lensing measurements or may indicate new physics beyond minimal ΛCDM, such as modified neutrino properties or evolving DE models (Section 2.3.5).
- **Cosmic dipole anomalies:** Tensions exist between the inferred cosmic dipole from the CMB and measurements from radio galaxies and QSOs. Separately, statistically significant directional variations in H_0 have been reported in both CMB and the local Universe, providing an alternative perspective on CMB anisotropic anomalies and bulk flow anomalies. These discrepancies could point to non-standard cosmic expansion or incomplete modeling of large-scale structure effects (Section 2.3.6).
- **Big Bang Nucleosynthesis (BBN) anomalies:** Discrepancies exist between deuterium and helium abundances inferred from BBN

and those predicted by CMB-based baryon density estimates, suggesting either measurement systematics or small deviations from standard physics during the early Universe (Section 2.3.7).

- **Lyman-α anomalies:** High-redshift Lyman-α forest measurements show mild tension with low-redshift constraints on the matter power spectrum, raising questions about the evolution of structure and thermal history of the Intergalactic Medium (IGM) (Section 2.3.8).
- **Integrated Sachs–Wolfe (ISW) and cosmic superstructures:** Measurements of the ISW effect, which probes late-time structure growth through correlations between CMB and large-scale structure data, have shown excess correlations on large scales, potentially linked to cosmic superstructures (Section 2.3.9).
- **Cosmic void anomalies:** Observations of cosmic voids have revealed unexpected properties in their size distribution and their contribution to the ISW effect, potentially suggesting deviations from the standard growth of structure (Section 2.3.11).
- **Fast Radio Burst (FRB) probes:** FRB observations have recently emerged as a powerful probe of cosmic tensions, offering a unique way to constrain the expansion history and large-scale bulk flows. Preliminary results suggest some inconsistencies with early universe predictions. It is crucial to emphasize that in estimating H_0 from FRBs, a prior assumption of the underlying cosmological model is required. Specifically, the H_0 values presented in the associated Whisker plot are computed under the assumption of a ΛCDM cosmology. Deviations from the standard ΛCDM framework are expected to yield different H_0 estimates, reflecting the model dependence inherent in such measurements. Furthermore, the constraints on H_0 have progressively tightened over time, primarily due to the increasing number of well-localized FRBs and improvements in the statistical methodologies applied to their analysis (Section 2.3.12).
- **Radio background excess:** Several observations of the diffuse radio sky have reported an unexplained excess in both the surface brightness and the anisotropy power of the radio background, which could be linked to new diffuse or low flux radio sources, PMFs, exotic decays, or residual systematics across a range of radio observations (Section 2.3.13).
- **Bulk flow anomalies:** Peculiar velocity measurements and bulk flows inferred from galaxy catalogs show a higher amplitude than predicted by ΛCDM, potentially pointing to the presence of large-scale structures beyond the standard model (Section 2.3.14).
- **Ultra Long Period Cepheids:** These variable stars have been proposed as potential standard candles, but their properties appear inconsistent with standard stellar evolution models, raising questions about distance ladder calibrations (Section 2.3.15).

Ongoing and upcoming surveys such as Euclid, The Rubin Observatory's Legacy Survey of Space and Time (LSST), and the Roman Space Telescope will play a pivotal role in clarifying these anomalies. Additionally, methodological advances, including cross-correlations between multiple probes and the application of Machine Learning (ML) techniques (Sections 3, 3.2–3.5), will help assess whether these tensions are genuine physical discoveries or the result of residual systematics. A deeper understanding of these anomalies is essential to determine whether extensions to the standard ΛCDM framework are required and to uncover the fundamental nature of DE, DM, and cosmic structure formation.

1.4. Data analysis: How to tackle the problem

The analysis of cosmological data has seen remarkable advancements, leveraging a wide range of statistical, computational, and interdisciplinary approaches. These methodologies have not only refined parameter constraints but also opened new avenues to tackle cosmological tensions such as the H_0 and S_8 discrepancies. These tensions challenge the completeness of the ΛCDM model, suggesting the possibility of new physics or unresolved systematics.

Cosmology simulators and MCMC techniques (Section 3.1) are foundational tools for exploring high-dimensional parameter spaces. They allow for robust testing of cosmological models against observational data while accounting for degeneracies and systematics. Advances in MCMC methods, such as nested sampling and Hamiltonian Monte Carlo, have improved the efficiency and accuracy of parameter estimation, particularly when combining data from the CMB, BAO, and SN datasets.

ML approaches (Section 3.2) have emerged as powerful tools in cosmological analysis. Neural networks, GP, and decision trees have demonstrated their utility in extracting patterns, accelerating data analysis, and refining model predictions. For example, ML techniques have been used to process large-scale structure data and improve constraints on DE models. Hybrid approaches, combining ML with traditional statistical methods, have further enhanced the reliability of these analyses by integrating the strengths of both paradigms.

Reconstruction methods (Section 3.3) have also played a critical role, enabling the inference of the Universe's expansion history from observational data. Techniques such as GP regression have been applied to reconstruct the Hubble parameter $H(z)$ and the growth of cosmic structures without assuming a specific cosmological model. These methods reduce systematic biases and provide model-independent insights into cosmological tensions.

Bio-inspired algorithms, particularly GA (Section 3.4), have introduced novel ways to optimize model selection and parameter estimation in cosmology. These algorithms, inspired by evolutionary processes in nature, use mechanisms such as selection, mutation, and crossover to identify optimal solutions in complex and high-dimensional parameter spaces. GAs are particularly well-suited for exploring cosmological models where traditional gradient-based methods may struggle, such as those involving nonlinear dynamics or multimodal likelihood functions. By iteratively refining a population of candidate solutions, GAs can efficiently locate regions of interest in the parameter space, even in the presence of degeneracies or non-Gaussian distributions. Applications of GAs in cosmology have been diverse. They have been employed to address key tensions, such as the H_0 and S_8 discrepancies, by testing alternative models including EDE, Interacting Dark Matter (IDM)-DE scenarios, and MG theories. For instance, GAs have been used to explore the parameter space of IDE models, identifying regions that minimize tensions with both early- and late-time observations. Their flexibility allows for the incorporation of priors from ML or other inference techniques, further enhancing their robustness. Moreover, hybrid approaches that combine GAs with ML have shown promise in improving the convergence and accuracy of solutions. These methods leverage the pattern recognition capabilities of neural networks or decision trees to guide the evolutionary search process, thereby reducing computational overhead while maintaining accuracy. In addition to model testing, GAs have proven effective in enhancing observational strategies. By simulating survey configurations and optimizing the allocation of observational resources, they help maximize the scientific output of upcoming missions. This includes optimizing survey strategies for WL, galaxy clustering, and other probes of large-scale structure. The adaptability of GAs also extends to their role in reconstructing the initial conditions of the Universe from observed data. By evolving populations of initial conditions, these algorithms can identify those that best reproduce observed structures, offering insights into the fundamental physics of the early Universe. Overall, bio-inspired algorithms like GAs represent a powerful addition to the cosmological toolkit, enabling the exploration of complex models and the refinement of observational strategies. Their continued integration with other advanced methods, such as ML and high-performance simulations, holds great potential for addressing the most pressing tensions in cosmology and uncovering new physics.

Cosmological simulations (Section 3.5) have become indispensable for interpreting observational data and testing theoretical models. High-resolution N-body simulations, hydrodynamic models, and semi-analytic methods provide a detailed understanding of the large-scale structure formation and the interplay of DM and DE. These simulations enable the calibration of observables such as WL signals, galaxy clustering, and BAO measurements, thereby improving the accuracy of cosmological parameter constraints.

Statistical tools, including profile likelihoods, have gained prominence in cosmology for estimating confidence intervals and assessing parameter significance. Unlike traditional Bayesian methods, profile likelihoods provide a frequentist alternative (Section 3.6) that is less sensitive to prior assumptions. This makes them particularly useful in scenarios where prior information is limited or where strong assumptions may bias the results. Profile likelihoods excel in analyzing models with complex parameter spaces, including those with non-Gaussian distributions or significant degeneracies between parameters. Such complexities often arise in cosmological contexts, for instance, when exploring EDE models, IDE scenarios, or the inclusion of additional relativistic species. These models frequently introduce additional degrees of freedom, leading to correlations that can obscure parameter constraints when traditional Bayesian approaches are employed. A key advantage of the profile likelihood approach is its ability to disentangle degeneracies and provide robust confidence intervals without relying on the full posterior distribution. This is achieved by profiling the nuisance parameters, effectively marginalizing them without requiring explicit integration. As a result, the profile likelihood method can highlight the true parameter dependencies and offer more transparent interpretations of the data. Applications of profile likelihoods in cosmology have included constraining the equation of state of DE, testing deviations from the standard ΛCDM model, and evaluating the statistical significance of cosmological tensions, such as those involving H_0 and S_8. For example, in the context of EDE, profile likelihoods have been used to assess whether parameter shifts can resolve these tensions or whether they indicate systematic effects in the data. The computational efficiency of profile likelihoods also makes them a valuable tool in high-dimensional analyses, particularly for next-generation cosmological surveys. Their ability to isolate relevant subspaces of parameter space enables efficient exploration of hypotheses while minimizing the computational cost associated with evaluating full posterior distributions. Furthermore, recent advances in computational methods have improved the applicability of profile likelihoods. Techniques such as adaptive mesh refinement and ML-assisted likelihood evaluations have reduced the computational demands of high-precision analyses. These innovations make profile likelihoods increasingly attractive for analyzing the large datasets expected from upcoming missions like the Simons Observatory, Euclid, and the Roman Space Telescope.

These methodologies, often used in combination, reflect a collaborative effort across theoretical, computational, and observational domains. For example, the integration of MCMC methods with ML-enhanced simulations and reconstruction techniques has provided a comprehensive framework for addressing persistent cosmological tensions. This synergy has also enabled the exploration of exotic scenarios, such as decaying DM, PMFs, and varying fundamental constants, which aim to explain anomalies in the current cosmological framework.

The ongoing advancements in data analysis tools and methodologies are pivotal for the next generation of cosmological surveys, including the Simons Observatory, CMB—Stage 4 (CMB-S4), Euclid, and the Roman Space Telescope. These surveys will generate unprecedented datasets that require state-of-the-art techniques to extract meaningful insights. A schematic is shown in Fig. 7 of these methods. By embracing these innovations, the cosmological community continues to push the boundaries of our understanding of the Universe, addressing existing tensions and paving the way for new discoveries in fundamental physics.

2. Observational cosmology and systematics

2.1. H0 tension: Measurements and systematics

Introduction: Adam Riess

It is cliché to say we live in the era of precision cosmology — but it is true. Over the past several decades, the type, scope, and precision of cosmological measurements have grown enormously. Two of the most powerful tools, SNIa, and BAOs, joined the cadre of first-rank indicators during this time. Other observables — such as the CMB, gravitational lensing, primordial abundances, and components of the distance ladder — have been refined and matured, sharpening our view of the Universe. It is an exhilarating time to be a cosmologist. The surprising and non-intuitive composition of the Universe demands the full use of our observational toolkit. Whether the correct cosmological model is the simplest form of ΛCDM or one with additional complexities will ultimately be determined by the quality of our measurements. In the following sections, you will read how the astronomical zoo of objects and features has been employed to produce precision tests of the Universe, with a level of control over systematic errors once known only to particle physics. To be fair, not every tool and technique has reached the same level of robustness (and some may never do so), but this is something you can judge for yourself as you explore the state of each art. Perhaps the biggest question for observational cosmology in the 2020s is what to make of the growing evidence of tensions. The first appearance of any tension or anomaly is usually attributed to experimental error or systematics — an assumption that makes sense when playing the odds. However, signals that may herald new physics will be treated the same unless critical thinking and extensive analysis follow. At present, one or more tensions have surpassed thresholds of statistical significance, reproducibility, and independent cross-checks, earning them the continued attention of the field. In the end, as Einstein once said, the Universe (or Lord) is subtle but not malicious. Our goal is to measure these subtleties.

2.1.1. The distance ladder

Coordinator: Louise Breuval

Contributors: Adam Riess, Giulia De Somma, Leandros Perivolaropoulos, Lluís Galbany, Lucas Macri, Richard I. Anderson, Siyang Li, and Vladas Vansevicius

The Hubble constant measures the present expansion rate of the Universe. This cosmological parameter represents the slope of the redshift-distance relation, $cz = H_0 D$, in the limit of $z \sim 0$. Only distant galaxies are sensitive to the Universe's expansion, unlike nearby systems which are dominated by local gravitational interactions. The best method to reach galaxies in this regime, called the *Hubble Flow* ($0.02 < z < 0.20$), is to build a distance ladder based on a succession of distance indicators. The most widely used and best calibrated distance ladder is based on three rungs. First, geometric distances are used to calibrate the period–luminosity relation of Cepheid variables in nearby galaxies. This law is, in turn, adopted to calibrate SNIa on the second rung, which is limited to the volume where both Cepheids and SNIa are observable. Finally, on the third rung, distances and redshifts of SNIa in the *Hubble Flow* directly measure H_0. Although Cepheids provide the most homogeneous and reliable set of distances to many nearby galaxies, they can be substituted by alternative standard candles such as TRGB stars [15,16], JAGB [17,18], or Mira variables [19,20]. On the second rung, SNIa can be replaced by SBF [21,22], SNII [23,24] or the Tully–Fisher relation [25]. These methods provide valuable independent checks of the distance ladder.

A Cepheid-SNIa distance ladder was included in the HST Key Project on the Extragalactic Distance Scale [27] result of $H_0 = 72 \pm 8\,\mathrm{km\,s^{-1}Mpc^{-1}}$(which calibrated multiple secondary distance indicators using Cepheids). Since then, this measurement was significantly

Fig. 7. Schematic of the different data analysis approaches used in the cosmology community.

improved using state-of-the-art data from later HST instruments, homogeneous calibration, and near-IR Cepheid observations (Fig. 8). The first rung of the distance ladder is currently supported by four geometric calibrators, each providing a direct absolute determination of the Cepheid luminosity: *Gaia* DR3 parallaxes of Cepheids and host clusters in the MW [28], detached eclipsing binaries distances in the Large and Small Magellanic Clouds (SMC) [29,30], and the water maser distance to NGC 4258 [31]. The second rung now comprises a total of 42 SNIa in 37 galaxies, where all hosts are observed with the same instrument (Wide Field Camera 3 (WFC3)) on the same HST, an investment of more than 1000 orbits of observing time. On the last rung, the Pantheon+ team provides $\sim$ 300 SNIa in the *Hubble Flow* with the highest quality data and calibration, standardized across many surveys [32,33]. These recent developments provided the most precise H_0 measurement from a simultaneous fit of the three rungs with $73.17 \pm 0.86\,\mathrm{km\,s^{-1}Mpc^{-1}}$ [34,35]. This HST-based measurement has recently been confirmed with observations of a subsample of SNIa host galaxies with JWST, which show excellent consistency between both telescopes [26] (Fig. 9). Regardless of the method, essential elements for a precise H_0 measurement in the late Universe include the use of near-infrared photometry to minimize the impact of dust [36] and consistent data to cancel flux calibration errors between rungs.

2.1.2. Cepheid variables as standard candles

Coordinator: Louise Breuval

Contributors: Adam Riess, Giulia De Somma, Leandros Perivolaropoulos, Lluís Galbany, Lucas Macri, Richard I. Anderson, Siyang Li, and Vladas Vansevicius

2.1.2.1. Cepheid variables as standard candles. Classical Cepheids are luminous evolved stars located in the instability strip region of the

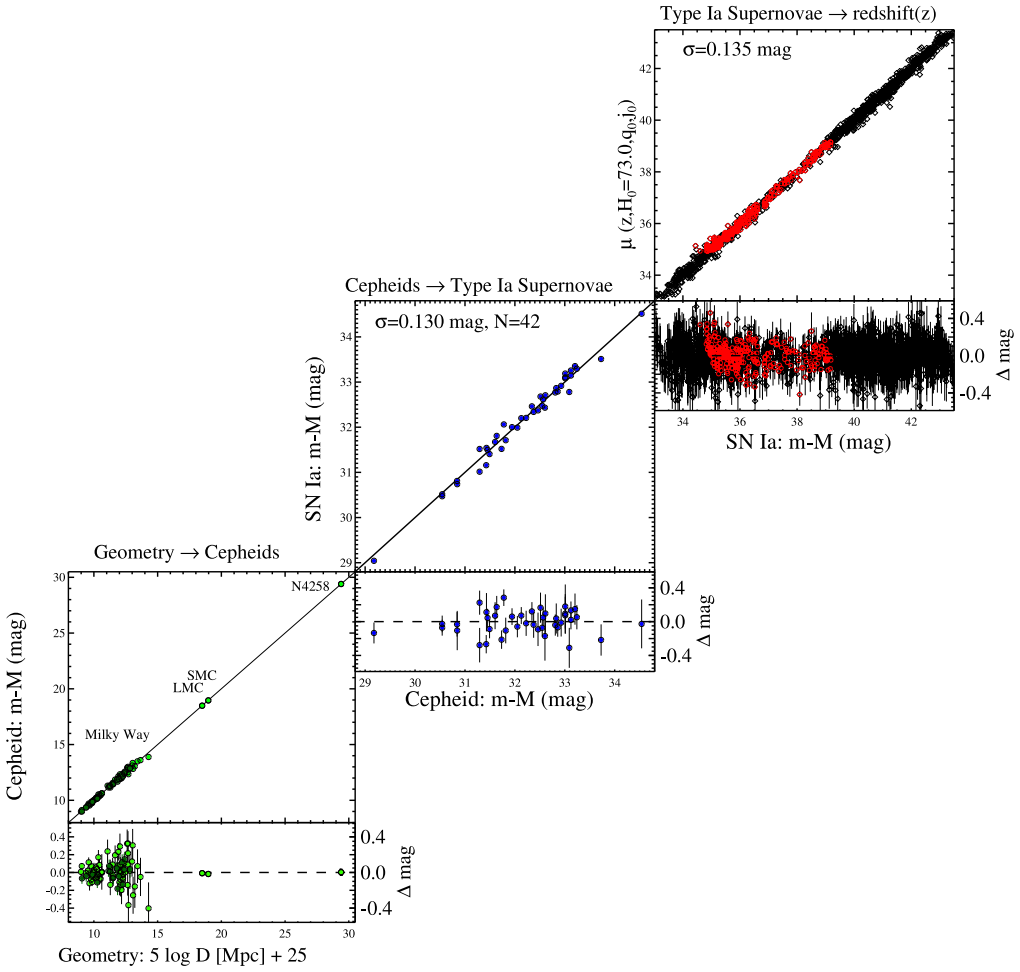

Fig. 8. The Cepheid-SNIa distance ladder [26]. The left-hand panel (first rung) shows the four anchor galaxies with geometric distances which are adopted to calibrate Cepheids. In the middle (second rung), 42 SNIa are calibrated with Cepheids. On the right-hand panel (third rung), redshifts and distances of SNIa in the Hubble Flow directly measure the expansion rate of the Universe.

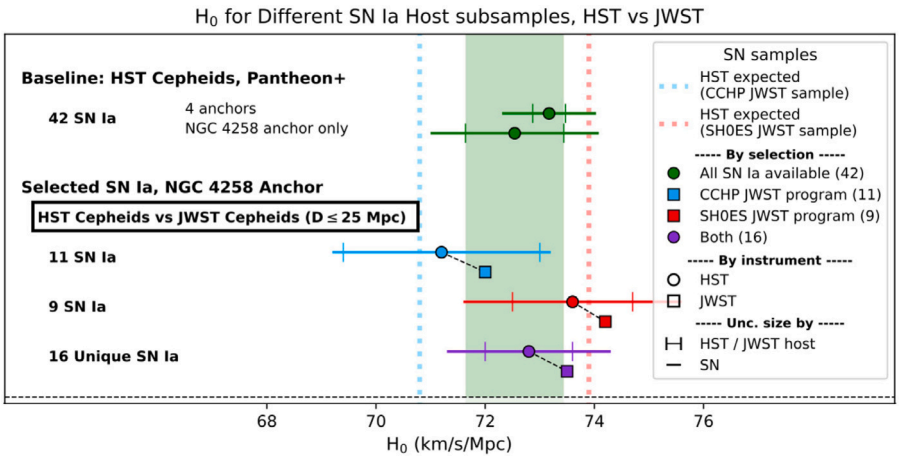

Fig. 9. Comparisons of H_0 between HST Cepheids (baseline, green circles) and JWST Cepheids (squares) for different SNIa host subsamples. The CCHP (blue) and SH0ES (red) subsamples selected for JWST observations produce a difference of 3–4 $\mathrm{km\,s^{-1}Mpc^{-1}}$ in H_0 owing to selection. The HST and JWST distance measurements themselves are in good agreement [26]. (For interpretation of the references to colour in this figure legend, the reader is referred to the web version of this article.)

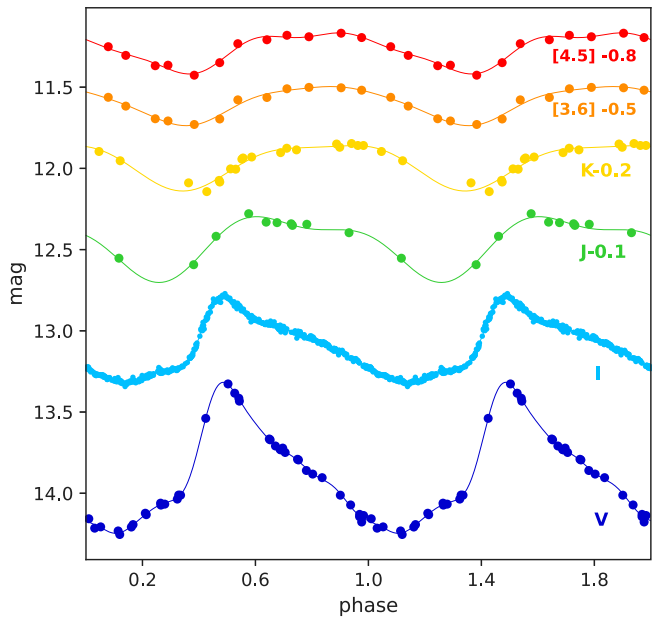

Fig. 10. Multi-band light curves for Cepheid OGLE-SMC-CEP-4697 based on a compilation of data from Refs. [37–39].

Hertzsprung–Russell diagram. These stars undergo regular radial pulsations driven by two mechanisms: the κ (opacity) and γ (adiabatic exponent, $\Gamma_3 - 1$) mechanisms, which operate in the partial ionization zones of abundant elements such as H, He, and He+ [40,41]. Cepheids are regarded as the "gold standard" for distance measurements due to their tight period–luminosity (P–L) relation [42], expressed as $M = a \log P + b$, where M is the absolute magnitude, P is the pulsation period, and a and b are constants. By measuring a Cepheid's P, its M can be determined, and its distance D (in Mpc) can be inferred using the distance modulus: $m - M = 5 \log_{10}(D) + 25$, where m is the apparent magnitude. From a theoretical perspective, the P–L relation arises from fundamental principles of stellar astrophysics [43]. The pulsation period is related to the mean density ρ of the star by $P \propto \rho^{-1/2}$, where $\rho \propto \mathcal{M}/R^3$ ($\mathcal{M}$ and R are the stellar mass and radius, respectively). The Stefan–Boltzmann law, $L \propto R^2 T_{\rm eff}^4$, and the mass–luminosity relation, $L \propto \mathcal{M}^{3.5}$, link the star's luminosity (L) and effective temperature ($T_{\rm eff}$) to its pulsation period, providing a direct foundation for the P–L relation.

Cepheids play a key role in the distance ladder [34]. Their P–L relation is locally calibrated with geometric distances and is used, in turn, to calibrate SNIa on the second rung. Cepheids are easy to identify due to their periodicity and are bright enough to be observed up to about 50 Mpc with the current generation of space telescopes. They are generally identified at optical wavelengths [44], where their pulsation amplitudes peak ($\sim$ 1 mag in the V band), allowing precise determination of their pulsation periods (Fig. 10). Follow-up observations in the near-infrared minimize the impact of interstellar dust on their magnitudes. P–L relations are typically constructed using intensity-averaged magnitudes over the pulsation cycle. These averages are derived either through extensive photometric sampling or by fitting random-phase measurements with template light curves [45,46]. Using mean magnitudes significantly reduces the P–L dispersion by a factor of $\sim$2 compared to random-phase measurements.

However, systematic uncertainties in Cepheid distances may arise due to differences between nearby calibrators and distant Cepheids observed in SNIa host galaxies. These include chemical composition, period range, crowding, dust properties, and potential nonlinearity of the P–L relation (see Ref. [47] for a comprehensive review). In the following sections, we outline the most significant systematics affecting Cepheid distances, and we propose solutions to mitigate them.

2.1.2.2. Improvements in reducing the systematics.

Photometric systems Combining multiple photometric systems to observe Cepheids in the first and second rung introduces a $1.4 - 1.8\%$ systematic error in distance measurements, as described in Ref. [48]. To mitigate this, it is advantageous to use the same telescope and instrument, thereby minimizing flux-calibration errors. Ground-based telescopes, while offering dedicated facilities with high availability [38], are impacted by atmospheric absorption and scattering. In contrast, space-based observatories like the HST and JWST provide superior image quality, are unaffected by weather, exhibit excellent long-term stability, and are not constrained by the day-night cycle. Prior to the launch of JWST, WFC3 on HST was the only instrument capable of resolving Cepheids in the most distant SNIa host galaxies at optical and near-infrared wavelengths [34]. While WFC3 is well-suited for observing both faint and bright targets, it suffers from a slight non-linearity in the infrared. Specifically, photons from faint stars (low count rates) are measured less efficiently than those from bright stars (high count rates), introducing a Count Rate Non-Linearity (CRNL). Though small, this bias is critical for achieving percent-level precision and amounts to 0.0077 ± 0.0006 mag/dex [49]. A CRNL correction is typically applied to bright Cepheids in anchor galaxies to ensure consistent calibration [34,35].

Crowding Separating Cepheids from their surrounding stellar populations is one of the most significant challenges in measuring Cepheids in SNIa host galaxies [15]. Contamination from redder stars, such as RGB and AGB stars along the line of sight, limits the precision of Cepheid measurements, especially in the near-infrared. A common approach to address crowding is to add artificial stars of known brightness at random positions near Cepheids and recover their magnitudes using the same photometric methods applied to real stars [44]. This allows for a statistical correction for crowding (although such corrections remove the bias, but not the added scatter or crowding noise). With the advent of JWST, the ability to separate Cepheids from background stars has improved significantly, resulting in a substantial reduction in crowding noise. Recent JWST observations of Cepheids in SNIa host galaxies including the anchor galaxy NGC 4258 [50,51] have demonstrated excellent agreement with prior HST measurements, achieving a mean difference of only 0.01 mag. Furthermore, JWST data reduced the scatter in the P–L relation by a factor of 2.5 (Fig. 11). This result decisively rules out Cepheid crowding from HST photometry as the cause of the Hubble tension, with a 8.2σ CL.

Metallicity The luminosity of Cepheids at a given period is known to correlate with their chemical composition, but the sign and magnitude of this dependence (γ) have historically been difficult to constrain [52–54]. Accounting for the metallicity dependence is essential in the distance ladder, particularly when calibrating Cepheids in the Magellanic Clouds, which are more metal-poor than typical SNIa host galaxies [35,48]. However, Cepheids in NGC 4258 and the MW resemble those in large spiral SNIa hosts, making metallicity differences negligible for determining H_0. Recent calibrations of the metallicity effect, leveraging accurate distances and expanded Cepheid samples, have converged on a consensus. These calibrations include studies using *Gaia* parallaxes and individual spectroscopic abundances of MW Cepheids [55–57] and combined analyses of MW and Magellanic Cloud Cepheids with geometric distances [35,58]. The derived metallicity dependence (γ) lies between -0.2 and -0.3 mag/dex, with the negative sign indicating that metal-rich Cepheids are intrinsically brighter than metal-poor ones. Recent theoretical studies have corroborated both the sign and magnitude of this effect [59,60], particularly for the Wesenheit index (a dereddened magnitude combining multiple filters [61]) employed in the SH0ES distance ladder [34]. For nearby galaxies, direct [Fe/H] abundances can be determined from high-resolution spectroscopy of Cepheids [56,62]. In more distant galaxies, metallicities are inferred from the [O/H] gradient measured via HII region spectroscopy [63–65] or optical Integral Field Spectroscopy (IFS) of calibrator galaxies [66]. These methods are consistent in the

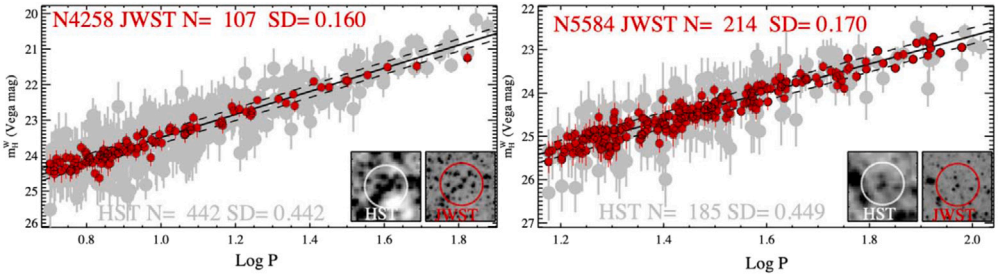

Fig. 11. Cepheid P–L relations in the Wesenheit index obtained from HST$F160W$ (gray) and JWST$F150W$ (red), showing the 2.5 reduction in scatter in NGC 4258 (left) and NGC 5584 (right). (For interpretation of the references to colour in this figure legend, the reader is referred to the web version of this article.)
Source: Figure taken from Ref. [51].

MW, where Cepheid spectroscopy agrees with HII region gradients to within $1\sigma \sim 0.05$ dex [34]. Because the metallicities of Cepheids in SNIa host galaxies closely match those in the anchor galaxies, the Hubble constant is only weakly affected by the metallicity effect. Neglecting the correction would change H_0 by just $0.5\,\mathrm{km\,s^{-1}Mpc^{-1}}$(in the higher H_0 direction) [34]. Although the impact on H_0 is minimal, the metallicity correction plays a crucial role in ensuring consistency among anchor galaxies while independently matching the radial dependence with *Gaia* parallaxes in the MW.

Binaries While crowding can be mitigated using artificial star measurements, unresolved companion stars physically associated with Cepheids can bias their measured flux, thereby affecting inferred distances. A significant fraction of Cepheids reside in binary or multiple systems [67], and unresolved companions typically increase the measured brightness of Cepheids. However, because unresolved binarity is equally present in both SNIa hosts and anchor galaxies, its effect largely cancels out in calibrated distances. In the Wesenheit index adopted in the SH0ES distance ladder, [68] used synthetic populations of binary Cepheids to estimate the impact of binarity, finding it to be a minor effect, contributing only 0.004 mag in distance modulus, or a 0.1% change in H_0. Similarly, [69] determined that the primary source of flux contamination arises from Cepheids located in open clusters, leading to an overestimate of H_0 by approximately 0.23%. However, the fraction of Cepheids in open clusters is relatively small (see also Refs. [46,70]). Thus, while binarity and clustering introduce minor biases, their overall impact on H_0 remains negligible at the current level of precision.

2.1.2.3. Perspectives.

Dust laws Dust has long been a critical systematic uncertainty in the distance ladder [71]. To correct for dust, one can either subtract $R_\lambda \times E(V-I)$ to Cepheid apparent magnitudes or adopt a reddening-free "Wesenheit" magnitude (see Ref. [34,61] for details). Additionally, to the uncertainties in the reddening $E(V-I)$ itself, the value of the R_V parameter is not independently known in each SNIa host galaxy and at each Cepheid position, but rather is assumed to match the MW [34,72]. However, the use of near-infrared observations greatly limits the impact of reddening, reducing the size of R_λ to ~ 0.4 and variations due to these different values of R_V to ± 0.03. Varying the reddening law across different hosts first requires subtracting the intrinsic color of Cepheids in order to separate the component of the color that results from dust reddening (see Sect. 6.3 and Appendix D in Ref. [34]). A complete sampling of the reddening curve at long and short wavelengths in each host as well as an improved characterization of the dependence of R_V with host properties such as mass, star formation rate, and color [73] can further reduce this source of uncertainty in Cepheid measurements.

Cepheid parallaxes Early measurements of trigonometric parallaxes were obtained with the Fine Guidance Sensor (FGS) on HST [74] and later by spatial scanning with HST/WFC3 [75,76] for ~10 MW Cepheids. The European Space Agency (ESA) *Gaia* mission now provides parallaxes for thousands of Cepheids with individual precision at the $\sim 5\%$ level [28]. The main systematic uncertainty in this method arises from the parallax zero-point, a small corrective term estimated with distant QSOs, LMC stars and binaries. The Early Data Release 3 constrained this term and characterized its dependence on magnitude, color, and position [77]. However, MW Cepheids are bright, resulting in limited sampling of the offset term for these stars. Fortunately, the parallax zero-point offset is an additive term, while the distance scale derived from parallaxes is multiplicative. This distinction allows for separation of the two terms, provided a sufficient range of Cepheid distances is available. The analysis of 75 MW Cepheids with high S/N and HST/WFC3 photometry in Ref. [78] yielded a residual parallax offset of $-14\,\mu$ as for Cepheid-like bright stars, which aligns well with the majority of independent studies for stars in this magnitude range [79]. MW Cepheids thus remain the strongest anchor of the distance ladder.

Greater individual precision can be achieved with Cepheids in open clusters by using the average parallax of cluster members [80,81]. Cluster members, being fainter than Cepheids, allow for a more accurate calibration of the parallax offset. In this magnitude range, studies by Refs. [82,83] find a zero-point consistent with zero, demonstrating good agreement between P–L relations derived from individual Cepheids and cluster members. These results further confirm the robust accuracy of *Gaia* parallaxes across a broad range of magnitudes.

New anchors for the cepheid distance ladder The distance ladder is currently supported by geometric distances in four galaxies: *Gaia* parallaxes in the MW [78,82], detached eclipsing binary (DEB) distances in the Large [29,48] and Small [30,35] Magellanic Clouds, and the water maser distance to NGC 4258 [31,84]. Adding new anchors to the Cepheid calibration would reduce uncertainties and strengthen the first rung of the distance ladder. A galaxy can serve as an anchor if it meets two conditions: (1) having Cepheid photometry measured in the same system (e.g., HST/WFC3) as the rest of the distance ladder and (2) having a sufficiently precise geometric distance. The two nearby galaxies, M31 and M33, are excellent candidates for this role, as they contain large Cepheid samples observed with HST/WFC3 [46,85]. However, they remain beyond the reach of late-type DEBs, which are too faint at these distances or suffer from imprecise geometric distances obtained with other methods [86]. On the other hand, early-type DEBs are brighter and could enable geometric distance measurements for M31 and M33 [87]. This method relies on model atmosphere theory, in contrast to the 1% precision surface brightness color relation used for late-type DEBs in the Magellanic Clouds. Significant advancements in these methods are anticipated [88,89], and they should soon provide additional robust anchors for the Cepheid distance ladder.

Future prospects Ongoing surveys (e.g., Zwicky Transient Facility (ZTF)) and the next generation of ground-based (Rubin, Extremely Large Telescope (ELT)) and space telescopes *(Roman)* will provide new insights into the Cepheid distance ladder [90,91]. These advancements will enable the discovery of new Cepheids through deep optical time-series observations of distant galaxies, extending the volume of the local Universe where Cepheids can be studied. High-precision photometry for bright stars in the MW and Magellanic Clouds will be measured by the PhotSat mission in optical bandpasses, which will also help

characterize the extinction law in different environments. Direct abundance measurements obtained with ground-based ELT will complement current datasets and extend the range of distances over which different metallicity tracers — such as Cepheids, blue supergiants, or HII regions — can be compared [62,63,92,93]. Expanding Cepheid samples in both nearby and distant galaxies will allow further tests of the linearity and universality of the P–L relation, a subject of ongoing debate [94–96]. In SNIa host galaxies, long-period Cepheids dominate as they are the brightest, while in nearby anchors, they may saturate or have invalid parallaxes. Conversely, P–L relations in nearby galaxies often include mostly short-period Cepheids. This period disparity could influence the inferred distances in the event of a P–L break. Recent studies [34,97,98] show no evidence for a non-linear P–L relation and demonstrate that allowing for different slopes does not improve the P–L fit. [34] also finds the P–L slope consistent with a single value within 1σ across the current sample of host galaxies. The significance of this effect will be confirmed with larger samples at greater distances. Additionally, the metallicity dependence of the P–L slope [55,59] will be clarified through observations in different environments.

2.1.3. Maser driven constraints

Coordinator: Cheng-Yu Kuo

Contributors: Dom Pesce, Jim Braatz, Mark Reid, and Violetta Impellizzeri

For the purpose of measuring H_0 using accurate distances external galaxies, the so-called *H_2O maser technique*, e.g., see Ref. [99,100] provides a novel tool that allows one to by-pass the traditional extragalactic distance ladders and measure the *angular-diameter distance* to a galaxy in a single step without relying on the CMB. This method involves sub-milliarcsecond resolution imaging and single-dish monitoring of the 22 GHz H_2O maser emission from sub-parsec circumnuclear disks at the center of active galaxies. These *disk maser* emissions, which arise from the $J_{K_-K_+} = 6_{16} - 5_{23}$ transition[1] of the ortho-H_2O molecule, usually have extremely high surface brightnesses, permitting mapping with Very Long Baseline interferometry (VLBI) that allows for a unique probe of the gas distribution and kinematics on sub-parsec scales at the centers of distant galaxies [102].

As revealed in the prototypical maser galaxy NGC 4258, e.g., see Ref. [103,105], the masing gas in a disk maser system often resides in a nearly edge-on thin disk around the central supermassive black hole (BH). The rotation curve of the gas can be nearly perfectly traced by Keplerian rotation, enabling black hole (BH) mass measurements to percent-level accuracy, e.g., see Ref. [106,107]. Given the assumption that the gas dynamics is dominated by the gravity of the central BH, the simplicity of disk geometry and kinematics allow one to use the orbital radii $r_{\rm sys} = v^2_{\rm sys}/a_{\rm sys}$ of the *systemic* maser components, see Fig. 12, e.g., see Ref. [106], as a standard ruler for measuring the angular-diameter distance $D_{\rm A}$ of the galaxy, e.g., see Ref. [105], where $v_{\rm sys}$ and $a_{\rm sys}$ standing for the orbital velocity and centripetal acceleration of a systemic maser component. By using $r_{\rm sys}$ as the standard ruler, one can easily show that the angular-diameter distance of a maser galaxy can be expressed as $D_{\rm A} = v_0^2 \sin(i)/a\Delta\theta$, where i and $\Delta\theta$ indicate the maser disk inclination and the angular radius of the systemic masers, respectively. As long as the masing components of the gas follow circular orbits, one can determine an accurate galaxy distance by measuring the four disk parameters including $a_{\rm sys}$, $v_{\rm sys}$, i, and $\Delta\theta$, where a_0 can be measured from single-dish monitoring of the maser lines, e.g., see Ref. [100] and the rest of the three parameters can be obtained by modeling the maser disk in three dimensions, e.g., see Ref. [108,109].

To apply this maser technique to galaxies in the local Universe, one has to first search for maser disks similar to NGC 4258 that allow for robust disk modeling. To this end, the Megamaser Cosmology Project (MCP; [111,112]) has carried out an extensive survey of H_2O megamaser emission from >4800 AGNs [113,114] within redshift $z \lesssim 0.05$, resulting in the detection of $\gtrsim$30 candidate disk masers [115]. The follow-up imaging of these candidates has increased the number of H_2O maser disks with high precision VLBI maps by a factor of $\gtrsim$4 over the past decade. The resultant Hubble constant (see Fig. 13) from this effort is $H_0 = 73.9 \pm 3.0\,{\rm km\,s^{-1}Mpc^{-1}}$ [110], a $\sim$4% uncertain H_0 estimate determined based on six "clean" disk maser systems that have the required spectral qualities for reliable disk modeling. This maser-based H_0 measurement is well consistent with the majority of direct, *late Universe* measurements of Hubble constant. Its uncertainty is currently dominated by measurement errors in the maser position obtained from VLBI observation and in the determination of the maser acceleration with the single-dish monitoring. The systematic uncertainties, which could result from non-circular orbits of the masing gas, e.g., see Ref. [108] or from the impacts of non-gravitational forces such as shocks in the maser disk, e.g., see Ref. [115–117], are currently negligible in comparison with measurement errors. It is expected that the accuracy of the maser-based H_0 measurement can be further improved to $\sim$1%, the long-term goal of the observational cosmology community, by measuring distances to $\gtrsim$50 maser galaxies, with $\sim$7% accuracy per measurement [118]. It is promising that this goal can be realized after the full array operation of the next-generation Very Large Array (ngVLA), which will bring about an order of magnitude improvement in sensitivity, permitting efficient detection of disk maser systems in a $\sim$30 times larger volume compared with the MCP [118] as well as significant improvement in VLBI maser position measurement.

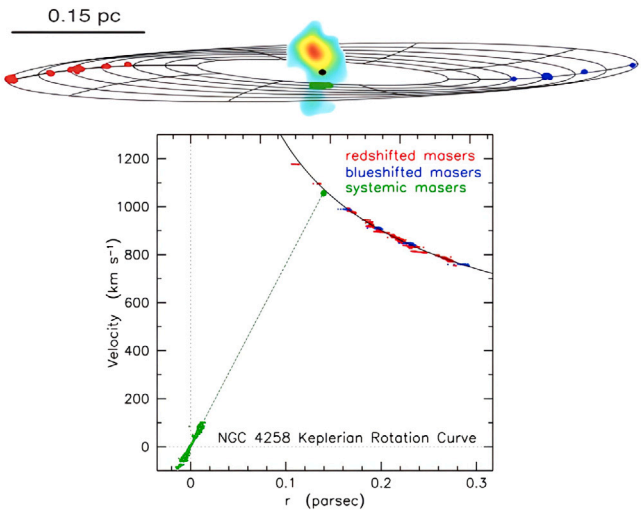

Fig. 12. The distribution and Keplerian rotation curve [103,104] of the 22 GHz H_2O masers in NGC 4258. The red, blue, and green dots in the plot represent the redshifted, blueshifted, and systemic maser components, respectively. (For interpretation of the references to colour in this figure legend, the reader is referred to the web version of this article.)

2.1.4. On the tip of the red giant branch method

Coordinator: Richard I. Anderson

Contributors: Adam Riess, Gagandeep S. Anand, Giulia de Somma, Ippocratis Saltas, Louise Breuval, Siyang Li, and Vladas Vansevicius

The TRGB method provides the most precise stellar alternative to classical Cepheids (Section 2.1.2) on the first and second rungs of the extragalactic distance ladder used to measure the Hubble constant [119]. Comparison between TRGB and Cepheid distances in supernova hosts shows very good agreement between both methods, Fig. 11 in Refs. [16] or [26]. Fig. 14 illustrates two paths to H_0 in which

[1] Here, J is the total angular momentum of the H_2O molecule, with K_- and K_+ representing the projections of J on two molecular axes, e.g., see Ref. [101].

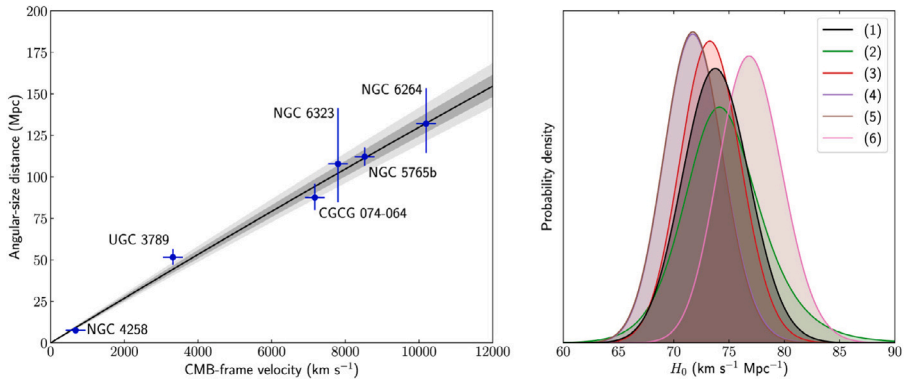

Fig. 13. Left panel: Hubble diagram for the six maser galaxies considered in the MCP H_0 measurement [110]. Assuming a fixed velocity uncertainty of 250 km s^{-1} associated with peculiar motions, the MCP constrains the Hubble constant to be $H_0 = (73.9 \pm 3.0)\,\mathrm{km\,s^{-1}Mpc^{-1}}$, independent of distance ladders and the CMB. Right panel: posterior distributions for H_0 from the five different peculiar velocity treatments considered in Ref. [110], with the *fiducial* treatment plotted in black.

the TRGB calibrates either SBF (Section 2.1.5) [22,120] measured in elliptical galaxies or SNIa (Section 2.1.7), e.g., see Ref. [15,121,122] measured in any type of galaxy for tracing the Universe's isotropic expansion in the Hubble flow. In both cases, the TRGB serves as an intermediary to translate the relative apparent magnitude differences of SBF or SNIa as a function of redshift to an absolute scale anchored to geometrically measured distances. As part of the past decade's unfurling Hubble tension, the TRGB method has seen major improvements and inspired deep investigations into systematics of late-Universe H_0 measurements. Here, we briefly review the astrophysical basis of the TRGB as a standard candle to determine luminosity distances, present methodological considerations relevant for determining TRGB distances to better than $\sim 5\%$, and consider likely future developments relevant for the H_0 tension in light of catalysts provided by new observational facilities and upcoming space missions. [123] provides further background and in-depth discussion.

2.1.4.1. The astrophysical basis. The TRGB as a standard candle is a robust empirical concept that is usefully supported by a solid understanding of the evolution of RGB stars. Empirically, the magnitude m_T is measured as the inflection point of a RGB LF [126,127]. Measuring m_T therefore requires a large number of stars to avoid stochastic effects and, in particular, cannot be done for each star separately. This characteristic is shared with the J-region AGB method [128,129] (Section 2.1.8) and distinguishes the TRGB as a *statistical* standard candle from pulsating stars, such as classical Cepheids, whose luminosity can be measured and calibrated *individually* [47,130].

The TRGB feature is astrophysically explained by the very rapid thermonuclear ignition of degenerate helium cores of low-mass first-ascent RGB stars, the so-called helium flash (HeF), see e.g., [133–137]. In particular, old RGB with masses $\lesssim 1.6\,M_\odot$ develop helium cores of nearly equal mass ($\sim 0.5\,M_\odot$), resulting in a nearly equal luminosity of the HeF that can be exploited as a standard candle. Younger, higher-mass giants reach lower luminosity due to lower electron degeneracy at higher core temperatures and lower densities. This mass limit corresponds to an age-effect: giants older than ~ 4 Gyr have nearly constant luminosity in $I-$band. Differences in chemical composition (metallicity) significantly affect TRGB luminosity and temperature due to line blanketing: the bolometric magnitude behaves as $M_{T,\mathrm{Bol}} \propto -0.19[\mathrm{Fe/H}]$ [136]. At the same time, higher metallicity results in cooler effective temperature. Hence, more metal-poor giants are brighter and bluer. Thankfully, the dependence on metallicity is partially mitigated in Cousins $I-$band where the bolometric correction ($M_I = M_\mathrm{Bol} - BC_I$) nearly compensates the change in luminosity for low-metallicity ($[\mathrm{Fe/H}] \in [-0.7, -2.0]$) giants. Color-based metallicity calibrations can further mitigate this issue, e.g., see Ref. [138,139]. Hence, the TRGB is a theoretically well-supported standard candle when low-metallicity ($[\mathrm{Fe/H}] < -0.7$) old (> 4 Gyr) RGB stars are observed in $I-$band. However, observations at infrared wavelengths require caution and additional study with respect to the aforementioned effects, in particular if the observed RGB populations exhibit diversity in age and/or chemical composition, see Fig. 15.

Theoretical predictions of the TRGB luminosity rely on stellar evolution models that require various assumptions and simplified treatment of stellar physics, including the modeling of opacities, diffusion, convection (mixing-length theory) and overshooting, mass-loss, electron screening, neutrino losses [140], nuclear reaction rates, among others [137,141]. In particular, the dominant uncertainties related to radiative opacity introduce systematics of up to 1.6%. Simultaneously varying radiative and conductive opacities, nuclear reaction rates (e.g., triple-alpha reaction), and neutrino losses affect the bolometric Tip luminosity by $\delta L/L \sim 10^{-3}$, depending on mass and metallicity [142]. Comparisons with observations are subject to larger uncertainties, notably related to the translation of bolometric luminosity to magnitude, which require stellar atmosphere models that are usually considered separately from the evolutionary models [137].

2.1.4.2. Methodological considerations and HST-based results.

The absolute calibration of the TRGB method requires measuring m_T in RGB populations of known distance to obtain $M_\mathrm{T} = m_\mathrm{T} - \mu_0$. The best available, geometrically measured, distances (in ascending order) are: trigonometric parallaxes from the ESA *Gaia* mission [143], the distances to the LMC and SMC measured by detached eclipsing binary stars [29,30], and the megamaser distance to NGC 4258 (M106) [31]. Importantly, the distance moduli $\mu_{0,i}$ of the LMC, SMC, and NGC 4258 are frequently used in distance ladders calibrated using stellar standard candles and hence their systematics are often shared among different H_0 measurements, e.g., see Ref. [34,35,144,145]. Comparing distances to other galaxies measured using an absolute calibration based on the same anchor, such as NGC 4258, thus yields the strongest test of distance systematics [e.g.,26,146]. As implied in Fig. 14, uncertainties in μ_0 propagate directly into H_0 measurements, as they set the absolute scale of the secondary tracers (SNIa, SBF) via the primary standard candle (here: TRGB). Basing an absolute TRGB calibration on the broadest possible set of "anchors" reduces possible bias and allows one to determine appropriate standardization procedures, e.g., to account for metallicity differences [121,138]. At present, the most accurate TRGB calibrations to date are obtained in the Magellanic Clouds [126,147] and NGC 4258 [16] using passbands similar to $I-$band, such as HST's ACS/F814 W or JWST's NIRCAM/F090 W. TRGB calibration based on *Gaia* parallaxes [148] has been achieved based on EDR3 parallaxes, which require correction for complex systematics, e.g., see Ref. [77,

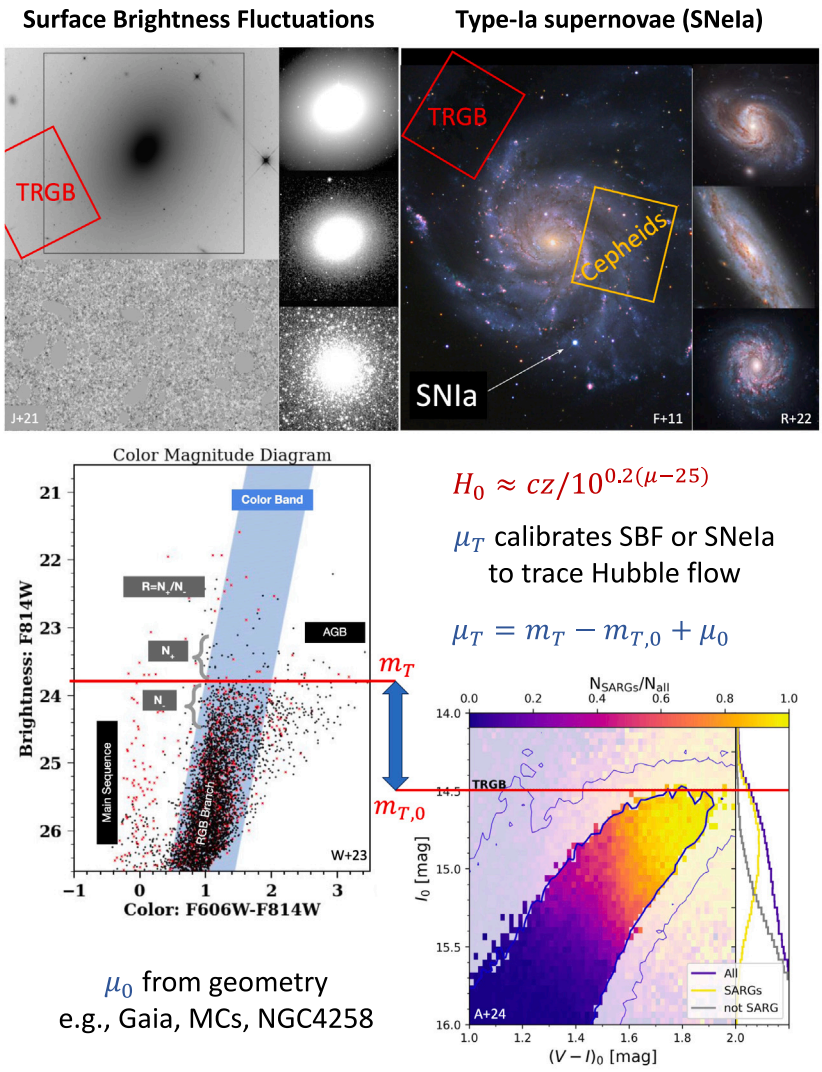

Fig. 14. Illustrations of extragalactic distance ladders built on the TRGB method. The scales considered increase upwards. *Bottom right:* The TRGB feature is calibrated based on color-magnitude diagrams of stars whose distances (μ_0) are known from geometric measurements, such as *Gaia* parallaxes, the Magellanic Clouds, or NGC4258. The choice and systematics of (the combination of) geometric anchors directly impact the Hubble constant by setting μ_0. *Center left:* The apparent magnitude of the TRGB feature is determined in other galaxies. Differences in the absolute magnitude between TRGB populations, either compared to the calibrating set or as field-to-field variations, must be mitigated by standardization. *Upper part, right:* The measured TRGB distances calibrate the fiducial absolute magnitude of SNIa in any type of galaxy. Cross-checks between multiple stellar standard candles can primarily be obtained in galaxies hosting young, intermediate-age, and old stellar populations at the same time. Note that TRGB fields should be placed on galaxy halos populated by old, metal-poor stars, whereas classical Cepheid fields target young stellar populations in supernova host galaxies. *Upper part, left:* Alternatively, the TRGB is used to calibrate the absolute scale of the SBF method for distance determination to elliptical galaxies that trace the Hubble flow. SBF exploits the fact that the variance of SBF decreases as d^2.
Figure credit: R.I. Anderson based on images as labeled from: J+21 [124]; F+11 B. J. Fulton, Las Cumbres Observatory; R+22 [34]; W+23 [125], A+24 [126].

78,83,149–152]. Furthermore, a parallax-based TRGB calibration has been obtained for ωCentauri [153]. The period–color relation of stars near the TRGB may provide a useful avenue to deal with (differential) reddening when calibrating the TRGB based on field RGs [147].

A critical element of determining accurate distances using standard candles is to ensure consistency between the absolute calibration and the standardized application in the target environments. However, there are measurable differences even between the I–band absolute magnitudes in the LMC and the SMC, and they reflect noticeably in the variability periods of the small-amplitude RGB stars that make up the RGB population at the Tip [126]. These ubiquitous small amplitude pulsations near the RGB Tip allow us to probe the intrinsic diversity (e.g., in age and metallicity) ofRGB populations that is not typically known a priori and thus constitute a difficult-to-control astrophysical systematic at the level of a couple of percent [147]. Additionally, a common feature of RGB populations in other galaxies is contamination by other stars, notably at higher luminosity (typically AGB stars). Unfortunately, the specifics and degree of such contamination differ from environment to environment (cf. CATs below) and are not reliably known a priori. The exception to this rule is globular clusters (GC), which rarely contain stars brighter than the TRGB, e.g., see Ref. [154], so that measuring $m_{\rm T}$ conceptually corresponds to searching for the brightest cluster star without knowing how much it differs from the HeF luminosity. As a result, GC-based values of $m_{\rm T}$ represent lower limits to the desired measurement of $m_{\rm T}$ and are furthermore also subject to variations in metallicity and age, depending on the photometric band. Thus, GC-based $m_{\rm T}$ values differ conceptually from the values of $m_{\rm T}$ measured in RGB populations of mixed age and metallicity. Further study is needed to assess to what degree such effects impact $M_{\rm T}$, and hence, H_0.

Extinction corrections are routinely applied for TRGB calibration in the Magellanic Clouds [155]. However, dust corrections to TRGB measurements in other galaxies typically, e.g., see Ref. [144] rely on

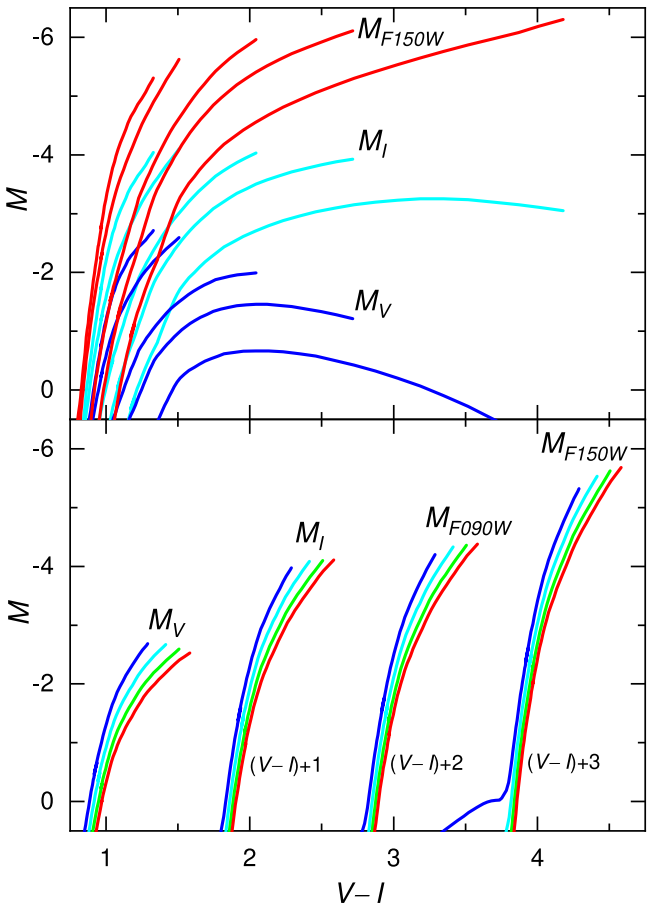

Fig. 15. Dependence of M_T on chemical composition and age based on PARSEC v.1.2S isochrones [131,132]. *Top:* 8 Gyr isochrones for increasing metallicity (from left to right: [M/H]= −2.2, −1.5, −0.7, −0.4, 0.0) in Johnson V (dark blue), Cousins I (cyan), and JWST/NIRCAM F150 W (red) passbands. *Bottom:* [M/H]= −1.5 isochrones for increasing ages (left to right) of 2 Gyr (blue), 4 Gyr (cyan), 8 Gyr (green), and 14 Gyr (red) in the Johnson V, Cousins I, JWST/NIRCAM F090 W and F150 W passbands, successively offset in color for visibility. (For interpretation of the references to colour in this figure legend, the reader is referred to the web version of this article.)

all-sky dust extinction maps [156,157] that account only for MW foreground dust and whose accuracy is limited in the vicinity of resolved galaxies. Recently, it has been pointed out [158] that small, albeit non-zero, extinction in galaxy halos leads to underestimated H_0 values and that dust extinction estimates based on background quasars [159] provide a possibility for correcting this one-sided systematic. Statistical corrections for local extinction have since been applied [16,122]. However, further study of extinction effects and their variation across circumgalactic media would be useful to provide improved corrections.

The TRGB magnitude (m_T) is measured either via an edge detection algorithm [119,127], such as a Sobel filter, or via a maximum likelihood fit of the LF [79,160,161]. When Sobel filters are used for edge detection, LFs are typically smoothed to some degree to reduce noise [127], and different weighting schemes have been considered in the literature [125,162]. Recently, it has been pointed out that both the LF smoothing and the Sobel response weighting introduce biases that depend on the shape of the observed LFs [126]. In particular, Sobel response weighting was shown to introduce the tip-contrast relation determined independently using observations [125]. Both issues can easily bias the measured value of m_T by 0.06 mag (∼ 3% in distance), and it is therefore crucial to apply the same TRGB measurement method in all target RGB populations to avoid bias. Similarly, observer choices, such as color cuts (notably near the Tip), can affect the measured m_T and should be decided based on objective criteria [122].

Field-to-field variations of m_T have been recently reported within the same galaxies. This led to the development of an unsupervised TRGB detection algorithm, called CATs (Comparative Analysis of TRGBs), which sought to reduce the impact of subjective observer choices on the measurement of m_T [122,125]. In the process, a tip-contrast relation was determined, which has since been shown to result from the use of weighted Sobel response curves [126]. Bias of TRGB distances can thus be avoided if either (a) unweighted Sobel filters are used to measure m_T [126], or (b) if an appropriate tip-contrast relation is used to standardize m_T a posteriori when weighted Sobel response curves are used [122]. Given the simpler algorithm and the non-uniqueness of the tip contrast, which depends on the measured m_T, it appears prudent to avoid Sobel filter weighting. First results from an I−band (F090 W) TRGB calibration using the JWST also support this approach [16].

In observations based on the *Hubble* Space Telescope or JWST, the placement of TRGB fields in target galaxies is crucial to ensure that the targeted RGB population is similar or standardizable to the RGB population that provides the absolute calibration [163], for an example, e.g., see Ref. [146]. Thanks to very large fields-of-view, observations with the ESA *Euclid* mission [164] or the future Nancy Grace Roman telescope[2] will allow us to integrate field-to-field variation analysis into TRGB algorithms, rendering them much more robust. However, the existence of field-to-field variations within a single galaxy highlights the need for TRGB standardization to account for differences between RGB populations in different galaxies.

The choice of photometric system The TRGB has been most commonly measured in the I−band where it is nearly flat and relatively insensitive to metallicity and age effects [119,145], cf. Fig. 15. There has been growing interest in NIR TRGB measurements due to the capabilities of the JWST and the intrinsically higher (1 − 2 mag) luminosity in the NIR [165,166], and several I−band and NIR observing programs are currently being analyzed with JWST (e.g., GO-1685, 1995, 2875, 3055). However, the (color) slope of the TRGB at NIR wavelengths requires additional consideration. Both empirical (see Refs. [165–172]) and theoretical approaches [137,173] have been considered for the time being, and further study is required to determine competitive and accurate TRGB distances at infrared wavelengths. Furthermore, K−corrections are expected to exceed 1% in distance for single-band JWST TRGB observations at distances above ∼ 70 Mpc for the F150 W passband and shorter wavelengths [158].

2.1.4.3. Implications for H_0 and the Hubble constant tension. Several studies have reported H_0 measurements involving the TRGB as a standard candle, with rather significant differences. To understand these differences, it is crucial to consider the differing assumptions and methods underlying each analysis. In particular, Refs. [121,144] applied different absolute TRGB calibrations and TRGB measurement methodologies to the same set of HST I−band TRGB observations in conjunction with the CSP SNIa dataset in the Hubble flow and measured $H_0 = 69.8 \pm 0.6 \pm 1.6\,\mathrm{km\,s^{-1}Mpc^{-1}}$ and $71.5 \pm 1.8\,\mathrm{km\,s^{-1}Mpc^{-1}}$, respectively. In an update to Ref. [144], Ref. [174](v3) employed JWST I−band (F090 W) TRGB measurements together with CSP SNIa and obtained $H_0 = 70.4 \pm 1.2 \pm 1.3 \pm 0.7\ \mathrm{km\,s^{-1}Mpc^{-1}}$. Ref. [122] corrected the tip-contrast TRGB systematic and replaced the CSP SNIa with Pantheon+ to ensure a consistent calibration between SNIa in host galaxies and the Hubble flow and found $72.94 \pm 1.98\,\mathrm{km\,s^{-1}Mpc^{-1}}$. Replacing HST entirely with JWST I−band TRGB observations of 17 unique SNIa yields $72.1 \pm 2.2 \pm 1.2\,\mathrm{km\,s^{-1}Mpc^{-1}}$ [26]. Recently, Ref. [120] replaced SNIa entirely with SBF calibrated by JWST I−band TRGB observations [16] and found $73.8 \pm 0.7 \pm 2.3\,\mathrm{km\,s^{-1}Mpc^{-1}}$, confirming the conclusion from Ref. [122] that at least half the difference between the H_0 values reported by Ref. [144] and Ref. [82] can be attributed to SNIa alone.

[2] https://roman.gsfc.nasa.gov

The prospects for further improvements of the TRGB method and, in turn, to increase the accuracy in H_0 are very promising. New wide-field space-based telescopes (Euclid, Roman) will allow us to comprehensively measure $m_{\rm T}$ in a very large number of galaxies, while JWST will allow to push the limits of TRGB distances. Potentially, *Roman* could allow to directly calibrate $m_{\rm T}$ in the LMC and SMC, circumventing differences among photometric systems. However, the target magnitudes are close to saturation ($\sim$ 6s at AB 15 mag in F087[3]). An SBF calibration based on the TRGB method will yield an accurate H_0 measurement fully independent of the Cepheid-SNIa distance ladder [22,120], if different geometric distances are used to calibrate the two types of standard candles. Future improvements in the *Gaia* astrometric solution will play an important role in this endeavor, as will synthetic *Gaia* photometry based on B_p and R_p spectra [175]. Pushing the TRGB to the limit using JWST may motivate infrared observations owing to the combination of RGB stars being brighter in the near-IR and JWST providing optimal sensitivity there, although it has been already shown that I-band JWST TRGB measurements are feasible out to at least 50 Mpc [22,176].

In order to ensure that stellar standard candles provide the clearest and most accurate picture of cosmic tensions, notably the Hubble constant tension, it is crucial to pursue the most direct and simple assessments of systematics. To this end, direct and detailed comparisons of distances measured using the TRGB method, classical Cepheids, and the JAGB method are preferred, cf. [26]. In contrast, trying to understand TRGB or Cepheid-based systematics from published values of H_0 is complicated by several other possible differences between distance ladder set ups, e.g., with respect to the treatment of peculiar motions and supernova standardization [122]. Cross-checks based on nearby galaxies, e.g., M31 [85], M33 [46,177], and other nearby galaxies (e.g., HST GO-17520), will be particularly insightful to this end as they provide the greatest possible precision for each of the standard candles and an optimal ability to investigate causes of systematic differences, e.g., using spectroscopy on future 30m-class telescopes, such as the ELT.

2.1.5. The surface brightness fluctuations method

Coordinator: Michele Cantiello

Contributors: Enzo Brocato, Gabriella Raimondo, John Blakeslee, Joseph Jensen, and Rebecca Habas

2.1.5.1. Introduction & state of the art. The SBF method is a powerful technique used to measure distances of elliptical galaxies out to $\sim$ 150 Mpc, and may reach distances as far as $\sim$ 300 Mpc with telescopes like the JWST [22]. Introduced in the late 1980s, the SBF method relies on the fact that the surface brightness of a galaxy exhibits small-scale variations due to the statistical distribution of stars [178–182]. When imaging a galaxy, the number of stars that fall within each detector pixel varies, causing pixel-to-pixel variations in the surface brightness. The amplitude of these fluctuations is inversely proportional to the square of the distance to the galaxy [183], allowing one to estimate distances from imaging alone.

In principle, the SBF method is straightforward. The only difficulty lies in isolating the signal fluctuations of the underlying Population II stars from contaminants such as globular clusters, star forming regions, and background galaxies. Once this is done, the absolute SBF magnitude can be calibrated in a given passband, $\overline{M}_\xi$, using galaxies at well-known distances [184] or through stellar populations numerical modeling [185]. The distance modulus $\mu_0 \equiv (m-M) = 5\log 10(D) + 25$ can then be inferred as usual: $\mu_0 = \overline{m}_\xi - \overline{M}_\xi$ where $\overline{m}_\xi$ is the ξ-band observed fluctuation magnitude and D is the distance in Mpc.

In practical terms, the SBF distance measurement involves several steps, summarized briefly here and illustrated in Fig. 16: (i) determining and subtracting the sky background; (ii) modeling and subtracting the galaxy (upper middle panel in Fig. 16); (iii) masking all potential sources of contamination to the fluctuation signal (e.g., globular clusters within the galaxy, background galaxies, dust patches, etc.; upper right panel); (iv) modeling the LF of sources in the frame to estimate the spurious fluctuation contribution from unexcised sources (lower left panel); and (v) power spectrum analysis of the residual masked frame, to measure the amplitude of the SBF signal (lower middle and right panels). Additional details on this procedure are available in the references cited in this review.

In recent years, the application of the SBF method has seen significant advancements, particularly with the contributions from the high-resolution space-based data from the HST. Recently, Refs. [21, 124] used HST/WFC3 data to measure highly accurate distances for a sample of $\sim$ 60 elliptical galaxies, taking particular care to analyze the $\overline{M}_{F110W}$ calibration, and succeeded in obtaining distances with median statistical uncertainties $\lesssim 4\%$.

From the ground, the Next Generation Virgo Cluster Survey (NGVS), a project based on 104 degrees^2 deep optical imaging from the CFHT [187], has provided a dataset ideal for SBF measurements in the Virgo Cluster. The NGVS has enabled detailed studies of galaxy distances in this cornerstone galaxy cluster [186], and represents a crucial survey, serving as a precursor for future large ground- and space-based surveys.

Most of the focus for the use of SBF has been on bright galaxies, where the method provides the lowest uncertainty, reaching levels $\lesssim$ 5% on single targets in well-designed observations. The advent of large area deep surveys has, however, led to the discovery of an increasingly large number of dwarf galaxies which play a fundamental role in Cosmology [188]. Several authors [189–191] have applied the SBF technique to smaller and fainter systems. These studies have demonstrated that $\overline{m}$ can be used to estimate distances to dwarf galaxies, although with relatively large errors compared to massive galaxies, providing a typical uncertainty of $\delta D/D \sim 15\%$. Despite the relatively larger error, these elusive galaxies are often challenging targets for distance measurement due to their low surface brightness and complex stellar populations. This has opened new avenues for using SBF to probe the Local Universe and improve the cosmic distance ladder.

2.1.5.2. The Hubble constant tension. In addition to providing distance estimates for individual galaxies, SBF can also be used to probe tensions in the measurement of the Hubble constant that have arisen between the CMB observations [192] and the value obtained from the late-Universe [34].

The SBF method, with its ability to provide distance measurements to galaxies beyond the 50 Mpc range, offers a unique perspective on this tension, independent of the classical Cepheid/SNIa route. This topic has been explored by Ref. [21] for a sample of bright galaxies between 20–100 Mpc, with $\overline{M}_{\rm F110W}$ calibrated using both Cepheids and TRGB distances. For both calibrations, the authors derived a value of H_0 that is fully consistent with the direct distance estimates in the local Universe. The work by Ref. [21] was based on a small sample, and this result should be corroborated with larger studies. That study, as well as some of the newly programmed ones [22], used SBF in near-IR passbands where the amplitude of fluctuations is "enhanced" because the brightest stars contributing to the signal are brighter compared to the optical bands. This enhancement is key for the recent results on H_0 and will be crucial for future observations, as it allows for reliable measurements for galaxies at larger distances.

A complementary approach to the H_0 tension uses SBF indirectly, as a calibration for SNIa distances. Rather than the Cepheid-SNIa route to Cosmology, one can use a Cepheid-SBF-SNIa route. This method has larger systematic and statistical uncertainties from the extra rung in the distance ladder, but offers the advantage of having a larger calibration sample of SNIa from the local Universe because of the larger overlap in galaxies that host SNIa and have SBF measurements. This approach was adopted by Ref. [193], who used a heterogeneous

[3] https://roman.gsfc.nasa.gov/science/apttables2021/table-timetosaturation.html

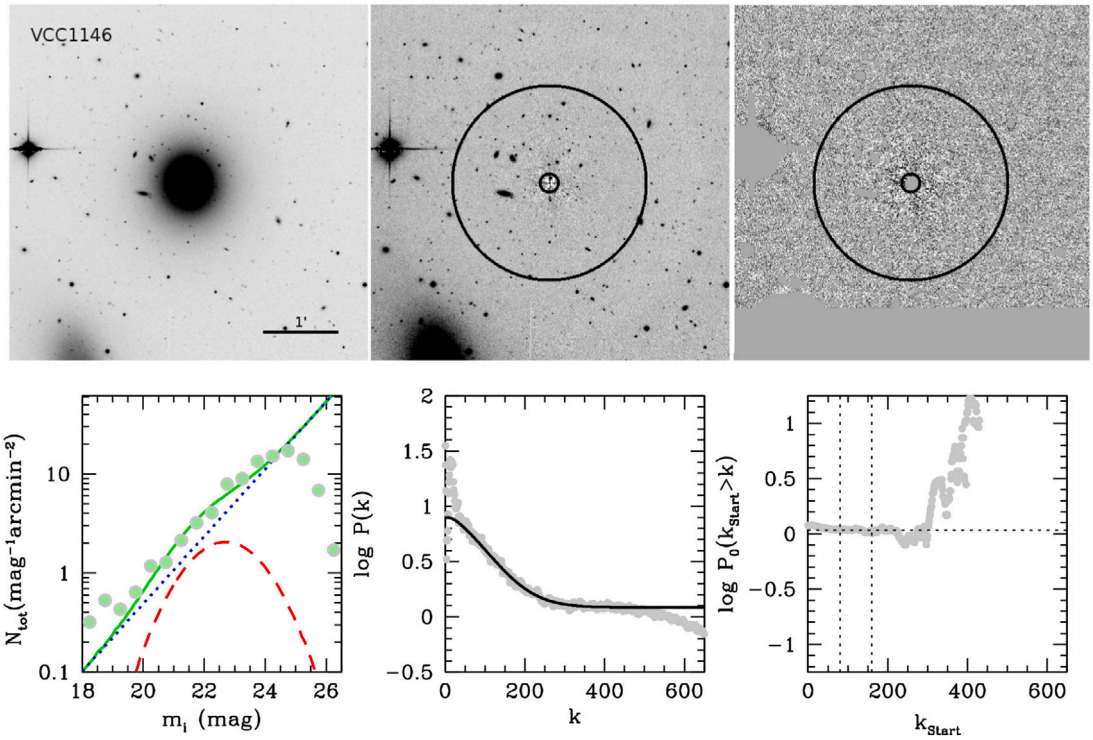

Fig. 16. SBF analysis for the galaxy VCC 1146. **Top row:** *i*-band image, residual image, and masked residual image (left to right). Black annuli in the second and third panels mark the inner and outer radii used for SBF measurements. **Bottom left:** Fitted LF for external sources. Green circles are observational data with a faint-end downturn from incompleteness. The solid green line shows the best fit, corrected for incompleteness, with blue dotted and red dashed curves representing the background galaxy and GC LFs. **Bottom middle:** Azimuthal average of the residual power spectrum (gray circles) and the fit (solid black line). **Bottom right:** Fitted P_0 values vs. k_{start}, with $k_{end} = 450$. Vertical lines at $k_{start} = 80$ and 160 show the range over which the fit is stable. The median P_0 in this range (dotted horizontal line) is adopted.
Source: Figure adapted from Ref. [186].

collection of SNIa and SBF measurements from existing literature, obtaining $H_0 = 71.1 \pm 2.4(\text{stat}) \pm 3.4(\text{sys})\,\text{km s}^{-1}\text{Mpc}^{-1}$. More recently, Ref. [194] used a very homogeneous sample of SBF measurements from Ref. [124], and found that the Hubble–Lemaître parameter derived from the revised SALT2 [32] parameter fit and calibrated with near-IR SBF distances is $H_0 = 73.3 \pm 1.0(\text{stat}) \pm 2.7(\text{sys})\,\text{km s}^{-1}\text{Mpc}^{-1}$. Note that the SNIa-independent estimate from Ref. [21], based on Cepheid zero-point calibration, yielded $H_0 = 73.3 \pm 0.7(\text{stat}) \pm 2.4(\text{sys})\,\text{km s}^{-1}\text{Mpc}^{-1}$, whereas the most recent recalibration, which relies on TRGB distances from JWST observations of Virgo and Fornax galaxies by Ref. [120], provided $H_0 = 73.8 \pm 0.7(\text{stat}) \pm 2.3(\text{sys})\,\text{km s}^{-1}\text{Mpc}^{-1}$.

2.1.5.3. Future prospects and projects. The SBF method is expected to become even more relevant in the future, taking advantage of the fact that most of the forthcoming facilities will operate in the near-IR regime, where the SBF signal is much stronger. The JWST, with its superior resolution and sensitivity, is expected to enable detailed SBF studies of distant galaxies, potentially reaching $\sim$ 300 Mpc [22]. The large sky surveys from the Vera Rubin Observatory's LSST and from the Euclid mission, will further enhance the capabilities of SBF by providing an enormous dataset for SBF, largely dominated by the dwarfs. This will allow astronomers to apply the SBF method to a much larger and more diverse sample of galaxies, improving the statistical robustness of the 3D mapping of the Universe within 40–70 Mpc.

On longer time scales, the Nancy Grace Roman Space Telescope (to be launched in the mid-late 2020s), will also play a crucial role in the advancement of SBF, due to its combination of wide-field, high-resolution, and infrared wavelength coverage. Roman will enable high-precision SBF measurements over large areas of the sky, potentially reaching the depth of the JWST, but over a wider area. The future 30–40 m class ground based telescopes, with their adaptive optics (AO), may also be more useful for SBF than the JWST. Correcting for atmospheric distortions using the AO systems could provide better FWHM resolutions than the JWST in certain passbands (e.g., *K*-band) which, combined with the huge telescope collecting area, would allow SBF to be applied to more and more distant systems. Although time-consuming, because of the specific requests of AO observations of extended objects and the needs for AO activation loops, observing a handful of well-chosen targets with one of these massive telescopes could allow one to discriminate between different cosmological models, independently from SNIa.

Beyond improved telescopes, SBF observations also benefit from improved numerical stellar population studies. Accurate models of stellar populations are essential for interpreting SBF measurements, reducing systematic uncertainties and deriving reliable *k*-corrections which cannot be ignored beyond $\sim$ 150 Mpc. Additionally, the application of SBF to blue, low-mass galaxies requires the calibration of $\overline{M}$ across a broader range of stellar populations and environments. Stellar population modeling will offer a reference to test and prove the reliability of the SBF method over a wide interval of population properties.

Theoretical efforts over the past 20 years have focused on incorporating stars in peculiar evolutionary stages, such as thermally pulsing AGB stars and hot HB stars in old-intermediate populations (e.g., see Ref. [185,195]). These efforts have also included the impact of α-elements and He-abundance enhancements. Advancements in this area will benefit from the insights gained by applying theories of late stellar evolution — dominated by poorly understood physics such as mass loss processes — to the observations in mid-infrared instruments like MIRI on the JWST. This will result in more refined stellar population models for distance estimates and a better understanding of these crucial stages of stellar evolution.

Future SBF measurements can also benefit from the adoption of ML techniques. ML methods require training on large samples that are not yet available, but when they are, ML algorithms can optimize the measurement of SBF, which is currently slow and heavily reliant on human

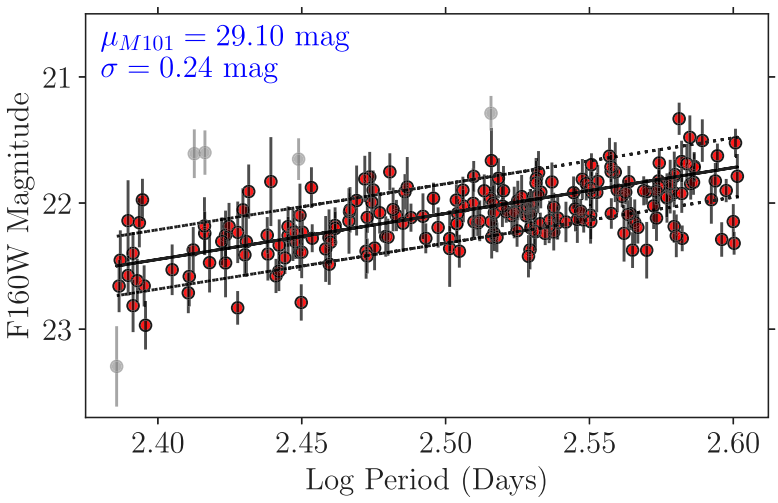

Fig. 17. Period–Luminosity Relation for short-period, presumed O-rich Miras in the SNIa host galaxy M101 from Ref. [20].

intervention. ML can further identify patterns and correlations in large datasets, improving the efficiency of SBF measurements and reducing measurement time. Sufficient training datasets will be available after the first years of Euclid or LSST public data releases.

In conclusion, the SBF method currently stands as a robust and versatile tool in extragalactic distance measurements. To date, the method's range of usefulness allows it to be adopted for tests on the H_0 tension, providing results that agree with the late-time/direct Hubble constant estimates. With advancements in telescope technology, data processing, and collaborative efforts, the SBF method is well-positioned to make significant contributions to resolving cosmic tensions, possibly even beyond the H_0 parameter, and enhancing our understanding of the Universe. By implementing the proposed future developments, the astronomical community can further refine the SBF technique and extend its applicability to new frontiers in extragalactic astronomy.

2.1.6. *Mira variables*

Coordinator: Caroline Huang

Contributors: Antonio Capodagli, Lucas Macri, and Massimo Marengo

Mira variables are fundamental-mode, thermally-pulsing AGB stars with periods ranging from $\sim 100-1000$ days or longer. They fall into a broader category of variables known as Long-Period Variables (LPVs), which includes semi-regular variables, and OGLE small-amplitude RGB stars, which are overtone or irregular pulsators. The pulsation of Miras is likely driven by a κ-mechanism similar to that found in Cepheids. As highly-evolved stars, they contribute to the chemical enrichment of the ISM through stellar mass loss, have low effective temperatures ($T_{\rm eff} < 3500$ K) with spectral intensity peaking between 1–2 μ m, and are often among the brightest stars in an intermediate-to-old population ($L \sim 10^4 L_\odot$). They are also ubiquitous as nearly all stars ($0.8 M_\odot < M < 8 M_\odot$) will experience a Mira phase in evolution.

Like other AGB stars, they may be classified into two main spectral types based on their photospheric carbon-to-oxygen ratio (C/O ratio). The exact boundaries are somewhat fluid, but typical C/O values are: C/O ratio $\gtrsim 1$ are classified as C-rich (C-type), C/O ratio $\lesssim 0.5$ are O-rich (M-type), and C/O ratio $\sim 0.5-1.0$ are intermediate, or S-type. While the identification of carbonaceous or silicate molecular features in stellar spectra is the gold standard for classification, in practice, spectra are difficult or expensive to obtain, and colors, or color-color diagrams, are typically used as a proxy for spectral type.

The first Period–Luminosity Relations (PLRs) derived for Miras used bolometric magnitudes [196,197]. Over the past several decades, Miras have been observed in bands ranging from optical to far-infrared have been used to measure distances to many Local Group galaxies (see reviews by Refs. [198–200] and references therein) and map the structure of the MW [201]. Studies of nearby dwarf galaxies have suggested that metallicity does not appear to have an observable effect on the pulsational properties of these stars [202,203], although possible metallicity effects have been suggested by theoretical models. Recently, nonlinear stellar pulsational models have shown significant improvements in matching theoretical predictions of long-period variable PLRs with observations [204] which may shed light on this apparent discrepancy in the future.

2.1.6.1. Application. For the purposes of this review, we will focus on the O-rich Miras, which are more commonly used as distance indicators because they follow PLRs with lower scatter in near-infrared wavelengths (~ 0.12 mag) compared to their C-rich counterparts. In order to create the PLRs, time-series observations — often with either an uneven, power-law spacing or monthly sampling — are also required in order to determine periods.

The first rung of Mira distance ladder uses *Hubble* Space Telescope observations of Miras in the water megamaser host galaxy NGC 4258 and ground-based near-infrared observations of Miras in the LMC [205,206] as "anchor" galaxies to obtain an absolute magnitude calibration [19]. In order to tie the ground-based observations to the HST photometric system, Ref. [207] used a photometric transformation derived from O-rich Mira spectra. Unlike the Cepheid distance ladder, there is currently no precise, parallax-based absolute magnitude calibration. This is due to the fact that Miras (as well as AGB stars in general, and other evolved stars such as red supergiants) exist at the intersection of many difficulties for *Gaia* — they are highly luminous, red, have angular sizes larger than their parallaxes, and are known to have photocenter variations, all of which can contribute to underestimated uncertainties and bias in the inversion of their parallaxes [208–211].

The second rung of the distance ladder is currently built on observations of Miras in two nearby Type Ia Supernova host galaxies — NGC 1559 and M101 (hosts of SN 2005df and SN 2011fe respectively, with PL relation for M101 shown in Fig. 17) [19,20]. Thus far, these are the only two SNIa host galaxies with Mira-based distances. The statistical uncertainty in the SNIa calibration is also the dominant source of error in the Mira-H_0 measurement (even after standardization, the uncertainty in SNIa peak magnitude is $\sim$ 0.1 mag). Thus the greatest reduction in uncertainty will be obtained from obtaining more observations of Miras in SNIa host galaxies.

2.1.6.2. Implications for hubble constant and hubble constant tension. The current most precise Mira-based measurement yields $H_0 = 72.37 \pm 2.97\,{\rm km\,s^{-1}Mpc^{-1}}$ ($\sim 4\%$ total uncertainty, including both statistical and systematic components) [20]. While it is not yet as precise as more established distance indicators, as an independent measurement, this

result does support the hypothesis that the local measurement of H_0 is greater than the early-Universe measurement with $\sim$ 95% confidence. In addition, it provides an important cross-check to distances made with other more established distance indicators such as Cepheids and TRGB.

2.1.6.3. Prospects. The next decade should be particularly exciting for using Miras and other LPVs as distance indicators. In the NIR/MIR bands accessible with HST, JWST and *Roman*, Miras have PLRs with smaller scatter than in the optical, nearly-sinusoidal light curves, and are relatively easy to identify as some of the brightest stars in resolved stellar populations. The Vera C. Rubin Observatory's LSST is expected to have sufficient depth and number of epochs to enable the detection of Miras at optical wavelengths (*griz*) [212] in galaxies out to $D \sim$ 10 Mpc [213].

2.1.7. Type Ia supernovae

Coordinator: Maria Vincenzi

Contributors: Jenny Wagner, Lluís Galbany, Luca Izzo, M. Pilar Ruiz Lapuente, and Sanjay Mandal

SNIa are thermonuclear explosions of carbon oxygen white dwarfs in close binary systems. Their peak brightness after various empirical corrections is highly homogeneous (r.m.s. <0.15 mag in B-band), hence their usage in cosmology as standardizable candles. SNIa have played and still play a crucial role in measurements of the Hubble constant, and they are typically used in two out of three rungs in the typical distance ladder. In the second rung, their luminosities are calibrated with stellar distance indicators, e.g., Cepheids or TRGB or JAGB, in the same galaxy. In the third rung, their brightness values calibrate the Hubble–Lemaître relation into what is now deemed the 'Hubble flow' (~100 to 600 Mpc, or $z < 0.15$), where the cosmological expansion dominates over the peculiar motions of galaxies. Ideally, one could remove the intermediate step (second rung), and go straight from geometric calibration to SN. Unfortunately, the rate of SN in the local Universe is not nearly frequent enough to provide multiple SN in the few galaxies used for geometric anchors (the MW, the LMC, or the mega-maser NGC 4258). Even with Cepheids/TRGB/JAGB as a go-between, the low rate of SN in the nearby Universe (roughly one per galaxy per 100 years) is the limiting component of the precision of H_0 measurements, for instance Ref. [34] utilizes every SNIa that pass cosmological quality requirements and Cepheid suitability within 40 Mpc. The most comprehensive three-rung ladder H_0 measurements using Cepheids are shown in Fig. 8.

2.1.7.1. SN Ia standardization and derivation of H_0. We review here the formalism for deriving the Hubble constant with SNIa in the local distance ladder, as presented by Ref. [34]. Using a set of Cepheids or TRGB distance moduli (μ_0) calibrated with geometric measurements such as parallax or megamasers (first rung in the distance ladder) and comparing these distances to brightnesses m_X of SNIa exploding in the same galaxies, we can estimate the single offset M_B, which describes the absolute magnitude of an SNIa (second rung). Following the SALT modeling framework [214,215],[4] SNIa standardized brightness, m_X,[5] is generally measured with the Tripp formula [218] such that:

$$m_X = m_B + \alpha x_1 - \beta c - \delta_{Bias} + \delta_{Host}\,, \tag{2.1}$$

where m_B, x_1 and c are all independent properties of each light curve derived using the SALT light-curve model, α and β are correlation coefficients that help standardize the brightness, δ_{Bias} is a correction due to selection effects and other biases as predicted by simulations, and δ_{Host} is a final correction due to residual correlations with host galaxy properties.

For a SNIa in the ith Cepheid host,

$$m_{X,i} = \mu_{0,i} + M_B\,, \tag{2.2}$$

where M_B is the fiducial SNIa absolute magnitude (assumed to be the same across the whole sample), and $\mu_{0,i}$ is the distance modulus derived from Cepheid measurements for the ith galaxy. The ladder is completed with a set of SNIa that measure the expansion rate quantified as the intercept, a_B, of the distance (or magnitude)–redshift relation. For an arbitrary expansion history and for $z > 0$ as

$$a_B = \log cz \left\{ 1 + \frac{1}{2}\left[1 - q_0\right] z - \frac{1}{6}\left[1 - q_0 - 3q_0^2 + j_0\right] z^2 + \mathcal{O}(z^3) \right\} - 0.2 m_X^{HF}\,, \tag{2.3}$$

measured from a set of SNIa (z, m_X^{HF}) in the Hubble flow, where z is the redshift due to expansion, q_0 is the deceleration parameter, and j_0 is the jerk parameter. Typically, for ΛCDM, j_0 is set to 1. The determination of H_0 follows from

$$\log H_0 = 0.2 M_B + a_B + 5\,. \tag{2.4}$$

Covariances between rungs are taken into account following the approach in Refs. [219,220]. Finally, q_0 (and j_0) can only be constrained from SNIa data, without the requirement of any additional information.

2.1.7.2. Systematics on the path to H_0 with SN Ia. H_0 measurements using SNIa are affected by various sources of systematic uncertainties.

Ref. [33] gives a comprehensive overview of many of these systematics and how they may affect measurements of H_0. In Fig. 18, adapted from Ref. [33], we show the impact on H_0 of applying 1σ shift of each systematic. We group the systematics into various categories: Redshifts, SN Physics, Selection, Calibration, and MW Dust. Before delving into each category of systematics in detail, it is crucial to understand which systematics H_0 is most sensitive to, and conversely, which have minimal impact due to being mitigated. The distance ladder is structured so that the same probe is used in two of its three rungs (e.g., Cepheids in the first and second rungs, and SNIa in the second and third rungs). If a systematic error disproportionately affects SNIa in the second and third rungs, or introduces significant differences in the SNIa populations between these rungs, it will have a substantial impact on H_0. Conversely, if a systematic introduces a consistent offset that affects all SNIa uniformly, the impact of that systematic will be negligible due to the cancellation effect inherent in this formalism. In other words, consistent offsets will cancel out, mitigating the effect of the systematic error.

Calibration: Since many of the same surveys measure SN in both the second and third rungs of the distance ladder, the effects of calibration systematics on H_0 is mitigated by the effect discussed above. As illustrated in Ref. [223] in the context of the latest SH0ES analysis, per-survey "gray" calibration offsets affect the uncertainty by $0.2\,\mathrm{km\,s^{-1}Mpc^{-1}}$at most. However, when different surveys are used for the second and third rungs, as shown in Ref. [15,225], this cancellation does not occur and the effects of calibration can be larger.

Redshifts: H_0 measurements are more sensitive to systematics related to redshift since redshift information is used only in the third rung of the distance ladder, with no systematic mitigation. Ref. [222] explore various bulk flow models in the nearby Universe, finding that changes in H_0 could be up to $0.2\,\mathrm{km\,s^{-1}Mpc^{-1}}$. They also note that including or excluding peculiar velocity corrections could lead to $\Delta H_0 \sim 0.5$. Additionally, Refs. [230,231] find redshift measurement biases causing uncertainties around $0.1\,\mathrm{km\,s^{-1}Mpc^{-1}}$.

SN Physics and Selection: SN intrinsic astrophysics and the role of SN dust remain one of the most poorly understood aspects of SNIa cosmology and can affect H_0 measurements [221,232]. Most analyses have found that these effects have a small impact on H_0 because the differences between SN sub-populations selected in the second and

[4] The SALT2 and SALT3 frameworks have been used in all most recent cosmological analyses. Other frameworks are also available, i.e., SnooPy [216], BayeSN [217].

[5] We call the standardized brightness m_X instead of m_B as in Ref. [34] to be clear that the brightness is standardized.

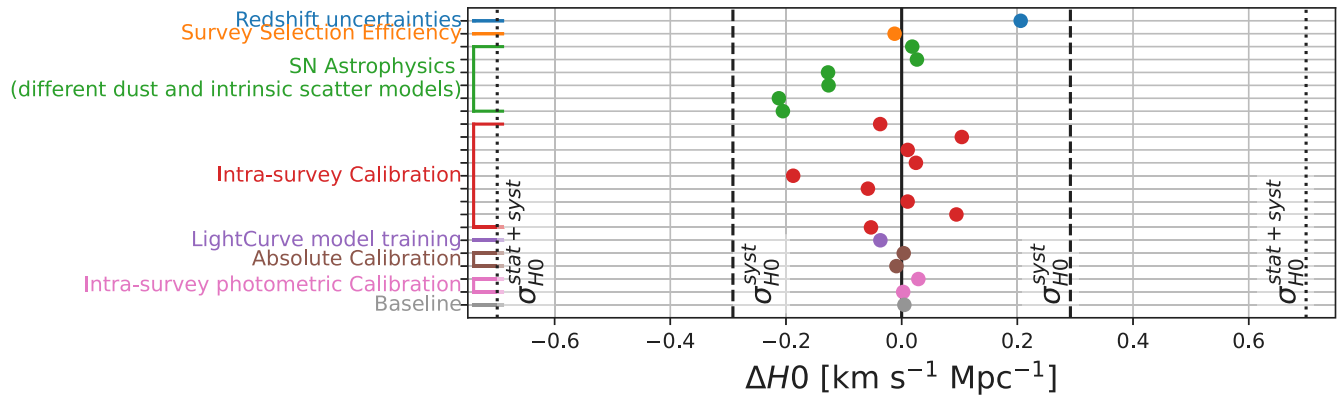

Fig. 18. Ref. [33], the impact on recovery of H_0 of the various systematic uncertainties tabulated. The units of these measurements are $\mathrm{km\,s^{-1}Mpc^{-1}}$. The dashed lines are given at ΔH_0 of 0.7, which is the entire contribution of the uncertainty in Ref. [34] from SN measurements. We labeled the different categories of systematic uncertainties.
Source: Adapted from

Table 1
A summary of the various cross-checks and systematics on the supernova component of the distance ladder. If two uncertainties are given, the first one is the statistical uncertainty and the second one is the systematic uncertainty.

Reference	Notes on the specific systematics check implemented	Result ($\mathrm{km\,s^{-1}Mpc^{-1}}$)
Optical SNIa:		
[221]	Uses spectral feature twinning process to improve standardization; checks dust modeling, intrinsic scatter modeling;	73.01 ± 0.92
[222]	Checks different models of peculiar velocities/bulk flows	$\sigma_{H_0} < 0.2$
[223]	Checks SNIa Calibration by allowing individual SN survey offsets	$\sigma_{H_0} < 0.2$
[224]	Checks impact of mass step, global vs. local correlations	$\sigma_{H_0} < 0.15$
[225]	Checks light-curve fitting method; also does NIR fits	73 ± 2
[194]	Uses 4-rung distance ladder, checks SNIa host demographic systematic	$74.6 \pm 0.9 \pm 2.7$
[226]	Uses ZTF data alone, check on SNIa calibration	76.94 ± 6.4
NIR SNIa:		
[227]	Uses literature NIR SN (restframe J) and peak fitting	72.8 ± 2.8
[36]	Uses literature NIR SN (restframe J and H band)	$72.3 \pm 1.4 \pm 1.4$
[228]	Uses RAISIN\+literature NIR SN (restframe Y band) and SNooPy fitting, check on dust	75.9 ± 2.2
[229]	Uses literature NIR SN and BayesN fitting	$74.82 \pm 0.97 \pm 0.84$

third rung are not expected to be significantly different. For example, Ref. [233] showed evidence for a correlation between standardized brightness and the age of the host galaxy (quantified estimating the specific star-formation at the SN location). In earlier measurements like Ref. [234], the third rung of SN had no galaxy-based selection applied. Only the second rung had this selection, tied to Cepheid discovery, which favored star-forming host galaxies. This would potentially lead to a bias in the recovery of H_0. The size of the bias would depend on the relative differential fraction of host-galaxy demographics between the second and third rung multiplied by the size of the correlation. Subsequent analyses [224] showed that this effect would likely be insufficient to explain the Hubble tension. Still, in the most recent SH0ES analysis [34], the selection of SN in the third rung of the distance ladder was done to be as similar as possible as the second rung. Only SN found in star-forming galaxies are selected, which thereby removed the sensitivity to this systematic. Yet, the impact of this change was less than the statistical uncertainty from the supernova component of the distance ladder. Similarly, significant differences in dust extinction and/or color-related effects between SN in the second and third rung could potentially bias H_0 measurements [235]. SN dust extinction and color-dependent corrections are encapsulated in the nuisance parameter β (see Eq. (2.1)). As a cross-check, the β parameter was fitted separately in SN used in the second and third rung, and it was found to be consistent [33]. This test, together with various NIR SN H_0 measurements, see Table 1 [36,227–229], suggests that dust or color-dependent effects are not expected to significantly bias H_0, or to be a significantly underestimated systematic in current H_0 measurements.

Other systematics: Additional systematic tests, such as changing the light-curve fitter or adding spectroscopic information, have shown consistent results, within $\approx 0.3\,\mathrm{km\,s^{-1}Mpc^{-1}}$, e.g., see Ref. [221,225]. Even when isolating data to a single survey, as in Ref. [229], the results remain consistent, though with larger uncertainties due to the smaller sample size.

2.1.7.3. Variants on the path to H_0 with Supernovae Ia. Some of the main cross-checks on the SNIa used for these analyses is varying the wavelength regime in which light curves are measured (i.e., optical to NIR) or the dataset used (i.e., the survey used to measure the light curves). As H_0 constraints are limited by the number of SN found within 40 Mpc, there is considerable overlap in the data between these various studies. The most popular path to check and improve the distance ladder with SNIa is by measuring NIR light curves. We list these papers in Table 1. Overall, even though the rest-frame band in which light curves are measured varies between these analyses, and the fitting method varies between these methods, there is generally very good agreement in the recovered values of H_0. One challenge multiple of these studies have found (e.g., [227,228]) is larger calibration offsets between samples than those found for optical studies. A benefit of this type of study is the possibility of improved precision of distance measurements from NIR data, but the quality of older light curves has not typically been good enough to evaluate this possibility.

An additional path is creating a "4-rung distance ladder", as done in Ref. [194]. SNIa used in the SH0ES distance ladder are those found in late-type galaxies. To avoid this specific sub-sample, one can add another rung in the distance ladder from SBF between TRGB/Cepheids and SN. The analysis of Ref. [194] improves on that of Ref. [193] because the latter follows a similar method, but uses an inhomogeneous set of SBF measurements. The inhomogeneous set significantly increases the scatter of the tie between SBF and SN measurements and appears to bias H_0 to lower values. Ref. [194] find a value of $H_0 = 74.6 \pm 2.8\,\mathrm{km\,s^{-1}Mpc^{-1}}$, in good agreement with the SH0ES value.

2.1.7.4. Inverse distance ladder to H_0 with supernova. The same set of SNIa used in the SH0ES distance ladder can also serve as uncalibrated relative distance indicators to constrain H_0 when combined with other probes like BAO. BAO constrain the expansion history $H(z)$ and extrapolate H_0. But this approach assumes the sound horizon from CMB constraints and is model-dependent, relying on ΛCDM to infer $H(z=0)$ from BAO data at $z \sim 0.5$. However, SNIa can address the latter issue. Instead of calibrating SNIa to the distance ladder, they can be calibrated to the BAO distance scale at typical BAO redshifts ($z \sim 0.5$), allowing SNIa to constrain the expansion history at later times ($z < 0.1$) without assuming ΛCDM. Studies such as Refs. [236–238] using this technique found $H_0 = 68.57 \pm 0.9\,\mathrm{km\,s^{-1}Mpc^{-1}}$, consistent with CMB under ΛCDM. Since BAOs obtain the physical scale from the sound speed in the early Universe, these low H_0 values have prompted discussions about the impact of the sound horizon value.

2.1.7.5. Improving measurements of H_0 in the future. Improving constraints on H_0 using SNIa and the distance ladder is challenging. The limiting factor in the past decade has been the fact that HST can discover Cepheids/TRGB within a radius of 40 Mpc, and there is one to three SNIa per year exploding within this volume. However, new telescopes like the JWST (or future instruments like the Nancy Grace Roman Space Telescope and the ELT) are already showing impressive improvements (both in quality and depth) in Cepheids, TRGB and JAGB measurements[6] as shown by Refs. [26,174], with exciting hints of shifts to lower H_0 values presented by Ref. [26], even though the statistics is still too low to draw firm conclusions.

The other path toward improving the constraint from SNIa is to improve the precision of the measurements. This is the path followed by papers like Refs. [221,239] which tried using spectral features to improve the standardization, or the large number of papers that measure SNIa in the NIR as better standard candles. The main challenge is that these new standardization approaches depend on the amount of data available for its application in past literature measurements. New types of measurements can be made for nearby SN in the future, but we cannot re-measure past SNIa.

2.1.8. J-regions of the asymptotic giant branch methods

Coordinator: Siyang Li

Contributors: Adam Riess, Bartek Zgirski, Caroline Huang, Dan Scolnic, Gagandeep S. Anand, Greg Sloan, Louise Breuval, Richard I. Anderson, and Stefano Casertano

The JAGB refers to a group of stars in a NIR color magnitude diagram (see Fig. 19) that contains thermally pulsating carbon-rich AGB stars with photospheric C/O greater than 1. The potential for using carbon stars (CS) as distance indicators was first realized in the 1980s [240–244], and the method was later revived in the 2000s [129,177,245–248]. These pioneering studies, among others, have proposed that the mean, median, mode, or model fit of a near-infrared J-region LF can be used as a standard candle to measure extragalactic distances. The basis for doing so originates from the expectation that only oxygen-rich AGB stars that have masses falling within a relatively narrow range can evolve into carbon-rich AGB stars, constrained by hot bottom burning and the efficiency of the 3rd dredge-up events.

2.1.8.1. Application. The JAGB method relies on a measurement of the CS infrared magnitude distribution in a color range between weakly pulsating CS that produce little dust and strongly pulsating CS (i.e., Mira variables) that produce significant amounts of amorphous carbon dust. The JAGB is typically measured in the "outer disk" of a galaxy where the stellar population is young enough to contain a substantial amount of carbon AGB stars and far enough from the center to minimize the effects of crowding and internal reddening [249]. The region is also typically chosen to be close enough to avoid sparser fields which increases the statistical uncertainty. In addition, the red background of galaxies can be similar to that of CS and contaminate the CS sample [248]. Consistent selection of fields is also important in maintaining consistent stellar populations.

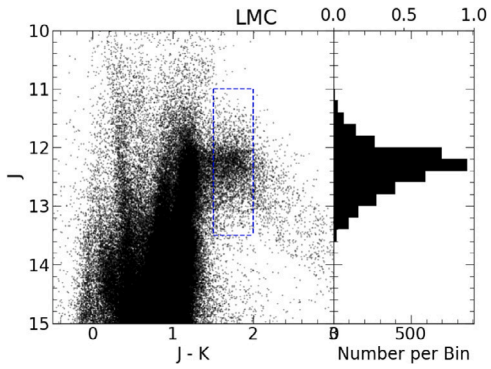

Fig. 19. J vs. J - K color-magnitude diagram of stars in the LMC using the sample from Ref. [250].

Several methods have been proposed to measure the JAGB reference magnitude in the outer disk; these are typically designed to measure some variation of the peak of the J-region LF. For instance, Refs. [129,247] use the mean and median, Ref. [177] smooth a binned J-region LF and take the mode, while Refs. [246,251] introduce maximum likelihood and binned versions of medians and calibrate their JAGB measurements using the skew parameter in a Lorentzian fit. Ref. [248] fit a Gaussian+Quadratic model to the LF. There is an important need for standardization of the technique to ensure accuracy.

2.1.8.2. Prospects. The JAGB method has the potential to independently support or refute local measurements of the Hubble constant from the second rung of the distance ladder. Recent studies have found JAGB-based Hubble constants of 74.7 ± 2.1 (stat) ± 2.3 (sys) $\mathrm{km\,s^{-1}Mpc^{-1}}$, with a full range spanning 71 to 78 $\mathrm{km\,s^{-1}Mpc^{-1}}$ depending on the measurement method used [18], and 67.96 ± 1.85 (stat) ± 1.90 (sys) $\mathrm{km\,s^{-1}Mpc^{-1}}$ [174,252], noting that the lower value here originates from galaxy subsample selection, see Ref. [26]. However, it is important to be aware that this method is still much less mature than other standard candles, such as Cepheids. For this method to be robust, several aspects will need to be better understood, such as the empirical effects of metallicity, molecular atmospheric diversity effects on photometry, and the shift of CS from weak to strong pulsations in the context of population diversity.

In addition, past literature has found evidence of non-uniform asymmetry in the J-region LF [79,246,251,253]. This can produce methodological variations (i.e., the mean will be different from the median, mode, and model fit). Non-uniformity of the asymmetry can also result in a mismatch in the degree of methodological variations across the distance ladder, thus increasing uncertainties of the method. It will be important to standardize this effect.

The JAGB method introduces observational flexibility for measuring H_0. JAGB only requires a single epoch while Cepheids need multiple epochs to measure their periods and mean magnitudes. CS are ubiquitous in most galaxies, unlike Cepheids which are generally observed in face-on spiral galaxies. In the near-infrared, JAGB stars are as bright as long-period Cepheids, making them competitive for reaching large distances. On the other hand, the metallicity dependence of Cepheids is very well calibrated [58], which is not yet the case for CS. The JAGB feature is also brighter than TRGB. However, JAGB stars are an intermediate-age (300 Myr - 1 Gyr [129]) population, and are

[6] Even a 25% increase in the Cepheid distance would allow a doubling in the number of usable SNIa in the second rung of the distance ladder (the volume of discovered SN will increase with distance cubed).

therefore not as ubiquitous as TRGB stars, which populate essentially every galaxy.

The JAGB is primarily measured in the NIR, typically in the J- and H-bands (or space-based equivalents: HST *F110W* [249], JWST, *F115W*, [17] & *F150W* [18]). It is important to understand whether either of these bands necessarily offers more consistency in color dependence over the other and whether either is sloped as a function of color. Multiple studies have found evidence of asymmetric LF and non-flat color dependence in both the J- and H- bands [79,246,251,253].

Increasing the SNIa sample size decreases fluctuations in H0 arising from cosmic variance and facilitates closer reversion to the mean (see Ref. [26]). Recently, Ref. [254] augmented the JAGB sample used to measure H0 by combining all available JAGB distances to SNIa host galaxies in the literature, as well as measuring new distances to galaxies from JWST Cycles 1 & 2 for a total of 15 galaxies hosting 18 SNIa. As in Ref. [18], they find methodical variations consequent of non-uniform asymmetry in the J-region LF; taking the middle measurement variant (as described in Ref. [18]) yields $H_0 = 73.3 \pm 1.4(\mathrm{stat}) \pm 2.0(\mathrm{sys})\,\mathrm{km\,s^{-1}Mpc^{-1}}$.

A powerful way to characterize, and potentially better standardize, variations in the JAGB method is to conduct a field-to-field comparison of the JAGB. This approach has been implemented for the TRGB by the Comparative Analysis for TRGBs (CATs) team [122,125,255]. They compared multiple fields in a given galaxy and developed a standardization procedure via a contrast ratio. Future missions, such as Roman, and more observations with JWST can obtain a larger field coverage that can be used to measure the JAGB and make a similar analysis possible.

2.1.9. The Hubble constant from Type II supernovae

Coordinator: Lluís Galbany

Contributors: Anil Kumar Yadav, Anto Idicherian Lonappan, David Benisty, Géza Csörnyei, Ismailov Nariman Zeynalabdi, and Vladas Vansevičius

With the currently ongoing tension between local and distant measurements of the Hubble constant, it is crucial to test and employ independent methods that adhere to a separate set of systematic uncertainties. SNII offer such independent routes with sufficient accuracy. SNII are the explosions of red supergiant stars, with multiple direct progenitor detections to date (e.g., see Refs. [256,257]). Given the well constrained progenitor type along with their relatively simple composition (with the red supergiant retaining its hydrogen envelope and being made up mostly of H and He before the explosion) and the recent advancements in the understanding of the explosion mechanism, multiple theoretically well-founded distance estimation techniques exist for SNII. The spectra of SNII are characterized by the presence of broad P-Cygni profiles, which allow constraining the photospheric properties. To date, three techniques have been used to measure the Hubble constant: the expanding photosphere method (EPM, [258]), the spectral modeling based techniques (either the spectral expanding atmosphere method SEAM [259] or the tailored EPM [260]) and the standardizable candle method (SCM, [261]). Of the three, SCM is an empirical technique, which employs the relation present between the luminosity and the expansion velocity of the supernova. On the other hand, EPM and SEAM both aim to constrain the physical parameters and the luminosity based on the spectra directly, providing a single step measurement tool. Both Refs. [23,262] demonstrated that SCM and EPM distance measurements up to redshifts of $z \approx 0.34$ are feasible, providing important alternative paths for cosmology, as depicted in Fig. 20.

2.1.9.1. Methods and approaches to measure H_0 using SNe II. The use of EPM for SNII, which essentially consists of estimating the size of the photosphere, then comparing it to the observed flux by assuming a blackbody spectrum, was first demonstrated by Ref. [258]. This initial exploration yielded $H_0 = 65 \pm 15\,\mathrm{km\,s^{-1}Mpc^{-1}}$. However, it was highlighted later by Ref. [263], SNII radiate with a much smaller surface flux than a blackbody of the same color temperature (the photosphere flux appears diluted), owing to the scattering dominated atmosphere of SNII and the fact that the thermalization layer from which the blackbody radiation is generated is deeper than the photosphere. To take this into account, the EPM was refined by incorporating a multiplicative ξ dilution factor, which relates the position of the thermalization layer to the photosphere, which was shown to depend largely only on the color temperature (see Refs. [264–266]). Systematic discrepancies between the different sets of dilution factors can explain differences on the scale of 20% in the inferred distance [267,268]. The EPM is to date one of the most frequently used distance estimation technique for SNII, with the latest H_0 estimate being $72.9^{+5.7}_{-4.3}\,\mathrm{km\,s^{-1}Mpc^{-1}}$ based on 12 SNII following Ref. [269], using the dilution factors from Ref. [265]. To rule out the possible systematic effects introduced by dilution factors, one has to carry out radiative transfer based spectral modeling of observations, which yields self-consistent results for the physical parameters.

This is achieved in both the customized EPM and in the SEAM, which incorporate radiative transfer modeling of spectra into the distance estimation process. In both techniques, the modeling of the complete spectral time series is carried out, which yields the relevant physical parameters at each epoch in a self-consistent way, avoiding the use of dilution factors. However, estimating a single radiative transfer model takes hours to days, hence estimating a distance this way is a time-consuming process. Due to this, until recent years, this method was only used for a handful of SN [259,260,270]. Recent advances in ML allowed for the faster estimation of radiative transfer models, hence significantly speeding up this modeling process, as described in Ref. [271]. This method was shown to provide internally consistent results [24] at a competitive precision [146] and yielded a Hubble constant of $H_0 = 74.9^{+1.9}_{-1.9}\,\mathrm{km\,s^{-1}Mpc^{-1}}$ based on the analysis of literature SN [272]. However, this method is currently largely limited to local redshifts: to date only a few SNII were observed far enough out into the Hubble flow in sufficient detail for the application of either tailored EPM or SEAM.

To date, the most widely used method for estimating H_0 using SNII is the SCM [23,261,273]. The method is based on an empirically found correlation between the luminosity and the photospheric expansion velocity of the objects [274,275], and in terms of philosophy is similar to the method employed for SNIa (e.g., see Ref. [34]). In contrast to the Ia's, however, to standardize SNII, spectroscopic information is required in the form of line velocity measurements. Over the years, the standardization has been further extended with color term accounting for the varying level of extinction present for different SN [276]. Recently, Ref. [23] applied this method with nine calibrator SN to estimate the Hubble constant by using SNII as the final rung of the distance ladder, obtaining $H_0 = 75.4^{+3.8}_{-3.7}\,\mathrm{km\,s^{-1}Mpc^{-1}}$. The method is still under further development, with the aim of increasing the currently available set of calibrators with high precision cases, and also with attempts to investigate the need for additional standardization terms based on spectroscopic information.

These results show that SNII indeed provides important and independent distance measures that can serve as the tools for a sanity check for multiple rungs of the distance ladder. With the steady increase in the number of objects with detailed observations, the coming years will see multiple SNII-based Hubble constant estimates with competitive precision, which will allow for an alternative look at the Hubble tension.

2.1.10. HII galaxy distance indicators

Coordinator: Ricardo Chávez

Contributors: Ana Luisa González Morán, David Fernández-Arenas, David Valls-Gabaud, Elena Terlevich, Fabio Bresolin, Iryna Vavilova,

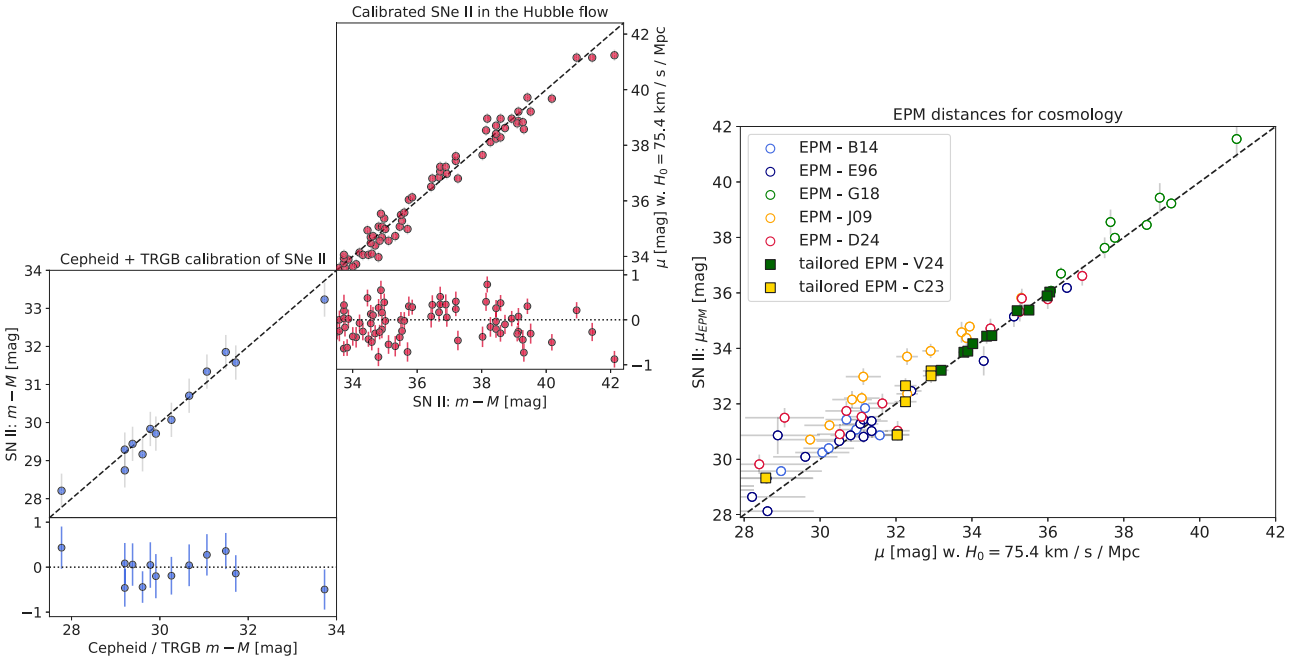

Fig. 20. SNII for Hubble parameter estimation. **Left:** The distance ladder formalism applied on SNII, as presented by Ref. [23]. The bottom panels with the blue dots depict the intermediate rung of the distance ladder, where the SNII brightnesses are calibrated through Cepheids and TRGB, along with the residuals after the standardization. The top panels with the red dots show the final rung of the distance ladder, where this standardization is applied on SNII in the Hubble flow which allow for a Hubble constant estimation, while the residuals are shown on the panel below. **Right:** SNII Hubble diagram using EPM distances, as updated from Ref. [277]. EPM distances do not require external calibration, hence they provide a single step measurement of H_0. The empty circles denote the EPM distances that employ dilution factors, while the filled squares mark the tailored EPM estimates that make use of radiative transfer modeling. The references for the distance estimates are as follows: B14 – [278], E96 – [264], G18 – [262], J09 – [267], D24 – [269], V24 – [272] and C23 – [24].

Ismailov Nariman Zeynalabdi, Manolis Plionis, Roberto Terlevich, Rodrigo Sandoval-Orozco, Spyros Basilakos, and Vladas Vansevičius

HII galaxies (HIIGs) are characterized by intense, compact episodes of star formation predominantly occurring within dwarf irregular galaxies, significantly enhancing their luminosity. These galaxies are spectroscopically identified based on the prominent equivalent width of their Balmer emission lines, specifically $EW(H\beta) > 50$ Å, which indicates their young age (less than 5 Myr). Similarly, Giant Extragalactic HII Regions (GEHRs) exhibit vigorous star formation but are typically found in the outer disks of late-type galaxies. The rest-frame optical spectra of both HIIGs and GEHRs display pronounced emission lines, indicative of gas ionization by massive Young Stellar Clusters (YSC) or Super Star Clusters (SSC), leading to similar spectral features [279–283].

Numerous studies have confirmed a consistent correlation, found by Ref. [281], between the luminosity of Balmer lines, such as $L(H\beta)$, and the ionized gas velocity dispersion, σ, measured through these emission lines, in both HIIGs and GEHRs. This relationship, known as the $L-\sigma$ relation [283–285], is recognized as a potent cosmological distance indicator [286–289], where GEHRs and nearby HIIGs are used as the "anchor" sample because their distances can be independently estimated from Cepheid variables or TRGB measurements. As a result, the $L-\sigma$ relation provides an exceptional method for utilizing this distance metric to investigate the Hubble flow over an extensive range of redshifts (z).

The characteristic strong emission lines within the rest-frame optical spectra of GEHRs and HIIGs render them effective tools for exploring nascent star formation at high redshifts. Using instruments such as NIRSpec [290] on board the JWST [291], it is possible to study these regions up to $z \sim 6.5$ through the Hα emission line, or even up to $z \sim 9$ using the Hβ and [OIII]$\lambda\lambda 4959, 5007$ Å emission lines. This capability enables the observation of luminous HIIGs that date back to the Epoch of Reionization (EoR) as shown in Fig. 21.

Using a dataset of 231 GEHRs and HIIGs, some observed with NIRSpec on the JWST up to $z \sim 7.5$, a study by Ref. [289] employs the MultiNest Bayesian inference algorithm [292–294] to derive constraints for various cosmological models. They used uniform, non-informative priors across all parameters for unbiased estimations. The derived constraints are detailed in Table 2, showing marginalized best-fit values and 1σ uncertainties for each parameter, with some parameters held constant during the analysis. The study explores a generalized parameter space $\theta = \{\alpha, \beta, h, \Omega_{\rm m}, w_0, w_a\}$, where $\theta_n = \{\alpha, \beta\}$ represents nuisance parameters of the $L-\sigma$ relation for GEHRs and HIIGs with α as the intercept and β as the slope. For the flat ΛCDM model, $\theta_c = \{h, \Omega_{\rm m}, -1, 0\}$ sets h as the reduced Hubble constant and $\Omega_{\rm m}$ as the total matter density, fixing the first two DE equation of state (DE EoS) parameters at $w_0 = -1$ and $w_a = 0$, corresponding to a cosmological constant (Λ). Adjusting w_0 allows for models with evolving DE EoS, akin to quintessence [295,296], while including w_a aligns with the CPL model [297–299].

The constraints derived on cosmological parameters, specifically $\{h, \Omega_{\rm m}, w_0\} = \{0.731 \pm 0.039, 0.302^{+0.12}_{-0.069}, -1.01^{+0.52}_{-0.29}\}$ (stat) from GHIIR and HIIG data, align closely with recent Pantheon+ results from 1550 SNIa, which produces $\{h, \Omega_{\rm m}, w_0\} = \{0.735 \pm 0.011, 0.334 \pm 0.018, -0.90 \pm 0.14\}$ [33]. This agreement emphasizes the validity and importance of HIIGs as distance indicators within the context of current cosmological studies.

The enduring validity of the $L-\sigma$ relation at high redshifts ($z > 3$), reaching into the EoR, suggests remarkable uniformity in HIIGs properties over vast cosmic timescales. This not only confirms the reliability of the $L-\sigma$ relation as a cosmological tool but also illuminates the fundamental processes underlying the formation and evolution of early Universe galaxies.

In our efforts to improve the accuracy of cosmological parameters using HIIGs, the addition of data from JWST, extending to $z \sim 9$

Table 2
Marginalized best-fit parameter values and associated 1σ uncertainties for the HIIGs and anchor samples. Values enclosed in parentheses indicate parameters that were held constant during the analysis.

Data set	α	β	h	Ω_m	w_0	w_a	N
HIIG	–	(5.022 ± 0.058)	–	$0.282^{+0.037}_{-0.045}$	(-1.0)	(0.0)	195
HIIG	–	(5.022 ± 0.058)	–	$0.278^{+0.092}_{-0.051}$	$-1.21^{+0.45}_{-0.40}$	(0.0)	195
HIIG	(33.268 ± 0.083)	(5.022 ± 0.058)	0.715 ± 0.018	$0.267^{+0.038}_{-0.048}$	(-1.0)	(0.0)	195
HIIG	(33.268 ± 0.083)	(5.022 ± 0.058)	0.718 ± 0.020	$0.278^{+0.091}_{-0.050}$	$-1.22^{+0.46}_{-0.40}$	(0.0)	195
Anchor+HIIG	33.28 ± 0.11	4.997 ± 0.089	0.730 ± 0.038	(0.3)	(-1.0)	(0.0)	231
Anchor+HIIG	33.28 ± 0.14	5.00 ± 0.11	0.730 ± 0.040	$0.335^{+0.044}_{-0.055}$	(-1.0)	(0.0)	231
Anchor+HIIG	33.29 ± 0.14	4.99 ± 0.11	0.731 ± 0.039	$0.302^{+0.12}_{-0.069}$	$-1.01^{+0.52}_{-0.29}$	(0.0)	231
Anchor+HIIG	33.29 ± 0.14	4.99 ± 0.11	0.730 ± 0.039	$0.321^{+0.10}_{-0.063}$	$-0.91^{+0.55}_{-0.33}$	$-0.71^{+0.65}_{-1.2}$	231

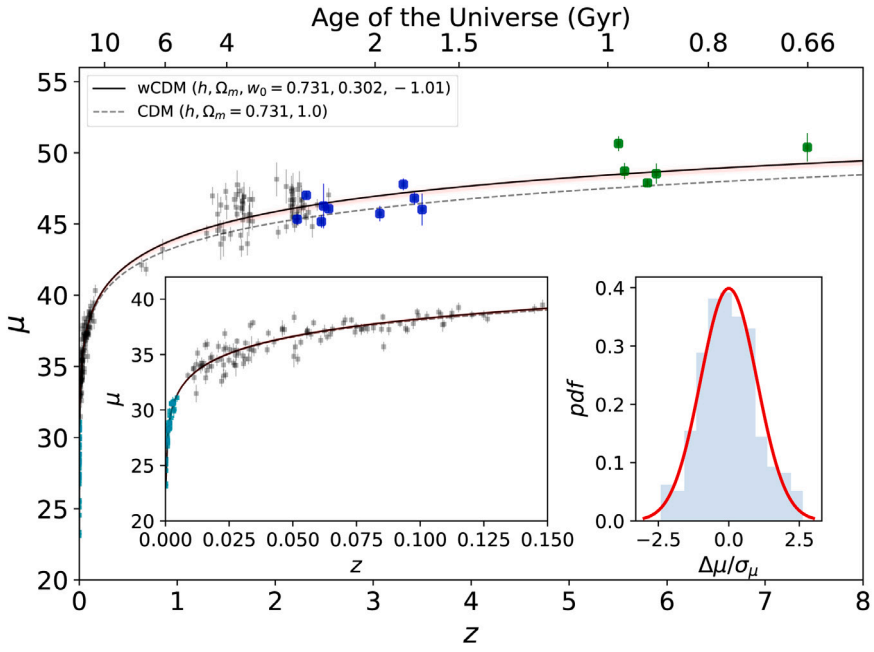

Fig. 21. Hubble diagram for GEHRs and HIIGs, here z is the redshift and μ is the distance modulus. In cyan we present the "anchor" sample of 36 GEHRs which have been analyzed in Ref. [300], in black we present the full sample of 181 HIIGs which have been analyzed in Ref. [289], while in blue we present the 9 new HIIGs from Ref. [301] and in green 5 new HIIGs studied with JWST by Ref. [302]. The black line is the cosmological model that best fits the data with the red shaded area representing the 1σ uncertainties to the model, while the gray dashed line is a flat cosmological model without DE. The inset at the left shows a close-up of the Hubble diagram for $z \lesssim 0.15$. The inset at the right presents the pulls PDF of the entire sample of GEHRs and HIIGs and the red line shows the best Gaussian fit to the PDF.
Source: Adapted from Ref. [289].

and beyond, is proving crucial. The JWST's exceptional sensitivity and resolution enable detailed observations of HIIGs at these higher redshifts, offering a unique view of the early Universe. This data range is essential for analyzing the dynamics of the Universe's expansion across various cosmological scenarios.

2.1.11. The baryonic Tully-Fisher relation approach

Coordinator: Khaled Said

Contributors: Benoit Famaey, Cláudio Gomes, Duško Borka, Esha Bhatia, Jenny G. Sorce, Maurice H.P.M. van Putten, Milan Milošević, Paolo Salucci, Paula Boubel, Predrag Jovanović, and Vesna Borka Jovanović

The BTFR [303–312] extends the classic Tully–Fisher (TF; [25,313–335]) relation by incorporating both the stellar and gas masses of galaxies, correlating a galaxy's baryonic mass (M_b) with its rotational velocity (V_{rot}). This relation provides critical insights into galaxy formation and dynamics and is crucial in testing and constraining models of galaxy evolution within both the ΛCDM framework and alternative theories [336–349].

The BTFR is defined as: $M_b \propto V_{rot}^x$, where M_b is the sum of stellar and gas masses, $M_b = M_* + M_{gas}$ and x is typically around 4, suggesting a deep connection between the visible matter and the dynamics of galaxies [303,350–352].

2.1.11.1. Historical context and development. The original TF relation, proposed by Ref. [313], established a link between the intrinsic brightness of spiral galaxies and their maximum rotational velocities. This relation has been pivotal in determining distances to galaxies and measuring the Hubble constant [353]. For example, Ref. [313] applied their TF relation to derive distances to the Virgo and Ursa Major clusters, estimating a Hubble constant of approximately $H_0 \approx 84\,\mathrm{km\,s^{-1}Mpc^{-1}}$ for Virgo and $H_0 \approx 75\,\mathrm{km\,s^{-1}Mpc^{-1}}$ for Ursa Major. The extension to the BTFR was motivated by the need to include galaxies with significant gaseous components, particularly dwarf galaxies [303]. Over the years, numerous studies have validated and expanded the BTFR, demonstrating its robustness and utility in various cosmological and astrophysical applications [312,347,354]. A crucial step toward the understanding of the physics of the TF and BTFR relationships has been the finding, in disk systems, of a family of *local* Tully–Fisher-like relationships [355–357], holding at various specific galactocentric radii and thus dubbed as the Radial Tully Fisher (RTF: for a review see Ref. [358]).

2.1.11.2. Theoretical models and their implications.

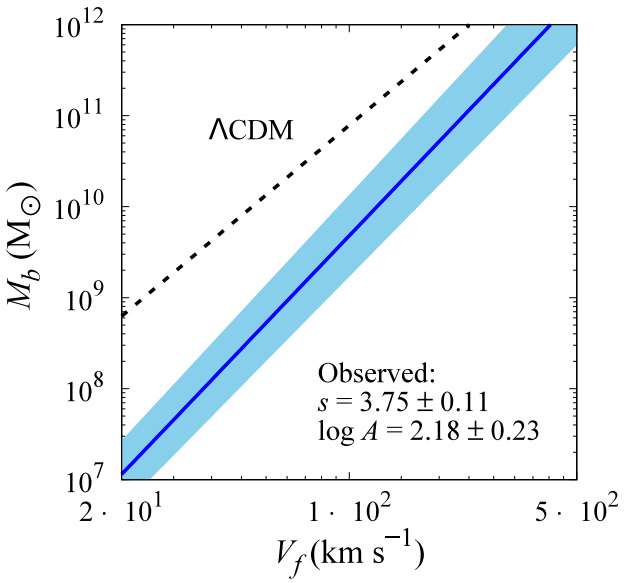

Fig. 22. Comparison between the BTFR obtained from error-weighted fits of galaxies with accurate distances from Ref. [359] to the BTFR predicted by ΛCDM cosmology. The observed BTFR (blue solid line) includes a light blue band representing the intrinsic scatter of 0.1 dex. The ΛCDM prediction is shown as a black dashed line. Both relations are plotted using equations from Ref. [359]: Eq. (6) for the observed BTFR and Eq. (6) for the ΛCDM prediction. [Reprinted under CC BY 4.0. from: V. Borka Jovanović, D. Borka, and P. Jovanović, Contrib. Astron. Obs. Skalnate Pleso 55/2, 24 - 33 (2025)].

The standard Λcdm model In the ΛCDM, the TF and BTFR are seen as consequences of the gravitational dynamics dictated by DM halos and baryonic matter. The rotational velocities of galaxies are thought to be influenced by both visible and DM, with the BTFR providing a means to probe these interactions [347]. However, as illustrated in Fig. 22, the observed slope and intrinsic scatter of the BTFR often differ from ΛCDM predictions, which typically forecast a lower slope and higher scatter [359]. This discrepancy poses challenges to the ΛCDM model and prompts further investigation into galaxy dynamics and mass distribution.

Modified gravity models Some studies propose that the BTFR can be explained without DM through modified theories like $f(R)$ theories of gravity [360–363]. Alternative gravitational theories, such as Modified Newtonian dynamics (MOND) and non-minimal matter-curvature coupling models, offer different perspectives on the BTFR. MOND, proposed by [364], adjusts Newtonian dynamics at low accelerations, predicting a BTFR with a slope exactly equal to 4, consistent with many observations [347,354]. MOND has made several successful predictions regarding the detailed shapes of rotation curves, galaxy dynamics, and galaxy lensing [365–367].

Another approach, non-minimal matter-curvature coupling model, generalizes the pure gravity sector by introducing a generic function of the curvature scalar, $f_1(R)$, and a non-minimal coupling between the matter Lagrangian and another generic function of the curvature scalar, $f_2(R)$ [368],

$$S = \int d^4x\sqrt{-g}\left(f_1(R) + f_2(R)\mathcal{L}\right)\,. \tag{2.5}$$

This model leads to an extra force term in the geodesics for a perfect fluid. In three dimensions and in the Newtonian limit, assuming that the total acceleration $\vec{a}$ is collinear with the 3-force, f, and in the limit of very small gravitational accelerations, the Newtonian acceleration, $\vec{a}_{\rm N}$, is $\vec{a}_{\rm N} \approx \frac{a}{a_{\rm E}}\vec{a}$, where $a_{\rm E}^{-1} = (2f)^{-1}\left(1 - \frac{f^2}{a^2}\right)$, which is remarkably similar to MOND's result. Furthermore, $a \approx \sqrt{a_{\rm E}GM}/r = v^2/r$, hence a Tully–Fisher relation appears with a luminosity of the form $L \sim v^4$ with $v^4 = a_{\rm E}GM$. Thus $a_{\rm E} = 10^{-10}\ \mathrm{ms}^{-2}$ as in MOND or $a_{\rm E} = (8.5 \pm 1.3) \times 10^{-10}\ \mathrm{ms}^{-2}$ [368]. This model has been shown to be consistent with several observations ranging from the cosmic version of the virial theorem at Abell 586 cluster [369], to Jeans instability in Bok globules [370,371], or to SN distance data and the BAO data allowing for an attempt to solve the Hubble tension [372].

A finite sensitivity of weak gravitation in galaxy dynamics to background cosmology may be detectable below the de Sitter acceleration scale [373] using SPARC [374] and large galaxy surveys such as MaNGA [375]. Redshift dependence would point to a potentially unified picture, linking BTFR to JWST observations of ultra-high redshift galaxies at cosmic dawn [376,377]. This approach may also place novel observational constraints on cosmological parameters, notably H_0 and the deceleration parameter q_0 [375].

2.1.11.3. Observations and cosmic tensions. Various studies have extensively explored the BTFR using data from large galaxy surveys. The Spitzer Photometry and Accurate Rotation Curves (SPARC), for example, includes measurements of 175 rotationally supported galaxies in the near-IR, minimizing the effect of star-halo degeneracy and providing precise baryonic mass and rotational velocity data [378,379]. Such robust datasets enable accurate fits to the BTFR and facilitate comparisons between observed galaxy properties and theoretical predictions. The BTFR for the SPARC sample aligns with a scale of $x = 4$. Research by Ref. [380] using the BTFR with a sample of 95 independent galaxies also challenges the Hubble constant value $H_0 < 70\,\mathrm{km\,s^{-1}Mpc^{-1}}$ with 95% confidence level. A More recent study by Ref. [25] demonstrated that using the BTFR allowed them to determine a Hubble constant of $H_0 = 75.5 \pm 2.5\,\mathrm{km\,s^{-1}Mpc^{-1}}$, which again challenges the standard cosmological model that suggests lower H_0 values [192]. Additionally, studies have shown variations in BTFR parameters across different distance bins, which could contribute to the understanding of the Hubble tension [381–386].

The RTF relationship, applied to a large sample of 843 local galaxies extending out to $z = 0.03$, has recently been used as a distance indicator to determine the maximum allowed variance of the $H(z)/H_0$ parameter [356]. They found that the maximum allowed local 'radial' variation is 1%, which is not enough to resolve the H_0 tension. In the near future, with the PROBES sample [387] (3000 objects) we will be able to use the RTF to test the hypothesis of a Giant Local Void at greater distances and investigate the anisotropy of the expansion of the Universe (see Ref. [356] for the present situation). Finally, the RTF can be applied at $z \sim 1 - 2$ to investigate a major part of the expansion history of the Universe [388].

The original TF relation is also useful for tracing the distance–redshift relation, provided that the relation is carefully calibrated. Unlike the BTFR, the TF relation is not universally linear, so studies typically introduce more complex models to account for the curvature and varying intrinsic scatter [333,389]. The Cosmicflows-4 (CF4) Tully–Fisher catalog [25] of ~10,000 spiral galaxies is currently the largest TF dataset, combining HI line widths with photometric magnitudes. There have been several published H_0 measurements using this dataset. For the full CF4 TF catalog, Ref. [25] derived $H_0 = 75.5 \pm 2.5\,\mathrm{km\,s^{-1}Mpc^{-1}}$ with an estimated systematic error of $\pm 3\,\mathrm{km\,s^{-1}Mpc^{-1}}$. Using an improved measurement methodology [389] and updated primary distance calibration [390], this was re-measured as $H_0 = 76.3 \pm 2.1\,(\mathrm{stat}) \pm 1.5\,(\mathrm{sys})\,\mathrm{km\,s^{-1}Mpc^{-1}}$, where the statistical error reflects the relatively small number of primary calibrators in the sample (~ 50 objects with CPLR and/or TRGB distances). These are in agreement with other recent H_0 measurements using the TF relation as the final rung of the distance ladder, which consistently return $H_0 > 70\,\mathrm{km\,s^{-1}Mpc^{-1}}$ (see Ref. [353] for a review). The next generation of Tully–Fisher datasets resulting from large surveys such as WALLABY [391], DESI [392], and FAST [393] will increase the precision of TF-derived measurements of the Hubble constant.

2.1.12. The Hubble tension in our Backyard: DESI and the nearness of the Coma cluster

Coordinator: Yukei Murakami

Contributors: Daniel Scolnic

The recent work by DESI [394] analyzed their first samples of early-type galaxies in the DESI peculiar velocity survey to study the fundamental plane (FP). FP is an empirical three-dimensional relation that links elliptical galaxies' radii, surface brightness, and the velocity dispersions [395,396][7]. This tight correlation serves as a standardization to measure distances to the galaxies over a large redshift range once the absolute distance scale is anchored to an independent, well-measured distance. In the DESI work [394], the Hubble Constant H_0 is measured with FP using an SBF measurement to the Coma cluster to calibrate the distance scale (i.e., distance ladder). Alternatively, recent study [397] showed that one can calibrate the FP in the early universe using Planck+ΛCDM inference of H_0 to measure the distance to the Coma cluster (inverse distance ladder). The inverse distance ladder with Planck+ΛCDM–calibration of FP places Coma at $\sim$ 10% further than the direct measurement of distance by SBF. In addition, the new SNIa distance, as well as other independent distance measurements to Coma collected over the past few decades, are all consistent with the SBF, creating a tension against Planck+ΛCDM–prediction. This discrepancy provides a unique opportunity to shed light on the implications of the Hubble Tension in our local universe.

2.1.12.1. DESI FP and inverse distance ladder. DESI has provided an extensive FP measurement and a Hubble diagram over the redshift range of $0.01 < z < 0.1$ using a sample of 4191 early-type galaxies in the Hubble flow and 226 galaxies in Coma [394]. The FP relation, which correlates a galaxy's velocity dispersion, surface brightness, and physical size, serves as a secondary distance indicator when calibrated with independent distance anchors. When the FP relation is calibrated using a near-infrared SBF distance of $D_{\rm Coma} = 99.1 \pm 5.8$ Mpc [124], DESI derives a value of $H_0 = 76.05 \pm 1.3\,{\rm km\,s^{-1}Mpc^{-1}}$. This result relates the Hubble constant and the Coma distance as $H_0 = (76.05 \pm 1.3) \times \left(\frac{99.1\ {\rm Mpc}}{D_{\rm Coma}}\right) {\rm km\,s^{-1}Mpc^{-1}}$. This relation can be used to obtain the distance to Coma predicted by Planck+ΛCDM, using the Planck-inferred value of the Hubble constant $H_0 = 67.4\ {\rm km\,s^{-1}Mpc^{-1}}$. The implied distance to Coma shifts to $D_{\rm Coma} = 111.8 \pm 1.8$ Mpc, a distance larger than any of the historical measurements that we discuss later.

2.1.12.2. Latest Coma distance with ATLAS SNe Ia. A recent analysis [397] compiled a sample of 10 spectroscopically confirmed SNIa within the Coma Cluster observed by the ATLAS survey [398] and YSE [399], as well as two additional SN previously included in the Pantheon+ dataset [32]. Applying the standardization and calibration methods established in the Pantheon+ analysis, the study derived a mean standardized peak brightness of $m_B^0 = 15.712 \pm 0.041$ mag for SN in Coma cluster. Using the absolute magnitude calibration of SNIa from the HST Cepheids [34], this results in a distance modulus of $\mu = 34.97 \pm 0.05$ mag, corresponding to $D_{\rm Coma} = 98.5 \pm 2.2$ Mpc. This measurement is in excellent agreement with the SBF distance used to calibrate DESI, with a significantly reduced uncertainty. The measured distance is at 4.6σ tension from the Planck-ΛCDMprediction.

2.1.12.3. New & historical measurements in tension with Λcdm. Historical measurements, as well as additional distance indicators and calibration methods further support a distance to Coma around 100 Mpc (see Fig. 23). A compilation of historical measurements summarized in [400], including I-band Tully–Fisher [319], K-band SBF [401], I-band SBF [402], $D_n - \sigma$ [403], FP [404] and Globular Cluster LF (GCLF) [405], produce an average of $D_{\rm Coma} = 95.1 \pm 3.1$ Mpc. The HST Key Project (KP) calibrated the FP relation using Cepheid variable stars, and its results, accounted for the recent updates, measure $D_{\rm Coma} = 85 \pm 8$ Mpc [406]. A more recent JWST measurement of TRGB and SBF, allows to re-calibrate the FP relation by HST-KP, which places Coma at 90 ± 9 Mpc. When combined with the SBF distance used in the DESI work and the new SNIa distance, these independent approaches yield a consensus distance of 98.0 ± 2.0 Mpc.

The tension between local and Planck-calibrated distances to Coma reflects a broader challenge in reconciling the local and early-universe distance scales. If Coma were truly at $D_{\rm Coma} > 110$ Mpc as ΛCDM-Planck calibration of DESI FP predicts, it would be inconsistent with decades of direct distance measurements based on a wide range of methodologies. The upcoming year 1 data release for DESI FP is expected to be significantly larger than the current study, and the targeted JWST observation of Coma galaxies (PI Jensen, GO 5989) is underway. When combined, these data will significantly reduce the statistical uncertainties in the FP-based H_0 or distance measurements, and the increased sky coverage in DESI data will allow FP to be calibrated with more than one galaxy clusters. Additionally, a few SNIa are being discovered in Coma every year, and the SNIa–based distance measurements are expected to be more robust in the next few years. Coma distance serves as an alternative or additional perspective on the issues surrounding the cosmological distance scales, and it showcases a new type of distance ladder analysis that is expected to develop rapidly in the coming years.

2.1.13. Cosmic chronometers

Coordinator: Michele Moresco

Contributors: Adrià Gómez-Valent, Anto Idicherian Lonappan, Arianna Favale, David Benisty, David Valls-Gabaud, Dinko Milakovic, Elena Tomasetti, Marek Biesiada, Rodrigo Sandoval-Orozco, Ruth Lazkoz, Sanjay Mandal, Swayamtrupta Panda, and Vavilova Iryna

CC have emerged in the last few years [182] as one of the most promising cosmological probes that can provide direct measurements of the expansion history of the Universe without the need to rely on any assumed cosmological model. The method [408], which is only based on the validity of the Cosmological Principle and on the assumption that General Relativity and standard physics hold in the environment of the galactic stars, proposes to derive the Hubble parameter $H(z)$ directly from the differential age evolution of the Universe (dt) in a redshift interval (dz), as:

$$H(z) = -\frac{1}{(1+z)}\frac{dz}{dt}\,. \tag{2.6}$$

To map the age evolution of the Universe, the best tracers that have been found are very massive ($\log_{10}(M/M_\odot) > 11$) and passively evolving galaxies since they have been proven to be extremely homogeneous systems, with synchronized formation, representing at each redshift the oldest population of galaxies [182]. Several authors have applied this method with different approaches to derive the differential age dt [409–417]. It currently counts more than 30 $H(z)$ measurements in the range $0 < z < 2.1$, with accuracy from ~10%–15% at the higher redshifts down to ~5% at the lower redshifts (see Fig. 24). See Refs. [182,418] for extensive reviews on the topic.

Since it provides a measurement of the Hubble parameter without assuming any cosmological model, recently, CCs have been widely employed in discussing the Hubble tension. To fully take advantage of the potential of these data, several different cosmology-independent techniques have been explored, from GP [419–431], to non-parametric smoothing [432,433], Weighted Polynomial Regression method [422], Padé approximations [427,434], and ANN architectures [431]; all these analysis provide a reconstruction of $H(z)$ independent of any cosmological model that can, in turn, be extrapolated to $z = 0$ for a determination of the Hubble constant H_0. The other alternative is, instead, to assume a cosmological model and derive cosmological constraints from

[7] See Section 2.1.11 for the Tully–Fisher relation, a late-type galaxy counterpart

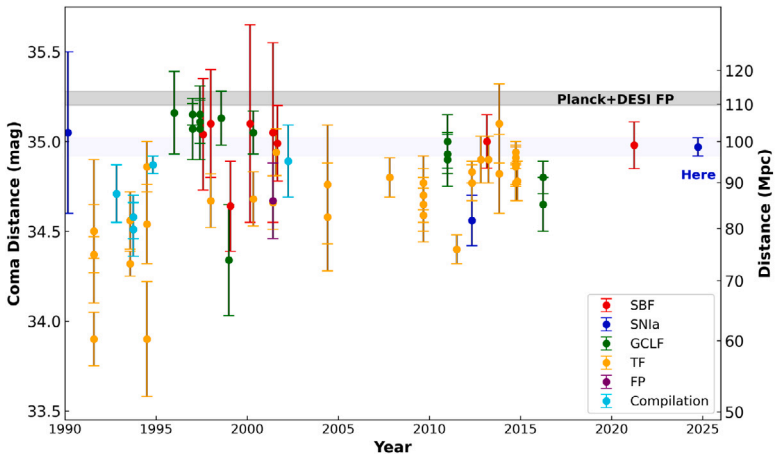

Fig. 23. Historical (1990 onward) distance modulus measurements of the Coma cluster (as reviewed in [406]). Only distance measurements that do not depend on redshift and H_0 are included. Figure taken from [397], and the rightmost point represents the SNIa distance measured in their work.

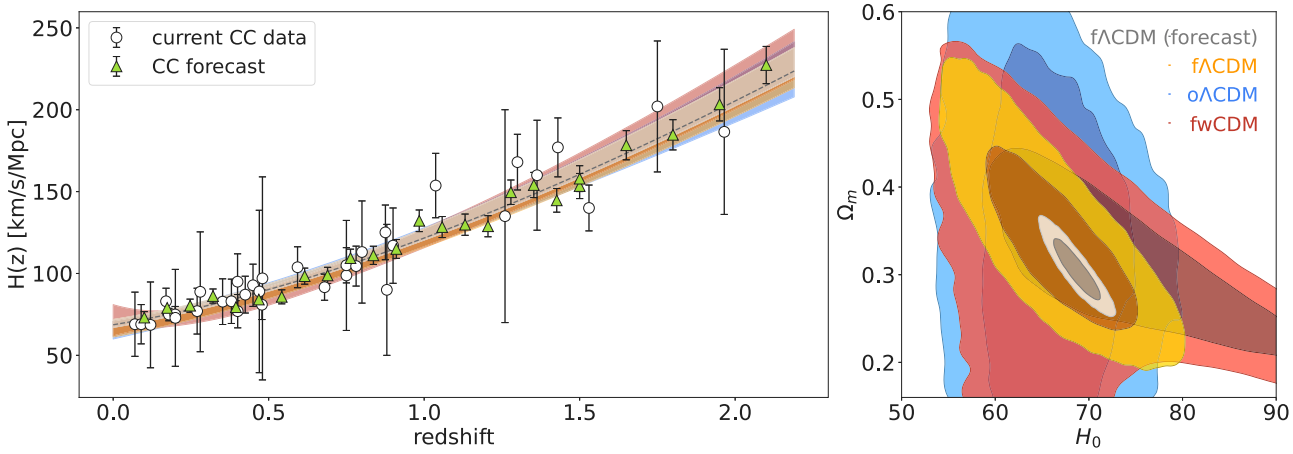

Fig. 24. Left plot. H(z) measurements obtained with the CC method from the literature (white points) and from future surveys (green points, from Refs. [182,407]). Right plot. Cosmological constraints in the Ω_m-H_0 plane; the different colors show the 68% CL results (also reported in the left panel) obtained by fitting current data with a flat ΛCDM (in blue), open ΛCDM (in yellow), and flat wCDM (in red) cosmological model, and future CC data with a flat ΛCDM model (in gray). (For interpretation of the references to colour in this figure legend, the reader is referred to the web version of this article.)

the parametric fit of the data [182,435,436]. Both these approaches, considering all the sources of statistical and systematic errors, give comparable results, yielding a constraint on the Hubble constant of $H_0 = 70.7 \pm 6.7\,\mathrm{km\,s^{-1}Mpc^{-1}}$ [429]. Future measurements, however, leveraging on much larger statistics (like from the ESA mission Euclid [437] or from future spectrographs like WST [407]) and better modeling of the data, promise to significantly improve these constraints, improving the accuracy from ∼8% to ∼2%. An example is given in Fig. 24, where current and future CC data are fitted with different cosmological models (flat ΛCDM, open ΛCDM, and wCDM) to provide constraints in the $\Omega_{\rm M}$-H_0 plane (for more details, see Refs. [182,407]).

A difference in H_0 can be reinterpreted also as a tension in the calibrators of the cosmic distance ladders, i.e., the absolute magnitude M of standard candles such as SNIa and the standard ruler represented by the comoving sound horizon at the baryon-drag epoch, r_d. Assuming CC as reliable CCs, it is also possible to use them to measure these distance calibrators independently from the CMB and the first rungs of the direct distance ladder. Thus, it is clear why CC plays an important role in the discussion. So far, the uncertainties for M and r_d derived by applying these calibrations are still too large to arbitrate the tension [424,429,438], but also this is bound to improve in the near future with the advent of upcoming surveys and data. Euclid [437], for instance, is expected to increase by 2 orders of magnitude the currently available statistics [182]. CCs have been used to calibrate baryon acoustic oscillations and SNIa [422–424,429,439–441] and also other standardizable objects like ultra-compact radio QSOs [420], GRBs or QSOs [430,438,442,443] which can be exploited to extend the ladder beyond the SNIa redshifts, $z > 2$.

Beyond the H_0 tension, CCs are also the ideal data to test and compare with different cosmological models, from the simplest to the more exotic ones. Among the litmus tests of the ΛCDM model, the $Om(z)$ diagnostic and its two-point version $Om(z_1, z_2)$ have a distinguishing feature [444] that depends only upon the expansion rate $H(z)$. Hence, CCs have been used [445,446] to perform tests of scenarios assuming either a cosmological constant or an evolving DE equation of state.

2.1.14. Strong lensing and time delay measurements

Coordinator: Tommaso Treu

Contributors: Alba Domi, Alexander Bonilla Rivera, Ali Övgün, Anowar J. Shajib, Clecio Roque De bom, David Valls-Gabaud, Dominique Sluse, Eoin O Colgain, Frédéric Courbin, Jenny Wagner, Lindita Hamolli, Predrag Jovanović, Sherry H. Suyu, Simon Birrer, Tanja Petrushevska, and Veronica Motta

Time variable sources that are multiply imaged — i.e., strongly lensed — provide an opportunity to measure absolute distances, and

therefore cosmological parameters including the Hubble constant H_0. The main advantages of this so-called time delay cosmography (TDC) with respect to other cosmological probes described in this white paper are: (i) it is a direct measurement of distances well into the Hubble flow; (ii) it is independent of all other types of distance measurements; (iii) it relies on well understood fundamental physics such as general relativity. In this section, we provide a brief summary of TDC, the current state of the art, and future prospects. The reader is referred to dedicated reviews for more extensive discussion, e.g., see Ref. [447–451].

The method was originally proposed for lensed SNIa by Refsdal in Ref. [452], well before the discovery of any actual strong gravitational lens. Since the mid-eighties it has been applied to lensed QSOs [447], and only recently — with the discovery of multiply imaged SN [453, 454] — it has been possible to fulfill Refsdal's dream [455,456].

TDC measures angular diameter distances, typically between $z = 0.5 - 3$, where the majority of deflector galaxies and lensed sources lie. More precisely, it measures the so-called time delay distance $D_{\Delta t} = (1 + z_d)\frac{D_d D_s}{D_{ds}}$, where D indicates angular diameter distance, and the subscripts s and d stand for source and deflector, respectively. In combination with stellar kinematics, it also measures D_d [457].

TDC is thus primarily sensitive to H_0. It is, however, also sensitive to other cosmological parameters, such as curvature or the DE equation of state, in a complementary way to probes such as the CMB and SNIa, breaking some of the degeneracies of those probes [458–461].

Several representative measurements using lensed QSOs prior to 2022 are summarized in Fig. 25. Already in 2020, just 7 lenses yielded H_0 at 2% precision [462,463], under standard assumptions about the mass density profile of the deflector. That measurement is in agreement with, and completely independent, of late Universe probes. If those assumptions are relaxed, and a parameterization of the mass density profile that is maximally degenerate with the Hubble constant via the mass-sheet degeneracy [464,465] is considered, the uncertainty increases to 8% for the same 7 lenses [466]. In 2023, the first lensed supernova [455] yielded an H_0 measurement with ~7% precision. Whereas this precision is very encouraging for a single system, especially given the complexity of modeling a cluster of galaxies, see also Ref. [456], it is not sufficient to distinguish between the early and late-time measurements and resolve the "Hubble tension". As more lensed SN are being discovered and analyzed, e.g., see Ref. [467–474], the precision is expected to improve rapidly, especially once the Roman and Rubin telescopes come on line [475].

In order to increase the precision on H_0 to the desired level of 1% under these weaker assumptions, three complementary approaches can be pursued [476]. The first is to increase the sample size. The Euclid, Roman, and Rubin Telescopes are expected to discover thousands of strong lenses, including lensed SN [477–480]. There is little doubt that large numbers of lenses will be discovered. The challenge will be to transform them into cosmological probes by obtaining the necessary additional data and computing the necessary cosmography grade models. Additional data include high-resolution images, time delays, deflector and source redshift, deflector kinematics, and supernova classification if relevant. Some of these data will be provided by the surveys themselves, e.g., high-resolution images by Roman and Euclid [475,481] and some time delays by Rubin [482], but others will require concerted follow-up effort. A coordinated follow-up for measuring precise time delays is critical. QSO time delays require high precision lightcurves minimally affected by microlensing [483,484], while SN require dedicated multi-color or spectroscopic follow-up [485,486]. The effort will be substantial, and it will require, e.g., repurposing a 4 m class telescope for time delays or building a dedicated satellite. The advent of ELTs will simplify matters, especially for high-resolution imaging and kinematics.

Modeling hundreds of lenses with precision sufficient for cosmography hundreds of lenses would be prohibitive at the moment, both in terms of human power and computing power. Fortunately, efforts are

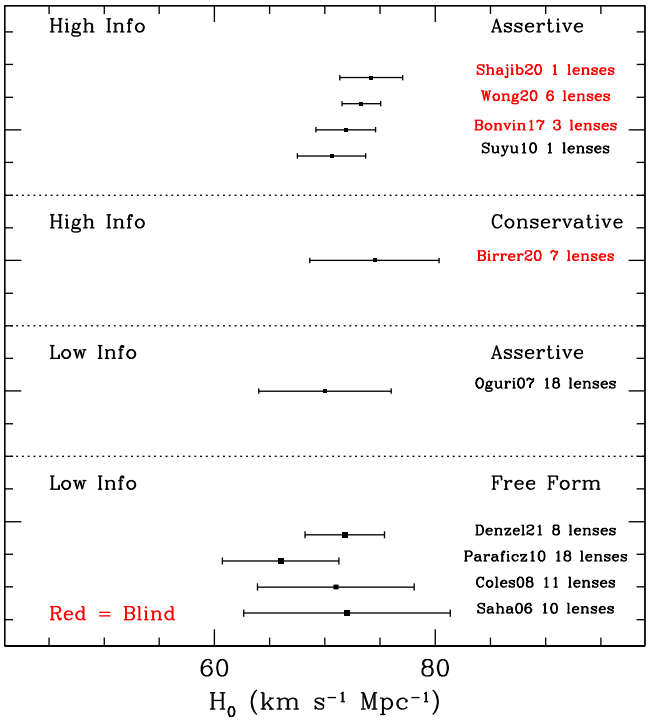

Fig. 25. The measurements are categorized according to (i) assumptions on the mass distribution of the main deflector, "assertive" and "conservative" for simply parameterized models or "free form" for pixilated models; (ii) to the amount of information used per lens, "low info" utilizes QSO positions and time delays, "high info" adds the extended surface brightness distribution of the multiple images of the QSO host galaxy (or "Einstein Ring"), stellar kinematics of the main deflector, and number counts or WL to estimate the line-of-sight convergence. For each measurement, the reference and the number of time delay lenses are given. The measurements shown in red were performed with blinding to prevent experimenter bias.
Source: The figure is taken from Ref. [449], see therein for details.

underway to develop automated pipelines [487–490], in some cases with the help of ML algorithms [491–493], to speed things up. The first results are promising, in the sense that models from independent automated pipelines are found to agree in their predicted time delays within the uncertainties, when the data contain sufficient information models that agree to within the uncertainties in predicted time delay can be found [494].

The second approach consists of increasing the precision per lens. In order to break the mass sheet degeneracy, non-lensing information is needed, for example, stellar kinematics of the deflector [461,495–497], the absolute luminosity of a lensed supernova Ia [498], or WL [499]. If the quality of the kinematics is sufficient, in principle, each lens can deliver distances to 2%–4% precision, limited by systematic errors in stellar velocity dispersion measurements [500].

The third approach consists of utilizing the much more abundant non-time delay lenses (a.k.a. "external samples") to learn about the internal structure of time delay lenses. This method has been shown to increase the precision of TDC significantly [466]. The key to using external samples without introducing biases is to understand the selection function of both the time delay and non-time delay lenses sufficiently well. At the moment, this is not a limiting factor [501] - statistical errors are larger - but the selection function will have to be properly modeled and understood in order to achieve 1% precision and accuracy on H_0, sufficient to solve the Hubble tension.

As more lensed SN are being discovered and analyzed, the precision is expected to improve rapidly, especially once the Roman and Rubin telescopes come online [502].

2.1.15. Extended QSO cosmologies

Coordinator: Maria Giovanna Dainotti

Contributors: Aleksander Łukasz Lenart, Catarina Marques, Celia Escamilla-Rivera, Giada Bargiacchi, Giovanni Montani, Rodrigo Sandoval-Orozco, and Swayamtrupta Panda

QSOs are one of the most luminous non-transient energy sources, whose use at cosmological scales allows us to study the Universe at higher redshifts, e.g., up to $z \sim 7$ [503,504]. At this redshift range, it is possible to reveal some interesting aspects and deviations from different cosmological models that can be indistinguishable at low z. In this path, some examples of the QSO cosmological use are: *(i)* the reverberation mapping technique [505,506], and *(ii)* the relation between variability in X-ray amplitude and black hole mass scatter [507]. However, there is a lack of a clear definition of QSOs to order the diversity of AGN objects [508], although recent studies have begun to streamline the various QSO categories [509,510] with particular emphasis on sources accreting at or above the Eddington limit [511]. There is a need to homogenize the modeling of broadband QSO spectra and examine and assess the evolution of QSO properties (Black Hole mass, Eddington ratio, viewing angle to the source) over a broad range of redshifts [512, 513]. Under such techniques, several QSO catalogs have been used to find cosmological constraints under certain theoretical assumptions, e.g., consistencies or inconsistencies between time delays from reverberation mapping of prominent emission lines extending beyond the cosmic noon [514] and impact of the inherent heterogeneity in the data set on cosmological parameter constraints [515], constraints using GRBs with QSO cosmology analysis for future landscapes [516].

Furthermore, studies including QSO catalogs combined with GRB observations achieve small uncertainties on cosmological parameters [517,518]. Moreover, combining the Risaliti-Lusso relation for QSO with SNIa can allow us to obtain corrections on the redshift evolution as a function of cosmology [519]. Recent studies have been going through the Risaliti-Lusso relation, which has been validated in Ref. [513], where $\Omega_{\mathrm{m},0}$ value seems larger when only it is considered QSO baselines [519–523], and some systematics in the QSOs measurements should be expected in future new cosmological probes [524]. Despite the systematics, this relation is a promising cosmological probe since its observed dispersion on average is ∼0.20–0.25 dex, and becomes significantly smaller when only the sources with the highest quality X-ray observations are considered [525], suggesting that intrinsically the X-ray to UV relation has a scatter lower than 0.1 dex, pointing to a tight, universal physical process regulating the energy flow between the accretion disk and the X-ray emitting region in QSOs. In this scheme, several studies related to extended theories of gravity have been performed and cosmologically constrained using QSO baselines, e.g., $f(T)$ cosmologies have been constrained through cosmography by considering non-flat and flat geometries [526] with GRB observables, using QSO objects [527] detected through high-quality UV and X-ray fluxes up to $z \sim 5.1$ [528]. In view of possible discrepancies among measurements of the matter critical parameter via sources with different z-ranges, it has been proposed a promising model in which $\Omega_{0,m}$ becomes a dynamical quantity. The proposed scenario relies on a metric $f(R)$-gravity in the so-called Jordan frame and dominant linear contribution is retained in the potential term of the non-minimally coupled scalar field (a small deviation is included too). It is such a dominant contribution that is responsible for a non-standard critical matter parameter [529]. From the cosmographic point of view, other analyses have highlighted a significant tension between the standard cosmological model and the best-fit cosmographic model, when using QSOs, SNIa, and GRBs [528], QSOs and SNIa [530], and QSOs combined with GRBs, BAO, and SNIa [531]. Also, some studies use QSOs as standard rulers [527] by their angular size–luminosity using very-long-baseline interferometry [532]. In addition, the joint analysis of spectroastrometry and reverberation mapping can measure AGN distances and provide a new way to measure H_0 [533]. Furthermore, recent results have considered QSO physics from UV, X-ray, and optical plane techniques behind the local observations as cosmological probes to study the H_0 tension [534]. Another application of QSOs in cosmology is the Sandage test of the cosmological redshift drift, i.e., a small dynamic change in the redshift of objects following the Hubble flow [535], which requires not only high instrumental resolution but also very bright targets. One of the main objectives of the QUBRICS (QUasars as BRIght beacons for Cosmology in the Southern Hemisphere) survey [536] is to provide a sample of bright targets for the Sandage test. The two brightest QSOs in this Golden Sample have started to be analyzed in the pilot program "An ESPRESSO Redshift Drift Experiment", which will be a complete end-to-end proof of concept for this experiment at ANDES in ELT, where the redshift drift signal is expected to be detected [537]. Although the Sandage test is a direct and real-time model-independent mapping of the expansion rate of the Universe, recent theoretical studies such as Refs. [538,539] show synergies with other cosmological probes, in particular regarding the characterization of the physical properties of DE.

Regarding the efforts to reach a higher precision in the determination of cosmological parameters, also a purely statistical approach has been employed. This is based on the fact that the normalized residuals of QSO logarithmic luminosities of the Risaliti-Lusso relation are not normally distributed. Hence, the Gaussian is not the most appropriate distribution to be used as cosmological likelihood. Indeed, Ref. [517] prove that the QSO have the logistic distribution as a best-fit. This is shown in the right upper panel of Fig. 26 along with the same investigation for GRBs (left upper panel) and SNIa (lower panels). Remarkably, the employment of this proper likelihood for QSOs, compared to the standard Gaussian one, reduces the uncertainty on H_0 up to 35%, on $\Omega_{\mathrm{m},0}$ up to 27%, on Ω_k up to 32%, and on w up to 31%, when non-flat and wCDM models are investigated by combining QSOs with GRBs, BAOs, and SNIa, where every single probe is fitted with its own best-fit cosmological likelihood [518]. Another approach aiming at inferring cosmological parameters with lower uncertainties consists of identifying a QSO sub-sample composed only of sources that better follow the Risaliti-Lusso relation, i.e., are closer to the best-fit relation. Indeed, this method allows us to reduce the intrinsic dispersion of the correlation, thus yielding a better precision of the cosmological parameters. Different techniques have been applied to select such a sub-sample [529,540,541] which have promoted QSOs as standalone cosmological probes, even with the same precision as SNIa.

2.1.16. GRBs as cosmological standard candles

Coordinator: Maria Giovanna Dainotti

Contributors: Aleksander Łukasz Lenart, Arianna Favale, Denitsa Staicova, Giada Bargiacchi, Hassan Abdalla, and Radosław Wojtak

Long-duration GRBs (LGRBs) could be used as standard candles, extending the capabilities of the Hubble diagram to measure distances further than currently possible with SNIa, thereby helping to constrain cosmological parameters. Phenomenological relations derived from spectral modeling, e.g., the Amati relation [542–544] can be used for this purpose. This relation connects the source-frame energy ($\mathrm{E}_{i,p}$), where the gamma-ray spectral energy peaks, with the isotropic-equivalent bolometric energy (E_{iso}) released during the prompt phase [545]. Another significant empirical correlation in the prompt emission is the Yonetoku relation [546] between E_{peak} with the intrinsic peak luminosity L_{iso}. This correlation has been validated for both LGRBs and short-duration GRBs (SGRBs) [546,547]. Given the large variability in the feature of the prompt emission, a more promising approach is obtained with the use of correlations involving the plateau emission [548], a relatively flat segment in the light curve (LC). The Dainotti relation relates the rest-frame time at the end of the plateau (T_a^*) and its corresponding luminosity (L_a). This relation succeeds in

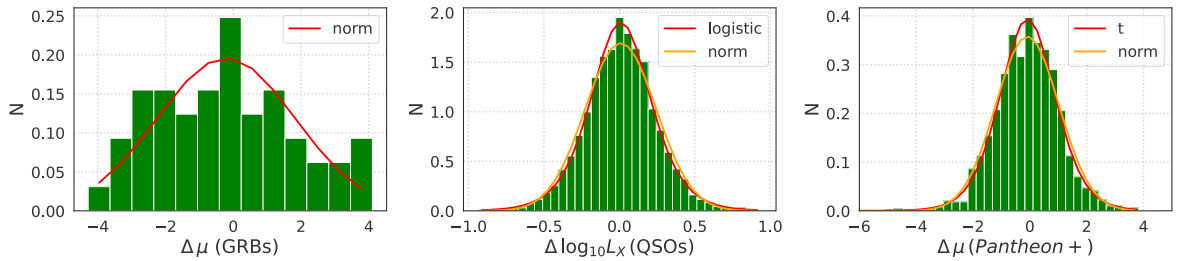

Fig. 26. Normalized residuals $\Delta\mu$ histogram for GRBs (left panel), QSOs (middle panel), and SNIa from Pantheon + samples (right panel). The red curve is the best-fit distribution, while the orange one is the Gaussian distribution. In the case of GRBs, the two coincide since the Gaussian is the best-fit distribution.

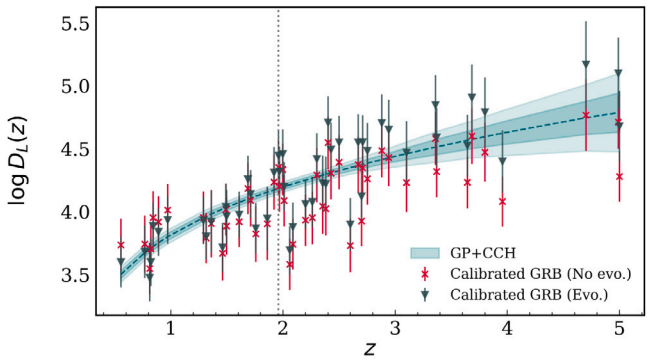

Fig. 27. The distance luminosity vs redshift when a calibration with CC is considered. *Source:* The figure has been taken by Ref. [430].

standardizing GRBs by utilizing the shape of their LCs. Indeed, around 500 GRBs observed by Swift exhibit a distinct, plateau phase in X-rays. The great advantage of this relation, compared to the ones in the prompt emission, is that the plateau phase can be attributed more straightforwardly to various theoretical models, including magnetar spin-down [549–552] and forward/reverse shock mechanisms [553–555].

This correlation was later updated in Refs. [556–558], and subsequently extended to a 3D correlation by incorporating the peak luminosity (L_{peak}) [556,559–561], the so-called 3D Dainotti relation. [558,559] demonstrated that this correlation is devoid of biases and it can be corrected for the redshift evolution.

Further studies by Refs. [560,562] confirmed the robustness of this correlation for high-quality LGRBs, which show well-defined plateau properties that obey the fundamental plane relation and constitute the so-called Gold sample. An improvement of this sample has been classified as the Platinum sample [563]. As a result, this correlation has been successfully applied as a cosmological tool [518,564–567], providing insights into the high-redshift Universe. GRBs, being at high-z, could be one of the important tools to differentiate between competing cosmological models. Indeed, Ref. [517] pinpointed traces of rising tension between flat ΛCDM and the equivalent model with $\Omega_k \neq 0$. There is a trend that reveals $\Omega_k < 0$, marking the importance of further studies in this direction at high-z.

The future cosmological role of GRBs has also been investigated in Ref. [566] where it has been determined how many GRBs are needed as stand-alone probes to achieve a comparable precision on $\Omega_{m,0}$ to the one obtained by SNIa only. They obtained the same error measurements derived using SNIa in 2011 and 2014 with 142 and 284 simulated optical GRBs, respectively, considering the error bars on the variables halved. These error limits will be reached in 2038 and in 2047, respectively. Using a doubled sample, obtained by the current ML approaches [568,569] allowing a LC reconstruction [570] and the estimates of GRB redshifts, with error bars halved, the same precision as SNIa in 2011 and 2014, is reached now and in 2026, respectively. If we need to reach the current precision of SNIa, it would require 18 years from now, but this estimate is very conservative since it does not consider the new redshifts from Euclid and JWST.

Indeed, in light of the existing cosmological tensions, such as the one on the Hubble constant, H_0, it has become fundamental to obtain unbiased cosmological distances via intermediate redshift probes. Thus, the calibration procedure of the GRB correlations must not be subject to strong model-dependent assumptions. Works have shown that this can be done by employing low-z probes, such as SNIa from the Pantheon Plus sample, a collection of 1701 SNIa, discussed already in the previous section, in combination with advanced statistical techniques such as GP [571] or cosmographical analyses [572,573]. On the other hand, data on the $H(z)$ obtained from CC can play the role of calibrating the ladders [429] (see Fig. 27) since these data only rely on General Relativity and the validity of the standard physics in the environment of the galaxy stars. Ref. [430] found that current data on CC can identify a subset of GRBs in the Platinum sample in $0.553 \leq z \leq 1.96$ that reveals a tight fundamental plane relation, with one of the lowest intrinsic scatter observed to date, $\sigma_{int} = 0.20^{+0.03}_{-0.05}$. This result is obtained considering a relation corrected for evolutionary effects and with parameters compatible with the magnetar model [550–552,574]. The GRB sub-sample pinpointed by this model-independent calibration can represent a valuable set of standardizable candles that is used to extend the cosmic distance ladder by providing unbiased luminosity distances up to $z = 5$. For QSO, calibrating with SNIa, varying only H_0 in the cases without and with correction for evolution, $H_0 = 73.76 \pm 2.18\,\mathrm{km\,s^{-1}Mpc^{-1}}$ and $H_0 = 69.82 \pm 2.27\,\mathrm{km\,s^{-1}Mpc^{-1}}$, respectively [519]. For GRBs, using the Gaussian priors, varying only H_0 in the cases without and with correction for evolution, $H_0 = 73.23 \pm 3.31\,\mathrm{km\,s^{-1}Mpc^{-1}}$ and $H_0 = 72.87 \pm 2.92\,\mathrm{km\,s^{-1}Mpc^{-1}}$, respectively [567].

Additionally, the 3D X-ray Dainotti relation has also been recently employed in cosmographic analyses to investigate the reliability of the standard cosmological model in a cosmology-independent way. In this concern, as mentioned in the previous section, GRBs combined with SNIa, QSOs, and BAO point toward a statistically significant discrepancy between the prediction of the concordance model and the observational data Ref. [531]. From another point of view, [575] constrained the transition epoch between a matter-dominated and a DE-dominated universe by using two cosmographic approaches and the combination of GRBs, SNIa, and BAO obtaining results compatible with the concordance model. Concerning instead the statistical analyses already mentioned for QSOs, the residuals of the distance moduli of GRBs remarkably prove to be effectively Gaussian, as reported in the upper left panel of Fig. 26, differently from the cases of QSOs and SNIa.

Given the importance of the 3D Dainotti relation, it is crucial to explore the existence of the same correlations but with different associated classes (not only the Platinum sample). The LGRBs associated with Supernovae Type Ib/c (GRB-SN) are interesting since they have been discussed in the literature as possible standard candles [563,576]. Ref. [577] investigate the existence of probable correlations among SN parameters and GRB prompt and afterglow features considering the largest compilation of GRB-v possible associations observed from 1997

up to 2021 and find a possible correlation between the GRB optical luminosity at the end of the plateau ($\log_{10} L_{a,opt}$) and the $\log_{10}$ of SN rest-frame peak time ($\log_{10} t_p^*$). The correlation can be expressed as $\log_{10} L_{a,opt} = (9.43 \pm 1.47) \log_{10} t_p^* - (13.60 \pm 11.89)$. The uncertainties on the fitting parameters (16%–87%) are too high to allow using this correlation for standardizing GRBs, thus new observations are needed to validate it. If confirmed, then it will represent a crucial support for cosmological analysis.

Another interesting application of GRB physics in cosmology comes from the search for quantum gravity models. Some such models predict an energy-dependent speed of light, which can be observed as simultaneously emitted high and low-energy photons arriving at different times. Such a tiny quantum effect is expected to be amplified by very high energies of the photons and cosmological distances, making GRBs a promising probe. In Refs. [578,579], the authors explored the use of different GRB time-delay datasets in combination with the Pantheon/Pantheon+ SNIa datasets, BAOs, and the CMB distance priors under different approximations for the intrinsic lag to constrain cosmological parameters and investigate the impact on the H_0 tension. The analysis revealed that the inclusion of such time-delay datasets still leads to a deviation in the parameter $c/H_0 r_d$, where c is the speed of light and r_d is the comoving sound horizon at the drag epoch. Such deviation can be interpreted as an artifact of the H_0 tension on the remaining quantities, demonstrating again that the tension is spread to the whole $H_0 - r_d - \Omega_{\rm m,0}$ plane. Such a dataset is not directly affected by the $E_p - E_{iso}$ correlation, but relies critically on the assumption of Lorentz Invariance Violation (LIV), which so far has not been detected. In the case where LIV is not zero, GRB time delays would be a new independent cosmological probe.

In addition, the constraints on the cosmological parameters can be obtained with the interaction of the gamma rays with their surrounding medium or other radiations. Gamma rays with energies above around 10 GeV are attenuated via interactions with the extragalactic background light (EBL) photons, resulting in electron-positron pair production. The attenuation effect was systematically measured in spectra of blazars and GRBs, using a wide range of instruments and techniques, e.g., see Ref. [580,581]. Since the attenuation scales with the comoving distance, these measurements can be used to constrain cosmological parameters, in particular H_0, given a model of the EBL based on integrating light from galaxies in deep cosmological surveys [582]. Recent joint modeling of the EBL and γ-ray attenuation yields $H_0 = 65.1^{+6.0}_{-4.9}\,\mathrm{km\,s^{-1}Mpc^{-1}}$, and $H_0 = 66.5^{+2.2}_{-2.1}\,\mathrm{km\,s^{-1}Mpc^{-1}}$when combined with the BAO observations and the BBN prior [583]. The H_0 measurements are independent of any external distance calibration, and the best-fit values are in close agreement with the CMB-based Planck value [192].

2.1.17. Gravitational wave constraints

Coordinator: Antonella Palmese

Contributors: Bangalore S. Sathyaprakash, Ivan de Martino, Matteo Tagliazucchi, Nicola Borghi, and Nicola Tamanini

The field of GW astronomy has recently facilitated novel measurements of the Universe's expansion rate by exploiting unique properties of compact binary mergers. By providing a distinct perspective on the Universe, in contrast to traditional astronomical and cosmological probes (such as electromagnetic radiation, cosmic rays, and neutrinos), GWs offer a complementary approach to addressing cosmological tensions.

Since 2015, a ground-based GW detector network, including the Laser Interferometer Gravitational Wave Observatory (LIGO) [584] and later Virgo [585] and KAGRA [586], has been detecting coalescences of compact object binaries, which so far include binary neutron star (BNS) [587], neutron star-black hole (NSBH) [588], and binary black hole (BBH) [589] mergers. It is anticipated that LIGO-Virgo-KAGRA (LVK) will complete their fourth and fifth observing runs (O4 and O5) by the early 2030s [590], after which a significantly upgraded detector network, called A$^\#$ [591,592] is expected to become operational. This will be followed by the deployment of next-generation (XG) observatories, such as the Cosmic Explorer [593–595] and Einstein Telescope (ET) [596]. Additionally, the Laser Interferometer Space Antenna (LISA) [597] is scheduled for launch in the next decade and will be sensitive to GWs from the inspiral and merger of binaries within the 0.1 mHz to 1 Hz frequency range, including massive BBHs and extreme mass ratio inspirals (EMRIs). LISA and XG observatories will observe mergers throughout the cosmos from an epoch before the first stars formed.

GW events can be used as "standard sirens" (StS; [598,599]), as they can act as absolute distance indicators. The GW signal of a compact binary merger is directly sensitive to the luminosity distance of the source and can therefore be combined with redshift information to act as a probe of the expansion of the Universe. Depending on where the redshift information is derived from, StSs are typically divided into different classes, with bright and dark StSs being the two main classes. In what follows, we briefly describe each method and the state of the field, including the latest measurements and systematics studies, and end with prospects for future measurements, focusing on H_0 constraints as a pathway to shed light on the Hubble tension.

2.1.17.1. Bright standard sirens. For bright StSs, an electromagnetic (EM) counterpart is identified, and the redshift is derived from its host galaxy, assuming that both are unique. So far, there exists only one EM counterpart that is confidently associated with a GW event, GW170817 [600]. This association has been used to derive the first StS measurement [601], finding $H_0 = 70^{+12}_{-8}\,\mathrm{km\,s^{-1}Mpc^{-1}}$, a $\sim 14\%$ precision measurement. Subsequent analyses have taken a more in-depth approach to estimate the peculiar velocity of the host galaxy [602–604]. Moreover, various works attempted to take advantage of the EM observations to constrain the viewing angle of the binary and break the distance–inclination angle degeneracy which exists when estimating these parameters from the GW data [605–608]. The latest of these measurements reached a $\sim 7\%$ precision and they are all consistent with both early and late-time measurements of H_0.

It is worth noting some of the major systematics that may affect future bright StS measurements. A StS analysis only using the GW data and the host galaxy spectroscopic redshift of a high-confidence EM counterpart provides an H_0 measurement which is not expected to first order to be affected by major systematic uncertainties, assuming that the peculiar velocities measurements are well constrained (also considering that their uncertainties will become less important as we move toward larger GW detector distance horizons [609]) and detector calibration errors are kept under control ($\lesssim 2\%$ [610]). Although GW selection effects are well understood and can be more easily modeled, selection effects from EM searches also need to be taken into account and may be coupled to binary parameters such as source luminosity distance and viewing angle [611]. Beyond selection effects, if including EM estimates of the viewing angle, H_0 measurements may also be affected by modeling uncertainties of the jet structure [612], kilonova geometry [613], or even a possible jet misalignment with the binary angular momentum [614].

Future bright StSs are most likely expected to arise from binary neutron star (BNS) and neutron star black hole (NSBH; which would prove valuable StSs [615]) mergers, but candidate EM counterparts to BBH mergers also exist [616–618]. Although the BBH EM counterparts association is currently uncertain [619,620], they may in the future be used to infer the Hubble constant along with other cosmological parameters [621–625].

2.1.17.2. Dark standard sirens. Most mergers detected by the LVK (currently in the order of $\sim$ 200 when including significant detection candidates from the ongoing observing run) do not have an associated EM counterpart and are mostly comprised of BBH mergers. In that case,

the redshift information necessary for an StS analysis may be taken from galaxy catalogs (e.g., see Refs. [626,627]), from the redshifted mass measured with the GW data [628,629], or a combination of the two [630–632].

In the first case, the redshift distribution of galaxies along the line of sight of a GW event's localization can be used to infer cosmological parameters, including H_0, from the distance–redshift relation. Various works have produced such measurements so far [633–641], in general finding a precision on H_0 down to $\sim$ 20% following the third LVK observing run, again in agreement with both *Planck* and SH0ES constraints. Even when combined with the bright StS available, the precision reaches $\sim$ 10% (when ignoring EM viewing angle constraints) and does not yet allow us to distinguish between the two leading H_0 measurements.

Golden dark sirens are a subclass of dark sirens when the catalog contains, or follow-up observations reveal, a single galaxy in the 3D localization volume. Although rare, they may provide exquisite few percent-level measurements of H_0 [642]. It is also possible to cross-correlate GW events with galaxy catalogs to infer cosmological parameters (e.g., see Ref. [643]). In all cases, the GW localization precision and the availability of extended spectroscopic galaxy catalogs [632] will be crucial to establish dark StS as a cosmological probe competitive with bright StSs.

In the second case, the source redshift is reconstructed at the statistical level by taking advantage of the presence of features in the distributions of the BBH population properties, such as the mass gap that may be explained by the theory of pair-instability supernova [644,645], or the overdensity peaks in the mass distribution observed in LVK data [646,647]. This "spectral sirens" approach has allowed constraints on H_0 at the $\sim$ 60% level [636] and on modified GW propagation [648,649]. These constraints are expected to significantly improve with XG detectors, as all BBH events can be used as spectral sirens. However, this poses a computational challenge, since the time required for a full cosmological and population analysis scales linearly with the number of events.

The major sources of systematics for dark sirens methods are expected from incorrect assumptions on the mass function [636]; while inferring cosmological parameters in conjunction may mitigate this effect [630], it is still crucial to correctly model the mass function including its potential evolution [629]. Other systematics may arise when using photometric redshifts [650,651], and host galaxy weighting or galaxy assumptions that do not match the true underlying distribution of merger hosts [652,653].

2.1.17.3. Prospects for ground-based detectors. Fig. 28 in Ref. [654] summarizes the prospect of terrestrial GW observatories in resolving the Hubble tension. The x-axis lists GW detector networks that are expected to become operational or newly built over the next decade or more. For each network, the y-axis shows the precision with which the Hubble constant would be measured, for four classes of binary merger events: BBH, NSBH and BNS as golden dark sirens, as well as BNS mergers with associated EM counterpart. For each network the figure also shows the number of events expected to be detected in each source class. A target precision of 2% could be achieved by the HLV network with dark sirens but is not guaranteed since the number of events expected is $\mathcal{O}(1)$. If the current median BNS merger rate holds, then the HLV network might observe $\sim$ 130 bright sirens and accomplish the 2% target. Assuming one ET detector and its synergy with Transient High Energy Sources and Early Universe Surveyor (THESEUS) [655] for bright StSs, one may achieve accuracy on H_0 of only $0.40\,\mathrm{km\,s^{-1}Mpc^{-1}}$ in the case of a non-flat ΛCDM model after five years of observations (which corresponds to $\sim$ 166 bright StSs detections with redshift below $z \sim 4.3$) [656]. ET alone, or a network of only two CE detectors, will not be able to accomplish the 2% target with dark sirens, although a network of two CE detectors could do so with bright sirens. A network consisting of an ET and at least one CE will determine H_0 to sub-percent precision with dark sirens of all source classes, as well as with hundreds of bright sirens. In the case of DE models, the accuracy on the Hubble constant may achieve 1% after 10 years of observations due to the correlations between H_0 and the DE parameters of the specific model under consideration [657]. It is also worth noting that bright sirens with XG will reach a percent level precision in distance in the local Universe, thus enabling precision measurements of σ_8 [658] which will inform our understanding of the S_8 tension, should it persist. With XG observatories we will enter the era of precision cosmology with GW observations.

2.1.17.4. LISA perspective. The LISA [659] will push GW cosmology at high redshift ($z \gtrsim 3$), mapping the expansion of the Universe in a still poorly charted cosmic epoch [660]. LISA will observe both bright sirens, in the form of massive black hole binary mergers with an identified EM counterpart [661,662], and dark sirens, in the form of extreme mass ratio inspirals (EMRIs) [663]. Independently these two populations of standard sirens are expected to deliver percent constraints on the Hubble constant [664–669]. Combined together, however, they should provide a one-percent, or even better, constraint on H_0 [670], making LISA a rightful competitor to solve the Hubble tension. The large redshift of LISA standard sirens will furthermore provide original tests of ΛCDM and of general relativity, delivering new potential insights on the nature of DE [665,671–675].

2.1.18. The cosmic microwave background radiation

Coordinator: Margherita Lembo and Martina Gerbino

Contributors: Anto Idicherian Lonappan, Chandra Shekhar Saraf, Enrico Specogna, Luca Caloni, Özgür Akarsu, Nils A. Nilsson, Paweł-Bielewicz, Simone Paradiso, and Venus Keus

2.1.18.1. Review of CMB basics and recent observations. The CMB plays a crucial role in shaping our understanding of modern physics and remains a powerful tool for advancing knowledge in cosmology and particle physics. The CMB dates back to roughly 380000 years after the Big Bang, at a redshift of $z_* \simeq 1100$, when CMB photons decoupled from electrons, close to the moment in the thermal history of the Universe when electrons and protons combined into neutral hydrogen atoms. Since then, CMB photons free stream with a nearby blackbody distribution with a temperature today of approximately $T \simeq 2.7$ K [676]. The CMB spectrum peaks around 100 GHz, within the microwave frequency range of the electromagnetic spectrum. Primordial density perturbations at the last scattering surface gave rise to temperature anisotropies in the CMB field of the order of $\Delta T/T \sim 10^{-5}$ [677]. The CMB radiation, because of its quadrupolar anisotropy, is indeed also partially linearly polarized due to Thompson scattering, with an amplitude of $\sim$ 10% of temperature anisotropies.

The polarization pattern is usually decomposed into so-called (curl-free) E-modes and (divergence-free) B-modes. On small angular scales, both the temperature and the polarization fields undergo a tiny distortion when they pass close to large distributions of matter. The weak gravitational lensing effect (CMB lensing) is one of the most important mechanisms that can generate secondary anisotropies in the CMB. In particular, it smears out anisotropies at small angular scales in temperature and E-mode polarization, and it gives rise to an additional B-mode contribution sourced by the lensed E-mode pattern.

The first full sky mapping of the CMB anisotropies was made by the COBE satellite [678], refined by WMAP [679] and finally by *Planck* [192], that delivered the state-of-the-art for full-sky CMB measurements both in temperature and polarization. At smaller (arcmin) angular scales in temperature and E-mode polarization, observations have been dominated in sensitivity by the ground-based experiments ACT and SPT; the search for B modes has been led so far by ground-based telescopes observing degree angular scales, i.e., BICEP/KECK, POLARBEAR/Simons Array.

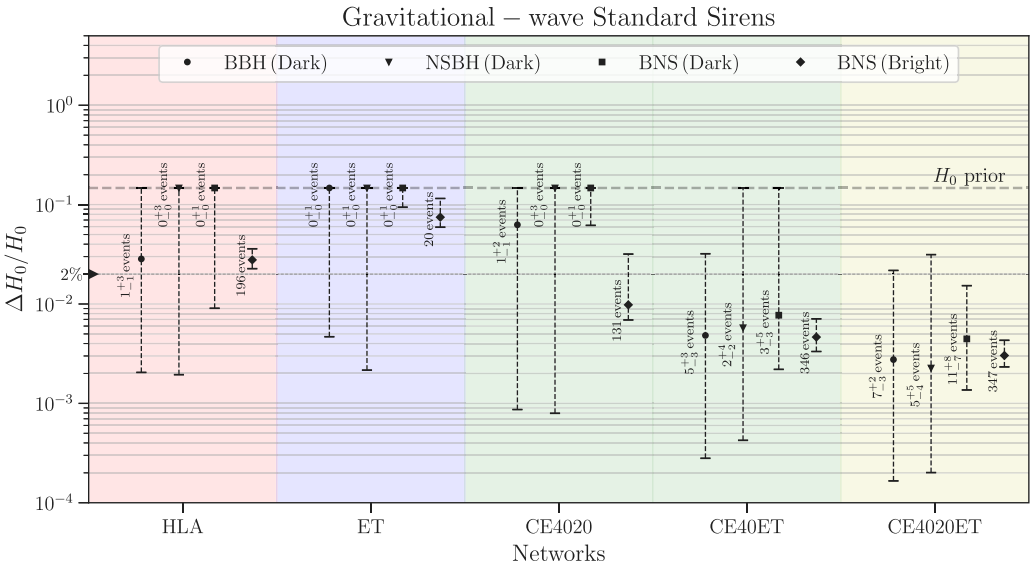

Fig. 28. Precision with which H_0 would be constrained by standard sirens with the HLV network upgraded to A# sensitivity and networks containing one or more XG observatories (see Section 2.1.17.3 text for details).
Source: Figure taken from Ref. [654].

Next-generation CMB experiments, both space-borne (e.g., LiteBIRD [680]) and ground-based (e.g., Simons Observatory [681] and CMB-S4 [682]), aim to achieve precise measurements of CMB polarization. A clear science goal is to detect the imprint on CMB pattern of primordial GWs, which are the smoking gun of an inflationary phase in the early Universe [680,683,684]. Moreover, improved measurements of CMB polarization would provide insights on potential new physics beyond the standard model [685–693]. CMB lensing is one of the most relevant observable of near-future CMB experiments, as it provides an invaluable tool to reconstruct the integrated distribution of matter in the Universe and to place stringent constraints on physical properties and effects mostly related to the late-time phases of the Universe, such as the growth of structures and neutrino masses (see e.g., *Planck* [694], ACT [695], SPT [696]).

2.1.18.2. CMB-driven constraints in the context of cosmological tensions. CMB observations allowed us to test the predictions of the standard cosmological model and to shape our knowledge of the Universe, its history, and composition. Despite its phenomenological success, the ΛCDM model is still incomplete in that, for example, fails to address the fundamental nature of the most abundant dark components. In addition, it has been facing challenges due to statistical tensions between results obtained with recent cosmological and astrophysical surveys of increased accuracy. Most notably, there is a severe ($> 5\sigma$) discrepancy in the value of the Hubble constant H_0 estimated with CMB observations with respect to the result obtained with local distance ladder measurements [34,192]. Furthermore, CMB and LSS measurements show a less severe albeit still intriguing disagreement on the amplitude of matter perturbations quantified via the σ_8 parameter [192, 697–699]. These discrepancies and their implications will be explored in more detail in the following subsections from the perspective of CMB observations.

2.1.18.3. Constraints on H_0 from CMB measurements. The Hubble tension is one of the major unresolved issues in modern cosmology. This tension refers to the discrepancy between local measurements of the Hubble constant, H_0, and the value inferred from early Universe observations assuming the ΛCDM model. Early Universe estimates of H_0 are driven by CMB observations made by the *Planck* satellite, which yields the value $H_0 = 67.27 \pm 0.60\,\mathrm{km\,s^{-1}Mpc^{-1}}$ at 68% CL, using a combination of TT,TE,EE+ lowE data [192] (see also Refs. [700,701] for re-analyses of *Planck* data, with no significant deviations of H_0 from the *Planck* result). On the other hand, the most sensitive local measurement of H_0 is obtained by the SH$_0$ES collaboration, which finds $H_0 = 73.04 \pm 1.04\,\mathrm{km\,s^{-1}Mpc^{-1}}$ exploiting type SNIa calibrated with Cepheids [34]. These two values are in 5σ tension.

Alternative CMB datasets, such as WMAP [679], ACT [702,703], and SPT [704], or CMB-independent probes, such as combinations of BBN with BAO measurements [705], yield H_0 values that align with those obtained from *Planck*. The analysis of ACT-DR6 data [703] yields a 68% CL value of $H_0 = 66.11 \pm 0.79\,\mathrm{km\,s^{-1}Mpc^{-1}}$ (ACT TT-TEEE+Planck-Sroll2 EE at large scales to constrain tau) consistent with measurements obtained by *Planck* satellite and lower than local measurements. Similarly, the combination of ACT-DR6 and WMAP data results in a value of $H_0 = 66.78 \pm 0.68\,\mathrm{km\,s^{-1}Mpc^{-1}}$ at 68% CL [703,706]. Additionally, the combination of ACT and WMAP data results in a value of $H_0 = 67.6 \pm 1.1\,\mathrm{km\,s^{-1}Mpc^{-1}}$ at 68% CL [702]. The same collaboration also reported an estimate of $H_0 = 68.3 \pm 1.1\,\mathrm{km\,s^{-1}Mpc^{-1}}$ from measurements of CMB lensing in combination with BAO data (6dF and SDSS) [695]. The SPT collaboration finds a compatible result, with a value of $H_0 = 68.3 \pm 1.5\,\mathrm{km\,s^{-1}Mpc^{-1}}$ at 68% CL [704], improved to $66.81 \pm 0.81\,\mathrm{km\,s^{-1}Mpc^{-1}}$ with the use of the latest unlensed EE and CMB lensing data in combination with a prior on the optical depth τ [707]. It is relevant to emphasize that all the results above are independent of *Planck* data. On the other hand, late-time measurements different from SH$_0$ES, including additional methods for calibrating SNIa at large distances (see Section 2.1.7) or observations independent of SNIa (see e.g., Section 2.1.9, Section 2.1.13, Section 2.1.10, Section 2.1.17), are all suggesting higher values of the Hubble parameter.

Depending on the combination of measurements, the tension ranges roughly from 4σ to 6σ. Fig. 29 shows a comprehensive list of CMB measurements of the Hubble parameter. It is important to emphasize that these results were derived under the assumption of the ΛCDM model. For example, as shown in Ref. [708], the uncertainty on H_0 increases when considering extensions to the ΛCDM framework.

Assuming a different cosmological model may lead to different estimates of H_0, either in the mean value or in the width (i.e., in the errorbar) of the PDF (or both) [3,709,710].

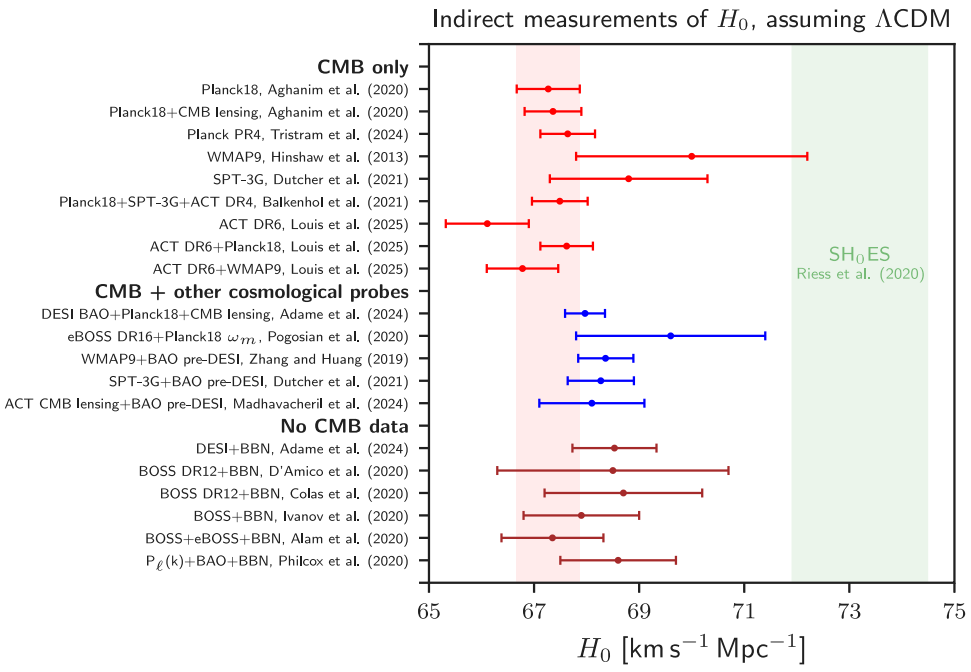

Fig. 29. Whisker plot with 68% CL constraints on the Hubble constant H_0 through different indirect measurements performed over the years. The constraints shown in this plot have been derived assuming ΛCDM model. If not specified, "BAO" refers to a combination of BAO data prior to DESI (see the corresponding paper for more details). The green vertical band corresponds to the H_0 value from SH$_0$ES team [34], while the red one corresponds to the value from *Planck* 2018 [192].
Source: This figure has been adapted from Fig. 1 of Ref. [709].

Since the value of H_0 inferred from CMB observations depends on the underlying cosmological model, this discrepancy with the local measurements of the Hubble parameter might be an indication of physics beyond the ΛCDM model. An alternative possibility, which will be discussed in Section 2.1.18.5, is that this tension is due to unknown systematics that affect either early-time or late-time observations (or both). However, given the vast array of independent probes of H_0, it seems quite unlikely that systematic effects may be the only responsible for this discrepancy. This further motivates the search for an explanation in terms of new physics. The landscape of theoretical scenarios to address the H_0 tension is broadly discussed in Section 4. Here, we just recall that the easiest extensions to ΛCDM are unable to solve the tension. More exotic scenarios, like those involving new BSM interactions between the components of the stress–energy tensor, the existence of new components or variation of fundamental constants, usually do not properly alleviate the tension, but rather yield estimates of H_0 with a larger uncertainty than the ΛCDM-based inference. Some models that gained visibility in the past, like those with strongly self-interacting neutrinos, require new physics that is at odds with complementary constraints from laboratory probes [711]. The search for new physics is still ongoing.

In order to understand the possible physical origin of this tension, we need first to discuss how CMB observations constrain H_0 (see Refs. [712,713]). The key quantity from which the Hubble constant is inferred is the angular scale of the sound horizon at recombination, which we assume to happen instantaneously at redshift $z_* \simeq 1100$. This is defined as

$$\theta_s \equiv \frac{r_s(z_*)}{D_{\rm A}(z_*)}\,, \tag{2.7}$$

where $r_s(z_*)$ and $D_{\rm A}(z_*)$ are the comoving sound horizon at recombination and the comoving angular diameter distance to recombination, respectively:

$$r_s(z_*) = S_k\left(\int_{z_*}^{\infty} \frac{c_s(z)}{H(z)}dz\right), \qquad D_A(z_*) = S_k\left(\int_0^{z_*} \frac{1}{H(z)}dz\right), \tag{2.8}$$

with

$$S_k(x) = \begin{cases} \frac{1}{\sqrt{|k|}}\sinh(\sqrt{|k|}x)\,, & \text{for } k<0 \\ x\,, & \text{for } k=0 \\ \frac{1}{\sqrt{|k|}}\sin(\sqrt{|k|}x)\,, & \text{for } k>0 \end{cases}. \tag{2.9}$$

Here, $c_s(z) = 1/\sqrt{3[1+R(z)]}$ is the sound speed of the acoustic waves in the baryon-photon plasma, where $R(z) = 3\rho_{\rm b}(z)/(4\rho_\gamma(z)) = 3\omega_{\rm b}/(4\omega_\gamma)(1+z)^{-1}$ denotes the ratio between the baryon and photon energy densities, and k is the spatial curvature of the Universe. Because of the so called "geometric degeneracy" [714], CMB anisotropy measurements alone do not constrain the curvature of the Universe. To a large extent, the degeneracy can be broken using CMB lensing effect. Tighter constraints can be imposed by analyzing CMB data in combination with other cosmological probes (see Section 2.1.18.4). The Hubble parameter, $H(z)$, is given in terms of the physical densities of DE, matter, photons, neutrinos and curvature as

$$H(z) = (100\ \text{km s}^{-1}\ \text{Mpc}^{-1}) \sqrt{\omega_{\rm DE}(z) + \omega_{\rm m,0}(1+z)^3 + \omega_\gamma(1+z)^4 + \omega_\nu(z) + \omega_k(1+z)^2}\,. \tag{2.10}$$

Within the ΛCDM model, $\omega_{\rm DE}(z) = \omega_\Lambda$ and $\omega_k = 0$. The only unknown quantities in Eqs. (2.8)–(2.10) are $\omega_{\rm b}$, $\omega_{\rm m,0}$ and ω_Λ. The radiation density ω_γ is fixed by the CMB temperature obtained from measurements of the CMB blackbody spectrum [676] and the neutrino density can be obtained at any time by properly integrating the neutrino distribution function[8].

[8] The parameter of the neutrino equation of state is not constant. Therefore, it is not possible to generally parameterize ω_ν via a simple scaling of the redshift, unless one considers the limiting cases of ultra-relativistic and non-relativistic neutrinos.

Then, H_0 is inferred from CMB data as follows (see Ref. [713] for more details). First, we determine the baryon and matter densities from their impact on CMB power spectra [715]. The baryon density affects the relative heights of the acoustic peaks and the diffusion damping in the CMB power spectrum, while the matter density is mostly determined via the "potential envelope" effect, i.e., the increase in power for modes that re-entered the horizon before matter–radiation equality. The characteristic scale of this power boost corresponds to the comoving size of the horizon at matter–radiation equality projected on the last scattering surface, which depends on the ratio between the matter and radiation densities. Since ω_Λ is negligible at redshifts $z \geq z_*$, we have everything we need to determine $r_s(z_*)$ via Eq. (2.8).

Then, we obtain the acoustic scale θ_s from the spacing between the acoustic peaks, and, using Eq. (2.7) we derive $D_{\rm A}(z_*)$. As a last step, we adjust ω_Λ in order to match the value of $D_{\rm A}(z_*)$ calculated via Eq. (2.8) with the one inferred as described above. Having determined the physical density of each component, we can finally reconstruct $H(z)$ via Eq. (2.10). For $z = 0$, this provides us with the value of H_0.

Note that θ_s is very tightly constrained by observations. In particular, it is measured to 0.03% accuracy by *Planck* data, which gives $100\theta_s = 1.04109 \pm 0.00030$ using a combination of TT,TE,EE+ lowE data [192]. Other CMB probes measure θ_s to be consistent with Planck, such as $10^4\theta_s = 104.056 \pm 0.031$ from ACT-DR6 (TTTEEE+Planck-Sroll2 EE [703]) and $100\theta_s = 1.04016 \pm 0.00067$ (SPT+WMAP [704]).

2.1.18.4. CMB in combination with other cosmological probes. The same acoustic oscillations that we observe in the CMB are also left imprinted in the galaxy power spectra in the form of BAO. The characteristic scale of BAO is the sound horizon at the drag epoch, $z_d \simeq 1059$ [192], i.e., the time when baryons were released from the drag of CMB photons. This characteristic scale provides us with a cosmological standard ruler that serves as an independent way to measure the expansion rate of the Universe and improve our bounds on the cosmological parameters. Notably, the inclusion of BAO data allows us to better constrain the spatial curvature of the Universe and break the aforementioned geometric degeneracy [714,716]. We refer to Section 2.1.19 for a more detailed discussion of BAO measurements of H_0. In what follows, we report an incomplete list of the most recent estimates of H_0 obtained with the combination of CMB and LSS data, to give a sample of the complementarity and constraining power of these combinations.

A recent analysis of DESI BAO data in combination with Planck PR4 primary anisotropies (using small, commander and CamSpec likelihoods), Planck and ACT-DR6 CMB lensing, leads to $H_0 = 68.17 \pm 0.28\,{\rm km\,s^{-1}Mpc^{-1}}$ [717]. A combined analysis of *Planck* CMB lensing, BOSS DR12 galaxy power spectra, and the PANTHEON+supernova constraints yields $H_0 = 64.8^{+2.2}_{-2.5}\,{\rm km\,s^{-1}Mpc^{-1}}$ [718], by imposing a BBN prior on physical baryon density and assuming ΛCDM cosmology. A multi-tracer full-shape analysis of luminous red galaxy (LRG) and emission line galaxy (ELG) samples from the eBOSS DR16 measures $H_0 = 70.0 \pm 2.3\,{\rm km\,s^{-1}Mpc^{-1}}$in the ΛCDM framework when combining the BBN prior and fixing the spectral tilt n_s to *Planck* value [719]. Another analysis of the BOSS DR12 data by fixing n_s and the baryon-to-DM ratio $\Omega_b/\Omega_{\rm DM}$ to *Planck* value gives $H_0 = 68.5 \pm 2.2\,{\rm km\,s^{-1}Mpc^{-1}}$ [720]. Adopting a forward modeling approach for the BOSS DR12 bispectrum monopole, with BBN prior on $\Omega_b h^2$, [721] found $H_0 = 67.6^{+2.2}_{-1.8}\,{\rm km\,s^{-1}Mpc^{-1}}$. Another study of the BOSS galaxy power spectrum with bispectrum monopole and quadrupole estimated $H_0 = 69.2 \pm 1.1\,{\rm km\,s^{-1}Mpc^{-1}}$ [722] within the ΛCDM model, using BBN and fixing spectral tilt to *Planck* value.

It is crucial to highlight that these results assume a ΛCDM cosmology. A combination of *Planck* TT,TE,EE+lowE, *Planck* lensing, BAO measurements from BOSS and eBOSS, and Pantheon+ SNIa data, assuming a non-flat ΛCDM model yielded $H_0 = 68.24 \pm 0.54\,{\rm km\,s^{-1}Mpc^{-1}}$ with $\Omega_k = 0.0004 \pm 0.0017$ [723]. A similar constraint of $H_0 = 68.53 \pm 0.56\,{\rm km\,s^{-1}Mpc^{-1}}$was found when treating $A_{\rm lens}$ as a free parameter (for more details, see the discussion on the $A_{\rm lens}$ anomaly in Section 2.1.18.5). Extending the analysis to non-flat wCDM model resulted in $H_0 = 67.95 \pm 0.66\,{\rm km\,s^{-1}Mpc^{-1}}$and $\Omega_k = 0.0016 \pm 0.0019$ (see Ref. [723] and references therein). To conclude this list of constraints, the take-home message is that the combination of CMB and LSS measurements provide estimates of H_0 which are in agreement with the (lower) value inferred from Planck alone. This is true also in case of combinations that do not include Planck anisotropies — or do not include Planck data at all — in their fit.

2.1.18.5. The role of potential systematic effects in CMB-based estimates of H_0. Unresolved systematic effects (hereafter systematics) in CMB measurements could potentially bias the cosmological constraints. This possibility has motivated a collective effort to examine potential sources of systematics within the CMB dataset.

Features in the *Planck* spectra (especially temperature and at small scales) have been also interpreted as hints to unsolved systematics. In this context, the $A_{\rm lens}$ anomaly in Planck data is noteworthy. First introduced in Ref. [724], $A_{\rm lens}$ is a phenomenological (somehow "unphysical") parameter used to rescale the effects of gravitational lensing on the CMB angular power spectra. Therefore, the expected value is $A_{\rm lens} = 1$. Interestingly, *Planck* data (primary anisotropies) show a preference for $A_{\rm lens} > 1$ at more than 2σ, increasing to more than 3σ when combined with BAO data [192]. Theoretical explanations for such values are challenging, as it would require either a closed universe, posing conflicts with other datasets and simple inflationary models, or more exotic solutions such as modifications to General Relativity. Furthermore, the lensing anomaly does not appear in *Planck* trispectrum data (i.e., in the lensing power spectrum), which offers an independent and complementary measurement of CMB lensing. If not indicative of new physics or not interpreted as a statistical fluke, the $A_{\rm lens}$ anomaly might arise from an undetected systematics error in *Planck* data and this systematic could potentially bias the measurement of the H_0 parameter. However, when the effect of $A_{\rm lens}$ is marginalized over in the analyses, the *Planck* and *Planck* + BAO constraints on H_0 shift only slightly toward higher values: $H_0 = 68.28 \pm 0.72\,{\rm km\,s^{-1}Mpc^{-1}}$and $H_0 = 68.23 \pm 0.49\,{\rm km\,s^{-1}Mpc^{-1}}$at 68% CL, respectively [192], not enough to provide a satisfying solution to the H_0 tension. If the $A_{\rm lens}$ anomaly is due to systematics which may impact the final H_0 constraints, it raises questions whether the same systematics can be fully captured by $A_{\rm lens}$ alone or if further modeling is needed. Moreover, recent analyses by ACT and SPT, which also find a lower value of H_0 than local measurements, find no deviation from the standard lensing effect predicted by the ΛCDM model [702,703,725], supporting the idea that the $A_{\rm lens}$ anomaly might not be the right solution to the tension.

The consistency of cosmological parameters estimated from different multipole ranges of Planck data has also been investigated extensively in the past years [726–728], sometimes claiming evidence for internal inconsistencies which may impact the H_0 estimates. However, it has been showed [715] that the shifts in cosmological parameters recovered from different ranges — mostly due to the combined effects in temperature of non-lensing-related residuals at high multipoles and power deficit at large scales ($\ell < 30$) - are not very significant and consistent with sample variance.

In the context of potential systematics in CMB data, it is also worth mentioning that the mild discrepancy seen between ACT-DR4 and both WMAP and Planck has been solved with the final data release of ACT. Indeed, ACT-DR6 finds very good agreement with both Planck Legacy data (PR3) and Planck PR4 (NPIPE) already at the power spectrum level [703]. In terms of cosmological parameters, the difference between the best fit values in ΛCDMobtained with ACT-DR6 and Planck is estimated to be within 1.6σ (for Planck Legacy) and 2.5σ (for Planck PR4), see [703,706] for details.

As far as SPT results are concerned, good agreement has been found [704] between SPT and Planck, both at the power spectrum level

(in TT over angular scales that are signal-dominated in both experiments) and at the cosmological parameter level (assuming ΛCDM). As noted by the SPT collaboration, this excellent agreement between two effectively independent experiments (given the negligible overlap between observed sky fractions and different sensitivity to angular scales) is a strong argument in favor of the robustness of the results and of the consistency of ΛCDM across different scales and spectra. A good agreement has been found also between SPT and WMAP. The agreement between SPT and ACT is acceptable [704], with the largest shift in recovered ΛCDM parameters being on θ (2σ larger in ACT than in SPT). However, a multi-dimensional statistical test results in no significant deviations to be noted and agree with an explanation in terms of statistical fluctuations.

Another crucial aspect of the CMB data analysis to be explored in the context of H_0 estimation is the possible impact of instrumental systematic effects. In CMB data analysis, particular care is devoted to the quantification of residual systematics, which are corrected for through the pipeline and/or propagated in the likelihood analysis either by incorporating it in the noise model or modeling specific residuals in the data vector. In this context, the use of end-to-end simulations is key. Among the different sources of systematics, beam characterization and instrument calibration (especially in polarization) are particularly worrisome. As an example, the determination of polarization efficiencies is considered one of the main limitations of the Planck data products [729]. Nevertheless, the use of a large suite of null tests and cross-checks on several data splits, and the comparison with realistic end-to-end simulations allow us to show, for all the data products released by the main CMB experiments, that possible biases of cosmological parameters — included H_0 — induced by residual systematics are small-to-negligible [702,704,707,729–732]. Similar analyses on dedicated simulations for next generation CMB experiments have recently shown that, even in the presence of unaccounted-for systematics (i.e., effects which have not been corrected for in the analysis pipeline) due to, e.g., beam chromaticity, bandpass mismatch, polarization angle miscalibration and incorrect calibration in polarization, the bias on H_0 is at the level of a small fraction of σ [733,734]. Therefore, we conclude that instrumental systematic effects cannot be the (only) source of discrepancy between the CMB-based estimate of H_0 and local measurements.

Finally, the interplay between instrumental systematics and foreground contamination can have non-linear effects on the final results, potentially biasing cosmological parameter estimates, including the Hubble constant. The presence of galactic and extragalactic foregrounds, such as dust emission and radio sources, complicates the separation of the CMB signal from other astrophysical contributions. This complexity underscores the need for precise modeling and mitigation strategies to ensure accurate parameter estimation, but it is unlikely the source of the H_0 tension.

2.1.18.6. S_8 tension. The amplitude of the CMB power spectrum, especially CMB lensing, places stringent constraints on the matter density and hence on σ_8. Here, we briefly address the tension related to the amplitude of matter clustering in the late Universe, described by the parameter $S_8 \equiv \sigma_8(\Omega_{\rm m,0}/0.3)^{0.5}$. For a more detailed discussion, refer to Section 2.2.

CMB-based estimates of S_8 are consistently larger than those derived from galaxy-based measurements [192,695,700–702,704,707]. Observations of weak gravitational lensing at low redshifts ($z \lesssim 0.5-1$) indeed suggest weaker matter clustering than predicted by the ΛCDM model with parameters inferred from CMB data. Simply put, the distribution of galaxies and matter in the late Universe appears smoother than expected based on the evolution of the fluctuations seen in the CMB. The CMB estimate of S_8 is model-dependent and can shift with other parameters that affect the growth and amplitude of matter fluctuations. Notably, the optical depth to reionization (τ), which carries the largest uncertainty among the ΛCDM parameters, and the sum of neutrino masses ($\sum m_\nu$), which is a derived parameter and is usually fixed. Uncertainties in these parameters affect the derived S_8 constraints. Additionally, *Planck*'s excess lensing anomaly, as discussed in Ref. [735], can mimic a larger S_8. However, the CMB-LSS tension persists even without *Planck*'s lensing excess, as shown by the latest ACT+WMAP analysis [703,706], which reports a high value of $S_8 = 0.857 \pm 0.020$ without an anomalous lensing amplitude, and SPT-3G analysis [707], which is independent of temperature data and reports $S_8 = 0.850 \pm 0.017$.

On the theoretical side, efforts to resolve the S_8 tension involve modifying the matter or gravity sectors of the ΛCDM model, leading to a range of alternative cosmological scenarios (see e.g., Sections 4.1 and 4.2 for more details). Although some models alleviate the S_8 tension, most fail to provide consistent solutions when all cosmological probes are considered. In particular, due to the correlation between H_0 and S_8, models that resolve the S_8 tension often worsen the H_0 tension, and vice versa [736–738]. For example, late-time dark sector transitions, which prefer a higher H_0 value, often result in lower $\Omega_{\rm m,0}$ to preserve the measured value of $\Omega_{\rm m,0}h^2$, leading to changes in structure growth and CMB anisotropies and typically yielding a higher σ_8 than ΛCDM due to extended matter domination. Similarly, EDE models that address the H_0 tension tend to increase σ_8 because they require a higher initial curvature perturbation amplitude to counterbalance the unclustered component. It is therefore crucial to perform joint analyses fitting a full array of multiple datasets, without fixing any of the parameters of the model. Simultaneously any solution to the S_8 tension must be consistent with the growth history (typically studied through the parameter $f\sigma_8(z)$), probed by e.g., BAO, galaxy power spectrum, and void measurements.

2.1.19. *Baryonic acoustic oscillations*

Coordinator: Florian Beutler

Contributors: Armando Bernui, David Benisty, Denitsa Staicova, Felipe Avila, Ignacio Sevilla-Noarbe, Özgür Akarsu, Maret Einasto, Mustapha Ishak, Nicola Deiosso, Rafael C. Nunes, Ruchika, Samuel Brieden, and Sveva Castello

BAO represent a characteristic scale in the distribution of galaxies, or more generally of any tracer of the matter density field [739,740]. This scale, known as the sound horizon r_d, originated from sound waves traveling through the early ($z \gtrsim 1060$) Universe before baryons and photons decoupled (see Refs. [741–743] for reviews of the subject). We can employ this scale as a standard ruler, which allows us to measure the expansion history of the Universe. In practice, the BAO features can be extracted from the two-point correlation function of galaxies, where it appears as a peak [744,745], or from the Fourier-space equivalent, the power spectrum, where it is manifested as a series of oscillations [746–748]. In the following, we will review the different methods to extract the BAO scale from the galaxy distribution. We will then discuss the most recent measurements from DESI.

2.1.19.1. Methods. The 3D position of a galaxy can be determined by measuring its location on the sky (in right ascension and declination) and its redshift. For this reason, measuring the BAO scale in the perpendicular direction to the line-of-sight and along the line-of-sight provides constraints on slightly different quantities. The angular component constrains the comoving angular diameter distance $D_{\rm M}/r_d = 1/\Delta\theta$, where $\Delta\theta$ is the angular separation of the pair of galaxies, while the line-of-sight component constrains the comoving Hubble distance $D_{\rm H}/r_d = 1/\Delta z$, where Δz is the redshift separation of the galaxy pair. In the Friedmann–Lemaître–Robertson–Walker (FLRW) metric, the comoving angular diameter distance $D_{\rm M}$, the related $D_{\rm A}$ and the Hubble distance $D_{\rm H}$ are given by

$$D_{\rm M} = \frac{c}{H_0\sqrt{|\Omega_K|}}\,\mathrm{sinn}\left[|\Omega_K|^{1/2}\int_0^z \frac{dz'}{E(z')}\right], \quad D_{\rm A} = \frac{D_{\rm M}}{1+z}, \quad D_{\rm H} = \frac{c}{H_0 E(z)}, \tag{2.11}$$

where $\mathrm{sinn}(x) \equiv \sin(x)$, x, $\sinh(x)$ for $\Omega_K < 0$, $\Omega_K = 0$, $\Omega_K > 0$ respectively, and $E(z)$ is the normalized Hubble function. Rather than separating D_M and D_H, often measurements are reported as a combination of the two given by $D_\mathrm{V} \equiv \left[z D_\mathrm{M}(z)^2 D_\mathrm{H}(z)\right]^{1/3}$. BAO constraints from photometric galaxy surveys usually have significant redshift uncertainties that only allow for constraints on D_M. One important point to note from the equations above is that BAO measurements always constrain distances relative to the sound horizon scale. This introduces degeneracies between cosmological parameters and the sound horizon scale r_d. In ΛCDM for example, BAO can only constrain $H_0 r_d$, and breaking this degeneracy is crucial to obtain measurements of H_0 and provide key information in light of the Hubble tension. We will discuss this further in Section 2.1.19.3.

The density field sources a velocity field that will displace galaxies away from their initial position, effectively leading to a redshift-dependent smoothing of the localized BAO feature. This effect can reduce the signal-to-noise by up to a factor of two at low redshift (e.g., see Ref. [749]) and also results in a sub-percent level systematic biasing of the BAO scale [750,751]. Given that the velocity field is sourced by the density, one can estimate the displacement of galaxies assuming standard gravity and correct for this effect [751,752]. Such techniques are known as density field reconstruction and are routinely applied to most spectroscopic BAO measurements.

The standard BAO analysis relies on converting the angular position and the redshift into Cartesian coordinates, from which the 3D clustering statistics can be calculated. This step requires adopting a fiducial cosmology, which typically is taken to be a flat ΛCDM model with parameters based on the CMB. The BAO analysis accounts for these assumptions by including geometric scaling parameters and so far studies with alternative models (e.g., EDE or MG) have not found that the fiducial cosmology assumptions inflict any significant bias in the standard BAO analysis [753–756]. Through density field reconstruction, the standard analysis also makes assumptions about the connection between the measured galaxy density field, the matter density field, and the large-scale velocity field. However, just like with the fiducial cosmology assumptions, the impact on the measurements has been shown to be negligible (e.g., see Refs. [757,758]). Assumptions about the number of relativistic particles, N_eff at high redshift have been shown to impact the BAO phase and could bias BAO measurements [759,760]. The standard analysis usually fixes this parameter to the standard model value. While a Planck prior on N_eff (within ΛCDM) reduces any potential bias to well below the uncertainties of current measurements, one still should be aware of these prior assumptions.

Given the priors implicit in the standard BAO analysis, alternative analysis methods have been developed that can (at least partly) avoid the assumption of a fiducial cosmology [761]. This technique often runs under the name *transverse BAO* [762,763], which should not be confused with the many angular BAO measurements in the literature which follow the standard analysis technique described above (see e.g., DES Y6 in Fig. 30). The basic idea of such methods is to bin the data into redshift bins and measure the angular BAO signature in those redshift bins through two-point angular-clustering statistics, avoiding the need to convert redshifts into distances. However, to account for the redshift evolution within the redshift bin one still needs to use a fiducial cosmology, and density field reconstruction is generally not applied in such cases. For this reason, such methods usually have much larger measurement uncertainties (see e.g., see Refs. [764–770]).

2.1.19.2. BAO measurements. The BAO feature has been measured both with photometric and spectroscopic surveys. Photometric surveys allow for a direct identification of a huge number of galaxies, but generally only provide poor photometric redshift information. Even for measurements of the angular BAO scale, the redshift information is necessary to split the sample into redshift bins, to avoid the smearing of the BAO signal due to its redshift evolution. Although the photometric redshift quality can be improved with an adequate subselection, this usually also reduces the number of galaxies in the sample [771]. To date, the best photometric BAO measurement comes from DES year-6 analysis using about 16 000 000 galaxies and yielding a 2.1% constraint on D_M/r_d [772]. Observational systematics for such measurements are dominated by uncertainties in the redshift distribution, which are nevertheless still below the statistical error budget.

Compared to photometric surveys, spectroscopic surveys have the advantage of providing precise redshift measurements and detailed spectral information. This is achieved through the identification of specific spectral lines or features, such as the Hα, Hβ, OII lines or the 4000 $\AA$ break for galaxies, and broad emission lines for QSOs. The Lyman-α (Lyα) forest represents a series of absorption features in the spectra of distant QSOs that can be used to map the distribution of intergalactic hydrogen gas and provides additional BAO measurements at higher redshift [773].

The first convincing detections of the BAO signal in the distribution of galaxies came from the 2-degree Field Galaxy Redshift Survey (2dFGRS) and the Sloan Digital Sky Survey (SDSS) in the early and mid-2000s [744,746,774], while the first detection in the Lyα forest was made by the BOSS [775]. There have been many more subsequent detections in other galaxy surveys [748,749,776–782]. The best constraints to date come from DESI, which measured the BAO signal in 8 independent redshift bins with a detection significance ranging from 3.3 to 9.1σ [745,783]. A comparison between these DESI measurements and previous BAO measurements is shown in Fig. 30.

Observational and instrumental systematics, such as fiber collisions [784], distortions due to peculiar velocities (Redshift-Space Distortions (RSD)), non-linear matter and galaxy clustering, atmospheric dispersion, and spectrograph calibration are critical factors in any analysis based on spectroscopic surveys datasets. Since the BAO signal is located on very large scales ($r_d \sim 150\,\mathrm{Mpc}$) and represents a distinguishable feature unlikely to be mimicked by any instrumental or physical process, BAO measurements have proven to be very robust (see e.g., see Ref. [758]). The galaxy clustering analysis of DESI identified the galaxy-halo connection (HOD) as the dominant systematic for their BAO measurement. However, all combined systematics still only added 5% to the final statistical error budget even for the highest precision BAO measurement (see table 13 and 15 in Ref. [783]).

The BAO signal is most commonly measured as a mixture of radial and transversal modes. Alternatively, the BAO signature can be extracted in a thin redshift bin using the two-point angular-clustering statistics (where the angular separation of pairs instead of the comoving distances are computed, avoiding converting redshifts into distances using a fiducial cosmology), providing a measurement of the transverse BAO, $\Delta\theta_\mathrm{BAO}(z)$. The finer the redshift bin, the purer this transverse contribution. If r_d is known, $\Delta\theta_\mathrm{BAO}(z)$ determines $D_\mathrm{M}(z)$, as explained in Section 2.1.19.1. Fig. 30 shows such transverse BAO measurements from SDSS data (labeled SDSS-tr) derived in Refs. [762,763,785–788]. However, for the remainder of this section, we will focus on the most recent DESI analysis.

2.1.19.3. BAO and the H_0 tension. One of the challenges in the use of BAO measurements in cosmology is the degeneracy between the sound horizon r_d and Hubble constant H_0. As mentioned in Section 2.1.19.1, this arises because all measurable quantities in the BAO data depend on the product $c/H_0 r_d$. The only way to decouple them is by using additional information beyond the BAO scale [713,718,789–796] or imposing an external prior on r_d from the CMB or BBN [699,713,797]. The 2024 DESI BAO results combined with a BBN prior from Ref. [798] yield a constraint of $H_0 = 68.53 \pm 0.80\,\mathrm{km\,s^{-1}Mpc^{-1}}$ [783]. This measurement is independent of the CMB and solely based on DESI BAO + BBN. While this value of the Hubble constant is slightly higher than the one preferred by Planck [192] as well as the one reported in previous data from SDSS [797], it is still in 3.4σ tension with the $SH0ES$ result of Ref. [78]. Fig. 31 shows the values for H_0 and $\Omega_{\mathrm{m},0}$ inferred from the DESI data, along with the $SH0ES$ results on H_0 as a shaded band. One

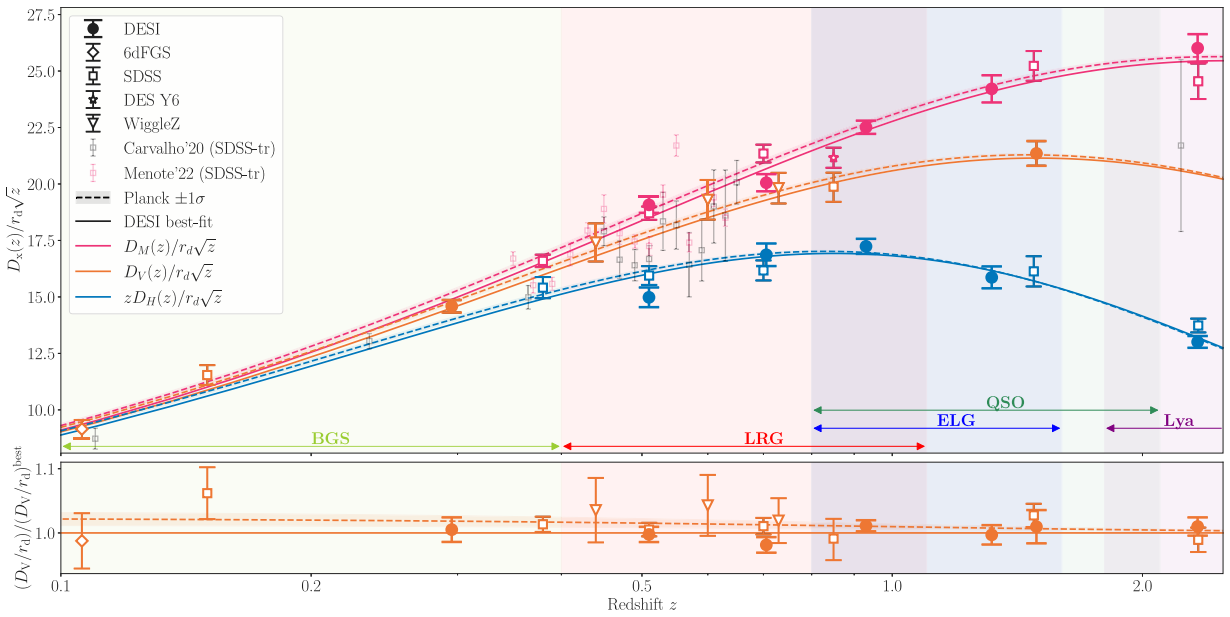

Fig. 30. DESI BAO measurements (filled circles) compared to prior BAO measurements (empty symbols) from spectroscopic (6dFGS, WiggleZ, SDSS) and photometric (DES Y6) surveys, where SDSS includes the MGS, BOSS DR12 and eBOSS DR16 galaxy and Lyman-α Samples. Additionally, we show the transverse BAO measured from SDSS catalogs (SDSS-tr) in thin redshift shells, neglecting the longitudinal modes. Note that these measurements are not official SDSS products, but were instead obtained independently in Refs. [763,785–788] (small gray squares) and Ref. [762] (small pink squares). Horizontal arrows and colored regions indicate the redshift range spanned by each DESI tracer type. Solid lines show BAO distances (scaled by $\sqrt{z}$ for improved visibility) as a function of redshift z for the standard flat ΛCDM DESI best-fit, and dashed lines indicate the Planck best-fit with shaded region denoting the $\pm1\sigma$ regime. **Upper panel:** Comparison between transverse (pink), radial (blue), and isotropic (orange) BAO measurements, where the latter is only displayed for data that does not exhibit an anisotropic measurement due to low signal-to-noise. **Lower panel:** Isotropic BAO distance residuals where the anisotropic BAO measurements from the upper panel (apart from DES-Y6 and SDSS-tr, which do not measure radial BAO) have been combined into an isotropic measurement (not shown in the upper panel to avoid redundancy). (For interpretation of the references to colour in this figure legend, the reader is referred to the web version of this article.)

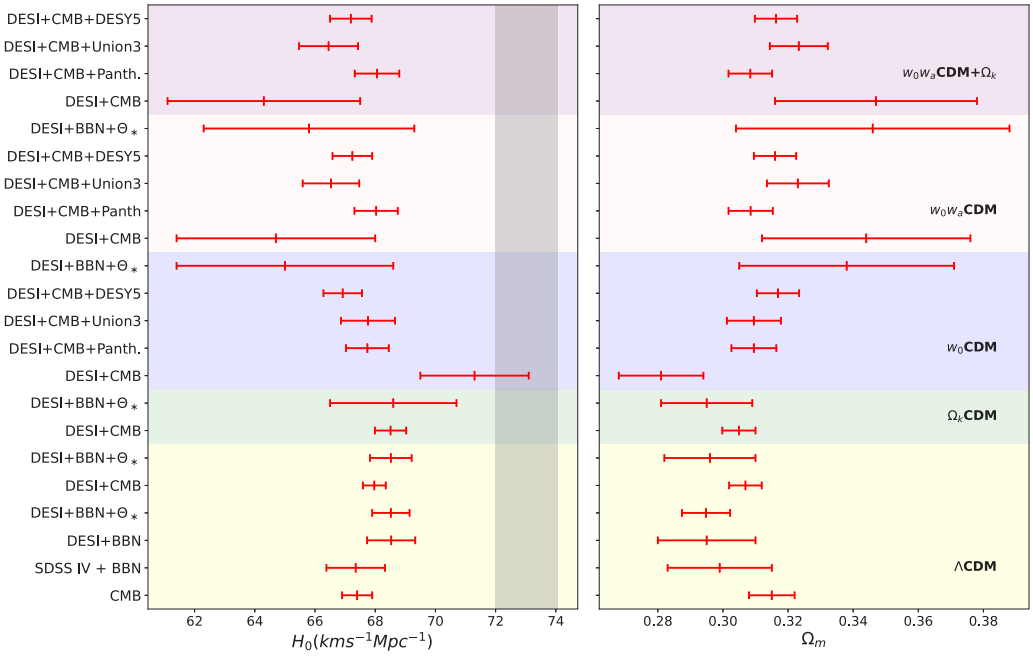

Fig. 31. 68% credible-interval constraints on the Hubble constant H_0 (left panel) and the matter density $\Omega_{m,0}$ (right panel), assuming different cosmological models and different combinations of datasets (on the plot, DESI, Planck 2018, Pantheon Plus, DESY5, Union3) and the BBN and θ_* priors. The gray band indicates the SH0ES measurement for H_0.

sees that only the w_0CDM model comes close to resolving the Hubble tension for the DESI+CMB dataset to the price of much lower matter density. A further look at the DESI results is presented in Fig. 32, where we show the 1σ posteriors for some of the models presented in Fig. 31. In this figure, the degeneracy between H_0 and $\Omega_{m,0}$ manifests as the covariance of the inferred data, which is particularly visible on the right panel of Fig. 32 zooming in on the DESI+BBN models. This leads to the known issue that, across different models, increasing H_0 generally decreases $\Omega_{m,0}$, and vice versa. On the plots, r_d is missing since it is not a free parameter for all tested models.

BAO measurements rely on a model-dependent extrapolation to redshift zero when constraining the Hubble constant. However, combining BAO with SNIa datasets and the CMB does constrain the redshift

evolution and makes it difficult to find extensions to ΛCDM that could resolve the Hubble tension [238,789,799–802].

Ref. [803] has found that marginalizing over r_d can lead to a degeneracy between H_0 and the primordial power spectrum and to a model-dependent H_0 measurement. A similar observation has been published in Ref. [804] showing that models that only reduce r_d cannot resolve the Hubble tension while at the same time remaining consistent with other cosmological datasets. A possible solution to this consists of working with the sound horizon as a free parameter (thus not making any assumption concerning the recombination physics) and using other quantities to break the degeneracy [805–807]. In these works, it was shown that while this approach can produce interesting results when examining ΛCDM alternatives, it does not solve the Hubble tension. Another approach consists in marginalizing over both r_d and H_0 [808], which integrates the quantity $c/H_0 r_d$ out of the likelihood (χ^2) and thus removes entirely the dependence on these parameters from the theoretical predictions. The results obtained in this way show a slight preference for Dynamical Dark Energy (DDE) models but they do not solve the Hubble tension.

While early BOSS and eBOSS Ly-α BAO results showed a 1.5 to 2.5σ tension with Planck-ΛCDM [789,797], the most recent Ly-α analysis in DESI [745] shows no tension anymore. However, DE density reconstructions using DESI BAO still suggest the possibility of zero or negative DE densities for $z \gtrsim 1.5$–2 in some dataset combinations [809]. Additionally, a shift of the Ly-α BAO peak at the 2.2σ and 3.5σ levels in real and redshift space, respectively, was recently suggested in Ref. [810]. The reasons behind these findings are yet to be understood, warranting further investigation. Since the comoving angular diameter distance to last scattering, $D_{\rm M}(z_*)$, is strictly constrained by CMB data almost model-independently, a lower $H(z)$ for $z \gtrsim 1.5$–2 due to vanishing or negative DE density should be compensated by a higher $H(z)$ for $z \lesssim 1.5-2$, provided that the pre-recombination Universe is not modified [801,802,811–813]. This results in a higher H_0 and correspondingly smaller $\Omega_{\rm m}$, which can reduce the S_8 value and address the most discussed tensions in the ΛCDM model [801,802,811–813].

The most recent DESI data release, DESI DR2, improves on the DR1 findings, analyzing over 14 million galaxies and QSOs from three years of observations (surpassing SDSS in the effective volume of all tracers). Compared to DR1, the precision of BAO measurements has increased by approximately a factor of two, with uncertainties reduced to about 0.24% for galaxy/QSO measurements and 0.65% at high redshift from the Lyman-α forest (which is now twice the DR1 sample). The DESI DR2 combined with a BBN prior yield $H_0 = 68.51 \pm 0.58\,{\rm km\,s^{-1}Mpc^{-1}}$-28% more precise than DR1. The cosmological analysis shows stronger evidence for evolving DE, with statistical significance amounting to $2.8\sigma, 3.8\sigma$ and 4.2σ depending on which datasets are combined with DESI (Pantheon +, Union3 or DES Y5) and 3.1σ for DESI+CMB. The results show a preference for a DE equation of state with $w_0 > -1$ and $w_a < 0$ and a possible phantom crossing in the past. While the degeneracy direction for the constraints in the $w_0 - w_a$ plane approximately points toward the ΛCDM solution, the statistical evidence consistently challenges the standard ΛCDM across multiple analysis approaches and dataset combinations [717].

2.1.19.4. Outlook. The DESI experiment is expected to publish its Y3 BAO analysis in 2025, while the final Y5 analysis should be made public in 2026/27 [814]. The final dataset will be three times larger than the current Y1 catalog, and proposals for a DESI extension until 2029 and a second phase (DESI-II) well into the 2030s are under consideration. At the same time, the Euclid mission has also started, with the first cosmology analysis expected in 2025/26 [164], and the Vera Rubin Observatory will see first light in 2025.

On a longer timescale, there have been several proposals for stage-V spectroscopic experiments with a start in the early to mid-2030s. These experiments increase the telescope aperture and the spectroscopic multiplexing capabilities with the aim of collecting hundreds of millions of galaxy redshifts (e.g., see Refs. [407,815–817]). After the DESI mission is completed, the BAO signal in the low redshift Universe ($z \lesssim 1$) will have been measured up to the sample variance limit over almost the entire sky available for cosmological measurements ($\sim$ 15 000 to 18 000 deg^2), see figure 16 in Ref. [818]. Future experiments therefore focus on the high redshift regime, where significant gains are still possible.

2.2. S8 tension: measurements and systematics

2.2.1. Weak lensing

Coordinator: Marika Asgari, Daniela Grandón, Cora Uhlemann

Contributors: David Sanchez Cid, Ignacio Sevilla, Judit Prat, Konrad Kuijken, Maciej Bilicki, Markus Michael Rau, Masahiro Takada, Nikolina Šarčević, and Shun-Sheng Li

Cosmic shear is one of the key probes of the LSS. A cosmic shear analysis measures the weak gravitational lensing signal [819–824] imprinted in the observed galaxy shapes by LSS (see Ref. [825–827] for a review and references therein). The strength of this signal depends directly on the total matter distribution between the source galaxies and the observer. Therefore, cosmic shear provides a precise mapping of the projected matter density field, capturing its statistical properties and enabling constraints on cosmological parameters.

To perform a cosmic shear analysis, we need a galaxy catalog that comprises two measurements: galaxy shapes (Section 2.2.1.1) and the redshift information (Section 2.2.1.2). The redshifts are used to divide source galaxies into tomographic bins. The redshift distribution in each bin determines the strength of the lensing effect and serves as an input for the theoretical predictions of the cosmic shear signal, which require prescriptions for baryonic effects (Section 2.2.1.3) and the intrinsic alignment of galaxies (Section 2.2.1.4). In addition, the tomographic analysis allows us to extract information about the evolution of structures and to disentangle the astrophysical systematics from the cosmological information.

The most commonly used estimator for the cosmic shear signal is the two-point statistic. In real space, the two-point shear correlation functions are measured as the average correlation between the shapes of galaxy pairs in parallel and orthogonal directions as a function of their angular separation [828]. Both of those correlations can be related to one angular convergence power spectrum, which is a line-of-sight projection of the matter power spectrum, and thus sensitive to non-linear effects on small scales and low redshifts. However, because the lensing field is a non-Gaussian random field, cosmic shear surveys have also implemented estimators that capture information beyond the traditional two-point statistics [829]. These higher-order or non-Gaussian statistics, such as the three-point shear correlation function [830–833], the bispectrum [834,835], the lensing convergence PDF [836–839] or its moments [840], and peak statistics [841–844], among others [845–848], have proven effective in enhancing the constraining power and promise to be valuable in Stage IV analysis [829,849].

Cosmic shear analysis is most sensitive to the S_8 parameter and the strength of the intrinsic alignment signal of galaxies. In fact, with the available data, S_8 is the only cosmological parameter that cosmic shear analysis can robustly constrain from two-point statistics. A joint analysis of two-point function and higher-order statistics however can improve constraints in $\Omega_{\rm m,0}$, as well as self-calibrate systematics and break degeneracies between cosmological and nuisance parameters. These surveys consistently infer S_8 values that are 1–3σ lower than what is expected from the CMB anisotropies.

The current generation of Stage III cosmic shear surveys — such as the KiDS [850,851], DES [852,853], the Subaru HSC Survey [854–856] and the Dark Energy Camera All Data Everywhere (DECADE; [857]) — have conducted multiple cosmic shear analyses from at least two separate data releases. These surveys consistently infer S_8 values that are 2–3σ lower than what is expected from the CMB anisotropies and

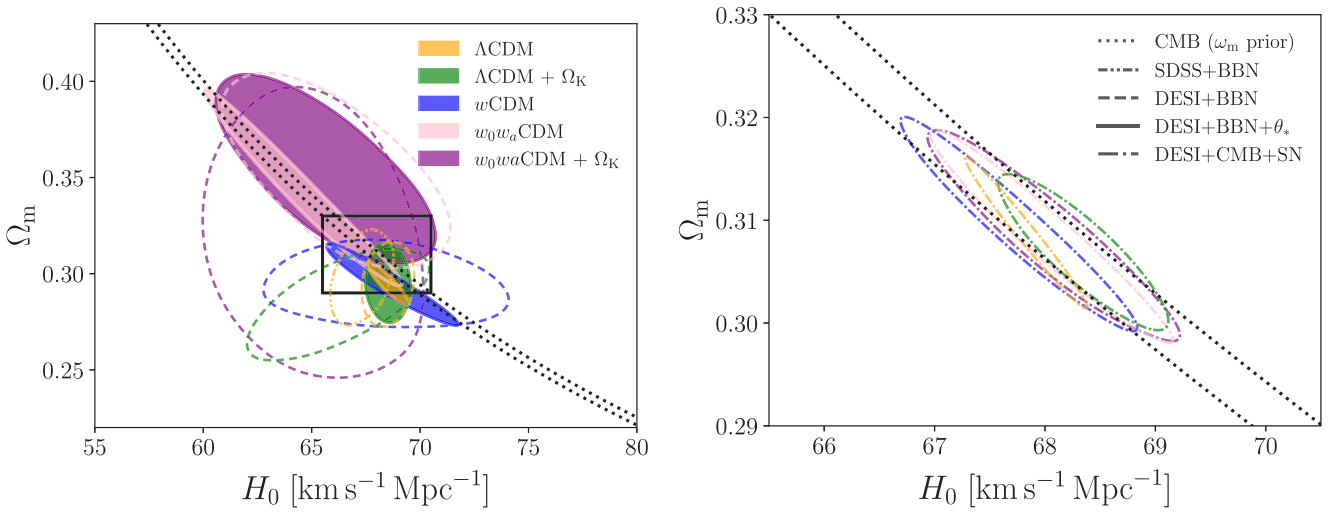

Fig. 32. Illustrations of the degeneracy between the Hubble constant and the matter density parameter ($\Omega_{\rm m,0}$) constrained by different data combinations (indicated by line style) for different models (indicated by color) at 1σ. "CMB" refers to Planck + ACT lensing data and "SN" to the Pantheon+ SNIa sample. The parameter region constrained by CMB alone is shown as a prior on $\omega_{\rm m}$ (black dotted contours) that is independent of the late-time model extensions considered here. The most constraining data combination (DESI+CMB+SN) is shown on the right as a zoom into the black rectangle on the left for better visibility. For conciseness, the SDSS BAO + BBN constraint (dash-dot-dotted) is shown for ΛCDM (orange) only. Note that the legends shown in the left and right panels apply to both simultaneously.

CMB lensing measurements by *Planck* and ACT [855,856,858–864]. A summary of these results is presented in Fig. 33. This disagreement in the S_8 value between early- and late-time probes, often referred to as the S_8 tension, was first observed between the tomographic analysis of the Canada France Hawaii Telescope Lensing Survey (CFHTLenS) [865] and the first *Planck* cosmology results [866], at the level of 2.3σ. More recently, the DES and KiDS teams collaborated on a unified analysis pipeline which resulted in a joint constraint with a slightly higher value of S_8, translating to a 1.7σ difference with *Planck* [867]. The most recent KiDS results (KiDS-Legacy) shows consistent results with Planck at the level of 1σ. The most recent KiDS results (KiDS-Legacy) show consistent results with Planck at the level of 1σ [868].

The "3 × 2pt" analysis has emerged in the past decade as a mature cosmological probe that extends cosmic shear by incorporating two additional two-point correlations: galaxy-galaxy lensing (the cross-correlation of lens galaxy positions and source galaxy shapes) and photometric galaxy clustering (the autocorrelation of lens galaxy positions). The primary advantage of this combination is its ability to break the degeneracy between $\Omega_{\rm m,0}$ and σ_8, enabling robust constraints on $\Omega_{\rm m,0}$ in addition to S_8, as well as improving the self-calibration of the nuisance parameters, especially of the intrinsic alignment and redshift parameters. The three major current-generation surveys have conducted this kind of analysis, with their results presented in Fig. 33. Generally, the S_8 values measured by 3 × 2pt have been found to be $\sim$ 1–2σ below the *Planck* value predicted assuming ΛCDM cosmology, thus with a slightly smaller tension with respect to the cosmic shear results.

A summary of the S_8 constraints from low-redshift probes, including lensing surveys, is shown in Fig. 4. In particular, results from peak count analyses — the most studied higher-order statistic — are presented for KiDS-1000 [841], DES Y3 [877], and HSC Y1 [842]. The most precise constraints on S_8 come from the DES Y3 peak counts analysis, yielding $S_8 = 0.797^{+0.015}_{-0.013}$, which is in 1.5σ tension with Planck 2018 [192]. The recently published KiDS-Legacy COSEBIs results report $S_8 = 0.815^{+0.016}_{-0.021}$, showing less than 1σ disagreement with Planck [868]. On the other hand, a shear two-point correlation function analysis using only blue (star-forming) galaxies in DES Y1 yields $S_8 = 0.822^{+0.019}_{-0.020}$ [878], indicating no tension with Planck CMB results. These findings highlight the importance of mitigating astrophysical systematics — such as intrinsic alignments — to better understand the nature of the s_8 discrepancy.

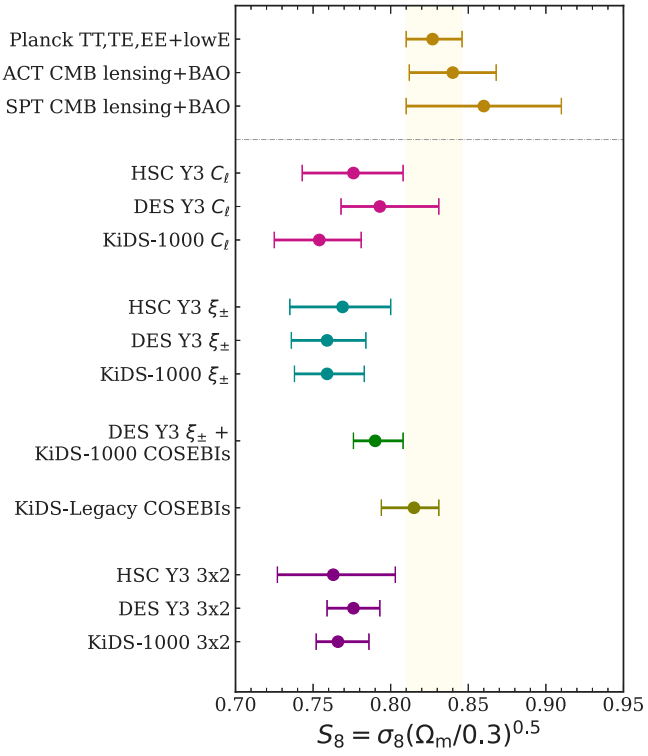

Fig. 33. The S_8 constraints derived from the Stage III WL surveys DES Y3 [861,862,869,870], HSC Y3 [864,871–873], KiDS-1000 [860,874,875] and KiDS-Legacy [868] from two-point shear statistics in harmonic space using C_l or in angular space using $\xi_\pm$, COSEBIS and 3 × 2-point statistics including galaxy clustering. Also shown is the joint constraint from DES Y3+KiDS-1000 [867]. We include the CMB measurements from the Planck satellite [694], ACT [695], and SPT [876] on top for comparison. The error bars denote 1-σ uncertainties.

The constraints on S_8 and other cosmological parameters can also be affected by the adopted statistical inference pipeline. Most cosmic shear analyses use a Gaussian likelihood, which is defined using the data, the theoretical predictions, and the data covariance matrix (for exceptions employing simulation-based inference (SBI), e.g., see Ref. [879–881]).

Studies have shown that an accurate estimation of the covariance matrix is crucial to avoid biases in cosmological constraints [882, 883]. Additionally, properly accounting for likelihood asymmetry in two-point functions is essential for robust parameter inference [884].

In this section, we focus on weak gravitational lensing and the associated systematics that influence cosmic shear cosmological constraints. These systematics can be broadly categorized as observational or theoretical. Observational systematics affect either the accuracy of shape measurements or the redshift distributions. On the theoretical side, achieving percent-level precision in predicting the matter power spectrum is required across a wide range of scales [885], determined by the survey depth and analysis choices. Since these scales extend into the nonlinear regime, an accurate nonlinear power spectrum prescription is necessary. Additionally, two key astrophysical systematics — intrinsic galaxy alignments and baryonic feedback — remain among the least understood aspects of theoretical modeling for this signal. Various modeling approaches have been developed to address these issues, which can generally be categorized into emulators based on N-body simulations [886,887], and the more widely used halo model-based approaches, see Ref. [888] for a recent review, such as `halofit` [889, 890] and `HMcode` [891,892]. While emulators may offer greater accuracy within the specific parameter range they are trained on, they lack the flexibility of halo model approaches, which are capable of extrapolating beyond this range. As a result, most cosmic shear analyses to date, including all of the flagship publications by current surveys have relied on the latter. To limit the contributions from small scales, suitable linear combinations of the signal can achieve a nulling of the effective WL kernel [893]. This can be used to perform scale cuts in physical rather than angular space and render predictions more robust to small-scale physics, e.g., see Ref. [894,895]. While this discussion focuses on current cosmic shear surveys, the next generation of cosmic shear observations (Stage IV surveys) is approaching [437,896,897]. As constraints tighten, more precise modeling and calibration will be required. Consequently, the interplay of these systematic effects will become increasingly important in future analyses.

2.2.1.1. Observational effects: Shape measurement and calibration. Extracting WL signals from observed galaxy images is a non-trivial task. The cosmic shear signal is typically orders of magnitude smaller than the intrinsic galaxy ellipticities, necessitating robust statistical measurements of a large number of galaxies. Furthermore, systematic biases introduced by various instrumental and measurement effects further complicate the process. While the statistical limitations are readily overcome with the ever-growing galaxy samples in ongoing and upcoming WL surveys; addressing the systematic biases remains a challenging task. This challenge is further exacerbated by increasingly stringent requirements driven by the growing statistical power of these surveys. For upcoming Stage IV surveys, the overall residual shear biases must be reduced to the order of 10^{-3}, compared to the current percent-level requirements of Stage III surveys, e.g., see Ref. [898]. Achieving this stringent requirement demands continuous development of shear measurement and calibration techniques, with particular attention to subtle effects arising from object detection, blending, selection, and redshift estimation.

Shape measurement and data-based calibration Given the critical importance of accurate shear measurement, the WL community has dedicated significant early efforts to developing robust shear measurement algorithms. A number of methods have now achieved an overall bias at the percent level. Broadly, these shear measurement methods can be categorized into two main classes: moment-based methods, e.g., see Ref. [899] and model-fitting methods, e.g., see Ref. [900, 901]. Moment-based methods estimate galaxy ellipticities from the second moments of observed galaxy images after correcting for the point-spread function (PSF) caused by instrumental and observational effects. Conversely, model-fitting methods employ forward modeling with PSF-convolved parametric galaxy profiles. These techniques are susceptible to specific biases. Moment-based methods are affected by missing pixels, and contamination by light from detected and undetected neighboring galaxies, whereas model-fitting approaches suffer from "model bias". Additionally, both are affected by common biases such as "noise bias" and selection effects, see Ref. [902] for a recent review. These biases need to be calibrated and corrected for shear measurement methods to meet the requirement of modern WL surveys.

A recent significant advancement in shear measurement algorithms is the introduction of self-calibration or meta-calibration procedures that serve as a first-order correction to the initial shear measurement, e.g., see Ref. [903,904]. These techniques, which can rely on model profiles, observed galaxy images, or priors from deep observations, have demonstrated the ability to control the residual shear bias to a percent or sub-percent level, nearly meeting the requirements of current Stage III surveys, e.g., see Ref. [905–907]. However, these data-based calibrations cannot correct biases introduced at the detection stage as required for the accuracy of Stage IV surveys, e.g., see Ref. [908].

Detection biases and simulation-based calibration Detection biases arise primarily from blending, where the light of neighboring galaxies overlaps in the image plane. Pixel noise and PSF convolution further exacerbate these effects, introducing shear-dependent detection biases, e.g., see Ref. [909–912]. Because these biases arise before shear measurement and are already imprinted in the data, they are difficult to calibrate using observations alone. Meta-calibration methods attempt to correct detection biases by introducing an additional detection step, known as metadetection, but this becomes challenging when accounting for redshift estimation [913]. Furthermore, the shear of galaxies varies with their environment and redshift, resulting in redshift-shear interplay effects that cannot be calibrated with observational data where the true shear is unknown, e.g., see Ref. [905,907]. Thus, simulation-based calibration is essential for shear measurement methods to meet the stringent requirements of Stage IV surveys. This approach originated from a series of community-wide blind challenges, where mock images with realistic galaxy properties and real data features were used to assess shear measurement algorithms [914–918]. With simulated images, where the ground truth is known, shear biases can be directly measured for any algorithm.

If the simulated images accurately replicate a survey's properties (e.g., resolution, PSF, signal-to-noise SNR, size and ellipticity distributions, source density, and clustering), the measured shear biases can be used to calibrate residual biases in real observations. This approach has been adopted by all Stage III surveys, e.g., see Ref. [905–907] and will remain vital for the Stage IV surveys.

Impact on S_8 tension and future direction Decades of dedicated work on shear measurement and calibration have significantly improved the accuracy of shear measurement. The latest KiDS cosmic shear analysis demonstrates that residual shear biases, primarily stemming from uncertainties in galaxy profiles, introduce only sub-percent uncertainties in S_8 estimates [919]. Shear measurement uncertainties are thus unlikely to be the main driver of the current S_8 tension.

Since shear measurement is closely tied to redshift estimation in real observations, developing a consistent, joint calibration of shear and redshift estimates using multi-band image simulations remains essential and will be a key focus for future simulation-based calibration, e.g., see Ref. [905,907]. Furthermore, due to the inherent limitations of image simulations — especially in capturing galaxy profile details — advancing shear measurement algorithms to reduce sensitivity to these intricacies remains a crucial goal.

2.2.1.2. Observational effects: Redshift measurement and calibration. WL measurements rely on two-dimensional (projected) quantities, meaning individual source redshifts are not strictly required. However, redshift estimates are essential for cosmic shear tomography, which enhances the signal and probes the time evolution of the growth of structures. Historically, the requirements for photometric redshifts of individual lensing sources have been relatively lenient, but upcoming surveys such

as *Euclid* [164] and LSST [897] demand higher precision, e.g., see Ref. [920] for a review.

Photometric redshift estimation Photometric redshift estimation is crucial for extracting cosmological information in optical surveys like LSST and *Euclid*. In contrast to spectroscopic redshift measurement, photometric redshift inference uses image, or photometric information. Broad band optical surveys like LSST and *Euclid* take images in 100–200 nanometer wide optical filter bands, which does not allow the recovery of atomic lines. This limitation means that redshift estimation must rely on the overall shape and characteristic features of a galaxy's spectral energy distribution (SED), for a review see Ref. [920,921]. Two primary approaches exist: ML and template fitting. ML methods [922–928] construct a direct mapping from observed photometry of individual galaxies to their redshift based on training data. While this training data does not need to spatially overlap, it has to be representative and complete in the color-redshift mapping being learned. Template fitting methods, e.g., see Ref. [929–935] match observed photometry to pre-existing SED models. It relies on accurate SED modeling and requires validation using similar calibration datasets. Although complementary, both techniques face challenges such as epistemic uncertainty in the SED and selection function models and incompleteness of accurate reference data at the faint end of the color-magnitude space, e.g., see Ref. [936–940].

Redshift distribution calibration for cosmic shear Beyond individual redshift estimates for cosmic shear sources, accurately calibrating their *redshift distributions* is crucial for interpreting observed signals with underlying cosmological models. For a given set of sources — usually selected in tomographic redshift bins — it is essential to recover their underlying *true* redshift distribution as closely as possible [941]. This is necessary to relate the observed signal to theoretical predictions, as the redshift distribution of sources determines the observed shape correlations via the matter power spectrum. Calibrating the redshift distribution in current WL surveys is challenging due to the faint nature of most cosmic shear sources and the limited availability of spectroscopic measurements. Consequently, a range of calibration methods have been developed, and efforts are ongoing to extend spectroscopic samples to better match the needs of cosmic shear surveys [937,942].

One of the earliest approaches for redshift distribution calibration, employed by e.g., the Deep Lens Survey (DLS) [943] or CFHTLenS [944], involved stacking photo-z posterior PDFs, derived with Bayesian Photometric Redshifts (BPZ) [945], to estimate the population distribution $\mathrm{d}N/\mathrm{d}z$. As Stage III surveys increased in statistical power, more reliable calibration methods were developed. These methods generally rely on either mapping the relation between colors and redshifts, or on the cross-correlation (clustering) approach. The former employs spectroscopic or narrow-filter multiband photometric calibration data to re-weight $\mathrm{d}N/\mathrm{d}z_{\mathrm{phot}}$, either directly in magnitude space [858,859,946], by incorporating additional properties, e.g., see Ref. [947], or via self-organizing maps (SOM) [948]. Two key ingredients are required for these calibration methods: spectroscopic data that closely match the cosmic shear sample (in magnitude, color, and redshift range) and a sufficient number of multi-band filters to break degeneracies in the color-redshift mapping. This is most readily achievable in KiDS, which covers nine bands and includes multiple deep calibration fields [949,950]. The DES redshift inference and calibration utilizes a mapping from deep multi-band to wide four-band data that is combined with spatial cross-correlations [951–953]. This choice is motivated by studies [940] that found that the photometric redshift biases from direct calibration strategies induced by the incompleteness in spectroscopic calibration samples are unacceptably high for DES. Similar to DES, the HSC calibration [954] relies on a combination of spectroscopic and narrow filter multiband calibration data as well as spatial cross-correlation measurements described in the following section. We note that the choice of photometric redshift calibration method and the incorporation of systematic effects is dictated by the survey specification and cannot be generalized across survey designs. However it can be concluded that the treatment of selection functions of calibration sources poses a major challenge for DES, HSC, and KiDS.

The cross-correlation method, also known as clustering redshifts, leverages the spatial correlation of galaxy positions to estimate $\mathrm{d}N/\mathrm{d}z$ for a photometric sample by measuring its angular cross-correlation with a reference sample that has known redshifts, e.g., see Ref. [955,956]. Either spectroscopic or high-fidelity photometric redshifts can serve as reference samples in this method. A major limitation of the clustering redshift approach is the availability of wide-angle calibration samples that extend to sufficiently high redshifts. As a result, its application in current cosmic shear surveys has been restricted primarily to the calibration of low-redshift bins [949,951,954].

Impact on S_8 tension and future direction Ref. [957] showed that an improved redshift calibration of the full sample or calibrations using different subsets change the S_8 obtained from the fiducial KiDS-1000 analysis at most at the level of 0.5σ. For upcoming surveys, photometric redshift estimation based on ML methods could benefit from training sample augmentation with simulated galaxies possessing otherwise unrepresented features [958]. The complex selection function of spectroscopic surveys presents a major challenge in the calibration of photometric redshifts, especially at the faint end of the color-magnitude space [940].

Computationally efficient approaches for the marginalization over photometric redshift uncertainties are crucial to tackling the challenge of running inference in high-dimensional parameter spaces. Strategies can involve simplified $n(z)$ parametrizations, such as in terms of shifts of a mean redshift Δz per bin, or a resampling approach using multiple MCMC chains at a fixed $n(z)$ sampled from the uncertainties. Ref. [959] showed that for the forecasted precision for HSC Y3, these methods recover statistically consistent error bars. However, when the constraining power of the full HSC survey (or other surveys of comparable or greater statistical power) is considered, the choice of the marginalization method may modify the 1σ uncertainties on $\Omega_{\mathrm{m},0} - S_8$ constraints by a few percent.

2.2.1.3. Astrophysical effects: Baryonic feedback. With the increasing precision of modern cosmological surveys, small-scale astrophysical processes — commonly referred to as baryonic feedback — have become increasingly relevant in WL analyses. Baryonic feedback, driven by galaxy formation, supernova explosions, and AGN, suppresses the total matter power spectrum on scales of $k \sim 1$–$10\,\mathrm{h\,Mpc^{-1}}$ by redistributing gas within and beyond halos and influencing through back-reaction [960]. Unlike gravity, which acts as a long-range force, baryonic effects follow an inside-out pattern: halos, stars, galaxies, and central supermassive black holes form on small scales through hierarchical structure formation, while supernova and AGN feedback modify the baryon distribution by, for example, expelling intrahalo gas into the IGM [961–965]. In particular, hydrodynamical simulations [966–970] indicate that AGN feedback is one of the most significant effects in suppressing the matter power spectrum at small scales. However, the spatial extent of the AGN ejected gas remains an open question — whether it affects a few Mpc or extends to tens of Mpc [969,971]. Below this maximum scale, the total matter distribution remains unchanged due to the conservation of mass and momentum. On smaller scales of $k > 10\,\mathrm{h\,Mpc^{-1}}$, baryonic effects such as gas cooling and star formation become efficient, leading to an upturn in the matter power spectrum [885]. Since these effects alter the total matter distribution, cosmic shear summary statistics — such as two-point correlation functions — are significantly affected compared to a purely collisionless scenario.

Mitigation strategies Despite the importance of baryonic feedback, modeling it from first principles remains challenging due to the complex and nonlinear nature of these processes. This introduces significant theoretical uncertainties in WL analyses. A common mitigation

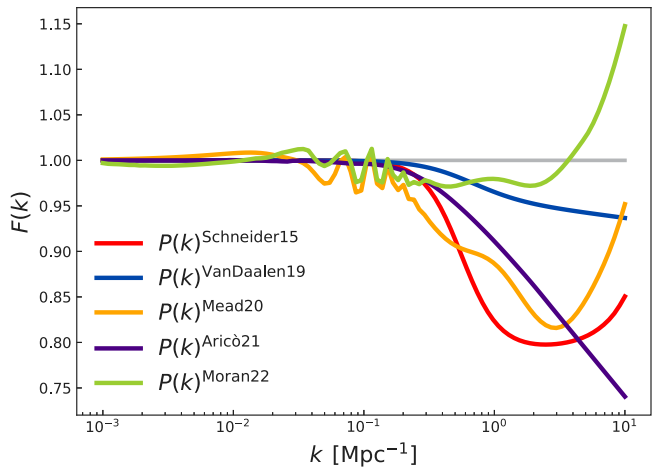

Fig. 34. Suppression of the total matter power spectrum on small scales due to baryonic effects for various baryon models [887,891,960,972,973]. All spectra were computed for a flat ΛCDM cosmology with $\Omega_c = 0.25$, $\Omega_b = 0.05$, $\Omega_k = 0.0$, $\sigma_8 = 0.81$, $n_s = 0.96$, and $h = 0.67$, assuming no massive neutrinos. The y-axis shows the ratio $F(k)$ of each model including modeling of baryons, to the nonlinear matter power spectrum without baryonic effects. The nonlinear power spectrum was computed using `pyccl.nonlin_matter_power` method, while baryonic suppression was modeled with the baryonic modules in `pyCCL` [974], all evaluated at $a = 1$ ($z = 0$) over the same k-range.
Source: Adapted from Ref. [975].

strategy is to apply scale cuts to the summary statistics, excluding small scale data where hydrodynamical simulations suggest feedback effects dominate [860–862,864,871]. While this method preserves the robustness of cosmological constraints, it comes at the cost of discarding high SNR scales that are rich in cosmological information, thereby limiting the constraining power of WL surveys. To fully exploit the potential of upcoming Stage IV surveys, it is crucial to incorporate baryonic effects into cosmological analyses rather than simply removing affected scales.

Several modeling strategies have been developed to address this issue by incorporating baryonic feedback into the total matter power spectrum. One widely used approach is the baryon correction model (BCM), which modifies the position of particles in N-body simulations using parametric prescriptions that approximate the impact of feedback on the DM halo profiles [887,962,972,976].

Another method integrates baryonic effects within the halo model framework by modifying density profiles and gas expulsion mechanisms [891,892,977]. Some of these models and their impact on the matter power spectrum are summarized in Fig. 34. Principal Component Analysis (PCA) and alternative basis function approaches provide a more data-driven way to capture a broad range of feedback scenarios [978]. The most detailed recipe comes from cosmological hydrodynamical simulations, which explicitly simulate baryonic physics using sub-grid prescriptions for unresolved processes such as supernova and AGN feedback [885]. However, discrepancies arise due to differences in sub-grid implementations, calibration strategies, and simulation methods. These variations lead to disagreements in both the amplitude and scale dependence of the suppression of the total matter power spectrum [971]. Consequently, an effective model for WL must be flexible enough to encompass the full range of plausible baryonic effects. Moreover, other nonlinear effects — including intrinsic alignments, nonlinear clustering, and reduced shear corrections — must be accounted for to ensure robust cosmological constraints. The aforementioned strategies provide a way to marginalize over baryonic feedback uncertainties while preserving small-scale cosmological information. However, degeneracies between baryonic feedback and cosmological parameters may degrade the constraints on S_8, highlighting the need of estimators beyond the two-point functions that can disentangle these effects while maximizing the constraining power of next-generation surveys.

Higher-order statistics of the WL field, such as bispectrum, peak counts [849,979] and the one-point lensing PDF [836], are more sensitive to non-Gaussian and smaller-scale structures than two-point correlations [847,980–982]. Thus, combining the two-point correlations with the higher-order statistics would allow us to obtain tighter constraints on cosmological parameters [842,846], while self-calibrating the baryonic effects [983].

Finally, multi-probe approaches — combining WL with X-ray, measurements of the Sunyaev–Zeldovich (SZ) effect (thermal tSZ and kinetic kSZ), and FRB observations — offer complementary constraints on the distribution of baryons in large-scale structures [984,985,985–988]. These techniques collectively help preserve cosmological information while minimizing biases from astrophysical processes.

Impact on cosmic tension and S_8 To explore the impact of baryons on the inferred S_8, Stage III surveys have conducted parameter inference with two-point functions down to small scales. They found that moderate to small baryonic effects are present in the data [976, 989–991]. In particular, Ref. [989] performed a joint cosmic shear analysis of the Stage III surveys DES-Y3, KiDS-1000 and HSC-DR1 using small scale data in harmonic space. This reanalysis implements a single pipeline that extends the cosmic shear angular power spectrum to scales up to $\ell < 4500$, using `BACCOemu` to model the non-linear regime and baryonic effects in the total matter power spectrum. Their resulting S_8 constraint is 1.8σ lower than *Planck*, however, [989] found a $\Omega_{m,0}$ tension between both data sets of 3.5σ. When analyzing the parameter space in terms of variables without an implicit dependence on the Hubble constant H_0, (S_{12}, w_m), the authors find no tension with *Planck*. On the other hand, Ref. [990] explore signatures of baryonic effects in the HSC Y3 two-point correlation functions $\xi_\pm$ down to small scales of 0.28 arcminutes (up to $k \sim 20h$ Mpc^{-1}). The theoretical modeling is implemented by means of a non-linear DM-only matter power spectrum emulator (similar to DarkEmulator [992]). The authors found no significant shift in the inferred S_8 when including the small scales. Moreover, the DM-only theory fits the observations within the statistical error of the survey, meaning baryons are not playing an important role in these measurements. Similar results were obtained for HSC Y1 data using multiple higher-order statistics at small scales [847]. These studies of cosmic shear data, together with other analyses from the Sunyaev-Zel'dovich observations, indicate that strong feedback scenarios are needed to reconcile the S_8 inferred from cosmic shear surveys with the value derived from *Planck* ΛCDM [993]. This translates into a large suppression of the matter power spectrum, of the order of ~25% at $k \sim 1$ h Mpc^{-1}. The latter, however, is larger than the suppression found from hydrodynamical simulations, and contradicts the constraints imposed by X-ray observations of the baryon mass fraction for cluster-scale halos [990,991]. Therefore, it is possible that baryons in combination with other non-linear effects and unmodeled systematics may explain the discrepancy between cosmic shear results and *Planck* ΛCDM cosmology, or extensions of ΛCDM and new physics are required.

2.2.1.4. Astrophysical effects: Intrinsic alignments of galaxies. Intrinsic alignments (IA) of galaxies represent a significant astrophysical effect that can systematically affect the measurement of cosmic shear and, consequently, the inference of cosmological parameters (see Ref. [994] for a comprehensive review). These alignments arise due to gravitational interactions and the tidal forces exerted by the large-scale structure of the Universe, causing the shapes of nearby galaxies to correlate with each other and with the surrounding matter density field.

For cosmic shear two-point correlation functions, intrinsic alignments can be categorized primarily into two types: intrinsic–intrinsic (II) alignments and gravitational–intrinsic (GI) and intrinsic-gravitational (IG) alignments. II alignments occur when the shapes of

physically close galaxies are directly influenced by the same gravitational tidal field, leading them to align with each other. GI and IG alignments describe the correlation between intrinsic galaxy shapes and the shear induced by gravitational lensing. GI refers to the correlation between the intrinsic shape of a foreground galaxy and the shear of a background galaxy, while IG represents the reverse case [995]. These terms are related through symmetry properties of the shear field, with IG often being treated as the transpose of GI in theoretical and numerical treatments.

Galaxy-galaxy lensing (GGL) probe, or the correlation between galaxy shapes and galaxy positions, is also sensitive to intrinsic alignments when the shape and the position catalog overlap in redshift. GGL is sensitive only to GI types of alignments and through a different kernel than for cosmic shear (see equations in e.g., Ref. [996]). Because of this, 3×2pt analyses significantly help to constrain the intrinsic alignment parameters. Recently, GGL shear-ratios have been used to fold in prior IA information to the cosmic shear analysis [861,862,997]. Recently, inverse galaxy-galaxy lensing has also been proposed as an additional probe to constrain IA parameters [998].

Modeling intrinsic alignments Intrinsic alignment (IA) models vary in complexity and scale-dependent effectiveness. The Nonlinear Alignment Model (NLA) [999] has been the standard approach to model red (elliptical) galaxies. This model assumes a linear coupling between the nonlinear tidal field and galaxy shapes, typically parameterized by an amplitude parameter alongside an optional redshift evolution parameter. In this framework, blue (spiral) galaxies are assumed to have negligible intrinsic alignments. However, the linear tidal shear assumption breaks down on small scales, necessitating more sophisticated models.

The Tidal Alignment and Tidal Torquing (TATT) model [1000] represents an important extension, introducing additional terms to capture the alignments of spiral galaxies where angular momentum plays a critical role. This model incorporates a separate amplitude parameter for the tidal torquing effect, along with its own redshift scaling parameter. In total, the basic TATT model typically employs four parameters: A_1 (tidal alignment amplitude), A_2 (tidal torquing amplitude), η_1 (alignment redshift scaling), and η_2 (torquing redshift scaling). A fifth parameter, $b_{\rm TA}$ (the linear bias of source galaxies), is frequently included to account for the clustered distribution of source galaxies in observational data. Many studies such as Refs. [1001–1003] demonstrate that while NLA fits measurements well above 6–8 Mpc/h, TATT extends this range down to 1–2 Mpc/h. These findings emerge from both simulation-based tests (N-body with semi-analytic IA components or hydrodynamic simulations) and direct fits to observational data.

For modeling at even smaller scales, the halo model describes alignments using one-halo and two-halo terms, based on galaxy correlations within and between DM halos [994,1004] while the Effective Field Theory (EFT) framework treats alignments as a tensor field and incorporates small-scale physics through free parameters. Ref. [1005] shows that EFT describes DM halo intrinsic alignments up to $k_{\rm max} = 0.30\ h$/Mpc at $z = 0$, significantly outperforming both NLA and TATT which they find to only reach $k_{\rm max} = 0.05\ h$/Mpc.

Despite these advances in model complexity, practical applications raise important questions about necessary sophistication. The DES Y3 cosmic shear analysis [861] found that NLA was sufficient to fit their data, even though TATT had been chosen for fiducial results in a blinded fashion. Similarly, Ref. [1001] found no significant evidence for non-zero tidal torquing amplitude (A_2) in Illustris TNG hydrodynamic simulations, challenging the need for TATT's full 5-parameter framework in typical applications. Moreover, it is important to note that increasing model complexity does not necessarily reduce biases. The interplay between IA and other uncertainties (e.g., from photometric redshift errors [1006]) can introduce additional complications. Recent work [1007] shows that jointly modeling IA and source redshift distributions via a shared LF can help mitigate such biases while maintaining consistency in WL analyses. Careful calibration and validation remain crucial to ensure these models accurately represent physical processes without introducing unintended distortions in cosmological analyses. To navigate these modeling challenges, researchers have developed strategic approaches for IA model selection. Ref. [1008] recently introduced a data-driven methodology to objectively determine which IA model best suits a particular analysis, providing a more systematic framework for model choice. In parallel, many cosmological studies have adopted a multi-model approach, presenting results across several IA formulations to demonstrate robustness and identify potential model-dependent biases. Below, we examine how these modeling decisions have shaped recent cosmological parameter constraints and what they reveal about the relative importance of IA modeling in contemporary WL analyses.

2.2.1.5. Modeling IA for higher order statistics. While IA modeling has primarily focused on two-point statistics, recent efforts have extended these frameworks beyond 2-point statistics. Analytical advances have provided foundations for modeling IA in bispectra [1009,1010] and the lensing PDF [1011], while Ref. [1012] demonstrated that high signal-to-noise peaks in aperture mass maps can experience deviations up to 30% for *Euclid*-like surveys due to IA effects. Many recent analyses employ simulation-based inference, which relies on map-level IA modeling and presents unique challenges. For example, Ref. [1013] showed that source clustering impacts non-Gaussian statistics significantly more than two-point functions [1014]. Current approaches address this either by implementing additional clustering terms in analytical predictions [1011] or by directly incorporating clustering effects in simulations [879]. The latter approach extends beyond traditional NLA implementation by using simulation-based clustering rather than tree-level perturbation theory, showing that modeling IA at the map level can also offer advantages for various summary statistics.

Impact on cosmic tension and S_8 Misestimations in intrinsic alignments can lead to significant biases in the structure growth parameter S_8, thereby affecting our understanding of cosmic tensions. Recent cosmic shear analyses, as illustrated in Fig. 35, demonstrate that among various analysis choices, the selection of IA model often produces shifts in the S_8 constraints, which will become substantial for Stage IV surveys [1015]. The TATT model (pink points) tends to yield somewhat lower S_8 values compared to the NLA model (blue points) across different analysis combinations. This difference, while modest, may be relevant when considering potential tensions between early and late-Universe probes, as indicated by the comparison with the reference line in the figure. The largest change comes from the joint analysis of data from the DES and KiDS, which revealed that transitioning from the NLA model to the more complex TATT model can lead to heightened tension in S_8 measurements. Quantitatively, the difference between the redshift-dependent NLA and TATT analysis results was 0.9σ in the S_8 marginalized posterior, but reached 1.3σ when comparing the maximum a posteriori (MAP) values in the full parameter space. This distinction is particularly significant as it indicates that the discrepancy arises from genuine differences in model physics rather than merely from differences in prior volumes or projection effects. These results highlight the importance of carefully considering IA modeling choices when interpreting cosmological constraints from WL surveys. 3×2pt analyses in DES Y3 were less susceptible to the IA model compared to statistics based on cosmic shear alone.

Future directions As WL analyses continue to advance, refining IA models and developing more realistic cosmological simulations will be essential for providing robust validation tests. These improvements will work synergistically with upcoming surveys such as LSST by the Vera C. Rubin Observatory, which will deliver high-quality imaging across unprecedented sky areas, enabling studies of IA with greater statistical power and tightening constraints on cosmic shear measurements.

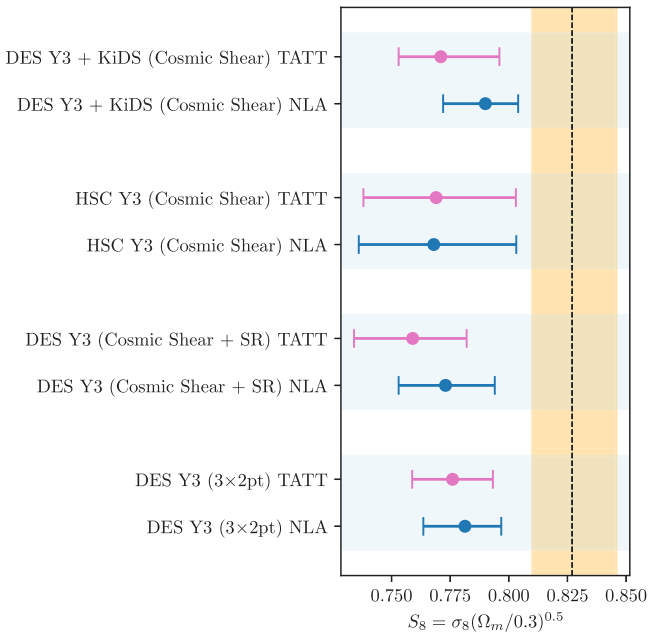

Fig. 35. Impact of IA model choice to S_8 in recent WL analyses assuming the ΛCDM model. The DES Y3 + KiDS results are from Ref. [867], HSC Y3 from Ref. [864], DES Y3 cosmic shear (COSEBIS and $\xi_\pm$)+ SR (shear-ratio) from Ref. [861,862] and DES Y3 3 × 2pt from Ref. [869]. The vertical dashed line is the *Planck* value with its corresponding uncertainty shaded in orange. All error bars correspond to 1-σ uncertainties.

Exciting new approaches are also already emerging from recent observations. Measurements have consistently found IA amplitudes lower than theoretical expectations, with blue galaxies showing negligible alignment signals [1016]. Building on these findings, [878] proposed an innovative strategy of conducting cosmic shear analysis exclusively with blue galaxies – potentially eliminating the need for complex IA modeling entirely. While this approach sacrifices approximately half the galaxy sample, reducing statistical power, it could significantly mitigate systematic uncertainties. The viability of this or other compromises will become clearer as theoretical understanding advances and next-generation survey data becomes available.

2.2.1.6. Confirmation bias and blinding. Modern cosmological analyses in surveys like DES, KiDS, and HSC are often highly complex and require the seamless interaction of large teams responsible for different parts of the analysis. Sources of epistemic error are difficult to control, which can lead to a dependence of cosmological parameter constraints on analysis choices. At the same time, complementary cosmological constraints like from the CMB might induce a subconscious bias in a select parameter subspace, like σ_8 and $\Omega_{m,0}$. In cases where the value of the cosmological parameters are revealed during the analysis, this might lead to 'confirmation bias', where analysis assumptions are subconsciously tuned toward a certain scientific narrative. The complexity of cosmological analysis combined with the significant dependency on analysis choices, therefore necessitates strict strategies to avoid this confirmation bias. The blinding strategies differ across surveys but generally consist of catalog-level blinding where a set of synthetic and encrypted multiplicative shear values are artificially added to obfuscate the true shear field and analysis-level blinding where the inferred parameter posteriors are altered to avoid a ready comparison with prior work [1017].

2.2.2. Galaxy cluster counts

Coordinator: Dominique Eckert

Contributors: Antonio da Silva, Filippo Bouchè, Francesco Pace, Iryna Vavilova, Jenny G. Sorce, Massimiliano Romanello, Radosław Wojtak, Sebastian Grandis, Shahab Joudaki, and Vittorio Ghirardini

2.2.2.1. Methodology. Galaxy clusters are the most massive gravitationally bound structures in the present Universe and originate from the largest fluctuations of the primordial matter distribution. Their mass and number density strongly depends on the underlying cosmological parameters [1018], such that galaxy cluster surveys are powerful probes of cosmological parameters. In this section, we describe the main steps that are needed to extract cosmological information from galaxy cluster surveys. We identify the major bottlenecks that need to be addressed to advance our cosmological knowledge with the use of this technique, and summarize the main recent results in the field.

The halo mass function and its cosmological dependency In the hierarchical structure formation scenario, small structures formed at high redshifts progressively merge under the influence of gravity to form the massive systems we see today. As such, the number density of halos and its time evolution trace the growth of structures in the Universe, which depends on the underlying cosmological model. The halo mass function describes the number of collapsed halos at a given time per unit volume and halo mass. Its shape, normalization, and redshift evolution are highly sensitive to cosmological parameters.

In mathematical terms, the halo mass function can be expressed in the following way:

$$\frac{\mathrm{d}n}{\mathrm{d}\ln M} = \frac{\rho_{\mathrm{m},0}}{M} f(\sigma) \left| \frac{\mathrm{d}\ln\sigma}{\mathrm{d}\ln M} \right| , \tag{2.12}$$

with $\rho_{\mathrm{m},0}$ the mean matter density of the Universe at present day, σ the mass variance on a mass scale M and $f(\sigma)$ a function characterizing different fitting (or theoretical) expressions. Often, $f(\sigma)$ is written in as $\nu f(\nu)$, where the peak height $\nu = \delta_{\mathrm{c}}/\sigma$ is a function of mass and time. Here, δ_{c} is the linearly extrapolated overdensity and can be evaluated within the framework of the spherical collapse model. Many different expressions exist for $f(\sigma)$ [1019–1024].

In Fig. 37 we present the dependence of the Tinker halo mass function [1022] on the matter power spectrum normalization σ_8 (left panel) and on the matter density $\Omega_{\mathrm{m},0}$. We see that the effect on the halo mass function is that of increasing the number of structures. A higher value of $\Omega_{\mathrm{m},0}$ implies also a higher σ_8 value. The two parameters are highly degenerate at the high-mass end, as shown by Fig. 36 where a $50\,\mathrm{deg}^2$ mock cluster counts survey is compared with DES+KiDS WL and the latest Planck collaboration data. The degeneracy between Ω, and σ_8 for galaxy cluster counts is clearly visible.

It is important to note that halo masses are usually defined within a spherical overdensity Δ with respect to either the critical density $\rho_{\mathrm{c}}(z)$ or the mean density of the Universe $\rho_{\mathrm{m}}(z)$. For a given overdensity Δ_{c} or Δ_{m}, the corresponding mass M_Δ and radius R_Δ are defined as the mass and radius within which the condition

$$\frac{M_\Delta}{4/3\pi R_\Delta^3} = \Delta_{\mathrm{c/m}}\ \rho_{\mathrm{c/m}}(z) , \tag{2.13}$$

is satisfied. The choice of the halo mass function and of the observational mass definition must therefore be adapted to the chosen spherical overdensity. Common choices for the definition of the overdensity are $500c$, $200c$, and $200m$.

Mass-observable scaling relations and the scatter around these relations While the halo mass function is highly sensitive to cosmological parameters, constraining it from galaxy cluster surveys is a challenging task. The main underlying issue is that halo mass is not a directly observable quantity. Samples of galaxy clusters are extracted from surveys of the baryonic component that fills these structures, whether it is in the form of hot gas (X-ray, Sunyaev-Zel'dovich effect) or stars (optical/IR). Galaxy cluster detection techniques and their primary

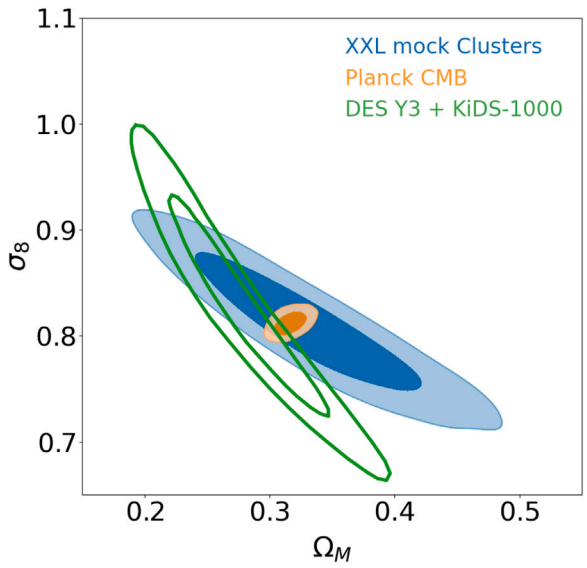

Fig. 36. $\Omega_{\rm m,0}-\sigma_8$ degeneracy in typical cosmic shear and cluster counts experiments. The blue curve and shaded area show the degeneracy of the expected $\Omega_{\rm m,0}-\sigma_8$ contours in a mock 50 deg^2 X-ray cluster count survey, whereas the green contours show the same degeneracy in the combined DES Y3 + KiDS-1000 cosmic shear estimate. We can see that the degeneracy is shallower in cluster counts experiments ($\sigma_8 \propto \Omega_{\rm m,0}^{-0.3}$) compared to cosmic shear ($\sigma_8 \propto \Omega_{\rm m,0}^{-0.5}$), such that any definition of S_8 that is optimal for either experiment will not perfectly follow the degeneracy of the other. For comparison, we add the *Planck* CMB $\Omega_{\rm m,0}-\sigma_8$ contours in orange. (For interpretation of the references to colour in this figure legend, the reader is referred to the web version of this article.)

observables are described in more detail in Section 2.2.2.2. In all cases, the primary observable of the survey is not directly the halo mass but rather a quantity that depends on it. The relation between survey observable and the halo mass, usually referred as a *scaling relation*, needs to be properly understood to turn the detected cluster samples into constraints on the halo mass function.

If galaxy clusters grow and evolve in a self-similar way [1025], the relations between observable quantities $\mathcal{O}$ and spherical overdensity halo mass M_Δ are expected to be power laws. While astrophysical effects such as mergers, cooling, and AGN feedback can cause deviations from the simple self-similar scenario, evidence suggests [1026–1029] that these relations can be well described by power laws with a log-normal intrinsic scatter $\sigma_{\log\mathcal{O}}$,

$$\log\mathcal{O} = A_{\mathcal{O}M} + B_{\mathcal{O}M}\left(\frac{M_\Delta}{M_{pivot}}\right) + \gamma_{\mathcal{O}M}\,E(z) \pm \sigma_{\log\mathcal{O}}\,, \tag{2.14}$$

with $E(z) = H(z)/H_0$. Here the parameters $A_{\mathcal{O}M}$ and $B_{\mathcal{O}M}$ are the normalization and the slope of the mass-observable scaling relation and $\gamma_{\mathcal{O}M}$ governs its redshift evolution. The scaling relation allows us to construct the probability of detecting a system with a measured observable $\mathcal{O}$ given the source's mass and redshift, $P(\mathcal{O}|M,z)$. A precise knowledge of these parameters is required to make accurate cosmological inferences from galaxy surveys. We discuss the associated issues in more detail in .

Selection function, forward modeling, likelihood function The cosmological analysis of galaxy cluster catalogs follows a Bayesian inference approach. A generative model for the data given unknown model parameters has to be postulated, and the PDF of the actual data as a function of the model parameters, the likelihood, has to be computed. The generative model assumed for a cluster catalog with observable $\hat{\mathcal{O}}$ and redshift z at a sky position θ is a Poisson realization of the density field

$$\frac{{\rm d}\tilde{n}}{{\rm d}\hat{\mathcal{O}}} = \frac{{\rm d}n}{{\rm d}\hat{\mathcal{O}}}\left(1 + b_{\rm eff}\delta(\theta,z)\right)\,, \tag{2.15}$$

with $b_{\rm eff}$ the effective bias, $\delta(\theta,z)$ the matter density contrast, and

$$\frac{{\rm d}n}{{\rm d}\hat{\mathcal{O}}} = \int {\rm d}\mathcal{O}\int {\rm d}M\,\frac{{\rm d}n}{{\rm d}M}\,P(\mathcal{O}|M,z)P(\hat{\mathcal{O}}|\mathcal{O},z,\theta)P({\rm sel}|\hat{\mathcal{O}},\mathcal{O},z,\theta)\,, \tag{2.16}$$

where $\frac{{\rm d}n}{{\rm d}\ln M}$ is the halo mass function (Eq. (2.12)), $P(\mathcal{O}|M,z)$ the observable mass relation and its scatter (Eq. (2.14)), $P(\hat{\mathcal{O}}|\mathcal{O},z,\theta)$ the effect of instrumental noise of the intrinsic observable $\mathcal{O}$, and $P({\rm sel}|\hat{\mathcal{O}},\mathcal{O},z,\theta)$ the selection function. The latter takes values between 0 and 1 based on the probability of including the cluster with properties $(\hat{\mathcal{O}},\mathcal{O},z,\theta)$.

The second term in Eq. (2.15) can be ignored for sufficiently high-mass and wide survey area samples, yielding the Poisson likelihood used by Refs. [736,1030–1036]. For smaller area surveys and lower mass surveys, the second term contributes significantly via the variance of the matter field. In such cases, a composite Gaussian-Poisson likelihood has to be used [1037–1044]. The resulting likelihood depends on the cosmological parameters via the halo mass function and the cosmological volume. It also depends on the nuisance parameters describing the observable mass relation and, potentially, the selection function. Marginalizing over sufficiently flexible observable mass relation parameterizations is crucial to accurately represent the cluster population, especially with regard to the halo mass.

2.2.2.2. Galaxy cluster surveys.

X-ray The vast majority of the baryonic content of galaxy clusters is in the form of a hot ($> 10^7$ [K]), highly ionized plasma that fills the system's gravitational potential well. Given the high temperatures involved, the intracluster medium (ICM) shines predominantly in the X-ray range through thermal bremsstrahlung and line emission. As such, galaxy clusters are luminous ($L_X = 10^{44} - 10^{45}$ [erg/s]) X-ray sources spanning a diameter of several arcmin. The overwhelming majority of extended X-ray sources in the extragalactic sky are galaxy clusters, such that X-ray surveys are powerful cluster detection machines. In the early 1990s, Röntgensatellit (ROSAT) [1045–1047] performed an all-sky X-ray survey and several deeper but small area surveys, e.g., ROSAT Deep Cluster Survey (RDCS) [1048] which allowed for the detection of several thousand clusters. This spurred the build-up of several sub-samples, either volume-limited (REXCESS) [1049], or flux-limited (HIFLUGCS) [1050,1051] with a well-understood selection function.

Deep follow-up observations of ROSAT-selected clusters with *XMM-Newton* and *Chandra* allowed to constrain cosmological parameters with cluster number counts by measuring the mass of these systems with better precision [1052]. *XMM-Newton*, thanks to its larger field-of-view, enabled to scan deeply (30–40 ks) several tens of square degrees, enabling the serendipitous detection of the fainter galaxy group population, extending the mass range used in the cosmological analysis. The XXL survey [1053] detected ~ 450 clusters over an area of 50 deg^2 [1037,1041]. More recently, *eROSITA* undertook several all-sky surveys, with the ultimate goal of detecting about 100,000 galaxy clusters. The results from the first of these all-sky surveys were recently released [1036] and provided the detection of $\sim 12,000$ clusters over half the sky.

Sunyaev-zel'dovich effect The thermal SZ effect [tSZ;1054] describes the inverse-Compton scattering of CMB photons off the hot electrons of the ICM. Photons crossing the path of a hot electron cloud occasionally encounter hot electrons and gain energy, which induces a modification of the spectral shape of the CMB, see Ref. [1055] for a review. At the peak frequency of the CMB, the tSZ effect takes the form of a *decrement* in the temperature of the CMB, as a fraction of the photons are upscattered to higher frequencies. At first order, the spectral signal of the tSZ depends only on the Compton parameter, y, which describes the average energy gain over the line of sight. The total integrated signal over the area of a cluster, Y_{SZ}, is proportional to the integrated thermal energy of the ICM [1056].

The advantage of the tSZ effect as a cluster detection technique is twofold. First, the signal is essentially independent of redshift, which

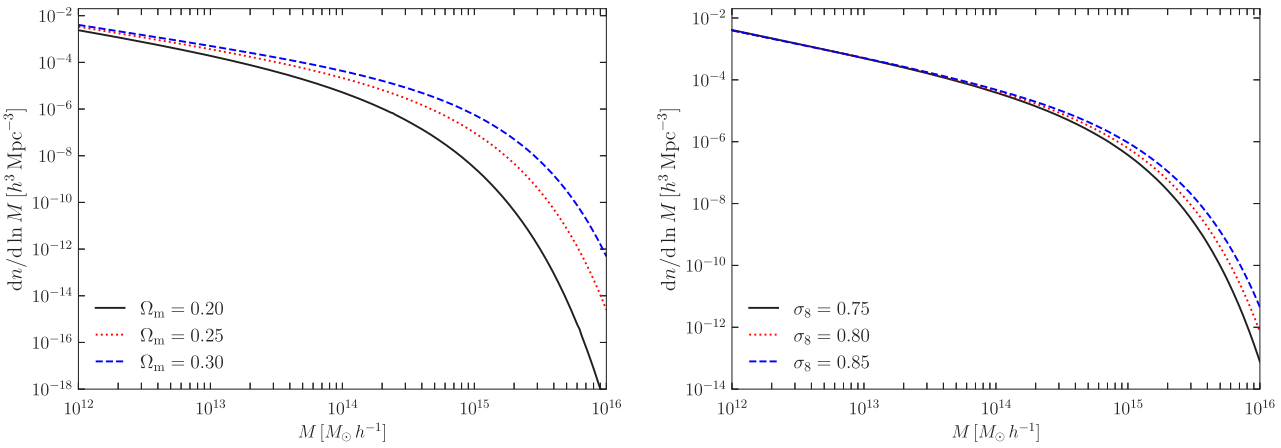

Fig. 37. Dependence of the Tinker mass function on matter density Ω_m (left panel) and on the matter spectrum normalization σ_8 (right panel) at $z = 0$.

makes it very efficient to detect high-redshift systems. Second, the primary tSZ observable, Y_{SZ}, is believed to be an excellent proxy of cluster mass [1057–1060]. In the past decade, the *Planck* survey yielded the detection of > 2000 galaxy clusters with this technique extending out to $z \sim 1$ [737,1061]. While *Planck* was very sensitive to the tSZ thanks to its wide frequency range and all-sky coverage, the detection efficiency of high-redshift sources was hampered by the poor *Planck* beam, such that the bulk of the detected systems are at redshift $z < 0.5$. Conversely, ground-based experiments have larger collecting areas and better angular resolution. SPT [1062–1064] and ACT [1065,1066] were now able to gather catalogs of several thousand galaxy clusters out to $z \sim 2$.

Optical/near-IR photometry While in the past couple of decades, a great deal of attention was devoted to the selection of galaxy clusters through the ICM, there is now renewed interest in the detection of galaxy clusters as overdensities of galaxies thanks to the new generation of optical and near-IR surveys like *Euclid* and *Rubin*. As their name suggests, galaxy clusters were originally defined as such based on the detection of overdensities of galaxies in the same region of the sky. Based on visual inspection of photometric plates, Abell (1989) [1067] constructed a catalog of more than 4000 clusters that has been used for more than two decades as a reference of the local large-scale structure. Since that time, sophisticated galaxy cluster detection algorithms have been developed which allowed to extract large samples of clusters from galaxy surveys. Modern detection algorithms are mainly split into two classes: red sequence and photometric redshifts. Red sequence cluster finders [1068–1070] take advantage of the predominance of passive red galaxies in clusters with respect to the field to search for overdensities of red galaxies. This method reduces spurious detections thanks to the use of the red sequence, which is known to trace rich environments [1071,1072]. Alternatively, methods based on photometric redshifts [720,1073] make use of galaxy SEDs to search for galaxy overdensities in three-dimensional space. These techniques rely on the availability of high-quality photometric redshifts but make no assumption on the existence of a red sequence. For a detailed comparison of various cluster finding algorithm, we refer to Ref. [1074].

The main advantage of optical cluster catalogs is their high sensitivity, with the deepest current catalogs containing more than 100,000 clusters (e.g., see Refs. [1075–1079]). Modern algorithms also provide an estimate of the cluster redshift as a direct byproduct. The primary observable of optical cluster finders is the number of member galaxies, or *richness* N. A standardized richness estimate is computed iteratively to include cluster members above a given absolute magnitude. Richness is known to correlate with halo mass [1080,1081], although with a large intrinsic scatter induced by projection effects and miscentering [1082,1083].

Shear selection The techniques discussed above all rely on detection through the baryonic content of clusters, whether it is in the form of gas or galaxies, whereas the vast majority of the mass is made of DM. In the past decade, direct detection of galaxy clusters as peaks in projected WL mass maps has become possible [906,1084–1087]. This technique allows to detect clusters directly through their total mass content rather than through a proxy that is related to the halo mass in a complex way. Thanks to the depth of the Subaru/HSC-SSP survey (∼ 30 galaxies per square arcmin), Ref. [1085] presented a sample of 65 shear-selected clusters within a ∼ 160 deg^2 area with a S/N greater than 4.7. All the most significant peaks were associated with galaxy overdensities or X-ray signals [1088]. More recently, the first cosmological constraints from shear-selected cluster samples were extracted from an area of ∼ 500 deg^2 [1086,1089]. While at the present day shear-selected cluster catalogs are much smaller than catalogs obtained from other techniques, upcoming lensing experiments like *Euclid* will yield much larger samples directly extracted from the projected mass distribution. The primary issue associated with shear selection is projection associated with correlated large-scale structure and halo orientation, such that the masses of the detected systems are expected to be over-estimated by ∼ 50% [1090]. Future works will need to model projection effects in detail to make accurate cosmological inferences from large samples of shear-selected systems.

2.2.2.3. *Mass calibration and systematics.*

Mass calibration techniques The number of galaxy clusters as an observable displays a direct degeneracy between the mean mass scale of the sample and the cosmological parameters, which dictate the number density of halos via the mass function and the cosmological volume. Number counts of galaxy clusters can thus only constrain cosmological parameters if the relation between halo mass and cluster observables is determined, a problem called mass calibration. Our knowledge of subgrid astrophysical processes limits the direct calibration of this relation on hydrodynamical simulation. It is thus very challenging to derive the degree of uncertainty on the mass calibration from pure simulation-based studies. The latter is, however, the main contributor to the final cosmological constraining power of cluster number counts experiments and should, therefore, be assessed in a reliable, empirical fashion.

In the context of a CDM cosmology, most of the halo mass is composed of DM. Empirical mass calibration can thus only proceed via measurements of the cluster's gravitational potential. Three techniques have been established to observe the cluster gravitational potential: *(i)* hydrostatic equilibrium; *(ii)* cluster galaxy dynamics; *(iii)* WL. Owing to its independence on the dynamical state, WL has become in recent years the method of choice to calibrate galaxy cluster mass, see Ref. [1091] for a review.

While WL is expected to be close to unbiased on average, the signal-to-noise of individual cluster mass measurement is usually very low. Mass calibration is thus integrated into the likelihood framework discussed above by considering the marginal PDF of the observable directly linked to halos mass $\hat{\mathcal{O}}_{\rm M}$ conditional on the observable one seeks to calibrate $\hat{\mathcal{O}}$ [1031,1032,1034,1035], reading

$$p(\mathcal{O}_{\rm M}|\hat{\mathcal{O}},z,\theta)=\left(\frac{{\rm d}n}{{\rm d}\hat{\mathcal{O}}}\right)^{-1}\frac{{\rm d}n}{{\rm d}\hat{\mathcal{O}}{\rm d}\hat{\mathcal{O}}_{\rm M}}\,, \tag{2.17}$$

with

$$\frac{{\rm d}n}{{\rm d}\hat{\mathcal{O}}{\rm d}\hat{\mathcal{O}}_{\rm M}}=\int{\rm d}\mathcal{O}\int{\rm d}\mathcal{O}_{\rm M}\int{\rm d}M\,\frac{{\rm d}n}{{\rm d}M}P(\mathcal{O},\mathcal{O}_{\rm M}|M,z)P(\hat{\mathcal{O}}|\mathcal{O},z,\theta)$$
$$P(\hat{\mathcal{O}}_{\rm M}|\mathcal{O}_{\rm M},z)P({\rm sel}|\hat{\mathcal{O}},\mathcal{O},z,\theta)\,, \tag{2.18}$$

where $P(\mathcal{O},\mathcal{O}_{\rm M}|M,z)$ is the joint scaling relation between mass calibration observable and primary observable, and $P(\hat{\mathcal{O}}_{\rm M}|\mathcal{O}_{\rm M},z)$ parameterized the measurement uncertainty on the mass calibration observable. Note that the correlation between the observable mass relation is crucial to account for physical selection effects [1092,1093]. The marginal relation $P(\mathcal{O}_{\rm M}|M,z)$ needs to be anchored, and its parameters tightly constraint within prior, such that the overall likelihood of the mass calibration depends only on the parameters of the primary observable mass relation, thus constraining them.

Mass calibration uncertainties For the sake of brevity, we shall focus on the systematic uncertainty affecting WL mass calibration. Given the advent of wide and deep photometric surveys, WL mass calibration has emerged as the principal way to calibrate cluster number count. Three sources of statistical uncertainty impact the WL signal of galaxy clusters: the shape noise due to the intrinsic ellipticity of source galaxies, the intrinsic heterogeneity of cluster mass profiles at the same mass (due to scatter around the concentration mass relation, varying degrees of substructure, orientation, triaxiality, etc.), and the statistical fluctuations in the line-of-sight integrated matter field [1094,1095]. Deeper and wider WL surveys can only reduce the first of these three noise sources.

WL mass calibration shares the systematics of the shear measurement and photometric redshift estimation inherent in the source catalogs from wide and deep photometric surveys. Furthermore, the displacement between the observed and true cluster position washes out the WL signal (mis-centering). As clusters are significant overdensities in the galaxy field, depending on the source background selection, a fraction of unlensed cluster members might contaminate the source sample and dilute the signal (cluster member contamination). Finally, baryonic effects do not only alter the total halo mass but also the halo mass profile that sources the lensing. The combined impact of these effects is summarized by establishing the relation between the WLL mass (that results from fitting the WL signal) and the halo mass on realistic WL simulations [1096–1098]. WL masses are biased low by 5%–10% depending on the fitting formula used and scatter around the true halo mass [1099–1101]. The systematic uncertainties of the aforementioned effects are distilled into an uncertainty on the bias of the WL mass [1034,1093,1102,1103]. Current understanding of baryon feedback puts a 2% lower limit on this uncertainty [1098]. Depending on the WL survey, photometric source redshift uncertainties increase this to 10% at high cluster redshifts. The other effects have a quantifiably smaller impact, as, for instance, mis-centering and cluster member contamination are partially controlled empirically [1034,1081,1093,1104].

Halo mass function The halo mass function described above only considers structures made by CDM. However, halos contain a certain amount of baryons. Neglecting this contribution leads to a systematic bias in determining the halo mass function. This can be easily understood by considering that baryons will change the total mass of the halo.

Hydrodynamical simulations found that the effects of baryons are different whether, in the simulations, radiative effects are taken into account or gas heating is only due to gravitational effects. For instance, models with AGN feedback decrease the abundance of clusters compared to DM-only simulations [1031]. The impact of baryons appears to depend on the halo mass. Considering an overdensity of 1500 times the critical density, baryons contribute up to 6%–7% to the total mass, while for 200 times the critical density, their contribution reduces to only about 1%.

In terms of number counts, [1105,1106] found that the number density of halos decreases up to 15% at low masses and redshifts, while being in broad agreement with that of DM-only simulations in the other cases. In addition, to better match X-ray and SZ observational studies, [1106] proposed fits to estimate the baryon contribution when moving from a halo defined as 200 times the critical density to one found using 500 times this density. The retrieved halo masses in the presence of baryons can also be corrected to match the expected halo masses in gravity-only simulations [1098,1107].

2.2.2.4. Results.

Cosmological parameters measurements and tensions Cosmological results on the mean matter density at present time, $\Omega_{\rm m}$, from cluster number counts agree with CMB results that it should be around 0.3. Recent results from eROSITA (0.29 ± 0.01 [1036]), SPT (0.29 ± 0.03 [1035]), WtG (0.26 ± 0.03 [1030]), XXL (0.31 ± 0.03 [1041]), *Planck* SZ (0.33 ± 0.03 [736]) and DES ($0.32^{+0.08}_{-0.07}$ [1108]), and UNIONS (0.29 ± 0.05 [1109]) are all consistent with the results from *Planck* CMB [192] of 0.315 ± 0.007.

Conversely, there is currently some disagreement between the values of σ_8 from cluster number counts obtained in various studies. While some studies find σ_8 in agreement with the CMB value of 0.811 ± 0.006 (eROSITA 0.88 ± 0.02 [1036]; SPT 0.82 ± 0.03 [1035]; WtG 0.83 ± 0.04 [1030]; XXL 0.84 ± 0.04 [1041]), *Planck* SZ found a value of 0.76 ± 0.03 [736] which is in tension with the CMB at the level of $\sim 2.5\sigma$.

Similar to the case of cosmic shear, and as highlighted in Fig. 37, consistency with CMB should be assessed by considering the entire multi-dimensional posterior distribution. For this reason, it is customary to consider the quantity, $S_8=\sigma_8\left(\frac{\Omega_{\rm m,0}}{0.3}\right)^{\alpha}$, with $\alpha=0.5$. We note, however, that the degeneracy between $\Omega_{\rm m,0}$ and σ_8 in cluster count experiments follows a slightly different slope from cosmic shear, with an index in the range 0.2 (e.g., SPT [1035]) to 0.4 (e.g., eROSITA, [1036]).

Considering only experiments including an internally calibrated WL mass-observable scaling relation, i.e., eROSITA, SPT, WtG, and XXL, the tension between $\Omega_{\rm m}$ and CMB measurements is at most 1.2-σ, thus showing a high level of consistency between experiments. The same exercise applied to σ_8 indicates a slightly higher level of tension (1.7 σ), such that potential systematics still remain at this level of precision.

Constraints on dark energy Cluster number counts are useful in providing constraints on the DE equation of state w. DE affects the growth of structures in the Universe at redshifts below ~ 1, thereby reducing the growth of massive halos. Most current studies on the DE equation of state from cluster counts assume a constant equation of state w and a flat universe. All the results published thus far are consistent with $w=-1$ (*Chandra* $w=-1.14\pm0.21$ [1052]; WtG $w=-0.98\pm0.15$ [1030]; SPT $w=-1.45\pm0.31$ [1035]; eROSITA $w=-1.12\pm0.12$ [1036]). Similar results were obtained constraining the gas mass fraction to be constant with time ($w=-1.13^{+0.17}_{-0.20}$ [1110]).

Alternative models The halo mass function, as discussed above, is a great tool to investigate the underlying cosmological model. For this reason, several authors studied its behavior in MG models, such as the normal branch of Dvali–Gabadadze–Porrati theory (nDGP) [1111] and $f(R)$ [1112] simulations. To model the HMF in MG scenarios, N-body simulations are required to calibrate the difference between the HMF in the MG simulations with respect to ΛCDM. Ref. [1111] studied the evolution of perturbations for the nDGP model, which is characterized by a time-varying gravitational constant. The numerical nDGP mass

function predicts up to three times more objects at very high masses, for strong deviations from ΛCDM, explained by the fact that the halo mass function is very sensitive to σ_8.

A similar approach, but which combines the benefits of the previous ones is that used by Refs. [1112,1113] to study the halo mass function in $f(R)$ models. The authors parameterize the modifications induced by $f(R)$ models both in the spherical collapse model and in the HMF, calibrating these modifications on N-body simulations. These modifications are a function of mass, and redshift. Finally, Ref. [1114] showed that the halo mass function is universal when expressed in terms of $\ln(\sigma^{-1})$ rather than the halo mass M.

2.2.2.5. Other cosmological probes from galaxy clusters: cluster clustering. The spatial distribution of galaxy clusters represents a valuable cosmological probe, depending on the composition of the Universe and on the nature of gravitational interaction. In particular, cluster clustering traces the growth rate of density perturbations, therefore it has been widely employed for inferring fundamental cosmological parameters, such as the matter density, $\Omega_{\rm m,0}$, and the amplitude of mass fluctuations on scales of $8\,h^{-1}$ Mpc, σ_8 [1115–1118], as well as the neutrino properties [1119] and deviations from the ΛCDM model, possibly described by the DDE parameters, i.e., w_0 and w_a [1120]. Moreover, it can be used to significantly improve the precision on the constraints from cluster weak gravitational lensing [1115] and number counts [1120], when analyzed in combination with them.

Despite the limit in the exploitation of the clustering properties due to the difficulty in collecting large homogeneous cluster samples, which leads to poorer statistics with respect to galaxy samples, cosmology with galaxy clusters presents a series of relevant advantages. First, galaxy clusters, being placed at the nodes of the filamentary structure of the cosmic web, are hosted by the latest and most massive virialized haloes formed by the hierarchical growth of cosmic structures. Therefore they are highly biased tracers, more clustered than galaxies [1018, 1121,1122]. While, in general, the galaxy bias is difficult to model properly, especially on small physical scales, and it is usually seen as a nuisance parameter in cosmological analyses based on galaxy statistics, the effective bias of galaxy cluster samples can be theoretically predicted [1117,1118,1123,1124], depending on the mass and the redshift of the hosting haloes [1125]. In turn, the cluster mass, mainly consisting of DM, can be linked to directly observable mass proxies, through the so-called mass-observable scaling relation [1018,1104,1126,1127]. However, the uncertainties on scaling relation parameters and their redshift evolution affect our ability to recover the true cluster mass and represent one of the limits of cosmological inference from galaxy clusters. This highlights the importance of having a robust WL mass calibration, capable of assessing the systematics caused by halo orientation, selection, and projection effects [1040,1081]. A second advantage is that galaxy clusters present lower peculiar velocities with respect to their host galaxies, reducing the small-scale distortions in the clustering signal, namely the Fingers of God effect, caused by nonlinear dynamics and incoherent motion within virialized structures [1128,1129].

Cluster clustering is traditionally investigated through the analysis of the two-point correlation function, $\xi(r)$, which measures the excess probability of finding a pair of objects in the volume elements δV_1 and δV_2, at the comoving separation r, relative to that expected from a random distribution. Increasing attention is being paid to higher-order statistics, and in particular, to the three-point correlation function, $\zeta(r_{12}, r_{13}, r_{23})$, which provides the probability of finding triplets of objects at comoving separations r_{12}, r_{13}, and r_{23}, and has been successfully applied for the detection of the BAO peak of galaxy clusters [1130]. These probes require the assumption of a fiducial cosmology to convert the observed angular and redshift coordinates into distances, which might be different from the true one, resulting in geometric distortions [1131], which have to be taken into account in the modeling of the clustering signal [1132,1133]. In recent years, the two-point redshift-space correlation function of a homogeneous sample of X-ray selected galaxy clusters from the XXL survey, carried out by the XMM-Newton satellite, has been used to measure a value of $\Omega_{\rm m,0}$ in full agreement with the ΛCDM model [1134]. On the other hand, optically selected clusters from the Sloan Digital Sky Survey (SDSS) have been employed to get an estimate of $f\sigma_8$, which was found consistent with General Relativity predictions [1116], to determine the distance–redshift relation, $\Omega_{\rm m,0}$ and H_0, from the BAO peak [1128,1135] and, in combination to stacked gravitational lensing, to constrain σ_8 [1115]. Moreover, from the 3D clustering of the Planck SZ selected galaxy clusters, the Planck mass bias, $b_{\rm SZ}$, and $\Omega_{\rm m,0}$, have been derived, while σ_8 was not constrained [1136]. The tomographic cluster autocorrelation from the Constrain Dark Energy with X-ray (CODEX) sample, after redshift-dependent richness selection, has been employed to explore the $\Omega_{\rm m,0} - \sigma_8$ degeneracy, putting constraints on the structure growth parameter, S_8 [1137]. Since cluster clustering is particularly sensitive to these parameters, independent constraints on S_8 have been put by measuring the two-point correlation function of the photometric clusters detected in the third data release of KiDS-DR3 [1117]. An equivalent approach consists in the study of the angular correlation function, $w(\theta)$, and its spherical harmonic counterpart, the angular power spectrum, C_ℓ [1138]. In particular, a first measurement of the auto-correlation cluster power spectrum and of the galaxy-galaxy cluster cross-spectrum has been performed on the SDSS-DR8 photometric sample [1124]. Moreover, from the tomographic study of $w(\theta)$ and C_ℓ of the same KiDS-DR3 catalog, competitive constraints on S_8 have been found [1118]. These results, being based on angular positions alone, are not affected by geometric distortions, highlighting the potential of angular cluster clustering as a cosmological probe in future photometric redshift surveys.

2.2.3. Galaxy clustering — Other probes

Coordinator: Chandra Shekhar Saraf

Contributors: Kishan Deka, and PawełBielewicz

2.2.3.1. Cross-correlations. The S_8 parameter can be measured from the redshift space clustering of galaxies by estimating the two- and three-point correlation functions or their Fourier counterparts, the galaxy power spectrum, and bispectrum. These statistics can be used to gain insights into the growth rate of cosmic structures, $f\sigma_8(z)$, from RSD at the effective redshift of the galaxy sample [1139–1141]. The galaxy clustering data can be combined with CMB surveys to yield constraints on σ_8 and S_8. Several studies [1142–1145] have reported values of σ_8 consistent with the CMB-only analyses. An illustrative schematic of estimating σ_8 parameter from cross-correlation measurements between *Planck* CMB lensing convergence map and DESI's Legacy Imaging Survey (DESI-LIS; [1146]) is shown in Fig. 38 (see Ref. [1147] for details on cross-correlation analysis). A cross-correlation between unWISE galaxies and ACT DR6 CMB lensing measurements found $S_8 = 0.813 \pm 0.021$, and $S_8 = 0.810 \pm 0.015$ with a combination of Planck and ACT cross-correlations [1144]. These measurements are fully consistent with the predictions from primary CMB measurements within our standard cosmology. Another study correlating Gaia–unWISE QSO catalog with *Planck* PR4 CMB lensing found $\sigma_8 = 0.7766 \pm 0.034$ and $\Omega_{\rm m,0} = 0.343^{+0.017}_{-0.019}$, which translates to $S_8 = 0.819 \pm 0.058$ [1143]. However, many cross-correlation analyses between CMB datasets and galaxy samples divided into narrow redshift bins [1148–1155] find low values of σ_8 and S_8 parameter (when $\Omega_{\rm m,0}$ is generally assumed to be consistent with the well constrained values from SN and CMB analyses), resulting in mild tension with *Planck* analysis. A tomographic cross-correlation of DES-Y3 data and CMB lensing from SPT and Planck estimated $S_8 = 0.734^{+0.035}_{-0.028}$ [1149]. Another cross-correlation of DESI Legacy Imaging survey LRGs and CMB lensing from *Planck* found $S_8 = 0.765 \pm 0.023$ and $S_8 = 0.790^{+0.024}_{-0.027}$ with ACT DR6 [1156].

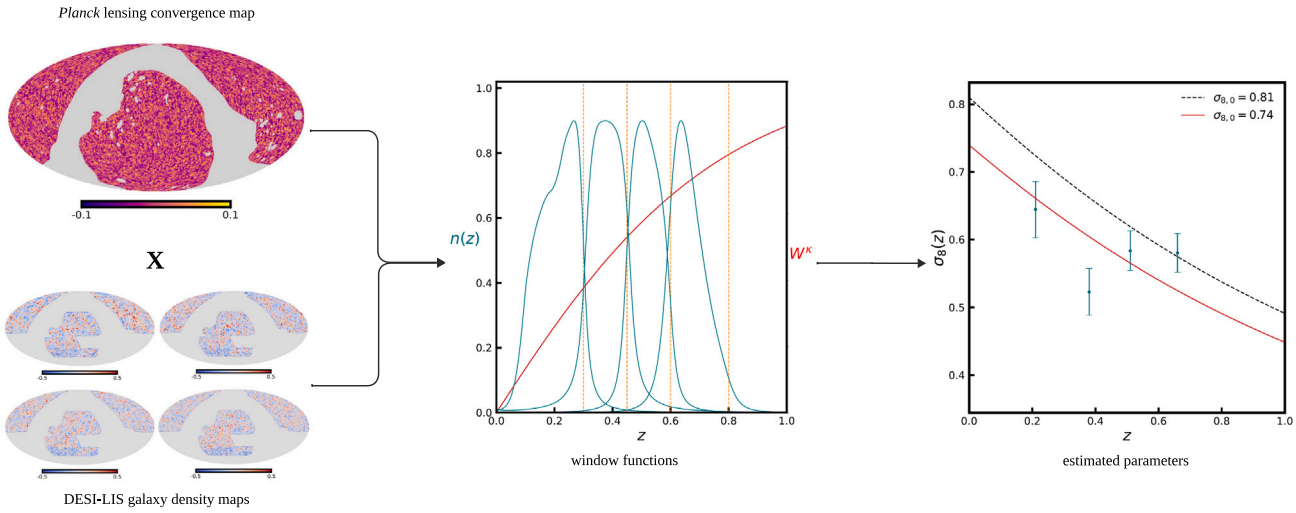

Fig. 38. An illustration of estimating σ_8 parameter from tomographic cross-correlation measurements between DESI-LIS galaxy survey and *Planck* lensing convergence map, assuming ΛCDM model [1157]. (a) The *Planck* lensing convergence map and DESI-LIS galaxy density maps in four tomographic bins, smoothed with a Gaussian beam of 60′ FWHM (only to better show the large scale distribution). (b) The galaxy redshift distribution for the four redshift bins (solid blue lines) and the CMB lensing kernel (solid red line). The vertical dashed orange lines mark the boundaries of redshift bins. (c) The σ_8 parameter estimated from cross-correlation measurements of four tomographic bins. The red line is the evolution of σ_8 parameter as estimated from cross-correlation data. The dashed black line is the evolution of σ_8 parameter measured from the *Planck* CMB data alone. (For interpretation of the references to colour in this figure legend, the reader is referred to the web version of this article.)

2.2.3.2. Full shape analyses. The σ_8 parameter can also be measured by fitting the full shape of the observed power spectrum from spectroscopic surveys as well as the galaxy bispectrum [721,1158–1162]. Furthermore, the σ_8 parameter can be translated into S_8 parameter with additional measurements of $\Omega_{m,0}$ (from power spectrum shape, SN or CMB). The measurements of S_8 parameters employing full shape analysis of the galaxy power spectrum [1158,1162] are in tension with *Planck* measurements [192], but with typically less than 3σ statistical significance. Recent constraints on the S_8 parameter from the BOSS galaxy bispectrum multipoles found $S_8 = 0.774^{+0.056}_{-0.053}$ [721] and $S_8 = 0.77 \pm 0.04$ [1161], which are statistically consistent with both CMB and WL measurements.

2.2.3.3. 3 × 2 pt analyses. The combined analysis of two-point statistics corresponding to galaxy clustering, galaxy-galaxy lensing, and cosmic shear is commonly known as the "3 × 2pt" analysis. The joint analyses provide us with an improved control of the systematic uncertainties such as galaxy bias and intrinsic alignments. The first 3 × 2pt analysis were published with the datasets from KiDS-450 × {2dFLenS + BOSS} [1163], KiDS-450 × GAMA [1164] and DES-Y1 [1165]. The DES-Y1 analysis used photometric galaxies as both lens and sources, finding $S_8 = 0.773^{+0.026}_{-0.020}$. The KiDS collaboration, on the other hand, used overlapping imaging and spectroscopic surveys, resulting in $S_8 = 0.742 \pm 0.035$ when combined with 2dFLenS + BOSS, and $S_8 = 0.800^{+0.029}_{-0.027}$ with GAMA survey.

The updated constraints on S_8 with 3 × 2pt analyses combining KiDS-1000 with {2dFLenS + BOSS} datasets gives $S_8 = 0.766^{+0.020}_{-0.014}$ [874], at 3.1σ tension with *Planck* constraints within the ΛCDM model. The recent measurements from the DES-Y3 datasets resulted in $S_8 = 0.776 \pm 0.017$ in the ΛCDM cosmology and $S_8 = 0.775^{+0.026}_{-0.024}$ assuming a wCDM model [869]. However, a joint analysis of DES-Y3 3 × 2pt data, *Planck* CMB anisotropy data (without lensing), eBOSS BAO and RSD measurements, and DES SNIa data provides $S_8 = 0.812 \pm 0.008$ in the ΛCDM model. A joint cosmic shear analysis of KiDS-1000 and DES Y3 data has obtained stringent constrain of $S_8 = 0.790^{+0.018}_{-0.014}$ [867]. Another 3 × 2pt analyses performed with the HSC-Y3 imaging data and SDSS BOSS DR11 spectroscopic galaxies yielded $S_8 = 0.775^{+0.043}_{-0.038}$ for the ΛCDM model [872]. The HSC-Y3 analysis is highly consistent with both KiDS-1000 and DES-Y3 measurements of S_8 within one standard deviation.

2.2.3.4. Systematics. The measurements of cosmological parameters from large-scale structure evolution at low redshifts require state-of-the-art analysis pipelines to correct for a large number of systematic effects. The observation sector can include effects such as atmospheric and extragalactic extinction, stellar contamination, airmass and blurring [1166], fiber collisions [1167], angular and radial modes systematics [1168].

For the cross-correlation between galaxy clustering and CMB, galaxy survey systematics such as photometric calibration errors, foreground contamination and catastrophic errors need to be modeled and mitigated for unbiased inferences [1152,1155,1169–1171]. In order to allow tomographic cross-correlations with photometric galaxy surveys, both precise individual galaxy photometric redshifts and accurate redshift distributions for the ensemble, require techniques for redshift determination. Typically, a subset of spectroscopically observed sources are used to train, validate and calibrate photometric redshifts and redshift distributions. The accuracy of the redshift distribution directly impacts the accuracy of estimated cosmological parameters. Biases in the mean redshifts of the tomographic bins will cause a bias in S_8. Recently, [1147,1157] have shown the importance of precise modeling of redshift error distributions and redshift bin mismatch of objects, when estimating σ_8 and S_8 parameters.

In the theory sector, the largest uncertainty comes from the accuracy of the models for non-linear clustering of galaxies. The cross-correlation measurements, full shape analyses, and the bispectrum multipoles, all depend on the accurate modeling of the non-linear regime in the redshift-space galaxy clustering. This uncertainty has been improved after the significant progress from the effective field theory of the large-scale structure which provides accurate description of galaxy clustering at large scales [719,722,1172–1180].

2.3. Other challenges

2.3.1. Systematics and the $A_{\rm lens}$ parameter

Coordinator: William Giarè

Contributors: Alessandro Melchiorri, Anto Idicherian Lonappan, Deng Wang, Elsa M. Teixeira, Enrico Specogna, Giulia Gubitosi, Ido Ben-Dayan, Matteo Forconi, Özgür Akarsu, and Rita B. Neves

On scales smaller than ten arcminutes, the interaction between CMB photons and the Universe's large-scale structure becomes significant, giving rise to second-order anisotropies. One of the most important contributions is the gravitational deflection, or lensing, experienced by CMB photons along their paths [1181]. At arcminute scales, lensing deflections distort the observed image of the CMB fluctuations, imprinting a distinctive non-Gaussian four-point correlation function (or trispectrum) in both the temperature and polarization anisotropies [1181]. This signal can be extracted with a high signal-to-noise ratio by correlating power in different directions on the sky, leading to a direct reconstruction of the power spectrum of the CMB lensing field, now measured at $\sim 40\sigma$ [694,695,1182,1183].

Although gravitational lensing does not alter the overall distribution of primary CMB anisotropies, it leaves distinctive signatures in the spectra of temperature and polarization anisotropies. The most relevant effects are the conversion of E-mode polarization to B-modes, the transfer of power to the damping tail, and the lensing-induced smoothing of the acoustic peaks and troughs in the TT, TE, and EE spectra. The degree of smoothing is directly tied to the amplitude of the power spectrum of the lensing potential, which is derived from the six ΛCDM parameters. As a result, interesting consistency tests have been proposed to verify whether the amplitude of lensing inferred through the high-ℓ smoothing of acoustic peaks matches the theoretical predictions of the standard cosmological model.

In Ref. [724], the phenomenological parameter $A_{\rm lens}$ was introduced to encompass various physical mechanisms that might affect the lensing amplitude. This parameter scales the amplitude of the lensing trispectrum, effectively accounting for the associated smoothing effects in the CMB temperature and polarization spectra. $A_{\rm lens}$ is defined such that $A_{\rm lens} = 1$ matches the standard ΛCDM prediction, whereas $A_{\rm lens} = 0$ corresponds to a scenario where CMB lensing is disregarded altogether. By allowing $A_{\rm lens}$ to remain a free parameter in theoretical models, its value can be directly constrained by data, potentially confirming or deviating from the ΛCDM predictions.

Focusing on the Planck-2018 data release (PR3), the analysis of the Planck `plik` likelihood for the TT, TE, and EE spectra at $\ell > 30$, combined with the `Commander` likelihood for the TT spectrum at $2 \leq \ell \leq 30$ and the `SimAll` likelihood for the EE spectrum at $2 \leq \ell \leq 30$, yields $A_{\rm lens} = 1.180 \pm 0.065$ [192]. This finding suggests an excess lensing signal at approximately 2.8σ, resulting from a significant improvement in χ^2 of approximately $\Delta\chi^2 \sim 9.7$. This improvement primarily originates from high-ℓ temperature and polarization data, particularly within the multipole range $600 < \ell < 1500$. As shown in Fig. 24 of Ref. [192], there is a visible preference for increased lensing smoothing in the oscillatory residuals in the TT spectrum at $1100 < \ell < 2000$.

Since 2018, the Planck data has undergone substantial reanalyses. The new Planck PR4 (`NPIPE`) CMB maps incorporate significant improvements, such as increased coverage of sky area at high frequencies, improved processing of time-ordered data, and approximately 8% more data accounted for in the lensing trispectrum reconstruction. Updated likelihoods for temperature and polarization spectra have been released following these developments. The latest versions of `CamSpec` [700] and `HiLLiPoP` [701] — two likelihoods already employed in various studies by the Planck collaboration — are now based on the Planck PR4 (`NPIPE`) maps, reducing small-scale noise compared to `plik` and enhancing the constraints on cosmological parameters by up to 10%. Both likelihoods indicate a shift toward $A_{\rm lens} = 1$. For `CamSpec`, the constraints on the lensing amplitude inferred from high-ℓ smoothing of acoustic peaks are summarized in Table 6 of Ref. [700]. Temperature and polarization data reduce the preference for $A_{\rm lens} > 1$ to less than 1.7σ while focusing solely on the TT spectrum increases the lensing anomaly to 2.3σ. Constraints on $A_{\rm lens}$ resulting from the new `HiLLiPoP` likelihood are summarized in Table 6 of Ref. [701]. They consistently agree with ΛCDM at 1σ.

These new reanalyses suggest that the preference for excess power smoothing has decreased in the `NPIPE` maps, lending weight to interpreting the lensing anomaly as systematics in the Planck PR3 data. The latter interpretation finds support in CMB experiments other than Planck. ACT and the SPT have released precise small-scale measurements of the spectra of temperature and polarization anisotropies [704,725,732], as well as precise reconstructions of the lensing trispectrum [695,1183,1184]. The Data Release 4 of the ACT constrains $A_{\rm lens} = 1.01 \pm 0.11$ in remarkable agreement with the baseline value (see Fig. 16 of Ref. [702]). Similarly, the SPT TT, TE, and EE spectra analysis gives $A_{\rm lens} = 0.87 \pm 0.11$, consistent with ΛCDM at 1.2σ. In this case, we refer to Table V of Ref. [704] and Table VII of Ref. [725] for earlier analyses involving only the EE and TE spectra (yielding $A_{\rm lens} = 0.98 \pm 0.12$).

Fig. 39 summarizes the 68% CL intervals for the parameter $A_{\rm lens}$, inferred over the years from the analysis of lensing-induced smoothing of the acoustic peaks and troughs in the TT, TE, and EE spectra measured by various experiments and likelihoods discussed so far.

2.3.2. Evidence for a nonvanishing Ω_k

Coordinator: Will Handley

The spatial curvature of the Universe, parameterized by Ω_k, is a fundamental parameter in cosmology, intimately tied to the geometry and fate of the Universe. While the inflationary paradigm predicts a value extremely close to zero, it is important to observationally test this prediction. In the standard cosmological model, Ω_k is degenerate with other parameters when using CMB data alone, such that CMB data do not provide strong constraints on curvature. However, the addition of external data sets, such as BAO measurements, can break this degeneracy.

The Planck 2018 data release presented an intriguing hint of a possible departure from a flat universe. Analyzing the TT,TE,EE+lowE data, the Planck team found a preference for negative values of Ω_k in the range $-0.095 < \Omega_k < -0.007$ at 99% confidence level, with $\Delta\chi^2_{\rm eff} = -11$ compared to the baseline ΛCDM model [192]. This preference was attributed to a combination of volume effects and better fits both the high-ℓ and low-ℓ data in closed models. Notably, closed models predict a higher lensing amplitude ($A_{\rm L}$), which can explain the preference for $A_{\rm L} > 1$ in Planck data, and also a better fit to the low-ℓ temperature power spectrum. Adding Planck lensing data to TT,TE,EE+lowE, the constraint on Ω_k shifts to $\Omega_k = -0.0106 \pm 0.0065$ at 68% confidence level, reducing the preference for closed models to less than 2σ. Finally, including BAO data results in $\Omega_k = 0.0007 \pm 0.0019$, consistent with a flat universe at 1σ [192].

However, this conclusion has been challenged in the literature. Ref. [1185] and Ref. [1186] show that there is Bayesian evidence for a closed universe, albeit not quantified in the Planck paper, and that the Planck lensing reconstruction is in tension with TT,TE,EE+lowE data at 2.5σ. In particular, the tension is driven by the preference for a higher value of $A_{\rm L}$ in closed models, which is not supported by the Planck lensing reconstruction. They argue that BAO data are also in tension with TT,TE,EE+lowE data, and that combining these datasets is not justified. Ref. [1187] conversely shows that the preference for $\Omega_k < 0$ is reduced when using the CamSpec likelihood, which uses more data than the Planck baseline likelihood, and argue that BAO data strongly prefer flat universes.

More recently, Ref. [1188] showed that the BAO scale measurements implicitly assume a fiducial ΛCDM cosmology, and that the

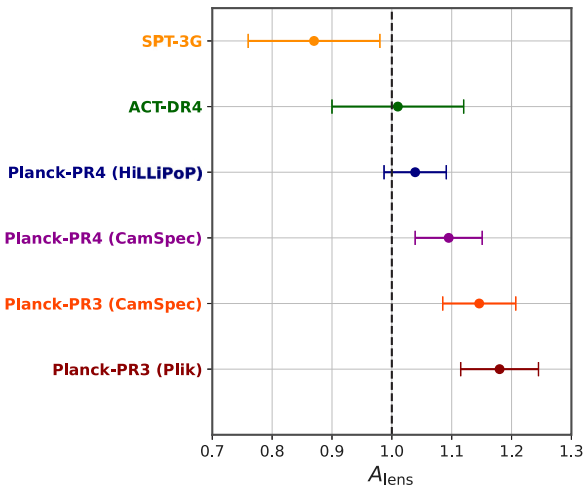

Fig. 39. The whisker plot summarizes the 68% CL intervals for the parameter $A_{\rm lens}$, inferred over the years from the analysis of lensing-induced smoothing of the acoustic peaks and troughs in the TT, TE, and EE spectra measured by various experiments with different likelihoods. Constraints based on the Planck-PR3 measurements indicate an excess of lensing, which is reduced in the recent Planck-PR4 updated likelihoods. Small-scale temperature and polarization spectra from ACT-DR4 and SPT-3G are in overall agreement with $A_{\rm lens} = 1$, consistently recovered within one standard deviation (or slightly more).

preference for a flat universe can be weakened when relaxing these assumptions. They find that using the full shape of the galaxy power spectra, the tension between BAO and Planck data in the Ω_k parameter is reduced to $\sim 1.5\sigma$.

The tension between Planck CMB data and BAO measurements in the context of non-vanishing curvature has motivated numerous works that explore its possible origin and its implications for cosmology. For example, Ref. [1189] used CC as an alternative dataset to break the geometric degeneracy, finding $\Omega_k = -0.0054 \pm 0.0055$, consistent with a flat universe. However, the tension between different H_0 measurements persists even in the context of non-flat models [1190–1192].

The curvature tension therefore remains an open problem in cosmology. Future observations, such as those from DESI, Euclid, and the Vera Rubin Observatory will provide more precise BAO measurements, which will allow us to test the robustness of the flat Universe assumption and potentially shed light on the origin of this discrepancy.

2.3.3. Anisotropic anomalies in the cosmic microwave background radiation

Coordinator: Leandros Perivolaropoulos

Contributors: András Kovács, Anto Idicherian Lonappan, Emanuela Dimastrogiovanni, Eoin Ó Colgáin, Frode K. Hansen, Giulia Gubitosi, Laura Mersini-Houghton, Marina Cortês, Nils A. Nilsson, Shahin Sheikh-Jabbari, and Venus Keus

The CMB, a relic from the early Universe, provides crucial insights into cosmology. Observations by COBE, WMAP, and *Planck* have revealed several anisotropic anomalies that may challenge the prevailing ΛCDM cosmological model and the cosmological principle, prompting a reevaluation of our understanding of the early Universe's structure and the inflationary paradigm [1193,1194].

One such anomaly is the unusually low quadrupole moment ($\ell = 2$) in the CMB power spectrum, which deviates from the predictions of cosmic variance and the ΛCDM model [726,1195]. This anomaly has implications for inflationary cosmology and may require theoretical adjustments. The low quadrupole moment was first observed by COBE and later confirmed by WMAP and *Planck*, with increasing precision. The statistical significance of this anomaly has been thoroughly investigated, and its persistence across multiple observations challenges our understanding of the primordial power spectrum and the inflationary paradigm. Theoretical efforts to explain the low quadrupole moment have included modifications to the inflation model, such as a running spectral index or a cutoff in the primordial power spectrum at large scales [1196,1197].

Another striking feature is the alignment of the quadrupole and octopole moments, which appears to be oriented with the ecliptic plane and the motion of the Solar System [1198,1199]. This alignment violates statistical isotropy and suggests potential cosmological or local explanations. The quadrupole–octopole alignment was first reported using WMAP data and later confirmed by *Planck*, with both missions providing strong evidence for its existence. The alignment has been studied extensively, with some proposing that it could be a signature of cosmic topology [1200], while others have investigated the possibility of local foreground contamination or systematic effects [1201,1202]. The statistical significance of this alignment and its potential origins remain active areas of research.

The upper and lower panels of Fig. 40 illustrate the derived quadrupole and octopole moments, respectively. The alignment of these moments with the ecliptic plane highlights one of the key anisotropic anomalies in the CMB. This alignment suggests a possible violation of statistical isotropy and indicates that there may be underlying cosmological or local causes for this observed pattern. Understanding the significance and origins of these alignments is crucial for interpreting the implications for the standard cosmological model and exploring potential new physics.

The CMB also exhibits a hemispherical power asymmetry, known as the dipolar power distribution, where one half of the celestial sphere has significantly more temperature fluctuations than the other [1204, 1205]. The scale and statistical significance of this asymmetry raise questions about the density variations in the early Universe. The hemispherical power asymmetry was first detected in WMAP data and later confirmed by *Planck*. The hemispherical asymmetry can be considered as two different anomalies as described in detail in Ref. [1205]. For larger scales, $\ell < 100$, the asymmetry can be modeled as a dipolar modulation of an isotropic field. The p-value of this modulation asymmetry has been reported as $0.1 - 1\%$, but considerably less significant when correcting for the choice of $\ell_{\rm max}$. The second hemispherical asymmetry, the angular clustering asymmetry, extends to much smaller scales. By estimating the CMB power spectrum locally in different parts of the sky, maps of the spatial distribution of the power spectrum can be estimated for different multipole ranges. When estimating a dipole for these local power spectrum maps at different scales, these dipoles are found to cluster. This clustering is found to persist at least to $\ell = 1000$ and only $1/1000$ simulations show similar clustering. The clustering direction is close to the direction of the large scale dipolar asymmetry. The origin of

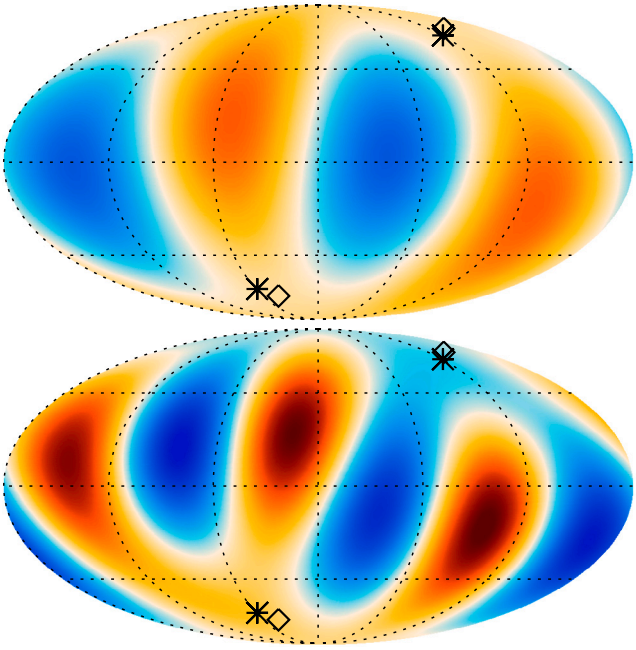

Fig. 40. Upper Panel: Derived quadrupole moment from the Planck SMICA map, showing the preferred axis of the quadrupole. Lower Panel: Derived octopole moment, indicating the alignment with the quadrupole. These alignments suggest a significant anomaly in the CMB, challenging the assumption of statistical isotropy. The plus and star symbols indicate the axes of the quadrupole and octopole, respectively, around which the angular momentum dispersion is maximized. The diamond symbols correspond to the quadrupole axes after correction for the kinematic quadrupole. From Ref. [1203].

this asymmetry remains unclear, with some proposing that it could be a signature of non-Gaussianity in the primordial perturbations [1206–1208], while others have explored the possibility of a super-horizon scale mode modulating the primordial power spectrum [1209].

Additionally, there is a parity asymmetry in the CMB, with a preference for odd-parity modes over even-parity modes, challenging the scale invariance of primordial fluctuations [1210,1211]. The parity asymmetry was first reported using WMAP data and later confirmed by *Planck*, with both missions providing evidence for a statistically significant difference between the power in odd and even multipoles. This asymmetry has been studied in the context of the primordial tensor-to-scalar ratio, with some suggesting that it could be a signature of chiral gravity [1212,1213]. The physical origin of this asymmetry and its implications for the inflationary model remain open questions.

The Cold Spot is another intriguing anomaly — a large, unusually cold region in the CMB, surrounded by a hot ring [1214–1216]. Both the WMAP and *Planck* missions identified it as a significant deviation from the Gaussian random field expectation ($\sim 3\sigma$), and its region has been studied extensively. To explain it, novel cosmological mechanisms [1217,1218], a cosmic texture [1219], a large void in the line-of-sight [1220], and a systematic effect [1214,1221] have all been investigated. Importantly, the *Eridanus supervoid* ($R \approx 200\ \mathrm{h}^{-1}\mathrm{Mpc}$, $\delta \approx -0.2$) was detected at $z < 0.3$ aligned with the Cold Spot, based on galaxy counts from multiple surveys [1222,1223]. This evidence is supported by reconstructions of the cosmic velocity field [1224] and WL analyses by the DES team [1225], suggesting a causal relation between these individually rare objects in the CMB and in the cosmic web. Yet, the statistical significance of the Cold Spot and its potential origins remain active areas of research.

Another very significant CMB anomaly, which potentially could give rise to many of the above mentioned anomalies, is the cooling of CMB photons around nearby galaxies. First discovered in Ref. [1226], the stacking of CMB temperatures in areas around the halos in nearby $z < 0.015$ late type spiral galaxies showed lower CMB temperatures compared to elsewhere on the sky. This was followed up in Ref. [1227] where it was shown that an attempt at modeling the discovered cooling of CMB photons around galactic halos gives rise to several of the observed anomalies. In particular, the hemispherical asymmetries and the cold spot arise naturally in such a scenario with the correct directions on the sky. Correlations are found between the largest scales of the CMB and the nearby galaxy distribution obtained from the 2MRS galaxy catalog [1228]. In Ref. [1221] a detailed study of the galaxies in the cold spot areas showed that the shape and size of the cold spot to a large degree could be explained by cooling of the galaxies in this area. In particular, the nearby large Eridanus group of galaxies is located at this position. In Ref. [1229], the cooling was found to correlate to the nearby cosmic density field. In Ref. [1230], the cooling is detected at the 5.7σ significance level when looking at galactic halos in the most massive nearby cosmic filaments. Even when correcting for the look-elsewhere-effect by allowing for different choices of galaxy properties, the detection is stronger than in any of 10.000 simulated CMB skies. Finally, Ref. [1231] shows that by masking the affected area on the sky, the estimate of the cosmological parameters is not significantly altered. The origin of the cooling of CMB photons in galactic halos is unknown, but in Ref. [1230], it is speculated whether DM could be involved.

The statistical independence and potential interconnections between these anomalies are crucial areas of investigation. For example, the relationship between the low quadrupole moment and the lack of large-angle correlations in the CMB is of particular interest [1232,1233]. The lack of large-angle correlations was first reported using COBE data and later confirmed by WMAP and *Planck*, with all three missions providing evidence for a significant deficit of correlations on angular scales greater than $\sim 60°$. This anomaly has been studied in the context of cosmic topology [1234,1235], with some proposing that it could be a signature of a non-trivial topology of the Universe. The relationship between the lack of large-angle correlations and the low quadrupole moment has also been investigated, with some suggesting that they may share a common origin [1236].

Collectively, these anomalies pose a significant challenge to the standard model of cosmology. While some of these anomalies may be the result of foreground contamination or systematic effects, their persistence across multiple observations and their statistical significance suggests that they may have a cosmological origin. The standard ΛCDM model, which assumes a flat, homogeneous, and isotropic Universe, struggles to explain these anomalies, and their existence may require modifications to the model or the development of new theoretical frameworks.

Upcoming observational missions, such as the *Euclid* space telescope and next-generation ground-based CMB experiments, have the potential to shed new light on these anomalies [437,682]. These missions will provide unprecedented sensitivity and angular resolution, allowing for a more detailed study of the CMB and its anomalies. In particular, the *Euclid* mission will provide detailed measurements of the large-scale structure of the Universe, which can be used to test models of the early Universe and the origin of the CMB anomalies. Next-generation CMB experiments, such as CMB-S4, will provide a significant improvement in sensitivity and angular resolution, allowing for a more detailed study of the CMB power spectrum and its anomalies.

Several theoretical frameworks and models have been proposed to explain these anomalies, such as the role of topology in large-angle CMB correlations [1235], the impact of a cosmological GW background [1237], and the effects of superhorizon isocurvature DE [1209]. Other models, including anisotropic k-essence [1238], loop quantum cosmology [1239], non-canonical anisotropic inflation [1240], and unexpected topology of temperature fluctuations [1234], have also been explored. These models aim to provide a theoretical framework that

can account for the observed anomalies while maintaining consistency with other cosmological observations.

The development of new theoretical models and advanced simulations will also be crucial in understanding the early Universe's complexities. Theoretical efforts to explain the CMB anomalies will require a deep understanding of the physics of the early Universe, including the dynamics of inflation, the generation of primordial perturbations, and the evolution of the Universe in the presence of DE and DM. Advanced simulations, such as those performed with the *Planck* Sky Model [1241], will be essential in understanding the impact of foreground contamination and systematic effects on the observed CMB anomalies.

In the early 2000's in the program of investigation of the selection of the initial conditions of our Universe [1242–1245], authors proposed to allow the wave-function of the Universe to propagate on the landscape of string theory and used quantum cosmology to derive the probability of our origin. This was the first work where the answer was derived from an underlying fundamental theory. It showed that in contrast to previous beliefs, the most likely Universe to spontaneously come into existence is the one that starts at very high energy. The authors proposed to use the quantum entanglement between branches of the wave function as a way to test the theory and, for the first time to have a handle to test the existence of the quantum multiverse [1218,1246]. Traces of earlier entanglement are imprinted as anomalies in our sky. The authors calculated and predicted a series of seven anomalies, including the Cold Spot, power asymmetry, alignments, and suppression of power in lowest multipoles, etc., all of which are by now observed. Status of the predicted anomalies against observations showed perfect agreement [1247–1250].

As cosmology continues to evolve, the anisotropic anomalies in the CMB serve as a reminder of the importance of critically examining our models and assumptions, driving us to deepen our understanding of the cosmos. The existence of these anomalies suggests that our current understanding of the early Universe and the origin of cosmic structure may be incomplete, and that new theoretical frameworks and observational efforts may be necessary to fully explain the observed features of the CMB. As we continue to study these anomalies and their implications for cosmology, we may uncover new insights into the fundamental nature of the Universe and the physical processes that shaped its evolution.

2.3.4. Hints of dynamical dark energy in DESI baryon acoustic oscillations and beyond

Coordinator: William Giarè

Contributors: Anton Chudaykin

DESI has recently released data from its first (DR1) [699,745,783,809,1251] and second (DR2) [717,1252–1254] year of BAO measurements, based on observations of tens of millions of extragalactic objects, including galaxies, QSOs, and Lyman-α forest tracers. These DESI BAO observations provide precise constraints on the transverse comoving distance, the Hubble rate, and their combination (all relative to the sound horizon at the drag epoch) across seven redshift bins in the range $0.1 < z < 4.2$.

One of the most notable results from DESI BAO observations concerns the nature of DE. As initially highlighted by the DESI collaboration's DR1 results [699,1251] and recently confirmed by DR2 results [717,1255], the combination of DESI BAO with CMB data from the *Planck* satellite and SNIa distance moduli measurements from three independent SNIa samples (i.e., the Pantheon-plus catalog [32,33], the Union3 compilation [1256], and five-year observations from DESy5 [1257–1259]) provides moderate to strong evidence for a time-evolving DE component, commonly referred to as DDE. One important aspect of this preference is that the data indicates a phantom crossing scenario, in which the dark energy equation of state crosses the $w = -1$ [1260]. While this behavior presents theoretical challenges for most simple scalar-field models, it can be realized in multi-field scenarios, alternative models of gravity [1261–1264]. The DESI preference for an evolving DE has been explored in the context of general scalar-tensor Horndeski theories [1265–1268] and in modified gravity models with non-minimal coupling [1266,1269].

Given the potential impact of these results on our understanding of the Universe, caution is essential, and thoroughly testing the robustness of these findings is of paramount importance. Unsurprisingly, a significant portion of the cosmology and high-energy physics community has actively engaged with this issue, clarifying and/or bringing up several aspects and concerns surrounding this preference toward DDE. In the following, we review some of the key results that have emerged from the consistency checks conducted over the past few months, highlighting both the strengths and weaknesses of the observed preference, while stressing aspects that warrant further clarification.

- **Parameterization of the Equation of State –** Barring, for the moment, any potential systematic issues in the different datasets involved in the analyses, a first key aspect that has undergone significant cross-checking [809,1269–1281] is the parameterization used to describe the DE EoS. Originally, the DESI collaboration parameterized the time evolution of the EoS using the linear CPL form, $w(a) = w_0 + w_a(1-a)$, arguing that various combinations of data indicate a consistent preference for a present-day quintessence-like EoS ($w_0 > -1$) that crosses the phantom barrier ($w_a < 0$). Specifically, within this parameterization, DESI DR1 BAO measurements, when combined with Planck CMB and DESy5 SNIa, yield a preference for DDE at a significance level of $\sim 3.9\sigma$. This preference decreases to $\sim 2.5\sigma$ ($\sim 3.5\sigma$) when replacing DESy5 with Pantheon-plus (Union3) [699]. Notably, within the same CPL parameterization, these results remain stable when substituting DESI DR1 BAO with the latest DR2 DESI measurements. The latter not only confirms the preference for DDE but also consistently strengthens it by approximately $\sim 0.3\sigma$ across all dataset combinations with BAO and SNIa. Although the CPL parameterization has been shown to match the background evolution of distances arising from the exact DE equations of motion with about 0.1% accuracy for viable cosmologies across a broad range of physics (including scalar fields, MG, and phase transitions see, e.g., Refs. [298,1282]) alternative parameterizations that deviate from CPL at both $z \ll 1$ and $z \gtrsim 1$ remain consistent with current observations. In Ref. [1283], it was argued that assuming the CPL parameterization is not the primary driver of this preference. When combining CMB, DESI BAO, and SNIa measurements within various EoS parameterizations, w_0 consistently remains in the quintessence regime, while the constraints on w_a indicate a preference for a dynamical evolution crossing into the phantom regime (see also Ref. [1280]). This result holds for both DESI DR1 and the latest DESI DR2 BAO measurements, as confirmed by the DESI collaboration in Ref. [1255]. In this sense, the preference is to be considered robust against different models.
- **DESI BAO measurements (and beyond)–** Since the preference for DDE was first highlighted by the DESI collaboration, the impact of DESI BAO DR1 data on this preference has been carefully scrutinized, with systematic effects in DESI BAO measurements remaining a topic of debate, see, e.g., Refs. [1265,1284–1287]. Notably, the DESI BAO measurement at $z = 0.71$ exhibits a $\sim 3\sigma$ tension with predictions from the Planck best-fit ΛCDM cosmology, making it a key driver of several hints for new physics, including (part of) the preference for DDE. However, it is crucial to emphasize that *(i)* the latest DESI DR2 BAO measurements not only confirm the preference for DDE but also consistently strengthen it by approximately $\sim 0.3\sigma$ across all dataset combinations with BAO and SNIa. While this increase in preference from DESI DR1 to DESI DR2 is not highly statistically significant, it definitively reinforces the signal, suggesting that the

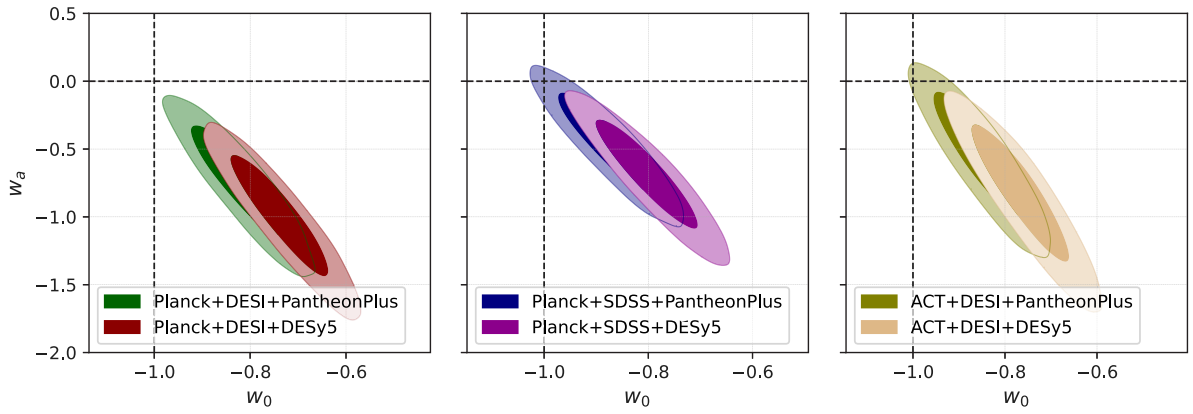

Fig. 41. Observational constraints in the w_0-w_a plane (at 68% and 95% CL) assuming a CPL parameterization for DE across different datasets. The left panel shows constraints from a combination of the Planck `Plik` likelihood for high-ℓ TT, TE, and EE PR3 spectra, the `Commander` and `SimAll` likelihoods for low-ℓ temperature and polarization (TT and EE), and Planck PR4 `NPIPE` combined with ACT-DR6 lensing likelihoods, along with DESI DR1 BAO and Pantheon-plus / DESy5 SNIa data. The middle panel examines the impact of replacing DESI BAO with SDSS BAO, while the right panel explores how the constraints shift when Planck is replaced with ACT-DR4 for temperature and polarization spectra and ACT-DR6 for lensing.

initial preference for DDE observed in DESI DR1 may not be merely a statistical fluctuation resulting from a preliminary one-year observation. *(ii)* In combined analyses of CMB, BAO, and SNIa data, the preference for DDE is not exclusively driven by DESI BAO, whether from DR1 or DR2. In fact, as reported in Ref. [1288], a similar shift toward DDE is observed when replacing DESI BAO measurements with SDSS BAO. Planck CMB combined with SDSS BAO and DESy5 SNIa indicates a preference for DDE at a statistical significance exceeding 2.5σ, see also Fig. 41. Likewise, Planck CMB combined with SDSS BAO and Union 3 points to a DDE component at $\gtrsim 2\sigma$ significance. The only combination where this preference is notably weakened below 2σ is when SDSS BAO and Pantheon-plus SNIa are analyzed together with Planck CMB. Importantly, across all independent datasets — each showing hints of deviation from a cosmological constant at varying levels of statistical significance — a consistent shift in parameter space is observed in the same direction, namely toward a quintessence-like equation of state in the present epoch that transitions into a phantom-like regime in the past. Overall, while DESI BAO data undoubtedly strengthen the preference for DDE, the other datasets involved in the analysis — most prominently SNIa distance modulus measurements — play an equally significant role in shaping this result. For further discussions on BAO data, we refer to Section 2.1.19.

- **SNIa–** It quickly became clear that SNIa data play a major role in driving the preference for DDE. Excluding DESI BAO and considering data combinations involving Planck CMB and either DESy5 or Union3 (i.e., without including any BAO surveys) already leads to a preference for DDE at $\sim$ 2–2.5σ (see, e.g., Refs. [1288, 1289]). Given the crucial role of SNIa measurements in this trend, the potential impact of systematic effects has been widely investigated [523,1290–1294], particularly for the DESy5 sample, which exhibits the strongest shift toward DDE. For instance, Ref. [1295] highlighted the influence of SNIa measurements, reporting a cross-correlation between the PantheonPlus and DESy5 supernova samples that suggested a calibration difference of $\sim$ 0.04 mag between low and high redshifts. Correcting for this offset brings the DESy5 sample into closer agreement with Planck's ΛCDM cosmology. Since the parameter space favored by the uncorrected DESy5 sample diverges from many other cosmological datasets, it has been suggested that the apparent evidence for DDE might primarily arise from systematic effects in DESy5 SNIa. In response to these concerns, the DES collaboration in Ref. [1296] showed that the debated $\sim$ 0.04 mag offset between Pantheon+ and DESy5 at low and high redshift is partly due to improvements in the modeling of supernova intrinsic scatter and host galaxy properties in DESy5 (which account for up to $\sim$ 43% of the offset) and partly ($\sim$ 38%) due to a misleading comparison. The latter arises because different selection functions characterize the DES subsets included in Pantheon+ and DES-SN5YR, leading to differences in individual supernova distance measurements due to distinct bias corrections. Therefore, while SNIa data do play a pivotal role in shaping the preference for DDE, these findings might warrant additional tests to carefully assess potential systematics before drawing definitive conclusions. For further discussions on SNIa data, we refer to Section 2.1.7.
- **Planck CMB data (and beyond):** The final dataset considered in these analyses is the CMB angular power spectra, measured by the Planck Collaboration. While a DDE component primarily affects the late-time evolution of the Universe, it also has a non-negligible impact on the CMB spectra. The most significant effect of DE dynamics on the CMB angular power spectrum is observed in the amplitude of the ISW plateau at very large angular scales. This amplitude is mainly determined by primordial inflationary parameters (A_s and n_s) and contributions from the late-time ISW effect, which is sensitive to DE dynamics (see also Section 2.3.9). Specifically, a phantom (quintessence) DE component suppresses (enhances) the decay of gravitational potentials that source the late ISW effect. Therefore, assessing the impact of Planck measurements on the preference for DDE is certainly worthwhile. As discussed in Ref. [1297], Planck data — particularly the large-scale temperature and E-mode polarization measurements — play a crucial role in reinforcing the preference for DDE reported by the DESI collaboration. Several studies in the literature [192, 1298–1303] have highlighted that temperature and polarization data at large angular scales ($\ell \lesssim 30$) drive a number of mild anomalies, including a latent preference for a phantom-like DE component [192,1298,1299]. As discussed in Ref. [1297], temperature and E-mode polarization anisotropy measurements at $\ell \lesssim 30$ are precisely the subsets of Planck data strengthening the shift toward DDE, as well. Notably, when Planck's large-scale data are excluded from the analysis or when considering alternative CMB experiments that are independent of Planck, the preference for DDE diminishes significantly. In these cases, no strong preference for DDE is observed when combining DESI with Pantheon-plus SNIa data, and the ΛCDM model remains consistent within (or close to) the 95% confidence level results. For instance, no convincing preference for DDE is found in any combination involving SPT data, whether using DESI BAO together with Pantheon-plus or DESy5, or even when including

Planck/WMAP large-scale temperature and polarization measurements. Similarly, in analyses involving ACT data, a preference for DDE is observed only when combining ACT with DESI BAO and DESy5 SNIa, while it gets diluted when replacing DESy5 with Pantheon-plus, see also Fig. 41. However, when Planck large-scale temperature and polarization measurements are combined with ACT small-scale temperature and polarization data, a preference for DDE (re-)emerges. Long story short, in the CMB front of the analysis, the shift toward DDE is primarily strengthened by Planck's large-scale data, while other CMB experiments generally weaken the case for DDE. Taking a conservative stance, this adds to broader concerns about potential systematic issues raised in other datasets discussed earlier.

2.3.5. Neutrino tensions

Coordinator: Gabriela Barenboim

Contributors: Adèle Poudou, Janusz Gluza, Mariana Melo, Matteo Forconi, Olga Mena, Rasmi Hajjar, Rishav Roshan, and Stefano Gariazzo

Neutrino physics is in its Golden Age era. Neutrinos possess unique characteristics that set them apart. Firstly, they are significantly lighter than other fermions by several orders of magnitude. Remarkably, no direct mass measurement has yet provided evidence for a non-zero neutrino mass; for all detected neutrinos, $E = pc$ within errors. Secondly, they have their own cosmological background. Neutrinos are often described as "elusive" due to their nature, yet they are incredibly abundant throughout the Universe. Their near absence of interaction is why we seldom detect their presence. This relic neutrino background has never been detected directly. Nevertheless, neutrinos are hot thermal relics, and their masses, even if tiny, affect the Universe's evolution, having its largest impact on the growth of structure at small scales due to the neutrino free steaming nature. Therefore, albeit indirectly, we can set an upper bound on them by cosmological observations. Although official Planck CMB results report $\sum m_i < 0.24$ eV [192], the addition of LSS data in the form of BAO allows reaching $\sum m_i < 0.09$ eV [1304] or even $\sum m_i < 0.072$ eV from the very recent DESI BAO survey observations [699,1305], all at 95% CL. Similar bounds are obtained when different likelihood approaches are adopted for analyzing Planck data [701], while the limits are relaxed when high-multipole CMB data are considered instead of Planck [1306].

Nevertheless, the tightest limits to date are those reported in Ref. [1307] after the addition to Planck and DESI observations of other background probes, such as CC, galaxy clusters angular diameter distances, and GRBs distance moduli. For instance, the combination of CMB with GRBs and DESI BAO provides $\sum m_\nu < 0.049$ eV. The most constraining bound is obtained when CMB, SNIa luminosity distances, DESI BAO, and all background probes are combined: this limit is 0.043 eV at 95% CL. Background probes are therefore able to provide strong bounds on the neutrino mass due to both the preferred higher mean value of the Hubble constant and the smaller errors on both H_0 and the matter mass-energy density $\Omega_{\rm m}$. Consequently, cosmological limits currently possess the highest constraining power on neutrino masses if the standard scenario is assumed for neutrino decoupling and if neutrinos are massive stable particles (see Fig. 42).

In the past, neutrinos were supposed to provide a possible explanation to the H_0 and σ_8 tensions, see e.g., [1308]. More recently, however, it has been shown that an increase in H_0 due to neutrino physics is normally related to an increase also in σ_8, see e.g., Fig. 34 in Ref. [192]. A solution to both tensions thanks to neutrinos seems therefore unlikely.

On the other hand, neutrino oscillations measured at terrestrial experiments while being insensitive to the overall neutrino mass scale, determine the value of two squared mass differences, the atmospheric $|\Delta m^2_{31}| \approx 2.55 \cdot 10^{-3}$ eV^2 and the solar $\Delta m^2_{21} \approx 7.5 \cdot 10^{-5}$ eV^2 splittings [1309,1310]. Since the sign of $|\Delta m^2_{31}|$ is unknown, two mass

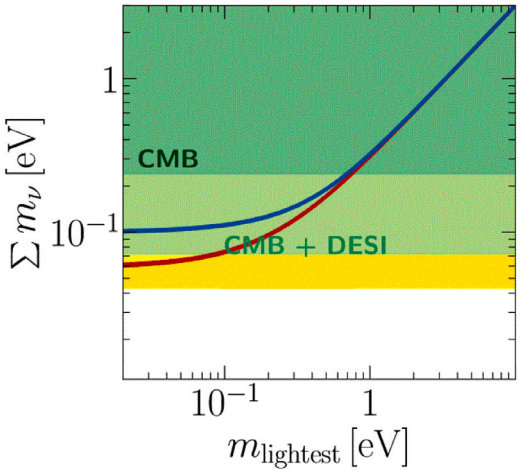

Fig. 42. The sum of the neutrino masses as a function of the lightest neutrino mass for normal (red) and inverted (blue) orderings. Cosmological constraints from CMB, CMB plus DESI, and including measurements from CC, distance moduli from GRBs, and angular diameter distances from galaxy clusters are also depicted by the shaded green and yellow regions. (For interpretation of the references to colour in this figure legend, the reader is referred to the web version of this article.)

orderings are possible, the *normal* (NO) and the *inverted* (IO) orderings:

$$\sum m_i = \begin{cases} \text{NO:} & m_\nu^2 + \sqrt{m_\nu^2 + \Delta m^2_{21}} + \sqrt{m_\nu^2 + \Delta m^2_{31}} \geq 0.058 \text{ eV}, \\ \text{IO:} & m_\nu^2 + \sqrt{|\Delta m^2_{31}| + m_\nu^2} + \sqrt{|\Delta m^2_{31}| + \Delta m^2_{21} + m_\nu^2} \geq 0.101 \text{ eV}. \end{cases} \tag{2.19}$$

Notice that not only some of the above-mentioned current cosmological limits are *below* the minimum sum of the neutrino masses allowed in the inverted hierarchical scenario, but also some of them are *below* the minimum mass required from neutrino oscillation probes. Very interestingly, several of the possible data combinations imply a neutrino mass limit at 2σ smaller than the minimum expected from oscillation experiments, i.e., $\sum m_\nu \lesssim 0.06$ eV, pointing toward a clear tension between cosmological and oscillation neutrino mass limits, see Ref. [1307]. Therefore, despite the fact that such tension has so far not been present [1311], not only one but several sets of cosmological measurements indicate a clear problem between these cosmological and terrestrial searches of neutrino masses. Cosmological constraints, therefore, at present, reflect some *tension regarding neutrino masses*:

- Through cosmological observations, we are about to rule out the minimum value of $\sum m_i$ allowed by neutrino oscillations. It is important to remember that cosmology does not directly measure neutrino masses but rather constrains the neutrino energy density, which is proportional to neutrino masses in the standard scenario. This relation could be altered by the presence of new physics: current cosmological bounds may point to the existence of very exotic cosmological scenarios (possibly related to dark sector physics) and/or non-standard neutrino physics since these bounds are extremely robust within simple extensions of the ΛCDM model; see, e.g., [1312]. Possible scenarios to relax the cosmological neutrino mass bounds include time-varying neutrino masses [1313], decaying neutrinos [1314–1317], strongly-interacting neutrinos [1318,1319], long-range neutrino forces [1320], among others [1321–1325].
- Using Planck 2018, BOSS Lyman-alpha, and DESI data, if negative neutrino masses are allowed in the fitting pipeline, a slightly better fit is obtained with $\sum m_i < 0$ than with $\sum m_i \geq 0$ [1324]. It should be noted, however, that the absolute sign of the mass of a fermion is a phase (i.e., is unobservable) and therefore this

preference for negative masses should be taken as an indication of an incomplete model rather than an actual physical measurement.

These tensions will need to be addressed in the coming years, and upcoming cosmological measurements, such as those from e.g., future observations by DESI or CMB-S4, will be able to test all the current tensions (and possibly additional ones; see below) while sharpening the cosmological neutrino mass limits.

Last but not least, the Karlsruhe Tritium Neutrino (KATRIN) experiment, a tritium beta decay experiment, may directly discover the electron neutrino mass, finding a positive signal.[9] Such a putative neutrino mass detection by KATRIN will show an additional clear *tension* with current cosmological mass limits. As previously stated, possible inconsistencies among laboratory and cosmological searches would definitely point to a much richer neutrino sector, to a departure from the standard model of cosmology, or to a combination of both. Such a situation would offer exciting possibilities to discover new physics. Neutrino physics has brought the first departure from Standard Model Physics and may also be the first one to falsify the current standard cosmological scenarios where they are hot thermal stable relics interacting exclusively via weak interactions.

2.3.6. Cosmic dipoles

Coordinator: M.M. Sheikh-Jabbari

Contributors: Dinko Milaković, Eoin Ó Colgáin, Francesco Sorrenti, Iryna Vavilova, Jenny Wagner, José Pedro Mimoso, Laura Mersini-Houghton, Leandros Perivolaropoulos, Lu Yin, Maciej Bilicki, and Manolis Plionis

Cosmological principle, the *assumption* that the Universe around us at cosmological scales is (statistically or on the average) homogeneous and isotropic, is the cornerstone of the modern cosmology, see Ref. [1328] for a recent review. CMB temperature fluctuations [192] have been regarded as a very precise verification of cosmic isotropy at the surface of last scattering at around $z \sim 1100$. However, the existence of a very small deviation from isotropy in the CMB is not ruled out theoretically [1329] and references therein or observationally [1328,1330–1335] and references therein. Such small anisotropies, if they exist and are not due to systematics, in principle can grow in time through the large structure formation, especially when we enter a nonlinear growth regime. It is therefore, prudent to thoroughly explore evidence for traces of anisotropy especially in late cosmology.

Any physical observable may be expanded in terms of spherical harmonics on the celestial sphere. The lowest mode is $\ell = 0$ which preserves isotropy. The next mode is $\ell = 1$, corresponding to dipoles of the physical observable in question. Given that deviations from spherical symmetry are expected to be small, one expects higher multipoles to have smaller contributions and hence harder to detect. On the other hand, the dipole component, which is the largest mode beyond isotropy, is observer dependent and can be a kinematical effect. For example, it is well established that the dipole in the CMB, which corresponds to $\sim 10^{-4} - 10^{-3}$ fluctuation in the CMB temperature (compared to usual 10^{-5} fluctuations), can be attributed to peculiar motion of the observer compared to the "CMB frame" that moves with the Hubble flow. So, exploring the dipoles in cosmic observables one should always note this frame dependence. The very local Universe is obviously not isotropic around us. One can ask how far one should look to be confident in the Hubble/CMB frame. It is established that this distance is larger than ~ 100 Mpc, as indicated also by the convergence scale of the acceleration dipole due to matter fluctuations traced by galaxies and clusters of galaxies distributions, first at Ref. [1336–1338] and later at Ref. [1339–1342]. The "bulk flow" in the Local Universe is a collective phenomenon due to the peculiar motions of matter structures [1343] that instead of moving in random directions, appear to follow an approximate dipole velocity flow, see Ref. [1344] and references therein. The existence of bulk flows that are too large for ΛCDM expectations may be taken as a sign of departure from isotropy that shows itself as a dipole in various cosmological observables.

2.3.6.1. Non-comoving cosmology, tilted cosmology. The cosmological dipole is a frame dependent notion. To distinguish kinematical and a non-kinematical (not removable by the choice of frame) one needs to study usual FLRW cosmological models in a non-comoving frame, see Ref. [1345–1349]. A related, but conceptually different, notion is the "tilt" introduced by King and Ellis [1350]. Suppose we choose a comoving frame, a frame in which metric does not have time-space off-diagonal elements, $g_{ti} = 0$. In this frame cosmic fluids may exhibit a momentum flow, i.e., the time-space component of energy momentum tensor T^t_i may be nonzero. Tilt may be different for different components of cosmic fluid, e.g., (pressureless) matter or radiation may have different tilts and hence there does not exist a Hubble or CMB frame. Tilt is a dynamical variable in cosmology, like the shear or Hubble parameter, e.g., see Ref. [1329,1351–1355] and references therein. This is in contrast with the non-comoving cosmology in which the dipole components are not dynamic ones. The existence of tilts yields dipole anisotropy in various cosmological observables.

2.3.6.2. Observational hints for cosmic dipoles. We start by recalling that typical cosmological observables are redshift (as a measure of distance), look-back time, Hubble expansion rate, deceleration/acceleration parameter, luminosity distance, angular diameter distance, and number counts. In an anisotropic cosmology, these quantities besides the redshift z also depend on line-of-sight. Redshift, the ratio of the frequency of the photon emitted by a source and the one observed by the observer minus one, receives a Doppler shift if there is a bulk flow of velocity v:

$$1 + z = (1 + z_0)\Delta\,, \qquad \Delta := (1 - v/c\cos\theta_{\rm LoS})/\sqrt{1 - v^2/c^2}\,, \tag{2.20}$$

where $1 + z_0 = 1/a$ is redshift when the source and observer have zero relative velocity and $\theta_{\rm LoS}$ denotes the line of sight angle. For more formal and detailed derivations and analysis see Refs. [1354,1356–1361].

2.3.6.3. Ellis-Baldwin test. A standard technique for searching for a dipole component in the distribution of sources in the sky is the seminal Ellis–Baldwin test [1362]. The number N per solid angle of a local source in the sky (say radio galaxies or QSO) in two frames moving with a relative velocity v and angle $\cos\theta_{\rm LoS}$ is given by

$$\frac{{\rm d}N}{{\rm d}\Omega}\Big|_{\rm obs} = \frac{{\rm d}N}{{\rm d}\Omega}\Big|_{\rm rest} \Delta^{2+k}\,, \tag{2.21}$$

where k is a constant parameterizing astrophysical characteristics of the source population.

2.3.6.4. Cosmic microwave background dipole. A dipole component in the CMB is customarily treated as purely kinematical, due to the motion of the observer. This may be viewed as the definition of "CMB frame", a frame in which the CMB has no dipole component. While one can always find such a frame, only in an isotropic universe all other cosmological observables are necessarily dipole free in the CMB frame. The heliocentric frame, in which our cosmological observations are made, is moving with respect to the CMB frame with velocity $v = (369.82 \pm 0.11)\,{\rm km s^{-1}}$ along the direction (in degrees) $(l, b) = (264.02 \pm 0.0085, 48.253 \pm 0.004)$ [192]. While the CMB dipole may be treated as kinematical, there have been persistent CMB quadrupole and octopole components which may be hints of deviations from the cosmological principle, see Refs. [1328,1330,1363] for reviews.

The Planck CMB data in the CMB frame may still show traces of a dipole once one makes a hemispherical split analysis (HSA) of the data. This method involves splitting the celestial sphere into two

[9] The current limit is $m_\beta < 0.45$ eV (90% CL) [1326], and the expected sensitivity is 0.2 eV (90% CL) [1327]

hemispheres and fitting ΛCDM to CMB data in each hemisphere. One then reads the values of H_0 and $\Omega_{\rm m,0}$ in each hemisphere, rotates the hemisphere separation plane in the sky, and records the ratio of the difference between the two values of H_0 in each hemisphere, ΔH_0, over the mean H_0 value over the whole sky, $\bar{H}_0$. This analysis has yielded a maximal value of $\Delta H_0/\bar{H}_0 \simeq 10\%$, roughly along 45° to the direction of the CMB kinematic dipole [1334], a direction close to the axis of the hemispherical power asymmetry, a well-recognized CMB anomaly [1330]. Intriguingly, this is the same level as the discrepancy in Hubble tension; however see Ref. [1364].

2.3.6.5. Maximum temperature asymmetry (MTA). is another dipolar anomaly in the CMB which is identified by examining the temperature differences between opposite pixels in the CMB sky map after subtracting the dipole component. MTA selects a preferred axis by maximizing the temperature difference between these opposite pixels and indicates a preferred direction in the CMB temperature fluctuations, signature of a dipole. See Ref. [1365] for MTA analysis in the WMAP 7-year data. The proximity of the MTA axis to the α dipole, DE dipole, and dark flow directions (see below) further strengthens the case for a potential underlying physical cause for these anisotropies.

2.3.6.6. Fine structure constant dipole. Initially reported by Ref. [1366], was identified through the analysis of QSO absorption spectra using the Very Large Telescope (VLT) and the Keck Observatory. The dipole suggests a spatial variation in the fine structure constant α across the sky, with a dipole axis pointing toward $(l, b) = (331°, -14°)$, and an amplitude $A = (0.97 \pm 0.21) \times 10^{-5}$. However, recent studies have reduced the significance of the α dipole to less than 4σ [1363,1367].

2.3.6.7. Type Ia supernovae dipole. SNIa are widely accepted as standard candles with a fairly good distribution over the sky [JLA, Pantheon(+), Union3, DES-5Y, ZTF]. The SNIa observations are of course made in the heliocentric frame, correcting for the presumed (peculiar) motion w.r.t. the CMB frame, assuming that a Hubble flow frame exists and that the far enough (farther than $\sim$ 100 Mpc SNIa) are already in the Hubble flow frame w.r.t us. This may obscure possible dipole components in the data in the heliocentric frame [1368]. SNIa data may be explored for a possible cosmological dipole component in 3 different kind of analyses:

(I) *Ellis–Baldwin test for SNIa* We still do not have enough observed SNIa to carry out this test. It may be feasible in some years.

(II) *HSA using a cosmographic expansion, dipole fitting method.* For relatively low redshift data, $z \lesssim 1$, one can expand Hubble parameter and luminosity distance in powers of z,

$$H = H_0 \left[1 + (1+q_0)z + \mathcal{O}(z^2)\right], \qquad D_{\rm L}(z) = \frac{cz}{H_0}\left[1 + \frac{1}{2}(1-q_0)z + \mathcal{O}(z^2)\right]. \tag{2.22}$$

One may now consider a dipole in H_0, i.e., $H_0(\theta) = H_0(1 + \mathcal{D}_H \cos\theta)$ or similarly in acceleration, $q_0(\theta) = q_0(1 + \mathcal{D}_q \cos\theta)$ and perform HSA. This test has been carried out for JLA [1369,1370] and Pantheon(+) [1348, 1368,1371–1373] datasets claiming for a small dipole in H_0 and a notable dipole for q_0 roughly along the CMB dipole in the heliocentric frame. See also, [1344,1374]. There have been analyses that claim not seeing a dipole see e.g., [33,1375–1382]. We need to wait for more SNIa data, e.g., the DES data and ZTF to confirm or refute these claims.

(III) *HSA and dipole fitting of ΛCDM into SNIa data.* This analysis started in 2010 in Ref. [1383] with the Union2 SNIa dataset and identified a significant anisotropy in the accelerating expansion rate in direction $(l, b) = (309^{\circ}{}^{+23^{\circ}}_{-3^{\circ}}, 18^{\circ}{}^{+11^{\circ}}_{-10^{\circ}})$. The anisotropy level $\Delta\Omega_{0m,\rm max} = 0.43 \pm 0.06$ was consistent with statistical isotropy in about 30% of simulations. The alignment with other observations like bulk velocity flows and CMB low multipole moments, fine structure constant, and DE dipole obtained through MTA method [1384] suggested a potential underlying physical cause.

Similar recent approaches use the luminosity distance and distance ladder relation $\mu = 5\log D_{\rm L}(z) + 25$ with $D_{\rm L}(z) = \frac{c}{H_0}\int^z {\rm d}z'/\sqrt{1-\Omega_{\rm m,0} + (1+z')^3\Omega_{\rm m,0}}$ and perform HSA. This has been carried out yielding a small variation $\Delta H_0 \lesssim$ few ${\rm km\,s^{-1}Mpc^{-1}}$ over the sky [1385], see also Refs. [1374,1386–1390] and Refs. [1372,1374, 1391] for further analysis. It would be instructive to repeat a similar analysis with other datasets like DES 5Y [1374,1389] or ZTF data release. Alternatively, one may repeat a similar analysis with absolute magnitudes of SNIa (instead of H_0 and $\Omega_{\rm m,0}$) [1392]. Analyzing the latest ZTF data release, particularly at low redshifts, may yield further valuable information. Ultimately, the combination of these different approaches and datasets will enhance our understanding of cosmic anisotropies and contribute to a more comprehensive picture of the Universe's large-scale structure.

2.3.6.8. Quasar (QSO) dipoles. QSO catalogs contain about 1000 times more data points compared to SNIa datasets, nonetheless, unlike the SNIa their standardizability [182,1393,1394] is still a matter of debate, see Refs. [524,1395–1397] and references therein. The 3 anisotropy/dipole searches mentioned above using SNIa data, can be repeated for the QSO samples. *Ellis–Baldwin test for QSO* has been carried out yielding a significant (up to 4.9σ) departure from isotropy [1398]: QSO of redshifts $z \gtrsim 1$ are not in Hubble/CMB frame, while in the heliocentric frame they move in the same direction as the CMB dipole, their peculiar velocity is few orders of magnitude bigger than the CMB velocity ${\rm 370\,km s^{-1}}$, see also Refs. [1399,1400]. This result is still under debate e.g., see Refs. [1401,1402] and references therein.

The HSA for QSO data with the dipole fitting method has also been carried out, in a cosmographic expansion and/or using Risaliti-Lusso [1394] X-ray/UV flux relation. This has also led to a $2-3\sigma$ level result for a dipole component in H_0 [1403].

2.3.6.9. Radio galaxy dipole. Radio galaxies are typically located at cosmological distances and hence within the standard cosmological principle paradigm, they are expected to be moving with the Hubble flow; they should not exhibit a flow in the CMB frame and CMB frame should be their rest frame. This was first put to the test in 2002 [1404], confirming the expectation. However, the same observation has been repeated with better accuracy, refuting the earlier result in about 3σ level [1405], finding radio galaxies moving with speed 4 times bigger than the CMB velocity in the heliocentric frame, and roughly in the same direction. Similar results have been reported in Refs. [1406–1413], see however Refs. [1414–1419].

2.3.6.10. Gamma-ray burst dipole. GRBs may also be used to perform similar dipole tests as in QSO or SNIa. However, a relatively low number of data points in GRB samples and their still debated standardizability [542,1420–1422] (see Ref. [516] for a recent review) puts limits on using GRBs as reliable cosmological observables. See Refs. [1403,1423] for the search of a dipole in H_0 through an HSA within ΛCDM and GRB data, reporting $2-3\sigma$ deviation from isotropy.

2.3.6.11. Cosmicflow-4 (CF4) bulk flow. A measure for a possible (non)kinematic dipole may be inferred from peculiar velocities of large catalogs of distant galaxies with known distances (which typically means cosmologically close $\lesssim$ 500 Mpc). Such large distance, non-random and coherent in direction velocity fields, if they exist, are called bulk flows. Bulk flows may be compared to the expected Hubble flow. CF4 (superseded CF2 and CF3) [1424] complies $\sim$ 56000 galaxies to this end, while reporting $H_0 = 74.6 \pm 0.8 \pm 3(Sys)$ ${\rm km\,s^{-1}Mpc^{-1}}$ also reports their peculiar velocities.[10] The amplitude and alignment of the inferred velocity field from the CF4 data is at $\sim 2-3\sigma$ discrepancy with respect to the ΛCDM model [1425]. While closer galaxies at around 50–100

[10] It is notable that this value for H_0 has independent systematics from those based on cosmic distance ladder.

Mpc seem to show no excess or deficit in their velocity fields compared to expected Hubble flow, farther ones show sizable excesses (by more than 3 times) [1426,1427] and in a direction compatible with the CMB dipole, confirming similar anomalies seen in CF3 [1428]. Similar bulk flows have also been reported from the low redshift part of Pantheon+ compilation ($0.015 \leq z \leq 0.06$); these flows are toward the Shapley supercluster [1344] (see also Ref. [1374]).

A specific kind of bulk flow (as defined above) has been given a different name, *dark flows*. Dark flows are associated with peculiar velocities of galaxy clusters that can be measured through fluctuations in CMB generated by the CMB photons off X-ray emitting gas inside clusters [1429]. Dark flows are found in scales larger than 300 Mpc and the dark flow dipole is a dipole found at the position of galaxy clusters in filtered maps of CMB temperature anisotropies [1430] see also Refs. [1431–1433], see however, Ref. [1434]. It is hard to accommodate dark flow dipoles in the ΛCDM cosmology.

2.3.6.12. Cosmological models accommodating the presence of cosmic dipoles. As discussed, dipoles can appear in various cosmological observables, such as the distribution of QSO and SNIa, distances, acceleration parameter, H_0, the fine-structure constant α. One can construct models that accommodate dipoles in some of these observables and/or introduce mechanisms to yield large-scale inhomogeneities or anisotropies in the Universe. Below, we discuss some of the prominent theoretical models that could explain the observed cosmic dipoles.

Off-Center observers in spherical cosmological scale inhomogeneities. Off-center observers situated in a spherically symmetric inhomogeneous universe can see a dipolar anisotropy due to the observer's position relative to the center of the inhomogeneity. This idea is explored in models where large-scale structures or voids introduce anisotropies due to the observer's peculiar location within the cosmic structure [1435,1436].

Primordial dipolar horizon scale perturbations. Primordial perturbations generated during the inflationary epoch can also have dipole anisotropy that can be imprinted on the largest scales and re-enter the horizon at later times, leading to observable dipolar anisotropies in the CMB and other cosmological observables. Such mechanisms can be related to specific inflationary models that predict large-scale anisotropies [1206,1437].

Nontrivial topology of the cosmos. The spatial topology of the Universe may play a role in creating cosmic dipoles. Nontrivial topologies, such as those involving multiply connected spaces, can introduce preferred directions and anisotropies on large scales which may be detectable in the distribution of galaxies, the CMB, and other cosmological datasets [1234,1438]. (Non-trivial topology may induce anisotropy through parity-violation without involving a dipole [1332,1439].)

Hubble scale topological defects. Hubble scale topological defect, such as a global monopole created by the DE scalar field at recent cosmological times, known as topological quintessence, can be another source of dipolar anisotropy in various observable (from the off-center observer viewpoint) [1363,1384,1440,1441]. This scenario may also explain the alignment of various observed dipoles, such as the QSO dipole, the SNIa dipole, and the α dipole.

Other physical mechanisms. Other physical mechanisms that can induce cosmic dipoles include:

- *Anisotropic Dark Energy*: Models with an anisotropic equation of state for DE can lead to directional dependencies in the expansion rate of the Universe, thereby creating dipolar anisotropies [1442–1444].

- *Large-Scale magnetic fields* can introduce anisotropies in the CMB and other observables, potentially explaining some of the observed dipoles [1445,1446].

- *Vector field models*: Inflationary models involving vector fields can naturally generate anisotropic perturbations [1447], leading to observable dipoles in various cosmological datasets [1448,1449].

- *Tilted models*: Tilted cosmological models, where observers have peculiar velocities relative to the cosmic rest frame, can lead to locally observed acceleration and dipole-like anisotropies in the deceleration parameter [1347,1352–1356,1369,1401,1450–1453].

These theoretical models provide a rich framework for understanding the observed cosmic dipoles. Future observations and more refined data will be crucial in testing these models and determining the true nature of the large-scale anisotropies in our Universe.

2.3.6.13. Conclusion and future directions. We briefly discussed dipoles in various cosmological observables, from the dipole in the distribution of astrophysical sources like SNIa, QSO, GRB and radio galaxies over the sky, to dipole in the coherent flows of matter (clusters and superclusters), to dipoles in the cosmological model observables like $H_0, \Omega_{\mathrm{m},0}$. Besides the dipoles we discussed here, there have been reports on an intrinsic (non-kinematical) dipole in the CMB [1454–1458], the dipole in the fine structure constant [1366,1384,1459] and in the distribution of baryon matter in the Universe using FRB [1460,1461]. Moreover, if the CMB dipole is interpreted as our departure from the Hubble flow it will induce 'time dilation dipole', a directionally-dependent time dilation over the sky. Detection of time dilation dipole can provide a new assessment of the cosmological principle [1462, 1463].

These dipoles, if of a cosmological origin and if not kinematical, hint at a breakdown of the cosmological principle, the very pillar of modern cosmology. Most of the dipoles discussed here may be individually of not a large statistical significance, nonetheless, the synergy between them suggests that they may not be dismissed. Future data with better sky coverage will be instrumental in establishing/refuting true cosmological dipoles. If established, one should take more serious steps in accommodating a cosmological dipole in the cosmological models, such first steps have been taken in [1352,1354].

2.3.7. Big bang nucleosynthesis

Coordinator: Nils Schöneberg

Contributors: Dinko Milaković, Ismailov Nariman Zeynalabdi, John Webb, Luca Izzo, and Venus Keus

BBN describes the process of generating the atomic nuclei of light elements shortly after the big bang as a result of the Universe cooling down beyond the point at which photo-disintegration of these nuclei becomes inefficient. Since the heavier elements need to be built up from lighter components,[11] the process of the nucleosynthesis only begins when the Deuterium photo-disintegration becomes inefficient, which occurs when the photon temperature is around $T \sim 100$ keV (corresponding to redshift $z \sim 5 \cdot 10^8$). For reviews see Refs. [1464–1467]. Not all stable elements are readily produced from BBN due to the instability of isobars with 5 or 8 baryons. In particular, the stable elements produced in significant proportion from BBN are hydrogen (^{1}H and ^{2}H), Helium (^{3}He and ^{4}He), and Lithium (^{6}Li and ^{7}Li), with the remaining elements produced only in tiny proportions compared to later stellar and cosmic-ray induced generation. As such, the primordial abundances of these heavier elements are almost impossible to measure, given that already for the small abundance of Lithium the post-BBN generation presents a significant systematic, see Section 2.3.7.1. Despite generally showing an excellent agreement between predicted and observed abundances, we discuss hints at possible tensions for these different elements in Section 2.3.7.1– Section 2.3.7.3. Furthermore, BBN can play a critical role in other tensions, see Section 2.3.7.4.

2.3.7.1. Lithium tension. The two stable isotopes of Lithium (^{6}Li and ^{7}Li) are produced only in very subdominant amounts, with ^{7}Li at

[11] The reason for this is that the direct n-particle fusion is suppressed by a power of η_b^n where $\eta_b \sim 6 \cdot 10^{-10}$ is the tiny baryon-to-photon ratio. As such, subsequent progressive 2-nuclei fusion processes are more relevant for the fusion of heavier elements, which makes the isobar stability gaps crucially important.

a level 10^{-9} times below that of hydrogen (^{1}H). At face value, the prediction of the ^{7}Li abundance from standard BBN is about 2–4 times higher than that measured in the atmospheres of metal-poor stars in the galactic halo, for example, see Ref. [1468] computes $^7\text{Li/H}=(4.94\pm 0.72)\cdot 10^{-10}$ (for a CMB-motivated baryon density, see also Refs. [1469–1473] for other such high computations) while Ref. [1474] measured $^7\text{Li/H}=(1.58^{+0.35}_{-0.28})\cdot 10^{-10}$ (see Ref. [1475] for a higher measurement in the SMC, possibly related to nova enrichment [1476]). See Ref. [1477] for a review. Naïvely this appears to be a large issue for standard BBN. However, there are a few caveats to take into account.

The observations of the ^{7}Li abundances are extrapolated to zero metallicity (iron abundance), but the plateau originally observed (the so-called Spite plateau) Ref. [1478,1479] appears to not persist at lower metallicities (increased scatter falling on average below the plateau), see for example Refs. [1477,1480,1481]. The issue is that Lithium can be burnt up in stellar environments, possibly even in metal-poor stars. In particular, convective mixing in metal-poor stars could bring the Lithium down to layers with a temperature above $3\cdot 10^6$ K sufficient for further burning, see for example Ref. [1482]. This stellar depletion argument is still under investigation, for a recent discussion see Ref. [1483] — In this case ^{6}Li would be burnt up and thus its abundance is used as a useful argument on whether such burning is expected to have taken place. However, the observation of ^{6}Li is even more difficult due to its even smaller abundance (and its ready generation through cosmic rays). Initial observations indicating a plateau at $^6\text{Li}/^7\text{Li}\sim 0.05$ (BBN predictions are at $\sim 10^{-4}$ Refs. [1465,1469]) would indicate that stellar burning could not have taken place [1484–1490], but newer observations currently only put upper bounds [1491–1494], overall making stellar depletion a likely explanation. See Ref. [1495] for another argument toward stellar processes and Ref. [1496] for possible observations of a truly primordial plateau.

Another argument could be made on the aspect of the nuclear reaction rates, though the rates appear to be consistent, see Ref. [1483] for a discussion. As such, while nuclear rates are unlikely to be the cause of the Lithium tension, stellar depletion could very well be an entirely sufficient explanation. Given this unclear footing of the Lithium tension, any claims of a "required" modification of standard BBN should be seen with great caution. Despite this, a range of non-standard BBN models have been proposed as possible solutions to the Lithium tension, such as for example Refs. [1481,1497–1509], and Ref. [1510] for a review.

2.3.7.2. Helium anomaly. Primordial ^{3}He is remarkably difficult to measure [1467] (see also Ref. [1511]) since ^{3}He is generally readily produced and depleted in stars. It is thus rarely used to constrain BBN. Conversely, ^{4}He is a crucial part of the BBN predictions that can be readily measured in ionized metal poor extragalactic HII regions. Since ^{4}He is produced in stellar cores, the primordial Helium mass fraction Y_P is usually found by extrapolating the ratio of $^4\text{He}/^1\text{H}$ from the measured systems as a function of metallicity to zero metallicity, which is presumed to represent the primordial value. These determinations from 214 systems [1512–1517] (which roughly average to $Y_P = 0.245\pm 0.003$ [1467]) generally agree extremely well with the value predicted from baryon abundance and neutrino abundance determinations from the *Planck* satellite under the standard BBN assumptions (giving $Y_P = 0.241 \pm 0.025$ [192]). The recent determination from the EMPRESS survey on the Subaru telescope by Ref. [1518] returns a much lower value ($Y_P = 0.2370\pm 0.0033$) compared to all previous results, including that of Ref. [1516] (which gets $Y_P = 0.2436\pm 0.0040$). This is interesting because Ref. [1518] uses the entire sample 1 of Ref. [1516] and the only difference is the addition of five additional extremely metal-poor galaxies (J1631+4426, J0133+1342, J0825+3532, J0125+0759, and J0935-0115). Four out of five of these galaxies lie significantly below the expected Helium mass fraction (from the fit of Ref. [1516]) given their metallicity, see Fig. 43. Taking the measurements at face value, one would conclude a non-zero lepton asymmetry [1519,1520] and a slight preference for additional relativistic degrees of freedom [1518, 1519]. However, such an analysis is yet to be independently confirmed. We also note that Ref. [1521] finds a higher-than-mean value.

2.3.7.3. Deuterium — A new tension? The final element that is produced in decent quantity from BBN is Deuterium (^{2}H, alternatively D). While the Deuterium measurements are largely consistent, see Fig. 43, its abundance can also be seen to be in tension with the baryon abundance determined from CMB data, depending on which modeling of the nuclear rates is performed [1471,1522,1523], thus requiring new measurements of nuclear rates to clear up the posited tension. In particular, the crucial rates for Deuterium are

$$^2\text{H} + {}^2\text{H} \to {}^3\text{H} + p^+ \ \text{(ddp)}\,, \qquad {}^2\text{H} + {}^2\text{H} \to {}^3\text{He} + n \ \text{(ddn)}\,. \tag{2.23}$$

Conversely, to probe the consistency with the CMB one can also check what nuclear rates would be preferred given the baryon abundance and neutrino number from the CMB (see Section 2.1.18) [1522,1524].

2.3.7.4. Impact of BBN on other tensions. While BBN is extremely self-consistent, it can also be used to support other tensions. For example, the combination of BAO+BBN data provides one of the tightest non-Planck determinations of a low H_0 value, see for example Refs. [699, 705,789,1525–1529] (from DESI DR1 [699], 68.51 ± 0.58 km s^{-1} Mpc^{-1} from DESI DR2, or $67.6^{+0.9}_{-1.0}$ km s^{-1} Mpc^{-1} from eBOSS (and 68.3 ± 0.7 km s^{-1} Mpc^{-1} when additionally including eBOSS ShapeFit [1526]), see also Section 2.1.19), recently reaching a precision of $H_0 = 68.52 \pm 0.62$ km s^{-1}Mpc^{-1} [699], which puts a significant strain on solutions of the Hubble tension that focus solely on the CMB. See also in particular Section 2.1.19. BBN data also aids in constraining dark radiation or varying constant solutions, see Sections 4.8 and 4.1.3 (although the latter is not tightly enough constrained to exclude it as a solution to the Hubble tension, see Ref. [1530]).

2.3.8. Anomalies with Lyman-α measurements

Coordinator: Vid Iršič

Contributors: Simeon Bird

Similarly to how galaxies trace the matter distribution at lower redshifts, the IGM has been used to trace the matter distribution at the time when first galaxies are forming ($z > 2$) (e.g., Ref. [1532]). The most well-studied observable of the IGM is the Lyman-α (Lyα) forest — a series of absorption lines in the spectra of QSOs, that arise due to the scattering of QSO light on the intervening neutral hydrogen atoms in the ground state. In the last two decades the Lyα forest has been measured in large spectroscopic surveys to study the precise position of the BAO [745,1533], full-shape RSD [1534,1535], as well as small-scale 1D clustering statistics [1536,1537]. The latter relies on the estimation of the 1D power spectrum along each QSO spectrum and then averaged over all the QSO spectra in the data sample [1538,1539]. This methodology has also been applied to smaller samples, with 10-100's of high-resolution and high signal-to-noise QSO spectra [1540–1543]. The highest precision constraints from the Lyα forest on the amplitude and shape of the matter power spectrum come from the measurements of the 1D flux power spectra.

The cosmological parameter inference from the 1D flux power spectra relies on state-of-the-art cosmological simulations [1544–1547] as well as a data compression technique [1548]. This method assumes that at $2 < z < 4$ and small scales (< 10 Mpc/h) the Lyα forest is constraining only two effective parameters — the amplitude and slope of the linear matter power spectrum at a pivot wavenumber and redshift, with the exact pivot point depending on the survey. This data compression has been shown to be valid also for some of the extensions of the ΛCDM model, such as cosmology with massive neutrinos or running of the spectral index [1549].

However, this methodology is typically valid when limited to scales > 1 Mpc/h or cosmological models that do not drastically change

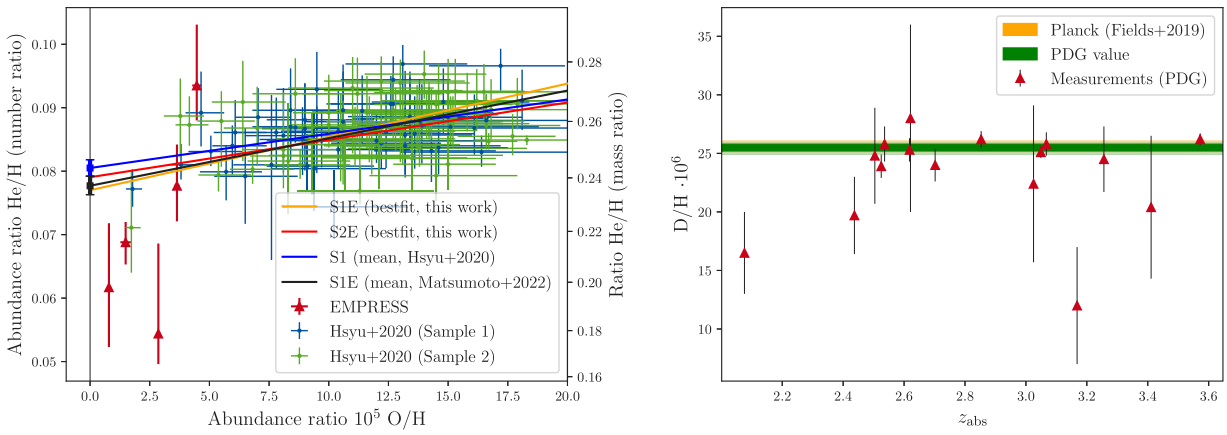

Fig. 43. Left: A comparison of the Helium abundance measurements from Ref. [1516] (Hysu+2020) to some recent fits of Ref. [1518] (Mastumoto+2022). For the fits, S1 is sample 1, S2 is sample 2, and E denotes the EMPRESS data. Right: A comparison of Deuterium abundance measurements from Ref. [1467](PDG) compared to the corresponding summary value and the Planck prediction according to Ref. [1531] (Fields+2019).

the behavior of the small-scale linear matter power spectrum (such as light DM models). In those cases, at least one more parameter can be extracted from the data corresponding, for example, to the scale of suppression of the matter power spectrum due to free-streaming nature of DM [1550]. This has been successfully used to produce bounds on various types of alternative DM models [1551–1555].

While the ongoing DESI survey will provide updated constraints, the current most precise measurements of the 1D flux power spectrum at 0.1–1.0 h Mpc^{-1} come from the SDSS-IV/eBOSS spectroscopic survey [1556]. A subsequent cosmological inference analysis [1553] reported a tension with the CMB inferred cosmological parameters, suggesting a hint of new physics in the form of a running of the spectral index. No non-statistical effects in the data analysis were identified that could explain the signal and significant effort was invested toward mitigation strategies of systematic effects. A later re-analysis of the eBOSS DR14 measurements used improved cosmological simulations and sampling techniques [1557] and pointed to possible internal tension in the data between lower redshift ($z < 2.5$) and higher redshift ($z > 2.5$) Lyα data. The analysis also proposed that the previous tension driving the constraints on the running of the spectral index can be completely alleviated at the expense of the increased tension in the amplitude of the matter clustering σ_8. The S8 tension between the amplitude of structure expected by the CMB and the amplitude of structure detected by WL at lower redshifts has also been detected at $z = 2$ by the Lyα analysis of Ref. [1557], with agreement between the measurements of the Lyα forest and WL.

Similarly, several analyses of high-resolution data pointed to a small tension between the CMB and Lyα forest from the high-resolution observations of QSO spectra [1558,1559]. A 2σ tension was reported between Planck CMB analysis and high redshift ($3 < z < 5.5$) Lyman-α forest data from XQ-100/MIKE/HIRES in Ref. [1560]. The study argued that several systematic effects in the data, such as QSO continuum mis-estimation, residual high column density systems not masked in the data selection, and astrophysical uncertainties in the mean transmission of the high redshift Lyman-α scattering could potentially alleviate the tension. A further study combining both high redshift XQ-100/MIKE/HIRES and low redshift eBOSS DR14 data [1561] showcased that the internal tension is strongest in the compressed parameter space of amplitude and slope of the linear matter power spectrum at pivot scale ($k_p \sim 1$ h Mpc^{-1}) and redshift ($z \sim 2.5$) as probed by the Lyman-α forest data. Both studies [1560,1561] further proposed that systematics in the data would pull in the direction of higher slope and lower amplitude (or vice-versa). Study of Ref. [1561] then argued that for that reason EDE models are severely penalized in this part of the parameter space and can thus be robustly excluded. A recent study by Ref. [1562] summarized these findings and proposed a new physics model of mixed ultra-light axions to solve the tension between eBOSS and Planck CMB data. While successful in explaining the results of the eBOSS survey, such a model would induce heavy suppression of matter power spectrum on smaller scales < 1 h^{-1} Mpc, that would be detected high redshift data [1541,1542]. These data sets access smaller scales and put stringent constraints on such on DM suppression, including mixed DM models [1563,1564].

The dependence of the Lyα 1D analysis on the cosmological simulations makes independent tests costly. Moreover, the cosmological parameter inference is not immune to astrophysical effects. While certain physical properties of the IGM are becoming well understood, and can be measured independently, such as the thermal history evolution [1565]; the impact of other effects, such as inhomogeneous helium reionization, on the 1D flux power spectrum is not yet fully understood [1566,1567]. Aside from the uncertainty of the astrophysics of the IGM, several observational systematic effects can potentially explain the differences between the current measurements.

Nevertheless, these anomalies in the Lyα forest data could offer a fascinating hint of new physics that can be tested and explored in a unique range of redshifts and clustering scales probed.

2.3.9. *Cosmic superstructures and the ISW anomalies*

Coordinator: Istvan Szapudi

Contributors: András Kovács, Christine Lee, Deng Wang, Maret Einasto, Mina Ghodsi, and Pekka Heinämäki

2.3.9.1. Galaxy superclusters. The largest structures in the cosmic web are superclusters of galaxies — overdensity regions that embed the richest galaxy clusters connected by filaments of poor clusters and galaxy groups [1568–1570]. Galaxies and galaxy systems form due to initial density perturbations of different scales. Perturbations of a scale of about $100h^{-1}$ Mpc give rise to the largest superclusters, the largest coherent systems in the Universe [1571]. The sizes of the richest and largest superclusters are up to almost $200h^{-1}$ Mpc [1570,1572,1573]. With their galaxies, groups, clusters, filaments, and gas, superclusters can be considered as miniature versions of universes. Therefore, they are ideal laboratories to study the properties and evolution of various elements of the cosmic web [1574,1575].

Superclusters as the connected overdensity regions in the cosmic web have been defined based on individual objects (typically optical or

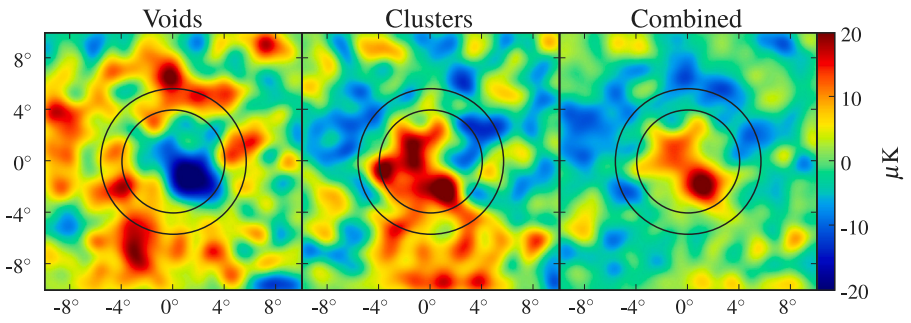

Fig. 44. The first stacking measurement of WMAP toward SDSS LRGs [1583] from 2008. The significance exceeded 4.4σ with $A \simeq 4$. The anomalous signal has been reproduced with Planck CMB maps and in most wide-angle LSS maps over different areas of the sky.

X-ray groups and clusters of galaxies) or luminosity-density or velocity fields [1570,1572,1576–1578].

The extreme cases of observed objects usually provide the most stringent tests for theories; this motivates the need for a detailed understanding of various properties of the richest superclusters [1579]. Various properties of superclusters can be used to test cosmological models, such as their abundance, masses, sizes, shapes, morphology, the properties of their high-density cores, and so on [1574,1580]. Recent observational results (e.g., DESI Collaboration [699]) have shown a tension in the Hubble value based on different observational probes, challenging the concordance model of the DE equation of state. Superclusters, representing the grand finale of hierarchical merging events, evolve at the forefront under the influence of two competing forces driven by DE and DM. They may provide a useful probe through their superior mass and extent. For example, the abundance of rich superclusters at a given epoch and the stacked signal through the ISW effect generated by large superclusters can be useful to constrain the DE equation of state [1581–1585]. In what follows, we focus on supercluster imprint on the CMB, and on the properties of supercluster planes, shells, and on the regularity in the supercluster distribution.

2.3.9.2. The ISW puzzle. When photons cross the decaying potential well of a supercluster, they become hotter; in voids, they become colder. This phenomenon is the ISW effect [1586]. The ISW puzzle consists of anomalous signal levels detected when stacking the CMB aligned with supervoids and superclusters. The effect has persisted since 2008 [1583].

The linear contribution to the late-time ISW CMB $T_{\rm ISW}$ is integrated over the line-of-sight from the present time ($z = 0$) to the surface of last scattering ($z_{\rm LS}$) [1586],

$$\frac{\Delta T_{\rm ISW}}{\overline{T}}(\hat{\boldsymbol{n}}) = 2\int_0^{z_{\rm LS}} \frac{a}{H(z)}\dot{\Phi}(\hat{\boldsymbol{n}}, \chi(z))\,\mathrm{d}z = -2\int_0^{z_{\rm LS}} a\,(1-f(z))\,\Phi(\hat{\boldsymbol{n}}, z)\,\mathrm{d}z\,, \tag{2.24}$$

where a is the scale factor, χ is the comoving distance, Φ is the gravitational potential, and $H(z)$ is the Hubble parameter. The second equality reveals the connection with the logarithmic growth function $f(\tau) \equiv d\ln D/d\ln a$ [14]. While the analogous non-linear Rees-Sciama effect [1587] happens in all models, the ISW effect gauges the divergence of growth history from the Einstein–de Sitter (EdS) model where it is zero.

The CMB stacked toward superclusters and supervoids creates hot and cold spots, respectively (c.f., Fig. 44). The ISW amplitude relative to concordance expectations, $A_{\rm ISW} \equiv \Delta T_{\rm obs}/\Delta T_{\Lambda\rm CDM}$ quantifies any anomalies when $A_{\rm ISW} \neq 1$. The first measurement to stack superstructures [1583] found $A_{\rm ISW} \simeq 4$ with the correct signs for supervoids and superclusters.

2.3.9.3. Summary of observations. Later stacking measurements, mainly based on voids, are consistent with $A_{\rm ISW} \approx 4$–5 [1582,1588–1591]. Cross-correlating the CMB with large-scale structure is typically consistent with the concordance model [1153,1592], although with less statistical power from a given data set. Stacking superstructures focuses on the highest signal-to-noise data in contrast with the unweighted average of the two-point statistics.

The BOSS redshift survey updated the void stacking measurements of the SDSS. Void finding techniques solving the "void-in-void" problem by combining voids into larger structures confirmed the earlier excess [1593,1594]. Algorithms with no merging identified no excess [1595]. Stacking [1596,1597] DES Year-1 and Year-3 photometric redshift data sets further corroborated earlier results by Ref. [1583]. Since DES covers a different part of the sky than the original SDSS, it lessens the likelihood of a statistical fluke. The combined DES and BOSS data sets [1594] yield the ultimate result $A_{\rm ISW} \approx 5.2 \pm 1.6$ in the redshift range of $0.2 < z < 0.9$. Fig. 45 summarizes the principal observations of the ISW tension.

2.3.9.4. The cold spot. The stacking measurements draw attention to the largest anomaly of the CMB, the Cold Spot (CS), an exceptionally cold of approximately 70 μ K area centered on Galactic coordinates $(l, b) \simeq (209°, -57°)$ [1193,1214,1598]. Could it be due to the ISW effect? The Eridanus void, found by Refs. [1222,1599] targeting an extended underdensity aligned with the CS, is the likely cause. While the full CS signal with substructures taken into account predicted by the concordance model $A_{\rm ISW} = 1$ [1223] is not enough to explain observations, the excess $A_{\rm ISW} \approx 4$–5 would suffice. Bayesian hypothesis testing overwhelmingly favors the hypothesis of the Eridanus void causing the CS over chance alignment [1222].

2.3.9.5. Avera and the ISW and hubble puzzles. The Average Expansion Rate Approximation (AvERA) model [13,13,14] simultaneously explains the excess ISW signal and Hubble constant anomaly, see Ref. [1600], where they fit $H_0 = 71.99^{+1.05}_{-1.03}\,\mathrm{km\,s^{-1}Mpc^{-1}}$ to SNIa. AvERA approximates emerging curvature models [1601–1603] with a modified N-body simulation. AvERA reverses the order of averaging and solving the Friedman equation; a minor but surprisingly consequential modification of the standard N-body algorithm. Its motivation is the Separate Universe Hypothesis (SUH), stating that an under- or overdense region evolves like a universe with modified cosmological parameters. Recent general relativistic simulations [1604] confirmed that emerging curvature in voids dominates the late cosmic expansion history as predicted by AvERA.

The final Hubble constant in AvERA depends slightly on the coarse-graining parameter. Between the extreme scales of the box size (no effect) and resolution (SUH breaks down), the final results are only mildly sensitive to coarse-graining: an order of magnitude change will alter the results by a few percent. The best fit, expressed as a mass scale of $\simeq 1 - 2 \times 10^{11} M_\odot$, reproduces the locally observed higher Hubble constant [13].

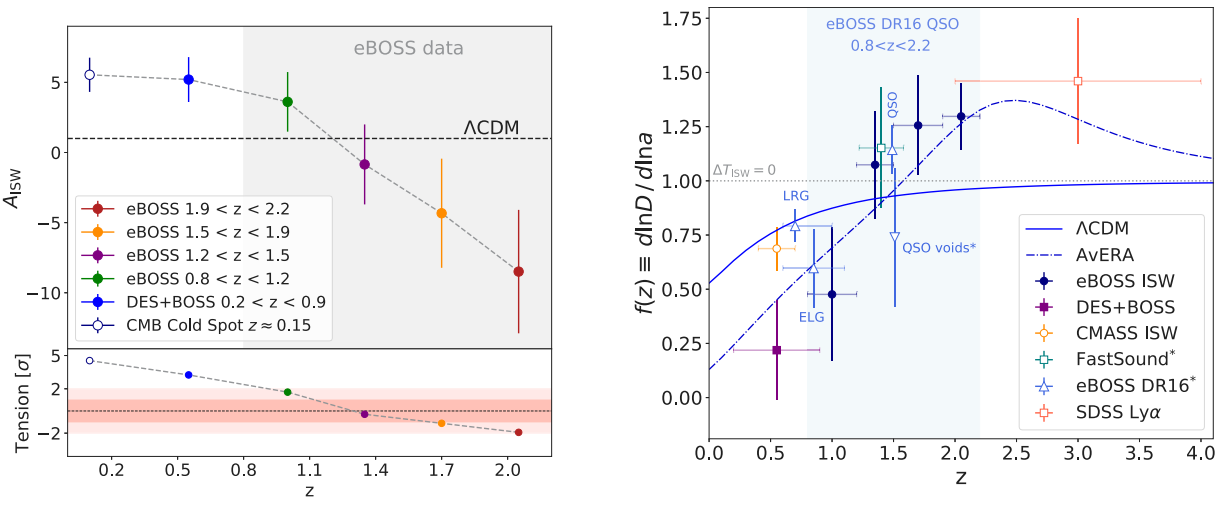

Fig. 45. These figures from Ref. [1605] sum up the ISW tension as of today. Left: Observed ISW amplitudes in different redshift bins. The excess ISW signal transitions around $z \lesssim 1.5$ and changes sign. The bottom panel displays the significance of the deviations compared to ΛCDM predictions (1σ and 2σ correspond to shaded bands). Right: Solid and dashed lines show the cosmic growth history in *Planck* 2018 ΛCDM cosmology and in AvERA as used by Ref. [1153]. Points with an asterisk display $f\sigma_8(z)$ constraints divided by the *Planck* $\sigma_8(z)$ value. The DES, BOSS, and eBOSS ISW anomalies have a consistent trend in terms of the re-scaled ΛCDM growth rate values ($A_{\rm ISW}(z) \times [1 - f^{\Lambda{\rm CDM}}(z)]$). The CMASS [1595] and eBOSS LRGs ISW amplitude is not significantly anomalous. Nevertheless, the eBOSS ELG, QSO, and high-z constraints from the FastSound and SDSS Lyα lean toward the *late complexity* trend predicted by the AvERA.

The AvERA expansion history is similar to concordance expectations with minor differences in detail. By definition, it starts on the same trajectory as a ΛCDM or EdS model at high z. Around $z \simeq 4$, the initial collapse of high-density regions accelerates growth compared to the concordance model. At lower redshifts, $z \simeq 1.5$, the voids start dominating. Their expansion stunts growth more effectively than Λ, thus the "void effect" explains the local higher Hubble constant. The higher derivative also produces an excess ISW effect [14] comparable to observations. Thus, the AvERA *explains the Hubble and ISW puzzles simultaneously*. In AvERA, the coarse-graining scale drives the local Hubble constant. While boosting the coarse-graining scale by a factor of two induces only a few percent change in H_0, a reasonable choice of a few times $10^{11} M_\odot$ (Lagrangian) achieves perfect consistency with the local measurements. The *late complexity* of AvERA expansion history affects S_8 as well, although this has not been investigated in detail.

AvERA has a robust and surprising prediction: a sign change of the ISW effect above $z \simeq 1.5$ [14]. In contrast, the concordance DE models predict an unmeasurably small ISW signal at the same redshift.

2.3.9.6. Opposite sign ISW effect. The eBOSS DR16 QSOs [1606] enabled the first look for ISW sign reversal [1605]. The data cover a crucial redshift range $0.8 < z < 2.2$ where ΛCDM and AvERA diverge: the first tends to zero while the latter predicts a sign change around $z \simeq 1.5$.

The concordance model signal was estimated with a QSO mock catalog from the Millennium-XXL for comparison with stacking 800 supervoids of the eBOSS DR16 QSO catalog. The excess signal $A_{\rm ISW} \approx 3.6 \pm 2.1$ in the redshift range of $0.8 < z < 1.2$ is comparable with earlier observations. At $1.5 < z < 2.2$, the AvERA-predicted opposite-sign ISW signal emerged in 2.7σ tension with the ΛCDM. Despite the moderate significance of these measurements, taken together with the excess at low redshift and the CMB CS, it suggests a more complex growth history than any variations of the concordance model. The observed *late complexity* (c.f., Fig. 45) consistent with AvERA implies that alternative models, such as emerging curvature, will explain the late expansion history of the Universe.

2.3.9.7. Supercluster complexes and planes. In several cases, the richest superclusters form complexes in which several very rich superclusters are almost connected. These are, for example, the Sloan Great Wall at redshift $z = 0.08$ and the BOSS Great Wall at redshift $z = 0.47$ with a length of over $250 h^{-1}$ Mpc [1573,1607–1609]. It has been questioned whether the presence of several such rich complexes in the local Universe is in agreement with the standard cosmological model [1583,1610–1612].

Also, in the local Universe galaxy superclusters are arranged on huge planes which span many hundreds of Mpc in space. Among these are the Local Supercluster Plane, discovered by Ref. [1613] in the distribution of superclusters. Rich optical and X-ray clusters, as well as luminous galaxies and radio galaxies in the local Universe are located on this plane [1572,1614–1616]. Perpendicular to the Local supercluster plane, [1617] discovered in the distribution of rich superclusters another plane — the Dominant supercluster plane. It is not yet clear whether the presence of such planes are in agreement with our standard cosmological model. For example, using constrained simulations of the local Universe in the $500 h^{-1}$ Mpc box [1618] found that a plane with the extent of approximately $100 h^{-1}$ Mpc can be recovered in simulations. However, 0.28% of random realizations of simulations only matched both underdense and overdense regions of the local Universe, and their simulation box was not large enough to test the presence of a supercluster plane hundreds of Mpc long. Also, they did not analyze the probability of finding two perpendicular supercluster planes. Refs. [1616,1619] speculate that such planes may be a signature of long, nearly straight strings.

2.3.9.8. Regularity in the distribution of rich superclusters and supercluster shells. Ref. [1572] analyzed for the first time the spatial distribution of superclusters based on the all-sky catalog of superclusters using various methods. In their study [1572] discovered that local rich superclusters are arranged in an almost regular pattern with the characteristic distance between superclusters $120–140 h^{-1}$Mpc, see also Ref. [1620] on the regularity periodogram of the local structures. The power spectrum of rich clusters has a bump at this scale, and the correlation function has a series of wiggles [1621–1623]. Rich superclusters are separated by giant voids or supervoids [1624,1625]. Superclusters are not arranged randomly in the cosmic web, and this makes projections smaller. As a result, supervoids are in some cases connected and form very large voids, as the Eridanus supervoid. Such huge structures can leave their signature to the CMB. These signatures are discussed in Section 2.3.9.2. In addition, Ref. [1626] detected a hint of the regularity with the scale

of about $400h^{-1}$Mpc in the distribution of QSO systems at redshift range $1 < z < 1.8$.

The Sloan Digital Sky Survey covers a part of the regular patterns of superclusters. Ref. [1627] showed that rich superclusters in the sky region, covered by the SDSS, are arranged in six intertwined shell-like structures with the same characteristic radius as found for the whole pattern of superclusters, approximately 120–140 h^{-1} Mpc [1627]. The centers and walls of these shells are marked by rich galaxy clusters in superclusters such as the Bootes supercluster, the Sloan Great Wall, the Corona Borealis supercluster, the Ursa Major supercluster, and other superclusters, see also Ref. [1628]. The most prominent of these shells was recently determined also using the CosmicFlows 4 data, and named "Ho'oleilana" [1629].

The huge sizes of these shells tell us that the origin of these shells, and regular pattern in the supercluster distribution should come from the very early Universe. Ref. [1627] concluded that the process behind these shells is still unknown. Ref. [1629] interpreted the shell which they named as HoÂ'oleilana as BAO shell. However, in the BAO shells the central mass is always much higher than the mass in shell walls [1630]. Analysis of the luminosities and masses of superclusters have shown that rich superclusters typically have mass-to-light ratios $M/L \approx 300$ [1608,1631,1632]. Therefore, we can estimate masses of superclusters in the HoÂ'oleilana using their luminosities provided by Ref. [1627] and this M/L value. The mass of the central cluster in the Bootes supercluster, Abell cluster A1795 is $M \approx 6.6$–$11.2 \times 10^{14} M_{\odot}$ [1633,1634]. The mass of the Bootes supercluster itself is the lowest among superclusters in this shell, $M_{Boo} \approx 0.1 \times 10^{16} M_{\odot}$. Masses of superclusters in the walls of this structure are more than a hundred times higher than the mass of the central cluster, A1795, of the order of $M_{scl} \approx 0.2$–$3.5 \times 10^{16} M_{\odot}$, and their total mass is at least $M_{tot} \approx 25 \times 10^{16} M_{\odot}$.

Therefore, masses of superclusters contradict the interpretation of Ho'oleilana as BAO shell, as proposed in Ref. [1629]. Ref. [1627] already provided arguments against BAO interpretation. Namely, the radius of the shell is larger than ≈ 109 h^{-1} Mpc, the BAO scale, and shell is wide, being in the interval of 120–140 h^{-1} Mpc. Ref. [1629] proposed that for the interpretation that this structure represents a BAO shell, the value of the Hubble constant should be approximately $77\,\mathrm{km\,s^{-1}Mpc^{-1}}$, see Ref. [1629] for details. However, so high value of H0 is very unlikely. Therefore it is still, even thirty years after discovery, an open question whether the presence of such structures can be explained within the ΛCDM cosmological model, and which processes in the very early Universe are behind this regularity.

2.3.10. JWST anomalies

Coordinator: Matteo Forconi

Contributors: William Giarè

One of the major challenges in testing the ΛCDM model is the lack of direct observations at high redshift ($z \gtrsim 10$). Current probes, such as BAO and SNIa, do not reach this regime, making it difficult to study the accuracy of the ΛCDM model around these epochs; this is particularly important considering that the large-scale structures we observe today largely emerged in the early stages of the Universe's evolution. The JWST, however, has been able to achieve this goal, offering a glimpse into these distant epochs of galaxy evolution history. Because of the expansion of our Universe, photons emitted by distant sources experience a non-negligible redshifting, such that UV light falls into the infrared spectrum today. Moreover, the farther away the source (i.e., the earlier in cosmic time), the fainter the observed signal. To address these observational challenges, JWST Near Infrared Camera (NIRCam) [1635] covers a wavelength range of $[0.6-5]\mu$ m, improving the coverage of its predecessor, HST, that was optimized for visible wavelengths. Coupled with a primary mirror which is nearly three times larger than that of HST, JWST significantly increases our ability to detect and resolve faint and very distant targets.

Recent JWST observations have identified a large population of photometric galaxy candidates [1636–1645]. Many of these galaxies are very bright [1637,1639,1646], with UV LFs that differ from previous theoretical and observational predictions [1641,1647–1651]. They are found at remarkably high redshifts ($z \geq 12$) [1641,1652–1655] and some exhibit extremely large stellar masses ($M \geq 10^{10.5} M_{\odot}$) [1656–1660]. The unveiling of these extreme objects is difficult to reconcile within the standard galaxy formation models and, by extension, the assumed underlying cosmology (ΛCDM) [1661–1663]. Moreover, JWST's ability to discover new SN candidates [1664–1669] introduces additional prospects for tackling tension in cosmology [1670,1671].

It is important to emphasize that these preliminary findings are from photometric data which, alone, are not enough to draw definitive conclusions. A major source of uncertainty is the difficulty in differentiating early star-forming galaxies from quiescent galaxies at lower redshifts [1672], as well as the spectral energy distribution templates used to interpret photometric bands may be unsuitable for very massive galaxies in the early Universe — though updated templates have been suggested, e.g., see Refs. [1673,1674]. Nonetheless, comparisons of photometric and spectroscopic redshifts in overlapping samples of galaxies with both measurements further validate these observations [1675–1682].

A way to alleviate this emerging tension is to reconsider the physics and assumptions behind the structure evolution and star formation process at high redshift [1683–1694]. Because measured stellar masses strongly depend on the Initial Mass Function (IMF), adopting a top-heavy IMF [1691,1695,1696] instead of the typical standard assumption of a Salpeter IMF [1697] could shift the inferred stellar masses. Additionally, increasing the gas temperatures can lead to a greater contribution to the brightness of early galaxies and consequently lowering the stellar mass estimates, although feedback effects might compensate this mechanism [1698]. Another critical factor is the star formation history and star formation efficiency ϵ. The results are highly sensitive to the model adopted [1699–1702]; a higher ϵ can explain large early galaxies by accelerating the reionization process [1703–1707] though this must be reconciled with constraints from lower-redshift data. Indeed, extremely high ϵ with minimal feedback is required to explain bright $z \sim 16$ JWST candidates [1708,1709].

These possible explanations deal with the complex physics relating star formation to the evolution of DM halos at high redshifts. However, emerging evidence suggests the issue might lie within our cosmological model. While it is premature to draw any definitive conclusions from these preliminary observations, if neither of the aforementioned possibilities can reconcile theory with the JWST data, it may be necessary to rethink the assumptions of the underlying cosmological model itself.

A common way to quantify discrepancies with JWST data is through the *Cumulative Stellar Mass Density* (e.g., see Refs. [1636,1656,1657,1710]), defined as

$$\rho_{\star}(\bar{M}) = \epsilon f_{\rm b} \int_{z_1}^{z_2} \int_{\bar{M}}^{\infty} \frac{dn_h}{dM} M\, dM \frac{dV}{V(z_1, z_2)}\,, \tag{2.25}$$

where $f_{\rm b} = \Omega_{\rm b}/\Omega_{\rm m}$ is the cosmic baryon fraction, ϵ is the efficiency of converting baryons into stars, V is the comoving volume of the Universe between redshift z_2 and z_1 and dn_h/dM is the mass function. For computing the mass function, the halo multiplicity [1019] is needed and one of the most used is the Sheth-Tormen alternative [1020,1122] due to its theoretical motivations for collapsed halos [1711,1712] and multiple successful N-body tests [1024,1713] (even though other phenomenological fitting mass functions exist [1714,1715]). A further assumption often made is to use a Top-Hat window function for smoothing the density field. In focusing on the cosmological framework, one typically sets ϵ to a fixed value (for a conservative approach usually $\epsilon = 0.2$ is enough). In principle, star formation efficiency can be a function of the halo mass [1716] and further adjustments to star formation physics might be needed for more precise computations [1660]. Nevertheless, for massive halos (e.g., CEERS observations [1656]), one

can approximate ϵ as a smoothly varying power law. If the mass range is short, this approximation does not affect greatly the assumptions for the model. Lastly, the cosmic baryon fraction is usually considered, instead of computing the baryon evolution in different halos [1717–1723]. If $f_{\rm b}$ is not a function of the halo mass, it plays a role of a multiplicative factor and a greater $f_{\rm b}$ can only push the theoretical predictions toward the observed data points. All these methodological choices and simplifications are widely used in the literature and allow to present conservative results that can be directly compared with similar works following the same approach.

One strategy for reconciling JWST data is to boost the halo mass function at the tail, thereby producing enough massive galaxies at early-times. This can be achieved with massive primordial black holes [1724,1725] with a fractional contribution of $f_{\rm PBH} \sim 10^{-3}$, consistent with current constraints [1726,1727]. Super massive primordial black holes not only can accelerate the structure formation process but they could also explain the observed super massive black holes that, otherwise, would have insufficient time to form from Pop III stellar remnants [1728–1736]. Other approaches involve modifying the primordial fluctuations through, for instance, rare density fluctuations from the inflaton field [1737], a blue tilted [1738,1739] or modified [1740] primordial power spectrum, or also introducing non-Gaussianities in the initial condition, affecting the abundance of DM halos [1741]. Barring self-interactions, the properties of DM halos around galaxies imply that $m_a > 10^{-21}$ eV i.e. that this particle is indistinguishable from a cold one on galactic scale [1742].

Axion-related solutions offer a further possibility for understanding JWST's detection of unusually massive galaxies [1743]. For example, axion miniclusters can boost early galaxy formation [1744] though their required masses exceeded super-radiance constraints. Alternatively, axions with masses between 10^{-22}eV $\lesssim m_a \lesssim 10^{-19}$ eV with delayed oscillations, can produce efficient axion field fragmentation driving the formation of more massive galaxies [1745]. Introducing a fuzzy DM component, usually modeled with axions, in the structure formation process can lead to suppression of small halos and galaxies, thus potentially alleviating tension if paired with altered star formation efficiency [1746]. Yet another axion-like solution is found in axion quark nuggets [1747].

These JWST observations can also be interpreted by invoking PMF [1748] or cosmic string loops with a tension below the limit imposed by CMB observations but above constraints from astrophysical probes (that can be avoided by adjusting the effective low radius cut-off) [1749–1751]. Observed massive galaxies also allow us to revisit the proprieties of Warm Dark Matter (WDM) particles [1752–1754]. Explored in the context of EDE, the fit to JWST observations is improved with respect to the one in the minimal ΛCDM framework. In fact, EDE leads to an increased n_s and simultaneously raises the fraction of EDE, that allows for a larger number of halos and massive galaxies, and, at the same time, achieving a non-negligible improvement toward easing the Hubble tension [1755–1758]. Another possibility to increase the predicted cumulative stellar mass density in agreement with JWST observations, is to employ alternatives in the DE sector such as phantom crossing in the DE equation of state [1759], a negative cosmological constant [1760–1762] a sign-switching model [1763] or a simple CPL parameterization [1764]. Conversely, interactive dark energy appears to exacerbate the tension [1755].

2.3.11. Cosmic voids

Coordinator: Dante Paz

Contributors: Alice Pisani, Carlos Correa, Cora Uhlemann, Maret Einasto, Mina Ghodsi, Nico Hamaus, Nico Schuster, Sofia Contarini, and Umut Demirbozan

2.3.11.1. Properties and identification of cosmic voids. Cosmic voids are vast underdense regions of the Universe. Since their discovery [1765–1768], they have been recognized as powerful cosmological laboratories [1769–1772]. Hence, they encode key information about the expansion history and geometry of the Universe [1772,1773]. The statistical properties of voids depend on two factors: (i) the matter tracers used to map the large-scale structure, namely, galaxies, and (ii) the method used to identify them from the spatial distribution of these tracers. Regarding the first factor, the non-trivial biased relation between galaxies and matter distribution in low-density environments has been studied intensively in recent years [1624,1774–1777]. Regarding (ii), there are different classes of void finders; for a comparison see Ref. [1778]. Some methods exploit the watershed transform technique, see for instance Refs. [1779,1780], others are based on dynamical properties [1781], and some methods identify low integrated density in spherical or free-shape regions, see for instance Ref. [1782]. Despite the intrinsic differences between all the methods, there is a consensus on the basic statistical properties of voids. Roughly speaking, voids are underdense regions with densities as low as $10-20\%$ of the average density of the Universe, their properties described here are almost exclusively governed by gravity [1604,1783–1785], and the motion of tracers around them is consistent with linear dynamics [1786,1787]. They can have diameters starting from few Mpc, spanning several tens of Mpc and the sizes of the largest voids may even exceed hundreds of Mpc [1572,1612,1788]. Such huge voids are delineated by the richest structures - galaxy superclusters, connected by a hierarchical pattern of filaments within these large voids [1612,1624].

2.3.11.2. Void size function as cosmological test. The evolution of underdense regions in the Universe, particularly isolated spherically symmetric density perturbations, involves several key stages. Initially, these regions expand until internal matter overtakes the outer shells, transitioning from linear to non-linear growth. As voids expand, their density decreases, forming spherical shapes with reverse top-hat density profiles, leading to super-Hubble bubbles with suppressed structure growth and boundary ridges. There are two modes of this void evolution: the void-in-void mode, where regions expand at all scales, and the void-in-cloud mode, where voids expand but surrounding matter density leads to contraction and eventual collapse [1786,1789]. The spherical expansion model, combined with excursion set theory, can model the void size function (VSF) — the number density of voids as a function of their comoving size [1789–1791]. The VSF depends on the power spectrum of fluctuations, the growth rate of structures, and the critical density threshold when expanding shells cross. Using the cosmological model, we can predict the abundance of voids of a given comoving size. By comparing this modeled function with observations of abundances at different redshift bins, it is possible to conduct cosmological tests.

2.3.11.3. The void-galaxy cross-correlation function. The cross-correlation function for voids and galaxies can also be used to perform an Alcock-Paczynski test, similar to the galaxy correlation function at BAO scales. The one void term can be interpreted as the stacked mean void profile and serves as a standard sphere at different redshifts to test the Universe's geometry and the relations between the angular diameter and the comoving distances. This profile, in combination with a model for RSD, can be used to test cosmological parameters and gravity models [1792–1795].

2.3.11.4. Redshift-space distortions in voids. The assumption of spherical symmetry for the galaxy distribution around voids breaks down in observations due to RSD acting along the line of sight. The general characteristics of RSD include an elongation of inner correlation contours toward larger scales (due to void expansion) and a flattening of the correlation levels at large scales due to the infall and lower expansion rates at the void outskirts. These anisotropic patterns encode valuable information about void dynamics and the galaxy velocity field. The first model for RSD in voids is the linear model, equivalent to the Kaiser factor in the galaxy autocorrelation [1794]. The pairwise velocity distribution can also be described with the Gaussian streaming

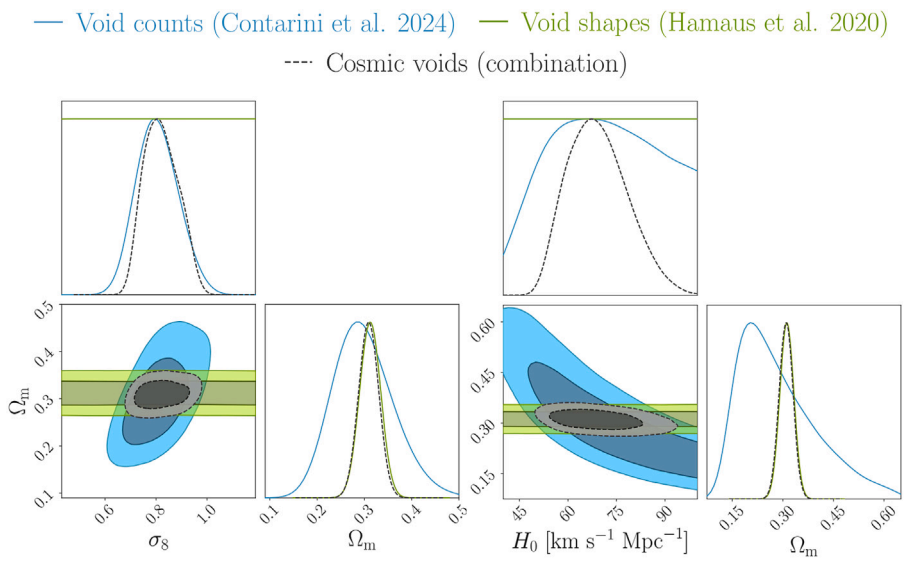

Fig. 46. Confidence contours from void counts (light blue, [1798]) and void shape distortions (green, [1799]) of the BOSS DR12 voids, and their combination (black) as independent constraints on Ω_m, H_0 and σ_8. Adapted from [1798], licensed under Creative Commons Attribution 4.0 International (CC BY 4.0). (For interpretation of the references to colour in this figure legend, the reader is referred to the web version of this article.)

model [1786]. For the impact of RSD in VSF and void-galaxy cross correlation see for instance [1796,1797].

2.3.11.5. An independent probe in the landscape of cosmic tensions. Recent studies have highlighted the potential to test the standard cosmological model using voids in upcoming redshift surveys, such as Euclid [1800–1802]. In a recent analysis presented in Ref. [1798], the void size function in the BOSS DR12 galaxies were examined. Through a combined analysis of void abundances and void-galaxy cross-correlations, these findings proved to be both competitive and compatible with cosmological constraints derived from other probes (see Fig. 46). Furthermore, recent studies of the CMB lensing imprints of cosmic voids have become a valuable test for the cosmological model. In particular, the BOSS survey reported up to 5.3σ [1803], DES reached up to 5.9σ [1804], the WISE–PanSTARRS combination obtained 13.3σ [1805], and the DESI Legacy Survey DR9 achieved up to 17σ [1806], all in excellent agreement with ΛCDM predictions. However, the achieved precision on the parameters does not yet allow for a decisive position in the context of current cosmological tensions. Nevertheless, these results emphasize the significance of cosmic voids as they provide an independent cosmological probe that comes at no extra costs in modern cosmological surveys.

2.3.12. Fast radio burst probes of cosmic tensions

Coordinator: Amanda Weltman

Contributors: Anthony Walters, Bing Zhang, Christo Venter, Shruti Bhatporia, and Surajit Kalita

2.3.12.1. Introduction to fast radio burst cosmology. FRB observations are relatively recently discovered bright transient events (typically observed for a few ms duration) detected in the radio spectrum [1807]. Of particular use to us in cosmology, is the observation that they originate at cosmological distance, apparently from host galaxies at these distances [1808], and thus they provide us with potentially very powerful probes of cosmology [1809,1810] as well as the IGM [1811, 1812].

To date, there have been approximately 800 observed FRBs with information available in the public domain. The majority of these have been detected by the Canadian Hydrogen Intensity Mapping Experiment (CHIME).[12] The primary open problem of FRB science is understanding their origins and the progenitor mechanism at work [1813]. Compelling evidence has accumulated for a magnetar engine, as exemplified by the only Galactic FRB 20200428D detected from a magnetar in the MW. On the other hand, some other engines for cosmological FRBs are still possible (see Refs. [1813–1815] for detailed reviews on FRB progenitor mechanisms). Perhaps the greatest open puzzle is the curious observation that while some FRBs appear to repeat, not all of them do, and there does not appear to be any pattern or periodicity to so-called FRB repeaters. While there may be some selection effects at work, it is likely that there are simply different classes of bursts and thus even more to discover about FRBs and with FRBs. Hence, multi-wavelength observations or detections of GWs [1816] and neutrinos from FRB sites will be important to better understand their progenitor mechanisms.

Recent searches for persistent radio emission from one-off and repeating FRBs identified a nearly unresolved source for FRB 20190714 A, with a peak brightness of 53 μJy/beam, marking the first detection of persistent radio emission potentially linked to a non-repeating FRB. Multi-wavelength follow-ups in ultraviolet, optical, X-ray, and gamma-ray bands set upper limits [1817], aiding the distinction between repeating and one-off FRBs. Persistent emission modeling can constrain central source energetics and test magnetar-driven emission scenarios. Follow-ups also refine host galaxy properties, localization, and redshift-dependent FRB characteristics, enhancing their use in cosmology.

2.3.12.2. Fundamental parameter inference from fast radio bursts. One of the key parameters in understanding FRBs is the dispersion measure (DM), which gives information about the ionized plasma along the path of the light ray. Broadly it gets contributions from each of the 4 environments along the line of sight, our Galaxy, its halo, the IGM, and the host galaxy as illustrated in Fig. 47. The $(1 + z_S)$ factor in the denominator of the last term accounts for the observed value of redshifted DM_{Host}. In general, DM_{IGM} contains the information of the underlying cosmology. The average DM_{IGM} is given by the following

[12] https://www.chime-frb.ca/catalog

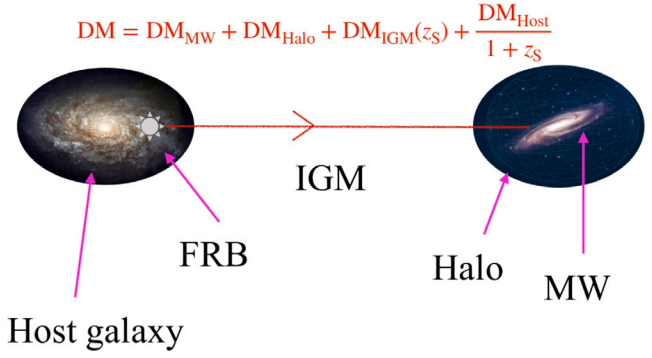

Fig. 47. Illustrative diagram indicating key components of contributing to measured DM of FRBs.

equation (now known as the Macquart relation [1812])

$$\langle \mathrm{DM_{IGM}}(z_\mathrm{S})\rangle = \frac{3c\Omega_\mathrm{b}H_0^2}{8\pi G m_\mathrm{p}}\int_0^{z_\mathrm{S}} \frac{f_\mathrm{IGM}(z)\chi(z)(1+z)}{H(z)}\mathrm{d}z, \tag{2.26}$$

where Ω_b is the baryonic matter density, m_p is the proton mass, f_IGM is the baryon mass fraction in the IGM, and $\chi(z)$ is the ionization fraction along the line of sight. As $\langle \mathrm{DM_{IGM}}\rangle$ contains cosmological parameters, this equation can be used to constrain their values. For instance, utilizing a set of mock FRBs, DE equation of state for wCDM cosmology was constrained [1818,1819] and predicted that with $\mathcal{O}(10^4)$ localized FRBs, this constraint can be tighter than the same obtained from BAO measurements.

FRBs have been observed over a relatively narrow redshift range to date, 100 MHz–8 GHz [1820,1821], and partly this is most likely a result of observation bias, where we can more easily observe the bursts that are closest to us. This has limited their potential in constraining cosmological parameters directly [1809], though using cosmology as a prior allows for IGM constraints, specifically a potential solution to the missing baryon problem [1811,1812]. Moreover, using a specific case of FRB 150418, earlier studies established a limit on the photon mass of $m_\gamma < 1.8\times10^{-14}\,\mathrm{eV\,c^{-2}}$ [1822] and this bound has been continuously strengthened with the inclusion of additional FRBs [1823,1824]. Furthermore, localized FRBs have been used to constrain the parameterized post-Newtonian (PPN) parameter [1825] and other fundamental constants like the fine-structure constant and the proton-to-electron mass ratio [1826,1827].

2.3.12.3. Hubble constant estimations using fast radio bursts. Several recent studies have leveraged FRBs with measured redshifts to constrain H_0 within a Bayesian framework. This approach compares the measured $\mathrm{DM_{IGM}}$ of localized FRBs with their theoretical predictions, yielding constraints on H_0 and other cosmological parameters. Ref. [1809] was among the first to investigate the utility of FRBs as cosmological probes through simulations. Their mock FRB catalog highlighted the challenge posed by DM variations due to IGM inhomogeneities. Notably, the most significant improvement was observed in the $\Omega_{\mathrm{b},0}h^2$ parameter when combining FRBs with CMB, BAO, SN, and H_0 data. Additionally, they found that FRBs offered limited constraints on the DE equation of state, while the curvature parameter (Ω_k) showed some improvement when combined with other data. Moving forward, Ref. [1812] leveraged 8 localized FRBs to constrain $\Omega_{\mathrm{b},0} = 0.051^{+0.021}_{-0.025}h_{70}^{-1}$ where $h_{70} = H_0/(70\,\mathrm{km\,s^{-1}\,Mpc^{-1}})$, consistent with values derived from CMB and BBN data. Another interesting work using a strong lensing effect with 10 FRBs found $H_0 \approx 70\,\mathrm{km\,s^{-1}Mpc^{-1}}$ [1828].

More recently, as more FRB data are available, these constraints have been revised to a great extent. Ref. [1829] analyzed 9 localized FRBs and found $H_0 = 62.3\pm9.1\,\mathrm{km\,s^{-1}Mpc^{-1}}$, assuming a homogeneous host galaxy contribution, which may limit the complete validation of the result. Subsequently, Ref. [1830] classified 18 localized FRBs based on host galaxy morphology and employed the IllustrisTNG simulation to estimate individual host contributions. This approach yielded $H_0 = 68.81^{+4.99}_{-4.33}\,\mathrm{km\,s^{-1}Mpc^{-1}}$. However, their model-based host DM values were lower than the actual reported values for some FRBs. Moreover, Ref. [1831] included 16 localized and 60 unlocalized FRBs detected by ASKAP, estimating $H_0 = 73^{+12}_{-8}\,\mathrm{km\,s^{-1}Mpc^{-1}}$. Their larger error bars, despite a substantial number of FRBs, likely reflect the inclusion of systematic uncertainties. Moving beyond, Ref. [1832] incorporated a scatter in the Macquart relation with 78 FRBs (21 localized) and obtained $H_0 = 85.3^{+9.4}_{-8.1}\,\mathrm{km\,s^{-1}Mpc^{-1}}$. Ref. [1833] employed a model-independent method with 18 localized FRBs and found $H_0 = 71\pm3\,\mathrm{km\,s^{-1}Mpc^{-1}}$. Conversely, Ref. [1834] estimated $H_0 = 95.8^{+7.8}_{-9.2}\,\mathrm{km\,s^{-1}Mpc^{-1}}$ using 24 localized FRBs with a wide flat prior on $\mathrm{DM_{Halo}}$. Furthermore, Ref. [1835] combined 12 unlocalized FRBs with BBN data, resulting in $H_0 = 80.4^{+24.1}_{-19.4}\,\mathrm{km\,s^{-1}Mpc^{-1}}$. Additionally, Ref. [1836] used a combination of 18 localized FRBs and the Pantheon dataset to estimate $H_0 = 65.5^{+6.4}_{-5.4}\,\mathrm{km\,s^{-1}Mpc^{-1}}$. Ref. [1837] propose a novel method using ANN architectures for 23 localized FRBs to estimate $H_0 = 67.3\pm6.6\,\mathrm{km\,s^{-1}Mpc^{-1}}$. Furthermore, utilizing Bayesian analysis with different likelihood functions and distinct host distributions for 64 localized FRBs, Ref. [1838] obtained H_0 values well above $70\,\mathrm{km\,s^{-1}Mpc^{-1}}$ aligning with the late-Universe H_0 values with 1σ error bars no longer overlap with those obtained from early-Universe measurements. More recently, accounting 98 localized FRBs, Ref. [1839] showed multiple estimates of H_0 utilizing different methodologies.

As we see, FRBs do offer preliminary constraints on cosmological parameters, although they currently lack the power to definitively resolve existing tensions in cosmology. While not as stringent as constraints derived from established probes like CMB and SNIa, FRB-derived constraints are significantly tighter than those obtained from GW observations. A primary contributor to the discrepancies in H_0 values reported by different researchers lies in the choice of models for IGM and host DM contributions, which remain largely unconstrained from observations. Future surveys aiming to detect a larger number of FRBs, with a substantial fraction localized to their host galaxies, hold promise for significantly improved constraints. These advancements could potentially contribute to resolving the current Hubble tension.

2.3.12.4. Understanding nature of dark matter using fast radio bursts. Beyond constraining the Hubble constant and other cosmological parameters related to the evolution of the Universe, FRBs hold promise for constraining the fraction of primordial mass black holes made up of DM (f_PBH). In this context, strong gravitational lensing of FRBs plays a crucial role. When light rays from FRBs pass near a massive object with mass M_L, they can be deflected, potentially producing multiple, time-delayed copies of the original burst. The time delays and magnification (μ) of these lensed images provide an estimate of the source's optical depth (τ), which is linked to f_PBH as follows

$$\tau(M_\mathrm{L}, z_\mathrm{S}) = \frac{3}{2}f_\mathrm{PBH}\Omega_\mathrm{c}\int_0^{z_\mathrm{s}}\mathrm{d}z_\mathrm{L}\frac{H_0^2}{cH(z_\mathrm{L})}\frac{D_\mathrm{L}D_\mathrm{LS}}{D_\mathrm{S}}(1+z_\mathrm{L})^2\left[y_\mathrm{max}^2(\mu)-y_\mathrm{min}^2(M_\mathrm{L},z_\mathrm{L})\right], \tag{2.27}$$

where D_L and D_S are respectively angular diameter distances to the lens object and the source from the observer, D_LS is the same between lens and source, y_min and y_max are minimum and maximum impact parameters, respectively. Ref. [1840] pioneered this method, setting an initial constraint of $f_\mathrm{PBH} < 0.08$ assuming FRB lensing by black holes exceeding mass $M > 20\,M_\odot$. Subsequent studies incorporated FRB microstructure [1841] and extended mass functions [1842] to refine these bounds. Notably, Ref. [1843] visualized using a null detection of lensed FRBs within a sample of 110 real FRB observations. Further investigations explored the impact of intervening plasma, which mimics the lensing effects. Ref. [1844] demonstrated this using 172 CHIME

FRBs, highlighting the need to account for such decoherence or scattering screens. More recently, Ref. [1845] analyzed 636 FRBs from CHIME and the absence of confirmed lensing events suggesting that MG might introduce a screening effect akin to the plasma scenario. In summary, FRBs offer constraints on $f_{\rm PBH}$ in the mass range of approximately $10^{-4} - 10^{4}\ M_{\odot}$ and these constraints are comparable or even surpassing existing experiments like OGLE, EROS, Icarus, and MACHO.

The landscape of FRB-based constraints is constantly evolving as new and more powerful radio telescopes come online. Arrays such as Hydrogen Intensity and Real-time Analysis eXperiment (HIRAX) [1846], Deep Synoptic Array (DSA)-2000 [1847], Bustling Universe Radio Survey Telescope in Taiwan (BURSTT) [1848] and Square Kilometer Array Observatory (SKAO) [1849] promise to detect a significantly larger number of FRBs, including potentially localized ones. This will undoubtedly lead to further refinements in our understanding of the Universe.

2.3.13. Radio background excess

Coordinator: Jack Singal

Contributors: Alan Kogut, Marco Regis, and Nicolao Fornengo

Throughout most of the electromagnetic spectrum the observed level of surface brightness and anisotropy of the sky background radiation is roughly consistent with that expected from known emission mechanisms from astrophysical and cosmological sources. This is the case for the backgrounds at infrared, e.g., see Ref. [1850], microwave, e.g., see Ref. [1434], optical/UV, e.g., see Ref. [1851], X-ray, e.g., see Ref. [1852], and gamma-ray, e.g., see Ref. [1853] wavelengths. However, in the radio region of the electromagnetic spectrum, both the observed surface brightness level of the photon background and the level of its anisotropy angular power are seemingly much larger than that which can be produced by known source classes, resulting in a tension that is, as of now, an anomaly.

As recently summarized in Ref. [1854], with the known structure resulting from Galactic diffuse emission subtracted, the surface brightness of the level of diffuse background radiation on the sky, from at least ∼20 MHz to 3 GHz, as a function of frequency ν is, in radiometric temperature units

$$T_{\rm BGND}(\nu) = 30.4 \pm 2.6{\rm K} \left(\frac{\nu}{310\ {\rm MHz}}\right)^{-2.66\pm0.04} + T_{\rm CMB}\,, \tag{2.28}$$

where $T_{\rm CMB}$ is the frequency-independent contribution of 2.725 K due to the CMB. This background level has been measured by the Absolute Radiometer for Cosmology, Astrophysics, and Diffuse Emission 2 (ARCADE 2) [1855,1856] at the high frequency end, and several radio maps at lower frequencies from which an absolute zero level calibration can be determined, including recently the Long Wavelength Array (LWA) [1857]. Because the spectral index of −2.6 is consistent with synchrotron radiation, this has been referred to as the radio synchrotron background (RSB). The RSB surface brightness level is shown in radiometric temperature units and spectral energy density units in Fig. 48.

This level of surface brightness is several times higher than can be produced by known classes of radio sources in the Universe. Studies of radio source counts show that the total emission from the known discrete extragalactic sources, particularly AGN and star-forming galaxies, is around a factor of five lower than the surface brightness level of the RSB [1863–1865]. Producing the surface brightness of the RSB with discrete extragalactic sources would require an enormous number of a new class of low-flux sources [1863].

For lines of sight far away from the Galactic plane, the RSB is considerably brighter than the expected contribution from models of Galactic diffuse emission [1866]. The possibility that the RSB originates from a larger spherical halo of radio emission surrounding our Galaxy is highly disfavored by several considerations, e.g., see Ref. [1854,1866] including that it would make our Galaxy highly atypical [1867]. Observational constraints on the polarization structure of the diffuse radio emission rule out the Local Bubble as an origin scenario [1868].

In a parallel situation to the surface brightness, the anisotropy level of the RSB, as measured at 140 MHz, is also higher than that which could result from models of known source classes [1869,1870]. The measured angular power spectrum of the diffuse radio emission is a power law (in K^2 or "$(\Delta T)^2_\ell$" units) with increasing ℓ with index $\beta = 2.17 \pm 0,08$ from $700 \lesssim \ell \lesssim 4000$ (angular scales from ∼2' to ∼20'), indicative of unclustered point sources, diffuse sources, or a large number of faint, clustered point sources [1870]. However, its level of anisotropy power rules out the former, given that the density of high flux point sources is constrained by source counts observations such as e.g., [1864]. This leaves very numerous but highly clustered point sources or diffuse sources as the source classes that can seemingly reproduce the level of the observed angular power spectrum of the RSB.

There are other observational constraints on possible origin scenarios for the RSB. Any possible source class and emission mechanism must not:

- overproduce the observed level of the background radiation at far-infrared wavelengths, given the known correlation between radio and far-infrared emission in galaxies, e.g., see Ref. [1871]. Any origin scenario involving galaxies or their components would need this correlation to evolve with redshift [1872,1873].
- overproduce the observed level of the X-ray background through inverse-Compton upscattering of the CMB and/or optical/UV background [1872]. If the RSB indeed originates from a synchrotron process, this puts a lower limit on the strength of the magnetic field in the sources from which the RSB originates of around 1μG at redshift $z = 0$. At higher redshifts this lower limit increases by a factor of up to $(1+z)^4$ due to the increase in the surface brightness level of the CMB at higher redshifts.
- overproduce the observed limits on the 21-cm absorption trough, due to the possible presence of the RSB at redshifts $z \sim 10$ increasing the temperature of the background relative to the temperature of the 21-cm transition, e.g., see Ref. [1874].
- overproduce the observed cross-correlation angular power spectrum between the RSB and optical source catalogs, indicating that the vast majority of its sources, if discrete, must be at $z \gtrsim 0.5$ [1873].

Some RSB origin scenarios that have been suggested include SN of massive population III stars [1875], emission from Alfvén reacceleration in merging galaxy clusters [1876], annihilating DM in halos or filaments [1877–1880] or ultracompact halos [1881], "dark" stars in the early Universe [1882,1883], dense nuggets of quarks [1884], accretion onto primordial black holes [1885–1887], decays to dark photons [1888], dark photon decays [1889,1890], and other injections of photons in the early Universe from processes [1891] including superconducting cosmic strings [1892] and decays of relic neutrinos [1893]. Some of these models likely violate one or more of the observational constraints discussed here, while others contain parameter spaces where they do not.

Upcoming observatories, and observations possible with current facilities, have the potential to further constrain and test RSB origin scenarios. A measurement, such as with the space-based LuSSE-Night [1894] to determine if the spectrum hardens below 10 MHz would be useful in this regard. The radio SZ effect [1895,1896] when combined with the well-known CMB SZ effect, would result in observed cluster radio emission having a null frequency at $700 \leq \nu \leq 800$ MHz, below which there would be an increment in the observed surface brightness in the direction of a cluster and above which there would be a decrement, each on the order of $\lesssim 1$ mk (both on top of the contribution from the background RSB). A detection or lack thereof at the required sensitivity in clusters of various redshifts would constrain the redshift(s) of the origin of the RSB. The radio background being far in excess, in both surface brightness and anisotropy angular power,

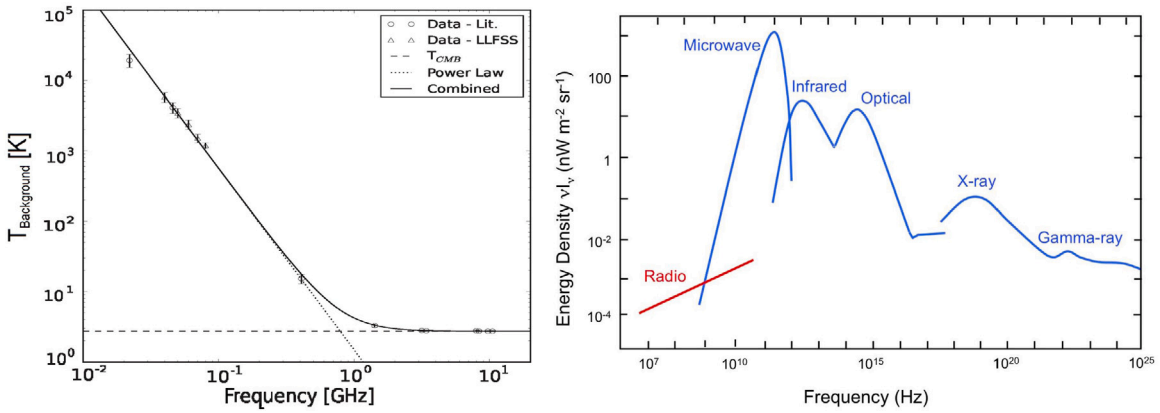

Fig. 48. Left: The radio sky zero level in radiometric temperature units, reproduced from Ref. [1857], as measured by several different instruments or surveys reporting an absolute zero-level calibration. Results are shown for ARCADE 2 at 3–10 GHz [1855,1856], Reich & Reich at 1.4 GHz, [1858], Ref. [1859] at 408 MHz, Ref. [1860] at 45 MHz, and Ref. [1861] at 22 MHz, as well as several points reported by Ref. [1857]. **Right**: The photon backgrounds in the Universe in units of spectral energy surface brightness density. Reproduced from Ref. [1862].

of that which is expected to be produced by known source classes and processes in the Universe is an intriguing issue.

2.3.14. Tension between the large scale bulk flow and the standard cosmological model

Coordinator: Richard Watkins

Contributors: Hume A. Feldman

The Cosmological Principle requires that the motions of galaxies averaged over a sphere of radius R (bulk flow) should go to zero as R becomes cosmologically large. Thus the determination of the Large-Scale Bulk Flow is an important probe of this principle and of the Standard Cosmological Model more generally. Estimating the bulk flow requires large catalogs of galaxy peculiar velocity measurements; in the last decade, the quantity and quality of this type of data has improved to where bulk flows can provide an important test of our understanding of the Universe.

2.3.14.1. Analyzing the bulk flow using the cosmic flows 4 catalog. The Cosmic Flows 4 (CF4) peculiar velocity catalog [1424] contains velocities and their uncertainties for 38,057 groups and individual galaxies; this represents most of the peculiar velocity data in existence. Analyzing the bulk flow using this data presents several significant challenges. First, we can only measure the radial component of the peculiar velocity. Second, peculiar velocities typically have large uncertainties; objects in the CF4 catalog typically have uncertainties that are around 15% of the redshift. This means that since distant galaxies have much larger absolute uncertainties, most of the information in the catalog is concentrated nearby. Thus care must be taken to ensure that the bulk flow estimate is not dominated by objects near the center of the volume. Finally, the CF4 survey has a very irregular distribution both radially and on the sky. Thus analyzing the bulk flow using the CF4 requires a method that can "even out" the distribution of the information in the volume of interest both so that the volume is uniformly sampled and so that radial flows do not make spurious contributions. The latter is particularly important given the current tension in the value of the Hubble constant. The use of an incorrect value of the Hubble constant in calculating peculiar velocities can result in phantom radial flows that can contribute to the bulk flow if the volume of interest is not sampled in an isotropic manner.

Ref. [1426] deals with these challenges by analyzing the CF4 catalog using the Minimum Variance (MV) method [1428,1897,1898]. The MV method generates estimates of the bulk flow components, in a volume of radius R, that is as close as possible to those that would be measured from an ideal (isotropic and well sampled) survey; thus it balances the information in the catalog so that the volume is evenly sampled. In addition, a constraint is put on the MV bulk flow estimates so that they are completely independent of the value of the Hubble constant. It should be noted that even though the analysis uses only radial velocity measurements, if it is assumed that the velocity field is irrotational (as it should be if it were generated via gravitational instability), then the MV method estimates reflect averages of the full three-dimensional velocities.

2.3.14.2. The bulk flow tension. Ref. [1426] determined that the largest radius for which the bulk flow could be estimated with the CF4 catalog is around $200h^{-1}$Mpc. Their bulk flow estimates as a function of radius are shown in Fig. 49 and displayed in Table 3. The figure shows both the estimates and uncertainties for the components of the bulk flow (in galactic coordinates) as well as the magnitude. Included in the figure (in red) is the expected magnitude of the bulk flow as a function of radius calculated using the Cosmological Standard Model. Contrary to expectations, they find that the bulk flow magnitude increases with increasing radius. In addition, they find that the bulk flow has a much larger magnitude than expected in the Cosmological Standard Model [192]. Indeed, they found the probability of obtaining a bulk flow as large or larger in the Standard Model for $R = 200$ h^{-1}Mpc to be 1.5×10^{-6}, equivalent to about 4.8σ. Ref. [1427] find a similar magnitude for the bulk flow (also using the MV method) but estimate larger uncertainties using cosmological simulation data. Ref. [1425] also analyzes the bulk flow from the CF4 catalog using a very different method and obtains a result that is consistent with the Standard model. However, it is difficult to discern the sensitivity of their bulk flow to different scale motions. Thus the large-scale bulk flow potentially poses a significant challenge to the standard model, but determining the strength of this challenge will require resolving differences in analysis methods.

2.3.15. Ultra long period cepheids

Coordinator: Ilaria Musella

Contributors: Giuliana Fiorentino, Marcella Marconi, Roberto Molinaro, and Vincenzo Ripepi

The Ultra Long Period Cepheids are pulsating stars characterized by periods longer than ~ 80 days with a mean absolute magnitude in the I band $-9 < M_I < -7$ mag. Thanks to their significant brightness they are observable at very long distances, up to cosmologically interesting scales. Thus they could represent competitive standard candles, not

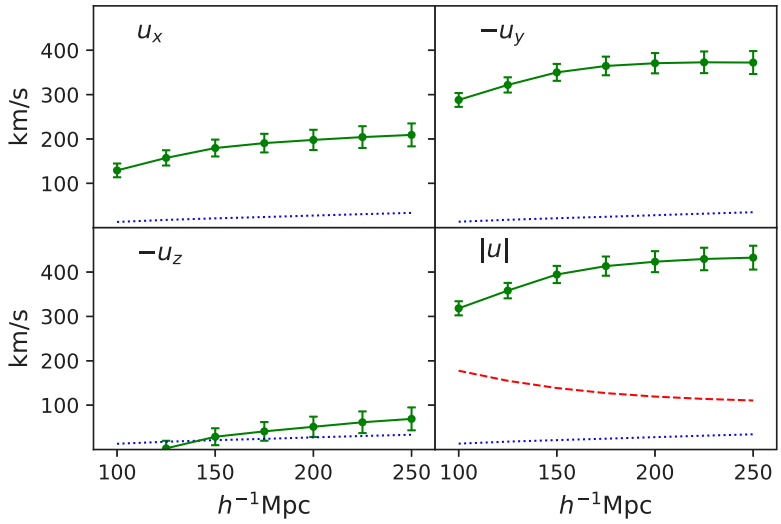

Fig. 49. The green points with error bars show the bulk flow components and magnitude estimated from the CF4 catalog as a function of radius R. The error bars indicate the uncertainty in the estimates due to measurement noise. The dotted blue lines show the theoretical standard deviation of the expected differences between the bulk flow estimates and the bulk flow from an ideal survey calculated using the cosmological standard model (not including measurement noise). The red dashed line indicates the theoretical expectation for the magnitude of the bulk flow calculated using the Cosmological Standard Model.
Source: The figure is reproduced with permission from Ref. [1426].

Table 3
Summary of Bulk Flows for $R = 150h^{-1}$ Mpc and $R = 200h^{-1}$ Mpc. The uncertainties include both the theoretical difference between the estimate and the bulk flow from an ideal survey and the measurement noise.

	$R = 150h^{-1}$ Mpc	$R = 200h^{-1}$ Mpc
Expectation (km/s)	139	120
Bulk Flow (km/s)	395 ± 29	427 ± 37
Direction	$l = 297° \pm 4°$	$l = 298° \pm 5°$
	$b = -4° \pm 3°$	$b = -7° \pm 4°$
χ^2 with 3 d.o.f.	20.19	29.84
Probability	1.54×10^{-4}	1.49×10^{-6}

requiring the combination with secondary distance indicators [1899–1905] to reach the Hubble flow. On this basis, using ULPs might reduce the possible effect of systematic errors on the calibration of the extragalactic distance scale and, in turn, on the local determination of H_0. Despite their expected important role in distance scale studies, their application as standard candles is still challenging due to the relatively small sample of ULPs with well-sampled light curves covering more than one cycle and some inconsistencies between theoretical evolutionary and pulsational predictions and the observed properties. Indeed, the number of known ULPs is 73 observed in different galaxies. In particular, only one has recently been discovered in our Galaxy in the Gaia DR3 catalog. Their position in the period–luminosity planes and the color-magnitude diagrams suggest that these objects represent the extension at higher luminosity and mass of the Classical Cepheids, but their mass–luminosity relation could be different according to their evolutionary stage. As recently suggested in Ref. [1905], the consistency between ULP and Classical Cepheids relations increases when the photometry accuracy improves, thus supporting the hypothesis that they are the same type of pulsating variables but with different mass and period ranges.

However, at such high luminosity and mass levels, stellar evolution does not predict the occurrence of the blue loop typical of the central helium-burning phase of intermediate-mass stars, so the population of the Instability Strip might correspond to the first crossing toward the RGB. Moreover, the observed pulsation period provides a strong constraint on the stellar mass at fixed temperature and luminosity. Current evolutionary tracks matching the observed position of the ULPs do not always provide a combination of mass, luminosity, and effective temperature consistent with the observed periodicity.

The agreement between the ULP and Classical Cepheid Wesenheit relations tends to confirm the Hubble constant value obtained based on Classical Cepheids, even if the remaining uncertainties on these objects' evolutionary and pulsational properties need to be solved and the dispersion of their Wesenheit relation has to be reduced to contribute to the understanding of the Hubble tension. To this aim, future theoretical and observational investigations will include different steps: to better understand the evolutionary status of the ULPs through a detailed comparison with updated sets of evolutionary tracks and isochrones, to produce an extended grid of nonlinear convective pulsation models covering the high mass and luminosity regime expected for these variable start to increase the number of ULPs and improve their photometric accuracy. In this respect, exploring the Gaia database to find new ULPs will be fundamental. Recently, the first MW ULP was found among the variables classified as Long Period Variables in Gaia DR3 and there are likely other misclassified ULPs. In addition, the forthcoming Rubin-LSST survey will also represent a fundamental opportunity to improve the photometry of the known Local Group ULPs and/or increase the sample.

3. Data analysis in cosmology

Coordinator: Agnieszka Pollo

The volume and complexity of data available for observational cosmology has increased greatly during the last years, and in the coming years, the amount of data generated by different ground-based and space observatories and experiments is expected to grow by orders of magnitude.

For example, the Early Data Release of DESI comprising 2 million spectra of extragalactic sources amounts to 80 TB, and it is only 2% of the expected full final DESI catalog [1906–1908]. Imaging data are even more voluminous: a single exposure of the Dark Energy Camera (DECam) produces an image of the size of a gigabyte [1909]; and the latest DES Data Release 2 [1910] was built upon 76,217 such single-epoch images. Similarly, one night of observations with the Subaru HSC camera results in several hundred gigabytes of data [1911], which translated into ~ 70 TB database already with the first data release of

the Hyper Suprime-Cam Subaru Strategic Program [1912], and several hundreds of terabytes after the third data release [1913].

All these numbers are expected to fade soon with the expected arrival of Euclid [164], Vera Rubin Observatory [897], or SKAO data.[13] In particular, Vera Rubin Observatory is expected to deliver more than 500 petabytes of imaging data per year, while for SKAOthe data volume is expected to exceed 700 petabytes per year.[14]

In addition to the expected multiwavelength and multimessenger observational or experimental data, there exists a whole additional realm of data useful for cosmology, i.e., simulations. Simulated catalogs are being used to test different cosmological scenarios, to probe mechanisms of baryonic interactions in the dark-matter-dominated Universe, especially at small, non-linear scales; and finally, to create mock realizations of real catalogs which can be used both for physical predictions and for tests of specific measurement techniques against a variety of biases introduced by observational strategy and technique. The creation of simulated catalogs is usually a multi-level process, requiring a lot of computational power and creating amounts of data much larger than the corresponding observational data themselves.

Using all types of data expected in the near future, both observed and simulated, to provide reliable scientific results, requires developing new approaches to data handling and analysis at different levels. Firstly, all these data need to be properly stored and transferred. Ideally, they should also be made publicly accessible in formats that are easy to handle for users from different scientific communities. Datasets observed at different wavelengths or coming from different experiments need to be cross-correlated to facilitate multi-messenger studies. Finally, scientific analysis of these data results in the creation of derived data sets, in amounts often exceeding the original data. Storage, transfer, and subsequent analysis of large amounts of data is not only costly but also requires a well thought out technological and strategic approach. ASTRONET Roadmap for years 2022-2035[15] indicates near-future big data as one of the biggest challenges that astronomy in Europe will face in the coming decade and recommends the development of a "Tiered" approach for data infrastructure, to optimize the use of available resources.

With new big data, unavoidably, come new methods, ideally fully automated and requiring little human intervention (e.g., see Ref. [1914]). It is therefore not surprising that a majority of sections in this chapter deal with different aspects of ML-based approaches to the data analysis, in order to speed up and optimize the science output, and to probe all possible parameter spaces. However, with the growing popularity of these methods, new challenges arise.

An old saying popular in ML community says "rubbish in, rubbish out"; it concisely summarizes the fact that the errors or biases that exist in the original data, also those unknown to the users, are unavoidably transferred to the results. Informed application of any machine-learning methods requires an in-depth understanding of the properties and limitations of the data. A related problem is a common "black box" approach to ML applications. Insufficient understanding of algorithms used may result in users not being aware of their limitations and applicability to a given scientific problem and given data. The next big challenges are related to the interpretability and reproducibility of the results obtained with the aid of machine-learning-based methods. In particular, reproducibility strengthens the importance of keeping codes and data open to the scientific community so that all the scientific results obtained can be independently verified. However, it cannot be forgotten that storage — especially long term storage — and computing power come with a cost, both monetary, and environmental. The latter aspect draws more and more attention especially now, when commercial ML and artificial intelligence projects fuel an increasing demand for resources.

Observational cosmology has already become an extremely data-intensive endeavor, and the future large, complex and interdependent data sets that will be generated by observatories, space missions, real and mock experiments, theoretical model simulations, and different types of numerical simulations will require new tools and approaches, and close co-operation between different fields of science. It is safe to say that cosmology and extragalactic astrophysics are now only at the beginning of this road.

3.1. Bayesian inference methods in cosmology

Coordinator: Jesús Torrado

Contributors: Alessandro Vadalà, Benjamin l'Huillier, Denitsa Staicova, Guadalupe Cañas-Herrera, Jenny G. Sorce, Laura Herold, Matías Leizerovich, Matteo Martinelli, Ruth Lazkoz, and Susana J. Landau

Modern cosmology has entered an era of precision measurements, where extracting robust constraints on theoretical models from increasingly complex datasets demands sophisticated statistical approaches. Monte Carlo (MC) methods have emerged as the cornerstone of parameter inference in cosmology, allowing researchers to efficiently explore high-dimensional parameter spaces and quantify uncertainties in a fully Bayesian framework. This section presents an overview of the most commonly used MC techniques in cosmological analyses, their strengths and limitations, and practical considerations for their implementation.

The goal of Bayesian parameter inference is to determine the posterior $p(\boldsymbol{\theta}|\boldsymbol{d},\mathcal{M})$, which is the probability of the parameters of model $\mathcal{M}$ taking some value $\boldsymbol{\theta}$, given the data $\boldsymbol{d}$. The posterior can be related to the likelihood of the data $\boldsymbol{d}$ being a realization of the model with given parameter values, i.e., $\mathcal{L}(\boldsymbol{d}|\boldsymbol{\theta},\mathcal{M})$, via the Bayes theorem

$$p(\boldsymbol{\theta}|\boldsymbol{d},\mathcal{M}) = \frac{\mathcal{L}(\boldsymbol{d}|\boldsymbol{\theta},\mathcal{M})\,\pi(\boldsymbol{\theta},\mathcal{M})}{\mathcal{Z}(\boldsymbol{d},\mathcal{M})}\,, \tag{3.1}$$

where $\pi(\boldsymbol{\theta},\mathcal{M})$ is the prior and $\mathcal{Z}(\mathbf{d},\mathcal{M})$ the model evidence. Since one typically cares about the constraints imposed on the model parameters, which are independent of the overall normalization of the posterior, the model evidence is often neglected as it contributes only a constant factor. However, as we will discuss below, this evidence becomes important for model selection. In standard parameter estimation contexts, we usually drop the explicit conditioning on the model $\mathcal{M}$. When required, lower-dimensional constraints, e.g., Bayesian credible intervals, are easily obtained by marginalization, i.e., integration of the posterior over the remaining parameters. By construction, the model evidence is the *marginal likelihood* over the full parameter space, $\mathcal{Z}(\boldsymbol{d}) = \int \mathcal{L}(\boldsymbol{d}|\boldsymbol{\theta})\pi(\boldsymbol{\theta})\,\mathrm{d}\boldsymbol{\theta}$, determining the probability of the data having been realized under the given model, whatever the values of its parameters (hence their usefulness for model comparison).

There are various Monte Carlo (MC) techniques aimed at determining the posterior $p(\boldsymbol{\theta}|\mathbf{d})$ by means of obtaining a fair sample from it. Below we offer a short review of the most popular MC algorithms used by the astrophysical and cosmological community, which is illustrated in Fig. 50. These approaches have diverse strengths, but also limitations, which we refer to as "sampling problems" below.

Moreover, the choice of prior $\pi(\boldsymbol{\theta})$ can lead to unwanted (and sometimes unknown) effects like prior dependence or projection/prior volume effects, which we refer to as "modeling problems" and will be discussed below in the context of cosmological tensions.[16]

[13] https://www.skao.int/

[14] https://www.skao.int/sites/default/files/documents/SKA-TEL-SKO-0001818-01_DataProdSummary-signed_0.pdf

[15] https://www.astronet-eu.org/wp-content/uploads/2023/05/Astronet_RoadMap2022-2035_Interactive.pdf

[16] Of course, the modeling of the likelihood $\mathcal{L}(d|\boldsymbol{\theta})$ is also often based on approximations and can lead to uncertainties. Since the likelihood is the basis of all parameter inference, not only MC approaches, we will not discuss those here.

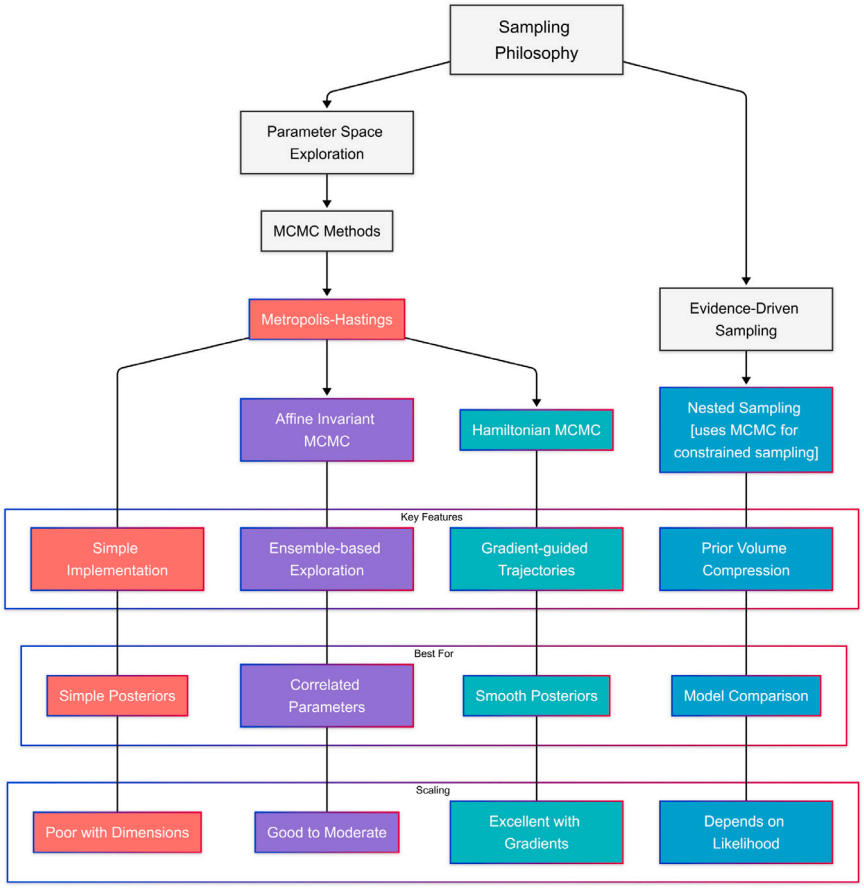

Fig. 50. A flowchart summarizing the main differences between different samplers.

3.1.1. Markov chain Monte Carlo sampling algorithms

MCMC algorithms explore the parameter space through a proposal-acceptance mechanism, building a *chain* of states, or points in parameter space, from which a (decorrelated) fair sample from the posterior can be extracted. Robust convergence tests (usually based on the stability of a single Markov chain or similarity between parallel ones), are crucial to avoid biased inferences and inaccurate error estimates, guaranteeing that the MCMC samples reliably represent the target posterior distribution.

The family of MCMC algorithms encompasses a large number of different approaches. They can be classified under different criteria: the strategy followed to propose new points, the acceptance–rejection test performed on the proposals, the distribution from which they effectively sample (not always the target distribution), whether they pre-condition the parameter space, and how.

In the simplest approach, at each step $\boldsymbol{\theta}$, a new state $\boldsymbol{\theta}'$ is drawn from a proposal density $q(\boldsymbol{\theta}'|\boldsymbol{\theta})$ and accepted with probability

$$\alpha = \min\left(1, \frac{\phi(\boldsymbol{\theta}')q(\boldsymbol{\theta}|\boldsymbol{\theta}')}{\phi(\boldsymbol{\theta})q(\boldsymbol{\theta}'|\boldsymbol{\theta})}\right), \tag{3.2}$$

where $\phi(\boldsymbol{\theta})$ is the target distribution, i.e., the posterior in a Bayesian framework. This test is called the *Metropolis–Hastings* (MH) criterion. Rejected proposals increase the *weight* of the current state within the chain. A typical choice for the proposal distribution is a multivariate normal $\boldsymbol{\theta}' \sim \mathcal{N}(\boldsymbol{\theta}, \boldsymbol{\Sigma}_T)$, with a variable dispersion covariance $\boldsymbol{\Sigma}_T$ tailored to parameter values at each step.

While unsophisticated, this method can produce accurate inference for simple distributions in large dimensions, but its efficiency depends critically on the choice of an appropriate proposal distribution, and otherwise deteriorates quickly for highly correlated or complex distributions.

Efficiency can be increased by using the current chain (or parallel chains) to compute an affine transformation that would decorrelate the posterior locally (or globally if sufficiently Gaussian). This affine transformation can be chosen so that proposals involve the re-calculation of only parts of the likelihood pipeline [1915] (as implemented in `MontePython` [1916,1917] and `Cobaya` [1918]). Parallelization, together with these strategies, can make MCMC well-suited for computationally expensive likelihood evaluations.

For more complicated posterior structures, such as curving degeneracies that would need a local transformation to be decorrelated, *ensemble methods* such as `emcee`[17] [1919] can use the information on the position of multiple walkers to automatically adapt proposals. More recently, the authors of `pocoMC`[18] [1920] have proposed the use of Sequential Monte Carlo (i.e., sequentially sampling from a family of distributions that interpolate between the prior and the posterior) while learning a generalized transformation that decorrelates arbitrary parameter spaces, using Normalizing Flows [1921]. `pocoMC` can compute model evidences along MC samples.

Slice sampling [1922] is an alternative adaptive approach to propose new Markov chain states, that automatically adjusts step sizes to the local shape of the distribution. For each parameter update, it samples uniformly from a randomly-oriented "slice" under the PDF curve, $S_y = \{\boldsymbol{\theta} : y < \phi(\boldsymbol{\theta})\}$, where y is uniformly drawn from $[0, \phi(\boldsymbol{\theta}_{\rm current})]$. A proposal $\boldsymbol{\theta}'$ is then uniformly sampled from this slice through a stepping-out and shrinking procedure. This adaptivity makes slice sampling particularly robust, requiring minimal tuning while maintaining

[17] https://github.com/dfm/emcee
[18] https://github.com/minaskar/pocomc

good mixing properties. The algorithm naturally accommodates different scales in different regions of the parameter space, though its efficiency can decrease in higher dimensions. A modern implementation combining slice sampling with an ensemble approach, with applications in cosmology and astronomy, is `zeus`[19] [1923]. Slice sampling has also been used to increase the efficiency and robustness of nested samplers (see below).

3.1.2. Hamiltonian Monte Carlo

Hamiltonian Monte Carlo (HMC), also known as *hybrid* Monte Carlo, is an MCMC approach that incorporates gradient information through an augmented parameter space with momentum variables. The system evolves according to Hamiltonian dynamics

$$\mathcal{H}(\boldsymbol{\theta}, \boldsymbol{p}) = -\ln \phi(\boldsymbol{\theta}) + \frac{1}{2}\boldsymbol{p}^T \boldsymbol{M}^{-1} \boldsymbol{p}\,, \tag{3.3}$$

where $\boldsymbol{M}$ is a mass matrix. In this approach, proposals for accepted/rejected new states are obtained by letting the current state evolve according to an energy-conserving trajectory for a set amount of time — in practice some number of steps of corresponding of small but finite duration. By following continuous trajectories determined by local dynamics, rather than diffusive random steps, HMC significantly reduces random-walk behavior, improving sampling efficiency for posterior with complicated geometries.

A key challenge in HMC is selecting an appropriate integration time for the dynamic evolution of the steps, i.e., the number and duration of finite steps. The No-U-Turn Sampler (NUTS) [1924] refines this approach by adaptively determining the trajectory length, ensuring efficient exploration without manual tuning. By dynamically terminating paths upon noticing signs of retracing, NUTS avoids redundant computations while preserving detailed balance, thus enhancing the efficiency, particularly in high-dimensional spaces.

In order to exploit the advantages of HMC, cosmological codes and likelihoods need to be able to compute derivatives with respect to input parameters and intermediate observables, respectively. The most common approach is to build these codes using *automatically-differentiable* numerical frameworks that are able to produce gradients for arbitrary inputs. The most capable and popular one at the time of writing this paper is the `Python` library `JAX` [1925]. There is a growing body of `JAX`-based cosmological and astronomical libraries (`JAX-COSMO`[20] [1926], `DISCO-DJ`[21] [1927]) and likelihoods (`candl`[22] [1928]), as well as machine-learning cosmological emulators (`CosmoPower-JAX`[23] [1929]). Another popular programming framework that allows for automatic-differentiation is `julia`,[24] that has been employed for example in `LimberJack.jl`[25] [1930], `Capse.jl`[26] [1931] and `Effort.jl`[27] [1932].

An implementation of NUTS that can be interfaced with `JAX`-based codes is `numpyro`[28] [1933]. Using `numpyro` and diverse `JAX`-based cosmological libraries and emulators, recent works [1934,1935] have reported efficiency gains of up to orders of magnitude, especially for parameter spaces of large dimensionality that are expected when performing inference on data from next-generation surveys.

3.1.3. Nested sampling

Nested sampling [1936] transforms the evidence calculation into a one-dimensional integral over prior mass X accumulated up to a given likelihood value

$$\mathcal{Z} = \int_0^1 \mathcal{L}(X)\,\mathrm{d}X \qquad \text{with} \qquad X(\lambda) = \int_{\mathcal{L}(\boldsymbol{\theta})>\lambda} \pi(\boldsymbol{\theta})\,\mathrm{d}\boldsymbol{\theta}\,, \tag{3.4}$$

where the likelihood is evaluated such that $\mathcal{L}(X(\lambda)) = \lambda$ for some likelihood-cutoff value λ. Numerically, this integral is computed as a weighted sum $\mathcal{Z} \sim \sum_{i=1}^{m} w_i L_i$, with $w_i \sim \Delta X$. The algorithm maintains a set of *live points* updated at every step: the one with the lowest likelihood is dropped (and referred to as a *dead* point), and a new one is sampled restricted to having a likelihood larger than that of the recently-dead point. The prior volume shrinkage ΔX is computed probabilistically and assigned the likelihood value of the dead point. In addition to the evidence calculation, the pool of dead points may be used to construct a fair sample from the posterior.

The procedure to sample a point from the prior subject to a minimum likelihood, i.e., within an *iso-likelihood* contour, is the main hurdle of the algorithm. Some implementations, such as `MultiNest`[29] [293], construct a minimal ellipsoid containing the set of live points, and sample uniformly from an enlarged version of it. `UltraNest`[30] [1937], implements a different sampling approach based on ellipsoids centered around the live points themselves, and includes more robust uncertainty estimation for the integrated evidence. Others, like `PolyChord`[31] [1938], propose new points by running a short affine-invariant MCMC chain (in particular using slice-sampling) from one of the current live points. MCMC-based approaches have better dimensionality scaling, but tend to be slower for simpler problems. Other modern implementations like `dynesty`[32] [1939] dynamically vary the number of live points to improve efficiency. All these approaches allow for efficient sampling of multi-modal distributions by using clustering algorithms to separate and evolve different subsets of live points in parallel.

In general, nested samplers are preferred when the geometry of the posterior distribution is complicated or exhibits multiple peaks. Due to its ability to compute the Bayesian evidence, nested sampling is also particularly valuable for model selection problems. Nested sampling can however be computationally very expensive for highly dimensional parameter spaces, but it parallelizes very efficiently up to the number of live points.

There have been in recent years various attempts at accelerating nested sampling using ML, focusing on efficiently sampling within iso-likelihood contours. `nautilus`[33] [1940] and `neuralike`[34] [1941] train a neural network on the spatial dependence of the likelihood in the vicinity of the current live set (only on the live set for `neuralike`) to construct an estimate of the iso-likelihood contour, and reject points predicted to be outside it before the true likelihood is evaluated. `nessai`[35] [1942] takes a similar approach, training a *normalizing flow* on the set of live points to find a transformation of the iso-likelihood contour into a much simpler hyper-sphere.

3.1.4. Practical considerations for choosing an MC sampler

The sampling methods discussed above differ in both their theoretical foundations and practical applications, each offering distinct advantages and limitations in cosmological parameter inference.

Traditional Metropolis–Hastings MCMC uses local random-walk proposals, leading to $O(\sqrt{d})$ scaling in dimensionality d. While simple and reliable, these proposals often require many likelihood evaluations, making them computationally expensive, especially for high-dimensional parameter spaces or when the likelihood poorly constrains

[19] https://github.com/minaskar/zeus
[20] https://github.com/DifferentiableUniverseInitiative/jax_cosmo
[21] https://github.com/ohahn/DISCO-EB
[22] https://github.com/Lbalkenhol/candl
[23] https://github.com/dpiras/cosmopower-jax
[24] https://github.com/JuliaLang/julia
[25] https://github.com/jaimerzp/LimberJack.jl
[26] https://github.com/CosmologicalEmulators/Capse.jl
[27] https://github.com/CosmologicalEmulators/Effort.jl
[28] https://github.com/pyro-ppl/numpyro
[29] https://github.com/farhanferoz/MultiNest
[30] https://github.com/JohannesBuchner/UltraNest
[31] https://github.com/PolyChord/PolyChordLite
[32] https://github.com/joshspeagle/dynesty
[33] https://github.com/johannesulf/nautilus
[34] https://github.com/igomezv/neuralike
[35] https://github.com/mj-will/nessai

the parameters. Non-Gaussian posteriors, particularly multi-modal distributions, can further challenge efficient parameter space exploration. A good dimensionality scaling can be retained for simple distributions using decorrelating affine-invariant transforms. For more complicated, highly non-Gaussian, and multi-modal distributions, ensemble and sequential MC approaches can help, especially when in combination with generalized decorrelating transforms such as NFs.

Slice sampling takes a geometric approach by sampling from level sets of the PDF, automatically adjusting to the local structure of the posterior. This self-adaptive behavior results in $O(d)$ scaling without requiring manual tuning, making it effective for problems with widely varying parameter scales, such as fitting galaxy LFs where parameters span multiple orders of magnitude. While computationally inexpensive in low dimensions, its efficiency can degrade in high-dimensional spaces.

HMC improves upon this by using gradient information to make physics-inspired proposals, achieving better $O(d^{1/4})$ scaling. This makes HMC particularly effective for problems with strong parameter correlations, such as hierarchical models in galaxy clustering. However, it requires differentiable likelihoods and careful tuning of integration parameters.

Nested sampling transforms the problem into a one-dimensional integration over nested likelihood contours. Despite its $O(d^3)$ scaling due to constrained sampling requirements when using simple acceptance/rejection sampling, it offers important advantages: direct computation of the evidence $\mathcal{Z}$ (essential for model comparison in DE studies) and natural handling of multi-modal distributions. This makes it particularly valuable in cosmology, GW physics, and gravitational lensing analyses. A better dimensionality scaling can be achieved by using slice-sampling for constrained sampling, or performing acceptance/rejection sampling on a surrogate model.

The choice of sampler often depends on specific requirements like parameter space dimensionality, likelihood characteristics, and the need for evidence calculations [1943–1946]. For problems in which the likelihood is extremely fast, $\mathcal{O}(< 10^{-2}\,\mathrm{s})$, and the dimensionality is of orders or a few 10 s, simple approaches should suffice, such as affine-invariant MCMC, or a non-boosted nested sampler if a model evidence estimate is needed. For harder problems (very high dimensionality, strong non-Gaussianity, multi-modality), the use of the more advanced methods discussed above, such as preconditioned Sequential Monte Carlo and ML-boosted nested samplers, can prove optimal. For extremely slow likelihoods, $\mathcal{O}(> 10\,\mathrm{s})$, the approaches discussed in Section 3.2 such as *surrogate posterior* methods or *simulation-based inference* may be the only viable option, at the cost of some statistical robustness.

An illustration of the problem of dimensionality and the complexity of the distribution can be seen Fig. 51. On it we show how the runtime and the accuracy scale with dimensions for a multi-dimensional Gaussian distribution and the Rosenbrock distribution. For the accuracy test, we use the Wasserstein distance metric [1947], which measures the true distributional similarity between sampler outputs and reference distributions. One can see that all samplers show excellent performance on Gaussian problems across dimensions, but exhibit a dramatic accuracy drop-off for Rosenbrock problems beyond 6–8 dimensions, reflecting the inherent challenge of sampling correctly from complex, highly correlated distributions in higher dimensions.

3.1.5. Cosmological inference frameworks

There exist a number of public codes facilitating the integration of MC samplers such as the ones mentioned above with cosmological inference pipelines: numerical codes to calculate cosmological observables (Boltzmann codes such as `CAMB` [1948], `CLASS` [1949], and `PyCosmo` [1950] and their extensions, as well as emulators) and experimental likelihoods for cosmological and astrophysical surveys and data.

The most used ones in the last years are `CosmoSIS`[36] [1951] `MontePython`[37] [1916,1917] and `Cobaya`[38] [1918] (which uses `GetDist`[39] [1952] for analyzing MC results). The choice for a particular one will be determined by the scientific problem at hand, since each provides a different combination of features and integrates different theoretical codes and experimental likelihoods.

Their use is thoroughly recommended since they facilitate not only the interfacing between the different parts of the inference pipeline, but also help in specifying the models and priors as well as the configuration of samplers and theoretical codes, and provide sane defaults for each. They usually either include in their source or automate the installation of cosmological codes and likelihoods, as well as MC samplers.

3.1.6. Modeling problems: Prior dependence and projection effects

Analyses of present-day data require a significant modeling effort in order to achieve accurate theoretical predictions that can be compared to data without biasing the results. This includes the modeling of complicated physics and systematic or non-linear effects, which require introducing additional parameters (nuisance parameters) that need to be kept free during the sampling of the corresponding posterior distribution. If the data is not sensitive to all parameters in such a high-dimensional spaces, this can lead to a flat likelihood surface $\mathcal{L}(D|\boldsymbol{\theta})$ in Eq. (3.1), which in turn can result in a sensitivity to the choice of prior $\pi(\boldsymbol{\theta})$. If the prior distribution is not informed by past experiments or theory, the dependence of the results on $\pi(\boldsymbol{\theta})$ may be unwanted and needs to be explored in a sensitivity analysis. A second — more subtle — dependence of the one-dimensional posteriors on the prior is introduced at marginalization. Since the marginalization procedure takes into account the posterior volume, for very flat or very non-Gaussian likelihood surfaces, there may be an (unwanted) up-weighting of regions with large (prior) volume. These so-called projection or prior volume effects can lead to shifts of the marginalized posterior away from the maximum-likelihood estimate or "best fit" point (see also Section 3.6), and may bias the constraints on the physics of the problem if the choice of prior was not sufficiently informed.

An example of this in the context of the σ_8 tension is the Effective Field Theory of Large Scale Structure (EFTofLSS) (e.g., see Refs. [1177, 1178,1953–1955]), a perturbation-theory based technique to describe the power spectrum of biased tracers up to mildly non-linear scales, that is applied to LSS measurements. In such an approach, several new parameters are introduced, as they enter the perturbative expansion of the galaxy density field. These parameters will be free parameters in the context of an MCMC analysis and, therefore, require a choice of prior. However, the arbitrary nature of the choice of such priors can become a problem for the analysis, since the inferred cosmological parameters can depend on the particular choice of prior. It has been shown how different prior choices, e.g., extending the range of allowed values to extreme intervals, can significantly affect the outcome of the analysis, with projection effects shifting some parameters, such as the primordial amplitude A_s and the amplitude of matter fluctuations, σ_8, with respect to their true values [1956,1957]. It was further demonstrated that different — albeit theoretically equivalent — choices of the EFT parameterization lead to discrepant inferred cosmological parameters [1957,1958]. Ref. [1959] confirms a significant impact of priors on the nuisance parameters on the inferred cosmological parameter using frequentist profile likelihoods. Approaches to choose well motivated priors on the EFT parameters include the use of a Jeffreys prior [719,1960] or simulation-inferred priors [1961–1963]. Such an effect hinders the robustness of the analysis results, as strong

[36] https://github.com/joezuntz/cosmosis?tab=readme-ov-file
[37] https://github.com/brinckmann/montepython_public
[38] https://github.com/CobayaSampler/cobaya
[39] https://github.com/cmbant/getdist

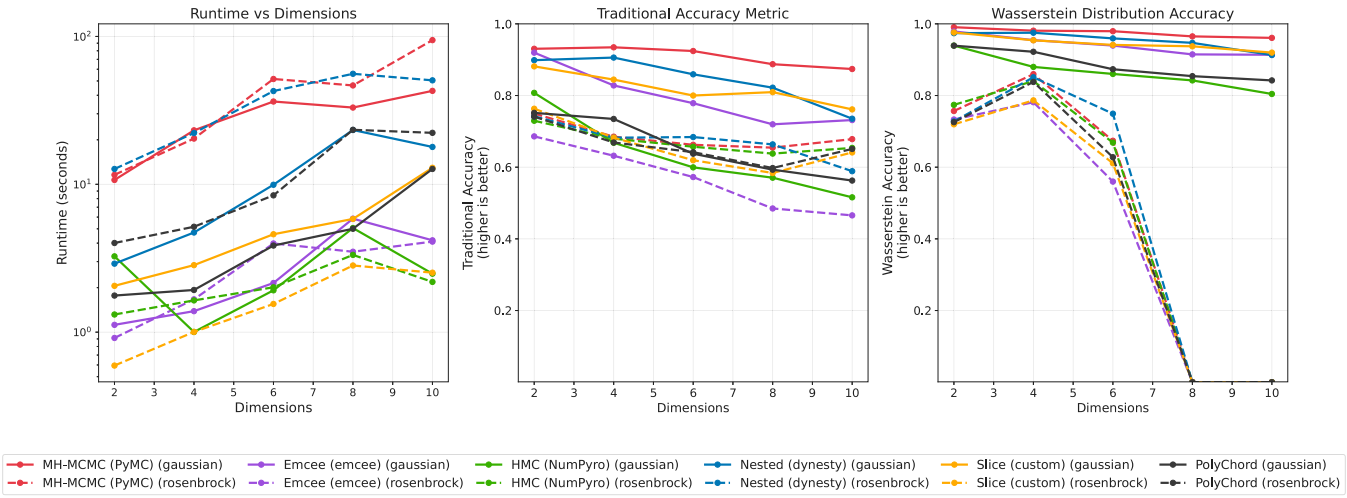

Fig. 51. Illustration of how different sampling methods scale with dimensionality and target distribution complexity. The left panel shows runtime scaling with increasing dimensions, while the middle and right panels display sampler accuracy using two different metrics. Results are shown for both a simple multivariate Gaussian distribution (solid lines) and the challenging banana-shaped Rosenbrock distribution (dashed lines). The traditional accuracy metric combines deviations from mean and function evaluation errors. The Wasserstein accuracy metric uses optimal transport theory to measure distributional similarity between samples and theoretical distributions.

assumptions, only partially motivated by theoretical considerations, need to be done on the choice of priors for the extra parameters.

A similar projection effect, shifting the values of parameters away from their true value, can be introduced also when considering priors on the baryon abundance $\Omega_{\rm b,0}\,h^2$. Several nuisance effects modeled in LSS observables require the value of this parameter, which is however not strongly constrained by LSS observations. For such a reason the choice of prior for the abundance of baryons can be significant for the analysis, as switching from a uniform prior to a Gaussian constrain as provided by BBN [798] can change the outcome in a significant way [1957].

In the context of the Hubble tension, an impact of prior effects on the inferred value of H_0 has been reported and explored for several extended models, for example: EDE (see Section 4.1.1) [1964–1970], NEDE (see Section 4.1.2) [1971,1972], number of relativistic species (see Section 4.1.3) [1973–1975], Brans–Dicke model (see Section 4.3.1) [1976] decaying DM (see Section 4.4.3) [1977] and more.

3.1.7. Model comparison criteria

The increasing complexity of cosmological models and datasets necessitates robust statistical frameworks for model comparison and consistency checks. Information criteria and Bayesian methods provide quantitative tools for selecting between competing models while accounting for model complexity and data support.

There exist several information criteria that can be used to compare models [1978]. Common criteria that balance goodness-of-fit of a model against its complexity are the Akaike Information Criterion (AIC) and the Bayesian Information Criterion

$$\mathrm{AIC} = -2\ln(\mathcal{L}_{\rm max}) + 2k\,, \qquad \mathrm{BIC} = -2\ln(\mathcal{L}_{\rm max}) + k\ln(N)\,, \tag{3.5}$$

where $\mathcal{L}_{\rm max}$ is the maximum likelihood, k is the number of free parameters, and N is the effective number of data points on which the likelihood is defined. When comparing a *test* model versus a *baseline* one (e.g., ΛCDM) using ICs (AIC and BIC), we compute the difference in criterion values as

$$\Delta\mathrm{IC}_{\rm test} = \mathrm{IC}_{\rm baseline} - \mathrm{IC}_{\rm test}\,.$$

The model with the *lowest IC* is preferred [1979], meaning, in this sign convention, $\Delta\mathrm{IC} > 0$ favors the test model, while $\Delta\mathrm{IC} < 0$ favors the baseline model. The value of $|\Delta\mathrm{IC}|$ indicates the strength of the preference: $|\Delta\mathrm{IC}| \geq 2$ (weak), $|\Delta\mathrm{IC}| \geq 6$ (medium), $|\Delta\mathrm{IC}| \geq 10$ (strong).

The Deviance Information Criterion (DIC) extends AIC to hierarchical models by accounting for parameter uncertainty:

$$\mathrm{DIC} = -2\ln(\mathcal{L}(\hat{\theta})) + 2p_D\,, \qquad \text{with} \qquad p_D = 2\left[\ln(\mathcal{L}(\hat{\theta})) - \langle\ln(\mathcal{L}(\theta))\rangle\right]\,, \tag{3.6}$$

where $\hat{\theta}$ is the posterior mean of the free parameters, p_D the effective number of them, and $\langle\ln(\mathcal{L}(\theta))\rangle$ the mean log-likelihood over the posterior samples. Unlike AIC and BIC, DIC uses the entire posterior distribution rather than just the maximum likelihood estimate, making it particularly suitable for Bayesian hierarchical models where the effective number of parameters may be less than the actual number due to prior constraints [1980].

The Bayes Factor (BF) provides a fully Bayesian approach to model comparison

$$\mathrm{BF}_{12} = \frac{\mathcal{Z}_1}{\mathcal{Z}_2} = \frac{\int \mathcal{L}_1(\theta_1)\pi_1(\theta_1)\,\mathrm{d}\theta_1}{\int \mathcal{L}_2(\theta_2)\pi_2(\theta_2)\,\mathrm{d}\theta_2}\,. \tag{3.7}$$

Jeffreys' scale is commonly used to interpret $\ln(\mathrm{BF}_{12})$ values: 0–1 indicates inconclusive evidence, 1–3 suggests positive evidence, 3–5 shows strong evidence, and values larger than 5 represent very strong evidence in favor of model 1 [1979,1981]. While AIC and BIC are easily computed from MCMC chains, Bayes factors require accurate evidence estimation, typically obtained through nested sampling or thermodynamic integration methods. As a fully Bayesian approach, the value of the Bayes Factor depends strongly on the choice of prior density, unlike for information criteria, so a prior sensitivity analysis is advisable.

3.1.8. Tension metrics

Tension metrics are statistical tools that are used to quantify the agreement (or lack thereof) between the estimation of cosmological parameters obtained with different data sets, beyond the widely applied *"rule of thumb"*. According to this rule the distance between two posterior 1-d distributions can be quantified in 1-dimensional standard deviations by $N_\sigma = (\mu_{\rm A} - \mu_{\rm B})/\sqrt{\sigma_{\rm A}^2 + \sigma_{\rm B}^2}$ where $\mu_{\rm A/B}$ and $\sigma_{\rm A/B}$ refer to the means and variances obtained with each data set. Most studied tension metrics can be grouped into two families: (i) those based on Bayesian evidence [1982,1983] and (ii) those based on the posterior distribution [1984–1986]. While group (i) answers the question about what hypothesis is preferred by the data under the assumed model, group (ii) intends to establish the statistical significance between the posteriors of data sets A and B within the parameter space of both

experiments. For each metric, an estimator is computed and a corresponding probability P is defined that quantifies the agreement or disagreement between data sets in terms of its corresponding equivalent 1-dimensional N_σ defined as: $P = \mathrm{Erf}(N_\sigma/\sqrt{2})$. In most cases the probability P is related to the *probability-to-exceed* (PTE) of an estimator Q that follows a χ^2_d distribution, defined as

$$\mathrm{PTE} = \int_Q^\infty \chi^2_d(x)\,\mathrm{d}x\,. \tag{3.8}$$

(i) Metrics defined on Bayesian evidence ($\mathcal{Z}$). The Bayesian ratio statistic R corresponding to two datasets A and B, and the combination AB of both of them, can be written as [1982]

$$R = \frac{\mathcal{Z}_{\rm AB}}{\mathcal{Z}_{\rm A}\mathcal{Z}_{\rm B}}\,. \tag{3.9}$$

$R \gg 1$ is interpreted as both datasets being consistent, while $R \ll 1$ means that the datasets are inconsistent. However, it has been shown that the R estimator depends on the choice of the prior and can therefore underestimate inconsistencies. This estimator has two primary contributions, one from the unlikeliness of two datasets being in agreement, the *information ratio* I, and another from their disagreement, the *suspiciousness* S [1983]

$$\ln I = \mathcal{D}_{\rm A} + \mathcal{D}_{\rm B} - \mathcal{D}_{\rm AB}\,, \qquad \ln S = \ln R - \ln I\,. \tag{3.10}$$

Here $\mathcal{D}$ refers to the Kullback–Leibler divergence between prior and posterior, quantifying the information gain/compression produced by the given data set. The suspiciousness estimator S remains unaltered under a change of the prior widths as long as this change does not significantly alter the posterior. In addition, if the posterior is a d-dimensional Gaussian, the quantity $d - 2\ln S$ follows a χ^2_d distribution. Under that approximation, the probability of two datasets being discordant by chance can be computed as the PTE of $d - 2\ln S$.

(ii) Metrics based on the posterior distribution. First, we discuss some metrics based on quadratic estimators that require Gaussian posteriors. For these, the probability P of the data sets agreeing is defined as P = 1 − PTE where PTE is the probability-to-exceed defined above. Let us call $\hat{\theta}_{\rm A}$ the mean of the parameters inferred with dataset A and $\hat{\theta}_{\rm B}$ the one obtained with dataset B, while $\hat{\Sigma}_{\rm A}$ and $\hat{\Sigma}_{\rm B}$ refer to their respective covariance matrices. The method called *parameter differences in standard form* relies on the quadratic estimator [1984]

$$Q_{\rm DM} = (\hat{\theta}_{\rm B} - \hat{\theta}_{\rm A})^T(\hat{\Sigma}_{\rm B} + \hat{\Sigma}_{\rm A})^{-1}(\hat{\theta}_{\rm B} - \hat{\theta}_{\rm A})\,, \tag{3.11}$$

This estimator follows a χ^2_ν distribution with $\nu = \mathrm{Rank}[\hat{\Sigma}_{\rm B} + \hat{\Sigma}_{\rm A}]$ and can be regarded as a generalization of the *rule of thumb*. The method called *parameter differences in updated form* measures how one data set updates the other and is based on [1984]

$$Q_{\rm UDM} = (\hat{\theta}_{\rm AB} - \hat{\theta}_{\rm A})^T(\hat{\Sigma}_{\rm AB} - \hat{\Sigma}_{\rm A})^{-1}(\hat{\theta}_{\rm AB} - \hat{\theta}_{\rm A})\,, \tag{3.12}$$

Here $\hat{\theta}_{\rm AB}$ are the inferred parameters obtained with the joint datasets A and B, while $\hat{\Sigma}_{\rm AB}$ is the respective covariance matrix. This estimator follows a χ^2_ν distribution with $\nu = rank[(\hat{\Sigma}_{\rm AB} - \hat{\Sigma}_{\rm A})]$ degrees of freedom. Next, we describe the *Goodness-of-fit loss* which evaluates the likelihood function at the maximum of the posterior of the joint distribution and of each distribution separately [1984]

$$Q_{\rm DMAP} = 2\ln\mathcal{L}_{\rm A}(\theta_{p,\rm A}) + 2\ln\mathcal{L}_B(\theta_{p,\rm B}) - 2\ln\mathcal{L}_{\rm AB}(\theta_{p,\rm AB})\,, \tag{3.13}$$

Here $\theta_{p,\rm A/B}$ are the Maximum a posteriori (MAP) parameters considering the dataset A/B. The estimator $Q_{\rm DMAP}$ follows a χ^2 distribution with $\Delta\nu = \nu^{\rm A} + \nu^{\rm B} - \nu^{\rm AB}$ degrees of freedom, where for a given data set/combination $\nu = N - \mathrm{tr}[\boldsymbol{\Sigma}_\pi^{-1}\boldsymbol{\Sigma}_p]$, with N being the effective number of data points defining the likelihood, and $\boldsymbol{\Sigma}_\pi$, $\boldsymbol{\Sigma}_p$ the covariance matrices of the prior and the posterior, respectively. This metric is effective at evaluating how well the theoretical prediction fits the data, but does not evaluate directly the disagreement between inferred parameters.

The next method, called *exact parameter shift* (EPS) does not require Gaussian posteriors and is based on the parameter difference probability [1984,1986]

$$P(\Delta\theta) = \int P_{\rm A}(\theta)P_{\rm B}(\theta - \Delta\theta)\,\mathrm{d}\theta\,, \tag{3.14}$$

where $\Delta\theta = \hat{\theta}_{\rm A} - \hat{\theta}_{\rm B}$ is the difference between the means of the posterior parameters that correspond to datasets A/B. The probability to identify the tension is calculated by summing over all the values of $P(\Delta\theta)$ over the iso-contour corresponding to no difference $\Delta\theta = 0$

$$\Delta = \int_{P(\Delta\theta)>P(\mathbf{0})} P(\Delta\theta)\,\mathrm{d}\Delta\theta\,. \tag{3.15}$$

Usually, this integral is computed numerically from the posterior samples. In cases of strong disagreement, this estimator may be difficult to compute.[42]

Many authors use the tools presented here to discuss tensions in the inferred value of cosmological parameters with recent data sets [699, 1987,1988]. It has been discussed [1987] that the different metrics answer different questions. For example, $Q_{\rm UDM}$ quantifies how a given data set updates the values of the inferred parameters of another data set, while $Q_{\rm DMAP}$ quantifies the difference of the goodness of fit between the individual and joint data sets to the underlying theoretical model. On the other hand, to quantify the tension between the value of inferred parameters, the appropriate metrics are $Q_{\rm DM}$ and EPS, emphasizing that the former requires posteriors to be sufficiently Gaussian, while the latter does not. Fig. 52 shows two examples of 2-d contours and posteriors that correspond to different data sets and the corresponding N_σ obtained with each metric, together with the ones computed with the 1-d *rule of thumb* for each parameter. If EPS can be computed, usually the equivalent N_σ that corresponds to DM and EPS indicate similar values, while there is a difference with the ones obtained using the *rule of thumb* [1987]. Note that the *rule of thumb* only quantifies the tension in a given parameter, while the metrics presented above quantify the disagreement in the whole parameter space.

3.2. Machine learning based inference techniques

Coordinator: Jurgen Mifsud

Contributors: Alba Domi, Anto Idicherian Lonappan, Benjamin L'Huillier, Celia Escamilla-Rivera, Clecio Roque De bom, Daniela Grandón, Daria Dobrycheva, David Valls-Gabaud, Denitsa Staicova, Elena Giusarma, Filippo Bouchè, Germano Nardini, Ippocratis Saltas, Iryna Vavilova, J Alberto Vazquez, Jacobo Asorey, Jenny G. Sorce, Judit Prat, Konstantinos Dialektopoulos, Leandros Perivolaropoulos, Luca Izzo, Luis A. Escamilla, Matteo Martinelli, Purba Mukherjee, Rahul Shah, and Ruth Lazkoz

In traditional approaches, analytical likelihood functions are employed to characterize the PDFs of observed data, enabling parameter estimation through posterior inference. However, certain datasets exhibit errors that cannot be adequately described by simple analytical distributions, such as multivariate Gaussian distributions. Consequently, the true likelihood in such cases is often complex and lacks an explicit analytical form, making traditional parameter inference methods challenging to implement. To address this issue, various likelihood-free techniques have been developed to circumvent the direct computation of likelihood functions.

[41] Reprinted from Physics Letters B, Volume 855, id.138844 Leizerovich, M., Landau, S.J., Scóccola, C.G. Tensions in cosmology: A discussion of statistical tools to determine inconsistencies Copyright (2024), with permission from Elsevier.

[42] We point out that in the case of strong disagreement, care must be taken with the sampling of the tails of the distributions.

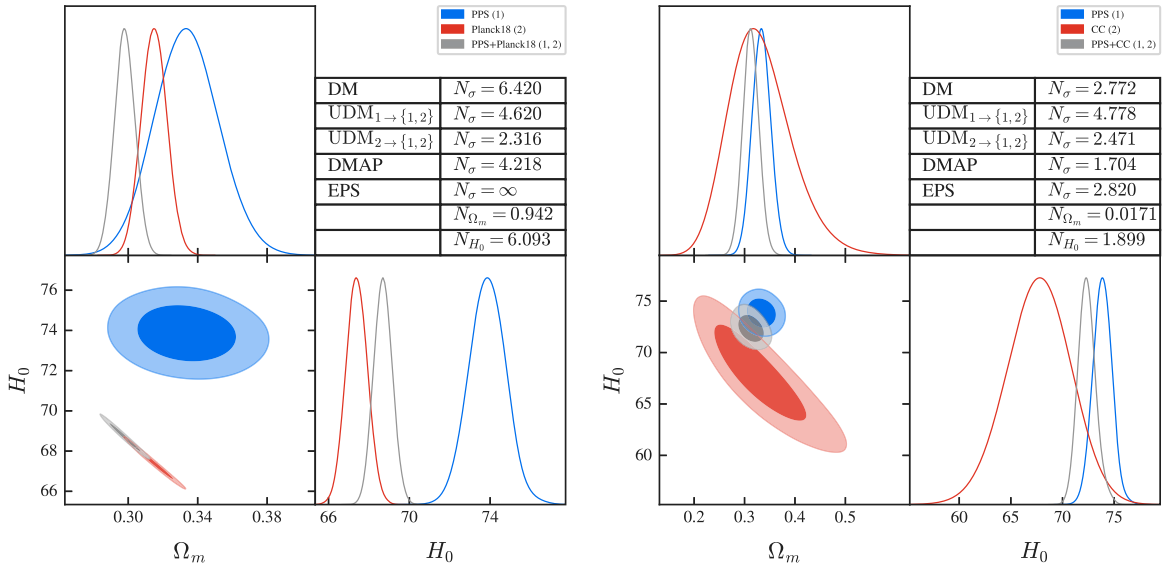

Fig. 52. Tensions metrics applied to **(a)** Planck 2018 vs Pantheon Plus + SH0ES (PPS), **(b)** CC vs Pantheon Plus + SH0ES. In all cases, blue contours correspond to PPS and gray contours to the joint analysis. N_σ refers to the 1-d standard deviations that correspond to a 1-d PDF associated with each metric estimator that quantifies the disagreement between different data sets (see the beginning of this subsection). Q_{UDM} quantifies how the parameters inferred from one dataset are updated when another is incorporated into the analysis. Q_{DMAP} is related to the difference in goodness of fit to the different data of the underlying model. Q_{DM} and EPS quantify the difference in the value of the inferred parameters. N_{Ω_m} and N_{H_0} quantify the tension in each inferred parameter applying the 1-d rule of thumb.[41].
Source: Adapted from Ref. [1987].

In standard Bayesian inference, posterior distributions are typically explored using methods such as MCMC sampling, variational inference, or other Bayesian computational techniques. These conventional approaches generally rely on evaluating the likelihood function for the models and parameters under consideration. However, for highly complex and computationally intensive models, the likelihood function may become intractable, and simulations can demand significant time and resources, rendering parameter inference impractical. Therefore, parameter estimation techniques that mitigate or overcome these challenges are highly beneficial, particularly in cosmological studies. Likelihood-free inference has emerged as a promising paradigm for Bayesian inference in scenarios involving complex generative models, leveraging only forward simulations to perform analysis.

With the current generation of large-scale structure observational programs, such as the European Space Agency's Euclid mission [437] and LSST [897], sub-percent-level precision measurements are anticipated. The upcoming decade is thus expected to witness an unprecedented increase in the quantity, diversity, and quality of multi-wavelength astronomical observations of the large-scale structure. This surge in data will necessitate the development of highly sophisticated computational tools. At this stage, the limitations may shift from data quality or availability to the capabilities of statistical and data-driven methodologies. ML techniques have demonstrated substantial potential in addressing the computational challenges associated with traditional statistical methods, positioning them as valuable tools for advancing cosmological analyses.

For instance, current ML techniques were adopted to the scatter in cluster mass estimates [1989] and to distinguish between standard and MG theories from statistically similar WL maps [1990]. Such techniques have also been found to be useful for the next generation CMB experiments [1991], N-body simulations [1992], cosmological parameters inference [1993], DE model comparison [1994], supernova classification [1995] and strong lensing probes [1996].

Cosmology is experiencing an unprecedented growth in the volume and complexity of astronomical datasets, driven by large-scale surveys like Euclid, LSST, and DESI. These datasets are used to construct data vectors for cosmological parameter inference, with which we can shed light on current parameter tensions within ΛCDM. To fully leverage the wealth of cosmological information encoded in these datasets, ML methods have emerged as a powerful tool.

In this section, we will discuss a number of ML based inference techniques, with an emphasis on those techniques which were adapted to address cosmological tensions. Neural networks are becoming ever more widely employed in physics, including in the field of cosmology. We refer the interested reader to a review of the core concepts surrounding the use of neural networks in Refs. [1997,1998]. In this section we discuss the cosmological applications of artificial neural networks (Section 3.2.1), convolutional neural networks (Section 3.2.2), Bayesian neural networks (Section 3.2.3), and deep learning (Section 3.2.4).

3.2.1. *Artificial neural networks*

The method by which ANN architectures [1661] are used to learn to mimic the iterative process by which an MCMC analysis takes place is described in this section together with some details of the adopted methodology to optimize the ANN structure for comparative analyses. ANNs are non-parametric techniques in the sense that they do not contain the cosmological parameters themselves, unlike the likelihood functions. This may extend cosmological analyses to otherwise overly complex systems, or reduce the computational requirements of regular cosmological model analyses making the approach more accessible. Inspired by biological neural networks, an ANN is a setup composed of a collection of neurons that are organized into layers [1999–2001]. This family of algorithms offers a powerful base on which to apply complex numerical tasks. ANNs are optimized to work in computer systems with a large number of threads which has become a feasible prospect in recent years with the development of very powerful graphical processing units (GPUs), thus making the process of training ANNs competitive with traditional techniques. In recent years, ANNs have become very useful in meeting the accuracy and computational efficiency required for analyses in cosmology. ANNs are constructed with input and output layers to represent the MCMC parameter set that is being sampled and output likelihood respectively. These layers are connected to a series of internal, or hidden, layers that are structured in a way to optimize

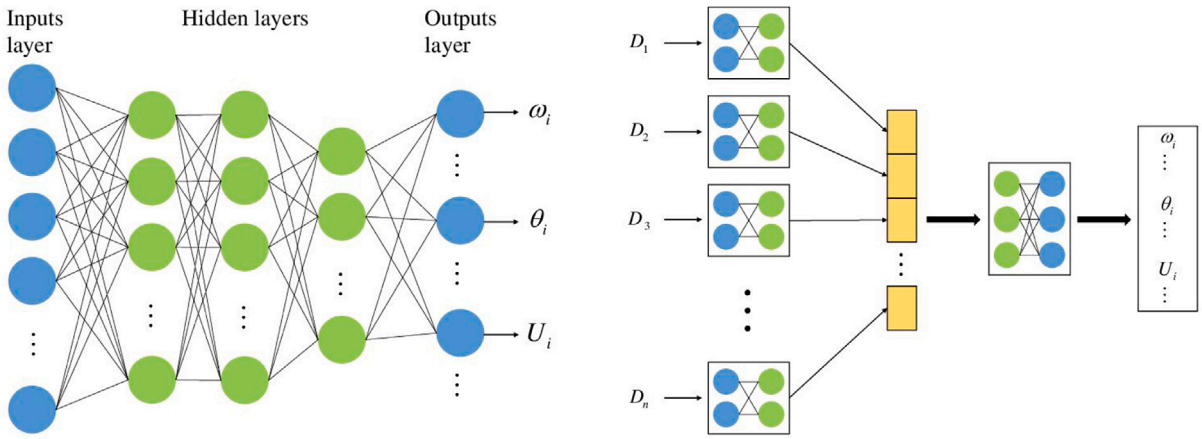

Fig. 53. The network structure used for parameter estimation in Ref. [2002]. The structure of the left panel is for one dataset, while the multi-branch network of the right panel is for multiple datasets $\{D_1, D_2, D_3, \ldots, D_n\}$ that are from different experiments.

how closely the ANN can imitate the MCMC iterations. Each layer in this network is composed of neurons, each of which is connected to the neurons of the layers preceding and after it, as illustrated in the left panel of Fig. 53 for a single data set.

For the task of inferring cosmological parameter constraints, the observational data is fed to the input layer, then the information of observational data passes through each hidden layer, and finally the cosmological parameters are outputted from the output layer. Specifically, each layer accepts a vector, the elements of which are called neurons, from the former layer as input, then applies a linear transformation and a nonlinear activation on the input, and finally propagates the current result to the next layer.

ANNs have been widely implemented as emulators of cosmological observables, such as the lensing power spectrum [2003,2004], CMB source functions [2005,2006], the CMB temperature anisotropies power spectrum and the matter power spectrum [2004,2007]. The main purpose of these applications is to accelerate the statistical analysis, when expensive Boltzmann codes and big volumes of data prevent us from efficiently sampling the posterior distributions. In particular, CosmicNet I aims to remove bottlenecks from Einstein–Boltzmann solvers (such as CLASS or CAMB) by training neural network emulators that learn the mapping from four ΛCDM parameters to source functions of CMB anisotropies. The resulting trained ANN model is then injected into the CLASS code for public use. This work was later extended to include extensions of a flat ΛCDM, such as DDE, spatial curvature. Emulators are crucial for summary statistics of cosmological probes that lack an analytical prescription that models their dependence on cosmology and other parameters. This is the case of higher-order statistics of cosmic fields, such as the peak counts (a distribution of local maxima in a field) and the one-point PDF. As emulators are only approximations of the target observables, recent works have explored how to propagate the uncertainty derived from such approximation, in order to safeguard parameter inference against biases [2008].

In recent years, likelihood-free analyses relied on ensembles of neural networks as density estimators of the sampling distribution of the data. In Refs. [2002,2009], a cosmological likelihood-free inference technique has been developed. The left panel of Fig. 54 depicts the schematic diagram of the likelihood-free architecture adopted in Ref. [2002] containing the main processes of training and parameter estimation. First, a class object for the cosmological model that contains the simulation method of the measurements is developed, where the simulation method here is used to generate the training set. Then, the initial parameters are set without any constraints in their selection. Subsequently, the training set will be simulated automatically, where two sampling methods can be considered to generate cosmological parameters: sampling uniformly in a hypercube or a hyper-ellipsoid. It should be noted that the posterior distribution is unknown before the first estimation using the ANN model. Thus, the cosmological parameters here cannot be generated in a hyper-ellipsoid. Therefore, the cosmological parameters are uniformly generated in a hypercube using the set of initial parameters. Consequently, an ANN model will be constructed automatically based on the respective training set. At the same time, the training set is then preprocessed before training the network, while noise will be automatically generated based on the observation errors and added to the training set. The training set will then be normalized, and the training set will be fed to the ANN model, consisting of thousands of epochs.

Cosmological parameters are then estimated using the well-trained ANN model. In simple terms, the ANN model actually learns a mapping between the data space of the measurements and the parameter space of cosmological parameters, as depicted in the right panel of Fig. 54 via a mapping between the data space of measurements and the cosmological parameter space. Therefore, in order to infer the respective posterior distribution, the corresponding distribution of the measurements is fed to the ANN model. Indeed, a large number of data-like samples of the measurements using the observational data are generated and fed to the ANN model to obtain the corresponding ANN chain, similar to the concept of an MCMC chain.

The ANN method in Refs. [2002,2009] was shown to be very successful in estimating cosmological parameters with one data set, which was then extended to multiple data sets by utilizing a multi-branch network The latter multi-branch network is illustrated in the right panel of Fig. 53, in which it was successfully tested with CMB, SNIa, and BAO datasets in Refs. [2002,2009], as illustrated in the derived results of Fig. 55 with the Planck 2015 data set. Thus, the ANN method was shown to be capable of estimating parameters using data sets of multiple experiments and is a direct competitor of the customary MCMC technique.

3.2.2. *Convolutional neural networks*

With the advent of precision cosmology, we are reaching an era in which it is extremely important to avoid any potential biases in the cosmological analysis when extracting cosmological parameters. For example, most of the time large-scale structure analyses are done using summary statistical observables like 2-point correlation functions, after assuming a cosmology to go from angular coordinates to Cartesian ones. This type of analysis can bias the cosmological parameters and a tomographic analysis can avoid this [2010].

One alternative to the use of summary statistics is the use of CNN architectures. They can be used to make direct inferences on cosmological parameters from astrophysical images. For instance, Ref. [2011] used CNNs to constrain axions as DM from 21 cm line intensity mapping

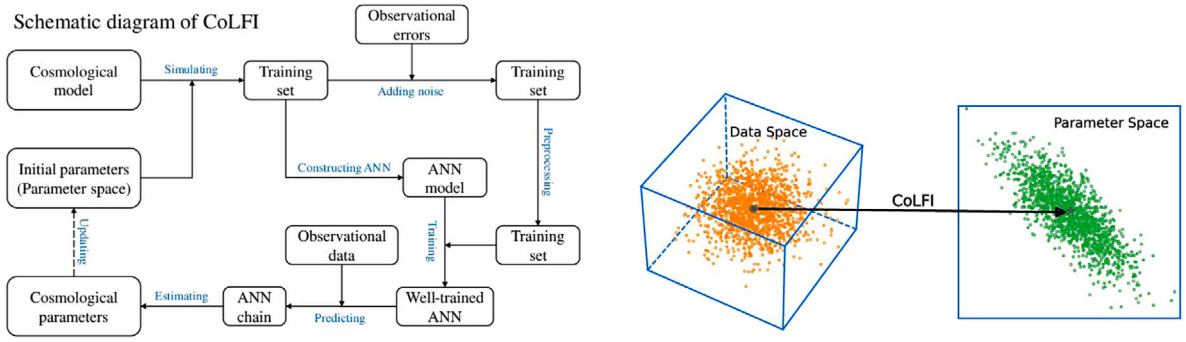

Fig. 54. The left panel depicts the schematic diagram of the likelihood-free architecture adopted in Ref. [2002]. In the right panel, a visualization of a mapping between the data space of measurements and the cosmological parameter space is illustrated.

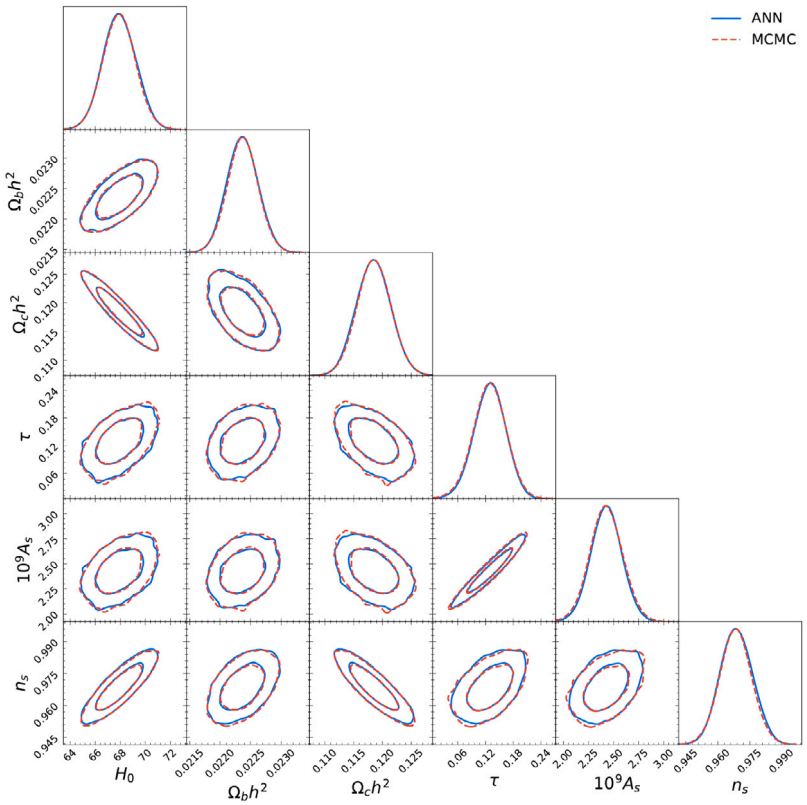

Fig. 55. One-dimensional and two-dimensional marginalized distributions [2002] constrained from Planck 2015 power spectrum. The blue solid lines are the results of the ANN method, the red dashed lines represent those of the MCMC method, and the gray circles are the fiducial values of the cosmological parameters.

probes. In Fig. 56 we show a schematic of the adopted CNN model architecture. It took as input a $64 \times 64 \times 128$ lightcone data cube where each voxel has dimension 4.68 cMpc×4.68 cMpc×1.48 Mhz (cMpc means co-moving Mpc).

If DM were described by axion-like particles (ALPs), the small scale structure would change the value of $\Omega_{m,0}$ leading to a change in H_0 and σ_8, potentially solving the potential tensions. To make a direct inference from CNNs, we need a training set of simulations of the given astrophysical image for different sets of parameters (e.g., axion mass or H_0). The input layer is basically the simulation with the angular maps and the frequency maps while the final output layer is the vector with the cosmological parameters inferred (in this case, the axion mass). The input layer is filtered and pooled down before being inputted as a vector to the connected neural network layers. The data is passed through the network a number of epochs updating the corresponding weights each time.

The inferred results, as depicted in Fig. 57, show that the CNN successfully recovered the true values of the axion mass in the testing data with a precision of $\sim$ 20% across a broad range of masses. To evaluate the uncertainty in the recovered values, 100 additional independent simulations were generated for both an axion model and a standard CDM model. For an axion mass of $M_X = 10^{-21}$ eV, a mass uncertainty of $^{+5.94}_{-4.80} \times 10^{-21}$ eV was inferred. It was further concluded that this method could potentially enable the detection of axion DM using SKAO1-Low with 68% confidence if the axion mass is $M_X < 1.86 \times 10^{-20}$ eV. However, these findings depend on the Planck 2015 cosmological parameters and the specific design parameters of future SKAO1-Low configurations.

A CNN was also adopted to perform the typically computationally expensive task of estimating the parameters of GW events. The considered CNN in Ref. [2012] is able to produce posterior distributions that in all cases are compatible with the already published results. The schematic of the respective CNN is depicted in Fig. 58, whereas

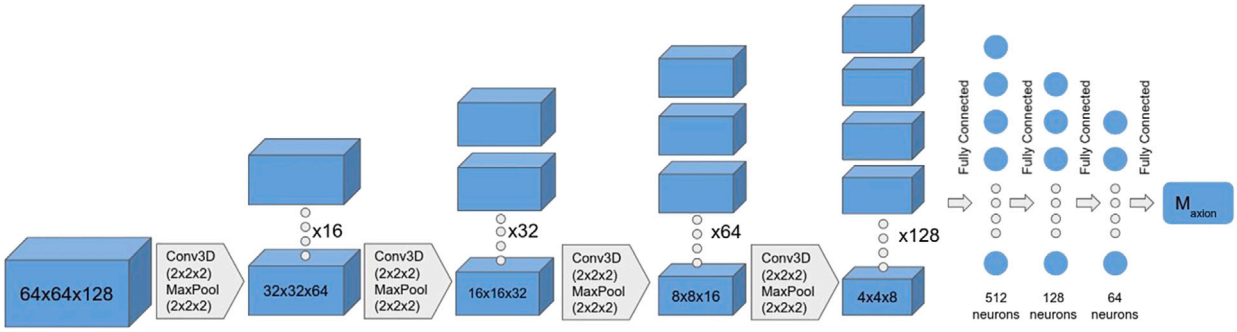

Fig. 56. The architecture of the CNN adopted in Ref. [2011], with input data cube of 64 × 64 × 128 voxels where each voxel has dimension 4.68 cMpc × 4.68 cMpc × 1.48 Mhz (cMpc means co-moving Mpc).

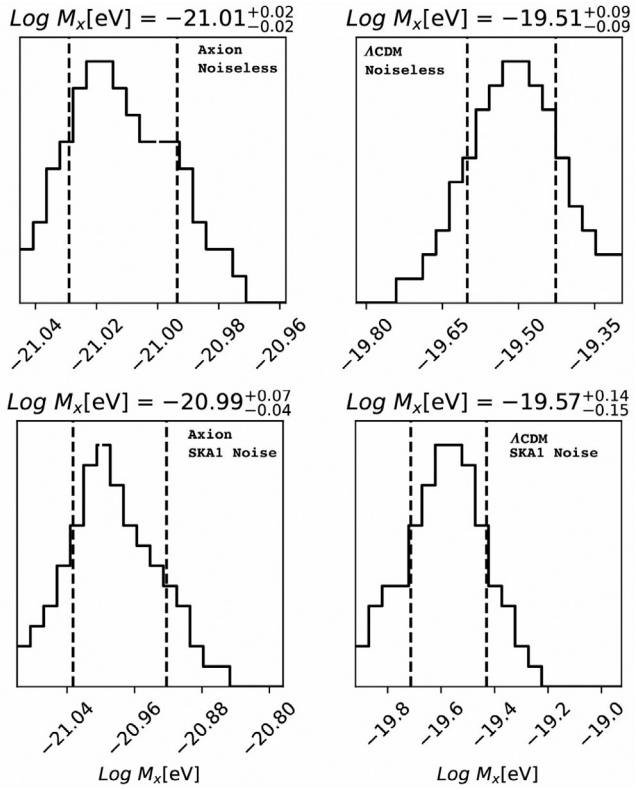

Fig. 57. The distribution of the CNN inferred predictions [2011] on 100 noiseless simulations fixed axion mass of 10^{-21} eV, along with the vertical dashed lines showing the 1-σ (68%) credible interval. We should remark that the CNN could predict the axion mass because the CNN is trained only with the data including axions.

the inferred results for the event GW200224_222234 are illustrated in Fig. 59. In the case of event GW200224_222234, all the estimated parameters were found to be in accordance with those published in the GWTC-3 catalog. Having said that, the effective spin was the worst performing parameter. Furthermore, the uncertainty yielded by the CNN on the sky position was found to be too large to accurately pinpoint the event, but it still is unbiased and is expected to produce a first alert for the instruments that look for electromagnetic counterparts to start pointing their instruments to a given patch in the sky. The latter would be more feasible with the upcoming more accurate pipelines which are expected to improve the precision of the sky localization. Overall, the GW event results indicate a good response from CNNs. One of the most important advantages is its computational efficiency, in which the CNN model could provide several posterior samples in a fraction of the time required by Bayesian inference methods, thus facilitating multi-messenger astronomy.

3.2.3. Bayesian neural networks

A BNN that outputs Gaussian PDFs was adopted in Ref. [2013]. The BNN has five input nodes for the five-band *grizy* photometry. A parameter grid search was performed in order to optimize for free parameters, including the number of epochs, number of layers, number of nodes per layer, learning rate, loss function, activation function, and optimizer. The BNN has a final output node that produces a mean and standard deviation assuming a Gaussian distribution for each photo-z prediction.

A key attribute of the BNN model is the production of photo-z uncertainties, which are needed for using photo-z results in cosmological analyses. It was also found that the BNN produces accurate uncertainties. In Ref. [2013], the HSC Public Data Release 2 [2014], which is designed to reach similar depths as LSST but over a smaller portion of the sky was adopted for the BNN. In total, the data consists of 286,401 galaxies with broadband grizy photometry and known spectroscopic redshifts. The considered galaxy sample covers a redshift of $0.01 < z < 4$, however the majority of the sample lies between $0.01 < z < 2.5$. In the BNN analysis of Ref. [2013], 80% of the galaxies were used for training, 10% for validation, and 10% for testing. The performance of the BNN technique is clearly illustrated in Fig. 60, in which the BNN was reported to have superior photo-z estimations with respect to other competing models.

The capability of BNNs was confronted in Refs. [2015,2016] on different avenues. The first is how effective BNNs can be in recognizing the distinct features in the power spectrum for a particular modification to the concordance model of cosmology, such as $f(R)$ or Dvali–Gabadadze–Porrati (DGP) [2017]. The second avenue that was exploited in Refs. [2015,2016] is their ability to detect a deviation from ΛCDM in the power spectrum irrespective of the particular modification. Two BNNs with the same architecture were trained in Refs. [2015,2016], the first for five labels divided between ΛCDM and the considered four extensions, whilst the second trained to distinguish between the two labels of ΛCDM and non-ΛCDM. Due to the fact that only four redshift bins were considered in these works, it was beneficial to treat the data as four separate time series and use one-dimensional convolutional layers.

The architecture of the network used to train both the five-label and two-label networks is depicted in the left panel of Fig. 61. Initially, the adopted structure consisted of three 1D convolutional flip out layers with 8, 16 and 32 filters, kernel sizes of 10, 5, and 2 with strides of 2, 2, and 1, respectively. Each of the first two 1D convolutional layers was followed by a max pooling layer with a pool size of 2 and a pooling stride of 2 for the first max pooling layer and a pooling stride of 1 for the second max pooling layer. After both of these max pooling layers there is a batch normalization layer. Following the final convolutional layer there is a global average pooling layer to reduce the filter size to

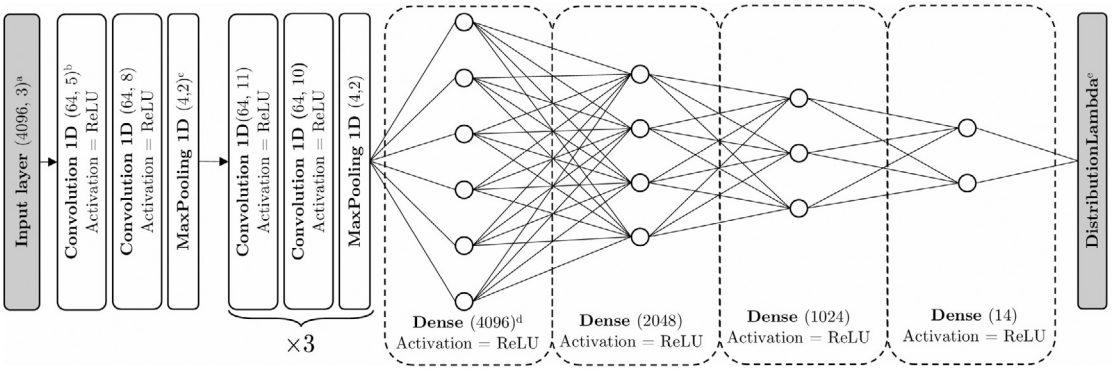

Fig. 58. Architecture of the CNN used in Ref. [2012]. The first set of layers are 1-dimensional convolutions and 1-dimensional maxpooling ones, followed by a set of fully connected dense layers. Between each of the dense layers, a dropout of 20% is applied to prevent overfitting during the training stage.

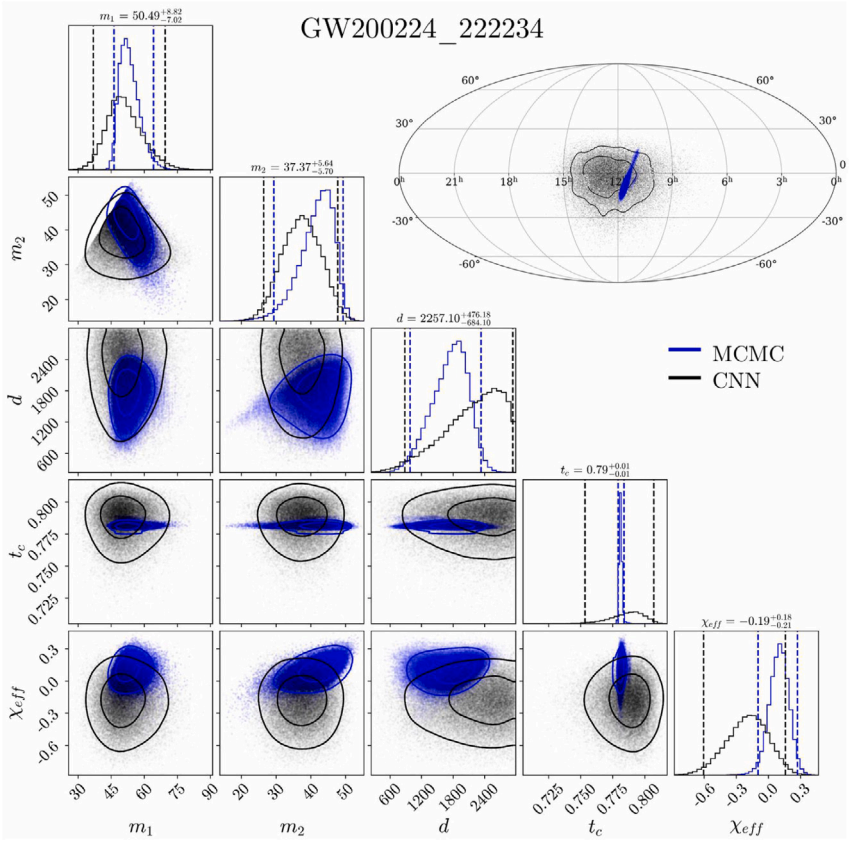

Fig. 59. Full posterior distribution inferred [2012] from the CNN and MCMC approaches for the GW200224_222234 event.

one in order to pass it to a dense layer with 32 nodes. Finally, after a further batch normalization there is a softmax layer consisting of five or two neurons for either the five- or two-label networks, respectively.

It was found that a five-label network trained to classify between ΛCDM, $f(R)$ gravity, DGP gravity, wCDM and a "random" class provided more reliable predictions than a two-label network trained to distinguish simply between ΛCDM and non-ΛCDM. While generally being less sensitive to variations in the noise distribution, it can also determine whether a power spectrum does not belong to any class included in the training set. Since the selection of the correct model is crucial when performing conventional statistical analyses such as with MCMCs, this ability could prove beneficial in indicating prospective models to consider. However, the network used in this work is currently limited to classification tasks while the notion of model selection on firm statistical grounds in the context of BNNs remains an open problem.

It could be concluded that BNNs may provide a powerful new means to search for hints of new physics in cosmological datasets. In particular, it is anticipated that they will serve as a powerful "filter", allowing us to narrow down the theory space before moving on to constrain model parameters with MCMCs while perhaps even signaling the presence of new physics that does not belong to any known model.

3.2.4. Deep learning

Neural networks have lately become ubiquitous in cosmology [2001,2009,2019–2032]. In this regard, the LADDER - Learning Algorithm for Deep Distance Estimation and Reconstruction - suite is a novel deep learning algorithm designed to learn the cosmic distance ladder in a model-independent, non-parametric manner [2018,

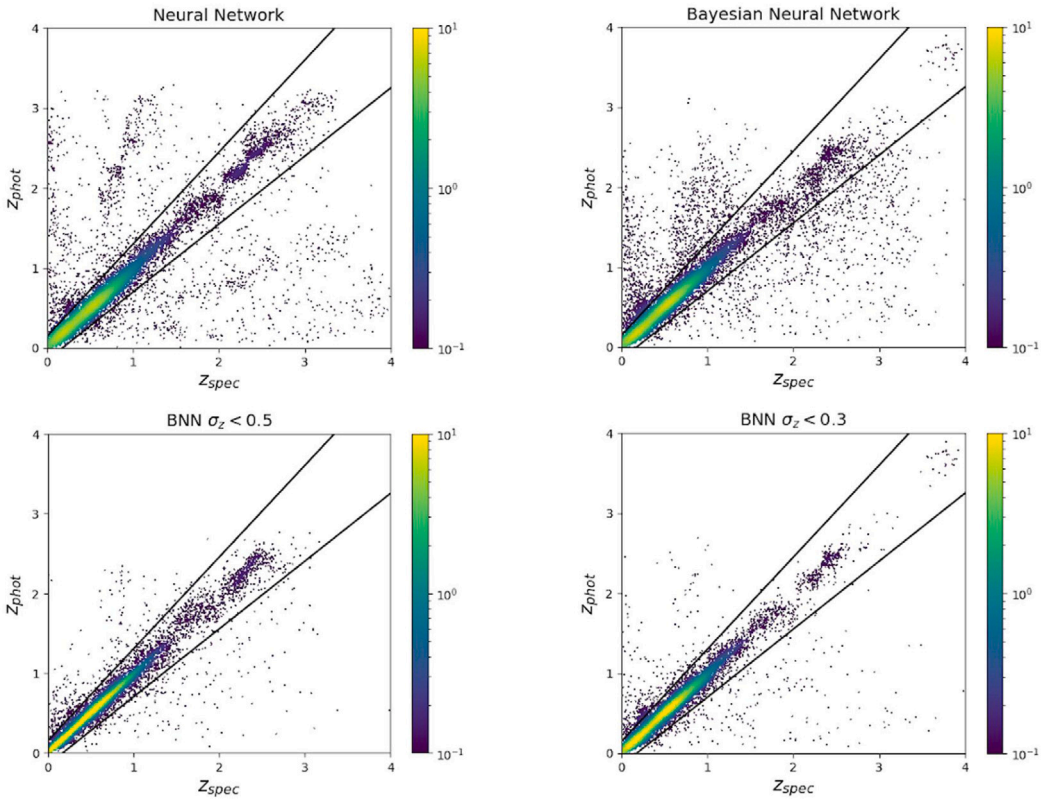

Fig. 60. Visualization of the neural network (top left) and BNN (top right) performance compared to the BNNN with outlier removal criteria $\sigma_z < 0.5$ (bottom left) and $\sigma_z < 0.3$ (bottom right) [2013].

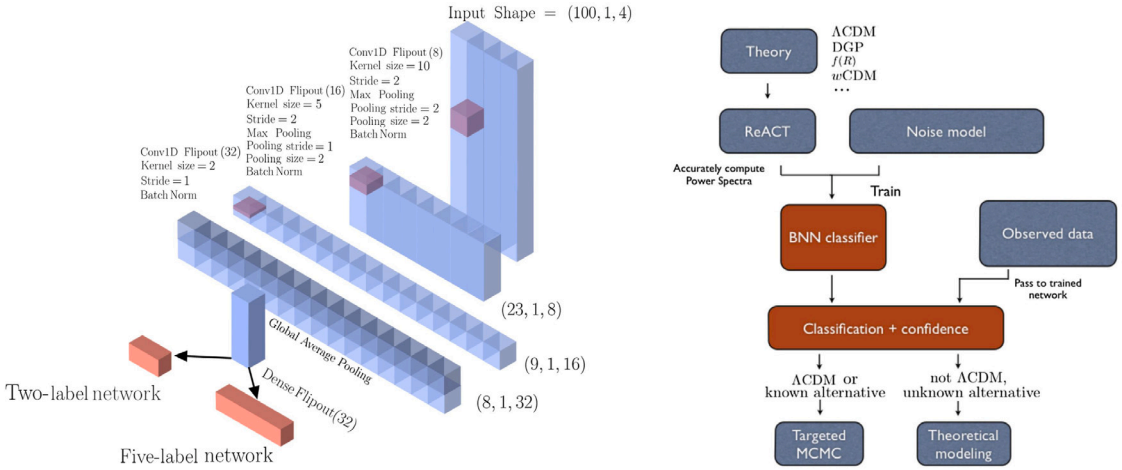

Fig. 61. The right panel illustrates the BNN workflow as adopted in Refs. [2015,2016], whilst the left panel depicts the corresponding BNN architecture employed for both the five-label and two-label classification tasks. The height of each block illustrates the dimension size for each layer, while the number of blocks per layer corresponds to the number of filters. The dense blocks embedded in the first three transparent layers indicate the kernels for the first three one-dimensional convolutional layers scaled by their respective size.

2018]. The schematic overview of the training algorithm is depicted in Fig. 62, whilst the corresponding algorithm is illustrated in Fig. 63. Trained on late-time datasets like the Pantheon SNIa dataset [2033], LADDER incorporates associated errors and complete covariance information. It interpolates from the joint distribution of a randomly chosen subset of the dataset to estimate target variables and errors simultaneously, effectively handling correlations and the sequential nature of the data. This leads to robust predictions resilient to input noise and outliers, even in data-sparse regions. Optimized by physically motivated metrics such as monotonicity and smoothness, LADDER leverages the Gaussian nature of the observations by employing the Kullback–Leibler (KL) divergence as the loss function during training.

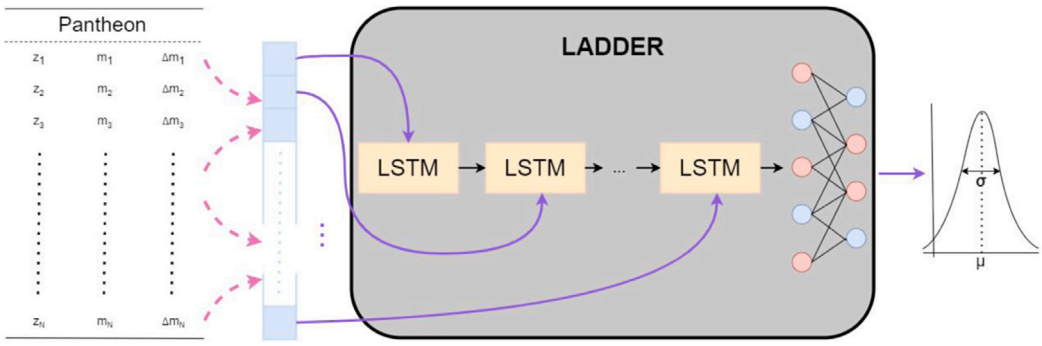

Fig. 62. Schematic overview of the deep learning algorithm adopted in Ref. [2018].

Algorithm1 LADDER - Learning Algorithm for Deep Distance Reconstruction and Estimation

Given $\mathcal{D}, \mathbf{C}_{\rm sys}$ and batch size B.
Initialize θ_0.
while not StopCondition **do**
  $l \leftarrow 0$
  for $i = 1, 2, \ldots B$ **do**
    Get K samples from $\mathcal{D}$
      $\{(z_1, m_1, \Delta m_1), \ldots (z_K, m_K, \Delta m_K)\}$
    $Y_i = (m_{j_1}, \Delta m_{j_1})$
    $\hat{m}_{j_2}, \hat{m}_{j_3}, \ldots \hat{m}_{j_K} \sim \mathcal{N}(m_{j_2}, m_{j_3}, \ldots m_{j_K}, \Sigma_m^K)$
    $X_i = (z_{j_1}, z_{j_2}, \hat{m}_{j_2}, \ldots z_{j_K}, \hat{m}_{j_K}) \quad z_{j_2} \leq z_{j_3} \ldots$
    $\mu, \sigma = f_{\theta_t}(X_i)_1, f_{\theta_t}(X_i)_2$
    $l \mathrel{+}= D_{KL}\left(\mathcal{N}(m_{j_1}, \Delta m_{j_1}), \mathcal{N}(\mu, \sigma)\right)$
  end for
  Compute $\nabla_{\theta_t} l \quad \forall \theta_t$
  $\theta_{t+1} = \theta_t + \eta \cdot \nabla_{\theta_t}$
  if ... **then**
    StopCondition $\leftarrow$ True
  end if
end while

Fig. 63. The deep learning algorithm adopted in Ref. [2018].

The LSTM network, found to perform best with the Pantheon dataset, is included in the LADDER suite, available publicly on GitHub (https://github.com/rahulshah1397/LADDER) under a MIT License and version 1.0 is archived in Zenodo [2018].

Having learned the cosmic distance ladder, LADDER is a powerful tool for cosmological applications. It can independently verify the consistency of SNIa datasets like Pantheon+ [32] and DES [1257], and serve as a pathology test for qualitatively different datasets, such as 2D vs. 3D BAO. Additionally, it acts as a model-independent calibrator for high-redshift datasets, including GRBs and QSOs. Moreover, previous ML approaches in cosmology struggled with stable error prediction at higher redshifts, rendering them unsuitable for precision cosmological tests. LADDER overcomes these challenges and shows promise in extrapolating beyond available data, useful for simulating intermediate-redshift data or augmenting current data to higher redshifts.

In Ref. [2034] LADDER is employed to recalibrate SDSS BAO and DESI BAO in a model-independent manner, which helps address the longstanding H_0 and S_8 tensions simultaneously. Traditionally, BAO distances are inferred using the sound horizon at the drag epoch (r_d), which is calibrated based on CMB data under the assumption of the ΛCDM model. In contrast, LADDER, trained on the Pantheon dataset, derives r_d purely from observational data without relying on cosmological model assumptions, instead incorporating merely an astrophysical prior on the absolute magnitude of SNIa (M_B). When combined with Planck 2018 data, this recalibrated BAO framework, along with Pantheon, yields joint constraints on ΛCDM that significantly alleviate the H_0 and S_8 tensions, due to an "in-plane shift", despite their negative correlation. These results highlight the potential biases introduced by CMB-based BAO calibration and demonstrate the robustness of data-driven approaches, offering a promising new avenue for precision cosmology.

Beyond conventional deep learning architectures, more advanced generative models have been developed to tackle complex challenges in cosmological inference. These methods, such as normalizing flows [2035] and diffusion models [2036,2037], extend deep learning capabilities by efficiently learning high-dimensional PDFs and accelerating likelihood-free inference. Unlike traditional MCMC approaches, which often struggle with computational inefficiency, generative models can rapidly approximate complex posteriors while maintaining high accuracy.

Normalizing flows have shown promise in addressing cosmological tensions, such as discrepancies in the Hubble constant and matter fluctuation amplitude (S_8). By modeling joint PDFs across datasets, they enhance uncertainty quantification and provide a robust statistical framework for analyzing these tensions [2038,2039]. One example is the EMUFLOW framework [2040], which utilizes normalizing flows to model joint posterior distributions from multiple datasets, enabling efficient constraint combination without increasing parameter space dimensionality. Additionally, methods employing normalizing flows

have been developed for non-Gaussian tension estimation, improving the quantification of agreement levels between different cosmological experiments and offering insights into discrepancies such as the H_0 tension [2041]. Further developments in normalizing flow architectures have introduced approaches that incorporate symmetries of the universe, such as translation and rotation equivariance, optimizing parameter inference for cosmological fields [2042]. Other extensions [2043] leverage hierarchical wavelet-based decompositions to improve robustness across spatial scales, while iterative flow-based techniques facilitate the transformation of complex PDFs into tractable forms, improving efficiency in cosmological data analysis.

Diffusion models, leveraging stochastic iterative denoising processes, have also been applied successfully to cosmological parameter inference. These models excel in uncertainty quantification and high-fidelity generative sampling of cosmological fields, particularly in large-scale structure and WL studies. A recent application integrates diffusion models with Hamiltonian Monte Carlo methods [2044,2045], enabling accurate posterior sampling and accelerated convergence in extracting key cosmological parameters such as $\Omega_{m,0}$ and S_8. The ability of diffusion models to reconstruct high-fidelity statistical distributions while remaining robust to observational noise makes them valuable tools for precision cosmology. As ML techniques continue to evolve, integrating generative models into cosmological inference is expected to enhance the precision and reliability of parameter estimation, especially for upcoming surveys like LSST and Euclid. These advancements underscore the growing role of deep learning-driven methodologies in shaping the future of cosmological analysis.

3.2.5. Conclusion

We reviewed the application of ML methods for the inference of cosmological parameters, emphasizing their versatility and capacity to address the inherent complexity of astronomical datasets. By integrating ML techniques into cosmological inference, we enable efficient and accurate predictions, facilitating faster convergence of traditional algorithms such as MCMC and advancing implicit likelihood or likelihood-free inference using deep learning. These innovations are particularly valuable in handling the high-dimensional, noisy, and often incomplete nature of cosmological data.

Across the subsections of this review, it is evident that the ML techniques considered provide powerful new tools to uncover potential signals of new physics within cosmological datasets. These methods act as a "filter", allowing researchers to effectively narrow down the theory space and refine subsequent analyses with standard techniques like MCMC. Furthermore, ML based approaches may even reveal evidence of new physics that does not fit within the framework of existing theoretical models, opening new avenues for exploration.

While alternative methodologies exist, we emphasize the transformative potential of advanced learning algorithms in optimizing the extraction of information from cosmological data. By demonstrating their utility, we aim to showcase how these novel approaches can complement or enhance traditional inference techniques. The innovative integration of ML into the cosmological framework promises to address current challenges, such as improving parameter constraints and identifying hidden structures or patterns in data, thereby paving the way for more accurate reconstructions of cosmological phenomena.

We also highlight the possibility of yet unexplored ML algorithms that may surpass the performance of those outlined in this review. This underscores the importance of continued exploration and innovation within the ML and cosmology communities. By encouraging the adoption and further development of ML based inference techniques, we aim to inspire new efforts to tackle unresolved questions in cosmology from fresh perspectives. Such endeavors would significantly improve the precision and reliability of cosmological analyses, contributing to a deeper understanding of the Universe's fundamental nature and addressing ongoing tensions in cosmological observations.

In conclusion, the integration of ML methods into cosmological research represents a paradigm shift, offering not only computational efficiency but also novel insights into the underlying physics of the Universe. We urge the community to actively engage in the exploration of these advanced tools, as they hold the potential to revolutionize the study of cosmology in the years to come.

3.3. Reconstruction techniques

Coordinator: Luis Escamilla, Daniela Grandón

Contributors: Adrià Gómez-Valent, Anil Kumar Yadav, Anjan Ananda Sen, Anto Idicherian Lonappan, Ariadna Montiel, Arianna Favale, Benjamin L'Huillier, Biesiada Marek, Celia Escamilla-Rivera, David Benisty, David Valls-Gabaud, Eoin Ó Colgáin, Filippo Bouchè, Iryna Vavilova, Isidro Gómez-Vargas, J. Alberto Vázquez, Jenny G. Sorce, Jenny Wagner, Jurgen Mifsud, Konstantinos Dialektopoulos, Luis E. Padilla, Matteo Martinelli, Miguel A. Sabogal, Purba Mukherjee, Rafael C. Nunes, Rahul Shah, Rocco D'Agostino, Ruth Lazkoz, Víctor H. Cárdenas, and Wojciech Hellwing

Reconstruction techniques have become crucial for understanding the phenomenology of DE, the expansion history, and the growth of large-scale structures in our Universe. They aim to capture specific features or general trends in the data, test a predefined physical model against observations, or explore a flexible, theory-agnostic framework to elucidate the phenomenology of cosmological functions. In general, reconstructions can be categorized into parametric and non-parametric approaches. They mainly differ in their underlying assumptions about a cosmological model and the functional form of the reconstructed quantity. The former imposes an explicit form on the function being reconstructed, thereby reducing uncertainties in the result. However, the a priori assumption of a specific model may limit the flexibility of the reconstruction and introduce biases regarding the properties of the cosmological function of interest. To mitigate this, some studies instead perform a non-parametric ("free-form") reconstruction within a theory-agnostic framework. Non-parametric reconstructions are particularly useful for gaining insights into the dynamics of cosmological functions when the true underlying function is not directly observable but can be inferred from observed data.

Many works on the parametric and non-parametric approaches investigate the impact of H_0 priors, to see whether the H_0 tension is also imprinted in the derived cosmological reconstructions. Hence, these techniques can shed light on the cosmological tensions and advance our understanding of their effects on a broader context. Moreover, a joint analysis of parametric and non-parametric reconstructions using cosmological observations is valuable to robustly identify departures from the ΛCDM model that emerge despite the differences of the methods used (e.g., see Ref. [2046–2048] for examples). In summary, these methods serve as data-driven frameworks to decode the phenomenology of cosmological functions from complex datasets, and offer an alternative approach to distinguish between competing cosmological models.

In what follows we present some examples of reconstructions and how they can be classified according to their methodology.

3.3.1. Parametric reconstructions

In a parametric reconstruction, the desired physical quantity is modeled using an analytical function with a set of free parameters that describe its behavior across cosmic time or spatial scales. The free parameters of the postulated function, and the cosmological parameters, are hence jointly inferred in light of the observational data. Hence, parameterizations are a crucial tool for modeling unknown physical phenomena in a mathematically tractable way. As an example, in the absence of a fundamental and well-defined theory of DE, several functions, i.e., $w(z)$, $\rho(z)$, have been parameterized in a broad number of different ways. These parametrizations track the dynamics of a

DE back in time simply extending the cosmological model with extra parameters. While parametric methods are computationally efficient and easy to interpret, they are inherently limited by the assumptions built into the chosen parameterization. A poorly chosen model may lead to biased results that fail to capture the true complexity of the underlying physics. As such, model selection criteria for various parametric candidates are critical in assessing the robustness of the results.

3.3.2. Phenomenological parameterizations

Phenomenological parameterizations focus on capturing specific behaviors, often without direct derivation from fundamental physics. Their primary goal is to test whether certain trends (such as evolving equations of state, deviations from General Relativity, or modified growth of structure) are compatible with observational data. These parameterizations provide a practical way to explore a broad range of possibilities without requiring a detailed theoretical foundation. Some well-known examples include:

- CPL parameterization [297,298] for the DE equation of state

$$w(z) = w_0 + w_a z/(1+z)\,, \tag{3.16}$$

  which is the general go-to parameterization used to test if any dynamic behavior can be present in DE (this parameterization is further explained in Section 2.3.4). The DESI collaboration recently employed this parameterization in their analysis of year-one BAO data [699] and found evidence suggesting a preference for a DDE model with a significance exceeding 2σ.
- The Jassal–Bagla–Padmanabhan (JBP) parameterization [2049], also for the DE equation of state

$$w(z) = w_0 + w_a z/(1+z)^2\,, \tag{3.17}$$

  which serves as a modification of the CPL designed to exhibit different behaviors at large redshifts.
- Interaction term between DE and DM [2050–2053]

$$Q = \xi H \rho_{\rm DM}\,, \tag{3.18}$$

  with the parameter ξ governing the strength of the interaction. It is proposed as a way to represent the interaction as a function of time (H) and energy density ($\rho_{\rm DM}$). Given its phenomenological nature, this approach can be extended further, as demonstrated in Ref. [2054], where the interaction term was modified to depend not only on DM but also on DE. In this case, the interaction takes the form $Q = \xi H(\rho_{\rm DM} - \alpha\rho_{\rm DE})$ with the new parameter α regulating the strength of the dependence on DE. Moreover, the authors in Ref. [2052] discuss the interaction between DM and DE in the context of the second law of thermodynamics and its consequences on DE evolution. For a more complete discussion on DE-DM interactions please refer to Section 4.4.3.
- A parametric form for the DE density $X(z)$ was developed by Refs. [2055–2057] and further tested in Refs. [2046,2058]. The quadratic parameterization corresponds to

$$X(z) \equiv \frac{\rho_{\rm DE}(z)}{\rho_{\rm DE}(0)} = 1 + (4x_1 - x_2 - 3)\left(\frac{z}{z_m}\right) - 2\,(2x_1 - x_2 - 1)\left(\frac{z}{z_m}\right)^2\,, \tag{3.19}$$

  where z_m is the maximum redshift in the data set, x_1 and x_2 are the free parameters of the model to be constrained in light of the data. When $x_1 = x_2 = 1$, the parameterization reduces to ΛCDM where the DE density is constant $X(z) = 1$. This approach aims to study evidence for DE evolution by allowing its energy density to change with redshift. Reconstructing $X(z)$, instead of $w(z)$, is advantageous since this quantity is more directly traced by the luminosity distance. A cubic parameterization was also explored in Ref. [2058] to allow for an extra degree of freedom and to investigate whether further transitions with respect to $X(z) = 1$ are found in the reconstruction.
- The growth rate parameterization [2059]

$$f(z) = \Omega_{m,0}(z)^{\gamma}\,, \tag{3.20}$$

  where γ is named the growth index, which for ΛCDM has a value of ~ 0.55. A recent application of this parameterization can be found in Ref. [2060], where an analysis using $f\sigma_8$ and Planck CMB revealed a tension of 4.2σ with the concordance model's expected value of $\gamma = 0.55$, suggesting a potential need for modifications to the way the standard model predicts structure growth.
- The gravitational slip [2061]

$$\eta = \frac{\Phi}{\Psi}\,, \tag{3.21}$$

  where Φ and Ψ are the metric potentials in the perturbed Einstein equations. If η deviates from 1 there may be an indication for MG. In Ref. [2062] four different models for η were analyzed using forecasts from WL, galaxy clustering, and supernova data to evaluate how effectively future surveys could constrain the slip parameter. Furthermore, in Ref. [2063] a deviation from GR was found using GW data along with the slip parameter.

As we can see, phenomenological parameterizations allow for a broad exploration of deviations from the standard model without committing to a specific underlying theory.

3.3.3. Physically motivated parameterizations

Physically motivated parameterizations, in contrast, are derived from fundamental theories and ensure consistency with known physics. These models are often constructed from Lagrangian formulations, field equations, or extensions of Einstein's General Relativity, ensuring that theoretical principles like energy conditions and stability constraints are satisfied. Some of these parameterizations which can be found in the literature are:

- Scalar fields for DE. A well-known one being the Quintessence [295], where a scalar field ϕ with a potential $V(\phi)$ leads to an equation of state

$$w(z) = \frac{\dot\phi/2 - V}{\dot\phi/2 + V}\,, \tag{3.22}$$

  having the peculiarity of behaving as, in which the kinetic term has the wrong sign, $\dot\phi^2/2 \to -\dot\phi^2/2$, leading to $w(z) > -1$. Complementary to it we have the Phantom scalar field [2064] where $w(z) < -1$. The combination of them, resulting in the interacting-two-scalar-field model named Quintom [2065–2067] has also been studied due to its peculiarity of being able to cross the Phantom-divide line ($w = -1$) [2068,2069]. K-essence scalar field [2070], which can be seen as an extension of Quintessence where non-canonical kinetic terms are included in the Lagrangian.
- Horndeski theories of MG [665,2071–2073], which provide the most general scalar-tensor theories leading to second-order field equations.
- $f(R)$ theories [2074] which modify the Ricci scalar in the Einstein–Hilbert action

$$S = \int d^4x\sqrt{-g}\left(\frac{1}{16\pi G}f(R) + \mathcal{L}_{\rm m}\right)\,, \tag{3.23}$$

  where the $f(R)$ can take many forms. In Ref. [2075] two different parameterizations for $f(R)$ were studied, them being $f(R) = R - 2\Lambda(1 - e^{-R/\Lambda b})$ and $f(R) = R - 2\Lambda\big(1 - \frac{1}{1+(R/\Lambda b)^n}\big)$, finding concordance with the standard model when using BAO, SN and CC data. Similarly, in Ref. [2076] a preference for the standard model is recovered when the two models $f(R) = R - \beta/R^n$ and $f(R) = R - \alpha\ln R - \beta$ are used in tandem with simulated GW data.

- For DM models, we encounter WDM [2077–2081], where a nonzero velocity dispersion modifies the matter power spectrum. Another example is Self-Interacting DM [2082–2085], in which a cross-section σ/m accounts for self-interactions, affecting structure formation at small scales while preserving the CDM behavior on larger scales.

Both phenomenological and physically motivated parameterizations aim to describe the evolution of cosmic components, test deviations from ΛCDM, and assess the viability of new models against observations. Phenomenological parameterizations provide a flexible way to analyze trends, while the physically motivated ones ensure consistency with fundamental physics. The choice between the two depends on whether the focus is on empirical data fitting or theoretical consistency.

3.3.4. Model-independent parameterizations

While both phenomenological and physically motivated parameterizations help constrain the behavior of cosmological functions, they inherently require assumptions about the functional form. However, these assumptions can limit the flexibility of the analysis, as the chosen parameterization may not fully capture the true underlying features of the function being reconstructed. To overcome this limitation, one can employ more sophisticated parameterization methods that minimize the number of underlying assumptions. Some of these approaches, referred to as model-independent methods, remain parametric but offer significantly greater flexibility, allowing them to capture a wider range of possible features in the data.

3.3.4.1. Basis representation. Basis-representation parameterizations provide a flexible and systematic way to reconstruct cosmological functions by expanding them in terms of a chosen set of basis functions. Common examples found in the literature include:

- Given its simplicity and ease of use, the Taylor expansion has been applied to many different cosmological functions. As an example, in Ref. [2086] the DE equation of state, through its pressure, was expressed as a truncated Taylor series

$$p = p_0 + \sum_{n=1}^{N-1} \frac{1}{n!} \frac{d^n p}{d\rho^n}\bigg|_0 (\rho - \rho_0) + \mathcal{O}[(\rho - \rho_0)^N]\,. \tag{3.24}$$

  This idea can be extended even further. By performing a Taylor expansion of the Hubble parameter around $z = 0$, one arrives at the cosmographic approach [2087–2090], which will be explored in more detail in a later subsection.
- In a manner similar to the Taylor series expansion, one can instead adopt a different basis, such as a Fourier series. In Ref. [2091], this approach was applied to the DE equation of state, revealing a preference for an oscillatory behavior at late-times. The equation of state was found to cross the phantom divide multiple times, which has been found to be a stable solution for the Kinetic Gravity Braiding model proposed in Ref. [2092], a minimally coupled Horndeski model. This however does not hold for other single scalar field models, where gravitational instabilities appear when crossing the phantom divide.
- The Padé approximation could be seen as an extension to the Taylor series, being itself a rational of two polynomial series. It has the advantage of a faster convergence rate, but potentially using more new terms/parameters. Its uses are well varied in the literature, going from the luminosity distance [434,2093–2096], the Hubble expansion rate [2096], the DE EoS [2095] and even $f(R)$ [2097]. In Ref. [2093] the luminosity distance was expressed as $d_{\rm L} = \frac{a_1 z}{1+b_1 z+b_2 z^2}$, which is usually called the $(1,2)$ Padé approximant for $d_{\rm L}$, finding some agreement with Planck's CMB data at small redshifts but allowing DE to be dynamical.
- Wavelet expansion. Wavelets work as a basis and have the peculiarity of being localized in frequency and configuration space, which is useful for capturing both global trends and local fluctuations. In Ref. [2098], a wavelet-basis was used for the DE EoS in the next manner

$$w(z_j) + 1 = \sum P_i \psi_i(z_j)\,, \tag{3.25}$$

  with z_j being the redshift points at which w is calculated, P_i the coefficients of the expansion and ψ_i the wavelet function. In this particular work the wavelets used were the Haar ones (where $\psi_i(x) = 1$ for $0 \le x \le 1/2$, $\psi_i(x) = -1$ for $1/2 < x \le 1$ and $\psi_i(x) = 0$ otherwise) and, using SNIa, WMAP and BAO data, a hint for dynamical DE was found.
- Reconstructions using an orthonormal basis set of functions (ONB) has been used to reconstruct the normalized cosmic expansion function, $H(z)/H_0$, from the Pantheon dataset [2099], without assuming a specific cosmology. In this approach, the luminosity distance function $D_{\rm L}(a, \boldsymbol{c})$ was expanded into orthonormal basis functions $\phi_\alpha(a)$ as

$$D_{\rm L}(a, \boldsymbol{c}) = \sum_{\alpha=0}^{N_{\rm B}-1} c_\alpha \phi_\alpha(a) = \boldsymbol{c} \circ \boldsymbol{\Phi}\,, \tag{3.26}$$

  where a is the scale factor. The c_α elements of $\boldsymbol{c} \in \mathbb{R}^{N_{\rm B}}$ denote the weights of the $N_{\rm B}$ basis functions. These terms are summed up in the short-hand notation of the right hand side. The choice of the ONB can be adapted to the problem at hand, as has been done in Ref. [2099], but other general choices like Chebycheff polynomials can be used. Then the values of c_α are obtained by minimizing the χ^2 function [2100]. Using a special ONB adapted to approximate a ΛCDM universe with its first few basis functions, [2099] showed that the reconstructed cosmic expansion function from the Pantheon set of SNIa still yields very broad confidence bounds, such that ΛCDM and other competitive models of DE are still statistically consistent with the dataset.

3.3.4.2. Interpolation methods. Another model-independent approach to parameterization, similar to the basis representation method, involves interpolation techniques. In this approach, a set of "positions" is defined and then connected in a specific manner, with the chosen connection method determining the type of interpolation used. These positions act as free parameters, whose optimal values are determined through Bayesian parameter inference algorithms, such as MCMC or Nested Sampling.

An example of such a class of methods consists in binning the function one wants to reconstruct and treat each one of its binned values as a free parameter of the analysis, e.g., one could aim at constraining the value of $w(z)$ at a given number of redshift z_i. This completely removes assumptions made on the trend of the function, but significantly increases the number of free parameters to take into account. When using this approach the bins are usually connected with hyperbolic tangents to preserve continuity. As a function it can be represented as

$$w(z) = w_1 + \sum_{i=1}^{N-1} \frac{w_{i+1} - w_i}{2} \left(1 + \tanh\left(\frac{z - z_i}{\xi}\right)\right), \tag{3.27}$$

where N is the number of bins, w_i the amplitude of the bin, z_i the position where the bin begins in the z axis and ξ is a hyperparameter which governs how "smooth" is the transition from one bin to the other (a higher value represents a higher smoothness). Being one of the most utilized model-independent interpolation methods it has a wide range of applications such as in reconstructing: the neutrino mass [2101]; the primordial power spectrum and inflaton potential [2102]; the DE energy density [2103,2104]; the DE EoS [2103,2105,2106]; the interaction kernel in an IDE model [2021,2107]; a DE perfect-fluid model [2108]. Another example of a binned analysis (or interpolation) is the reconstruction of the functions $\mu(z)$ and $\Sigma(z)$, which describe deviations from General Relativity (e.g., see Refs. [2109–2111]). In

Refs. [2112,2113], joint constraints on these functions and on the DE density parameter $\Omega_{\rm DE}(z)$ were obtained combining CMB, BAO, and SN data. The results of this analysis show hints for deviations from General Relativity, mainly in the $\Sigma(z)$ function which encodes deviations from the gravitational lensing effect expected in the standard model, while also reducing both H_0 tension to $\sim 2\sigma$ (when comparing the inferred value of $H_0 = 69.44 \pm 1.3\,{\rm km\,s^{-1}Mpc^{-1}}$with the SH0ES one) and the S_8 tension (by inferring a value of $S_8 = 0.780 \pm 0.033$ which is in line with DES Y3's measured value of $S_8 = 0.769 \pm 0.016$).

Another choice of interpolation is commonly referred to as "nodal reconstruction" [2114]. Here the interpolations are done using linear, cubic, or higher order splines, to fill in the gaps between a certain number of nodes. The simplest example is the linear interpolation, that is, given two coordinates (z_i, f_i) and (z_{i+1}, f_{i+1}), the function behaves as follows

$$f(z) = f_i + \frac{f_{i+1} - f_i}{z_{i+1} - z_i}(z - z_i), \quad z \in [z_i, z_{i+1}]\,. \tag{3.28}$$

This method has been used to reconstruct several important cosmological quantities, i.e., the primordial power spectrum [2115–2118], the DE energy density and the DE EoS [2103,2119], the expansion rate of the Universe [2120] and the neutrino mass [2101]; just to mention a few.

An unusual type of interpolation makes use of GP. The mathematical formalism behind it was already presented in Section 3.1, and further details of its applications in reconstruction will be discussed in the following subsection. This interpolation works in a similar manner to the nodal reconstruction, but with the obvious distinction that the connection between the varying nodes is made through GP. This approach can mitigate some issues that the other two approaches present, such as the choice of the bins' width and positions [2121], while also presenting the advantage of being infinitely differentiable. Given its relatively new implementation it has not been used widely. In Ref. [2121] was first implemented with the equation of state parameter, and in Ref. [1994] was used to reconstruct the interaction kernel of an IDE model.

3.3.5. Cosmography

The degeneracy among various theories proposed in recent years to explain DE has driven the investigation of methods that enable the study of cosmic expansion without relying on predefined cosmological models. This is the case of the well-known cosmographic approach [2087–2090], which depends only on the cosmological principle and uses series expansions of the luminosity distance around the current time. The power of the cosmographic method arises from the fact that it involves observables that can be directly compared with data and guarantees independence from any assumed DE equation of state. Thus, the cosmographic method has been extensively utilized to distinguish between various theoretical models that appear similar when compared to observations [2122–2125].

However, the cosmographic method faces two main challenges that may limit its effectiveness as an accurate tool for describing cosmic expansion. The first challenge is the necessity for a substantial amount of data to distinguish between the cosmological constant and a DDE. The second issue concerns the use of high-redshift data to explore potential deviations from the standard cosmological model. The latter aspect conflicts with the core principle of the standard cosmographic technique, which relies on a Taylor expansion series centered around $z = 0$. As a result, large error propagations due to convergence issues often compromise the effectiveness of the method. Over time, various alternatives to the standard cosmographic method have been explored to address these limitations. One approach involves using auxiliary variables and developing expansion series for cosmological observables based on re-parametrizations of the redshift variable converging as $z \gg 1$ [434,1394,2126].

An alternative way to tackle the aforementioned challenges is to utilize rational polynomials that can heal convergence problems typical of the standard Taylor-based cosmography. A prominent example of this technique is offered by Padè polynomials, which can be calibrated to maximize the convergence radius, thereby enabling a more stable fitting process at high redshifts [2093–2095]. The benefits of Padè polynomials have recently been exploited in various theoretical contexts to explore potential deviations from Einstein's gravity [2096,2127,2128]. Furthermore, the cosmographic method based on Padè polynomials, as well as the auxiliary y-redhift parameterization, has been adopted to evaluate in a model-independent way the cosmological tensions in the H_0 and σ_8 measurements suggested by recent observations [2129]. Another strategy to extend the convergence radius of the cosmographic series and address the subjectivity in truncating the expansion, which may still be an issue with the Padé method, involves using Chebyshev polynomials. It has been shown that these polynomials can significantly reduce the uncertainties in higher-order terms of the cosmographic series, thus offering a precise description of the Universe's evolution at late-times [2130,2131].

The Weighted Function Regression Method, first employed in Ref. [422], addresses the subjectivity involved in choosing the truncation order of cosmographical expressions. It does so by considering all cosmographical orders when reconstructing cosmological functions, and it applies robust Bayesian weights to penalize the use of additional parameters. In practice, the contribution of higher orders can be neglected since their weights are significantly suppressed. This method has been used to reconstruct the Hubble and deceleration functions, as well as to estimate the Hubble and deceleration parameters in a model-independent way with low-redshift data, see Ref. [422,2132], respectively.

3.3.6. Non-parametric methods

Non-parametric reconstructions are data-driven methods that do not rely on a specific functional form of the reconstructed function and hence strive to minimize model assumptions. In other words, the aim is to describe the data without imposing strong a priori constraints. Among the most common applications of non-parametric methods we find GP regression, ANNs, the local regression smoothing method, and the iterative smoothing method. These methods vary in their flexibility to reconstruct highly non-linear relations between variables and how the uncertainties on the reconstruction are obtained. We proceed to describe them and their applications in cosmology.

3.3.6.1. Gaussian processes. Both powerful and versatile tools in ML and statistical analysis [2133,2134], GP are a Bayesian technique that generalizes distributions over functions, extending Gaussian distributions into function space [2135]. This approach allows for the reconstruction of a function $f(x)$ at every point x using an observational data set $\left\{\left(x_i,\, f(x_i) + \sigma_i\right) \mid i = 1, \ldots, N\right\}$, without needing to assume a predetermined specific functional parameterization. The reconstructed function and its derivatives are Gaussian random variables with a mean $\mu(x)$ and variance $\mathrm{cov}\,[f(x), f(x)]$ at each data point x. The functions at different points x and $\tilde{x}$ are related by a covariance function $K(x, \tilde{x})$, commonly referred to as a kernel, which depends on a small set of hyperparameters. Although there is a wide range of covariance functions available in the literature [2134,2136], the hyperparameters are generally constant, as their values characterize the function's smoothness rather than modeling such behavior. Most cosmological applications of GP use a zero mean function and optimize the hyperparameters [2137]. A strict Bayesian approach is to marginalize over the hyperparameters. As for the mean function, while stationary processes can be described by a constant mean function, non-stationary ones such as the cosmic distances or growth may not. The authors in Ref. [2138] showed how marginalizing over a *reasonable* family of mean functions and over the hyperparameters yields a robust and unbiased result. An application of this *full marginalization* approach

is to use GP as a forward model. One can generate *untrained* GP by sampling the hyperparameters, and calculating the likelihood. This allows forward modeling of quantities such as the growth rate $f\sigma_8(z)$ and distances while combining several datasets [2138–2144]. In cosmology, GP techniques have been successfully employed to reconstruct the dynamics of cosmological functions with minimal physical assumptions about the Universe's geometry or the nature of its main components. These include the background the expansion rate of the Universe $H(z)$ [419,422,423,429,2047,2145–2149] as can be seen in Fig. 64, the deceleration parameter $q(z)$ [1376,2150–2152], the distance duality relation [2153–2155], and the cosmological jerk parameter [2156]. To explore the dynamics of DE, examples include reconstructions of the DE energy density [2046,2058,2142], the scalar field dynamics [2157], the equation of state $w(z)$ [425,2158,2159], and interaction between DE and DM [2160–2163]. These applications have served to study MG models [2147,2147,2164–2176], cosmic curvature [2177–2184], and GWs [672,2185–2187], inflaton speed of sound's profile [2188], and many other perspectives [424,430,2101,2189–2198]. In particular, the authors in Ref. [2188] adopt a slightly different approach. They demonstrated how mildly-informative physical priors can be imposed on a GP reconstruction in a Bayesian way so that robust constraints on physical parameters can be extracted along with a non-parametric reconstruction. In summary, all these applications have proven particularly valuable for testing the robustness of ΛCDM and identifying potential deviations from our current understanding of the Universe.

3.3.6.2. Artificial neural networks. ANNs have also seen a steep increase in their application to cosmology (for further information on this please refer to Section 3.2.1, Section 3.2.2, Section 3.2.3 and Section 3.2.4). The two main advantages of ANNs over other non-parametric techniques are that they can capture (highly) non-linear relations in complex datasets, and in principle do not require the data to follow a specific statistical distribution. For this reason, the cosmological community has developed various neural network reconstructions of cosmological functions. Some cosmological functions reconstructed with ANNs include the distance modulus $\mu(z)$ from the Pantheon and Pantheon+ compilation [1994,2018,2020,2023,2025,2034] and the Hubble function $H(z)$ [2001,2020,2026,2199,2200]. In particular, a novel approach was developed in Ref. [1994] where the authors train a recurrent neural network to learn the mapping from redshift z to distance modulus $\mu(z)$ using the Pantheon SNIa sample. This model, combined with a BNN, is also able to propagate the uncertainties into the predicted function $\hat{\mu}(z)$ and thereby into cosmological constraints. This approach was also implemented to calibrate GRBs at high redshift [2021]. Other applications include ANNs reconstructions using LSST simulated data [2201], CNNs to reconstruct the BAO signal [2202], ANNs for growth data $f\sigma_8$ [2001,2199], and velocities of rotation curves [2203]. For visual reference, in Fig. 64 an ANN was used to reconstruct $H(z)$. Other approaches generate ANN models for small datasets and their errors using feedforward neural networks with Monte Carlo Dropout and hyperparameter grid optimization [2001] or GAs [2023].

As with other non-parametric reconstruction methods, the goal is to generate an ANN model based on observational data and then compare the resulting reconstruction with theoretical predictions from parametric methods to allow for robust conclusions. In this direction, different cosmological models have been analyzed using neural network reconstructions. Examples include ΛCDM [2001,2020,2184], the CPL model [1994,2001,2020,2201], Chaplygin gas models [1994], and Horndeski gravity [2026], among others.

3.3.6.3. Iterative smoothing method. The authors in Ref. [2204] used this non-parametric method to smooth supernova data using a Gaussian smoothing function. This method aims to reconstruct cosmological quantities such as the expansion rate, $H(z)$, and the equation of state of DE, $w(z)$, in a model-independent manner. The only assumptions made by this method are the smoothing scale and a guess background model for the quantity under study. However, it is necessary to use a bootstrapping method to determine the optimal guess model. In Ref. [2204], the authors used an iterative method to estimate the guess model. They started with a simple cosmological model, such as ΛCDM, as the initial guess model and then the results were used as the next step in the iteration. With each iteration, it was expected the guess model to become more accurate, thus giving a result that is less and less biased toward the initial guess model used. Indeed, it was noted that using different models for the initial guess does not affect the final result as long as the process is iterated several times.

The method requires careful consideration of the smoothing scale. A very small smoothing scale gives an accurate but noisy guess model, therefore after a few iterations, the result will become too noisy to be of any use. It is better to use a larger smoothing scale for smoother results. On the other hand, the bias of the final result decreases with each iteration, since with each iteration one gets closer to the true model. The bias decreases non-linearly with the number of iterations. In Ref. [2204], points out that after about 10 iterations, for moderate values of the smoothing scale, the bias is acceptably small. Also, beyond this, the bias still decreases with the number of iterations but the decrease is negligible while the process takes more time and results in larger errors on the parameters. In Refs. [2205–2207] the method was improved to reconstruct the distance modulus in a model-independent way and then employed in Refs. [2208,2209], to name just a few examples. In particular, this method was applied to reconstruct the cosmic expansion history and growth to test curvature, DE, and GR [2207,2210–2212].

3.3.6.4. Local regression smoothing and simulation extrapolation (Loess+Simex). The LOcally wEighted Scatterplot Smoothing (Loess), also known as local polynomial regression, is a non-parametric method for data analysis that does not require specifying a predefined relationship between dependent and independent variables. It generalizes standard least-squares methods and is widely used for non-parametric simple regression in various disciplines. *Loess* aims to depict the global trend of a dataset by fitting low-degree polynomials to subsets of data around each observation, giving more weight to points closer to the target observation using a Kernel-based weighting system. Typically, first or second-order polynomials are used since higher orders do not significantly enhance results and increase computational complexity. The process is applied iteratively to cover the entire data range, resulting in a comprehensive trend depiction. Important aspects of the method include selecting the number of data points for each fit through a smoothing parameter called span, s, determining the polynomial degree, and choosing the weight function form. Additionally, confidence intervals are constructed by calculating the variance of the fitted values, assuming Gaussian distributed errors. Despite some bias in the estimation, the cross-validation technique provides accurate confidence intervals around the *Loess* curve. To account for the observational errors on real data, additional methods are needed. To this end, the authors in Ref. [2213] proposed to combine the *Loess* method with the simulation-extrapolation method, also called *Simex*, which is a simulation-based method designed to minimize bias resulting from the inclusion of covariates that are prone to errors. Estimates are derived by introducing additional measurement errors, using a form of resampling. This resampling helps identify the pattern of measurement error. After estimating the pattern, final estimates are obtained by extrapolating back to the scenario where there is no measurement error.

Loess and *Simex* were first used together in cosmology in Ref. [2213] to reconstruct the expansion history $H(z)$. Later, this technique was also used to reconstruct galaxy rotation curves [2214], the distance modulus [2215], and other cosmological quantities [2048,2216,2217], with also accurate results.

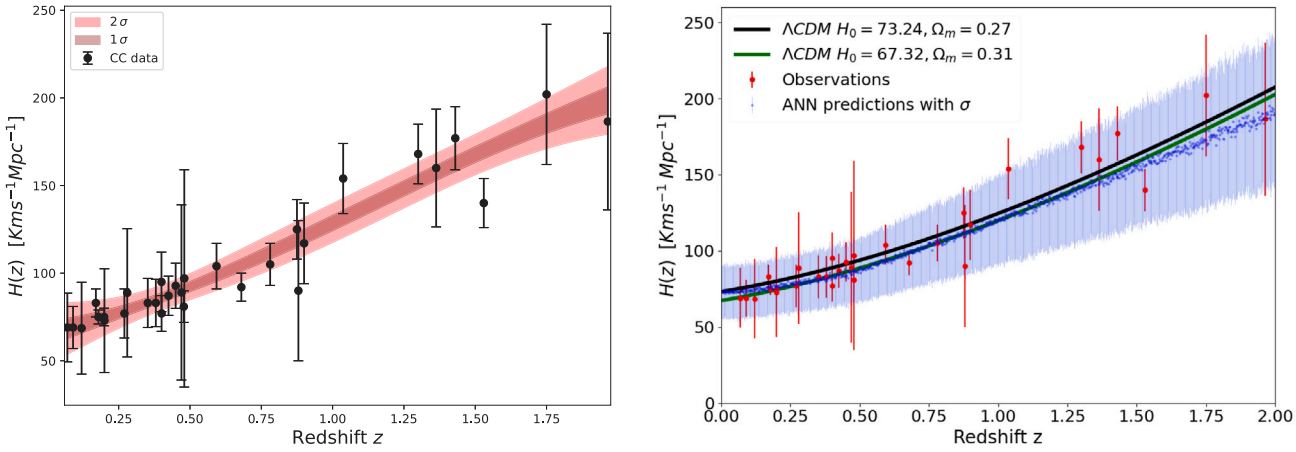

Fig. 64. Non-parametric reconstructions of the Hubble function $H(z)$ using CCs. Two different approaches were used: GP regression (left) and ANNs (right). The ANN reconstruction was made following the approach in Ref. [2001]. The analysis models observational uncertainties using Monte Carlo Dropout, as also employed in Refs. [1994,2184,2201]. The cosmic chronometer data from [410] and theoretical predictions from the ΛCDM model are included for reference.

3.4. Bio-inspired algorithms in model selection

Coordinator: Reginald Christian Bernardo

Contributors: Anto Idicherian Lonappan, Antonio da Silva, Arrianne Crystal Velasc, Celia Escamilla-Rivera, David Valls-Gabaud, Dinko Milakovic, Erika Antonette Enriquez, Filippo Bouche, Isidro Gómez-Vargas, J. Alberto Vázquez, Jenny G. Sorce, John K. Webb, Jurgen Mifsud, and Renier Mendoza

We briefly discuss GAs (Sections 3.4.1–3.4.2), their applications to cosmology (Section 3.4.3) and potential relevance to the understanding of cosmological tensions (Section 3.4.4).

3.4.1. Genetic algorithm

A GA is a biology-inspired optimization strategy that mainly takes elements of natural evolution in order to single out one solution that is the fittest from a pool of similarly naturally selected individual solutions. GAs are powerful optimization methods, called meta-heuristic because they do not use derivatives to find the optimum, and they guarantee to find the best solution under certain conditions, despite the challenges posed by local optimality [2218]. This has been used in a wide variety of scientific problems such as in high energy physics [2219] and GW astronomy [2220], and is known to be able to find global optimum and resolve tiny differences between seemingly degenerate solutions to a problem. GA is particularly well-suited to bypass issues related to complex, high-dimensional parameter spaces and multimodal functions. In cosmology, it was introduced as a means to overcome the bias in selecting a cosmological model in order to infer the properties of DE [2221]. This was then followed by Ref. [2222] and Ref. [2223], which has further marketed GA as an alternative tool for cosmological analysis through the estimation of uncertainty. An excellent recent introduction to GA for cosmological parameter estimation is given in Ref. [2224].

GAs operate with a population of individuals (possible solutions), where each individual is characterized by a chromosome, which in turn is described by a set of genes. These individuals make up the population that evolves over successive generations. The key ingredients of GA are described in Table 4, while the evolutionary process is illustrated in Fig. 65.

In essence, GAs sample from a population of individuals ranked by a fitness scale. The fittest individuals are more likely to survive and reproduce through crossover and mutation, creating offspring with improved traits. The best or elite individuals are stored to guarantee that the population is improving through the generations. This iterative process continues until the optimal solution, or the fittest individual,

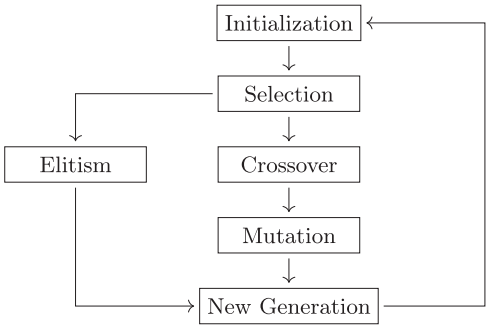

Fig. 65. Flowchart illustrating the key steps in GAs [2225].

emerges. In cosmology, the gene can be thought of as each cosmological parameter, such as w_0 and w_a in CPL cosmology, and the chromosome as the string of genes, e.g., $(H_0, \Omega_{m,0}, w_0, w_a)$ [2224]. A GA can, of course, be applied in a variety of ways; notably, in the pioneering works [2221–2223] the GA has been used in the context of grammatical evolution (GE), where the elements and key ingredients of GAs are utilized to search for solutions within function spaces, alleviating the arbitrariness of cosmological parameterization. More recently, GAs have been used to eliminate the arbitrary choice of a kernel function in GP regression [2226] and to optimize neural networks [2023]. It has also found applications in spectroscopic modeling [2227–2229], and in conjunction with information criteria for model selection [2230].

3.4.2. Machine learning and GA variants

In this section, we dig a little further into the details on GAs in order to get a better grip of its intricacies, and use it as a template to introduce some of its more familiar variants that have also been considered in the field. The basic steps of GAs are summarized in the pseudocode shown in Algorithm 1, based on the notation in Ref. [2223] and Ref. [2225].

Algorithm 1 highlights that GAs are fundamentally an optimization strategy, inspired by the principles of natural selection and genetics. In cosmology, however, particularly through the lens of grammatical evolution, GAs transcend traditional optimization by serving as an ML method. The resulting combined method utilizes the adaptive search capabilities of GA and GE to incrementally evolve a grammar that approximates cosmological functions, such as cosmic expansion and growth rates, from input data. By discovering functional forms that capture the underlying dynamics of cosmological phenomena,

Table 4
Key ingredients of GAs [2225].

Fitness-function	Determines the fitness of individuals in a population. This function can be tailored to the specific problem, such as minimizing the Euclidean distance or optimizing the likelihood in cosmological applications. The fitness function is a predefined metric used to rank solutions.
Selection	Defines the portion of the population that will advance to the next generation. A common method is the 'roulette wheel' selection, where fitter individuals have higher chances of being selected for reproduction.
Elitism	Ensures that the individuals that passed the selection process can be directly added to the next generation. Elitism guarantees that the best fitness value will not get worse after every generation.
Crossover	Refers to the process of combining the genetic information of two parents to produce offspring. This mechanism allows for the exchange of genes between individuals, promoting the inheritance of favorable traits while introducing genetic diversity into the population.
Mutation	Involves the random alteration of an individual's genes. This step is crucial for introducing new genetic variations, ensuring that the population does not stagnate and continues to evolve toward better solutions. This allows GAs to escape local solutions and obtain global solutions.

Algorithm 1 GA pseudocode.

Notation: f: fitness function, $[b_1, b_2]$: population range, D: population dimension, r: mutation rate, N: population size,
G: max. number of generations, m: individual index, t: generation index, $M(t)$: population at generation t, m^*: best solution
Input: f, $[b_1, b_2]$, D, r, N, G
Output: m^*, $f(m^*)$

```
Define the maximum number G of generations and the mutation rate r
Set the generation counter t ← 0
Generate an initial random population M(0) consisting of N individuals having dimension D and range [b1, b2]
while t < G do
    Compute and save the fitness f(m) of each individual m in the current population M(t)
    Sort M(t) with respect to the fitness of each m
    Define selection probabilities p(m) for each m in M(t)
    Choose a proportion of M(t) based on the selection probabilities p(m)
    Apply crossover on parent individuals to produce offspring
    Apply mutation on offspring with a probability based on the mutation rate r
    Store the new generation M(t + 1) of individuals
    Select the elite individuals in M(t + 1) to be preserved for the next generations
    t ← t + 1
end while
Return the best individual m* of the final generation and its fitness f(m*)
```

GAs in this context demonstrate their dual role in both optimizing and learning, revealing intricate patterns that may be governing our Universe. This versatility is notably owed to the pioneering works of Refs. [2221–2223], which fully fleshed out GA's flexibility for extracting insights on the elusive DE given late-time data. This opens up GAs to the same wealth of applications ML has been applied to in cosmology, such as in the calibration of very high redshift observables [2021], non-parametric cosmological reconstructions [2215], Bayesian deep learning for DE [1994,2231,2232], and in testing the validity of routines such as the cosmographic approach [2233].

Other than ML, another broad scientific discipline where GAs are prominent is optimization, specifically under the categories of metaheuristic, nature-inspired, and evolutionary algorithms. Within this realm, GAs have various variants, such as memetic algorithms, which are designed to prevent premature convergence by incorporating local search strategies [2234]. Given their inherently distributed nature, GAs stand to benefit significantly from the advent of quantum computers and their parallelism. Quantum GAs exploit quantum mechanical phenomena such as superposition and entanglement to implement quantum evolutionary concepts and operators [2235]: quantum chromosomes, entangled crossovers, quantum elitism, etc. The quantum nature of these algorithms introduces a non-zero probability of adding new genetic material to the population, thereby mitigating premature convergence [2236].

In recent years, several quantum GAs have been developed [2236–2239], featuring either a fully quantum architecture or the integration of quantum operators within a classical GA framework. Implementing these innovative GAs on actual quantum devices has yielded enhanced performances compared to their classical counterparts, despite the limitations of today's noisy quantum hardware [2236,2238]. The first application of quantum GAs in cosmological analysis is currently underway, aiming at minimizing the chi-squared function of different cosmological probes: SNIa, baryon acoustic oscillations, CMB [2240]. This development marks a significant step forward, combining the strengths of quantum computing and GAs to tackle complex problems in cosmology.

One of the more familiar variants of GAs in the astrophysics and cosmology community is particle swarm optimization (PSO). PSO is inspired by the social behavior of birds flocking or fish schooling, where each particle (or candidate solution) adjusts its position in the search space based on its own experience and the experience of neighboring particles. The algorithm involves iteratively updating the velocities and positions of the particles, guiding them toward the best solutions found so far. This method has been used in Ref. [2241] to infer cosmological parameters given CMB data and in Ref. [2242] to calibrate semi-analytic galaxy formation models in a fixed cosmological background. PSO has been employed even earlier in astrophysics, such as in Ref. [2243] to search for periodic orbits in three-dimensional galactic potentials. Recently, the method has found application in GW analysis as seen in Refs. [2244].

It is now becoming clearer that GA and PSO approaches are only the tip of the iceberg, or perhaps an opening to Pandora's box, of mathematical optimization techniques available for astrophysical and cosmological research. The recent review by Refs. [2244] discusses several optimization methods, including particle swarm optimization, in high energy and astrophysics applications. In the following sections, we shall introduce a Bayesian tool inspired by PSO, the Approximate Bayesian Computation-Sequential Monte Carlo (ABC-SMC) [2245–2247], which has been applied recently in cosmological model selection and parameter estimation [2248,2249]. Work on a comparative study of nature-inspired optimization methods applied to cosmological parameter estimation, including MCMC, GA, Improved Multi-Operator Differential Evolution [2250], and the Philippine Eagle Optimization Algorithm [2251], is in progress, showing optimistic results for parameter estimation and cosmological reconstruction [2252].

3.4.3. GA for cosmology

In cosmology, GAs have mostly been used in the context of grammatical evolution [2221–2223]. This was motivated by the fact that the Universe's most dominant component at late-times is dark, and a non-parametric reconstruction via GA-GE seems particularly well

suited for such a problem. In grammatical evolution, one deals with a set of grammar functions, often polynomials are considered as well as trigonometric, logarithm, and exponential functions, that are exposed to the GA optimization scheme. The output of GA-GE is thus a functional approximation of the "true" function that has spawned the observed data; this can then be characterized with a fundamental model, such as ΛCDM or w_0w_aCDM CPL, if the data were cosmological in nature. Uncertainty estimation in the context of GA-GE was also studied in Refs. [2221–2223], suggesting various converging estimates by a Fisher matrix formalism, bootstrapping *a la* Monte Carlo, and a path integral approach.

Recently, GA-GE and other ML strategies were used in Ref. [2253] to draw insights from late-time expansion data. As with any ML approach, however, the output of the reconstruction via GA-GE can generally be quite dependent on the choice of the hyperparameters, for GA-GE, this would be the grammar functions. This can be put to good use if there is prior knowledge of the functional behavior of the underlying fundamental model, such as in Ref. [2254] where trigonometric grammar functions have been utilized to search for oscillating features in the primordial power spectrum. This turned out to be a promising avenue to address simultaneously the tensions in the Hubble constant and the matter power spectrum [2255,2256]. Furthermore, the GA-GE approach has been applied to SN, baryon acoustic oscillations, CC, RSD, and normalized Hubble rate measurements to symbolically reconstruct the cosmological functions in Ref. [2257], and was also used to forecast constraints on the ΛCDM model in Refs. [2258–2260].

Another way to use GAs in cosmology that has gained some traction recently is to directly use it to estimate the cosmological parameters, e.g., phenomenological DE parameters w_0 and w_a, in a given model [2224]. In this way, the uncertainty can similarly be estimated using a Fisher matrix approach or via bootstrapping, resulting in an approximation to the posterior of the cosmological parameters, that can be used with MCMC to strengthen the robustness of the analysis. We illustrate this very briefly with a quick GA computation (Fig. 66), to show the constraints obtained by GAs and MCMC in spatially-curved ΛCDM and flat CPL given cosmic chronometer measurements [2261] and SN observations [32,33,2262]. For the GA parameters, we consider the likelihood $\mathcal{L}$ as a fitness function, a "tournament" type selection with a rate of 30%, an adaptive mutation rate of $(80\%, 20\%)$, and a "scattered" crossover type with a probability of 50%. In our notation for adaptive mutation, the first number in the tuple (a, b) denotes the fraction a of the genes in a chromosome that are going to be mutated for low quality solutions (ranked accordingly by fitness), and the second number corresponds to the fraction b of chromosomes that are to be mutated for high quality ones.

In non-flat ΛCDM, it can be seen that the GA and MCMC results agree with each other on the inferred cosmological parameter space to a high degree, including correlations [2263]. The GA output population can furthermore be used to chip in to the results; as shown in this case it is also consistent with MCMC. However, in the more complex CPL model, the analogous constraints reveal a slight hint of disassociation between the results of MCMC and GA, particularly with the DE parameters. The disagreement is not to be worried about regardless since the deviations are well within the inferred confidence regions of either method. This quick exercise nonetheless shows GA in action in cosmological parameter estimation, and reinforces one of our messages that GAs can act as a supporting tool to MCMC for cosmological analysis. This is especially true for models that are more complex than ΛCDM, despite the different nature of MCMC methods that sample the posterior distribution, while GAs maximize the likelihood.

GAs and their variants have been considered in applications that assess improve the output of other methods, such as in optimizing Neural Networks [2023,2029] and speeding up Bayesian inference [1941]. Similarly ABC-SMC and GA have been applied to tackle the issue of kernel selection of GP [2264] when it is applied for cosmological reconstruction [2226,2265]; leading toward an ML hybrid that no longer depends on any one arbitrary choice of a kernel function. Furthermore, ABC-SMC has shown to be quite useful for parametric reconstruction and model selection, as shown in Ref. [2248], in the end catering to its users with one model and its parameters that best suit the data. Another notable application of GAs is given in Ref. [2266] to test the viability of an emergent universe scenario using Planck data and BBN.

3.4.4. GA for cosmological tensions

We emphasize that GAs for cosmological parameter estimation are not meant as a replacement for MCMC. GAs are rather a support tool for the traditional MCMC, offering unique advantages given its ability to navigate complex, non-linear, and high-dimensional parameter space, for example, to have faster parameter estimations and more information to define the priors of an MCMC. Subsequently, GAs can become very useful in tackling cosmological tensions and systematics, especially given the fact that biases might not be traceable by other methods. This has been teased out in recent results to be discussed.

Ref. [2254] used GAs to search for local features in the primordial power spectrum using Planck data. GAs were applied as a reconstruction tool by using its main ingredients in a grammar space of functions, such that the overall implementation looks for the most suitable parameterization of the power spectrum all while constraining the parameters of each parameterization. It resulted in significant improvements to the fit, compared with prior Planck likelihoods [2254]. Such local features were shown to be able to reduce simultaneously both the Hubble and the σ_8 tensions, giving a possible unified fundamental solution to the cosmic tensions traceable to inflation [2255,2256]. Notably, GA's capacity to break degeneracy between otherwise acceptable solutions has proven to be an invaluable lens for identifying local features in the primordial power spectrum.

On the other hand, Ref. [2267] used GAs to constrain the comoving sound horizon at the baryon drag epoch. They also checked it against traditional recombination codes or numerical fitting via the Eisenstein-Hu approach. GAs were again applied in an independent cosmological model fashion by working on grammar functions. Subsequently, GA constraints to the sound horizon at baryon drag prevented usual cosmological parameter biases that affect traditional methods. Because the Hubble constant from BAO measurements relies on constraints to the sound horizon at baryon drag epoch, GAs may well be able to help in understanding the cosmic tensions and the role of systematics. The observable is also directly influenced by the matter density, giving this a route for GA to chip into the σ_8 tension.

Ref. [2268] furthermore used GAs to test cosmology at the perturbative level. They used GAs to constrain growth rate observations, based on a synthetic ΛCDM cosmological model. GAs led easily to the reconstruction of the underlying cosmology and ruled out other often considered phenomenological and MG models including wCDM, designer $f(R)$, and the Hu-Sawicki model. This impressive application highlights another aspect of GAs — the ability to see a signal through noise, even when the noise is as huge as in growth rate observations. [2269] used GAs together with cosmological background and perturbations data, leading to a support for phantom DE behavior in the dark sector in order to alleviate the cosmic tensions.

Ref. [2249] used a GA variant ABC to pit together Hubble constant priors that are representative of the Hubble tension. This has seen the solution consistently evolve toward the direction of the Planck values, independent of the shape of the priors and the data sets (CCs, SN, and RSD) used in combination. However, this is heavily influenced by the use of CCs which were considered as a baseline data set in the analysis, since CCs prefer low values of the Hubble constant. Nonetheless, this serves as another example of when GAs can be used to choose which priors are more consistent for given data sets. An earlier work has used ABC in the same vein [2248], but in a more extensive way by using the GA variant to select between ΛCDM and phenomenological

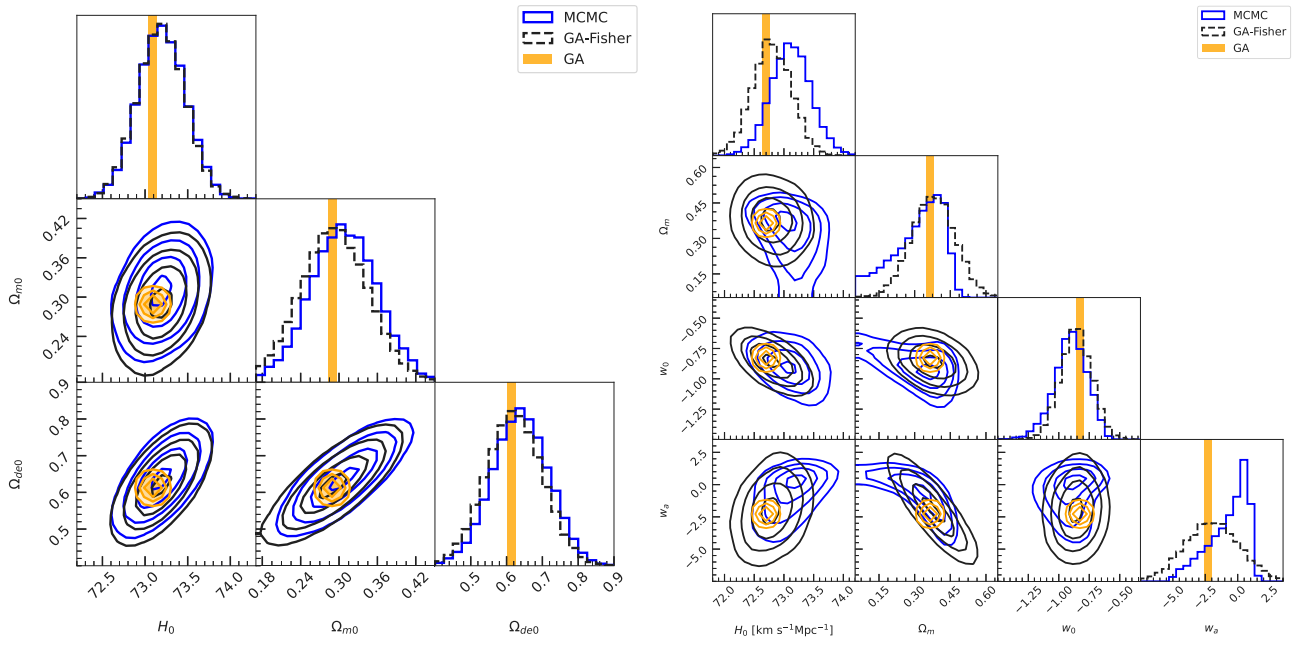

(a) Curved ΛCDM (b) CPL (w_0w_aCDM)

Fig. 66. Constraints on a spatially-curved ΛCDM and a flat CPL (w_0w_aCDM) models with CCs [2261] and SN [32,33,2262]; blue corresponds to MCMC results; black to GA-Fisher (GA Fisher matrix uncertainty estimation hybrid); orange are the localized samples (trimmed outliers) in the GA final population containing the best solution. (For interpretation of the references to colour in this figure legend, the reader is referred to the web version of this article.)

parameterizations of DE, sometimes referred to as XCDM. The results of this work have been quite intriguing, all evolved toward XCDM with a preference for Hubble constant values consistent with the Planck constraint, regardless of the choice of priors, including Hubble constant priors, and data sets considered. However, this has similarly relied on CCs as an anchor of the data, and the resulting low values of the Hubble constant may be traced to this.

Fig. 67 presents a comparison of H_0 and $S_8 = \sigma_8\sqrt{\Omega_{\rm m,0}/0.3}$ [6] constraints from MCMC, GA, and ABC-SMC using a combination of late-time data. The results highlight the ability of GAs, discussed extensively in this review, to address cosmological tensions by corroborating MCMC outcomes and even providing its own distinctive results. All cases examined show remarkable consistency between GAs and MCMC, with GAs successfully capturing correlations within the parameter space. Notably, all independent methods considered generally support a low S_8 and a high H_0, although this conclusion is contingent on the datasets used. Additionally, ABC, which compares ΛCDM and wCDM while constraining their parameters, demonstrated narrower posterior distributions compared to MCMC, particularly when the algorithm extends over numerous generations before selecting a preferred model [2248]. Nonetheless, ABC constraints remain consistent due to the method's capacity to mitigate prior dependence [2248,2249].

To sum up, GAs offer several significant advantages as they are particularly effective for solving complex optimization problems where traditional methods falter. GAs are robust and flexible, capable of finding optimal or near-optimal solutions in large, multi-dimensional search spaces. GAs are also inherently parallel, allowing to explore multiple solutions simultaneously and increase the likelihood of discovering high quality solutions efficiently. Understandably, GAs also have some disadvantages, such as computational efficiency, requiring significant processing power and time, especially for large-scale problems. Its performance also relies heavily on the choice of its hyperparameters such as population size, mutation rate, and crossover rate. Regardless, this is certainly one method that the community may find worth further investing into, for its flexibility and applicability to an incredible range of scenarios, embodied by the various ways GAs and their variants have been applied in astrophysics and cosmology.

When looking for a needle in a haystack, one may turn to MCMC to identify the most probable region where the needle could be. Reversely, one may turn to GAs to identify this needle, systematically sifting through the haystack and evolving toward the solution with precision and persistence. This needle may well be the solution to the cosmic tensions, if not a huge hint to this cosmological conundrum.

3.5. *Inference from cosmological simulations*

Coordinator: Lei Zu

Contributors: Alan Heavens, Andrew Liddle, Anto Idicherian Lonappan, Antonio da Silva, Benjamin L'Huillier, Chi Zhang, Daniela Grandón, David Benisty, Elena Giusarma, Filippo Bouchè, Houzun Chen, Jenny G. Sorce, Jenny Wagner, Jurgen Mifsud, Luz Ángela García, Marika Asgari, Nikolaos E. Mavromatos, Oleksii Sokoliuk, Ruth Lazkoz, Vasiliki A. Mitsou, and Wojciech Hellwing

In this section, we explore cosmological simulation and their connection to cosmological tensions. We begin by introducing the role of cosmological simulations in modeling nonlinear scale physics and the relevant tools. Next, we examine how cosmological simulations serve as a powerful tool for investigating physics beyond the ΛCDM. Finally, we discuss key observations and associated tensions at small scales, showing how cosmological simulations bridge theoretical predictions and observational data.

3.5.1. *Cosmological simulation*

When studying the large-scale structure evolution of the Universe, the density perturbation $\delta = \frac{\delta\rho_{\rm m}}{\rho_{\rm m}}$ becomes much greater than unity ($\delta \gg 1$) at small scales like $k \gtrsim 1$ h/Mpc. In this nonlinear regime, linear perturbation theory fails to accurately describe the evolution of structures. To overcome this limitation, N-body simulations, a particle based method, are employed to model the behavior of phase space particles-representing a group of DM particles within a given cosmological

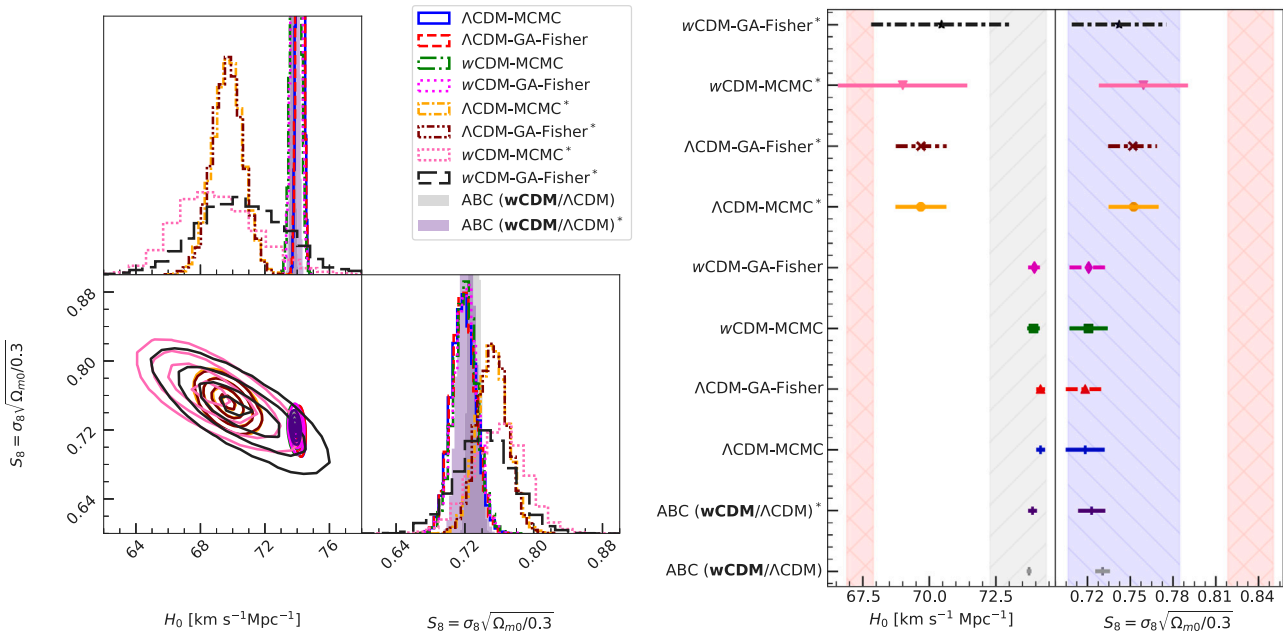

Fig. 67. H_0 and $S_8 = \sigma_8\sqrt{\Omega_{m,0}/0.3}$ constraints on a spatially-flat ΛCDM and wCDM models using MCMC, GA, and ABC. Data sets used are CCs [2261], standardized distances (Pantheon+ /SH0ES [32,33,2262]), growth rate measurements (compiled in Ref. [2270]), and baryon acoustic oscillations (DESI year-1 [699]). Red vertical bands are from Planck [192], blue from KiDS-450 [697,850,858,903], and gray from Ref. [34]. An asterisk in the superscript in the label denotes that the Pantheon+ /SH0ES data was not considered. In the ABC label, the bold faced model is the preferred one. (For interpretation of the references to colour in this figure legend, the reader is referred to the web version of this article.)

framework. Additionally, some cosmological simulations incorporate hydrodynamics to account for the effects of baryons. These simulations produce detailed predictions of structure formation, enabling direct comparisons with observational data. While computationally intensive, cosmological simulations are essential for understanding the Universe at scales dominated by nonlinear effects. They serve as a critical link between theoretical cosmological models and observations. By providing insights into nonlinear physics, cosmological simulations play a pivotal role in addressing tensions between the standard ΛCDM model and observational data.

3.5.2. Nonlinear effects

N-body simulations describe structure formation at scales dominated by the nonlinear effects of gravity. In these simulations, "particles" represent DM, characterized by properties such as mass, position and velocity. The initial conditions for these simulations are derived from theoretical models of the early Universe, typically set at high redshifts ($z \sim 100$) when the Universe was nearly homogeneous. On small scales like $k \gtrsim 10$ h/Mpc, hydrodynamic effects become significant. The inclusion of hydrodynamics is necessary in simulations to accurately capture the influence of baryonic processes. **GADGET** (GAlaxies with DM and Gas intEracT) is one of the most widely used N-body and hydrodynamics simulation codes [2271–2273]. It combines N-body methods for gravitational interactions with Smoothed Particle Hydrodynamics (SPH) for modeling gas dynamics, enabling the study of both collisionless systems (e.g., DM) and hydrodynamic phenomena. Building on **GADGET**, other advanced codes have been developed, such as **AREPO** [2274], which uses a moving mesh approach instead of SPH, and **GIZMO** [2275], which replaces modern SPH with a mesh-free hydrodynamics solver for improved accuracy. **SWIFT** is also a fully open-source highly-parallel, versatile, and modular coupled hydrodynamics, gravity, cosmology, and galaxy-formation code [2276]. In addition, Adaptive Mesh Refinement based codes such as **RAMSES** (Refined Adaptive Mesh with Static Expansion) [2277] are also extensively used for cosmological and astrophysical simulations. Due

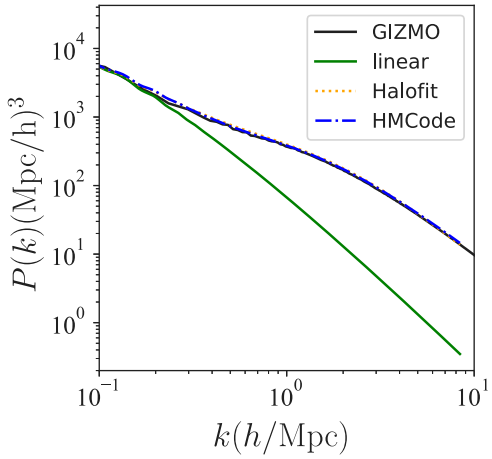

Fig. 68. The matter power spectrum with the same ΛCDM cosmological parameters for $k \sim 0.1$–10 h/Mpc at $z = 0$. The green solid line shows the linear results. The black solid line represents the N-body simulation results by using the publicly available code **GIZMO** while the orange dotted (blue dash-dotted) line is calculated by the nonlinear analytical code Halofit (HMCode). (For interpretation of the references to colour in this figure legend, the reader is referred to the web version of this article.)

to the computational intensity of high-resolution simulations, several groups have made their results publicly available. Examples include the **Millennium Simulation** [2278], **Horizon Run Simulations** [2279], **Illustris and IllustrisTNG** [2280,2281], **Bolshoi Simulation** [2282], **EAGLE** [2283,2284], **Quijote Simulations** [2285]. Researchers can utilize these simulated results for their own science targets.

Using some N-body simulation results as benchmarks [1021,2286], several semi-analytic models are developed to predict the nonlinear matter power spectrum, such as Halofit [889,890] and HMCode [891, 2287]. These semi-analytic models significantly reduce computational

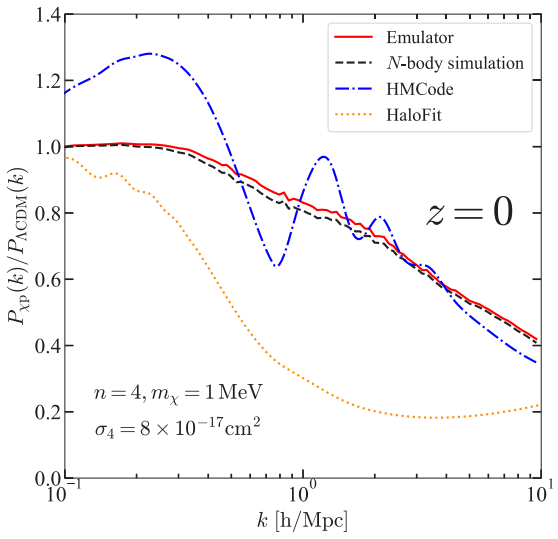

Fig. 69. The ratio of the nonlinear matter power spectrum at $z = 0$ in DM-proton scattering scenario [2290]. The red solid lines denote the emulator developed in Ref. [2290], the black dashed lines are the N-body simulation results from GIZMO, the blue dashed-dotted lines are the correction from HMCode and the orange dotted lines are the correction from HaloFit.

time while remaining applicable across a wide range of cosmological parameters. Halofit employs simulation results to construct fitting formulas, while HMCode, a refined version of the halo model, introduces modifications that enhance its consistency with simulation outcomes. Additionally, ML techniques have been increasingly applied as emulator to predict nonlinear structure formation. For example, the **Quijote Simulations** have been widely employed in ML applications for cosmology, providing large-scale training datasets for deep learning models aimed at improving parameter inference and nonlinear structure formation predictions [2288,2289].

Fig. 68 shows the matter power spectrum in the standard ΛCDM model for $k \sim 0.1$–10 h/Mpc at $z = 0$. The linear matter power spectrum (green solid line) significantly underestimates the power at nonlinear scales $k > 0.1$ h/Mpc. Nonlinear results from N-body simulations (black solid line, GIZMO) align closely with analytical models such as Halofit (orange dotted line) and HMCode (blue dash-dotted line). Within the ΛCDM framework, both Halofit and HMCode achieve accuracy within 10% compared to the N-body simulation. HMCode also exhibits superior performance when incorporating extensions beyond ΛCDM, such as baryonic feedback, WDM, massive neutrinos, DDE, and MG [891, 2287]. However, if the initial matter power spectrum or the late-time dynamical evolution significantly deviates from the ΛCDM scenario, the reliability of HMCode predictions is doubtful. As shown in Fig. 69, when addressing new physics beyond ΛCDM, at nonlinear scales, both HMCode and Halofit fail to provide accurate nonlinear corrections, see Ref. [2290] for details. In such cases, conducting cosmological simulations correctly becomes essential to study the structure evolution in the specific model.

3.5.3. Cosmological simulations beyond ΛCDM

To explore new physics beyond the ΛCDM framework at nonlinear scales, various groups have developed cosmological simulations in different cosmological scenarios. One of the most studied extensions is the WDM model. The free-streaming motion of WDM, due to its thermal velocity, suppresses structure formation on small scales. Numerous cosmological simulations of WDM [1722,2291–2293] have investigated the resulting mass distributions and halo properties. These studies reveal suppressed mass distributions below a scale determined by the mass of WDM particle, and shallower density slopes systematically compared to CDM.

Another critical area of interest is the total mass of neutrinos, which influences the evolution of the total energy density and introduces free-streaming effects. Several studies have incorporated massive neutrinos into cosmological simulation codes using additional particle sets or relativistic approaches [2294–2296]. A higher total neutrino mass results in a stronger suppression of the matter power spectrum at small scales. For instance, the suppression of the total matter power spectrum at $k \sim 1$ h/Mpc is approximately 5% for $m_\nu = 0.06$ eV, and increases to 25% for $m_\nu = 0.3$ eV, see Ref. [2295] for details.

In addition to neutrino effects, cosmological simulations have also been extended to study alternative gravity models and DE effects beyond CDM. Various computational tools have been developed to simulate structure formation under MG theories, including ECOSMOG [2297], MG-GADGET [2298], ME-GADGET [2299], and MG-AREPO [2300], MG-PCOLA [2301], MG-QUIJOTE [2302]. ECOSMOG incorporates MG models, including $f(R)$ gravity, chameleon models, and symmetron theories, using an AMR framework to achieve high-resolution nonlinear simulations. ME-GADGET allows for an arbitrary phenomenological (with varying $H(a)$ and $G_N(a)$) and IDM (with varying $m_{DE}(a)$) models to be used in the gravity-only simulation setting. MG-PCOLA is a fast N-body solver extending the COLA method to MG, balancing speed and accuracy for large-scale structure studies. Recent MG-PCOLA simulations incorporating massive neutrinos reveal that their inclusion leads to additional suppression of structure growth. In particular, in scalar-tensor models, this suppression enhances the damping of small-scale power beyond what is expected from standard neutrino free-streaming, reinforcing the interplay between neutrinos and MG. MG-QUIJOTE is a large suite of MG simulations tailored for ML applications and parameter inference, covering various MG scenarios and offering a benchmark dataset for cosmological studies.

Furthermore, if DM has additional non-gravitational interactions — for instance, with baryons/electrons [2290,2303,2304], neutrinos [2305–2307], or dark radiation [2308–2310] — this will introduce additional pressure that suppresses small-scale structure formation. These interactions modify the Boltzmann equation in the early Universe by adding energy and momentum exchange terms, creating a pressure that counteracts gravitational collapse. This suppression occurs primarily during the early Universe, when matter densities are high enough to trigger collisions. As the Universe expands, the interaction rate falls below the Hubble rate, i.e., DM decouples. After that, the interactions become negligible on galactic scales. Thus the primary deviations between IDM and CDM arise during the early Universe, influencing the initial conditions for structure formation. A common approach involves calculating the linear evolution of the matter power spectrum first, including DM interactions, during the early phase when density perturbations remain small and linear theory is applicable. These results are then used as initial conditions (at $z \sim 100$) for later cosmological simulations when DM interactions can be neglected. Notably, interactions often imprint unique oscillation features in the initial power spectrum, similar to those observed in baryons. However, these oscillations diminish during nonlinear evolution as the Universe evolves. As a result, these distinctive oscillation structures are expected to be observable primarily at high redshifts [2290,2310,2311].

3.5.4. Cosmological simulations in nonlinear observation and cosmic tension

Cosmological simulations model particle behavior and predict DM properties at nonlinear scales, providing a crucial tool for comparing theoretical predictions with observations such as WL, Lyman-α, halo density profile, upcoming cosmic 21 cm, and so on. Various discrepancies between ΛCDM model and observations have emerged at different scales, including the S_8 tension, core-cusp problem, too-big-to-fail problem, the diversity of dwarf galaxy rotation curves, missing satellites problem, and so on. Cosmological simulations serve as a

powerful bridge between theory and observations, helping to address discrepancies and exploring the physics beyond standard ΛCDM. In this section, we discuss key nonlinear observations and the related tensions between ΛCDM and the measurements.

3.5.4.1. Weak lensing. WL provides a direct method for mapping the late-time large-scale structure of the Universe by statistically analyzing the shape distortions of numerous background galaxies induced by foreground matter fields. By calculating the two-point correlation functions of the shapes of galaxy pairs, WL measurements have widely been used for exploring the matter distributions in our local Universe. WL is sensitive to the scale down to $k \gtrsim 1$ h/Mpc at low redshift(typically $z < 2$), where nonlinear gravitational evolution significantly affects the matter power spectrum [855,856,860,862,869]. On smaller scales ($k \gtrsim 10$ h/Mpc), baryonic processes, such as gas cooling, feedback from star formation, and AGN, leading significantly systematic uncertainties to WL measurement. To mitigate uncertainties in baryonic physics, many analyses mask or marginalize over these small-scale regions [862,869, 989]. Several other approaches have been developed to address this uncertainty. For example, one method that preserves small-scale measurements is the Bayesian Model Averaging (BMA) framework presented in Ref. [849]. In this approach, BMA combines the individual posterior distributions of multiple competing baryonic feedback models derived from hydrodynamical simulations to provide robust cosmological constraints. Furthermore, the nonlinear evolution of cosmic structures at late-times introduces strong non-Gaussianities in the matter density field, requiring estimators beyond two-point functions to capture this additional information [829]. These estimators, often referred to as higher-order or non-Gaussian statistics, are useful for breaking parameter degeneracies [2312,2313], self-calibrating systematics [983], and overall improving cosmological constraints compared to two-point functions [837,842,844,847,2314,2315]. The theoretical modeling of these estimators relies heavily on cosmological simulations, both to characterize their dependence on cosmological parameters and to build the likelihoods, where the covariance matrix is typically estimated from hundreds of simulations at a fixed cosmology [883]. An alternative to adding estimators of higher-order statistics is to use the full information from the field using Bayesian hierarchical modeling, e.g., see Ref. [2316–2320], or Bayesian simulation-based inference based on neural compression of the field, e.g., see Ref. [2321,2322], which avoid the need to estimate covariance matrices. Both these approaches rely heavily on simulations. We refer the reader to Section 2.1 for a detailed discussion on WL.

In ΛCDM framework, WL surveys have reported an S_8 tension (see Section 2.1 for details): the S_8 parameter measured from WL survey is lower than the value inferred from Planck CMB data, with a significance of 2-3σ [859,869,2323]. Despite some uncertainties in observational measurements, various beyond ΛCDM models have been proposed to address this issue, such as suppressed small-scale matter power due to interactions between DM and dark radiation [2310,2324–2326], DM-baryon interactions [2327], or DM-neutrino scattering [2328,2329]. Cosmological simulations play a crucial role in addressing these issues. Upcoming more precise large scale surveys like Vera C. Rubin Observatory [897], Euclid [437] and China Space Station Telescope (CSST) [2330] are expected to provide crucial insights and help resolve these tensions.

3.5.4.2. Lyman-α forest. Lyman-α forest refers to a series of absorption lines observed in the spectra of distant QSOs. These lines are caused by the interaction of light from the QSO with intervening clouds of neutral hydrogen gas along the line of sight. As a result, the Lyman-α forest is widely used as a tracer of neutral hydrogen gas distribution and, by extension, the underlying matter distribution, assuming a correlation between mass and neutral gas. The Lyman-α forest probes the matter power spectrum in the mildly nonlinear regime over a broad range of redshifts, down to scales of 1–80 h/Mpc (at $z = 2 - 6$ in ground-based observation) [2331–2333]. Compared to WL surveys, the Lyman-α forest is sensitive to smaller scale structures at higher redshifts. Since the Lyman-α forest mainly traces the IGM in the cosmic web, directly correlated with the neutral hydrogen gas distribution, its signal is highly influenced by the baryonic physics [2334]. High-precision hydrodynamical simulations that accurately account for baryonic physics are essential for studying the Lyman-α forest. Using these simulation results, researchers can investigate physics beyond the ΛCDM, including WDM [1550,1553,2333,2335], fuzzy DM [1551,1563,2336] and neutrino mass [2337,2338]. Recent simulations suggest that small tensions may exist between ΛCDM cosmological simulation and Lyman-α observation (see Section 2.3.8 for the anomalies in Lyman-α measurements), which can be explained by mechanisms such as the dark photon heating or DM-neutrino interaction [2339,2340]. An improved understanding of baryonic physics is crucial to addressing these issues and refining our interpretation of Lyman-α observation.

3.5.4.3. Cosmic 21 cm. The cosmic 21 cm signal refers to the hyperfine transition of neutral hydrogen atoms, which emits or absorbs radiation at a wavelength of 21 cm (frequency of 1.42 GHz). This signal is a powerful tool for probing the evolution of the Universe at high redshift, across a wide range of cosmic epochs, from the Dark Ages (prior to star formation) to the EoR and beyond [2341,2342]. The 21 cm signal traces the distribution of matter and can map the evolution of large-scale structures over cosmic time. Although the angular resolution of the 21 cm signal is limited to tracing ionized bubbles on scales of several Mpc, which corresponds to very large structures, it remains a powerful tool for exploring the nonlinear scale structure. The small scale structure significantly impacts the halo collapsing. In general, any model that suppresses or modifies the amplitude of DM fluctuations on small scales could affect the 21 cm cosmic dawn signal. Several previous works have discussed using the future cosmic 21 cm data to probe the physics beyond ΛCDM [2343–2348]. One key advantage of the cosmic 21 cm signal is its ability to trace the mass distribution at very high redshifts, where the original information is preserved due to limited impact from structure formation [2311,2349]. By modeling the dynamics of DM and the feedback of baryons, cosmological simulations play a pivotal role in understanding and interpreting the cosmic 21 cm signal [2311,2348,2350]. Upcoming cosmic 21 cm observations, such as the Low-Frequency Array (LOFAR) [2351], the Hydrogen Epoch of Reionization Array (HERA) [2352], and the SKAO [2353], are expected to open a new window into the high redshift Universe and provide novel insights into the nature of DM.

3.5.4.4. Dwarf galaxy scale puzzles. At small scales, such as those of dwarf galaxies, significant tensions exist between predictions from N-body simulations and observational data [2354]. Several key discrepancies are summarized below:

Core-cusp Problem Gravity only N-body simulations of DM in a CDM Universe predict that DM halos should have a "cusp" — a sharp rise in density toward their center, known as Navarro–Frenk–White profile, or NFW [2355]. However, observations of low-mass galaxies of different luminosity and morphology [358] indicate that their DM halos instead have a core, a central region with nearly constant density [2356,2357].

Diversity Problem for Rotation Curves Simulations predict that galaxies with the same maximum circular velocity should have similar halo density profiles. However, observations reveal a significant variation in the central densities of these galaxies [2358, 2359].

Missing Satellites Problem Simulations predict a large number of small DM halos, but observations show a much smaller number of dwarf satellite galaxies around larger galaxies, such as the MW [2360,2361].

Too-Big-to-Fail Problem The number of massive DM subhalos predicted by simulations is inconsistent with the number of observed bright satellite galaxies in systems like the MW [2362, 2363].

These small-scale issues highlight a disconnect between N-body simulations and observations, particularly in our local group. They suggest that gravity-only CDM N-body simulations are insufficient to fully describe the Universe on these scales. Several hypotheses have been proposed to resolve these discrepancies, involving both astrophysical processes and modifications to the standard ΛCDM model. Stellar and supernova feedback can redistribute baryonic matter, influencing the gravitational potential and altering the density profile of the DM and the halo mass function [2364,2365]. The feedback process can also eject gas from massive subhalos, suppressing star formation to explain the too big to fail problem [2366–2370]. Another way to solve this small-scale puzzle requires modifications to ΛCDM. Several models have been proposed such as Self-Interacting DM (SIDM) [2082] and fuzzy DM [2371]. SIDM introduces DM-DM interactions that redistribute energy, forming cores in halos, and leading to more diverse halo density profiles and a different subhalo mass function. N-body simulations incorporating SIDM have been used to test these predictions and compare them with the observations. Many SIDM simulations were performed and used to discuss the DM halo distribution after the first proposal [2372–2377]. Early studies constrained the SIDM cross section through observations, such as strong lensing [2378]. The results show that the parameter space for the SIDM model to solve the small scale problem have already been constrained. However, subsequent simulations with higher resolution and improved algorithms revealed that earlier constraints may have been overestimated [2379–2382]. For fuzzy DM, the introduction of ultra-light bosons with kiloparsec-scale wavelength naturally suppresses structure formation at these scales. Unlike classical particles, fuzzy DM behaves more like a wave, requiring the solution of quantum-mechanical wave equations in N-body simulations. Studies have shown that fuzzy DM naturally forms solitonic cores at the centers of halos due to quantum pressure while simultaneously suppressing small-scale structure formation as a consequence of the uncertainty principle [2383–2385]. This provides a compelling explanation for the core-cusp problem and the missing satellites problem. For now, resolving small-scale issues remains an ongoing challenge, as both baryonic feedback processes and alternative DM properties beyond CDM have their own strengths and limitations. High-resolution cosmological simulations, combined with advanced algorithms to incorporate baryonic physics and additional DM interactions, provide a crucial tool for understanding these small-scale puzzles. These simulations become a bridge between the theoretical predictions from proposed models and the observational data. They help us better understand the existing cosmological tensions.

3.6. Profile likelihoods in cosmology

Coordinator: Adrià Gómez-Valent

Contributors: Elisa G. M. Ferreira, Emil Brinch Holm, Giacomo Galloni, Laura Herold, Paolo Campeti, Sophie Henrot-Versillé, Vivian Poulin, and William Giarè

3.6.1. Motivation

In cosmology, it is very common to encounter high-dimensional parameter spaces. Efficient exploration of these spaces through the sampling of their corresponding multivariate distributions is commonly achieved using Monte Carlo techniques. In these analyses, statistical information is contained in the resulting MCMC, from which one can infer the posterior distribution and other derived Bayesian products. In parameter spaces of dimension greater than two one cannot visualize the posterior distribution in the original parameter space. One needs to apply the so-called marginalization technique to project the results into spaces of lower dimension and compute the marginalized posterior distributions of the individual parameters and their constraints at the desired confidence level. This is also done to obtain the contour plots in all the two-dimensional planes of interest. Marginalization is extremely efficient and is a very practical tool that eases the visualization and interpretation of the results in Bayesian analyses. However, when the original (non-marginalized) PDF has non-Gaussian features, the marginalized posterior distributions obtained do not exclusively reflect how the parameters are distributed based on their ability to explain the data but also according to their integrated probability weight. This introduces volume (or marginalization) effects, which can potentially bias conclusions in a significant way. In other words, if deviations from Gaussianity are large, the marginalized posterior can hide points in parameter space that fit the data well. Another potential drawback of the marginalization method is the impact of the prior, which, even if assumed to be flat, is still informative in all cases. For instance, a flat prior on a variable x or on its logarithm, $\log x$, might induce important changes in the constraints of a model, even if the boundaries of the priors are perfectly consistent. This is due to volume effects, again. Hence, volume effects can significantly impact the interpretation of results extracted from MCMCs. Detecting these biases is of utmost importance. In the context of cosmology, accurately quantifying these biases is essential, e.g., for a correct assessment of cosmological tensions in the ΛCDM model and beyond, as well as in data compression performed by galaxy and WL surveys, see Section 3.6.4 for details.

A mismatch between the point in parameter space that maximizes the original posterior distribution and the point constructed with the values of the parameters that maximize the individual one-dimensional posteriors already hints at the non-negligible impact of marginalization effects. One can investigate the impact of marginalization effects using the profile likelihood (PL). The PL is a method from frequentist statistics to construct parameter intervals, and therefore, by construction inherently independent of a prior. It ensures, in particular, that the results (on the parameter inference) do not depend on the choice of the parameterization of the problem. This part of the work aims to explain the basics of PLs and is organized as follows. In Section 3.6.2 we describe how to build confidence intervals using PLs. In Section 3.6.3 we describe several methods to compute them, both approximately from the MCMCs or, more precisely, using advanced numerical optimization techniques with the help of concrete codes. Finally, in Section 3.6.4 we give some examples of applications of the PLs in cosmology, providing a rich list of references.

3.6.2. Confidence intervals from profile likelihoods

While Bayesian credible intervals are statements about the degree of belief of the value of the true parameter, frequentist confidence intervals are based on the *coverage*: frequentist confidence intervals are said to *cover* the true value of the parameter with a confidence level α if — after repetition of the experiment — a fraction α of the experiments contain the true value of the parameter (e.g., see Ref. [1467] for a review, or Ref. [2386] in the context of cosmology). Confidence intervals with correct coverage can be constructed using the *Neyman construction* [2387]. This construction requires knowledge of the full PDF $P(\hat{\boldsymbol{\mu}}|\boldsymbol{\mu}_{\rm true})$, where $\hat{\boldsymbol{\mu}}$ are the maximum likelihood estimates (MLE) of the model parameters $\boldsymbol{\mu}$ estimated from observations and $\boldsymbol{\mu}_{\rm true}$ the (hypothetical) true values of these parameters. Since this probability is typically not known a priori, it needs to be estimated by generating mock realizations of the data. This makes the Neyman construction computationally expensive. Fortunately, a theorem by Wilks [2388] helps in many practical applications, which states: In the limit of a large data set, the log-likelihood ratio

$$\Delta\chi^2 = -2\log R(\boldsymbol{x},\boldsymbol{\mu})\,, \qquad R(\boldsymbol{x},\boldsymbol{\mu}) = \frac{\mathcal{L}(\boldsymbol{x}|\boldsymbol{\mu})}{\mathcal{L}(\boldsymbol{x}|\hat{\boldsymbol{\mu}})}\,, \tag{3.29}$$

follows a χ^2-distribution. Here $\mathcal{L}$ is the likelihood function and $\boldsymbol{x}$ is the data vector. In this case, the Neyman construction can be replaced by a much simpler *graphical construction* based on the profile likelihood. Wilks theorem holds trivially if the p.d.f. is Gaussian (for every possible value of the true parameters). We note, however, that Wilks' theorem holds for the full-dimensional likelihood (for any possible value of the true parameters) and not the profile likelihood. Although this effect vanishes in the large data limit, it is often very difficult to assess whether this limit is reached in practice [2389], and the confidence intervals are, therefore, only approximate (see Ref. [2386] for checks of the asymptotic assumptions in cosmology).

The profile likelihood for a parameter of interest μ (in one dimension) can be obtained by evaluating Eq. (3.29) for different values of μ. In the presence of other cosmological parameters and nuisance parameters, $\boldsymbol{\nu}$, the profile likelihood is calculated by setting μ to various values within a range of interest and minimizing $\chi^2(\mu, \boldsymbol{\nu}) = -2\log\mathcal{L}(\mu, \boldsymbol{\nu})$ with respect to all parameters $\boldsymbol{\nu}$. The global MLE, or "best-fit", corresponds to the minimum value $\chi^2_{\rm min}$ by design. A graphical frequentist confidence interval for μ can now be constructed using the difference $\Delta\chi^2(\mu) = \chi^2(\mu) - \chi^2_{\rm min}$. When μ is far from its physical boundary, a confidence interval at confidence level α is obtained by applying a fixed threshold $\Delta\chi^2_{\rm th}$ to $\Delta\chi^2(\mu)$. This threshold is chosen such that the cumulative distribution function of the χ^2 distribution with one degree of freedom equals α. Notable values are $\Delta\chi^2_{\rm th} = 1$ for 68% CL and $\Delta\chi^2_{\rm th} = 3.84$ for 95% CL [2390]. This method is applicable to both parabolic (i.e., for a Gaussian-distributed parameter) and non-parabolic $\Delta\chi^2(\mu)$ because of the invariance of the MLE under reparameterization.

When the parameter estimate is near its physical boundary, the conventional graphical profile likelihood construction for frequentist confidence intervals can be inadequate. It may result in empty intervals and fail to maintain the frequentist coverage property if the choice between an upper limit or a two-sided interval is made based on the data (the so-called "flip-flopping"). An adapted Neyman construction, also known as Feldman-Cousins (FC) prescription [2391] in the particle-physics literature, addresses these issues. To describe this method, we restrict the discussion to one-dimensional data x and a single model parameter μ for clarity. For each value of μ (with an unknown true value) and each observable x, we compute the likelihood ratio $R(x, \mu)$, with μ (and its MLE $\hat{\mu} \equiv \mu_{\rm best}$) restricted to its physically allowed values. The *confidence belt* at the desired CL α is constructed by selecting an *acceptance interval* $[x_1, x_2]$ for each μ satisfying

$$\begin{cases} R(x_1, \mu) = R(x_2, \mu)\,, \\ \int_{x_1}^{x_2} P(x|\mu)\, dx = \alpha\,, \end{cases} \tag{3.30}$$

where $P(x|\mu)$ is the p.d.f. of x given μ, and values of x are added to the acceptance interval in order of decreasing likelihood ratio. The confidence belt is formed by the union of all acceptance intervals $[x_1(\mu), x_2(\mu)]$. Intersecting the confidence belt with a line at $x = x_0$, where x_0 is the value of x minimizing χ^2 (i.e., the value observed in an experiment), yields the confidence interval $[\mu_1, \mu_2]$ for μ. The adapted Neyman or FC prescription provides a method to determine the endpoints of confidence intervals, which smoothly transitions between an upper limit and a two-sided interval, ensuring exact frequentist coverage even for parameters with non-Gaussian p.d.f.'s (and if Wilks' theorem does not hold). This is in contrast to the conservatism (over-coverage) inherent in Bayesian limits in the same context [2391,2392]. While overcoverage might not be as problematic as undercoverage, it reduces the ability to reject false hypotheses. This highlights the value of examining frequentist intervals.

If the p.d.f. of the parameter is Gaussian and the MLE of the parameter near a physical boundary at $\mu = 0$, then $\mu_{\rm best} = \max(0, x)$ and the likelihood ratio in simply becomes [2391]

$$R(x, \mu) = \begin{cases} \exp(-(x-\mu)^2/2), & \text{for } x \geq 0\,, \\ \exp(x\mu - \mu^2/2), & \text{for } x < 0\,, \end{cases} \tag{3.31}$$

where x and μ are in units of σ, the width of the parabolic fit to $\Delta\chi^2(\mu)$. Then, the confidence interval can be derived by solving Eq. (3.30), with $P(x|\mu)$ being a Gaussian with mean μ and unit variance. If, however, the p.d.f. of the parameter is non-Gaussian and Wilks' theorem does not hold, a full Neyman construction of the confidence intervals using simulations for several input values of the parameter of interest is necessary, e.g., see Ref. [2393,2394] for details.

With the necessary modifications, this entire treatment can be generalized to multiple dimensions. For example, under the assumption of Gaussianity, the iso-χ^2 curves for a two-dimensional case will be ellipses on the parameter space, whose angle of the major axis depends on the correlation of the two parameters of interest. Furthermore, if no physical boundary is close to the absolute minimum of χ^2 and if we consider the limit of a large data set, it is possible to adopt a graphical approach to derive the 68% and 95% confidence regions, as we mentioned for the one-dimensional case. This time, one must search for $\Delta\chi^2_{\rm th} = 2.3$ for 68% CL and $\Delta\chi^2_{\rm th} = 5.99$ for 95% CL regions. Similarly to the one-dimensional case, if Wilks' theorem does not hold, one should adopt a full Neyman construction to extract the confidence regions.

3.6.3. Calculation of profile likelihoods

Computing a profile likelihood for a single parameter involves a series of M optimizations, typically with $M \sim \mathcal{O}(10)$, in the $N-1$ dimensional parameter space. Furthermore, these cannot be reused for profiles in other parameters, unlike an MCMC, which simultaneously produces parameter constraints for all varied parameters. Since the optimizations themselves are moderately difficult, constructing a full profile likelihood analysis of several parameters can be very computationally demanding. In this subsection, we present some of the strategies adopted in the literature to accommodate the often high computational cost of computing profile likelihoods.

3.6.3.1. Optimization strategies. A converged set of MCMC chains of course contains information about the likelihood values at a large number of points in parameter space. Although MCMC algorithms are poor optimizers [1974], they can be used to estimate profile likelihoods by binning their points along the parameter θ being profiled. The bin around a fixed value of $\theta = \theta_0$ can be defined, for example, by a homogeneous central binning, as is done in Refs. [1944,1976,2395–2397], or by taking the n points of the MCMC that have a value of θ closest to the fixed value θ_0, as done in Ref. [2398], with n a fixed fraction of the total amount of MCMC points. Due to the finite sampling of the MCMC, the largest likelihood value found in each bin will generally be smaller than its optimized value at θ_0, which leads to noise in the profile likelihood curve. The great advantage of this approach, however, is that it has no computational cost if an MCMC is already given, so it can be used as an inexpensive initial test to check for marginalization and prior effects [1976], see also Ref. [2396]. Furthermore, such a profile can be used as the starting point for explicit optimizations at each fixed value of the profiled parameter.

When the binned MCMC is not adequately accurate, the profile likelihood can be computed by explicit optimization in the parameter subspace with the profiled parameter taking on a series of fixed values. Generally speaking, the most efficient optimization algorithms explore the parameter space for the highest likelihood value by using the gradient of the likelihood with respect to parameter space. Examples of such gradient-based optimizations algorithms often used in cosmology include the MIGRAD optimizer of the MINUIT package, which is a variable metric algorithm using the finite-difference estimates of the first derivative of the likelihood function [2399]. Refs. [2400–2404], amongst others, used MINUIT to construct profile likelihoods and found it to be computationally efficient.

In some cases, however, the cosmological likelihood functions are noisy, for example, due to approximation switching in the underlying theory code or insufficient precision settings, leading to inefficiency

in the gradient-based algorithms. For example, Refs. [710,1969,2397, 2405] found that gradient-free methods outperformed the gradient-based ones. The most popular gradient-free method employed in the literature is simulated annealing [2406], which works by running an MCMC using the modified likelihood $\tilde{L} \equiv L^{1/T}$ with an iteratively decreasing temperature T. The decreasing temperature enhances the peak structures in the likelihoods and eventually traps the MCMC close to the best fit. Simulated annealing has been used for profile likelihood construction in Refs. [1959,1967–1970,1972,1977,2397,2398], amongst others. Unfortunately, simulated annealing is very sensitive to its hyperparameters, which include the initial point of the optimization, the covariance matrix of the proposal distribution of the MCMC, and the rate at which the temperature decreases. Broadly speaking, three approaches have been suggested to inform the initial point and covariance matrix:

- *Running fixed-parameter MCMCs to obtain information.* Refs. [1967–1969] run individual MCMCs for each fixed value of the profiled parameter and use the best fit and covariance matrices of their chains in the optimization. This method produces great initial points and local covariance matrices, although with the disadvantage of the added computational cost of running the additional MCMCs.
- *Using information from an existing MCMC.* The CAMEL [2407] and PROSPECT codes [2398] assume the user to have a converged MCMC in the full parameter space before constructing the profile. Using this, it uses the binned MCMC profile likelihood estimate discussed in the preceding subsection, and furthermore constructs individual covariance matrices from the points in each bin. This method usually gives great initial points and local covariances matrices, but can be sensitive to the quality of the initial MCMC.
- *Optimizing the profile sequentially and reusing information from previous optimizations.* The Procoli code [2397] also assumes the availability of a converged MCMC at the beginning and uses its maximum a posteriori point and covariance matrix to find the global best fit. Procoli then carries out optimizations at equidistant points along the profiled parameter direction sequentially, using the result of the previous iteration as the initial point of the next. This method yields great initial points, at the sacrifice of the parallelization of the optimizations.

3.6.3.2. Publicly available profile likelihood codes. At the time of writing, there exist several publicly available tools for computing profile likelihoods in cosmology; here, we present them in order of the recency of their release.

- cobaya fork [2400]: Can be used with cobaya [1918]. Initializes points from an existing MCMC as described above. Usable as a sampler inside cobaya, making it easy to use if an MCMC has already been run with cobaya.[43]
- Procoli [2397]: Can be used with MontePython [1916,1917]. Uses the sequential strategy described above. Additionally allows for the extraction of individual χ^2 values for each experiment used in the data.[44]
- Prospect [2398]: Can be used with MontePython and cobaya. Uses an assumed precomputed MCMC as initialization, as described in the last section. Introduces an automatic step size tuning scheme, and comes with a snapshot checkpoint scheme that enables efficient parallelization and inspections of the run.[45]
- Camel [2407]: Code written in C++. The minimization algorithm is based on MINUIT [2399].[46]

All of the above codes (except Camel) work directly with the cosmology-specifying parameter files of MontePython or cobaya, respectively, that have been used, for example, in a complementary Bayesian analysis. They therefore also work with the theory codes already available in these, such as CLASS [1949] and, in the case of cobaya, CAMB [1948]. They also employ the GetDist code [1952] for analysis.

While the brute-force computation of full triangle plots of profile likelihoods, analogous to the most common product of the Bayesian analysis, is computationally unfeasible, future advances in gradient-based inference and emulators of likelihood codes are expected to make extensive profile likelihood analyses more broadly available. For example, already available is the neural network emulator CONNECT[47] [2408] has a run-mode that efficiently computes full triangle plots of profile likelihoods using gradient-based optimization, as explored in Ref. [2409].

3.6.4. Applications of profile likelihood in cosmology

- *EDE & NEDE:* Due to the complicated parameter structure of EDE (see Section 4.1.1), volume effects can have a strong impact on the constraints of this model. Using PLs, Refs. [1967,1968] showed that tight upper limits on EDE from CMB and LSS in Bayesian analyses, which questioned the ability of EDE to resolve the Hubble tension, are partially driven by prior volume effects, while in a frequentist analysis EDE presents a viable solution to the tension. Ref. [1969] uses PLs to explore the interplay between EDE and massive neutrinos. In Ref. [1970], both a Bayesian and PL analysis under an updated *Planck* CMB pipeline give tight upper limits on the fraction of EDE. Moreover, Ref. [1972] constrained the NEDE (see Section 4.1.2) model and showed that the frequentist analysis gives greater evidence of the model due to volume effects in the Bayesian posterior associated with the ΛCDM limit.
- *EFTofLSS:* Ref. [1959] studied the impacts of priors on the nuisance parameters of the EFTofLSS analysis method applied to full-shape power spectrum from galaxy surveys. They found that the priors usually employed to constrain the parameters to their physical regime were informative and had a significant effect on the constraining power of the analysis method.
- *Decaying dark matter:* Ref. [1977] studied a model where a fraction of the DM is allowed to decay into dark radiation. With two new parameters, the abundance of the decaying part of the CDM and its lifetime, series volume effects are found in the limits of parameter space that recover the ΛCDM model; these include the case of infinite lifetime and vanishing abundance. In particular, whereas the Bayesian analyses prefer either of these limits, [1977] shows that the best fit is associated with a narrow log-likelihood peak at a lifetime corresponding to decays just around recombination.
- *Phenomenological transition of dark matter to dark radiation:* Ref. [2398] tested the PROSPECT code on a model where a fraction of the DM transitions to dark radiation, characterized by three parameters: The fraction of DM that transitions, the central redshift of the transition, and a parameter that controls the shape of the transition [2410]. The ΛCDM limit is recovered in many limits of parameter space, leading to significant volume effects and parameterization dependencies that were diagnosed with profile likelihoods.
- *Lensing*: A complete study of the so-called $A_{\rm L}$ tension in the $\Lambda{\rm CDM} + A_{\rm L}$ has been done in Ref. [727].
- *Neutrino*: One of the prototypical applications of profile likelihood in cosmology is for neutrinos. Since neutrino mass constraints are close to the boundary $\sum m_\nu > 0$ and the non-Gaussian posteriors

[43] https://github.com/ggalloni/cobaya/tree/profile_sampler
[44] https://github.com/tkarwal/procoli
[45] https://github.com/AarhusCosmology/prospect_public
[46] http://camel.in2p3.fr/wiki/pmwiki.php
[47] https://github.com/AarhusCosmology/connect_public

found MCMC data analysis, profile likelihood was used to obtain the confidence interval on the sum of the neutrino mass. This has been done in the context of WMAP5, Sloan Digital Sky Survey (SDSS), and HST in Ref. [2395] and for *Planck* data in Ref. [2404]. In Ref. [2411] and Ref. [2412], they study the effect of priors in constraining the number of neutrino species using cosmological data and no evidence for deviations from the standard number of neutrino using profile likelihood. In Ref. [2411] was also highlighted the link with $A_{\rm lens}$ on the current limit. Refs. [1286,2413] explore the preference for "negative" neutrino masses with profile likelihoods.

- *Number of relativistic species,* $N_{\rm eff}$: Profile likelihood was used to test the possibility that extra relativistic species are present beyond the standard model prediction. A discrepancy between the posterior and profile likelihood confidence interval was found in $N_{\rm eff}$ in Refs. [1973,1974], indicating volume effects when using Wilkinson Microwave Anisotropy Probe (WMAP7) and HST data. It was applied to Planck data in Ref. [1975].
- *Gravitational wave energy density*: Constraints on the primordial GW density using CMB data and a study of the impact on cosmic string models has also been derived in Ref. [2414].
- *Tensor-to-scalar ratio*: Profile likelihood was used to analyze the tensor-to-scalar ratio, r, with current data. In Ref. [2403] the most recent *Planck* and BICEP/Keck CMB data was used in order to gain a clearer perspective on the discrepancy between Bayesian and frequentist upper limits on r previously found by the SPIDER collaboration [2394]. A similar analysis was done in Ref. [2400] combining CMB data from Planck PR4 and BICEP/Keck, and GW data from LIGO-Virgo-KAGRA. With the goal of testing the impact of MG theories on r, in Ref. [2415] combining data from CMB from *Planck* DR4 and BICEP/Keck and BAO data from 6dF Galaxy Survey, SDSS DR7 and eBOSS, the Bayesian and frequentist upper limits on r were obtained.
- *Inflation*: The advantages of using a profile likelihood, and more in general, of constructing frequentist confidence intervals with the FC prescription, are particularly evident when trying to constrain inflationary models. This typically allows for more informative constraints and physics insights, especially on models with numerous additional parameters, which are typically degenerate and hard to constrain simultaneously, especially with current data. An example is provided by the latest constraints from *Planck* and BICEP/Keck on axion-U(1) inflation [2402] and by forecasted constraints on axion-SU(2) inflation parameters for the future CMB satellite survey *LiteBIRD* [2393]. Another example is given by the attempt to constrain the spectral tilt of tensor primordial perturbations with the latest CMB and GW interferometers data [2400]. Profile likelihoods were also used to search for features in the primordial power spectrum imprinted in CMB and large-scale structure formation observables, using data from *Planck* and WiggleZ [2416].
- *Brans–Dicke model with cosmological constant:* The Brans–Dicke model with a constant positive vacuum energy density, the so-called BD-ΛCDM model, has been confronted with observations multiple times in the last years [2417–2421]. In Ref. [2420] the authors showed that in the absence of the Planck 2018 high-ℓ CMB polarization and lensing data, but still under a very rich dataset including the Planck 2018 full temperature and low-ℓ polarization likelihoods, together with the state-of-the-art data on SNIa, BAO, CC and RSD, it is possible to loosen the H_0 tension in BD-ΛCDM, while keeping $\sigma_8 \sim 0.790$. In Ref. [1976] the author tested the impact of volume effects in BD-ΛCDM through the analysis of the profile distribution and showed that they do not play a major role in this model.
- *Coupled quintessence:* Coupled quintessence was firstly studied in Refs. [2051,2422] considering a scalar-mediated interaction (fifth force) between DM particles, with the scalar field playing the role of DE. Constraints on this model have been reported e.g., in Refs. [2423–2429]. Volume effects have been recently quantified in Ref. [1976] for the case of a Peebles-Ratra potential [295,2430] using the profile distributions built directly from the MCMC. Their impact on the results are found to be small.
- *Neutrino-Dark Matter Interactions:* Ref. [2396] studied a model featuring scatter-like interactions between neutrinos and DM. Allowing the interaction strength and the total neutrino mass to vary, the model can have up to two parameters more than ΛCDM. A profile likelihood analysis was employed to test possible volume effects. In this case, no relevant volume effects were found. The profile likelihood supported the results derived by marginalizing over the parameter space, confirming a mild preference for non-vanishing interactions when small-scale CMB data are considered [2431,2432].
- *Baryon Acoustic Oscillations:* Profile likelihood has been used, sometimes in combination with Bayesian methods, to quantify BAO errors in determining the fitting scale in surveys. This has been done in the context of many surveys, like the Sloan Digital Sky Survey (SDSS) BOSS [2433] and the eBOSS [2434], or DES [2435,2436]. In [2437], they extend this method to add noise and compare different approaches to determine the error in determining the BAO scale. Profile likelihood was also used to fit the Lyman-α (Lyα) forest 3D correlation function [2438]. Using mocks, they found that profile likelihood is a good approximation for fitting the BAO peak from the Lyα forest correlation functions and is in full agreement with the Bayesian analysis (which is not the case for frequentist maximum likelihood estimators, which assume Gaussianity).

4. Fundamental physics

Coordinator: Vivian Poulin

Cosmology stands at a crossroads. The concordance ΛCDM model, which had shown a great level of success in describing a wide variety of cosmological observations, is being challenged by high precision data as reviewed in Section 2. However, the ΛCDM model has raised profound questions about the nature of its dominant components –DM and DE– as well as the mechanism at the origin of the primordial fluctuations (usually described by inflation) that remains largely unknown. Barring the existence of unknown systematic errors, these observational issues thus present a crucial opportunity to explore new physics beyond the ΛCDM paradigm. This section examines the collective efforts of the scientific community to interpret the implications of observations that challenge the ΛCDM model, with a particular focus on what the H_0 and S_8 tensions may reveal about fundamental physics.

At the core of the ΛCDM value of H_0 is the angular size of the sound horizon at recombination $\theta_s(z_*) = r_s(z_*)/D_{\rm A}(z_*)$, that CMB data have determined at $\mathcal{O} \sim 0.1\%$ precision [192]. In the flat FLRW metric, the angular diameter distance to recombination $D_{\rm A}(z_*)$ that carries information about H_0 can be computed as

$$D_{\rm A}(z_*) = (1+z_*)^{-1} \int_0^{z_*} \frac{dz}{H(z)}\,, \tag{4.1}$$

where under flat ΛCDM, $H(z) = H_0\sqrt{\Omega_{\rm r}(1+z)^4 + \Omega_{\rm m,0}(1+z)^3 + \Omega_\Lambda}$. Extracting the angular diameter distance from $\theta_s(z_*)$ requires knowledge of the sound horizon

$$r_s(z_*) = \int_{z_*}^{\infty} \frac{c_s(z)dz}{H(z)}\,, \quad \text{with} \quad c_s(z) = \frac{1}{\sqrt{3(1+4\rho_{\rm b}(z)/3\rho_{\rm r}(z))}}\,. \tag{4.2}$$

A value of $r_s(z_*)$ can be computed within a model, given knowledge of the cosmological parameters. Within ΛCDM, *Planck* data have allowed us to determine $r_s(z_*) = 144.39 \pm 0.3$ Mpc (TTTEEE+lowE) from the complex structure of peaks and troughs [192]. The value of H_0 is then

adjusted in order to match the corresponding value of $\theta_s(z_*)$, which yields $H_0 = 67.27 \pm 0.6\,\mathrm{km\,s^{-1}Mpc^{-1}}$. Similarly, the value of S_8 can be inferred from the linear matter power spectrum $P(k)$ given a set of cosmological parameters reconstructed from a fit to a given dataset as

$$S_8 \equiv \sqrt{\frac{\Omega_{\mathrm{m},0}}{0.3}} \times \left\{ \sigma_8 \equiv \int_0^\infty \frac{k^3}{2\pi^3} P(k) W_8^2(k) d\ln k \right\}, \tag{4.3}$$

where $W_8(k)$ is a window function describing a sphere of radius $R = 8\mathrm{Mpc}/h$ in Fourier space. Under the ΛCDM model fit to *Planck* data, it yields $S_8 = 0.834 \pm 0.016$.

The solutions to the H_0 discrepancy generally fall into two categories based on the requirement to leave the precisely measured value of $\theta_s(z_*)$ unaffected [709,710,713]. First, there are those that reduce the value of the sound horizon $r_s(z_*)$ such as to compensate for the shorter angular diameter distance implied by a larger H_0. Those typically correspond to early-time (pre-recombination) modifications and include for instance include, new relativistic species, EDE, or modified recombination scenarios. Second, late-time solutions modify the expansion history after recombination such that the angular diameter distance to recombination remains unaffected. These include e.g., phantom DE, IDE, or decaying DM. Both avenues offer advantages and disadvantages: the former scenarios may more easily adjust the shape of the expansion history that is constrained by BAO and SNIa (beyond the mere value of H_0), but will be strongly constrained by CMB observations, while the latter scenarios can more easily leave the CMB unaffected by exploiting the geometrical degeneracy, but are strongly constrained by late-time observations [710].

Resolving the S_8 tension, on the other hand, requires suppressing structure growth, which can be done through new DM interactions, evolving DE models, or modifications to general relativity. Yet, it remains to be established precisely what scales and what cosmic era must be affected in order to achieve concordance between all our LSS observations: is the tension solely appearing at small scales, that are potentially affected by large uncertainties related to non-linear and baryonic effects, or does it also appear on large-scales at late-times, where the physics is much more linear and under control? Answering these questions will drive the community effort to find a solution to the tension. Moreover, there is a clear interplay between the H_0 and S_8 tensions. First, simply because the definition of the physical scale k involved in S_8 in Eq. (4.3) is trivially influenced by the value of h: as the power spectrum as a strong dependence on the scale k (falling like k^{-3}) tension in S_8 may appear due to different values of h in the analysis, fooling us in comparing different physical scales [2439–2441]. However, even when corrected (e.g., through the use of $R = 12$ Mpc as an absolute scale [2439]), the tension can be influenced by the new physics introduced to resolve the Hubble tension. This stems from the observation that distance indicators, that provide measurements of $\Omega_{\mathrm{m},0}$ and H_0, necessarily imply a measurement of the physical matter density $\omega_{\mathrm{m},0} \equiv \Omega_{\mathrm{m},0}h^2$ [804,2442,2443]. Hence, a larger value of h will automatically imply a larger value of $\omega_{\mathrm{m},0}$, leading to earlier matter domination and thus a larger amplitude of fluctuations today.

Finding a solution to either or both tensions is an active area of research. As we illustrate within each section, understanding and resolving these tensions will not only improve the precision in measuring fundamental cosmological parameters but also offer a window into the fundamental physics governing the Universe [709]. Whether these tensions indicate systematic biases in data or genuine hints of new physics, they represent one of the most exciting frontiers in modern cosmology, potentially unlocking new insights into DM, DE, and the laws of gravity.

4.1. Early-time proposals

4.1.1. Early dark energy and variants

Coordinator: Laura Herold

Contributors: Adrià Gómez-Valent, Alexander Reeves, Alireza Talebian, David Benisty, Elisa G. M. Ferreira, Gabriela Garcia-Arroyo, Ivonne Zavala, Joan Solà Peracaula, Lu Yin, Luis Anchordoqui, Luz Ángela García, Matteo Forconi, Nikolaos Mavromatos, Rafaela Gsponer, and Vivian Poulin

4.1.1.1. Introduction and motivation. EDE models (for reviews see Refs. [2444–2446]) are a promising class of models proposed to resolve the Hubble tension with new physics. The central idea behind EDE is to introduce an additional component to the energy density of the Universe at early-times, which increases the expansion rate $H(z)$ before recombination z^*. This leads to a decrease of the (comoving) size of the sound horizon: $r_s(z^*) = \int_{z^*}^\infty c_s(z)/H(z)\mathrm{d}z$, where c_s is the sound speed in the baryon-photon plasma. To understand why this increases H_0 at present times, note that the angular size of the sound horizon $\theta_s = r_s/D_\mathrm{A}$ is directly and precisely observed by the CMB, e.g., see Ref. [192]. Hence, to maintain the same size of θ_s, the (comoving) angular diameter distance reduces, $D_\mathrm{A}(z^*) = \int_0^{z^*} \mathrm{d}z/H(z)$, and leads to an increase of H_0.

All EDE-type solutions to the Hubble tension have in common a DE-like rapid expansion with an equation of state $w \simeq -1$ around z^*, which peaks at some critical redshift z_c and is followed by a phase in which the background energy density decays or dilutes (see Fig. 70, left). EDE models often take the form of a cosmological scalar, whose background dynamics follow the homogeneous Klein–Gordon equation: the field is initially frozen in its potential, such that the background energy density is constant. The fractional contribution of the field to the total energy density, $\rho_\mathrm{EDE}/\rho_\mathrm{Tot}$, increases over time in a manner similar to that of DE. Eventually, Hubble friction dropping below a critical value, or a phase transition changing the shape of the potential, releases the scalar, at which point the field becomes dynamical, and the background energy density dilutes away faster than matter. The contribution of EDE to the Hubble rate is therefore localized before recombination, where it efficiently acts to reduce the size of the sound horizon.

EDE-like models have already been studied before the appearance of the Hubble tension, e.g., in the context of quintessence models [2447–2450] or in the context of recurring DE [2451]. The (axion-like) EDE model has gained significant attention as a proposed solution to the Hubble tension [2452–2454]. To fully resolve the tension, a fractional EDE contribution of $\sim 10\%$ around the time of matter–radiation equality is required [2455], reflecting the percentage difference in H_0 estimates between *Planck* [192] and SH0ES [34]. Although EDE models present a promising class of solutions when compared to other proposed solutions [710,713,2456], the improvement in observational constraints from the CMB and LSS in the last few years poses challenges to this class of models.

4.1.1.2. The axion-like EDE model. The originally proposed EDE model [2452–2454] consists of a scalar field ϕ in a potential of the form

$$V(\phi) = V_0[1 - \cos(\phi/f)]^n, \tag{4.4}$$

where $V_0 = m^2 f^2$ with m and f being referred to as "mass" and "decay constant", respectively. The index n is typically fixed to $n = 3$ as this provides the best fit to the data [2445,2455]. The parameters m and f, along with the initial value of the scalar field in the potential, $\theta_i = \phi_i/f$, need to be fit from the data. This "particle-physics parameterization" is often traded for the "phenomenological parameterization", which consists of f_EDE, the maximum fraction of EDE, $f_\mathrm{EDE} \equiv \rho_\mathrm{EDE}(z_c)/\rho_\mathrm{Tot}(z_c)$, at

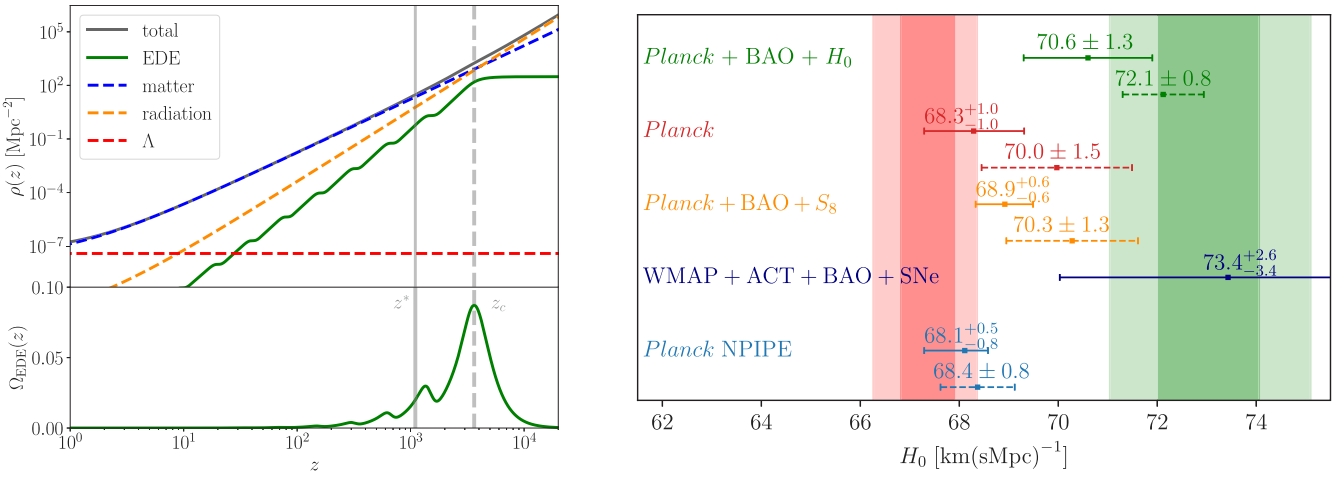

Fig. 70. *Left:* Energy densities, $\rho(z)$, of different components of the Universe as indicated in the legend. EDE (green) plays a subdominant rule at all redshifts, z. The fractional energy density $\Omega_{\rm EDE}(z)$ (bottom subplot) peaks at the critical redshift, z_c, and decays around recombination, z^*. *Right:* A comparison of constraints on H_0 within the axion-like EDE model under different data sets as indicated in the figure, where solid (dashed) lines represent Bayesian (frequentist) constraints (see text).
Source: The constraints are taken from Refs. [1968,1970,2454,2457,2458].

the critical redshift, z_c, which is determined by the onset of oscillations, along with the initial value of the scalar field θ_i.

Predictions for EDE cosmologies have been found using the effective fluid theory approach [2454] and by directly solving the linearized scalar field evolution equations [2455,2459]. Extensions of `CLASS` [1949] using the latter approach are publicly available.[48][49] `CAMB` [1948] includes EDE using the effective fluid approximation.[50]

The axion-like EDE model faces some theoretical challenges: the desired degeneracy between $f_{\rm EDE}$ and H_0, and with that, the ability of EDE to solve the tension sensitively depends on the choice of the parameters z_c and θ_i. Since there is no a priori reason for these parameters to have specific values, this leads to a "fine-tuning" problem. Moreover, the shape of the potential with index $n = 3$ is considered fine-tuned itself since it requires that lower-order terms in the axion-like potential are zero. Therefore, the axion-like EDE model is often seen as a phenomenological model of EDE. Nonetheless, there are approaches to derive the axion-like EDE model from fundamental theories such as string theory [2460–2462] or to motivate $n = 3$ by higher-order instanton corrections [2463].

4.1.1.3. EDE variants. From the axion-like EDE model, we learned valuable lessons about the challenges of EDE as a solution to the Hubble tension. In order to have the maximal possible leverage to resolve the tension, we need a specific form of potential, EDE needs to become relevant around matter–radiation equality and it needs to decay sufficiently fast before recombination. These theoretical challenges, or "fine-tunings", have inspired many variants of EDE, which will be presented here.

Several EDE models consist of **slow-rolling scalar fields** minimally coupled to the metric, with different shapes of potentials [2447,2464–2466]. Rock 'n' Roll EDE assumes a power law potential of the form $V(\phi) \sim \phi^{2n}$, which approximates the axion-like potential for small ϕ/f [2467]. Acoustic DE generalizes the EDE model by using a phenomenological fluid description of EDE parameterized by the sound speed c_s^2 and equation-of-state parameter $w_{\rm ADE}$ [2468].

A class of axion-like EDE models arises in the **string-inspired Chern–Simons (CS) gravity** [2469], which characterizes the low energy limit of string theory [2470]. In the simplest of such models [2471–2474], it leads to the generic form of Running Vacuum Model (RVM) inflation [2475–2478]. In the specific context of string-inspired CS gravity, it is called Stringy RVM (StRVM) [2473,2479], in which there is a pre-RVM-inflationary era dominated by a stiff-fluid of gravitational (Kalb-Ramond) axions that characterize the massless gravitational string multiplet. At the end of such eras, condensation of primordial chiral GWs leads to a condensation of the gravitational anomaly CS term that couples the model to string axions that are either of Kalb-Ramond type or arise from compactification [2480]. The condensed CS term leads to linear terms in the axion potential [2481, 2482], responsible for RVM inflation, while the nonperturbative instanton effects lead to additional periodic modulations. In the context of the StRVM [2471–2473], the coefficient of the linear axion term is not a constant, but an RVM-type functional of even powers of the Hubble parameter. This differentiates the model from other linear axion monodromy models that arise from brane compactification [2483]. In Refs. [2481,2482] it was shown that the CS condensate leads to a *metastable* EDE, as there are imaginary parts in the effective action, pointing to a finite-lifetime of the respective vacua. Notably, different forms of the StRVM can also help alleviate, in modern eras, the Hubble and growth-of-structure tensions [2484,2485]. In the framework of α-attractors in inflation [2486–2488], a potential for EDE was proposed in Ref. [2489] that can reproduce various cases based on its functional form.

Unified models of EDE and late DE have been proposed in Refs. [2490–2492]. Ref. [2490] introduces a model where a scalar field can explain both EDE and late DE in a joined manner in the context of α-attractors. In Ref. [2491], a unified model of EDE and late DE is introduced, which can also enhance the primordial GW spectrum at PTA scales. Moreover, the EDE scalar potential can arise from a D-brane moving in the compact dimensions of warped compactifications in the context of D-brane models of cosmology. Ref. [2492] used a dynamical system approach to analyze a unified model of EDE and late DE. Scaling EDE is characterized by a constant EDE fraction in both the radiation- and matter-dominated epochs. This behavior is naturally found in quintessence models with exponential potentials and dates back to the concept of scalar field DE [296]; see also Ref. [2493,2494]. The very tight constraints imposed by the CMB disfavor this type of models as a solution to the tension [2448,2450,2495,2496], even when allowing for a coupling between EDE and DM [2428]. In the case of tracker solutions, [2497] studied EDE using quintessence and K-essence in the tracker regimes.

The possibility of **EDE field coupling to other particles** was also explored. Refs. [2459,2498,2499] introduce a model with a coupling

[48] https://github.com/PoulinV/AxiCLASS
[49] https://github.com/mwt5345/class_ede
[50] https://github.com/cmbant/CAMB/tree/master

between EDE and DM. The coupling modifies the scalar potential, including a matter contribution and a modulation of the DM mass. In a similar spirit, the coupled scalar DM to EDE has been studied in Refs. [2428,2500,2501]. The waterfall EDE model was explored in Ref. [2502], in which the EDE phase ends through spontaneous symmetry breaking. This mechanism has the potential to generate a dark-photon-DM component. In Ref. [2503], the EDE phase is realized and ended similarly to the warm inflation model. The possibility of EDE coupling to neutrinos was studied in Refs. [2504,2505] with the coupling to neutrinos being a natural trigger for the EDE field at around the matter–radiation equality when the neutrinos become non-relativistic. The possibility of these models not being able to solve the Hubble tension was raised in Ref. [2506] and later disputed in Ref. [2507]. Emerging DE models consider a non-negligible contribution of the DE density during the radiation domination era. This effect is introduced through an evolving equation of state that, at early-times, mimics radiation and at late-times asymptotically reaches $\omega \to -1$ [2508–2510]. This phenomenological emergent DE model [2511] shows promising results when confronted with data [808].

Instead of using a specific EDE model, one can use a **model-independent reconstruction** of the EDE expansion history. Ref. [2495] uses a tomographic approach, in which $\rho_{\rm EDE}$ is grouped into redshift bins z and constrained by confronting this model with data. They find that the tightest upper bound on $\rho_{\rm EDE}$ occurs around the CMB decoupling, whereas much weaker constraints are obtained before and after recombination, leaving room for the EDE model to alleviate the Hubble tension. Ref. [2108] determine $\rho_{\rm EDE}$ in scale-factor bins, finding that the maximum $\rho_{\rm EDE}$ is reached at about $z \sim 10^5$, which is different from the z_c derived with the standard approach. Alternatively, a parametric equation of state can be fit [2512]. Moreover, different microphysics of EDE could have important effects [2513]. In Ref. [2514], a phenomenological model is proposed that can mimic the EDE phase through multiple transitions in the vacuum DE density.

4.1.1.4. Constraints on EDE from CMB, BAO and SN. In the following sections, we will discuss observational constraints on the axion-like EDE model from different data sets (see Fig. 70, right, for a whisker plot). When analyzing EDE with *Planck* primary and lensing CMB [726], BAO [777,2515,2516], SNIa [2033], and the H_0 measurement of the SH0ES collaboration [48,2517], these data sets generally prefer high values of $f_{\rm EDE}$ and high values of H_0 consistent with direct measurements.[51] The goodness of fit, i.e., the χ^2, reduces compared to ΛCDM, albeit with three extra parameters compared to ΛCDM. This is mainly driven by the ability of EDE to accommodate higher H_0 values by reducing r_s, which in turn leads to higher values of n_s and $\omega_{\rm cdm}$. Ref. [2454] uses the effective fluid description of the axion-like EDE model, Planck 2015 [726] and SH0ES 2018 [2517] and obtains $f_{\rm EDE} \sim 5\%$ at $z_c \sim 5000$ and $H_0 = 70.6 \pm 1.3\,{\rm km\,s^{-1}Mpc^{-1}}$ ($\Delta\chi^2 = -14.2$, first errorbar in Fig. 70), whereas in Ref. [2455] using the scalar field description and updating to the SH0ES 2019 value [48] results in $f_{\rm EDE} \sim 10\%$ at $z_c \sim 3700$ and $H_0 = 71.49 \pm 1.20\,{\rm km\,s^{-1}Mpc^{-1}}$ ($\Delta\chi^2 = -20.3$).[52] Updating to Planck 2018 data, [1965,2459] also use the scalar field description yielding $f_{\rm EDE} \sim 14\%$ at $z_c \sim 3800$ and $H_0 = 71.2 \pm 1.1\,{\rm km\,s^{-1}Mpc^{-1}}$ ($\Delta\chi^2 = -16.2$) while updating to DDESI BAO yields $H_0 = 71.7 \pm 0.76\,{\rm km\,s^{-1}Mpc^{-1}}$. Finally, those constraints were recently updated with Planck 2020 NPIPE data [1970] yielding $H_0 = 71.24 \pm 0.77\,{\rm km\,s^{-1}Mpc^{-1}}$ for $f_{\rm EDE} = 0.107 \pm 0.023$ at $\log_{10}(z_c) = 3.585^{+0.049}_{-0.15}$ ($\Delta\chi^2 = -28.0$).

4.1.1.5. EDE and LSS. Confronting the EDE model with LSS data can impose stringent constraints on $f_{\rm EDE}$. This can be understood as LSS data typically prefer lower values of the amplitude of clustering σ_8 and the related parameter S_8 compared to CMB data (the so-called "S_8 discrepancy"). Ref. [2454] find $S_8 = 0.838 \pm 0.015$ for Planck, BOSS BAO, Pantheon and SH0Es data, and more recently Ref. [2442] find $S_8 = 0.831 \pm 0.012$ for Planck, DESI BAO, Pantheon+ and SH0ES data. However, $f_{\rm EDE}$ typically correlates positively with the amount of late-time clustering due to increased $\omega_{\rm cdm}$ in models with higher $f_{\rm EDE}$ which compensates for the EDE-induced boost to the early Integrated Sachs–Wolfe (eISW) effect to maintain a good fit to the CMB [2455,2518–2520]. Including LSS data thus weakens the evidence for EDE compared to using CMB data alone by providing an independent constraint on the clustering amplitude [2457].

Several studies have shown that the combination of BOSS full-shape and BAO data [777,1527,2515,2521–2523] (based on the effective field theory of LSS, e.g., see Refs. [1177,1178]) alongside the CMB give tight upper bounds on $f_{\rm EDE}$ [1173,2524,2525] when not including any direct measurements of H_0. WL data have also been explored in the context of the EDE model. For example, see Ref. [2457] where DES-YI 3 × 2pt data [1165], as well as S_8 priors from KiDS and HSC [855,858,859], were used to derive tight upper limits of $f_{\rm EDE} < 0.060$ and $H_0 = 68.92^{+0.57}_{-0.59}\,{\rm km\,s^{-1}Mpc^{-1}}$ while giving high values of $S_8 = 0.8060 \pm 0.0082$ when combined with *Planck* [192] leading to the conclusion that LSS data can rule out the EDE model (fifth errorbar in Fig. 70). In contrast, [1965] examine the EDE model in the context of KiDS [859] and DES [698] data and find that a one-parameter EDE model, which fixes $\{z_c, \theta_i\}$, does not lead to a significantly worsened S_8 discrepancy compared to ΛCDM and advocate for caution when combining datasets that are statistically discrepant. Furthermore, [1966] argue that the stringent constraints found when combining CMB data with BOSS full-shape and BAO likelihoods can be traced to a potential tension in the power spectrum amplitude A_s between *Planck* and BOSS which is present even in ΛCDM. Thus, while it is clear that LSS data can play an important role in constraining the EDE model, the existence of subtle inconsistencies between CMB and LSS data, present even within the ΛCDM framework, complicates the interpretation.

It is also worth mentioning the important role that the use of σ_8 as a cosmological parameter might play in this discussion. The σ_8 parameter is computed as a convolution of the matter power spectrum and a window function at a characteristic scale $R_8 \equiv 8\ {\rm h^{-1}}$ Mpc. Thus, σ_8 provides information about the amplitude of the power spectrum at a scale that changes in models with different values of H_0. To address this issue, [2439] suggested using the parameter σ_{12}, which is computed at a fixed scale $R_{12} = 12$ Mpc that does not depend on h. In Ref. [1976] it is shown that despite the positive correlation between σ_8 and $f_{\rm EDE}$ in fitting analyses with CMB+BAO+SNIa, the correlation between σ_{12} and $f_{\rm EDE}$ is negligible.

Attempts have been made to address both the H_0 and S_8 tensions simultaneously by expanding the EDE model parameter space to include components that reduce the amplitude of clustering at late-times. For example, Refs. [1969,2428] allow for a free neutrino mass in the EDE model finding that current data limits the effectiveness of massive neutrinos to suppress structure formation at small scales due to the stringent constraint placed on the sum of neutrino masses from the *Planck* 2018 data which is not much weakened in the context of EDE. Other works have also considered a coupling between EDE and DM in order to try to decrease the value of $\omega_{\rm cdm}$ and make the growth of large-scale structures less efficient at late-times [2428,2459,2498].

4.1.1.6. Prior effects and frequentist constraints. Due to the complicated parameter structure of the EDE model, the tight upper limits on EDE from CMB and LSS are not only driven by physical effects but also affected by prior volume (or projection) effects in the MCMC posterior. These prior effects arise due to the nested parameter structure of the model: while $f_{\rm EDE}$ controls the fraction of EDE, z_c and θ_i are auxiliary parameters describing the model in more detail. When $f_{\rm EDE}$ approaches zero, the ΛCDM limit is recovered, and z_c, θ_i becomes redundant and

[51] All data combinations and model implementations in this section use the same SNIa sample and BAO data, but differ in H_0 and *Planck* data.

[52] All central intervals in this section are quoted at 68% CL while all upper limits are quoted at 95% CL

unconstrained. This leads to a larger prior volume at $f_{\rm EDE} \approx 0$ than at $f_{\rm EDE} > 0$ and a non-Gaussian posterior, which in turn can lead to a preference for the ΛCDM limit in the marginalized posterior. In Refs. [1965,1966] (and Ref. [1971] for NEDE) the influence of prior effects was illustrated by fixing z_c, θ_i in the analysis and varying only $f_{\rm EDE}$ along with the ΛCDM parameters, which leads to larger allowed values of $f_{\rm EDE} = 0.0523^{+0.026}_{-0.036}$ when using the same BOSS full-shape data [720,1145,1172] with the effective field theory of LSS [1177, 1178] combined with BAO and CMB [1434].

Since these effects are related to the prior, which is an inherently Bayesian quantity, Refs. [1967,1968] constructed frequentist constraints based on the profile likelihood, which are independent of priors and only depend on the likelihood (top three dashed error bars in Fig. 70). Using *Planck* CMB [1434] and BOSS full-shape power spectrum data [720,1145,1172,2526] based on the effective field theory of LSS, the profile likelihood yields higher values of $f_{\rm EDE} = 0.087 \pm 0.037$ and $H_0 = 70.57 \pm 1.36\,{\rm km\,s^{-1}Mpc^{-1}}$ ($\Delta\chi^2 = -5.6$) than the constraints from Bayesian posteriors. Additionally, including SH0ES data pushes the inferred $H_0 = 72.1 \pm 0.8\,{\rm km\,s^{-1}Mpc^{-1}}$ even further up. Even when additionally including 3×2pt data from DES [869], the profile likelihood yields moderately high values of $f_{\rm EDE} \approx 6\%$ and $H_0 = 70.28 \pm 1.33\,{\rm km\,s^{-1}Mpc^{-1}}$. This shows that the Bayesian constraints from CMB and LSS are partially driven by prior effects and indicates that more data is necessary to fully rule out or detect EDE. These results agree with Ref. [1976], which uses an approximate profile distribution obtained from MCMC samples, which is computationally cheaper than computing a profile likelihood. In a Bayesian context, [1173] explores the impact of priors on constraints from the effective field theory of LSS on EDE. Using a Jeffreys prior on nuisance parameters mitigates projection effects from the effective field theory of LSS, resulting in smaller overall volume projection effects on EDE when combined with other datasets. Ref. [2527] utilizes a neural network to obtain a data-driven parameterization of EDE.

4.1.1.7. Ground-based CMB experiments and alternative CMB pipelines. The *Planck* experiment offers high-precision measurements of the large- to intermediate-scale CMB temperature and polarization power spectra. Ground-based CMB experiments such as ACT and SPT can improve over *Planck* data, especially at small scales ($\ell \gtrsim 2000$) and in polarization measurements [732]. Constraining EDE with data from the ACT Data Release 4 (TT, TE, and EE power spectra) [732] combined with large-scale *Planck* TT [192,729,1434], *Planck* CMB lensing [694], and BAO data [777,1145,2515] yields $f_{\rm EDE} = 0.091^{+0.020}_{-0.036}$ and $H_0 = 70.9^{+1.0}_{-2.0}\,{\rm km\,s^{-1}Mpc^{-1}}$ [710,2458,2528]. The combination of ACT, WMAP [1193], BAO, Pantheon [2033] in a Bayesian analysis leads to $f_{\rm EDE} = 0.158^{+0.015}_{-0.094}$ and $H_0 = 73.43^{+2.6}_{-3.4}\,{\rm km\,s^{-1}Mpc^{-1}}$ [2458] (seventh errorbar in Fig. 70). The combination of data sets ACT DR4, SPT-3G TEEE 2018 [725,2529], and *Planck* TT650TEEE [192] gives a similar preference for EDE [2529–2531]. Hence, replacing *Planck* data with ACT data leads to a preference of high values of $f_{\rm EDE}$ and H_0 without the inclusion of any H_0 prior [2532–2534]. However, the inclusion of SPT temperature and *Planck* temperature TT at $\ell > 650$ strongly decreases this preference, with $f_{\rm EDE} < 0.071$ in a Bayesian analysis [1964].

This preference for EDE diminishes with recent ACT DR6 data, finding $f_{\rm EDE} < 0.12$ for ACT combined with *Planck*, and even lower for ACT alone [703,706]. For ACT DR6 alone, the EDE model does not show any improvement in fit compared to ΛCDM, suggesting that the preference for EDE in the previous ACT DR4 could be due to a statistical fluctuation in the EE and TE power spectra.

The most commonly used *Planck* likelihood for multipoles $\ell > 30$ is the `Plik` likelihood [729]. The `CAMSPEC` [2535] and `Hillipop` [701] likelihoods are alternative likelihoods, which differ in data cuts and analysis choices. Ref. [1970] use the `CAMSPEC` likelihood with the *Planck* PR4 NPIPE maps [2536] along with BAO data from BOSS [1145], SDSS [2515] and 6dFGS [777] and supernova data from Pantheon+ [33] to constrain the EDE model. They find low values of $H_0 = 68.11^{+0.47}_{-0.82}\,{\rm km\,s^{-1}Mpc^{-1}}$ and $f_{\rm EDE} < 0.061$ in a Bayesian analysis, and similarly $H_0 = 68.37 \pm 0.75\,{\rm km\,s^{-1}Mpc^{-1}}$ and $f_{\rm EDE} < 0.094$ in a frequentist analysis (bottom two errorbars in Fig. 70). Using the `Hillipop` likelihood, Ref. [2446] find similarly tight constraints on EDE, as well as Ref. [2537]. Hence, both alternative *Planck* likelihoods pose a challenge to the axion-like EDE model's ability to solve the H_0 tension.

4.1.1.8. Complementary EDE observables. If EDE existed in the early Universe, it is natural to expect evidence other than the H_0 tension of this deviation from ΛCDM. In this section, we discuss possible such signatures in data sets different from the commonly used data discussed above. Galaxies and small-scale LSS probes could provide important insight into EDE models. For example, EDE cosmologies predict **more massive clusters and an increased abundance of galaxy-mass haloes** at higher redshifts [1756]. Refs. [1755,1757,2538] propose that EDE cosmologies could accommodate the massive high-redshift JWST galaxies. However, while the fit to JWST data improves, EDE possibly worsens the fit to Hubble Space Telescope data. **Lyman-α forest** data from SDSS eBOSS [1556] and MIKE/HIRAS [2333] give tight upper limits on EDE [1561] due to the preference of lower values of n_s than *Planck*. However, the Lyman-α forest data shows a discrepancy with *Planck* data [1562], which warrants further investigation. Furthermore, an expansion rate differing from ΛCDM would affect the relation between redshift and age, which can be constrained by the **age of ancient objects** in the Universe [2539]. Hence, improved age constraints will be able to constrain EDE cosmologies.

Measurements of the CMB anisotropies along with other CMB observables could hold clues about deviations from ΛCDM. For example, if EDE would couple to photons in a parity-violating manner, it could explain the tentative evidence of **cosmic birefringence** observed in *Planck* data [689,693,2540]. The EDE field with the potential in Eq. (4.4) predicts a unique shape of the EB power spectra, which is not favored by *Planck* data and hence constrains a possible parity-violating coupling of EDE to photons [691,2541–2543]. Moreover, **spectral distortions** are sensitive to physics in the (pre-) recombination era. Since EDE is dynamical during this epoch, spectral distortion measurements could be sensitive to distinct EDE signatures [2544].

Theoretical considerations and the requirement of a consistent UV completion can place constraints on EDE models. For example, Ref. [2545] employed the **axion weak gravity conjecture**[53] to derive an upper bound on the axion decay constant. Specifically, for $n = 1$ in the potential Eq. (4.4), this leads to $f < 0.008\,M_{\rm Pl}$, which is not consistent with the typically assumed parameter values. Potential ways to circumvent or relax this constraint exist [2545]. Moreover, EDE cosmologies typically prefer **higher values of n_s** close to unity, which would point to a scale invariant Harrison–Zeldovich spectrum [2519,2531,2548–2550] and would have important implications for inflation [2551,2552].

Hence, while EDE models provide a promising class of models to resolve the Hubble tension, theoretical considerations and new data provide challenges to these models.

4.1.2. New early dark energy and variants

Coordinator: Florian Niedermann

Contributors: Martin S. Sloth, and Mathias Garny

NEDE is a theoretical framework to address the Hubble tension where a scalar field ψ undergoes a phase transition between BBN

[53] The axion weak gravity conjecture is part of a broader program known as the "swampland". This program aims to define the boundary between effective field theories that are consistent with quantum gravity and those that exist in the "swampland" of incompatible theories. The precise statement of the axion weak gravity conjecture remains a topic of debate [2546,2547].

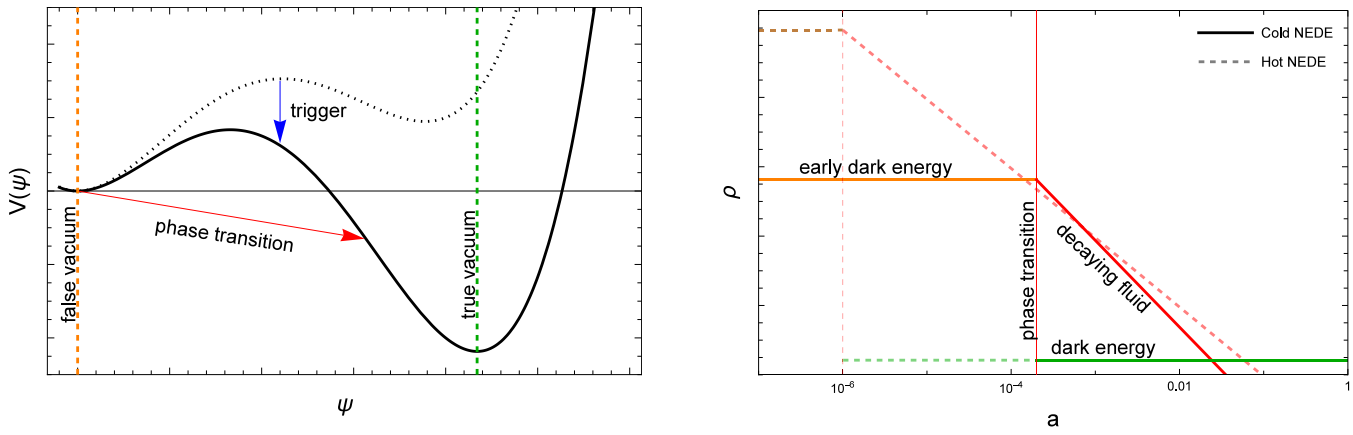

(a) Microscopic picture (b) Cosmological fluid model

Fig. 71. Schematic representation of the NEDE framework, explaining its microphysics and phenomenology. Left: The NEDE field decays in a triggered first-order phase transition, giving rise to an energy injection before recombination. EDE is identified with the field's vacuum energy before the transition, and DE with the true vacuum after the transition. Right: On cosmological length scales, a fluid description can be applied. Cold and Hot NEDE energy densities are represented as the solid and dashed lines, respectively.

and recombination on a time scale that is short compared to the Hubble time, such as, e.g., a first-order phase transition [2553,2554]. In contrast to other phenomenological approaches to the Hubble tension, NEDE is rooted in concrete microphysics, which is operative at the eV scale. Current CMB temperature and polarization measurements are sensitive to the precise mechanism triggering the phase transition, and, therefore, the phenomenology differs depending on the concrete NEDE realization. The two main examples are Cold and Hot NEDE, where the trigger of the phase transition is a second scalar field or the temperature of a dark sector, respectively. In the case of Cold NEDE, the phenomenology shares some features with other EDE-type models, but differs both at background and perturbation level, particularly after the phase transition. On the other hand, Hot NEDE is more similar to strongly interacting dark radiation (SIDR) models, and can be viewed as a UV completion of these types of models, explaining naturally the creation of extra radiation after BBN in a supercooled phase transition. In a nutshell, the idea is summarized in Fig. 71, where the left panel explains the field-theoretic idea and the right panel depicts the cosmological model. Initially, the NEDE field ψ is stuck in a false minimum of its potential. It is separated from the true minimum by a large potential barrier. The (false) vacuum energy associated with ψ constitutes an early DE component (orange line). However, as the trigger mechanism kicks in, the barrier shrinks, initiating a strong first-order phase transition. This corresponds to the nucleation of bubbles that separate the true from the false vacuum. Eventually, all of space is converted to the true vacuum. In the case of a fast phase transition, this can be described in a fluid model in terms of an abruptly decaying early DE component (red line). It leaves behind a residual vacuum energy, which can be identified with DE (green line). As a closely related idea, we mention ChainEDE, which relies on a series of a large number of first-order phase transitions to address the H_0 tension [2555].

4.1.2.1. Cold new early dark energy. Cold NEDE introduces an additional, ultralight scalar field ϕ to trigger the phase transition [1971, 2554]. Its effective potential valid at low energies is

$$V(\psi,\phi) = \frac{\lambda}{4}\psi^4 + \frac{\beta}{2}M^2\psi^2 - \frac{1}{3}\alpha M\psi^3 + \frac{1}{2}m^2\phi^2 + \frac{1}{2}\tilde{\lambda}\phi^2\psi^2 \dots , \tag{4.5}$$

where α, β, λ, and $\tilde{\lambda}$ are dimensionless EFT parameters. The model introduces a hierarchy of scales, where the trigger field ϕ is an ultralight field with mass $m \sim 10^{-27}$ eV and the tunneling field ψ is much heavier with mass $M \sim$ eV. A possible high-energy completion has been argued to be possible within a multi-axion framework, where the small masses are protected through an approximate shift symmetry [2556]. In terms of its cosmological fluid description, Cold NEDE introduces four additional parameters: the fluid's maximal energy fraction, $f_{\rm NEDE}$, the redshift z_* of the phase transition, the equation of state parameter of the post-phase transition fluid, $w_{\rm NEDE}$, and the relic abundance of the trigger field today Ω_ϕ.

The phenomenological model has been implemented in the Boltzmann code `TriggerCLASS`[54] and tested extensively against cosmological data in the literature. Most work has been done in the limit where $\Omega_\phi \ll 1$, corresponding to a subdominant trigger field. For example, using Planck 2018 [192], Pantheon [2033], and BAO [777, 1145,2515] data, the H_0 tension was found to be reduced to 2σ when employing the $Q_{\rm DMAP}$ tension measure [710] (with a value for H_0 taken from Ref. [78]). This result was supported later in Ref. [1972] in a profile likelihood approach, which gets around prior volume issues, that are otherwise are known to drive the posteriors for $f_{\rm NEDE}$ toward small values [1971] (see also the discussion in Section 4.1.1 for more details). Without including a prior on H_0, it was found that $H_0 = 69.56^{+1.16}_{-1.29}$ km s^{-1}Mpc^{-1}and $f_{\rm NEDE} = 0.076^{+0.040}_{-0.035}$ at 68% CL, amounting to a 2σ indication for a non-vanishing fraction of NEDE. Including the SH0ES prior, $H_0 = 71.62^{+0.78}_{-0.76}$ km s^{-1}Mpc^{-1}and $f_{\rm NEDE} = 0.136^{+0.024}_{-0.026}$ was obtained at 68% CL, which amounts to a 5σ evidence for a non-vanishing fraction of NEDE. The model has also been studied in the presence of additional LSS [1972,2557] and ground-based CMB data [2458,2558,2559], broadly matching the baseline results cited above, although it should be noted that axiEDE and Cold NEDE respond differently to ACT and SPT data [2458]. Recently the assumption $\Omega_\phi \ll 1$ was dropped in Ref. [2556]. In that case, the trigger field can make a sizable contribution to the energy budget today in the form of a fuzzy DM component (for a phenomenologically similar model see also Ref. [2560]). With their non-vanishing pressure fluctuations, the trigger field's perturbations act against gravitational collapse on small scales as required for solving also the S_8 tension. As a result, the model was found to simultaneously reduce both tensions[55] below 2σ (with the above choice of datasets $S_8 = 0.818^{+0.023}_{-0.017}$ was obtained).

4.1.2.2. Hot new early dark energy. In Hot NEDE [2562,2563], the phase transition is triggered by the decreasing dark sector temperature T_d, and the sound horizon is lowered due to the dark radiation

[54] https://github.com/NEDE-Cosmo/TriggerCLASS.git

[55] This is another important difference at the phenomenological level between axiEDE (and other EDE type models) and NEDE. While axiEDE is known to worsen the S_8 tension, NEDE has the potential to resolve both the H_0 tension and the S_8 tension.

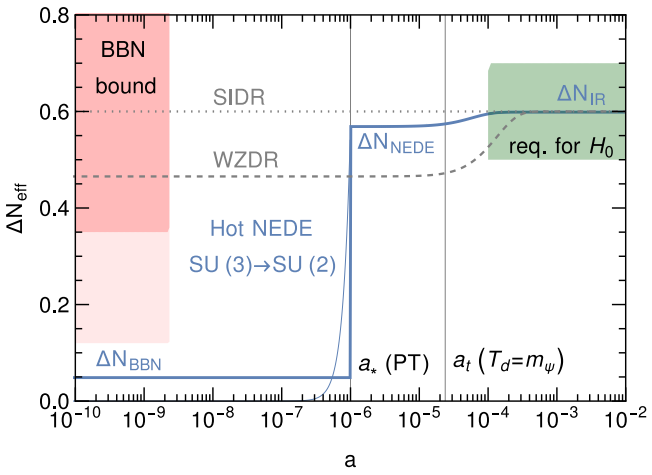

Fig. 72. Evolution of $\Delta N_{\rm eff}$ in Hot NEDE with a supercooled Coleman–Weinberg phase transition (PT) between the BBN and recombination epochs, leading to a strong increase ($\Delta N_{\rm BBN} \to \Delta N_{\rm NEDE}$) due to the latent heat being converted into relativistic $SU(2)$ dark gauge and Higgs bosons during the PT, and a second slight increase due to the dark Higgs becoming non-relativistic ($\Delta N_{\rm NEDE} \to \Delta N_{\rm IR}$). This evolution is intimately linked to the underlying Coleman–Weinberg model. Also shown are bounds from BBN, and the values required to solve the H_0 tension around recombination, as well as two models featuring extra dark radiation but no phase transition (SIDR and WZDR [2561]).

generated from the latent heat, i.e., the false vacuum energy released into the dark sector during the transition [2564] (for a comparison to Cold NEDE see Table 5). If the phase transition occurs between BBN and recombination, this setup naturally reconciles SIDR-type solutions to the Hubble tension with BBN bounds on extra radiation [2564] (see Fig. 72). It furthermore differs from SIDR at the perturbation level, and makes complementary predictions. In particular, the model predicts oscillatory features on small scales in the matter power spectrum alongside a Stochastic Gravitational Wave Background (SGWB) signal that can be looked for in Lyman-α forest data and pulsar timing arrays, respectively.

Hot NEDE can be realized by the well-known Coleman–Weinberg mechanism of spontaneous symmetry breaking within a dark sector featuring a dark Higgs field ψ that transforms under a dark gauge symmetry $SU(N)$. This setup naturally leads to the required supercooled first-order phase transition, breaking the initial $SU(N)$ to $SU(N-1)$, as well as to self-interactions described by the non-Abelian gauge symmetry. The dynamics is captured by the effective potential [2564]

$$V(\psi;T_d) = B\psi^4\left(\ln\frac{\psi^2}{v^2} - \frac{1}{2}\right) - \frac{\mu_{\rm eff}^2}{2}\psi^2\left(1 - \frac{\psi^2}{2v^2}\right) + \Delta V_{\rm thermal}(\psi;T_d)\,, \tag{4.6}$$

where the dimensionless parameter $B \sim g^4$ depends on the gauge coupling g. During the NEDE phase transition, ψ picks up a super-eV expectation value v. Due to an approximate conformal symmetry (controlled by the soft breaking parameter $\mu_{\rm eff} \sim$ eV), the phase transition exhibits a significant amount of supercooling, where the latent heat dominates over the dark radiation plasma, giving rise to an EDE component. In a more fundamental picture, ψ is the modulus of a dark sector Higgs multiplet, breaking an initial $SU(N)$ gauge symmetry to $SU(N-1)$. The corresponding massless gauge bosons alongside the light Higgs degrees of freedom are then populated during the phase transition, reheating the dark sector and introducing a sizable increase in the effective number of relativistic degrees of freedom, $\Delta N_{\rm eff}$. Although both Cold and Hot NEDE feature an EDE component, their phenomenology differs significantly. In particular, the Hot NEDE phase transition occurs before the CMB epoch at redshifts $z_* \gtrsim 10^5$ (see the right panel in Fig. 71). As a result, Hot NEDE lowers the sound horizon r_s (and thus increases H_0 as explained in Section 4.1.1) through the energy injection provided by the strongly interacting dark sector plasma *after* the phase transition and, on a phenomenological level, is thus more akin to SIDR models (with mass threshold effects) such as Ref. [2561]. However, its main phenomenological advantage is that it gets around BBN constraints on $\Delta N_{\rm eff}$, which otherwise would rule out SIDR models as solutions to the Hubble tension [2564,2565], see Fig. 72 (for other ideas to avoid BBN bounds see Refs. [2566–2574]). A first test against cosmological data [2564] showed that the model reduces the $Q_{\rm DMAP}$ tension to 2.8σ. Moreover, it was found that $H_0 = 96.13^{+0.62}_{-1.00}$ km s^{-1}Mpc^{-1} and $H_0 = 71.17 \pm 0.83$ km s^{-1}Mpc^{-1} without and with including a Gaussian prior on H_0, respectively (datasets as for cold NEDE except for the prior on H_0 taken from Ref. [34]).

4.1.3. Extra relativistic degrees of freedom

Coordinator: Sunny Vagnozzi

Contributors: Adèle Poudou, Alexander Bonilla Rivera, Biswajit Karmakar, Branko Dragovic, Davide Pedrotti, Diego Rubiera-Garcia, László Árpád Gergely, Leila L. Graef, Luca Visinelli, Luis Anchordoqui, Marcin Postolak, Margus Saal, Mariana Melo, Matteo Forconi, Özgür Akarsu, Salvatore Capozziello, Sebastian Bahamonde, Shouvik Roy Choudhury, Simony Santos da Costa, Stefano Gariazzo, Thejs Brinckmann, Utkarsh Kumar, Vivian Poulin, William Giarè, and Wojciech Hellwing

Introducing extra relativistic species (ERS, also referred to as "dark radiation") is one of the most well-motivated and straightforward extensions of the ΛCDM model, but also one of the simplest ways of raising the inferred value of H_0 [2575]. The ESR energy density is most easily parameterized via the effective number of neutrino species $N_{\rm eff}$ [2576], controlling the relation between the total radiation energy density ρ_r and the photon energy density ρ_γ [2577,2578]

$$\rho_r = \rho_\gamma\left[1 + \frac{7}{8}\left(\frac{4}{11}\right)^{\frac{4}{3}} N_{\rm eff}\right]\,. \tag{4.7}$$

In the presence of only three standard neutrinos undergoing instantaneous decoupling, $N_{\rm eff} = 3$. However, in the standard cosmological model, $N_{\rm eff}^{\rm SM}$ is slightly larger than 3, owing to the fact that the neutrino decoupling process is not instantaneous. The latest determinations yield $N_{\rm eff}^{\rm SM} \simeq 3.044$ [2579–2582]. After electron-positron annihilation, the only relativistic particles in the standard cosmological model are neutrinos and photons. However, several well-motivated extensions of the Standard Model of particle physics predict the existence of additional particles which could be relativistic at epochs of cosmological interest, including but not limited to light sterile neutrinos [2583–2587], Goldstone bosons [2588,2589], axions, axion-like particles, and ultra-light DM [2453,2453,2590–2600], light or massless dark photons [2601–2609], and so on [2610,2611]: such particles lead to a value of $\Delta N_{\rm eff} = N_{\rm eff} - N_{\rm eff}^{\rm SM} \neq 0$. It is worth noting that a non-zero value of $\Delta N_{\rm eff}$ does not necessarily imply the existence of new particles. For instance, it could be associated with a non-standard distribution of standard neutrinos, or the presence of neutrino asymmetries (i.e., a non-zero chemical potential) [2612,2613]. In addition, a SGWB, possibly at the origin of the signal detected in pulsar timing array data [2614–2617], could also provide a significant contribution to $N_{\rm eff}$ [2618–2628]. Moreover, $\Delta N_{\rm eff}$ can in principle be negative, for instance, in low-reheating scenarios following inflation, where the reheating temperature $T_{\rm rh}$ can be as low as a few MeV, leading to incomplete thermalization of standard neutrinos [2629–2632].

A non-zero value of $\Delta N_{\rm eff}$ leads to a host of signatures at both the times of BBN and recombination. ERS increases the physical radiation density and thereby raises the pre-recombination expansion rate $H(z)$ before recombination (as well as after, although by then the radiation component is sub-dominant). At the BBN epoch, this pushes the freeze-out of nuclear interactions toward higher temperatures, raising the yield of light elements. At recombination, the presence of ERS leads to

Table 5
Comparison of Cold and Hot NEDE, both relying on a fast-triggered phase transition before recombination to address the Hubble tension.

NEDE model	Cold NEDE	Hot NEDE
model family	EDE	(stepped) strongly interacting dark radiation
physics lowering r_s	false vacuum energy	latent heat released as SIDR
trigger	ultralight field	dark sector temperature
redshift of phase transition	$10^3 \lesssim z_* \lesssim 10^4$	$10^5 \lesssim z_* \lesssim 10^9$
equation of state parameter	$w_{\rm NEDE} > 1/3$ ($\sim 2/3$)	$w_{\rm NEDE} = 1/3$
microphysics	axion-like particle	dark sector Higgs

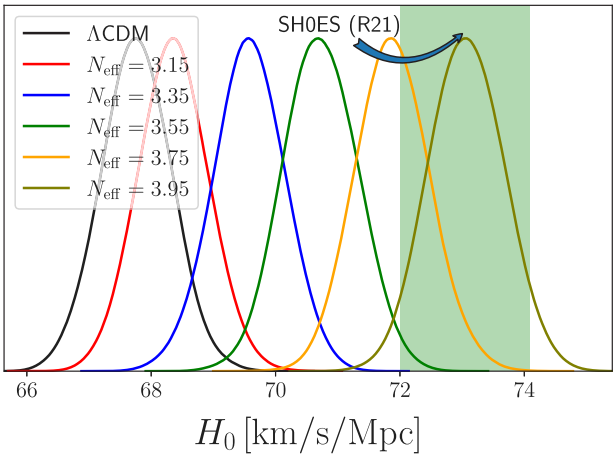

Fig. 73. Posterior distributions for H_0 inferred from a combination of *Planck* 2018, SDSS BAO, and *PantheonPlus* SNIa data for different fixed values of $N_{\rm eff}$. The green shaded region corresponds to the *R21* measurement $H_0 = 73.04 \pm 1.04\,{\rm km\,s^{-1}Mpc^{-1}}$as inferred by the SH0ES team in Ref. [34].

a variety of direct and indirect signatures on the CMB: however, once the redshift of matter–radiation equality $z_{\rm eq}$ and the acoustic angular scales θ_s are fixed, the only remaining effects of $\Delta N_{\rm eff}$ on the CMB power spectra consist of an increased (Silk) damping of the higher acoustic peaks and a phase-shift of the acoustic peaks toward larger scales (e.g., see Refs. [2633–2635]). All these effects indeed lead to some of the tightest cosmological constraints on $\Delta N_{\rm eff}$: current BBN and CMB inferences both broadly indicate $\Delta N_{\rm eff} \lesssim 0.2-0.3$, while next-generation cosmological surveys will be able to improve the sensitivity of $\Delta N_{\rm eff}$ by almost an order of magnitude [681,682].

Increasing $N_{\rm eff}$ while keeping the physical baryon and DM densities ω_b and ω_c fixed has the effect of increasing the pre-recombination expansion rate, thus decreasing the comoving sound horizon at recombination r_s, which then requires a higher value of H_0 in order to keep θ_s fixed. This is the reason why ERS are one of the most economical ways of raising H_0 and are generally considered a benchmark model in this sense. These effects lead to a positive correlation between $N_{\rm eff}$ and H_0 [712,2636], with an increase in the former leading to an increase in the latter, as captured by the following linear relation [2637], as can be seen in Fig. 73

$$\Delta H_0 = H_0|_{\Delta N_{\rm eff}\neq 0} - H_0|_{\Lambda{\rm CDM}} \simeq 5.9\,\Delta N_{\rm eff}\,, \tag{4.8}$$

as calibrated to *Planck* 2018 CMB, BAO, and *Pantheon* SNIa measurements in 2020. This relation, first obtained in Ref. [2637], was illustrated in Ref. [2520] in the H_0-σ_8 plane, together with the analogous relation for several tension-resolving candidate models.

From Eq. (4.8) we see that increasing H_0 to a level that solves the Hubble tension requires $N_{\rm eff} \gtrsim 4$, corresponding to the effect of an extra fully thermalized neutrino which, importantly, is completely excluded by BBN and CMB considerations. The main reason why the CMB excludes high values of $N_{\rm eff}$ is that they disproportionately alter the damping scale r_d, in turn altering the ratio r_s/r_d, which is tightly constrained especially by high-multipole polarization measurements to be close to its ΛCDM value (see e.g., the discussion in Ref. [713]). Moreover, the neutrino drag/phase shift effect [2638,2639] is also altered to an extent that is incompatible with the data. This is why the simplest, 7-parameter ΛCDM+$N_{\rm eff}$ model fails to solve the Hubble tension, despite constituting a useful benchmark [709,2640,2641]. Within the simplest 7-parameter ΛCDM+$N_{\rm eff}$ model one infers $N_{\rm eff} = 2.89\pm0.19$, $H_0 = 66.3\pm 1.4\,{\rm km\,s^{-1}Mpc^{-1}}$, and $S_8 = 0.831 \pm 0.013$ from *Planck* 2018 temperature, polarization, and lensing data, whereas further adding SDSS BAO and *Pantheon* SNIa data change these numbers to $N_{\rm eff} = 3.00 \pm 0.17$, $H_0 = 67.4 \pm 1.1\,{\rm km\,s^{-1}Mpc^{-1}}$, and $S_8 = 0.823 \pm 0.011$ respectively (in what follows, the switch from *Pantheon* to *PantheonPlus* SNIa data is not expected to bring about significant changes).

The cosmological evolution of ERS characterized by Eq. (4.7) is de facto equivalent to that of massless neutrinos, and for this reason we can refer to the ΛCDM+$N_{\rm eff}$ model as describing *free-streaming* ERS. It is worth noting that the above considerations hold for some of the simplest dark radiation models, including light sterile neutrinos [2642], models with lepton asymmetries/non-zero neutrino chemical potential [2643,2644], thermal axions [2593], and so on. Relaxing the assumption that ERS are free-streaming can potentially help address the above shortcomings. The simplest possibility for such a *self-interacting dark radiation* is one where the ERS component is strongly self-coupled and therefore constitutes a perfect fluid [2645], whose Boltzmann hierarchy can be truncated to the first moment (with vanishing anisotropic stress). Nevertheless, when confronted with cosmological data, such a scenario fails to solve the Hubble tension [710], as it is unable to reduce the neutrino drag and Silk damping effects to an extent that is allowed by the data while raising H_0 sufficiently. When confronted with *Planck* 2018 and SDSS BAO data, one finds $H_0 = 68.67 \pm 0.84\,{\rm km\,s^{-1}Mpc^{-1}}$. Other natural extensions envisage the possibility of both free-streaming and self-interacting ERS, for instance within the "dark sector equilibration" model of Ref. [2646], and the "recoupling" or "instantaneous decoupling" models (such as in atomic DM [2647–2649] or twin Higgs [2650]) of Ref. [2325], which, however, can only partially alleviate the tension, leading to figures very similar to the previous ones. Yet another possibility to undo the unwanted effects of free-streaming ERS and improve the tension-solving ability of self-interacting dark radiation features scattering between the latter and the DM component: however, this model can only partially alleviate the Hubble tension and is disfavored from a model-comparison perspective due to its higher statistical complexity [710]. In this case, one finds $H_0 = 68.55 \pm 0.92\,{\rm km\,s^{-1}Mpc^{-1}}$from a fit to *Planck* 2018 and SDSS BAO data [710].

A class of models that has received considerable interest in this context features non-standard interactions that do not involve the dark radiation components, but the otherwise standard neutrino species. Non-standard neutrino interactions, for instance via a four-point contact interaction mediated by a sufficiently massive ($m \gtrsim 1\,{\rm keV}$) mediator, as studied in [1319,2325,2651–2663] can suppress or delay neutrino free-streaming, and, with it, the free-streaming-induced phase shift. for fixed values of the sound horizon r_s (which is mostly unaffected by these interactions), the position of the first acoustic peak would therefore be at higher multipoles. Reversing it to the observed position requires a higher value of H_0. It has been shown that a

combination of self-interacting neutrinos, additional dark radiation components ($N_{\rm eff} \sim 4$), and large neutrino masses ($M_\nu \sim 1\,$eV) can offset the unwanted effects of dark radiation on the damping tail of the CMB, and allow for large values of H_0 while not spoiling the fit to CMB temperature data [1318]. A fit to the latter and BAO data reveals a bi-modal distribution for the interaction strength, with stronger values of the interaction strength ($\sim 10^9$ times that of the weak interaction strength) being the tension-solving ones. Nevertheless, this solution is strongly challenged from both the data and theoretical perspectives. From the data side, small-scale polarization data strongly disfavor these models with strong self-interaction strength [2657,2658], which are also partially challenged by BAO data (due to the fact that r_s is unchanged) [1319]. In particular, when confronted against *Planck* 2018, SDSS BAO, and *PantheonPlus* SNIa data, one infers $H_0 = 67.3^{+2.2}_{-2.1}\,{\rm km\,s^{-1}Mpc^{-1}}$ and $H_0 = 66.7^{+2.2}_{-2.1}\,{\rm km\,s^{-1}Mpc^{-1}}$ for the moderately interacting and strongly interacting modes respectively [2657,2658]. Finally, from the model-building side, a model in which all three neutrinos self-interact equally is excluded by laboratory constraints [2664], while constructing a phenomenologically viable model has proven challenging [2663]. EFT analyses of BOSS data reveal support for a strongly interacting neutrino mode [2661], although an analysis combined with CMB data still disfavors the strongly self-interacting neutrino model where all 3 neutrinos are interacting [1319]. Interestingly, parameter degeneracies allow for a lower value of the scalar spectral index in the interacting neutrino model, which can be leveraged to allow for inflationary models that are otherwise ruled out within ΛCDM, such as natural inflation and Coleman–Weinberg inflation [2655,2659,2663]. It is worth noticing that large values of $N_{\rm eff}$ are in tension with BBN, unless this extra dark radiation is generated after the BBN epoch. This is the scenario studied in Ref. [2665], where a fraction of the DM abundance results from the decay of an unstable and initially thermally decoupled heavy particle, which decays into a DM particle (initially relativistic and therefore contributing to $N_{\rm eff}$, before becoming cold once the Universe has expanded sufficiently) and a Standard Model particle such as neutrinos or photons. In this case, one finds in the best case $H_0 = 69.08 \pm 0.71\,{\rm km\,s^{-1}Mpc^{-1}}$ and $S_8 = 0.850 \pm 0.008$ from a fit to *Planck* 2018, SDSS BAO, and *Pantheon* SNIa data.

Although the simplest self-interacting neutrino models appear to be ruled out, the framework remains a very interesting benchmark one and gives a good idea of possible ingredients one might want to consider in order to make non-minimal ERS models viable. Motivated by these considerations, various works have explored models of eV-scale Majorons, pseudo-Goldstone bosons associated with the spontaneous breaking of a global $U(1)$ lepton number symmetry. The Majoron enjoys weak couplings to neutrinos, although in the theoretically best motivated coupling limit, it cannot induce the four-point contact interactions mentioned earlier. The resulting phenomenology is instead dominated by inverse neutrino decays and Majoron decays. Overall, these effects still damp neutrino free-streaming, although with a different time dependence, which leads to a better performance of the model when confronted against cosmological data. It should be noted that Majoron decays also lead to a value of $\Delta N_{\rm eff} \sim 0.11$ [2666]. Nevertheless, although relatively successful, Majoron models fall short of completely solving the Hubble tension [2667], with $H_0 = 70.06^{+2.21}_{-2.31}\,{\rm km\,s^{-1}Mpc^{-1}}$ from a fit to *Planck* 2018, SDSS BAO, and *Pantheon* SNIa data. A fit to *Planck* 2018 and SDSS BAO data instead leads to $H_0 = 70.18 \pm 0.61\,{\rm km\,s^{-1}Mpc^{-1}}$, whereas the S_8 values inferred within the model are not available [2668].

The above are only examples of some of the ERS models considered in the literature, and it is beyond our scope to give a full list of examples. Other interesting possibilities which have been considered in the literature involve self-interacting sterile neutrinos [2669–2672], or the so-called stepped fluids [2561,2673–2675]. The latter are a particular class of self-interacting ERS models, consisting of a mix of massless and massive particles: when the temperature of the dark sector drops below the mass of a massive species, the latter deposits entropy in the lighter ones, leading to a "step" in the ERS energy density. Concrete Lagrangian realizations of these classes of models have been studied, for instance, within the context of "Wess-Zumino dark radiation", and have been found to be relatively promising in alleviating the Hubble tension, although current data sets do not show a strong preference for the model [2565]. From a fit to *Planck* 2018, SDSS BAO, and *Pantheon* SNIa data, one finds $H_0 = 69.3^{+0.9}_{-1.3}\,{\rm km\,s^{-1}Mpc^{-1}}$ and $S_8 = 0.829 \pm 0.011$ for the Wess-Zumino dark radiation model, whereas for a more general stepped dark radiation model these change to $H_0 = 68.8^{+1.3}_{-1.5}\,{\rm km\,s^{-1}Mpc^{-1}}$ and $S_8 = 0.823 \pm 0.013$ respectively [2561].

Overall, despite the fact that there is no consensus ERS model that solves the Hubble tension, many of these models possess interesting features that could guide the community in the right direction. It would therefore not be surprising if ERS were to play at least some role in the Hubble tension. These and related aspects are being actively investigated.

4.2. Late-time proposals

4.2.1. Late dark energy

Coordinator: Rafael C. Nunes

Contributors: Abdolali Banihashemi, Adrià Gómez-Valent, Anil Kumar Yadav, Anjan Ananda Sen, Anne Christine Davis, Arianna Favale, Benjamin L'Huillier, Branko Dragovic, Brooks Thomas, Carlos G. Boiza, Carsten van de Bruck, Celia Escamilla-Rivera, Cláudio Gomes, Cristian Moreno, Daniele Oriti, David Benisty, David Tamayo, Davide Pedrotti, Elsa Teixeira, Emmanuel N. Saridakis, Gaetano Lambiase, Giulia De Somma, Hsu-Wen Chiang, Hussain Gohar, Ilim Cimdiker, Jaume Haro, Javier Rubio, Joan Solà Peracaula, Juan García-Bellido, Jurgen Mifsud, Kathleen Sammut, Keith R. Dienes, Laur Järv, Laura Mersin, Leandros Perivolaropoulos, Leila L. Graef, Lilia Anguelova, Luis A. Escamilla, Luz Ángela García, Mahdi Najafi, Margus Saal, Mariam Bouhmadi-López, Masoume Reyhani, Mina Ghodsi Yengejeh, Nikolaos E. Mavromatos, Nima Khosravi, Oem Trivedi, Özgür Akarsu, Paloma Morilla, Paolo Salucci, Purba Mukherjee, Rahul Shah, Ronaldo C. Batista, Ruth Lazkoz, Salvatore Capozziello, Sanjay Mandal, Sebastian Bahamonde, Simony Santos da Costa, Suresh Kumar, Utkarsh Kumar, Víctor H. Cárdenas, Vasiliki A. Mitsou, Vincenzo Salzano, Vivian Poulin, and Wojciech Hellwing

4.2.1.1. Current status of simplified DE model parameterizations circa 2024. The key property of DE is its EoS, defined as $w \equiv \frac{P_x}{\rho_x}$. Extensions of the ΛCDM model, where w can either be a constant or a dynamical function of cosmic time, represent the simplest parametric approaches for testing deviations from the ΛCDM framework. Fig. 74 presents the current state-of-the-art constraints on the EoS, w, at the 68% CL, inferred from various dataset combinations under the assumption of the wCDM model [2676]. The figure is adapted from Ref. [1298]. As widely discussed in the literature, models with $w < -1$, when constrained using CMB data alone, tend to predict higher values of H_0, due to a strong degeneracy between w and H_0 [2677]. To achieve a more robust analysis, a joint dataset combination of CMB+BAO+SN+CC yields $H_0 = 68.6^{+1.7}_{-1.5}\,{\rm km\,s^{-1}Mpc^{-1}}$, which is in good agreement with the ΛCDM.

Robust and up-to-date analyses of simple extensions to the well-known dynamic $w(z)$CDM models are presented in Refs. [1283,2678]. The results include the most recent BAO measurements obtained by DESI. The preference for the $w(z)$CDM model remains robust, regardless of the parameterization used, but none of the parameterizations are able to resolve the H_0 tension. Similar or identical simple parametric models within the $w(z)$CDM class have been discussed in the literature. In general, while certain datasets may favor a dynamic parameterization of DE, these models are not capable of resolving the tension in H_0.

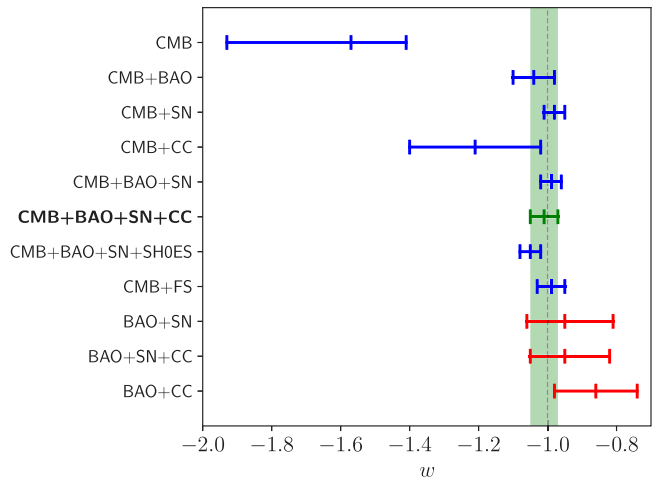

Fig. 74. The whisker plot summarizes the 68% CL intervals for the DE EoS parameter, w, inferred from various dataset combinations under the assumption of the wCDM model. Results that incorporate CMB data are represented by blue bars, except for the final consensus dataset combination (CMB+BAO+SN+CC), which is shown in green. In contrast, results obtained without the CMB data are depicted in red. The green band highlights the 68% CL interval derived from the final consensus dataset combination, yielding $w = -1.013^{+0.038}_{-0.043}$. The gray vertical dashed line marks the cosmological constant value, $w = -1$. (For interpretation of the references to colour in this figure legend, the reader is referred to the web version of this article.)
Source: Figure taken from Ref. [1298].

4.2.1.2. Challenges for late dark energy models from BAO and SNIa data on deformations of $H(z)$ and the ultra-late physics transition approach. LDE models aim to resolve the Hubble tension by introducing degrees of freedom that deform the Planck18 ΛCDM form of $E(z) \equiv H(z)/H_0$, reconciling the early sound horizon scale with late-time Cepheid calibrators. However, these models face significant challenges in simultaneously fitting the SH0ES H_0 value, the sound horizon scale at recombination, and distances from SNIa and anisotropic BAO at $z \in [0.01, 2.5]$. Many models also exacerbate the growth tension [3,769,1298,1363,2466,2532–2534,2679–2693].

Recent analyses also propose a rapid transition in the effective gravitational constant, $G_{\rm eff}$, at ultra-late times ($z_t \lesssim 0.01$) to address the tension [72,386,2682,2684,2694–2698]. This is based on the mismatch in absolute magnitude ($M_{\rm B}$) between CMB and local Universe observations. The luminosity distance–redshift relation

$$\mu(z) = m_{\rm B}(z) - M_{\rm B} = 5\log_{10}\left(\frac{d_{\rm L}(z)}{10\,{\rm pc}}\right),$$

suggests SNIa luminosities at $z > z_t$ are consistent with constant $G_{\rm eff}$ [1363]. A sudden transition in $G_{\rm eff}$ at z_t could explain the $\Delta M_{\rm B} \approx -0.2$ mag deviation in local SN needed to reconcile high- and low-redshift H_0 values. This model addresses the H_0 tension and suggests reduced growth of density perturbations without affecting ΛCDM background expansion [386,1363,2694,2695]. Future GW, astrophysical, and cosmological perturbation analyses may test this hypothesis in the context of physical models [2695,2696,2699]. The ultra-late $G_{\rm eff}$ transition provides a compelling alternative framework warranting further investigation.

On the other hand, when the inverse distance ladder is built with angular (or 2D) BAO, instead of anisotropic (or 3D) BAO, the phenomenology required to solve the Hubble tension is completely different. Angular BAO data are claimed to be less subject to model dependencies, since in contrast to anisotropic BAO analyses, no fiducial model is used to convert redshifts and angles into distances of a tracer map. Despite being obtained from the same parent catalogs, 2D and 3D BAO data are known to be in tension [764–766,768,769,2190], pointing to the existence of unaccounted-for systematic errors in one or both data sets or an underestimation of their uncertainties. When angular BAO is employed in the fitting analysis, it is possible to find a late-time solution to both the Hubble and growth tensions without violating the constancy of $M_{\rm B}$ [769]. The latter requires the effective DE density to become negative at $z \gtrsim 1.5-2$ to compensate for the late-time increase of $H(z)$ and not spoil the description of the CMB. This possibility has been recently realized in the context of a model with a sign-switching cosmological constant [801,802,811,812,2700–2702] and even more effectively in the model presented in Ref. [2485].

4.2.1.3. Holographic dark energy and gravity–thermodynamics correspondence models. The holographic principle, rooted in quantum gravity, proposes that a system's entropy is determined by its surface area rather than its volume. Holographic dark energy (HDE) utilizes this principle to describe late-time DE as an infrared cutoff for specific HDE models. Various alternative HDE formulations exist, including the Tsallis and Barrow models, each with distinct energy density equations and parameters [2703–2721]. Moreover, choices for the infrared cutoff can vary, ranging from simple options such as the Hubble horizon to more intricate ones like the Granda–Oliveros or Nojiri–Odintsov cutoffs. Beyond theoretical motivations, HDE models potentially resolve tensions in H_0 measurements. Fitting these models to comprehensive datasets yields values consistent with recent observations, possibly enhanced by incorporating sterile neutrinos [2722].

On the other hand, modified cosmology based on gravity-thermodynamics correspondence [2723–2726] is another way to explore the Universe's evolution. The relationship between black hole quantities and conventional thermodynamics [2727,2728] has been extended to cosmic horizons [2729], with a range of applications [2723,2725,2726]. In particular, these concepts have been used for entropic force cosmological models [2730–2735], in which entropic force terms account for the Universe's accelerated expansion. Furthermore, modifications to holographic dark energy models have been made using different notions of entropy [2736–2738] coming from statistical mechanics and thermodynamics. Indeed, the fundamental limit established by the Bekenstein entropy bound [2739] has had important consequences for understanding fundamental aspects of geometry and possible ways of reducing the Hubble tension [2740] consistent with data from Refs. [2741,2742].

The H_0 and σ_8 tension can be concurrently relieved by the modified cosmology employing Tsallis–Cirto nonextensive entropy [2736], as demonstrated in Ref. [2743]. The authors demonstrate how a phantom effective DE, which is recognized as one of the adequate processes that might relieve H_0 tension, can be obtained for specific Tsallis–Cirto parameter choices. Furthermore, given the same parameter choice, they find an enhanced friction term and an effective Newton's constant smaller than the conventional one, therefore solving the σ_8 tension. In Ref. [2744], the σ_8 tension is examined using Jacobson's method [2723] in the nonextensive setting. Additionally, Hubble tension can be relieved in entropic force cosmological models [2731,2745] because the interaction terms naturally arise from reversible and irreversible processes across the horizons in the evolution equations. Nevertheless, further work needs to be done to develop these approaches. Moreover, a wide range of holographic dark energy models have been utilized to examine these cosmological tensions, for example, Tsallis holographic dark energy [2746]. Addressing these cosmological challenges will require further research on gravity–thermodynamic relationship to cosmological applications.

4.2.1.4. Modeling late dark energy: Examining the phantom, tracker, quintom, multifield descriptions and their clustering properties. Phantom-scalar-field DE cosmologies are usually denoted by an EoS that satisfies $w < -1$ [2064,2747]. However, the current observations have shown a good agreement with the standard ΛCDM model. Within these observational analyses, some suggestions invoke the presence of a phantom divide boundary. Furthermore, these phantom scalar field DE models

have introduced scalar fields ϕ to study the dynamics of evolving DE through this phantom divided boundary, however, within this scheme, we experiment with issues like fine-tuning [2748]. To find a viable solution, tracker DE scenarios have been analyzed [295,2749], where ϕ controls the energy density and it is possible to obtain attractor background solutions. Some parametrizations in this regard [2750–2752] are used to verify if this model can solve (or relax) the H_0 tension. To introduce a phantom scalar field term, we consider a gravitational action as

$$S = \frac{1}{2\kappa^2}\int d^4x\sqrt{-g}\left(R + \mathcal{L}_\phi(\phi, \partial_\mu\phi) + \mathcal{L}_{\rm m}\right), \tag{4.9}$$

where $\mathcal{L}_\phi$ is the Lagrangian for a phantom scalar field. Considering a flat FLRW metric, we can vary Eq. (4.9) with respect to the metric and ϕ to obtain the gravitational field equations and the Klein–Gordon equation. In this scheme, it is standard to consider a new set of hyperbolic polar coordinates which can ease the numerical solutions [2751].

From the perspective of this ansatz, it was reported that this kind of phantom/tracker model does not address the Hubble tension when considering a compressed Planck likelihood, given a $H_0 = 69.1^{+0.5}_{-0.6}\,{\rm km\,s^{-1}Mpc^{-1}}$ [2751] value, which is in a 3σ CL tension with the latest local result [34]. However, Ref. [2753] explored the possibility of reconstructing the constraints using the full Planck [192] likelihood in addition to model-independent CMB baselines, e.g., ACTPol DR4 [702], the SPT-3G [725] and the WMAP9 [2754] datasets, showing that phantom tracker scalar field cosmologies can reduce the statistical tension on H_0 to below 3σ.

However, quintom DE, featuring two scalar fields with distinct kinetic energies, blends quintessence and phantom characteristics, and has been shown to be a framework of interest. Model-independent techniques reveal a fluctuating EoS, crossing the phantom divide line ($w_{\rm DE} = -1$) multiple times. Quintom models offer a promising alternative to standard quintessence and phantom models, potentially providing a more accurate fit with fewer parameters. Several studies explore quintom's potential in resolving the H_0 tension, with analyses coupling the phantom component to DM and examining various quintessence, phantom, and quintom models. These studies yield various estimates of the Hubble constant, suggesting the possibility of reducing the tension by up to 2.6 σ [1263,2066,2067,2069,2091,2103,2106,2755–2765].

Multifield models of cosmic acceleration arise from the coupling of several scalar fields to gravity. The standard action that describes this system is

$$S = \frac{1}{2\kappa^2}\int d^4x\sqrt{-g}\left[R - G_{IJ}(\{\phi^L\})\partial_\mu\phi^I\partial^\mu\phi^J - V(\{\phi^L\})\right], \tag{4.10}$$

where $g_{\mu\nu}$ is the four-dimensional space–time metric and G_{IJ} is the metric on the manifold parameterized by the scalars ϕ^I with $I = 1, 2, \ldots, n$. When the field-space metric G_{IJ} has curvature, such multifield models can lead to novel effects, compared to single-scalar field models, in the context of both cosmological inflation and LDE. Specifically, for LDE models of this type, see Refs. [2766–2771].

The qualitatively new features of the multifield case arise from solutions of the background equations of motion, whose field-space trajectories are (strongly) non-geodesic. In the case of two fields, that is, when $n = 2$, the deviation from a geodesic is measured by the turning rate of the background trajectory $(\phi_0^1(t), \phi_0^2(t))$ in field space, $\Omega = -N_I D_t T^I$, where T^I and N_I are unit vectors, respectively, tangent and normal to the trajectory; also $D_t T^I \equiv \dot\phi_0^J \nabla_J T^I$. Strongly non-geodesic trajectories are characterized by large turning rates. Multifield models of LDE, whose background solutions have such rapid-turning field-space trajectories, can have an equation of state parameter w very close to -1 and, despite that, can be observationally distinct from a cosmological constant [2768–2771]. This is because the speed of sound c_s of the dark-energy perturbations around the background solution can be (significantly) reduced compared to the speed of light.

DE perturbations around the exact background solution of Ref. [2770] were studied in Ref. [2771]. It was shown there that the speed of sound of these perturbations is significantly reduced. Combining that with an equation of state parameter $w \approx -1$, as well as incorporating matter in the exact background solution, it was further argued in Ref. [2771] that this model of multifield DE is very promising for alleviating simultaneously the σ_8 and Hubble tensions.

More generally, a low sound speed of DE perturbations is a natural possibility of any k-essence model [1263,2772,2773] and also phantom models [1264]. In this case, DE perturbations can grow on small scales and impact the structure formation, see Ref. [2774] for a review. Recent efforts in understanding the effects of DE perturbations in structure formation include Refs. [2775–2778], but we still need an accurate determination of their impact on nonlinear observables.

With more freedom in the perturbative sector, clustering DE models could circumvent the usual trend seen in late DE models of worsening the growth tension. However, some explorations of this case were conducted only for non-phantom EoS. Recent analyses of this scenario indicate that DE with low sound speed worsens the S_8 tension [2779] and the very low c_s values are not allowed by current data [2780].

4.2.1.5. Running vacuum models. Quantum fluctuations in the expanding Universe induce the running of the vacuum energy density (VED). An example, motivated by dualities in string theory is Ref. [2781] where the spacetime vacuum is such that its trans-Planckian modes are coupled and track the Hubble expansion rate [2782–2786]. The running character of the vacuum was originally motivated using renormalization group arguments in curved spacetime [2787–2789], but more formal calculations have been recently performed in the context of QFT in curved spacetime using adiabatic regularization and renormalization techniques [2790–2792] as well as effective low-energy string theory [2471,2472,2479]. See Refs. [2793,2794] for dedicated reviews of the RVM within the QFT approach and [2473] for the stringy version. The running VED takes the following form

$$\rho_{\rm vac}(H) = \frac{3}{8\pi G}(c_0 + \nu H^2 + \tilde\nu\dot H) + \mathcal{O}(H^4). \tag{4.11}$$

In contrast to the rigid energy density $\rho_\Lambda = \Lambda/8\pi G$ associated with the cosmological constant in ΛCDM, $\rho_{\rm vac}$ also receives dynamical contributions from the quantized matter fields. For $\nu, \tilde\nu \neq 0$ the VED becomes dynamical. Eq. (4.11) lies at the core of the class of RVMs. The higher-order terms $\mathcal{O}(H^4)$ can explain inflation with a graceful exit without the need of *ad hoc* scalar fields [2475–2477,2477,2795,2796]. Here we just focus briefly on the low-energy terms appearing in Eq. (4.11), which are controlled by the parameters ν and $\tilde\nu$. Their values depend on the masses and non-minimal couplings (in the case of the scalar fields) of the various particle species of the theory, and they are expected to be $\lesssim \mathcal{O}(10^{-4} - 10^{-2})$, although they are ultimately determined from observations. In spite of being small, the running of the vacuum can leave a non-negligible imprint on the post-inflationary stages of cosmic expansion both at the background and perturbation levels. The time evolution of $\rho_{\rm vac}$ may imply either the non-conservation of matter and/or the time-evolution of the gravitational coupling G and other fundamental "constants" of nature, and this can lead to a variety of scenarios explored in the literature [2797–2802]. The RVMs are able to accommodate the wealth of cosmological data at our disposal and have a positive bearing on the cosmological tensions. The RVMs were actually the first to point out significant hints of DE (vacuum) dynamics in the Universe using a large amount of cosmological data, almost one decade before the advent of DESI [2803,2804], see also Refs. [2803–2809] and Refs. [2810–2813]. The most updated constraints on these models can be found in the recent works Refs. [2814,2815], where the authors analyze the RVMs in light of a complete dataset under the simplified assumption $\tilde\nu = \nu/2$ and show that coupling between DM and the running vacuum can significantly loosen the growth tension, especially when the vacuum dynamics is activated at $z \sim 1$, and also that a joint

running of $\rho_{\rm vac}$ and G can strongly mitigate both the growth and H_0 tensions. This is also true in the Brans–Dicke model [2418–2420,2816].

The stringy version of the RVM [2471–2473,2479] provides both early- and late-dark-energy models within string theory [2817,2818]. This model, a Chern–Simons modification of GR [2469], results in a vacuum energy density with logarithmic corrections in the Hubble parameter, $H^2 \ln H$. These corrections, arising from quantum graviton effects in an expanding Universe [2819], help alleviate the H_0 and growth-of-structure tensions [2484], and can dominate logarithmic corrections from matter QFT effects [2790–2792].

4.2.1.6. Emergent dark energy. Dynamic DE models are gaining attention over the simple cosmological constant, Λ, to reconcile discrepancies between CMB and SH_0ES data [2508,2820]. One such model is Critically Emergent Dark Energy (CEDE), where DE emerges as a critical phenomenon [2821–2823]. In CEDE, DE density grows from zero in a phase transition, with an order parameter sensitive to photon thermal baths. Below a critical redshift, z_c, DE self-interaction dominates, leading to universal order. This model uses Ginzburg–Landau theory to describe phase transitions and derives DE density dependence below z_c as [2823,2824]

$$\kappa^2\rho_{\rm DE}(z)/3H_0^2 = (1-\Omega_{\rm m,0}-\Omega_{\rm r,0})\sqrt{1-z/z_c}\,. \tag{4.12}$$

Confronting this phantom-like model with the CMB data [729], yields $H_0 = 70.0^{+1.2}_{-2.7}\,{\rm km\,s^{-1}Mpc^{-1}}$with less χ^2 than ΛCDM. Adding SN data [2033] and/or BAO data [776,777,2433,2515], pushes z_c toward larger values where practically ΛCDM is restored; and the H_0 posterior shrinks to the tension zone of Planck18. CEDE offers richer predictions beyond phantom-like DE. Considering the specific scale dependence of DE density fluctuations in this model [2825], it alleviates both low-ℓ/high-ℓ inconsistencies in the CMB angular power spectrum and the $A_{\rm L}$ anomaly reported by Planck [192]. Assuming CEDE, 1σ posterior intervals of cosmological parameters are constrained with $\ell < 800$ and $\ell > 800$ overlap. Additionally, in this framework, $A_{\rm L}$ is consistent with unity well within the 1σ region.

Another Phenomenologically Emergent Dark Energy (PEDE) model developed to address the Hubble tension is [2508]

$$\Omega_{\rm DE}(z) = \Omega_{\rm DE,0}\left[1-\tanh\left(\log_{10}(1+z)\right)\right]\,. \tag{4.13}$$

The lack of additional parameters makes the model especially intriguing. However, Ref. [2826] argues that while the PEDE model fits background data well, it fails to match cluster-scale observations compared to ΛCDM at the perturbation level. Various authors further analyzed this model statistically with diverse cosmological datasets and in extended frameworks [1270,2187,2192,2511,2690,2827–2834]. However, it offers a worse fit to the combined datasets in comparison to ΛCDM [710]. As extensions of the PEDE model, include the generalized emergent dark energy (GEDE) [2511,2820] and the modified emergent dark energy (MEDE) models [2835]. Both the MEDE & GEDE frameworks can help in reducing the H_0 tension to $\lesssim 3\sigma$ CL.

4.2.1.7. Vacuum metamorphosis. The Vacuum Metamorphosis (VM) model, proposed to explain the late-time accelerated expansion of the Universe, is based on non-perturbative quantum gravitational effects [2836–2838]. It features a minimally coupled, ultra-light scalar field with mass $m \sim 10^{-33}$ eV. The model's key aspect is a gravitational phase transition occurring when the Ricci scalar curvature R reaches the order of the scalar field's squared mass, m^2, which is related to the current matter density parameter $\Omega_{\rm m,0}$. In this framework, the gravitational phase transition occurs at the critical redshift $z_t = -1 + \frac{3\Omega_{\rm m,0}}{4(1-M)}$, where M is a free parameter of the theory.

This transition leads to an effective radiation component in the Universe post-transition, resulting in a De-Sitter phase, distinct from the ΛCDM scenario. In the original VM scenario, there is no cosmological constant at high redshifts, and the matter density parameter $\Omega_{\rm m,0}$ is given by $\left[\frac{4}{3}\left(3M(1-M-\Omega_k-\Omega_{\rm r,0})\right)^3\right]^{1/4}$, where $\Omega_k = -k/H_0^2$ and $\Omega_{\rm r,0}$ is the radiation density parameter. Joint analysis with *Planck* 2018 + BAO + Pantheon yields $H_0 = 74.21 \pm 0.66\,{\rm km\,s^{-1}Mpc^{-1}}$ [2839], which resolves the H_0 tension within 1σ. An extension of the VM model, namely the VM-VEV model, includes a cosmological constant at high redshifts, represented by the vacuum expectation value of the massive scalar field. This extension requires additional conditions such as the transition occurring in the past ($z_t \geq 0$) and the DE density being non-negative post-transition i.e., $\Omega_{\rm DE}(z > z_t) \geq 0$, respectively. Joint analysis with *Planck* 2018 + BAO + Pantheon leads to $H_0 = 73.26 \pm 0.32\,{\rm km\,s^{-1}Mpc^{-1}}$ [2839]. While the VM & VM-VEV models can align H_0 with the SH0ES value, they exhibit a poorer fit to low-redshift data, such as BAO and Pantheon, compared to ΛCDM.

4.2.1.8. Others DE frameworks and their implications for the H_0 tension. Rather than initially adopting a particular physical model for DE, given our lack of clear insight into its origin, we can opt for an exploratory approach utilizing a probing function to represent the DE density. The DDE model, generalized to $w(z) = \sum_n w_n x(z)$, where the parameters w_n are fixed by observations and $x(z)$ is a function of redshift that can correspond to both phantom and non-phantom fields, has been shown to alleviate the σ_8 tension [2840] as well as the H_0 tension. It is worth noting that the H_0 tension improves further when the neutrino mass $\sum_\nu m_\nu$ is taken into account [2841]. Another approach was initiated in Refs. [2055,2056,2842], where the authors used both linear and quadratic probe functions for $X(z) = \frac{\rho_{\rm DE}(z)}{\rho_{\rm DE}(0)}$. For ΛCDM, $X(z) = 1$, while $X(z) \neq 1$ for *any* redshift z indicates DE evolution. A quadratic probe function used in the literature is proposed in Ref. [2057]. This perspective shows that such an approach may prefer $X(z)$ decreasing with z, even taking negative values for $z > 1$. Using the most recent BAO observations from the DESI [699], the same trend was found in Ref. [809]. This trend, including the possibility of a negative $X(z)$, poses a challenge for DE modeling and may have profound implications in light of recent cosmological tensions and the foundations of standard cosmology.

A pseudo-Rip DE scenario, leading to asymptotically de Sitter behavior, is proposed in Ref. [2843]. This model appears to be statistically favored over the consensus ΛCDM model according to some Bayesian discriminators. The equation of state parameter, typically evaluated at the present time, is given by $w_0 = -1 - \frac{\eta\lambda{\rm sech}(2\lambda)}{3\arctan(\sinh(\lambda))}$, where η is a free parameter of the model. It is concluded that the pseudo-Rip ΛCDM model significantly improves the description of late-time ($z \lesssim 2.5$) data more decisively than that at higher redshifts.

Late-time DE transitions at redshifts $z \ll 0.1$ [2532] can make the predicted value of H_0 compatible with SH0ES measurements. Conversely, in Ref. [2844], a model-independent constraint on late-time models shows strong evidence against homogeneous new physics over the ΛCDM model. Surprisingly, despite the absence of H_0 and $M_{\rm B}$ tensions in the local Universe, Ref. [2845] argues that late-time data solutions to the H_0 tension require a smaller sound horizon at the recombination era. Additional discussions on r_d scales and H_0 tension can be found in Refs. [769,2846]. The authors in Ref. [2847] argue that new physics at low redshifts cannot resolve the H_0 tension.

It is important to emphasize that simple scalar field quintessence models have been widely studied for their ability to address the coincidence problem through tracking behavior. A possibility is to use generalized axion-like models with inverse-cosine-like potential [2848–2851], which provides natural entrance and exit of the tracking regime within a single-field framework. While it is not ruled out, the Hubble tension can be slightly reduced [2852]. Also, a different approach to tackle the late acceleration of the Universe is by invoking a modified Chaplygin gas [2853–2856], being the simplest case when its equation of state deviates from that of a cosmological constant by a simple power law of its energy density. This was analyzed from a perturbation point of view in Ref. [2857].

We also highlight that the cosmological stasis framework [2858–2860] is a phenomenon arising within many BSM cosmologies in which

the abundances Ω_i of multiple cosmological energy components with different equation of state parameters w_i remain constant across extended periods despite cosmic expansion. This occurs due to dynamical feedback within the equations of motion for the corresponding energy densities, with the stasis state serving as a global dynamical attractor. Such systems evolve toward stasis irrespective of initial conditions and remain in stasis until some underlying mechanism alters the dynamical feedback. Most importantly, the effective equation of state parameter $w_{\rm eff} = \sum_i \Omega_i w_i$ for the Universe remains constant during stasis but nevertheless generically differs from the canonical values associated with, e.g., matter, radiation, or vacuum energy. Stasis at either early or late-times (relative to recombination) can therefore potentially broaden the scope of possibilities for reconciling cosmological tensions. In a similar context, we can also mention the effects of the backreaction of super-Hubble cosmological fluctuations on the late-time accelerated expansion [2861]. Some works suggested that this mechanism could drive a dynamical self-regulating relaxation of the cosmological constant, as first speculated in Ref. [2862]. This behavior could potentially result in an oscillatory effective DE [2863]. A discussion on the tension problem within these scenarios can be found in Ref. [2863], which also provides further references on these models.

4.2.2. Dark energy models exhibiting a rapid density transition from negative to positive values in the late universe

Coordinator: Özgür Akarsu, Rafael C. Nunes

Contributors: Adrià Gómez-Valent, Alexander Zhuk, Anil Kumar Yadav, Anjan Ananda Sen, Antonio De Felice, Branko Dragovic, Davide Pedrotti, Emmanuel N. Saridakis, Emre Özülker, Eoin Ó Colgáin, Hanyu Cheng, J. Alberto Vázquez, Joan Solà Peracaula, Jurgen Mifsud, Laur Järv, Leandros Perivolaropoulos, Leila L. Graef, Luca Visinelli, Luis Anchordoqui, M.M. Sheikh-Jabbari, Nihan Katırcı, Ruth Lazkoz, and Suresh Kumar

The possible need for DE assuming negative density values at high redshifts was first highlighted by BOSS collaboration [789], detecting $\Lambda > 0$ for $z < 1$ but favoring $\rho_{\rm DE} < 0$ for $z > 1.6$, particularly based on Ly-α BAO measurements at $z_{\rm eff} \approx 2.34$, which exhibited a 2.5σ tension with Planck-ΛCDM [192] and suggested a non-monotonic $H(z)$ evolution that is difficult to reconcile with strictly $\rho_{\rm DE} \geq 0$ in GR. Independently, Ref. [444] proposed that this discrepancy with Planck-ΛCDM, known as the Ly-α BAO anomaly, could be explained by an MG model in which $\Lambda > 0$ is dynamically screened, leading to an effective $\rho_{\rm DE}$ passing below zero, accompanied by a singularity in its EoS parameter $w_{\rm DE}$, at $z \sim 2.3$. This discrepancy was later reduced to $\sim 1.5\sigma$ with the completed eBOSS [1533]. However, model-independent/non-parametric reconstructions of $\rho_{\rm DE}$, using the BAO data, consistently favor $\rho_{\rm DE}$ crossing below zero or vanishing for $z \gtrsim 1.5-2$. Moreover, such reconstructions of $w_{\rm DE}$ — though inherently unable to capture a sign change in DE density — persistently favor $w_{\rm DE} \sim -1$ for $z \lesssim 1-1.5$ but trend toward large negative values below -1 at $z \sim 1.5-2$ — which is expected right after a DE density smoothly transitions from negative to positive as the Universe expands, therefore potentially indicating a sign change in $\rho_{\rm DE}$. The recent DESI Ly-α BAO data shows no tension with Planck-ΛCDM [699]. However, while DESI BAO data — when analyzed using the CPL parameterization — provides more than 3σ evidence for dynamical DE [699], a less noted but significant finding is that non-parametric reconstructions of DE density also indicate the possibility of vanishing or negative values for $z \gtrsim 1.5-2$ [809,2864], consistent with trends observed in pre-DESI BAO data, e.g., SDSS BAO [2145,2162,2864].

It was not immediately recognized that addressing the Ly-α anomaly could naturally be linked to the H_0 and S_8 tensions, both of which emerged sometime after the Ly-α anomaly was first identified. A brief explanation of this connection is as follows [801,811]: If a DE model leaves the pre-recombination Universe remains unaltered, as in the standard ΛCDM model, then the comoving sound horizon at last scattering, $r_* = \int_{z_*}^{\infty} c_{\rm s} H(z)^{-1} {\rm d}z$, is expected to remain effectively unchanged from its ΛCDM counterpart. The Planck CMB spectra provide precise, nearly model-independent measurements of the angular scale of the sound horizon, $\theta_* = r_*/D_M(z_*)$, and the present-day physical matter density, $\Omega_{\rm m,0}h^2$, derived from the peak structure and damping tail. Consequently, in DE models featuring negative DE densities at high redshifts, say, for $z > z_\dagger$, both the comoving angular diameter distance to last scattering, $D_M(z_*) = c\int_0^{z_*} H(z)^{-1}{\rm d}z$, and $\Omega_{\rm m,0}h^2$ must remain consistent with their Planck-ΛCDM inferred values. This requires that any suppression of $H(z)$ at $z > z_\dagger$, due to negative DE density, must be compensated by an enhancement of $H(z)$ at $z < z_\dagger$ to maintain consistency with the Planck-ΛCDM-inferred $D_M(z_*)$. As a result, this mechanism naturally increases H_0 (implying a fainter $M_{\rm B}$) and decreases $\Omega_{\rm m,0}$ relative to Planck-ΛCDM. A later transition (i.e., smaller $z_\dagger$) leads to a prolonged phase of suppression, or similarly, more negative DE density values lead to more suppression; both effects amplify the enhancement in H_0 and reduction in $\Omega_{\rm m,0}$, provided the transition occurs before the negative DE density becomes dominant — beyond which expansion would halt and contraction would ensue. This framework also predicts higher σ_8 values because the suppressed $H(z)$ at $z > z_\dagger$ reduces cosmic friction, thereby enhancing structure formation at high redshifts [2696,2865]. However, the lower present-day matter density leads to reduced $S_8 = \sigma_8\sqrt{\Omega_{\rm m,0}/0.3}$ values, potentially resolving the S_8 tension. This reduced cosmic friction enhances structure formation for $z > z_\dagger$ [801], potentially explaining the JWST anomaly [1755,1759,2866,2867] — where deep-space observations at $z \gtrsim 5$ indicate stronger structure growth than predicted by Planck-ΛCDM.

In the rapidly growing literature, fitting within the framework outlined above, Refs. [2700,2868] are the earliest studies explicitly connecting the Ly-α anomaly with the H_0 tension. Ref. [2868] assumed that the Universe is consistent with Planck-ΛCDM for $z \gtrsim 4$ and reconstructed $H(z)$ using low-redshift data, including Ly-α BAO. They found that the DE density reaches a minimum within a certain redshift range and becomes negative for $z \gtrsim 2$, accompanied by higher H_0 values, and argued that this behavior can be most simply explained by an AdS-like cosmological constant ($\Lambda < 0$) combined with an evolving DE component. Ref. [2700] proposed that inertial mass density, $\varrho \equiv \rho + p$, maybe more fundamental than energy density and introduced a DE parameterization with a minimal dynamical deviation from the usual vacuum energy/cosmological constant ($\varrho = 0$) in the form $\varrho \propto \rho^\lambda$, referred to as graduated dark energy (gDE) ($\varrho = {\rm const}$, simple-gDE [2869]). gDE exhibits a wide range of behaviors depending on λ; notably, for large negative λ, it serves as a phenomenological model for an AdS-to-dS-like transition in DE. It was shown via gDE that joint observational data, including but not limited to Planck-CMB and Ly-α BAO, suggest $\lambda \sim -18$, indicating a behavior analogous to a rapid AdS-to-dS transition at $z_\dagger \sim 2$, consequently alleviating both the H_0 tension and the Ly-α anomaly. With this constraint on λ, gDE resembles a smooth step-like function, yielding $\rho_{\rm gDE}/\rho_{\rm c0} \sim -0.7$ with $w_{\rm DE} \gtrsim -1$ for $z_\dagger \gtrsim 2$ before rapidly switching sign at $z_\dagger \sim 2$ and settling at $\rho_{\rm gDE}/\rho_{\rm c0} \approx 0.7$ with $w_{\rm DE} \lesssim -1$ for $0 \leq z \lesssim 2$.[56] This led to the conjecture that around $z_\dagger \sim 2$, the Universe underwent a period of rapid

[56] For a minimally interacting DE with $\rho_{\rm DE}$ transitioning from negative to positive at $z_\dagger$ as the Universe expands (z decreases), physical consistency demands $\rho_{\rm DE} < 0$ with $w_{\rm DE} > -1$ just before the transition and $\rho_{\rm DE} > 0$ with $w_{\rm DE} < -1$ just after, ensuring a smooth crossing through $\rho_{\rm DE} = 0$ while maintaining the continuity equation. Since $p_{\rm DE}$ remains finite, $w_{\rm DE}$ exhibits a singularity at $z = z_\dagger$, with $\lim_{z\to z_\dagger^\pm} w(z) = \pm\infty$. However, this is a safe singularity — $\rho_{\rm DE}$ remains finite, and $w_{\rm DE}$ diverges solely because $\rho_{\rm DE}$ crosses zero while $p_{\rm DE}$ remains finite and nonzero. Consequently, given that $H^2 \propto \rho_m + \rho_{\rm DE}$, H and other kinematical parameters evolve smoothly; in scalar field realizations, the sound speed remains luminal, further reinforcing the regularity of the crossing [2870]. By contrast, the alternative scenario of sign-changing $\rho_{\rm DE}$ — where $\rho_{\rm DE} < 0$ with $w_{\rm DE} < -1$ just before the transition and

mirror AdS-to-dS transition in vacuum energy — rapid sign-switching cosmological constant, Λ_s, from negative to positive while preserving the magnitude — or a similar phenomenon.

The Λ_sCDM framework [801,802,811,812,1325,2872] extends ΛCDM by replacing the usual cosmological constant (Λ) with a dynamically evolving counterpart (Λ_s) that undergoes a mirror AdS-to-dS transition in the late Universe, while leaving other standard cosmological components — such as CDM, baryons, pre-recombination physics, BBN, and inflation paradigm — unchanged. This transition can typically be described using sigmoid-like functions, such as the smooth approximation of the signum function, $\operatorname{sgn} x \approx \tanh(kx)$, where $k > 1$ and x represents either redshift (z) or scale (a). An example is $\Lambda_s(z) = \Lambda_{s0} \tanh[\nu(z_\dagger - z)]/\tanh[\nu z_\dagger]$, where $\nu > 1$ controls the sharpness of the transition, $\Lambda_{s0} > 0$ is the present-day value, and $z_\dagger$ denotes the transition redshift. For a rapid transition (e.g., $\nu \gtrsim 10$) occurring at $z_\dagger \sim 2$, this function effectively behaves as $\Lambda_s \approx \Lambda_{s0}$ for $z \lesssim 2$ and $\Lambda_s \approx -\Lambda_{s0}$ for $z \gtrsim 2$. In the limiting case $\nu \to \infty$, the transition becomes instantaneous, $\Lambda_s(z) \to \Lambda_{s0} \operatorname{sgn}[z_\dagger - z]$, defining the *abrupt* Λ_sCDM model, which extends ΛCDM by a single additional parameter, serving as an idealized representation of a rapid mirror AdS-to-dS transition. Abrupt Λ_sCDM [801,802,811,812,1325,2872] has emerged as one of the most promising and economical extensions of ΛCDM; introduces only a single additional parameter, $z_\dagger \sim 2$ (estimated through robust observational analyses), beyond ΛCDM, resolving major cosmological tensions — including those in H_0, M_B, and S_8 — as well as the BAO Ly-α anomaly, while yielding an age of the Universe consistent with estimates from the oldest globular clusters. Additionally, when allowing variations in m_ν and $N_{\rm eff}$, it predicts values consistent with the standard model of particle physics [1325], suggesting that it may avoid the recently proposed anomaly in which cosmological data (such as DESI BAO), within the ΛCDM framework, appears to favor $m_\nu < 0$ [1307,1324,2386,2873–2875] (see Section 2.3.5). From a physical perspective, Λ_sCDM is identical to ΛCDM for $z < z_\dagger$, featuring a dS-like cosmological constant after the transition, but introduces a minimal modification by adopting an AdS-like cosmological constant for $z > z_\dagger$, i.e., for all redshifts prior to the transition. However, from a phenomenological perspective — viz., in terms of the Universe's expansion dynamics and observational signatures — the impact of this modification is effectively confined to redshifts $z \lesssim z_\dagger \sim 2$. Specifically, Λ_sCDM replicates the $H(z)$ of ΛCDM for $z < z_\dagger$ — albeit with systematically larger values — introduces $H(z)$ deformation around $z \sim z_\dagger$, and becomes nearly indistinguishable from ΛCDM at higher redshifts ($z \gtrsim 3$). Consequently, from a phenomenological standpoint, Λ_sCDM is a post-recombination/late-time modification to ΛCDM. Abrupt Λ_sCDM, the simplest phenomenological realization of the Λ_sCDM framework, has been extensively studied [801,802,811,812,1325]. However, its abrupt transition at $z = z_\dagger$ introduces a discontinuity, leading to a type II (sudden) singularity [2876] at $z = z_\dagger$, though Ref. [2696] has shown this has negligible impact on cosmic structure formation and evolution. Nonetheless, this singularity suggests that the abrupt Λ_sCDM model should be interpreted as an idealized approximation, effectively serving as a proxy for a rapid yet smooth transition.[57]

We refer readers to Refs. [425,444,769,789,802,1288,1291,1292,1325,2046,2103,2104,2224,2248,2465,2485,2508,2689,2701,2821,2822,2868–2870,2872,2878–2910] for further theoretical and observational studies — including model agnostic reconstructions (see Section 3.3) — that explore DE with negative densities, often consistent with an AdS-like cosmological constant, at $z \gtrsim 1.5-2$, and aimed at addressing major cosmological tensions. Phantom DE models, which typically feature $\rho_{\rm DE}$ that decreases with redshift but are conventionally assumed to yield $\rho_{\rm DE} > 0$, are known to mitigate the H_0 tension. Among these, the *phantom crossing model*, proposed phenomenologically in Ref. [2911] (DMS20 [813]), stands out. A recent analysis, which considered this model as a particular example of the broader Omnipotent DE class [813], reaffirmed its success while also revealing that its ability to assume negative densities for $z \gtrsim 2$ — mimicking an AdS-like cosmological constant beyond sufficiently high z — is central to its effectiveness. IDE models [768,800,2427,2912–2922] (see Section 4.2.3) offer an alternative approach to resolving the H_0 tension; however, model-independent reconstructions of the IDE kernel [2162] suggest that negative DE densities at $z \gtrsim 2$ persist as a possibility.

While late-Universe rapid AdS-to-dS (or analogous) transitions in DE, as proposed by Λ_sCDM, were initially viewed as challenging to reconcile with a robust physical mechanism, the remarkable phenomenological success of this approach — despite its simplicity — has prompted deeper theoretical inquiries. Even established frameworks, upon re-examination, have been found to accommodate such transitions within previously overlooked solution spaces, prompting researchers to adopt a fresh perspective on familiar theories. For instance, Λ_sCDM$^+$ [2701,2899,2900] proposes a stringy realization of Λ_sCDM; it was shown that, despite the AdS swampland conjecture suggesting that a late-universe AdS-to-dS transition is unlikely due to the arbitrarily large separation between AdS and dS vacua in moduli space, such a transition can nonetheless be realized through the Casimir forces of fields inhabiting the bulk.[58] Building on the same theoretical framework, Λ_sCDM$_\pm$ [2926] extends Λ_sCDM$^+$ by allowing the AdS phase to have arbitrary depths, considering different curvature radii in the AdS and dS phases. It was demonstrated in Ref. [2897] that, in various formulations of GR, a Λ_s can arise naturally through an overall signature change of the metric. Λ_sVCDM [802,2872] advances the Λ_sCDM framework into a theoretically complete physical cosmology, offering a fully predictive description of the Universe, including the AdS-to-dS transition epoch itself. It was shown that

$\rho_{\rm DE} > 0$ with $w_{\rm DE} > -1$ just afterward — leads to singularities in both $w_{\rm DE}$ and $\rho_{\rm DE}$, as $\lim_{z\to z_\dagger^\pm} w_{\rm DE}(z) = \mp\infty$ and $\lim_{z\to z_\dagger^\pm} \rho_{\rm DE}(z) = \mp\infty$, thereby leading to a breakdown of the spacetime metric. Thus, only the first scenario is physically viable, predicting a phantom-like phase ($w_{\rm DE} < -1$) following the transition. Consequently, the tendency of model-agnostic reconstructions of $w_{\rm DE}(z)$ and various EoS parameterizations (e.g., CPL) to favor large negative values beyond -1 for $z \sim 1.5-2$ may indicate negative or vanishing DE densities for $z \gtrsim 1.5-2$. For further discussion, see Refs. [813,2696,2870,2871]

[57] A well-defined formulation necessitates a smooth transition, enabling a detailed study of perturbations but introducing theoretical challenges. A rapid AdS-to-dS transition can sharply increase $\dot{H}$, inducing transient super-acceleration ($\dot{H} > 0$), which may affect cosmological observables and, within GR, is often linked to ghost instabilities and WEC violations. These impose constraints on the transition's rapidity in GR but may be circumvented in type-II minimally MG theories such as VCDM [2877,2878]. For further discussion, see [802,2870,2872].

[58] By combining swampland conjectures with observational data, it was proposed that the cosmological hierarchy problem — i.e., the smallness of DE density in Planck units — could be understood as an asymptotic field-space limit corresponding to the decompactification of a micron-sized extra (dark) dimension [2923]. Within this framework, Casimir forces from fields inhabiting the dark dimension can drive an AdS-to-dS transition [2899], forming the basis of the Λ_sCDM$_\pm$ and Λ_sCDM$^+$. Specifically, a 5D Einstein–de Sitter gravity action compactified on a circle induces a runaway potential inherited from the 5D cosmological term [2924]. If the 5D cosmological constant is small, the quantum contribution of the lightest 5D modes — identified with Casimir energy [2925] — becomes significant. A minimal setup requires a 5D mass spectrum comprising the graviton, three generations of light right-handed neutrinos, and a real scalar field φ with a potential featuring two local minima [2899]. At $z_\dagger \sim 2$, φ undergoes quantum tunneling from the false to the true vacuum [2900], acquiring a larger mass and suppressing its Casimir energy contribution. This modifies the balance of fermionic and bosonic degrees of freedom, triggering the AdS-to-dS transition. The deep infrared fields of the dark sector contribute to the effective number of relativistic neutrino-like species.

the mirror AdS-to-dS transition can be effectively realized within a type-II minimally MG framework called VCDM [2877,2878], through a specific Lagrangian incorporating an auxiliary scalar field with a smoothly sewed two-segmented linear potential. Ref. [2903] demonstrated that the teleparallel $f(T)$ gravity, specifically its exponential infrared form [2927], which has shown significant promise in addressing the H_0 tension [2928,2929] in its solution space giving phantom-like effective DE, admits previously overlooked solution spaces, which accommodate an alternative scenario where the effective DE transitions smoothly from negative to positive at $z_\dagger \sim 1.5$, while remaining consistent with CMB power spectra. Building on these insights, $f(T)$-Λ_sCDM successfully maps the background dynamics of Λ_sCDM into the $f(T)$ gravity framework [2904], further establishing a theoretical foundation for AdS-to-dS-like transitions in the late Universe. Ph-Λ_sCDM [2870], introduced a phantom DE model, which is a specific realization of a general scalar field with a hyperbolic tangent potential that induces smooth AdS-to-dS, 0-to-dS, and dS-to-dS transitions. Despite its negative kinetic term, the step-like potential prevents pathologies like unbounded energy growth, Big Rip, and WEC violations, ensuring smooth evolution of cosmological parameters. Notably, the AdS-to-dS transition in DE density does not precisely parallel that of the potential, persisting longer due to the kinetic term's contribution. Even if different realizations of Λ_sCDM yield identical background dynamics, they still exhibit differences. GR-based Λ_sCDM models [801,811,812,2870], Λ_sVCDM [802,2872], and $f(T)$-Λ_sCDM differ in their predictions for linear perturbations, while the string-inspired Λ_sCDM$^+$ [2701,2899, 2900,2926] predicts a modest excess in the total effective number of neutrino species, with $N_{\rm eff} = 3.294$. Such distinguishing features are invaluable, as they provide a means to compare and ultimately discriminate between these alternative realizations using observational data. Other than the models explicitly realizing/resembling the background dynamics of Λ_sCDM, there exist various other approaches that fit within the broader paradigm outlined earlier. These include brane-world models [444,2881,2882], multiple axion models [2930, 2931], energy–momentum log gravity [2887], bimetric gravity [2909], Horndeski gravity [2898], holographic DE [2906], Granda–Oliveros holographic DE [2907], composite DE (wXCDM) [2485,2908], inspired by the ΛXCDM framework [2932] — extends the abrupt Λ_sCDM model by introducing two free parameters that allow $w_{\rm DE}$ to take arbitrary constant values before and after the transition[59] — , the Omnipotent DE concept [813], with its specific realization DMS20 [2911], represents a class of DE models characterized by non-monotonic densities and transitions across $w_{\rm DE} = -1$, DE pressure parametrizations [2933, 2934], which yield $w_{\rm DE}$ similar DMS20, the Lotka–Volterra model of two interacting fluids [2896], running Barrow entropy [2895], multiple-transition vacuum DE models [2514], and scenarios invoking a modification of the gravitational constant between super- and sub-horizon regimes, motivated by the Hořava–Lifshitz proposal or the Einstein-aether framework [2935].

Thus, a rapidly growing body of literature has emerged within this class of models — particularly in recent years — with many having been tested against a variety of observational datasets, consistently revealing a strong correlation between the redshift of the sign change in the DE density, $z_\dagger$, and the model's ability to address major cosmological tensions, especially those involving H_0 and S_8. To provide insight, we highlight several representative observational constraints. The abrupt Λ_sCDM model, using the combined Planck+BAOtr+KiDS1000+SNIa+
SH0ES dataset, yields $z_\dagger = 1.72^{+0.09}_{-0.12}$, predicting $H_0 = 73.16 \pm 0.64\,{\rm km\,s^{-1}\,Mpc^{-1}}$ and $S_8 = 0.774 \pm 0.009$, thereby fully resolving both tensions [812]. When analyzed with the Planck+SNIa+SH0ES combination, the same model gives $z_\dagger = 1.83^{+0.11}_{-0.19}$, $H_0 = 72.07 \pm 0.88$, and $S_8 = 0.786 \pm 0.011$, still strongly alleviating both tensions, albeit trending slightly toward ΛCDM values — as expected for higher $z_\dagger$, which reduces the impact of the AdS-like phase [802]. The Λ_sCDM$^+$, the string-theory-inspired realization, analyzed with the same combined dataset as the first case, yields a higher transition redshift of $z_\dagger = 2.105 \pm 0.264$; yet, due to its enhanced $N_{\rm eff} = 3.249$, it predicts an even larger Hubble constant, $H_0 = 74.04 \pm 0.71$, thus also fully resolving the Hubble tension [2701]. The wXCDM model, the two-parameter extension of the abrupt Λ_sCDM, yields a slightly lower transition redshift $z_\dagger = 1.46 \pm 0.02$, predicting $H_0 = 70.94 \pm 0.56\,{\rm km\,s^{-1}\,Mpc^{-1}}$ and $S_8 = 0.784 \pm 0.009$ based on the Planck+BAOtr+DESY5 SN+CC+$f\sigma_{12}$+SH0ES dataset, thereby successfully addressing both tensions, while differing in that it features an EoS parameter crossing from $w_{\rm DE} < -1$ to $w_{\rm DE} > -1$ across the transition from negative to positive energy density [2908]. These examples show that, despite variations in dataset and model details, scenarios featuring AdS-to-dS or analogous transitions with $z_\dagger \sim 1.5$–2 consistently succeed in addressing both the H_0 and S_8 tensions. Further insights come from Λ_sCDM$_\pm$, the extension of Λ_sCDM$^+$ that allows arbitrary AdS depths, revealing a degeneracy whereby deeper AdS phases permit higher $z_\dagger$ values while still resolving the H_0 tension [2926]. Even the few observational findings highlighted here provide a compelling case for continued theoretical and observational investigation of this class of models.

If future observations continue to support these models, the implications for theoretical physics would be profound, as an AdS-like cosmological constant is a theoretical sweet spot, favored by the AdS/CFT correspondence [2936] and string theory frameworks [2937]. Recent work [2938] has demonstrated that a supersymmetric vacuum in string theory can naturally produce an AdS-like cosmological constant at present-day energy scales, motivating DE scenarios where the field evolves on a potential with an AdS minimum rather than the standard dS minimum. Such a negative cosmological constant could shape both the current cosmic acceleration and the Universe's long-term evolution, offering a compelling link between fundamental theory and observations. In this direction, Ref. [2888] examined a DE model consisting of an AdS-like cosmological constant and a DE component with an EoS parameter w_ϕ, finding no evidence for an AdS-like cosmological constant and a mild preference for an effective phantom DE component, though ΛCDM remains favored. Ref. [2939] (see also [2891]) extends wCDM and CPL-CDM by introducing an AdS-like cosmological constant, demonstrating improvements in both data fits and alleviation of the H_0 tension, while further studies [1760–1762] show that this model can also address the JWST anomaly. Indeed, the models discussed in this section are expected to generally enhance structure formation at high z, making them natural candidates for explaining the JWST anomaly [1755,1759,2866,2867]. However, their rigorous quantitative analysis of perturbation evolution and cosmic structuring is necessary. The evolution of cosmic structures and linear perturbations in the (abrupt) Λ_sCDM model has been studied in Refs. [1763,2696,2865]. Specifically, Ref. [1763] found that for $\Omega_{\Lambda,0} = -0.7$ and $\Omega_{\rm m,0} = 0.3$, Λ_sCDM predicts up to an 80% increase in cluster density for turnaround redshifts $z_{\rm max} \gtrsim 2$, suggesting a potential explanation to the JWST anomaly. Ref. [2696] demonstrated that even in abrupt Λ_sCDM (the most extreme case), the transition itself has no significant impact on bound structures, preserving model viability. Additionally, Ref. [2865] showed that the growth index remains $\gamma \sim 0.55$ as in

[59] The wXCDM model [2485,2908], inspired by ΛXCDM [2932], introduces a composite DE scenario with two components: X (for $z > z_\dagger$) and Y (for $z < z_\dagger$). Y behaves as running vacuum energy with a quintessence-like EoS ($w_Y \gtrsim -1$), while X, termed 'phantom matter' (PM), has a phantom-like EoS ($w_X \leq -1$) but negative energy density, mimicking effective string action terms at low energies [2473]. The Kalb-Ramond axion and gravitational Chern–Simons term generate a 'phantom vacuum' [2479], where PM enhances structure formation at high z, potentially explaining the JWST anomaly. The de Sitter vacuum is restored via gChS condensates, and data support $w_Y > -1$, $w_X < -1$, aligning with DESI results [699].

ΛCDM. However, Planck CMB data predicts $\Omega_{\rm m,0} = 0.28$ for $\Lambda_{\rm s}$CDM and $\Omega_{\rm m,0} = 0.32$ for ΛCDM, leading to growth rates of $f = 0.49$ and $f = 0.53$ at $z = 0$, respectively. Notably, $\Lambda_{\rm s}$CDM predicts a value closer to $f = 0.48$, recently obtained from LSS data when γ is treated as a free parameter in ΛCDM [2060], indicating its potential to resolve the structure growth anomaly. DESI data (combination with other datasets) have further validated DE models incorporating an AdS-like cosmological constant [2901,2905], while obviating the need for phantom DE in the DE sector [2905]. The post-reionization HI 21-cm signal is explored as a probe for an AdS-like cosmological constant in the DE sector [2940]. In summary, a negative cosmological constant in the DE sector is physically motivated, consistent with current data, and may yield distinctive cosmological and astrophysical signatures — including the possibility of a bouncing future universe [2941].

Ref. [2942] suggested that a promising approach to resolving cosmological tensions may involve combining early- and late-time new physics to better fit the data. Ref. [2902] explored a hybrid model integrating abrupt $\Lambda_{\rm s}$CDM with a varying electron mass mechanism, identifying it as a promising candidate. However, they found that this combination does not improve the tension, as the two models push $\Omega_{\rm m,0}$ in opposite directions. Ref. [1325] analyzed the $\Lambda_{\rm s}$CDM+$N_{\rm eff}$+$\sum m_\nu$ and ΛCDM + $N_{\rm eff}$+$\sum m_\nu$ models, allowing variations in $N_{\rm eff}$ and $\sum m_\nu$ within abrupt $\Lambda_{\rm s}$CDM and ΛCDM. They found that $\Lambda_{\rm s}$CDM+$N_{\rm eff}$+$\sum m_\nu$ consistently fits the data better while preserving the success of $\Lambda_{\rm s}$CDM and predicting standard neutrino properties. In contrast, when ΛCDM + $N_{\rm eff}$+$\sum m_\nu$ yields high H_0 values, it does so at the cost of large $\Delta N_{\rm eff}$, whereas $\Lambda_{\rm s}$CDM+$N_{\rm eff}$+$\sum m_\nu$ achieves similarly high H_0 values while remaining consistent with the standard $N_{\rm eff}$. This suggests that the $\Lambda_{\rm s}$CDM+$N_{\rm eff}$+$\sum m_\nu$ alleviates the need for pre-recombination new physics, at least concerning neutrino properties.

4.2.3. Interacting dark energy

Coordinator: Carsten van de Bruck

Contributors: Amare Abebe, Dario Bettoni, David Benisty, David Tamayo, Denitsa Staicova, Diego Rubiera-Garcia, Emmanuel Saridakis, Emre Özülker, Kay Lehnert, Leila L. Graef, Lu Yin, Luis Anchordoqui, Marcel A. van der Westhuizen, Marco de Cesare, Nikolaos E. Mavromatos, Oem Trivedi, Oleksii Sokoliuk, Purba Mukherjee, Rahul Shah, Sveva Castello, Vitor da Fonseca, and Yuejia Zhai

4.2.3.1. Introduction. In this subsection, we discuss models with an interaction between DE and DM. Such IDE models have been introduced to address problems of the ΛCDM model, including the H_0 and S_8 tensions (for comprehensive reviews, e.g., see Ref. [709,2943,2944]). Some IDE models can reduce the H_0 tension from 5σ to 3.6σ [709].

In a general model, the conservation equations for DM and DE take the form

$$\nabla_\mu T^{\mu\nu}_{\rm (DM)} = Q^\nu\,, \quad \text{and} \quad \nabla_\mu T^{\mu\nu}_{\rm (DE)} = -Q^\nu\,, \tag{4.14}$$

ensuring that the total energy–momentum tensor of DM and DE remains conserved, namely, $\nabla_\mu(T^{\mu\nu}_{\rm (DM)} + T^{\mu\nu}_{\rm (DE)}) = 0$. Often, the resulting background equations are written in the form

$$\dot\rho_{\rm DM} + 3H\rho_{\rm DM} = Q\,, \quad \text{and} \quad \dot\rho_{\rm DE} + 3H(\rho_{\rm DE} + p_{\rm DE}) = -Q\,. \tag{4.15}$$

In order for IDE models to be viable candidates for addressing the H_0 and σ_8 tensions, special attention must be given to the physicality of the parameter space [2945]. In these models, there is not always a mechanism to halt the energy transfer when either the DM or DE density becomes zero (i.e., $Q \neq 0$ in Eq. (4.15) when $\rho_{\rm DE/DM} = 0$), which can lead to negative energies. The case of $Q > 0$ corresponds to an energy transfer from DE to DM. It has been reported that CMB observations seem to favor an energy transfer from DE to DM, WL measurements and thermodynamical considerations suggest an energy transfer from DM to DE [2050,2946–2948].

One well studied class of models is coupled quintessence, in which $Q^\nu = \beta\dot\phi^\nu T^\mu_{({\rm DM})\mu}$ and $Q = -\beta T^\mu_{({\rm DM})\mu}\dot\phi$, where ϕ is the DE scalar field and $T^\mu_{({\rm DM})\mu}$ denotes the trace of the DM energy–momentum tensor [2051, 2422,2949]. There also exists an extension of these models in which DM and DE are disformally coupled [2950–2953]. Such scalar field theories of IDE may alleviate the Hubble tension but do not fully solve it [2427,2429,2954].

Other, more phenomenological approaches propose a coupling of the form $Q^\mu = Qu^\mu_{\rm DM}/a$ or $Q^\mu = Qu^\mu_{\rm DE}/a$ [2955,2956] (in these expressions, a is the scale factor and $u^\mu_{\rm DM}$ or $u^\mu_{\rm DE}$ are the four-velocity of DM or DE fluid, respectively). The interaction Q is usually written as $Q = \xi H\rho_{\rm DE}$ or $\xi H\rho_{\rm DM}$, where ξ is a dimensionless coupling constant, determining the size and direction of energy/momentum flow. The case $Q = \xi H\rho_{\rm DE}$ was recently studied in Ref. [2957] (see also [2913] for a previous study), assuming an equation of state of DE $w_{\rm DE} = -0.999$, using the CMB data provided by Planck, WMAP and ACT. Different dataset combinations resulted in consistent results, showing evidence for a non-zero coupling and a Hubble expansion rate H_0 consistent with local measurements. Using Planck alone, the analysis results in $H_0 = 71.6 \pm 2.1\,{\rm km\,s^{-1}Mpc^{-1}}$, ACT alone results in $H_0 = 72.6^{+3.4}_{-2.6}\,{\rm km\,s^{-1}Mpc^{-1}}$and the combination of ACT and Planck results in $H_0 = 71.4^{+2.5}_{-2.8}\,{\rm km\,s^{-1}Mpc^{-1}}$. In Ref. [2958], the assumption about the equation of state was relaxed, allowing for a dynamical evolution via the parameterization $w_{\rm DE}(a) = w_0 + w_a(1-a)$. It was found that models featuring a dynamical phantom equation of state ($w_0 < -1$) perform worse than the non-dynamical case. On the other hand, models featuring a dynamical quintessence equation of state ($w(a) > -1$ at any redshift) perform better in attempting to increase the value of H_0 compared to the respective non-dynamical case. However, when considering the joint analysis of CMB, BAO SDSS, and SN data, no significant increase in H_0 to solve the Hubble tension was found, while it is a promising solution considering DESI BAO data [800].

In the following, we present a number of other IDE models.

4.2.3.2. Models.

Nonlinear interacting dark energy This class of models is an extension of the models discussed above. A general form of the nonlinear IDE models is given by $Q = 3H\xi F(\rho_{\rm DE}, \rho_{\rm DM})$, where F is a nonlinear function of the energy densities and ξ is a free constant parameter. Generally, when $Q > 0$, the H_0 tension worsens and the S_8 alleviates; conversely, when $Q < 0$, the H_0 tension alleviates and the S_8 worsens [2945]. The authors of Ref. [2959] investigate nonlinear IDE as an interaction between DM and a scalar field, in Ref. [2960] a model is discussed that could be interpreted as a particular case of a running vacuum model $\Lambda(H)$.

Power laws IDE models with the general form $Q = 3H\xi\rho^p_{\rm DM}\rho^s_{\rm DE}(\rho_{\rm DM} + \rho_{\rm DE})^r$, where p, s and r integers, were studied in Ref. [2961], and observational constraints for specific cases provided in Ref. [2962]. Observational constraints of $Q = 3H\xi\left(\rho_{\rm DM} + \rho_{\rm DE} + \frac{\rho_{\rm DM}\rho_{\rm DE}}{\rho_{\rm DM}+\rho_{\rm DE}}\right)$ are discussed in Ref. [2963]. The model $Q = \gamma\rho^\alpha_{\rm DM}\rho^\beta_{\rm DE}$, using CMB, BAO, RSD, and SNIa data, predicts lower values of $f(z)\sigma_8(z)$ at $z < 1$ comparing to ΛCDM, which alleviates the tension of ΛCDM with various RSD data [2964]. Other model types, such as exponential models $Q = 3H\xi\rho_{\rm DE}\exp\left(\rho_{\rm DE}/\rho_{\rm DM} - 1\right)$ [2965], and logarithmic models $Q = 3H\xi\rho_{\rm DE}\log(\rho_{\rm DE}/\rho_{\rm DM})$ and $Q = 3H\xi\rho_{\rm DE}\log(\rho_{\rm DM}/\rho_{\rm DE})$ [2966], were studied but showed no significant promising results.

Models with the forms $Q = 3H\xi\rho_{\rm DE}\sin(\rho_{\rm DE}/\rho_{\rm DM} - 1)$ and $Q = 3H\xi\rho_{\rm DE}[1 + \sin(\rho_{\rm DE}/\rho_{\rm DM} - 1)]$ have gained special attention for their potential to alleviate the H_0 tension [2967]. Analysis with Planck 2018 gives $H_0 = 72.67^{+5.43}_{-8.26}\,{\rm km\,s^{-1}Mpc^{-1}}$at 68% CL, and Planck 2018+BAO gives $H_0 = 69.17^{+1.52}_{-1.71}\,{\rm km\,s^{-1}Mpc^{-1}}$at 68% CL. Hence, for Planck 2018 and Planck 2018+BAO, the H_0 tension with respect to SH0ES ($H_0 = 73.0 \pm 1.0\,{\rm km\,s^{-1}Mpc^{-1}}$) is reduced down to 0.05σ, 2σ respectively; notably, for Planck 2018 alone case the tension is completely solved.

However, these results should be interpreted with caution due to potential biases and uncertainties. Additionally, a theoretical justification for the specific form of Q is necessary to ensure that it is not merely an ad hoc model.

Diffusion interactions A diffusive interaction between DE and DM was introduced in Refs. [2968–2970]. The diffusion of energy density between DE into DM uses a non-conserved stress energy tensor $T^{\mu\nu}$ with a source current j^μ, $\nabla_\mu T^{\mu\nu}_{(\mathrm{m})} = \gamma^2 j^\nu$, where γ^2 is the coupling diffusion coefficient of the fluid. The current j^μ is a time-like covariant conserved vector field $\nabla_\mu j^\mu = 0$ which describes the conservation of the number of particles in the system. In a homogeneous expansion, the modified Friedman equations read

$$\dot{\rho}_{\mathrm{DM}} + 3H\rho_{\mathrm{DM}} = \frac{\gamma}{a^3}\,, \quad \dot{\rho}_\Lambda = -\frac{\gamma}{a^3}\,, \tag{4.16}$$

The contribution of the current goes as $\sim a^{-3}$ since the current is covariantly conserved. In this way, there is a compensation between DE and DM. Ref. [2971] introduces cases with a diffusion constant that could be represented for a scalar field ϕ or a perfect fluid, leading to late-time forms of DE and a DE density parameter that could be interpreted as a perturbation of the ΛCDM model.

Another example of diffusion interactions is represented by models where the energy–momentum transfer vector comes from a potential, $Q_\mu = \nabla_\mu J$. This class of models finds a natural embedding within unimodular gravity. In fact, in unimodular gravity the total energy–momentum of matter fields need not be conserved in general [2972]. The energy density of DE is then identified with the potential J up to an arbitrary integration constant, $\rho_{\mathrm{DE}} = J + \Lambda_0$, and the equation of state is $w_{\mathrm{DE}} = -1$ identically. Models of this kind have been proposed to describe effective diffusion processes due to an underlying discrete spacetime structure [2973,2974]. In Ref. [2889] it was argued that such diffusive interactions — with energy transfer from DM to DE — can alleviate the Hubble tension, see Refs. [2975–2977] for a more detailed analysis. This class of models is also formally equivalent to "interacting vacuum models", which have been studied within the context of general relativity [2978,2979]. Embedding minimally IDE with $w_{\mathrm{DE}} = -1$ within UG has the following advantages: (*i*) the vacuum energy does not gravitate in UG removing the age-old problem regarding the puzzling absence of the vacuum energy density in cosmological observations [2980,2981], (*ii*) the well-known perturbative large-scale instability studied in Ref. [2955] does not exist in UG [2982], (*iii*) since the DE is an effective source in UG rather than a physical one, ρ_{DE} can attain negative values opening up a large phenomenological landscape to address the cosmological tensions. Moreover, it opens up a path for quantum gravity motivated interaction terms; e.g., see Refs. [2972–2974].

An important aspect often forgotten in the study of such diffusive models is to study the effect of large-scale structure formation in such a fluid environment. Growth-rate analyses can shed light on whether such a model alleviates the σ_8 tension or not.

Metastable dark energy Models of metastable DE have been analyzed in several works, see for instance Refs. [709,2983–2993]. In particular, in Refs. [2983,2985], phenomenological models in this context were investigated, considering the case of a constant DE decay rate, depending only on the intrinsic properties of DE and the type of decay channel. The following cases of metastable DE decaying in three distinct ways were considered: (I) exponentially; (II) into DM; (III) into dark radiation. Among these models, model II showed slightly better consistency [2985]. This model is sometimes called metastable IDE [709], since it is described by Eq. (4.15) with $Q = \Gamma\rho_{\mathrm{DE}}$, where Γ is the DE decay rate.

In Ref. [2985] it was shown that despite the fit for this model against Pantheon + BAO data providing higher values for H_0, when the CMB distance priors from Planck 2018 are included, the Hubble tension is restored. Later on, in Ref. [2986], a full analysis was performed using different combinations of data from Planck 2018, BAO, DES, R19 [48,192]. A larger value of H_0 was then supported, solving the tension with R20 [78] within 1σ. Future data with higher precision must provide us with a clearer understanding of the performance of these models concerning the tension. Some discussion on motivations for metastable IDE arising from quantum mechanics can be found in Refs. [2987,2988]. We can also find some examples from field theory descriptions, as in Refs. [2984,2989–2991], for instance.

Another model of metastable EDE is provided by the so-called Chern–Simons gravity inspired from string theory, studied in Refs. [2471,2473,2481]. It has been shown that, under some conditions, condensation of chiral GWs in early epochs of the Universe, can lead to a non-trivial condensate of the Chern–Simons gravitational anomaly term. The latter is characterized by the presence of imaginary parts, which are such that they lead to a metastable EDE, with a lifetime that can be in the phenomenologically right ballpark of larger than 50–60 e-foldings. The model, which also leads to RVM type inflation, due to the non-linear H^4 dependence of the (real part of the) pertinent vacuum energy density, can also help alleviate the Hubble and growth-of-structure tensions in modern eras [2484].

Elastic dark energy interactions In DE-DM elastic interactions models the two species interact via velocity or momentum transfer. There are various ways of implementing these exchanges [2994–2996] but here, for the sake of concreteness, we focus on the particular realization presented in Ref. [2996] and further developed in Refs. [2997–2999] (see Ref. [3000] for a short review), which is based on the following phenomenological implementation of the coupling

$$\nabla_\nu T^{\mu\nu}_{\mathrm{DM}} = \alpha\left(u^\mu_{\mathrm{DM}} - u^\mu_{\mathrm{DE}}\right)\,, \quad \nabla_\nu T^{\mu\nu}_{\mathrm{de}} = -\alpha\left(u^\mu_{\mathrm{DM}} - u^\mu_{\mathrm{DE}}\right)\,, \tag{4.17}$$

where α measures the strength of the interaction. It is clear that the interaction is active only when there is relative motion between the two species, i.e., at sub-Hubble scales while, at the largest scales, where the two fluids share a common reference frame, the interaction is absent. This means, in turn, that no modifications to the background evolution are produced. As a consequence, these models are not designed to address the H_0 tension but have an impact on relaxing the σ_8 one. In fact, at the level of linear perturbation, Euler equation receives a new contribution proportional to the relative velocity between the two species with a time dependent interaction rate $\Gamma_\alpha = \alpha a^4/\Omega_{\mathrm{DM}}$ in the case of DM and further weighted by the relative abundance of DM to DE $R = a^{3w}\Omega_{\mathrm{DM}}/(1+w)/\Omega_{\mathrm{DE}}$ in the case of DE. Since the interaction grows with the Universe expansion as a^4, eventually, $\Gamma_\alpha \sim H$ and the interaction with DE becomes relevant starting to exert a drag on DM which suppresses its clustering. This allows for the onset of a dark-coupling epoch at late-time as desired and as suggested by data that points toward a suppression in the clustering at $z \lesssim 2$. By considering Planck 2018 data releases, SNIa and Baryon Acoustic Oscillations data it has been shown that the interaction can indeed reduce the value of σ_8 and does so without affecting Ω_m ($\sigma_8 = 0.753^{+0.011+0.022}_{-0.011-0.021}$, $\Omega_m = 0.311^{+0.007+0.014}_{-0.007-0.013}$) and that the presence of the interaction is strongly favored [2997,2998]. The fact that no correlations between the interacting parameter and background ones is introduced is a particularly welcome feature since it implies no worsening of the H_0 tension. Remarkably, the inclusion of S_8 data allows for a constraint at percent level of the interaction by surveys like JPAS, Euclid, and DESI [2997] while SKAO-like experiments should have enough sensitivity to detect the interaction parameter [3001]. Finally, it is worth mentioning that the inclusion of massive neutrinos does not spoil the detection prospects for this model [3002] and that other implementations and analyses reach similar conclusions [2999,3003,3004].

Fading dark matter If the swampland conjecture for DE is correct, it would lead to the prediction that the ΛCDM model, where DE is constant, cannot be veracious [3005,3006]. Quite independently of swampland considerations, there have been proposals for a rolling scalar field as the source ofDE. If this were the case, the swampland

distance conjecture suggests that the rolling field would lead at late-times to an exponentially light tower of states. Identifying this tower as residing in the dark sector yields a natural coupling of the scalar field to the DM, leading to a continually reducing DM mass as the scalar field rolls in the recent cosmological epoch. It has been shown that the way in which the tower of light states evolves over time could help to reduce (though not fully eliminate) the H_0 tension [3007]. More unambiguously, the coupling of the scalar field to the DM leads to a reduction of mass, or fading of DM, which is compensated by a bigger value of DE. The latter becomes more noticeable in the present accelerating epoch, leading to an increase in H_0. Salam-Sezgin 6-dimensional supergravity [3008] and its string realization of Cvetič-Gibbons-Pope [3009] can bring to fruition the fading DM model [3010, 3011].

Late-time interacting constant/dynamical dark energy Late-time dark energy interacting with DM has been extensively explored in the context of the H_0 and σ_8 tensions. Numerous studies have been carried out in the context of the Hubble tension using different forms of the interaction term and Λ/constant EoS late-time dark energy, and by imposing various theoretical bounds on the parameter space to prevent instabilities [768,2913–2916,2918–2920,2942,2944,2967, 3012–3028]. Similarly in the context of the clustering tension significant studies include [2716,2916–2918,2920,3016,3026,3029–3033]. In Ref. [2958] an interacting setup with interaction proportional to the DE density ($Q \propto \rho_{\rm de}$), was investigated in the light of late-time DDE assuming a CPL parameterization in the context of the Hubble tension, and found no significant scope of alleviation of the tension with various combinations of datasets in either the phantom or quintessence regimes. In Ref. [2828], using the same form of interaction, various other parametrizations of LDE (MEDE, CPL, JBP) were considered. It was reported here that a quintessence EoS in such an interacting scenario does not help with the Hubble tension, and noticeably makes the σ_8 tension worse. However, a phantom EoS, although did not affect the Hubble tension, showed significant scope in alleviating the σ_8 tension (especially for the CPL and JBP parametrizations). The inclusion of RSD data in this scenario helped obtain tighter constraints on certain parameters, but resulted in a relatively less pronounced relaxation of the clustering tension, which might indicate ΛCDM bias in RSD data. A phenomenological parameterization, where a scalar field depends linearly on the number of e-folds, was used to test its interaction with DM [2948]. However, the constrained interacting dark energy (CIDER) model, with a background identical to the standard ΛCDM model, appears to better address the σ_8 tension [2426,3034].

Late-time singularities Depending on the choice for the interacting term Q, late-time singularities, for which infinities in the Hubble factor (or on its derivatives) appear, may arise at finite future times [2123,3035–3041]. Since some of them represent possible ends for the Universe, this undermines the consistency of the theory. Furthermore, they have been shown to occur for both linear and non-linear forms of Q.

4.2.3.3. Modeling and observational aspects of IDE models. In this section, we present some other aspects of IDE models, such as N-body structure formation simulations of certain IDE models, and comparing IDE models to data.

Marginalization approach to IDE A recent estimate of IDE contribution from Pantheon and Pantheon Plus, CC and transversal BAO [3012] has shown evidence for up to 2σ deviation from ΛCDM. This study has been done in the framework of the marginalization approach which aims to circumvent the Hubble tension by integrating H_0 and r_d out of the model, leaving only Ω_m, w and ξ as parameters. The results show a strong dependence on the used SNIa dataset and whether it is Cepheids calibrated or not, with the latter remaining compatible with ΛCDM.

N-Body simulations of IDE Several simulations of the structure formation were run up to date under the IDE ansatz, namely works of Refs. [2299,3022], where they have considered several cases of IDE and derived such probes of the LSS as matter power spectrum, halo mass function, concentration-mass relation, and halo bias. The most interesting parameter is the concentration-mass relation, namely c_{200} that can be related to the X-ray data and galaxy rotation curves, which via the maximum likelihood method imposes the redshift evolving constraints on the DE-DM coupling parameter ξ, with the joint posterior distribution giving a best fit of $\xi = 0.071 \pm 0.034$.

Distinguishing IDE from modified gravity A word of caution is required when constraining IDE models based on large-scale structure observables. Models involving a fifth force acting on DM lead to a breaking of the weak equivalence principle for this component and thus a deviation in the Euler equation, affecting the growth of cosmic structure f. However, the resulting observational signatures on current and forecasted measurements of $f\sigma_8$ present a strong degeneracy with gravity modifications in the Poisson equation [3042,3043]. WL, which is sensitive to the sum of the two gravitational potentials describing the geometry of the Universe, is also generically unable to break this degeneracy. This indicates that standard large-scale structure analyses may not be able to distinguish IDE from gravity modifications, leading to a potential ambiguity among models proposed to address cosmological tensions.

Luckily, the two scenarios can be disentangled by considering measurements of gravitational redshift [3044,3045], an observable accessible in two-point correlations by the coming generation of galaxy surveys [3046,3047]. This effect is sensitive to the gravitational potential encoding the distortion of time and appearing in the Euler equation, thus providing a direct test of the weak equivalence principle and a clear way to discriminate between the two scenarios.

Model-independent reconstructions of IDE kernel In Ref. [2162], the interaction kernel $Q(z)$, which governs the energy exchange between DM and DE, is reconstructed within a fully model-independent framework, without imposing any predefined functional form. Employing both binned step-function reconstructions and GP interpolation, the authors infer the redshift evolution of $Q(z)$ directly from observational data, including BAO, CC, and the Pantheon+ supernova sample. The reconstructed kernel displays nontrivial features — most notably, multiple sign changes and mild oscillatory behavior at the 1σ level — suggesting dynamic and potentially reversible energy transfer between the dark components. As a result of this evolving interaction, the effective DE density is found to cross zero and become negative at redshifts $z \gtrsim 2$, demonstrating that IDE scenarios do not necessarily exclude negative DE densities at high redshift (see Section 4.2.2), despite the conventional assumption that DE remains positive in IDE models.

Application of the parameterized post-Friedmann framework in IDE Understanding the interaction of DE necessitates examining both the expansion history of the Universe and the growth of cosmic structures [3048,3049]. It has been observed that in the IDE scenario, calculating perturbations often results in divergent curvature perturbations on superhorizon scales, posing a significant problem for IDE cosmology [3050–3052].

To address this issue, the parameterized post-Friedmann (PPF) framework is an effective theory that treats DE perturbations based solely on the fundamental properties of DE [3053–3057]. This approach extends the parameterized PPF framework, originally designed for uncoupled DE, and can mitigate the instability in IDE cosmology [3058]. Consequently, the entire parameter space of IDE models can be explored using observational data [2722,3023,3059–3063].

A generalized framework to study IDE models is also provided by the effective theory of IDE [3064]. This formalism relies on a model-independent approach at the level of the action and provides a description of linear cosmological perturbations in scalar-tensor theories of gravity with a homogeneous and isotropic background. This allows for a direct comparison with cosmological data to constrain a rich non-standard phenomenology [3043,3065].

4.3. Modified gravity

4.3.1. Modified gravity in light of cosmic tensions

Coordinator: Francesco Bajardi, Micol Benetti, Salvatore Capozziello

Contributors: Adrià Gómez-Valent, Alessandro Vadalà, Ali Övgün, Amare Abebe, Andronikos Paliathanasis, Anil Kumar Yadav, Araceli Soler Oficial, Christian Pfeifer, Daniel Blixt, David Benisty, Diego Rubiera-Garcia, Duško Borka, Emmanuel N. Saridakis, Erik Jensko, Francisco S. N. Lobo, Gabriel Farrugia, Gaetano Lambiase, Giovanni Montani, Giuseppe Sarracino, Hussain Gohar, Ilim Cimdiker, Inês S. Albuquerque, Ismael Ayuso, Joan Solà Peracaula, Konstantinos F. Dialektopoulos, László Á. Gergely, Marcin Postolak, Marco de Cesare, Maria Caruana, Mariaveronica De Angelis, Nihan Katırcı, Nils A. Nilsson, Noemi Frusciante, Pierros Ntelis, Predrag Jovanović, Rebecca Briffa, Rocco D'Agostino, Saeed Rastgoo, Sanjay Mandal, Sergei D. Odintsov, Tiago B. Gonçalves, Tiziano Schiavone, Vesna Borka Jovanović, and Vincenzo Salzano

The shortcomings exhibited by GR on different energy scales question its validity as the best theory to describe the gravitational interaction [3066]. Indeed, at the quantum level it shows problems with its extension to a quantum theory of gravity [3067,3068], since it is non-renormalizable [3069], and the prediction of infinite gravitational tidal forces, by the existence of singularities [3070]. In the large-scale scenario, the observed Universe's accelerating expansion [27,34] cannot be predicted within the context of the standard model of cosmology without introducing the cosmological constant, whose theoretical value assessed by Quantum Field Theory differs from the value inferred by the Friedman equations [2980,3071]. The repulsive force driving the Universe expansion is dubbed "Dark Energy", whose existence, to date, is only based on indirect observations [3072,3073]. In addition, on galactic scales, the dynamics of the farthest stars orbiting around the center of galaxies (and, generally, incompatibilities on the LSS) represents a further open issue [3074,3075] currently addressed to a never-detected form of matter called "Dark Matter" [3076,3077].

These incompatibilities therefore open up the possibility of new (or rather, extended) scenarios, and here we will examine possible modifications to gravity.

Among the most important and widely considered approaches to address the aforementioned problems related to the unknown nature of DE and DM, as well as cosmological tensions, are modifications to GR itself. These can broadly be split into two main categories, whose features will be considered in detail in the next sections. The first category, referred to as *extended theories of gravity*, includes extensions of the Einstein–Hilbert action by other curvature terms (see Ref. [3078] for a review on the topic). The second category, referred to as *alternative theories of gravity* consists of models modifying the basic principles of GR, such as the Equivalence principle or Lorentz invariance. The main purpose of modified theories of gravity is to address GR shortcomings on different scales, providing a different view to describe gravity, potentially able to fix issues related to cosmology [3079] and the quantum formalism of the gravitational interaction [3067]. Extended and alternative theories of gravity naturally introduce extra degrees of freedom with respect to GR, which might potentially accommodate cosmic tensions. Several promising MG models involve modifications to the Einstein–Hilbert gravitational action, such as incorporating higher-order curvature invariants [3080–3082], establishing connections between geometry and scalar fields [2072,3083–3085], or introducing additional geometric features to spacetime beyond curvature, such as torsion (Poincaré gauge gravity and teleparallel gravity) [3086,3087] or non-metricity (metric-affine gravity and symmetric teleparallel gravity) [3088,3089], or non-linear connections (Finsler gravity) [3090, 3091]. Different classes of MG theories are outlined in Fig. 75.

4.3.1.1. Extended theories of gravity. One of the famous examples of GR extensions is the $f(R)$ gravity models, where the Ricci scalar R in the Einstein–Hilbert action is replaced by a general function $f(R)$. This modification leads to fourth-order field equations, which can explain cosmic acceleration without invoking DE [3038,3092–3101]. Various formulations of this theory have been explored, some of which can produce deviations in the Newtonian potential [3102], potentially addressing phenomena like the galaxy rotation curves without resorting to DM. Notably, the Starobinsky model [2074], which introduces a quadratic term in the scalar curvature to explain cosmic inflation, has attracted significant attention within this framework. Extra degrees of freedom in $f(R)$ gravity affect the Hubble function $H(z)$, providing deviations from the ΛCDM paradigm. In the equivalent scalar-tensor representation in the Jordan frame of $f(R)$ gravity, in Ref. [3103] it is shown that the scalar field dynamics may lead to a definition of an effective Hubble constant $H_0^{\rm eff}(z)$ that depends on the redshift z. In this regard, the non-minimal coupling between the scalar field and the metric plays a crucial role. Notably, $H_0^{\rm eff}(z)$ may successfully address the Hubble tension since it could reconcile measurements and estimates of H_0 obtained at different redshifts, from local probes at $0 \lesssim z \lesssim 2$ to CMB at $z \sim 1100$. Accordingly, the general scalar field potential is computed in Ref. [3103], as well as the respective $f(R)$ functional form in the low-redshift regime within $f(R)$ quadratic gravity. Furthermore, Ref. [3104,3105] shows that a rescaling of the Universe's expansion rate can emerge without presupposing a specific dependence on the redshift (as done in Ref. [3103]). Indeed, it is just the non-minimally coupled scalar field of the scalar-tensor representation responsible for the Hubble constant scaling. Then, the additional DDE source was implemented in the $f(R)$ gravity to provide a smooth transition between a quintessence regime and phantom fluids, resulting in an effective Hubble constant that exhibits a plateau behavior for $z \gtrsim 5$ matching the Planck prediction. For equivalent approaches, see also Refs. [3106–3109]. These scenarios with $H_0^{\rm eff}(z)$ were motivated by binned analysis of the SNIa Pantheon sample and BAOs [516,1670,3110], pointing out a slowly decreasing trend of the Hubble constant. In Ref. [3111], by exploiting the $f(R)$ gravity correspondence with a scalar-tensor theory, the authors provide a condition in which the H_0 tension is alleviated. Specifically, this condition is based on the existence of a metastable de Sitter point that occurs for redshifts near the recombination.

The Einstein–Hilbert action could be extended also by introducing dynamical scalar fields non-minimally coupled with the geometry [3112]. Scalar-tensor theories are often taken into account to address the dynamics of the early Universe, in the framework of the inflationary paradigm [3113]. In fact, inflation is usually conceived as generated by a scalar field ϕ, called the inflaton, which is supposed to be responsible for the accelerating expansion of the early Universe. According to this picture, inflation should be led by some scalar field driving the cosmic acceleration between 10^{-34} and 10^{-35} s after the Big Bang, generating an isotropic and homogeneous Universe. The theory of inflation describes also the production of particles after the early-time accelerating expansion (reheating) [3114–3116]. Moreover, to tackle the cosmological constant problem or the evolution of cosmological vacuum energy, new degrees of freedom for the gravitational field have to be considered.

In this scenario, Horndeski theory represents the most general scalar-tensor theory with second-order field equations in four dimensions [2071,3117]. It encompasses a wide range of models and offers a comprehensive framework for modifying the gravitational interaction by incorporating an extra degree of freedom through a scalar field [3118–3120]. This results in significant and intriguing consequences for both inflation and DE physics. The detection of the GW170817 event together with the electromagnetic counterpart [587] provides one of the most stringent constraints on scalar-tensor theories that propose an unusual speed of GWs. This imposes severe limits on Galileons and extends to other scalar-tensor theories, including the quartic and quintic sectors of Horndeski's theory [3121–3124]. Nevertheless, it has been noted that since the energy scales observed at

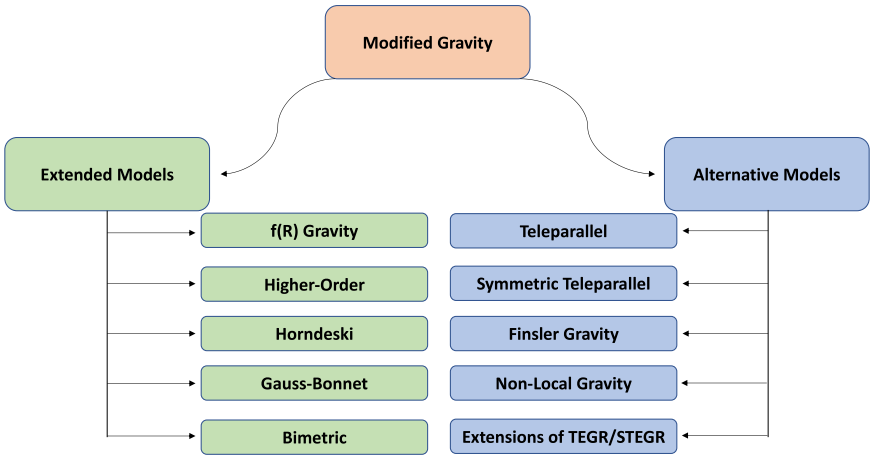

Fig. 75. A summary of the MG roadmap, outlining the potential extensions of GR.

LIGO lie very close to the typical cutoff of these types of theories, the translation of the bound on the speed of GWs to a cosmological setting might be non-trivial [3125].

Scalar-Tensor models have been taken into account also to address the H_0 tension problem. For instance, in Ref [3126]. Planck 2018 data are used to constrain the simplest models of scalar-tensor theories, accommodating a higher value for H_0 and therefore alleviating the tension between Planck/BAO and distance-ladder measurement from SNIa data. The capability of scalar-tensor and bi-scalar–tensor modified theories to alleviate the tension is also considered in Refs. [3127,3128], and other works [3129–3131].

Even when limiting the analysis to Horndeski models that respect the GWs' speed bound, observational constraints on H_0 using Planck data alone have been shown to yield values that are consistent with local determinations at 2σ for the Galileon Ghost Condensate [3132] and 1σ for the Generalized Cubic Covariant Galileon [2909,3133]. More recent studies have also considered Horndeski gravity to specifically address cosmic tensions, showing that particular setups free of ghost instabilities could lead to interesting late-time features possibly alleviating the H_0 tension [2898,3134].

Cosmic tensions have also been addressed in the context of the time-honored Brans–Dicke (BD) theory [3135,3136], which is the prototype of the large family of scalar-tensor theories (see also Ref. [2072]). BD gravity embodies the first historical attempt at incorporating a dynamical gravitational coupling to GR. It also constitutes the simplest scalar-tensor theory which can be embedded within the much broader class of Horndeski models [2071] and, in fact, many of these models reduce to BD at cosmological scales [2417]. Apart from the metric tensor, BD gravity involves a new (scalar) degree of freedom, φ, which controls the strength (and the possible time evolution) of the gravitational interaction $G_\varphi = G/\varphi$, with G being the (locally measured) Newton constant transforming the gravitational coupling constant into a new dynamic variable [3137]. The scalar field φ is non-minimally coupled to gravity via the Ricci scalar and its dynamics is controlled by a dimensionless parameter $\omega_{\rm BD}$, the BD parameter (or equivalently $\epsilon_{\rm BD} \equiv 1/\omega_{\rm BD}$).

Let us denote by BD-ΛCDM the Brans–Dicke counterpart of the standard ΛCDM, which represents the BD model with a cosmological constant, Λ. The cosmological term Λ is actually not present in the original BD theory, but in modern times Λ is obviously needed to trigger the late-time observed acceleration of the Universe. The BD-ΛCDM extension of the original BD model has been recently tested in the light of a large set of cosmological data of various sorts [2420], such as SNIa+BAO+$H(z)$+CMB+LSS, where $H(z)$ may include or not the SH0ES prior on H_0. If the latter is included, one finds [2420] that the BD-ΛCDM model is remarkably successful in reducing the H_0 and σ_8 tensions to inconspicuous levels of $\sim 1.5\sigma$ (when the high-l polarization and lensing data from Planck 2018 are not considered) [2420]. Notice that The RVM is mimicked by the BD-ΛCDM model, particularly the type-II RVM version with variable G_φ [2418,2814–2816]. The BD-ΛCDM turns out to fit the cosmological data significantly better than the standard ΛCDM model, and this is confirmed by different statistical criteria (see Refs. [2419,2420,2814,2816] for details). On the other hand, adding a constant potential for the scalar field does not correspond to the usual vacuum energy in BD theory. An explicit detailed theoretical and observational investigation of this BD extension of ΛCDM model, studied in Ref. [3138], reveals that the model does not alleviate the tensions with no significant deviations from ΛCDM.

Values of the effective cosmological gravitational coupling G_φ about $\sim$ 7–9% larger than G are preferred at $\sim 3\sigma$ CL This is possible thanks to the fact that φ remains below 1 throughout the entire cosmic evolution, while preserving the matter and radiation energy densities very close to the typical ΛCDM values. As a result, one finds higher $H(z)$ values during all the stages of the cosmic history without changing dramatically the abundances of the matter species in the pre- and post-recombination epochs. The lowering of the sound horizon at the baryon-drag epoch, r_d, is accompanied by an increase in the Hubble parameter. This helps to alleviate the H_0 tension in good agreement with other relevant background datasets, such as e.g., BAO and SNIa. In order not to spoil the correct fit to the CMB temperature data, the model is prone to yield values of the spectral index n_s that are considerably larger (viz. closer to 1 from below) than the standard ΛCDM model. This causes, however, no problem since the dynamics of φ can compensate for the changes in the matter power spectrum introduced by this fact (cf. Sec. 3 of Ref. [2420]). Remarkably, the model is able to cut back the σ_8 tension at the same time. The relief of this tension can be accomplished by means of a negative value of $\epsilon_{\rm BD}$, or alternatively through a positive value, provided that sufficiently massive (light) neutrinos are allowed [2420]. In both cases one finds $|\epsilon_{\rm BD}| \lesssim \mathcal{O}(10^{-3})$. The BD parameter has a direct impact on the LSS data through the linear perturbation equations. For instance, for $\epsilon_{\rm BD} < 0$ the friction term in the equation of the matter density contrast grows, and the source term decreases. Both effects contribute in sync to the lowering of σ_8, thus providing a physical explanation for a possible solution to the growth tension. It goes without saying that the compatibility between the larger cosmological value obtained for the gravitational coupling and the value measured locally, G, should be possible provided one can find an appropriate screening mechanism. Different studies show that these mechanisms are possible, although other works find that their implementation may not be so straightforward [3139].

Another way to extend the GR action is to introduce higher-order curvature invariants [3140–3150]. This is the case of Gauss–Bonnet

gravity, where the action includes a specific combination of curvature invariants known as the Gauss–Bonnet term. In this context, particularly intriguing are theories incorporating quadratic curvature terms, as they stem from GR viewed as an Effective Field Theory aiming to construct effective models toward quantum gravity. Notably, certain combinations of higher-order contractions of the Riemann tensor yield a topological surface term in four dimensions, known as the Gauss–Bonnet topological scalar, $\mathcal{G}$. In four dimensions, this scalar equates to the Euler density, which, according to the generalized Gauss–Bonnet theorem, provides the Euler characteristic when integrated over the manifold. The Gauss–Bonnet invariant is often utilized for its topological properties to simplify dynamics. However, in four dimensions, to render its contribution non-trivial, it is typically coupled to a dynamical scalar field [3151–3155] or incorporated as a function in the gravitational action [3156–3159]. This approach, where a function $f(\mathcal{G})$ is added to the scalar curvature, can mimic the behavior of a cosmological constant at late-times and, in the limit $f(\mathcal{G}) = 0$, GR is restored. Another avenue involves considering higher dimensions where $\mathcal{G}$ is non-trivial and coupling the Gauss–Bonnet invariant to a constant diverging when $D = 4$. Gauss–Bonnet gravity has been studied to address the H_0-tension [3160,3161], finding that can be greatly resolved within 2σ level.

Bimetric gravity [3162] is a consistent theory of non-linearly interacting spin-2 fields, one massless and one massive, which allows for a broad range of cosmological expansion histories and is compatible with cosmological as well as local tests of gravity [3163–3165]. In its most general form, the theory features four additional parameters in addition to the standard ΛCDM ones. There are no free functions, unlike several other MG theories. Studies based on a restricted class of two-parameter models have shown that the value of H_0 inferred from the inverse distance ladder is only slightly increased compared to ΛCDM [2884]; however, such models do not comply with the constraints required for a working screening mechanism [3164]. A more recent analysis [2909] based on more general three-parameter models has shown that, using (model-independent) transverse 2D BAO data in combination with SN and CMB, results in a value of H_0 which is closer to the SH0ES value. On the other hand, using 3D BAO data produces a lower H_0 value, suggesting a potential bias in the latter. A study of the S_8 tension has not been performed at present, since a framework for structure formation in bimetric gravity has not yet been developed.

Functors of actions theories (FAT), is part of the extensions of gravity theories, and they predict the existence of *actionions*, i.e., the actionic fluctuations and field-particles, which are analogs of energetic fluctuations and field particles. In light of deviations from DE equations of state, $w_0 \simeq -1.1$, FAT predicts the existence of actionic fluctuations which are of the order of one tenth of the observed volume [3166, 3167].

4.3.1.2. Alternative theories of gravity. The second class of modifications revises the basic foundations of GR, such as the Equivalence Principle, metric compatibility, Lorentz invariance, *etc.*. One such approach involves considering a more general geometric framework with an affine connection different from the Levi-Civita one, thereby introducing both torsion and non-metricity into spacetime. Torsion is associated with the antisymmetric part of the connection, while non-metricity arises from the non-vanishing covariant derivative of the metric tensor. Within this framework, the Riemann tensor and its contractions in GR can be expressed in terms of torsion, non-metricity, or a combination of both. The gravity formulations characterized by curvature, torsion, and non-metricity are dynamically equivalent, differing only by a boundary term in their respective actions, reason for which they are often termed the "geometric trinity of gravity" [3168]. This classical equivalence involving boundary terms that do not affect the field equations (and are thus omitted from the action formulation), is viewed from the perspective of GR as motivated by the possibility of formulating GR as a gauge theory [3086,3087,3169,3170].

In this framework, a consistent gravitational theory can be formulated by promoting torsion over curvature as the sole governing factor of spacetime, resulting in a theory that precisely mirrors the dynamics of GR. This theory, known as the "Teleparallel Equivalent of General Relativity" (TEGR) [3171], has garnered significant attention in recent years, undergoing extensive analysis [3086,3087,3170,3172–3174]. TEGR presents a theoretical framework that interprets gravity as a consequence of torsion within the fabric of spacetime. In this context, gravitational interactions are described through a set of tetrad fields, also referred to as "vierbeins", which form the basis for depicting spacetime geometry. These tetrad fields define a torsion tensor, serving as the source of gravity in the theory and representing the antisymmetric component of the Christoffel connection.

An extensively studied model alongside TEGR is the "Symmetric Teleparallel Equivalent of General Relativity" (STEGR), which describes spacetime through non-metricity. Non-metricity allows for the consideration that spacetime may not adhere to the metric compatibility condition, a fundamental assumption in GR. While torsion arises directly from the antisymmetry of the affine connection, non-metricity emerges when the covariant derivative of the metric tensor is non-zero, denoted as $\nabla_\sigma g_{\mu\nu} \neq 0$. As consisting of field equations entirely equivalent to those of GR, both TEGR and STEGR fall short of addressing the limitations GR imposes on larger scales. Consequently, similar to $f(R)$ gravity within the metric formalism, modifications to the Lagrangian density of TEGR can be explored in various ways [3175], including introducing new torsion [3176,3177] and non-metricity invariants [3178], coupling these to additional scalar or axion fields [3179] or introducing an arbitrary function of the torsion scalar, leading to $f(T)$ gravity [3180,3181]. The latter has been proposed as a potential solution to late-time cosmological issues, such as the Universe's accelerated expansion [3182,3183]. The characteristics of gravity theories including torsion and non-metricity, such as $f(T)$, $f(Q)$ (with T being the torsion scalar and Q the non-metricity scalar) gravity, new general relativity and many more, are currently under investigation, particularly concerning their applications in cosmology and astrophysics [2127,3184–3207]. Specifically, in the context of cosmological tensions, Refs. [2175,2176,3208] explores methods to address the H_0 tension within $f(T)$ models; in Refs. [3209,3210] it is shown how to alleviate both the H_0 and σ_8 tensions simultaneously within torsional gravity from the perspective of effective field theory; in Ref. [3211] the evolution of scalar perturbations in $f(T)$ gravity and its effects on the CMB anisotropy is evaluated to show that $f(T)$ models do not provide tension on the Hubble constant that prevails in the ΛCDM cosmology; in Ref. [3212] the authors demonstrate that the $f(T)$ models prefer a higher value of H_0 with respect to the Planck prediction, in better agreement with local estimates. Similar effects can be achieved in some classes of the beyond-generalized Proca model that, at the background level, resembles $f(T)$ theory [3213]. Finally, in Refs. [3214–3216] solutions to the tensions were proposed in the framework of $f(Q)$ gravity.

In another class of these models, Finsler gravity [3090,3217–3221] offers an intriguing new way to derive the gravitational field of many particle systems, when they are modeled as a kinetic gas, instead of as a (perfect) fluid [3222,3223]. The dynamics of a kinetic gas is described by a 1-particle distribution function (1PDF) on the 1-particle phase space of spacetime, which takes the velocity distribution of the gas particles into account. Usually, when the gravitational field of a kinetic gas is derived, one obtains the energy–momentum tensor of the gas by averaging the 1PDF over the velocity distribution of the particles. By means of this averaging procedure, the information about the velocity distribution of the gas particles are lost and the gravitational field is derived from an effective fluid energy momentum-tensor as a source term in the Einstein equations. Finsler spacetime geometry describes gravity in terms of a curved 1-particle phase space of a curved spacetime (technically the tangent or co-tangent bundle). Here, the

1PDF directly sources the gravitational field of the kinetic gas without losing information through velocity averaging. The contribution of the velocity (kinetic energy) distribution of the gas to its gravitational field is fully taken into account in Finslerian gravity, rather than being averaged away [3222,3223]. The first promising solutions of Finsler gravity in the cosmological context have been obtained [3224], which show a linearly expanding Universe as a vacuum background solution. Further studies are ongoing to demonstrate that the contribution of the kinetic energy of a many-particle system to its gravitational field can be the solution to the Hubble tension and our understanding of DE.

It is worth pointing out that some alternative theories propose that gravity is mediated by a graviton with a small non-zero mass m_g. Experimental limits on m_g are set using models such as the Yukawa potential and dispersion relations, tested on astrophysical and cosmological scales. In addition to detectors like LIGO/Virgo or LISA, graviton mass limits can be derived from electromagnetic observations of gravitational systems, such as constraints on S-stars orbits [3225,3226], or from Schwarzschild precession of S2 in Yukawa gravity [3227], consistent with LIGO data.

Some theories of gravity relax the assumption of nonminimal coupling between the geometry and matter sources. This happens, for instance, in $f(R,\mathcal{L}_{\rm m})$ [368,3228], $f(R,\mathcal{T})$ [3229], $f(R,T_{\mu\nu}T^{\mu\nu})$ [3230–3233], and $f(R,\mathcal{T},R_{\mu\nu}T^{\mu\nu})$ [3234,3235] theories of gravity, where $\mathcal{L}_{\rm m}$ is the matter Lagrangian density, and $\mathcal{T}$ the trace of the energy–momentum tensor $T_{\mu\nu}$ (in its standard definition). Additionally, one can construct similar nonminimal coupled theories in the torsional framework, such as in $f(T,\mathcal{L}_{\rm m})$ [3236,3237] and in $f(T,\mathcal{T})$ [3238] theories of gravity, where T is the torsion scalar.

A characteristic of these theories with nonminimal geometry–matter coupling is that the covariant divergence of the matter energy–momentum tensor can in general be nonzero (though the standard continuity equation can be recovered in particular models). A new avenue has been recently opened by modifying the introduction of the material source in the usual EH action, such as matter-type modified theories of gravity with $f(\mathcal{L}_{\rm m},\mathcal{T},T_{\mu\nu}T^{\mu\nu})$, since these theories are equivalent to nonminimal interaction models in GR [3239]. Depending on the form of interaction determined by f function, some nontrivial dynamics easing cosmological tensions [2162], difficult to achieve via simple interaction kernels can be achieved, these DE models have effects on early and late-times of the Universe and hence may address the current tensions within ΛCDM model. The extra two degrees of freedom have the potential to offer more room to accommodate cosmic tensions. However, this also provides a challenge, given that Einstein–Boltzmann codes are commonly prepared to deal with at most one extra degree of freedom, it is, at the moment, more challenging to compute the evolution of perturbations and constrain these theories.

So far, studies have focused on the simplest classes of models. An example of studying dynamics of scalar perturbations, using the quasistatic approximation, is in Ref. [3240] for $f(R,\mathcal{T}) = R + f_2(\mathcal{T})$ models with $f_2(\mathcal{T}) \propto \mathcal{T}^{1/2}$ to ensure the usual matter continuity equation. This work finds that there is a strong scale k dependence of the matter perturbations, not supported by observations.

A more recent work Ref. [3241] reports on the possibility of $f(R,\mathcal{T}) = R + \lambda\mathcal{T}$ alleviating the σ_8 tension, while increasing the H_0 tension. In the Hu–Sawicki model of $f(R)$ gravity the σ_8-tension observations worsen [2840], while it might be alleviated in viscosity in the DM model (in modified cosmological models, massive neutrinos suppress the matter power spectrum on the small length scales, which implies that the bounds on neutrino mass get modified too) [3242–3245].

To conclude, it is worth noticing that most alternative/extended theories of gravity may be subject to screening mechanisms, such as the *chameleon* mechanism [3246,3247], which can be encountered in several scalar-tensor theories [3248,3249] as well as in MG models [3250–3262] that can be recast in terms of an additional scalar field (e.g., see Ref. [3263]), like $f(R)$ gravity. In this case, the scalar field is coupled to the matter fields so that its mass is environment-dependent. As long as the matter density is high enough, the scalar field acquires a heavy mass around the potential minimum, strongly reducing the range of the fifth force it mediates, and making it essentially unobservable, see however [3264,3265].

On the contrary, on cosmological scales, far from regions with higher densities, the scalar field has a lighter mass, effectively mediating the additional gravitational interaction. Another screening mechanism is the *symmetron* screening [3266], where the potential of the scalar field $V(\phi)$ breaks the parity symmetry in low-density regions, which instead is restored at smaller scales. In this mechanism, the scalar field has a vacuum expectation value (VEV) that depends on local matter density, becoming larger in low-density regions and smaller in high-density regions. Moreover, the coupling of the scalar field to matter is proportional to the VEV, so that the scalar couples with gravitational strength in the low-mass-density regions, while it is decoupled, and then screened, in the high-density ones. In Ref. [3267] it has been concluded that symmetron screening cannot be used to alleviate the Hubble tension.

Finally, the Vainshtein mechanism [3268] is important for some MG models, such as massive gravity, Dvali–Gabadadze–Porrati (DGP), or Galileon theory. The Vainshtein mechanism manifests itself at nonlinear scales, below a certain radius known as the Vainshtein radius. Nearby massive bodies GR are recovered through a strong kinetic self-coupling, weakening the interaction with matter and reducing the propagation of the extra degree of freedom. Recently, it was shown that bimetric gravity can alleviate the H_0 tension (refer to Section 4.2), and could potentially alleviate also the S_8 tension [2909].[60]

According to the latest observations, one of the most promising extended gravity models is the generalized cubic covariant Galileon model. Using only CMB data, provides $H_0 = 72^{+8}_{-5}\,\mathrm{km\,s^{-1}Mpc^{-1}}$, $\sigma_8 = 0.88^{+0.07}_{-0.05}$ at a 95% confidence level [3133] and $S_8 = 0.84 \pm 0.10$. At the same time, the tensions are restored by combining the CMB data with external datasets.

In the framework of alternative theories, particularly encouraging is the Δ_4 model, which is a specific non-local gravity model providing non-local quantum corrections to standard GR. This model predicts the values $H_0 = 70.3 \pm 0.9\,\mathrm{km\,s^{-1}Mpc^{-1}}$ and $\sigma_8 = 0.82 \pm 0.02$ [3271], using the CMB, BAO and SN datasets, which is higher than Planck predictions, in better agreement with the local estimates. The related S_8 value is $S_8 = 0.81 \pm 0.02$.

All in all, although there is not a universally accepted MG model that resolves the cosmological tensions, many of these models offer promising aspects that could help guide future research. Most of the models considered in this section provide a higher value for H_0, though implications on σ_8 should be further explored. As cosmological data continue to improve, these theories will be subject to increasingly stringent tests, potentially leading to a deeper understanding of the fundamental nature of gravity and the Universe. Therefore, it is quite possible that extended/alternative theories could contribute, at least in part, to addressing the H_0 and σ_8 tensions.

4.3.2. Early modifications to gravity

Coordinator: Emmanuel N. Saridakis, Konstantinos F. Dialektopoulos

Contributors: Andrzej Borowiec, Alfio Maurizio Bonanno, Ali Övgün,

[60] However, it must be noted that drawing accurate predictions for the formation of LSS in bimetric gravity is challenging, so at present the S_8 tension can only be addressed under some simplifying assumptions. Regarding the H_0 tension the alleviation comes with the drawback that more parameters are introduced and bimetric gravity is preferred by AIC [3269] but ΛCDM is preferred by BIC [3270] with the latter giving a stronger penalty for introducing more parameters to the model in consideration.

Andreas Lymperis, Andreas Papatriantafyllou, Anil Kumar Yadav, Antonio Racioppi, Athanasios Bakopoulos, Athanasios Chatzistavrakidis, Branko Dragovic, Carlos G. Boiza, Charalampos Tzerefos, Chiara De Leo, Christian Pfeifer, Cláudio Gomes, Damianos Iosifidis, Daniele Oriti, David Benisty, Davide Pedrotti, Despoina Totolou, Diego Rubiera-Garcia, Elias Vagenas, Elisa Fazzari, Elvis Baraković, Flavio Bombacigno, Fotios K. Anagnostopoulos, Francisco S. N. Lobo, Gaetano Lambiase, Genly Leon, Gerasimos Kouniatalis, Giannis Papagiannopoulos, Giovanni Otalora, Giulia De Somma, Giuseppe Gaetano Luciano, Gonzalo J. Olmo, José Pedro Mimoso, Jurgen Mifsud, Kathleen Sammut, László Árpád Gergely, Laur Järv, Manolis Plionis, Manuel Gonzalez-Espinoza, Manuel Hohmann, Margus Saal, Maria Petronikolou, Miguel A. S. Pinto, Nikolaos E. Mavromatos, Nikolaos Petropoulos, Oem Trivedi, Özgür Akarsu, Petros Asimakis, Saeed Rastgoo, Salvatore Capozziello, Saurya Das, Sebastian Bahamonde, Simony Santos da Costa, Spyros Basilakos, Stylianos A. Tsilioukas, Supriya Pan, Thanasis Karakasis, Tiago B. Gonçalves, Tomi Koivisto, Vasilios Zarikas, Vedad Pasic, Xin Ren, Yuejia Zhai, and Yu-Min Hu

MG is a quite general framework that can offer alleviation to the tensions, since apart from late-time solutions (which were analyzed in the previous subsection) one can apply it at early-times too [3272]. In order to solve the Hubble tension, it is possible to introduce modifications to the standard cosmological model. The general idea is that new assumptions at pre- and post-recombination are needed. For this reason, changing some of these assumptions, i.e., changing the cosmological model before or after the recombination epoch, may be the solution to obtain a different value of H_0. One possible solution is to consider a MG scenario before the recombination epoch. Since the BAO data constrain Hr_d, the final goal is to obtain a lower value of the sound horizon at the drag epoch r_d and thus a higher value of H_0. Some constraints from models adhering to this approach are shown in Table 6.

The expression of the sound horizon is $r_d = \int_{z_d}^{\infty} dz c_s(z)/H(z)$, where at sufficiently high redshift the sound speed $c_s(z)$ can be considered almost constant and equal to $c/\sqrt{3}$. To decrease the value of r_d we need that, in a certain redshift interval $z \in (z_1, z_2)$, the expansion of the Universe is higher with respect to the ΛCDM case in the same value. An example of this approach can be found in Ref. [3273], where it is shown that the Hubble tension can be reduced by assuming a MG model acting at early-times with a scalar field non-minimally coupled to the Ricci scalar. Furthermore, in Ref. [3274], they explore the possibility of obtaining a lower value of the sound horizon, and consequently a higher value of H_0, by using a MG model that allows for a phenomenological shift in the effective Planck mass on cosmological scales before recombination, through a non-minimal coupling of a scalar field with gravity.

In Refs. [2471,2473,2479] it was proposed that the dynamics of the early Universe is described by a Chern–Simons (CS) gravitational model, characterized by gravitational anomalies, which arises in the low-energy limit of string theory [2470,2480], after appropriate compactification to (3+1) spacetime dimensions. The model involves the graviton and Kalb-Ramond (KR), or gravitational, axion field (assuming a constant dilaton). The latter couples to the anomalous terms. Chiral primordial GW can condense under some circumstances, leading to a non-trivial condensate of the CS terms [2481,3275,3276], and hence a linear axion potential, resembling the axion monodromy situation in string-theory models [2483]. Such linear-axion potentials lead to inflation [2481,2818], which however are of the so-called RVM type [2476]. This means that the corresponding vacuum energy density contains dominant terms of order H^4 (where H is the Hubble parameter, which is almost constant during inflation).

It is such non-linear terms that drive the RVM inflation. In Ref. [2481], it was shown that the CS condensates are *metastable*, in the sense that they contain imaginary parts [2482], which can determine the duration of the RVM inflation. The model contains a pre-RVM-inflationary era characterized by stiff-KR-axion-matter dominance. It is during such an epoch that chiral GWs are formed, by either non-spherically-symmetric mergers of primordial (rotating) black holes, or collapses of domain walls, the latter arising, for instance, from dynamical breaking of supergravity [3277,3278], which can characterize the early epochs of such string-inspired models after the Big Bang [2473].

The detailed transition from such an era to the RVM inflation is discussed in Ref. [2481], using a dynamical system approach. The model can also lead to post-inflationary late-eras DE modifications, involving vacuum energy terms of the form $H^2\ln(H)$, which are held responsible for the simultaneous alleviation of H_0 and growth-of-structure tensions [2484].

The simplest generalization of Einstein's theory are the so-called $f(R)$ theories, which can be further generalized by including a non-minimal coupling between the matter Lagrangian and another generic function of the curvature [368]

$$S = \int d^4x\sqrt{-g}\left(f_1(R) + f_2(R)\mathcal{L}\right) .$$

This model gives rise to an extra force term in the geodesics for a perfect fluid. In fact, stemming from the Liouville theorem in phase space, the flux density of particles is shown to be covariantly conserved, and the Boltzmann H-theorem is still preserved as the entropy vector flux is a non-decreasing function of the spacetime coordinates likewise in general relativity. Despite the distribution function being formally equivalent to Einstein theory for a homogeneous and isotropic universe, some quantities differ, namely as the effects of the non-minimal coupling appear on the radiation density evolution and on the matter Lagrangian choice, which is no longer degenerate, for instance, Ref. [3279]. In these theories, the baryon asymmetry is generated through an effective coupling between the Ricci scalar and the net baryon current, which dynamically breaks CPT invariance, thus matching the observed asymmetry for very small deviations from general relativity. Moreover, the resulting temperatures are compatible with the subsequent formation of the primordial abundances of light elements [3280]. Hence, among others, this scenario allows for a good agreement with SN distance data and the BAO data for different exponents in a power-law type non-minimal coupling function, thus alleviating the Hubble tension [372].

A consistent gauge theory of gravity and spacetime based on the Lorentz symmetry was found rather recently [3281–3283]. Addressing the problem of time, the theory predicts that the space that emerges via spontaneous breaking of the Lorentz symmetry could be massive [3281, 3284,3285]. This would be the minimal explanation of the missing mass in the Universe, and a slight extension of the scenario might alleviate the H_0 tension through a cosmic spin as has been discussed also in the context of Poincaré models of gravity [3285–3288]. An ultraviolet completion mentioned in Ref. [3289] leads to modifications of early cosmology, whereas the relevance of a different description of nonperturbative effects to the cosmological tensions was speculated in Ref. [3290]. Ref. [3291] rewrites the higher curvature theories using a gauge theory of gravity.

As a subcase of metric-affine and gauge theories of gravity, teleparallel gravity has also been well-studied in the early Universe. The Teleparallel Equivalent of General Relativity (TEGR) describes gravitational interactions as the torsion of the connection of spacetime. Several teleparallel inflationary scenarios have been proposed in the literature, in order to change the early-Universe evolution and eventually alleviate the H_0 tension, and here we briefly summarize some of them. Born–Infeld inspired inflation originates from the work of Born and Infeld, who proposed a finite self-energy for point-like particles to avoid divergences in physics. This approach has influenced various gravity theories, including Eddington-inspired Born–Infeld gravity, which addresses singularities like black holes and the big bang. In teleparallel cosmology, Born–Infeld inspired models use an $f(T)$ gravity Lagrangian, featuring a scaling parameter $\lambda_{\rm BI}$ that induces inflation without an inflaton field [3182,3292,3293]. This model aligns with

the CMB and transitions to standard ΛCDM at later times, providing a comprehensive framework for early Universe dynamics [3294–3298].

In Loop Quantum Cosmology within the FLRW framework, the matter bounce scenario is described by a modified Friedmann equation, resulting in a non-singular bounce at $t = 0$. This model can be reformulated in terms of $f(T)$ gravity [3299–3307]. The Lagrangian can be adjusted to fit observations by varying the critical density ρ_{cr}. Scalar fields, affecting spectral indices and power spectra, are crucial for matching CMB observations and ensuring reheating. Perturbations reveal additional degrees of freedom, impacting the scalar and tensor power spectra, with the tensor-scalar ratio potentially exceeding observed bounds, dependent on scalar field dynamics.

Higgs inflation explores the coupling of the Higgs field with gravitational theories like GR, TEGR, and STEGR. The Higgs potential $V(\phi) = \frac{\lambda}{4}(\phi^2 - v^2)^2$ can be coupled with the torsion scalar T to investigate inflationary scenarios. In this context, a particular action is used, incorporating kinetic and potential functions [3308]. Some studies reveal issues, such as a high tensor-to-scalar ratio or failing to achieve inflationary models. Despite these challenges, alternative scalar field couplings and potential functions may yield more practical inflationary models, suggesting further exploration is necessary for natural inflation in teleparallel gravity.

When the canonical quantization techniques of Loop Quantum Gravity are applied to cosmological scenarios, one finds that the big bang singularity is generically resolved by a big bounce [3309–3314]. This happens even when different quantization prescriptions are used, which leads to various nonsingular models of loop quantum cosmologies [3315–3319] (known as LQC, mLQC-I, and mLQC-II [3317]) that differ in their concrete pre-bounce and post-bounce dynamics. In Ref. [3320], it has been found that the effective dynamics of those three quantum-corrected models can be accurately approximated by a 3-parameter family of metric-affine $f(R)$ theories of gravity [3321], where two of the parameters can be set by constraints at the bounce and at low curvatures (GR limit), while the third one can be determined (numerically) by fitting the background evolution. Interestingly, the non-perturbative dynamics of all three models are dominated by a logarithmic correction [3322]. Additionally, the best fit value of the free parameter can be well approximated by elementary combinations of the bounce density and the Barbero-Immirzi parameter. On the other hand, it is possible to recover regular big-bounce scenarios also in the presence of a dynamical Barbero-Immirzi field, when a purely torsional Nieh–Yan term on a FLRW background [3323,3324] and its non-metrical generalization in Bianchi-I cosmologies [3325] are taken into account. This idea naturally leads to projective-invariant metric-affine formulations of Chern–Simons MG, for which big bounce and de Sitter solutions arise [3326]. A peculiar aspect of these models is that they predict the coupling of metric tensor modes to torsion tensor components, leading to torsional birefringence and the possibility of distinguishing the usual metric version of Chern–Simons gravity from its metric-affine counterpart via the quasinormal mode emission of compact objects [3327] (see also Ref. [3328]).

Axions and Axion-Like Particles (ALPs) provide well-motivated candidates to address important problems in cosmology, maintaining at the same time a significant discovery potential in current and future experiments. Among their uses, they can serve as candidates for DE within the quintessence scenario [3329,3330]. ALPs arise naturally in string-inspired models [2480], often not single but as a plethora of light pseudoscalar fields [3331]. Their characteristic sinusoidal potential generates models of EDE that can potentially resolve the Hubble tension [2454,2455,3332]. Remarkably, although these models are loosely inspired by string theory, recent attempts highlight the potential of embedding them into stable type IIB string compactifications [2461,2462], which would provide a fundamental starting point. The appearance of multiple ALPs in stringy scenarios allows for alignment mechanisms that combine them and can lead to models where at different stages of the cosmological evolution different ALPs act as inflaton, QCD axion, and quintessence [3333,3334]. Pseudoscalar fields were also considered in the context of teleparallel and symmetric teleparallel gravity, where they couple to the CP-violating quadratic terms that can be formed with the torsion tensor or/and the non-metricity tensor [3179,3335,3336]. Such additional fields could contribute to the cosmological dynamics in the early Universe [3179,3337] and can also lead to GW velocity birefringence [3338,3339], which can be tested using multi-messenger approaches [3340].

DM creation during or after inflation can be associated with irreversible thermodynamic processes [3341–3343]. Refs. [3344,3345] proposed an alternative cosmology based on the irreversible thermodynamics of open systems, in which the explanation for the production of macroscopic matter and entropy in the early Universe relies on a reinterpretation of the matter energy–momentum tensor that includes an irreversible creation term. However, this contrasts with the covariant conservation of the energy–momentum tensor in GR.

In the last decade, several MG theories that contain nonminimal couplings between geometry and matter have been proposed, such as $f(R,\mathcal{L}_m)$ [3228], $f(R,T)$ [3229], $f(R,T_{\mu\nu}T^{\mu\nu})$ [3230–3233] and $f(R,T,R_{\mu\nu}T^{\mu\nu})$ [3234] theories of gravity, where R and $R_{\mu\nu}$ are the Ricci scalar and tensor, $\mathcal{L}_m$ the matter Lagrangian density, and T the trace of the energy–momentum tensor $T_{\mu\nu}$. A property of all these theories is that the matter energy–momentum tensor is not conserved. This feature allowed Harko [3346] to physically interpret such non-conservation as an irreversible energy flow from the gravitational field to the matter sector that could result in particle creation, by using the thermodynamics of open systems approach. The effects and implications of the irreversible matter creation processes on the late cosmological evolution have been studied on some of these modified theories of gravity [3346–3349] (see Ref. [3350] for a review). It was shown in Ref. [3239] that if such theories include the Ricci scalar R in the Einstein–Hilbert form, i.e., assuming minimal geometry–matter coupling — they are effectively equivalent to nonminimal interaction models within the framework of GR. These MG theories could be further explored in the context of the early Universe DM creation that can eventually lead to alleviation of the H_0 tension.

ΛCDM paradigm is very efficient in describing our Universe; however, it is broadly acknowledged that the model ought to break down and exhibit limitations in at least the two extreme phases of the Universe, namely its very early and very late phases. In the very early Universe, Planck scale or quantum gravity effects are expected to set in, resulting in potentially significant conclusions, some of which may be measurable. While proposals for quantum gravity abound, and one can in principle take any theory and examine its implications for the above stages of the Universe, here we will primarily be interested in a virtual model-independent prediction of theories of quantum gravity, namely the Generalized Uncertainty Principle (GUP). The GUP predicts significant changes to several thermodynamic quantities, while it leaves some others intact [3351–3354].

A generic and often-used version of GUP is

$$[x_i, p_j] = i\hbar\left[1 - \alpha\left(p\delta_{ij} + \frac{p_i p_j}{p}\right) + \alpha^2\left(p^2\delta_{ij} + 3p_i p_j\right)\right] \tag{4.18}$$

$$\Delta x \Delta p \geq \frac{\hbar}{2}\left[1 - 2\alpha\langle p\rangle + 4\alpha^2\langle p\rangle^2\right] \ , \tag{4.19}$$

where the dimensional parameter α can be traded off with a dimensional one α_0, via $\alpha = \alpha_0 \ell_{Pl}/\hbar$, where $\ell_{Pl} \simeq 10^{-35}$ m is the standard Planck length and $1 \leq \alpha_0 \leq 10^{15}$, the upper bound dictated by the fact that no Planck scale effects have been observed at the LHC, which has a characteristic length scale of 10^{-20} m $\simeq 10^{15}\,\ell_{Pl}$ (corresponding to 10 TeV of energy), which the "new length scale" $\alpha_0\ell_{Pl}$ should not exceed.

It follows that quantum gravity effects can in principle take effect right from the electroweak to the Planck scale. Since our focus is in the very early Universe, we will be concerned near the Planck

scale. As explained in Ref. [3351] the standard Heisenberg Uncertainty Principle and the GUP can be translated into a corresponding time–energy uncertainty relation. This, coupled with the first Friedmann equation, can in turn be used to estimate the Planck energy, mass, density, time, temperature, and effective number density. Since the GUP terms can differ significantly from the standard Heisenberg one near the Planck scale, it is not surprising that many of the quantities alluded to above undergo significant changes in the early Universe. Perhaps the most significant among them is the Planck energy density, whose ratio to the observed DE density increases by at least a factor of 4 to about 10^{119}.

Additionally, the same uncertainty principle can in fact affect the Friedmann equations and cosmological predictions in the radiation dominated era, as shown in Refs. [3352,3353]. There, an interaction term coupling baryon current and space–time was used to satisfy the first two Sakharov conditions, which along with the modified Friedmann equations break thermal equilibrium and thus satisfy the third and last Sakharov condition. The results can provide a rich phenomenology.

In the GUP approach, where a modification to the canonical algebra of the system leads to minimal uncertainties in the configuration and/or momenta, the evolution of the FLRW Universe with canonical variables (c, p) in the presence of scalar matter field ϕ with its momentum p_ϕ, can be described by the action of the GUP modified Wheeler–deWitt equation on the wave function of the Universe Ψ, $\left(\partial_\phi^2 + \widehat{\Theta}_{\rm GUP}\right)\Psi = 0$, where $\widehat{\Theta}_{\rm GUP}$ is a self-adjoint operator. In one approach [3355], which is equivalent to a cut-off in the length, $[\mathbf{q}, \mathbf{p}] = i\left(1 + \beta\mathbf{p}^2\right)$, using suitable wave-packets for the deep Planckian regime, it is found that the wave-packets do not fall in the classical singularity and the GUP Universe exhibit a stationary behavior in approaching the Planckian region. This implies that no bounce is present in this model. In another approach using GUP-modified Friedmann equations [3356], it is found that the DE density scales as $\tilde{\alpha}H^4$, where $\tilde{\alpha}$ is a GUP parameter associated to the minimum length, and H is the Hubble parameter. This means that this approach to GUP cannot explain the acceleration of the present Universe, since the energy density decreases very quickly. It is worth mentioning that GUP comes in various forms and a recent proposal based on a different modification of algebra (minimal momenta) [3357] together with an improved prescription may be a better approach. The reason is that (1) the momenta of gravitational field are related to the metric or triads so it is more natural to have minimal values in those quantities, and (2) without an improved scheme, just like LQC, one might obtain incorrect classical or asymptotic limits and hence the theory might not also be correct in the Planckian regime.

The Asymptotic Safety approach to Quantum Gravity offers a potential solution to the problem of quantizing the gravitational field. This approach is grounded in the existence of an ultraviolet non-Gaussian fixed point for the couplings of the $\sqrt{g}R$ and $\sqrt{g}$ operators in the Euclidean theory [3358]. A direct consequence of this fixed point is the dynamic suppression of Newton constant G at very high energies, which has significant implications for early cosmological models. In Ref. [3359], a comprehensive cosmological evolution from the inflationary phase to a late de Sitter phase is discussed. Additionally, [3360] proposes the idea that the Universe originates from a state of zero entropy and evolves toward an accelerated expansion phase.

Following Ref. [3361], one can also expect various modifications to the Effective Action at the inflationary scale. In particular, it has been shown in Ref. [3362] that an $f(R)$ Lagrangian of the form $L = R + \alpha R^{3/2} + \frac{R^2}{6m^2} - \Lambda$ represents a modification of the well-known Starobinsky quadratic Lagrangian. This modification arises due to the presence of higher curvature relevant operators generated by the renormalized flow near the non-Gaussian fixed point. The predicted scalar-to-tensor ratio r is significantly higher than in the standard Starobinsky model, making it a potential target for testing in future CMB missions like LiteBIRD.

The cosmological evolution of the early Universe is tested at temperature $T \lesssim 1$ MeV through the prediction of BBN. For temperatures $T \gg 1$ MeV, it is not excluded that new physics occurred, offering the possibility that non-standard cosmologies might have played a relevant role in the interplay between particle physics and cosmology. The Ice Cube experiment, for example, has revealed a high-energy astrophysical neutrino flux, with energies $\sim O(1)$ PeV [3363,3364]. Among the various scenarios to explain this phenomenon, it has been proposed the minimal model of DM decay [3365]. This interaction is also able to generate the correct abundance of DM in the Universe [3365]. In the standard cosmological model, the rate of DM decay, needed to obtain the correct DM relic abundance, differs by several orders of magnitude as compared with that needed to explain the Ice Cube data, making the four-dimensional operator unsuitable. However, such a discrepancy can be reconciled in modified cosmologies, so that the Ice Cube neutrino rate and DM relic density can be consistently explained [3366–3368].

In Fig. 76 we summarize the various early modified gravity theories that have been proposed to alleviate the tensions, while some corresponding predictions for H_0 and σ_8 are summarized in Table 6.

4.4. Matter sector solutions

4.4.1. Cold dark matter

Coordinator: Luca Visinelli

Contributors: Andrzej Borowiec, Anil Kumar Yadav, Branko Dragovic, Davide Pedrotti, Goran S. Djordjevic, Ioannis D. Gialamas, Ippocratis Saltas, Ivan De Martino, Janusz Gluza, Jenny G. Sorce, Jenny Wagner, Krishna Naidoo, Marcin Postolak, Martti Raidal, Mehmet Demirci, Paolo Salucci, Pran Nath, Reggie C. Pantig, Riccardo Della Monica, Rishav Roshan, Sebastian Trojanowski, Torsten Bringmann, Venus Keus, and Wojciech Hellwing

4.4.1.1. Motivation and evidences. The circular velocity of stars in a spiral galaxy can be inferred from the measurements of the Doppler shift of atomic lines at different distances R from the galactic center, leading to a velocity distribution $v = v(R)$ known as the *rotation curve*. The distribution of the luminous matter in virialized objects does not match that of the gravitational matter, demanding an additional non-luminous component.

Historically, this "missing mass problem" in the late Universe led to the proposition that there is a yet undetected form of matter [3369–3373]. Subsequently, CMB observations revealed a missing mass in the power spectrum already at redshift $z = 1100$, which could also be attributed to the same form of matter we call DM today. Evidence for the presence of DM in the Universe spans from galactic (rotation curves of spiral galaxies) to extra-galactic (clusters of galaxies, weak gravitational lensing observations) to cosmological scales (LSS, acoustic peaks in the CMB, BBN, non-linear growth of inhomogeneities. See Ref. [3374] for a historic reconstruction and Refs. [358,3375–3379] for reviews. N-body simulations with DM only reproduce well the LSS [2355,3074,3380] and are advancing to incorporate the essential *gastrophysics* effects [2280,3381].

The role of DM in addressing cosmic tensions is of profound interest from both theoretical and observational perspectives. If discovered, a DM particle would be a relic from a period before BBN, for which we currently have no direct data. The properties of DM — such as its clustering power spectrum, free-streaming velocity, and particle characteristics — would enable us to better model the pre-BBN epoch and differentiate between various "early Universe" proposals aimed at resolving these tensions. Furthermore, some theories that address the H_0 tension explicitly involve interactions between DM and other components, including DE. Pinning down the properties of DM is crucial for understanding its interactions with other particles, including those in exotic DE models.

Table 6
Early modifications to gravity: predictions.

Model	H_0	σ_8
Early MG and the sound horizon [2445]	> 70	< 0.8
String-inspired Chern–Simons modifications [2484]	$71.27^{+0.76}_{-0.73}$	$0.816^{+0.017}_{-0.015}$
Non-minimally coupled models [372]	$70.59^{+0.52}_{-0.53}$	–
Axions and Axion-like particles [3340]	70.6 ± 1.3	–

Fig. 76. Possible early modifications to gravity.

4.4.1.2. Theory. The evidence supporting the existence of non-baryonic DM is compelling across all observed astrophysical scales. While alternative theories are still under consideration, the notion of CDM has emerged as the dominant framework. DM might exist as macroscopic objects or as a particle, either fundamental or composite, proposed in extensions beyond the SM framework. A non-exhaustive summary of the properties (scattering cross section and target mass) of some candidates is provided in Fig. 77, inspired by previous work in Refs. [3382–3384].

Macroscopic DM One of the earliest propositions on the nature of DM is that it could appear in the form of known astrophysical objects of mass M such as planets or stellar black holes [3385,3386]. This conjecture has been challenged by gravitational microlensing surveys, which collectively exclude these objects as the main DM component over the mass range $10^{-11} \lesssim M/M_\odot \lesssim 10$ [3387–3390].

Along with known astrophysical objects, massive DM candidates consist of primordial black holes which are produced in the early Universe by a plethora of mechanisms at different mass scales. Stable primordial black holes possess a mass $M \gtrsim 5 \times 10^{14}$ g so that their Page time [3391] exceeds the age of the Universe, making them suitable DM candidates. A more stringent bound $M \gtrsim 10^{17}$ g is obtained from the non-observation of Hawking emission in the extragalactic γ-ray flux and in X-ray detectors [3392–3395]. Lensing constraints also apply to primordial black holes, leaving an open window of opportunity where primordial black holes are the DM in the mass range $M \in [10^{17}\text{-}10^{22}]$ g under the assumption of a monochromatic mass function.

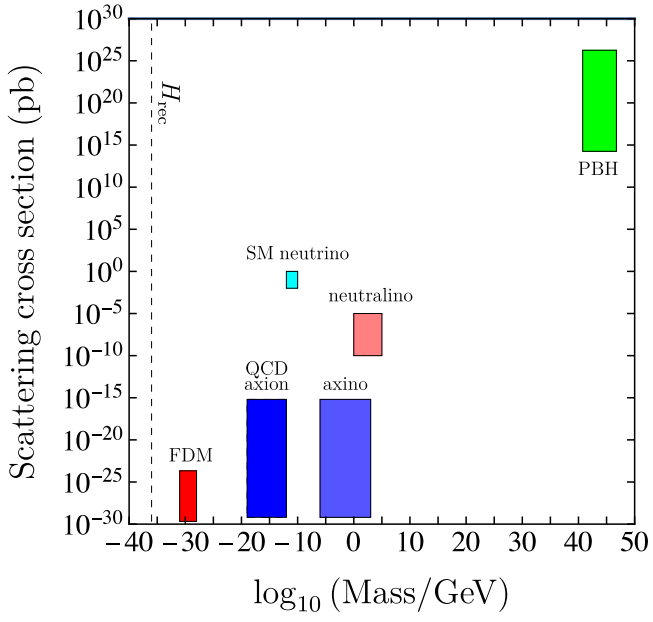

Fig. 77. An estimate of the scattering cross section for some DM candidates, as a function of the DM mass. The plot is inspired from Refs. [3382–3384]. As a comparison, the SM neutrino is also included.

Particle DM An intriguing possibility is that DM results from a completely new sector of physics not comprised within the SM. This includes candidates such as sterile neutrinos, axions, supersymmetric particles (gravitinos, neutralinos, axinos), weakly/feebly/strongly interacting massive particles, Q-balls, or ultralight scalars. Generally speaking, DM particles should be (i) non-relativistic at recombination, (ii) neutral or feebly charged, (iii) stable over cosmological timescales, (iv) feebly interacting with the SM. Interactions between the dark and visible sectors can help alleviate cosmological tensions. For example, a model in which dark matter interacts with the baryon sector yields $S_8 = 0.794\,(0.804)^{+0.009}_{-0.010}$ for the marginalized posterior (maximum of the full posterior), when fit to *Planck* 2018, SDSS BAO, and DES-Y3 data at 1σ CL [2327]. In a scenario where dark matter feebly interacts with photons, a fit to *Planck* 2018 + SDSS BAO leads to $S_8 = 0.803 \pm 0.021$ and $H_0 = 67.70 \pm 0.43\ \mathrm{km\,s^{-1}Mpc^{-1}}$ at 1σ CL [3396]. While the upper limit for the mass m of a particle candidate is the Planck mass, the lower limit for a fermionic species is provided by the Gunn–Tremaine condition [3397], which reads $m \gtrsim 100\,\mathrm{eV}$ from consideration on dwarf spheroidal galaxies [3398]. For a bosonic species, the lower mass limit is often considered as the Hubble rate at matter–radiation equality, $m \gtrsim 10^{-27}$ eV, from the consideration that the ultralight field should oscillate by the time at which the matter component becomes relevant over radiation. Some particle models that have been explored include the following. Explaining the missing mass across cosmic times and scales by a single extension of the known cosmological model has motivated the search for further corroborations of its existence and led particle physicists to investigate potential particle candidates.

Flavor discrete symmetry models The SM fails to explain neutrino masses, mixings, and DM with the WIMP paradigm comprehensively. Standing at this juncture, it is certainly a tempting challenge to find a common origin of these two seemingly uncorrelated sectors and much effort goes beyond the SM of particle physics to explore scenarios that can accommodate a candidate of DM and explain non-zero neutrino masses and mixing [3399]. Typically, models based on non-Abelian discrete flavor or modular symmetries are considered to explain observed neutrino mixing, and breaking of the same symmetry may lead to the residual symmetry, which at the same time stabilizes the DM [3399,3400]. For example, in models based on the A_4 discrete group, light neutrino masses can be associated with tree-level type-I seesaw mechanism and the one-loop contributions accommodating viable DM candidates responsible for observed relic abundance of DM [3401]. In such models, constraints coming from the lepton flavor violating processes are also important, restricting DM masses and leaving ranges of DM parameters that can be probed in collider studies.

Supersymmetry Since B and L-violating operators in the SM have dimension $d \geq 5$, the renormalizable Lagrangian possesses an accidental global B-L symmetry [3402–3405], which is imposed in supersymmetric extensions of the SM to avoid experimental consequences such as a large proton decay rate. Such a symmetry leads to an R-parity which is conserved in scattering and decay processes, leading to supersymmetric particles to be produced in pairs. The same R-parity leads to the stability of the lightest supersymmetric particle, which could be a DM candidate if it is neutral. Supersymmetry, first postulated to address the hierarchy problem, has thus long provided us with a long list of DM candidates [3406]. These include neutralinos [3407–3413], sneutrinos [3414,3415], gravitinos [3416–3426], and axinos [3427, 3428], massive spin-2 particles [3429–3433] resulting from modifications of gravity, and Kaluza–Klein excitations [3434–3436] found in theories incorporating extra dimensions. However, some of the simplest versions of the theory are under stress due to the non-observation of any supersymmetric particles in collider experiments. The lightest neutralino, among others, is an example of a much broader category of particle DM candidates dubbed weakly interacting massive particles (WIMPs), produced thermally in the early Universe.

Weakly interacting massive particles (WIMPs) WIMPs, some of the most studied DM candidates, are hypothesized to have been produced in the early Universe as they were initially in thermal equilibrium with the primordial bath. As the Universe expanded and cooled, the production of WIMPs ceased and they "froze out" of thermal equilibrium. The freeze-out temperature is defined as the point when the Hubble expansion rate exceeds the WIMP annihilation rate. The leftover density of WIMPs after freeze-out, i.e., their relic density, depends on their annihilation cross-section. The annihilation cross-section needed for WIMPs to achieve the observed DM density today is naturally of the same order of magnitude as the weak nuclear force cross-section. This coincidence is known as the "WIMP miracle" because it suggests that WIMPs could naturally account for DM without needing highly tuned parameters. Since the WIMP miracle provides a compelling argument for them as the leading DM candidate, many direct and indirect detection experiments are built to probe the typical WIMP mass range of $\sim \mathcal{O}(\mathrm{GeV})$ to $\sim \mathcal{O}(100\,\mathrm{GeV})$ [3375,3376]. Even though direct and indirect experiments continue to constrain the parameter space for the vanilla WIMPs scenario - as for most DM models - exciting new directions in the WIMP paradigm, such as CP-violating DM [3437], multi-component DM [3438], pseudo-Goldstone DM [3439], have been proposed which not only provide viable DM candidates but also address other shortcomings of the SM [3440]. Even if the WIMP miracle is not realized, loopholes exist such as coannihilation [3407,3441,3442], annihilation to slightly heavier states [3441], p-wave annihilation, resonances [3441,3443], and Sommerfeld enhancement [3444,3445].

Sub-gev thermal DM The WIMP paradigm can be generalized to lower DM masses and coupling constants, and various sub-GeV DM candidates have been proposed that can also be produced thermally in the early Universe [3446–3448]. In this case, their mass is typically bounded from below to $m > \mathcal{O}(\mathrm{MeV})$ by astrophysical constraints and BBN, while even stronger indirect detection bounds are present for light DM candidates annihilating to SM species via s-wave channels, see the recent review in Ref. [3449]. In other models, however, dedicated direct detection techniques are needed to probe them [3450], and multiple accelerator-based searches are ongoing and planned [3451].

Sterile neutrinos A minimal extension of the SM with the addition of a Weyl fermion N as a sterile neutrino could provide viable DM candidates. This particle couples to the SM through a Yukawa term such as $\sim yNLH$, where L is a left-handed lepton doublet and H is the SM Higgs doublet, which could give rise to the small neutrino masses through the seesaw mechanism [3452–3455] and possible lead to baryogenesis via the leptogenesis mechanism [3456]. Sterile neutrinos of mass $m < m_e$ might decay into three active neutrinos, thus constraining the sterile mixing angle θ for a given m [3457]. The abundance of sterile neutrino DM is fixed through a freeze-in mechanism in which active neutrinos oscillate into N before decoupling [3458]. Possible caveats include a finite lepton asymmetry [3459] or the presence of self-interactions [3460–3462].

The QCD axion The QCD axion [3463,3464] is a light pseudoscalar coupled with the SM gluons, introduced to solve the strong-CP problem through the Peccei–Quinn mechanism [3465]. The interaction with the gluon leads to a mixing of the axion with the neutral pions and to a small mass $m_a \sim 6\,\mu\mathrm{eV}(10^{12}\,\mathrm{GeV}/f_a)$, where f_a is the energy scale at which the infrared description breaks. Because of its interaction with the gluon that induces a coupling with the charged pions, this particle inevitably couples with the SM photon. Models that generalize the Peccei–Quinn mechanism leading to a very light axion and a prediction for the axion–photon coupling $g_{a\gamma\gamma}$ have been long studied and constitute the benchmark for laboratory axion searches, such as the KSVZ [3466,3467] and the DFSZ axion [3468,3469]. A nonrelativistic population of cosmic QCD axions is produced through the vacuum misalignment mechanism [3470–3472], leading to a number density in axions with a large occupation number at the time $T_{\mathrm{osc}} \sim \mathrm{GeV}$ at which coherent oscillations in the field begin. This population of

axions can possibly address the DM abundance for given values of the mass m_a and of the initial value of the axion field $\theta_i f_a$ [3473–3475]. The uncertainties in the assessment of the axion parameters can be divided into cosmological [3476,3477], particle content [3478,3479], and theoretical [3480], see Refs. [2591,3481] for reviews. A robust experimental search is currently ongoing worldwide to try and detect this particle [2596,3482].

Ultralight bosons Ultralight bosons or "fuzzy" DM (FDM) with masses in the range $m \sim 10^{-23}$-10^{-18} eV would possess a de Broglie wavelength of astronomical size [2371,3483,3484]. An ultralight scalar, naturally generated in string theory, is generally considered to be real or pseudo-scalar field minimally coupled to the metric, and acquires a small mass from various UV mechanisms [3331,3485]. When the Universe cools below a certain critical temperature, the field starts to roll down and oscillates about the minimum of its potential [2590,3486–3488]. N-body cosmological simulations have shown the formation of a DM core within each virialized halo, which is supported against gravitational collapse by the internal quantum pressure due to the Heisenberg uncertainty principle on the de Broglie scale, surrounded by an interference pattern representing the oscillation in the density and velocity fields of the DM particles [2383,3489–3493]. A lower bound on the boson mass is derived by considering the quantum pressure introduced at cosmological scales, which suppresses the power spectrum of linear inhomogeneities at large wavelengths and leads to a lower bound $m \gtrsim 10^{-21}$ eV [1551,1552,1563,3494,3495]. Stronger constraints on the mass and the abundance of ultralight scalars are placed from a variety of observations which involve detection strategies at astronomical or cosmological scales [2336,3378,3496–3504], which could nevertheless depend on the details of cosmology and the astrophysics involved. An issue with FDM candidates lies in that such particles cannot produce the very large regions of about constant density observed at the center of large galaxies [1742,3505]. Ultralight bosons coupled to a dark energy fluid can help relieve both the H_0 and S_8 tensions. For instance, a model fit to *Planck* 2018, lensing, Pantheon, SH0ES, and WiggleZ LSS data results in $H_0 = 68.81^{+1.60}_{-0.67}$ km s^{-1}Mpc^{-1}and $S_8 = 0.7993^{+0.0410}_{-0.0140}$ at 1σ CL [3506].

4.4.1.3. Experimental efforts.

Laboratory searches Given the vast landscape of particle DM candidates, several techniques have been implemented for their searches. Here, we highlight the detection of WIMPs and axions in underground detectors.

If DM is in the form of WIMPs with a small coupling to SM nucleons, it is possible to detect a small event rate R based on DM-nucleon elastic scattering, totaling $R \sim N_T n_{\rm DM} \sigma_A v$. Here, N_T is the number of nucleon targets in the experiment, $n_{\rm DM}$ is the number density of DM in the Solar system, $v \sim 220$ km/s is the relative velocity, and σ_A is the scattering cross section off a nucleon of atomic number A. For spin-independent (SI) interactions, the DM scattering cross section is often quoted in terms of $\sigma_{\rm SI} \approx \sigma_A/A^4$ [3375,3507]. For spin-dependent (SD) scatterings, the enhancement with the target mass is more modest and reads $\sigma_A \approx \sigma_{\rm SD}\, A^2(J+1)/J$, where J is the spin of the nucleus. The most sensitive experiments include liquid xenon-based detectors: XENONnT [3508], LUX-ZEPLIN (LZ) [3509], and PandaX-4T [3510], which all set a bound on the SI DM-nucleon cross section $\sigma_{\rm SI} \lesssim 10^{-47}$ cm^2 for the DM mass $m \sim 40$ GeV. The argon-based detector DarkSide-50 [3511] is the most sensitive in targeting the SI cross section for WIMP masses below about 3 GeV, with proposed experiments including DarkSide-20k [3512] and ArDM [3513]. Note, that the results depend on several assumptions on: (i) the distribution of DM in the solar system and around the Earth, (ii) the universal coupling between the WIMP and the nucleons, (iii) the mass range of the mediator, (iv) the knowledge of the nuclear form factors, (v) the effective theory used to model the interaction, (vi) the absence of self-interactions, (vii) the scattering process being elastic. All of these caveats have been thoroughly investigated in the literature in relation to realistic DM models.

The laboratory search for the QCD axion and other light bosons proceeds by means of resonant cavities in a "haloscope" [3514,3515], light shining through wall experiments [3516–3519], dielectric haloscopes [3520], and DM radio searches [3521]. In a resonant cavity, a galactic axion converts into a microwave photon through the interaction with the virtual photon of an external magnetic field [3522–3528]. DM radio searches are employed in DMRadio/ABRACADABRA [3529] and, for light axions not related to the QCD theory, with SuperMAG [3530]. Scalar fields produced in the Sun are searched through helioscopes: CAST [3531] and IAXO [3532].

Indirect detection Indirect detection of DM involves observing the potential byproducts of DM interactions rather than revealing a new particle. This method relies on DM particles annihilating or decaying into SM particles, which are then detected in astronomical and terrestrial instruments. The byproducts of these interactions typically include (1) gamma rays [3533,3534], high-energy photons that can travel vast distances and are easier to trace back to their source; (2) Neutrinos [3535–3537], which are nearly massless and interact very weakly with matter, making them hard to detect but potentially useful for indirect detection; and (3) Charged cosmic rays [3538–3540] such as electrons, positrons, protons, and antiprotons. An excess of these particles in cosmic rays could indicate DM interactions [3541].

Different detectors and observatories are used to identify the potential signals from DM interactions. Instruments like the Fermi Gamma-ray Space Telescope observe the sky for gamma-ray emissions, focusing on high DM density regions like the Galactic Center or dwarf spheroidal and dwarf spirals [3542–3546]. Facilities such as IceCube in Antarctica detect neutrinos by observing the Cherenkov radiation produced when neutrinos interact with ice [3547,3548]. Instruments like the Alpha Magnetic Spectrometer (AMS-02) on the International Space Station measure the flux of cosmic rays, looking for anomalies that could indicate DM annihilation or decay [3549].

One key challenge for indirect detection is to distinguish potential DM signals from astrophysical backgrounds. For instance, gamma rays can be produced by various astrophysical sources like pulsars, supernova remnants, or AGN, while neutrinos are produced in the Sun and in the atmosphere. Cosmic rays have numerous sources, including the Sun and SN, making it difficult to attribute any observed excess to DM. For this, fingerprints are searched through cross-correlation studies using data from different wavelengths and types of particles to identify coincident excesses that could point at DM, and spectrum analysis where the energy spectrum of detected particles is analyzed to identify features characteristic of DM annihilation or decay.

Currently, there is no definitive detection of DM through indirect methods, but some intriguing signals and excesses warrant further investigation. For instance, Fermi has observed a gamma-ray excess in the Galactic Center which could be due to DM annihilation [3550]. Also, the AMS-02 has detected an excess of positrons in cosmic rays, which might indicate DM [3549], although astrophysical sources like pulsars are a competing explanation. Future instruments and missions, such as the Cherenkov Telescope Array (CTA) [3551–3555] and the next-generation neutrino observatories will provide more sensitive measurements and potentially offer clearer insights into the nature of DM.

Inferring the distribution and amount of DM by its gravitational interactions is a complementary route to the detection of byproducts. Gravitational lensing is a very suitable probe because it only relies on light deflection, with no further need for the modeling of luminous matter effects. Since the first detection of a strongly lensed QSO [3556, 3557], strong gravitational lensing has successfully constrained masses of galaxies and galaxy clusters to about 10% [3558,3559]. While the initial lens modeling of the light-deflecting mass density profiles overestimated the DM inferred from strong lensing, increasing complexity of the lens models has reduced the amount of DM necessary to produce the observed, highly magnified and distorted images of background

galaxies [3560]. Yet, open questions still remain whether the amount of substructures observed in galaxy clusters agree with ΛCDM [3561–3565].

4.4.2. Warm dark matter

Coordinator: Supriya Pan

Contributors: Biswajit Karmakar, Branko Dragovic, Cláudio Gomes, Cora Uhlemann, Davide Pedrotti, Emmanuel N. Saridakis, Ioannis D. Gialamas, Janusz Gluza, Massimiliano Romanello, Mehmet Demirci, Pran Nath, Reggie C. Pantig, Riccardo Della Monica, Torsten Bringmann, Venus Keus, Weiqiang Yang, and Wojciech Hellwing

4.4.2.1. Constraints on WDM from observation of high-redshift galaxies and reionization. The introduction of WDM particles, with a mass of the order of a few keV, can alleviate some of the challenges of the ΛCDM model at the kpc scales, namely the Missing Satellites problem or the Too-Big-to-Fail problem [2354]. Indeed, during the structure formation process, the higher thermal velocity of non-collisional WDM particles determines a flow from overdense to underdense regions, canceling the cosmic perturbations with a physical size smaller than the so-called free streaming length, $\lambda_{\rm FS}$. This leads to a suppression in the matter power spectrum, $P(k)$, which becomes more important with decreasing WDM particle mass, m_χ, and has macroscopic consequences on the number density of low-mass haloes.

In addition to baryonic effects related to the star formation efficiency in DM haloes, small-scale modifications in the halo mass function can also alter the high-z number density of faint galaxies, resulting in a turn-over in the rest frame galaxy ultraviolet LF (UV LF) [3566,3567] and in a delay in the galaxy formation [3568,3569]. From the comparison between the abundance of faint galaxies and the number density of DM haloes predicted in the context of WDM cosmologies, it is possible to derive a lower limit on m_χ, independent of the baryonic physics involved in the galaxy formation process [3570].

In turn, the progressive steepening of the UV LF faint-end slope at high redshift confirms the fundamental role of faint galaxies during the EoR, when the intergalactic hydrogen passed from a neutral to an ionized state for the effect of energetic photons emitted by the primeval sources of light, at $z \gtrsim 6$. Indeed, the UV LF is directly linked to the star formation rate (SFR) [3571] and so to the existence of a hot stellar population that acts as a source of ionizing photons responsible for the reheating of the IGM [3572–3574]. In particular, their number density is given by $\dot{N}_{\rm ion} = f_{\rm esc}\xi_{\rm ion}\rho_{\rm UV}$, where the UV luminosity density, $\rho_{\rm UV}$, derived from the integral of the UV LF, is multiplied by two quantities, namely the ionizing photon production efficiency, $\xi_{\rm ion}$, and the escape fraction, $f_{\rm esc}$. The former describes how efficiently it is possible to get ionizing photons from a UV continuum radiation field and depends on different astrophysical quantities, such as the initial mass function (IMF), the metallicity and the age of the stellar population. The latter is defined as the fraction of ionizing photons that escape from the emitting galaxies and contribute to the phase transition of the IGM. Due to the lack of information about the geometry of the ISM in high-z galaxies, $f_{\rm esc}$ is not well constrained and it is difficult to model properly. Moreover, as a multiplicative factor of the total ionizing photons budget, it degenerates with the WDM particles mass, thus summarizing most of our uncertainties about the reconstruction of the reionization history in both ΛCDM and ΛWDM scenarios [3575,3576]. Despite these astrophysical uncertainties, constraints on m_χ can be obtained through observations of the LF [3577–3579] and the SFR density [1754] up to high redshift, and from the comparison of the expected electron scattering optical depth, $\tau_{\rm es}$, positive with an ionized IGM, with empirical data from Planck [3580].

4.4.2.2. Candidates. Traditionally, WDM is defined as a fermion with 2 degrees of freedom that decouples relativistically and has a temperature to match the observed DM relic density with zero chemical potential. This allows to express observational limits on the free-streaming length as constraints on the mass of the DM particle. Lyman-α observations, for example, firmly exclude $m_{\rm WDM} > 1.9\,{\rm keV}$ [3581] (though sometimes more aggressive bounds have been derived, reaching up to $m_{\rm WDM} > 5.3\,{\rm keV}$ [1553]).

From the theoretical point of view, an excellent WDM candidate consists of a fermion that is a singlet under the standard model gauge group, commonly referred to as sterile (or right-handed) neutrino [3582,3583]. The resulting mixing with active neutrinos, through the neutrino portal, is constrained to mixing angles too small for sterile neutrinos to fully thermalize in the early Universe. Instead, DM production proceeds via oscillations, combined with neutral and charged current interactions of the active neutrinos with the SM heat bath [3458]. Parameter regions for which this mechanism produces the correct DM abundance in its simplest form are excluded [3584]. These bounds can be evaded by enhancing the production through oscillations by introducing a large primordial lepton asymmetry [3459], new self-interactions of the SM [3461,3585] or sterile neutrinos [3462,3586]. Further alternative scenarios that remain viable include the decay of a new scalar state combined with subsequent entropy injection [3587–3589] and thermal production via extended gauge sectors [3590–3593]. Common to these scenarios is that the WDM mass bounds in general become model-dependent, and therefore have to be re-expressed by using model-independent bounds on the free-streaming length (for the case of self-interacting sterile neutrinos, notably, the bound on the sound-horizon due to late kinetic decoupling can be more stringent [3462]).

Fuzzy dark matter (FDM): Fuzzy DM (FDM), also known as wave DM, quantum wave dark matter, or ultra-light axion DM, is an interesting area of research that bridges concepts from quantum mechanics, astrophysics, and cosmology, which offers potential solutions to some longstanding puzzles in our understanding of the Universe. It is a theoretical model proposing that DM consists of ultra-light particles with boson masses on the order of $m_{\rm b} = 10^{-22}\,{\rm eV}$ [2383,3486].

Unlike traditional particle DM models, fuzzy DM behaves more like a wave due to its extremely low mass. This wave-like nature leads to unique quantum mechanical effects on large scales [3594,3595]. This wave-like behavior of FDM results in a quantum pressure that opposes gravitational collapse on small scales. This can suppress the formation of small-scale structures, potentially addressing the "missing satellites problem" observed in the MW and other galaxies. In terms of halo structure, the density of DM halos is predicted to have a central core with a soliton-like structure. This differs from the sharp cusps predicted by CDM models and can help resolve some discrepancies between observations and simulations of galactic cores. While ultra-light, FDM behaves like a CDM on cosmological scales, providing a good fit for large-scale structure formation and CMB observations. Some works show hints that ultralight axions can improve consistency between CMB and galaxy clustering data, potentially reducing the S_8 tension [3596]. Tensions between the former and Lyman-alpha constraints could be alleviated with a component of ultralight or WDM [1562]. Regarding astrophysical tests, precise measurements of the distribution and movement of stars in galaxies, the structure of DM halos, and gravitational lensing effects can be done. The low mass end for ultralight DM has been ruled out by the dynamics of ultra-faint dwarf galaxies based on stellar kinematics in virialized halos [3502] and the Lyman-alpha forest [1551] using hydrodynamical simulations, where uncertainties in the modeling remain. Recently, constraints on the soliton mass using the Event Horizon Telescope (EHT) results for the black hole shadows of M87* and Sgr. A* was found [3597], confirming the theoretical model of FDM. It was also tested and constrained using the motion of the S2 star around Sgr. A* [3504]. How the FDM soliton evolves while being accreted on a black hole helps determine the stages of accretion flow [3598]. Not only for black holes, the effect of solitonic quantum wave DM was also explored through wormhole

solutions [3599]. Indeed, these studies explored how the effects of FDM can manifest through astrophysical objects, acting as an alternative method for Earth-based laboratory detection.

Based on the existing literature, it is clear that WDM models are potentially reached since some indications for alleviating the S_8 tension have been noted. However, the models in this category are not fully explored widely unlike other cosmological models. We anticipate that WDM remains a potentially rich area that needs to be investigated widely aiming to understand how the tensions on H_0 and S_8 can be relieved.

4.4.3. Interacting and decaying dark matter

Coordinator: Elsa M. Teixeira

Contributors: Amare Abebe, Amin Aboubrahim, Andrzej Borowiec, Anil Kumar Yadav, Branko Dragovic, Brooks Thomas, Davide Pedrotti, Emmanuel N. Saridakis, Emre Özülker, Gaspard Poulot, Ioannis D. Gialamas, Ivonne Zavala Carrasco, Jose A. R. Cembranos, Keith R. Dienes, Luis Anchordoqui, Marcin Postolak, Nikolaos E. Mavromatos, Paolo Salucci, Pran Nath, Rafael C. Nunes, Reggie C. Pantig, Riccardo Della Monica, Rishav Roshan, Simony Santos da Costa, Tomi Koivisto, Torsten Bringmann, Víctor H. Cárdenas, Vasiliki A. Mitsou, Venus Keus, Vivian Poulin, William Giarè, and Wojciech Hellwing

4.4.3.1. Interacting dark matter. Models of IDM replace the CDM component in ΛCDM by posing either a self-interaction between DM particles or interactions between DM and the other species in the Universe. Consequently, the mass of the DM particles bears some dependence on such interaction, defined in an FLRW background as

$$\dot{\rho}_{\rm IDM} + 3H\rho_{\rm IDM} = Q_i\,, \tag{4.20}$$

where Q_i embodies the interaction between DM and the ith species with energy density ρ_i (whose conservation equation will include a symmetric interacting term to ensure energy conservation). One key feature in favor of several models of IDM is that they can exhibit suppression of the matter power spectrum in relation to its ΛCDM counterpart. This effect is relevant in terms of attempts to address the cosmological tensions, particularly the S_8 tension, even upon including constraints from the CMB data. In the following, we present various types of IDM models and discuss their relevance for the resolution of cosmic tensions.

Dark matter interactions with baryonic matter Theoretical models often consider DM-baryonic matter (DM-BM) scattering to modify the evolution of density perturbations. For instance, velocity-dependent cross-sections in these interactions can impact the growth rate of cosmic structures, affecting the matter power spectrum and, hence, the derived value for the S_8 parameter [2327,3600,3601]. These interactions may also modify the reionization history through changes in the ionization fraction, optical depth, and CMB data-derived cosmological parameters [3602]. Recent simulations suggest even weak DM-BM interactions can leave observable effects on large-scale structures and the Lyman-α forest [3603]. Screened DM models propose local environment-dependent interaction strengths [3263] while models like matter bounce scenarios propose alternatives to the standard inflationary paradigm [3604,3605]. These DM-BM interaction models must balance improving cosmological fits without violating constraints from other astrophysical observations, such as galaxy clustering and WL surveys, thereby representing a promising but challenging research avenue [3606]. Further observational data from upcoming missions and theoretical refinement are needed to assess their viability as a potential solution to the cosmological discrepancies [3607].

Recent astrophysical evidence shows discrepancies between observed mass distributions in galaxies and predictions from the collisionless ΛCDM model [3375]. Notably, a constant density region is often found in galaxies' innermost areas, contrary to the expected cuspy density profile [358,2355,2357,2364,3608,3609]. Additionally, DM halo parameters correlate with the structural parameters of the luminous component, such as the half-light radius R_{50} and stellar mass $M_\star$ [3610–3614]. This entanglement between the dark and luminous components suggests some interaction between DM and BM [3615], occurring only where the product of DM and BM densities exceeds a threshold [3615,3616]. Outside these regions, DM halos retain their original NFW profiles. The DM-BM interaction, observed over several Gyrs, does not affect the formation of galaxy dark halos but gradually modifies the halo density over time, erasing the initial cusp. This process may be observable in the recent mass distribution of high-redshift galaxies [3615]. While the macroscopic effects of this interaction are clearer, the microscopic processes remain uncertain. Numerous candidates for IDM have been proposed (e.g., see Refs. [3617–3620]), and investigations continue. Observations suggest these interactions could occur in secluded regions of galaxies, such as stars, molecular clouds, neutron stars, black holes, and central supermassive black holes, aligning with various studies (e.g., see Refs. [3621,3622]).

Dark matter interactions with photons In Ref. [2674], an extension of the ΛCDM model is proposed where DM couples with photons (γ), resulting in a nonconservation of particle numbers. This model suggests that DM particles gradually decay into photons over time without significant scattering processes, slightly deviating from the standard cosmic evolution. It offers a potential solution to the cosmic tensions (see Fig. 4). Based on the theoretical study of couplings between DM and relativistic relics in Ref. [3623], a lower limit on the DM mass has been derived [3624] for DM-γ interactions: $m_\chi > 8.7$ keV at 95% CL (assuming it saturates 100% of the observed relic density). Alternatively, one could derive a bound on the abundance of such DM candidates depending on the mass [3593]. Observational constraints on DM-γ scattering cross-section were derived in Ref. [3625], with $\sigma_{\rm DM-\gamma} \leq 2.25 \times 10^{-6}\sigma_{\rm Th}, (m_{\rm DM}/{\rm GeV})$ at 95% CL. A multi-IDM framework, including interactions with photons, was explored in Ref. [3396], simultaneously addressing the H_0 and S_8 tensions. The prospects for testing DM-γ interactions through CMB spectral distortions have been discussed in Ref. [3626]. The black hole shadow, a dark region observed against a bright background, is closely related to the photonsphere, the region where photons orbit the black hole. By performing backward tracing techniques, one can study how the shadow deviates from the classical prediction due to DM effects. Studies like Refs. [3627,3628] have shown that DM-γ interactions in the photonsphere can alter the shadow's shape, illustrating how astrophysical objects can be used as independent DM probes. Numerous studies have since explored different DM models and their effects on black hole properties [3504, 3597,3629–3658], concluding that significant DM concentrations are necessary for observable effects on a black hole's shadow [3659].

Dark matter interaction with dark radiation The possibility that the multiple cosmic discrepancies are tied to the existence of a dark sector filled with a thermal bath of dark relativistic species, also known as dark radiation (DR), interacting with DM has been widely explored (e.g., see Ref. [2561,2565,2673,2674,3660–3667]). In the standard model, the effective number of neutrinos accounting for the three neutrino species, $N_{\rm eff} = 3$. Still, the presence of DR can modify this value, reducing the sound horizon and adjusting the inverse distance ladder calibration of the BAO and SNIa. This is discussed extensively in Section 4.1.3.

The DR-DM interaction has two primary effects: it introduces a drag term in the DM Euler equation, reducing the growth of DM perturbations and potentially explaining the low S_8 values measured by WL surveys; and it influences DR perturbation dynamics, reducing their free-streaming, which can result in a larger contribution to $N_{\rm eff}$ and align with H_0 measurements from the SH_0ES experiment. Various models embody these ideas, such as the "non-Abelian DM model" [3660,3661,3663], "partially acoustic DM" [3662], "cannibal DM" [3664], stepped-dark radiation [2561,2565,2673,3665–3667], and neutrino-DM interaction [2329]. Interestingly, these models may

also address other CDM issues, such as the cusp/core problem, the so-called "too big to fail" (TBTF) issue, and the missing satellites problem (see Ref. [2354] for a review). Indeed, Ref. [3668] is the first particle-physics proposal to address all three problems simultaneously. The model in Ref. [3669] integrates this into DR as sterile neutrinos, introducing late-time effects that influence H_0/σ_8. Ref. [3670] offers a comprehensive Lagrangian-level classification of DM-DR interaction models, showing how CDM can mimic a WDM cut-off in the matter power spectrum. Alternatively, model-independent analyses can be conducted through the "effective field theory of structure formation" (ETHOS) [2308,2309], which provides a mapping from Lagrangian parameters of DM-DR models to phenomenological parameters of the linear power spectrum, with numerical simulations extending this to the full non-linear power spectrum.

Dark matter interaction with dark energy Interactions within the dark sector may help resolve various tensions simultaneously by leveraging on the unknown nature of DE and DM (see Section 4.2.3 for a more thorough account of IDE models). For instance, in Refs. [3671–3673], the authors show that by applying fluid approximation methods for rapidly oscillating scalar field DM coupled to scalar field DE through a Lagrangian approach, DM can effectively be treated as a fluid on cosmological scales under the appropriate Hubble-averaged behavior. These models are expected to help alleviate cosmic tensions, namely on S_8, due to their contributions in suppressing the matter power spectrum on small scales, and on H_0 through the modified background dynamics.

A recent paper proposed a cosmological model of DM and DE based on a particle physics Lagrangian [3506] to address cosmic tensions. The model involves two interacting ultralight scalar fields, one for DM and one for DE, with a coupling between them and was tested against various cosmological data sets, including Planck [192,729,1434], BAO [777,797,1145,2515,3674,3675], and Pantheon and SH0ES data [33,34]. It demonstrated an ability to alleviate the H_0 tension, reducing the discrepancy to about $\sim 2\sigma$, and also resolved the S_8 tension.

4.4.3.2. Decaying dark matter. Another approach posits instead that a fraction of the DM sector is undergoing a decay process into another species, falling under the broad heading of decaying DM (DDM) models. This scenario is motivated by theoretical considerations, can explain specific experimental results, and addresses small-scale issues in the CDM paradigm. Initially developed in the 1980s, the DDM model has gained renewed interest in light of cosmic tensions. Accordingly, such models conventionally contain two extra parameters: the lifetime of DDM τ plus the initial fraction of DDM to total DM $f_{\rm DDM}$. The decay is expressed in FLRW as

$$\dot{\rho}_{\rm DDM} + 3H\rho_{\rm DDM} = -\Gamma_i\,\rho_{\rm DDM}\,, \tag{4.21}$$

where Γ_i is the decay width of DDM (related to its lifetime as $\Gamma = \tau^{-1}$) into the species ρ_i. There are several variations of the DDM hypothesis. However, these scenarios alone are unlikely to resolve the H_0 tension, which would require, for example, assuming an earlier decay of DM.

Dark matter decays into dark decay products Various scenarios involving the decay of an unstable component of multicomponent DM into dark radiation have been proposed to address the H_0 and S_8 tensions [2571,3676–3683]. For short-lived particles ($\Gamma \gtrsim 10^6$ Gyr^{-1}), DM decays into dark radiation at early-times ($t \ll t_{\rm LS} \sim 1.17 \times 10^{13}$ s, where $t_{\rm LS}$ denotes the time of last scattering), increasing the expansion rate and reducing the sound horizon size r_s, thus increasing H_0 [2571,3676,3677]. Since the angular size of the sound horizon at the last scattering surface $\theta_{\rm LS} \equiv r_{\rm LS}/D_M(t_{\rm LS})$ is a CMB observable that must be kept fixed, a reduction of $r_{\rm LS}$ simultaneously decreases the comoving angular diameter distance from a present-day observer to the last scattering surface $D_M(t_{\rm LS})$, and increases H_0. For long-lived particles, DM is depleted into radiation after $t_{\rm LS}$, shifting matter-DE equality to earlier times and allowing a late-time increase in H_0 [3678,3679]. Moreover, two-body decays that transfer energy from DM to DR, reducing the late Universe matter content, help accommodate local S_8 measurements [3680–3682]. For $\Gamma \gtrsim H_0 \sim 0.7$ Gyr^{-1}, most unstable DM particles have decayed by redshift $z = 3$, impacting observations like those from IceCube if sterile neutrinos play the role of DR [3684,3685]. If $\Gamma \lesssim H_0$, only a fraction of DM particles have decayed. Recent CMB data severely constrain the fraction of unstable DM in these scenarios [3593,3686–3691]. Short-lived particles are constrained by CMB polarization [3690,3691], and low redshift DM depletion reduces CMB lensing power, conflicting with Planck data [3686–3688]. Including BAO measurements further tighten constraints on the fraction of long-lived particles [3689,3690]. Current bounds make a decaying DM solution to the H_0 tension unlikely, though a combination of scenarios with multiple decaying DM particles (for example decays into a combination CDM and WDM [3692]) at different epochs may effectively ease this tension.

More promising is the role that DDM can play regarding the S_8 tension, especially in models where the (dark) decay products are massive particles. These products get a velocity kick $\epsilon \equiv v/c$ from the decay, suppressing structure growth on scales below their free-streaming length while behaving like regular CDM at the background level, thus avoiding the strong constraints from BAO data. These scenarios have been tested against various cosmological data [3681,3682], including the full shape of BOSS power spectrum [3693] and KiDS WL measurements [3694], and shown to reduce the S_8 tension to $\sim 1.5\sigma$ for lifetimes $\Gamma^{-1} \simeq 120$ Gyr and velocity kick $\epsilon \simeq 1.2\%$ [3693]. In addition, depending on the lifetime and kinetic energy of the decay, DDM can address or mitigate various tensions related to small-scale structures and galaxy formation [3695–3699] such as the missing satellites problem [2360,2361], by estimating the power spectrum cut-off scale.

It is also worthwhile to move beyond the specific idea of decaying particle DM and consider a more generic parameterization to describe the potential conversion of a DM component to DR, with a transition rate that may not necessarily follow exponential decay [2326,2410]. This approach includes traditional decaying DM but also encompasses scenarios such as merging primordial black holes (PBHs) or late-time DM self-annihilation in the presence of long-range forces. In these generalized scenarios, the S_8 and H_0 tensions can be mitigated in somewhat different ways, though a complete resolution of these tensions remains unlikely.

Dynamical dark matter DDM models the decay of a DM ensemble across epochs, balancing the collective lifetimes against cosmological abundances among various DM components [3700]. One realization of such a DDM ensemble that has been extensively studied consists of a tower of dark Kaluza–Klein states associated with a large extra dimension; such a tower then allows for the possibility of "intra-ensemble" decays from heavier to lighter dark states [3701,3702]. Such decays can modify the DM velocity distribution over time [3702] and potentially address the S_8 tension [3703,3704]. This idea has recently found new relevance within the Swampland program [3705], which suggests an extra mesoscopic dimension ("dark dimension") in the micron range [2923], leading to a tower of weakly interacting light DM particles which are KK excitations of the graviton [3706]. While DDM scenarios of this sort may potentially address the S_8 tension, they are also subject to constraints on the expansion rate at late-times from, e.g., SNIa [3707].

Dark sectors with varying equations of state In the case of soft DM and soft DE [3708,3709] one considers that effectively the dark sectors have a different equation of state at large scales, namely at scales entering the Friedmann equations, and a different one at intermediate scales, namely at scales entering the perturbation equations, features that are typical in soft materials [3710]. In this case, the perturbative-level properties are slightly changed, and one can easily alleviate the S_8 tension. It has also been shown that such scenarios can be compatible with JWST observations, offering a potential explanation

for the unexpectedly rapid emergence of massive galaxies at high redshifts [3711].

Some applications of decaying dark matter DM decaying during or after recombination can alter the CMB power spectrum by injecting energy that reionises the IGM, constraining the DM lifetime to $\tau_{\rm DM} \gtrsim 10^{25}$ s for photon or e^+e^- decay products [192,3593,3712,3713]. Additionally, null detections of diffuse X/γ-rays impose strict constraints on the DM lifetime. In DM-dominated galaxies or clusters, e^+e^- decay products can produce radio waves through electromagnetic interactions, observable by radio telescopes like the SKAO [3714], providing a better probe for decaying DM compared to current gamma-ray observations. A recent study [3715] found that DM decay width $\Gamma_{\rm DM} \gtrsim 10^{-30}$ s^{-1} is detectable with SKAO. These constraints were used in Refs. [3716,3717] to understand the scale of Quantum Gravity, assuming that it breaks all approximate global symmetries, including DM stability. Moreover, null detection of X-ray signals has ruled out minimal DM models like νMSM [3718] for DM produced from active-sterile oscillation and has severely constrained the DM mass above the MeV scale for feebly interacting massive particles produced from gauge boson decays [3719].

4.5. Other solutions

4.5.1. Estimates based on a possible local void

Coordinator: Indranil Banik

Contributors: Alireza Talebian, Bahman Khanpour, Ebrahim Yusofi, Harry Desmond, Paolo Salucci, Richard Stiskalek, Sahar Mohammadi, Sandeep Haridasu, Sergij Mazurenko, Sveva Castello, and Vasileios Kalaitzidis

Cosmic voids may help to alleviate the Hubble tension. A void effectively adds negative mass to a localized region of an otherwise homogeneous universe. The repulsive gravitational effect of this negative mass causes matter to flow away from the void, further deepening it and enhancing its repulsive effect. Recent studies in a void-dominated late universe [3720–3723] indicate that cosmic voids achieve maximum entropy and thermal equilibrium [3724,3725]. This hierarchical evolution may lead to the formation of large spherical cosmic voids through the merging of smaller sub-voids via the void-in-void process [1789,1798,3726]. Studies suggest that clusters and voids can exert positive pressure individually [3722,3725]. Their coexistence in the Universe's web-like structure results in opposing pressures: overdensities generate positive pressure that pulls them closer together, while voids create negative expansion pressure that separates galaxies. The outflow from a local void could inflate observed redshifts and thus estimates of H_0, though this effect is not sufficient to solve the Hubble tension in ΛCDM [3727,3728].

Near-infrared observations covering 90% of the sky suggest that we live inside the Keenan–Barger–Cowie (KBC) void [3729]. The results are deep enough to cover most of the galaxy LF, making them representative of the underlying matter distribution. The KBC void or Local Hole is evident throughout the electromagnetic spectrum, including in X-rays [3730,3731], optical [3732,3733], infrared [3729,3734–3741], and radio wavelengths [1407,3742]. Comparison with the Millennium XXL simulation [3743] suggests that the KBC void is 6σ discrepant with ΛCDM [3744]. Since the underlying observations are galaxy number counts in redshift space, the results are unaffected by the assumed H_0.

Various proposals have been made arguing that gravitationally driven outflows from the KBC void could solve the Hubble tension [3745–3749]. In a homogeneously expanding universe, we would expect that $cz' = \dot{a} = H_0$, where $z' \equiv {\rm d}z/{\rm d}r$ is the rate at which z rises with r. However, if we are located near the center of a large void, the outflow velocity would rise from zero at the void center to some maximum further out, before gradually decaying away. The initial rise with r would inflate cz'. To estimate how much, we note that the KBC void has an underdensity in redshift space of $\delta_{\rm obs} = 46 \pm 6\%$ (see figure 11 of Ref. [3729]). The actual underdensity is about half as much because of RSD [3750], the reduction in distance to any fixed redshift due to outflow from a local void inflating cz'. The reduced volume reduces the number counts, making the underdensity appear deeper in redshift space than it actually is. Accounting for this and assuming the required reduction in comoving density from the nearly homogeneous early Universe must be due to an increase in comoving volume, [3744] argued in their Eq (5) that

$$\frac{cz'}{H_0} = \left(1 - \delta_{\rm obs}\right)^{-1/6} . \tag{4.22}$$

Thus, we would generally expect the locally estimated H_0 (actually cz') to exceed H_0 estimated from the CMB or other high-redshift probes by $11 \pm 2\%$. This is only a rough estimate — the actual result depends on how the void has evolved over cosmic history. This must differ from the growth of voids in ΛCDM given that density fluctuations on the KBC void's comoving scale of 300 Mpc are very well observed at the time of recombination and match ΛCDM expectations [701], implying that density perturbations on these scales grow faster than in ΛCDM. It is suggested that this is caused by a modification to gravity on length scales $\gtrsim$ 100 Mpc, which would not affect the early Universe as its smaller age reduced the cosmic horizon, the distance that light and gravity could have traveled [3744].

A further argument for this scenario is the observed bulk flow curve out to $z = 0.083$ or about 350 Mpc [1426] based on the CF4 galaxy catalog [1424]. The bulk flow measures the average vector velocity of tracers within a spherical region centered on the Sun, albeit using only line of sight velocities. Ref. [1426] argue that the observed bulk flow on the largest probed scales is roughly quadruple the ΛCDM expectation and thus in $> 5\sigma$ tension with it (see also Section 2.3.14). The bulk flow curve in a full-sky survey is independent of the assumed H_0, which sets the monopole of the velocity field, while the bulk flow is a function of the orthogonal dipole. There are additional subtleties when the sky coverage is not complete, but since CF4 covers most of the sky, a slight adjustment to the estimator is sufficient to deal with the small unobserved regions of the sky, which mainly lie at low Galactic latitudes (see figure 2 of Ref. [1424]). However, the sky coverage becomes less complete at $z \gtrsim 0.05$ as CF4 mostly relies on SDSS. There can be spurious effects even at lower z because CF4 is reliant on combining surveys, each with their own zero-point and limited sky coverage.

The local void scenario was explored in great detail by Ref. [3744], who constructed semi-analytic models of a small initial underdensity at $z = 9$ and evolved it to today. Those authors used Milgromian MOND [364–366] to enhance the gravity from any given (under)density distribution, allowing the exploration of self-consistent models with enhanced structure growth on the relevant scales. A good joint fit was obtained to the density profile of the KBC void and the observed magnitude of the Hubble tension. An important conclusion was that our location in the void needs to be fine-tuned at the 2% level, which is not a strong argument against the model [3744]. The velocity field in their model was recently calculated in more detail [3751]. The predicted bulk flow curve was found to agree well with the observations of Ref. [1426], which are themselves in good agreement with the measurements reported by Ref. [1427]. The rising bulk flow curve implies we are located fairly close to the void center, minimizing any impact on the CMB quadrupole due to gravitational lensing [3752,3753]. Ongoing work aims to perform this peculiar velocity inference at the field level rather than relying on the bulk flow summary statistic.

The H_0 tension should disappear at high z once the density returns to the cosmic mean and the void's impact gradually decays. Indeed, the ages of the oldest Galactic stars and CCs (Section 2.1.13) suggest a low H_0 consistent with the CMB value and well below the local cz' [438,441,3754,3755]. In fact, the Hubble tension is largely a mismatch between the local cz' and H_0 estimated in other ways, typically from higher z data [3756]. This can be done assuming ΛCDM,

leading to the concept of $H_0(z)$, the value of H_0 inferred from data in a narrow redshift range centered on z. Although ΛCDM predicts a flat curve, there is evidence for a declining trend [516,1290,3103,3104,3110,3757,3758]. The most recent analyses carefully minimize covariance between H_0 estimates from different redshift bins, finding 6σ evidence for a declining trend [3759,3760]. Similar techniques can be applied to construct simulated $H_0(z)$ curves that map the decay of the void's impact on z [3761]. Their figure 3 shows good agreement with the observed $H_0(z)$ [3759,3760].

BAO observables also deviate from ΛCDM in the manner predicted by the local void scenario [3762]. These discrepancies (especially in DESI data; [699]) have alternatively been interpreted in terms of the DE density varying with time [1283,1284,3763]. Regardless of the interpretation, the Hubble tension seemingly becomes weaker at high redshift, and not merely due to larger uncertainties [2689]. A recent study examined a variable DE fluid with a quadratic EoS in a late-time context [3723,3725,3764]. Such an EoS may emerge from cluster/void mergers and could represent a redshift-dependent EoS parameter for cosmic acceleration [3721–3723,3725].

The main issue facing the void model at the moment is that the Hubble tension does not clearly decay at high z in the analysis of SN [3765], though there are some hints of such a decay [516,3110,3759]. While the BAO ruler has a fixed comoving size at $z \lesssim 1000$, SN are not standard candles but merely standardizable [3766]. The intrinsic SN luminosity depends on color and stretch, or how rapidly the light curve decays [33,218]. There are not enough SN in host galaxies with Cepheid distances to reliably constrain these dependencies, which must be obtained jointly with the other cosmological parameters in the Hubble flow sample. This is usually done assuming some parameterized form for the relation between luminosity distance and redshift derived from an isotropic and homogeneous Friedmann cosmological model [3767,3768], though with an additional free parameter in the DE equation of state w [3769–3771]. SN calibrated through the distance ladder, in combination with BAO data and the *Planck* distance priors [192], suggest compatibility with a homogeneous cosmology and indicate that a potential local void would not significantly impact the measurement of H_0 from SN [3772–3774] — but this would need to be confirmed by less model-dependent approaches as a cross-check [3775,3776]. A particular concern is that the typical stretch and color of SN exhibit strong trends with z [3777–3779]. Due to the need to calibrate how both affect the intrinsic SN luminosity, these trends may mask the decaying away of the excess redshift induced by a local void [3761]. One might think that neglecting an actually present local void would cause the optimal homogeneous Friedmann model to provide a poor fit to the data, but the SN magnitude uncertainties are artificially inflated such that the reduced $\chi^2 = 1$, completely hiding any such issue [3780]. The results also change slightly if we assume that it is the color rather than magnitude that has an extra unknown source of noise, for instance, due to dust [3781]. There is ongoing work on revising the SN fitting procedure to allow a local void to inflate redshifts in the nearby Universe, jointly considering cosmological and standardization parameters.

While the KBC void could potentially solve the Hubble tension, it is not evident in the reconstructed local density field [2317] and its existence has not been validated kinematically [3765,3782]. A recent analysis of galaxies using the Radial Tully–Fisher (RTF) relation [355] provides a very promising way to investigate the possibility [356]. They demonstrated comprehensively that a local void capable of alleviating the Hubble tension is highly unlikely to reside at $z \lesssim 0.01$ (as suggested by Ref. [3739]) because it would have been evident in the analysis of the local cosmic expansion through the RTF distance indicator. This agrees with previous studies over the same redshift range using standard SN distance indicators and datasets [3765,3782] — though a plausible local void would inflate redshifts much further out [3761]. Remarkably, the RTF indicator could easily become the best distance indicator for $z \lesssim 0.15$, where it could be applied to a galaxy sample several times larger than SN datasets. In each galaxy, the RTF method would provide multiple distance measurements, each as accurate as those obtained from SN.

The KBC void is unique among solutions to the Hubble tension in that it was proposed long before the Hubble tension became known. Its large size and depth and the anomalous bulk flow curve all suggest that structure formation on scales of several hundred Mpc is more efficient than expected in ΛCDM, as also suggested by the high redshift, mass, and collision velocity of the El Gordo interacting galaxy clusters [3783,3784]. If so, the Hubble tension might be resolved without adjusting the background cosmology, preserving its excellent fit to high-redshift datasets and the ages of the oldest stars [441,456,3754]. In the future, important tests will be provided by techniques that extend beyond the void radius. For instance, peculiar velocity reconstructions using galaxy scaling relations already constrain cz' out to $z = 0.1$ [389,390,394,397]. Extending them to $z \gtrsim 0.3$ would test the predicted decaying of the void's effect at larger z [3761]. BAO measurements suffer the opposite problem: they are most accurate at $z \gtrsim 0.5$, well beyond the void's influence [699]. It is crucial to extend BAO measurements to $z \lesssim 0.2$, where a local void should have an appreciable impact [3762]. More detailed analyses of existing datasets would also help, for instance obtaining bulk flow measurements using SN to check results obtained so far using galaxies and extend them further out [1388,1390,1391,2844,3785,3786]. The inferred bulk flows can serve as a consistency check on measurements using the far more numerous galaxies.

4.5.2. *Primordial magnetic fields*

Coordinator: Karsten Jedamzik

Contributors: Alireza Talebian, Anto Idicherian Lonappan, Cláudio Gomes, Gaetano Lambiase, Iryna Vavilova, Levon Pogosian, and Tom Abel

The possible existence of PMFs in the early Universe has been a research topic for decades (for further reviews see Refs. [3787–3789]). The underlying question is if magnetic fields observed in galaxies, clusters of galaxies, filaments, and in particular voids of the extragalactic medium [3790–3796] could be the result of a magnetogenesis process in the very early Universe which magnetized the Universe already well before recombination. The alternative would be that all/or most of the observed magnetic fields are due to astrophysical processes such as dynamos and outflows. The impact of a putative PMFs on the CMB has therefore been studied in great detail [687,3797–3838,3838–3843]. Most proposed effects result in upper limits around comoving $\sim 1\,$nG, which is however a field strength about two orders of magnitude stronger than that required for cluster magnetic fields $\sim 1\mu$G to be explained entirely by a PMFs [3844]. It has been realized that the anisotropies in the CMB are particularly sensitive to one effect, the creation of small-scale baryon inhomogeneities by PMFs [3845,3846].

A PMF of comoving field strength $\sim 0.05\,$nG on comoving length scales $\sim$kpc produces slightly non-linear baryon inhomogeneities on such scales during recombination. This is possible since kpc scales are well below the photon mean free path such that magnetic pressure is counter-acted only by the small baryon pressure and not the photon pressure. This process is often referred to as "baryon clumping".

Note that any PMF is characterized by a continuous spectrum, containing initially magnetic power on a large range of scales, either with a scale-invariant spectrum due to inflationary magnetogenesis or a very blue Batchelor spectrum due to magnetogenesis during cosmic phase transitions. In the latter scenario the bulk of the PMF is dissipated as the Universe expands, and a comoving $\sim 0.05\,$nG field left shortly before recombination results in a $\sim 0.01\,$nG field at the present epoch, approximately the value to explain cluster magnetic fields. The process of PMF-induced baryon clumping has been studied numerically and allowed to set stringent upper limits on the final total present PMF strength of $\sim 0.01\,$nG for a Batchelor spectrum [3847]. This upper limit

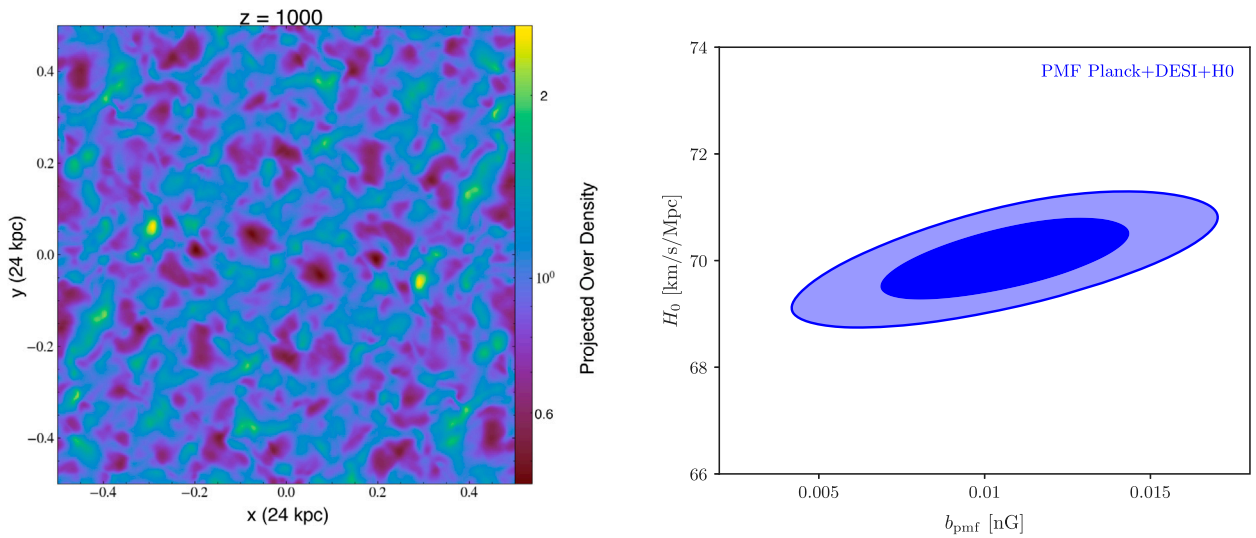

Fig. 78. *Left:* Results of an MHD simulation [3852] starting at redshift $z = 4500$ with an initial comoving magnetic field of 0.526 nG with Batchelor spectrum and initially vanishing density perturbations and peculiar flows. The figure shows the (projected) density fluctuations generated at $z = 1000$ by the stochastic magnetic field. *Right:* Preliminary results of a MCMC comparing the theoretical prediction of a ΛCDM model with a PMF with Batchelor spectrum to the combination of Planck CMB data [192], DESI-1Y BAO data [699], and the SH0ES [34] Hubble constant determination. It is seen that a final magnetic field of $B \approx 0.01$ nG is preferred leading to Hubble constants of $H_0 \approx 70\ \mathrm{km\,s^{-1}Mpc^{-1}}$, significantly larger than those predicted in ΛCDM without a PMF. This field strength is close to that needed to explain observed cluster magnetic fields entirely by a PMF.

may be subject to factor two changes when the newer Planck CMB data and/or a more realistic treatment of the PMF effects on the CMB are employed.

Recombination in a clumpy baryon medium proceeds faster than in a homogeneous medium due to the non-linearity in the recombination rate (i.e., $\alpha_e\langle n_e n_p\rangle > \alpha_e\langle n_e\rangle\langle n_p\rangle$ where α_e is the recombination coefficient and n_e, n_p are electron- and proton- density, respectively, with $n_e \approx n_p$). Recombination therefore occurs earlier when PMFs are present, such that the sound horizon $r_\star$ is reduced [3848]. A reduction of the sound horizon compared to ΛCDM is the ingredient utilized by essentially all early-time solutions for the Hubble tension (see Section 4.1.1 for an explanation). The effect of baryon clumping on the CMB has been analyzed by several groups [3848–3851]. Here the clumping was treated in toy three-zone models, averaging the ionization fraction from three different and independent regions with the average density the same as in an homogeneous universe. Due to the absence of detailed knowledge of the PMFs generated baryon PDF function, i.e., the probability to find a baryon at a certain density, and its evolution, non-evolutionary models with an ad hoc PDF were chosen. In Ref. [3848] it was found that when Planck data in combination with three late-time H_0 determinations was confronted to such clumping models, clumping was preferred at the $\sim 3\sigma$ CL with inferred $H_0 \approx 69.8$–$71\ \mathrm{km\,s^{-1}Mpc^{-1}}$depending on the chosen baryon PDF. Though the fit to the CMB data was slightly worse than in ΛCDM it was still reasonably good (a PTE value of 0.17 compared to 0.20 for ΛCDM without PMFs). On the other hand, when other data is included, such as BAO and SN, slightly lower $H_0 \approx 69.7$–$70.6\ \mathrm{km\,s^{-1}Mpc^{-1}}$were inferred. It is now known that the combination of Planck CMB data and BAO data essentially disallows H_0 as high as the SH0ES value $H_0 \approx 73\ \mathrm{km\,s^{-1}Mpc^{-1}}$in all early-type solutions to the Hubble tension if the physical matter density parameter $\Omega_m h^2$ has a value comparable to the one in the best-fit ΛCDM model [804]. When the model was confronted only to CMB data (Planck in combination with SPT-3G and/or ACT), but no late-time H_0 measurements were used, clumping was no further detected but only limited from above [3849–3851]. It was argued that clumping is heavily constrained by the reduced Silk damping in conflict with the ACT data [3849], see below however.

These promising trends tempted a recent much more sophisticated study of recombination in the presence of PMFs [3852]. Instead of using three-zone models, MHD simulations of PMFs before, during, and after recombination were performed automatically leading to the correct baryon PDF and its evolution. The simulations were performed down to redshift $z = 10$, providing a direct connection between the magnitude of clumping during recombination and the PMF total strength at the onset of structure formation. A chemistry solver coupled to the MHD simulations was used to self-consistently compute the ionization fraction in each volume element. The average perturbation of the ionization fraction compared to a homogeneous no-PMF model was computed and can be used to compute the anisotropies in the CMB in a magnetized universe. The study revealed the possible importance of two further effects, namely the mixing of Lyman-alpha photons between different regions, and enhanced Lyman-alpha photon loss due to peculiar motions of the baryon fluid. Whereas the second effect was found to be subdominant for weak magnetic fields (final field ~ 0.01 nG for Batchelor spectrum) the almost complete mixing of Lyman-alpha photons from regions at different densities leads to a further reduction of the ionization fraction during recombination. It also results in an enhancement of Silk damping such that magnetized models often have virtually identical Silk damping to non-magnetized ones.

The left panel of Fig. 78 shows the projected baryon overdensity, i.e., $(\rho - \langle\rho\rangle)/\langle\rho\rangle$ of a magnetized universe at $z = 1000$, with density clumps entirely created by the existing stochastic PMF with Batchelor spectrum. There is currently no other than PMF explanation for the putative existence of baryon isocurvature density fluctuations before recombination as other scenarios (pre-existing isocurvature fluctuations) are ruled out by BBN or are not volume-filling enough (isocurvature fluctuations due to cosmic strings). The right panel of Fig. 78 shows the result if a magnetized ΛCDM model is compared to Planck, DESI, and SH0ES data. It is found that a universe without PMFs is essentially ruled out by this data combination. Moreover, the predicted Hubble constant is around $70\ \mathrm{km\,s^{-1}Mpc^{-1}}$. Though this value does not match the SH0ES value it is in accordance with other observational determinations of H_0 [174,252]. It is intriguing to realize that the final present day magnetic field $B_0 \approx 0.01$ nG is essentially that required to explain the origin of cluster magnetic fields. It furthermore is also an explanation of the putative observations of an extragalactic field by γ-ray observations. Further observational advances in small-scale CMB anisotropy experiments (ACT, SPT-3G, S4) and γ-ray observations of a

compact-size halo of powerful blazars (CTA with sensitivity less 0.1 TeV and sufficient angular resolution [3853]) have the potential to establish that the early Universe had already been magnetized.

4.5.3. Feasibility of inflationary models to ameliorate the cosmic tensions

Coordinator: Jaume de Haro, Luis A. Anchordoqui

Contributors: Ali Övgün, Alireza Talebian, Andrew R. Liddle, Andrzej Borowiec, Anil Kumar Yadav, Anto Idicherian Lonappan, Antonio Racioppi, Benjamin L'Huillier, Carsten Van De Bruck, Cláudio Gomes, Cristian Moreno-Pulido, Dario Bettoni, David Benitsy, Deng Wang, Denitsa Staicova, Diego Rubiera-Garcia, Elias C. Vagenas, Emanuela Dimastrogiovanni, Emmanuel N. Saridakis, Giulia Gubitosi, Giuseppe Fanizza, Goran S. Djordjević, Ido Ben-Dayan, Ignatios Antoniadis, Ioannis D. Gialamas, Javier Rubio, Joan Solà Peracaula, Juan Garcia-Bellido, Laura Mersini-Houghton, Leila L. Graef, M.M. Sheikh-Jabbari, Margus Saal, Marina Cortês, Micol Benetti, Milan Milošević, Nikolaos E. Mavromatos, Nils A. Nilsson, Octavian Postavaru, Oem Trivedi, Özgür Akarsu, Petar Suman, Rishav Roshan, Salvatore Samuele Sirletti, Saurya Das, Simony Santos Da Costa, and Venus Keus

4.5.3.1. Modeling the inflationary expansion and its generalities in connection to the cosmic tensions. Inflation was first suggested to solve the flatness and horizon problems [3854]. The simplest inflationary model, known as "vanilla" or single-field inflation, describes the expansion of the Universe using a single scalar field ϕ with a suitable potential $V(\phi)$. The dynamics of this field are governed by the conservation and Friedmann equations. The most popular approximation for the scalar field is the so-called **slow-roll approximation**, with the potential energy dominating the energy density of the Universe, i.e., $\dot{\phi}^2 \ll V(\phi)$ and $\ddot{\phi} \ll 3H\dot{\phi}$, where H is the Hubble rate. This leads to an approximately exponential expansion, with the scale factor evolving as $a(t) \sim e^{Ht}$. It is possible to define the slow roll parameters: $\epsilon = M_{\rm Pl}^2\ [V'(\phi)/V(\phi)]^2/2$ and $\eta = M_{\rm Pl}^2\ [V''(\phi)/V(\phi)]$. Using them, one can relate inflationary observables, such as the scalar spectral index $n_s \approx 1 - 6\epsilon + 2\eta$ and the tensor-to-scalar ratio $r \approx 16\epsilon$, to the shape of the inflaton potential $V(\phi)$ [3855]. A point worth noting at this juncture is that an approach to addressing the H_0 tension involves studying the slow-rolling dynamics of a self-interacting scalar field, which can lead to an emerging H as a function of redshift; however, it should also be noted that while the scalar field could be responsible for a quintessence slow-rolling, it has not been associated thus far to inflationary models [3107].

Vanilla inflation predicts a nearly scale-invariant spectrum of scalar perturbations with a slight red tilt, quantified by the scalar spectral index $n_s \approx 0.96$–0.98. However, the slow-roll approximation is only one way to go, there are other examples such as fast-roll approximation [3856], constant-roll [3857,3858], rapid-turn inflation [3859, 3860], scalar field inflation in the presence of a non-minimal coupling between matter and curvature [3861] symmergent inflation [3862, 3863], gauge-field inflation [1447,3864,3865,3865–3889], s-dual inflation [3890,3891], nonlinear electrodynamics inflation [3892–3900], and symmergent gravity theory [3862,3863].

Many inflationary models predict primordial non-Gaussianities, which play a crucial role in understanding the early Universe's evolution and testing the inflationary paradigm. Non-Gaussianities are quantified by the non-linearity parameter $f_{\rm NL}$, which measures the amplitude of non-Gaussian fluctuations in the primordial curvature perturbations. These fluctuations require analysis of higher-order correlation functions, such as the bispectrum, beyond the two-point correlation function used for Gaussian fluctuations. Previous CMB experiments, including WMAP and early releases of the Planck data, aimed to detect these non-Gaussianities. The most recent constraints from the Planck 2018 results provide $f_{\rm NL}$ values for the standard templates: $f_{\rm NL}^{\rm local} = -0.9 \pm 5.1$, $f_{\rm NL}^{\rm equilateral} = -26 \pm 47$, and $f_{\rm NL}^{\rm orthogonal} = -38 \pm 24$, what indicates no statistically significant detection of primordial non-Gaussianities yet. However, it is important to keep in mind that multi-field or exotic single field inflationary models can lead to strongly scale-dependent non-Gaussianity [3901], which could evade large-scale constraints while still significantly affecting small scales. Such scale-dependent primordial non-Gaussianities could actually alleviate the S_8 tension in the non-linear regime of structure formation, without affecting the linear regime [3902].

Future CMB surveys, such as those planned with the Simons Observatory, CMB-S4, and the Euclid mission, promise significantly improved constraints on $f_{\rm NL}$. The Simons Observatory aims to achieve sensitivity levels that could reduce the uncertainties on $f_{\rm NL}$ to around $\Delta f_{\rm NL} \sim 1$. Similarly, CMB-S4, with its planned deep and wide CMB observations, is expected to further tighten these constraints and provide unprecedented precision in measuring primordial non-Gaussianities. The Euclid mission, primarily designed for large-scale structure surveys, will complement CMB observations by probing the distribution of galaxies and the large-scale structure of the Universe, thereby offering additional avenues to constrain $f_{\rm NL}$. These upcoming observations are expected to enhance our ability to test a broader range of inflationary models and deepen our understanding of models that could alleviate the S_8 tension.

4.5.3.2. Classes of inflationary models with ramifications for the cosmic tensions. There are numerous extensions or alternatives to vanilla inflation, justified in various ways. In this subsection, we summarize the generalities of inflationary models that have a connection to the cosmic tensions and call attention to the role these specific models have in ameliorating the tensions.

Higgs inflation In the simplest Higgs inflation model [3903], the Standard Model Higgs field is coupled non-minimally to gravity through a large dimensionless parameter, leading effectively to an almost flat Einstein-frame potential able to support inflation for a sufficient number of e-folds (for a review, see Ref. [3904]). One of the appealing aspects of this scenario is its minimalist approach, as it does not require the introduction of new fields or couplings beyond the Standard Model content. In particular, the reheating stage can be computed in detail, leading, in terms of the number of last e-folds $N_\star$, to precise predictions for the spectral tilt $n_s = 1 - 2/N_\star \simeq 0.966$ and the tensor-to-scalar ratio $r = 12/N_\star^2 \simeq 0.0033$ [3905–3907]. Additionally, the scenario offers a compelling connection with accelerator experiments, providing a detailed description of the power spectrum across a vast range of scales [3908,3909]. The MCMC analysis of current cosmological data confirms the model's observational viability and demonstrates that for the interval $N_\star \in [54.5, 60]$, it can break down the $H_0 - \sigma_8$ correlation [3910]. Specifically, considering an instantaneous transition to radiation-domination, the H_0 tension is reduced to approximately 3σ [76], constraining $H_0 = 67.94 \pm 0.45\,{\rm km\,s^{-1}Mpc^{-1}}$, while the value of $\sigma_8 = 0.793 \pm 0.003$ is in complete agreement with the KiDS-1000 results [3911]. The constrained $S_8 = 0.8019 \pm 0.0097$ is in 2σ with Planck, DES and KiDS-1000 data.

Several extensions of the minimal Higgs inflation scenario have been considered in the literature [3912–3919]. The so-called Higgs-Dilaton model addresses the current accelerated expansion of the Universe by introducing a unimodular constraint that manifests itself as the strength of a runaway Einstein-frame potential for a dilaton field [3912]. A significant feature of this scenario is the existence of specific consistency relations between the spectral tilt of primordial density perturbations, the tensor-to-scalar ratio, and the DE equation of state [3913]. Predictions of these relations are in tension with direct measurements of H_0 using low-redshift SN, but they align well with current CMB observations and large-scale structure data, offering distinctive signatures that could be tested by future galaxy surveys [3920–3922].

Starobinsky inflation Starobinsky cosmology is renowned as an excellent large-field slow-roll inflationary model [2074], aligning very well with CMB observations [3923,3924]. The key feature of the

Starobinsky potential, essential for achieving slow-roll inflation, is its asymptotic behavior, where $V_s(\phi) \to$ const. as $\phi \to \infty$. Despite its celebrated success, the model does not seem to align well with proposals that could resolve the cosmic tensions. For example, it was noted in Ref. [3925] that Starobinsky inflation can hardly coexist with an EDE fraction ~ 0.06, which is only able to reduce the H_0 tension down to about 3σ.

Brane inflation A theory that stems from the string theory, involves the interaction between branes in higher-dimensional space. Inflation occurs due to the motion of branes within a compactified extra-dimensional space, such as in the Klebanov–Strassler throat. The separation between branes acts as the inflaton, and their eventual collision ends inflation. This scenario can lead to observable levels of non-Gaussianity in the CMB power spectrum and the distribution of large-scale structures in the Universe, as well as potentially detectable GWs. The dynamics of the inflaton in brane inflation are governed by the Dirac–Born–Infeld (DBI) action, which is a type of non-canonical action [3926–3930]. Matrix inflation (a.k.a. M-flation) [3931] may also be viewed as a multi-brane version of the brane-inflation scenarios.

Tachyon cosmological models of inflation, based on the dynamics of a D3-brane in the bulk of the second Randall-Sundrum model, have been extensively considered [3932]. Particle creation and reheating in a braneworld inflationary scenario with a tachyon field were extended to include matter in the bulk. It has been demonstrated how the interaction of the tachyon with the U(1) gauge field drives the cosmological creation of massless particles and where estimates have been found for the resulting reheating at the end of inflation [3933]. A holographic braneworld scenario with a D3-brane located at the holographic boundary of an asymptotic AdS_5 bulk [3934] has shown significantly better agreement with Planck data [3923].

The cosmic tensions have been addressed in several models based on brane inflation. For example, in Ref. [2882] it was shown that phantom braneworld prefers a higher value of H_0 providing a much better fit to the local measurements. In addition, in Ref. [3935] it was pointed out that the simplest D-term inflation can be consistent with the cosmic string bound provided by observations of gravitational. Consistency with observations requires a spectral index $n_s = 1$ in accordance with the pre-recombination proposals to alleviate the H_0 tension (e.g., EDE).

Quintessential inflation After the discovery of the current cosmic acceleration [48,2980,3936,3937], several theoretical mechanisms were developed to explain it. Quintessence models broadly encompass scenarios with one or more scalar fields with appropriate potential/dynamics that can drive the late-time cosmic acceleration, allowing for much richer possibilities beyond that simple case, in which one gets a dynamical equation of state parameter. An important feature of quintessential models is the need to examine ghosts and other non-physical features of their perturbations [1264]. For recent applications in cosmology, see Refs. [3938–3940]. One of the simplest ways to do it is the so-called *quintessential inflation* [3941–3947], where the inflaton field is the only responsible for both accelerated phases. Several authors developed and improved the original Peebles–Vilenkin model [3948–3951], also embedding it in more fundamental frameworks [3952–3955]. In particular, α-attractors quintessential-inflation parameters can be constrained by stage IV surveys [3956] and they have been tested using *Planck* and low-redshift data [3957] and scale invariant models [3922]. Of particular interest here, the quintessential inflation, coming from the Lorentzian distribution introduced in Refs. [3958, 3959], agrees with the recent observations and is in agreement with the SH0ES H_0 measurement [3960]. Indeed by confronting the model to cosmological observations, one obtains $H_0 = 72.25 \pm 0.74\,\mathrm{km\,s^{-1}Mpc^{-1}}$ at 68% CL [3960,3961].

K-essence, multifield inflation, and their generalizations K-essence extends the standard model by including a non-canonical kinetic term in the Lagrangian, $P(\phi, X)$, where $X = \frac{1}{2}\partial_\mu\phi\partial^\mu\phi$ [2070,2772,3962–3964]. K-essence models can help address cosmic tensions through their unique equation of state properties and field dynamics affecting both early and late Universe evolution. In Ref. [3965] researchers demonstrate how k-essence can modify the expansion history in ways that specifically target both the Hubble and structure growth tensions. Similarly, Ref. [3966] examines how an EDE model triggered by the radiation-matter transition can be realized in k-essence. K-essence's theoretical flexibility makes it particularly valuable for tension resolution, as shown in Refs. [3967,3968], where k-essence is shown to maintain consistency with both observational constraints and theoretical requirements. The multifield dynamics have been further studied in Ref. [3969]. The generalized k-essence can further contribute to models affecting the sound speed of perturbations and the equation of state, which can modify cosmological distance ladder and thus influence tension-related parameters [2780,3970,3971].

Uniform five-dimensional inflation Compact extra dimensions can obtain large size by higher dimensional inflation, relating the weakness of the actual gravitational force to the size of the observable Universe [2924,3703]. A solution to the horizon problem implies that the fundamental scale of gravity must be smaller than 10^{13} GeV which can be realized in a brane-world framework for any number of extra dimensions. However, the requirement of (approximate) flat power spectrum of primordial density fluctuations consistent with present observations make this simple proposal possible only for one extra dimension at around the micron scale [2924,3972]. Consistency with 2018 *Planck* CMB data is supported by numerical simulations [3973–3975]. After the end of five-dimensional inflation, the radion modulus can be stabilized at a vacuum with positive energy of the order of the present DE scale. An attractive mechanism for radion stabilization is based on the contribution to the Casimir energy of fields propagating in the bulk: the graviton, a real scalar field, and three right-handed neutrinos [2899]. The scalar field has a potential holding two local minima with very small differences in vacuum energy and bigger curvature (mass) of the lower one, and thus when the false vacuum tunnels to its true vacuum state, the field becomes more massive and its contribution to the Casimir energy becomes exponentially suppressed [2900]. The tunneling process then changes the difference between the total number of fermionic and bosonic degrees of freedom contributing to the quantum corrections of the vacuum energy, yielding a sign-switching cosmological constant, Λ_s, see Section 4.2.2. Despite the fact that when inflation comes to an end radion stabilization necessitates a dark sector with $\Delta N_{\rm eff} \sim 0.25$ (i.e., saturating *Planck*'s upper limit [192]), in the style of Ref. [812], uniform five-dimensional inflation could help simultaneously resolve the H_0, S_8, and M_B tensions [2701,2926].

Running vacuum models The RVM approach (see Refs. [2477, 2793,2794] and references therein), is a framework for an effective description of cosmology, and it has implications for the time evolution of the fundamental constants [2797,2802]. The RVM framework [2473] is based upon the idea that the cosmological vacuum energy densities and pressure are functions of even powers of the Hubble parameter $H(t)$ (and, under circumstances, also of logarithmic non-polynomial corrections of $H(t)$). In the cosmic vacuum, which characterizes inflation, a de Sitter equation of state $p(H(t)) = -\rho(H(t))$, with

$$\rho(H(t)) = \frac{\Lambda(H(t))}{\kappa^2} = \frac{3}{\kappa^2}\left(c_0 + \nu\, H^2 + \alpha\, \frac{H^4}{H_I^2} + \cdots\right), \tag{4.23}$$

is satisfied, although, during each post-inflationary era, the total energy density and pressure is supplemented by the corresponding contributions of matter and/or radiation, as recent quantum-field-theory calculations in the RVM context have shown [2790–2792,3976]. We remark that the coefficients ν and α are considered as constants during each epoch of the Universe's evolution; H_I is the scale of inflation, which, according to data in Ref. [3923], is currently set to $H_I \lesssim 10^{-5}\, M_{\rm Pl}$, in order of magnitude. The important feature of the RVM framework is that inflation does not require any external inflaton fields, but it is mainly due to the non-linear gravitational dynamics due to the H^4 and higher-order terms in the expression of $\rho(H(t))$ [2475,2476],

which dominate the early Universe eras. Note that the RVM can provide a smooth evolution of the Universe, and can also account for its thermodynamic history and properties [2478,3977].

This generic framework finds a concrete realization in the context of Quantum Field Theory (QFT) in curved spacetime when the vacuum energy density is renormalized using the adiabatic renormalization method, in which a subtraction is performed at an off-shell scale M subsequently identified with the Hubble rate $H(t)$ at each cosmic epoch. This eliminates the quartic mass contributions $\sim m^4$ (hence the need for fine tuning) and induces a dynamics of the vacuum energy of the above form [2790–2792,3976]. An alternative realization, termed "Stringy RVM" (StRVM), is found when RVM is embedded in string theory cosmologies, under the assumption [2471,2473,2479] that the early Universe consists of fields appearing in the bosonic massless ground-state multiplet of superstrings. The model assumes that the dilaton is stabilized to a constant value, through the minimization of an appropriate potential, possibly induced by string loops [2472]. The pertinent string-inspired, low-energy gravitational theory is a Chern–Simons (CS) gravity [2469,3978]. The CS nature of gravity arises from the linear coupling of the string-model independent axion [2470, 2480] to the CS gravitational anomaly, which is due to the Green–Schwarz counterterms [3979] that modify the antisymmetric-tensor field strength as a consequence of the requirement of cancellation of gauge and gravitational anomalies in the extra dimensional string space. In the StRVM, the gravitational anomalies in the primordial Universe are not assumed to be canceled, although such a cancellation occurs at the exit from RVM inflation, after the generation of chiral fermionic matter [2471,2473,2479], due to the decay of the RVM vacuum. The RVM inflation in the StRVM is induced by condensates of the gravitational CS term due to condensation of primordial GW, which are formed during a pre-inflationary epoch [2473,2479]. An estimate for the CS condensate can be provided within a second quantization of weak GW formalism [2481,3275,3276]. It is found to be proportional to $H^4(t)$, which during inflation varies very slowly with the cosmic time. As shown in Ref. [2481], the formation of the CS condensate provides an approximately linear KR-axion monodromy potential, leading to inflation in the sense that the latter corresponds to a saddle point of the evolution of an appropriate dynamical system of variables. This result is general and refers to all scenarios with linear axion potentials, such as those obtained, for instance, from appropriate compactifications of string theories [2483].

Finally, let us notice the intriguing potential implication of this framework on the alleviation of cosmological tensions [2484,2485]. Indeed, in the context of StRVM, quantum graviton corrections induce in general corrections to the effective vacuum energy density of the non-polynomial form $H^{2n}\ln(H)$, $n \in \mathbb{Z}^+$. Such corrections have been computed explicitly in the context of dynamically broken supergravity models [2819], which can also be cast in an RVM format [3980] and can describe a pre-RVM inflationary epoch of StRVM. In cases such corrections survive in modern epochs, they can provide a resolution of the Hubble and, under some circumstances, also of the growth-of-structure tension: $H_0 = 71.27^{+0.76}_{-0.73}$ and $\sigma_8 = 0.816^{+0.017}_{-0.015}$ [2484]. See also the "phantom matter" proposal of Ref. [2485], inspired by the StRVM approach and providing a potential resolution of both tensions. Subdominant logarithmic corrections on H can also arise within the conventional RVM, by integrating out matter fields in QFT of fermions and bosons in expanding spacetimes [2790–2792,3976].

In a related context to the RVM, we can mention the works from Ref. [3981,3982] on the back-reaction effect of super-Hubble cosmological fluctuations. Ref. [3981] examines a scenario in which a large bare cosmological constant drives early accelerated expansion and shows that the backreaction effect of infrared fluctuations can reduce it. Such kind of models are expected to have an impact on the H_0 tension problem, as discussed in Ref. [2863].

4.6. The cosmological principle

Coordinator: Eoin Ó Colgáin

Contributors: Alexander Bonilla Rivera, András Kovács, Anil Kumar Yadav, Antonio da Silva, Asta Heinesen, Daniele Oriti, Dario Bettoni, David Benisty, David L. Wiltshire, Diego Rubiera-Garcia, Dinko Milakovic, Duško Borka, Ebrahim Yusofi, Elias C. Vagenas, Giuseppe Fanizza, Goran S. Djordjević, Hassan Abdalla, Ido Ben-Dayan, Iryna Vavilova, Jenny G. Sorce, Jenny Wagner, Jessica Santiago, John K. Webb, José Pedro Mimoso, Juan Garcia-Bellido, Laura Mersini-Houghton, Leandros Perivolaropoulos, M.M. Sheikh-Jabbari, Maciej Bilicki, Marie-Noëlle Cé lérier, Marina Cortês, Milan Milošević, Nihan Katırcı, Nils A. Nilsson, Özgür Akarsu, Predrag Jovanović, Saurya Das, Tajron Jurić, Víctor H. Cárdenas, Valerio Marra, Vesna Borka Jovanović, and Wojciech Hellwing

In recent years the status of the cosmological principle (CP), a fundamental assumption in modern cosmology, has become less clear cut. However, what stymies debate is the absence of a consensus definition of the CP. The CP is commonly presented as the idea that the Universe is *isotropic* (the same in every direction for a comoving observer who is at rest with respect to the *cosmic fluid* of the expanding Universe) and *homogeneous* (the same at every point on a hypersurface corresponding to a given cosmic time) at suitably large scales. Homogeneity implies that there is no special location, such as a preferred observing position or center, while isotropy states that there is no special direction, such as an axis. These two statements do not automatically imply one another, and the possible departures from each of them are currently among the most prominent research topics in cosmology.

Unfortunately, the terminology is loose and it is always possible to find a definition that is perfectly untestable. First, what is meant by large scales is rarely discussed. Secondly, given that we have only one vantage point in the Universe, testing homogeneity is difficult. In particular, depending on how one defines the latter, one could end up with a claimed "large scale" varying from $\sim 70\ h^{-1}$ Mpc [3983–3985] up to $\sim 260\ h^{-1}$ Mpc [3986]. Thirdly, even when scientists argue that there is an anomaly with the CP, great care is required to separate ΛCDM predictions from generic predictions of isotropic/homogeneous Universes. For example, $\sim 260\ h^{-1}$ Mpc [3986] is a claimed upper bound for the homogeneity scale in a ΛCDM universe. Moreover, homogeneity is also challenged by large structures [1607,3987–3990], but one inevitably must compare to the predictions of a specific FLRW model, i.e., ΛCDM, and often, one either finds comparable structures in simulations or one can question the statistics [1611,1612,3991–3993]. Finally, a point very rarely discussed, and which may pass by as a minimal assumption, is the very existence of a "cosmic fluid". Besides how harmless those words might sound, what this actually assumes is the existence of a *unique reference frame* which is at rest with respect to the average distribution of the CMB, baryonic matter, DM and DE simultaneously in different time periods of the history of the Universe. Looking closely at this definition, one then opens Pandora's box, in which to start, we have a lack of proper and robust definition of averages in GR, followed by questions regarding averaging scales and even if the averaging scales should be the same or not for different fluids.[61] Admittedly, these are excellent theoretical questions, but if one approaches cosmology at a granular scale, constructing an observationally testable model is impossible. In cosmology one should not lose

[61] Applying the CP for a void-dominated cosmology [3720–3723], involving superclusters and cosmic voids, necessitates that cosmic voids tend toward achieving maximum symmetry. The result of such an evolution would be a vast spherical cosmic void, which is formed by the merging of smaller sub-voids (void-in-void process) [1789,1798,3726]. The density of the largest cosmic voids will be closer and closer to that of the Universe, making the CP more applicable to the present void-dominated Universe.

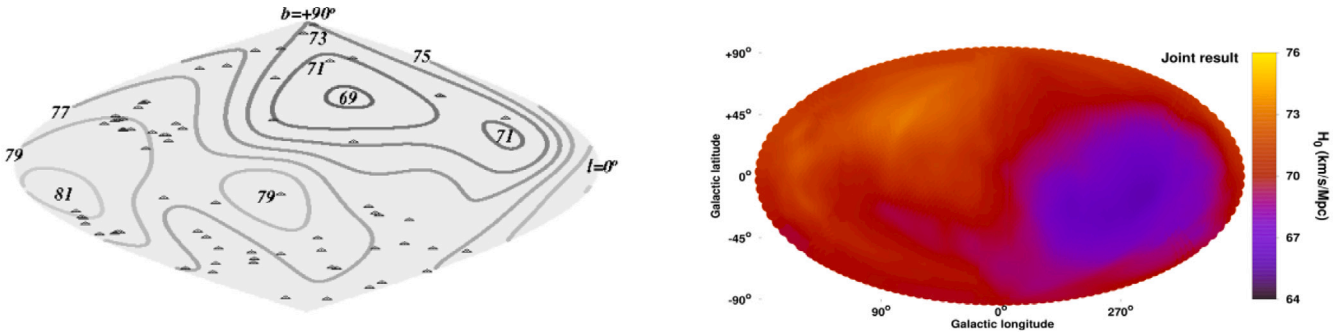

(a) HST Key Project (b) Galaxy cluster scaling

Fig. 79. Left: Angular variations of H_0 on the sky in galactic coordinates in the aftermath of the HST Key Project. Reproduced from Figure 1 (a) of Ref. [3994]. Right: Angular variations of H_0 on the sky in galactic coordinates from galaxy cluster scaling relations. Reproduced from Figure 7 of Ref. [3995].

track of the *grossly* simplified assumptions - justifiable on the relatively poor quality of astronomical data - being made.

The Universe is a gravitating system. Gravity is GR, at least in a minimal setting. This necessitates a choice for a spacetime metric $g_{\mu\nu}$ to insert on the left hand side of Einstein's equation. Here the modus operandi is to start from the most symmetric possibility. This leads one to a maximally symmetric spacetime in 4D, namely Minkowski, anti-de Sitter, and de Sitter metrics. From these three, the latter is the only physically relevant possibility and appears in the asymptotic future of any universe with late-time accelerated expansion. The pursuit of symmetry also leads one to the *perfect cosmological principle* (PCP), according to which the Universe is homogeneous and isotropic in space *and* time. This means that the Universe in the large is also unchanging with time. The PCP was the basis of the steady-state cosmology, an alternative to the Big Bang theory [3996,3997], but this required a physically contrived scenario whereby the density of matter remained unchanged due to a continuous creation of matter.

4.6.1. FLRW spacetime

In pursuit of a more physical model, one can always pursue classes of less restrictive spacetimes. The concession one makes is reducing maximal symmetry in the 4D spacetime to maximal symmetry in a 3D space. This leads one to the FLRW metric, a cornerstone of modern cosmology. The FLRW spacetime metric $g_{\mu\nu}$ is given by Ref. [3767]

$$ds^2 = g_{\mu\nu}dx^\mu dx^\nu = -c^2dt^2 + a(t)^2\left(\frac{dr^2}{1-kr^2} + r^2(d\theta^2 + \sin^2\theta\, d\phi^2)\right), \tag{4.24}$$

where $a(t)$ is the scale factor, k represents the spatial curvature, and (t, r, θ, ϕ) are the comoving coordinates. Combining FLRW with GR, the Einstein equation reduces to the Friedmann equation,[62] which has an important consequence that the Hubble constant $H_0 = H(z = 0)$ arises as an integration constant [3758]. Note, Eq. (4.24) simply specifies the spacetime and not the model. However, once one fully specifies the model, e.g., ΛCDM, the onus is on the astronomy and cosmology communities to demonstrate that H_0 is a constant in cosmic time or redshift. If H_0 is not constant in a given model, one runs into a "Hubble tension" problem, e.g., see Refs. [34,192].

This then brings us to the simplest way to test the metric in Eq. (4.24). H_0 can be determined model independently in the local Universe $z \lesssim 0.2$ using Cepheids, TRGB, or other possible primary distance indicators in order to calibrate SNIa [34,144]. Note that working locally, one can safely decouple the cosmological model [220]. In short, one should make sure that there are no statistically significant angular variations of H_0 between different directions on the sky, because as discussed, H_0 must be a constant. Already, galaxy cluster scaling relations point to $\sim 9\%$ changes in H_0 in the local Universe [3995,4000,4001]. Evidently, if the precision on H_0 is $\sim 5 - -10\%$, this is no problem, but it may become problematic if one pursues $\sim 1\%$ precision. Since nobody builds the distance ladder on galaxy clusters, it is imperative to recover this result in SNIa. Preliminary results exist, but given the relatively small size of SNIa samples, which become worse when restricted to lower redshifts, angular H_0 variations at low redshifts are consistent with statistical fluctuations ($< 2\sigma$) [1344,1374] (see also Refs. [1380,1385,1390,3994,4002]).[63] Given the better statistics in cosmicflows (CF) data, a data set comprising SNIa alongside other distance indicators, the observation of an anisotropic H_0 has recently been pushed to 3.9σ [4006]. It should be stressed that there is no guarantee that one can get to a $> 3\sigma$ variation in H_0 from SNIa alone, but the test can and should be done. Note that a statistically significant angular variation in H_0 would make both the Hubble constant and the Hubble tension ill-defined. Since, S_8 is a parameter within the ΛCDM model, and the model builds upon FLRW, a breakdown of FLRW would also make S_8 tension ill-defined[64].

In addition, locally, there are also claims from the CF program that there are anisotropic bulk flows [1343], which may no longer converge to ΛCDM expectations [1426] (see also Refs. [1425,1427]), thereby echoing a kinematic SZ anomaly, one disputed by the *Planck* collaboration [4008], from a decade previously [1429,1431,1432,4009]. An upgrade of CF data to include WALLABY [391,4010,4011], FAST [393] and DESI data [394] recently found that the homogeneity scale is not yet recovered at 300 h^{-1} Mpc [4012], thereby strictly violating the 260 h^{-1} bound [3986]. In tandem, the inferred bulk flow was larger than ΛCDM predictions, but remained consistent with the model. Note, in Ref. [1426] an isotropic expansion or constant H_0 is assumed, but the bulk flow becomes anomalously large. CF data makes use of a host of distance indicators, including SNIa, so one can in principle recover the same result from SNIa alone.[65] Here it is worth noting that SNIa redshifts are typically corrected for peculiar velocities of the host galaxy, so it is imperative to make sure that anomalously

[62] The Friedmann equation can be derived by moving to the accelerated frame using the scale factor [3998,3999].

[63] One can also fit a dipole to SNIa [1391,4003–4005]. One may find [4005] that SNIa and CMB are not in the same frame, but that the difference can be interpreted as a bulk peculiar velocity $v_{\rm bulk}$ consistent with ΛCDM expectations. Note, these analyses are typically biased toward the lowest redshift SNIa, so one needs to study the redshift dependence of $v_{\rm bulk}$ in shells, where overlap is expected with the cosmicflows program [1426].

[64] As an aside, since an anisotropy makes a contribution to the energy budget of the Universe scaling as a^{-6}, which is relevant in the early Universe, it is plausible a new anisotropic cosmological model can be found that alleviates the tension with larger local H_0 determinations, e.g., see Refs. [1364,4007].

large bulk flows are not simply swept under the rug to reinforce an isotropic expansion (see criticism of SNIa peculiar velocity corrections in Refs. [4013,4014]). Another cautionary note on making peculiar velocities corrections regards the non-linearities that arise on local scales. This is an extremely delicate subject, especially given that the boundary scales where linear and non-linear regimes are applicable, together with the regime where perturbation theory is no longer valid, are still under investigation. In order to avoid this point, one must go to high redshift sources.

The other way to test the CP model independently is through aberration and Doppler effects with a large sample of sources. Although the Ellis–Baldwin test [1362] was outlined last century, the test only became feasible this century [1398,1404–1407,1410–1414,1419,4015,4016]. While there may be outliers [1414,1417,1418,1463,4017,4018], there is a growing consensus that radio galaxy and QSO data sets do not inhabit the same rest frame as the CMB [1398,1405–1407,1411–1413,1419,4015,4016]. Nevertheless, these are challenging studies, both technically and sociologically, thus it is always conceivable that observational [1402,1463,4018,4019] and or theoretical systematics [1360,4020] (however see Ref. [4021]) are at play. The earliest studies have typically employed frequentist statistics, but later papers have provided a Bayesian interpretation [1400,1419,1463]. Taken at face value, the disagreement between CMB and radio galaxies/QSOs on the cosmic dipole points to a breakdown of the CP — and, therefore, of FLRW. The problem is interpreting this result. At what scales or redshifts does this happen? How badly is FLRW broken? None of this would be obvious without corroborating FLRW anomalies in the local Universe.

So where are we now on FLRW? Both in the local Universe $z \lesssim 0.2$ and large samples of radio galaxies/QSOs with assumed median redshifts of $z \sim 1$ we see hints of a violation of FLRW. Given the rich structures in the local Universe [1343,4022,4023], variations in H_0, or alternatively bulk flows, are expected. See Fig. 79. The important question is whether these effects deviate from the expectations of the ΛCDM model. On the other hand, a mismatch in the cosmic dipole, could easily be explained by a relatively local effect and not an FLRW violation at large scales. Thus, it is of interest to study the Hubble diagram out to $z \sim 1$ in order to check if one recovers an FLRW universe. One could adopt the ΛCDM model, e.g., see Refs. [1385,1403,4002,4024], and check that variations in H_0 become less significant as effective redshifts of SNIa samples, etc, increase, but one can also tackle this problem model independently through cosmography [2086] up to $z = 1$, the radius of convergence of the expansion [2126]. See Refs. [1382,4025] for preliminary studies in this direction. Note, cosmography introduces additional parameters, especially if one wants to describe models beyond FLRW [1358], so one will require large data sets to conduct these studies. Nevertheless, the motivation should be clear. Current hints of FLRW violation at low and high redshift need to be connected in a common framework. The big question that needs to be addressed is how good is FLRW as an approximation to the physical Universe? While few scientists outside the field of cosmology, especially relativists, would challenge the assertion that FLRW is an approximate symmetry, since there is no argument that it is fundamental, this may be cold comfort for precision cosmology. $\sim 9\%$ variations in H_0 [3995,4000,4001], suggest that FLRW is a good approximation to $\lesssim 10\%$. This is easy to square with the perceived isotropy of the CMB, when one factors in residual asymmetries in CMB data or CMB anomalies [1330]. A subset of the latter has persisted through three independent satellite experiments, namely COBE [677], WMAP [2754] and *Planck* [192], allowing one to make the case that the Universe is unlikely to be statistically isotropic based on CMB data alone [1332]. Unsurprisingly, H_0 can vary by up to $\sim 10\%$ along the axis of the hemispherical power asymmetry [1333,1334], a recognized CMB anomaly, and attempts to recover the CMB dipole from aberration and Doppler boosts are contaminated at lower multipoles (larger scales) by this anomaly (see Fig. 3 of Ref. [4026]).[66] In addition, it is evident that WMAP/*Planck* CMB data prefers a *phenomenological* Bianchi model over ΛCDM [4029–4032],[67] which is only possible if there is a residual anisotropy in the data. Nevertheless, it is not clear if beyond FLRW models, especially the models in Section 4.6.2, can rival FLRW cosmology. This is not a statement about fits to data, this is the statement that at a purely technical level one would need a complete understanding of cosmological perturbation theory in these models. Given the anomalies in this white paper, it is hard not to contemplate that precision cosmology, defined through models where fitting parameters are constrained at the $\sim 1\%$ error, may be at a crossroads. See Ref. [1328] for a recent overview of observations and the key claim that we have exceeded the precision where the approximate nature of the FLRW assumption is evident.

4.6.2. Moving beyond FLRW

In light of these FLRW anomalies, there is a growing interest in exploring more general metrics that relax the assumptions of homogeneity and isotropy. In this respect, if the CP is relaxed so that the homogeneity holds but not isotropy, then the corresponding exact solutions of Einstein's field equations are given by the class of cosmological models called Bianchi universes, named after the Italian mathematician Luigi Bianchi who first classified these spaces [1364,4033–4035]. Homogeneity in space implies that Einstein's field equations reduce from partial to ordinary differential equations in time, making Bianchi models exact solutions. A complete list of all such solutions for all Bianchi cosmological models from type I to type IX and for perfect fluid is given by Ref. [4036]. Bianchi universes also contain, as a subclass, the standard isotropic FLRW universes. Although Bianchi models were previously considered to be inconsistent with observations, recent studies highlighted above challenge the isotropy assumption and revive interest in these models, which therefore remain widely studied [4037,4038]. Ref. [1364,4035] presents an observational analysis of Bianchi type-I, -V, and -XI spacetime extensions of the ΛCDM model. This section discusses some of the alternative metrics that have been proposed to address these issues.

4.6.2.1. Lemaître–tolman–bondi (LTB) metric.

The LTB metric [4039–4041] describes a spherically symmetric but radially inhomogeneous universe. It is given by

$$ds^2 = -c^2 dt^2 + \frac{R'(r,t)^2}{1+2E(r)} dr^2 + R(r,t)^2 (d\theta^2 + \sin^2\theta\, d\phi^2), \tag{4.25}$$

where $R(r,t)$ is the radius of the spherical shell at time t and radial coordinate r, and $E(r)$ is an arbitrary function related to the energy of the shells. The LTB metric allows for variations in the density and expansion rate along different radial directions, providing a more flexible framework to model inhomogeneities in the Universe [4039–4041]. The series of N-body simulations discussed in Ref. [4042] explores the development of large-scale structures against an LTB background that incorporates a cosmological constant, specifically within the ΛLTB model framework.

Spherical inhomogeneities in LTB models can emerge either due to matter voids or due to Hubble scale spherical inhomogeneities of DE. In the latter case, such inhomogeneities can be supported by topological considerations, particularly in the context of recently formed global monopoles. These topological defects arise when the vacuum

[65] Indeed, restricting the CF data to SNIa, one confirms the large bulk flow, but large errors make this consistent with ΛCDM expectations. We thank Rick Watkins for private communication.

[66] For this reason, it is customary to remove large scales, e.g. see Refs. [4027,4028].

[67] These phenomenological Bianchi models cannot be seen as deformations of the ΛCDM model since the cosmological parameters adopt different values.

manifold of the quintessence scalar field has non-trivial π_2 topological properties [4043,4044]. This scenario corresponds to the "Topological Quintessence" class of models, which may support deviations from the FLRW metric on cosmological scales.

In the context of topological quintessence, a global monopole formed during a recent phase transition with a core size comparable to the present Hubble scale could induce the observed accelerated expansion of the Universe. The monopole's scalar field is trapped near a local maximum of its potential in a cosmologically large region of space. This setup leads to an inhomogeneous but isotropic DE distribution, where the core of the monopole exhibits an effective cosmological constant-like behavior, while the outer regions revert to a matter-dominated Einstein–de Sitter universe.

An off-center observer within such a topological quintessence framework would naturally observe cosmic dipoles due to the asymmetric positioning relative to the monopole core. This asymmetry can manifest as dipoles in various cosmological observations, including the CMB and large-scale velocity flows [1361,4045,4046].

Recent numerical simulations have explored the dynamics of such global monopoles minimally coupled to gravity in an expanding universe with initially homogeneous matter. These studies show that when the energy density of the monopole core starts dominating the background density, the spacetime in the core begins to accelerate its expansion in accordance with a ΛCDM model with an effective inhomogeneous spherical DE density parameter $\Omega_\Lambda(r)$ [1440]. Away from the core, the Universe appears as an Einstein–de Sitter Universe, while near the core, $\Omega_\Lambda(r)$ reaches a maximum.

These findings suggest that topological quintessence models could provide viable explanations for certain cosmological observations and anomalies. The key is that the presence of a large-scale topological defect could naturally introduce the observed anisotropies without requiring exotic modifications of gravity or the introduction of multiple new fields.

4.6.2.2. Bianchi metrics. Bianchi models [4033,4047–4052] generalize the FLRW metric by allowing for anisotropies while maintaining homogeneity. They are classified into nine different types based on their symmetry properties. For example, the Bianchi I metric is given by

$$ds^2 = -c^2dt^2 + a(t)^2dx^2 + b(t)^2dy^2 + c(t)^2dz^2\,, \tag{4.26}$$

where $a(t)$, $b(t)$, and $c(t)$ are scale factors along the x, y, and z axes, respectively. These models can describe universes that have directional dependencies in their expansion rates, which might help explain certain observed anisotropies [1328,4053–4055]. See Ref. [1364,4035] for observational analysis of Bianchi type-I extension of the ΛCDM model.

4.6.3. Mc-Vittie spacetime

The McVittie metric is the exact solution of Einstein's field equations describing a black hole or a massive object immersed in an expanding cosmological spacetime [4056,4057]. The metric can be written by

$$ds^2 = -(1-\Phi_N)\,dt^2 + a(t)^2\left[\frac{dr^2}{1-\Phi_N} + r^2\,d\Omega^2\right]\,, \tag{4.27}$$

where $\Phi_N = 2GM/(rc^2)$. In the low-energy limit ($\Phi_N \ll 1$ and $rH \ll 1$) the equation of motion reads [4058–4060]: $\ddot{r}/r = -GM/r^3 + \ddot{a}/a$. For the de Sitter–Schwarzschild metric the $\ddot{a}/a$ changes to $\Lambda c^2/3$. For $z \approx 0.67$ the $\ddot{a}/a$ acts as an attractive force for early cosmic times while for the de Sitter–Schwarzschild metric only the constant term $\Lambda c^2/3$ remains. Galaxy groups in the local Universe are bounds on the interplay between the expansion force and the Newtonian attraction [4061]. This gives another setup to determine the Hubble constant [4062–4068].

4.6.3.1. Inhomogeneous general relativity solutions. Beyond the specific cases of LTB and Bianchi metrics, there are more general inhomogeneous solutions in GR that do not assume any specific symmetry. These solutions can be constructed using various techniques, such as analytic or perturbative methods or numerical relativity. One notable example of an exact solution of the GR field equations, obtained with a dust gravitational source, is the Szekeres model, which generalizes the matter (+ cosmological constant) dominated FLRW solution by dropping any symmetry in the metric

$$ds^2 = -c^2dt^2 + e^{2\alpha}dx^2 + e^{2\beta}(dy^2 + dz^2)\,, \tag{4.28}$$

where α and β are functions of both spatial and temporal coordinates. These models allow for full inhomogeneity and anisotropy, providing a more general framework to describe the Universe [4069]. The Szekeres models can be divided into three classes: quasi-spherical, quasi-plane and quasi-hyperbolic. The quasi-spherical Szekeres class of solutions, which includes the LTB model as a subclass, can therefore be viewed as a generalization of this LTB model where the spheres of constant $\{t, x\}$ coordinates are non-concentric and exhibit each a given mass dipole whose direction is rotated from one sphere to the other. However, the surfaces x = const within a space t = const might be quasi-spherical in regions of the space and quasi-hyperbolic elsewhere, with a zero curvature at the boundaries. Every class possesses the FLRW solutions as a limit for particular forms of the functions defining its metric which can be obtained at some large scale for any of the classes, quasi-spherical, quasi-plane and quasi-hyperbolic. Hence, the possibility to use the Szekeres model for representing the inhomogeneous late Universe with a transition to homogeneity (FLRW) at some larger scale. These models have been used to study various cosmological phenomena, including the formation of large-scale structures and the impact of inhomogeneities on the CMB. Now, in the era of precision cosmology, their application to the analysis of the largest cosmological data sets will have to be performed [4070].

4.6.3.2. Fully model independent cosmographic approach. Another possibility to test the CP in a fully covariant, model independent way without imposing any a priori metric, is using the general cosmographic approach developed by Kristian and Sachs [4071] (see also Refs. [1358, 1361,4072]). Its only assumption is that the galaxies can be described in terms of a pressureless dust fluid following flow lines that can be described in terms of a unique congruence — an assumption made by all of the other theoretical approaches as well. The idea then lies on the fact that the matter flow, and its kinematical parameters — the expansion Θ, the shear σ_{ab} and the vorticity ω_{ab} – are a direct probe to the expansion of the Universe. One then can Taylor expand the generalized luminosity distance in redshift and obtain the generalized Hubble and deceleration parameters, which are now naturally directional dependent quantities. For an observer boosted with respect to the matter frame (one must always assume this is the case and directly measure the boost velocity), the generalized Hubble parameter has been proven to contain a monopole, a dipole induced only by the boost velocity, and a quadrupole component [1361]. This approach also provides a fully covariant non-perturbative generalization of the perturbative result obtained by Ref. [4073] in which they develop a way to disentangle the intrinsic dipole from a kinematically originated one [1361], a very important need in order to test the CP.

4.6.3.3. Timescape cosmology. A new study of the Pantheon+ catalog has now claimed that an inhomogeneous alternative [4074–4077] to the models discussed above fits better than ΛCDM with strong to very strong Bayesian evidence ($\ln B \sim 3$–5) [3776]. Positive evidence ($\ln B \sim$ 1–2) remains even when restricted to SNIa with $z > z_{\rm min} = 0.06$. In contrast to models based on a single metric, timescape combines small scale FLRW geometries — regionally valid on scales of $\sim$ 3–30 Mpc — via a Buchert average [4078–4080]. A closure condition is needed to supplement the Buchert equations, without which its physical interpretation is open to debate [1602,4081]. Timescape extends the Strong Equivalence Principle to a Cosmological Equivalence Principle to apply on small scales over which average isotropic motion in empty space is operationally indistinguishable from average isotropic expansion in nonempty space [4082], leading to the quasilocal Hubble

expansion condition as a closure relation for Buchert averages. The predicted variance in local Hubble expansion can be calibrated [4076] and tested observationally, leading to a potential resolution of the Hubble tension [3775], and a natural framework for resolving dipole anomalies in terms of small scale non-kinematic differential expansion [4083]. This appears to be consistent with new analysis of void statistics in numerical relativity simulations using the full Einstein equations [1604].

The timescape and ΛCDM expansion histories differ by $\sim$ 1–3% over small redshift ranges, but can be distinguished with a long enough lever arm. Independent projections made for the Euclid mission in 2014 [4084] show that with Euclid BAOs plus 1000 independent SNIa distances, the FLRW expansion history and the timescape alternative can be definitively tested via the Clarkson–Bassett–Lu (CBL) test [4085]. The new Pantheon+ results for SNIa [3776] have been independently confirmed independently with the DES survey [4086], where it was found that for events with $z > z_{\rm min} = 0.033$ timespace is preferred over ΛCDM with $\ln B = 1.7$. Based on simple geometric scaling arguments, the DES analysis [4086] finds that BAOs strongly favor ΛCDM over timescape. However, in timescape the BAO must be extracted directly from raw galaxy clustering data [4087], and independently recalibrated from the CMB anisotropy spectrum and the sound speed in the primordial plasma. The nonbaryonic to baryonic matter densities ratio for timescape still has large uncertainties [4076]. Thus reanalysis of the matter model in the early Universe in conjunction with constraints from a variety of forthcoming datasets is an urgent goal for implementing the CBL test to definitively decide between FLRW and timescape by 2030.

4.6.3.4. Constraints from observations. Detailed cosmological observations have imposed constraints on some of the alternative models described above. For instance, the Generalized LTB model with inhomogeneous isotropic DE has been studied to understand its consistency with observations such as the Union2 SNIa data and the CMB multipoles [1435]. More recently, Ref. [3774] confronted ΛLTB models to a host of data sets finding that the models could not resolve Hubble tension. It has been shown that for such models to be consistent with observations, the size of the inhomogeneity must be large, typically on the order of a few Gpc. Additionally, the observer must be located relatively close to the center of the inhomogeneity to avoid large dipole anisotropies.

The exploration of these alternative metrics is crucial for addressing the current tensions in cosmology. By considering more general spacetimes, we can test the robustness of the CP and potentially uncover new physics that could reconcile discrepancies between observations and the standard model. As high-precision data continue to pour in, the development and testing of these models will be an essential part of the future of cosmology.

4.6.4. What needs to happen going forward

Even though a more precise definition of the CP took a little while to be developed [4088,4088] following the pioneering works of Vesto Slipher [4089], Henrietta Swan Leavitt [4090], Georges Lemaître [4091] and Edwin Hubble [4092], it was formulated in a time when, more than a principle, it was a *need* for cosmology to go forward. Its historical importance and scientific contribution to the advancement of cosmology is undeniable. But, given the amount of present and future data, continuing to apply it without a proper investigation of its validity and limitations is no longer a matter of science, but faith.

Here we develop a brief list of the necessary requirements in order to properly test the CP:

- Robust data with large sky coverage, in order to test for possible directional dependent effects;
- Model independent techniques for cleaning up possible foreground contamination which does not assume (or imposes) the CP;
- Model independent analysis and parameter estimation;
- The practice of clearly and forthrightly stating all of the (explicit and implicit) assumptions made throughout the analysis;
- A robust model independent theoretical method connected to observations, in a way that allows for the interpretation of the data.

Note that angular variations of H_0 on the sky and the cosmic dipole can both be studied independently. The former will benefit from large SNIa samples with excellent sky coverage from ZTF, Vera Rubin observatory, and Romans space telescope. The SKAO will provide large radio galaxy samples allowing a definitive conclusion on the cosmic dipole anomaly [1408,4093].

4.7. Quantum gravity phenomenology

Coordinator: Giulia Gubitosi

Contributors: Christian Pfeifer, Elias C. Vagenas, Gaetano Lambiase, Manuel Hohmann, Nikolaos E. Mavromatos, Saurya Das, and Vasiliki A. Mitsou

One might reasonably conjecture that at least some of the MG models discussed in the previous sections of this review might emerge in an appropriate limit from quantum gravity. In fact, for some of the models the connection is more apparent, as is the case, for example, of Hořava-Lifshitz gravity [4094], that introduces anisotropic scaling between space and time at high energies. This leads to a power-counting renormalizable theory of gravity that deviates from GR at short distances. This model has been proposed by Hořava in Ref. [4094], where an effective Quantum Gravity approach not requiring the Lorentz invariance at fundamental ultraviolet scales has been formulated. This invariance, however, emerges at large distances. It mainly aims to solve the high-energy issues suffered by GR through a spacetime foliation capable of reproducing the causal structure out of the quantum regime. Basic foundations and applications of this approach can be found e.g., in Refs. [3604,4095–4105]. This model is potentially capable of addressing the H_0 tension, as demonstrated in Ref. [4106]. Specifically, the authors obtain a positive result on the cosmic tensions between the Hubble constant H_0 and the cosmic shear S_8 due to a shift of H_0 toward a higher value. Moreover, in Ref. [4107] the authors show that up to 36% of the Hubble tension can be explained by Lorentz-violating effects in a Hořava–Lifshitz scenario. This, in fact, is a common feature of theories involving gravitational Lorentz violation, where local G no longer equals cosmological G [4108].

However, a full-fledged fundamental theory of quantum gravity is still elusive. This motivates the adoption of a bottom-up approach, that is complementary to the top-down approach attempting to formulate fundamental theories and then working out their predictions in specific limits. In this bottom-up approach, possible features of the quantum interaction and dynamics of gravity as well as particles and fields propagating on a quantum spacetime are described at an effective level via phenomenological models. This field of research, called quantum gravity phenomenology, successfully leads to observable predictions whose confirmation or constraints serve as guidelines for building a fundamental theory of quantum gravity, as it is explained in detail in the review in Ref. [3067] and white papers in Refs. [3068,4109].

In the following, we will outline how phenomenological models of quantum gravity can affect the understanding of cosmological tensions and how cosmological observations may lead to the discovery of quantum aspects of gravity.

4.7.1. QG modified gravitational dynamics

4.7.1.1. Hubble tension and generalized uncertainty principle. The GUP was originally motivated by considerations coming from string theory [4110] and from the analysis of the relation between gravitational and quantum theories in black hole physics [4111]. Subsequent work found relations to noncommutative geometry [4112,4113]. Recently, in Ref. [4114] it was shown that the deformation parameter entering the GUP can be related to the coefficients of the standard model extension (SME) in the gravity sector [4115] and in this case, stringent bounds on the GUP parameter can be inferred from SME parameters.

The idea of GUP was suggested as a possible explanation of the Hubble tension in Refs. [4116,4117]. GUP introduces Planck-scale corrections to the standard relations between canonical variables, due to the interplay between the quantum theory and general relativity. Therefore, it is expected that such GUP corrections will be relevant during the very early/Planck epochs of cosmology, and leave their fingerprints on the quantum fluctuations. As these GUP-modified quantum fluctuations propagate in a cosmological spacetime, they affect primordial fluctuations during cosmic inflation. Since these fluctuations are encoded in the CMB anisotropies [4118,4119], one expects to read the GUP corrections in the CMB power spectrum. In particular, one can select the cosmological spacetime to be the isotropic and homogeneous FLRW Universe with Hamiltonian, in natural units, of the form [4120,4121]

$$\mathcal{H}_{\rm FLRW}(p_a,a) = N\frac{p_a^2}{24a} + 6Nka - N\rho a^3 + \kappa\Pi\,, \tag{4.29}$$

where a and p_a are, respectively, the scale factor which plays the role of the generalized coordinate operator and the generalized canonical momentum conjugate to the scale factor. Note that N is the lapse function and Π is its conjugate momentum, while κ is its corresponding coefficient. Then, one introduces the GUP-modified canonical momentum [4122–4125]

$$P_a = p_a\left(1+\lambda_1 p_a + \lambda_2 p_a^2 + \mathcal{O}(p_a^3)\right), \tag{4.30}$$

and substitutes it in the Hamiltonian $\mathcal{H}_{\rm FLRW}(p_a,a)$, in order to obtain the GUP-modified Hamiltonian (keeping terms up to 2nd order in momentum)

$$\mathcal{H}^{\rm GUP}_{\rm FLRW}(p_a,a) = \frac{1}{24}\frac{p_a^2(1+2\lambda_1 p_a + 2\lambda_2 p_a^2 + \lambda_1^2 p_a^2)}{a} + 6ka - \rho a^3 + \kappa\Pi\,. \tag{4.31}$$

By combining the GUP-modified Hamiltonian equations, one finds the GUP-modified Hubble function to be [4126]

$$H_{\rm GUP} = H\left[1 + 48\lambda_1 a^2 H + \left(864\lambda_2 + 576\lambda_1^2\right)a^4H^2\right]^{1/2}, \tag{4.32}$$

where H is the standard Hubble function.

As already mentioned, CMB will include signatures of the GUP corrections, and thus, the fingerprints of quantum gravity. Therefore, on the one hand, the GUP-modified Hubble parameter, i.e., $H_{\rm GUP}$, can represent the one obtained by the Planck collaboration which utilizes the CMB data [192], H_{CMB}. On the other hand, the unmodified Hubble parameter H, can be assumed to be the one obtained from the HST which utilizes the SNIa data [48]. In this case, we dub it $H_{\rm SN}$. Based on this, the above expression for the GUP-modified Hubble parameter becomes

$$H_{CMB} = H_{\rm SN}\left[1 + 48\lambda_1 a^2 H_{\rm SN} + \left(864\lambda_2 + 576\lambda_1^2\right)a^4H_{\rm SN}^2\right]^{1/2}. \tag{4.33}$$

It is evident that the GUP can, in principle, provide at least a partial explanation of the Hubble tension problem. Detailed analyses are currently ongoing.

4.7.2. Quantum gravity effects on the physics of particles and fields

4.7.2.1. Propagation of particles and fields on quantum spacetime. One intensively studied aspect of the interaction between quantum spacetime and particles and fields is a modification of their propagation properties. Usually, this is studied in terms of a modified dispersion relation (MDR) of the particles, which encodes a modified light cone and mass shell structure. One distinguishes two cases: the Lorentz invariance violating (LIV) case [4127], where just an MDR is considered, and the deformed relativity (DSR) case [4128,4129], where the MDR is supplemented by a modified energy–momentum conservation law and deformed (most often non-linear) Lorentz transformations between observers which leave the MDR invariant and transform the deformed energy–momentum conservation in a covariant way.

In the context of cosmology, the most interesting consequence of an MDR is a different time of arrival of photons of different energy, when they are emitted simultaneously at the same spacetime event at redshift z [4130], such as GRBs [4131,4132] or AGNs [4133]. Such a time delay can be thought of analogously as to what happens when electromagnetic radiation propagates through an optical non-trivial medium and photons of different energy are affected differently by the medium.

In general, such an MDR for photons can be parameterized in the form [4134]

$$E^2 = p^2(1 + f(E,\mathbf{p},E_{\rm QG},z))\,, \tag{4.34}$$

where f is a function that parametrizes the Planck scale modification in terms of the energy E of the photon at emission, its comoving momentum $\mathbf{p} = P/a(t)$, the quantum gravity energy scale $E_{\rm QG}$ (which might or might not be the Planck scale) and possibly the redshift. For two different photons, emitted with an energy E_1 and E_2, to leading non-vanishing order in $E_{\rm QG}$, this leads to a time delay of the form

$$\Delta t_{\rm QG} = t_2 - t_1 = \frac{1}{H_0}\frac{E_2^n - E_1^n}{E_{\rm QG}^n}\kappa(z)\,, \tag{4.35}$$

where $\kappa(z)$ is the redshift distance function to the source at redshift z. It depends on the choice of the MDR model, i.e., in the choice of the function f and on the choice of the cosmological model and its parameters. Some examples are

- non-critical string-inspired models with redshift dependent $E_{\rm QG}$ [4135–4137] or the Jacob-Piran model [4138] with constant $E_{\rm QG}$, with $\kappa(z) = \int_0^z \frac{(1+z')^n}{E_{\rm QG}^n(z')H(z')}dz'$.
- For $n = 1$ in Eq. (4.35), DSR models like κ-Poincare in the bicrossproduct basis [4139], where the redshift distance function reads $\kappa(z) = \int_0^z dz'\frac{1}{(z'+1)H(z')}$ or in more general DSR models in FLRW spacetime, where the redshift distance function is described by the three-parameter (η_1,η_2,η_3) model [4140]

$$\kappa(z) = \int_0^z dz'\left(\frac{(z'+1)}{H(z')}\left[\eta_1 + \eta_2\left(1-\left(1-\frac{H(z')I(z')}{z'+1}\right)^2\right) + \eta_3\left(1-\left(1-\frac{H(z')I(z')}{z'+1}\right)^4\right)\right]\right), I(z') = \int_0^{z'}\frac{dz''}{H(z'')}$$

Taking into account these time delay effects in the analysis of the Hubble tension might lead to an alleviation of the present tensions [4141–4143]. More detailed analyses remain a future prospect.

4.7.2.2. Interactions of particles and fields on quantum spacetime. Another relevant feature related to quantum gravity effects on particles concerns modifications of relativistic interactions, that might induce changes to the predictions of the particle content of the Universe.

In LIV models, the combination of MDR with the expected standard conservation of energy and momentum gives rise to strong modifications to interaction thresholds [4127], with effects for example on the opacity of the Universe to high-energy particles [4144,4145].

Going beyond LIV, an important ingredient for self-consistent DSR models is a modified energy momentum conservation. In a process in which two particles with 4-momenta p and q collide, the center of mass energy is not given by the simple sum of their momenta, since this would not be invariant under modified Lorentz transformations, but

given by a modified addition law, to first order of the form [4129]

$$(p \oplus q)_\mu = p_\mu + q_\mu + \frac{1}{E_{\rm QG}} f(p,q)_\mu \,, \tag{4.36}$$

where the precise expression of $f(p,q)_\mu$ depends on the model under consideration. In general, it is a non-linear function of p and q.

This modified energy–momentum conservation law leads as well to modifications in relativistic threshold reactions, however they would be much weaker than in the LIV case, typically only relevant for particles of Planck-scale energy. While these effects have no direct link to cosmological tensions, their concomitant presence with the propagation effects discussed above might help constrain the specific form of MDR modification that is compatible with observations.

4.8. Varying fundamental constants and their role in the hubble tension

Coordinator: Jens Chluba

Contributors: Catarina Marques, Dan Grin, Gabriel Lynch, Leo Vacher, Nils Schöneberg, Ruchika, and Vitor da Fonseca

Fundamental physical constants need not be constant, neither spatially nor temporally. This seemingly simple statement has profound implications for a wide range of physical processes and interactions, and can be probed through a number of observations, see Ref. [4146–4148] for a broad review. Studies of fundamental constants (FCs) and their possible temporal and spatial variations are thus of utmost importance, and could provide a glimpse at physics beyond the standard model, possibly shedding light on the presence of additional scalar fields and their couplings to the standard sector, e.g., see Ref. [4149,4150].

In the cosmological context, the fine-structure constant, $\alpha_{\rm EM}$, and electron rest mass, $m_{\rm e}$, are the most interesting, although variations of Newton's constant have also been considered [4151–4153] subject to some recent theoretical and observational constraints [4154,4155]. The former can be directly probed with measurements of the CMB temperature and polarization anisotropies, e.g., see Ref. [4156–4163] through their effect on the cosmological recombination history and photon scattering rate. A detailed description of individual physical effects on the CMB power spectra is given in Ref. [4164], with calculations of the cosmological recombination history carried out using `CosmoRec` [4165]. In short, *increasing* $\alpha_{\rm EM}$ and/or $m_{\rm e}$ leads to *earlier* recombination. This is primarily driven by the changes to the atomic energy levels, which scale as $E \propto \alpha_{\rm EM}^2 m_{\rm e}$, thereby enforcing a higher temperature for recombination to occur. Beyond this leading dependence, several subtle effects are encountered leading to differences in how $\alpha_{\rm EM}$ and $m_{\rm e}$ variations affect the CMB signals. Crucially, the effect of $\alpha_{\rm EM}$ and $m_{\rm e}$ on the Thomson scattering rate, $\sigma_{\rm T} \propto \alpha_{\rm EM}^2/m_{\rm e}^2$, has to be carefully taken into account to yield consistent constraints [4164,4166]. For additional discussion of the effects on recombination see Ref. [4167].

Analyzing *Planck* 2013 data, the values of $\alpha_{\rm EM}$ and $m_{\rm e}$ around recombination were proven to coincide with those obtained in the lab to within $\simeq$ 0.4% for $\alpha_{\rm EM}$ and $\simeq$ 1%–6% for $m_{\rm e}$ [4168]. These limits are $\simeq$ 2–3 orders of magnitude weaker than constraints obtained from other "local" measurements [4169–4172] and those from BBN [4173]; however, the CMB is sensitive to very different phases in the history of the Universe, centered around the time of last scattering some 380,000 years after the Big Bang, thereby complementing these measurements. In addition, CMB measurements can be used to probe spatial variations of the FCs at cosmological distances [4174,4175], opening yet another avenue for exploration.

With the *Planck* 2013 results in mind, no significant surprises were expected from the analysis of improved CMB data of the *Planck* 2015 and 2018 releases. It, however, turned out that when considering models with varying $m_{\rm e}$, the geometric degeneracy becomes significant and can accommodate shifts in the value of the Hubble parameter when multiple probes are combined [4166]. The same geometric freedom is *not* encountered when varying $\alpha_{\rm EM}$ due to the modified dependence of the visibility function on this parameter. Indeed, when allowing $m_{\rm e}$ to depart from the standard (local) value, a non-standard value of $\Delta m_{\rm e}/m_{\rm e} = 1.0191 \pm 0.0059$ ($\simeq 3.2\sigma$ significance) can be traded for a reduction of the Hubble tension, suggesting that new physics may be at work (see Fig. 80 for illustration). The addition of extra degrees of freedom that influence the post-recombination Universe such as Ω_k or w_0/w_a to variations of the electron mass allows to further ease the Hubble tension with a $\sim 3.6\sigma$ preference, robust to SN data and BBN constraints [710,1530,2456].

This finding has spurred an increased interest in studying VFCs in this context, with scenarios that allow for varying $m_{\rm e}$, e.g., see Ref. [4166,4176–4179] for additional discussion, ranking high in model comparisons [710]. Since VFCs can be caused by the presence of scalar fields, e.g., see Ref. [4149,4180,4181], a natural question is whether the same scalar field could also be causing effects relating to EDE, possibly indicating a 'two sides of the same coin' interplay. Constraints using the synergy of cosmological and local data have been put on a variety of well-motivated scalar fields models allowing for physical changes in $\alpha_{\rm EM}$ [4182–4186]. However, local data, such as atomic clocks, are putting very strong constraints on such models such that they are mostly unable to produce significant variations of $\alpha_{\rm EM}$ during the recombination era [4187], while such constraints on varying $m_{\rm e}$ models are less restrictive [1530]. In addition, VFCs could play a role in solving the Hubble tension even in light of the recent DESI measurements [1530,2902,4188–4190], although a general mechanism causing early recombination could simply be the main cause of the tensions [4190].

Given the state of affairs, it will be extremely important to ask how different cosmological probes can be combined to shed light on the physical origin of the Hubble tension. One important avenue forward is to directly constrain the electron recombination history, given its crucial role in the formation of the CMB anisotropies [739,4191–4196]. This has recently been achieved using a non-perturbative and model-independent approach [4188], providing a clear target for theoretical exploration. Indeed, the cosmological data prefers early recombination over the standard recombination history obtained using `CosmoRec`, very much like what is caused by varying $m_{\rm e}$ or models with early structure formation [4188]. This data-driven result may therefore indicate new physics in the redshift one thousand Universe, but at this point cannot distinguish the physical cause of this finding.

One way of directly probing the recombination history is through measurements of the cosmological recombination radiation (CRR) [2544,4175,4197–4199]. This tiny spectral distortion signal is created by photons emitted in the hydrogen and helium recombination eras, and thus directly depends on the time and duration of the recombination process. It was shown in Refs. [2544,4175] that various extensions to ΛCDM can in principle be distinguished with future CMB spectrometer measurements as envisioned for the ESA Voyage 2050 program [4200]. Should the Hubble tension persist, then this will provide the ultimate test for various theoretical models. In addition, one can expect the observational uncertainties in the cosmological recombination history to hamper our ability to answer questions about extensions to ΛCDM. A measurement of the CRR is therefore highly motivated even beyond questions about the Hubble tension, and provides a direct probe of one of the main pillars in our interpretation of CMB data.

4.9. Local new physics solutions to the Hubble and growth tensions

Coordinator: Leandros Perivolaropoulos

Contributors: Bhuvnesh Jain, Harry Desmond, Indranil Banik, Jeremy Sakstein, Nick Samaras, Radosław Wojtak, and Ruchika

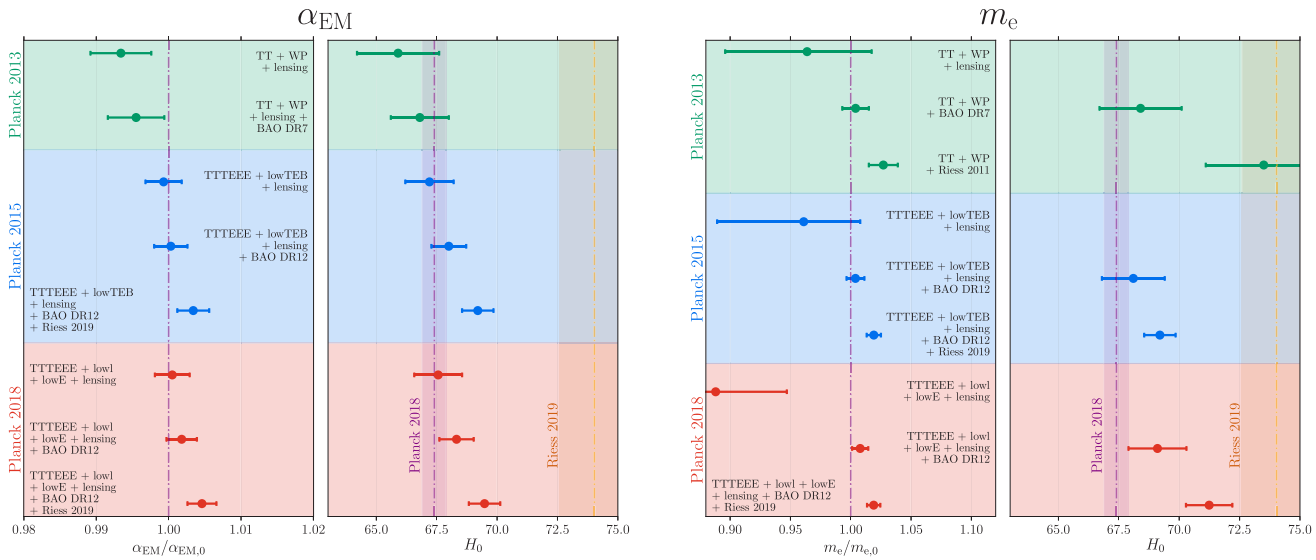

Fig. 80. Constraints on the fundamental constants using various combinations of *Planck* data together with their H_0 values and errors. *Left:* results from the fine structure constant $\alpha_{\rm EM}$. *Right:* similar results but for the effective electron mass m_e. Here, we have redacted the constraint for H_0 from CMB data only because the error bars are so large. For the m_e MCMC analysis, we have widened the prior on the Hubble constant such that $H_0 > 20\,{\rm km\,s^{-1}Mpc^{-1}}$. The figure is from Ref. [4166], which illustrated that varying m_e can alleviate the Hubble tension.

A recent comprehensive analysis provides new insights into the Hubble tension, suggesting that the core of the problem may lie in the distance ladder measurements rather than in conflicts between early and late Universe observations [3756]. This study compiled and analyzed two distinct groups of H_0 measurements: those based on the distance ladder approach, and those derived from one-step methods independent of both the distance ladder and the sound horizon scale. The analysis revealed a significant discrepancy between these two groups. Distance ladder-based measurements yielded a best-fit $H_0 = 72.8 \pm 0.5\,{\rm km\,s^{-1}Mpc^{-1}}$, while one-step measurements resulted in $H_0 = 69.0 \pm 0.48\,{\rm km\,s^{-1}Mpc^{-1}}$. Notably, when two outlier measurements were removed from the one-step sample, the best-fit value reduced to $H_0 = 68.3 \pm 0.5\,{\rm km\,s^{-1}Mpc^{-1}}$, which is fully consistent with sound horizon-based measurements like those from *Planck* CMB observations. A Kolmogorov–Smirnov test yielded a p-value of 0.0001, indicating that the two samples are not drawn from the same underlying distribution.

Since the distance ladder is the only method for measuring H_0 that is based on local physics (via calibrators of SNIa), these findings lend support to the hypothesis of local physics solutions to the Hubble tension. They suggest that the discrepancy may not be between early and late-time measurements, but rather between distance ladder measurements and all other H_0 determinations. This points to either a systematic effect influencing all distance ladder measurements or new physics differentially impacting rungs of the ladder.

Such an intriguing class of potential solutions to the Hubble tension involves new physics acting in the local part of the distance ladder (first and second rungs). This idea was first developed by Ref. [4201], who identified that screened fifth forces (for reviews see Refs. [4202–4206]) may have a differential impact on different rungs of the ladder such that their neglect could bias the inference of H_0. Ref. [4201] developed a range of phenomenological screening models, in which the degree of screening (and hence the effective value of Newton's constant, $G_{\rm eff}$) is set by various gravitational properties of the galaxies used to calibrate SNIa and their environments. This included a novel screening mechanism governed by the local DM density arising from the viable DE candidate of baryon–DM interactions [3605,4207]. Ref. [4201] determined ranges for the screening proxies such that the anchor galaxies of the Cepheid PLR (the MW, LMC, and N4258) are screened while some of the galaxies used to infer the SNIa absolute magnitude are not. Since Cepheid pulsation periods are reduced and luminosities increased by an unscreened fifth force, the standard analysis neglecting the fifth force would then underestimate the distance to the SNIa-calibrator galaxies, which at fixed redshift would overestimate H_0.

[235,4208] present another perspective by analyzing the extinction models used for SnIa in the calibration galaxies. Their study suggests that the standard extinction model developed by [232] for the Pantheon+ SnIa compilation underestimates the brightness of reddened supernovae in high stellar-mass calibration galaxies. They propose a modified extinction model that assumes a Milky Way-like distribution of the total-to-selective extinction coefficient R_B in all calibration galaxies, which is also consistent with the extinction corrections employed for Cepheids, and a modified shape of the reddening distribution. This approach yields a lower value of the derived Hubble constant, reducing the tension with the Planck measurement assuming a flat ΛCDM cosmology from 5.2σ to 2.8σ. This result highlights the importance of accurately modeling local astrophysical effects, such as dust extinction, to resolve the Hubble tension. Different extinction properties in the calibration galaxies do not necessitate violations of the Copernican principle, but they may likely result from the fact that the calibration galaxies are not a representative sample of galaxies in the Hubble flow (the former are solely late-type galaxies, whereas the latter include all morphological types). This selection bias can propagate to the SNIa sector via environment-dependent properties, whose physical origin is currently the subject of intense research.

A detailed modification to the SH0ES analysis pipeline allowing for this effect revealed that the Hubble tension could be eliminated with a fifth-force strength $(G_{\rm eff} - G)/G \approx 0.1$ in some of the screening models. However, an important constraint derives from the consistency of Cepheid and TRGB distances to galaxies where both can be measured. The fifth force affects TRGB distances oppositely to Cepheid distances [4201], so the fact that these distances agree under GR implies that they will disagree under a strong fifth force. This requires $(G_{\rm eff} - G)/G \lesssim 0.05$ in the most effective models, preventing this theory from reducing the H_0 tension below the 2σ level. Other constraints were studied, but found not to yield such a strong bound. Nevertheless, in conjunction with some other effects (of which a myriad are presented in this white paper), the tension could be resolved.

Ref. [4201] only addressed the Cepheid-calibrated distance ladder. The principal alternative is TRGB, which yields a slightly smaller H_0 value of $70–72\,{\rm km\,s^{-1}Mpc^{-1}}$ under the assumption of GR. The model was

extended to the TRGB calibration in Ref. [4209], where it was shown to be fully effective at solving the Hubble tension in that case. This requires the LMC (the anchor galaxy of the TRGB absolute magnitude) to be less screened than the SNIa calibrators. As the LMC is the least massive of the SH0ES anchors — and TRGB stars tend to be found in higher-mass galaxies than Cepheids, which are young stars found in star-forming disks — significant regions of the MG parameter space can solve both the TRGB tension and reduce the Cepheid tension to $\sim 2.5\sigma$. Note that the SNIa themselves are assumed screened in all these analyses, as would typically be expected in viable MG models due to their dense environments — discussion of possible effects on SNIa may be found in Appendix B of Ref. [4201]. Variants of the model are studied in Ref. [3267,4210].

An alternative to screening is the more recent idea that new physical phenomena or transitions in the form of physical laws occur locally, specifically at distances $\lesssim 40$ Mpc or redshifts $z \lesssim 0.01$, affecting the connection between the distance ladder's second rung (SNIa calibration by Cepheids or TRGB) and third rung (Hubble flow SNIa). These Local Physics Transitions (LPTs) are assumed to involve abrupt changes of fundamental constants like the gravitational constant G or the fine structure constant. They can affect the calibrators and SNIa used in the first and second rungs of the distance ladder, leading to a different behavior compared to that in the Hubble flow (at larger scales).

The simplest class of this paradigm involves an abrupt transition in the value of G while the other fundamental constants remain fixed. Refs. [2682,2695] propose that a rapid transition in G at a redshift $z_t \approx 0.01$ could resolve the Hubble tension. This G-step model (GSM) could imply that SNIa have lower luminosity $L_<$ at local scales (second rung of distance ladder) than the luminosity $L_>$ of distant SNIa in the Hubble flow (third rung). The ratio that would be required to solve the Hubble tension is $L_>/L_< = 1.15$, leading to a higher inferred value of H_0 due to the degeneracy between the SNIa $L_>$ and H_0 in the Hubble flow.

The LPT paradigm was studied in Ref. [2695] through a reanalysis of the SH0ES data. By allowing for a transition in the absolute magnitude of SNIa at a distance of about 50 Mpc, they find that the best-fit value of H_0 drops significantly from $H_0 = 73.04 \pm 1.04\,\mathrm{km\,s^{-1}Mpc^{-1}}$ to $H_0 = 67.32 \pm 4.64\,\mathrm{km\,s^{-1}Mpc^{-1}}$, in full consistency with the *Planck* value. This model also shows a substantial improvement in the fit to the data when an additional constraint from the inverse distance ladder is included. Another study further tested and confirmed that the Cepheid and SNIa datasets do not disfavor such a transition [4211].

Assuming $L - A \propto G^\gamma$ (where A, γ are constants and L is the SNIa absolute luminosity), an exponent $\gamma < 0$ ($\gamma > 0$) would mean that a lower (higher) value of G is required at $z \gtrsim 0.01$ to solve the Hubble tension, leading also to a potential resolution (exacerbation) of the growth rate tension [2682].

Recent constraints on G variation between the present time and recombination suggest that $|\Delta G/G| < 0.05$ at 2σ, where $\Delta G \equiv G_> - G_<$ [4153]. These studies assume ΛCDM expansion and that all other fundamental constants remain unchanged; relaxing these could weaken the constraints. Using the strong constraints of Ref. [4153], requiring $L_>/L_< = 1.15$ with $A = 0$ requires $\gamma \notin [-4.5, 2.8]$.

Early studies assumed that $L \propto M_{\rm Ch}$ (where $M_{\rm Ch}$ is the Chandrasekhar mass), which implies $\gamma = -3/2$ [4212–4214]. However, this does not account for the standardization procedure required for turning SNIa into standard candles; building a semi-analytic model to account for this, more recent studies use a simplified SNIa standardization procedure (no full use of light curve stretch and no use of color) and approximate semi-analytical arguments (no hydrodynamical simulation) to suggest that $\gamma \simeq 1.46$ with $A = 0$ [4201,4215,4216]. Both approaches make significant simplifications to the underlying physics; a fully reliable analysis should use full 3D hydrodynamical simulations of SNIa with a range of properties and obtain their light curves, properly treat MG effects on white dwarf structure, and adopt a standardization protocol identical to that employed empirically, also producing uncertainties on γ and A.

It is thus possible that $\gamma \notin [-4.5, 2.8]$ could be viable in the GSM. $\gamma < 0$ is however also strongly constrained: a sharp rise in G up to 150 Myr ago ($z \lesssim 0.01$) would have dramatic unobserved effects on neutron stars by causing them to contract, thereby releasing vast amounts of energy [4217]. This is however also based on significant simplifying assumptions that may not hold in practice. In particular, roughly constant neutron star and binary formation rate over time is assumed, all galaxies are assumed similar to the MW, higher black hole formation at early-times due to more massive stars and low metallicity is ignored, etc.

Further strong challenges to the GSM are presented in Ref. [4155]. Their main criticisms relate to the expansion of the Earth's orbit around the Sun coupled with lower G leading to a 10% increase in the number of days per year that is not seen in the geochronometric and cyclostratigraphic records, a higher helioseismic age of the Sun due to higher G over the vast majority of its history creating a mismatch with the ages of the oldest meteorite samples from the early Solar System, and a sharp drop in Solar insolation on the Earth in the geologically recent past due to a drop in G, leading to a large temperature drop.

Even if $\gamma \notin [-4.5, 2.8]$ were to be conclusively ruled out or SNIa modeling found to require $\gamma < 0$ which is then ruled out by neutron stars, or the tests in Ref. [4155] were verified, the possibility of a simultaneous transition of G with other fundamental constants [4218–4220] like the fine structure constant would remain, keeping the general LPT paradigm alive. Transitions of the type envisaged by the paradigm could be produced by theories such as Dilaton and Kaluza–Klein theories [4180], TeVeS-like theories [4221], or varying α theories [4222]. Note that the above constraints do not apply to the screening models discussed at the start of this section because screening naturally hides the fifth force locally and there is no universal change to fundamental constants like G.

In conclusion, the proposed local physics modifications discussed here, including both the screened fifth force model and transitions in the effective gravitational constant, appear to constitute a promising approach to the resolution of the Hubble tension. These results underscore the importance of further investigation of new physics in the local Universe that could affect the calibration of the cosmic distance ladder, and of constraints on such physics from other sources.

5. Discussion and future opportunities

The problem of cosmic tensions poses several challenges and a number of opportunities in more deeply assessing possible systematics in observational surveys, developing new data analysis tool kits to refine our treatment of these data products, and developing more robust physical models that can build on the successes of the concordance model and pose new questions and give new solutions to the next decade of cosmology. To meet these challenges, a community-wide effort will be needed involving advances in each separate field, but also strongly and more interconnected relationships between these disciplines.

The coming decade will bring a number of pivotal surveys and observatories that aim to confront the central questions posed by the last decades of concordance physics. This may bring additional unforeseen discoveries in the cosmic history of the Universe, as well as new tools from the increasingly dominant spectrum of ML and statistical physics toolkits, and possibly a new paradigm in our perspective of fundamental physics as an explanation of the driver of cosmic evolution. In Section 5.1 the most significant observatories and survey prospects are discussed in the context of the coming decade of observational cosmology. In Section 5.2 several key areas of development are identified which will be crucial to meeting the growing observational, statistical, and fundamental physics challenges of the upcoming decade of cosmology. Finally, we close in Section 5.3 with a summary of the

central themes of this work and an outlook perspective on the impact of cosmic tensions over the next few years.

5.1. Future survey prospects

Cosmology has undergone astounding advancements in the last few decades, due in part to the rapid progress of robust surveys, including unprecedented instrument precision and impressive new approaches to statistical analyses. These advancements have enabled a wider spectrum of tests of theoretical models, as well as unforeseen discoveries such as the accelerating expansion of the Universe in the late 1990s and the unexpectedly high number of galaxies imaged in the Hubble Deep Field. The next decade is set to extend this discovery potential with a swath of exciting missions nearing completion.

The dynamics of future surveys have pivoted to extreme precision surveys with vastly expanded mission objectives. These include measurements reaching much closer to the early Universe, such as the potential detection of the first luminous objects in the Universe through the 21-cm hydrogen line, the possible detection of signatures of inflation in the CMB, and significant reductions in the uncertainty of current CMB measurements. There are also a host of surveys that will track the spatial distribution of galaxies in the Universe to unprecedented levels in terms of the number of galaxies and the precision of these measurements. These surveys will facilitate even deeper investigations into the large-scale structure of the cosmos, providing more information on the nature and evolution of DE and DM.

There is a vast array of planned observational surveys and measurements for the coming decade, which will add to the already considerable number of active survey collaborations. Below, we describe some of the major planned and ongoing missions and survey analyses.

5.1.1. Cosmic microwave background

A key focus of the next generation of cosmological surveys is the study of the CMB. Building on decades of groundbreaking discoveries, future CMB experiments are poised to address some of the most pressing challenges in modern cosmology, including the persistent tensions in the Hubble constant and the amplitude of matter fluctuations (S_8). Upcoming CMB missions aim to achieve unprecedented precision in measurements of the CMB's temperature and polarization anisotropies, offering unique insights into the physics of the early Universe and its evolution.

The H_0 tension stems from a significant discrepancy between the value of the Hubble constant inferred from early Universe observations, such as the CMB, and local measurements using the cosmic distance ladder. Future CMB experiments will refine measurements of the sound horizon at the baryon drag epoch — a critical calibration scale for early-time H_0 estimates. These high-precision data will test proposed solutions to the H_0 tension, including EDE models, extra relativistic species, or modifications to pre-recombination physics, by either validating or ruling out scenarios that alter the expansion history before recombination.

The S_8 tension, which reflects a discrepancy in the amplitude of matter clustering, is another key focus of upcoming CMB experiments. By producing high-resolution maps of the CMB lensing power spectrum, they will directly probe the distribution of DM and the growth of large-scale structures. These measurements will be critical for cross-checking WL and galaxy clustering observations, helping to clarify whether the S_8 tension arises from unknown systematics in late-time surveys or signals a breakdown in the standard cosmological model.

Additionally, CMB experiments will probe primordial B-mode polarization, providing a unique window into the inflationary era and the energy scale of the early Universe. These observations could also inform models that connect the physics of inflation to current cosmological tensions, such as scenarios involving new scalar fields or MG.

Future CMB missions will also contribute to our understanding of DE and neutrino physics. Improved measurements of secondary anisotropies, such as the Sunyaev–Zel'dovich effect, will enable detailed studies of galaxy clusters and baryonic feedback processes, while precise constraints on the sum of neutrino masses and extra relativistic species will help refine models of the early Universe. By combining these capabilities with cross-correlations to other cosmological probes, such as BAO and WL surveys, CMB experiments will play a pivotal role in addressing cosmological tensions and advancing our understanding of the fundamental properties of the Universe.

Below, we highlight some of the major planned and ongoing CMB-focused missions and their scientific goals:

- **South Pole Telescope — 3rd Generation (SPT-3G)**: The SPT-3G [4223] is the latest upgrade to the SPT, focusing on high-resolution studies of the CMB from the exceptional observational site at the South Pole. This third-generation camera, featuring over 16,000 detectors, has significantly improved sensitivity, enabling deeper and more precise measurements of CMB temperature and polarization anisotropies. What sets SPT-3G apart is its ability to perform high-resolution surveys over small sky patches, optimized for studies of galaxy clusters via the Sunyaev–Zel'dovich effect, as well as gravitational lensing of the CMB. These measurements are critical for understanding the distribution of DM and large-scale structure formation. Additionally, SPT-3G contributes to constraints on the sum of neutrino masses and potential new physics beyond the standard cosmological model. The compact field-of-view and deep integration capabilities make SPT-3G uniquely suited for detecting subtle signals, such as CMB lensing, and studying small-scale anisotropies.
- **Atacama Cosmology Telescope (ACT)**: Located in the Atacama Desert of Chile, ACT [4224] is a ground-based observatory dedicated to high-resolution studies of the CMB. The telescope has been instrumental in mapping CMB temperature and polarization anisotropies and probing large-scale structure. The ACT Data Release 4 (DR4) provided high-sensitivity maps of the CMB, including measurements of temperature, E-mode polarization, and cross-correlations, covering over 17,000 square degrees of the sky. DR4 data significantly refined estimates of cosmological parameters, including constraints on H_0, σ_8, and the sum of neutrino masses. It also included improved measurements of the lensing power spectrum, advancing our understanding of the distribution of matter in the Universe. The forthcoming ACT Data Release 6 (DR6) is expected to feature even more precise maps with reduced noise levels and expanded sky coverage. DR6 aims to provide improved constraints on primordial B-mode polarization, enhancing our ability to test inflationary physics. Additionally, it will enable more detailed studies of secondary anisotropies, such as the Sunyaev–Zel'dovich effect, and cross-correlations with galaxy surveys.
- **PolarBear and Simons Array**: PolarBear, along with its successor, the Simons Array [4225], is focused on high-resolution measurements of the CMB's polarization anisotropies. Located in the Atacama Desert, Chile, these experiments aim to detect B-mode polarization caused by gravitational lensing and primordial GWs. The Simons Array, an upgraded version of PolarBear, consists of multiple telescopes with advanced detectors for improved sensitivity. These measurements will refine constraints on the tensor-to-scalar ratio r, test inflationary models, and map the lensing power spectrum, shedding light on the distribution of DM and the evolution of large-scale structure.
- **SPIDER**: SPIDER [2394] is a balloon-borne experiment designed to detect the large-scale polarization of the CMB, focusing on B-modes linked to primordial GWs. By operating above the atmosphere, SPIDER achieves reduced contamination from ground-based noise and atmospheric effects. Its payload consists of multiple telescopes equipped with cryogenic polarimeters, optimized

for observing large angular scales. SPIDER has already completed successful flights, with future missions planned to improve sensitivity and expand sky coverage.

- **Ali Cosmic Polarization Telescope (AliCPT)**: AliCPT [4226] is a ground-based CMB experiment located at the high-altitude Ali Observatory in Tibet. AliCPT focuses on measuring the polarization of the CMB at large angular scales, particularly the B-modes associated with primordial GWs. Its high-altitude location minimizes atmospheric contamination, allowing for precise measurements.
- **Q&U Bolometric Interferometer for Cosmology (QUBIC)**: QUBIC [4227] is an international collaboration designed to measure the B-mode polarization of the CMB using bolometric interferometry. It uniquely combines the sensitivity of bolometric detectors with the spatial filtering capabilities of interferometry, allowing for precise measurements of polarization anisotropies. Located at high altitude in Argentina, QUBIC targets primordial B-modes associated with inflation, as well as lensing-induced B-modes, providing critical constraints on the tensor-to-scalar ratio r. The first module began operations in 2022.
- **The Simons Observatory (SO)**: The Simons Observatory [681] is a next-generation ground-based experiment located in the Atacama Desert, Chile. It will consist of three small-aperture telescopes (SATs) and one large-aperture telescope (LAT), all equipped with advanced cryogenic detector arrays. The primary goal of the observatory is to measure the CMB temperature and polarization anisotropies with high precision across a wide range of angular scales. SO will target the primordial B-mode polarization of the CMB, providing critical tests of inflationary physics and insights into the early Universe's energy scale. It will also probe secondary anisotropies, such as the Sunyaev–Zel'dovich effect, to map the growth of large-scale structure. The observatory will place constraints on the sum of neutrino masses and search for new physics beyond the standard model. Additionally, SO will refine measurements of cosmological parameters like H_0 and S_8, addressing key tensions in the ΛCDM model. The Simons Observatory is expected to begin operations in the mid-2020s.
- **Cosmology Large Angular Scale Surveyor (CLASS)**: The CLASS experiment [4228] is designed to study the polarization of the CMB on large angular scales. Located in the Atacama Desert, Chile, CLASS employs a series of telescopes equipped with cryogenic detectors to measure the faint polarization signals from the early Universe. The experiment focuses on detecting the reionization and recombination bumps in the CMB polarization power spectrum, aiming to constrain primordial GWs and the optical depth of reionization. CLASS's innovative strategy includes observing large sky patches with rapid rotation to minimize systematic errors caused by atmospheric and instrumental noise.
- **GroundBIRD**: GroundBIRD [4229] is a ground-based experiment designed to measure the polarization of the CMB on large angular scales. Located at the Teide Observatory in Spain, it uses fast rotation and superconducting detectors to reduce atmospheric noise and systematic errors. The experiment focuses on detecting B-mode polarization signals, particularly those associated with primordial GWs. GroundBIRD's innovative observing strategy, which involves continuous scanning with a rotating cryostat, enhances its sensitivity to large-scale polarization while minimizing contamination.
- **BICEP/Keck Array and BICEP Array**: The BICEP/Keck Array and its successor, the BICEP Array [4230], are focused on detecting B-mode polarization of the CMB with high sensitivity. Operating from the South Pole, these experiments target large-scale polarization signals to constrain the tensor-to-scalar ratio r and probe the inflationary epoch. The BICEP Array incorporates advanced detector technology and expanded frequency coverage to improve sensitivity and reduce systematic uncertainties.
- **The Lite satellite for the study of B-mode polarization and Inflation from cosmic background Radiation Detection (LiteBIRD)**: The LiteBIRD probe [2393,4231–4234] aims to measure the unique imprints of B-mode polarization in CMB photons, which are related to primordial GWs and inflation. It will succeed the Planck mission in conducting full-sky surveys. Expected to launch in late 2029, LiteBIRD is a Japanese initiative by JAXA involving collaborations with agencies in North America and Europe. Positioned at the Lagrange point L2 in the Sun-Earth system, it will conduct a three-year survey. The relic CMB radiation features E-mode polarization, linked to scalar perturbations, and B-mode polarization, associated with tensor perturbations. While the Cosmic Background Imager provided the first detailed E-mode polarization map, the B-mode signal remains undetected. LiteBIRD will take cosmic-variance-limited measurements of E-mode polarization to study large-scale correlations, shedding light on initial conditions for cosmological perturbations and providing insights into physics beyond the standard model. Regarding B-mode polarization, LiteBIRD will aim for a tensor-to-scalar ratio limit of $r < 0.001$. A positive detection would have a profound impact on fundamental physics, offering insights into inflationary physics, parity violation, and primordial cosmological magnetism.
- **CMB — Stage 4 (CMB-S4)**: The CMB-S4 observatory [682] will operate telescopes at both the South Pole and the Atacama Desert in Chile, enabling deep microwave observations over small and large sky fields. It will employ advanced superconducting detector array technologies to reduce galactic foreground contamination. Expected to start operations in the late 2020s, though currently on hold, CMB-S4 aims to measure primordial GWs associated with the early rapid expansion of density fluctuations, characterized by the B-mode polarization of the CMB. This would provide critical information about cosmic inflation and fundamental physics, targeting a tensor-to-scalar ratio of $r < 0.002$, an order of magnitude improvement over current limits. CMB-S4 will constrain the sum of neutrino masses, critical for understanding the sterile neutrino theory and the inverted neutrino mass hierarchy. Beyond neutrino physics, it will impose stringent limits on possible light particles beyond the standard model, addressing extra effective degrees of freedom. On DM, CMB-S4 will probe CMB anisotropies for potential signals of WIMP annihilation, placing constraints on their masses, while exploring non-thermal DM effects on lensing power spectra. Another key goal is probing DE, with precision measurements of ΛCDM cosmological parameters such as H_0 and S_8, enabling comparisons with other early-time probes. Additionally, CMB-S4 will generate higher-resolution maps of matter distribution in the Universe by measuring distortions in CMB photons caused by gravitational lensing from the surface of last scattering. This will significantly enhance future galaxy surveys.
- **Cosmic Microwave Background - High Definition (CMB-HD)**: CMB-HD [4235,4236] is a proposed next-generation ground-based observatory that aims to revolutionize cosmology with its unparalleled resolution and sensitivity. Unlike other CMB experiments, CMB-HD focuses on small-scale anisotropies, achieving an angular resolution of 0.5 arcminutes and surveying over 50% of the sky. This capability allows it to probe previously inaccessible signals and extend our understanding of the Universe to finer detail. CMB-HD's primary science goals include precise measurements of the Sunyaev–Zel'dovich effects to map galaxy clusters, their gas content, and baryonic physics. It will also produce detailed maps of the small-scale CMB lensing power spectrum, offering new insights into the distribution of DM and the growth of large-scale structure. By detecting primordial B-mode polarization, CMB-HD will constrain the tensor-to-scalar ratio r

to test inflationary physics at energy scales far beyond current limits. Additionally, CMB-HD will place stringent constraints on the sum of neutrino masses, light relics, and possible deviations from the ΛCDM model.

- **Probe of Inflation and Cosmic Origins (PICO)**: PICO [4237] is a proposed next-generation satellite mission designed to provide a comprehensive, all-sky measurement of the CMB. Operating from space, PICO will avoid the challenges of atmospheric contamination and cross-calibration issues that affect ground-based experiments. Its observations will span a broad frequency range from 20 GHz to 800 GHz, enabling highly accurate foreground removal and calibration consistency across the entire sky. A key advantage of PICO's space-based platform is its ability to precisely measure the optical depth to reionization, τ. This measurement, critical for understanding the early history of star formation and the growth of cosmic structures, is less accessible to ground-based telescopes due to the need for absolute calibration. By combining this capability with its unparalleled sensitivity to B-mode polarization, PICO will constrain the tensor-to-scalar ratio r to levels below 0.001, providing definitive tests of inflationary models. In addition to probing inflation, PICO will deliver high-resolution maps of the E-mode polarization and CMB lensing power spectrum, offering insights into the distribution of DM and large-scale structure. It will also place stringent constraints on the sum of neutrino masses, detect potential signals from light relics, and test extensions to the ΛCDM model. If approved, PICO will complement ground-based experiments by addressing systematic challenges and providing the calibration accuracy and sensitivity only possible from space.
- **Polarized Radiation Imaging and Spectroscopy Mission (PRISM)**: PRISM [4238] is a proposed satellite mission designed to provide extremely sensitive, all-sky measurements of the CMB's temperature and polarization anisotropies. With its advanced instrumentation and broad frequency coverage, PRISM aims to enhance our understanding of both early and late-time cosmology. A key goal of the mission is to detect primordial B-mode polarization, which would provide direct evidence of inflation and constrain the energy scale of the early Universe. PRISM's ability to refine measurements of the CMB power spectrum and polarization will enable tighter constraints on the sound horizon at the baryon drag epoch, directly addressing the H_0 tension by testing EDE models and other modifications to pre-recombination physics. Additionally, PRISM's high sensitivity to secondary anisotropies, such as CMB lensing, will improve measurements of the lensing power spectrum, aiding investigations into the S_8 tension and the growth of large-scale structure. If approved, PRISM would complement ground-based and balloon-borne experiments by avoiding atmospheric contamination, offering a clean and highly detailed dataset for cosmological studies.

5.1.2. Baryon acoustic oscillations

The study of BAO has become a cornerstone of modern cosmology, providing a powerful method for measuring the expansion history of the Universe. BAO are the relic imprints of sound waves that propagated in the early Universe, leaving a characteristic scale in the large-scale distribution of galaxies and matter. This standard ruler has proven invaluable for calibrating cosmic distances and constraining key cosmological parameters, including the Hubble constant and the DE equation of state.

As the precision of cosmological measurements continues to improve, future BAO experiments are poised to deliver new insights into the late-time Universe. By mapping the three-dimensional distribution of galaxies, QSOs, and other tracers across an extensive redshift range, these experiments will probe the dynamics of cosmic expansion and the growth of large-scale structure. This enhanced precision will enable a deeper exploration of the H_0 and S_8 tensions, testing whether they arise from unaccounted systematics or new physics beyond the ΛCDM model.

In addition to refining our understanding of DE and its influence on cosmic acceleration, upcoming BAO surveys will provide complementary constraints on modifications to gravity and potential extensions to standard cosmology. Synergies with other probes, such as WL and CMB lensing, will further bolster the ability to test fundamental physics and the consistency of the cosmological model.

Below, we describe some of the major planned and ongoing BAO-focused missions and their scientific objectives:

- **Dark Energy Spectroscopic Instrument (DESI)**: DESI [814] is a state-of-the-art spectroscopic survey currently operating on the Mayall 4-meter telescope at Kitt Peak National Observatory. Its primary goal is to create the most detailed three-dimensional map of the Universe by observing tens of millions of galaxies and QSOs across a wide redshift range. DESI's high-precision BAO measurements will provide critical constraints on the cosmic distance scale and the expansion history of the Universe, directly addressing the H_0 tension. Additionally, RSD analyses from DESI will help probe the growth rate of large-scale structures, contributing to our understanding of the S_8 tension and testing potential modifications to gravity.
- **Canadian Hydrogen Intensity Mapping Experiment (CHIME)**: CHIME [4239] is a revolutionary radio interferometer located at the Dominion Radio Astrophysical Observatory in Canada. Designed to operate in the 400–800 MHz band, it maps the large-scale structure of the Universe using the 21 cm hydrogen line, covering a redshift range of $0.8 < z < 2.5$. By using intensity mapping techniques, CHIME provides precise measurements of the BAO scale, complementing optical surveys like DESI and HIRAX. The experiment's wide field-of-view and innovative cylindrical reflector design enable it to conduct highly efficient surveys, making CHIME a key player in refining the cosmic distance scale.
- **BAO from Integrated Neutral Gas Observations (BINGO)**: BINGO [4240] is a 21 cm intensity mapping experiment specifically designed to measure BAO in the redshift range $0.13 < z < 0.48$. Located in Brazil, it utilizes a compact array of radio antennas to map the large-scale distribution of neutral hydrogen. BINGO is optimized to minimize instrumental noise and systematics, providing precise constraints on the expansion history of the Universe and DE. The project is currently under construction and expected to begin operations in the mid-2020s.
- **Euclid**: The Euclid mission [4241], led by ESA, is designed to create a detailed three-dimensional map of the Universe, enabling precise measurements of the BAO scale across a wide redshift range ($0.7 < z < 2.0$). Its near-infrared spectroscopic survey will provide accurate redshifts for tens of millions of galaxies, establishing a robust standard ruler for cosmological distances. By focusing on high-redshift galaxy clustering, Euclid will refine the expansion history and DE equation of state. Its spectroscopic data will also complement optical BAO studies, bridging gaps in redshift coverage and enhancing multi-probe analyses with other cosmological surveys.
- **Prime Focus Spectrograph (PFS):** The PFS survey [4242,4243] is a spectroscopic survey operating on the 8-meter Subaru Telescope. It is designed to observe 2,400 objects simultaneously within a 1.2 deg^2 field of view, covering wavelengths from the near-ultraviolet to the near-infrared. With its wide field and spectral coverage, PFS focuses on three primary science programs: cosmology, galaxy evolution, and galactic archeology. For cosmology, PFS will observe approximately 4 million emission-line galaxies (ELGs) over 1,200 deg^2, covering redshifts from 0.8 to 2.4. Unlike other surveys, it will uniquely map ELGs at $2.0 < z < 2.4$, complementing DESI. PFS will provide high-precision measurements of BAO and the Alcock–Paczyński (AP) effect, enabling

constraints on the Hubble expansion history and testing potential evolution in dark energy out to $z = 2.4$. By combining these results with lower-redshift BAO constraints, PFS will determine the dark energy density to approximately 7% accuracy per redshift bin. Additionally, RSD measurements will reconstruct the growth rate of cosmic structure, $f\sigma_8(z)$, with 6% accuracy up to $z = 2.4$, allowing for a precise determination of the sum of neutrino masses, with an uncertainty of $\sigma(\sum m_\nu) = 0.02$.

- **Roman Space Telescope (formerly WFIRST)**: The Roman Space Telescope [896], led by NASA, is a highly ambitious mission designed to address key questions about DE, exoplanets, and the structure of the Universe. Through its High Latitude Survey, Roman will map the large-scale distribution of galaxies and perform WL and BAO analyses with unprecedented precision. This mission will provide robust constraints on the expansion history, DE dynamics, and the growth of cosmic structures.
- **Rubin Observatory's Legacy Survey of Space and Time (LSST)**: The Rubin Observatory [4244], in its final construction phase in northern Chile, will conduct the LSST, a 10-year survey of $18,000\,\mathrm{deg}^2$ of the sky across six wavelength bands. Public data release is expected approximately two years after first light in 2025. LSST will address a broad range of fundamental questions, including: (1) Is DE dynamical, as characterized by the w_0-w_a parameterization? (2) Can the expansion history and large-scale structure help distinguish between exotic energy densities and MG? (3) What are the properties of DM, as revealed by microlensing searches? (4) Do DM halos exist without hosting galaxies? (5) Are matter fluctuations in the late Universe consistent with CMB-derived constraints? LSST is expected to profoundly impact our understanding of DE, DM, and fundamental physics.
- **SKAO (Square Kilometer Array Observatory)**: SKAO [4245] is a next-generation radio telescope array under development, with sites in South Africa and Australia. Its unprecedented sensitivity and angular resolution will enable precise 21-cm intensity mapping, allowing for detailed BAO measurements across a wide redshift range. These data will be instrumental in tracing the evolution of cosmic expansion and structure growth, providing crucial information for resolving the H_0 and S_8 tensions and testing the consistency of the ΛCDM model. (see Section 5.1.5)
- **The Hydrogen Intensity and Real-time Analysis eXperiment (HIRAX)**: HIRAX [1846] is a radio interferometer array under construction in South Africa, optimized for intensity mapping of the 21-cm hydrogen line. HIRAX will measure BAO across a redshift range of $0.8 < z < 2.5$, directly probing the expansion history during the period of cosmic acceleration driven by DE. These measurements will complement optical BAO surveys, refining constraints on DE models and addressing potential new physics.
- **Dark Energy Spectroscopic Instrument - Phase II (DESI-II)**: DESI-II [4246] is a proposed extension of the highly successful DESI survey, aiming to build on its existing infrastructure to further refine cosmological measurements. By expanding its redshift coverage and increasing the volume of observed galaxies and QSOs, DESI-II will provide even more precise measurements of the BAO and RSD. The extended survey will target fainter galaxies and higher redshift objects, allowing for a deeper exploration of the late-time Universe's expansion history and the growth of cosmic structures.
- **The 4-meter Multi-Object Spectroscopic Telescope (4MOST)**: 4MOST [4247], based at the ESO's VISTA telescope in Chile, is designed to conduct massive spectroscopic surveys of galaxies and QSOs over large sky areas. Its multi-object spectrograph will enable precise BAO measurements and RSD analyses, improving constraints on the cosmic expansion rate and structure growth. 4MOST will work synergistically with imaging surveys like LSST to provide redshift information critical for cosmological studies, including cross-correlation analyses to probe the S_8 tension.
- **Spectro-Photometer for the History of the Universe, Epoch of Reionization, and Ices Explorer (SPHEREx)**: SPHEREx [4248] is a NASA mission designed to perform an all-sky spectral survey. By mapping galaxies across a wide range of redshifts, SPHEREx will measure BAO and RSD signals, enabling precise constraints on the expansion history and the growth of cosmic structure. Its unique spectral coverage will complement optical surveys and provide new insights into the physics.
- **CO Mapping Array Project (COMAP)**: COMAP [4249] is a pioneering experiment focused on intensity mapping of carbon monoxide (CO) lines at high redshift. COMAP will trace the large-scale structure of the Universe during the epoch of galaxy formation, providing a complementary approach to BAO measurements. These data will help refine constraints on the expansion history and test models of DE and MG.
- **Packed Ultra-Wideband Mapping Array (PUMA)**: PUMA [4250] is a proposed next-generation radio interferometer optimized for detecting BAO and measuring RSD over a wide redshift range of $2 < z < 6$. Using 21 cm intensity mapping, PUMA will map the large-scale distribution of neutral hydrogen, providing unprecedented insights into the Universe's expansion history and the growth of cosmic structure. Its innovative design, featuring a densely packed array of antennas, will enable high sensitivity and wide bandwidth, making it a critical experiment for studying DE, testing modifications to gravity, and resolving tensions in cosmological parameters. Expected to begin operations in the 2030s, PUMA will complement optical BAO surveys and push the boundaries of cosmological research.

5.1.3. *Weak lensing experiments*

WL is a cornerstone tool for investigating cosmological tensions, particularly the S_8 discrepancy, which reflects a persistent difference between the amplitude of matter fluctuations inferred from early- and late-Universe observations. WL measures the subtle distortions in galaxy shapes caused by the gravitational lensing effect of intervening mass distributions, providing a direct probe of the growth of cosmic structures. By combining the clustering amplitude σ_8 with the matter density parameter $\Omega_{\mathrm{m},0}$, the derived parameter $S_8 = \sigma_8\sqrt{\Omega_{\mathrm{m},0}/0.3}$ becomes a critical test of the ΛCDM model.

In addition to its crucial role in addressing the S_8 tension, WL data also contribute to resolving the H_0 tension. Synergistic analyses that combine WL with other cosmological probes, such as CMB lensing and BAO measurements, enable a multi-probe approach to jointly constrain both early- and late-Universe parameters. This integrated strategy improves the robustness of results and provides deeper insights into the underlying physics driving these tensions.

Below, we highlight planned and ongoing WL experiments and their contributions to addressing the S_8 tension:

- **Kilo-Degree Survey (KiDS)**: KiDS [860] provided high-precision WL and photometric redshift measurements across $1350\,\mathrm{deg}^2$, with a strong focus on controlling systematics such as shear calibration, photometric redshifts, and intrinsic galaxy alignments. Using high-quality imaging from the Very Large Telescope (VLT) and tomographic redshift binning, KiDS delivered some of the most precise S_8 constraints, highlighting a persistent tension with ΛCDM predictions. Its integration with external datasets, such as galaxy clustering and CMB lensing maps, enabled multi-probe analyses and established a strong foundation for addressing the S_8 tension in future surveys.
- **Dark Energy Survey (DES)**: DES [4251] observed $5000\,\mathrm{deg}^2$ of the southern sky, combining WL and galaxy clustering to provide robust S_8 constraints. With precise photometric redshift calibration and careful control of systematics, DES advanced studies

of large-scale structure growth. Its cross-correlations with CMB lensing maps and tomographic analyses tested ΛCDM predictions and explored extensions like evolving DE. DES's extensive data and methodological innovations set a high standard for future WL surveys.

- **Hyper Suprime-Cam (HSC)**: HSC [854], conducted on the Subaru Telescope, delivered WL data over $1400\,\mathrm{deg}^2$ with exceptional resolution and depth, enabling precise studies of cosmic shear. Its high-resolution imaging allowed detailed analyses of smaller-scale structures and provided key insights into S_8, revealing persistent tensions with ΛCDM predictions. The survey's innovative techniques for photometric redshift estimation and systematic error control ensured high accuracy in its results. HSC also contributed significantly to cross-correlation studies with galaxy clustering and CMB lensing, further refining constraints on the growth of structure and testing extensions to the standard cosmological model.
- **Super-pressure Balloon-borne Imaging Telescope (SuperBIT)**: SuperBIT [4252] is a stratospheric, balloon-borne telescope designed for high-resolution, wide-field imaging, enabling precise WL measurements of galaxy clusters. By operating above most of Earth's atmosphere, it minimizes atmospheric distortions, delivering exceptional data quality. SuperBIT's observations are critical for mapping the distribution of DM and studying large-scale structure formation, providing complementary insights to ground- and space-based surveys. Its unique capabilities contribute to addressing the S_8 tension by offering an independent probe of structure growth.
- **Euclid**: Euclid's high-resolution optical and near-infrared imaging capabilities [4241] are designed to map the weak gravitational lensing of billions of galaxies over $15,000\,\mathrm{deg}^2$ of the sky. Its ability to probe redshifts up to $z \sim 2.5$ makes it uniquely suited for tomographic studies of structure growth, providing tight constraints on the S_8 parameter. By achieving unparalleled depth and resolution in WL, Euclid will play a crucial role in testing modifications to ΛCDM, such as evolving DE models and MG theories. Its combination of imaging and spectroscopic data will enable synergy with Rubin LSST and CMB lensing maps, further enhancing our understanding of cosmic structure formation.
- **Rubin Observatory's Legacy Survey of Space and Time (LSST)**: The Rubin Observatory [4244] will survey $18,000\,\mathrm{deg}^2$ of the sky over a 10-year period, providing deep, multi-band imaging across six optical filters. Rubin's LSST high precision in WL and galaxy clustering measurements will allow detailed tomographic studies of structure growth and yield tighter constraints on S_8. Its ability to detect millions of faint galaxies at high redshifts will improve our understanding of the evolution of cosmic structures and test potential extensions to ΛCDM. Rubin's LSST rich dataset will also facilitate cross-correlations with CMB and other WL surveys, strengthening the multi-probe approach to resolving cosmological tensions.
- **Roman Space Telescope (formerly WFIRST)**: The Roman Space Telescope's High Latitude Survey [896] will deliver high-resolution WL data over $2000\,\mathrm{deg}^2$, focusing on the distribution of DM and the growth of cosmic structures. Its combination of near-infrared imaging and spectroscopy enables precise photometric redshift estimation, essential for tomographic studies of WL. Roman's unparalleled sensitivity at high redshifts ($z \sim 2$) will refine measurements of the S_8 parameter, providing stringent tests of ΛCDM and its alternatives, such as evolving DE and MG models. Its synergy with Euclid and Rubin's LSST will enhance cross-calibration efforts and improve constraints on cosmic structure formation across a wide range of scales and epochs.
- **Square Kilometer Array Observatory (SKAO)**: SKAO [4245], utilizing 21-cm intensity mapping and WL, will provide unique and independent constraints on S_8 by probing the distribution of DM and the growth of structures. Its radio-based approach will extend WL studies to higher redshifts and larger scales, offering a complementary perspective to optical surveys. By addressing potential systematics in traditional probes, SKAO will play a crucial role in testing deviations from ΛCDM and enhancing multi-probe strategies to resolve cosmological tensions.
- **Einstein Telescope (ET) and Cosmic Explorer (CE)**: These proposed third-generation GW observatories [594,4253–4255], expected to begin operations in the mid to late 2030s, will achieve unprecedented sensitivity in detecting GWs. In addition to their primary focus on GW astrophysics, they will enable measurements of WL effects on GW signals. This innovative approach provides a novel and independent method to probe the S_8 parameter, offering insights into the growth of cosmic structures and testing extensions to the standard cosmological model. Their unique capabilities will complement traditional WL surveys, further enriching multi-probe cosmological studies. (see Section 5.1.4)

5.1.4. Gravitational waves as probes of cosmological tensions

GWs offer a revolutionary perspective in addressing cosmological tensions, functioning as "standard sirens" that enable the measurement of cosmic distances independently of electromagnetic calibrations. By directly determining the luminosity distance to GW events, particularly those accompanied by electromagnetic counterparts (e.g., binary neutron star mergers), this method bypasses systematics associated with traditional distance ladder techniques. For a recent review on the capabilities of GW observatories see [654].

In addition to these "bright sirens", GWs from events lacking identifiable electromagnetic counterparts, termed "dark sirens", can also contribute to cosmology. By correlating the GW signal with galaxy catalogs to infer host redshifts, dark sirens expand the scope of GW cosmology, providing complementary constraints on the Hubble constant and other cosmological parameters. Furthermore, advancements in spectroscopic observations of host galaxies have introduced "spectroscopic sirens", which refine redshift measurements associated with GW events. These high-precision techniques enhance the reliability of constraints on the expansion history and reduce uncertainties linked to host galaxy identification.

Beyond H_0, GWs contribute to understanding large-scale structure formation through WL of GWs by intervening matter. These lensing effects provide unique insights into the amplitude of matter fluctuations, addressing the S_8 tension. Additionally, third-generation observatories such as the ET and the Cosmic Explorer will extend GW observations to higher redshifts ($z \sim 10$), probing the early Universe's expansion history and potential deviations from the ΛCDM model. The integration of GW observations with traditional cosmological probes, such as BAO, CMB, and WL, opens new pathways for multi-messenger cosmology. Together, these complementary approaches promise to resolve key tensions and deepen our understanding of the fundamental physics of the Universe.

Below, we highlight ongoing and planned GW experiments and their contributions to addressing cosmological tensions.

- **LIGO-Virgo-KAGRA Network**: The collaboration between the LIGO, Virgo, and KAGRA interferometers [590] has already achieved a remarkable number of significant detections, including the merger of a neutron star with an unknown compact object. This success is attributed to substantial sensitivity improvements, stemming from upgrades to individual detectors and the synergistic effect of combined observations. The fourth observation run (O4) is scheduled to conclude in the summer of 2025, after which further upgrades will be implemented. These upgrades will include advancements such as reduced thermal noise, new test mass mirrors, and the installation of a larger beamsplitter in the LIGO detectors. These enhancements will significantly increase

the network's overall sensitivity, enabling a larger detection volume and improved precision in measurement. As the number of detections grows, the uncertainty in key cosmological parameters like H_0 will decrease. Specifically, for neutron star–neutron star (NS–NS) mergers, the uncertainty in H_0 estimates is expected to improve by approximately $15\%/\sqrt{N}$, where N is the number of detections. This progress underscores the pivotal role of the LIGO-Virgo-KAGRA network in refining our understanding of the Universe.

- **Laser Interferometer Space Antenna (LISA)**: LISA [597] will be the first space-based GW detector, consisting of three spacecraft in a triangular configuration, separated by millions of kilometers, and following a heliocentric orbit. Scheduled for launch in the mid-2030s, LISA will primarily focus on astrophysical phenomena, including high-redshift mergers, extreme mass ratio inspirals, galactic binaries, and planetary objects. However, its contributions to cosmology will be equally groundbreaking. One of LISA's key cosmological objectives is to dramatically expand the catalog of dark sirens. These GW events, devoid of electromagnetic counterparts, serve as alternative standard candles, independent of the traditional cosmological distance ladder. By leveraging statistical methods with galaxy catalogs or identifying electromagnetic counterparts where possible, LISA will test the distance–redshift relation on cosmological scales, providing new constraints on DE models. With sensitivity extending to redshifts as high as $z \sim 10$, LISA will open a window to the Universe's distant past, offering unprecedented opportunities to explore the nature of DE at scales inaccessible to current methods. Furthermore, LISA's observations will enable precise and independent measurements of H_0, contributing to resolving the persistent cosmological tensions.
- **Einstein Telescope (ET)**: ET [4253–4255] is a proposed next-generation GW observatory designed to achieve unprecedented sensitivity through advancements in quantum noise suppression, cryogenics, and interferometry. With a triangular configuration and a planned underground location to minimize seismic noise, the ET represents a significant leap forward from current ground-based detectors. A pathfinder prototype [4256], established at Maastricht University in 2021, has already demonstrated promising results in key enabling technologies, paving the way for the full-scale project. Like LISA, the ET will test the distance–redshift relation on cosmological scales and provide independent measurements of H_0, free from the assumptions of the traditional distance ladder [654]. This will primarily be achieved through the detection of binary compact object coalescences, which serve as robust standard sirens. Beyond H_0, the ET will be uniquely equipped to detect SGWBs of cosmological origin, offering a direct window into the early Universe. These observations could shed light on fundamental processes such as inflation, the formation of primordial black holes, phase transitions in the early Universe, and potential topological defects. The ET's ability to probe these phenomena would significantly deepen our understanding of the Universe's origins and evolution, making it a cornerstone of future GW astronomy and cosmology.
- **Cosmic Explorer (CE)**: The proposed CE observatory [594,595] will build on the design principles of LIGO, but with significantly enhanced capabilities. Its arms, each spanning 40 km, will dramatically improve sensitivity, particularly in the low-frequency range. This enhanced sensitivity will enable the detection of black hole-black hole mergers at unprecedented distances and increase the detection rate to as many as 10^5 events per year. With its ability to observe GWs in the 5–4000 Hz frequency band, CE will produce an unparalleled map of the GW sky, reaching back to high redshifts of $z \sim 20$ [4257,4258]. By probing this deep into the Universe's history, CE will offer complementary insights into binary mergers, tracing their origins to the first stars and providing critical information on the star formation rate and galaxy evolution over cosmic time. In addition to astrophysical discoveries, CE will play a pivotal role in cosmology. By observing a vast catalog of dark sirens, CE will enable precise inferences of H_0 and provide a valuable independent check on the expansion history of the Universe. This makes CE an essential component of next-generation GW astronomy and its intersection with cosmology.
- **TianQin**: TianQin [4259,4260] is a proposed Chinese space-based GW observatory designed to detect GWs in the millihertz frequency range. It will consist of three spacecraft in a geocentric orbit, forming an equilateral triangle with arm lengths of approximately 10^5 km. TianQin's primary scientific objectives include the detection of signals from supermassive black hole mergers, extreme mass ratio inspirals (EMRIs), and SGWBs. One of TianQin's unique features is its orbit near the Earth, which facilitates precise laser interferometry while minimizing challenges associated with deep-space communication. Similar to LISA, TianQin will employ advanced laser metrology and drag-free control to achieve exceptional sensitivity to low-frequency GWs. In the context of cosmology, TianQin will contribute significantly to resolving cosmological tensions. By expanding the catalog of both bright and dark sirens, TianQin will enable independent measurements of H_0 and test the distance–redshift relation on cosmological scales. Additionally, its observations will probe the early Universe, offering insights into the SGWB and potential new physics beyond the standard model. TianQin is expected to launch in the 2030s, complementing other space-based observatories and advancing the era of precision GW cosmology.
- **Taiji**: Taiji [4261] is a proposed Chinese space-based GW observatory designed to detect GWs in the millihertz frequency band. Unlike TianQin, which operates in a geocentric orbit, Taiji will be positioned at the Sun-Earth Lagrange point L_2, providing a quieter observational environment and allowing for longer baselines. Its design includes three spacecraft forming an equilateral triangle with arm lengths of 3×10^6 km, optimized for detecting low-frequency GWs. Taiji's scientific goals include probing the evolution of the Universe at redshifts as high as $z \sim 20$ and detecting GWs from sources such as massive black hole binaries, intermediate-mass black hole mergers, and the SGWB. Its high sensitivity will also enable the study of rare cosmic phenomena inaccessible to other observatories, offering an unparalleled view of early-Universe processes. In cosmology, Taiji will contribute to addressing key tensions, including the H_0 discrepancy, by expanding the catalog of dark sirens and providing precise measurements of the distance–redshift relation. Additionally, Taiji will enhance our understanding of DE and inflation by exploring signals from primordial GWs, phase transitions, and primordial black holes. Scheduled for launch in the 2030s, Taiji complements the capabilities of both TianQin and LISA, focusing on high-redshift phenomena and deepening our understanding of the early Universe while advancing China's leadership in GW astronomy.
- **DECi-hertz Interferometer Gravitational Wave Observatory (DECIGO)**: DECIGO [4262] is a proposed Japanese space-based GW observatory designed to fill the frequency gap between ground-based detectors like LIGO and Virgo and low-frequency observatories like LISA. With a target frequency range centered around decihertz (0.1–10 Hz), DECIGO will enable the study of intermediate-mass black hole binaries, early Universe GW backgrounds, and other phenomena inaccessible to existing detectors. The DECIGO mission will consist of three spacecraft forming a triangular configuration with arm lengths of 1,000 km, operating in a heliocentric orbit. The observatory will use highly sensitive laser interferometry and drag-free control technologies to

achieve unprecedented precision in GW detection. A prototype mission, B-DECIGO, is planned to demonstrate key technologies in Earth orbit before the full-scale DECIGO mission launches. In cosmology, DECIGO will provide unique insights by detecting GWs from primordial sources such as phase transitions, cosmic strings, and inflation. Its sensitivity to the SGWB will allow for constraints on the physics of the early Universe, offering a direct window into energy scales far beyond those probed by CMB. DECIGO will also expand the catalog of standard sirens, enabling precise measurements of H_0 and the distance–redshift relation, which are crucial for resolving cosmological tensions. DECIGO's ability to study GWs from $z \sim 1000$ to the present will bridge the gap between early-Universe physics and late-time structure formation, providing complementary data to missions like LISA, Taiji, and TianQin. Expected to launch in the mid-2030s, DECIGO represents a major advancement in GW astronomy, with profound implications for cosmology and fundamental physics.

- **Pulsar Timing Arrays (PTAs)**: Pulsar Timing Arrays are an innovative approach to detecting low-frequency GWs in the nanohertz frequency band. Unlike ground- or space-based interferometers, PTAs utilize the precise timing of millisecond pulsars as natural clocks to measure distortions in spacetime caused by passing GWs. International collaborations, such as the North American Nanohertz Observatory for Gravitational Waves (NANOGrav) [4263], the European Pulsar Timing Array (EPTA), the Parkes Pulsar Timing Array (PPTA) [4264], and the International Pulsar Timing Array (IPTA) [4265], form a global network to maximize sensitivity and coverage. PTAs are particularly sensitive to GWs produced by supermassive black hole binaries (SMBHBs), which emit at nanohertz frequencies during their inspiral phase. Additionally, PTAs can probe the SGWB arising from the superposition of signals from numerous SMBHBs or from cosmological sources, such as cosmic strings, phase transitions, or inflation. In cosmology, PTAs provide unique insights by constraining the evolution of structure and the formation of massive galaxies. These measurements complement other GW observatories by covering a distinct frequency range, extending the spectrum of observable GWs. PTAs can also indirectly contribute to addressing the H_0 tension by improving our understanding of galaxy mergers and structure growth. Recent breakthroughs, such as the NANOGrav 15-year data release, have hinted at the first detection of a SGWB. These results, if confirmed, would open a new window into the Universe's evolution and provide evidence for processes occurring at very high energy scales, far beyond the reach of current particle accelerators. PTAs represent an essential component of the global GW detection strategy, providing a unique and complementary perspective to ground- and space-based observatories. With the advent of next-generation radio telescopes like SKAO, the sensitivity of PTAs is expected to dramatically improve, enabling more precise measurements and extending the range of detectable sources.

5.1.5. 21 Cm cosmology

The 21 cm line, arising from the hyperfine transition of neutral hydrogen (HI), provides a powerful and versatile tool for probing the Universe's structure and evolution across a wide range of redshifts. This signal serves as a unique tracer of the IGM and large-scale structure, enabling the study of key epochs such as the cosmic dawn, the EoR, and the post-reionization era. Unlike traditional probes, 21 cm cosmology captures three-dimensional information, offering tomographic insights into the distribution of matter and its interaction with radiation fields over cosmic time. The potential of the 21 cm line extends beyond mapping large-scale structure. It offers a novel avenue to address key cosmological tensions, including constraints on H_0 and the amplitude of matter fluctuations S_8. Moreover, the sensitivity of 21 cm surveys to high-redshift phenomena makes them an invaluable complement to other cosmological probes such as CMB, BAO, and WL.

In this part, we outline the current and future 21 cm experiments, their capabilities, and their expected contributions to cosmology. Special emphasis is placed on their role in addressing fundamental questions about the early Universe, the formation of cosmic structures, and the underlying physics driving cosmic tensions:

- **Low-Frequency Array (LOFAR)**: LOFAR [2351] is a cutting-edge radio interferometer designed to observe the Universe at low radio frequencies, operating primarily in the range of 10 MHz to 240 MHz. With its core located in the Netherlands and stations distributed across Europe, LOFAR provides high-resolution imaging and wide-field observations. A key focus of LOFAR is probing the 21 cm hydrogen signal from the EoR, offering insights into the period when the first stars and galaxies ionized the IGM. By mapping the structure of neutral hydrogen during this era, LOFAR aims to uncover the processes governing cosmic reionization and the emergence of the first luminous sources. Additionally, LOFAR's sensitivity to low-frequency signals makes it a valuable tool for studying other phenomena, including cosmic magnetism, DM, and the large-scale structure of the Universe. The array's modular and scalable design allows it to complement ongoing and future surveys.
- **Murchison Widefield Array (MWA)**: MWA [4266] is a cutting-edge low-frequency radio interferometer located in Western Australia, designed to observe the Universe at frequencies between 80 MHz and 300 MHz. With its compact configuration of 4,096 dipole antennas spread across 1.5 kilometers, the MWA excels at capturing wide-field, low-frequency observations. A primary objective of the MWA is to detect the 21 cm hydrogen signal from the EoR, enabling a detailed study of the processes that ionized the early Universe and the formation of the first stars and galaxies. Additionally, the MWA probes large-scale cosmic structures, providing insights into the distribution of matter and the role of DE in cosmic evolution. The array is a precursor instrument to the SKAO and serves as a testbed for developing advanced techniques in calibration, foreground removal, and signal extraction. Its location at the radio-quiet Murchison Radio-astronomy Observatory ensures minimal interference, enhancing its sensitivity to faint cosmological signals. Beyond cosmology, the MWA is also used to study solar physics, ionospheric science, and transient phenomena, making it a versatile instrument for advancing astrophysical research.
- **Hydrogen Epoch of Reionization Array (HERA)**: HERA [2352] is a dedicated radio interferometer designed specifically to study the 21 cm hydrogen signal from the EoR. Located in the radio-quiet Karoo region of South Africa, HERA consists of 350 closely packed parabolic dishes, each 14 m in diameter, optimized for high sensitivity to faint cosmological signals at redshifts corresponding to the EoR ($6 < z < 12$). HERA's primary goal is to provide a detailed characterization of the IGM during the EoR, tracing the formation and evolution of the first luminous sources — stars, galaxies, and black holes — and their impact on the ionization state of the Universe. By mapping fluctuations in the 21 cm emission, HERA will constrain the timing and progression of reionization, offering insights into the astrophysical processes driving it. The array's design prioritizes simplicity and precision calibration, which are critical for mitigating systematics and isolating the faint EoR signal from overwhelming foreground contamination. As a successor to PAPER, HERA incorporates lessons learned from earlier experiments, significantly improving sensitivity and resolution. HERA is expected to complement other 21 cm experiments like LOFAR, MWA, and SKAO by focusing specifically on the EoR. Its measurements will also provide valuable data for testing models of cosmic structure formation, the

properties of the first galaxies, and potential new physics beyond the standard cosmological model.

- **The Radio Experiment for the Analysis of Cosmic Hydrogen (REACH)**: REACH [4267] is an innovative experiment designed to detect the globally averaged 21 cm signal from neutral hydrogen, targeting the cosmic dawn and the EoR. What sets REACH apart is its novel calibration techniques and an advanced antenna design aimed at mitigating the impact of instrumental systematics and foreground contamination, long-standing challenges in 21 cm cosmology. By achieving unprecedented precision in isolating the faint cosmological signal, REACH opens a new window into the thermal and ionization history of the early Universe. Beyond its methodological advancements, REACH has the potential to address broader cosmological tensions. Its ability to constrain the timing and physics of reionization provides indirect insights into the nature of DM and DE. Additionally, deviations in the 21 cm signal from standard theoretical predictions could indicate new physics, such as interactions between baryons and DM or non-standard early heating mechanisms. These contributions place REACH at the forefront of innovative probes for resolving foundational challenges in cosmology.
- **Canadian Hydrogen Intensity Mapping Experiment (CHIME)**: Located at the Dominion Radio Astrophysical Observatory in Canada, CHIME [4239] operates in the 400–800 MHz band, corresponding to a redshift range of 0.8 to 2.5. Its primary goal is to map neutral hydrogen intensity across this range to measure the expansion history of the Universe. By producing the largest three-dimensional map of hydrogen intensity in this critical epoch, CHIME provides unprecedented insights into the large-scale structure of the Universe and probes cosmic evolution during the dark ages through the 21 cm transition line. In addition to tracing the evolution of structure, CHIME offers statistical constraints on BAO using the Hydrogen Intensity Mapping technique. These measurements enable synergistic analyses with other cosmological surveys, enhancing the precision of constraints on fundamental parameters like H_0 and the amplitude of matter fluctuations S_8. Since beginning operations in 2018, CHIME has already yielded significant data, with planned upgrades set to further improve the precision and resolution of intensity maps.
- **Giant Metrewave Radio Telescope (GMRT)**: Located near Pune, India, the GMRT [4268] is an array of 30 fully steerable parabolic dishes, each 45 m in diameter, operating in the frequency range of 50 MHz to 1.5 GHz. It is one of the most sensitive radio telescopes for low-frequency observations and plays a significant role in 21 cm cosmology. GMRT has been used extensively to study the 21 cm hydrogen signal from the Cosmic Dawn and the EoR. Its ability to probe neutral hydrogen at different redshifts provides critical insights into the thermal and ionization history of the IGM and the formation of the first luminous sources. In addition to EoR studies, GMRT contributes to understanding large-scale structures, galaxy formation, and the properties of DE and DM. As an established facility, GMRT continues to produce high-impact results and serves as a vital complement to ongoing and upcoming experiments such as LOFAR, HERA, and SKAO.
- **Five-hundred-meter Aperture Spherical Telescope (FAST)**: FAST [4269], located in Guizhou, China, is the world's largest single-dish radio telescope, with an aperture of 500 m. Operating in the frequency range of 70 MHz to 3 GHz, FAST is a highly versatile instrument capable of a broad range of astrophysical studies, including 21 cm observations. Its massive collecting area provides unparalleled sensitivity, making it an invaluable tool for studying neutral hydrogen in the Universe. FAST contributes to 21 cm cosmology by probing the large-scale distribution of hydrogen gas, investigating the EoR, and tracing the evolution of cosmic structures during the Cosmic Dawn. Its ability to perform both single-dish and interferometric measurements allows it to complement other instruments in the global effort to constrain models of cosmic evolution. Beyond 21 cm studies, FAST is used for pulsar searches, extragalactic surveys, and studies of ISM dynamics. With its extraordinary sensitivity and high precision, FAST is poised to make new contributions to our understanding of the early Universe and fundamental physics.
- **Hydrogen Intensity and Real-time Analysis eXperiment (HIRAX)**: Building on the technology of CHIME, HIRAX [1846] is located near the SKAO site in South Africa and is designed to achieve similar scientific objectives in the southern sky. Operating in the 400–800 MHz frequency band, HIRAX aims to map neutral hydrogen intensity over the redshift range of 0.8 to 2.5, providing critical insights into the evolution of the Universe during this epoch. The array consists of 1,000 closely packed 6 m radio dishes, which will create a high-resolution hydrogen intensity map of the southern sky using the 21 cm emission line. Initially conceived as a demonstration of SKAO technology, HIRAX has evolved into an ambitious project, poised to deliver a detailed three-dimensional map of large-scale structure in this redshift range. A primary science goal of HIRAX is to measure BAO signature in the matter distribution, enabling precise constraints on the expansion history of the Universe. HIRAX's southern sky coverage complements CHIME's northern sky observations, offering an opportunity for joint analyses to refine measurements of cosmological parameters, including H_0 and S_8.
- **Square Kilometre Array Observatory (SKAO)**: The SKAO [4245] is expected to begin operations for Phase 1 in the late 2020s, with sites located in Australia (covering low-frequency observations) and South Africa (mid-frequency observations). Together, these will form the world's largest radio telescope system, with a total collecting area of approximately 1 km^2, enabling unprecedented sensitivity and resolution. Operating across a frequency range of 50 MHz to 14 GHz, the SKAO will span a physical radius of roughly 3,000 km, hosting hundreds of radio dishes and over 100,000 antennas. By producing the most comprehensive 21 cm hydrogen intensity maps to date, the SKAO will probe the large-scale structure of the Universe, reaching back to the first galaxies and stars. This ambitious project will provide new insights into the EoR, the emergence of the first luminous sources, and the role of DE in shaping cosmic evolution. Additionally, it will complement other observational probes, offering synergies with WL, BAO, and CMB experiments to refine our understanding of cosmological tensions.

5.1.6. *Type Ia supernovae and distance ladder*

SNIa play a pivotal role in modern cosmology as highly reliable standard candles for measuring cosmic distances. By leveraging the uniform intrinsic luminosity of these SNIa, calibrated through the cosmic distance ladder, precise determinations of H_0 are possible. The cosmic distance ladder comprises several hierarchical steps: (1) geometric distance measurements using Cepheid variables, TRGB stars, masers, etc.; (2) calibration of SNIa luminosities based on these measurements; and (3) application of SNIa to measure H_0 in the Hubble flow, where cosmic expansion dominates. Recent advancements in distance ladder measurements have refined the determination of H_0, notably through Cepheid-calibrated SNIa in the SH0ES project, which reports a value significantly higher than early Universe estimates from the CMB. This discrepancy, known as the Hubble tension, remains one of the most pressing challenges in cosmology. Complementary approaches, including TRGB, Mira variables, and SBF methods, offer alternative calibrations and independent cross-checks, helping to ensure robustness and reduce systematic biases. However, all these methods consistently yield higher H_0 values than those derived from early Universe probes, highlighting the tension.

Future surveys and advanced instrumentation promise to transform SNIa measurements and distance ladder studies. JWST's unprecedented resolution has already begun improving Cepheid observations in crowded fields, while upcoming missions aim to reduce systematic uncertainties further. New facilities will also increase the number and diversity of SNIa observations, extending measurements to higher redshifts and improving statistical power. Below, we highlight ongoing and planned SN and distance ladder experiments and their contributions to addressing cosmological tensions.

- **Dark Energy Survey (DES)**: DES [4251], conducted from 2013 to 2019, used the 4-meter Blanco Telescope at Cerro Tololo Inter-American Observatory (CTIO) to observe approximately $5000\,\mathrm{deg}^2$ of the southern sky. DES contributed significantly to supernova cosmology by discovering and monitoring thousands of SNIa across a broad redshift range ($z \sim 0.01$ to 1.2). Its high-quality photometry enabled precise constraints on H_0 and DE properties. DES complements other distance ladder experiments by providing a statistically robust dataset of SNIa at intermediate redshifts, improving constraints on the cosmic expansion history and addressing potential systematics in supernova cosmology.
- **The Gaia mission**: Gaia [143], operating since 2013, has revolutionized the cosmic distance ladder by providing precise parallaxes for millions of stars, including Cepheid variables and TRGB stars. These highly accurate measurements are critical for calibrating the absolute luminosities of SNIa and improving the determination of the Hubble constant. Gaia's unparalleled astrometric precision significantly reduces uncertainties in the local distance scale and mitigates systematic biases in SNIa calibrations. By anchoring the first rung of the distance ladder, Gaia plays a key role in addressing the Hubble tension and refining our understanding of cosmic expansion.
- **Zwicky Transient Facility (ZTF)**: The ZTF [4270], operating since 2018 at the Palomar Observatory, utilizes a 48-inch Schmidt Telescope with a wide field of view ($47\,\mathrm{deg}^2$) for high-cadence transient surveys. ZTF has been instrumental in discovering and monitoring nearby SNIa, providing critical data for calibrating the distance ladder. By targeting local SNIa, ZTF supports precise measurements of H_0 and cross-validates calibrations derived from other standard candles, such as Cepheids and TRGB stars. Its extensive dataset complements space-based missions like Gaia and JWST by increasing the sample size of well-observed SNIa.
- **Nearby Supernova Factory (SNfactory)**: The SNfactory [4271], an international collaboration, focuses on obtaining detailed spectrophotometry of low-redshift SNIa. Using the SuperNova Integral Field Spectrograph (SNIFS) on the University of Hawaii's 2.2-meter telescope, SNfactory has been essential in characterizing the diversity of SNIa and improving standardization techniques. SNfactory's precise spectrophotometric data reduce systematic uncertainties in SNIa luminosities, refining the calibration of the distance ladder and improving constraints on H_0.
- **Asteroid Terrestrial-impact Last Alert System (ATLAS)**: Although primarily designed for asteroid detection, ATLAS [4272], operating on multiple telescopes in Hawaii, South Africa, and Chile, has made substantial contributions to supernova cosmology. Its wide field of view and high-cadence observations are well-suited for identifying and monitoring nearby SNIa. ATLAS's discoveries provide valuable data for calibrating the distance ladder, especially at low redshifts, complementing ground-based and space-based missions in improving the accuracy of H_0 measurements and addressing cosmological tensions.
- **James Webb Space Telescope (JWST)**: JWST [291], launched in 2021, provides unparalleled near-infrared imaging and spectroscopy, enabling precise observations of Cepheid variables and TRGB stars in crowded fields. These measurements significantly enhance the calibration of SNIa and improve the accuracy of H_0. JWST's ability to observe faint objects at high resolution allows it to extend the cosmic distance ladder to greater distances and reduce systematic uncertainties. By complementing ground- and space-based surveys, JWST plays a crucial role in addressing the Hubble tension and probing potential new physics beyond ΛCDM.
- **Rubin Observatory's Legacy Survey of Space and Time (LSST)**: The Rubin Observatory [4244], currently under construction in Chile, will conduct the LSST, a ten-year survey covering approximately $18,000\,\mathrm{deg}^2$ of the southern sky. With its 8.4-meter aperture and a 9.6-square-degree field of view, Rubin's LSST will discover and monitor hundreds of thousands of SNIa across a broad redshift range ($z \sim 0.01$ to 1.2). Rubin's LSST will revolutionize supernova cosmology by significantly increasing the sample size and improving statistical precision in measuring H_0. Its high-cadence, multi-band photometry will mitigate systematics such as dust extinction and host-galaxy effects, and its synergy with spectroscopic follow-up surveys will ensure robust classifications and redshift measurements.
- **Roman Space Telescope (formerly WFIRST)**: The Roman Space Telescope [896], scheduled for launch in the late 2020s, will perform a High Latitude Survey to observe thousands of SNIa across a broad redshift range ($z \sim 0.1$ to 2.0). With its wide field of view and high-resolution imaging in the near-infrared, Roman will extend the cosmic distance ladder, improving the precision and accuracy of the Hubble constant. Roman's deep multi-band photometry will reduce systematics like dust extinction and enhance the calibrations of standard candles. By complementing ground-based surveys such as Rubin's LSST and incorporating follow-up spectroscopy, Roman will play a critical role in resolving the Hubble tension.
- **Extremely Large Telescope (ELT)**: The ELT [4273], currently under construction in Chile, will leverage its 39-meter aperture and advanced adaptive optics to achieve unprecedented precision in SNIa observations. By providing high-resolution imaging and spectroscopy, the ELT will play a vital role in calibrating the distance ladder through Cepheids, TRGB stars, and direct measurements of SNIa in the local Universe. The ELT's ability to observe SNIa at higher redshifts will complement space-based surveys like Rubin's LSST and Roman, reducing systematic uncertainties and improving the determination of the Hubble constant.
- **Future Extremely Large Telescopes (GMT and TMT)**: Beyond the ELT, upcoming ground-based observatories such as the Giant Magellan Telescope (GMT) [4274] and the Thirty Meter Telescope (TMT) [4275] will significantly enhance SNIa and distance ladder measurements. With their large apertures of 24.5 meters (GMT) and 30 meters (TMT), these telescopes will provide unparalleled resolution and sensitivity, enabling precise observations of Cepheids, TRGB stars, and SNIa in both the local and high-redshift Universe. These telescopes will extend the reach of the distance ladder by detecting fainter Cepheids and SNIa at greater distances, improving calibration precision and reducing systematic uncertainties. Their advanced instrumentation will complement space-based missions like JWST and Roman by providing high-resolution follow-up spectroscopy and imaging, further refining H_0 and contributing to resolving the Hubble tension.

5.1.7. Time delay cosmography

The strong lensing of QSOs and SN offers a unique opportunity to measure the expansion rate of the Universe across different redshifts. This approach leverages the variable nature of these objects, enabling the use of the time-delay method — an independent high-redshift cosmological probe that does not rely on the distance ladder. The technique involves observing multiple images of a strongly lensed source, such as a QSO or SN, produced by an intermediary lensing

galaxy. The mass profile of this galaxy, combined with the respective distances between the observer, lens, and source, determines the offsets of the lensed images and is crucial for obtaining precise estimates of cosmological parameters.

This method relies on the time delays between light rays traveling along different paths, caused by both geometric differences in the light geodesics and the distribution of matter within the lensing galaxy. By accurately measuring these delays, the time-delay method provides an estimate of the Hubble constant, independent of large-scale structure parameters.

Strong lensing is inherently challenging due to the specific alignment required between the observer, lens, and source. Moreover, the rarity of suitable QSOs or SN reduces the probability of detection. Despite these challenges, over 300 strongly lensed QSOs have been identified to date, typically in the redshift range $\sim$ 1–3, with lensing galaxies found at redshifts $\sim$ 0.2–0.8. The lensed images are usually separated by a few arcseconds, well within the resolution capabilities of modern ground-based telescopes. Time delays ranging from a few days to a year are sufficient for accurate measurements, making the time-delay method a powerful tool for cosmology.

Below, we highlight ongoing and planned experiments leveraging the time-delay method and their contributions to measuring H_0 and addressing cosmological tensions.

- **Very Large Telescope Interferometer (VLTI)**: The VLTI [4276], operated by the European Southern Observatory (ESO), provides ultra-high angular resolution imaging through its interferometric array of telescopes. With its ability to resolve fine details in strongly lensed QSOs, VLTI plays a critical role in time-delay cosmography by enabling precise measurements of the lensing geometry and time delays. Its high spatial resolution is particularly useful for modeling lensing galaxies and reducing systematic uncertainties in the determination of H_0.
- **Atacama Large Millimeter/submillimeter Array (ALMA)**: ALMA [4277], located in Chile, offers unparalleled sensitivity and resolution for observing lensed submillimeter galaxies and QSOs. By measuring time delays in radio and submillimeter wavelengths, ALMA provides a complementary approach to optical time-delay cosmography, reducing systematic biases and refining constraints on the Hubble constant.
- **Keck Observatory**: The Keck Observatory [4278], located on Maunakea, Hawaii, features two 10-meter telescopes equipped with advanced adaptive optics systems. These capabilities allow Keck to obtain high-resolution imaging and spectroscopy of strongly lensed QSOs and SN, essential for precise time-delay measurements. Keck's sensitivity and angular resolution enable detailed modeling of lensing galaxies and accurate determination of light path geometries, contributing to independent constraints on H_0. Its role as a follow-up instrument for time-delay cosmography complements surveys like Rubin's LSST and Euclid, providing critical data for refining cosmological models.
- **Subaru Telescope**: The Subaru Telescope [4242], a 8.2-meter optical-infrared telescope located on Maunakea, Hawaii, plays a key role in observing strong lensing systems for time-delay cosmography. Equipped with instruments such as the HSC, Subaru excels at wide-field imaging and detailed follow-up of lensed systems. Subaru's capabilities allow it to identify and resolve lensed QSO systems and SN, particularly in crowded fields, enabling precise time-delay measurements. Its contributions to modeling lensing mass distributions and improving light path geometries are vital for reducing systematic uncertainties in the determination of H_0. Subaru serves as a valuable complement to space-based missions like Roman and ground-based facilities like Keck.
- **Euclid**: The Euclid mission [4241], covering a $14,000\,\mathrm{deg}^2$ area of the sky, is expected to observe approximately 170,000 strong lensing events during its lifetime. These events will provide valuable insights into the properties of DM halos in dwarf galaxies, the mass distribution within galaxies, and galaxy cluster structures in the redshift range $0 < z < 2$. Strong lensing events are inherently rare and require robust detection methods. To address this challenge, Euclid employs CNNs, which are trained on extensive simulated datasets to extract image features and identify strong lensing properties. These advanced pipelines allow for precise identification of lensing phenomena, including sharp Einstein rings, which are expected to be detectable down to an angular resolution of 0.5 arcseconds. Additionally, Euclid is anticipated to detect up to $\sim$ 2300 strongly lensed QSO sources, enabling precise measurements of time delays. The time-delay cosmography enabled by Euclid's high-resolution imaging will place stringent constraints on H_0, making it one of the most powerful tools for addressing cosmological tensions.
- **Rubin Observatory's Legacy Survey of Space and Time (LSST)**: The Rubin Observatory's [4244] unparalleled depth and sky coverage will enable the discovery of up to ten million QSOs over its operational lifetime, spanning a redshift range of $z \sim 0$–7. This extensive dataset will have profound implications for QSO-related physics, including strong lensing and time-delay cosmography. Rubin's LSST is expected to detect approximately $\sim$ 2600 time-delayed lensing systems, assuming optimistic projections. These systems will play a pivotal role in refining measurements of H_0 and probing the dynamical properties of DE at high redshifts. With its deep and wide survey capabilities, Rubin's LSST will significantly enhance the statistical precision of time-delay cosmography, providing critical insights into the expansion history of the Universe.
- **Roman Space Telescope (formerly WFIRST)**: The Roman Space Telescope [896], set to launch in the late 2020s, will make significant contributions to time-delay cosmography through its deep, high-resolution near-infrared imaging and wide field of view. Roman is expected to detect thousands of strongly lensed QSOs and SN, enabling precise measurements of time delays across a broad redshift range. With its exceptional sensitivity, Roman will identify and characterize lensing systems with high precision, including detailed modeling of lensing galaxies. These observations will reduce uncertainties in the Hubble constant H_0 and provide crucial constraints on the properties of DE. Roman's synergy with other surveys, such as Rubin's LSST, will further enhance the statistical power and accuracy of time-delay cosmography.
- **Square Kilometre Array Observatory (SKAO)**: The SKAO [4245], with its radio arrays in South Africa and Australia, will enable high-resolution observations of strongly lensed radio sources. By detecting and monitoring time-delayed radio-lensed systems, SKAO will provide independent measurements of H_0. Its sensitivity to faint radio signals and ability to resolve sub-arcsecond structures make it a powerful tool for time-delay cosmography.
- **Extremely Large Telescope (ELT)**: The ELT [4273], currently under construction in Chile, will leverage its 39-meter aperture to achieve unparalleled angular resolution and sensitivity. This will allow for detailed imaging and spectroscopy of strongly lensed QSOs and supernovae, facilitating precise time-delay measurements. The ELT's advanced instrumentation will help model lensing galaxies with greater accuracy, reducing uncertainties in the determination of the Hubble constant.
- **Thirty Meter Telescope (TMT)**: The TMT [4275], planned for construction in Hawaii or the Canary Islands, will provide high-resolution imaging and spectroscopic capabilities, enabling detailed observations of strongly lensed systems. By resolving lensed images with extreme precision, the TMT will contribute to time-

delay cosmography by improving measurements of H_0 and probing the dynamics of DE.

- **Giant Magellan Telescope (GMT)**: The GMT [4274], under construction in Chile, will utilize its segmented 24.5-meter primary mirror to achieve exceptional imaging and spectroscopic capabilities. Its high resolution and sensitivity will support time-delay cosmography by enabling precise modeling of lensed systems and accurate measurements of H_0, particularly at intermediate redshifts.

5.1.8. Fast radio bursts (FRBs)

FRBs are extremely bright, short-duration radio transients lasting only a few milliseconds, with the potential to serve as powerful tools for probing cosmology. Their extragalactic origin is supported by their large dispersion measures, which are observed to evolve with redshift. A significant number of FRBs have been localized to host galaxies, allowing their redshifts to be determined and their origins, such as possible magnetar emissions, to be studied.

Localized FRBs provide valuable insights into several cosmological phenomena, including the baryon fraction in the IGM, strong lensing events, the equivalence principle, the expansion history of the Universe, and the cosmic reionization history. The interaction of FRBs with the IGM makes them excellent probes of baryonic matter in these regions, as the interaction of radio signals with gas distributions offers a new perspective on the "missing baryon problem". Regarding the Hubble constant H_0, FRBs alone face degeneracies that limit their ability to directly constrain H_0. However, combining FRB data with complementary datasets such as CMB, BBN, or GW measurements breaks these degeneracies and enables precise cosmological constraints.

Below, we highlight the list of ongoing and planned experiments leveraging FRBs to address cosmological tensions and improve our understanding of the Universe's evolution.

- **Canadian Hydrogen Intensity Mapping Experiment (CHIME)**: CHIME [4239], situated in British Columbia, Canada, is a pioneering radio telescope designed to monitor transient radio signals, including FRBs. Its fixed-cylinder design and wide field of view allow CHIME to observe the sky continuously, detecting thousands of FRBs annually across a range of redshifts. This high detection rate enables the identification of rare FRBs suitable for cosmological studies, such as those with high dispersion measures or unique signatures that indicate strong lensing events. CHIME's advanced time-domain sensitivity is optimized for detecting short-duration radio transients, making it a valuable tool for measuring the arrival times of FRBs with high precision. These capabilities allow CHIME to constrain propagation effects, such as delays caused by intervening structures, which can be cross-referenced with GW studies to extract cosmological information. Its unparalleled FRB detection volume provides a complementary dataset for investigating the evolution of the cosmic expansion when paired with optical and GW experiments.
- **Australian Square Kilometer Array Pathfinder (ASKAP)**: ASKAP [4279], located in Western Australia, is a cutting-edge radio telescope optimized for detecting and localizing FRBs. Its unique combination of wide field-of-view and interferometric imaging capabilities allows ASKAP to efficiently detect and pinpoint FRBs to sub-arcsecond accuracy. This precise localization is critical for identifying host galaxies and determining redshifts of FRB sources. ASKAP's advanced beamforming technology enables the detection of high-redshift FRBs, providing insights into the IGM and the evolution of the cosmic expansion. Its ability to associate FRBs with host galaxies allows for independent constraints on H_0 when combined with other cosmological probes.
- **Upgrade of the Molonglo Observatory Synthesis Telescope (UTMOST)**: UTMOST [4280], located in Australia, is a reconfigured radio telescope optimized for detecting FRBs. Its high-cadence observing strategy makes it ideal for the real-time discovery and timing of FRBs, particularly at low redshifts. Although less sensitive than newer facilities, UTMOST's rapid response capability enables timely follow-up studies and statistical surveys of FRBs. By characterizing nearby FRBs, UTMOST complements high-sensitivity instruments such as ASKAP and FAST, contributing to our understanding of the local FRB population and its cosmological implications.
- **MeerKAT**: MeerKAT [4281], situated in South Africa, is a highly sensitive radio telescope designed for high-resolution imaging and precision timing, making it an invaluable tool for studying FRBs. Its wide frequency coverage and long baselines enable MeerKAT to detect faint and distant FRBs, particularly those at high redshifts, offering insights into the early Universe. MeerKAT excels in pinpointing FRB host galaxies and measuring dispersion measures with high precision. This allows for a detailed study of the large-scale structure of the Universe and the evolution of baryonic matter over cosmic time. MeerKAT also plays a complementary role to SKAO by serving as a pathfinder and refining techniques for future large-scale FRB surveys. Its contributions to the Hubble constant determination and reionization studies position MeerKAT as a crucial instrument for resolving cosmological tensions.
- **Five-hundred-meter Aperture Spherical Telescope (FAST)**: FAST [4269], located in Guizhou, China, is the world's largest single-dish radio telescope, offering unparalleled sensitivity for detecting faint and distant FRBs. Its ability to detect FRBs with extremely high signal-to-noise ratios enables precise measurements of dispersion measures and localization for follow-up studies. FAST contributes significantly to cosmology by detecting high-redshift FRBs and analyzing their interaction with the IGM. Its sensitivity allows it to probe the cosmic expansion and test reionization models, complementing large-scale surveys such as SKAO and CHIME. FAST's unique capabilities make it a critical instrument for advancing FRB-based cosmological studies.
- **Deep Synoptic Array (DSA-110)**: The DSA-110 [4282], located in California, is a dedicated radio array designed exclusively for detecting and localizing FRBs. With 110 antennas operating in the 1.28 GHz band, the array achieves sub-arcsecond localization accuracy, enabling precise identification of FRB host galaxies. DSA-110's focus on real-time detection and localization provides critical insights into the redshift distribution of FRBs and their cosmological applications. By linking FRBs to their host environments, DSA-110 contributes to breaking degeneracies in cosmological parameter estimation, particularly when combined with other datasets such as GW observations and optical surveys.
- **Giant Metrewave Radio Telescope (GMRT)**: The GMRT [4268], located in Pune, India, has been instrumental in studying FRBs at low radio frequencies. Its unique sensitivity and wide frequency coverage make it a valuable tool for characterizing the spectral properties of FRBs and their interaction with the IGM. GMRT has been used for follow-up observations of FRBs detected by other instruments, particularly at frequencies below 800 MHz. These observations complement higher-frequency detections by telescopes like CHIME and ASKAP, providing new insights into FRB emission mechanisms and their propagation through cosmic structures. While not a dedicated FRB facility, GMRT's versatility and precision continue to support advancements in FRB cosmology.
- **Very Large Array Low-band Ionosphere and Transient Experiment (VLITE)**: VLITE [4283], operating on the Very Large Array (VLA), focuses on low-frequency transient detection, including FRBs. Its ability to monitor the sky continuously allows it to

identify faint FRBs and investigate their spectral properties at lower frequencies.

- **Square Kilometre Array Observatory (SKAO)**: The SKAO [4245], under construction in South Africa and Australia, is poised to become the largest and most sensitive radio telescope array in the world. Its exceptional capabilities will enable precise localization of FRBs at sub-arcsecond resolution and direct measurement of their redshifts, significantly advancing FRB cosmology. By detecting and studying FRBs across a broad redshift range, SKAO will provide insights into the evolution of the IGM, reionization history, and cosmic expansion. Its ability to map dispersion measures over cosmic time will complement other datasets, such as GW observations and optical surveys, to break degeneracies in cosmological parameters, including H_0. While its primary focus is on large-scale structure studies through 21 cm intensity mapping, SKAO's FRB-specific contributions, including redshift localization and host galaxy characterization, make it a new instrument for addressing cosmological tensions.
- **Next Generation Deep Synoptic Array (DSA-2000)**: DSA-2000 [4284], a planned expansion of the DSA-110, will feature 2000 antennas, dramatically increasing sensitivity and detection rates for FRBs. This next-generation array will provide precise localization for tens of thousands of FRBs across a wide redshift range. With its enhanced capabilities, DSA-2000 will enable detailed studies of the cosmic expansion, baryon distribution, and reionization history.
- **Low-Frequency Array (LOFAR2.0)**: LOFAR2.0 [1148], an upgraded version of the Low-Frequency Array, will provide enhanced sensitivity and temporal resolution for detecting FRBs at low frequencies. Its broad frequency coverage and improved capabilities will allow it to probe previously inaccessible redshift ranges for FRBs, making it a unique tool for studying the early Universe. LOFAR2.0's ability to detect low-frequency FRBs will contribute to understanding their emission mechanisms and their interaction with the IGM.
- **APERTure Tile In Focus (Apertif)**: Apertif [4285], an upgrade to the Westerbork Synthesis Radio Telescope (WSRT) in the Netherlands, provides wide-field imaging for detecting FRBs. Its combination of sensitivity and survey speed enables it to identify transient events, contributing to population studies of FRBs and complementing other instruments in the field.
- **Burst Transient Telescope (BURSTT)**: BURSTT is a planned experiment designed to search for FRBs with enhanced detection rates and localization capabilities. Its wide field of view will make it particularly effective in identifying high-redshift FRBs and improving constraints on their cosmological applications.
- **Canadian Hydrogen Observatory and Radio-transient Detector (CHORD)**: CHORD [4286], a planned successor to CHIME, will combine higher sensitivity with improved localization capabilities for FRBs. CHORD is expected to detect tens of thousands of FRBs across a broad redshift range, providing critical insights into the evolution of cosmic structures and addressing cosmological tensions.
- **Pathfinder for Real-time Extragalactic Cosmic Intensity Survey Experiment (PRECISE)**: PRECISE is a dedicated pathfinder for FRB studies, focusing on real-time detection and precise localization of FRBs. It will enhance the study of their host galaxies and the IGM, making it a valuable addition to the next generation of FRB experiments.

5.1.9. *Line-intensity mapping*

The large-scale structure of the Universe can be surveyed through the radiation intensity emitted by gas clouds, in a manner similar to galaxy surveys, but without resolving individual sources. This approach significantly accelerates the survey process. While many surveys focus exclusively on the 21 cm line associated with the hyperfine transition of neutral hydrogen, line-intensity mapping (LIM) extends this technique to include additional spectral lines, such as carbon monoxide (CO) and ionized carbon (CII), which provide complementary tracers of large-scale structure and galaxy evolution. The intensity distribution maps derived from LIM can be translated into matter fluctuation power spectra and enable studies across a broader range of cosmic epochs.

Unlike traditional 21 cm experiments, which focus specifically on the neutral hydrogen distribution, LIM captures the integrated emission of multiple spectral lines, making it a more versatile approach. This broader capability allows LIM to probe different phases of the ISM and the EoR, as well as to reduce parameter degeneracies by spanning a wider range of redshifts and tracers.

This innovative technique employs angular resolution observations to trace the spatial distribution of matter, even at high redshifts where traditional galaxy surveys face challenges. If foreground contamination can be effectively mitigated, line-intensity mapping has the potential to (1) provide wide redshift coverage, averaging out cosmological parameter degeneracies across different redshifts, (2) yield large-scale information that could reveal signatures of inflation and gravitational effects, and (3) access matter density modes that are less affected by non-linear physics. By complementing 21 cm experiments, LIM plays a critical role in addressing cosmological tensions, such as the H_0 and S_8 discrepancies. Its ability to combine data from multiple spectral lines and explore different epochs of cosmic evolution allows it to test new models of DE, modifications to gravity, and other potential extensions to the standard cosmological model.

The further development of this technique will require advancements in millimeter-wave detectors and the refinement of data analysis methods to mitigate astrophysical and modeling systematics. Below, we identify the key ongoing and planned experiments leveraging line-intensity mapping to study cosmic large-scale structures and the EoR using this method.

- **The Hobby-Eberly Telescope Dark Energy Experiment (HETDEX)**: HETDEX [4287] is a groundbreaking survey leveraging line-intensity mapping of Lyman-α emitters to study the large-scale structure of the Universe. By mapping the intensity distribution of Lyman-α emission over the redshift range $1.9 < z < 3.5$, HETDEX provides insights into the matter power spectrum and the evolution of cosmic structures during a pivotal epoch in the Universe's history. HETDEX's line-intensity mapping measurements play a crucial role in addressing cosmological tensions by offering independent constraints on large-scale structure and its growth, as well as the expansion history of the Universe. Additionally, HETDEX's use of intensity mapping reduces reliance on resolving individual sources, enabling efficient surveys of faint, distant cosmic structures.
- **CO Mapping Array Project (COMAP)**: COMAP [4249] is a pioneering experiment designed to map the large-scale structure of the Universe through intensity mapping of the CO rotational transition lines. By targeting the $z \sim 2.4 - 3.4$ redshift range, COMAP traces the distribution of molecular gas in galaxies during the peak of star formation activity, offering insights into galaxy evolution and the assembly of cosmic structures. COMAP plays a crucial role in addressing cosmological tensions by providing independent constraints on the large-scale matter distribution and the expansion history.
- **CarbON CII line in post-rEionization and ReionizaTiOn epoch (CONCERTO)**: CONCERTO [4288] is a state-of-the-art experiment designed to study the large-scale structure of the Universe using line-intensity mapping of the [CII] emission line. Operating in the redshift range $4.5 < z < 8.5$, CONCERTO aims to trace the distribution of ionized carbon during the EoR and the early stages of galaxy formation. By capturing the integrated [CII] signal from unresolved sources, it provides a unique probe of the

ISM and star formation in high-redshift galaxies. CONCERTO's sensitivity to high-redshift structures complements other intensity mapping experiments and traditional surveys, enabling a more detailed understanding of reionization-era physics and its connection to late-time cosmological parameters. Furthermore, by probing large-scale modes, CONCERTO helps refine models of DE, inflation, and modifications to gravity, providing new insights into the underlying causes of cosmological tensions.

- **Spectro-Photometer for the History of the Universe, Epoch of Reionization, and Ices Explorer (SPHEREx)**: This proposed all-sky survey aims to provide spatial distribution data using various tracers to explore different cosmic eras [4248]. The survey will utilize the Hα, Hβ, and [OIII] lines to probe $0.1 < z < 5$, $0.5 < z < 2$, and $0.5 < z < 3$, respectively, mapping low-redshift gas clouds. The higher redshift range, spanning $5.2 < z < 8$, will be investigated using the Lyman-α line, providing a direct probe of the EoR. By spanning a wide range of redshifts and utilizing multiple spectral lines, SPHEREx can help address cosmological tensions, such as the H_0 and S_8 discrepancies, by providing independent measurements of large-scale structure growth and the expansion history of the Universe.
- **Tomographic Ionized-Carbon Mapping Experiment (TIME)**: TIME [4289] is designed to probe the EoR by mapping the redshifted 157.7 μm emission line of singly ionized carbon ([CII]) over the redshift range $5 \lesssim z \lesssim 9$. In addition, it observes carbon monoxide (CO) rotational transitions from galaxies at intermediate redshifts $0.5 \lesssim z \lesssim 2$. These measurements aim to trace the early stages of galaxy formation and star formation history, providing a complementary view of large-scale structure during key epochs in cosmic evolution.
- **The Cosmic Dawn Intensity Mapper (CDIM)**: CDIM [4290] is a proposed space-based mission designed to explore the large-scale structure of the Universe through line-intensity mapping of multiple spectral lines. By targeting key tracers such as hydrogen Lyman-α, Hα, Hβ, and [OIII], CDIM will probe a wide redshift range, spanning from the EoR ($6 < z < 10$) to the era of peak star formation ($z \sim 2$). These measurements will provide a comprehensive view of the distribution of ionized and molecular gas, as well as star formation processes. CDIM's ability to map the matter distribution across a wide range of redshifts and tracers reduces parameter degeneracies and systematic uncertainties. By bridging the gap between early- and late-time probes, CDIM provides complementary data to galaxy surveys and CMB experiments. Additionally, its sensitivity to faint, diffuse emission makes it a powerful tool for studying large-scale modes that are less accessible with traditional surveys.
- **Fred Young Submillimeter Telescope (CCAT-prime)**: CCAT-prime [4291], equipped with the advanced Prime-Cam instrument, is designed to perform line-intensity mapping of emission lines such as [CII] at redshifts relevant to the EoR and cosmic dawn. By tracing the [CII] line, along with other potential tracers, CCAT-prime aims to explore the star formation history, the ISM, and the role of galaxies in reionizing the early Universe. Its high-altitude site and state-of-the-art instrumentation provide exceptional sensitivity for mapping large-scale structure during key phases of cosmic evolution.

5.1.10. Potential new probes

As our understanding of the Universe deepens, new observational techniques and theoretical frameworks are being developed to challenge existing paradigms and explore unresolved tensions in cosmology. These potential new probes leverage advanced technologies and novel methodologies to address persistent discrepancies in key cosmological parameters, such as the Hubble constant H_0, the amplitude of matter fluctuations S_8, etc. By pushing the boundaries of precision measurements and theoretical modeling, these probes aim to uncover new physics or systematic effects that may underlie these tensions.

This section explores these innovative probes, highlighting their potential contributions to resolving the current challenges in cosmology and paving the way for new discoveries about the Universe.

- **Visible and Infrared Survey Telescope for Astronomy (VISTA)**: VISTA [4292] is a ground-based facility dedicated to wide-field surveys in the visible and near-infrared wavelengths. Equipped with an advanced infrared camera, VISTA is uniquely suited to mapping the large-scale structure of the Universe by detecting galaxies and QSOs at high redshifts. Its unprecedented sensitivity and wide-field capabilities allow it to probe the cosmic web, trace the distribution of matter, and explore the evolution of structures over cosmic time. By providing precise measurements of galaxy clustering and WL signals, VISTA contributes to addressing key cosmological tensions, such as those related to the amplitude of matter fluctuations S_8 and the Hubble constant H_0. Furthermore, its ability to survey large areas of the sky with high resolution offers unique opportunities to identify deviations from standard cosmological models, potentially unveiling signatures of new physics.
- **Transient High-Energy Sky and Early Universe Surveyor (THESEUS)**: THESEUS [655] is a proposed space-based mission designed to explore the high-energy transient sky and study the early Universe. By detecting GRBs from the first generation of stars (Pop III stars) and other energetic phenomena, THESEUS provides a unique probe into the era of cosmic reionization and early star formation. THESEUS combines wide-field monitoring and precise localization of GRBs with follow-up spectroscopy, enabling measurements of the cosmic star formation rate and the chemical enrichment history of the Universe. Its ability to observe the high-energy sky at unprecedented sensitivity offers a complementary approach to resolving cosmological tensions, such as refining constraints on the matter density parameter ($\Omega_{\mathrm{m},0}$) and testing models of DE. By bridging the gap between high-energy astrophysics and cosmology, THESEUS represents a transformative tool for uncovering new physics and deepening our understanding of the early Universe.
- **Quasars as Geometric Rulers**: QSOs, the luminous cores of AGN, offer a novel approach to cosmological measurements by serving as geometric rulers. Their variability over time, combined with precise measurements of time delays in gravitationally lensed QSOs, enables the determination of absolute distances in the Universe. This method bypasses many of the traditional assumptions in standard candles or rulers, providing an independent means of measuring H_0 and testing the expansion history of the Universe. In addition to their role in time-delay cosmography, QSOs also probe the large-scale structure of the Universe through clustering and absorption-line studies. This dual utility allows QSOs to contribute to resolving tensions in cosmological parameters, such as H_0 and S_8. Their utility as geometric rulers and tracers of structure represents a powerful avenue for exploring deviations from the standard cosmological model.
- **Redshift Drift with ANDES (ArmazoNes High Dispersion Echelle Spectrograph)**: ANDES, a planned instrument for the ELT, offers a unique opportunity to measure the redshift drift — a direct, model-independent observation of the Universe's expansion history. By observing spectral lines of distant QSOs and tracking their subtle changes over decades, ANDES aims to detect the tiny redshift drift predicted by the standard cosmological model. This groundbreaking method provides a direct probe of the dynamics of the Universe, bypassing the need for distance ladder calibrations or assumptions about standard candles or rulers. By directly measuring the acceleration or deceleration

of cosmic expansion, ANDES will place new constraints on DE, modifications to gravity, and the fundamental properties of the Universe. Its unparalleled precision makes it a new tool for addressing unresolved tensions in cosmological parameters.

- **CMB Spectral Distortions**: Deviations from a perfect blackbody spectrum of the CMB encode information about energy injections in the early Universe. These distortions arise due to processes such as Silk damping of primordial perturbations, decaying or annihilating particles, and early structure formation. The two primary types of distortions, μ-distortions (sensitive to energy injections at $z \gtrsim 10^5$) and y-distortions (from later energy injections), provide a complementary approach to testing the standard ΛCDM model. Measurements of spectral distortions could reveal signatures of new physics, including primordial non-Gaussianity, modifications to the recombination history, or interactions between DM and radiation. Future space missions such as *PIXIE* and *PRISM* aim to achieve the required sensitivity to detect these distortions, opening new avenues for cosmological exploration.
- **Lunar Astronomy**: Lunar astronomy [4293], leveraging the unique environment of the Moon, presents a groundbreaking opportunity to probe the cosmos in ways that are challenging or impossible from Earth. The Moon's lack of atmosphere eliminates atmospheric distortions, enabling precise observations across a wide range of wavelengths, including radio, infrared, and X-rays. Furthermore, the Moon's far side provides an unparalleled radio-quiet environment, ideal for low-frequency observations of the early Universe, including the cosmic dawn and the EoR. Lunar observatories have the potential to address cosmological tensions by providing high-precision measurements of large-scale structure, the CMB, and the 21 cm signal from neutral hydrogen. Additionally, their stable environment offers the possibility of ultra-long-term observations, enabling direct measurements of cosmological parameters such as the Hubble constant and constraints on the nature of DE. By extending observational capabilities beyond Earth-based and space-based platforms, lunar astronomy could transform our understanding of the Universe.

5.2. Recommendations

The open question of **cosmic tensions presents a unique opportunity** to reassess how observational measurements in cosmology are reconciled with physical models through diverse data analysis approaches. This may signal a turning point in our understanding of how to interpret measurements, particularly in the presence of potential systematics at a fundamental level. Such a systematic effect would need to manifest across all phenomena in local distance ladder measurements or be ubiquitous in early-time measurements. Another possibility is the emergence of new, independent measurements that do not rely on either the distance ladder or early Universe constraints. In particular, advances in GW astronomy, where standard sirens provide a novel approach to constructing distance scales, hold great promise. While this method remains in its early stages and has yet to reach the precision required to compete with traditional approaches, its continued development — particularly with upcoming detectors such as LISA and third-generation ground-based observatories — could play a crucial role in resolving cosmic tensions in the future.

A key tool in analyzing observational data and potential systematics, alongside the exploration of fundamental physics theories, is the application of data analysis methods. Traditionally, data analysis has relied on Bayesian statistical techniques, both for interpreting observational data and for comparing physical models. However, there is growing interest in developing frequentist approaches more broadly, given their reduced dependence on prior information. At the same time, there is strong motivation to advance statistical methods that leverage the broad range of ML techniques. These include supervised learning approaches such as GP, as well as unsupervised methods like neural networks. The development of toolkits based on these statistical frameworks holds significant potential, both in enhancing the extraction of information from observational data and in refining model-building strategies. In particular, such tools could provide valuable insights into fundamental physics by systematically addressing the open issues surrounding cosmic tensions. It will be essential to integrate these methodologies into standard analysis pipelines for upcoming large-scale surveys.

A plethora of physically motivated fundamental physics theories have been studied in recent years, with particular attention given to their connection to resolving the open problem of cosmic tensions and associated questions within the standard model of cosmology. These efforts have focused on further developing geometric gravity, exploring potential physics beyond the standard model of particle physics, and investigating emergent phenomenology and possible quantum gravity effects. On the other hand, many practical theories in these approaches were originally motivated by theoretical or semi-physical considerations. The further integration of the growing body of observational evidence into the development of new classes of physical theories will drive the next generation of cosmological models, aligning them with the most pressing questions from observational surveys. Additionally, the use and advancement of model-building toolkits will contribute to the creation of physically motivated theoretical models that address cosmic tensions while preserving the successes of the current standard model of cosmology.

The breadth of observational surveys has been reviewed in Section 2, where their potential systematics are discussed in detail. In Section 3, recent developments in traditional data analysis approaches are examined alongside discussions of emerging statistical tools that are expected to become competitive in the coming years, including those based on ML methods. The development of new physically motivated fundamental theories is explored in Section 4, with a focus on their potential to resolve cosmological tensions while preserving the successful elements of the current standard model of cosmology. The future of the field will depend not only on the advancement of each of these areas individually but also on the ability of the community to integrate these diverse approaches into a coherent framework to address the growing challenges posed by cosmic tensions. This effort will require close collaboration between observational cosmologists, data analysts, and fundamental physicists. In the coming decade, it will be essential to:

- Leverage next-generation observational surveys to improve the precision of key cosmological parameters and systematically test for hidden systematics.
- Incorporate advanced statistical techniques, including ML-based inference methods and profile likelihood approaches, into standard cosmological pipelines.
- Continue developing theoretical models that remain consistent with observational constraints while addressing the root causes of cosmological tensions.
- Encourage interdisciplinary collaboration between observational, computational, and theoretical communities to ensure that different approaches are synthesized into a cohesive framework.

Resolving the cosmic tensions represents a defining challenge for the cosmology community. Success in this endeavor will require a concerted effort across multiple fronts, balancing innovative new techniques with a rigorous assessment of existing methodologies. By systematically integrating new data, analysis techniques, and theoretical advancements, the next decade of cosmological research has the potential to transform our understanding of the Universe's fundamental properties.

Challenges in observational cosmology:

- **Cepheid variables** — The next generation of ground- and space-based optical surveys will provide deep time-series observations of distant galaxies, expanding the volume over which the universality of the period–luminosity relation can be tested. These observations will also improve our understanding of the impact of metallicity in different environments. As new Cepheids are discovered and observational precision increases, reducing uncertainties in Cepheid measurements will require better constraints on dust reddening, zero-point corrections in Cepheid parallaxes, and new geometric anchors in the distance ladder.
- **Masers** — Systematics in megamaser-hosting galaxies, such as non-circular orbits and non-gravitational forces, do not significantly impact constraints on cosmological parameters. However, the primary challenge for maser-based techniques lies in discovering new high-quality megamaser-hosting galaxies suitable for precise distance measurements.
- **Tip of the Red Giant Branch (TRGB)** — This method relies on a statistical approach to standardizing TRGB stars, making the calibration process a critical aspect of the analysis. The main challenges in applying the TRGB method include (1) potential imbalances between TRGB and calibrating galaxy brightness intensities, (2) the need for accurate calibration of the target field, and (3) effective outlier detection methods for poorly sampled LFs.
- **Mira variables** — Oxygen-rich Mira stars can serve as anchors in the first rung of the distance ladder for calibrating absolute magnitudes. However, their luminosity, color, large angular size, and surface variations introduce significant uncertainties in parallax measurements. On the second rung, the number of known Mira stars remains low, presenting an opportunity for future observations to expand their use in distance calibration.
- **Type Ia supernovae** — SNIa primarily appear in the second and third rungs of the three-rung distance ladder. Their systematics are among the most extensively studied and best mitigated. However, the effects of (1) calibration systematics, (2) redshift-dependent biases in the third rung, and (3) stellar physics and sample selection may each contribute to potential changes in the estimates of certain cosmological parameters. Another challenge in this sector is the potential expansion of the distance ladder framework to include higher or lower rungs.
- **J-regions of the asymptotic giant branch (JAGB)** — This is a relatively new but promising method for extending the distance ladder. The primary challenges for establishing this approach as a robust distance indicator include a better understanding of the effects of metallicity, atmospheric influences on photometry, and variations in pulsation across different stellar populations.
- **Type II supernovae** — SNII offer an independent path to circumvent SNIa systematics while introducing different systematic considerations. This method has the potential to achieve greater precision with the addition of further calibrators and a better understanding of how spectroscopic data can be leveraged to improve the standardization procedure.
- **Surface brightness fluctuations (SBF) methods** — SBF-based methods have shown promise in constraining distances to very distant galaxies, relying primarily on imaging data. The next generation of optical telescopes will provide opportunities to refine these techniques further. Given the statistical nature of the approach, a deeper understanding of stellar population studies and peculiar evolutionary stages will help reduce systematic uncertainties. Addressing these factors will enable SBF to continue improving as a robust method for constraining cosmological parameters.
- **Cosmic chronometers** — This method has the advantage of being theoretically economical in terms of its underlying assumptions while providing a direct numerical measurement of the Hubble parameter in redshift space. Beyond the need to increase the number of measurements using this approach, some systematic challenges include (1) uncertainties in stellar metallicity estimates, (2) errors in star formation history modeling and underlying assumptions, and (3) contamination by young or star-forming outliers.
- **HII galaxies** — These galaxies are characterized by bursts of massive star formation, and their strong emission in specific spectral lines makes them valuable probes for high-redshift cosmology. However, for this method to become more robust, several systematics need to be addressed, including (1) improved physical modeling of emission line width profiles, (2) better understanding of stellar age effects, (3) corrections for extinction-induced deformations in emission lines, and (4) refined metallicity distribution calibrations.
- **Baryonic Tully–Fisher relation methods** — The Tully–Fisher and BTFR can be applied to cosmology to constrain the Hubble constant, given an underlying cosmological model. While this method offers good control over systematics, the relatively small number of observed galactic objects currently limits its competitiveness compared to other techniques. This limitation will be addressed with upcoming large-scale surveys. On the modeling side, further development may help reduce model dependence, for instance, by incorporating ML techniques into the analysis.
- **Strong lensing and time-delay cosmography** — Strong lensing provides a distance-ladder-independent method for measuring H_0 through time-delay cosmography. However, several systematics currently limit its precision, including uncertainties in lens mass modeling, the impact of line-of-sight structures, and degeneracies in the inferred time delays. Additionally, assumptions about mass profile parametrizations can introduce biases in cosmological constraints. Improving this technique will require higher-resolution imaging, better characterizations of lens environments, and larger statistical samples of well-measured lensing systems to reduce both statistical and systematic uncertainties.
- **Gravitational wave astronomy** — Free from electromagnetic radiation, GW cosmology provides uniquely independent methods to constrain cosmological parameters, separate from all other approaches. Standard sirens offer the additional advantage of serving as absolute distance indicators, making them independent of a cosmological model in determining the Hubble constant. However, an electromagnetic counterpart is required to identify the host galaxy, which is then used to infer certain galactic properties; alternatively, statistical methods utilizing galaxy catalogs can be employed. On the other hand, dark sirens suffer from potential systematics related to assumptions about galactic properties.
- **Cosmic microwave background (CMB) radiation** — Like other observatories, CMB experiments are subject to instrumentation systematics and internal tensions, which can be more pronounced given the precision of the measurements and the vast volume of data collected. Ensuring consistency between high- and low-multipole analyses in cosmological parameter estimation remains a critical challenge for future CMB surveys. The next generation of CMB experiments will aim to minimize instrumental and astrophysical systematics, improving constraints on fundamental physics. By reducing these contamination effects, it may even become possible to robustly measure B-mode polarization, which remains a crucial target for detecting primordial GWs and probing inflationary physics.
- **Baryon acoustic oscillations (BAO)** — This method enables robust cosmological analyses based on millions of extragalactic

objects. However, its statistical nature introduces a number of systematics that must be carefully accounted for. One key challenge is that the source density field is displaced due to peculiar motions, particularly in low-redshift regions, which is corrected using density field reconstruction techniques. As more galaxies are observed with higher precision, these reconstruction methods must continue to improve. Another important aspect of BAO surveys is the reliance on an underlying fiducial cosmology to transform between coordinate systems. While the influence of this model is relatively small, developing techniques to further reduce this dependence remains a priority. Additionally, BAO measurements are taken relative to the sound horizon, introducing another model-dependent feature that should be further refined to minimize its impact.

- **Galaxy clustering** — The growth of large-scale structures can be inferred from the statistical clustering of galaxies in redshift space, which depends on estimates of correlation functions and power spectra. The statistical nature of these measurements introduces several systematics, including those originating from measurement techniques (such as atmospheric and extragalactic extinction corrections), galaxy survey systematics (such as calibration errors and foreground contamination), and uncertainties in nonlinear modeling for redshift-space galaxy clustering.
- **Large-scale structure and higher-order statistics** — Beyond two-point statistics such as the galaxy correlation function and power spectrum, higher-order statistics and cosmic web topology provide additional tools to probe cosmology. Measurements of cosmic voids, filament structures, and the bispectrum offer sensitivity to non-Gaussianities and potential modifications to gravity. The main challenges in this sector include modeling nonlinear structure formation, correcting for observational systematics, and integrating these statistics into existing cosmological frameworks.
- **Weak lensing** — Weak gravitational lensing surveys rely on statistically significant samples of galaxies, introducing several challenges that must be addressed. These include uncertainties in individual galaxy redshift estimates due to the inherent limitations of photometric redshift determinations, systematic biases in shear and shape ellipticity measurements, and difficulties in accurately modeling nonlinearities in the matter power spectrum. Improving these aspects will be essential for maximizing the precision of WL constraints on cosmological parameters.
- **Galaxy cluster counts** — Galaxy clusters are the largest gravitationally bound structures in the Universe and are highly sensitive to cosmic evolution and the underlying cosmological parameters. Aside from the challenge of distinguishing how different cosmological models affect cluster evolution, a major issue in this method is the mass calibration problem. This refers to the relationship between the total halo mass and observable cluster properties, which is crucial for using cluster counts as a cosmological probe. The primary method for determining halo masses is WL, which itself introduces additional systematic uncertainties. As survey data become more precise, the mass calibration problem will increasingly become a limiting factor in the effectiveness of this approach.
- **Quasar and GRB distance ladder** — Both QSOs and GRBs have shown strong potential as probes of the high-redshift Universe, providing constraints across multiple cosmological parameters. However, their precision remains limited compared to other methods, partly due to systematics related to the physical nature of the sources, which remain an active area of discussion in the literature. Resolving these open questions would significantly enhance the statistical power of cosmological parameter constraints when these data are used in combination with other survey observations.
- **Fast radio bursts (FRBs)** — The relatively recent discovery of FRBs provides a powerful new probe of cosmological models. These events have shown promising potential to independently constrain the Hubble constant, as well as other cosmological parameters, particularly offering insights into the matter density parameter within ΛCDM. However, systematics related to the modeling of DM contributions and the IGM remain crucial open questions for this technique. Refinements in these areas will be necessary to improve its precision.
- **Radio background excess** — The discrepancy between the expected emission from known astrophysical and cosmological sources and the observed brightness in the electromagnetic spectrum presents an anomaly in the radio segment of the spectrum. Resolving this requires a careful balance in accounting for infrared radiation production in early galaxies, X-ray contributions affecting inverse Compton scattering of CMB photons, the depth of the 21 cm signal, and constraints from the cross-correlated angular power spectrum with optical sources. The next generation of observatories has the potential to refine and test possible explanations for this excess signal.
- **Bulk flow measurements** — The average peculiar velocity of a statistically significant sample of galaxies should diminish at sufficiently high redshifts. However, measurements of bulk flows face several challenges, including large uncertainties in peculiar velocity estimates and biases in the spatial distribution of observed galaxies. Recent studies have suggested that bulk flow magnitudes increase with distance, a result that appears counterintuitive. Addressing this challenge will require the continued development of bulk flow measurement techniques, as well as improved observational data quality at higher redshifts.
- **Cosmic dipole and anisotropies** — The observed CMB dipole is expected to be consistent with the dipole measured in other astrophysical tracers. However, discrepancies in dipole measurements using different observational datasets suggest the possibility of systematic effects or new physics. Additionally, potential anisotropies in cosmological parameters such as H_0 and S_8 challenge the assumption of statistical isotropy. Addressing these issues requires improved methodologies and cross-correlations between independent datasets to test for underlying systematics or signatures of new physics.
- **Cross-correlations between cosmological probes** — Combining different observational techniques provides a means to reduce systematics and improve cosmological parameter constraints. Key cross-correlations include (1) WL and galaxy clustering to calibrate galaxy bias and structure formation models, (2) CMB lensing and large-scale structure to refine DM distribution models, and (3) standard sirens and BAO measurements to independently test the cosmic expansion history. As observational precision improves, cross-correlations will become increasingly important in resolving cosmological tensions.
- **21 cm intensity mapping** — The neutral hydrogen 21 cm signal provides a powerful method to trace the large-scale structure of the Universe across a wide range of redshifts. This technique has the potential to probe the cosmic dawn, reionization, and the post-reionization epochs, offering insights into the distribution of matter over cosmic time. However, several challenges must be addressed, including foreground contamination from astrophysical sources, calibration uncertainties, and the need for precise theoretical modeling of the signal's evolution.
- **Line-intensity mapping (LIM)** — LIM provides a promising method to trace large-scale structure by measuring integrated emission from spectral lines such as CO and Lyman-α rather than relying on resolved galaxy surveys. This method has the potential to map cosmic structure at high redshifts, but faces

challenges such as foreground contamination and the need for precise theoretical modeling.

- **Sunyaev-Zel'dovich (SZ) and X-ray surveys** — Measurements of galaxy clusters using the SZ effect and X-ray emission offer valuable constraints on cosmic structure formation and expansion. However, systematic uncertainties related to gas physics, temperature profiles, and mass calibration remain key challenges.
- **Multi-messenger cosmology** — Observations across multiple cosmic messengers, including electromagnetic signals, GWs, and high-energy particles, provide new opportunities for constraining cosmological parameters and testing fundamental physics. By combining information from different observational channels, multi-messenger approaches can help break degeneracies inherent in individual methods. However, challenges remain, including the low detection rates of some sources, difficulties in precise localization, and uncertainties in the modeling of extreme astrophysical environments.
- **Neutrino Cosmology** — Neutrinos remain among the least understood fundamental particles, and their extremely weak interactions make direct measurements of their properties exceptionally difficult. A key open question is whether these particles have a nonzero mass. Moreover, terrestrial neutrino oscillation experiments provide constraints that appear to contrast with indirect cosmological measurements, potentially hinting at physics beyond the Standard Model in the neutrino sector. Reconciling these discrepancies will require further advancements in both laboratory-based and cosmological neutrino studies.

Challenges in the development of numerical and data analysis tools:

- **Model constraints in conjunction with Bayesian statistics** — Bayesian statistical methods have been widely used to constrain cosmological model parameters against observational data, and they now feature a broad suite of tools designed to meet these challenges. However, as survey data volumes increase and cosmological models become more complex, the computational demands of traditional Bayesian approaches are becoming increasingly problematic. This motivates the development of more efficient algorithms and novel implementations of Bayesian inference techniques to maintain accuracy while improving computational feasibility.
- **Frequentist approaches** — Profile likelihoods provide a standard statistical method for analyzing cosmological models with high-dimensional parameter spaces, particularly when the likelihood surfaces exhibit non-Gaussian features. This approach involves running multiple traditional MCMC analyses for fixed parameters to construct a profile likelihood. Several community tools already implement this method, some incorporating ML techniques to enhance performance. However, due to the computationally intensive nature of this approach, further work on accelerating the sampling process will be crucial for making it more practical for a wider range of applications.
- **Hybrid Bayesian-Frequentist approaches** — While Bayesian inference dominates cosmological data analysis, frequentist methods such as profile likelihoods and bootstrapping offer complementary insights, particularly in scenarios where priors strongly influence results. Hybrid approaches that combine these frameworks can provide more robust parameter constraints, reduce sensitivity to prior assumptions, and improve statistical interpretability in high-dimensional cosmological models.
- **Fast approximate inference techniques** — Traditional Bayesian inference methods such as MCMC can be computationally prohibitive, especially for high-dimensional cosmological models. Alternative approaches such as Hamiltonian Monte Carlo, Variational Inference, and Neural Density Estimation offer promising routes to accelerate parameter estimation while maintaining accuracy. Developing and benchmarking these techniques for cosmological applications is an open challenge.
- **Cosmology simulator inference techniques** — The vast amount of information contained in the large-scale structure of the Universe presents a significant challenge for traditional simulation and analysis methods. Extracting cosmological parameters from these simulations is particularly difficult, as non-Gaussian and higher-order effects may become increasingly relevant for improving accuracy. Recent advances, including neural network architectures and decision tree learning approaches, have shown promise in addressing these challenges. However, the availability of community tools and a robust comparison of different inference techniques remain open issues that need further exploration.
- **Computational challenges in large-scale simulations** — Cosmological simulations are essential for understanding structure formation and model testing. However, the increasing size of observational datasets and complexity of simulations present major computational challenges. Key issues include (1) optimizing numerical algorithms for high-performance computing architectures, (2) improving resolution and scalability in N-body and hydrodynamical simulations, and (3) reducing computational costs while maintaining accuracy in statistical inference from simulations.
- **Reconstruction techniques** — The use of observational survey data to reconstruct physical models is still in its early stages; however, powerful techniques have already been developed and made publicly available. The development of more mature and statistically robust reconstruction methods, including those leveraging ML approaches, will be an important aspect of progress in this direction. A major challenge for these techniques lies in effectively utilizing the wide variety of available datasets, which may include background, perturbative, and other physical aspects of cosmological models.
- **Genetic algorithm model selection** — GAs provide a mechanism to explore an otherwise infinite model space within a finite time by applying selection criteria. These methods primarily rely on Bayesian constraint analyses, but practical toolkits for their implementation are not yet publicly available in the literature. The development of such toolkits is essential for advancing this technique into a more comprehensive classification framework. Additionally, combining GAs with other, faster constraint methods may enhance their suitability for practical model selection analyses.
- **Machine learning for theoretical model selection** — The increasing complexity of cosmological models necessitates efficient methods for exploring large parameter spaces. ML techniques, such as deep learning classifiers and GP regression, are being developed to identify viable theoretical models by learning patterns in high-dimensional likelihood landscapes. However, challenges remain in ensuring interpretability, robustness, and generalization across different datasets.
- **Calibration and validation of machine learning in cosmology** — ML algorithms are increasingly used for inference, parameter estimation, and anomaly detection in cosmological datasets. However, ensuring that these models generalize well across different observational conditions, remain unbiased, and do not overfit to specific datasets is a key challenge. Benchmarking ML models against traditional methods and developing interpretable AI approaches will be crucial for their broader adoption in cosmology.
- **Dark siren cosmology** — The number of standard sirens without an associated electromagnetic counterpart continues to grow.

These sources can also be used to constrain cosmological parameters, albeit through a statistical reconstruction of their population properties using galaxy catalogs. However, the simultaneous modeling of cosmology and mass distributions introduces computational challenges that must be addressed to extract robust constraints.

- **Spectroscopical sirens** — The use of spectroscopic data from host galaxies associated with GW events offers a promising avenue for improving the precision of standard siren measurements. By obtaining redshift information through spectroscopic observations, it is possible to reduce uncertainties in distance measurements and break degeneracies in cosmological parameter estimation. However, challenges remain in accurately identifying the host galaxy among multiple candidates, mitigating observational systematics in spectroscopic measurements, and optimizing survey strategies to maximize the detection of viable spectroscopical sirens.
- **Systematics mitigation in statistical inference** — The increasing precision of cosmological surveys requires robust methods to identify and mitigate systematics in data analysis. Key challenges include (1) the impact of prior choices on Bayesian inference, (2) biases introduced by incomplete or inhomogeneous datasets, and (3) uncertainties in the modeling of astrophysical and instrumental effects. The development of statistical techniques that can cross-validate results across different datasets while minimizing these biases remains an important open problem.
- **Big Bang Nucleosynthesis numerical estimates** — The precision of BBN predictions for primordial element abundances has significantly improved in recent years. Advanced numerical codes have revealed tensions in some species ratios that were not apparent in previous lower-order calculations. Future numerical developments incorporating these higher-order effects will be crucial for reassessing these tensions and refining BBN constraints on early Universe physics.
- **Cross-correlations and multi-probe statistical methods** — Combining multiple cosmological probes is essential for breaking degeneracies and improving parameter constraints. However, this requires sophisticated statistical frameworks to account for systematics, survey-specific biases, and correlated uncertainties across datasets. Developing robust cross-correlation pipelines that integrate WL, large-scale structure, and CMB measurements is a key challenge for upcoming surveys.
- **Data-driven approaches for systematics mitigation** — Systematic uncertainties remain a major challenge in cosmology, particularly in photometric redshift estimation, instrumental biases, and survey calibration. ML, GP, and hybrid statistical methods can provide real-time corrections for systematics, but require careful validation to ensure robustness across different datasets.
- **High-volume and high-dimensional data processing** — The increasing size of cosmological datasets from next-generation surveys requires the development of scalable numerical methods and high-performance computing techniques. Challenges include managing high-dimensional parameter spaces, optimizing data compression without loss of information, and implementing real-time data processing pipelines for massive observational datasets.

Challenges in fundamental physics:

- **Early-time physics** — The early Universe provides a compelling regime for introducing exotic physics that remains shielded by recombination. Mechanisms such as early scalar fields, additional neutrino species, or modified expansion histories primarily affect the sound horizon at recombination, which in turn impacts inferences of the Hubble constant. These early modifications also present opportunities for testing inflationary scenarios. However, a significant challenge remains in explaining the evolution of large-scale structure, ensuring that any proposed early-time physics can simultaneously produce the correct growth rate to remain consistent with all cosmological observations.
- **Inflation** — Phenomenological models successfully provide a spectrum of scenarios that can alleviate some tensions even under the assumption of Gaussian fields. However, it remains crucial to construct physically realistic explicit models that respect fundamental physical principles such as locality, causality, and unitarity, while also approximating key features of these phenomenological models. As future galaxy surveys improve precision on possible non-Gaussian features associated with primordial conditions, it will become increasingly important to develop accurate numerical simulations and theoretical descriptions of the nonlinear aspects of the evolution of these fields.
- **Big Bang Nucleosynthesis (BBN) tensions** — BBN predictions generally exhibit strong agreement with ΛCDM in the production rates of primordial species. However, discrepancies remain, particularly for lithium isotopes, and increasingly for helium and deuterium, when compared with their relative abundances inferred from observations of the oldest stars. These discrepancies may stem from stellar astrophysics rather than cosmological considerations, but they could also signal challenges for early Universe dynamics in non-standard cosmological models. Resolving these tensions requires improved modeling of stellar evolution, nuclear reaction rates, and alternative BBN scenarios.
- **Primordial magnetic fields** — The possible existence of non-negligible PMFs could have influenced CMB anisotropies and small-scale inhomogeneities in the large-scale structure of the Universe. Various realizations of these fields have shown promise in addressing aspects of cosmic tensions, particularly in modifying early-Universe physics. However, more precise small-scale measurements of CMB anisotropies are needed to robustly test these scenarios and establish whether PMFs play a significant cosmological role.
- **Quantum decoherence in the early Universe** — The classical nature of primordial perturbations is assumed in standard cosmology, yet their quantum mechanical origin requires a consistent explanation of decoherence processes. Understanding how quantum fluctuations transitioned to classical density perturbations and testing for potential residual quantum signatures remains an unresolved issue in fundamental physics.
- **Parity violations in cosmology** — Parity-violating interactions, such as those arising in extensions to general relativity or axion-like particles coupled to gravity, could leave unique imprints on the CMB polarization or large-scale structure. The detection of a nonzero cosmic birefringence signal, or deviations in E/B-mode power spectra, could offer evidence for such interactions. However, current observational constraints remain inconclusive, and refining the observational tests for parity violation remains an open challenge.
- **Nonflat spatial curvature** — The cosmological curvature parameter is a fundamental aspect of the FLRW geometric background and is predicted to be zero in most inflationary models. However, any possible nonzero value remains highly degenerate with other cosmological parameters in standard analyses. Methods to break this degeneracy, such as BAO measurements or other observational techniques, could provide important insights into potential departures from the standard model and their role in addressing cosmological tensions.
- **Testing the Cosmological Principle** — The standard model of cosmology assumes large-scale homogeneity and isotropy. However, several observations, including cosmic dipoles, bulk flows, and peculiar velocity anomalies, suggest that these assumptions

may need to be tested more rigorously. Developing more precise observational tests and statistical methodologies to assess the validity of the cosmological principle remains an important challenge in the field.

- **Nonvanishing cosmic dipoles** — The cosmic dipole represents the largest expected deviation from isotropy if the cosmological principle is broken at any level. Potential dipole signals have been investigated in various datasets, including the CMB, QSO distributions, fine-structure constant measurements, SNIa, radio galaxies, GRBs, and bulk flow studies. Recent observations have hinted at slight nonvanishing dipoles in some of these probes. To assess the validity and implications of such findings, it is necessary to develop more robust cosmological backgrounds that can accommodate or rule out these potential departures from isotropy.
- **CMB anisotropy anomalies** — Several features in the CMB anisotropic power spectrum exhibit mild tensions with the predictions of the ΛCDM model. Early Universe modifications that explain or incorporate these features more naturally may offer new insights into fundamental physics beyond standard cosmology. These anomalies include: (1) a stronger-than-expected ISW effect in certain analyses, (2) non-Gaussian features in the CMB, such as the Cold Spot, (3) a slight hemispherical asymmetry in the CMB power spectrum, (4) an unexpected lack of large-scale CMB temperature correlations, (5) a higher-than-predicted lensing parameter, and (6) a moderate inconsistency between parameter values derived from high- and low-multipole regions of the CMB power spectrum. Understanding whether these features stem from new physics or residual systematics remains an important challenge for upcoming surveys.
- **Anomalous Integrated Sachs–Wolfe (ISW) effect** — The ISW effect arises from the interaction of CMB photons with evolving gravitational potentials associated with large-scale structure. Observations suggest a discrepancy between the predicted ISW signal in ΛCDM and its measured imprint in cosmic superstructures and supervoids, both in amplitude and sign. This may indicate a more complex growth history than expected in the concordance model. Understanding whether this excess signal can be reconciled within ΛCDM, or if it points to new physics, remains an open question.
- **The nature of dark matter** — The connection between the fundamental properties of DM and cosmic evolution has significant implications both for the early Universe, through thermal and non-thermal relic physics, and for the late Universe, influencing the formation of large-scale structure. Modeling how the thermal history and other fundamental characteristics of DM may lead to deviations from standard cosmology via solutions of the Boltzmann equation will be crucial in assessing whether DM plays a role in alleviating cosmological tensions.
- **Axion-like particles and ultralight fields** — The existence of ultralight scalar fields, such as axion-like particles, could impact the evolution of the Universe through novel interactions with DM, DE, or radiation. These fields have been proposed to address cosmic tensions by altering the expansion rate or structure growth. Developing observational tests for their presence and impact remains a crucial task.
- **Complex dark sector interactions** — Many extensions to ΛCDM propose that DM and DE may not be independent, but instead part of a larger dark sector with self-interactions or couplings to other fields. These models introduce new forces in the dark sector that could impact structure formation, cosmic expansion, and small-scale clustering. However, constraining these interactions remains difficult, as current probes (e.g., CMB, BAO, WL) primarily test gravitational effects rather than direct couplings.
- **Modified gravity** — Extensions beyond ΛCDM may involve modifications to gravity, ranging from mild to radical departures from General Relativity. The literature is rich with competing formulations of MG theories, but many are disfavored at smaller scales and exhibit strong degeneracies both among themselves and with scalar-tensor theories. Additionally, MG theories often introduce challenges such as unwanted fifth-force effects. On the other hand, these theories provide an avenue for constructing alternative cosmological models independent of ΛCDM, which could yield departures from concordance cosmology in both early- and late-time evolution.
- **Late-time physics** — Measurements in the local Universe place strict constraints on the cosmic expansion profile, leaving little room for significant deviations from ΛCDM. However, recent results from large-scale surveys suggest possible hints of dynamical properties in DE at late-times. While numerous competing theories focus on late-time modifications, many of their observational properties remain highly degenerate. To address this issue, the development of more distinct and testable theoretical models, as well as more precise predictions from specific scenarios, would be beneficial.
- **Exotic dark energy models** — The majority of DE models assume a scalar-field-driven component, but alternative formulations involving vector or tensor fields have been proposed. These include vector–tensor theories, emergent gravity models, and Lorentz-violating DE frameworks. Understanding the observational signatures and constraints on these exotic models is an open challenge.
- **Variation of fundamental constants** — The possible variation of fundamental constants could arise from various exotic physics scenarios, including non-Standard Model particle interactions, MG, or coupled scalar fields, among others. Temporal or spatial variations in fundamental constants would have profound consequences for fundamental physics, potentially impacting atomic structure, nuclear reactions, and cosmological evolution. Observational efforts have primarily focused on detecting variations in the fine-structure constant and the electron mass, as these have shown promise in providing an alternative explanation for the Hubble tension. However, current CMB observations lack the precision to distinguish between models that allow for varying fundamental constants. Addressing this challenge will require next-generation observatories with significantly improved sensitivity to such effects.
- **Higher-dimensional cosmological models** — Theories incorporating extra spatial dimensions, such as brane-world scenarios and string-inspired cosmologies, propose modifications to gravity that could influence cosmic expansion, the dark sector, or structure formation. Developing testable predictions for these theories and determining their viability in explaining cosmic tensions remains a key theoretical challenge.
- **Cosmological quantum gravity** — It is expected that classical gravity breaks down at high energy scales, but the impact of UV-complete quantum gravity theories on cosmological observables remains unclear. In particular, it is uncertain whether such effects could resolve the Hubble tension or other cosmic anomalies. Possible quantum gravitational effects, such as the GUP, Lorentz invariance violations, or nonlinear modifications, could provide a new perspective on cosmic tensions as manifestations of non-classical physics. However, fully developed quantum gravity models that remain consistent with small-scale physics while simultaneously addressing these challenges are still in early stages of development.
- **Testing the equivalence principle on cosmological scales** — The equivalence principle, a cornerstone of general relativity, has been tested at small scales with high precision. However,

cosmological tests remain limited. Anomalies in the behavior of standard sirens, WL, or cosmic dipoles could indicate potential violations. Future large-scale surveys will play a crucial role in refining these tests.

- **Relic neutrinos and direct detection** — The cosmic neutrino background (CνB) is a fundamental prediction of Big Bang cosmology, yet it has never been directly detected. Cosmological observations place strong constraints on its properties, but upcoming laboratory experiments and indirect probes may provide the first evidence for relic neutrinos. If detected, these neutrinos could offer crucial insights into early-Universe physics, including possible deviations from the Standard Model.

By confronting these challenges, the cosmology community will be poised to revolutionize our understanding of the Universe, ensuring that future cosmological models remain consistent with increasingly precise observations while harnessing the full power of advanced statistical and computational methodologies.

5.3. Conclusions

The issue of cosmic tensions has emerged over the past decade as a significant challenge to the ΛCDM concordance model, which also faces underlying consistency issues and additional anomalies. While this is not unexpected for a phenomenological framework, the mounting observational discrepancies suggest that a new concordance model may ultimately be required to resolve these tensions. Despite the long-standing success of ΛCDM, the breadth and persistence of cosmic tensions represent the most serious and potentially insurmountable test for the standard cosmological paradigm.

Among these challenges, the continued statistical significance of the Hubble constant tension has solidified its status as a defining question in cosmology. This tension not only tests the robustness of the concordance model but also probes the ability of the cosmology community to reconcile local (late-time) measurements with global (early-time) constraints. The latter, being model-dependent, introduces additional complexities, while the former is subject to astrophysical systematics that may exert only a limited influence on the magnitude of the discrepancy. However, the widespread and consistent detection of the Hubble tension across independent measurement techniques casts doubt on the plausibility of a single cross-survey systematic effect that could fully account for the discrepancy. In Section 2.1, we review the diverse range of methods used to infer H_0. Many of these techniques rely on the distance ladder to measure the Hubble flow, including refined SNIa analyses, Cepheid variable calibrations, TRGB and JAGB methods, SNII measurements, Mira variables, and the SBF technique. Additionally, CCs provide a direct means of measuring the Hubble parameter to comparable redshifts. Collectively, these approaches yield a consistently high value of H_0, a result reinforced by distance-ladder-independent methods such as maser-driven constraints and estimates based on the BTFR. Furthermore, higher-redshift techniques — including HII galaxy distance indicators, time-delay strong lensing, FRBs, QSOs and GRBs Hubble diagrams — further substantiate the discrepancy. Another promising avenue for constraining H_0 lies in GW-based measurements using standard sirens, which provide an independent approach free from electromagnetic systematics. This method continues to improve and has already delivered encouraging results, potentially adding new insights into the nature and expression of the Hubble tension. On the other hand, every CMB-based survey — including Planck, ACT, and SPT — consistently yields a significantly lower value of the Hubble constant, assuming a ΛCDM cosmological framework. This lower range of H_0 values is further reinforced through the combination of baryon acoustic oscillation data and constraints from BBN. The core of the Hubble tension thus lies in the stark contrast between low-redshift measurements, which suggest a higher H_0, and early-Universe estimates derived from the CMB and similarly high-redshift probes, which favor a lower value.

The Hubble tension serves as a critical test of ΛCDM— or any alternative cosmological model — spanning from the primordial Universe to the present day. A closely related parameter that traces the expansion and structure formation history of the Universe is S_8, which encapsulates both the total matter density and the amplitude of matter fluctuations on scales of $8\,h^{-1}$ Mpc. This parameter is widely regarded as an effective measure of cosmic structure growth and is examined in Section 2.2. Similar to the Hubble tension, a statistical discrepancy emerges in the observed values of S_8 when comparing CMB-based primary anisotropy measurements with local probes such as WL, galaxy clustering, and galaxy cluster abundance studies. The S_8 parameter is also closely connected to the $f\sigma_8$ parameter, which is constrained through RSD, as well as other structure growth parameters, including the growth index, growth parameter, and growth rate. CMB-based measurements yield a relatively high and stable estimate of S_8 across multiple experiments, including different data subsets from the Planck mission's legacy release. In contrast, independent analyses from WL surveys, galaxy clustering, RSD, and galaxy count-based approaches predominantly indicate a lower S_8 value at a statistically significant level. When considered alongside the Hubble tension, the potential S_8 tension presents an even greater challenge to ΛCDM and alternative cosmological models, further testing their predictive power and ability to fully reconcile current observational data.

Additionally, several anomalies and challenges arising from the confrontation between ΛCDM and observational data have become increasingly apparent. These issues, described in Section 3, include the $A_{\rm lens}$ anomaly, which suggests an excess lensing amplitude in the Planck data and a potential deviation from ΛCDM predictions. This is further compounded by a slight preference for a closed universe in spatial curvature parameter constraints within the ΛCDM framework. Other CMB anisotropy anomalies include the low quadrupole moment and its alignment with the octupole, hemispherical asymmetry, and the Cold Spot anomaly. Beyond the CMB, additional unresolved questions concern the exact nature of cosmological neutrino physics, potential deviations from the cosmological principle due to large-scale bulk flows, and anomalies in the primordial abundances of certain species in the early Universe. More broadly, discrepancies have emerged in Lyman-α measurements, the ISW effect, radio synchrotron background observations, and the possible existence of large cosmic voids.

The vast amount of observational data related to cosmic expansion, large-scale structure formation, and the evolution of fundamental parameters presents a formidable challenge for the data analysis and theoretical modeling community. Traditional implementations of MCMC methods are increasingly struggling to distinguish between competing cosmological scenarios due to the complexity of their parameter dependencies and the high dimensionality of their parameter spaces. In Section 3, novel approaches to MCMC methods are discussed alongside alternative data analysis techniques. Frequentist parameter inference through profile likelihoods offers an intriguing pathway to mitigating prior volume effects that can dominate posterior constraints in Bayesian approaches. However, this method is even more computationally demanding than standard MCMC, making it impractical for certain classes of models beyond ΛCDM. Similarly, extracting cosmological information from large-scale simulations has become computationally intractable using conventional methods, necessitating the development of novel tools. ML techniques, particularly deep generative models, have shown significant promise in constraining cosmological parameters with improved efficiency. More broadly, ML inference frameworks have begun replacing traditional MCMC techniques, leveraging various neural network architectures to refine parameter estimation. In parallel, model selection methodologies have incorporated GAs as a systematic approach for exploring complex model spaces against observational constraints. These rapidly evolving techniques are proving essential

Table 7
List of notation conventions used in the White Paper (unless otherwise stated).

Definition	Meaning
$\hbar = c = k_B = 1$	Natural units
$\kappa^2 \equiv 8\pi G = M_{\rm Pl}^{-2}$	Gravitational constant
$\ln := \log_e,\ \log := \log_{10}$	Logarithm conventions
$(-\,+\,+\,+)$	Metric signature
$g_{\mu\nu}$	Metric tensor
$G_{\mu\nu} \equiv R_{\mu\nu} - \frac{1}{2} g_{\mu\nu} R$	Einstein tensor
Λ	Cosmological constant
$ds^2 = -dt^2 + a^2(t)\left[\frac{dr^2}{1-kr^2} + r^2\left(d\theta^2 + \sin^2\theta d\phi^2\right)\right]$	Friedmann–Lemaître–Robertson–Walker (FLRW) spacetime metric
$a(t)$	Scale factor
$a_0 = 1$	Scale factor today (set to unity)
t	Cosmic (proper) time
$\tau(t) = \int_0^t \frac{dt'}{a(t')}$	Conformal time
$\dot{} \equiv \frac{d}{dt}$	Cosmic time derivative
$' \equiv \frac{d}{d\tau}$	Conformal time derivative
$T^{\mu\nu} = \frac{2}{\sqrt{-g}} \frac{\delta \mathcal{L}_m}{\delta g_{\mu\nu}}$	Energy–momentum tensor of the Lagrangian density $\mathcal{L}$
$z = -1 + \frac{1}{a}$	Cosmological redshift
$H(z) = \frac{\dot{a}}{a}$	Hubble parameter
H_0	Hubble constant
$h \equiv H_0/100\,\mathrm{km\,s^{-1}Mpc^{-1}}$	Dimensionless reduced Hubble constant
$\rho_m,\ \rho_b,\ \rho_r$	Energy density of total matter, baryonic matter, and radiation
$\rho_{\rm DM},\ \rho_{\rm DE}$	Energy density of dark matter and dark energy
Ω_m	Present-day matter density parameter
$\Omega_r = 2.469 \times 10^{-5} h^{-2}(1 + 0.2271 N_{\rm eff})$	Present-day radiation density parameter
$\Omega_{\rm DM},\ \Omega_{\rm DE}$	Present-day density parameters of dark matter and dark energy
$\Omega_{\rm CDM}$	Present-day density parameters of cold dark matter
$\Omega_m(z) = \frac{\kappa^2 \rho_m}{3H^2}$	Matter density parameter
$\Omega_r(z) = \frac{\kappa^2 \rho_r}{3H^2}$	Relativistic content density parameter
$\Omega_{\rm DE}(z) = \frac{\kappa^2 \rho_{\rm DE}}{3H^2}$	Dark energy density parameter
$w \equiv \frac{p}{\rho}$	Equation of state (EoS) parameter
c_s	Sound speed
$r_s \equiv \int_0^\tau c_s(\tau')d\tau'$	Sound horizon
$r_d \equiv r_s(\tau_d)$	Sound horizon at drag epoch
σ_8	Amplitude of mass fluctuations on scales of $8\,h^{-1}$ Mpc
$S_8 = \sigma_8 \sqrt{\Omega_m/0.3}$	Weighted amplitude of matter fluctuations

in addressing the challenges posed by next-generation observatories, which are producing unprecedented volumes of data and introducing a vast array of potential new physics scenarios.

The increasingly robust expression of cosmic tensions — spanning the Hubble constant, large-scale structure growth, and various other anomalies — necessitates a reevaluation of potential new physics within both current and future observational surveys. The cosmology community has proposed a wide range of possible directions for addressing these challenges, which are reviewed in Section 4. Early-Universe modifications have the advantage of introducing exotic dynamics prior to recombination, beyond the reach of direct electromagnetic observations. However, while altering the sound horizon can help reconcile certain tensions, these modifications may introduce inconsistencies with the early growth of large-scale structure. Addressing this issue requires exploring different realizations of new physics in this sector alongside novel data analysis techniques, such as frequentist parameter inference. On the other hand, late-time modifications to cosmology have also shown promise in addressing cosmic tensions through diverse mechanisms, including additional fields, modifications to gravitational physics, and other extensions to the standard paradigm. However, the significantly more detailed and structured nature of late-Universe observations places stringent constraints on the evolution of such models, restricting the amplitude of any new physics in this regime. An alternative to modifying gravity in the field equations is to reconsider the behavior of the matter sector, such as through interacting or decaying DM scenarios, or more intricate physics governing DM properties. Beyond standard modifications to cosmic evolution, alternative explanations have been explored, including the role of large cosmic voids, the influence of PMFs, and variations in the dynamics of cosmic inflation. The severity of these tensions has also revived interest in non-standard cosmological geometries that challenge aspects of the cosmological principle, though such proposals remain in early stages of development. Similarly, while quantum gravity theories have not yet demonstrated a direct resolution to cosmic tensions, the potential variation of fundamental constants has been shown to meaningfully impact both the inferred Hubble constant and the growth of large-scale structures, with broader implications across multiple areas of fundamental physics. Ultimately, reconciling early- and late-time cosmological observations, alongside non-standard phenomenology, may necessitate a combination of modifications to the concordance model.

However, it remains crucial to break the strong degeneracy among different classes of modified cosmologies and ensure that proposed models not only fit existing data but also yield new, testable predictions while preserving the well-established successes of the concordance framework across both astrophysical and cosmological scales.

The coming years will see an explosion of high-precision observational data from upcoming surveys, as reviewed in Section 5.1. New CMB experiments, such as LiteBIRD and CMB-S4, have the potential to detect primordial GWs and refine measurements of CMB anisotropies, which may provide key insights into fundamental physics. In parallel, large-scale structure surveys — including those conducted by Euclid, the Roman Space Telescope, and the Rubin Observatory — will probe the evolution of cosmic structure and the nature of DE in unprecedented detail. WL studies, RSD, and clustering analyses will provide complementary information on cosmic structure formation, while 21 cm intensity mapping from SKAO, FAST, and CHIME will open a new observational window into the cosmic dawn. Additionally, radio astronomy efforts, such as FRB surveys with UTMOST and MeerKAT, will offer independent constraints on cosmic expansion and structure evolution. Beyond electromagnetic probes, the next generation of GW observatories — including the LIGO-Virgo-KAGRA network, the ET, Cosmic Explorer, and the space-based LISA mission — will provide direct insight into gravitational radiation, potentially offering novel constraints on early-Universe physics and cosmic expansion. Additionally, advances in standard siren measurements may provide an independent means of resolving the Hubble tension. Meanwhile, improvements in the cosmic distance ladder, enabled by JWST, ELT, and other facilities, will refine local measurements of H_0 with increasing precision. As the volume of observational data continues to grow exponentially, computational advancements will play an increasingly critical role in extracting cosmological information. The limitations of traditional MCMC methods necessitate the development of alternative approaches, such as frequentist inference through profile likelihoods, deep generative models, and other ML techniques. These innovations have already shown promise in improving parameter estimation and accelerating statistical inference, while model selection algorithms, including GAs, offer systematic strategies for exploring vast cosmological parameter spaces. The integration of artificial intelligence and high-performance computing will be essential in processing and analyzing the unprecedented data streams expected from next-generation observatories.

The comprehensive review presented in this White Paper, along with the collaborative efforts that shaped it, reflects a growing consensus within the cosmology community on the key directions that must be pursued in the coming years. As detailed in Section 5.2, these efforts span observational challenges, advancements in data analysis techniques, and the theoretical development of new physics models. Crucially, resolving cosmic tensions will require a synergistic approach, combining observational precision, computational innovation, and theoretical creativity. The next decade of cosmology will be pivotal in shaping our understanding of the Universe, with the potential to refine the current paradigm or uncover new physics that reshapes our fundamental model of cosmic evolution.

6. Conventions

The White Paper spans research communities in observational, data analysis, and fundamental physics areas which observe vastly different notational traditions. A big effort was made to homogenize this notation across the breadth of communities in the separate sections of this project. These notation conventions are defined in Table 7. Any deviations from this notation convection are noted in the specific subsections in which they occur.

7. List of acronyms

ACT	Atacama Cosmology Telescope
AGN	Active Galactic Nucleus
AGB	Asymptotic Giant Branch
ANN	Artificial Neural Network
BAO	Baryon Acoustic Oscillations
BTFR	Baryonic Tully–Fisher Relation
BNN	Bayesian Neural Network
BBN	Big Bang Nucleosynthesis
BOSS	Baryon Oscillation Spectroscopic Survey
CC	Cosmic chronometers
CDM	Cold Dark Matter
CMB	Cosmic Microwave Background Radiation
CNN	Convolutional Neural Network
CPL	Chevallier–Polarski–Linder
DDE	Dynamical Dark Energy
DE	Dark Energy
DM	Dark Matter
eBOSS	Extended Baryon Oscillation Spectroscopic Survey
EDE	Early Dark Energy
EFTofLSS	Effective Field Theory of Large Scale Structure
ELT	Extremely Large Telescope
EoR	Epoch of Reionization
EoS	Equation of State
ESA	European Space Agency
ET	Einstein Telescope
DES	Dark Energy Survey
DESI	The Dark Energy Spectroscopic Instrument
FLRW	Friedmann–Lemaître–Robertson–Walker
FRB	Fast Radio Burst
CMB-S4	CMB—Stage 4
GA	Genetic Algorithm
GP	Gaussian processes
GR	General relativity
GRB	Gamma-ray burst
GUP	Generalized Uncertainty Principle
GW	Gravitational Wave
HST	Hubble Space Telescope
HSC	Hyper Suprime-Cam
IDE	Interacting Dark Energy
IDM	Interacting Dark Matter
IGM	Intergalactic Medium
ISM	Interstellar Medium
ISW	Integrated Sachs–Wolfe
LDE	Late Dark Energy
LF	Luminosity Function
LISA	Laser Interferometer Space Antenna
LMC	Large Magellanic Clouds
JAGB	J-region Asymptotic Giant Branch
JWST	James Webb Space Telescope
KiDS	Kilo-Degree Survey
LIGO	Laser Interferometer Gravitational Wave Observatory
LSS	Large Scale Structure
LSST	Legacy Survey of Space and Time
MG	Modified Gravity
MCMC	Markov chain Monte Carlo
ML	Machine Learning
MW	Milky Way galaxy
MOND	Modified Newtonian dynamics

NEDE	New Early Dark Energy
PMF	Primordial Magnetic Field
PDF	Probability Density function
RGB	Red Giant Branch
QSO	QSO
RSD	Redshift-Space Distortions
RVM	Running Vacuum Model
SBF	Surface Brightness Fluctuations
SGWB	Stochastic Gravitational Wave Background
SKAO	Square Kilometer Array Observatory
SMC	Small Magellanic Clouds
SN	Supernovae
SNIa	Type Ia supernovae
SNII	Type II supernovae
SPT	South Pole Telescope
SPT-3G	South Pole Telescope - 3rd Generation
SZ	Sunyaev–Zeldovich
TRGB	Tip of the Red Giant Branch
WDM	Warm Dark Matter
WL	Weak Lensing
WMAP	Wilkinson Microwave Anisotropy Probe
ZTF	Zwicky Transient Facility

CRediT authorship contribution statement

Eleonora Di Valentino: Conceptualization, Data curation, Formal analysis, Funding acquisition, Investigation, Methodology, Project administration, Resources, Software, Supervision, Validation, Visualization. **Jackson Levi Said:** Conceptualization, Data curation, Formal analysis, Funding acquisition, Investigation, Methodology, Project administration, Resources, Software, Supervision, Validation, Visualization.

Declaration of competing interest

The authors declare that they have no known competing financial interests or personal relationships that could have appeared to influence the work reported in this paper.

Acknowledgments

This paper is based upon work from COST Action CA21136 *Addressing observational tensions in cosmology with systematics and fundamental physics* (CosmoVerse) supported by COST (European Cooperation in Science and Technology). EDV is supported by a Royal Society Dorothy Hodgkin Research Fellowship. JLS would also like to acknowledge funding from "Xjenza Malta" as part of the "Technology Development Programme" DTP-2024-014 (CosmicLearning) Project and the "XM-TÜBÄ° TAK R&I Programme" BridgingCosmology project. AGV is funded by "la Caixa" Foundation, Spain (ID 100010434) and the European Union's Horizon 2020 research and innovation programme under the Marie Sklodowska-Curie grant agreement No 847648, with fellowship code LCF/BQ/PI23/11970027. AP acknowledges support from the Polish National Science Centre through the grant 2023/50/A/ST9/00579. AP is supported by National Science Foundation Grant No. 2308193. CvdB is supported by the Lancaster–Sheffield Consortium for Fundamental Physics under STFC grant: ST/X000621/1. CU was supported by UKRI STFC ST/W001020/1 and European Union ERC StG, LSS_BeyondAverage, 101075919. DE acknowledges support from the Swiss National Science Foundation (SNSF), Switzerland under grant agreement 200021_212576. EMT is supported by funding from the European Research Council (ERC) under the European Union's HORIZON-ERC-2022 (grant agreement no. 101076865). ENS acknowledges the contribution of the LISA CosWG. This project has received funding from the European Research Council under the European Union's Horizon 2020 research and innovation programme (grant agreement 853291). FB acknowledges the support of the Royal Society through the University Research Fellowship. The work of FN is supported by VR Starting Grant 2022-03160 of the Swedish Research Council. GB is supported by the Spanish grants CIPROM/2021/054 (Generalitat Valenciana) and PID2023-151418NB-I00 funded by MCIU/AEI/10.13039/501100011033. IS acknowledges NASA, United States grants N4-ADAP24-0021 and 24-ADAP24-0074, and this research was supported in part by grant NSF PHY-2309135 to the Kavli Institute for Theoretical Physics (KITP). JT is supported by a Ramón *y* Cajal contract by the Spanish Ministry for Science, Innovation and Universities with Ref. RYC2023-045660-I. JM would also like to acknowledge funding from "Xjenza Malta" as part of the "Technology Development Programme" DTP-2024-014 (CosmicLearning) Project. KS acknowledges support from the Australian Government through the Australian Research Council Centre of Excellence for Gravitational Wave Discovery (OzGrav), through project number CE230100016. K.F.D. was supported by the PNRR-III-C9-2022–I9 call, with project number 760016/27.01.2023, and funding from "Xjenza Malta" as part of the "XM-TÜBÄ° TAK R&I Programme" BridgingCosmology project. LZ is supported by the NAWA Ulam fellowship (No. BPN/ULM/2023/1/00107/U/00001) and the National Science Centre, Poland (research grant No. 2021/42/E/ST2/00031). LG acknowledges financial support from AGAUR, CSIC, MCIN and AEI 10.13039/50110 0011033 under projects PID2023-151307NB-I00, PIE 20215AT016, CEX2020-001058-M, ILINK23001, COOPB2304, and 2021-SGR-01270. LV acknowledges support by the National Natural Science Foundation of China (NSFC) through the grant No. 123506 10240 "Astrophysical Axion Laboratories", and also thanks INFN through the "QGSKY" Iniziativa Specifica project. The work of LAA is supported by the US National Science Foundation Grant PHY-2412679. MA acknowledges the UK Science and Technology Facilities Council (STFC) under grant number ST/Y002652/1 and the Royal Society, United Kingdom under grant numbers RGSR2222268 and ICAR1231094. MG acknowledges support from the European Union (ERC, RELiCS, project number 101116027) and the PRIN (Progetti di ricerca di Rilevante Interesse Nazionale) number 2022WJ9J33. MF is funded by the PRIN (Progetti di ricerca di Rilevante Interesse Nazionale) number 2022WJ9J33. MC, GR, and RH acknowledge support from the project "INAF-EDGE" (Large Grant 12-2022, P.I. L. Hunt), from the ASI-INAF agreement "Scientific Activity for the Euclid Mission" (n.2024-10-HH.0; WP8420) and from the INAF "Astrofisica Fondamentale" GO-grant 2024 (PI M. Cantiello). MM acknowledges support from MIUR, PRIN 2022 (grant 2022NY2ZRS 001) and from the grant ASI n. 2024-10-HH.0 "Attività scientifiche per la missione Euclid – fase E". RCN thanks the financial support from the CNPq under the project No. 304306/2022-3 and FAPERGS under the project No. 23/2551-0000848-3. RCB is supported by an appointment to the JRG Program at the APCTP through the Science and Technology Promotion Fund and Lottery Fund of the Korean Government, and was also supported by the Korean Local Governments in Gyeongsangbuk-do Province and Pohang City. RC acknowledges support from the CONAHCYT research grant CF2022-320152. This project has received funding from the European Research Council (ERC) under the European Union's Horizon 2020 research and innovation programme (Grant Agreement No. 947660). RIA is funded by the SNSF Eccellenza Professorial Fellowship PCEFP2_194638. SK acknowledges funding by the National Center for Science, Poland, grant no. 2023/49/B/ST9/02777. SL is supported by the National Science Foundation Graduate Research Fellowship Program under grant No. DGE2139757. SV acknowledges support from the Istituto Nazionale di Fisica Nucleare (INFN) through the Commissione Scientifica Nazionale 4 (CSN4) Iniziativa Specifica "Quantum Fields in Gravity, Cosmology and Black Holes"

(FLAG), and from the University of Trento and the Provincia Autonoma di Trento (PAT, Autonomous Province of Trento) through the UniTrento Internal Call for Research 2023 grant "Searching for Dark Energy off the beaten track" (DARKTRACK, grant agreement no. E63C22000500003). SP acknowledges the financial support from the Department of Science and Technology, Philippines (DST), Govt. of India under the Scheme "Fund for Improvement of S&T Infrastructure (FIST)" (File No. SR/FST/MS-I/2019/41). TT acknowledges support from the National Science Foundation, United States, the National Areonautics and Space Administration, and the Gordon and Betty Moore Foundation, United States. VP is supported by funding from the European Research Council (ERC) under the European Union's HORIZON-ERC-2022 (grant agreement no. 101076865) and from the European Union's Horizon 2020 research and innovation program under the Marie Skłodowska-Curie grant agreement no. 860881-HIDDeN. AD acknowledges the support of the European Union's Horizon 2021 research and innovation programme under the Marie Sklodowska-Curie grant agreement No. 101068013 (QGRANT). AK has been supported by a *Lendület* excellence grant by the Hungarian Academy of Sciences (MTA). This project has received funding from the European Union's Horizon Europe research and innovation programme under the Marie Skłodowska-Curie grant agreement number 101130774. Funding for this project was also available in part through the Hungarian Ministry of Innovation and Technology NRDI Office grant OTKA NN147550. ARL was supported by FCT through the Investigador FCT Contract CEECIND/02854/2017 and the research project PTDC/FIS-AST/0054/2021. AP is grateful for the support of Vicerrectoría de Investigación *y* Desarrollo Tecnológico (Vridt) at Universidad Católica del Norte through Núcleo de Investigación Geometría Diferencial *y* Aplicaciones, Resolución Vridt No - 096/2022 and Resolución Vridt No - 098/2022. AP was supported by the Proyecto Fondecyt Regular 2024, Folio 1240514, Etapa 2024. AB acknowledges support from the National Science Center, project no. UMO-2022/45/B/ST2/01067. ABR is supported by the Fundação Carlos Chagas Filho de Amparo à Pesquisa do Estado do Rio de Janeiro (FAPERJ), Grant No E-26/200.149/2025 é 200.150/2025 (304809) AJS received support from NASA, United States through STScI grants HST-GO-16773 and JWST-GO-2974. AM acknowledges the financial support by Conacyt-Mexico through the Post- doc Project I1200/311/2023. AB acknowledges the fellowship of the Brazilian research agency CNPq. AH is funded by the Carlsberg foundation. BSS acknowledges National Science Foundation awards AST-2307147, PHY-2207638, PHY-2308886 and PHY-2309064. B. L. acknowledges the support of the National Research Foundation of Korea, South Korea (NRF-2022R1F1A1076338), the Partenariat Hubert Curien STAR with the National Research Foundation of Korea (RS-2023-00259422), and of the Korea Institute for Advanced Study (KIAS) grant funded by the government of Korea. The research activities of BT is supported in part by the U.S. National Science Foundation under Grant PHY-2014104. CGB is supported by the Spanish Grant PID2023-149016NB-I00 (MINECO/AEI/FEDER, UE) and the Basque government Grant No. IT1628-22 (Spain). CM is supported by an FCT fellowship, grant number 2023.03984. CZ is supported by the China Scholarship Council for 1 year study at SISSA. CP acknowledges the financial support by the excellence cluster QuantumFrontiers of the German Research Foundation (Deutsche Forschungsgemeinschaft, DFG) under Germany's Excellence Strategy – EXC-2123 QuantumFrontiers – 390837967 and was funded by the Deutsche Forschungsgemeinschaft (DFG, German Research Foundation), Germany - Project Number 420243324. D.B. acknowledges support from projects PID2021-122938NB-I00 funded by the Spanish "Ministerio de Ciencia e Innovación" and FEDER "A way of making Europe", PID2022-139841NB-I00 funded by the Spanish "Ministerio de Ciencia e Innovación" and SA097P24 funded by Junta de Castilla *y* León. DS acknowledges support from Bulgarian National Science Fund, Republic of Bulgaria grant number KP-06-N58/5. DRG acknowledges support from grant PID2022-138607NBI00, funded by MCIN/AEI/10.13039/501100011033. DB acknowledges funding from the Ministry of Science, Technological Development and Innovations of the Republic of Serbia, Project contract No. 451-03-136/2025-03/200017. The work of EG was supported in part by grant NSF PHY-2309135 to the Kavli Institute for Theoretical Physics (KITP). EF is supported by "Theoretical Astroparticle Physics" (TAsP), iniziativa specifica INFN and by the research grant number 2022E2J4RK "PANTHEON: Perspectives in Astroparticle and Neutrino THEory with Old and New messengers"under the program PRIN 2022 funded by the Italian Ministero dell'Università e della Ricerca (MUR). EDMF is supported by World Premier International Research Center Initiative (WPI Initiative), MEXT, Japan. FA thanks CNPq and Fundação Carlos Chagas Filho de Amparo á Pesquisa do Estado do Rio de Janeiro (FAPERJ), Processo SEI 260003/014913/2023 for financial support. The work of FB was supported by the post-doctoral grant CIAPOS/2021/169. FP acknowledges partial support from the INFN grant InDark and from the Italian Ministry of University and Research (MUR), PRIN 2022 'EXSKALIBUR – Euclid-Cross-SKA: Likelihood Inference Building for Universe's Research', Grant No. 20222BBYB9, CUP C53D2300131 0006, and from the European Union – Next Generation EU. FP also acknowledges support from the FCT project "BEYLA – BEYond LAmbda" with ref. number PTDC/FIS-AST/0054/2021. FSNL acknowledges support from the Fundação para a Ciência e a Tecnologia (FCT) Scientific Employment Stimulus contract with reference CEECINST/00032/2018, and funding through the research grants UIDB/04434/2020, UIDP/04434/2020 and PTDC/FIS-AST/0054/2021. GL was funded by Agencia Nacional de Investigación *y* Desarrollo (ANID) through Proyecto Fondecyt Regular 2024, Folio 1240514, Etapa 2024. He also thanks Vicerrectorá de Investigación *y* Desarrollo Tecnológico (VRIDT) at Universidad Católica del Norte for support through Núcleo de Investigación Geometría Diferencial *y* Aplicaciones (Resolución VRIDT NÂ° 096/2022). GG acknowledges the financial support from the COSMOS network (www.cosmosnet.it) through the ASI (Italian Space Agency) Grants 2016-24-H.0 and 2016-24-H.1- 2018. GDS acknowledges support from INAF-ASTROFIT fellowship and Istituto Nazionale di Fisica Nucleare (INFN), Naples Section, for specific initiatives QGSKY and Moonlight2, as well as GAIA DPAC funds from INAF and ASI (PI: M.Lattanzi). GJO acknowledges financial support from the Spanish Grants PID2020-116567GB-C21, PID2023-149560NB-C21 funded by MCIN/AEI/10.13039/501100011033, by CEX2023-001292-S funded by MCIU/AEI, and by i-COOP23096 funded by CSIC. GSDj acknowledges the support by the Ministry of Science, Technological Development and Innovation of the Republic of Serbia under contract 451-03-137/2025-03/ 200124 and support by the ICTP - SEENET-MTP NT03 Project TECOM-GRASP. GCH acknowledges support through the ESA research fellowship programm. HAF was partially supported by National Science Foundation grant AST-1907404. The work of IDG was supported by the Estonian Research Council, Estonia grants MOB3JD1202, RVTT3, RVTT7, and by the CoE program TK202 "Fundamental Universe". The work of IAM is supported by the Basque Government, Spain Grant IT1628-22, by Grant PID2021-123226NB-I00 (funded by MCIN/AEI/10.13039/5011000 11033 and by "ERDF A way of making Europe"). IDM acknowledges support from the grant PID2021-122938NB-I00 funded by MCIN/AEI/10.130 39/501100011033 and from the grant SA097P24 funded by Junta de Castilla *y* León and by "ERDF A way of making Europe". JA acknowledges support from the Diputación General de Aragón-Fondo Social Europeo (DGA-FSE) Grant No. 2020-E21-17R of the Aragon Government. JG and BK have been supported in part by the Polish National Science Center (NCN) under grant 2020/37/B/ST2/02371. JR is supported by a Ramón *y* Cajal contract of the Spanish Ministry of Science and Innovation with Ref. RYC2020-028870-I. This research was further supported by the project PID2022-139841NB-I00 of MICIU/AEI/10.13039/501100011033 and FEDER, UE. JS is

supported by the Taiwan National Science & Technology Council. JARC is supported by the project PID2022-139841NB-I00 funded by MICIU/AEI/10.13039/501100011033 and by ERDF/EU. JJ acknowledge partial support from STScI, United States under grants HST-GO-16262 and JWST-GO-03055. JGB acknowledges support from the Spanish Research Project PID2021-123012NB-C43 [MICINN-FEDER], and the Centro de Excelencia Severo Ochoa Program, Spain CEX2020-001007-S at IFT. KL is a recipient of the John and Pat Hume Scholarship and acknowledges support from the Friedrich Naumann Foundation for Freedom and from the Swiss Study Foundation. The research activities of KRD are supported in part by the U.S. National Science Foundation through its employee IR/D program as well as by the U.S. Department of Energy under Grant DE-FG02-13ER41976/DE-SC0009913. LLG acknowledges support from Conselho Nacional de Desenvolvimento Cientıfico e Tecnologico (CNPq), Grant No. 307636/2023-2 and from the Fundacao Carlos Chagas Filho de Amparo a Pesquisa do Estado do Rio de Janeiro (FAPERJ) Grant No. E-26/204.598/2024. LY acknowledges support from YST Program of APCTP and Natural Science Foundation of Shanghai 24ZR1424600. LC acknowledges support from FCT - Fundação para a Ciência e a Tecnologia through the projects with DOI identifiers 10.54499/2023.11681.PEX and 10.54499/2024.00249.CERN. MB is supported by the Polish National Science Center through grants no. 2020/38/E/ST9/00395 and 2020/39/B/ST9/03494. MGE acknowledges the financial support of FONDECYT de Postdoctorado, NÂ° 3230801. MdC acknowledges support from INFN iniziativa specifica GeoSymQFT. The work of MR is supported by the European Union – Next Generation EU and by the Italian Ministry of University and Research (MUR) via the PRIN 2022 project n. 20228WHTYC. ME was supported by the Estonian Ministry of Education and Research (grant TK202, "Foundations of the Universe"), by Estonian Research Council, Estonia grant PRG2172, and by the European Union's Horizon Europe research and innovation programme (EXCOSM, grant No. 101159513). The work of MBL, CGB & PM is supported by the Spanish Grant PID2023-149016NB-I00 (MINECO/AEI/FEDER, UE). This work is also supported by the Basque government Grant No. IT1628-22 (Spain). MC was supported by FCT through the Investigador FCT Contract No. CEECIND/02581/2018 and the research project PTDC/FIS-AST/0054/2021. MM acknowledges funding by the Agenzia Spaziale Italiana, Italy (ASI) under agreement no. 2018-23-HH.0 and support from INFN/Euclid Sezione di Roma. MASP acknowledges support from the FCT through the Fellowship UI/BD/154479/2022, through the Research Grants UIDB/04434/ 2020 and UIDP/04434/2020, and through the project with reference PTDC/FIS-AST/0054/2021 ("BEYond LAmbda"). MASP also acknowledges support from the MICINU through the project with reference PID2023-149560NB-C21. MAS received support from the CAPES scholarship. MK was funded through SASPRO2 project AGE of Gravity: Alternative Geometries of Gravity, which has received funding from the European Union's Horizon 2020 research and innovation programme under the Marie Skłodowska-Curie grant agreement No. 945478. MM acknowledges the support by the Ministry of Science, Technological Development and Innovation of the Republic of Serbia under contract 451-03-137/2025-03/ 200124. MI acknowledges that this material is based upon work supported in part by the Department of Energy, Office of Science, under Award Number DE-SC0022184 and also in part by the U.S. National Science Foundation under grant AST2327245. NF acknowledge support from the Research grant TAsP (Theoretical Astroparticle Physics) funded by INFN, Italy. NF is supported by the European Union – Next Generation EU and by the Italian Ministry of University and Research (MUR) via the PRIN 2022 project n. 20228WHTYC. The Work of NEM. is supported in part by the UK Science and Technology Facilities research Council (STFC) under the research grant ST/X000753/1. NAN was financed by IBS, United States under the project code IBS-R018-D3, and acknowledges support from PSL/Observatoire de Paris. NS is supported by the Charles University Grant Agency (GAUK) - 94224. PS is supported by Science and Technology Facilities Council, United Kingdom (STFC) training grant ST/X508287/1. PJ acknowledges funding from the Ministry of Science, Technological Development and Innovations of the Republic of Serbia, Project contract No. 451-03-136/2025-03/200002. RG acknowledges the support from the SNF 200020_175751 and 200020_207379 "Cosmology with 3D Maps of the Universe" research grant. RH work has been supported by the Spanish grants FPU19/03348 of MU, MCIN/AEI/10.13039/501100011033 grants PID2020-113644GB-I00, PID2023-148162NB-C22, by the European Union's Horizon 2020 research and innovation program under the Marie Sklodowska-Curie grants HORIZON-MSCA-2021-SE-01/ 101086085-ASYMMETRY and H2020-MSCA-ITN-2019/ 860881-HIDDeN and by the Generalitat Valenciana grants PROMETEO/2019/ 083 and CIPROM/2022/69. RH acknowledges funding from the Italian National Institute of Astrophysics (INAF) through large grant PRIN 12-2022 "INAF-EDGE" (PI L. Hunt). RR acknowledges financial support from the STFC Consolidated Grant ST/X000583/1. RBN acknowledges funding by the Royal Society, United Kingdom through the University Research Fellowship Renewal URF R 221005. RK is supported by Project SA097P24 funded by Junta de Castilla *y* Leon. SB is supported by "Agencia Nacional de Investigación *y* Desarrollo" (ANID), Grant "Becas Chile postdoctorado al extranjero" No. 74220006. ST is supported by the National Science Centre, Poland (research grant No. 2021/42/E/ST2/00031). SSC acknowledges support from the Istituto Nazionale di Fisica Nucleare (INFN) through the Commissione Scientifica Nazionale 4 (CSN4) Iniziativa Specifica "Quantum Fields in Gravity, Cosmology and Black Holes" (FLAG) and from the Fondazione Cassa di Risparmio di Trento e Rovereto (CARITRO Foundation) through a Caritro Fellowship (project "Inflation and dark sector physics in light of next-generation cosmological surveys"). SJL is supported by grant PIP 11220200100729CO CONICET and grant 20020170100129BA UBACYT. SP is supported by the international Gemini Observatory, a program of NSF NOIRLab, which is managed by the Association of Universities for Research in Astronomy (AURA) under a cooperative agreement with the U.S. National Science Foundation, on behalf of the Gemini partnership of Argentina, Brazil, Canada, Chile, the Republic of Korea, and the United States of America. SP acknowledges the financial support of the Conselho Nacional de Desenvolvimento Científico e Tecnológico (CNPq) Fellowships 300936/2023-0 and 301628/2024-6. TP acknowledges the financial support from the Slovenian Research Agency (grants I0-0033, P1-0031, J1-8136, J1-2460 and Z1-1853). TB was supported by ICSC – Centro Nazionale di Ricerca in High Performance Computing, Big Data and Quantum Computing, funded by European Union – NextGenerationEU. TS is supported by the Della Riccia foundation grant 2025 and the Galileo Galilei Institute Boost Fellowship 2024. TK was supported by the Estonian Research Council, Estonia grants CoE TK202 "Foundations of the Universe" and PRG2608 "Space - Time - Matter". VM thanks CNPq (Brazil) and FAPES (Brazil) for partial financial support. VAM is supported by Generalitat Valenciana via the Excellence Grant 164CIPROM/2021/073, by the Spanish MICIN/AEI/10.13039/501100011033 and the EU/FEDER via grant PID2021-122134NB-C21, and by the Spanish MCIU/AEI via the Severo Ochoa project CEX2023-001292-S. VP acknowledges the support by the Ministry of Education and Science of the Federation of Bosnia and Herzegovina, under Project Number 05-35-2467-1/23. VK acknowledges financial support from Research Ireland Grant 21/PATH-S/9475 (MOREHIGGS) under the SFI-IRC Pathway Programme. Report number: DIAS-STP-25-05. VM acknowledges support from ANID FONDECYT Regular grant number 1231418, Millennium Science Initiative AIM23-0001, and Centro de Astrofísica de Valparaíso CIDI N21. VBJ acknowledges funding from the Ministry of Science, Technological Development and Innovations of the Republic of Serbia, Project contract No. 451-03-136/2025-03/200017. WY has been supported by the National Natural Science Foundation of China under Grant No. 12175096, and Liaoning Revitalization Talents Program under Grant

no. XLYC1907098. WY is supported via the research projects 'COLAB' funded by the National Science Center, Poland, under agreement number UMO-2020/39/B/ST9/03494. "YH is funded by NSFC under the grant No. 12347137 and the China Postdoctoral Science Foundation, China under Grant No. 2024M753076".

Afternote: The opinions and conclusions expressed herein are those of the authors, and do not represent any funding agencies.

Data availability

The data that has been used is confidential.

References

[1] CosmoVerse Network, CA21136 - Addressing observational tensions in cosmology with systematics and fundamental physics, CosmoVerse Network, https://www.cost.eu/actions/CA21136.
[2] CosmoVerse Network, CA21136 - Addressing observational tensions in cosmology with systematics and fundamental physics, CosmoVerse Network, https://cosmoversetensions.eu/.
[3] E. Abdalla, et al., Cosmology intertwined: A review of the particle physics, astrophysics, and cosmology associated with the cosmological tensions and anomalies, JHEAp 34 (2022) 49–211, arXiv:2203.06142 [astro-ph.CO].
[4] E. Di Valentino, et al., Snowmass2021 - Letter of interest cosmology intertwined I: Perspectives for the next decade, Astropart. Phys. 131 (2021) 102606, arXiv:2008.11283 [astro-ph.CO].
[5] E. Di Valentino, et al., Snowmass2021 - Letter of interest cosmology intertwined II: The Hubble constant tension, Astropart. Phys. 131 (2021) 102605, arXiv:2008.11284 [astro-ph.CO].
[6] E. Di Valentino, et al., Cosmology intertwined III: $f\sigma_8$ and S_8, Astropart. Phys. 131 (2021) 102604, arXiv:2008.11285 [astro-ph.CO].
[7] E. Di Valentino, et al., Snowmass2021 - Letter of interest cosmology intertwined IV: The age of the universe and its curvature, Astropart. Phys. 131 (2021) 102607, arXiv:2008.11286 [astro-ph.CO].
[8] CosmoVerse Network Seminars, CA21136 - Addressing observational tensions in cosmology with systematics and fundamental physics, CosmoVerse Network Seminars, https://cosmoversetensions.eu/for-scientists/cosmoverse-seminars/.
[9] CosmoVerse Network Conferences, CA21136 - Addressing observational tensions in cosmology with systematics and fundamental physics, CosmoVerse Network Conferences, https://cosmoversetensions.eu/category/event/conferences/.
[10] CosmoVerse Network School, CA21136 - Addressing observational tensions in cosmology with systematics and fundamental physics, CosmoVerse Network School, https://cosmoversetensions.eu/event/cosmoverseschoolcorfu/.
[11] CosmoVerse Network Training Series, CA21136 - Addressing observational tensions in cosmology with systematics and fundamental physics, CosmoVerse Network Training Series, https://cosmoversetensions.eu/for-scientists/training-series/.
[12] CosmoVerse Network Training Series, CA21136 - Addressing observational tensions in cosmology with systematics and fundamental physics, CosmoVerse Network Training Series, https://cosmoversetensions.eu/for-scientists/journal-club/.
[13] G. Rácz, L. Dobos, R. Beck, I. Szapudi, I. Csabai, Concordance cosmology without dark energy, Mon. Not. R. Astron. Soc. 469 (1) (2017) L1–L5, arXiv:1607.08797 [astro-ph.CO].
[14] R. Beck, I. Csabai, G. Rácz, I. Szapudi, The integrated Sachs–Wolfe effect in the AvERA cosmology, Mon. Not. R. Astron. Soc. 479 (3) (2018) 3582–3591, arXiv:1801.08566 [astro-ph.CO].
[15] W.L. Freedman, et al., The Carnegie-Chicago Hubble Program. VIII. An independent determination of the Hubble constant based on the tip of the red giant branch, Astrophys. J. 882 (2019) 34, arXiv:1907.05922 [astro-ph.CO].
[16] G.S. Anand, et al., Tip of the red giant branch distances with JWST: An absolute calibration in NGC 4258 and first applications to type Ia Supernova hosts, Astrophys. J. 966 (1) (2024) 89, arXiv:2401.04776 [astro-ph.CO].
[17] A.J. Lee, W.L. Freedman, I.S. Jang, B.F. Madore, K.A. Owens, First JWST observations of JAGB stars in the SN Ia host Galaxies: NGC 7250, NGC 4536, NGC 3972, Astrophys. J. 961 (1) (2024) 132, arXiv:2312.02282 [astro-ph.GA].
[18] S. Li, A.G. Riess, S. Casertano, G.S. Anand, D.M. Scolnic, W. Yuan, L. Breuval, C.D. Huang, Reconnaissance with JWST of the J-region asymptotic giant branch in distance ladder galaxies: From irregular luminosity functions to approximation of the Hubble constant, Astrophys. J. 966 (1) (2024) 20, arXiv:2401.04777 [astro-ph.CO].
[19] C.D. Huang, A.G. Riess, W. Yuan, L.M. Macri, N.L. Zakamska, S. Casertano, P.A. Whitelock, S.L. Hoffmann, A.V. Filippenko, D. Scolnic, Hubble space telescope observations of Mira variables in the type Ia supernova host NGC 1559: An alternative candle to measure the Hubble constant, Astrophys. J. 889 (2020) 5, arXiv:1908.10883 [astro-ph.CO].
[20] C.D. Huang, et al., The Mira distance to M101 and a 4% measurement of H_0, Astrophys. J. 963 (2) (2024) 83, arXiv:2312.08423 [astro-ph.CO].
[21] J.P. Blakeslee, J.B. Jensen, C.-P. Ma, P.A. Milne, J.E. Greene, The Hubble constant from infrared surface brightness fluctuation distances, Astrophys. J. 911 (1) (2021) 65, arXiv:2101.02221 [astro-ph.CO].
[22] G.S. Anand, R.B. Tully, Y. Cohen, D.I. Makarov, L.N. Makarova, J.B. Jensen, J.P. Blakeslee, M. Cantiello, E. Kourkchi, G. Raimondo, The population II extragalactic distance scale: A TRGB distance to the Fornax cluster with JWST, Astrophys. J. 973 (2) (2024) 83, arXiv:2405.03743 [astro-ph.CO].
[23] T. de Jaeger, L. Galbany, A.G. Riess, B.E. Stahl, B.J. Shappee, A.V. Filippenko, W. Zheng, A 5 per cent measurement of the Hubble–Lemaître constant from Type II supernovae, Mon. Not. R. Astron. Soc. 514 (3) (2022) 4620–4628, arXiv:2203.08974 [astro-ph.CO].
[24] G. Csörnyei, C. Vogl, S. Taubenberger, A. Flörs, S. Blondin, M.G. Cudmani, A. Holas, S. Kressierer, B. Leibundgut, W. Hillebrandt, Consistency of Type IIP supernova sibling distances, Astron. Astrophys. 672 (2023) A129, arXiv:2302.03112 [astro-ph.SR].
[25] E. Kourkchi, R.B. Tully, H.M. Courtois, A. Dupuy, D. Guinet, Cosmicflows-4: the baryonic Tully–Fisher relation providing ∼10 000 distances, Mon. Not. R. Astron. Soc. 511 (4) (2022) 6160–6178, arXiv:2201.13023 [astro-ph.GA].
[26] A.G. Riess, et al., JWST validates HST distance measurements: Selection of supernova subsample explains differences in JWST estimates of local H_0, Astrophys. J. 977 (1) (2024) 120, arXiv:2408.11770 [astro-ph.CO].
[27] HST Collaboration, W.L. Freedman, et al., Final results from the Hubble Space Telescope key project to measure the Hubble constant, Astrophys. J. 553 (2001) 47–72, arXiv:astro-ph/0012376.
[28] Gaia Collaboration, Gaia Data Release 3. Summary of the content and survey properties, Astron. Astrophys. 674 (2023) A1, arXiv:2208.00211 [astro-ph.GA].
[29] G. Pietrzyński, et al., A distance to the Large Magellanic Cloud that is precise to one per cent, Nature 567 (7747) (2019) 200–203.
[30] D. Graczyk, G. Pietrzyński, I.B. Thompson, W. Gieren, B. Zgirski, S. Villanova, M. Górski, P. Wielgórski, P. Karczmarek, W. Narloch, B. Pilecki, M. Taormina, R. Smolec, K. Suchomska, A. Gallenne, N. Nardetto, J. Storm, R.-P. Kudritzki, M. Kałuszyński, W. Pych, A distance determination to the small magellanic cloud with an accuracy of better than two percent based on late-type eclipsing binary stars, Astrophys. J. 904 (1) (2020) 13, arXiv:2010.08754 [astro-ph.GA].
[31] M.J. Reid, D.W. Pesce, A.G. Riess, An improved distance to NGC 4258 and its implications for the Hubble constant, Astrophys. J. Lett. 886 (2) (2019) L27, arXiv:1908.05625 [astro-ph.GA].
[32] D. Scolnic, et al., The Pantheon+ analysis: The full data set and light-curve release, Astrophys. J. 938 (2) (2022) 113, arXiv:2112.03863 [astro-ph.CO].
[33] D. Brout, et al., The Pantheon+ analysis: Cosmological constraints, Astrophys. J. 938 (2) (2022) 110, arXiv:2202.04077 [astro-ph.CO].
[34] A.G. Riess, et al., A comprehensive measurement of the local value of the Hubble constant with 1 km/s/Mpc uncertainty from the Hubble Space Telescope and the SH0ES Team, Astrophys. J. Lett. 934 (1) (2022) L7, arXiv:2112.04510 [astro-ph.CO].
[35] L. Breuval, A.G. Riess, S. Casertano, W. Yuan, L.M. Macri, M. Romaniello, Y.S. Murakami, D. Scolnic, G.S. Anand, I. Soszyński, Small magellanic cloud cepheids observed with the Hubble space telescope provide a new anchor for the SH0ES distance ladder, Astrophys. J. 973 (1) (2024) 30, arXiv:2404.08038 [astro-ph.CO].
[36] L. Galbany, et al., An updated measurement of the Hubble constant from near-infrared observations of Type Ia supernovae, Astron. Astrophys. 679 (2023) A95, arXiv:2209.02546 [astro-ph.CO].
[37] V. Scowcroft, W.L. Freedman, B.F. Madore, A. Monson, S.E. Persson, J. Rich, M. Seibert, J.R. Rigby, The Carnegie Hubble program: the distance and structure of the SMC as revealed by mid-infrared observations of cepheids, Astrophys. J. 816 (2) (2016) 49, arXiv:1502.06995 [astro-ph.GA].
[38] I. Soszyński, A. Udalski, M.K. Szymański, D. Skowron, G. Pietrzyński, R. Poleski, P. Pietrukowicz, J. Skowron, P. Mróz, S. Kozłowski, Ł. Wyrzykowski, K. Ulaczyk, M. Pawlak, The OGLE collection of variable stars. Classical cepheids in the Magellanic system, Acta Astron. 65 (4) (2015) 297–312, arXiv:1601.01318 [astro-ph.SR].
[39] V. Ripepi, M.-R.L. Cioni, M.I. Moretti, M. Marconi, K. Bekki, G. Clementini, R. de Grijs, J. Emerson, M.A.T. Groenewegen, V.D. Ivanov, R. Molinaro, T. Muraveva, J.M. Oliveira, A.E. Piatti, S. Subramanian, J.T. van Loon, The VMC survey - XXV. The 3D structure of the small magellanic cloud from classical cepheids, Mon. Not. R. Astro. Soc. 472 (1) (2017) 808–827, arXiv:1707.04500 [astro-ph.GA].
[40] S.A. Zhevakin, Physical basis of the pulsation theory of variable stars, Ann. Rev. Astron. Astrophys.. 1 (1963) 367–400.
[41] J.P. Cox, Theory of Stellar Pulsation. (PSA-2), Volume 2, vol. 2, Princeton University Press, 1980.
[42] H.S. Leavitt, E.C. Pickering, Periods of 25 variable stars in the small magellanic cloud, Harv. Obs.. Circ. 173 (1912) 1–3.
[43] H. Shapley, Studies based on the colors and magnitudes in stellar clusters. IX. Three notes on cepheid variation, Astrophys. J. 49 (1919) 24–41.

[44] S.L. Hoffmann, et al., Optical identification of cepheids in 19 host galaxies of type Ia supernovae and NGC 4258 with the Hubble Space Telescope, Astrophys. J. 830 (1) (2016) 10, arXiv:1607.08658 [astro-ph.SR].

[45] L. Inno, N. Matsunaga, M. Romaniello, G. Bono, A. Monson, I. Ferraro, G. Iannicola, E. Persson, R. Buonanno, W. Freedman, W. Gieren, M.A.T. Groenewegen, Y. Ita, C.D. Laney, B. Lemasle, B.F. Madore, T. Nagayama, Y. Nakada, M. Nonino, G. Pietrzyński, F. Primas, V. Scowcroft, I. Soszyński, T. Tanabé, A. Udalski, New NIR light-curve templates for classical Cepheids, Astron. Astrophys. 576 (2015) A30, arXiv:1410.5460 [astro-ph.SR].

[46] L. Breuval, A.G. Riess, L.M. Macri, S. Li, W. Yuan, S. Casertano, T. Konchady, B. Trahin, M.J. Durbin, B.F. Williams, A 1.3% distance to M33 from Hubble Space Telescope cepheid photometry, Astrophys. J. 951 (2) (2023) 118, arXiv:2304.00037 [astro-ph.CO].

[47] R.I. Anderson, On cepheid distances in the H_0 measurement, 2024, http://dx.doi.org/10.48550/arXiv.2403.02801, arXiv e-prints, arXiv:2403.02801, arXiv:2403.02801 [astro-ph.SR].

[48] A.G. Riess, S. Casertano, W. Yuan, L.M. Macri, D. Scolnic, Large magellanic cloud cepheid standards provide a 1% foundation for the determination of the Hubble constant and stronger evidence for physics beyond ΛCDM, Astrophys. J. 876 (1) (2019) 85, arXiv:1903.07603 [astro-ph.CO].

[49] A.G. Riess, G. Narayan, A. Calamida, Calibration of the WFC3-IR count-rate nonlinearity, sub-percent accuracy for a factor of a million in flux, 2019, p. 1, Instrument Science Report WFC3 2019-1, 13 pages.

[50] A.G. Riess, G.S. Anand, W. Yuan, S. Casertano, A. Dolphin, L.M. Macri, L. Breuval, D. Scolnic, M. Perrin, R.I. Anderson, Crowded no more: The accuracy of the Hubble constant tested with high-resolution observations of cepheids by JWST, Astrophys. J. Lett. 956 (1) (2023) L18, arXiv:2307.15806 [astro-ph.CO].

[51] A.G. Riess, G.S. Anand, W. Yuan, S. Casertano, A. Dolphin, L.M. Macri, L. Breuval, D. Scolnic, M. Perrin, I.R. Anderson, JWST observations reject unrecognized crowding of cepheid photometry as an explanation for the Hubble tension at 8σ confidence, Astrophys. J. Lett. 962 (1) (2024) L17, arXiv:2401.04773 [astro-ph.CO].

[52] R.C. Kennicutt Jr., et al., The HST key project on the extragalactic distance scale. 13. The metallicity dependence of the cepheid distance scale, Astrophys. J. 498 (1998) 181, arXiv:astro-ph/9712055.

[53] S. Sakai, L. Ferrarese, R. Kennicutt, A. Saha, The effect of metallicity on cepheid - based distances, Astrophys. J. 608 (2004) 42–61, arXiv:astro-ph/0402499.

[54] L.M. Macri, K.Z. Stanek, D. Bersier, L. Greenhill, M. Reid, A new cepheid distance to the maser-host galaxy NGC 4258 and its implications for the Hubble constant, Astrophys. J. 652 (2006) 1133–1149, arXiv:astro-ph/0608211.

[55] V. Ripepi, G. Catanzaro, R. Molinaro, M. Gatto, G. De Somma, M. Marconi, M. Romaniello, S. Leccia, I. Musella, E. Trentin, G. Clementini, V. Testa, F. Cusano, J. Storm, Cepheid metallicity in the Leavitt Law (C-metall) survey - I. HARPS-N@TNG spectroscopy of 47 classical cepheids and 1 BL her variables, Mon. Not. R. Astro. Soc. 508 (3) (2021) 4047–4071, arXiv:2108.11391 [astro-ph.GA].

[56] A. Bhardwaj, et al., High-resolution spectroscopic metallicities of Milky Way cepheid standards and their impact on the Leavitt Law and the Hubble constant, Astrophys. J. Lett. 955 (1) (2023) L13, arXiv:2309.03263 [astro-ph.SR].

[57] E. Trentin, V. Ripepi, R. Molinaro, G. Catanzaro, J. Storm, G. De Somma, M. Marconi, A. Bhardwaj, M. Gatto, V. Testa, I. Musella, G. Clementini, S. Leccia, Cepheid metallicity in the Leavitt Law (C- MetaLL) survey. IV. The metallicity dependence of cepheid period-luminosity relations, Astron. Astrophys. 681 (2024) A65, arXiv:2310.03603 [astro-ph.SR].

[58] L. Breuval, A.G. Riess, P. Kervella, R.I. Anderson, M. Romaniello, An improved calibration of the wavelength dependence of metallicity on the cepheid Leavitt Law, Astrophys. J. 939 (2) (2022) 89, arXiv:2205.06280 [astro-ph.GA].

[59] R.I. Anderson, H. Saio, S. Ekström, C. Georgy, G. Meynet, On the effect of rotation on populations of classical cepheids II. Pulsation analysis for metallicities 0.014, 0.006, and 0.002, Astron. Astrophys. 591 (2016) A8, arXiv:1604.05691 [astro-ph.SR].

[60] G. De Somma, M. Marconi, R. Molinaro, V. Ripepi, S. Leccia, I. Musella, An updated metal-dependent theoretical scenario for classical cepheids, Astrophys. J. Suppl. 262 (1) (2022) 25, arXiv:2206.11154 [astro-ph.SR].

[61] B.F. Madore, The period-luminosity relation. IV - Intrinsic relations and reddenings for the large magellanic cloud cepheids, Astrophys. J. 253 (1982) 575–579.

[62] M. Romaniello, et al., The iron and oxygen content of LMC Classical Cepheids and its implications for the extragalactic distance scale and Hubble constant - Equivalent width analysis with Kurucz stellar atmosphere models, Astron. Astrophys. 658 (2022) A29, arXiv:2110.08860 [astro-ph.CO]; Erratum: Astron. Astrophys. 662 (2022) C1.

[63] D. Zaritsky, R.C. Kennicutt, J.P. Huchra, H II regions and the abundance properties of spiral galaxies, Astrophys. J. 420 (1994) 87.

[64] A.G. Riess, W.-D. Li, P.B. Stetson, A.V. Filippenko, S. Jha, R.P. Kirshner, P.M. Challis, P.M. Garnavich, R. Chornock, Cepheid calibrations from the Hubble Space Telescope of the luminosity of two recent type Ia supernovae and a re-determination of the Hubble constant, Astrophys. J. 627 (2005) 579–607, arXiv:astro-ph/0503159.

[65] A.G. Riess, et al., Cepheid calibrations of modern type Ia supernovae: Implications for the Hubble constant, Astrophys. J. Suppl. 183 (2009) 109–141, arXiv:0905.0697 [astro-ph.CO].

[66] L. Galbany, et al., Nearby supernova host galaxies from the CALIFA Survey: II. SN environmental metallicity, Astron. Astrophys. 591 (2016) A48, arXiv:1603.07808 [astro-ph.GA].

[67] P. Kervella, A. Gallenne, N. Remage Evans, L. Szabados, F. Arenou, A. Mérand, Y. Proto, P. Karczmarek, N. Nardetto, W. Gieren, G. Pietrzynski, Multiplicity of Galactic Cepheids and RR Lyrae stars from Gaia DR2. I. Binarity from proper motion anomaly, Astron. Astrophys. 623 (2019) A116, arXiv:1903.03632 [astro-ph.SR].

[68] P. Karczmarek, G. Hajdu, G. Pietrzyński, W. Gieren, W. Narloch, R. Smolec, G. Wiktorowicz, K. Belczynski, Synthetic population of binary cepheids. II. The effect of companion light on the extragalactic distance scale, Astrophys. J. 950 (2) (2023) 182, arXiv:2303.15664 [astro-ph.GA].

[69] R.I. Anderson, A.G. Riess, On cepheid distance scale bias due to stellar companions and cluster populations, Astrophys. J. 861 (1) (2018) 36, arXiv:1712.01065 [astro-ph.SR].

[70] B.J. Mochejska, L.M. Macri, D.D. Sasselov, K.Z. Stanek, The direct project: influence of blending on the cepheid distance scale. I. Cepheids in m31, Astron. J. 120 (2000) 810, arXiv:astro-ph/9908293.

[71] B. Follin, L. Knox, Insensitivity of the distance ladder Hubble constant determination to Cepheid calibration modelling choices, Mon. Not. R. Astron. Soc. 477 (4) (2018) 4534–4542, arXiv:1707.01175 [astro-ph.CO].

[72] L. Perivolaropoulos, F. Skara, Hubble tension or a transition of the cepheid SnIa calibrator parameters? Phys. Rev. D 104 (12) (2021) 123511, arXiv:2109.04406 [astro-ph.CO].

[73] C. Hahn, T.K. Starkenburg, D. Anglés-Alcázar, E. Choi, R. Davé, C. Dickey, K.G. Iyer, A.H. Maller, R.S. Somerville, J.L. Tinker, L.Y.A. Yung, IQ collaboratory. III. The empirical dust attenuation framework-taking hydrodynamical simulations with a grain of dust, Astrophys. J. 926 (2) (2022) 122, arXiv:2106.09741 [astro-ph.GA].

[74] G.F. Benedict, B.E. McArthur, M.W. Feast, T.G. Barnes, T.E. Harrison, R.J. Patterson, J.W. Menzies, J.L. Bean, W.L. Freedman, Hubble space telescope fine guidance sensor parallaxes of galactic cepheid variable stars: Period-luminosity relations, Astron. J. 133 (2007) 1810–1827, arXiv:astro-ph/0612465; Erratum: Astron. J. 133 (2007) 2980.

[75] S. Casertano, et al., Parallax of galactic cepheids from spatially scanning the wide field camera 3 on the Hubble Space Telescope: The Case of SS Canis Majoris, Astrophys. J. 825 (1) (2016) 11, arXiv:1512.09371 [astro-ph.SR].

[76] A.G. Riess, et al., New parallaxes of galactic cepheids from spatially scanning the Hubble space telescope: Implications for the Hubble constant, Astrophys. J. 855 (2) (2018) 136, arXiv:1801.01120 [astro-ph.SR].

[77] L. Lindegren, U. Bastian, M. Biermann, A. Bombrun, A. de Torres, E. Gerlach, R. Geyer, J. Hernández, T. Hilger, D. Hobbs, S.A. Klioner, U. Lammers, P.J. McMillan, M. Ramos-Lerate, H. Steidelmüller, C.A. Stephenson, F. van Leeuwen, Gaia early data release 3. Parallax bias versus magnitude, colour, and position, Astron. Astrophys. 649 (2021) A4, arXiv:2012.01742 [astro-ph.IM].

[78] A.G. Riess, S. Casertano, W. Yuan, J.B. Bowers, L. Macri, J.C. Zinn, D. Scolnic, Cosmic distances calibrated to 1% precision with Gaia EDR3 parallaxes and Hubble Space Telescope photometry of 75 Milky Way Cepheids confirm tension with ΛCDM, Astrophys. J. Lett. 908 (1) (2021) L6, arXiv:2012.08534 [astro-ph.CO].

[79] S. Li, S. Casertano, A.G. Riess, A maximum likelihood calibration of the tip of the red giant branch luminosity from high latitude field giants using Gaia early data release 3 parallaxes, Astrophys. J. 939 (2) (2022) 96, arXiv:2202.11110 [astro-ph.GA].

[80] R.I. Anderson, L. Eyer, N. Mowlavi, Cepheids in open clusters: An 8-D all-sky census, Mon. Not. R. Astron. Soc. 434 (2013) 2238, arXiv:1212.5119 [astro-ph.GA].

[81] L. Breuval, et al., The Milky Way cepheid Leavitt Law based on Gaia DR2 parallaxes of companion stars and host open cluster populations, Astron. Astrophys. 643 (2020) A115, arXiv:2006.08763 [astro-ph.SR].

[82] A.G. Riess, L. Breuval, W. Yuan, S. Casertano, L.M. Macri, J.B. Bowers, D. Scolnic, T. Cantat-Gaudin, R.I. Anderson, M.C. Reyes, Cluster cepheids with high precision Gaia parallaxes, low zero-point uncertainties, and Hubble Space Telescope photometry, Astrophys. J. 938 (1) (2022) 36, arXiv:2208.01045 [astro-ph.CO].

[83] M.C. Reyes, R.I. Anderson, A 0.9% calibration of the galactic cepheid luminosity scale based on Gaia DR3 data of open clusters and cepheids, Astron. Astrophys. 672 (2023) A85, arXiv:2208.09403 [astro-ph.GA].

[84] W. Yuan, L.M. Macri, A.G. Riess, T.G. Brink, S. Casertano, A.V. Filippenko, S.L. Hoffmann, C.D. Huang, D. Scolnic, Absolute calibration of cepheid Period–Luminosity relations in NGC 4258, Astrophys. J. 940 (1) (2022) 64, arXiv:2203.06681 [astro-ph.GA].

[85] S. Li, A.G. Riess, M.P. Busch, S. Casertano, L.M. Macri, W. Yuan, A sub-2% distance to M31 from photometrically homogeneous near-infrared cepheid Period–Luminosity relations measured with the Hubble Space Telescope, Astrophys. J. 920 (2) (2021) 84, arXiv:2107.08029 [astro-ph.CO].

[86] A.L. Argon, L.J. Greenhill, J.M. Moran, M.J. Reid, K.M. Menten, M. Inoue, The IC133 water vapor maser in the galaxy M33: A geometric distance, Astrophys. J. 615 (2004) 702–719, arXiv:astro-ph/0407486.

[87] A.Z. Bonanos, et al., The first DIRECT distance determination to a detached eclipsing binary in M33, Astrophys. J. 652 (2006) 313–322, arXiv:astro-ph/0606279.

[88] M. Taormina, R.-P. Kudritzki, J. Puls, B. Pilecki, E. Sextl, G. Pietrzyński, M.A. Urbaneja, W. Gieren, Toward early-type eclipsing binaries as extragalactic milestones. II. NLTE spectral analysis and stellar parameters of the detached O-type system OGLE-LMC-ECL-06782 in the LMC, Astrophys. J. 890 (2) (2020) 137, arXiv:2001.04762 [astro-ph.SR].

[89] A. Salsi, N. Nardetto, D. Mourard, D. Graczyk, M. Taormina, O. Creevey, V. Hocdé, F. Morand, K. Perraut, G. Pietrzynski, G.H. Schaefer, Progress on the calibration of surface brightness-color relations for early- and late-type stars, Astron. Astrophys. 652 (2021) A26, arXiv:2106.01073 [astro-ph.SR].

[90] C.-C. Ngeow, A. Bhardwaj, J.-Y. Henderson, M.J. Graham, R.R. Laher, M.S. Medford, J. Purdum, B. Rusholme, Zwicky transient facility and globular clusters: The period-luminosity and period-wesenheit relations for Type II Cepheids, Astrophys. J. 164 (4) (2022) 154, arXiv:2208.03404 [astro-ph.SR].

[91] W. Narloch, G. Hajdu, G. Pietrzyński, W. Gieren, P. Wielgórski, B. Zgirski, P. Karczmarek, M. Górski, D. Graczyk, Period-luminosity relations for galactic classical cepheids in the sloan bands, Astrophys. J. 953 (1) (2023) 14, arXiv:2306.06326 [astro-ph.GA].

[92] F. Bresolin, W. Gieren, R.-P. Kudritzki, G. Pietrzynski, M.A. Urbaneja, G. Carraro, Extragalactic chemical abundances: do HII regions and young stars tell the same story? The case of the spiral galaxy NGC 300, Astrophys. J. 700 (2009) 309–330, arXiv:0905.2791 [astro-ph.CO].

[93] F. Bresolin, R.-P. Kudritzki, M.A. Urbaneja, The metallicity and distance of NGC 2403 from blue supergiants, Astrophys. J. 940 (1) (2022) 32, arXiv:2209.13135 [astro-ph.GA].

[94] C.-C. Ngeow, S.M. Kanbur, S. Nikolaev, J. Buonaccorsi, K.H. Cook, D.L. Welch, Further empirical evidence for the non-linearity of the period-luminosity relations as seen in the Large Magellanic Cloud Cepheids, Mon. Not. R. Astron. Soc. 363 (2005) 831–846, arXiv:astro-ph/0507601.

[95] A. Sandage, G.A. Tammann, B. Reindl, New period-luminosity and period-color relations of classical Cepheids: III. Cepheids in SMC, Astron. Astrophys. 493 (2009) 471–479, arXiv:0810.1780 [astro-ph].

[96] M. Kodric, et al., Properties of M31. II: A Cepheid disk sample derived from the first year of PS1 PAndromeda data, AJ 145 (2013) 106, arXiv:1301.6170 [astro-ph.CO].

[97] A. Bhardwaj, S.M. Kanbur, L.M. Macri, H.P. Singh, C.-C. Ngeow, E.E.O. Ishida, Large magellanic cloud near-infrared synoptic survey - III. A statistical study of non-linearity in the Leavitt Laws, Mon. Not. R. Astro. Soc. 457 (2) (2016) 1644–1665, arXiv:1601.00953 [astro-ph.GA].

[98] D. Kushnir, A. Sharon, A cepheid systematics-free test of H_0 to $\lesssim 2.5\%$ accuracy using SH0ES photometry, 2024, arXiv:2404.16102 [astro-ph.CO].

[99] C. Kuo, J.A. Braatz, M.J. Reid, F.K.Y. Lo, J.J. Condon, C.M.V. Impellizzeri, C. Henkel, The megamaser cosmology project. V. An angular diameter distance to NGC 6264 at 140 Mpc, Astrophys. J. 767 (2013) 155, arXiv:1207.7273 [astro-ph.CO].

[100] C.Y. Kuo, J.A. Braatz, K.Y. Lo, M.J. Reid, S.H. Suyu, D.W. Pesce, J.J. Condon, C. Henkel, C.M.V. Impellizzeri, The megamaser cosmology project. VI. Observations of NGC 6323, Astrophys. J. 800 (1) (2015) 26, arXiv:1411.5106 [astro-ph.GA].

[101] B. Cooke, M. Elitzur, Water masers in late-type stars, Astrophys. J. 295 (1985) 175–182.

[102] K.Y. Lo, Mega-masers and galaxies, Annu. Rev. Astron. Astrophys. 43 (1) (2005) 625–676.

[103] A.L. Argon, L.J. Greenhill, M.J. Reid, J.M. Moran, E.M.L. Humphreys, Toward a new geometric distance to the active galaxy NGC4258. 1. VLBI monitoring of water maser emission, Astrophys. J. 659 (2007) 1040–1062, arXiv:astro-ph/0701396.

[104] J. Kormendy, L.C. Ho, Coevolution (or not) of supermassive black holes and host galaxies, Ann. Rev. Astron. Astrophys.. 51 (2013) 511–653, arXiv:1304.7762 [astro-ph.CO].

[105] J.R. Herrnstein, J.M. Moran, L.J. Greenhill, P.J. Diamond, M. Inoue, N. Nakai, M. Miyoshi, C. Henkel, A. Riess, A geometric distance to the galaxy NGC 4258 from orbital motions in a nuclear gas disk, Nature 400 (1999) 539–541, arXiv:astro-ph/9907013.

[106] C.Y. Kuo, J.A. Braatz, J.J. Condon, C.M.V. Impellizzeri, K.Y. Lo, I. Zaw, M. Schenker, C. Henkel, M.J. Reid, J.E. Greene, The megamaser cosmology project. III. Accurate masses of seven supermassive black holes in active galaxies with circumnuclear megamaser disks, Astrophys. J. 727 (2011) 20, arXiv:1008.2146 [astro-ph.CO].

[107] F. Gao, J.A. Braatz, M.J. Reid, J.J. Condon, J.E. Greene, C. Henkel, C.M.V. Impellizzeri, K.Y. Lo, C.Y. Kuo, D.W. Pesce, J. Wagner, W. Zhao, The megamaser cosmology project. IX. Black hole masses for three maser galaxies, Astrophys. J. 834 (1) (2017) 52, arXiv:1610.06802 [astro-ph.GA].

[108] M.J. Reid, J.A. Braatz, J.J. Condon, K.Y. Lo, C.Y. Kuo, C.M.V. Impellizzeri, C. Henkel, The megamaser cosmology project: IV. A direct measurement of the Hubble constant from UGC 3789, Astrophys. J. 767 (2013) 154, arXiv:1207.7292 [astro-ph.CO].

[109] F. Gao, J.A. Braatz, M.J. Reid, K.Y. Lo, J.J. Condon, C. Henkel, C.Y. Kuo, C.M.V. Impellizzeri, D.W. Pesce, W. Zhao, The megamaser cosmology project VIII. A geometric distance to NGC 5765b, Astrophys. J. 817 (2) (2016) 128, arXiv:1511.08311 [astro-ph.GA].

[110] D.W. Pesce, et al., The megamaser cosmology project. XIII. Combined Hubble constant constraints, Astrophys. J. Lett. 891 (1) (2020) L1, arXiv:2001.09213 [astro-ph.CO].

[111] M.J. Reid, J.A. Braatz, J.J. Condon, L.J. Greenhill, C. Henkel, K.Y. Lo, The megamaser cosmology project: I. VLBI observations of UGC 3789, Astrophys. J. 695 (2009) 287–291, arXiv:0811.4345 [astro-ph].

[112] J.A. Braatz, M.J. Reid, E.M.L. Humphreys, C. Henkel, J.J. Condon, K.Y. Lo, The megamaser cosmology Project. II. The angular-diameter distance to UGC 3789, Astrophys. J. 718 (2010) 657–665, arXiv:1005.1955 [astro-ph.CO].

[113] C.Y. Kuo, A. Constantin, J.A. Braatz, H.H. Chung, C.A. Witherspoon, D. Pesce, C.M.V. Impellizzeri, F. Gao, L. Hao, J.H. Woo, I. Zaw, Enhancing the H_2O megamaser detection rate using optical and mid-infrared photometry, Astrophys. J. 860 (2) (2018) 169, arXiv:1712.04204 [astro-ph.GA].

[114] C.Y. Kuo, J.Y. Hsiang, H.H. Chung, A. Constantin, Y.Y. Chang, E.d. Cunha, D. Pesce, W.T. Chien, B.Y. Chen, J.A. Braatz, I. Zaw, S. Matsushita, J.C. Lin, A more efficient search for H_2O megamaser galaxies: The power of X-ray and mid-infrared photometry, Astrophys. J. 892 (1) (2020) 18, arXiv:1911.10721 [astro-ph.GA].

[115] D.W. Pesce, J.A. Braatz, J.J. Condon, F. Gao, C. Henkel, E. Litzinger, K.Y. Lo, M.J. Reid, The megamaser cosmology project. VII. Investigating disk physics using spectral monitoring observations, Astrophys. J. 810 (1) (2015) 65, arXiv:1507.07904 [astro-ph.GA].

[116] A.E. Bragg, L.J. Greenhill, J.M. Moran, C. Henkel, Accelerations of water masers in ngc4258, Astrophys. J. 535 (2000) 73, arXiv:astro-ph/0001543.

[117] E.M.L. Humphreys, M.J. Reid, L.J. Greenhill, J.M. Moran, A.L. Argon, Toward a new distance to the active galaxy ngc 4258: II. Centripetal accelerations and investigation of spiral structure, Astrophys. J. 672 (2008) 800–816, arXiv:0709.0925 [astro-ph].

[118] J. Braatz, D. Pesce, J. Condon, M. Reid, H2O megamaser cosmology with the ngVLA, Bull. Am. Astron. Soc. 51 (3) (2019) 446.

[119] M.G. Lee, W.L. Freedman, B.F. Madore, The tip of the red giant branch as a distance indicator for resolved galaxies, Astrophys. J. 417 (1993) 553.

[120] J.B. Jensen, J.P. Blakeslee, M. Cantiello, M. Cowles, G.S. Anand, R.B. Tully, E. Kourkchi, G. Raimondo, The TRGB-SBF Project. III. Refining the hst surface brightness fluctuation distance scale calibration with JWST, 2025, arXiv:2502.15935 [astro-ph.CO].

[121] G.S. Anand, R.B. Tully, L. Rizzi, A.G. Riess, W. Yuan, Comparing tip of the red giant branch distance scales: An independent reduction of the Carnegie-Chicago Hubble program and the value of the Hubble constant, Astrophys. J. 932 (1) (2022) 15, arXiv:2108.00007 [astro-ph.CO].

[122] D. Scolnic, A.G. Riess, J. Wu, S. Li, G.S. Anand, R. Beaton, S. Casertano, R.I. Anderson, S. Dhawan, X. Ke, CATS: The Hubble constant from standardized TRGB and type Ia supernova measurements, Astrophys. J. Lett. 954 (1) (2023) L31, arXiv:2304.06693 [astro-ph.CO].

[123] S. Li, R.L. Beaton, The tip of the red giant branch distance ladder and the Hubble constant, 2024, arXiv:2403.17048 [astro-ph.CO].

[124] J.B. Jensen, et al., Infrared surface brightness fluctuation distances for massive and type Ia supernova host galaxies, Astrophys.. J. Supp. 255 (2) (2021) 21, arXiv:2105.08299 [astro-ph.CO].

[125] J. Wu, D. Scolnic, A.G. Riess, G.S. Anand, R. Beaton, S. Casertano, X. Ke, S. Li, Comparative analysis of TRGBs (CATs) from unsupervised, multi-halo-field measurements: Contrast is key, Astrophys. J. 954 (1) (2023) 87, arXiv:2211.06354 [astro-ph.CO].

[126] R.I. Anderson, N.W. Koblischke, L. Eyer, Small-amplitude red giants elucidate the nature of the tip of the red giant branch as a standard candle, Astrophys. J. Lett. 963 (2) (2024) L43, arXiv:2303.04790 [astro-ph.CO].

[127] D. Hatt, et al., The Carnegie-Chicago Hubble Program. II. The distance to IC 1613: The tip of the red giant branch and RR Lyrae Period–luminosity relations, Astrophys. J. 845 (2) (2017) 146, arXiv:1703.06468 [astro-ph.CO].

[128] S. Nikolaev, M.D. Weinberg, Stellar populations in the large magellanic cloud from 2mass, Astrophys. J. 542 (2000) 804–818, arXiv:astro-ph/0003012.

[129] B.F. Madore, W.L. Freedman, Astrophysical distance scale: The AGB J-band method. I. Calibration and a first application, Astrophys. J. 899 (1) (2020) 66, arXiv:2005.10792 [astro-ph.GA].

[130] R.I. Anderson, The span of space, Nat. Phys. 20 (11) (2024) 1841–1841.

[131] J. Tang, A. Bressan, P. Rosenfield, A. Slemer, P. Marigo, L. Girardi, L. Bianchi, New PARSEC evolutionary tracks of massive stars at low metallicity: testing canonical stellar evolution in nearby star-forming dwarf galaxies, Mon. Not. R. Astro. Soc. 445 (4) (2014) 4287–4305, arXiv:1410.1745 [astro-ph.SR].

[132] Y. Chen, A. Bressan, L. Girardi, P. Marigo, X. Kong, A. Lanza, PARSEC evolutionary tracks of massive stars up to 350 $M_\odot$ at metallicities $0.0001 \leq Z \leq 0.04$, Mon. Not. R. Astro. Soc. 452 (1) (2015) 1068–1080, arXiv:1506.01681 [astro-ph.SR].

[133] M. Salaris, S. Cassisi, The tip of the red giant branch as a distance indicator: results from evolutionary models, Mon. Not. R. Astron. Soc. 289 (1997) 406, arXiv:astro-ph/9703186.
[134] M. Salaris, S. Cassisi, A. Weiss, Red giant branch stars: the theoretical framework, Publ. Astron. Soc. Pac. 114 (2002) 375, arXiv:astro-ph/0201387.
[135] M. Salaris, S. Cassisi, Evolution of Stars and Stellar Populations, Wiley, 2005.
[136] S. Cassisi, M. Salaris, Old Stellar Populations: How to Study the Fossil Record of Galaxy Formation, Wiley-VCH Verlag GmbH, 2013.
[137] A. Serenelli, A. Weiss, S. Cassisi, M. Salaris, A. Pietrinferni, The brightness of the red giant branch tip. theoretical framework, a set of reference models, and predicted observables, Astron. Astrophys. 606 (2017) A33, arXiv:1706.09910 [astro-ph.SR].
[138] L. Rizzi, R.B. Tully, D. Makarov, L. Makarova, A.E. Dolphin, S. Sakai, E.J. Shaya, Tip of the red giant branch distances. 2. Zero-point calibration, Astrophys. J. 661 (2007) 815–829, arXiv:astro-ph/0701518.
[139] I.S. Jang, M.G. Lee, The tip of the red giant branch distances to type Ia supernova host galaxies. IV. Color dependence and zero-point calibration, Astrophys. J. 835 (1) (2017) 28, arXiv:1611.05040 [astro-ph.GA].
[140] E. Farag, F.X. Timmes, M.T. Chidester, S. Anandagoda, D.H. Hartmann, Stellar neutrino emission across the Mass–Metallicity plane, Astrophys. J. Suppl. 270 (1) (2024) 5, arXiv:2310.13142 [astro-ph.SR].
[141] S. Cassisi, Modelling of red giant stars: The state-of-the-art, Eur. Phys. J. Web Conf. 160 (2017) 04002.
[142] I.D. Saltas, E. Tognelli, New calibrated models for the tip of the red giant branch luminosity and a thorough analysis of theoretical uncertainties, Mon. Not. R. Astron. Soc. 514 (2) (2022) 3058–3073, arXiv:2203.02499 [astro-ph.SR].
[143] Gaia Collaboration, T. Prusti, et al., The Gaia mission, Astron. Astrophys. 595 (Gaia Data Release 1) (2016) A1, arXiv:1609.04153 [astro-ph.IM].
[144] W.L. Freedman, Measurements of the Hubble constant: Tensions in perspective, Astrophys. J. 919 (1) (2021) 16, arXiv:2106.15656 [astro-ph.CO].
[145] B.F. Madore, W.L. Freedman, K. Owens, Astrophysical distance scale VII: A self-consistent, multi-wavelength calibration of the slopes and relative zero points for the run of luminosity with color of stars defining the tip of the red giant branch, 2023, arXiv:2311.05048 [astro-ph.GA].
[146] G. Csörnyei, R.I. Anderson, C. Vogl, S. Taubenberger, S. Blondin, B. Leibundgut, W. Hillebrandt, Reeling in the Whirlpool galaxy: Distance to M 51 clarified through Cepheids and the Type IIP supernova 2005cs, Astron. Astrophys. 678 (2023) A44, arXiv:2305.13943 [astro-ph.GA].
[147] N.W. Koblischke, R.I. Anderson, Calibrating and standardizing the tip of the red giant branch in the small magellanic cloud using small-amplitude red giants, Astrophys. J. 974 (2) (2024) 181, arXiv:2406.19375 [astro-ph.SR].
[148] S. Li, S. Casertano, A.G. Riess, A Gaia data release 3 view on the tip of the red giant branch luminosity, Astrophys. J. 950 (2) (2023) 83, arXiv:2304.06695 [astro-ph.GA].
[149] J. Maíz Apellániz, M. Pantaleoni González, R.H. Barbá, Validation of the accuracy and precision of Gaia EDR3 parallaxes with globular clusters, Astron. Astrophys. 649 (2021) A13, arXiv:2101.10206 [astro-ph.IM].
[150] Y. Huang, H. Yuan, T.C. Beers, H. Zhang, The parallax zero-point of Gaia early data release 3 from LAMOST primary red clump stars, Astrophys. J. Lett. 910 (1) (2021) L5, arXiv:2101.09691 [astro-ph.GA].
[151] F. Ren, X. Chen, H. Zhang, R. de Grijs, L. Deng, Y. Huang, Gaia EDR3 parallax zero-point offset based on W Ursae majoris-type eclipsing binaries, Astrophys. J. Lett. 911 (2) (2021) L20, arXiv:2103.16096 [astro-ph.SR].
[152] S. Khan, R.I. Anderson, A. Miglio, B. Mosser, Y.P. Elsworth, Investigating Gaia EDR3 parallax systematics using asteroseismology of cool giant stars observed by Kepler, K2, and TESS. II. Deciphering Gaia parallax systematics using red clump stars, Astron. Astrophys. 680 (2023) A105, arXiv:2310.03654 [astro-ph.SR].
[153] J. Soltis, S. Casertano, A.G. Riess, The parallax of ω centauri measured from Gaia EDR3 and a direct, geometric calibration of the tip of the red giant branch and the Hubble constant, Astrophys. J. Lett. 908 (1) (2021) L5, arXiv:2012.09196 [astro-ph.GA].
[154] S. Jang, A.P. Milone, E.P. Lagioia, M. Tailo, M. Carlos, E. Dondoglio, M. Martorano, A. Mohandasan, A.F. Marino, G. Cordoni, Y.W. Lee, Integrated photometry of multiple stellar populations in globular clusters, Astrophys. J. 920 (2) (2021) 129, arXiv:2107.14246 [astro-ph.GA].
[155] D.M. Skowron, J. Skowron, A. Udalski, M.K. Szymański, I. Soszyński, Ł. Wyrzykowski, K. Ulaczyk, R. Poleski, S. Kozłowski, P. Pietrukowicz, P. Mróz, K. Rybicki, P. Iwanek, M. Wrona, M. Gromadzki, OGLE-ing the magellanic system: Optical reddening maps of the large and small magellanic clouds from red clump stars, Astrophys. J. Suppl. 252 (2) (2021) 23, arXiv:2006.02448 [astro-ph.SR].
[156] D.J. Schlegel, D.P. Finkbeiner, M. Davis, Maps of dust IR emission for use in estimation of reddening and CMBR foregrounds, Astrophys. J. 500 (1998) 525, arXiv:astro-ph/9710327.
[157] E.F. Schlafly, D.P. Finkbeiner, Measuring reddening with SDSS Stellar spectra and recalibrating SFD, Astrophys. J. 737 (2011) 103, arXiv:1012.4804 [astro-ph.GA].
[158] R.I. Anderson, Relativistic corrections for measuring Hubble's constant to 1% using stellar standard candles, Astron. Astrophys. 658 (2022) A148, arXiv:2108.09067 [astro-ph.CO].
[159] J.E.G. Peek, B. Ménard, L. Corrales, Dust in the circumgalactic medium of low-redshift galaxies, Astrophys. J. 813 (1) (2015) 7, arXiv:1411.3333 [astro-ph.GA].
[160] B. Mendez, M. Davis, J. Moustakas, J. Newman, B.F. Madore, W.L. Freedman, Deviations from the local Hubble flow. 1. The tip of the red giant branch as a distance indicator, Astron. J. 124 (2002) 213, arXiv:astro-ph/0204192.
[161] D. Makarov, L. Makarova, L. Rizzi, R.B. Tully, A.E. Dolphin, S. Sakai, E.J. Shaya, Tip of the red giant branch distances. 1. optimization of a maximum likelihood algorithm, Astron. J. 132 (2006) 2729–2742, arXiv:astro-ph/0603073.
[162] B.F. Madore, V. Mager, W.L. Freedman, Sharpening the tip of the red giant branch, Astrophys. J. 690 (2009) 389–393, arXiv:0809.2598 [astro-ph].
[163] R.L. Beaton, G. Bono, V.F. Braga, M. Dall'Ora, G. Fiorentino, I.S. Jang, C.E. Martínez-Vázquez, N. Matsunaga, M. Monelli, J.R. Neeley, M. Salaris, Old-aged primary distance indicators, Space Sci. Rev. 214 (8) (2018) 113, arXiv:1808.09191 [astro-ph.GA].
[164] Euclid Collaboration, Y. Mellier, et al., Euclid. i. Overview of the Euclid mission, 2024, arXiv:2405.13491 [astro-ph.CO].
[165] M.J.B. Newman, K.B.W. McQuinn, E.D. Skillman, M.L. Boyer, R.E. Cohen, A.E. Dolphin, O.G. Telford, An empirical calibration of the tip of the red giant branch distance method in the near infrared. I. Hubble Space Telescope WFC3/IR F110W and F160W filters, Astrophys. J. 966 (2) (2024) 175, arXiv:2403.03086 [astro-ph.GA].
[166] M.J.B. Newman, K.B.W. McQuinn, E.D. Skillman, M.L. Boyer, R.E. Cohen, A.E. Dolphin, O.G. Telford, An empirical calibration of the tip of the red giant branch distance method in the near infrared. II. JWST NIRCam wide filters, Astrophys. J. 975 (2) (2024) 195, arXiv:2406.03532 [astro-ph.CO].
[167] E. Valenti, F.R. Ferraro, L. Origlia, The red giant branch in the near - infrared color - magnitude diagrams. 1: The calibration of photometric indices, Mon. Not. R. Astron. Soc. 351 (2004) 1204, arXiv:astro-ph/0403563.
[168] J.J. Dalcanton, et al., Resolved near-infrared stellar populations in nearby galaxies, Astrophys. J. Suppl. 198 (2012) 6, arXiv:1109.6893 [astro-ph.CO].
[169] P.-F. Wu, R.B. Tully, L. Rizzi, A.E. Dolphin, B.A. Jacobs, I.D. Karachentsev, Infrared tip of the red giant branch and distances to the Maffei/IC 342 group, Astron. J. 148 (2014) 7, arXiv:1404.2987 [astro-ph.GA].
[170] B.F. Madore, et al., The near-infrared tip of the red giant branch. I. A calibration in the isolated dwarf Galaxy IC 1613, Astrophys. J. 858 (1) (2018) 11, arXiv:1803.01278 [astro-ph.GA].
[171] T.J. Hoyt, W.L. Freedman, B.F. Madore, M. Seibert, R.L. Beaton, D. Hatt, I.S. Jang, M.G. Lee, A.J. Monson, J.A. Rich, The near-infrared tip of the red giant branch. II. An absolute calibration in the large magellanic cloud, Astrophys. J. 858 (1) (2018) 12, arXiv:1803.01277 [astro-ph.GA].
[172] M.J. Durbin, R.L. Beaton, J.J. Dalcanton, B.F. Williams, M.L. Boyer, MCR-TRGB: A multiwavelength-covariant, robust tip of the red giant branch measurement method, Astrophys. J. 898 (1) (2020) 57, arXiv:2006.08559 [astro-ph.GA].
[173] K.B.W. McQuinn, M. Boyer, E.D. Skillman, A.E. Dolphin, Using the tip of the red giant branch as a distance indicator in the near infrared, Astrophys. J. 880 (1) (2019) 63, arXiv:1904.01571 [astro-ph.GA].
[174] W.L. Freedman, B.F. Madore, I.S. Jang, T.J. Hoyt, A.J. Lee, K.A. Owens, Status report on the Chicago-Carnegie Hubble program (CCHP): Three independent astrophysical determinations of the Hubble constant using the james webb space telescope, 2024, arXiv:2408.06153 [astro-ph.CO].
[175] Gaia Collaboration, Gaia data release 3. The galaxy in your preferred colours: Synthetic photometry from Gaia low-resolution spectra, Astron. Astrophys. 674 (2023) A33, arXiv:2206.06215 [astro-ph.SR].
[176] D.R. Weisz, et al., The JWST resolved stellar populations early release science program. II. Survey overview, Astrophys. J. Suppl. 268 (1) (2023) 15, arXiv:2301.04659 [astro-ph.GA].
[177] A.J. Lee, L. Rousseau-Nepton, W.L. Freedman, B.F. Madore, M.-R.L. Cioni, T.J. Hoyt, I.S. Jang, A. Javadi, K.A. Owens, The astrophysical distance scale. V. A 2% distance to the local group spiral M33 via the JAGB method, tip of the red giant branch, and Leavitt Law, Astrophys. J. 933 (2) (2022) 201, arXiv:2205.11323 [astro-ph.GA].
[178] J. Tonry, D.P. Schneider, A new technique for measuring extragalactic distances, Astron. J. 96 (1988) 807.
[179] J.L. Tonry, E.A. Ajhar, G.A. Luppino, Observations of surface-brightness fluctuations in virgo, Astron. J. 100 (1990) 1416.
[180] J.P. Blakeslee, A. Jordan, S. Mei, P. Cote, L. Ferrarese, L. Infante, E.W. Peng, J.L. Tonry, M.J. West, The ACS Fornax Cluster Survey. V. Measurement and recalibration of surface brightness fluctuations and a precise value of the Fornax–Virgo relative distance, Astrophys. J. 694 (2009) 556–572, arXiv:0901.1138 [astro-ph.CO].
[181] J.B. Jensen, J.P. Blakeslee, Z. Gibson, H.-c. Lee, M. Cantiello, G. Raimondo, N. Boyer, H. Cho, Measuring infrared surface brightness fluctuation distances with HST WFC3: Calibration and advice, Astrophys. J. 808 (1) (2015) 91, arXiv:1505.00400 [astro-ph.GA].

[182] M. Moresco, et al., Unveiling the universe with emerging cosmological probes, Living Rev. Rel. 25 (1) (2022) 6, arXiv:2201.07241 [astro-ph.CO].

[183] M. Cantiello, J.P. Blakeslee, Surface brightness fluctuations, 2023, arXiv:2307.03116 [astro-ph.CO].

[184] J.L. Tonry, A. Dressler, J.P. Blakeslee, E.A. Ajhar, A.B. Fletcher, G.A. Luppino, M.R. Metzger, C.B. Moore, The sbf survey of galaxy distances. 4. sbf magnitudes, colors, and distances, Astrophys. J. 546 (2001) 681–693, arXiv:astro-ph/0011223.

[185] G. Raimondo, Joint analysis of near-infrared properties and surface brightness fluctuations of LMC star clusters, Astrophys. J. 700 (2009) 1247–1261, arXiv:0907.1408 [astro-ph.GA].

[186] M. Cantiello, et al., The Next Generation Virgo Cluster Survey (ngvs). III. A catalog of surface brightness fluctuation distances and the three-dimensional distribution of galaxies in the Virgo cluster, Astrophys. J. 966 (1) (2024) 145, arXiv:2403.16235 [astro-ph.GA].

[187] L. Ferrarese, P. Côté, J.-C. Cuillandre, S.D.J. Gwyn, E.W. Peng, L.A. MacArthur, P.-A. Duc, A. Boselli, S. Mei, T. Erben, A.W. McConnachie, P.R. Durrell, J.C. Mihos, A. Jordán, A. Lançon, T.H. Puzia, E. Emsellem, M.L. Balogh, J.P. Blakeslee, L. van Waerbeke, R. Gavazzi, B. Vollmer, J.J. Kavelaars, D. Woods, N.M. Ball, S. Boissier, S. Courteau, E. Ferriere, G. Gavazzi, H. Hildebrandt, P. Hudelot, M. Huertas-Company, C. Liu, D. McLaughlin, Y. Mellier, M. Milkeraitis, D. Schade, C. Balkowski, F. Bournaud, R.G. Carlberg, S.C. Chapman, H. Hoekstra, C. Peng, M. Sawicki, L. Simard, J.E. Taylor, R.B. Tully, W. van Driel, C.D. Wilson, T. Burdullis, B. Mahoney, N. Manset, The Next Generation Virgo Cluster Survey (NGVS). I. Introduction to the survey, Astrophys. J. Suppl. 200 (1) (2012) 4.

[188] L.V. Sales, A. Wetzel, A. Fattahi, Baryonic solutions and challenges for cosmological models of dwarf galaxies, Nat. Astron. 6 (8) (2022) 897–910, arXiv:2206.05295 [astro-ph.GA].

[189] J.P. Blakeslee, M. Cantiello, Independent analysis of the distance to NGC, 1052-DF2, Res. Notes the Am. Astron. Soc. 2 (3) (2018) 146, arXiv:1808.02176 [astro-ph.GA].

[190] S.G. Carlsten, R.L. Beaton, J.P. Greco, J.E. Greene, Using surface brightness fluctuations to study nearby satellite galaxy systems: Calibration and methodology, Astrophys. J. 879 (1) (2019) 13, arXiv:1901.07575 [astro-ph.GA].

[191] Y.J. Kim, M.G. Lee, Calibration of surface brightness fluctuations for dwarf galaxies in the hyper suprime-cam gi filter system, Astrophys. J. 923 (2) (2021) 152, arXiv:2110.02522 [astro-ph.GA].

[192] Planck Collaboration, N. Aghanim, et al., Planck 2018 results. VI. Cosmological parameters, Astron. Astrophys. 641 (2020) A6, arXiv:1807.06209 [astro-ph.CO]; Erratum: Astron. Astrophys. 652 (2021) C4.

[193] N. Khetan, et al., A new measurement of the Hubble constant using type Ia supernovae calibrated with surface brightness fluctuations, Astron. Astrophys. 647 (2021) A72, arXiv:2008.07754 [astro-ph.CO].

[194] P. Garnavich, C.M. Wood, P. Milne, J.B. Jensen, J.P. Blakeslee, P.J. Brown, D. Scolnic, B. Rose, D. Brout, Connecting infrared surface brightness fluctuation distances to type Ia supernova hosts: Testing the top rung of the distance ladder, Astrophys. J. 953 (1) (2023) 35, arXiv:2204.12060 [astro-ph.CO].

[195] C. Chung, S.-J. Yoon, H. Cho, S.-Y. Lee, Y.-W. Lee, Yonsei Evolutionary Population Synthesis (YEPS) model. III. Surface brightness fluctuation of normal and helium-enhanced simple stellar populations, Astrophys. J. Suppl. 250 (2) (2020) 33, arXiv:2009.00625 [astro-ph.GA].

[196] I.S. Glass, T.L. Evans, A period-luminosity relation for Mira variables in the large magellanic cloud, nature 291 (5813) (1981) 303–304.

[197] M.W. Feast, I.S. Glass, P.A. Whitelock, R.M. Catchpole, A period-luminosity-colour relation for Mira variables, Mon. Not. R. Astro. Soc. 241 (1989) 375–392.

[198] P.A. Whitelock, Asymptotic giant branch variables as extragalactic distance indicators, IAU Symp. 289 (2013) 209, arXiv:1210.7307 [astro-ph.CO].

[199] P.A. Whitelock, Asymptotic giant branch variables in nearby galaxies, in: F. Kerschbaum, M. Groenewegen, H. Olofsson (Eds.), Why Galaxies Care About AGB Stars: A Continuing Challenge through Cosmic Time, in: IAU Symposium, vol. 343, 2019, pp. 275–282, arXiv:1809.10077 [astro-ph.GA].

[200] C.D. Huang, The Mira distance ladder, 2024, arXiv:2401.09581 [astro-ph.CO].

[201] P. Iwanek, R. Poleski, S. Kozłowski, I. Soszyński, P. Pietrukowicz, M. Ban, J. Skowron, P. Mróz, M. Wrona, A. Udalski, M.K. Szymański, D.M. Skowron, K. Ulaczyk, M. Gromadzki, K. Rybicki, M. Ratajczak, A three-dimensional map of the Milky Way using 66,000 Mira variable stars, Astrophys. J. Suppl. 264 (1) (2023) 20, arXiv:2212.00035 [astro-ph.GA].

[202] M.L. Boyer, K.B.W. McQuinn, M.A.T. Groenewegen, A.A. Zijlstra, P.A. Whitelock, J.T. van Loon, G. Sonneborn, G.C. Sloan, E.D. Skillman, M. Meixner, I. McDonald, O.C. Jones, A. Javadi, R.D. Gehrz, N. Britavskiy, A.Z. Bonanos, An infrared census of DUST in nearby galaxies with spitzer (DUSTiNGS). IV. Discovery of high-redshift AGB analogs, Astrophys. J. 851 (2) (2017) 152, arXiv:1711.02129 [astro-ph.SR].

[203] S.R. Goldman, M.L. Boyer, K.B.W. McQuinn, P.A. Whitelock, I. McDonald, J.T. van Loon, E.D. Skillman, R.D. Gehrz, A. Javadi, G.C. Sloan, O.C. Jones, M.A.T. Groenewegen, J.W. Menzies, An infrared census of dust in nearby galaxies with spitzer (DUSTiNGS). V. The period-luminosity relation for dusty metal-poor AGB stars, Astrophys. J. 877 (1) (2019) 49, arXiv:1902.07362 [astro-ph.SR].

[204] M. Trabucchi, P.R. Wood, N. Mowlavi, G. Pastorelli, P. Marigo, L. Girardi, T. Lebzelter, Modelling long-period variables - II. Fundamental mode pulsation in the non-linear regime, Mon. Not. R. Astro. Soc. 500 (2) (2021) 1575–1591, arXiv:2010.13654 [astro-ph.SR].

[205] W. Yuan, L.M. Macri, S. He, J.Z. Huang, S.M. Kanbur, C.-C. Ngeow, Large magellanic cloud near-infrared synoptic survey. V. Period-luminosity relations of Miras, Astron. J. 154 (4) (2017) 149, arXiv:1708.04742 [astro-ph.SR].

[206] W. Yuan, L.M. Macri, A. Javadi, Z. Lin, J.Z. Huang, Near-infrared Mira period-luminosity relations in M33, Astron. J. 156 (3) (2018) 112, arXiv:1807.03544 [astro-ph.SR].

[207] C.D. Huang, et al., A near-infrared Period–Luminosity relation for Miras in NGC 4258, an anchor for a new distance ladder, Astrophys. J. 857 (1) (2018) 67, arXiv:1801.02711 [astro-ph.CO].

[208] A. Chiavassa, B. Freytag, M. Schultheis, Heading Gaia to measure atmospheric dynamics in AGB stars, Astron. Astrophys. 617 (2018) L1, arXiv:1808.02548 [astro-ph.SR].

[209] A. Chiavassa, K. Kravchenko, F. Millour, G. Schaefer, M. Schultheis, B. Freytag, O. Creevey, V. Hocdé, F. Morand, R. Ligi, S. Kraus, J.D. Monnier, D. Mourard, N. Nardetto, N. Anugu, J.B. Le Bouquin, C.L. Davies, J. Ennis, T. Gardner, A. Labdon, C. Lanthermann, B.R. Setterholm, T. ten Brummelaar, Optical interferometry and Gaia measurement uncertainties reveal the physics of asymptotic giant branch stars, Astron. Astrophys. 640 (2020) A23, arXiv:2006.07318 [astro-ph.SR].

[210] M. Andriantsaralaza, S. Ramstedt, W.H.T. Vlemmings, E. De Beck, Distance estimates for AGB stars from parallax measurements, Astron. Astrophys. 667 (2022) A74, arXiv:2209.03906 [astro-ph.SR].

[211] A. Ahmad, B. Freytag, S. Höfner, Properties of self-excited pulsations in 3D simulations of AGB stars and red supergiants, Astron. Astrophys. 669 (2023) A49, arXiv:2211.07682 [astro-ph.SR].

[212] T. Konchady, L.M. Macri, X. Yan, J.Z. Huang, The M33 synoptic stellar survey. III. Miras and LPVs in griJHK$_S$, Mon. Not. R. Astro. Soc. 531 (1) (2024) 110–132, arXiv:2405.00503 [astro-ph.GA].

[213] W. Yuan, Period-Luminosity Relations of Cepheid and Mira Variables and Their Application to the Extragalactic Distance Scale (PhD thesis), Texas A&M University, 2017, https://oaktrust.library.tamu.edu/items/26f6e9a7-5e4c-47ea-ac3e-1645a5b6ab5a/full.

[214] SNLS Collaboration, J. Guy, et al., SALT2: Using distant supernovae to improve the use of type Ia supernovae as distance indicators, Astron. Astrophys. 466 (2007) 11–21, arXiv:astro-ph/0701828.

[215] W.D. Kenworthy, et al., SALT3: An improved type Ia supernova model for measuring cosmic distances, Astrophys. J. 923 (2) (2021) 265, arXiv:2104.07795 [astro-ph.CO].

[216] C.R. Burns, et al., The Carnegie supernova project: Light curve fitting with SNooPy, Astron. J. 141 (2011) 19, arXiv:1010.4040 [astro-ph.CO].

[217] K.S. Mandel, G. Narayan, R.P. Kirshner, Type Ia supernova light curve inference: hierarchical models in the optical and near infrared, Astrophys. J. 731 (2011) 120, arXiv:1011.5910 [astro-ph.CO].

[218] R. Tripp, A two-parameter luminosity correction for type Ia supernovae, Astron. Astrophys. 331 (1998) 815–820.

[219] SNLS Collaboration, A. Conley, et al., Supernova constraints and systematic uncertainties from the first 3 years of the supernova legacy survey, Astrophys. J. Suppl. 192 (2011) 1, arXiv:1104.1443 [astro-ph.CO].

[220] S. Dhawan, D. Brout, D. Scolnic, A. Goobar, A.G. Riess, V. Miranda, Cosmological model insensitivity of local H_0 from the cepheid distance ladder, Astrophys. J. 894 (1) (2020) 54, arXiv:2001.09260 [astro-ph.CO].

[221] Y.S. Murakami, A.G. Riess, B.E. Stahl, W.D. Kenworthy, D.-M.A. Pluck, A. Macoretta, D. Brout, D.O. Jones, D.M. Scolnic, A.V. Filippenko, Leveraging SN Ia spectroscopic similarity to improve the measurement of H $_0$, JCAP 11 (2023) 046, arXiv:2306.00070 [astro-ph.CO].

[222] E.R. Peterson, et al., The pantheon+ analysis: Evaluating peculiar velocity corrections in cosmological analyses with nearby type Ia supernovae, Astrophys. J. 938 (2) (2022) 112, arXiv:2110.03487 [astro-ph.CO].

[223] S.R. Brownsberger, D. Brout, D. Scolnic, C.W. Stubbs, A.G. Riess, Dependence of cosmological constraints on gray photometric zero-point uncertainties of supernova surveys, Astrophys. J. 944 (2) (2023) 188, arXiv:2110.03486 [astro-ph.CO].

[224] D.O. Jones, et al., Should type Ia supernova distances be corrected for their local environments? Astrophys. J. 867 (2) (2018) 108, arXiv:1805.05911 [astro-ph.CO].

[225] CSP Collaboration, C.R. Burns, et al., The carnegie supernova project: Absolute calibration and the Hubble constant, Astrophys. J. 869 (1) (2018) 56, arXiv:1809.06381 [astro-ph.CO].

[226] S. Dhawan, et al., A uniform type Ia supernova distance ladder with the Zwicky transient facility: Absolute calibration based on the tip of the red giant branch method, Astrophys. J. 934 (2) (2022) 185, arXiv:2203.04241 [astro-ph.CO].

[227] S. Dhawan, S.W. Jha, B. Leibundgut, Measuring the Hubble constant with type Ia supernovae as near-infrared standard candles, Astron. Astrophys. 609 (2018) A72, arXiv:1707.00715 [astro-ph.CO].

[228] D.O. Jones, et al., Cosmological results from the RAISIN survey: Using type Ia supernovae in the near infrared as a novel path to measure the dark energy equation of state, Astrophys. J. 933 (2) (2022) 172, arXiv:2201.07801 [astro-ph.CO].
[229] S. Dhawan, S. Thorp, K.S. Mandel, S.M. Ward, G. Narayan, S.W. Jha, T. Chant, A BayeSN distance ladder: H0 from a consistent modelling of type Ia supernovae from the optical to the near-infrared, Mon. Not. R. Astron. Soc. 524 (1) (2023) 235–244, arXiv:2211.07657 [astro-ph.CO].
[230] A. Carr, T.M. Davis, D. Scolnic, D. Scolnic, K. Said, D. Brout, E.R. Peterson, R. Kessler, The Pantheon+ analysis: Improving the redshifts and peculiar velocities of type Ia supernovae used in cosmological analyses, Publ. Astron. Soc. Austral. 39 (2022) e046, arXiv:2112.01471 [astro-ph.CO].
[231] C.L. Steinhardt, A. Sneppen, B. Sen, VizieR online data catalog: revised redshifts of the pantheon supernovae Ia (Steinhardt+, 2020), 2022, http://dx.doi.org/10.26093/cds/vizier.19020014, VizieR On-line Data Catalog: J/ApJ/902/14. Originally published in: 2020ApJ...902...14S.
[232] B. Popovic, D. Brout, R. Kessler, D. Scolnic, The Pantheon+ analysis: Forward modeling the dust and intrinsic color distributions of type Ia supernovae, and quantifying their impact on cosmological inferences, Astrophys. J. 945 (1) (2023) 84, arXiv:2112.04456 [astro-ph.CO].
[233] M. Rigault, et al., Confirmation of a star formation bias in type Ia supernova distances and its effect on measurement of the Hubble constant, Astrophys. J. 802 (1) (2015) 20, arXiv:1412.6501 [astro-ph.CO].
[234] A.G. Riess, L. Macri, S. Casertano, H. Lampeitl, H.C. Ferguson, A.V. Filippenko, S.W. Jha, W. Li, R. Chornock, A 3% solution: Determination of the Hubble constant with the Hubble space telescope and wide field camera 3, Astrophys. J. 730 (2011) 119, arXiv:1103.2976 [astro-ph.CO]; Erratum: Astrophys. J. 732 (2011) 129.
[235] R.a. Wojtak, J. Hjorth, Consistent extinction model for type Ia supernovae in Cepheid-based calibration galaxies and its impact on H0, Mon. Not. R. Astron. Soc. 533 (2) (2024) 2319–2334, arXiv:2403.10388 [astro-ph.CO].
[236] DES Collaboration, E. Macaulay, et al., First cosmological results using type Ia supernovae from the dark energy survey: Measurement of the Hubble constant, Mon. Not. R. Astron. Soc. 486 (2) (2019) 2184–2196, arXiv:1811.02376 [astro-ph.CO].
[237] S.M. Feeney, H.V. Peiris, A.R. Williamson, S.M. Nissanke, D.J. Mortlock, J. Alsing, D. Scolnic, Prospects for resolving the Hubble constant tension with standard sirens, Phys. Rev. Lett. 122 (6) (2019) 061105, arXiv:1802.03404 [astro-ph.CO].
[238] DES Collaboration, R. Camilleri, et al., The dark energy survey supernova program: An updated measurement of the Hubble constant using the inverse distance ladder, Mon. Not. R. Astron. Soc. 537 (2) (2025) 1818–1825, arXiv:2406.05049 [astro-ph.CO].
[239] P. Ruiz-Lapuente, J.I. González Hernández, 'SNe Ia twins for life': Toward a precise determination of H_0, Astrophys. J. 977 (2) (2024) 180, arXiv:2312.10334 [astro-ph.CO].
[240] H.B. Richer, Observations of a complete sample of C stars in the large magellanic cloud, Astrophys. J. 243 (1981) 744.
[241] H.B. Richer, D.R. Crabtree, C.J. Pritchet, Luminous late-type stars in NGC 205, Astrophys. J. 287 (1984) 138–147.
[242] H.B. Richer, C.J. Pritchet, D.R. Crabtree, Luminous late-type stars in Ngc 300, Astrophys. J. 298 (1985) 240–248.
[243] C.J. Pritchet, H.B. Richer, D. Schade, D. Crabtree, H.K.C. Yee, The late-type Stellar content of NGC 55, Astrophys. J. 323 (1987) 79.
[244] K.H. Cook, M. Aaronson, J. Norris, Carbon and m stars in nearby galaxies: A preliminary survey using a photometric technique, Astrophys. J. 305 (1986) 634.
[245] P. Battinelli, S. Demers, The standard candle aspect of carbon stars, Astron. Astrophys. 442 (1) (2005) 159–163.
[246] P. Ripoche, J. Heyl, J. Parada, H. Richer, Carbon stars as standard candles: I. The luminosity function of carbon stars in the Magellanic clouds, Mon. Not. R. Astro. Soc. 495 (3) (2020) 2858–2866, arXiv:2005.05539 [astro-ph.SR].
[247] W.L. Freedman, B.F. Madore, Astrophysical distance scale II. Application of the JAGB Method: A nearby galaxy sample, Astrophys. J. 899 (1) (2020) 67, arXiv:2005.10793 [astro-ph.GA].
[248] B. Zgirski, G. Pietrzyński, W. Gieren, M. Górski, P. Wielgórski, P. Karczmarek, F. Bresolin, P. Kervella, R.-P. Kudritzki, J. Storm, D. Graczyk, G. Hajdu, W. Narloch, B. Pilecki, K. Suchomska, M. Taormina, The araucaria project. distances to nine galaxies based on a statistical analysis of their carbon stars (JAGB Method), Astrophys. J. 916 (1) (2021) 19.
[249] A.J. Lee, Carbon stars as standard candles: An empirical test for the reddening, metallicity, and age sensitivity of the J-region Asymptotic Giant Branch (JAGB) method, Astrophys. J. 956 (1) (2023) 15, arXiv:2305.02453 [astro-ph.GA].
[250] L.M. Macri, C.-C. Ngeow, S.M. Kanbur, S. Mahzooni, M.T. Smitka, Large magellanic cloud near-infrared synoptic survey. I. Cepheid variables and the calibration of the Leavitt Law, Astron. J. 149 (2015) 117, arXiv:1412.1511 [astro-ph.SR].
[251] J. Parada, J. Heyl, H. Richer, P. Ripoche, L. Rousseau-Nepton, Carbon stars as standard candles – II. The median J magnitude as a distance indicator, Mon. Not. R. Astron. Soc. 501 (1) (2021) 933–947, arXiv:2011.11681 [astro-ph.GA].
[252] A.J. Lee, W.L. Freedman, B.F. Madore, I.S. Jang, K.A. Owens, T.J. Hoyt, The Chicago-Carnegie Hubble program: The JWST J-region Asymptotic Giant Branch (JAGB) extragalactic distance scale, 2024, arXiv:2408.03474 [astro-ph.GA].
[253] J. Parada, J. Heyl, H. Richer, P. Ripoche, L. Rousseau-Nepton, Carbon stars as standard candles – III. Un-binned maximum likelihood fitting and comparison with TRGB estimations, Mon. Not. R. Astron. Soc. 522 (1) (2023) 195–210, arXiv:2303.16934 [astro-ph.GA].
[254] S. Li, A.G. Riess, D. Scolnic, S. Casertano, G.S. Anand, JAGB 2.0: Improved constraints on the J-region Asymptotic Giant Branch-based Hubble constant from an expanded sample of JWST observations, 2025, arXiv:2502.05259 [astro-ph.CO].
[255] S. Li, A.G. Riess, D. Scolnic, G.S. Anand, J. Wu, S. Casertano, W. Yuan, R. Beaton, R.I. Anderson, Standardized luminosity of the tip of the red giant branch utilizing multiple fields in NGC 4258 and the CATs algorithm, Astrophys. J. 956 (1) (2023) 32, arXiv:2306.10103 [astro-ph.GA].
[256] S.J. Smartt, Progenitors of core-collapse supernovae, Ann. Rev. Astron. Astrophys. 47 (2009) 63–106, arXiv:0908.0700 [astro-ph.SR].
[257] C.D. Kilpatrick, et al., SN 2023ixf in Messier 101: A variable red supergiant as the progenitor candidate to a Type II Supernova, Astrophys. J. Lett. 952 (1) (2023) L23, arXiv:2306.04722 [astro-ph.SR].
[258] R.P. Kirshner, J. Kwan, Distances to extragalactic supernovae, Astrophys. J. 193 (1974) 27.
[259] E.A. Baron, P.E. Nugent, D. Branch, P.H. Hauschildt, Type IIP supernovae as cosmological probes: A SEAM distance to SN 1999em, Astrophys. J. Lett. 616 (2004) L91–L94, arXiv:astro-ph/0410153.
[260] L. Dessart, D.J. Hillier, Distance determinations using Type II supernovae and the expanding photosphere method, Astron. Astrophys. 439 (2005) 671, arXiv:astro-ph/0505465.
[261] M. Hamuy, P.A. Pinto, Type II supernovae as standardized candles, Astrophys. J. Lett. 566 (2002) L63–L65, arXiv:astro-ph/0201279.
[262] E.E.E. Gall, et al., An updated Type II supernova Hubble diagram, Astron. Astrophys. 611 (2018) A25, arXiv:1705.10806 [astro-ph.CO].
[263] R.V. Wagoner, Effects of scattering on continuous radiation from supernovae and determination of their distances, Astrophys. J. Lett. 250 (1981) L65–L69.
[264] R.G. Eastman, B.P. Schmidt, R. Kirshner, The atmospheres of Type II supernovae and the expanding photosphere method, Astrophys. J. 466 (1996) 911.
[265] L. Dessart, D.J. Hillier, Quantitative spectroscopy of photospheric-phase Type II supernovae, Astron. Astrophys. 437 (2005) 667, arXiv:astro-ph/0504028.
[266] C. Vogl, S.A. Sim, U.M. Noebauer, W.E. Kerzendorf, W. Hillebrandt, Spectral modeling of Type II supernovae. I. Dilution factors, Astron. Astrophys. 621 (2019) A29, arXiv:1811.02543 [astro-ph.HE].
[267] M.I. Jones, Distance determination to 12 Type II supernovae using the expanding photosphere method, Rev. Mex. Astron. Astrof. Ser. Conf. 35 (2009) 310, arXiv:0810.5538 [astro-ph].
[268] E.E.E. Gall, R. Kotak, B. Leibundgut, S. Taubenberger, W. Hillebrandt, M. Kromer, Applying the expanding photosphere and standardized candle methods to Type II-Plateau supernovae at cosmologically significant redshifts: the distance to SN 2013eq, Astron. Astrophys. 592 (2016) A129, arXiv:1603.04730 [astro-ph.CO].
[269] G. Dhungana, et al., Cosmological distance measurement of twelve nearby Supernovae IIP with ROTSE-IIIb, Astrophys. J. 962 (1) (2024) 60, arXiv:2308.00916 [astro-ph.HE].
[270] L. Dessart, et al., Using quantitative spectroscopic analysis to determine the properties and distances of Type II-Plateau Supernovae: SNe 2005cs and 2006bp, Astrophys. J. 675 (2008) 644, arXiv:0711.1815 [astro-ph].
[271] C. Vogl, W.E. Kerzendorf, S.A. Sim, U.M. Noebauer, S. Lietzau, W. Hillebrandt, Spectral modeling of Type II supernovae II. A machine learning approach to quantitative spectroscopic analysis, Astron. Astrophys. 633 (2020) A88, arXiv:1911.04444 [astro-ph.HE].
[272] C. Vogl, et al., No rungs attached: a distance-ladder free determination of the Hubble constant through Type II supernova spectral modelling, 2024, arXiv:2411.04968 [astro-ph.CO].
[273] T. de Jaeger, B.E. Stahl, W. Zheng, A.V. Filippenko, A.G. Riess, L. Galbany, A measurement of the Hubble constant from Type II supernovae, Mon. Not. R. Astron. Soc. 496 (3) (2020) 3402–3411, arXiv:2006.03412 [astro-ph.CO].
[274] M.A. Hamuy, Type II Supernovae as Distance Indicators (PhD thesis), University of Arizona, 2001.
[275] M. Hamuy, Observed and physical properties of core-collapse supernovae, Astrophys. J. 582 (2003) 905–914, arXiv:astro-ph/0209174.
[276] SNLS Collaboration, P. Nugent, et al., Towards a cosmological Hubble diagram for Type II-P supernovae, Astrophys. J. 645 (2006) 841–850, arXiv:astro-ph/0603535.
[277] T. de Jaeger, L. Galbany, The pursuit of the Hubble constant using Type II supernovae, 2023, arXiv:2305.17243 [astro-ph.CO].
[278] S. Bose, B. Kumar, Distance determination to eight galaxies using expanding photosphere method, Astrophys. J. 782 (2014) 98, arXiv:1401.5115 [astro-ph.CO].

[279] L. Searle, W.L.W. Sargent, Inferences from the composition of two dwarf blue galaxies, Astrophys. J. 173 (1972) 25.

[280] J. Bergeron, Characteristics of the blue stars in the dwarf galaxies I Zw 18 and II Zw 40., Astrophys. J. 211 (1977) 62–67.

[281] R. Terlevich, J. Melnick, The dynamics and chemical composition of giant extragalactic H II regions, Mon. Not. R. Astro. Soc. 195 (1981) 839–851.

[282] D. Kunth, G. Ostlin, The most metal-poor galaxies, Astron. Astrophys. Rev. 10 (2000) 1–79, arXiv:astro-ph/9911094.

[283] R. Chávez, R. Terlevich, E. Terlevich, F. Bresolin, J. Melnick, M. Plionis, S. Basilakos, The L–σ relation for massive bursts of star formation, Mon. Not. R. Astron. Soc. 442 (4) (2014) 3565–3597, arXiv:1405.4010 [astro-ph.GA].

[284] J. Melnick, R. Terlevich, M. Moles, Giant H II regions as distance indicators-ii. application to h ii galaxies and the value of the Hubble constant, Mon. Not. R. Astro. Soc. 235 (1988) 297–313.

[285] V. Bordalo, E. Telles, The L-sigma relation of local HII galaxies, Astrophys. J. 735 (2011) 52, arXiv:1104.4719 [astro-ph.CO].

[286] M. Plionis, R. Terlevich, S. Basilakos, F. Bresolin, E. Terlevich, J. Melnick, R. Chavez, A strategy to measure the dark energy equation of state using the HII galaxy Hubble relation & X-ray AGN clustering: Preliminary results, Mon. Not. R. Astron. Soc. 416 (2011) 2981, arXiv:1106.4558 [astro-ph.CO].

[287] R. Chávez, M. Plionis, S. Basilakos, R. Terlevich, E. Terlevich, J. Melnick, F. Bresolin, A.L. González-Morán, Constraining the dark energy equation of state with HII galaxies, Mon. Not. R. Astron. Soc. 462 (3) (2016) 2431–2439, arXiv:1607.06458 [astro-ph.CO].

[288] A.L. González-Morán, R. Chávez, R. Terlevich, E. Terlevich, F. Bresolin, D. Fernández-Arenas, M. Plionis, S. Basilakos, J. Melnick, E. Telles, Independent cosmological constraints from high-z H II galaxies, Mon. Not. R. Astron. Soc. 487 (4) (2019) 4669–4694, arXiv:1906.02195 [astro-ph.GA].

[289] R. Chávez, R. Terlevich, E. Terlevich, A.L. González-Morán, D. Fernández-Arenas, F. Bresolin, M. Plionis, S. Basilakos, R. Amorín, M. Llerena, Mapping the Hubble flow from z-0 to z-7.5 with H II galaxies, Mon. Not. R. Astro. Soc. 538 (2) (2025) 1264–1271, arXiv:2404.16261 [astro-ph.CO].

[290] B. Dorner, G. Giardino, P. Ferruit, C. Alves de Oliveira, S.M. Birkmann, T. Böker, G. De Marchi, X. Gnata, J. Köhler, M. Sirianni, P. Jakobsen, A model-based approach to the spatial and spectral calibration of NIRSpec onboard JWST, Astron. Astrophys. 592 (2016) A113, arXiv:1606.05640 [astro-ph.IM].

[291] J.P. Gardner, et al., The James Webb space telescope, Space Sci. Rev. 123 (2006) 485, arXiv:astro-ph/0606175.

[292] F. Feroz, M.P. Hobson, Multimodal nested sampling: an efficient and robust alternative to MCMC methods for astronomical data analysis, Mon. Not. R. Astron. Soc. 384 (2008) 449, arXiv:0704.3704 [astro-ph].

[293] F. Feroz, M.P. Hobson, M. Bridges, MultiNest: an efficient and robust Bayesian inference tool for cosmology and particle physics, Mon. Not. R. Astron. Soc. 398 (2009) 1601–1614, arXiv:0809.3437 [astro-ph].

[294] F. Feroz, M.P. Hobson, E. Cameron, A.N. Pettitt, Importance nested sampling and the MultiNest algorithm, Open J. Astrophys.. 2 (1) (2019) 10, arXiv:1306.2144 [astro-ph.IM].

[295] B. Ratra, P.J.E. Peebles, Cosmological consequences of a rolling homogeneous scalar field, Phys. Rev. D 37 (1988) 3406.

[296] C. Wetterich, Cosmology and the fate of dilatation symmetry, Nuclear Phys. B 302 (1988) 668–696, arXiv:1711.03844 [hep-th].

[297] M. Chevallier, D. Polarski, Accelerating universes with scaling dark matter, Internat. J. Modern Phys. D 10 (2001) 213–224, arXiv:gr-qc/0009008.

[298] E.V. Linder, Exploring the expansion history of the universe, Phys. Rev. Lett. 90 (2003) 091301, arXiv:astro-ph/0208512.

[299] P.J.E. Peebles, B. Ratra, The cosmological constant and dark energy, Rev. Modern Phys. 75 (2003) 559–606, arXiv:astro-ph/0207347.

[300] D. Fernández Arenas, E. Terlevich, R. Terlevich, J. Melnick, R. Chávez, F. Bresolin, E. Telles, M. Plionis, S. Basilakos, An independent determination of the local Hubble constant, Mon. Not. R. Astron. Soc. 474 (1) (2018) 1250–1276, arXiv:1710.05951 [astro-ph.CO].

[301] M. Llerena, R. Amorín, L. Pentericci, A. Calabrò, A.E. Shapley, K. Boutsia, E. Pérez-Montero, J.M. Vílchez, K. Nakajima, Ionized gas kinematics and chemical abundances of low-mass star-forming galaxies at z $\sim$ 3, Astron. Astrophys. 676 (2023) A53, arXiv:2303.01536 [astro-ph.GA].

[302] A. de Graaff, et al., Ionised gas kinematics and dynamical masses of z $\gtrsim$ 6 galaxies from JADES/NIRSpec high-resolution spectroscopy, Astron. Astrophys. 684 (2024) A87, arXiv:2308.09742 [astro-ph.GA].

[303] S.S. McGaugh, J.M. Schombert, G.D. Bothun, W.J.G. de Blok, The baryonic Tully-Fisher relation, Astrophys. J. Lett. 533 (2000) L99–L102, arXiv:astro-ph/0003001.

[304] E.F. Bell, R.S. de Jong, Stellar mass-to-light ratios and the Tully-Fisher relation, Astrophys. J. 550 (2001) 212–229, arXiv:astro-ph/0011493.

[305] S. Gurovich, S.S. McGaugh, K.C. Freeman, H. Jerjen, L. Staveley-Smith, W.J.G. De Blok, The baryonic tully fisher relation, Publ. Astron. Soc. Austral. 21 (4) (2004) 412, arXiv:astro-ph/0411521.

[306] S.S. McGaugh, The baryonic Tully-Fisher relation of galaxies with extended rotation curves and the stellar mass of rotating galaxies, Astrophys. J. 632 (2005) 859–871, arXiv:astro-ph/0506750.

[307] D. Pfenniger, Y. Revaz, The baryonic Tully-Fisher relation revisited, Astron. Astrophys. 431 (2005) 511, arXiv:astro-ph/0409621.

[308] A. Begum, J.N. Chengalur, I.D. Karachentsev, M.E. Sharina, Baryonic Tully-Fisher relation for extremely low mass galaxies, Mon. Not. R. Astron. Soc. 386 (2008) 138, arXiv:0801.3606 [astro-ph].

[309] C. Trachternach, W.J.G. de Blok, S.S. McGaugh, J.M. van der Hulst, R.J. Dettmar, The baryonic Tully-Fisher relation and its implication for dark matter halos, Astron. Astrophys. 505 (2009) 577, arXiv:0907.5533 [astro-ph.CO].

[310] D.V. Stark, S.S. McGaugh, R.A. Swaters, A first attempt to calibrate the baryonic Tully-Fisher relation with gas dominated galaxies, Astron. J. 138 (2009) 392, arXiv:0905.4528 [astro-ph.CO].

[311] S. Gurovich, K. Freeman, H. Jerjen, L. Staveley-Smith, I. Puerari, The slope of the baryonic Tully-Fisher relation, Astron. J. 140 (2010) 663, arXiv:1004.4365 [astro-ph.CO].

[312] D. Zaritsky, et al., The baryonic Tully-Fisher relationship for S^4G galaxies and the "condensed" baryon fraction of galaxies, Astron. J. 147 (2014) 134, arXiv:1402.6315 [astro-ph.GA].

[313] R.B. Tully, J.R. Fisher, A new method of determining distances to galaxies, Astron. Astrophys. 54 (1977) 661–673.

[314] M.J. Pierce, R.B. Tully, Distances to the Virgo and Ursa Major clusters and a determination of H 0, Astrophys. J. 330 (1988) 579.

[315] P. Teerikorpi, The inverse Tully-Fisher relation, Astrophys. Lett. Commun. 31 (1995) 263.

[316] R. Giovanelli, M. Haynes, T. Herter, N. Vogt, L.d. Costa, W. Freudling, J. Salzer, G. Wegner, The i-band Tully-Fisher relation for cluster galaxies: data presentation, Astron. J. 113 (1997) 22–52, arXiv:astro-ph/9610117.

[317] R. Giovanelli, M. Haynes, T. Herter, N. Vogt, L.d. Costa, W. Freudling, J. Salzer, G. Wegner, The i-band Tully-Fisher relation for cluster galaxies: a template relation, its scatter and bias corrections, Astron. J. 113 (1997) 53–79, arXiv:astro-ph/9610118.

[318] S. Courteau, H.-W. Rix, Maximal disks and the Tully-Fisher relation, ASP Conf. Ser. 136 (1998) 196, arXiv:astro-ph/9707290.

[319] T.R. Brent, M.J. Pierce, Distances to galaxies from the correlation between luminosities and linewidths. 3. Cluster template and global measurements of h0, Astrophys. J. 533 (2000) 744–780, arXiv:astro-ph/9911052.

[320] I.D. Karachentsev, S.N. Mitronova, V.E. Karachentseva, Y.N. Kudrya, T.H. Jarrett, The 2MASS Tully-Fisher relation for flat edge - on galaxies, Astron. Astrophys. 396 (2002) 431–438, arXiv:astro-ph/0209189.

[321] A.G. Bedregal, A. Aragon-Salamanca, M.R. Merrifield, The Tully-Fisher relation for s0 galaxies, Mon. Not. R. Astron. Soc. 373 (2006) 1125–1140, arXiv:astro-ph/0609076.

[322] E. Noordermeer, M.A.W. Verheijen, The high mass end of the Tully-Fisher relation, Mon. Not. R. Astron. Soc. 381 (2007) 1463, arXiv:0708.2822 [astro-ph].

[323] C.M. Springob, K.L. Masters, M.P. Haynes, R. Giovanelli, C. Marinoni, SFI++ II: A New I-band Tully-Fisher catalog, derivation of peculiar velocities and dataset properties, Astrophys. J. Suppl. 172 (2007) 599–614, arXiv:0705.0647 [astro-ph]; Erratum: Astrophys. J. Suppl. 182 (2009) 474–475.

[324] M.J. Williams, M. Bureau, M. Cappellari, The Tully-Fisher relations of early-type spiral and s0 galaxies, Mon. Not. R. Astron. Soc. 409 (2010) 1330, arXiv:1007.4072 [astro-ph.GA].

[325] P. Mocz, A. Green, M. Malacari, K. Glazebrook, The Tully-Fisher relation for 25,000 SDSS Galaxies as function of environment, Mon. Not. R. Astron. Soc. 425 (2012) 296, arXiv:1206.1662 [astro-ph.CO].

[326] R.B. Tully, H.M. Courtois, Cosmicflows-2: I-band Luminosity - HI linewidth calibration, Astrophys. J. 749 (2012) 78, arXiv:1202.3191 [astro-ph.CO].

[327] T.D. Rawle, J.R. Lucey, R.J. Smith, J.T.C.G. Head, S0 galaxies in the coma cluster: environmental dependence of the s0 offset from the Tully-Fisher relation, Mon. Not. R. Astron. Soc. 433 (2013) 2667, arXiv:1305.6929 [astro-ph.CO].

[328] J.G. Sorce, H.M. Courtois, R.B. Tully, M. Seibert, V. Scowcroft, W.L. Freedman, B.F. Madore, S.E. Persson, A. Monson, J. Rigby, Calibration of the mid-infrared Tully-Fisher relation, Astrophys. J. 765 (2013) 94, arXiv:1301.4833 [astro-ph.CO].

[329] J.G. Sorce, R.B. Tully, H.M. Courtois, T.H. Jarrett, J.D. Neill, E.J. Shaya, From spitzer galaxy photometry to Tully–Fisher distances, Mon. Not. R. Astron. Soc. 444 (1) (2014) 527–541, arXiv:1408.0729 [astro-ph.GA].

[330] S. Torres-Flores, C. Mendes de Oliveira, H. Plana, P. Amram, B. Epinat, The Tully-Fisher relations for Hickson compact group galaxies, Mon. Not. R. Astron. Soc. 432 (2013) 3085, arXiv:1304.4493 [astro-ph.CO].

[331] K. Said, R.C. Kraan-Korteweg, T.H. Jarrett, On how to extend the NIR Tully–Fisher relation to be truly all-sky, Mon. Not. R. Astron. Soc. 447 (2) (2015) 1618–1629, arXiv:1411.7361 [astro-ph.GA].

[332] K. Said, R.C. Kraan-Korteweg, T.H. Jarrett, L. Staveley-Smith, W.L. Williams, NIR Tully–Fisher in the zone of avoidance – III. Deep NIR catalogue of the HIZOA galaxies, Mon. Not. R. Astron. Soc. 462 (3) (2016) 3386–3400, arXiv:1607.08596 [astro-ph.GA].

[333] E. Kourkchi, R.B. Tully, G.S. Anand, H.M. Courtois, A. Dupuy, J.D. Neill, L. Rizzi, M. Seibert, Cosmicflows-4: The calibration of optical and infrared Tully–Fisher relations, Astrophys. J. 896 (1) (2020) 3, arXiv:2004.14499 [astro-ph.GA].

[334] R. Bell, K. Said, T. Davis, T.H. Jarrett, Calibration of the Tully–Fisher relation in the WISE W1 (3.4 μm) and W2 (4.6 μm) bands, Mon. Not. R. Astron. Soc. 519 (1) (2022) 102–120, arXiv:2205.13136 [astro-ph.GA].

[335] P. Boubel, M. Colless, K. Said, L. Staveley-Smith, Large-scale motions and growth rate from forward-modelling Tully–Fisher peculiar velocities, Mon. Not. R. Astron. Soc. 531 (1) (2024) 84–109, arXiv:2301.12648 [astro-ph.CO].

[336] D.J. Eisenstein, A. Loeb, An analytical model for the triaxial collapse of cosmological perturbations, Astrophys. J. 439 (1995) 520, arXiv:astro-ph/9405012.

[337] S.S. McGaugh, W.J.G. de Blok, Testing the dark matter hypothesis with low surface brightness galaxies and other evidence, Astrophys. J. 499 (1998) 41, arXiv:astro-ph/9801123.

[338] S.S. McGaugh, W.J.G. de Blok, Testing the hypothesis of modified dynamics with low surface brightness galaxies and other evidence, Astrophys. J. 499 (1998) 66–81, arXiv:astro-ph/9801102.

[339] H.J. Mo, S. Mao, S.D.M. White, The formation of galactic disks, Mon. Not. R. Astron. Soc. 295 (1998) 319, arXiv:astro-ph/9707093.

[340] M. Steinmetz, J. Navarro, The cosmological origin of the Tully-Fisher relation, Astrophys. J. 513 (1999) 555–560, arXiv:astro-ph/9808076.

[341] F.C. van den Bosch, Semi-analytical models for the formation of disk galaxies: I. Constraints from the Tully-Fisher relation, Astrophys. J. 530 (2000) 177, arXiv:astro-ph/9909298.

[342] L. Mayer, B. Moore, The baryonic mass - velocity relation: Clues to feedback processes during structure formation and the cosmic baryon inventory, Mon. Not. R. Astron. Soc. 354 (2004) 477, arXiv:astro-ph/0309500.

[343] O.Y. Gnedin, D.H. Weinberg, J. Pizagno, F. Prada, H.-W. Rix, Dark matter Halos of disk galaxies: Constraints from the Tully-Fisher relation, Astrophys. J. 671 (2007) 1115–1134, arXiv:astro-ph/0607394.

[344] F. Governato, B. Willman, L. Mayer, A. Brooks, G. Stinson, O. Valenzuela, J. Wadsley, T.R. Quinn, Forming disk galaxies in lambda-cdm simulations, Mon. Not. R. Astron. Soc. 374 (2007) 1479–1494, arXiv:astro-ph/0602351.

[345] V. Avila-Reese, J. Zavala, C. Firmani, H.M. Hernandez-Toledo, On the baryonic, stellar, and luminous scaling relations of disk galaxies, Astron. J. 136 (2008) 1340–1360, arXiv:0807.0636 [astro-ph].

[346] A.A. Dutton, The baryonic Tully-Fisher relation and galactic outflows, Mon. Not. R. Astron. Soc. 424 (2012) 3123, arXiv:1206.1855 [astro-ph.CO].

[347] S. McGaugh, The baryonic Tully-Fisher relation of gas rich galaxies as a test of LCDM and MOND, Astron. J. 143 (2012) 40, arXiv:1107.2934 [astro-ph.CO].

[348] M. Aumer, S. White, T. Naab, C. Scannapieco, Towards a more realistic population of bright spiral galaxies in cosmological simulations, Mon. Not. R. Astron. Soc. 434 (2013) 3142, arXiv:1304.1559 [astro-ph.GA].

[349] H. Desmond, R.H. Wechsler, The Tully–Fisher and mass–size relations from halo abundance matching, Mon. Not. R. Astron. Soc. 454 (1) (2015) 322–343, arXiv:1506.00169 [astro-ph.GA].

[350] F. Lelli, et al., Gas dynamics in tidal dwarf galaxies: Disc formation at z = 0, Astron. Astrophys. 584 (2015) A113, arXiv:1509.05404 [astro-ph.GA].

[351] P. Salucci, C.S. Frenk, M. Persic, A physical distance indicator for spiral galaxies and the determination of H(0), Mon. Not. R. Astron. Soc. 262 (1993) 392.

[352] A. Lapi, P. Salucci, L. Danese, Precision scaling relations for disk galaxies in the local universe, Astrophys. J. 859 (1) (2018) 2, arXiv:1804.06086 [astro-ph.GA].

[353] K. Said, Tully-Fisher relation, 2023, arXiv:2310.16053 [astro-ph.CO].

[354] S.S. McGaugh, A novel test of the modified newtonian dynamics with gas rich galaxies, Phys. Rev. Lett. 106 (2011) 121303, arXiv:1102.3913 [astro-ph.CO]; Erratum: Phys. Rev. Lett. 107 (2011) 229901.

[355] I.A. Yegorova, P. Salucci, The radial Tully-Fisher relation for spiral galaxies. 1, Mon. Not. R. Astron. Soc. 377 (2007) 507–515, arXiv:astro-ph/0612434.

[356] B.S. Haridasu, P. Salucci, G. Sharma, Radial Tully–Fisher relation and the local variance of Hubble parameter, Mon. Not. R. Astron. Soc. 532 (2) (2024) 2234–2247, arXiv:2403.06859 [astro-ph.CO].

[357] J.-P. Fontaine, P. Salucci, E. Karukes, The radial Tully-Fisher relations in dwarf spiral galaxies, in: Proceedings of the 53rd Rencontres de Moriond on Cosmology 2018, 2020, pp. 363 – 364, https://www.scopus.com/inward/record.uri?eid=2-s2.0-85089624578&partnerID=40&md5=e364fc57db93bf5425ab83b4aa5fadbd.

[358] P. Salucci, The distribution of dark matter in galaxies, Astron. Astrophys. Rev. 27 (1) (2019) 2, arXiv:1811.08843 [astro-ph.GA].

[359] F. Lelli, S.S. McGaugh, J.M. Schombert, The small scatter of the baryonic Tully–Fisher relation, Astrophys. J. Lett. 816 (1) (2016) L14, arXiv:1512.04543 [astro-ph.GA].

[360] V. Borka Jovanović, S. Capozziello, P. Jovanović, D. Borka, Recovering the fundamental plane of galaxies by $f(R)$ gravity, Phys. Dark Univ. 14 (2016) 73–83, arXiv:1610.03336 [astro-ph.GA].

[361] S. Capozziello, P. Jovanović, V.B. Jovanović, D. Borka, Addressing the missing matter problem in galaxies through a new fundamental gravitational radius, JCAP 06 (2017) 044, arXiv:1702.03430 [gr-qc].

[362] S. Capozziello, D.s. Borka, V. Borka Jovanović, P. Jovanović, Galactic structures from gravitational radii, Galaxies 6 (1) (2018) 22.

[363] S. Capozziello, V.B. Jovanović, D.s. Borka, P. Jovanović, Constraining theories of gravity by fundamental plane of elliptical galaxies, Phys. Dark Univ. 29 (2020) 100573, arXiv:2004.11557 [gr-qc].

[364] M. Milgrom, A modification of the Newtonian dynamics as a possible alternative to the hidden mass hypothesis, Astrophys. J. 270 (1983) 365–370.

[365] B. Famaey, S. McGaugh, Modified Newtonian Dynamics (MOND): Observational phenomenology and relativistic extensions, Living Rev. Rel. 15 (2012) 10, arXiv:1112.3960 [astro-ph.CO].

[366] I. Banik, H. Zhao, From galactic bars to the Hubble tension: Weighing up the astrophysical evidence for milgromian gravity, Symmetry 14 (7) (2022) 1331, arXiv:2110.06936 [astro-ph.CO].

[367] B. Famaey, A. Durakovic, Modified Newtonian Dynamics (MOND), 2025, arXiv:2501.17006 [astro-ph.GA].

[368] O. Bertolami, C.G. Boehmer, T. Harko, F.S.N. Lobo, Extra force in f(R) modified theories of gravity, Phys. Rev. D 75 (2007) 104016, arXiv:0704.1733 [gr-qc].

[369] O. Bertolami, C. Gomes, The Layzer-Irvine equation in theories with non-minimal coupling between matter and curvature, JCAP 09 (2014) 010, arXiv:1406.5990 [astro-ph.CO].

[370] C. Gomes, Jeans instability in non-minimal matter-curvature coupling gravity, Eur. Phys. J. C 80 (7) (2020) 633, arXiv:2008.10026 [gr-qc].

[371] C. Gomes, K. Ourabah, Quantum kinetic theory of Jeans instability in non-minimal matter-curvature coupling gravity, Eur. Phys. J. C 83 (1) (2023) 40, arXiv:2204.07871 [gr-qc].

[372] M. Barroso Varela, O. Bertolami, Hubble tension in a nonminimally coupled curvature-matter gravity model, JCAP 06 (2024) 025, arXiv:2403.11683 [gr-qc].

[373] M.H.P.M. van Putten, Evidence for galaxy dynamics tracing background cosmology below the de sitter scale of acceleration, Astrophys. J. 848 (1) (2017) 28, arXiv:1709.05944 [astro-ph.GA].

[374] M.H.P.M. van Putten, Self-similar galaxy dynamics below the de Sitter scale of acceleration, Mon. Not. R. Astro. Soc. 481 (1) (2018) L26–L29, arXiv:1804.06212 [astro-ph.GA].

[375] G.-M. Lee, M.H.P.M. van Putten, Prospects for high-resolution probes of galaxy dynamics tracing background cosmology in MaNGA, New Astron. 117 (2025) 102360, arXiv:2501.11882 [astro-ph.CO].

[376] M.H.P.M. van Putten, Galaxy dynamics tracing quantum cosmology beyond CDM below the de sitter scale of acceleration, Chinese J. Phys. 91 (2024) 377–381, arXiv:2408.06399 [gr-qc].

[377] M.H.P.M. van Putten, The fast and furious in JWST high- z galaxies, Phys. the Dark Universe 43 (2024) 101417, arXiv:2312.16692 [astro-ph.CO].

[378] F. Lelli, S.S. McGaugh, J.M. Schombert, M.S. Pawlowski, The relation between stellar and dynamical surface densities in the central regions of disk galaxies, Astrophys. J. Lett. 827 (1) (2016) L19, arXiv:1607.02145 [astro-ph.GA].

[379] F. Lelli, S.S. McGaugh, J.M. Schombert, SPARC: Mass models for 175 disk galaxies with spitzer photometry and accurate rotation curves, Astron. J. 152 (2016) 157, arXiv:1606.09251 [astro-ph.GA].

[380] J. Schombert, S. McGaugh, F. Lelli, Using the baryonic Tully–Fisher relation to measure H O, Astron. J. 160 (2) (2020) 71, arXiv:2006.08615 [astro-ph.CO].

[381] M. Puech, F. Hammer, H. Flores, R. Delgado-Serrano, M. Rodrigues, Y. Yang, The baryonic content and Tully-Fisher relation at z˜0.6, Astron. Astrophys. 510 (2010) A68, arXiv:0903.3961 [astro-ph.CO].

[382] S.H. Miller, K. Bundy, M. Sullivan, R.S. Ellis, T. Treu, The assembly history of disk galaxies: I - The Tully-Fisher relation to z˜1.3 from deep exposures with DEIMOS, Astrophys. J. 741 (2011) 115, arXiv:1102.3911 [astro-ph.CO].

[383] E.M. Di Teodoro, F. Fraternali, S.H. Miller, Flat rotation curves and low velocity dispersions in kmos star-forming galaxies at z $\tilde{1}$, Astron. Astrophys. 594 (2016) A77, arXiv:1602.04942 [astro-ph.GA].

[384] I. Shivaei, et al., The MOSDEF survey: Dynamical and baryonic masses and kinematic structures of star-forming galaxies at $1.4 \leq z \leq 2.6$, Astrophys. J. 819 (2016) 80, arXiv:1511.03272 [astro-ph.GA].

[385] C.M.S. Straatman, et al., ZFIRE: The evolution of the stellar mass Tully-Fisher relation to redshift $2.0 < Z < 2.5$ with MOSFIRE, Astrophys. J. 839 (2017) 57, arXiv:1703.00016 [astro-ph.GA].

[386] G. Alestas, I. Antoniou, L. Perivolaropoulos, Hints for a gravitational transition in Tully–Fisher data, Universe 7 (10) (2021) 366, arXiv:2104.14481 [astro-ph.CO].

[387] C. Stone, S. Courteau, N. Arora, M. Frosst, T. Jarrett, PROBES-I: A compendium of deep rotation curves and matched multiband photometry, Astrophys. J. Suppl. 262 (2022) 33, arXiv:2209.09912 [astro-ph.GA].

[388] G. Sharma, V. Upadhyaya, P. Salucci, S. Desai, Tully-Fisher relation of late-type galaxies at $0.6 \leq z \leq 2.5$, Astron. Astrophys. 689 (2024) A318, arXiv:2406.08934 [astro-ph.GA].

[389] P. Boubel, M. Colless, K. Said, L. Staveley-Smith, An improved Tully–Fisher estimate of H0, Mon. Not. R. Astron. Soc. 533 (2) (2024) 1550–1559, arXiv:2408.03660 [astro-ph.CO].

[390] D. Scolnic, P. Boubel, J. Byrne, A.G. Riess, G.S. Anand, Calibrating the Tully-Fisher relation to measure the Hubble constant, 2024, arXiv:2412.08449 [astro-ph.CO].

[391] B.S. Koribalski, et al., WALLABY – an SKA pathfinder H i survey, Astrophys. Space Sci. 365 (7) (2020) 118, arXiv:2002.07311 [astro-ph.GA].

[392] C. Saulder, et al., Target selection for the DESI peculiar velocity survey, Mon. Not. R. Astron. Soc. 525 (1) (2023) 1106–1125, arXiv:2302.13760 [astro-ph.CO].

[393] C.-P. Zhang, M. Zhu, P. Jiang, C. Cheng, J. Wang, J. Wang, J.-L. Xu, X.-L. Liu, N.-P. Yu, L. Qian, H. Yu, M. Ai, Y. Jing, C. Xu, Z. Liu, X. Guan, C. Sun, Q. Yang, M. Huang, Q. Hao, FAST Collaboration, The FAST all sky H I survey (FASHI): The first release of catalog, Sci. China Phys., Mech., Astron. 67 (1) (2024) 219511, arXiv:2312.06097 [astro-ph.GA].

[394] K. Said, et al., DESI peculiar velocity survey – fundamental plane, 2024, arXiv:2408.13842 [astro-ph.CO].

[395] S. Djorgovski, M. Davis, Fundamental properties of elliptical galaxies, Astrophys. J. 313 (1987) 59.

[396] A. Dressler, S.M. Faber, D. Burstein, R.L. Davies, D. Lynden-Bell, R.J. Terlevich, G. Wegner, Spectroscopy and photometry of elliptical galaxies: A large scale streaming motion in the local universe, Astrophys. J. Lett. 313 (1987) L37–L42.

[397] D. Scolnic, et al., The Hubble tension in our own backyard: DESI and the nearness of the coma cluster, Astrophys. J. Lett. 979 (1) (2025) L9, arXiv:2409.14546 [astro-ph.CO].

[398] A. Rest, H.J. Weiland, C.W. Stubbs, S.J. Smartt, K.W. Smith, B. Stalder, A.N. Heinze, L. Denneau, J.L. Tonry, ATLAS: A high-cadence all-sky survey system, Publ. Astron. Soc. Pac. 130 (988) (2018) 064505.

[399] Young Supernova Experiment Collaboration, D.O. Jones, et al., The young supernova experiment: survey goals, overview, and operations, Astrophys. J. 908 (2) (2021) 143, arXiv:2010.09724 [astro-ph.HE].

[400] D. Carter, et al., The HST/ACS Coma Cluster Survey: I - survey objectives and design, Astrophys. J. Suppl. 176 (2008) 424, arXiv:0801.3745 [astro-ph].

[401] J.B. Jensen, J.L. Tonry, G.A. Luppino, The infrared surface brightness fluctuation distances to the hydra and coma clusters, Astrophys. J. 510 (1999) 71, arXiv:astro-ph/9807326.

[402] B. Thomsen, W.A. Baum, M. Hammergren, G. Worthey, The distance to the coma cluster from surface brightness fluctuations, Astrophys. J. Lett. 483 (1997) L37–L40, arXiv:astro-ph/9704121.

[403] M.D. Gregg, The coma - leo I distance ratio and the Hubble constant, New Astron. 1 (1997) 363, arXiv:astro-ph/9703031.

[404] J. Hjorth, N.R. Tanvir, Calibration of the fundamental plane zero-point in the Leo-I group and an estimate of the Hubble constant, Astrophys. J. 482 (1997) 68–74, arXiv:astro-ph/9701025.

[405] J.J. Kavelaars, W.E. Harris, D.A. Hanes, J.E. Hesser, C.J. Pritchet, The globular cluster systems in the coma ellipticals. I: the luminosity function in ngc 4874, and implications for Hubble's constant, Astrophys. J. 533 (2000) 125, arXiv:astro-ph/9911206.

[406] R. de Grijs, G. Bono, Clustering of local group distances: publication bias or correlated measurements? VII. A distance framework out to 100 Mpc, Astrophys. J. Suppl. 248 (1) (2020) 6, arXiv:2004.00114 [astro-ph.GA].

[407] WST Collaboration, V. Mainieri, et al., The Wide-field Spectroscopic Telescope (WST) science white paper, 2024, arXiv:2403.05398 [astro-ph.IM].

[408] R. Jimenez, A. Loeb, Constraining cosmological parameters based on relative galaxy ages, Astrophys. J. 573 (2002) 37–42, arXiv:astro-ph/0106145.

[409] J. Simon, L. Verde, R. Jimenez, Constraints on the redshift dependence of the dark energy potential, Phys. Rev. D 71 (2005) 123001, arXiv:astro-ph/0412269.

[410] D. Stern, R. Jimenez, L. Verde, M. Kamionkowski, S.A. Stanford, Cosmic chronometers: Constraining the equation of state of dark energy. I: H(z) measurements, JCAP 02 (2010) 008, arXiv:0907.3149 [astro-ph.CO].

[411] M. Moresco, Raising the bar: new constraints on the Hubble parameter with cosmic chronometers at z ∼ 2, Mon. Not. R. Astron. Soc. 450 (1) (2015) L16–L20, arXiv:1503.01116 [astro-ph.CO].

[412] M. Moresco, L. Pozzetti, A. Cimatti, R. Jimenez, C. Maraston, L. Verde, D. Thomas, A. Citro, R. Tojeiro, D. Wilkinson, A 6% measurement of the Hubble parameter at $z \sim 0.45$: direct evidence of the epoch of cosmic re-acceleration, JCAP 05 (2016) 014, arXiv:1601.01701 [astro-ph.CO].

[413] A.L. Ratsimbazafy, S.I. Loubser, S.M. Crawford, C.M. Cress, B.A. Bassett, R.C. Nichol, P. Väisänen, Age-dating luminous red galaxies observed with the Southern African large telescope, Mon. Not. R. Astron. Soc. 467 (3) (2017) 3239–3254, arXiv:1702.00418 [astro-ph.CO].

[414] N. Borghi, M. Moresco, A. Cimatti, A. Huchet, S. Quai, L. Pozzetti, Toward a better understanding of cosmic chronometers: Stellar population properties of passive galaxies at intermediate redshift, Astrophys. J. 927 (2) (2022) 164, arXiv:2106.14894 [astro-ph.GA].

[415] K. Jiao, N. Borghi, M. Moresco, T.-J. Zhang, New observational H(z) data from full-spectrum fitting of cosmic chronometers in the LEGA-C survey, Astrophys. J. Suppl. 265 (2) (2023) 48, arXiv:2205.05701 [astro-ph.CO].

[416] E. Tomasetti, M. Moresco, N. Borghi, K. Jiao, A. Cimatti, L. Pozzetti, A.C. Carnall, R.J. McLure, L. Pentericci, A new measurement of the expansion history of the universe at z = 1.26 with cosmic chronometers in VANDELS, Astron. Astrophys. 679 (2023) A96, arXiv:2305.16387 [astro-ph.CO].

[417] R. Jimenez, M. Moresco, L. Verde, B.D. Wandelt, Cosmic chronometers with photometry: a new path to H(z), JCAP 11 (2023) 047, arXiv:2306.11425 [astro-ph.CO].

[418] M. Moresco, Addressing the Hubble tension with cosmic chronometers, 2023, arXiv:2307.09501 [astro-ph.CO].

[419] V.C. Busti, C. Clarkson, M. Seikel, Evidence for a lower value for H_0 from cosmic chronometers data? Mon. Not. R. Astron. Soc. 441 (2014) 11, arXiv:1402.5429 [astro-ph.CO].

[420] S. Cao, X. Zheng, M. Biesiada, J. Qi, Y. Chen, Z.-H. Zhu, Ultra-compact structure in intermediate-luminosity radio quasars: building a sample of standard cosmological rulers and improving the dark energy constraints up to z ˜ 3, Astron. Astrophys. 606 (2017) A15, arXiv:1708.08635 [astro-ph.CO].

[421] H. Yu, B. Ratra, F.-Y. Wang, Hubble parameter and baryon acoustic oscillation measurement constraints on the Hubble constant, the deviation from the spatially flat ΛCDM model, the deceleration–acceleration transition redshift, and spatial curvature, Astrophys. J. 856 (1) (2018) 3, arXiv:1711.03437 [astro-ph.CO].

[422] A. Gómez-Valent, L. Amendola, H_0 from cosmic chronometers and type Ia supernovae, with Gaussian processes and the novel weighted polynomial regression method, JCAP 04 (2018) 051, arXiv:1802.01505 [astro-ph.CO].

[423] B.S. Haridasu, V.V. Luković, M. Moresco, N. Vittorio, An improved model-independent assessment of the late-time cosmic expansion, JCAP 10 (2018) 015, arXiv:1805.03595 [astro-ph.CO].

[424] A. Gómez-Valent, Measuring the sound horizon and absolute magnitude of SNIa by maximizing the consistency between low-redshift data sets, Phys. Rev. D 105 (4) (2022) 043528, arXiv:2111.15450 [astro-ph.CO].

[425] A. Bonilla, S. Kumar, R.C. Nunes, Measurements of H_0 and reconstruction of the dark energy properties from a model-independent joint analysis, Eur. Phys. J. C 81 (2) (2021) 127, arXiv:2011.07140 [astro-ph.CO].

[426] E. Ó Colgáin, M.M. Sheikh-Jabbari, Elucidating cosmological model dependence with H_0, Eur. Phys. J. C 81 (10) (2021) 892, arXiv:2101.08565 [astro-ph.CO].

[427] T. Liu, S. Cao, S. Zhang, C. Zheng, W. Guo, Revisiting the Hubble constant, spatial curvature, and cosmography with strongly lensed quasar and Hubble parameter observations, Astrophys. J. 939 (1) (2022) 37, arXiv:2204.07365 [astro-ph.CO].

[428] Y. Yang, X. Lu, L. Qian, S. Cao, Potentialities of Hubble parameter and expansion rate function data to alleviate Hubble tension, Mon. Not. R. Astron. Soc. 519 (4) (2023) 4938–4950, arXiv:2204.01020 [astro-ph.CO].

[429] A. Favale, A. Gómez-Valent, M. Migliaccio, Cosmic chronometers to calibrate the ladders and measure the curvature of the universe. A model-independent study, Mon. Not. R. Astron. Soc. 523 (3) (2023) 3406–3422, arXiv:2301.09591 [astro-ph.CO].

[430] A. Favale, M.G. Dainotti, A. Gómez-Valent, M. Migliaccio, Towards a new model-independent calibration of gamma-ray bursts, JHEAp 44 (2024) 323–339, arXiv:2402.13115 [astro-ph.CO].

[431] Y. Yang, T. Liu, J. Huang, X. Cheng, M. Biesiada, S.-m. Wu, Simultaneous measurements on cosmic curvature and opacity using latest HII regions and H(z) observations, Eur. Phys. J. C 84 (1) (2024) 3, arXiv:2401.03413 [astro-ph.CO].

[432] N. Rani, D. Jain, S. Mahajan, A. Mukherjee, M. Biesiada, Revisiting dark energy models using differential ages of galaxies, JCAP 03 (2017) 005, arXiv:1612.07492 [astro-ph.CO].

[433] Z. Li, J.E. Gonzalez, H. Yu, Z.-H. Zhu, J.S. Alcaniz, Constructing a cosmological model-independent Hubble diagram of type Ia supernovae with cosmic chronometers, Phys. Rev. D 93 (4) (2016) 043014, arXiv:1504.03269 [astro-ph.CO].

[434] S. Capozziello, R. D'Agostino, O. Luongo, High-redshift cosmography: auxiliary variables versus Padé polynomials, Mon. Not. R. Astron. Soc. 494 (2) (2020) 2576–2590, arXiv:2003.09341 [astro-ph.CO].

[435] M. Moresco, L. Verde, L. Pozzetti, R. Jimenez, A. Cimatti, New constraints on cosmological parameters and neutrino properties using the expansion rate of the universe to z˜1.75, JCAP 07 (2012) 053, arXiv:1201.6658 [astro-ph.CO].

[436] M. Moresco, R. Jimenez, L. Verde, A. Cimatti, L. Pozzetti, C. Maraston, D. Thomas, Constraining the time evolution of dark energy, curvature and neutrino properties with cosmic chronometers, JCAP 12 (2016) 039, arXiv:1604.00183 [astro-ph.CO].

[437] EUCLID Collaboration, R. Laureijs, et al., Euclid definition study report, 2011, arXiv:1110.3193 [astro-ph.CO].

[438] F. Cogato, M. Moresco, L. Amati, A. Cimatti, An analytical late–universe approach to the weaving of modern cosmology, Mon. Not. R. Astron. Soc. 527 (3) (2023) 4874–4888, arXiv:2309.01375 [astro-ph.CO].

[439] A. Heavens, R. Jimenez, L. Verde, Standard rulers, candles, and clocks from the low-redshift universe, Phys. Rev. Lett. 113 (24) (2014) 241302, arXiv:1409.6217 [astro-ph.CO].

[440] L. Verde, J.L. Bernal, A.F. Heavens, R. Jimenez, The length of the low-redshift standard ruler, Mon. Not. R. Astron. Soc. 467 (1) (2017) 731–736, arXiv:1607.05297 [astro-ph.CO].

[441] W. Guo, Q. Wang, S. Cao, M. Biesiada, T. Liu, Y. Lian, X. Jiang, C. Mu, D. Cheng, Newest measurements of Hubble constant from DESI 2024 baryon acoustic oscillation observations, Astrophys. J. Lett. 978 (2) (2025) L33, arXiv:2412.13045 [astro-ph.CO].

[442] L. Amati, R. D'Agostino, O. Luongo, M. Muccino, M. Tantalo, Addressing the circularity problem in the $E_p - E_{iso}$ correlation of gamma-ray bursts, Mon. Not. R. Astron. Soc. 486 (1) (2019) L46–L51, arXiv:1811.08934 [astro-ph.HE].

[443] J.-J. Wei, F. Melia, Model-independent distance calibration and curvature measurement using quasars and cosmic chronometers, Astrophys. J. 888 (2) (2020) 99, arXiv:1912.00668 [astro-ph.CO].

[444] V. Sahni, A. Shafieloo, A.A. Starobinsky, Model independent evidence for dark energy evolution from baryon acoustic oscillations, Astrophys. J. Lett. 793 (2) (2014) L40, arXiv:1406.2209 [astro-ph.CO].

[445] X. Zheng, X. Ding, M. Biesiada, S. Cao, Z. Zhu, What are $Omh^2(z_1, z_2)$ and $Om(z_1, z_2)$ diagnostics telling us in light of $H(z)$ data? Astrophys. J. 825 (1) (2016) 17, arXiv:1604.07910 [astro-ph.CO].

[446] X. Zheng, M. Biesiada, X. Ding, S. Cao, S. Zhang, Z.-H. Zhu, Statistical analysis with cosmic-expansion-rate measurements and two-point diagnostics, Eur. Phys. J. C 78 (3) (2018) 274, arXiv:1803.09106 [astro-ph.CO].

[447] T. Treu, P.J. Marshall, Time delay cosmography, Astron. Astrophys. Rev. 24 (1) (2016) 11, arXiv:1605.05333 [astro-ph.CO].

[448] S.H. Suyu, T.-C. Chang, F. Courbin, T. Okumura, Cosmological distance indicators, Space Sci. Rev. 214 (5) (2018) 91, arXiv:1801.07262 [astro-ph.CO].

[449] T. Treu, S.H. Suyu, P.J. Marshall, Strong lensing time-delay cosmography in the 2020s, Astron. Astrophys. Rev. 30 (1) (2022) 8, arXiv:2210.15794 [astro-ph.CO].

[450] S.H. Suyu, A. Goobar, T. Collett, A. More, G. Vernardos, Strong gravitational lensing and microlensing of supernovae, Space Sci. Rev. 220 (1) (2024) 13, arXiv:2301.07729 [astro-ph.CO].

[451] S. Birrer, M. Millon, D. Sluse, A.J. Shajib, F. Courbin, S. Erickson, L.V.E. Koopmans, S.H. Suyu, T. Treu, Time-delay cosmography: measuring the Hubble constant and other cosmological parameters with strong gravitational lensing, Space Sci. Rev. 220 (5) (2024) 48, arXiv:2210.10833 [astro-ph.CO].

[452] S. Refsdal, On the possibility of determining Hubble's parameter and the masses of galaxies from the gravitational lens effect, Mon. Not. R. Astron. Soc. 128 (4) (1964) 307–310.

[453] XXX Collaboration, R.M. Quimby, M. Oguri, A. More, S. More, T.J. Moriya, M.C. Werner, M. Tanaka, G. Folatelli, M.C. Bersten, K. Nomoto, Detection of the gravitational lens magnifying a type Ia supernova, Science 344 (6) (2014) 396–399, arXiv:1404.6014 [astro-ph.CO].

[454] P.L. Kelly, et al., Multiple images of a highly magnified supernova formed by an early-type cluster galaxy lens, Science 347 (2015) 1123, arXiv:1411.6009 [astro-ph.CO].

[455] P.L. Kelly, et al., Constraints on the Hubble constant from supernova Refsdal's reappearance, Science 380 (6649) (2023) abh1322, arXiv:2305.06367 [astro-ph.CO].

[456] C. Grillo, L. Pagano, P. Rosati, S.H. Suyu, Cosmography with supernova Refsdal through time-delay cluster lensing: Independent measurements of the Hubble constant and geometry of the universe, Astron. Astrophys. 684 (2024) L23, arXiv:2401.10980 [astro-ph.CO].

[457] I. Jee, E. Komatsu, S.H. Suyu, D. Huterer, Time-delay cosmography: Increased leverage with angular diameter distances, JCAP 04 (2016) 031, arXiv:1509.03310 [astro-ph.CO].

[458] E.V. Linder, Lensing time delays and cosmological complementarity, Phys. Rev. D 84 (2011) 123529, arXiv:1109.2592 [astro-ph.CO].

[459] S.H. Suyu, et al., Cosmology from gravitational lens time delays and Planck data, Astrophys. J. Lett. 788 (2014) L35, arXiv:1306.4732 [astro-ph.CO].

[460] T. Collett, F. Montanari, S. Rasanen, Model-independent determination of H_0 and Ω_{K0} from strong lensing and type Ia supernovae, Phys. Rev. Lett. 123 (23) (2019) 231101, arXiv:1905.09781 [astro-ph.CO].

[461] A.J. Shajib, T. Treu, A. Agnello, Improving time-delay cosmography with spatially resolved kinematics, Mon. Not. R. Astron. Soc. 473 (1) (2018) 210–226, arXiv:1709.01517 [astro-ph.CO].

[462] DES Collaboration, A.J. Shajib, et al., STRIDES: a 3.9 per cent measurement of the Hubble constant from the strong lens system DES J0408-5354, Mon. Not. R. Astron. Soc. 494 (4) (2020) 6072–6102, arXiv:1910.06306 [astro-ph.CO].

[463] M. Millon, et al., TDCOSMO. I. An exploration of systematic uncertainties in the inference of H_0 from time-delay cosmography, Astron. Astrophys. 639 (2020) A101, arXiv:1912.08027 [astro-ph.CO].

[464] E.E. Falco, M.V. Gorenstein, I.I. Shapiro, On model-dependent bounds on H 0 from gravitational images : application to Q 0957+561 A, B, Astrophys. J. Lett. 289 (1985) L1–L4.

[465] J. Wagner, Generalised model-independent characterisation of strong gravitational lenses IV: formalism-intrinsic degeneracies, Astron. Astrophys. 620 (2018) A86, arXiv:1809.03505 [astro-ph.CO].

[466] S. Birrer, et al., TDCOSMO - IV. hierarchical time-delay cosmography – joint inference of the Hubble constant and galaxy density profiles, Astron. Astrophys. 643 (2020) A165, arXiv:2007.02941 [astro-ph.CO].

[467] A. Goobar, et al., iPTF16geu: A multiply imaged, gravitationally lensed type Ia supernova, Science 356 (2017) 291–295, arXiv:1611.00014 [astro-ph.CO].

[468] A. Goobar, et al., Uncovering a population of gravitational lens galaxies with magnified standard candle SN Zwicky, Nat. Astron. 7 (2023) 1098–1107, arXiv:2211.00656 [astro-ph.CO]; Erratum: Nature Astron. 7 (2023) 1137–1137.

[469] S.A. Rodney, G.B. Brammer, J.D.R. Pierel, J. Richard, S. Toft, K.F. O'Connor, M. Akhshik, K.E. Whitaker, A gravitationally lensed supernova with an observable two-decade time delay, Nat. Astron. 5 (11) (2021) 1118–1125, arXiv:2106.08935 [astro-ph.CO].

[470] W. Chen, P.L. Kelly, M. Oguri, T.J. Broadhurst, J.M. Diego, N. Emami, A.V. Filippenko, T.L. Treu, A. Zitrin, Shock cooling of a red-supergiant supernova at redshift 3 in lensed images, nature 611 (7935) (2022) 256–259, arXiv:2306.12985 [astro-ph.GA].

[471] P. Kelly, A. Zitrin, M. Oguri, J. Diego, H. Williams, T. Broadhurst, W. Chen, A. Koekemoer, J. Pierel, L. Strolger, T. Treu, Strongly lensed SN in MACS 2129 galaxy-cluster field, Transient Name Serv. AstroNote 169 (2022) 1.

[472] B.L. Frye, et al., The JWST discovery of the triply imaged type Ia "Supernova H0pe" and observations of the galaxy cluster PLCK G165.7+67.0, Astrophys. J. 961 (2) (2024) 171, arXiv:2309.07326 [astro-ph.GA].

[473] J.D.R. Pierel, et al., Lensed type Ia Supernova 'Encore' at z = 2: The first instance of two multiply imaged supernovae in the same host galaxy, Astrophys. J. Lett. 967 (2) (2024) L37, arXiv:2404.02139 [astro-ph.CO].

[474] J.D.R. Pierel, et al., Jwst photometric time-delay and magnification measurements for the triply imaged type Ia 'SN H0pe' at z= 1.78, Astrophys. J. 967 (1) (2024) 50, arXiv:2403.18954 [astro-ph.CO].

[475] J.D.R. Pierel, S. Rodney, G. Vernardos, M. Oguri, R. Kessler, T. Anguita, Projected cosmological constraints from strongly lensed supernovae with the Roman Space Telescope, Astrophys. J. 908 (2) (2021) 190, arXiv:2010.12399 [astro-ph.CO].

[476] S. Birrer, T. Treu, TDCOSMO - V. Strategies for precise and accurate measurements of the Hubble constant with strong lensing, Astron. Astrophys. 649 (2021) A61, arXiv:2008.06157 [astro-ph.CO].

[477] M. Oguri, P.J. Marshall, Gravitationally lensed quasars and supernovae in future wide-field optical imaging surveys, Mon. Not. R. Astron. Soc. 405 (2010) 2579–2593, arXiv:1001.2037 [astro-ph.CO].

[478] T. Petrushevska, Strongly lensed supernovae in well-studied galaxy clusters with the Vera C. Rubin observatory, Symmetry 12 (12) (2020) 1966, arXiv:2011.14122 [astro-ph.CO].

[479] LSST Dark Enrgy Science Collaboration, N. Arendse, S. Dhawan, A.S. Carracedo, H.V. Peiris, A. Goobar, R. Wojtak, C. Alves, R. Biswas, S. Huber, S. Birrer, Detecting strongly lensed type Ia supernovae with LSST, Mon. Not. R. Astron. Soc. 531 (3) (2024) 3509–3523, arXiv:2312.04621 [astro-ph.CO].

[480] T.E. Collett, The population of galaxy-galaxy strong lenses in forthcoming optical imaging surveys, Astrophys. J. 811 (1) (2015) 20, arXiv:1507.02657 [astro-ph.CO].

[481] X.-L. Meng, T. Treu, A. Agnello, M.W. Auger, K. Liao, P.J. Marshall, Precision cosmology with time delay lenses: high resolution imaging requirements, JCAP 09 (2015) 059, arXiv:1506.07640 [astro-ph.CO].

[482] K. Liao, et al., Strong lens time delay challenge: II. Results of TDC1, Astrophys. J. 800 (1) (2015) 11, arXiv:1409.1254 [astro-ph.IM].

[483] P. Jovanovic, A.F. Zakharov, L.C. Popovic, T. Petrovic, Microlensing of the X-ray, UV and optical emission regions of quasars: Simulations of the time-scales and amplitude variations of microlensing events, Mon. Not. R. Astron. Soc. 386 (2008) 397, arXiv:0801.4473 [astro-ph].

[484] M. Millon, et al., TDCOSMO - II. Six new time delays in lensed quasars from high-cadence monitoring at the MPIA 2.2 m telescope, Astron. Astrophys. 642 (2020) A193, arXiv:2006.10066 [astro-ph.CO].

[485] D.A. Goldstein, P.E. Nugent, D.N. Kasen, T.E. Collett, Precise time delays from strongly gravitationally lensed type Ia supernovae with chromatically microlensed images, Astrophys. J. 855 (1) (2018) 22, arXiv:1708.00003 [astro-ph.CO].

[486] J. Bayer, S. Huber, C. Vogl, S.H. Suyu, S. Taubenberger, D. Sluse, J.H.H. Chan, W.E. Kerzendorf, HOLISMOKES - V. Microlensing of Type II supernovae and time-delay inference through spectroscopic phase retrieval, Astron. Astrophys. 653 (2021) A29, arXiv:2101.06229 [astro-ph.CO].

[487] A. Etherington, et al., Automated galaxy–galaxy strong lens modelling: No lens left behind, Mon. Not. R. Astron. Soc. 517 (3) (2022) 3275–3302, arXiv:2202.09201 [astro-ph.CO].

[488] DES Collaboration, T. Schmidt, et al., STRIDES: automated uniform models for 30 quadruply imaged quasars, Mon. Not. R. Astron. Soc. 518 (1) (2023) 1260–1300, arXiv:2206.04696 [astro-ph.CO].

[489] R. Legin, Y. Hezaveh, L. Perreault-Levasseur, B. Wandelt, A framework for obtaining accurate posteriors of strong gravitational lensing parameters with flexible priors and implicit likelihoods using density estimation, Astrophys. J. 943 (1) (2023) 4, arXiv:2212.00044 [astro-ph.IM].

[490] A.J. Shajib, T. Treu, S. Birrer, A. Sonnenfeld, Dark matter haloes of massive elliptical galaxies at z ∼ 0.2 are well described by the Navarro-Frenk-White profile, Mon. Not. R. Astro. Soc. 503 (2) (2021) 2380–2405, arXiv:2008.11724 [astro-ph.GA].

[491] A. Adam, L. Perreault-Levasseur, Y. Hezaveh, M. Welling, Pixelated reconstruction of foreground density and background surface brightness in gravitational lensing systems using recurrent inference machines, Astrophys. J. 951 (1) (2023) 6, arXiv:2301.04168 [astro-ph.IM].

[492] LSST Dark Energy Science Collaboration, J.W. Park, S. Wagner-Carena, S. Birrer, P.J. Marshall, J.Y.-Y. Lin, A. Roodman, Large-scale gravitational lens modeling with bayesian neural networks for accurate and precise inference of the Hubble constant, Astrophys. J. 910 (1) (2021) 39, arXiv:2012.00042 [astro-ph.IM].
[493] S. Schuldt, R. Cañameras, Y. Shu, S.H. Suyu, S. Taubenberger, T. Meinhardt, L. Leal-Taixé, HOLISMOKES – IX. Neural network inference of strong-lens parameters and uncertainties from ground-based images, Astron. Astrophys. 671 (2023) A147, arXiv:2206.11279 [astro-ph.IM].
[494] S. Ertl, S. Schuldt, S.H. Suyu, T. Schmidt, T. Treu, S. Birrer, A.J. Shajib, D. Sluse, TDCOSMO X. Automated modeling of 9 strongly lensed quasars and comparison between lens modeling software, Astron. Astrophys. 672 (2023) A2, arXiv:2209.03094 [astro-ph.CO].
[495] T. Treu, L.V.E. Koopmans, The internal structure of the lens pg1115+080: breaking degeneracies in the value of the Hubble constant, Mon. Not. R. Astron. Soc. 337 (2002) L6, arXiv:astro-ph/0210002.
[496] A. Yıldırım, S.H. Suyu, A. Halkola, Time-delay cosmographic forecasts with strong lensing and JWST stellar kinematics, Mon. Not. R. Astron. Soc. 493 (4) (2020) 4783–4807, arXiv:1904.07237 [astro-ph.CO].
[497] TDCOSMO Collaboration, A.J. Shajib, et al., TDCOSMO. XII. Improved Hubble constant measurement from lensing time delays using spatially resolved stellar kinematics of the lens galaxy, Astron. Astrophys. 673 (2023) A9, arXiv:2301.02656 [astro-ph.CO].
[498] S. Birrer, S. Dhawan, A.J. Shajib, The Hubble constant from strongly lensed supernovae with standardizable magnifications, Astrophys. J. 924 (1) (2022) 2, arXiv:2107.12385 [astro-ph.CO].
[499] N. Khadka, S. Birrer, A. Leauthaud, H. Nix, Breaking the mass-sheet degeneracy in strong lensing mass modelling with weak lensing observations, Mon. Not. R. Astron. Soc. 533 (1) (2024) 795–806, arXiv:2404.01513 [astro-ph.CO].
[500] A. Yıldırım, S.H. Suyu, G.C.F. Chen, E. Komatsu, TDCOSMO - XIII. Cosmological distance measurements in light of the mass-sheet degeneracy: Forecasts from strong lensing and integral field unit stellar kinematics, Astron. Astrophys. 675 (2023) A21, arXiv:2109.14615 [astro-ph.CO].
[501] A. Sonnenfeld, S.-S. Li, G. Despali, R. Gavazzi, A.J. Shajib, E.N. Taylor, Strong lensing selection effects, Astron. Astrophys. 678 (2023) A4, arXiv:2301.13230 [astro-ph.GA].
[502] M. Pascale, et al., SN H0pe: The first measurement of H_0 from a multiply imaged type Ia supernova, discovered by JWST, Astrophys. J. 979 (1) (2025) 13, arXiv:2403.18902 [astro-ph.CO].
[503] E. Lusso, et al., Quasars as standard candles III. Validation of a new sample for cosmological studies, Astron. Astrophys. 642 (2020) A150, arXiv:2008.08586 [astro-ph.GA].
[504] F. Wang, J. Yang, X. Fan, J.F. Hennawi, A.J. Barth, E. Banados, F. Bian, K. Boutsia, T. Connor, F.B. Davies, R. Decarli, A.-C. Eilers, E.P. Farina, R. Green, L. Jiang, J.-T. Li, C. Mazzucchelli, R. Nanni, J.-T. Schindler, B. Venemans, F. Walter, X.-B. Wu, M. Yue, A luminous quasar at redshift 7.642, Astrophys. J. Lett. 907 (1) (2021) L1, arXiv:2101.03179 [astro-ph.GA].
[505] D. Watson, K.D. Denney, M. Vestergaard, T.M. Davis, A new cosmological distance measure using AGN, Astrophys. J. Lett. 740 (2011) L49, arXiv:1109.4632 [astro-ph.CO].
[506] M. Haas, R. Chini, M. Ramolla, F. Pozo Nuñez, C. Westhues, R. Watermann, V. Hoffmeister, M. Murphy, Photometric AGN reverberation mapping - an efficient tool for BLR sizes, black hole masses, and host-subtracted AGN luminosities, Astron. Astrophys. 535 (2011) A73, arXiv:1109.1848 [astro-ph.CO].
[507] F. La Franca, S. Bianchi, G. Ponti, E. Branchini, G. Matt, A new cosmological distance measure using active galactic nucleus X-ray variability, Astrophys. J. Lett. 787 (2014) L12, arXiv:1404.2607 [astro-ph.CO].
[508] M.L. Martínez-Aldama, A. del Olmo, P. Marziani, J.W. Sulentic, C.A. Negrete, D. Dultzin, M. D'Onofrio, J. Perea, Extreme quasars at high redshift, Astron. Astrophys. 618 (2018) A179, arXiv:1807.11006 [astro-ph.GA].
[509] P. Marziani, D. Dultzin, J.W. Sulentic, A. Del Olmo, C.A. Negrete, M.L. Martínez-Aldama, M. D'Onofrio, E. Bon, N. Bon, G.M. Stirpe, A main sequence for quasars, Front. Astron. Space Sci. 5 (2018) 6, arXiv:1802.05575 [astro-ph.GA].
[510] S. Panda, P. Marziani, B. Czerny, The Quasar Main Sequence explained by the combination of Eddington ratio, metallicity and orientation, Astrophys. J. 882 (2) (2019) 79, arXiv:1905.01729 [astro-ph.HE].
[511] S. Panda, P. Marziani, High Eddington quasars as discovery tools: current state and challenges, Front. Astron. Space Sci. 10 (2023) arXiv:2210.15041 [astro-ph.GA], https://www.frontiersin.org/journals/astronomy-and-space-sciences/articles/10.3389/fspas.2023.1130103.
[512] R. Prince, K. Hryniewicz, S. Panda, B. Czerny, A. Pollo, Viewing angle observations and effects of evolution with redshift, black hole mass, and eddington ratio in quasar-based cosmology, Astrophys. J. 925 (2) (2022) 215, arXiv:2106.03877 [astro-ph.GA].
[513] M.G. Dainotti, G. Bardiacchi, A.L. Lenart, S. Capozziello, E.O. Colgain, R. Solomon, D. Stojkovic, M.M. Sheikh-Jabbari, Quasar standardization: Overcoming selection biases and redshift evolution, Astrophys. J. 931 (2) (2022) 106, arXiv:2203.12914 [astro-ph.HE].
[514] S. Cao, M. Zajaček, S. Panda, M.L. Martínez-Aldama, B. Czerny, B. Ratra, Standardizing reverberation-measured C iv time-lag quasars, and using them with standardized Mg ii quasars to constrain cosmological parameters, Mon. Not. R. Astron. Soc. 516 (2) (2022) 1721–1740, arXiv:2205.15552 [astro-ph.CO].
[515] S. Cao, M. Zajaˇcek, B. Czerny, S. Panda, B. Ratra, Effects of heterogeneous data sets and time-lag measurement techniques on cosmological parameter constraints from Mg ii and C iv reverberation-mapped quasar data, Mon. Not. R. Astron. Soc. 528 (4) (2024) 6444–6469, arXiv:2309.16516 [astro-ph.CO].
[516] M.G. Dainotti, B. De Simone, T. Schiavone, G. Montani, E. Rinaldi, G. Lambiase, M. Bogdan, S. Ugale, On the evolution of the Hubble constant with the SNe Ia pantheon sample and baryon acoustic oscillations: A feasibility study for GRB-cosmology in 2030, Galaxies 10 (1) (2022) 24, arXiv:2201.09848 [astro-ph.CO].
[517] G. Bargiacchi, M.G. Dainotti, S. Nagataki, S. Capozziello, Gamma-ray bursts, quasars, baryonic acoustic oscillations, and supernovae Ia: new statistical insights and cosmological constraints, Mon. Not. R. Astron. Soc. 521 (3) (2023) 3909–3924, arXiv:2303.07076 [astro-ph.CO].
[518] M.G. Dainotti, G. Bargiacchi, M.g. Bogdan, A.L. Lenart, K. Iwasaki, S. Capozziello, B. Zhang, N. Fraija, Reducing the uncertainty on the Hubble constant up to 35% with an improved statistical analysis: different best-fit likelihoods for type Ia supernovae, baryon acoustic oscillations, quasars, and gamma-ray bursts, Astrophys. J. 951 (1) (2023) 63, arXiv:2305.10030 [astro-ph.CO].
[519] A.L. Lenart, G. Bargiacchi, M.G. Dainotti, S. Nagataki, S. Capozziello, A bias-free cosmological analysis with quasars alleviating H_0 tension, Astrophys. J. Suppl. 264 (2) (2023) 46, arXiv:2211.10785 [astro-ph.CO].
[520] T. Yang, A. Banerjee, E.O. Colgáin, Cosmography and flat ΛCDM tensions at high redshift, Phys. Rev. D 102 (12) (2020) 123532, arXiv:1911.01681 [astro-ph.CO].
[521] N. Khadka, B. Ratra, Quasar X-ray and UV flux, baryon acoustic oscillation, and Hubble parameter measurement constraints on cosmological model parameters, Mon. Not. R. Astron. Soc. 492 (3) (2020) 4456–4468, arXiv:1909.01400 [astro-ph.CO].
[522] G. Bargiacchi, M. Benetti, S. Capozziello, E. Lusso, G. Risaliti, M. Signorini, Quasar cosmology: dark energy evolution and spatial curvature, Mon. Not. R. Astron. Soc. 515 (2) (2022) 1795–1806, arXiv:2111.02420 [astro-ph.CO].
[523] E.O. Colgáin, M.M. Sheikh-Jabbari, R. Solomon, G. Bargiacchi, S. Capozziello, M.G. Dainotti, D. Stojkovic, Revealing intrinsic flat ΛCDM biases with standardizable candles, Phys. Rev. D 106 (4) (2022) L041301, arXiv:2203.10558 [astro-ph.CO].
[524] M. Zajaˇcek, B. Czerny, N. Khadka, M.L. Martínez-Aldama, R. Prince, S. Panda, B. Ratra, Effect of extinction on quasar luminosity distances determined from UV and X-ray flux measurements, Astrophys. J. 961 (2) (2024) 229, arXiv:2305.08179 [astro-ph.GA].
[525] A. Sacchi, et al., Quasars as high-redshift standard candles, Astron. Astrophys. 663 (2022) L7, arXiv:2206.13528 [astro-ph.CO].
[526] H. Shabani, A. De, T.-H. Loo, E.N. Saridakis, Cosmology of f(Q) gravity in non-flat universe, Eur. Phys. J. C 84 (3) (2024) 285, arXiv:2306.13324 [gr-qc].
[527] M. Sabiee, M. Malekjani, D. Mohammad Zadeh Jassur, f(T) cosmology against the cosmographic method: A new study using mock and observational data, Mon. Not. R. Astron. Soc. 516 (2) (2022) 2597–2613, arXiv:2212.04113 [astro-ph.CO].
[528] E. Lusso, E. Piedipalumbo, G. Risaliti, M. Paolillo, S. Bisogni, E. Nardini, L. Amati, Tension with the flat ΛCDM model from a high-redshift Hubble diagram of supernovae, quasars, and gamma-ray bursts, Astron. Astrophys. 628 (2019) L4, arXiv:1907.07692 [astro-ph.CO].
[529] M.G. Dainotti, A.L. Lenart, M.G. Yengejeh, S. Chakraborty, N. Fraija, E. Di Valentino, G. Montani, A new binning method to choose a standard set of quasars, Phys. Dark Univ. 44 (2024) 101428, arXiv:2401.12847 [astro-ph.HE].
[530] G. Bargiacchi, G. Risaliti, M. Benetti, S. Capozziello, E. Lusso, A. Saccardi, M. Signorini, Cosmography by orthogonalized logarithmic polynomials, Astron. Astrophys. 649 (2021) A65, arXiv:2101.08278 [astro-ph.CO].
[531] G. Bargiacchi, M.G. Dainotti, S. Capozziello, Tensions with the flat ΛCDM model from high-redshift cosmography, Mon. Not. R. Astron. Soc. 525 (2) (2023) 3104–3116, arXiv:2307.15359 [astro-ph.CO].
[532] R.A. Preston, D.D. Morabito, J.G. Williams, J. Faulkner, D.L. Jauncey, G. Nicolson, A VLBI survey at 2.29 GHz, Astron. J. 90 (1985) 1599–1603.
[533] J.-M. Wang, Y.-Y. Songsheng, Y.-R. Li, P. Du, Z.-X. Zhang, A parallax distance to 3C 273 through spectroastrometry and reverberation mapping, Nat. Astron. 4 (2020) 517–525, arXiv:1906.08417 [astro-ph.CO].
[534] R. Sandoval-Orozco, C. Escamilla-Rivera, R. Briffa, J. Levi Said, f(T) cosmology in the regime of quasar observations, Phys. Dark Univ. 43 (2024) 101407, arXiv:2309.03675 [astro-ph.CO].
[535] A. Sandage, The change of redshift and apparent luminosity of galaxies due to the deceleration of selected expanding universes, Astrophys. J. 136 (1962) 319.
[536] G. Calderone, K. Boutsia, S. Cristiani, A. Grazian, R. Amorin, V. D'Odorico, G. Cupani, F. Fontanot, M. Salvato, Finding the brightest cosmic beacons in the southern hemisphere, Astrophys. J. 887 (2) (2019) 268, arXiv:1909.06391 [astro-ph.IM].

[537] J. Liske, et al., Cosmic dynamics in the era of extremely large telescopes, Mon. Not. R. Astron. Soc. 386 (2008) 1192–1218, arXiv:0802.1532 [astro-ph].
[538] C.M.J. Marques, C.J.A.P. Martins, C.S. Alves, Fundamental cosmology from ANDES precision spectroscopy, Mon. Not. R. Astron. Soc. 522 (4) (2023) 5973–5979, arXiv:2305.01446 [astro-ph.IM].
[539] ANDES Collaboration, C.J.A.P. Martins, et al., Cosmology and fundamental physics with the ELT-ANDES spectrograph, Exper. Astron. 57 (1) (2024) 5, arXiv:2311.16274 [astro-ph.CO].
[540] M.G. Dainotti, G. Bargiacchi, A.L. Lenart, S. Nagataki, S. Capozziello, Quasars: Standard candles up to z = 7.5 with the precision of supernovae Ia, Astrophys. J. 950 (1) (2023) 45, arXiv:2305.19668 [astro-ph.CO].
[541] M.G. Dainotti, G. Bargiacchi, A.L. Lenart, S. Capozziello, The scavenger hunt for quasar samples to be used as cosmological tools, Galaxies 12 (1) (2024) 4, arXiv:2401.11998 [astro-ph.CO].
[542] L. Amati, et al., Intrinsic spectra and energetics of BeppoSAX gamma-ray bursts with known redshifts, Astron. Astrophys. 390 (2002) 81, arXiv:astro-ph/0205230.
[543] L. Amati, The E(p,i) - E(iso) correlation in grbs: updated observational status, re-analysis and main implications, Mon. Not. R. Astron. Soc. 372 (2006) 233–245, arXiv:astro-ph/0601553.
[544] L. Amati, F. Frontera, C. Guidorzi, Spectrum-energy correlations in gamma-ray bursts confront extremely energetic fermi GRBs, Astron. Astrophys. 508 (2009) 173–180, arXiv:0907.0384 [astro-ph.HE].
[545] F.F. Dirirsa, S. Razzaque, F. Piron, M. Arimoto, M. Axelsson, D. Kocevski, F. Longo, M. Ohno, S. Zhu, Spectral analysis of fermi-LAT gamma-ray bursts with known redshift and their potential use as cosmological standard candles, Astrophys. J. 887 (2019) 13, arXiv:1910.07009 [astro-ph.HE].
[546] D. Yonetoku, T. Murakami, T. Nakamura, R. Yamazaki, A.K. Inoue, K. Ioka, Gamma-ray burst formation rates inferred from the spectral peak energy-peak luminosity relation, Astrophys. J. 609 (2004) 935, arXiv:astro-ph/0309217.
[547] T. Aldowma, S. Razzaque, Deep neural networks for estimation of gamma-ray burst redshifts, Mon. Not. R. Astron. Soc. 529 (3) (2024) 2676–2685, arXiv:2401.11005 [astro-ph.HE].
[548] M.G. Dainotti, V.F. Cardone, S. Capozziello, A time - luminosity correlation for gamma ray bursts in the X - rays, Mon. Not. R. Astron. Soc. 391 (2008) 79, arXiv:0809.1389 [astro-ph].
[549] B.D. Metzger, D. Giannios, T.A. Thompson, N. Bucciantini, E. Quataert, The proto-magnetar model for gamma-ray bursts, Mon. Not. R. Astron. Soc. 413 (2011) 2031, arXiv:1012.0001 [astro-ph.HE].
[550] A. Rowlinson, P.T. O'Brien, B.D. Metzger, N.R. Tanvir, A.J. Levan, Signatures of magnetar central engines in short GRB lightcurves, Mon. Not. R. Astron. Soc. 430 (2013) 1061, arXiv:1301.0629 [astro-ph.HE].
[551] A. Rowlinson, B.P. Gompertz, M. Dainotti, P.T. O'Brien, R.A.M.J. Wijers, A.J. van der Horst, Constraining properties of GRB magnetar central engines using the observed plateau luminosity and duration correlation, Mon. Not. R. Astron. Soc. 443 (2) (2014) 1779–1787, arXiv:1407.1053 [astro-ph.HE].
[552] G. Stratta, M.G. Dainotti, S. Dall'Osso, X. Hernandez, G. De Cesare, On the magnetar origin of the GRBs presenting X-ray afterglow plateaus, Astrophys. J. 869 (2) (2018) 155, arXiv:1804.08652 [astro-ph.HE].
[553] Z.L. Uhm, A.M. Beloborodov, On the mechanism of gamma-ray burst afterglows, Astrophys. J. Lett. 665 (2007) L93, arXiv:astro-ph/0701205.
[554] Z.L. Uhm, B. Zhang, R. Hascoet, F. Daigne, R. Mochkovitch, I.H. Park, Dynamics and afterglow light curves of grb blast waves with a long-lived reverse shock, Astrophys. J. 761 (2012) 147, arXiv:1208.2347 [astro-ph.HE].
[555] R. Hascoet, F. Daigne, R. Mochkovitch, The prompt–early afterglow connection in gamma-ray bursts: implications for the early afterglow physics, Mon. Not. R. Astron. Soc. 442 (1) (2014) 20–27, arXiv:1401.0751 [astro-ph.HE].
[556] M.G. Dainotti, R. Willingale, S. Capozziello, V.F. Cardone, M. Ostrowski, Discovery of a tight correlation for gamma ray burst afterglows with 'canonical' light curves, Astrophys. J. Lett. 722 (2010) L215, arXiv:1009.1663 [astro-ph.HE].
[557] M.G. Dainotti, M. Ostrowski, R. Willingale, Toward a standard gamma ray burst: tight correlations between the prompt and the afterglow plateau phase emission, Mon. Not. R. Astron. Soc. 418 (2011) 2202, arXiv:1103.1138 [astro-ph.HE].
[558] M.G. Dainotti, V. Petrosian, J. Singal, M. Ostrowski, Determination of the intrinsic luminosity time correlation in the X-ray afterglows of gamma-ray bursts, Astrophys. J. 774 (2013) 157, arXiv:1307.7297 [astro-ph.HE].
[559] M.G. Dainotti, V. Petrosian, R. Willingale, P. O'Brien, M. Ostrowski, S. Nagataki, Luminosity–time and luminosity–luminosity correlations for GRB prompt and afterglow plateau emissions, Mon. Not. R. Astron. Soc. 451 (4) (2015) 3898–3908, arXiv:1506.00702 [astro-ph.HE].
[560] M.G. Dainotti, S. Postnikov, X. Hernandez, M. Ostrowski, A fundamental plane for long gamma-ray bursts with X-ray plateaus, Astrophys. J. Lett. 825 (2) (2016) L20, arXiv:1604.06840 [astro-ph.HE].
[561] M.G. Dainotti, X. Hernandez, S. Postnikov, S. Nagataki, P. Obrien, R. Willingale, S. Striegel, A study of the gamma-ray burst fundamental plane, Astrophys. J. 848 (2) (2017) 88, arXiv:1704.04908 [astro-ph.HE].
[562] M.G. Dainotti, S. Nagataki, K. Maeda, S. Postnikov, E. Pian, A study of gamma ray bursts with afterglow plateau phases associated with supernovae, Astron. Astrophys. 600 (2017) A98, arXiv:1612.02917 [astro-ph.HE].
[563] M.G. Dainotti, A. Lenart, G. Sarracino, S. Nagataki, S. Capozziello, N. Fraija, The X-ray fundamental plane of the Platinum Sample, the Kilonovae and the SNe Ib/c associated with GRBs, Astrophys. J. 904 (2) (2020) 97, arXiv:2010.02092 [astro-ph.HE].
[564] V.F. Cardone, S. Capozziello, M.G. Dainotti, An updated gamma ray bursts Hubble diagram, Mon. Not. R. Astron. Soc. 400 (2) (2009) 775–790, arXiv:0901.3194 [astro-ph.CO].
[565] M.G. Dainotti, V.F. Cardone, E. Piedipalumbo, S. Capozziello, Slope evolution of GRB correlations and cosmology, Mon. Not. R. Astron. Soc. 436 (2013) 82, arXiv:1308.1918 [astro-ph.HE].
[566] M.G. Dainotti, V. Nielson, G. Sarracino, E. Rinaldi, S. Nagataki, S. Capozziello, O.Y. Gnedin, G. Bargiacchi, Optical and X-ray GRB fundamental planes as cosmological distance indicators, Mon. Not. R. Astron. Soc. 514 (2) (2022) 1828–1856, arXiv:2203.15538 [astro-ph.CO].
[567] M.G. Dainotti, A.L. Lenart, A. Chraya, G. Sarracino, S. Nagataki, N. Fraija, S. Capozziello, M. Bogdan, The gamma-ray bursts fundamental plane correlation as a cosmological tool, Mon. Not. R. Astron. Soc. 518 (2) (2023) 2201–2240, arXiv:2209.08675 [astro-ph.HE].
[568] M.G. Dainotti, et al., Inferring the redshift of more than 150 GRBs with a machine-learning ensemble model, Astrophys. J. Suppl. 271 (1) (2024) 22, arXiv:2401.03589 [astro-ph.CO].
[569] M.G. Dainotti, A. Narendra, A. Pollo, V. Petrosian, M. Bogdan, K. Iwasaki, J.X. Prochaska, E. Rinaldi, D. Zhou, Gamma-ray bursts as distance indicators by a statistical learning approach, Astrophys. J. Lett. 967 (2) (2024) L30, arXiv:2402.04551 [astro-ph.HE].
[570] M.G. Dainotti, R. Sharma, A. Narendra, D. Levine, E. Rinaldi, A. Pollo, G. Bhatta, A stochastic approach to reconstruct gamma ray burst lightcurves, Astrophys. J. 267 (2) (2023) 42, arXiv:2305.12126 [astro-ph.HE].
[571] N. Liang, Z. Li, X. Xie, P. Wu, Calibrating gamma-ray bursts by using a gaussian process with type Ia supernovae, Astrophys. J. 941 (1) (2022) 84, arXiv:2211.02473 [astro-ph.CO].
[572] O. Luongo, M. Muccino, Kinematic constraints beyond $z \simeq 0$ using calibrated GRB correlations, Astron. Astrophys. 641 (2020) A174, arXiv:2010.05218 [astro-ph.CO].
[573] Y. Mu, B. Chang, L. Xu, Cosmography via Gaussian process with gamma ray bursts, JCAP 09 (2023) 041, arXiv:2302.02559 [astro-ph.CO].
[574] N. Rea, M. Gullon, J.A. Pons, R. Perna, M.G. Dainotti, J.A. Miralles, D.F. Torres, Constraining the GRB-magnetar model by means of the Galactic pulsar population, Astrophys. J. 813 (2) (2015) 92, arXiv:1510.01430 [astro-ph.HE].
[575] A.C. Alfano, S. Capozziello, O. Luongo, M. Muccino, Cosmological transition epoch from gamma-ray burst correlations, JHEAp 42 (2024) 178–196, arXiv:2402.18967 [astro-ph.CO].
[576] Z. Cano, Gamma-ray burst supernovae as standardizable candles, Astrophys. J. 794 (2014) 121, arXiv:1407.2589 [astro-ph.HE].
[577] M.G. Dainotti, B. De Simone, M.I. Khadir, K. Kawaguchi, T.J. Moriya, T. Takiwaki, N. Tominaga, A. Gangopadhyay, The quest for new correlations in the realm of the gamma-ray Burst—Supernova connection, Astrophys. J. 938 (1) (2022) 41, arXiv:2208.10958 [astro-ph.HE].
[578] D. Staicova, Impact of cosmology on Lorentz Invariance Violation constraints from GRB time-delays, Cl.. Quant. Grav. 40 (19) (2023) 195012, arXiv:2305.06504 [gr-qc].
[579] D. Staicova, Probing for Lorentz invariance violation in pantheon plus dominated cosmology, Universe 10 (2) (2024) 75, arXiv:2401.06068 [gr-qc].
[580] Fermi-LAT Collaboration, S. Abdollahi, et al., A gamma-ray determination of the Universe's star formation history, Science 362 (6418) (2018) 1031–1034, arXiv:1812.01031 [astro-ph.HE].
[581] MAGIC Collaboration, V.A. Acciari, et al., Measurement of the extragalactic background light using MAGIC and Fermi-LAT gamma-ray observations of blazars up to z=1, Mon. Not. R. Astron. Soc. 486 (3) (2019) 4233–4251, arXiv:1904.00134 [astro-ph.HE].
[582] A. Domínguez, R. Wojtak, J. Finke, M. Ajello, K. Helgason, F. Prada, A. Desai, V. Paliya, L. Marcotulli, D. Hartmann, A new measurement of the Hubble constant and matter content of the universe using extragalactic background light γ-ray attenuation, Astrophys. J. 885 (2) (2019) 137, arXiv:1903.12097 [astro-ph.CO].
[583] A. Domínguez, et al., A new derivation of the Hubble constant from γ-ray attenuation using improved optical depths for the fermi and cta era, Mon. Not. R. Astron. Soc. 527 (3) (2023) 4632–4642, arXiv:2306.09878 [astro-ph.HE].
[584] LIGO Scientific Collaboration, J. Aasi, et al., Advanced LIGO, Cl.. Quant. Grav. 32 (2015) 074001, arXiv:1411.4547 [gr-qc].
[585] VIRGO Collaboration, F. Acernese, et al., Advanced Virgo: a second-generation interferometric gravitational wave detector, Cl.. Quant. Grav. 32 (2) (2015) 024001, arXiv:1408.3978 [gr-qc].
[586] KAGRA Collaboration, T. Akutsu, et al., Overview of KAGRA: Calibration, detector characterization, physical environmental monitors, and the geophysics interferometer, PTEP 2021 (5) (2021) 05A102, arXiv:2009.09305 [gr-qc].
[587] LIGO Scientific, Virgo Collaboration, B.P. Abbott, et al., GW170817: Observation of gravitational waves from a binary neutron star inspiral, Phys. Rev. Lett. 119 (16) (2017) 161101, arXiv:1710.05832 [gr-qc].

[588] LIGO Scientific, KAGRA, VIRGO Collaboration, R. Abbott, et al., Observation of gravitational waves from two neutron star–black hole coalescences, Astrophys. J. Lett. 915 (1) (2021) L5, arXiv:2106.15163 [astro-ph.HE].
[589] LIGO Scientific, Virgo Collaboration, B.P. Abbott, et al., Observation of gravitational waves from a binary black hole merger, Phys. Rev. Lett. 116 (6) (2016) 061102, arXiv:1602.03837 [gr-qc].
[590] KAGRA, LIGO Scientific, Virgo Collaboration, B.P. Abbott, et al., Prospects for observing and localizing gravitational-wave transients with advanced LIGO, Advanced Virgo and KAGRA, Living Rev. Rel. 19 (2016) 1, arXiv:1304.0670 [gr-qc].
[591] P. Fritschel, K. Kuns, J. Driggers, A. Effler, B. Lantz, D. Ottaway, S. Ballmer, K. Dooley, R. Adhikari, M. Evans, B. Farr, G. Gonzalez, P. Schmidt, S. Raja, Report from the LSC Post-O5 Study Group, Tech. Rep. T2200287, LIGO, 2022, https://dcc.ligo.org/LIGO-T2200287/public.
[592] VIRGO Collaboration, F. Acernese, et al., Advanced virgo plus: Future perspectives, J. Phys. Conf. Ser. 2429 (1) (2023) 012040.
[593] D. Reitze, et al., Cosmic explorer: The U.S. contribution to gravitational-wave astronomy beyond LIGO, Bull. Am. Astron. Soc. 51 (7) (2019) 035, arXiv:1907.04833 [astro-ph.IM].
[594] M. Evans, et al., A horizon study for cosmic explorer: Science, observatories, and community, 2021, arXiv:2109.09882 [astro-ph.IM].
[595] M. Evans, et al., Cosmic explorer: A submission to the NSF MPSAC ngGW subcommittee, 2023, arXiv:2306.13745 [astro-ph.IM].
[596] E.T. Steering Committee, ET Design Report Update 2020, Tech. Rep. ET-0007A-20, Einstein Telescope, 2020, https://apps.et-gw.eu/tds/?content=3&r=17245.
[597] LISA Collaboration, P. Amaro-Seoane, et al., Laser interferometer space antenna, 2017, arXiv:1702.00786 [astro-ph.IM].
[598] B.F. Schutz, Determining the Hubble constant from gravitational wave observations, Nature 323 (1986) 310–311.
[599] D.E. Holz, S.A. Hughes, Using gravitational-wave standard sirens, Astrophys. J. 629 (2005) 15–22, arXiv:astro-ph/0504616.
[600] LIGO Scientific, Virgo, Fermi GBM, INTEGRAL, IceCube, AstroSat Cadmium Zinc Telluride Imager Team, IPN, Insight-Hxmt, ANTARES, Swift, AGILE Team, 1M2H Team, Dark Energy Camera GW-EM, DES, DLT40, GRAWITA, Fermi-LAT, ATCA, ASKAP, Las Cumbres Observatory Group, OzGrav, DWF (Deeper Wider Faster Program), AST3, CAASTRO, VINROUGE, MASTER, J-GEM, GROWTH, JAGWAR, CaltechNRAO, TTU-NRAO, NuSTAR, Pan-STARRS, MAXI Team, TZAC Consortium, KU, Nordic Optical Telescope, ePESSTO, GROND, Texas Tech University, SALT Group, TOROS, BOOTES, MWA, CALET, IKI-GW Follow-up, H.E.S.S., LOFAR, LWA, HAWC, Pierre Auger, ALMA, Euro VLBI Team, Pi of Sky, Chandra Team at McGill University, DFN, ATLAS Telescopes, High Time Resolution Universe Survey, RIMAS, RATIR, SKA South Africa/MeerKAT Collaboration, B.P. Abbott, et al., Multi-messenger observations of a binary neutron star merger, Astrophys. J. Lett. 848 (2) (2017) L12, arXiv:1710.05833 [astro-ph.HE].
[601] LIGO Scientific, Virgo, 1M2H, Dark Energy Camera GW-E, DES, DLT40, Las Cumbres Observatory, VINROUGE, MASTER Collaboration, B.P. Abbott, et al., A gravitational-wave standard siren measurement of the Hubble constant, Nature 551 (7678) (2017) 85–88, arXiv:1710.05835 [astro-ph.CO].
[602] C. Nicolaou, O. Lahav, P. Lemos, W. Hartley, J. Braden, The impact of peculiar velocities on the estimation of the Hubble constant from gravitational wave standard sirens, Mon. Not. R. Astron. Soc. 495 (1) (2020) 90–97, arXiv:1909.09609 [astro-ph.CO].
[603] S. Mukherjee, G. Lavaux, F.c.R. Bouchet, J. Jasche, B.D. Wandelt, S.M. Nissanke, F. Leclercq, K. Hotokezaka, Velocity correction for Hubble constant measurements from standard sirens, Astron. Astrophys. 646 (2021) A65, arXiv:1909.08627 [astro-ph.CO].
[604] C. Howlett, T.M. Davis, Standard siren speeds: improving velocities in gravitational-wave measurements of H_0, Mon. Not. R. Astron. Soc. 492 (3) (2020) 3803–3815, arXiv:1909.00587 [astro-ph.CO].
[605] C. Guidorzi, et al., Improved constraints on H_0 from a combined analysis of gravitational-wave and electromagnetic emission from GW170817, Astrophys. J. Lett. 851 (2) (2017) L36, arXiv:1710.06426 [astro-ph.CO].
[606] K. Hotokezaka, E. Nakar, O. Gottlieb, S. Nissanke, K. Masuda, G. Hallinan, K.P. Mooley, A.T. Deller, A Hubble constant measurement from superluminal motion of the jet in GW170817, Nat. Astron. 3 (10) (2019) 940–944, arXiv:1806.10596 [astro-ph.CO].
[607] S. Dhawan, M. Bulla, A. Goobar, A.S. Carracedo, C.N. Setzer, Constraining the observer angle of the kilonova AT2017gfo associated with GW170817: Implications for the Hubble constant, Astrophys. J. 888 (2) (2020) 67, arXiv:1909.13810 [astro-ph.HE].
[608] A. Palmese, R. Kaur, A. Hajela, R. Margutti, A. McDowell, A. MacFadyen, Standard siren measurement of the Hubble constant using GW170817 and the latest observations of the electromagnetic counterpart afterglow, Phys. Rev. D 109 (6) (2024) 063508, arXiv:2305.19914 [astro-ph.CO].
[609] A. Palmese, O. Graur, J.T. Annis, S. BenZvi, E. Di Valentino, J. Garcia-Bellido, S.G.A. Gontcho, R. Keeley, A. Kim, O. Lahav, S. Nissanke, K. Paterson, M. Sako, A. Shafieloo, Y.-D. Tsai, Gravitational wave cosmology and astrophysics with large spectroscopic galaxy surveys, Bull. Am. Astron. Soc. 51 (3) (2019) 310, arXiv:1903.04730 [astro-ph.CO].
[610] H.-Y. Chen, Systematic uncertainty of standard sirens from the viewing angle of binary neutron star inspirals, Phys. Rev. Lett. 125 (20) (2020) 201301, arXiv:2006.02779 [astro-ph.HE].
[611] H.-Y. Chen, C. Talbot, E.A. Chase, Mitigating the counterpart selection effect for standard sirens, Phys. Rev. Lett. 132 (19) (2024) 191003, arXiv:2307.10402 [astro-ph.CO].
[612] G. Gianfagna, L. Piro, F. Pannarale, H. Van Eerten, F. Ricci, G. Ryan, Potential biases and prospects for the Hubble constant estimation via electromagnetic and gravitational-wave joint analyses, Mon. Not. R. Astron. Soc. 528 (2) (2024) 2600–2613, arXiv:2309.17073 [astro-ph.HE].
[613] J. Heinzel, M.W. Coughlin, T. Dietrich, M. Bulla, S. Antier, N. Christensen, D.A. Coulter, R.J. Foley, L. Issa, N. Khetan, Comparing inclination dependent analyses of kilonova transients, Mon. Not. R. Astron. Soc. 502 (2) (2021) 3057–3065, arXiv:2010.10746 [astro-ph.HE].
[614] M. Müller, S. Mukherjee, G. Ryan, Be careful in multimessenger inference of the Hubble constant: A path forward for robust inference, Astrophys. J. Lett. 977 (2) (2024) L45, arXiv:2406.11965 [astro-ph.CO].
[615] S. Vitale, H.-Y. Chen, Measuring the Hubble constant with neutron star black hole mergers, Phys. Rev. Lett. 121 (2) (2018) 021303, arXiv:1804.07337 [astro-ph.CO].
[616] M.J. Graham, et al., Candidate electromagnetic counterpart to the binary black hole merger gravitational wave event S190521g, Phys. Rev. Lett. 124 (25) (2020) 251102, arXiv:2006.14122 [astro-ph.HE].
[617] M.J. Graham, et al., A light in the dark: searching for electromagnetic counterparts to black hole–black hole mergers in LIGO/Virgo O3 with the Zwicky transient facility, Astrophys. J. 942 (2) (2023) 99, arXiv:2209.13004 [astro-ph.HE].
[618] T. Cabrera, et al., Searching for electromagnetic emission in an AGN from the gravitational wave binary black hole merger candidate S230922g, Phys. Rev. D 110 (12) (2024) 123029, arXiv:2407.10698 [astro-ph.HE].
[619] G. Ashton, K. Ackley, I.M.n. Hernandez, B. Piotrzkowski, Current observations are insufficient to confidently associate the binary black hole merger GW190521 with AGN J124942.3 + 344929, Cl.. Quant. Grav. 38 (23) (2021) 235004, arXiv:2009.12346 [astro-ph.HE].
[620] A. Palmese, M. Fishbach, C.J. Burke, J.T. Annis, X. Liu, Do LIGO/Virgo black hole mergers produce AGN flares? the case of GW190521 and prospects for reaching a confident association, Astrophys. J. Lett. 914 (2) (2021) L34, arXiv:2103.16069 [astro-ph.HE].
[621] S. Mukherjee, A. Ghosh, M.J. Graham, C. Karathanasis, M.M. Kasliwal, I. Magaña Hernandez, S.M. Nissanke, A. Silvestri, B.D. Wandelt, First measurement of the Hubble parameter from bright binary black hole GW190521, 2020, arXiv:2009.14199 [astro-ph.CO].
[622] V. Gayathri, J. Healy, J. Lange, B. O'Brien, M. Szczepanczyk, I. Bartos, M. Campanelli, S. Klimenko, C.O. Lousto, R. O'Shaughnessy, Measuring the Hubble constant with GW190521 as an eccentric black hole merger and its potential electromagnetic counterpart, Astrophys. J. Lett. 908 (2) (2021) L34, arXiv:2009.14247 [astro-ph.HE].
[623] H.-Y. Chen, C.-J. Haster, S. Vitale, W.M. Farr, M. Isi, A standard siren cosmological measurement from the potential GW190521 electromagnetic counterpart ZTF19abanrhr, Mon. Not. R. Astron. Soc. 513 (2) (2022) 2152–2157, arXiv:2009.14057 [astro-ph.CO].
[624] C.R. Bom, A. Palmese, Standard siren cosmology with gravitational waves from binary black hole mergers in active galactic nuclei, Phys. Rev. D 110 (8) (2024) 083005, arXiv:2307.01330 [astro-ph.CO].
[625] L.M.B. Alves, A.G. Sullivan, Y. Yang, G. V., Z. Marka, S. Marka, I. Bartos, Determining the Hubble constant with AGN-assisted black hole mergers, Mon. Not. R. Astron. Soc. 531 (3) (2024) 3679–3683, arXiv:2009.13739 [astro-ph.HE].
[626] J.R. Gair, et al., The Hitchhiker's guide to the galaxy catalog approach for dark siren gravitational-wave cosmology, Astron. J. 166 (1) (2023) 22, arXiv:2212.08694 [gr-qc].
[627] R. Gray, et al., Cosmological inference using gravitational wave standard sirens: A mock data analysis, Phys. Rev. D 101 (12) (2020) 122001, arXiv:1908.06050 [gr-qc].
[628] W.M. Farr, M. Fishbach, J. Ye, D. Holz, A future percent-level measurement of the Hubble expansion at redshift 0.8 with advanced LIGO, Astrophys. J. Lett. 883 (2) (2019) L42, arXiv:1908.09084 [astro-ph.CO].
[629] J.M. Ezquiaga, D.E. Holz, Spectral sirens: Cosmology from the full mass distribution of compact binaries, Phys. Rev. Lett. 129 (6) (2022) 061102, arXiv:2202.08240 [astro-ph.CO].
[630] S. Mastrogiovanni, D. Laghi, R. Gray, G.C. Santoro, A. Ghosh, C. Karathanasis, K. Leyde, D.A. Steer, S. Perries, G. Pierra, Joint population and cosmological properties inference with gravitational waves standard sirens and galaxy surveys, Phys. Rev. D 108 (4) (2023) 042002, arXiv:2305.10488 [astro-ph.CO].
[631] R. Gray, et al., Joint cosmological and gravitational-wave population inference using dark sirens and galaxy catalogues, JCAP 12 (2023) 023, arXiv:2308.02281 [astro-ph.CO].

[632] N. Borghi, M. Mancarella, M. Moresco, M. Tagliazucchi, F. Iacovelli, A. Cimatti, M. Maggiore, Cosmology and astrophysics with standard sirens and galaxy catalogs in view of future gravitational wave observations, Astrophys. J. 964 (2) (2024) 191, arXiv:2312.05302 [astro-ph.CO].
[633] DES, LIGO Scientific, Virgo Collaboration, M. Soares-Santos, et al., First measurement of the Hubble constant from a Dark Standard Siren using the dark energy survey galaxies and the LIGO/Virgo binary–black-hole merger GW170814, Astrophys. J. Lett. 876 (1) (2019) L7, arXiv:1901.01540 [astro-ph.CO].
[634] LIGO Scientific, Virgo, VIRGO Collaboration, B.P. Abbott, et al., A gravitational-wave measurement of the Hubble constant following the second observing run of advanced LIGO and Virgo, Astrophys. J. 909 (2) (2021) 218, arXiv:1908.06060 [astro-ph.CO].
[635] LIGO Scientific, Virgo Collaboration, R. Abbott, et al., GW190814: Gravitational waves from the coalescence of a 23 solar mass black hole with a 2.6 solar mass compact object, Astrophys. J. Lett. 896 (2) (2020) L44, arXiv:2006.12611 [astro-ph.HE].
[636] LIGO Scientific, Virgo, KAGRA Collaboration, R. Abbott, et al., Constraints on the cosmic expansion history from GWTC–3, Astrophys. J. 949 (2) (2023) 76, arXiv:2111.03604 [astro-ph.CO].
[637] A. Palmese, C.R. Bom, S. Mucesh, W.G. Hartley, A standard siren measurement of the Hubble constant using gravitational-wave events from the first three ligo/virgo observing runs and the DESI legacy survey, Astrophys. J. 943 (1) (2023) 56, arXiv:2111.06445 [astro-ph.CO].
[638] DESI Collaboration, W. Ballard, et al., A dark siren measurement of the Hubble constant with the LIGO/Virgo gravitational wave event GW190412 and DESI Galaxies, Res. Notes AAS 7 (11) (2023) 250, arXiv:2311.13062 [astro-ph.CO].
[639] V. Alfradique, et al., A dark siren measurement of the Hubble constant using gravitational wave events from the first three LIGO/Virgo observing runs and DELVE, Mon. Not. R. Astron. Soc. 528 (2) (2024) 3249–3259, arXiv:2310.13695 [astro-ph.CO].
[640] C.R. Bom, V. Alfradique, A. Palmese, G. Teixeira, L. Santana-Silva, A. Santos, P. Darc, A dark standard siren measurement of the Hubble constant following LIGO/Virgo/KAGRA O4a and previous runs, Mon. Not. R. Astro. Soc. 535 (1) (2024) 961–975, arXiv:2404.16092 [astro-ph.CO].
[641] A. Finke, S. Foffa, F. Iacovelli, M. Maggiore, M. Mancarella, Cosmology with LIGO/Virgo dark sirens: Hubble parameter and modified gravitational wave propagation, JCAP 08 (2021) 026, arXiv:2101.12660 [astro-ph.CO].
[642] S. Borhanian, A. Dhani, A. Gupta, K.G. Arun, B.S. Sathyaprakash, Dark sirens to resolve the Hubble–Lemaître tension, Astrophys. J. Lett. 905 (2) (2020) L28, arXiv:2007.02883 [astro-ph.CO].
[643] C.C. Diaz, S. Mukherjee, Mapping the cosmic expansion history from LIGO-Virgo-KAGRA in synergy with DESI and SPHEREx, Mon. Not. R. Astron. Soc. 511 (2) (2022) 2782–2795, arXiv:2107.12787 [astro-ph.CO].
[644] J.R. Bond, W.D. Arnett, B.J. Carr, The evolution and fate of very massive objects, Astrophys. J. 280 (1984) 825–847.
[645] M. Zevin, S.S. Bavera, C.P.L. Berry, V. Kalogera, T. Fragos, P. Marchant, C.L. Rodriguez, F. Antonini, D.E. Holz, C. Pankow, One channel to rule them all? Constraining the origins of binary black holes using multiple formation pathways, Astrophys. J. 910 (2) (2021) 152, arXiv:2011.10057 [astro-ph.HE].
[646] KAGRA, VIRGO, LIGO Scientific Collaboration, R. Abbott, et al., Population of merging compact binaries inferred using gravitational waves through GWTC-3, Phys. Rev. X 13 (1) (2023) 011048, arXiv:2111.03634 [astro-ph.HE].
[647] I. Magaña Hernandez, A. Palmese, Evidence of a new feature in the binary black hole mass distribution at 70M⊙ from gravitational-wave observations, Phys. Rev. D 111 (8) (2025) 083031, arXiv:2407.02460 [astro-ph.HE].
[648] M. Mancarella, E. Genoud-Prachex, M. Maggiore, Cosmology and modified gravitational wave propagation from binary black hole population models, Phys. Rev. D 105 (6) (2022) 064030, arXiv:2112.05728 [gr-qc].
[649] K. Leyde, S. Mastrogiovanni, D.A. Steer, E. Chassande-Mottin, C. Karathanasis, Current and future constraints on cosmology and modified gravitational wave friction from binary black holes, JCAP 09 (2022) 012, arXiv:2202.00025 [gr-qc].
[650] DES Collaboration, A. Palmese, et al., A statistical standard siren measurement of the Hubble constant from the LIGO/Virgo gravitational wave compact object merger GW190814 and dark energy survey galaxies, Astrophys. J. Lett. 900 (2) (2020) L33, arXiv:2006.14961 [astro-ph.CO].
[651] C. Turski, M. Bilicki, G. Dálya, R. Gray, A. Ghosh, Impact of modelling galaxy redshift uncertainties on the gravitational-wave dark standard siren measurement of the Hubble constant, Mon. Not. R. Astron. Soc. 526 (4) (2023) 6224–6233, arXiv:2302.12037 [gr-qc].
[652] G. Perna, S. Mastrogiovanni, A. Ricciardone, Investigating the impact of galaxies' compact binary hosting probability for gravitational-wave cosmology, 2024, arXiv:2405.07904 [astro-ph.CO].
[653] A.G. Hanselman, A. Vijaykumar, M. Fishbach, D.E. Holz, Gravitational-wave dark siren cosmology systematics from galaxy weighting, Astrophys. J. 979 (1) (2025) 9, arXiv:2405.14818 [astro-ph.CO].
[654] H.-Y. Chen, J.M. Ezquiaga, I. Gupta, Cosmography with next-generation gravitational wave detectors, Cl.. Quant. Grav. 41 (12) (2024) 125004, arXiv:2402.03120 [gr-qc].
[655] THESEUS Collaboration, L. Amati, et al., The THESEUS space mission: science goals, requirements and mission concept, Exper. Astron. 52 (3) (2021) 183–218, arXiv:2104.09531 [astro-ph.IM].
[656] M. Califano, I. de Martino, D. Vernieri, S. Capozziello, Constraining ΛCDM cosmological parameters with Einstein telescope mock data, Mon. Not. R. Astron. Soc. 518 (2023) 3372–3385, arXiv:2205.11221 [astro-ph.CO].
[657] M. Califano, I. de Martino, D. Vernieri, S. Capozziello, Exploiting the Einstein telescope to solve the Hubble tension, Phys. Rev. D 107 (12) (2023) 123519, arXiv:2208.13999 [astro-ph.CO].
[658] A. Palmese, A.G. Kim, Probing gravity and growth of structure with gravitational waves and galaxies' peculiar velocity, Phys. Rev. D 103 (10) (2021) 103507, arXiv:2005.04325 [astro-ph.CO].
[659] LISA Collaboration, M. Colpi, et al., LISA Definition Study Report, 2024, arXiv:2402.07571 [astro-ph.CO].
[660] LISA Cosmology Working Group Collaboration, P. Auclair, et al., Cosmology with the laser interferometer space antenna, Living Rev. Rel. 26 (1) (2023) 5, arXiv:2204.05434 [astro-ph.CO].
[661] A. Klein, et al., Science with the space-based interferometer eLISA: Supermassive black hole binaries, Phys. Rev. D 93 (2) (2016) 024003, arXiv:1511.05581 [gr-qc].
[662] A. Mangiagli, C. Caprini, M. Volonteri, S. Marsat, S. Vergani, N. Tamanini, H. Inchauspé, Massive black hole binaries in LISA: Multimessenger prospects and electromagnetic counterparts, Phys. Rev. D 106 (10) (2022) 103017, arXiv:2207.10678 [astro-ph.HE].
[663] S. Babak, J. Gair, A. Sesana, E. Barausse, C.F. Sopuerta, C.P.L. Berry, E. Berti, P. Amaro-Seoane, A. Petiteau, A. Klein, Science with the space-based interferometer LISA. V: Extreme mass-ratio inspirals, Phys. Rev. D 95 (10) (2017) 103012, arXiv:1703.09722 [gr-qc].
[664] N. Tamanini, C. Caprini, E. Barausse, A. Sesana, A. Klein, A. Petiteau, Science with the space-based interferometer eLISA. III: Probing the expansion of the universe using gravitational wave standard sirens, JCAP 04 (2016) 002, arXiv:1601.07112 [astro-ph.CO].
[665] LISA Cosmology Working Group Collaboration, E. Belgacem, et al., Testing modified gravity at cosmological distances with LISA standard sirens, JCAP 07 (2019) 024, arXiv:1906.01593 [astro-ph.CO].
[666] A. Mangiagli, C. Caprini, S. Marsat, L. Speri, R.R. Caldwell, N. Tamanini, Massive black hole binaries in LISA: Constraining cosmological parameters at high redshifts, Phys. Rev. D 111 (8) (2025) 083043, arXiv:2312.04632 [astro-ph.CO].
[667] C.L. MacLeod, C.J. Hogan, Precision of Hubble constant derived using black hole binary absolute distances and statistical redshift information, Phys. Rev. D 77 (2008) 043512, arXiv:0712.0618 [astro-ph].
[668] D. Laghi, N. Tamanini, W. Del Pozzo, A. Sesana, J. Gair, S. Babak, D. Izquierdo-Villalba, Gravitational-wave cosmology with extreme mass-ratio inspirals, Mon. Not. R. Astron. Soc. 508 (3) (2021) 4512–4531, arXiv:2102.01708 [astro-ph.CO].
[669] M. Toscani, O. Burke, C. Liu, N.B. Zamel, N. Tamanini, F. Pozzoli, Strongly lensed extreme mass-ratio inspirals, Phys. Rev. D 109 (6) (2024) 063505, arXiv:2307.06722 [astro-ph.CO].
[670] N. Tamanini, Late time cosmology with LISA: probing the cosmic expansion with massive black hole binary mergers as standard sirens, J. Phys. Conf. Ser. 840 (1) (2017) 012029, arXiv:1612.02634 [astro-ph.CO].
[671] C. Caprini, N. Tamanini, Constraining early and interacting dark energy with gravitational wave standard sirens: the potential of the eLISA mission, JCAP 10 (2016) 006, arXiv:1607.08755 [astro-ph.CO].
[672] R.-G. Cai, N. Tamanini, T. Yang, Reconstructing the dark sector interaction with LISA, JCAP 05 (2017) 031, arXiv:1703.07323 [astro-ph.CO].
[673] M. Corman, A. Ghosh, C. Escamilla-Rivera, M.A. Hendry, S. Marsat, N. Tamanini, Constraining cosmological extra dimensions with gravitational wave standard sirens: From theory to current and future multimessenger observations, Phys. Rev. D 105 (6) (2022) 064061, arXiv:2109.08748 [gr-qc].
[674] L. Speri, N. Tamanini, R.R. Caldwell, J.R. Gair, B. Wang, Testing the quasar Hubble diagram with LISA standard sirens, Phys. Rev. D 103 (8) (2021) 083526, arXiv:2010.09049 [astro-ph.CO].
[675] C. Liu, D. Laghi, N. Tamanini, Probing modified gravitational-wave propagation with extreme mass-ratio inspirals, Phys. Rev. D 109 (6) (2024) 063521, arXiv:2310.12813 [astro-ph.CO].
[676] D.J. Fixsen, The temperature of the cosmic microwave background, Astrophys. J. 707 (2009) 916–920, arXiv:0911.1955 [astro-ph.CO].
[677] COBE Collaboration, G.F. Smoot, et al., Structure in the COBE differential microwave radiometer first year maps, Astrophys. J. Lett. 396 (1992) L1–L5.
[678] J.C. Mather, et al., A preliminary measurement of the cosmic microwave background spectrum by the Cosmic Background Explorer (COBE) satellite, Astrophys. J. Lett. 354 (1990) L37–L40.
[679] WMAP Collaboration, C.L. Bennett, et al., First year Wilkinson Microwave Anisotropy Probe (WMAP) observations: preliminary maps and basic results, Astrophys. J. Suppl. 148 (2003) 1–27, arXiv:astro-ph/0302207.
[680] LiteBIRD Collaboration, E. Allys, et al., Probing cosmic inflation with the LiteBIRD cosmic microwave background polarization survey, PTEP 2023 (4) (2023) 042F01, arXiv:2202.02773 [astro-ph.IM].

[681] Simons Observatory Collaboration, P. Ade, et al., The Simons observatory: Science goals and forecasts, JCAP 02 (2019) 056, arXiv:1808.07445 [astro-ph.CO].
[682] CMB-S4 Collaboration, K.N. Abazajian, et al., CMB-S4 Science Book, first ed., 2016, arXiv:1610.02743 [astro-ph.CO].
[683] M. Kamionkowski, E.D. Kovetz, The quest for B modes from inflationary gravitational waves, Ann. Rev. Astron. Astrophys.. 54 (2016) 227–269, arXiv:1510.06042 [astro-ph.CO].
[684] M.C. Guzzetti, N. Bartolo, M. Liguori, S. Matarrese, Gravitational waves from inflation, Riv. Nuovo Cimento 39 (9) (2016) 399–495, arXiv:1605.01615 [astro-ph.CO].
[685] M. Gerbino, A. Gruppuso, P. Natoli, M. Shiraishi, A. Melchiorri, Testing chirality of primordial gravitational waves with Planck and future CMB data: no hope from angular power spectra, JCAP 07 (2016) 044, arXiv:1605.09357 [astro-ph.CO].
[686] BICEP2, Keck Arrary Collaboration, P.A.R. Ade, et al., BICEP2 / Keck Array IX: New bounds on anisotropies of CMB polarization rotation and implications for axionlike particles and primordial magnetic fields, Phys. Rev. D 96 (10) (2017) 102003, arXiv:1705.02523 [astro-ph.CO].
[687] L. Pogosian, A. Zucca, Searching for primordial magnetic fields with CMB B-modes, Cl.. Quant. Grav. 35 (12) (2018) 124004, arXiv:1801.08936 [astro-ph.CO].
[688] N. Bartolo, G. Orlando, M. Shiraishi, Measuring chiral gravitational waves in chern-simons gravity with CMB bispectra, JCAP 01 (2019) 050, arXiv:1809.11170 [astro-ph.CO].
[689] Y. Minami, E. Komatsu, New extraction of the cosmic birefringence from the planck 2018 polarization data, Phys. Rev. Lett. 125 (22) (2020) 221301, arXiv:2011.11254 [astro-ph.CO].
[690] T. Namikawa, et al., Atacama cosmology telescope: constraints on cosmic birefringence, Phys. Rev. D 101 (8) (2020) 083527, arXiv:2001.10465 [astro-ph.CO].
[691] G. Choi, W. Lin, L. Visinelli, T.T. Yanagida, Cosmic birefringence and electroweak axion dark energy, Phys. Rev. D 104 (10) (2021) L101302, arXiv:2106.12602 [hep-ph].
[692] A. Greco, N. Bartolo, A. Gruppuso, Cosmic birefrigence: cross-spectra and cross-bispectra with CMB anisotropies, JCAP 03 (03) (2022) 050, arXiv:2202.04584 [astro-ph.CO].
[693] E. Komatsu, New physics from the polarized light of the cosmic microwave background, Nat. Rev. Phys. 4 (7) (2022) 452–469, arXiv:2202.13919 [astro-ph.CO].
[694] Planck Collaboration, N. Aghanim, et al., Planck 2018 results. VIII. Gravitational lensing, Astron. Astrophys. 641 (2020) A8, arXiv:1807.06210 [astro-ph.CO].
[695] ACT Collaboration, M.S. Madhavacheril, et al., The Atacama cosmology telescope: DR6 gravitational lensing map and cosmological parameters, Astrophys. J. 962 (2) (2024) 113, arXiv:2304.05203 [astro-ph.CO].
[696] SPT-3G Collaboration, L. Balkenhol, et al., Constraints on ΛCDM extensions from the SPT-3G 2018 EE and TE power spectra, Phys. Rev. D 104 (8) (2021) 083509, arXiv:2103.13618 [astro-ph.CO].
[697] S. Joudaki, et al., KiDS-450: Testing extensions to the standard cosmological model, Mon. Not. R. Astron. Soc. 471 (2) (2017) 1259–1279, arXiv:1610.04606 [astro-ph.CO].
[698] M. Asgari, et al., KiDS+VIKING-450 and DES-Y1 combined: Mitigating baryon feedback uncertainty with COSEBIs, Astron. Astrophys. 634 (2020) A127, arXiv:1910.05336 [astro-ph.CO].
[699] DESI Collaboration, A.G. Adame, et al., DESI 2024 VI: cosmological constraints from the measurements of baryon acoustic oscillations, JCAP 02 (2025) 021, arXiv:2404.03002 [astro-ph.CO].
[700] E. Rosenberg, S. Gratton, G. Efstathiou, CMB power spectra and cosmological parameters from Planck PR4 with CamSpec, Mon. Not. R. Astron. Soc. 517 (3) (2022) 4620–4636, arXiv:2205.10869 [astro-ph.CO].
[701] M. Tristram, et al., Cosmological parameters derived from the final Planck data release (PR4), Astron. Astrophys. 682 (2024) A37, arXiv:2309.10034 [astro-ph.CO].
[702] ACT Collaboration, S. Aiola, et al., The Atacama Cosmology Telescope: DR4 maps and cosmological parameters, JCAP 12 (2020) 047, arXiv:2007.07288 [astro-ph.CO].
[703] ACT Collaboration, T. Louis, et al., The Atacama Cosmology Telescope: DR6 power spectra, likelihoods and ΛCDM parameters, 2025, arXiv:2503.14452 [astro-ph.CO].
[704] SPT-3G Collaboration, L. Balkenhol, et al., Measurement of the CMB temperature power spectrum and constraints on cosmology from the SPT-3G 2018 TT, TE, and EE dataset, Phys. Rev. D 108 (2) (2023) 023510, arXiv:2212.05642 [astro-ph.CO].
[705] N. Schöneberg, J. Lesgourgues, D.C. Hooper, The BAO+BBN take on the Hubble tension, JCAP 10 (2019) 029, arXiv:1907.11594 [astro-ph.CO].
[706] ACT Collaboration, E. Calabrese, et al., The Atacama cosmology telescope: DR6 constraints on extended cosmological models, 2025, arXiv:2503.14454 [astro-ph.CO].
[707] SPT-3G Collaboration, F. Ge, et al., Cosmology from CMB lensing and delensed EE power spectra using 2019–2020 SPT-3G polarization data, Phys. Rev. D 111 (8) (2025) 083534, arXiv:2411.06000 [astro-ph.CO].
[708] SPT-3G Collaboration, K. Prabhu, et al., Testing the ΛCDM cosmological model with forthcoming measurements of the cosmic microwave background with SPT-3G, Astrophys. J. 973 (1) (2024) 4, arXiv:2403.17925 [astro-ph.CO].
[709] E. Di Valentino, O. Mena, S. Pan, L. Visinelli, W. Yang, A. Melchiorri, D.F. Mota, A.G. Riess, J. Silk, In the realm of the Hubble tension—a review of solutions, Cl.. Quant. Grav. 38 (15) (2021) 153001, arXiv:2103.01183 [astro-ph.CO].
[710] N. Schöneberg, G. Franco Abellán, A. Pérez Sánchez, S.J. Witte, V. Poulin, J. Lesgourgues, The H0 Olympics: A fair ranking of proposed models, Phys. Rep. 984 (2022) 1–55, arXiv:2107.10291 [astro-ph.CO].
[711] J.M. Berryman, et al., Neutrino self-interactions: A white paper, Phys. Dark Univ. 42 (2023) 101267, arXiv:2203.01955 [hep-ph].
[712] J.L. Bernal, L. Verde, A.G. Riess, The trouble with H_0, JCAP 10 (2016) 019, arXiv:1607.05617 [astro-ph.CO].
[713] L. Knox, M. Millea, Hubble constant hunter's guide, Phys. Rev. D 101 (4) (2020) 043533, arXiv:1908.03663 [astro-ph.CO].
[714] G. Efstathiou, J.R. Bond, Cosmic confusion: Degeneracies among cosmological parameters derived from measurements of microwave background anisotropies, Mon. Not. R. Astron. Soc. 304 (1999) 75–97, arXiv:astro-ph/9807103.
[715] Planck Collaboration, N. Aghanim, et al., Planck intermediate results. LI. Features in the cosmic microwave background temperature power spectrum and shifts in cosmological parameters, Astron. Astrophys. 607 (2017) A95, arXiv:1608.02487 [astro-ph.CO].
[716] D.J. Eisenstein, H.-j. Seo, M.J. White, On the robustness of the acoustic scale in the low-redshift clustering of matter, Astrophys. J. 664 (2007) 660–674, arXiv:astro-ph/0604361.
[717] DESI Collaboration, M.A. Karim, et al., DESI DR2 Results II: Measurements of baryon acoustic oscillations and cosmological constraints, 2025, arXiv:2503.14738 [astro-ph.CO].
[718] O.H.E. Philcox, G.S. Farren, B.D. Sherwin, E.J. Baxter, D.J. Brout, Determining the Hubble constant without the sound horizon: A 3.6% constraint on H0 from galaxy surveys, CMB lensing, and supernovae, Phys. Rev. D 106 (6) (2022) 063530, arXiv:2204.02984 [astro-ph.CO].
[719] R. Zhao, et al., A multitracer analysis for the eBOSS galaxy sample based on the effective field theory of large-scale structure, Mon. Not. R. Astron. Soc. 532 (1) (2024) 783–804, arXiv:2308.06206 [astro-ph.CO].
[720] G. D'Amico, J. Gleyzes, N. Kokron, K. Markovic, L. Senatore, P. Zhang, F. Beutler, H. Gil-Marín, The cosmological analysis of the SDSS/BOSS data from the effective field theory of large-scale structure, JCAP 05 (2020) 005, arXiv:1909.05271 [astro-ph.CO].
[721] SimBIG Collaboration, C. Hahn, M. Eickenberg, S. Ho, J. Hou, P. Lemos, E. Massara, C. Modi, A. Moradinezhad Dizgah, L. Parker, B.R.-S. Blancard, Cosmological constraints from the nonlinear galaxy bispectrum, Phys. Rev. D 109 (8) (2024) 083534, arXiv:2310.15243 [astro-ph.CO].
[722] G. D'Amico, Y. Donath, M. Lewandowski, L. Senatore, P. Zhang, The BOSS bispectrum analysis at one loop from the effective field theory of large-scale structure, JCAP 05 (2024) 059, arXiv:2206.08327 [astro-ph.CO].
[723] J. de Cruz Perez, C.-G. Park, B. Ratra, Updated observational constraints on spatially flat and nonflat ΛCDM and XCDM cosmological models, Phys. Rev. D 110 (2) (2024) 023506, arXiv:2404.19194 [astro-ph.CO].
[724] E. Calabrese, A. Slosar, A. Melchiorri, G.F. Smoot, O. Zahn, Cosmic microwave weak lensing data as a test for the dark universe, Phys. Rev. D 77 (2008) 123531, arXiv:0803.2309 [astro-ph].
[725] SPT-3G Collaboration, D. Dutcher, et al., Measurements of the E-mode polarization and temperature-E-mode correlation of the CMB from SPT-3G 2018 data, Phys. Rev. D 104 (2) (2021) 022003, arXiv:2101.01684 [astro-ph.CO].
[726] Planck Collaboration, N. Aghanim, et al., Planck 2015 results. XI. CMB power spectra, likelihoods, and robustness of parameters, Astron. Astrophys. 594 (2016) A11, arXiv:1507.02704 [astro-ph.CO].
[727] F. Couchot, S. Henrot-Versillé, O. Perdereau, S. Plaszczynski, B. Rouillé d'Orfeuil, M. Spinelli, M. Tristram, Relieving tensions related to the lensing of the cosmic microwave background temperature power spectra, Astron. Astrophys. 597 (2017) A126, arXiv:1510.07600 [astro-ph.CO].
[728] G.E. Addison, Y. Huang, D.J. Watts, C.L. Bennett, M. Halpern, G. Hinshaw, J.L. Weiland, Quantifying discordance in the 2015 planck CMB spectrum, Astrophys. J. 818 (2) (2016) 132, arXiv:1511.00055 [astro-ph.CO].
[729] Planck Collaboration, N. Aghanim, et al., Planck 2018 results. V. CMB power spectra and likelihoods, Astron. Astrophys. 641 (2020) A5, arXiv:1907.12875 [astro-ph.CO].
[730] Planck Collaboration, Y. Akrami, et al., Planck 2018 results. II. Low frequency instrument data processing, Astron. Astrophys. 641 (2020) A2, arXiv:1807.06206 [astro-ph.CO].
[731] Planck Collaboration, N. Aghanim, et al., Planck 2018 results. III. High frequency instrument data processing and frequency maps, Astron. Astrophys. 641 (2020) A3, arXiv:1807.06207 [astro-ph.CO].

[732] ACT Collaboration, S.K. Choi, et al., The atacama cosmology telescope: a measurement of the cosmic microwave background power spectra at 98 and 150 GHz, JCAP 12 (2020) 045, arXiv:2007.07289 [astro-ph.CO].
[733] S. Giardiello, A.J. Duivenvoorden, E. Calabrese, G. Galloni, M. Hasselfield, J.C. Hill, A. La Posta, T. Louis, M. Madhavacheril, L. Pagano, Modeling beam chromaticity for high-resolution CMB analyses, Phys. Rev. D 111 (4) (2025) 043502, arXiv:2411.10124 [astro-ph.CO].
[734] S. Giardiello, et al., The Simons observatory: impact of bandpass, polarization angle and calibration uncertainties on small-scale power spectrum analysis, JCAP 09 (2024) 008, arXiv:2403.05242 [astro-ph.CO].
[735] E. Di Valentino, S. Bridle, Exploring the tension between current cosmic microwave background and cosmic shear data, Symmetry 10 (11) (2018) 585.
[736] Planck Collaboration, P.A.R. Ade, et al., Planck 2015 results. XXIV. Cosmology from Sunyaev-Zeldovich cluster counts, Astron. Astrophys. 594 (2016) A24, arXiv:1502.01597 [astro-ph.CO].
[737] Planck Collaboration, P.A.R. Ade, et al., Planck 2015 results. xxvii. The Second Planck catalogue of Sunyaev-Zeldovich sources, Astron. Astrophys. 594 (2016) A27, arXiv:1502.01598 [astro-ph.CO].
[738] SPT Collaboration, T. de Haan, et al., Cosmological constraints from galaxy clusters in the 2500 square-degree SPT-SZ survey, Astrophys. J. 832 (1) (2016) 95, arXiv:1603.06522 [astro-ph.CO].
[739] P.J.E. Peebles, J.T. Yu, Primeval adiabatic perturbation in an expanding universe, Astrophys. J. 162 (1970) 815–836.
[740] R.A. Sunyaev, Y.B. Zeldovich, Small-scale fluctuations of relic radiation, Astrophys. Space Sci. 7 (1) (1970) 3–19.
[741] D.J. Eisenstein, W. Hu, Baryonic features in the matter transfer function, Astrophys. J. 496 (1998) 605, arXiv:astro-ph/9709112.
[742] B.A. Bassett, R. Hlozek, Baryon acoustic oscillations, 2009, arXiv:0910.5224 [astro-ph.CO].
[743] D.H. Weinberg, M.J. Mortonson, D.J. Eisenstein, C. Hirata, A.G. Riess, E. Rozo, Observational probes of cosmic acceleration, Phys. Rep. 530 (2013) 87–255, arXiv:1201.2434 [astro-ph.CO].
[744] SDSS Collaboration, D.J. Eisenstein, et al., Detection of the Baryon acoustic peak in the large-scale correlation function of SDSS luminous red galaxies, Astrophys. J. 633 (2005) 560–574, arXiv:astro-ph/0501171.
[745] DESI Collaboration, A.G. Adame, et al., DESI 2024 IV: Baryon acoustic oscillations from the Lyman alpha forest, JCAP 01 (2025) 124, arXiv:2404.03001 [astro-ph.CO].
[746] 2dFGRS Collaboration, S. Cole, et al., The 2dF galaxy redshift survey: Power-spectrum analysis of the final dataset and cosmological implications, Mon. Not. R. Astron. Soc. 362 (2005) 505–534, arXiv:astro-ph/0501174.
[747] SDSS Collaboration, W.J. Percival, et al., Baryon acoustic oscillations in the sloan digital sky survey data release 7 galaxy sample, Mon. Not. R. Astron. Soc. 401 (2010) 2148–2168, arXiv:0907.1660 [astro-ph.CO].
[748] BOSS Collaboration, F. Beutler, et al., The clustering of galaxies in the completed SDSS-III baryon oscillation spectroscopic survey: baryon acoustic oscillations in the fourier space, Mon. Not. R. Astron. Soc. 464 (3) (2017) 3409–3430, arXiv:1607.03149 [astro-ph.CO].
[749] BOSS Collaboration, L. Anderson, et al., The clustering of galaxies in the SDSS-III baryon oscillation spectroscopic survey: baryon acoustic oscillations in the data releases 10 and 11 galaxy samples, Mon. Not. R. Astron. Soc. 441 (1) (2014) 24–62, arXiv:1312.4877 [astro-ph.CO].
[750] K.T. Mehta, H.-J. Seo, J. Eckel, D.J. Eisenstein, M. Metchnik, P. Pinto, X. Xu, Galaxy bias and its effects on the baryon acoustic oscillations measurements, Astrophys. J. 734 (2011) 94, arXiv:1104.1178 [astro-ph.CO].
[751] N. Padmanabhan, X. Xu, D.J. Eisenstein, R. Scalzo, A.J. Cuesta, K.T. Mehta, E. Kazin, A 2 per cent distance to z=0.35 by reconstructing baryon acoustic oscillations - I. Methods and application to the sloan digital sky survey, Mon. Not. R. Astron. Soc. 427 (3) (2012) 2132–2145, arXiv:1202.0090 [astro-ph.CO].
[752] D.J. Eisenstein, H.-j. Seo, E. Sirko, D. Spergel, Improving cosmological distance measurements by reconstruction of the baryon acoustic peak, Astrophys. J. 664 (2007) 675–679, arXiv:astro-ph/0604362.
[753] J.L. Bernal, T.L. Smith, K.K. Boddy, M. Kamionkowski, Robustness of baryon acoustic oscillation constraints for early-universe modifications of ΛCDM cosmology, Phys. Rev. D 102 (12) (2020) 123515, arXiv:2004.07263 [astro-ph.CO].
[754] S. Sanz-Wuhl, H. Gil-Marín, A.J. Cuesta, L. Verde, BAO cosmology in non-spatially flat background geometry from BOSS+eBOSS and lessons for future surveys, JCAP 05 (2024) 116, arXiv:2402.03427 [astro-ph.CO].
[755] J. Pan, D. Huterer, F. Andrade-Oliveira, C. Avestruz, Compressed baryon acoustic oscillation analysis is robust to modified-gravity models, JCAP 06 (2024) 051, arXiv:2312.05177 [astro-ph.CO].
[756] BOSS Collaboration, M. Vargas-Magaña, et al., The clustering of galaxies in the completed SDSS-III Baryon oscillation spectroscopic survey: theoretical systematics and baryon acoustic oscillations in the galaxy correlation function, Mon. Not. R. Astron. Soc. 477 (1) (2018) 1153–1188, arXiv:1610.03506 [astro-ph.CO].
[757] P. Carter, F. Beutler, W.J. Percival, J. DeRose, R.H. Wechsler, C. Zhao, The impact of the fiducial cosmology assumption on BAO distance scale measurements, Mon. Not. R. Astron. Soc. 494 (2) (2020) 2076–2089, arXiv:1906.03035 [astro-ph.CO].
[758] S.-F. Chen, et al., Baryon acoustic oscillation theory and modelling systematics for the DESI 2024 results, Mon. Not. R. Astron. Soc. 534 (1) (2024) 544–574, arXiv:2402.14070 [astro-ph.CO].
[759] D. Baumann, D. Green, M. Zaldarriaga, Phases of new physics in the BAO spectrum, JCAP 11 (2017) 007, arXiv:1703.00894 [astro-ph.CO].
[760] D. Baumann, F. Beutler, R. Flauger, D. Green, A. Slosar, M. Vargas-Magaña, B. Wallisch, C. Yèche, First constraint on the neutrino-induced phase shift in the spectrum of baryon acoustic oscillations, Nat. Phys. 15 (2019) 465–469, arXiv:1803.10741 [astro-ph.CO].
[761] E. Sanchez, A. Carnero, J. Garcia-Bellido, E. Gaztanaga, F. de Simoni, M. Crocce, A. Cabre, P. Fosalba, D. Alonso, Tracing the sound horizon scale with photometric redshift surveys, Mon. Not. R. Astron. Soc. 411 (2011) 277–288, arXiv:1006.3226 [astro-ph.CO].
[762] R. Menote, V. Marra, Baryon acoustic oscillations in thin redshift shells from BOSS DR12 and eBOSS DR16 galaxies, Mon. Not. R. Astron. Soc. 513 (2) (2022) 1600–1608, arXiv:2112.10000 [astro-ph.CO].
[763] G.C. Carvalho, A. Bernui, M. Benetti, J.C. Carvalho, E. de Carvalho, J.S. Alcaniz, The transverse baryonic acoustic scale from the SDSS DR11 galaxies, Astropart. Phys. 119 (2020) 102432, arXiv:1709.00271 [astro-ph.CO].
[764] D. Camarena, V. Marra, A new method to build the (inverse) distance ladder, Mon. Not. R. Astron. Soc. 495 (3) (2020) 2630–2644, arXiv:1910.14125 [astro-ph.CO].
[765] R.C. Nunes, S.K. Yadav, J.F. Jesus, A. Bernui, Cosmological parameter analyses using transversal BAO data, Mon. Not. R. Astron. Soc. 497 (2) (2020) 2133–2141, arXiv:2002.09293 [astro-ph.CO].
[766] R.C. Nunes, A. Bernui, BAO signatures in the 2-point angular correlations and the Hubble tension, Eur. Phys. J. C 80 (11) (2020) 1025, arXiv:2008.03259 [astro-ph.CO].
[767] R. Arjona, S. Nesseris, Novel null tests for the spatial curvature and homogeneity of the universe and their machine learning reconstructions, Phys. Rev. D 103 (10) (2021) 103539, arXiv:2103.06789 [astro-ph.CO].
[768] A. Bernui, E. Di Valentino, W. Giarè, S. Kumar, R.C. Nunes, Exploring the H0 tension and the evidence for dark sector interactions from 2D BAO measurements, Phys. Rev. D 107 (10) (2023) 103531, arXiv:2301.06097 [astro-ph.CO].
[769] A. Gómez-Valent, A. Favale, M. Migliaccio, A.A. Sen, Late-time phenomenology required to solve the H0 tension in view of the cosmic ladders and the anisotropic and angular BAO datasets, Phys. Rev. D 109 (2) (2024) 023525, arXiv:2309.07795 [astro-ph.CO].
[770] M. Benetti, L.L. Graef, J.S. Alcaniz, The H_0 and σ_8 tensions and the scale invariant spectrum, JCAP 07 (2018) 066, arXiv:1712.00677 [astro-ph.CO].
[771] DES Collaboration, J. Mena-Fernández, et al., Dark Energy Survey: Galaxy sample for the baryonic acoustic oscillation measurement from the final dataset, Phys. Rev. D 110 (6) (2024) 063514, arXiv:2402.10697 [astro-ph.CO].
[772] DES Collaboration, T.M.C. Abbott, et al., Dark Energy Survey: A 2.1% measurement of the angular baryonic acoustic oscillation scale at redshift zeff=0.85 from the final dataset, Phys. Rev. D 110 (6) (2024) 063515, arXiv:2402.10696 [astro-ph.CO].
[773] P. McDonald, D. Eisenstein, Dark energy and curvature from a future baryonic acoustic oscillation survey using the Lyman-alpha forest, Phys. Rev. D 76 (2007) 063009, arXiv:astro-ph/0607122.
[774] 2dFGRS Collaboration, W.J. Percival, et al., The 2dF Galaxy redshift survey: The power spectrum and the matter content of the universe, Mon. Not. R. Astron. Soc. 327 (2001) 1297, arXiv:astro-ph/0105252.
[775] BOSS Collaboration, A. Slosar, et al., Measurement of baryon acoustic oscillations in the Lyman-alpha forest fluctuations in BOSS data release 9, JCAP 04 (2013) 026, arXiv:1301.3459 [astro-ph.CO].
[776] C. Blake, et al., The WiggleZ dark energy survey: mapping the distance-redshift relation with baryon acoustic oscillations, Mon. Not. R. Astron. Soc. 418 (2011) 1707–1724, arXiv:1108.2635 [astro-ph.CO].
[777] F. Beutler, C. Blake, M. Colless, D.H. Jones, L. Staveley-Smith, L. Campbell, Q. Parker, W. Saunders, F. Watson, The 6dF Galaxy Survey: Baryon acoustic oscillations and the local Hubble constant, Mon. Not. R. Astron. Soc. 416 (2011) 3017–3032, arXiv:1106.3366 [astro-ph.CO].
[778] BOSS Collaboration, L. Anderson, et al., The clustering of galaxies in the SDSS-III baryon oscillation spectroscopic survey: measuring D_A and H at z=0.57 from the baryon acoustic peak in the data release 9 spectroscopic galaxy sample, Mon. Not. R. Astron. Soc. 439 (1) (2014) 83–101, arXiv:1303.4666 [astro-ph.CO].
[779] BOSS Collaboration, A. Font-Ribera, et al., Quasar-Lyman α forest cross-correlation from BOSS DR11 : Baryon acoustic oscillations, JCAP 05 (2014) 027, arXiv:1311.1767 [astro-ph.CO].
[780] BOSS Collaboration, A.J. Ross, et al., The clustering of galaxies in the completed SDSS-III baryon oscillation spectroscopic survey: Observational systematics and baryon acoustic oscillations in the correlation function, Mon. Not. R. Astron. Soc. 464 (1) (2017) 1168–1191, arXiv:1607.03145 [astro-ph.CO].

[781] eBOSS Collaboration, R. Neveux, et al., The completed SDSS-IV extended Baryon Oscillation Spectroscopic Survey: BAO and RSD measurements from the anisotropic power spectrum of the quasar sample between redshift 0.8 and 2.2, Mon. Not. R. Astron. Soc. 499 (1) (2020) 210–229, arXiv:2007.08999 [astro-ph.CO].

[782] eBOSS Collaboration, A. de Mattia, et al., The completed SDSS-IV extended Baryon Oscillation Spectroscopic Survey: measurement of the BAO and growth rate of structure of the emission line galaxy sample from the anisotropic power spectrum between redshift 0.6 and 1.1, Mon. Not. R. Astron. Soc. 501 (4) (2021) 5616–5645, arXiv:2007.09008 [astro-ph.CO].

[783] DESI Collaboration, A.G. Adame, et al., DESI 2024 III: baryon acoustic oscillations from galaxies and quasars, JCAP 04 (2025) 012, arXiv:2404.03000 [astro-ph.CO].

[784] D. Bianchi, A. Burden, W.J. Percival, D. Brooks, R.N. Cahn, J.E. Forero-Romero, M. Levi, A.J. Ross, G. Tarle, Unbiased clustering estimates with the DESI fibre assignment, Mon. Not. R. Astron. Soc. 481 (2) (2018) 2338–2348, arXiv:1805.00951 [astro-ph.CO].

[785] G.C. Carvalho, A. Bernui, M. Benetti, J.C. Carvalho, J.S. Alcaniz, Baryon Acoustic Oscillations from the SDSS DR10 galaxies angular correlation function, Phys. Rev. D 93 (2) (2016) 023530, arXiv:1507.08972 [astro-ph.CO].

[786] J.S. Alcaniz, G.C. Carvalho, A. Bernui, J.C. Carvalho, M. Benetti, Measuring baryon acoustic oscillations with angular two-point correlation function, Fundam. Theor. Phys. 187 (2017) 11–19, arXiv:1611.08458 [astro-ph.CO].

[787] E. de Carvalho, A. Bernui, G.C. Carvalho, C.P. Novaes, H.S. Xavier, Angular baryon acoustic oscillation measure at $z = 2.225$ from the SDSS quasar survey, JCAP 04 (2018) 064, arXiv:1709.00113 [astro-ph.CO].

[788] E. de Carvalho, A. Bernui, F. Avila, C.P. Novaes, J.P. Nogueira-Cavalcante, BAO angular scale at zeff=0.11 with the SDSS blue galaxies, Astron. Astrophys. 649 (2021) A20, arXiv:2103.14121 [astro-ph.CO].

[789] BOSS Collaboration, E. Aubourg, et al., Cosmological implications of baryon acoustic oscillation measurements, Phys. Rev. D 92 (12) (2015) 123516, arXiv:1411.1074 [astro-ph.CO].

[790] G.S. Farren, O.H.E. Philcox, B.D. Sherwin, Determining the Hubble constant without the sound horizon: Perspectives with future galaxy surveys, Phys. Rev. D 105 (6) (2022) 063503, arXiv:2112.10749 [astro-ph.CO].

[791] O.H.E. Philcox, B.D. Sherwin, G.S. Farren, E.J. Baxter, Determining the Hubble constant without the sound horizon: Measurements from galaxy surveys, Phys. Rev. D 103 (2) (2021) 023538, arXiv:2008.08084 [astro-ph.CO].

[792] E.J. Baxter, B.D. Sherwin, Determining the Hubble constant without the sound horizon scale: Measurements from CMB lensing, Mon. Not. R. Astron. Soc. 501 (2) (2021) 1823–1835, arXiv:2007.04007 [astro-ph.CO].

[793] S. Brieden, H. Gil-Marín, L. Verde, A tale of two (or more) h's, JCAP 04 (2023) 023, arXiv:2212.04522 [astro-ph.CO].

[794] A. Krolewski, W.J. Percival, A. Woodfinden, New method to determine the Hubble parameter from cosmological energy-density measurements, Phys. Rev. Lett. 134 (10) (2025) 101002, arXiv:2403.19227 [astro-ph.CO].

[795] N. Arendse, et al., Cosmic dissonance: are new physics or systematics behind a short sound horizon? Astron. Astrophys. 639 (2020) A57, arXiv:1909.07986 [astro-ph.CO].

[796] J.-Q. Jiang, Y.-S. Piao, Can the sound horizon-free measurement of H_0 constrain early new physics? 2025, arXiv:2501.16883 [astro-ph.CO].

[797] eBOSS Collaboration, S. Alam, et al., Completed SDSS-IV extended baryon oscillation spectroscopic survey: Cosmological implications from two decades of spectroscopic surveys at the apache point observatory, Phys. Rev. D 103 (8) (2021) 083533, arXiv:2007.08991 [astro-ph.CO].

[798] N. Schöneberg, The 2024 BBN baryon abundance update, JCAP 06 (2024) 006, arXiv:2401.15054 [astro-ph.CO].

[799] W.J. Percival, S. Cole, D.J. Eisenstein, R.C. Nichol, J.A. Peacock, A.C. Pope, A.S. Szalay, Measuring the baryon acoustic oscillation scale using the SDSS and 2dFGRS, Mon. Not. R. Astron. Soc. 381 (2007) 1053–1066, arXiv:0705.3323 [astro-ph].

[800] W. Giarè, M.A. Sabogal, R.C. Nunes, E. Di Valentino, Interacting dark energy after DESI baryon acoustic oscillation measurements, Phys. Rev. Lett. 133 (25) (2024) 251003, arXiv:2404.15232 [astro-ph.CO].

[801] O. Akarsu, S. Kumar, E. Özülker, J.A. Vazquez, A. Yadav, Relaxing cosmological tensions with a sign switching cosmological constant: improved results with planck, BAO, and Pantheon data, Phys. Rev. D 108 (2) (2023) 023513, arXiv:2211.05742 [astro-ph.CO].

[802] O. Akarsu, A. De Felice, E. Di Valentino, S. Kumar, R.C. Nunes, E. Özülker, J.A. Vazquez, A. Yadav, Cosmological constraints on ΛsCDM scenario in a Type II minimally modified gravity, Phys. Rev. D 110 (10) (2024) 103527, arXiv:2406.07526 [astro-ph.CO].

[803] T.L. Smith, V. Poulin, T. Simon, Assessing the robustness of sound horizon-free determinations of the Hubble constant, Phys. Rev. D 108 (10) (2023) 103525, arXiv:2208.12992 [astro-ph.CO].

[804] K. Jedamzik, L. Pogosian, G.-B. Zhao, Why reducing the cosmic sound horizon alone can not fully resolve the Hubble tension, Commun. Phys. 4 (2021) 123, arXiv:2010.04158 [astro-ph.CO].

[805] L. Pogosian, G.-B. Zhao, K. Jedamzik, Recombination-independent determination of the sound horizon and the Hubble constant from BAO, Astrophys. J. Lett. 904 (2) (2020) L17, arXiv:2009.08455 [astro-ph.CO].

[806] D. Benisty, D. Staicova, Testing late-time cosmic acceleration with uncorrelated baryon acoustic oscillation dataset, Astron. Astrophys. 647 (2021) A38, arXiv:2009.10701 [astro-ph.CO].

[807] D. Staicova, De models with combined $H_0 \cdot r_d$ from BAO and CMB dataset and friends, Universe 8 (12) (2022) 631, arXiv:2211.08139 [astro-ph.CO].

[808] D. Staicova, D. Benisty, Constraining the dark energy models using baryon acoustic oscillations: An approach independent of H0 · rd, Astron. Astrophys. 668 (2022) A135, arXiv:2107.14129 [astro-ph.CO].

[809] DESI Collaboration, R. Calderon, et al., DESI 2024: reconstructing dark energy using crossing statistics with DESI DR1 BAO data, JCAP 10 (2024) 048, arXiv:2405.04216 [astro-ph.CO].

[810] F. Sinigaglia, F.-S. Kitaura, K. Nagamine, Y. Oku, The negative baryon acoustic oscillation shift in the Lyα forest from cosmological simulations, Astrophys. J. Lett. 971 (1) (2024) L22, arXiv:2407.03918 [astro-ph.CO].

[811] O. Akarsu, S. Kumar, E. Özülker, J.A. Vazquez, Relaxing cosmological tensions with a sign switching cosmological constant, Phys. Rev. D 104 (12) (2021) 123512, arXiv:2108.09239 [astro-ph.CO].

[812] O. Akarsu, E. Di Valentino, S. Kumar, R.C. Nunes, J.A. Vazquez, A. Yadav, Λ_sCDM model: A promising scenario for alleviation of cosmological tensions, 2023, arXiv:2307.10899 [astro-ph.CO].

[813] S.A. Adil, O. Akarsu, E. Di Valentino, R.C. Nunes, E. Özülker, A.A. Sen, E. Specogna, Omnipotent dark energy: A phenomenological answer to the Hubble tension, Phys. Rev. D 109 (2) (2024) 023527, arXiv:2306.08046 [astro-ph.CO].

[814] DESI Collaboration, A. Aghamousa, et al., The DESI Experiment Part I: Science,targeting, and survey design, 2016, arXiv:1611.00036 [astro-ph.IM].

[815] D.J. Schlegel, et al., The MegaMapper: A stage-5 spectroscopic instrument concept for the study of inflation and dark energy, 2022, arXiv:2209.04322 [astro-ph.IM].

[816] D.J. Schlegel, et al., Astro2020 APC White Paper: The MegaMapper: a z > 2 spectroscopic instrument for the study of inflation and dark energy, Bull. Am. Astron. Soc. 51 (7) (2019) 229, arXiv:1907.11171 [astro-ph.IM].

[817] R. Ellis, et al., SpecTel: A 10-12 meter class spectroscopic survey telescope, 2019, arXiv:1907.06797 [astro-ph.IM].

[818] DESI Collaboration, A.G. Adame, et al., Validation of the scientific program for the dark energy spectroscopic instrument, Astron. J. 167 (2) (2024) 62, arXiv:2306.06307 [astro-ph.CO].

[819] B. Jain, U. Seljak, Cosmological model predictions for weak lensing: Linear and nonlinear regimes, Astrophys. J. 484 (1997) 560, arXiv:astro-ph/9611077.

[820] N. Kaiser, Weak gravitational lensing of distant galaxies, Astrophys. J. 388 (1992) 272.

[821] N. Kaiser, Weak lensing by galaxy clusters, 1999, arXiv:astro-ph/9912569.

[822] J. Miralda-Escude, The correlation function of galaxy ellipticities produced by gravitational lensing, Astrophys. J. 380 (1991) 1.

[823] R.D. Blandford, A.B. Saust, T.G. Brainerd, J.V. Villumsen, The distortion of distant galaxy images by large-scale structure, Mon. Not. R. Astron. Soc. 251 (4) (1991) 600–627.

[824] L. Van Waerbeke, F. Bernardeau, Y. Mellier, Efficiency of weak lensing surveys to probe cosmological models, Astron. Astrophys. 342 (1999) 15–33, arXiv:astro-ph/9807007.

[825] M. Bartelmann, M. Maturi, Weak gravitational lensing, in: Ground-based and Airborne Telescopes VII, vol. 12, 2017, p. 32440, arXiv:1612.06535 [astro-ph.CO].

[826] M. Kilbinger, Cosmology with cosmic shear observations: a review, Rep. Progr. Phys. 78 (2015) 086901, arXiv:1411.0115 [astro-ph.CO].

[827] J. Prat, D. Bacon, Weak gravitational lensing, 2025, arXiv:2501.07938 [astro-ph.CO].

[828] P. Schneider, L. van Waerbeke, M. Kilbinger, Y. Mellier, Analysis of two-point statistics of cosmic shear: I. Estimators and covariances, Astron. Astrophys. 396 (2002) 1–20, arXiv:astro-ph/0206182.

[829] Euclid Collaboration, V. Ajani, et al., Euclid preparation. XXVIII. Forecasts for ten different higher-order weak lensing statistics, Astron. Astrophys. 675 (2023) A120, arXiv:2301.12890 [astro-ph.CO].

[830] L. Porth, S. Heydenreich, P. Burger, L. Linke, P. Schneider, A road map to cosmological parameter analysis with third-order shear statistics - III. Efficient estimation of third-order shear correlation functions and an application to the KiDS-1000 data, Astron. Astrophys. 689 (2024) A227, arXiv:2309.08601 [astro-ph.CO].

[831] M. Takada, B. Jain, The Three - point correlation function in cosmology, Mon. Not. R. Astron. Soc. 340 (2003) 580–608, arXiv:astro-ph/0209167.

[832] S. Heydenreich, L. Linke, P. Burger, P. Schneider, A roadmap to cosmological parameter analysis with third-order shear statistics - I. Modelling and validation, Astron. Astrophys. 672 (2023) A44, arXiv:2208.11686 [astro-ph.CO].

[833] A. Halder, O. Friedrich, S. Seitz, T.N. Varga, The integrated three-point correlation function of cosmic shear, Mon. Not. R. Astron. Soc. 506 (2) (2021) 2780–2803, arXiv:2102.10177 [astro-ph.CO].

[834] W.R. Coulton, J. Liu, M.S. Madhavacheril, V. Böhm, D.N. Spergel, Constraining neutrino mass with the tomographic weak lensing bispectrum, JCAP 05 (2019) 043, arXiv:1810.02374 [astro-ph.CO].

[835] I. Kayo, M. Takada, B. Jain, Information content of weak lensing power spectrum and bispectrum: including the non-Gaussian error covariance matrix, Mon. Not. R. Astron. Soc. 429 (2013) 344–371, arXiv:1207.6322 [astro-ph.CO].
[836] L. Castiblanco, C. Uhlemann, J. Harnois-Déraps, A. Barthelemy, Unleashing cosmic shear information with the tomographic weak lensing PDF, 2024, http://dx.doi.org/10.33232/001c.121302, arXiv:2405.09651 [astro-ph.CO].
[837] L. Thiele, G.A. Marques, J. Liu, M. Shirasaki, Cosmological constraints from the Subaru Hyper Suprime-Cam year 1 shear catalogue lensing convergence probability distribution function, Phys. Rev. D 108 (12) (2023) 123526, arXiv:2304.05928 [astro-ph.CO].
[838] B. Giblin, Y.-C. Cai, J. Harnois-Déraps, Enhancing cosmic shear with the multiscale lensing probability density function, Mon. Not. R. Astron. Soc. 520 (2) (2023) 1721–1737, arXiv:2211.05708 [astro-ph.CO].
[839] J. Liu, M.S. Madhavacheril, Constraining neutrino mass with the tomographic weak lensing one-point probability distribution function and power spectrum, Phys. Rev. D 99 (8) (2019) 083508, arXiv:1809.10747 [astro-ph.CO].
[840] DES Collaboration, M. Gatti, et al., Dark energy survey year 3 results: Cosmology with moments of weak lensing mass maps, Phys. Rev. D 106 (8) (2022) 083509, arXiv:2110.10141 [astro-ph.CO].
[841] J. Harnois-Deraps, et al., KiDS-1000 and DES-Y1 combined: cosmology from peak count statistics, Mon. Not. R. Astron. Soc. 534 (4) (2024) 3305–3330, arXiv:2405.10312 [astro-ph.CO].
[842] G.A. Marques, J. Liu, M. Shirasaki, L. Thiele, D. Grandón, K.M. Huffenberger, S. Cheng, J. Harnois-Déraps, K. Osato, W.R. Coulton, Cosmology from weak lensing peaks and minima with Subaru Hyper Suprime-Cam Survey first-year data, Mon. Not. R. Astron. Soc. 528 (3) (2024) 4513–4527, arXiv:2308.10866 [astro-ph.CO].
[843] N. Martinet, J.G. Bartlett, A. Kiessling, B. Sartoris, Constraining cosmology with shear peak statistics: tomographic analysis, Astron. Astrophys. 581 (2015) A101, arXiv:1506.02192 [astro-ph.CO].
[844] J. Liu, A. Petri, Z. Haiman, L. Hui, J.M. Kratochvil, M. May, Cosmology constraints from the weak lensing peak counts and the power spectrum in CFHTLenS data, Phys. Rev. D 91 (6) (2015) 063507, arXiv:1412.0757 [astro-ph.CO].
[845] DES Collaboration, D. Gruen, et al., Density split statistics: Cosmological constraints from counts and lensing in cells in DES Y1 and SDSS data, Phys. Rev. D 98 (2) (2018) 023507, arXiv:1710.05045 [astro-ph.CO].
[846] S. Cheng, G.A. Marques, D. Grandón, L. Thiele, M. Shirasaki, B. Ménard, J. Liu, Cosmological constraints from weak lensing scattering transform using HSC Y1 data, JCAP 01 (2025) 006, arXiv:2404.16085 [astro-ph.CO].
[847] D. Grandón, G.A. Marques, L. Thiele, S. Cheng, M. Shirasaki, J. Liu, Impact of baryonic feedback on HSC-Y1 weak lensing non-Gaussian statistics, Phys. Rev. D 110 (10) (2024) 103539, arXiv:2403.03807 [astro-ph.CO].
[848] J. Armijo, G.A. Marques, C.P. Novaes, L. Thiele, J.A. Cowell, D. Grandón, M. Shirasaki, J. Liu, Cosmological constraints using Minkowski functionals from the first year data of the Hyper Suprime-Cam, Mon. Not. R. Astron. Soc. 537 (4) (2025) 3553–3560, arXiv:2410.00401 [astro-ph.CO].
[849] D. Grandón, E. Sellentin, Stage IV baryonic feedback correction for non-Gaussianity inference, Mon. Not. R. Astron. Soc. 536 (2025) 2064–2071, arXiv:2407.20448 [astro-ph.CO].
[850] K. Kuijken, et al., Gravitational lensing analysis of the kilo degree survey, Mon. Not. R. Astron. Soc. 454 (4) (2015) 3500–3532, arXiv:1507.00738 [astro-ph.CO].
[851] K. Kuijken, et al., The fourth data release of the Kilo-Degree Survey: ugri imaging and nine-band optical-IR photometry over 1000 square degrees, Astron. Astrophys. 625 (2019) A2, arXiv:1902.11265 [astro-ph.GA].
[852] DES Collaboration, M. Gatti, et al., Dark energy survey year 3 results: weak lensing shape catalogue, Mon. Not. R. Astron. Soc. 504 (3) (2021) 4312–4336, arXiv:2011.03408 [astro-ph.CO].
[853] DES, NOAO Data Lab Collaboration, T.M.C. Abbott, et al., The dark energy survey data release 1, Astrophys. J. Suppl. 239 (2) (2018) 18, arXiv:1801.03181 [astro-ph.IM].
[854] H. Aihara, et al., The hyper suprime-cam SSP survey: Overview and survey design, Publ. Astron. Soc. Jap. 70 (2018) S4, arXiv:1704.05858 [astro-ph.IM].
[855] HSC Collaboration, C. Hikage, et al., Cosmology from cosmic shear power spectra with Subaru hyper suprime-cam first-year data, Publ. Astron. Soc. Jap. 71 (2) (2019) 43, arXiv:1809.09148 [astro-ph.CO].
[856] T. Hamana, et al., Cosmological constraints from cosmic shear two-point correlation functions with HSC survey first-year data, Publ. Astron. Soc. Jap. 72 (1) (2020) 16, arXiv:1906.06041 [astro-ph.CO]; Erratum: Publ. Astron. Soc. Jap. 74 (2022) 488–491.
[857] D. Anbajagane, et al., The DECADE cosmic shear project iv: cosmological constraints from 107 million galaxies across 5,400 deg^2 of the sky, 2025, arXiv:2502.17677 [astro-ph.CO].
[858] H. Hildebrandt, et al., KiDS-450: Cosmological parameter constraints from tomographic weak gravitational lensing, Mon. Not. R. Astron. Soc. 465 (2017) 1454, arXiv:1606.05338 [astro-ph.CO].
[859] H. Hildebrandt, et al., KiDS+VIKING-450: Cosmic shear tomography with optical and infrared data, Astron. Astrophys. 633 (2020) A69, arXiv:1812.06076 [astro-ph.CO].
[860] KiDS Collaboration, M. Asgari, et al., KiDS-1000 Cosmology: Cosmic shear constraints and comparison between two point statistics, Astron. Astrophys. 645 (2021) A104, arXiv:2007.15633 [astro-ph.CO].
[861] DES Collaboration, L.F. Secco, et al., Dark energy survey year 3 results: Cosmology from cosmic shear and robustness to modeling uncertainty, Phys. Rev. D 105 (2) (2022) 023515, arXiv:2105.13544 [astro-ph.CO].
[862] DES Collaboration, A. Amon, et al., Dark energy survey year 3 results: Cosmology from cosmic shear and robustness to data calibration, Phys. Rev. D 105 (2) (2022) 023514, arXiv:2105.13543 [astro-ph.CO].
[863] DES Collaboration, M.A. Troxel, et al., Dark energy survey year 1 results: Cosmological constraints from cosmic shear, Phys. Rev. D 98 (4) (2018) 043528, arXiv:1708.01538 [astro-ph.CO].
[864] R. Dalal, et al., Hyper suprime-cam year 3 results: Cosmology from cosmic shear power spectra, Phys. Rev. D 108 (12) (2023) 123519, arXiv:2304.00701 [astro-ph.CO].
[865] T. Erben, H. Hildebrandt, L. Miller, L. van Waerbeke, C. Heymans, H. Hoekstra, T.D. Kitching, Y. Mellier, J. Benjamin, C. Blake, C. Bonnett, O. Cordes, J. Coupon, L. Fu, R. Gavazzi, B. Gillis, E. Grocutt, S.D.J. Gwyn, K. Holhjem, M.J. Hudson, M. Kilbinger, K. Kuijken, M. Milkeraitis, B.T.P. Rowe, T. Schrabback, E. Semboloni, P. Simon, M. Smit, O. Toader, S. Vafaei, E. van Uitert, M. Velander, CFHTLenS: the Canada-France-Hawaii Telescope Lensing Survey - imaging data and catalogue products, Mon. Not. R. Astro. Soc. 433 (3) (2013) 2545–2563, arXiv:1210.8156 [astro-ph.CO].
[866] Planck Collaboration, P.A.R. Ade, et al., Planck 2013 results. XVI. Cosmological parameters, Astron. Astrophys. 571 (2014) A16, arXiv:1303.5076 [astro-ph.CO].
[867] Kilo-Degree Survey, DES Collaboration, T.M.C. Abbott, et al., DES Y3 + KiDS-1000: Consistent cosmology combining cosmic shear surveys, Open J. Astrophys.. 6 (2023) 2305.17173, arXiv:2305.17173 [astro-ph.CO].
[868] A.H. Wright, et al., KiDS-Legacy: Cosmological constraints from cosmic shear with the complete kilo-degree survey, 2025, arXiv:2503.19441 [astro-ph.CO].
[869] DES Collaboration, T.M.C. Abbott, et al., Dark Energy Survey Year 3 results: Cosmological constraints from galaxy clustering and weak lensing, Phys. Rev. D 105 (2) (2022) 023520, arXiv:2105.13549 [astro-ph.CO].
[870] DES Collaboration, C. Doux, et al., Dark energy survey year 3 results: cosmological constraints from the analysis of cosmic shear in harmonic space, Mon. Not. R. Astron. Soc. 515 (2) (2022) 1942–1972, arXiv:2203.07128 [astro-ph.CO].
[871] X. Li, et al., Hyper Suprime-Cam Year 3 results: Cosmology from cosmic shear two-point correlation functions, Phys. Rev. D 108 (12) (2023) 123518, arXiv:2304.00702 [astro-ph.CO].
[872] S. Sugiyama, et al., Hyper Suprime-Cam Year 3 results: Cosmology from galaxy clustering and weak lensing with HSC and SDSS using the minimal bias model, Phys. Rev. D 108 (12) (2023) 123521, arXiv:2304.00705 [astro-ph.CO].
[873] H. Miyatake, et al., Hyper Suprime-Cam Year 3 results: Cosmology from galaxy clustering and weak lensing with HSC and SDSS using the emulator based halo model, Phys. Rev. D 108 (12) (2023) 123517, arXiv:2304.00704 [astro-ph.CO].
[874] C. Heymans, et al., KiDS-1000 Cosmology: Multi-probe weak gravitational lensing and spectroscopic galaxy clustering constraints, Astron. Astrophys. 646 (2021) A140, arXiv:2007.15632 [astro-ph.CO].
[875] KiDS, Euclid Collaboration, A. Loureiro, et al., KiDS and Euclid: Cosmological implications of a pseudo angular power spectrum analysis of KiDS-1000 cosmic shear tomography, Astron. Astrophys. 665 (2022) A56, arXiv:2110.06947 [astro-ph.CO].
[876] SPT Collaboration, F. Bianchini, et al., Constraints on Cosmological Parameters from the 500 deg^2 SPTpol Lensing Power Spectrum, Astrophys. J. 888 (2020) 119, arXiv:1910.07157 [astro-ph.CO].
[877] DES Collaboration, D. Zürcher, et al., Dark energy survey year 3 results: Cosmology with peaks using an emulator approach, Mon. Not. R. Astron. Soc. 511 (2) (2022) 2075–2104, arXiv:2110.10135 [astro-ph.CO].
[878] DES Collaboration, J. McCullough, et al., Dark Energy Survey Year 3: Blue Shear, 2024, arXiv:2410.22272 [astro-ph.CO].
[879] DES Collaboration, M. Gatti, et al., Dark Energy Survey Year 3 results: Simulation-based cosmological inference with wavelet harmonics, scattering transforms, and moments of weak lensing mass maps. Validation on simulations, Phys. Rev. D 109 (6) (2024) 063534, arXiv:2310.17557 [astro-ph.CO].
[880] M. von Wietersheim-Kramsta, K. Lin, N. Tessore, B. Joachimi, A. Loureiro, R. Reischke, A.H. Wright, KiDS-SBI: Simulation-based inference analysis of KiDS-1000 cosmic shear, Astron. Astrophys. 694 (2025) A223, arXiv:2404.15402 [astro-ph.CO].
[881] C.P. Novaes, L. Thiele, J. Armijo, S. Cheng, J.A. Cowell, G.A. Marques, E.G.M. Ferreira, M. Shirasaki, K. Osato, J. Liu, Cosmology from HSC Y1 weak lensing data with combined higher-order statistics and simulation-based inference, Phys. Rev. D 111 (8) (2025) 083510, arXiv:2409.01301 [astro-ph.CO].
[882] R. Reischke, et al., KiDS-Legacy: Covariance validation and the unified OneCovariance framework for projected large-scale structure observables, 2024, arXiv:2410.06962 [astro-ph.CO].

[883] E. Sellentin, A.F. Heavens, Parameter inference with estimated covariance matrices, Mon. Not. R. Astron. Soc. 456 (1) (2016) L132–L136, arXiv:1511.05969 [astro-ph.CO].
[884] E. Sellentin, C. Heymans, J. Harnois-Déraps, The skewed weak lensing likelihood: why biases arise, despite data and theory being sound, Mon. Not. R. Astron. Soc. 477 (4) (2018) 4879–4895, arXiv:1712.04923 [astro-ph.CO].
[885] N.E. Chisari, M.L.A. Richardson, J. Devriendt, Y. Dubois, A. Schneider, A.L. Brun, R.S. Beckmann, S. Peirani, A. Slyz, C. Pichon, The impact of baryons on the matter power spectrum from the Horizon-AGN cosmological hydrodynamical simulation, Mon. Not. R. Astron. Soc. 480 (3) (2018) 3962–3977, arXiv:1801.08559 [astro-ph.CO].
[886] Euclid Collaboration, M. Knabenhans, et al., Euclid preparation: IX. EuclidEmulator2 – power spectrum emulation with massive neutrinos and self-consistent dark energy perturbations, Mon. Not. R. Astron. Soc. 505 (2) (2021) 2840–2869, arXiv:2010.11288 [astro-ph.CO].
[887] G. Aricò, R.E. Angulo, S. Contreras, L. Ondaro-Mallea, M. Pellejero-Ibañez, M. Zennaro, The BACCO simulation project: a baryonification emulator with neural networks, Mon. Not. R. Astron. Soc. 506 (3) (2021) 4070–4082, arXiv:2011.15018 [astro-ph.CO].
[888] M. Asgari, A.J. Mead, C. Heymans, The halo model for cosmology: a pedagogical review, 2023, http://dx.doi.org/10.21105/astro.2303.08752, arXiv:2303.08752 [astro-ph.CO].
[889] VIRGO Consortium Collaboration, R.E. Smith, J.A. Peacock, A. Jenkins, S.D.M. White, C.S. Frenk, F.R. Pearce, P.A. Thomas, G. Efstathiou, H.M.P. Couchmann, Stable clustering, the halo model and nonlinear cosmological power spectra, Mon. Not. R. Astron. Soc. 341 (2003) 1311, arXiv:astro-ph/0207664.
[890] R. Takahashi, M. Sato, T. Nishimichi, A. Taruya, M. Oguri, Revising the halofit model for the nonlinear matter power spectrum, Astrophys. J. 761 (2012) 152, arXiv:1208.2701 [astro-ph.CO].
[891] A. Mead, S. Brieden, T. Tröster, C. Heymans, hmcode-2020: improved modelling of non-linear cosmological power spectra with baryonic feedback, Mon. Not. R. Astron. Soc. 502 (1) (2021) 1401–1422, arXiv:2009.01858 [astro-ph.CO].
[892] A. Mead, C. Heymans, L. Lombriser, J. Peacock, O. Steele, H. Winther, Accurate halo-model matter power spectra with dark energy, massive neutrinos and modified gravitational forces, Mon. Not. R. Astron. Soc. 459 (2) (2016) 1468–1488, arXiv:1602.02154 [astro-ph.CO].
[893] F. Bernardeau, T. Nishimichi, A. Taruya, Cosmic shear full nulling: sorting out dynamics, geometry and systematics, Mon. Not. R. Astron. Soc. 445 (2) (2014) 1526–1537, arXiv:1312.0430 [astro-ph.CO].
[894] P.L. Taylor, F. Bernardeau, T.D. Kitching, k-cut cosmic shear: Tunable power spectrum sensitivity to test gravity, Phys. Rev. D 98 (8) (2018) 083514, arXiv:1809.03515 [astro-ph.CO].
[895] A. Barthelemy, S. Codis, C. Uhlemann, F. Bernardeau, R. Gavazzi, A nulling strategy for modelling lensing convergence in cones with large deviation theory, Mon. Not. R. Astron. Soc. 492 (3) (2020) 3420–3439, arXiv:1909.02615 [astro-ph.CO].
[896] D. Spergel, et al., Wide-field infrarred survey telescope-astrophysics focused telescope assets WFIRST-AFTA 2015 report, 2015, arXiv:1503.03757 [astro-ph.IM].
[897] LSST Collaboration, v. Ivezić, et al., LSST: from science drivers to reference design and anticipated data products, Astrophys. J. 873 (2) (2019) 111, arXiv:0805.2366 [astro-ph].
[898] R. Massey, et al., Origins of weak lensing systematics, and requirements on future instrumentation (or knowledge of instrumentation), Mon. Not. R. Astron. Soc. 429 (2013) 661, arXiv:1210.7690 [astro-ph.CO].
[899] N. Kaiser, G. Squires, T.J. Broadhurst, A method for weak lensing observations, Astrophys. J. 449 (1995) 460–475, arXiv:astro-ph/9411005.
[900] L. Miller, T.D. Kitching, C. Heymans, A.F. Heavens, L. Van Waerbeke, Bayesian galaxy shape measurement for weak lensing surveys. 1. Methodology and a fast fitting algorithm, Mon. Not. R. Astron. Soc. 382 (2007) 315, arXiv:0708.2340 [astro-ph].
[901] G.M. Bernstein, R. Armstrong, Bayesian lensing shear measurement, Mon. Not. R. Astron. Soc. 438 (2) (2014) 1880–1893, arXiv:1304.1843 [astro-ph.CO].
[902] R. Mandelbaum, Weak lensing for precision cosmology, Ann. Rev. Astron. Astrophys.. 56 (2018) 393–433, arXiv:1710.03235 [astro-ph.CO].
[903] I. Fenech Conti, R. Herbonnet, H. Hoekstra, J. Merten, L. Miller, M. Viola, Calibration of weak-lensing shear in the kilo-degree survey, Mon. Not. R. Astron. Soc. 467 (2) (2017) 1627–1651, arXiv:1606.05337 [astro-ph.CO].
[904] E. Huff, R. Mandelbaum, Metacalibration: Direct self-calibration of biases in shear measurement, 2017, arXiv:1702.02600 [astro-ph.CO].
[905] DES Collaboration, N. MacCrann, et al., Dark energy survey y3 results: blending shear and redshift biases in image simulations, Mon. Not. R. Astron. Soc. 509 (3) (2021) 3371–3394, arXiv:2012.08567 [astro-ph.CO].
[906] X. Li, et al., The three-year shear catalog of the subaru hyper suprime-cam ssp survey, Publ. Astron. Soc. Jap. 74 (2) (2022) 421–459–459, arXiv:2107.00136 [astro-ph.CO].
[907] S.-S. Li, et al., KiDS-Legacy calibration: unifying shear and redshift calibration with the SKiLLS multi-band image simulations, Astron. Astrophys. 670 (2023) A100, arXiv:2210.07163 [astro-ph.CO].
[908] H. Hoekstra, A. Kannawadi, T.D. Kitching, Accounting for object detection bias in weak gravitational lensing studies, Astron. Astrophys. 646 (2021) A124, arXiv:2010.04178 [astro-ph.CO].
[909] N. Kaiser, A new shear estimator for weak lensing observations, Astrophys. J. 537 (2000) 555, arXiv:astro-ph/9904003.
[910] G.M. Bernstein, M. Jarvis, Shapes and shears, stars and smears: optimal measurements for weak lensing, Astron. J. 123 (2002) 583–618, arXiv:astro-ph/0107431.
[911] C.M. Hirata, U. Seljak, Shear calibration biases in weak lensing surveys, Mon. Not. R. Astron. Soc. 343 (2003) 459–480, arXiv:astro-ph/0301054.
[912] J. Hartlap, S. Hilbert, P. Schneider, H. Hildebrandt, A bias in cosmic shear from galaxy selection: results from ray-tracing simulations, Astron. Astrophys. 528 (2011) A51, arXiv:1010.0010 [astro-ph.CO].
[913] E.S. Sheldon, M.R. Becker, N. MacCrann, M. Jarvis, Mitigating shear-dependent object detection biases with metacalibration, Astrophys. J. 902 (2) (2020) 138, arXiv:1911.02505 [astro-ph.CO].
[914] C. Heymans, et al., The shear Testing programme. 1. Weak lensing analysis of simulated ground-based observations, Mon. Not. R. Astron. Soc. 368 (2006) 1323–1339, arXiv:astro-ph/0506112.
[915] R. Massey, et al., The Shear TEsting Programme 2: Factors affecting high precision weak lensing analyses, Mon. Not. R. Astron. Soc. 376 (2007) 13–38, arXiv:astro-ph/0608643.
[916] S. Bridle, et al., Results of the GREAT08 Challenge: An image analysis competition for cosmological lensing, Mon. Not. R. Astron. Soc. 405 (2010) 2044, arXiv:0908.0945 [astro-ph.CO].
[917] T.D. Kitching, et al., Image analysis for cosmology: results from the GREAT10 star challenge, Astrophys.. J. Supp. 205 (2013) 12, arXiv:1210.1979 [astro-ph.IM].
[918] R. Mandelbaum, et al., The third gravitational lensing accuracy testing (GREAT3) challenge handbook, Astrophys. J. Suppl. 212 (2014) 5, arXiv:1308.4982 [astro-ph.CO].
[919] S.-S. Li, et al., KiDS-1000: Cosmology with improved cosmic shear measurements, Astron. Astrophys. 679 (2023) A133, arXiv:2306.11124 [astro-ph.CO].
[920] J.A. Newman, D. Gruen, Photometric redshifts for next-generation surveys, Ann. Rev. Astron. Astrophys.. 60 (2022) 363–414, arXiv:2206.13633 [astro-ph.CO].
[921] M. Salvato, O. Ilbert, B. Hoyle, The many flavours of photometric redshifts, Nat. Astron. 3 (2019) 212–222, arXiv:1805.12574 [astro-ph.GA].
[922] R. Tagliaferri, G. Longo, S. Andreon, S. Capozziello, C. Donalek, G. Giordano, Neural networks for photometric redshifts evaluation, in: Neural Nets. Lecture Notes in Computer Science, Volume 2859. ISBN 978-3-540-20227-1. Springer Berlin Heidelberg, 2003. p. 226-234, Springer Berlin Heidelberg, Berlin, Heidelberg, 2003, pp. 226–234.
[923] A.A. Collister, O. Lahav, ANNz: Estimating photometric redshifts using artificial neural networks, Publ. Astron. Soc. Pac. 116 (2004) 345–351, arXiv:astro-ph/0311058 [astro-ph].
[924] D.W. Gerdes, A.J. Sypniewski, T.A. McKay, J. Hao, M.R. Weis, R.H. Wechsler, M.T. Busha, ArborZ: Photometric redshifts using boosted decision trees, Astrophys. J. 715 (2010) 823–832, arXiv:0908.4085 [astro-ph.CO].
[925] M. Carrasco Kind, R.J. Brunner, TPZ: photometric redshift PDFs and ancillary information by using prediction trees and random forests, Mon. Not. R. Astro. Soc. 432 (2) (2013) 1483–1501, arXiv:1303.7269 [astro-ph.CO].
[926] C. Bonnett, Using neural networks to estimate redshift distributions. An application to CFHTLenS, Mon. Not. R. Astro. Soc. 449 (2015) 1043–1056, arXiv:1312.1287 [astro-ph.CO].
[927] M.M. Rau, S. Seitz, F. Brimioulle, E. Frank, O. Friedrich, D. Gruen, B. Hoyle, Accurate photometric redshift probability density estimation - method comparison and application, Mon. Not. R. Astro. Soc. 452 (4) (2015) 3710–3725, arXiv:1503.08215 [astro-ph.CO].
[928] B. Hoyle, Measuring photometric redshifts using galaxy images and deep neural networks, Astron. Comput. 16 (2016) 34–40, arXiv:1504.07255 [astro-ph.IM].
[929] S. Arnouts, S. Cristiani, L. Moscardini, S. Matarrese, F. Lucchin, A. Fontana, E. Giallongo, Measuring and modelling the redshift evolution of clustering: the Hubble deep field north, Mon. Not. R. Astro. Soc. 310 (1999) 540–556, arXiv:astro-ph/9902290 [astro-ph].
[930] N. Benitez, Bayesian photometric redshift estimation, Astrophys. J. 536 (2000) 571–583, arXiv:astro-ph/9811189.
[931] O. Ilbert, et al., Accurate photometric redshifts for the cfht legacy survey calibrated using the vimos vlt deep survey, Astron. Astrophys. 457 (2006) 841–856, arXiv:astro-ph/0603217.
[932] R. Feldmann, C.M. Carollo, C. Porciani, S.J. Lilly, P. Capak, Y. Taniguchi, O. Le Fèvre, A. Renzini, N. Scoville, M. Ajiki, H. Aussel, T. Contini, H. McCracken, B. Mobasher, T. Murayama, D. Sanders, S. Sasaki, C. Scarlata, M. Scodeggio, Y. Shioya, J. Silverman, M. Takahashi, D. Thompson, G. Zamorani, The Zurich extragalactic bayesian redshift analyzer and its first application: COSMOS, Mon. Not. R. Astro. Soc. 372 (2006) 565–577, arXiv:astro-ph/0609044 [astro-ph].

[933] N. Greisel, S. Seitz, N. Drory, R. Bender, R.P. Saglia, J. Snigula, Photometric redshifts and model spectral energy distributions of galaxies from the SDSS-III BOSS DR10 data, Mon. Not. R. Astro. Soc. 451 (2015) 1848–1867, arXiv:1505.01157.

[934] B. Leistedt, D.J. Mortlock, H.V. Peiris, Hierarchical Bayesian inference of galaxy redshift distributions from photometric surveys, Mon. Not. R. Astro. Soc. 460 (2016) 4258–4267, arXiv:1602.05960.

[935] A.I. Malz, D.W. Hogg, How to obtain the redshift distribution from probabilistic redshift estimates, Astrophys. J. 928 (2) (2022) 127, arXiv:2007.12178 [astro-ph.CO].

[936] C.E. Cunha, D. Huterer, H. Lin, M.T. Busha, R.H. Wechsler, Spectroscopic failures in photometric redshift calibration: cosmological biases and survey requirements, Mon. Not. R. Astro. Soc. 444 (2014) 129–146, arXiv:1207.3347 [astro-ph.CO].

[937] J.A. Newman, et al., Spectroscopic needs for imaging dark energy experiments, Astropart. Phys. 63 (2015) 81–100, arXiv:1309.5384 [astro-ph.CO]; Erratum: Astropart. Phys. 65 (2015) 112–113.

[938] D.C. Masters, D.K. Stern, J.G. Cohen, P.L. Capak, J.D. Rhodes, F.J. Castander, S. Paltani, The complete calibration of the color-redshift relation (C3R2) survey: Survey overview and data release 1, Astrophys. J. 841 (2) (2017) 111, arXiv:1704.06665 [astro-ph.CO].

[939] D.C. Masters, D.K. Stern, J.G. Cohen, P.L. Capak, S.A. Stanford, N. Hernitschek, A. Galametz, I. Davidzon, J.D. Rhodes, D. Sanders, B. Mobasher, F. Castander, K. Pruett, S. Fotopoulou, The complete calibration of the color-redshift relation (C3R2) survey: Analysis and data release 2, Astrophys. J. 877 (2) (2019) 81, arXiv:1904.06394 [astro-ph.GA].

[940] W.G. Hartley, et al., The impact of spectroscopic incompleteness in direct calibration of redshift distributions for weak lensing surveys, Mon. Not. R. Astro. Soc. 496 (4) (2020) 4769–4786, arXiv:2003.10454 [astro-ph.GA].

[941] Z. Ma, W. Hu, D. Huterer, Effects of photometric redshift uncertainties on weak-lensing tomography, Astrophys. J. 636 (1) (2006) 21–29, arXiv:astro-ph/0506614 [astro-ph].

[942] D. Masters, P. Capak, D. Stern, O. Ilbert, M. Salvato, S. Schmidt, G. Longo, J. Rhodes, S. Paltani, B. Mobasher, H. Hoekstra, H. Hildebrandt, J. Coupon, C. Steinhardt, J. Speagle, A. Faisst, A. Kalinich, M. Brodwin, M. Brescia, S. Cavuoti, Mapping the galaxy color-redshift relation: Optimal photometric redshift calibration strategies for cosmology surveys, Astrophys. J. 813 (2015) 53, arXiv:1509.03318 [astro-ph.CO].

[943] M.J. Jee, J.A. Tyson, M.D. Schneider, D. Wittman, S. Schmidt, S. Hilbert, Cosmic shear results from the deep lens survey - I: Joint constraints on omega_m and sigma_8 with a two-dimensional analysis, Astrophys. J. 765 (2013) 74, arXiv:1210.2732 [astro-ph.CO].

[944] J. Benjamin, L. Van Waerbeke, C. Heymans, M. Kilbinger, T. Erben, H. Hildebrandt, H. Hoekstra, T.D. Kitching, Y. Mellier, L. Miller, B. Rowe, T. Schrabback, F. Simpson, J. Coupon, L. Fu, J. Harnois-Déraps, M.J. Hudson, K. Kuijken, E. Semboloni, S. Vafaei, M. Velander, CFHTLenS tomographic weak lensing: quantifying accurate redshift distributions, Mon. Not. R. Astro. Soc. 431 (2013) 1547–1564, arXiv:1212.3327 [astro-ph.CO].

[945] N. Benítez, BPZ: Bayesian photometric redshift code, 2011, Astrophysics Source Code Library, record ascl:1108.011.

[946] M. Lima, C.E. Cunha, H. Oyaizu, J. Frieman, H. Lin, E.S. Sheldon, Estimating the redshift distribution of photometric galaxy samples, Mon. Not. R. Astro. Soc. 390 (1) (2008) 118–130, arXiv:0801.3822 [astro-ph].

[947] DES Collaboration, B. Hoyle, et al., Dark energy survey year 1 results: Redshift distributions of the weak lensing source galaxies, Mon. Not. R. Astron. Soc. 478 (1) (2018) 592–610, arXiv:1708.01532 [astro-ph.CO].

[948] A.H. Wright, H. Hildebrandt, J.L. van den Busch, C. Heymans, Photometric redshift calibration with self-organising maps, Astron. Astrophys. 637 (2020) A100, arXiv:1909.09632 [astro-ph.CO].

[949] H. Hildebrandt, J.L. van den Busch, A.H. Wright, C. Blake, B. Joachimi, K. Kuijken, T. Tröster, M. Asgari, M. Bilicki, J.T.A. de Jong, A. Dvornik, T. Erben, F. Getman, B. Giblin, C. Heymans, A. Kannawadi, C.A. Lin, H.Y. Shan, KiDS-1000 catalogue: Redshift distributions and their calibration, Astron. Astrophys. 647 (2021) A124, arXiv:2007.15635 [astro-ph.CO].

[950] A.H. Wright, et al., The fifth data release of the kilo degree survey: Multi-epoch optical/NIR imaging covering wide and legacy-calibration fields, Astron. Astrophys. 686 (2024) A170.

[951] J. Myles, et al., Dark energy survey year 3 results: redshift calibration of the weak lensing source galaxies, Mon. Not. R. Astro. Soc. 505 (3) (2021) 4249–4277, arXiv:2012.08566 [astro-ph.CO].

[952] R. Cawthon, et al., Dark energy survey year 3 results: calibration of lens sample redshift distributions using clustering redshifts with BOSS/eBOSS, Mon. Not. R. Astro. Soc. 513 (4) (2022) 5517–5539, arXiv:2012.12826 [astro-ph.CO].

[953] M. Gatti, et al., Dark energy survey year 3 results: clustering redshifts - calibration of the weak lensing source redshift distributions with redMaGiC and BOSS/eBOSS, Mon. Not. R. Astro. Soc. 510 (1) (2022) 1223–1247, arXiv:2012.08569 [astro-ph.CO].

[954] M.M. Rau, R. Dalal, T. Zhang, X. Li, A.J. Nishizawa, S. More, R. Mandelbaum, H. Miyatake, M.A. Strauss, M. Takada, Weak lensing tomographic redshift distribution inference for the Hyper Suprime-Cam Subaru Strategic Program three-year shape catalogue, Mon. Not. R. Astron. Soc. 524 (4) (2023) 5109–5131, arXiv:2211.16516 [astro-ph.CO].

[955] M. Schneider, L. Knox, H. Zhan, A. Connolly, Using galaxy two-point correlation functions to determine the redshift distributions of galaxies binned by photometric redshift, Astrophys. J. 651 (1) (2006) 14–23, arXiv:astro-ph/0606098 [astro-ph].

[956] J.A. Newman, Calibrating redshift distributions beyond spectroscopic limits with cross-correlations, Astrophys. J. 684 (2008) 88–101, arXiv:0805.1409 [astro-ph].

[957] J.L.v.d. Busch, et al., KiDS-1000: Cosmic shear with enhanced redshift calibration, Astron. Astrophys. 664 (2022) A170, arXiv:2204.02396 [astro-ph.CO].

[958] LSST Dark Energy Science Collaboration, I. Moskowitz, E. Gawiser, J.F. Crenshaw, B.H. Andrews, A.I. Malz, S. Schmidt, Improving photometric redshift estimates with training sample augmentation, Astrophys. J. Lett. 967 (1) (2024) L6, arXiv:2402.15551 [astro-ph.IM].

[959] T. Zhang, M.M. Rau, R. Mandelbaum, X. Li, B. Moews, Photometric redshift uncertainties in weak gravitational lensing shear analysis: models and marginalization, Mon. Not. R. Astron. Soc. 518 (1) (2022) 709–723, arXiv:2206.10169 [astro-ph.CO].

[960] M.P. van Daalen, J. Schaye, C.M. Booth, C.D. Vecchia, The effects of galaxy formation on the matter power spectrum: A challenge for precision cosmology, Mon. Not. R. Astron. Soc. 415 (2011) 3649–3665, arXiv:1104.1174 [astro-ph.CO].

[961] J. Sunseri, Z. Li, J. Liu, Effects of baryonic feedback on the cosmic web, Phys. Rev. D 107 (2) (2023) 023514, arXiv:2212.05927 [astro-ph.CO].

[962] A. Schneider, R. Teyssier, J. Stadel, N.E. Chisari, A.M.C. Le Brun, A. Amara, A. Refregier, Quantifying baryon effects on the matter power spectrum and the weak lensing shear correlation, J. Cosmol. Astropart. Phys. 2019 (3) (2019) 020, arXiv:1810.08629 [astro-ph.CO].

[963] G. Aricò, R.E. Angulo, C. Hernández-Monteagudo, S. Contreras, M. Zennaro, M. Pellejero-Ibañez, Y. Rosas-Guevara, Modelling the large-scale mass density field of the universe as a function of cosmology and baryonic physics, Mon. Not. R. Astro. Soc. 495 (4) (2020) 4800–4819, arXiv:1911.08471 [astro-ph.CO].

[964] A. Schneider, N. Stoira, A. Refregier, A.J. Weiss, M. Knabenhans, J. Stadel, R. Teyssier, Baryonic effects for weak lensing. Part I. Power spectrum and covariance matrix, J. Cosmol. Astropart. Phys. 2020 (4) (2020) 019, arXiv:1910.11357 [astro-ph.CO].

[965] J.M. Sullivan, U.s. Seljak, S. Singh, An analytic hybrid halo + perturbation theory model for small-scale correlators: baryons, halos, and galaxies, J. Cosmol. Astropart. Phys. 2021 (11) (2021) 026, arXiv:2104.10676 [astro-ph.CO].

[966] A.M.C. Le Brun, I.G. McCarthy, J. Schaye, T.J. Ponman, Towards a realistic population of simulated galaxy groups and clusters, Mon. Not. R. Astro. Soc. 441 (2) (2014) 1270–1290, arXiv:1312.5462 [astro-ph.CO].

[967] I.G. McCarthy, S. Bird, J. Schaye, J. Harnois-Deraps, A.S. Font, L. van Waerbeke, The BAHAMAS project: the CMB-large-scale structure tension and the roles of massive neutrinos and galaxy formation, Mon. Not. R. Astro. Soc. 476 (3) (2018) 2999–3030, arXiv:1712.02411 [astro-ph.CO].

[968] S. Kaviraj, C. Laigle, T. Kimm, J.E.G. Devriendt, Y. Dubois, C. Pichon, A. Slyz, E. Chisari, S. Peirani, The Horizon-AGN simulation: evolution of galaxy properties over cosmic time, Mon. Not. R. Astro. Soc. 467 (4) (2017) 4739–4752, arXiv:1605.09379 [astro-ph.GA].

[969] M.P. van Daalen, I.G. McCarthy, J. Schaye, Exploring the effects of galaxy formation on matter clustering through a library of simulation power spectra, Mon. Not. R. Astron. Soc. 491 (2) (2020) 2424–2446, arXiv:1906.00968 [astro-ph.CO].

[970] J. Schaye, R. Kugel, M. Schaller, J.C. Helly, J. Braspenning, W. Elbers, I.G. McCarthy, M.P. van Daalen, B. Vandenbroucke, C.S. Frenk, J. Kwan, J. Salcido, Y.M. Bahé, J. Borrow, E. Chaikin, O. Hahn, F. Huško, A. Jenkins, C.G. Lacey, F.S.J. Nobels, The FLAMINGO project: cosmological hydrodynamical simulations for large-scale structure and galaxy cluster surveys, Mon. Not. R. Astro. Soc. 526 (4) (2023) 4978–5020, arXiv:2306.04024 [astro-ph.CO].

[971] N.E. Chisari, et al., Modelling baryonic feedback for survey cosmology, Open J. Astrophys.. 2 (1) (2019) 4, arXiv:1905.06082 [astro-ph.CO].

[972] A. Schneider, R. Teyssier, A new method to quantify the effects of baryons on the matter power spectrum, J. Cosmol. Astropart. Phys. 2015 (12) (2015) 049–049, arXiv:1510.06034 [astro-ph.CO].

[973] K.R. Moran, K. Heitmann, E. Lawrence, S. Habib, D. Bingham, A. Upadhye, J. Kwan, D. Higdon, R. Payne, The Mira–Titan Universe – IV. High-precision power spectrum emulation, Mon. Not. R. Astron. Soc. 520 (3) (2023) 3443–3458, arXiv:2207.12345 [astro-ph.CO].

[974] LSST Dark Energy Science Collaboration, N.E. Chisari, et al., Core cosmology library: precision cosmological predictions for LSST, Astrophys. J. Suppl. 242 (1) (2019) 2, arXiv:1812.05995 [astro-ph.CO].

[975] N. Šarčević, Modelling and mitigating the systematics in weak lensing measurements, 2024, http://dx.doi.org/10.5281/zenodo.14602273.

[976] G. Aricò, R.E. Angulo, M. Zennaro, S. Contreras, A. Chen, C. Hernández-Monteagudo, DES Y3 cosmic shear down to small scales: Constraints on cosmology and baryons, Astron. Astrophys. 678 (2023) A109, arXiv:2303.05537 [astro-ph.CO].
[977] C. Fedeli, The clustering of baryonic matter. I: a halo-model approach, J. Cosmol. Astropart. Phys. 2014 (4) (2014) 028, arXiv:1401.2997 [astro-ph.CO].
[978] H.-J. Huang, T. Eifler, R. Mandelbaum, S. Dodelson, Modelling baryonic physics in future weak lensing surveys, Mon. Not. R. Astron. Soc. 488 (2) (2019) 1652–1678, arXiv:1809.01146 [astro-ph.CO].
[979] J.C. Broxterman, et al., The FLAMINGO project: baryonic impact on weak gravitational lensing convergence peak counts, Mon. Not. R. Astron. Soc. 529 (3) (2024) 2309–2326, arXiv:2312.08450 [astro-ph.CO].
[980] S. Foreman, W. Coulton, F. Villaescusa-Navarro, A. Barreira, Baryonic effects on the matter bispectrum, Mon. Not. R. Astron. Soc. 498 (2) (2020) 2887–2911, arXiv:1910.03597 [astro-ph.CO].
[981] N. Martinet, T. Castro, J. Harnois-Déraps, E. Jullo, C. Giocoli, K. Dolag, Impact of baryons in cosmic shear analyses with tomographic aperture mass statistics, Astron. Astrophys. 648 (2021) A115, arXiv:2012.09614 [astro-ph.CO].
[982] T. Lu, Z. Haiman, The impact of baryons on cosmological inference from weak lensing statistics, Mon. Not. R. Astron. Soc. 506 (3) (2021) 3406–3417, arXiv:2104.04165 [astro-ph.CO].
[983] E. Semboloni, H. Hoekstra, J. Schaye, Effect of baryonic feedback on two- and three-point shear statistics: prospects for detection and improved modelling, Mon. Not. R. Astron. Soc. 434 (2013) 148, arXiv:1210.7303 [astro-ph.CO].
[984] W. Elbers, et al., The FLAMINGO project: the coupling between baryonic feedback and cosmology in light of the S8 tension, Mon. Not. R. Astron. Soc. 537 (2) (2025) 2160–2178, arXiv:2403.12967 [astro-ph.CO].
[985] DES Collaboration, L. Bigwood, et al., Weak lensing combined with the kinetic Sunyaev–Zel'dovich effect: a study of baryonic feedback, Mon. Not. R. Astron. Soc. 534 (1) (2024) 655–682, arXiv:2404.06098 [astro-ph.CO].
[986] I.S. Khrykin, et al., FLIMFLAM DR1: The first constraints on the cosmic baryon distribution from eight fast radio burst sight lines, Astrophys. J. 973 (2) (2024) 151, arXiv:2402.00505 [astro-ph.GA].
[987] A. Amon, et al., Consistent lensing and clustering in a low-S_8 universe with BOSS, DES Year 3, HSC Year 1, and KiDS-1000, Mon. Not. R. Astro. Soc. 518 (1) (2023) 477–503, arXiv:2202.07440 [astro-ph.CO].
[988] K.-G. Lee, M. Ata, I.S. Khrykin, Y. Huang, J.X. Prochaska, J. Cooke, J. Zhang, A. Batten, Constraining the cosmic baryon distribution with fast radio burst foreground mapping, Astrophys. J. 928 (1) (2022) 9, arXiv:2109.00386 [astro-ph.CO].
[989] C. García-García, M. Zennaro, G. Aricò, D. Alonso, R.E. Angulo, Cosmic shear with small scales: DES-Y3, KiDS-1000 and HSC-DR1, JCAP 08 (2024) 024, arXiv:2403.13794 [astro-ph.CO].
[990] R. Terasawa, et al., Exploring the baryonic effect signature in the hyper suprime-cam year 3 cosmic shear two-point correlations on small scales: The S8 tension remains present, Phys. Rev. D 111 (6) (2025) 063509, arXiv:2403.20323 [astro-ph.CO].
[991] A. Amon, G. Efstathiou, A non-linear solution to the S_8 tension?, Mon. Not. R. Astron. Soc. 516 (4) (2022) 5355–5366, arXiv:2206.11794 [astro-ph.CO].
[992] T. Nishimichi, et al., Dark Quest. I. Fast and accurate emulation of halo clustering statistics and its application to galaxy clustering, Astrophys. J. 884 (2019) 29, arXiv:1811.09504 [astro-ph.CO].
[993] S. Amodeo, et al., Atacama cosmology telescope: modeling the gas thermodynamics in BOSS CMASS galaxies from kinematic and thermal Sunyaev-Zel'dovich measurements, Phys. Rev. D 103 (6) (2021) 063514, arXiv:Amodeo:2020mmu [astro-ph.CO]; Erratum: Phys. Rev. D 107 (2023) 063514.
[994] C. Lamman, E. Tsaprazi, J. Shi, N.N. Šarčević, S. Pyne, E. Legnani, T. Ferreira, The Ia guide: A breakdown of intrinsic alignment formalisms, 2023, http://dx.doi.org/10.21105/astro.2309.08605, arXiv:2309.08605 [astro-ph.CO].
[995] M.A. Troxel, M. Ishak, The intrinsic alignment of galaxies and its impact on weak gravitational lensing in an era of precision cosmology, Phys. Rep. 558 (2014) 1–59, arXiv:1407.6990 [astro-ph.CO].
[996] J. Prat, J. Zuntz, C. Chang, T. Tröster, E. Pedersen, C. García-García, E. Phillips-Longley, J. Sanchez, D. Alonso, X. Fang, E. Gawiser, K. Heitmann, M. Ishak, M. Jarvis, E. Kovacs, P. Larsen, Y.Y. Mao, L. Medina Varela, M. Paterno, S.D. Vitenti, Z. Zhang, LSST Dark Energy Science Collaboration, The catalog-to-cosmology framework for weak lensing and galaxy clustering for LSST, Open J. Astrophys. 6 (2023) 13, arXiv:2212.09345 [astro-ph.CO].
[997] DES Collaboration, C. Sánchez, et al., Dark energy survey year 3 results: Exploiting small-scale information with lensing shear ratios, Phys. Rev. D 105 (8) (2022) 083529, arXiv:2105.13542 [astro-ph.CO].
[998] D.N. Cross, C. Sánchez, Inverse galaxy-galaxy lensing: Magnification, intrinsic alignments, and cosmology, Phys. Rev. D 110 (12) (2024) 123534, arXiv:2410.00714 [astro-ph.CO].
[999] S. Bridle, L. King, Dark energy constraints from cosmic shear power spectra: impact of intrinsic alignments on photometric redshift requirements, New J. Phys. 9 (2007) 444, arXiv:0705.0166 [astro-ph].
[1000] J. Blazek, N. MacCrann, M.A. Troxel, X. Fang, Beyond linear galaxy alignments, Phys. Rev. D 100 (10) (2019) 103506, arXiv:1708.09247 [astro-ph.CO].
[1001] S. Samuroff, R. Mandelbaum, J. Blazek, Advances in constraining intrinsic alignment models with hydrodynamic simulations, Mon. Not. R. Astron. Soc. 508 (1) (2021) 637–664, arXiv:2009.10735 [astro-ph.CO].
[1002] DES Collaboration, S. Samuroff, et al., The Dark Energy Survey Year 3 and eBOSS: constraining galaxy intrinsic alignments across luminosity and colour space, Mon. Not. R. Astron. Soc. 524 (2) (2023) 2195–2223, arXiv:2212.11319 [astro-ph.CO].
[1003] DES Collaboration, K. Hoffmann, et al., Modeling intrinsic galaxy alignment in the MICE simulation, Phys. Rev. D 106 (12) (2022) 123510, arXiv:2206.14219 [astro-ph.CO].
[1004] M.C. Fortuna, H. Hoekstra, B. Joachimi, H. Johnston, N.E. Chisari, C. Georgiou, C. Mahony, The halo model as a versatile tool to predict intrinsic alignments, Mon. Not. R. Astron. Soc. 501 (2) (2021) 2983–3002, arXiv:2003.02700 [astro-ph.CO].
[1005] T. Bakx, T. Kurita, N.E. Chisari, Z. Vlah, F. Schmidt, Effective field theory of intrinsic alignments at one loop order: a comparison to dark matter simulations, J. Cosmol. Astropart. Phys. 10 (2023) 005, arXiv:2303.15565 [astro-ph.CO].
[1006] C.D. Leonard, M.M. Rau, R. Mandelbaum, Photometric redshifts and intrinsic alignments: Degeneracies and biases in the 3×2pt analysis, Phys. Rev. D 109 (8) (2024) 083528, arXiv:2401.06060 [astro-ph.CO].
[1007] LSST Dark Energy Science Collaboration, N. Šarčević, C.D. Leonard, M.M. Rau, Joint modelling of astrophysical systematics for cosmology with LSST cosmic shear, 2024, arXiv:2406.03352 [astro-ph.CO].
[1008] A. Campos, S. Samuroff, R. Mandelbaum, An empirical approach to model selection: weak lensing and intrinsic alignments, Mon. Not. R. Astron. Soc. 525 (2) (2023) 1885–1901, arXiv:2211.02800 [astro-ph.CO].
[1009] P.M. Merkel, B.M. Schäfer, A theoretical estimate of intrinsic ellipticity bispectra induced by angular momenta alignments, Mon. Not. R. Astron. Soc. 445 (3) (2014) 2918–2929, arXiv:1409.5197 [astro-ph.CO].
[1010] P.A. Burger, et al., KiDS-1000 cosmology: Combined second- and third-order shear statistics, Astron. Astrophys. 683 (2024) A103, arXiv:2309.08602 [astro-ph.CO].
[1011] A. Barthelemy, A. Halder, Z. Gong, C. Uhlemann, Making the leap. Part I. Modelling the reconstructed lensing convergence PDF from cosmic shear with survey masks and systematics, J. Cosmol. Astropart. Phys. 03 (2024) 060, arXiv:2307.09468 [astro-ph.CO].
[1012] J. Harnois-Déraps, N. Martinet, R. Reischke, Cosmic shear beyond 2-point statistics: Accounting for galaxy intrinsic alignment with projected tidal fields, Mon. Not. R. Astron. Soc. 509 (2022) 3868–3868, arXiv:2107.08041 [astro-ph.CO].
[1013] DES Collaboration, M. Gatti, et al., Detection of the significant impact of source clustering on higher order statistics with DES Year 3 weak gravitational lensing data, Mon. Not. R. Astron. Soc. 527 (1) (2024) L115–L121, arXiv:2307.13860 [astro-ph.CO].
[1014] KiDS-1000, Euclid Collaboration, L. Linke, et al., Euclid and KiDS-1000: Quantifying the impact of source-lens clustering on cosmic shear analyses, Astron. Astrophys. 693 (2025) A210, arXiv:2407.09810 [astro-ph.CO].
[1015] E. Krause, T. Eifler, J. Blazek, The impact of intrinsic alignment on current and future cosmic shear surveys, Mon. Not. R. Astron. Soc. 456 (1) (2016) 207–222, arXiv:1506.08730 [astro-ph.CO].
[1016] DES Collaboration, S. Samuroff, et al., Dark energy survey year 1 results: constraints on intrinsic alignments and their colour dependence from galaxy clustering and weak lensing, Mon. Not. R. Astron. Soc. 489 (4) (2019) 5453–5482, arXiv:1811.06989 [astro-ph.CO].
[1017] DES Collaboration, J. Muir, et al., Blinding multiprobe cosmological experiments, Mon. Not. R. Astron. Soc. 494 (3) (2020) 4454–4470, arXiv:1911.05929 [astro-ph.CO].
[1018] S.W. Allen, A.E. Evrard, A.B. Mantz, Cosmological parameters from observations of galaxy clusters, Ann. Rev. Astron. Astrophys. 49 (2011) 409–470, arXiv:1103.4829 [astro-ph.CO].
[1019] W.H. Press, P. Schechter, Formation of galaxies and clusters of galaxies by selfsimilar gravitational condensation, Astrophys. J. 187 (1974) 425–438.
[1020] R.K. Sheth, G. Tormen, Large scale bias and the peak background split, Mon. Not. R. Astron. Soc. 308 (1999) 119, arXiv:astro-ph/9901122.
[1021] A. Jenkins, C.S. Frenk, S.D.M. White, J.M. Colberg, S. Cole, A.E. Evrard, H.M.P. Couchman, N. Yoshida, The Mass function of dark matter halos, Mon. Not. R. Astron. Soc. 321 (2001) 372, arXiv:astro-ph/0005260.
[1022] J.L. Tinker, A.V. Kravtsov, A. Klypin, K. Abazajian, M.S. Warren, G. Yepes, S. Gottlober, D.E. Holz, Toward a halo mass function for precision cosmology: The Limits of universality, Astrophys. J. 688 (2008) 709–728, arXiv:0803.2706 [astro-ph].
[1023] W.A. Watson, I.T. Iliev, A. D'Aloisio, A. Knebe, P.R. Shapiro, G. Yepes, The halo mass function through the cosmic ages, Mon. Not. R. Astron. Soc. 433 (2013) 1230, arXiv:1212.0095 [astro-ph.CO].
[1024] G. Despali, C. Giocoli, R.E. Angulo, G. Tormen, R.K. Sheth, G. Baso, L. Moscardini, The universality of the virial halo mass function and models for non-universality of other halo definitions, Mon. Not. R. Astron. Soc. 456 (3) (2016) 2486–2504, arXiv:1507.05627 [astro-ph.CO].

[1025] N. Kaiser, Evolution and clustering of rich clusters, Mon. Not. R. Astron. Soc. 222 (1986) 323–345.
[1026] N. Truong, et al., Cosmological hydrodynamical simulations of galaxy clusters: X-ray scaling relations and their evolution, Mon. Not. R. Astron. Soc. 474 (3) (2018) 4089–4111, arXiv:1607.00019 [astro-ph.CO].
[1027] A.-R. Pop, et al., Sunyaev-Zel'dovich effect and X-ray scaling relations of galaxies, groups and clusters in the IllustrisTNG simulations, 2022, arXiv:2205.11528 [astro-ph.GA].
[1028] A. Pellissier, O. Hahn, C. Ferrari, Rhapsody-C simulations – Anisotropic thermal conduction, black hole physics, and the robustness of massive galaxy cluster scaling relations, Mon. Not. R. Astron. Soc. 522 (1) (2023) 721–749, arXiv:2301.02684 [astro-ph.CO].
[1029] J. Braspenning, et al., The FLAMINGO project: galaxy clusters in comparison to X-ray observations, Mon. Not. R. Astron. Soc. 533 (3) (2024) 2656–2676, arXiv:2312.08277 [astro-ph.GA].
[1030] A.B. Mantz, et al., Weighing the giants – IV. Cosmology and neutrino mass, Mon. Not. R. Astron. Soc. 446 (2015) 2205–2225, arXiv:1407.4516 [astro-ph.CO].
[1031] SPT Collaboration, S. Bocquet, et al., Mass calibration and cosmological analysis of the SPT-SZ galaxy cluster sample using velocity dispersion σ_v and X-ray Y_X measurements, Astrophys. J. 799 (2) (2015) 214, arXiv:1407.2942 [astro-ph.CO].
[1032] SPT Collaboration, S. Bocquet, et al., Cluster cosmology constraints from the 2500 deg^2 SPT-SZ survey: inclusion of weak gravitational lensing data from magellan and the hubble space telescope, Astrophys. J. 878 (1) (2019) 55, arXiv:1812.01679 [astro-ph.CO].
[1033] I.-N. Chiu, M. Klein, J. Mohr, S. Bocquet, Cosmological constraints from galaxy clusters and groups in the eROSITA final equatorial depth survey, Mon. Not. R. Astron. Soc. 522 (2) (2023) 1601–1642, arXiv:2207.12429 [astro-ph.CO].
[1034] DES, SPT Collaboration, S. Bocquet, et al., SPT clusters with DES and HST weak lensing. I. Cluster lensing and Bayesian population modeling of multiwavelength cluster datasets, Phys. Rev. D 110 (8) (2024) 083509, arXiv:2310.12213 [astro-ph.CO].
[1035] SPT, DES Collaboration, S. Bocquet, et al., SPT clusters with DES and HST weak lensing. II. Cosmological constraints from the abundance of massive halos, Phys. Rev. D 110 (8) (2024) 083510, arXiv:2401.02075 [astro-ph.CO].
[1036] V. Ghirardini, et al., The SRG/eROSITA all-sky survey: Cosmology constraints from cluster abundances in the western Galactic hemisphere, Astron. Astrophys. 689 (2024) A298, arXiv:2402.08458 [astro-ph.CO].
[1037] XXL Collaboration, F. Pacaud, et al., The XXL Survey: XXV. Cosmological analysis of the C1 cluster number counts, Astron. Astrophys. 620 (2018) A10, arXiv:1810.01624 [astro-ph.CO].
[1038] DES Collaboration, M. Costanzi, et al., Modelling projection effects in optically selected cluster catalogues, Mon. Not. R. Astron. Soc. 482 (1) (2019) 490–505, arXiv:1807.07072 [astro-ph.CO].
[1039] DES Collaboration, T.M.C. Abbott, et al., Dark Energy Survey Year 1 Results: Cosmological constraints from cluster abundances and weak lensing, Phys. Rev. D 102 (2) (2020) 023509, arXiv:2002.11124 [astro-ph.CO].
[1040] DES Collaboration, C. To, et al., Dark energy survey year 1 results: cosmological constraints from cluster abundances, weak lensing, and galaxy correlations, Phys. Rev. Lett. 126 (2021) 141301, arXiv:2010.01138 [astro-ph.CO].
[1041] C. Garrel, et al., The XXL survey - XLVI. Forward cosmological analysis of the C1 cluster sample, Astron. Astrophys. 663 (2022) A3, arXiv:2109.13171 [astro-ph.CO].
[1042] G.F. Lesci, et al., AMICO galaxy clusters in KiDS-DR3: Cosmological constraints from counts and stacked weak lensing, Astron. Astrophys. 659 (2022) A88, arXiv:2012.12273 [astro-ph.CO].
[1043] Y. Park, T. Sunayama, M. Takada, Y. Kobayashi, H. Miyatake, S. More, T. Nishimichi, S. Sugiyama, Cluster cosmology with anisotropic boosts: validation of a novel forward modelling analysis and application on SDSS redMaPPer clusters, Mon. Not. R. Astron. Soc. 518 (4) (2022) 5171–5189, arXiv:2112.09059 [astro-ph.CO].
[1044] T. Sunayama, et al., Optical cluster cosmology with SDSS redMaPPer clusters and HSC-Y3 lensing measurements, Phys. Rev. D 110 (8) (2024) 083511, arXiv:2309.13025 [astro-ph.CO].
[1045] W. Voges, et al., The ROSAT all - sky survey bright source catalogue, Astron. Astrophys. 349 (1999) 389, arXiv:astro-ph/9909315.
[1046] S. Borgani, P. Rosati, P. Tozzi, C. Norman, Cosmological constraints from the rosat deep cluster survey, Astrophys. J. 517 (1999) 40, arXiv:astro-ph/9901017.
[1047] R. Piffaretti, M. Arnaud, G.W. Pratt, E. Pointecouteau, J.B. Melin, The MCXC: a Meta-Catalogue of X-ray detected Clusters of galaxies, Astron. Astrophys. 534 (2011) A109, arXiv:1007.1916 [astro-ph.CO].
[1048] S. Borgani, P. Rosati, P. Tozzi, S.A. Stanford, P.E. Eisenhardt, C. Lidman, B. Holden, R. Della Ceca, C. Norman, G. Squires, Measuring omega_m with the rosat deep cluster survey, Astrophys. J. 561 (2001) 13–21, arXiv:astro-ph/0106428.
[1049] H. Bohringer, et al., The representative XMM-newton cluster structure survey (REXCESS) of an X-ray luminosity selected galaxy cluster sample, Astron. Astrophys. 469 (2007) 363–377, arXiv:astro-ph/0703553.
[1050] T.H. Reiprich, H. Boehringer, The Mass function of an X-ray flux-limited sample of galaxy clusters, Astrophys. J. 567 (2002) 716–740, arXiv:astro-ph/0111285.
[1051] G. Schellenberger, T.H. Reiprich, HICOSMO – cosmology with a complete sample of galaxy clusters – I. Data analysis, sample selection and luminosity–mass scaling relation, Mon. Not. R. Astron. Soc. 469 (3) (2017) 3738–3761, arXiv:1705.05842 [astro-ph.CO].
[1052] A. Vikhlinin, et al., Chandra cluster cosmology project III: cosmological parameter constraints, Astrophys. J. 692 (2009) 1060–1074, arXiv:0812.2720 [astro-ph].
[1053] M. Pierre, et al., The XXL Survey - I. Scientific motivations – XMM-Newton observing plan – Follow-up observations and simulation programme, Astron. Astrophys. 592 (2016) A1, arXiv:1512.04317 [astro-ph.CO].
[1054] R.A. Sunyaev, Y.B. Zeldovich, The Observations of relic radiation as a test of the nature of X-Ray radiation from the clusters of galaxies, Comments Astrophys. Space Phys. 4 (1972) 173–178.
[1055] T. Mroczkowski, et al., Astrophysics with the spatially and spectrally resolved sunyaev-zeldovich effects: a millimetre/submillimetre probe of the warm and hot universe, Space Sci. Rev. 215 (1) (2019) 17, arXiv:1811.02310 [astro-ph.CO].
[1056] A.V. Kravtsov, A. Vikhlinin, D. Nagai, A new robust low-scatter x-ray mass indicator for clusters of galaxies, Astrophys. J. 650 (2006) 128–136, arXiv:astro-ph/0603205.
[1057] D. Nagai, A.V. Kravtsov, A. Vikhlinin, Effects of galaxy formation on thermodynamics of the intracluster medium, Astrophys. J. 668 (2007) 1–14, arXiv:astro-ph/0703661.
[1058] M. Arnaud, E. Pointecouteau, G.W. Pratt, Calibration of the galaxy cluster M_500-Y_X relation with XMM-Newton, Astron. Astrophys. 474 (2007) L37, arXiv:0709.1561 [astro-ph].
[1059] D.P. Marrone, et al., LoCuSS: the Sunyaev-Zel'dovich effect and weak lensing mass scaling relation, Astrophys. J. 754 (2012) 119, arXiv:1107.5115 [astro-ph.CO].
[1060] Planck Collaboration, P.A.R. Ade, et al., Planck Early Results XI: Calibration of the local galaxy cluster Sunyaev-Zeldovich scaling relations, Astron. Astrophys. 536 (2011) A11, arXiv:1101.2026 [astro-ph.CO].
[1061] Planck Collaboration, P.A.R. Ade, et al., Planck 2013 results. XXIX. The Planck catalogue of Sunyaev-Zeldovich sources, Astron. Astrophys. 571 (2014) A29, arXiv:1303.5089 [astro-ph.CO].
[1062] R. Williamson, et al., An SZ-selected sample of the most massive galaxy clusters in the 2500-square-degree South Pole Telescope survey, Astrophys. J. 738 (2011) 139, arXiv:1101.1290 [astro-ph.CO].
[1063] SPT Collaboration, L.E. Bleem, et al., Galaxy Clusters Discovered via the Sunyaev-Zel'dovich Effect in the 2500-square-degree SPT-SZ survey, Astrophys. J. Suppl. 216 (2) (2015) 27, arXiv:1409.0850 [astro-ph.CO].
[1064] SPT, DES Collaboration, L.E. Bleem, et al., Galaxy clusters discovered via the thermal Sunyaev-Zel'dovich effect in the 500-square-degree SPTpol survey, Open J. Astrophys. 7 (2024) astro.2311.07512, arXiv:2311.07512 [astro-ph.CO].
[1065] M. Hasselfield, et al., The Atacama Cosmology Telescope: Sunyaev-Zel'dovich selected galaxyclusters at 148 GHz from three seasons of data, J. Cosmol. Astropart. Phys. 07 (2013) 008, arXiv:1301.0816 [astro-ph.CO].
[1066] ACT, DES Collaboration, M. Hilton, et al., The atacama cosmology telescope: a catalog of >4000 Sunyaev–Zel'dovich galaxy clusters, Astrophys. J. Suppl. 253 (1) (2021) 3, arXiv:2009.11043 [astro-ph.CO].
[1067] G.O. Abell, H.G. Corwin Jr., R.P. Olowin, A Catalog of rich clusters of galaxies, Astrophys. J. Suppl. 70 (1989) 1.
[1068] SDSS Collaboration, B. Koester, et al., A MaxBCG catalog of 13,823 galaxy clusters from the sloan digital sky survey, Astrophys. J. 660 (2007) 239–255, arXiv:astro-ph/0701265.
[1069] SDSS Collaboration, E.S. Rykoff, et al., REDMAPPER I: algorithm and SDSS DR8 catalog, Astrophys. J. 785 (2014) 104, arXiv:1303.3562 [astro-ph.CO].
[1070] M. Oguri, A cluster finding algorithm based on the multiband identification of red sequence galaxies, Mon. Not. R. Astron. Soc. 444 (1) (2014) 147–161, arXiv:1407.4693 [astro-ph.CO].
[1071] C.P. Haines, et al., LoCuSS: The slow quenching of star formation in cluster galaxies and the need for pre-processing, Astrophys. J. 806 (1) (2015) 101, arXiv:1504.05604 [astro-ph.GA].
[1072] P.A.A. Lopes, A.L.B. Ribeiro, S.B. Rembold, NoSOCS in SDSS – IV. The role of environment beyond the extent of galaxy clusters, Mon. Not. R. Astron. Soc. 437 (3) (2014) 2430–2447, arXiv:1310.6309 [astro-ph.CO].
[1073] F. Sarron, N. Martinet, F. Durret, C. Adami, Evolution of the cluster optical galaxy luminosity function in the CFHTLS : breaking the degeneracy between mass and redshift, Astron. Astrophys. 613 (2018) A67, arXiv:1712.09481 [astro-ph.GA].
[1074] Euclid Collaboration, R. Adam, et al., Euclid preparation. III. Galaxy cluster detection in the wide photometric survey, performance and algorithm selection, Astron. Astrophys. 627 (627) (2019) A23, arXiv:1906.04707 [astro-ph.CO].
[1075] DES Collaboration, M. Costanzi, et al., Methods for cluster cosmology and application to the SDSS in preparation for DES Year 1 release, Mon. Not. R. Astron. Soc. 488 (4) (2019) 4779–4800, arXiv:1810.09456 [astro-ph.CO].

[1076] Z.L. Wen, J.L. Han, Clusters of galaxies up to z=1.5 identified from photometric data of the Dark Energy Survey and unWISE, Mon. Not. R. Astron. Soc. 513 (3) (2022) 3946–3959, arXiv:2204.11215 [astro-ph.CO].
[1077] M. Maturi, F. Bellagamba, M. Radovich, M. Roncarelli, M. Sereno, L. Moscardini, S. Bardelli, E. Puddu, AMICO galaxy clusters in KiDS-DR3: sample properties and selection function, Mon. Not. R. Astron. Soc. 485 (2019) 498, arXiv:1810.02811 [astro-ph.CO].
[1078] M. Oguri, et al., An optically-selected cluster catalog at redshift 0.1< z< 1.1 from the Hyper Suprime-Cam Subaru Strategic Program S16A data, Publ. Astron. Soc. Jap. 70 (2018) S20, arXiv:1701.00818 [astro-ph.CO].
[1079] Z.L. Wen, J.L. Han, A catalog of 1.58 million clusters of galaxies identified from the DESI legacy imaging surveys, Astrophys. J. Suppl. 272 (2) (2024) 39, arXiv:2404.02002 [astro-ph.CO].
[1080] M. Simet, T. McClintock, R. Mandelbaum, E. Rozo, E. Rykoff, E. Sheldon, R.H. Wechsler, Weak lensing measurement of the mass–richness relation of SDSS redMaPPer clusters, Mon. Not. R. Astron. Soc. 466 (3) (2017) 3103–3118, arXiv:1603.06953 [astro-ph.CO].
[1081] DES Collaboration, T. McClintock, et al., Dark energy survey year 1 results: weak lensing mass calibration of redMaPPer galaxy clusters, Mon. Not. R. Astron. Soc. 482 (1) (2019) 1352–1378, arXiv:1805.00039 [astro-ph.CO].
[1082] C. Ge, M. Sun, E. Rozo, N. Sehgal, A. Vikhlinin, W. Forman, C. Jones, D. Nagai, X-ray scaling relations from a complete sample of the richest maxBCG clusters, Mon. Not. R. Astron. Soc. 484 (2) (2019) 1946–1971, arXiv:1803.05007 [astro-ph.GA].
[1083] DES Collaboration, V. Wetzell, et al., Velocity dispersions of clusters in the Dark Energy Survey Y3 redMaPPer catalogue, Mon. Not. R. Astron. Soc. 514 (4) (2022) 4696–4717, arXiv:2107.07631 [astro-ph.CO].
[1084] S. Miyazaki, T. Hamana, R.S. Ellis, N. Kashikawa, R.J. Massey, J. Taylor, A. Refregier, A subaru weak lensing survey I: cluster candidates and spectroscopic verification, Astrophys. J. 669 (2007) 714, arXiv:0707.2249 [astro-ph].
[1085] S. Miyazaki, et al., A large sample of shear selected clusters from the Hyper Suprime-Cam Subaru Strategic Program S16A wide field mass maps, Publ. Astron. Soc. Jap. 70 (2018) S27, arXiv:1802.10290 [astro-ph.CO].
[1086] K.-F. Chen, et al., Weak-lensing shear-selected galaxy clusters from the hyper suprime-cam subaru strategic program: I. Cluster catalog, selection function and mass–observable relation, 2024, arXiv:2406.11966 [astro-ph.CO].
[1087] G. Leroy, S. Pires, G.W. Pratt, C. Giocoli, Fast multi-scale galaxy cluster detection with weak lensing: Towards a mass-selected sample, Astron. Astrophys. 678 (2023) A125, arXiv:2304.01812 [astro-ph.CO].
[1088] M.E. Ramos-Ceja, et al., The eROSITA Final Equatorial-Depth Survey (eFEDS) - A complete census of X-ray properties of Subaru Hyper Suprime-Cam weak lensing shear-selected clusters in the eFEDS footprint, Astron. Astrophys. 661 (2022) A14, arXiv:2109.07836 [astro-ph.CO].
[1089] I.-N. Chiu, et al., Weak-lensing shear-selected galaxy clusters from the hyper suprime-cam subaru strategic program: II. Cosmological constraints from the cluster abundance, 2024, arXiv:2406.11970 [astro-ph.CO].
[1090] K.-F. Chen, M. Oguri, Y.-T. Lin, S. Miyazaki, Mass bias of weak lensing shear-selected galaxy cluster samples, Astrophys. J. 891 (2) (2020) 139, arXiv:1911.11480 [astro-ph.GA].
[1091] K. Umetsu, Cluster–galaxy weak lensing, Astron. Astrophys. Rev. 28 (1) (2020) 7, arXiv:2007.00506 [astro-ph.CO].
[1092] DES Collaboration, H.-Y. Wu, et al., Optical selection bias and projection effects in stacked galaxy cluster weak lensing, Mon. Not. R. Astron. Soc. 515 (3) (2022) 4471–4486, arXiv:2203.05416 [astro-ph.CO].
[1093] DES, eROSITA-DE Collaboration, S. Grandis, et al., The SRG/eROSITA All-Sky Survey - Dark Energy Survey year 3 weak gravitational lensing by eRASS1 selected galaxy clusters, Astron. Astrophys. 687 (2024) A178, arXiv:2402.08455 [astro-ph.CO].
[1094] H. Hoekstra, How well can we determine cluster mass profiles from weak lensing? Mon. Not. R. Astron. Soc. 339 (2003) 1155, arXiv:astro-ph/0208351.
[1095] D. Gruen, S. Seitz, M.R. Becker, O. Friedrich, A. Mana, Cosmic variance of the galaxy cluster weak lensing signal, Mon. Not. R. Astron. Soc. 449 (4) (2015) 4264–4276, arXiv:1501.01632 [astro-ph.CO].
[1096] D.E. Applegate, A. von der Linden, P.L. Kelly, M.T. Allen, S.W. Allen, P.R. Burchat, D.L. Burke, H. Ebeling, A. Mantz, R.G. Morris, Weighing the Giants – III. Methods and measurements of accurate galaxy cluster weak-lensing masses, Mon. Not. R. Astron. Soc. 439 (1) (2014) 48–72, arXiv:1208.0605 [astro-ph.CO].
[1097] SPT Collaboration, J.P. Dietrich, et al., Sunyaev–Zel'dovich effect and X-ray scaling relations from weak lensing mass calibration of 32 South Pole Telescope selected galaxy clusters, Mon. Not. R. Astron. Soc. 483 (3) (2019) 2871–2906, arXiv:1711.05344 [astro-ph.CO].
[1098] S. Grandis, S. Bocquet, J.J. Mohr, M. Klein, K. Dolag, Calibration of bias and scatter involved in cluster mass measurements using optical weak gravitational lensing, Mon. Not. R. Astron. Soc. 507 (4) (2021) 5671–5689, arXiv:2103.16212 [astro-ph.CO].
[1099] M.R. Becker, A.V. Kravtsov, On the accuracy of weak lensing cluster mass reconstructions, Astrophys. J. 740 (2011) 25, arXiv:1011.1681 [astro-ph.CO].
[1100] Y.M. Bahe, I.G. McCarthy, L.J. King, Mock weak lensing analysis of simulated galaxy clusters: bias and scatter in mass and concentration, Mon. Not. R. Astron. Soc. 421 (2012) 1073–1088, arXiv:1106.2046 [astro-ph.CO].
[1101] Euclid Collaboration, C. Giocoli, et al., Euclid preparation - XXXII. Evaluating the weak-lensing cluster mass biases using the Three Hundred Project hydrodynamical simulations, Astron. Astrophys. 681 (2024) A67, arXiv:2302.00687 [astro-ph.CO].
[1102] I.-N. Chiu, et al., The eROSITA Final Equatorial-Depth Survey (eFEDS) - X-ray observable-to-mass-and-redshift relations of galaxy clusters and groups with weak-lensing mass calibration from the Hyper Suprime-Cam Subaru Strategic Program survey, Astron. Astrophys. 661 (2022) A11, arXiv:2107.05652 [astro-ph.CO].
[1103] F. Kleinebreil, et al., The SRG/eROSITA All-Sky Survey - Weak lensing of eRASS1 galaxy clusters in KiDS-1000 and consistency checks with DES Y3 and HSC-Y3, Astron. Astrophys. 695 (2025) A216, arXiv:2402.08456 [astro-ph.CO].
[1104] F. Bellagamba, et al., AMICO galaxy clusters in KiDS-DR3: weak-lensing mass calibration, Mon. Not. R. Astron. Soc. 484 (2) (2019) 1598–1615, arXiv:1810.02827 [astro-ph.CO].
[1105] W. Cui, S. Borgani, K. Dolag, G. Murante, L. Tornatore, The effects of baryons on the halo mass function, Mon. Not. R. Astron. Soc. 423 (2012) 2279, arXiv:1111.3066 [astro-ph.CO].
[1106] S. Bocquet, A. Saro, K. Dolag, J.J. Mohr, Halo mass function: Baryon impact, fitting formulae and implications for cluster cosmology, Mon. Not. R. Astron. Soc. 456 (3) (2016) 2361–2373, arXiv:1502.07357 [astro-ph.CO].
[1107] T. Castro, S. Borgani, K. Dolag, V. Marra, M. Quartin, A. Saro, E. Sefusatti, On the impact of baryons on the halo mass function, bias, and cluster cosmology, Mon. Not. R. Astron. Soc. 500 (2) (2020) 2316–2335, arXiv:2009.01775 [astro-ph.CO].
[1108] DES, SPT Collaboration, M. Costanzi, et al., Cosmological constraints from DES Y1 cluster abundances and SPT multiwavelength data, Phys. Rev. D 103 (4) (2021) 043522, arXiv:2010.13800 [astro-ph.CO].
[1109] C.T. Mpetha, et al., Cosmology from UNIONS weak lensing profiles of galaxy clusters, 2025, arXiv:2501.09147 [astro-ph.CO].
[1110] SPT Collaboration, A.B. Mantz, et al., Cosmological constraints from gas mass fractions of massive, relaxed galaxy clusters, Mon. Not. R. Astron. Soc. 510 (1) (2021) 131–145, arXiv:2111.09343 [astro-ph.CO].
[1111] F. Schmidt, Cosmological simulations of normal-branch braneworld gravity, Phys. Rev. D 80 (2009) 123003, arXiv:0910.0235 [astro-ph.CO].
[1112] M. Kopp, S.A. Appleby, I. Achitouv, J. Weller, Spherical collapse and halo mass function in $f(R)$ theories, Phys. Rev. D 88 (8) (2013) 084015, arXiv:1306.3233 [astro-ph.CO].
[1113] S. Hagstotz, M. Costanzi, M. Baldi, J. Weller, Joint halo-mass function for modified gravity and massive neutrinos – I. Simulations and cosmological forecasts, Mon. Not. R. Astron. Soc. 486 (3) (2019) 3927–3941, arXiv:1806.07400 [astro-ph.CO].
[1114] S. Gupta, W.A. Hellwing, M. Bilicki, J.E. García-Farieta, Universality of the halo mass function in modified gravity cosmologies, Phys. Rev. D 105 (4) (2022) 043538, arXiv:2112.03699 [astro-ph.CO].
[1115] M. Sereno, A. Veropalumbo, F. Marulli, G. Covone, L. Moscardini, A. Cimatti, New constraints on $\sigma 8$ from a joint analysis of stacked gravitational lensing and clustering of galaxy clusters, Mon. Not. R. Astron. Soc. 449 (4) (2015) 4147–4161, arXiv:1410.5438 [astro-ph.CO].
[1116] F. Marulli, A. Veropalumbo, J.E. García-Farieta, M. Moresco, L. Moscardini, A. Cimatti, C3 cluster clustering cosmology I. New constraints on the cosmic growth rate at z ∼ 0.3 from redshift-space clustering anisotropies, Astrophys. J. 920 (1) (2021) 13, arXiv:2010.11206 [astro-ph.CO].
[1117] G.F. Lesci, et al., AMICO galaxy clusters in KiDS-DR3: Constraints on cosmological parameters and on the normalisation of the mass-richness relation from clustering, Astron. Astrophys. 665 (2022) A100, arXiv:2203.07398 [astro-ph.CO].
[1118] M. Romanello, et al., AMICO galaxy clusters in KiDS-DR3: Cosmological constraints from the angular power spectrum and correlation function, Astron. Astrophys. 682 (2024) A72, arXiv:2310.12224 [astro-ph.CO].
[1119] M.C.A. Cerbolini, B. Sartoris, J.-Q. Xia, A. Biviano, S. Borgani, M. Viel, Constraining neutrino properties with a Euclid-like galaxy cluster survey, J. Cosmol. Astropart. Phys. 06 (2013) 020, arXiv:1303.4550 [astro-ph.CO].
[1120] B. Sartoris, et al., Next generation cosmology: constraints from the euclid galaxy cluster survey, Mon. Not. R. Astron. Soc. 459 (2) (2016) 1764–1780, arXiv:1505.02165 [astro-ph.CO].
[1121] L. Moscardini, S. Matarrese, H.J. Mo, Constraining cosmological parameters with the clustering properties of galaxy clusters in optical and x-ray bands, Mon. Not. R. Astron. Soc. 327 (2001) 422, arXiv:astro-ph/0009006.
[1122] R.K. Sheth, H.J. Mo, G. Tormen, Ellipsoidal collapse and an improved model for the number and spatial distribution of dark matter haloes, Mon. Not. R. Astron. Soc. 323 (2001) 1, arXiv:astro-ph/9907024.
[1123] E. Branchini, S. Camera, A. Cuoco, N. Fornengo, M. Regis, M. Viel, J.-Q. Xia, Cross-correlating the γ-ray sky with catalogs of galaxy clusters, Astrophys. J. Suppl. 228 (1) (2017) 8, arXiv:1612.05788 [astro-ph.CO].
[1124] K. Paech, N. Hamaus, B. Hoyle, M. Costanzi, T. Giannantonio, S. Hagstotz, G. Sauerwein, J. Weller, Cross-correlation of galaxies and galaxy clusters in the Sloan Digital Sky Survey and the importance of non-Poissonian shot noise, Mon. Not. R. Astron. Soc. 470 (3) (2017) 2566–2577, arXiv:1612.02018 [astro-ph.CO].

[1125] J.L. Tinker, B.E. Robertson, A.V. Kravtsov, A. Klypin, M.S. Warren, G. Yepes, S. Gottlober, The large scale bias of dark matter halos: numerical calibration and model tests, Astrophys. J. 724 (2010) 878–886, arXiv:1001.3162 [astro-ph.CO].
[1126] N. Okabe, Y.-Y. Zhang, A. Finoguenov, M. Takada, G.P. Smith, K. Umetsu, T. Futamase, LoCuSS: calibrating mass-observables scaling relations for cluster cosmology with subaru weak lensing observations, Astrophys. J. 721 (2010) 875–885, arXiv:1007.3816 [astro-ph.CO].
[1127] S. Giodini, L. Lovisari, E. Pointecouteau, S. Ettori, T.H. Reiprich, H. Hoekstra, Scaling relations for galaxy clusters: properties and evolution, Space Sci. Rev. 177 (2013) 247–282, arXiv:1305.3286 [astro-ph.CO].
[1128] A. Veropalumbo, F. Marulli, L. Moscardini, M. Moresco, A. Cimatti, An improved measurement of baryon acoustic oscillations from the correlation function of galaxy clusters at z ∼ 0.3, Mon. Not. R. Astron. Soc. 442 (4) (2014) 3275–3283, arXiv:1311.5895 [astro-ph.CO].
[1129] F. Marulli, A. Veropalumbo, L. Moscardini, A. Cimatti, K. Dolag, Redshift-space distortions of galaxies, clusters and AGN: testing how the accuracy of growth rate measurements depends on scales and sample selections, Astron. Astrophys. 599 (2017) A106, arXiv:1505.01170 [astro-ph.CO].
[1130] M. Moresco, A. Veropalumbo, F. Marulli, L. Moscardini, A. Cimatti, C3: cluster clustering cosmology. II. First detection of the baryon acoustic oscillations peak in the three-point correlation function of galaxy clusters, Astrophys. J. 919 (2) (2021) 144, arXiv:2011.04665 [astro-ph.CO].
[1131] C. Alcock, B. Paczynski, An evolution free test for non-zero cosmological constant, Nature 281 (1979) 358–359.
[1132] F. Marulli, D. Bianchi, E. Branchini, L. Guzzo, L. Moscardini, R.E. Angulo, Cosmology with clustering anisotropies: disentangling dynamic and geometric distortions in galaxy redshift surveys, Mon. Not. R. Astron. Soc. 426 (2012) 2566, arXiv:1203.1002 [astro-ph.CO].
[1133] BOSS Collaboration, F. Beutler, et al., The clustering of galaxies in the SDSS-III Baryon Oscillation Spectroscopic Survey: Testing gravity with redshift-space distortions using the power spectrum multipoles, Mon. Not. R. Astron. Soc. 443 (2) (2014) 1065–1089, arXiv:1312.4611 [astro-ph.CO].
[1134] F. Marulli, et al., The XXL Survey: XVI. The clustering of X-ray selected galaxy clusters at z˜0.3, Astron. Astrophys. 620 (2018) A1, arXiv:1807.04760 [astro-ph.CO].
[1135] A. Veropalumbo, F. Marulli, L. Moscardini, M. Moresco, A. Cimatti, Measuring the distance–redshift relation with the baryon acoustic oscillations of galaxy clusters, Mon. Not. R. Astron. Soc. 458 (2) (2016) 1909–1920, arXiv:1510.08852 [astro-ph.CO].
[1136] G.F. Lesci, A. Veropalumbo, M. Sereno, F. Marulli, L. Moscardini, C. Giocoli, Mass bias and cosmological constraints from Planck cluster clustering, Astron. Astrophys. 674 (2023) A80, arXiv:2302.14074 [astro-ph.CO].
[1137] V. Lindholm, A. Finoguenov, J. Comparat, C.C. Kirkpatrick, E. Rykoff, N. Clerc, C. Collins, S. Damsted, J.I. Chitham, N. Padilla, Clustering of CODEX clusters, Astron. Astrophys. 646 (2021) A8, arXiv:2012.00090 [astro-ph.CO].
[1138] P.J.E. Peebles, Statistical analysis of catalogs of extragalactic objects. I. Theory, Astrophys. J. 185 (1973) 413–440.
[1139] eBOSS Collaboration, A. Tamone, et al., The Completed SDSS-IV extended Baryon Oscillation Spectroscopic Survey: Growth rate of structure measurement from anisotropic clustering analysis in configuration space between redshift 0.6 and 1.1 for the Emission Line Galaxy sample, Mon. Not. R. Astron. Soc. 499 (4) (2020) 5527–5546, arXiv:2007.09009 [astro-ph.CO].
[1140] Z. Li, Y.P. Jing, P. Zhang, D. Cheng, Measurement of redshift-space power spectrum for BOSS galaxies and the growth rate at redshift 0.57, Astrophys. J. 833 (2) (2016) 287, arXiv:1609.03697 [astro-ph.CO].
[1141] S. Alam, S. Ho, M. Vargas-Magaña, D.P. Schneider, Testing general relativity with growth rate measurement from Sloan Digital Sky Survey – III. Baryon Oscillations Spectroscopic Survey galaxies, Mon. Not. R. Astron. Soc. 453 (2) (2015) 1754–1767, arXiv:1504.02100 [astro-ph.CO].
[1142] ACT Collaboration, G.S. Farren, et al., The atacama cosmology telescope: cosmology from cross-correlations of unWISE galaxies and ACT DR6 CMB lensing, Astrophys. J. 966 (2) (2024) 157, arXiv:2309.05659 [astro-ph.CO].
[1143] G. Piccirilli, G. Fabbian, D. Alonso, K. Storey-Fisher, J. Carron, A. Lewis, C. García-García, Growth history and quasar bias evolution at z < 3 from Quaia, J. Cosmol. Astropart. Phys. 06 (2024) 012, arXiv:2402.05761 [astro-ph.CO].
[1144] D. Alonso, G. Fabbian, K. Storey-Fisher, A.-C. Eilers, C. García-García, D.W. Hogg, H.-W. Rix, Constraining cosmology with the Gaia-unWISE Quasar Catalog and CMB lensing: structure growth, J. Cosmol. Astropart. Phys. 11 (2023) 043, arXiv:2306.17748 [astro-ph.CO].
[1145] BOSS Collaboration, S. Alam, et al., The clustering of galaxies in the completed SDSS-III Baryon Oscillation Spectroscopic Survey: cosmological analysis of the DR12 galaxy sample, Mon. Not. R. Astron. Soc. 470 (3) (2017) 2617–2652, arXiv:1607.03155 [astro-ph.CO].
[1146] DESI Collaboration, A. Dey, et al., Overview of the DESI legacy imaging surveys, Astron. J. 157 (5) (2019) 168, arXiv:1804.08657 [astro-ph.IM].
[1147] C.S. Saraf, P. Bielewicz, M. Chodorowski, Effect of redshift bin mismatch on the cross correlation between the DESI Legacy Imaging Survey and the Planck CMB lensing potential, Astron. Astrophys. 690 (2024) A338, arXiv:2406.02857 [astro-ph.CO].
[1148] S.J. Nakoneczny, et al., Cosmology from LOFAR Two-metre Sky Survey Data Release 2: Cross-correlation with the cosmic microwave background, Astron. Astrophys. 681 (2024) A105, arXiv:2310.07642 [astro-ph.CO]; Astron. Astrophys. 686 (2024) C2 (erratum).
[1149] DES, SPT Collaboration, C. Chang, et al., Joint analysis of Dark Energy Survey Year 3 data and CMB lensing from SPT and Planck. II. Cross-correlation measurements and cosmological constraints, Phys. Rev. D 107 (2) (2023) 023530, arXiv:2203.12440 [astro-ph.CO].
[1150] M. White, et al., Cosmological constraints from the tomographic cross-correlation of DESI Luminous Red Galaxies and Planck CMB lensing, J. Cosmol. Astropart. Phys. 02 (02) (2022) 007, arXiv:2111.09898 [astro-ph.CO].
[1151] Z. Sun, J. Yao, F. Dong, X. Yang, L. Zhang, P. Zhang, Cross-correlation of Planck cosmic microwave background lensing with DESI galaxy groups, Mon. Not. R. Astron. Soc. 511 (3) (2022) 3548–3560, arXiv:2109.07387 [astro-ph.CO].
[1152] A. Krolewski, S. Ferraro, M. White, Cosmological constraints from unWISE and Planck CMB lensing tomography, J. Cosmol. Astropart. Phys. 12 (12) (2021) 028, arXiv:2105.03421 [astro-ph.CO].
[1153] Q. Hang, S. Alam, J.A. Peacock, Y.-C. Cai, Galaxy clustering in the DESI Legacy Survey and its imprint on the CMB, Mon. Not. R. Astron. Soc. 501 (1) (2021) 1481–1498, arXiv:2010.00466 [astro-ph.CO].
[1154] J.A. Peacock, M. Bilicki, Wide-area tomography of CMB lensing and the growth of cosmological density fluctuations, Mon. Not. R. Astron. Soc. 481 (1) (2018) 1133–1148, arXiv:1805.11525 [astro-ph.CO].
[1155] DES Collaboration, T. Giannantonio, et al., CMB lensing tomography with the DES Science Verification galaxies, Mon. Not. R. Astron. Soc. 456 (3) (2016) 3213–3244, arXiv:1507.05551 [astro-ph.CO].
[1156] N. Sailer, et al., Cosmological constraints from the cross-correlation of DESI Luminous Red Galaxies with CMB lensing from Planck PR4 and ACT DR6, 2024, arXiv:2407.04607 [astro-ph.CO].
[1157] C.S. Saraf, P. Bielewicz, Tomographic cross correlations between galaxy surveys and the CMB gravitational lensing potential - Effect of the redshift bin mismatch, Astron. Astrophys. 687 (2024) A150, arXiv:2311.15261 [astro-ph.CO].
[1158] T. Simon, P. Zhang, V. Poulin, Cosmological inference from the EFTofLSS: the eBOSS QSO full-shape analysis, J. Cosmol. Astropart. Phys. 07 (2023) 041, arXiv:2210.14931 [astro-ph.CO].
[1159] Y. Kobayashi, T. Nishimichi, M. Takada, H. Miyatake, Full-shape cosmology analysis of the SDSS-III BOSS galaxy power spectrum using an emulator-based halo model: A 5% determination of $\sigma 8$, Phys. Rev. D 105 (8) (2022) 083517, arXiv:2110.06969 [astro-ph.CO].
[1160] S.-F. Chen, Z. Vlah, M. White, A new analysis of galaxy 2-point functions in the BOSS survey, including full-shape information and post-reconstruction BAO, J. Cosmol. Astropart. Phys. 02 (02) (2022) 008, arXiv:2110.05530 [astro-ph.CO].
[1161] M.M. Ivanov, O.H.E. Philcox, G. Cabass, T. Nishimichi, M. Simonović, M. Zaldarriaga, Cosmology with the galaxy bispectrum multipoles: Optimal estimation and application to BOSS data, Phys. Rev. D 107 (8) (2023) 083515, arXiv:2302.04414 [astro-ph.CO].
[1162] O.H.E. Philcox, M.M. Ivanov, BOSS DR12 full-shape cosmology: ΛCDM constraints from the large-scale galaxy power spectrum and bispectrum monopole, Phys. Rev. D 105 (4) (2022) 043517, arXiv:2112.04515 [astro-ph.CO].
[1163] S. Joudaki, et al., KiDS-450 + 2dFLenS: Cosmological parameter constraints from weak gravitational lensing tomography and overlapping redshift-space galaxy clustering, Mon. Not. R. Astron. Soc. 474 (4) (2018) 4894–4924, arXiv:1707.06627 [astro-ph.CO].
[1164] E. van Uitert, et al., KiDS+GAMA: cosmology constraints from a joint analysis of cosmic shear, galaxy–galaxy lensing, and angular clustering, Mon. Not. R. Astron. Soc. 476 (4) (2018) 4662–4689, arXiv:1706.05004 [astro-ph.CO].
[1165] DES Collaboration, T.M.C. Abbott, et al., Dark Energy Survey year 1 results: Cosmological constraints from galaxy clustering and weak lensing, Phys. Rev. D 98 (4) (2018) 043526, arXiv:1708.01530 [astro-ph.CO].
[1166] BOSS Collaboration, A.J. Ross, et al., The clustering of galaxies in the SDSS-III baryon oscillation spectroscopic survey: analysis of potential systematics, Mon. Not. R. Astron. Soc. 424 (2012) 564, arXiv:1203.6499 [astro-ph.CO].
[1167] C. Hahn, R. Scoccimarro, M.R. Blanton, J.L. Tinker, S.A. Rodríguez-Torres, The effect of fibre collisions on the galaxy power spectrum multipoles, Mon. Not. R. Astron. Soc. 467 (2) (2017) 1940–1956, arXiv:1609.01714 [astro-ph.CO].
[1168] A. de Mattia, V. Ruhlmann-Kleider, Integral constraints in spectroscopic surveys, J. Cosmol. Astropart. Phys. 08 (2019) 036, arXiv:1904.08851 [astro-ph.CO].
[1169] C.S. Saraf, P. Bielewicz, M. Chodorowski, Cross-correlation between Planck CMB lensing potential and galaxy catalogues from HELP, Mon. Not. R. Astron. Soc. 515 (2) (2022) 1993–2007, arXiv:2106.02551 [astro-ph.CO].
[1170] A.R. Pullen, S. Alam, S. He, S. Ho, Constraining gravity at the largest scales through CMB lensing and galaxy velocities, Mon. Not. R. Astron. Soc. 460 (4) (2016) 4098–4108, arXiv:1511.04457 [astro-ph.CO].
[1171] S. Joudaki, et al., CFHTLenS revisited: assessing concordance with Planck including astrophysical systematics, Mon. Not. R. Astron. Soc. 465 (2) (2017) 2033–2052, arXiv:1601.05786 [astro-ph.CO].

[1172] M.M. Ivanov, M. Simonović, M. Zaldarriaga, Cosmological parameters from the BOSS galaxy power spectrum, J. Cosmol. Astropart. Phys. 05 (2020) 042, arXiv:1909.05277 [astro-ph.CO].
[1173] R. Gsponer, R. Zhao, J. Donald-McCann, D. Bacon, K. Koyama, R. Crittenden, T. Simon, E.-M. Mueller, Cosmological constraints on early dark energy from the full shape analysis of eBOSS DR16, Mon. Not. R. Astron. Soc. 530 (3) (2024) 3075–3099, arXiv:2312.01977 [astro-ph.CO].
[1174] S.-F. Chen, Z. Vlah, E. Castorina, M. White, Redshift-space distortions in lagrangian perturbation theory, J. Cosmol. Astropart. Phys. 03 (2021) 100, arXiv:2012.04636 [astro-ph.CO].
[1175] DESI Collaboration, S. Ramirez-Solano, et al., Full Modeling and parameter compression methods in configuration space for DESI 2024 and beyond, J. Cosmol. Astropart. Phys. 01 (2025) 129, arXiv:2404.07268 [astro-ph.CO].
[1176] M. Maus, et al., A comparison of effective field theory models of redshift space galaxy power spectra for DESI 2024 and future surveys, J. Cosmol. Astropart. Phys. 01 (2025) 134, arXiv:2404.07272 [astro-ph.CO].
[1177] D. Baumann, A. Nicolis, L. Senatore, M. Zaldarriaga, Cosmological non-linearities as an effective fluid, J. Cosmol. Astropart. Phys. 07 (2012) 051, arXiv:1004.2488 [astro-ph.CO].
[1178] J.J.M. Carrasco, M.P. Hertzberg, L. Senatore, The effective field theory of cosmological large scale structures, JHEP 09 (2012) 082, arXiv:1206.2926 [astro-ph.CO].
[1179] R.A. Porto, L. Senatore, M. Zaldarriaga, The lagrangian-space effective field theory of large scale structures, J. Cosmol. Astropart. Phys. 05 (2014) 022, arXiv:1311.2168 [astro-ph.CO].
[1180] M. Lewandowski, L. Senatore, F. Prada, C. Zhao, C.-H. Chuang, EFT of large scale structures in redshift space, Phys. Rev. D 97 (6) (2018) 063526, arXiv:1512.06831 [astro-ph.CO].
[1181] A. Lewis, A. Challinor, Weak gravitational lensing of the CMB, Phys. Rep. 429 (2006) 1–65, arXiv:astro-ph/0601594.
[1182] J. Carron, M. Mirmelstein, A. Lewis, CMB lensing from Planck PR4 maps, J. Cosmol. Astropart. Phys. 09 (2022) 039, arXiv:2206.07773 [astro-ph.CO].
[1183] ACT Collaboration, F.J. Qu, et al., The atacama cosmology telescope: a measurement of the DR6 CMB lensing power spectrum and its implications for structure growth, Astrophys. J. 962 (2) (2024) 112, arXiv:2304.05202 [astro-ph.CO].
[1184] SPT Collaboration, Z. Pan, et al., Measurement of gravitational lensing of the cosmic microwave background using SPT-3G 2018 data, Phys. Rev. D 108 (12) (2023) 122005, arXiv:2308.11608 [astro-ph.CO].
[1185] E. Di Valentino, A. Melchiorri, J. Silk, Planck evidence for a closed Universe and a possible crisis for cosmology, Nat. Astron. 4 (2) (2019) 196–203, arXiv:1911.02087 [astro-ph.CO].
[1186] W. Handley, Curvature tension: evidence for a closed universe, Phys. Rev. D 103 (4) (2021) L041301, arXiv:1908.09139 [astro-ph.CO].
[1187] G. Efstathiou, S. Gratton, The evidence for a spatially flat Universe, Mon. Not. R. Astron. Soc. 496 (1) (2020) L91–L95, arXiv:2002.06892 [astro-ph.CO].
[1188] A. Glanville, C. Howlett, T.M. Davis, Full-shape galaxy power spectra and the curvature tension, Mon. Not. R. Astron. Soc. 517 (2) (2022) 3087–3100, arXiv:2205.05892 [astro-ph.CO].
[1189] S. Vagnozzi, A. Loeb, M. Moresco, Eppur è piatto? The cosmic chronometers take on spatial curvature and cosmic concordance, Astrophys. J. 908 (1) (2021) 84, arXiv:2011.11645 [astro-ph.CO].
[1190] S. Vagnozzi, E. Di Valentino, S. Gariazzo, A. Melchiorri, O. Mena, J. Silk, The galaxy power spectrum take on spatial curvature and cosmic concordance, Phys. Dark Univ. 33 (2021) 100851, arXiv:2010.02230 [astro-ph.CO].
[1191] C.-G. Park, B. Ratra, Using the tilted flat-ΛCDM and the untilted non-flat ΛCDM inflation models to measure cosmological parameters from a compilation of observational data, Astrophys. J. 882 (2019) 158, arXiv:1801.00213 [astro-ph.CO].
[1192] C.-G. Park, B. Ratra, Measuring the Hubble constant and spatial curvature from supernova apparent magnitude, baryon acoustic oscillation, and Hubble parameter data, Astrophys. Space Sci. 364 (8) (2019) 134, arXiv:1809.03598 [astro-ph.CO].
[1193] WMAP Collaboration, C.L. Bennett, et al., Nine-year wilkinson microwave anisotropy probe (WMAP) observations: final maps and results, Astrophys. J. Suppl. 208 (2013) 20, arXiv:1212.5225 [astro-ph.CO].
[1194] Planck Collaboration, R. Adam, et al., Planck 2015 results. I. Overview of products and scientific results, Astron. Astrophys. 594 (2016) A1, arXiv:1502.01582 [astro-ph.CO].
[1195] WMAP Collaboration, G. Hinshaw, et al., First year Wilkinson Microwave Anisotropy Probe (WMAP) observations: The Angular power spectrum, Astrophys. J. Suppl. 148 (2003) 135, arXiv:astro-ph/0302217.
[1196] C.R. Contaldi, M. Peloso, L. Kofman, A.D. Linde, Suppressing the lower multipoles in the CMB anisotropies, J. Cosmol. Astropart. Phys. 07 (2003) 002, arXiv:astro-ph/0303636.
[1197] J.M. Cline, P. Crotty, J. Lesgourgues, Does the small CMB quadrupole moment suggest new physics? J. Cosmol. Astropart. Phys. 09 (2003) 010, arXiv:astro-ph/0304558.
[1198] D.J. Schwarz, G.D. Starkman, D. Huterer, C.J. Copi, Is the low-l microwave background cosmic? Phys. Rev. Lett. 93 (2004) 221301, arXiv:astro-ph/0403353.
[1199] C.J. Copi, D. Huterer, D.J. Schwarz, G.D. Starkman, On the large-angle anomalies of the microwave sky, Mon. Not. R. Astron. Soc. 367 (2006) 79–102, arXiv:astro-ph/0508047.
[1200] A. de Oliveira-Costa, M. Tegmark, Cmb multipole measurements in the presence of foregrounds, Phys. Rev. D 74 (2006) 023005, arXiv:astro-ph/0603369.
[1201] A. Slosar, U. Seljak, Assessing the effects of foregrounds and sky removal in WMAP, Phys. Rev. D 70 (2004) 083002, arXiv:astro-ph/0404567.
[1202] A. Hajian, Analysis of the apparent lack of power in the cosmic microwave background anisotropy at large angular scales, 2007, arXiv:astro-ph/0702723.
[1203] Planck Collaboration, P.A.R. Ade, et al., Planck 2013 results. XXIII. Isotropy and statistics of the CMB, Astron. Astrophys. 571 (2014) A23, arXiv:1303.5083 [astro-ph.CO].
[1204] H.K. Eriksen, F.K. Hansen, A.J. Banday, K.M. Gorski, P.B. Lilje, Asymmetries in the cosmic microwave background anisotropy field, Astrophys. J. 605 (2004) 14–20, arXiv:astro-ph/0307507; Astrophys. J. 609 (2004) 1198 (erratum).
[1205] Planck Collaboration, P.A.R. Ade, et al., Planck 2015 results. XVI. Isotropy and statistics of the CMB, Astron. Astrophys. 594 (2016) A16, arXiv:1506.07135 [astro-ph.CO].
[1206] A.L. Erickcek, M. Kamionkowski, S.M. Carroll, A hemispherical power asymmetry from inflation, Phys. Rev. D 78 (2008) 123520, arXiv:0806.0377 [astro-ph].
[1207] F. Schmidt, L. Hui, Cosmic microwave background power asymmetry from non-gaussian modulation, Phys. Rev. Lett. 110 (2013) 011301, arXiv:1210.2965 [astro-ph.CO]; Phys. Rev. Lett. 110 (2013) 059902 (erratum).
[1208] F.K. Hansen, T. Trombetti, N. Bartolo, U. Natale, M. Liguori, A.J. Banday, K.M. Gorski, Isotropic non-Gaussian gNL-like toy models that reproduce cosmic microwave background anomalies, Astron. Astrophys. 626 (2019) A13, arXiv:1806.08531 [astro-ph.CO].
[1209] C. Gordon, W. Hu, A Low CMB quadrupole from dark energy isocurvature perturbations, Phys. Rev. D 70 (2004) 083003, arXiv:astro-ph/0406496.
[1210] K. Land, J. Magueijo, The axis of evil, Phys. Rev. Lett. 95 (2005) 071301, arXiv:astro-ph/0502237.
[1211] J. Kim, P. Naselsky, Lack of angular correlation and odd-parity preference in CMB data, Astrophys. J. 739 (2011) 79, arXiv:1011.0377 [astro-ph.CO].
[1212] A. Lue, L.-M. Wang, M. Kamionkowski, Cosmological signature of new parity violating interactions, Phys. Rev. Lett. 83 (1999) 1506–1509, arXiv:astro-ph/9812088.
[1213] S.H.S. Alexander, Is cosmic parity violation responsible for the anomalies in the WMAP data? Phys. Lett. B 660 (2008) 444–448, arXiv:hep-th/0601034.
[1214] P. Vielva, E. Martinez-Gonzalez, R.B. Barreiro, J.L. Sanz, L. Cayon, Detection of non-Gaussianity in the WMAP 1 - year data using spherical wavelets, Astrophys. J. 609 (2004) 22–34, arXiv:astro-ph/0310273.
[1215] M. Cruz, L. Cayon, E. Martinez-Gonzalez, P. Vielva, J. Jin, The non-gaussian cold spot in the 3-year wmap data, Astrophys. J. 655 (2007) 11–20, arXiv:astro-ph/0603859.
[1216] S. Nadathur, M. Lavinto, S. Hotchkiss, S. Räsänen, Can a supervoid explain the Cold Spot? Phys. Rev. D 90 (10) (2014) 103510, arXiv:1408.4720 [astro-ph.CO].
[1217] K.T. Inoue, J. Silk, Local voids as the origin of large-angle cosmic microwave background anomalies I, Astrophys. J. 648 (2006) 23–30, arXiv:astro-ph/0602478.
[1218] R. Holman, L. Mersini-Houghton, T. Takahashi, Cosmological avatars of the landscape I: Bracketing the SUSY breaking scale, Phys. Rev. D 77 (2008) 063510, arXiv:hep-th/0611223.
[1219] M. Cruz, M. Tucci, E. Martinez-Gonzalez, P. Vielva, The non-gaussian cold spot in wmap: significance, morphology and foreground contribution, Mon. Not. R. Astron. Soc. 369 (2006) 57–67, arXiv:astro-ph/0601427.
[1220] L. Rudnick, S. Brown, L.R. Williams, Extragalactic radio sources and the WMAP cold spot, Astrophys. J. 671 (2007) 40–44, arXiv:0704.0908 [astro-ph].
[1221] D.G. Lambas, F.K. Hansen, F. Toscano, H.E. Luparello, E.F. Boero, The CMB Cold Spot as predicted by foregrounds around nearby galaxies, Astron. Astrophys. 681 (2024) A2, arXiv:2310.13755 [astro-ph.CO].
[1222] I. Szapudi, et al., Detection of a supervoid aligned with the cold spot of the cosmic microwave background, Mon. Not. R. Astron. Soc. 450 (1) (2015) 288–294, arXiv:1405.1566 [astro-ph.CO].
[1223] R. Mackenzie, T. Shanks, M.N. Bremer, Y.-C. Cai, M.L.P. Gunawardhana, A. Kovács, P. Norberg, I. Szapudi, Evidence against a supervoid causing the CMB Cold Spot, Mon. Not. R. Astron. Soc. 470 (2) (2017) 2328–2338, arXiv:1704.03814 [astro-ph.CO].
[1224] H.M. Courtois, R.B. Tully, Y. Hoffman, D. Pomarede, R. Graziani, A. Dupuy, Cosmicflows-3: cold spot repeller? Astrophys. J. Lett. 847 (1) (2017) L6, arXiv:1708.07547 [astro-ph.CO].
[1225] DES Collaboration, A. Kovács, et al., The DES view of the Eridanus supervoid and the CMB cold spot, Mon. Not. R. Astron. Soc. 510 (1) (2022) 216–229, arXiv:2112.07699 [astro-ph.CO].
[1226] H.E. Luparello, E.F. Boero, M. Lares, A.G. Sánchez, D.G. Lambas, The cosmic shallows – I. Interaction of CMB photons in extended galaxy haloes, Mon. Not. R. Astron. Soc. 518 (4) (2022) 5643–5652, arXiv:2206.14217 [astro-ph.CO].

[1227] F.K. Hansen, E.F. Boero, H.E. Luparello, D.G. Lambas, A possible common explanation for several cosmic microwave background (CMB) anomalies: A strong impact of nearby galaxies on observed large-scale CMB fluctuations, Astron. Astrophys. 675 (2023) L7, arXiv:2305.00268 [astro-ph.CO].
[1228] J.P. Huchra, et al., The 2MASS redshift survey - description and data release, Astrophys. J. Suppl. 199 (2012) 26, arXiv:1108.0669 [astro-ph.CO].
[1229] M. Cruz, E. Martínez-González, C. Gimeno-Amo, B.J. Kavanagh, M. Tucci, Unexplained correlation between the Cosmic Microwave Background temperature and the local matter density distribution, J. Cosmol. Astropart. Phys. 04 (2025) 079, arXiv:2407.17599 [astro-ph.CO].
[1230] F.K. Hansen, D.G. Lambas, H.E. Luparello, F. Toscano, L.A. Pereyra, A 5.7σ detection confirming the existence of a possibly dark matter related CMB foreground in nearby cosmic filaments, 2024, arXiv:2411.15307 [astro-ph.CO].
[1231] F. Toscano, F.K. Hansen, D.G. Lambas, H. Luparello, P. Fosalba, E. Gaztañaga, Are CMB derived cosmological parameters affected by foregrounds associated to nearby galaxies? Phys. Rev. D 111 (8) (2025) 083528, arXiv:2410.24026 [astro-ph.CO].
[1232] C.J. Copi, D. Huterer, D.J. Schwarz, G.D. Starkman, No large-angle correlations on the non-Galactic microwave sky, Mon. Not. R. Astron. Soc. 399 (2009) 295–303, arXiv:0808.3767 [astro-ph].
[1233] D. Sarkar, D. Huterer, C.J. Copi, G.D. Starkman, D.J. Schwarz, Missing power vs low-l alignments in the cosmic microwave background: no correlation in the standard cosmological model, Astropart. Phys. 34 (2011) 591–594, arXiv:1004.3784 [astro-ph.CO].
[1234] J.P. Luminet, J. Weeks, A. Riazuelo, R. Lehoucq, J.P. Uzan, Dodecahedral space topology as an explanation for weak wide - angle temperature correlations in the cosmic microwave background, Nature 425 (2003) 593, arXiv:astro-ph/0310253.
[1235] R. Aurich, H.S. Janzer, S. Lustig, F. Steiner, Do we live in a small universe? Cl. Quant. Grav. 25 (2008) 125006, arXiv:0708.1420 [astro-ph].
[1236] C. Copi, D. Huterer, D. Schwarz, G. Starkman, The uncorrelated universe: statistical anisotropy and the vanishing angular correlation function in WMAP years 1-3, Phys. Rev. D 75 (2007) 023507, arXiv:astro-ph/0605135.
[1237] C.J. Hogan, Gravitational waves from light cosmic strings: backgrounds and bursts with large loops, Phys. Rev. D 74 (2006) 043526, arXiv:astro-ph/0605567.
[1238] L.P. Chimento, M.I. Forte, Anisotropic k-essence cosmologies, Phys. Rev. D 73 (2006) 063502, arXiv:astro-ph/0510726.
[1239] S. Tsujikawa, M. Sami, R. Maartens, Observational constraints on braneworld inflation: the effect of a gauss-bonnet term, Phys. Rev. D 70 (2004) 063525, arXiv:astro-ph/0406078.
[1240] M.-a. Watanabe, S. Kanno, J. Soda, Inflationary universe with anisotropic hair, Phys. Rev. Lett. 102 (2009) 191302, arXiv:0902.2833 [hep-th].
[1241] J. Delabrouille, et al., The pre-launch Planck Sky Model: a model of sky emission at submillimetre to centimetre wavelengths, Astron. Astrophys. 553 (2013) A96, arXiv:1207.3675 [astro-ph.CO].
[1242] L. Mersini-Houghton, Cosmological implications of the string theory landscape, AIP Conf. Proc. 878 (1) (2006) 315–322, arXiv:hep-ph/0609157.
[1243] L. Mersini-Houghton, Can we predict Lambda for the non-SUSY sector of the landscape, Cl. Quant. Grav. 22 (2005) 3481–3490, arXiv:hep-th/0504026.
[1244] A. Kobakhidze, L. Mersini-Houghton, Birth of the universe from the landscape of string theory, Eur. Phys. J. C 49 (2007) 869–873, arXiv:hep-th/0410213.
[1245] R. Holman, L. Mersini-Houghton, Why the universe started from a low entropy state, Phys. Rev. D 74 (2006) 123510, arXiv:hep-th/0511102.
[1246] R. Holman, L. Mersini-Houghton, T. Takahashi, Cosmological avatars of the landscape. II. CMB and LSS signatures, Phys. Rev. D 77 (2008) 063511, arXiv:hep-th/0612142.
[1247] E. Di Valentino, L. Mersini-Houghton, Testing predictions of the quantum landscape multiverse 1: the starobinsky inflationary potential, J. Cosmol. Astropart. Phys. 03 (2017) 002, arXiv:1612.09588 [astro-ph.CO].
[1248] E. Di Valentino, L. Mersini-Houghton, Testing predictions of the quantum landscape multiverse 2: the exponential inflationary potential, J. Cosmol. Astropart. Phys. 03 (2017) 020, arXiv:1612.08334 [astro-ph.CO].
[1249] E. Di Valentino, L. Mersini-Houghton, Testing predictions of the quantum landscape multiverse 3: the hilltop inflationary potential, Symmetry 11 (4) (2019) 520, arXiv:1807.10833 [astro-ph.CO].
[1250] L. Mersini-Houghton, Predictions of the quantum landscape multiverse, Cl. Quant. Grav. 34 (4) (2017) 047001, arXiv:1612.07129 [hep-th].
[1251] DESI Collaboration, K. Lodha, et al., DESI 2024: Constraints on physics-focused aspects of dark energy using DESI DR1 BAO data, Phys. Rev. D 111 (2) (2025) 023532, arXiv:2405.13588 [astro-ph.CO].
[1252] DESI Collaboration, M.A. Karim, et al., DESI DR2 results I: baryon acoustic oscillations from the lyman alpha forest, 2025, arXiv:2503.14739 [astro-ph.CO].
[1253] DESI Collaboration, U. Andrade, et al., Validation of the DESI DR2 measurements of baryon acoustic oscillations from galaxies and quasars, 2025, arXiv:2503.14742 [astro-ph.CO].
[1254] A. Brodzeller, et al., Construction of the damped Lyα absorber catalog for DESI DR2 Lyα BAO, 2025, arXiv:2503.14740 [astro-ph.CO].
[1255] DESI Collaboration, K. Lodha, et al., Extended dark energy analysis using DESI DR2 BAO measurements, 2025, arXiv:2503.14743 [astro-ph.CO].
[1256] D. Rubin, et al., Union through UNITY: cosmology with 2,000 SNe using a unified Bayesian framework, 2023, arXiv:2311.12098 [astro-ph.CO].
[1257] DES Collaboration, T.M.C. Abbott, et al., The dark energy survey: cosmology results with ~1500 new high-redshift type ia supernovae using the full 5 yr data set, Astrophys. J. Lett. 973 (1) (2024) L14, arXiv:2401.02929 [astro-ph.CO].
[1258] DES Collaboration, B.O. Sánchez, et al., The dark energy survey supernova program: light curves and 5 yr data release, Astrophys. J. 975 (1) (2024) 5, arXiv:2406.05046 [astro-ph.CO].
[1259] DES Collaboration, M. Vincenzi, et al., The dark energy survey supernova program: cosmological analysis and systematic uncertainties, Astrophys. J. 975 (1) (2024) 86, arXiv:2401.02945 [astro-ph.CO].
[1260] DESI Collaboration, K. Lodha, et al., Extended dark energy analysis using DESI DR2 BAO measurements, 2025, arXiv:2503.14743 [astro-ph.CO].
[1261] A. Vikman, Can dark energy evolve to the phantom? Phys. Rev. D 71 (2005) 023515, arXiv:astro-ph/0407107.
[1262] S.M. Carroll, M. Hoffman, M. Trodden, Can the dark energy equation-of-state parameter w be less than −1? Phys. Rev. D 68 (2003) 023509, arXiv:astro-ph/0301273.
[1263] W. Hu, Crossing the phantom divide: Dark energy internal degrees of freedom, Phys. Rev. D 71 (2005) 047301, arXiv:astro-ph/0410680.
[1264] P. Creminelli, G. D'Amico, J. Norena, F. Vernizzi, The effective theory of quintessence: the w<-1 side unveiled, J. Cosmol. Astropart. Phys. 02 (2009) 018, arXiv:0811.0827 [astro-ph].
[1265] A. Chudaykin, M. Kunz, Modified gravity interpretation of the evolving dark energy in light of DESI data, Phys. Rev. D 110 (12) (2024) 123524, arXiv:2407.02558 [astro-ph.CO].
[1266] G. Ye, M. Martinelli, B. Hu, A. Silvestri, Non-minimally coupled gravity as a physically viable fit to DESI 2024 BAO, 2024, arXiv:2407.15832 [astro-ph.CO].
[1267] M. Ishak, et al., Modified gravity constraints from the full shape modeling of clustering measurements from DESI 2024, 2024, arXiv:2411.12026 [astro-ph.CO].
[1268] A. Chudaykin, M. Kunz, J. Carron, Modified gravity constraints with Planck ISW-lensing bispectrum, 2025, arXiv:2503.09893 [astro-ph.CO].
[1269] W.J. Wolf, P.G. Ferreira, C. García-García, Matching current observational constraints with nonminimally coupled dark energy, Phys. Rev. D 111 (4) (2025) L041303, arXiv:2409.17019 [astro-ph.CO].
[1270] A. Hernández-Almada, M.L. Mendoza-Martínez, M.A. García-Aspeitia, V. Motta, Phenomenological emergent dark energy in the light of DESI Data Release 1, Phys. Dark Univ. 46 (2024) 101668, arXiv:2407.09430 [astro-ph.CO].
[1271] DESI Collaboration, M. Malekjani, Z. Davari, S. Pourojaghi, Cosmological constraints on dark energy parametrizations after DESI 2024: Persistent deviation from standard ΛCDM cosmology, Phys. Rev. D 111 (8) (2025) 083547, arXiv:2407.09767 [astro-ph.CO].
[1272] O.F. Ramadan, J. Sakstein, D. Rubin, DESI constraints on exponential quintessence, Phys. Rev. D 110 (4) (2024) L041303, arXiv:2405.18747 [astro-ph.CO].
[1273] Y. Carloni, O. Luongo, M. Muccino, Does dark energy really revive using DESI 2024 data? Phys. Rev. D 111 (2) (2025) 023512, arXiv:2404.12068 [astro-ph.CO].
[1274] K.V. Berghaus, J.A. Kable, V. Miranda, Quantifying scalar field dynamics with DESI 2024 Y1 BAO measurements, Phys. Rev. D 110 (10) (2024) 103524, arXiv:2404.14341 [astro-ph.CO].
[1275] F.J. Qu, K.M. Surrao, B. Bolliet, J.C. Hill, B.D. Sherwin, H.T. Jense, Accelerated inference on accelerated cosmic expansion: New constraints on axion-like early dark energy with DESI BAO and ACT DR6 CMB lensing, 2024, arXiv:2404.16805 [astro-ph.CO].
[1276] A. Notari, M. Redi, A. Tesi, Consistent theories for the DESI dark energy fit, J. Cosmol. Astropart. Phys. 11 (2024) 025, arXiv:2406.08459 [astro-ph.CO].
[1277] P. Adolf, M. Hirsch, S. Krieg, H. Päs, M. Tabet, Fitting the DESI BAO data with dark energy driven by the Cohen-Kaplan-Nelson bound, J. Cosmol. Astropart. Phys. 08 (2024) 048, arXiv:2406.09964 [astro-ph.CO].
[1278] J.-Q. Jiang, D. Pedrotti, S.S. da Costa, S. Vagnozzi, Nonparametric late-time expansion history reconstruction and implications for the Hubble tension in light of recent DESI and type Ia supernovae data, Phys. Rev. D 110 (12) (2024) 123519, arXiv:2408.02365 [astro-ph.CO].
[1279] B.R. Dinda, R. Maartens, Model-agnostic assessment of dark energy after DESI DR1 BAO, J. Cosmol. Astropart. Phys. 01 (2025) 120, arXiv:2407.17252 [astro-ph.CO].
[1280] W.J. Wolf, C. García-García, P.G. Ferreira, Robustness of dark energy phenomenology across different parameterizations, 2025, arXiv:2502.04929 [astro-ph.CO].
[1281] A. Sousa-Neto, C. Bengaly, J.E. González, J. Alcaniz, No evidence for dynamical dark energy from DESI and SN data: a symbolic regression analysis, 2025, arXiv:2502.10506 [astro-ph.CO].
[1282] R. de Putter, E.V. Linder, Calibrating dark energy, J. Cosmol. Astropart. Phys. 10 (2008) 042, arXiv:0808.0189 [astro-ph].
[1283] W. Giarè, M. Najafi, S. Pan, E. Di Valentino, J.T. Firouzjaee, Robust preference for dynamical dark energy in DESI BAO and SN measurements, J. Cosmol. Astropart. Phys. 10 (2024) 035, arXiv:2407.16689 [astro-ph.CO].

[1284] Z. Wang, S. Lin, Z. Ding, B. Hu, The role of LRG1 and LRG2's monopole in inferring the DESI 2024 BAO cosmology, Mon. Not. R. Astron. Soc. 534 (4) (2024) 3869–3875, arXiv:2405.02168 [astro-ph.CO].

[1285] E.O. Colgáin, M.G. Dainotti, S. Capozziello, S. Pourojaghi, M.M. Sheikh-Jabbari, D. Stojkovic, Does DESI 2024 confirm ΛCDM? 2024, arXiv:2404.08633 [astro-ph.CO].

[1286] D. Naredo-Tuero, M. Escudero, E. Fernández-Martínez, X. Marcano, V. Poulin, Critical look at the cosmological neutrino mass bound, Phys. Rev. D 110 (12) (2024) 123537, arXiv:2407.13831 [astro-ph.CO].

[1287] D. Sapone, S. Nesseris, Outliers in DESI BAO: robustness and cosmological implications, 2024, arXiv:2412.01740 [astro-ph.CO].

[1288] W. Giarè, T. Mahassen, E. Di Valentino, S. Pan, An overview of what current data can (and cannot yet) say about evolving dark energy, Phys. Dark Univ. 48 (2025) 101906, arXiv:2502.10264 [astro-ph.CO].

[1289] DES Collaboration, T.M.C. Abbott, et al., Dark Energy Survey: implications for cosmological expansion models from the final DES Baryon Acoustic Oscillation and Supernova data, 2025, arXiv:2503.06712 [astro-ph.CO].

[1290] E.O. Colgáin, M.M. Sheikh-Jabbari, R. Solomon, M.G. Dainotti, D. Stojkovic, Putting flat ΛCDM in the (Redshift) bin, Phys. Dark Univ. 44 (2024) 101464, arXiv:2206.11447 [astro-ph.CO].

[1291] M. Malekjani, R.M. Conville, E.O. Colgáin, S. Pourojaghi, M.M. Sheikh-Jabbari, On redshift evolution and negative dark energy density in Pantheon + Supernovae, Eur. Phys. J. C 84 (3) (2024) 317, arXiv:2301.12725 [astro-ph.CO].

[1292] E.O. Colgáin, S. Pourojaghi, M.M. Sheikh-Jabbari, Implications of DES 5YR SNe dataset for ΛCDM, Eur. Phys. J. C 85 (3) (2025) 286, arXiv:2406.06389 [astro-ph.CO].

[1293] E.O. Colgáin, M.M. Sheikh-Jabbari, DESI and SNe: dynamical dark energy, Ω_m tension or systematics? 2024, arXiv:2412.12905 [astro-ph.CO].

[1294] A. Notari, M. Redi, A. Tesi, BAO vs. SN evidence for evolving dark energy, J. Cosmol. Astropart. Phys. 04 (2025) 048, arXiv:2411.11685 [astro-ph.CO].

[1295] G. Efstathiou, Evolving dark energy or supernovae systematics? Mon. Not. R. Astron. Soc. 538 (2) (2025) 875–882, arXiv:2408.07175 [astro-ph.CO].

[1296] DES Collaboration, M. Vincenzi, et al., Comparing the DES-SN5YR and Pantheon+ SN cosmology analyses: Investigation based on "Evolving Dark Energy or Supernovae systematics?", 2025, arXiv:2501.06664 [astro-ph.CO].

[1297] W. Giarè, Dynamical dark energy beyond planck? Constraints from multiple CMB probes, DESI BAO and type-ia supernovae, 2024, arXiv:2409.17074 [astro-ph.CO].

[1298] L.A. Escamilla, W. Giarè, E. Di Valentino, R.C. Nunes, S. Vagnozzi, The state of the dark energy equation of state circa 2023, J. Cosmol. Astropart. Phys. 05 (2024) 091, arXiv:2307.14802 [astro-ph.CO].

[1299] W. Giarè, E. Di Valentino, A. Melchiorri, Measuring the reionization optical depth without large-scale CMB polarization, Phys. Rev. D 109 (10) (2024) 103519, arXiv:2312.06482 [astro-ph.CO].

[1300] I. Ben-Dayan, U. Kumar, M. Shimon, A. Verma, Impact of low ell's on large scale structure anomalies, J. Cosmol. Astropart. Phys. 02 (2025) 069, arXiv:2409.15457 [astro-ph.CO].

[1301] Z.-Y. Peng, Y.-S. Piao, Dark energy and lensing anomaly in Planck CMB data, 2025, arXiv:2502.04641 [astro-ph.CO].

[1302] C.-G. Park, B. Ratra, Is excess smoothing of Planck CMB ansiotropy data partially responsible for evidence for dark energy dynamics in other $w(z)$CDM parametrizations? 2025, arXiv:2501.03480 [astro-ph.CO].

[1303] C.-G. Park, J. de Cruz Perez, B. Ratra, Is the w_0w_aCDM cosmological parameterization evidence for dark energy dynamics partially caused by the excess smoothing of Planck CMB anisotropy data? 2024, arXiv:2410.13627 [astro-ph.CO].

[1304] E. Di Valentino, S. Gariazzo, O. Mena, Most constraining cosmological neutrino mass bounds, Phys. Rev. D 104 (8) (2021) 083504, arXiv:2106.15267 [astro-ph.CO].

[1305] J.-Q. Jiang, W. Giarè, S. Gariazzo, M.G. Dainotti, E. Di Valentino, O. Mena, D. Pedrotti, S.S. da Costa, S. Vagnozzi, Neutrino cosmology after DESI: tightest mass upper limits, preference for the normal ordering, and tension with terrestrial observations, J. Cosmol. Astropart. Phys. 01 (2025) 153, arXiv:2407.18047 [astro-ph.CO].

[1306] E. Di Valentino, S. Gariazzo, W. Giarè, O. Mena, Impact of the damping tail on neutrino mass constraints, Phys. Rev. D 108 (8) (2023) 083509, arXiv:2305.12989 [astro-ph.CO].

[1307] D. Wang, O. Mena, E. Di Valentino, S. Gariazzo, Updating neutrino mass constraints with background measurements, Phys. Rev. D 110 (10) (2024) 103536, arXiv:2405.03368 [astro-ph.CO].

[1308] J. Hamann, J. Hasenkamp, A new life for sterile neutrinos: resolving inconsistencies using hot dark matter, J. Cosmol. Astropart. Phys. 10 (2013) 044, arXiv:1308.3255 [astro-ph.CO].

[1309] P.F. de Salas, D.V. Forero, S. Gariazzo, P. Martínez-Miravé, O. Mena, C.A. Ternes, M. Tórtola, J.W.F. Valle, 2020 global reassessment of the neutrino oscillation picture, JHEP 02 (2021) 071, arXiv:2006.11237 [hep-ph].

[1310] I. Esteban, M.C. Gonzalez-Garcia, M. Maltoni, T. Schwetz, A. Zhou, The fate of hints: updated global analysis of three-flavor neutrino oscillations, JHEP 09 (2020) 178, arXiv:2007.14792 [hep-ph].

[1311] S. Gariazzo, O. Mena, T. Schwetz, Quantifying the tension between cosmological and terrestrial constraints on neutrino masses, Phys. Dark Univ. 40 (2023) 101226, arXiv:2302.14159 [hep-ph].

[1312] E. di Valentino, S. Gariazzo, O. Mena, Model marginalized constraints on neutrino properties from cosmology, Phys. Rev. D 106 (4) (2022) 043540, arXiv:2207.05167 [astro-ph.CO].

[1313] C.S. Lorenz, L. Funcke, E. Calabrese, S. Hannestad, Time-varying neutrino mass from a supercooled phase transition: current cosmological constraints and impact on the Ω_m-σ_8 plane, Phys. Rev. D 99 (2) (2019) 023501, arXiv:1811.01991 [astro-ph.CO].

[1314] M. Escudero, J. Lopez-Pavon, N. Rius, S. Sandner, Relaxing cosmological neutrino mass bounds with unstable neutrinos, JHEP 12 (2020) 119, arXiv:2007.04994 [hep-ph].

[1315] Z. Chacko, A. Dev, P. Du, V. Poulin, Y. Tsai, Determining the neutrino lifetime from cosmology, Phys. Rev. D 103 (4) (2021) 043519, arXiv:2002.08401 [astro-ph.CO].

[1316] Z. Chacko, A. Dev, P. Du, V. Poulin, Y. Tsai, Cosmological Limits on the Neutrino Mass and Lifetime, JHEP 04 (2020) 020, arXiv:1909.05275 [hep-ph].

[1317] G. Franco Abellán, Z. Chacko, A. Dev, P. Du, V. Poulin, Y. Tsai, Improved cosmological constraints on the neutrino mass and lifetime, JHEP 08 (2022) 076, arXiv:2112.13862 [hep-ph].

[1318] C.D. Kreisch, F.-Y. Cyr-Racine, O. Doré, Neutrino puzzle: Anomalies, interactions, and cosmological tensions, Phys. Rev. D 101 (12) (2020) 123505, arXiv:1902.00534 [astro-ph.CO].

[1319] D. Camarena, F.-Y. Cyr-Racine, Strong constraints on a simple self-interacting neutrino cosmology, Phys. Rev. D 111 (2) (2025) 023504, arXiv:2403.05496 [astro-ph.CO].

[1320] I. Esteban, J. Salvado, Long range interactions in cosmology: implications for neutrinos, J. Cosmol. Astropart. Phys. 05 (2021) 036, arXiv:2101.05804 [hep-ph].

[1321] I.M. Oldengott, G. Barenboim, S. Kahlen, J. Salvado, D.J. Schwarz, How to relax the cosmological neutrino mass bound, J. Cosmol. Astropart. Phys. 04 (2019) 049, arXiv:1901.04352 [astro-ph.CO].

[1322] G. Dvali, L. Funcke, Small neutrino masses from gravitational θ-term, Phys. Rev. D 93 (11) (2016) 113002, arXiv:1602.03191 [hep-ph].

[1323] G. Barenboim, H. Sanchis, W.H. Kinney, D. Rios, Bound on thermal y distortion of the cosmic neutrino background, Phys. Rev. D 110 (12) (2024) 123535, arXiv:2407.18102 [astro-ph.CO].

[1324] N. Craig, D. Green, J. Meyers, S. Rajendran, No νs is good news, JHEP 09 (2024) 097, arXiv:2405.00836 [astro-ph.CO].

[1325] A. Yadav, S. Kumar, C. Kibris, O. Akarsu, Λ_sCDM cosmology: alleviating major cosmological tensions by predicting standard neutrino properties, J. Cosmol. Astropart. Phys. 01 (2025) 042, arXiv:2406.18496 [astro-ph.CO].

[1326] KATRIN Collaboration, M. Aker, et al., Direct neutrino-mass measurement based on 259 days of KATRIN data, Science 388 (6743) (2025) adq9592, arXiv:2406.13516 [nucl-ex].

[1327] G. Drexlin, V. Hannen, S. Mertens, C. Weinheimer, Current direct neutrino mass experiments, Adv. High Energy Phys. 2013 (2013) 293986, arXiv:1307.0101 [physics.ins-det].

[1328] P.K. Aluri, et al., Is the observable Universe consistent with the cosmological principle? Cl. Quant. Grav. 40 (9) (2023) 094001, arXiv:2207.05765 [astro-ph.CO].

[1329] G. Ellis, R. Maartens, M. MacCallum, Relativistic Cosmology, Cambridge University Press, 2012, https://books.google.it/books?id=IgkhAwAAQBAJ.

[1330] D.J. Schwarz, C.J. Copi, D. Huterer, G.D. Starkman, CMB Anomalies after Planck, Cl. Quant. Grav. 33 (18) (2016) 184001, arXiv:1510.07929 [astro-ph.CO].

[1331] P. Fleury, C. Clarkson, R. Maartens, How does the cosmic large-scale structure bias the Hubble diagram? J. Cosmol. Astropart. Phys. 03 (2017) 062, arXiv:1612.03726 [astro-ph.CO].

[1332] J. Jones, C.J. Copi, G.D. Starkman, Y. Akrami, The Universe is not statistically isotropic, 2023, arXiv:2310.12859 [astro-ph.CO].

[1333] P. Fosalba, E. Gaztanaga, Explaining cosmological anisotropy: evidence for causal horizons from CMB data, Mon. Not. R. Astron. Soc. 504 (4) (2021) 5840–5862, arXiv:2011.00910 [astro-ph.CO].

[1334] S. Yeung, M.-C. Chu, Directional variations of cosmological parameters from the Planck CMB data, Phys. Rev. D 105 (8) (2022) 083508, arXiv:2201.03799 [astro-ph.CO].

[1335] Euclid Collaboration, A. Kashlinsky, et al., Euclid preparation - XLVI. The near-infrared background dipole experiment with Euclid, Astron. Astrophys. 689 (2024) A294, arXiv:2401.17945 [astro-ph.CO].

[1336] M. Plionis, Large-scale optical dipole anisotropy, Mon. Not. R. Astro. Soc. 234 (1988) 401–416.

[1337] M. Plionis, R. Valdarnini, Evidence for large-scale structure on scales ≡300 h^{-1}Mpc, Mon. Not. R. Astro. Soc. 249 (1991) 46.

[1338] R. Scaramella, G. Vettolani, G. Zamorani, The distribution of clusters of galaxies within 300 MPC H -1 and the crossover to an isotropic and homogeneous universe, Astrophys. J. Lett. 376 (1991) L1.

[1339] E. Branchini, M. Plionis, Reconstructing positions and peculiar velocities of galaxy clusters within 20000 km/sec. I: the cluster 3-D dipole, Astrophys. J. 460 (1996) 569, arXiv:astro-ph/9501028.

[1340] M. Plionis, E. Kolokotronis, The x-ray cluster dipole, Astrophys. J. 500 (1998) 1, arXiv:astro-ph/9707147.

[1341] M. Rowan-Robinson, et al., The IRAS PSCz dipole, Mon. Not. R. Astron. Soc. 314 (2000) 375, arXiv:astro-ph/9912223.

[1342] D.D. Kocevksi, H. Ebeling, B. Tully, C.R. Mullis, The dipole anisotropy of the first all-sky X-ray cluster sample, in: A.P. Fairall, P.A. Woudt (Eds.), Nearby Large-Scale Structures and the Zone of Avoidance, in: Astronomical Society of the Pacific Conference Series, vol. 329, 2005, p. 89.

[1343] Y. Hoffman, D. Pomarede, R. Brent Tully, H. Courtois, The dipole repeller, 2017, http://dx.doi.org/10.1038/s41550-016-0036, arXiv:1702.02483 [astro-ph.CO].

[1344] M. Lopes, A. Bernui, C. Franco, F. Avila, Bulk flow motion detection in the local universe with pantheon+ type ia supernovae, Astrophys. J. 967 (1) (2024) 47, arXiv:2405.11077 [astro-ph.CO].

[1345] J.A.R. Cembranos, A.L. Maroto, H. Villarrubia-Rojo, Non-comoving cosmology, J. Cosmol. Astropart. Phys. 06 (2019) 041, arXiv:1903.11009 [astro-ph.CO].

[1346] C.G. Tsagas, M.I. Kadiltzoglou, K. Asvesta, The deceleration parameter in "tilted" Friedmann universes: Newtonian vs relativistic treatment, Astrophys. Space Sci. 366 (9) (2021) 90, arXiv:2105.09267 [gr-qc].

[1347] C.G. Tsagas, The deceleration parameter in 'tilted' universes: generalising the Friedmann background, Eur. Phys. J. C 82 (6) (2022) 521, arXiv:2112.04313 [gr-qc].

[1348] K. Asvesta, L. Kazantzidis, L. Perivolaropoulos, C.G. Tsagas, Observational constraints on the deceleration parameter in a tilted universe, Mon. Not. R. Astron. Soc. 513 (2) (2022) 2394–2406, arXiv:2202.00962 [astro-ph.CO].

[1349] J. Santiago, C.G. Tsagas, Timelike vs null deceleration parameter in tilted Friedmann universes, 2022, arXiv:2203.01126 [gr-qc].

[1350] A.R. King, G.F.R. Ellis, Tilted homogeneous cosmological models, Comm. Math. Phys. 31 (1973) 209–242.

[1351] C.G. Tsagas, A. Challinor, R. Maartens, Relativistic cosmology and large-scale structure, Phys. Rep. 465 (2008) 61–147, arXiv:0705.4397 [astro-ph].

[1352] C. Krishnan, R. Mondol, M.M. Sheikh-Jabbari, Dipole cosmology: the Copernican paradigm beyond FLRW, J. Cosmol. Astropart. Phys. 07 (2023) 020, arXiv:2209.14918 [astro-ph.CO].

[1353] C. Krishnan, R. Mondol, M.M. Sheikh-Jabbari, A tilt instability in the cosmological principle, Eur. Phys. J. C 83 (9) (2023) 874, arXiv:2211.08093 [astro-ph.CO].

[1354] E. Ebrahimian, C. Krishnan, R. Mondol, M.M. Sheikh-Jabbari, Towards a realistic dipole cosmology: the dipole ΛCDM model, Cl. Quant. Grav. 41 (14) (2024) 145007, arXiv:2305.16177 [astro-ph.CO].

[1355] A. Allahyari, E. Ebrahimian, R. Mondol, M.M. Sheikh-Jabbari, Big Bang in dipole cosmology, Eur. Phys. J. C 85 (2) (2025) 119, arXiv:2307.15791 [astro-ph.CO].

[1356] C.G. Tsagas, M.I. Kadiltzoglou, Deceleration parameter in tilted Friedmann universes, Phys. Rev. D 92 (4) (2015) 043515, arXiv:1507.04266 [gr-qc].

[1357] A. Heinesen, T. Buchert, Solving the curvature and Hubble parameter inconsistencies through structure formation-induced curvature, Cl. Quant. Grav. 37 (16) (2020) 164001, arXiv:2002.10831 [gr-qc]; Class. Quant. Grav. 37 (2020) 229601 (erratum).

[1358] A. Heinesen, Multipole decomposition of the general luminosity distance 'Hubble law' – a new framework for observational cosmology, J. Cosmol. Astropart. Phys. 05 (2021) 008, arXiv:2010.06534 [astro-ph.CO].

[1359] A. Heinesen, H.J. Macpherson, A prediction for anisotropies in the nearby Hubble flow, J. Cosmol. Astropart. Phys. 03 (03) (2022) 057, arXiv:2111.14423 [astro-ph.CO].

[1360] C. Guandalin, J. Piat, C. Clarkson, R. Maartens, Theoretical systematics in testing the cosmological principle with the kinematic quasar dipole, Astrophys. J. 953 (2) (2023) 144, arXiv:2212.04925 [astro-ph.CO].

[1361] R. Maartens, J. Santiago, C. Clarkson, B. Kalbouneh, C. Marinoni, Covariant cosmography: the observer-dependence of the Hubble parameter, J. Cosmol. Astropart. Phys. 09 (2024) 070, arXiv:2312.09875 [astro-ph.CO].

[1362] G.F.R. Ellis, J.E. Baldwin, On the expected anisotropy of radio source counts, Mon. Not. R. Astro. Soc. 206 (1984) 377–381.

[1363] L. Perivolaropoulos, F. Skara, Challenges for ΛCDM: an update, New Astron. Rev. 95 (2022) 101659, arXiv:2105.05208 [astro-ph.CO].

[1364] O. Akarsu, E. Di Valentino, S. Kumar, M. Ozyigit, S. Sharma, Testing spatial curvature and anisotropic expansion on top of the ΛCDM model, Phys. Dark Univ. 39 (2023) 101162, arXiv:2112.07807 [astro-ph.CO].

[1365] A. Mariano, L. Perivolaropoulos, CMB Maximum temperature asymmetry Axis: Alignment with other cosmic asymmetries, Phys. Rev. D 87 (4) (2013) 043511, arXiv:1211.5915 [astro-ph.CO].

[1366] J.K. Webb, J.A. King, M.T. Murphy, V.V. Flambaum, R.F. Carswell, M.B. Bainbridge, Indications of a spatial variation of the fine structure constant, Phys. Rev. Lett. 107 (2011) 191101, arXiv:1008.3907 [astro-ph.CO].

[1367] M.R. Wilczynska, et al., Four direct measurements of the fine-structure constant 13 billion years ago, Sci. Adv. 6 (17) (2020) eaay9672, arXiv:2003.07627 [astro-ph.CO].

[1368] R. Mohayaee, M. Rameez, S. Sarkar, Do supernovae indicate an accelerating universe? Eur. Phys. J. ST 230 (9) (2021) 2067–2076, arXiv:2106.03119 [astro-ph.CO].

[1369] J. Colin, R. Mohayaee, M. Rameez, S. Sarkar, Evidence for anisotropy of cosmic acceleration, Astron. Astrophys. 631 (2019) L13, arXiv:1808.04597 [astro-ph.CO].

[1370] R. Mohayaee, M. Rameez, S. Sarkar, Cosmological inference from within the peculiar local universe, Universe 10 (5) (2024) 209, arXiv:2003.10420 [astro-ph.CO].

[1371] A.K. Singal, Peculiar motion of Solar system from the Hubble diagram of supernovae Ia and its implications for cosmology, Mon. Not. R. Astron. Soc. 515 (4) (2022) 5969–5980, arXiv:2106.11968 [astro-ph.CO].

[1372] N. Horstmann, Y. Pietschke, D.J. Schwarz, Inference of the cosmic rest-frame from supernovae Ia, Astron. Astrophys. 668 (2022) A34, arXiv:2111.03055 [astro-ph.CO].

[1373] J.A. Cowell, S. Dhawan, H.J. Macpherson, Potential signature of a quadrupolar hubble expansion in Pantheon+supernovae, Mon. Not. R. Astron. Soc. 526 (1) (2023) 1482–1494, arXiv:2212.13569 [astro-ph.CO].

[1374] R. Mc Conville, E.O. Colgáin, Anisotropic distance ladder in Pantheon+supernovae, Phys. Rev. D 108 (12) (2023) 123533, arXiv:2304.02718 [astro-ph.CO].

[1375] U. Andrade, C.A.P. Bengaly, J.S. Alcaniz, B. Santos, Isotropy of low redshift type Ia Supernovae: A Bayesian analysis, Phys. Rev. D 97 (8) (2018) 083518, arXiv:1711.10536 [astro-ph.CO].

[1376] C.A.P. Bengaly, Evidence for cosmic acceleration with next-generation surveys: A model-independent approach, Mon. Not. R. Astron. Soc. 499 (1) (2020) L6–L10, arXiv:1912.05528 [astro-ph.CO].

[1377] W. Rahman, R. Trotta, S.S. Boruah, M.J. Hudson, D.A. van Dyk, New constraints on anisotropic expansion from supernovae Type Ia, Mon. Not. R. Astron. Soc. 514 (1) (2022) 139–163, arXiv:2108.12497 [astro-ph.CO].

[1378] A. Salehi, H. Farajollahi, M. Motahari, P. Pashamokhtari, M. Yarahmadi, S. Fathi, Are Type Ia supernova powerful tool to detect anisotropic expansion of the Universe? Eur. Phys. J. C 80 (8) (2020) 753.

[1379] J.P. Hu, Y.Y. Wang, F.Y. Wang, Testing cosmic anisotropy with Pantheon sample and quasars at high redshifts, Astron. Astrophys. 643 (2020) A93, arXiv:2008.12439 [astro-ph.CO].

[1380] S. Dhawan, A. Borderies, H.J. Macpherson, A. Heinesen, The quadrupole in the local Hubble parameter: first constraints using Type Ia supernova data and forecasts for future surveys, Mon. Not. R. Astron. Soc. 519 (4) (2023) 4841–4855, arXiv:2205.12692 [astro-ph.CO].

[1381] D. Sapone, S. Nesseris, C.A.P. Bengaly, Is there any measurable redshift dependence on the SN Ia absolute magnitude? Phys. Dark Univ. 32 (2021) 100814, arXiv:2006.05461 [astro-ph.CO].

[1382] C.A.P. Bengaly, J.S. Alcaniz, C. Pigozzo, Testing the isotropy of cosmic acceleration with the Pantheon+ and SH0ES datasets: A cosmographic analysis, Phys. Rev. D 109 (12) (2024) 123533, arXiv:2402.17741 [astro-ph.CO].

[1383] I. Antoniou, L. Perivolaropoulos, Searching for a cosmological preferred axis: union2 data analysis and comparison with other probes, J. Cosmol. Astropart. Phys. 12 (2010) 012, arXiv:1007.4347 [astro-ph.CO].

[1384] A. Mariano, L. Perivolaropoulos, Is there correlation between fine structure and dark energy cosmic dipoles? Phys. Rev. D 86 (2012) 083517, arXiv:1206.4055 [astro-ph.CO].

[1385] C. Krishnan, R. Mohayaee, E.O. Colgáin, M.M. Sheikh-Jabbari, L. Yin, Hints of FLRW breakdown from supernovae, Phys. Rev. D 105 (6) (2022) 063514, arXiv:2106.02532 [astro-ph.CO].

[1386] B. Bahr-Kalus, D.J. Schwarz, M. Seikel, A. Wiegand, Constraints on anisotropic cosmic expansion from supernovae, Astron. Astrophys. 553 (2013) A56, arXiv:1212.3691 [astro-ph.CO].

[1387] D. Zhao, Y. Zhou, Z. Chang, Anisotropy of the Universe via the Pantheon supernovae sample revisited, Mon. Not. R. Astron. Soc. 486 (4) (2019) 5679–5689, arXiv:1903.12401 [astro-ph.CO].

[1388] B. Kalbouneh, C. Marinoni, J. Bel, Multipole expansion of the local expansion rate, Phys. Rev. D 107 (2) (2023) 023507, arXiv:2210.11333 [astro-ph.CO].

[1389] L. Tang, H.-N. Lin, L. Liu, X. Li, Consistency of Pantheon+ supernovae with a large-scale isotropic universe*, Chin. Phys. C 47 (12) (2023) 125101, arXiv:2309.11320 [astro-ph.CO].

[1390] J.P. Hu, Y.Y. Wang, J. Hu, F.Y. Wang, Testing the cosmological principle with the Pantheon+ sample and the region-fitting method, Astron. Astrophys. 681 (2024) A88, arXiv:2310.11727 [astro-ph.CO].

[1391] F. Sorrenti, R. Durrer, M. Kunz, The dipole of the Pantheon+SH0ES data, J. Cosmol. Astropart. Phys. 11 (2023) 054, arXiv:2212.10328 [astro-ph.CO].

[1392] L. Perivolaropoulos, Isotropy properties of the absolute luminosity magnitudes of SnIa in the Pantheon+ and SH0ES samples, Phys. Rev. D 108 (6) (2023) 063509, arXiv:2305.12819 [astro-ph.CO].

[1393] G. Risaliti, E. Lusso, A hubble diagram for quasars, Astrophys. J. 815 (2015) 33, arXiv:1505.07118 [astro-ph.CO].

[1394] G. Risaliti, E. Lusso, Cosmological constraints from the Hubble diagram of quasars at high redshifts, Nat. Astron. 3 (3) (2019) 272–277, arXiv:1811.02590 [astro-ph.CO].

[1395] N. Khadka, B. Ratra, Do quasar X-ray and UV flux measurements provide a useful test of cosmological models? Mon. Not. R. Astron. Soc. 510 (2) (2022) 2753–2772, arXiv:2107.07600 [astro-ph.CO].

[1396] N. Khadka, M. Zajaˇcek, R. Prince, S. Panda, B. Czerny, M.L. Martínez-Aldama, V.K. Jaiswal, B. Ratra, Quasar UV/X-ray relation luminosity distances are shorter than reverberation-measured radius–luminosity relation luminosity distances, Mon. Not. R. Astron. Soc. 522 (1) (2023) 1247–1264, arXiv:2212.10483 [astro-ph.CO].
[1397] E.O. Colgáin, M.M. Sheikh-Jabbari, L. Yin, Do high redshift QSOs and GRBs corroborate JWST? 2024, arXiv:2405.19953 [astro-ph.CO].
[1398] N.J. Secrest, S. von Hausegger, M. Rameez, R. Mohayaee, S. Sarkar, J. Colin, A test of the cosmological principle with quasars, Astrophys. J. Lett. 908 (2) (2021) L51, arXiv:2009.14826 [astro-ph.CO].
[1399] A.K. Singal, Peculiar motion of the solar system derived from a dipole anisotropy in the redshift distribution of distant quasars, Mon. Not. R. Astron. Soc. 488 (1) (2019) L104–L108, arXiv:1405.4796 [astro-ph.CO].
[1400] L. Dam, G.F. Lewis, B.J. Brewer, Testing the cosmological principle with CatWISE quasars: a bayesian analysis of the number-count dipole, Mon. Not. R. Astron. Soc. 525 (1) (2023) 231–245, arXiv:2212.07733 [astro-ph.CO].
[1401] R. Kothari, M. Panwar, G. Singh, P. Tiwari, P. Jain, A study of dipolar signal in distant Quasars with various observables, Eur. Phys. J. C 84 (1) (2024) 75, arXiv:2208.14397 [astro-ph.CO].
[1402] A. Abghari, E.F. Bunn, L.T. Hergt, B. Li, D. Scott, R.M. Sullivan, D. Wei, Reassessment of the dipole in the distribution of quasars on the sky, J. Cosmol. Astropart. Phys. 11 (2024) 067, arXiv:2405.09762 [astro-ph.CO].
[1403] O. Luongo, M. Muccino, E.O. Colgáin, M.M. Sheikh-Jabbari, L. Yin, Larger H0 values in the CMB dipole direction, Phys. Rev. D 105 (10) (2022) 103510, arXiv:2108.13228 [astro-ph.CO].
[1404] C. Blake, J. Wall, Detection of the velocity dipole in the radio galaxies of the nrao vla sky survey, Nature 416 (2002) 150–152, arXiv:astro-ph/0203385.
[1405] J. Colin, R. Mohayaee, M. Rameez, S. Sarkar, High redshift radio galaxies and divergence from the CMB dipole, Mon. Not. R. Astron. Soc. 471 (1) (2017) 1045–1055, arXiv:1703.09376 [astro-ph.CO].
[1406] A.K. Singal, Large peculiar motion of the solar system from the dipole anisotropy in sky brightness due to distant radio sources, Astrophys. J. Lett. 742 (2011) L23, arXiv:1110.6260 [astro-ph.CO].
[1407] M. Rubart, D.J. Schwarz, Cosmic radio dipole from NVSS and WENSS, Astron. Astrophys. 555 (2013) A117, arXiv:1301.5559 [astro-ph.CO].
[1408] C.A.P. Bengaly, T.M. Siewert, D.J. Schwarz, R. Maartens, Testing the standard model of cosmology with the SKA: the cosmic radio dipole, Mon. Not. R. Astron. Soc. 486 (1) (2019) 1350–1357, arXiv:1810.04960 [astro-ph.CO].
[1409] A.K. Singal, Large disparity in cosmic reference frames determined from the sky distributions of radio sources and the microwave background radiation, Phys. Rev. D 100 (6) (2019) 063501, arXiv:1904.11362 [physics.gen-ph].
[1410] T.M. Siewert, M. Schmidt-Rubart, D.J. Schwarz, Cosmic radio dipole: Estimators and frequency dependence, Astron. Astrophys. 653 (2021) A9, arXiv:2010.08366 [astro-ph.CO].
[1411] N.J. Secrest, S. von Hausegger, M. Rameez, R. Mohayaee, S. Sarkar, A challenge to the standard cosmological model, Astrophys. J. Lett. 937 (2) (2022) L31, arXiv:2206.05624 [astro-ph.CO].
[1412] J.D. Wagenveld, H.-R. Klöckner, D.J. Schwarz, The cosmic radio dipole: Bayesian estimators on new and old radio surveys, Astron. Astrophys. 675 (2023) A72, arXiv:2305.15335 [astro-ph.CO].
[1413] A.K. Singal, Resolution of the incongruency of dipole asymmetries within various large radio surveys – implications for the Cosmological Principle, Mon. Not. R. Astron. Soc. 528 (4) (2024) 5679–5691, arXiv:2312.12785 [astro-ph.CO].
[1414] C. Gibelyou, D. Huterer, Dipoles in the sky, Mon. Not. R. Astron. Soc. 427 (2012) 1994–2021, arXiv:1205.6476 [astro-ph.CO].
[1415] C.A.P. Bengaly, R. Maartens, N. Randriamiarinarivo, A. Baloyi, Testing the cosmological principle in the radio sky, J. Cosmol. Astropart. Phys. 09 (2019) 025, arXiv:1905.12378 [astro-ph.CO].
[1416] C. Murray, The effects of lensing by local structures on the dipole of radio source counts, Mon. Not. R. Astron. Soc. 510 (2) (2022) 3098–3101, arXiv:2112.06689 [astro-ph.CO].
[1417] Y.-T. Cheng, T.-C. Chang, A. Lidz, Is the radio source dipole from NVSS consistent with the cosmic microwave background and ΛCDM? Astrophys. J. 965 (1) (2024) 32, arXiv:2309.02490 [astro-ph.CO].
[1418] P. da Silveira Ferreira, V. Marra, Tomographic redshift dipole: testing the cosmological principle, J. Cosmol. Astropart. Phys. 09 (2024) 077, arXiv:2403.14580 [astro-ph.CO].
[1419] O.T. Oayda, V. Mittal, G.F. Lewis, T. Murphy, A Bayesian approach to the cosmic dipole in radio galaxy surveys: joint analysis of NVSS & RACS, Mon. Not. R. Astron. Soc. 531 (4) (2024) 4545–4559, arXiv:2406.01871 [astro-ph.CO].
[1420] B.E. Schaefer, The hubble diagram to redshift >6 from 69 gamma-ray bursts, Astrophys. J. 660 (2007) 16–46, arXiv:astro-ph/0612285.
[1421] S. Basilakos, L. Perivolaropoulos, Testing GRBs as standard candles, Mon. Not. R. Astron. Soc. 391 (2008) 411–419, arXiv:0805.0875 [astro-ph].
[1422] N. Liang, W.K. Xiao, Y. Liu, S.N. Zhang, A cosmology independent calibration of gamma-ray burst luminosity relations and the hubble diagram, Astrophys. J. 685 (2008) 354, arXiv:0802.4262 [astro-ph].
[1423] S. Cao, N. Khadka, B. Ratra, Standardizing Dainotti-correlated gamma-ray bursts, and using them with standardized Amati-correlated gamma-ray bursts to constrain cosmological model parameters, Mon. Not. R. Astron. Soc. 510 (2) (2022) 2928–2947, arXiv:2110.14840 [astro-ph.CO].
[1424] R.B. Tully, et al., Cosmicflows-4, Astrophys. J. 944 (1) (2023) 94, arXiv:2209.11238 [astro-ph.CO].
[1425] Y. Hoffman, A. Valade, N.I. Libeskind, J.G. Sorce, R.B. Tully, S. Pfeifer, S. Gottlöber, D. Pomarède, The large-scale velocity field from the Cosmicflows-4 data, Mon. Not. R. Astro. Soc. 527 (2) (2024) 3788–3805, arXiv:2311.01340 [astro-ph.CO].
[1426] R. Watkins, T. Allen, C.J. Bradford, A. Ramon, A. Walker, H.A. Feldman, R. Cionitti, Y. Al-Shorman, E. Kourkchi, R.B. Tully, Analysing the large-scale bulk flow using cosmicflows4: increasing tension with the standard cosmological model, Mon. Not. R. Astron. Soc. 524 (2) (2023) 1885–1892, arXiv:2302.02028 [astro-ph.CO].
[1427] A.M. Whitford, C. Howlett, T.M. Davis, Evaluating bulk flow estimators for CosmicFlows–4 measurements, Mon. Not. R. Astron. Soc. 526 (2) (2023) 3051–3071, arXiv:2306.11269 [astro-ph.CO].
[1428] S. Peery, R. Watkins, H.A. Feldman, Easily interpretable bulk flows: continuing tension with the standard cosmological model, Mon. Not. R. Astron. Soc. 481 (1) (2018) 1368–1375, arXiv:1808.07772 [astro-ph.CO].
[1429] A. Kashlinsky, F. Atrio-Barandela, D. Kocevski, H. Ebeling, A measurement of large-scale peculiar velocities of clusters of galaxies: results and cosmological implications, Astrophys. J. Lett. 686 (2009) L49–L52, arXiv:0809.3734 [astro-ph].
[1430] F. Atrio-Barandela, A. Kashlinsky, H. Ebeling, D.J. Fixsen, D. Kocevski, Probing the dark flow signal in Wmap 9 -year and planck cosmic microwave background maps, Astrophys. J. 810 (2) (2015) 143, arXiv:1411.4180 [astro-ph.CO].
[1431] A. Kashlinsky, F. Atrio-Barandela, H. Ebeling, A. Edge, D. Kocevski, A new measurement of the bulk flow of X-ray luminous clusters of galaxies, Astrophys. J. Lett. 712 (2010) L81–L85, arXiv:0910.4958 [astro-ph.CO].
[1432] A. Kashlinsky, F. Atrio-Barandela, H. Ebeling, Measuring the dark flow with public X-ray cluster data, Astrophys. J. 732 (2011) 1, arXiv:1012.3214 [astro-ph.CO].
[1433] F. Atrio-Barandela, On the statistical significance of the bulk flow measured by the PLANCK satellite, Astron. Astrophys. 557 (2013) A116, arXiv:1303.6614 [astro-ph.CO].
[1434] Planck Collaboration, N. Aghanim, et al., Planck 2018 results. I. Overview and the cosmological legacy of Planck, Astron. Astrophys. 641 (2020) A1, arXiv:1807.06205 [astro-ph.CO].
[1435] J. Grande, L. Perivolaropoulos, Generalized LTB model with inhomogeneous isotropic dark energy: observational constraints, Phys. Rev. D 84 (2011) 023514, arXiv:1103.4143 [astro-ph.CO].
[1436] H. Alnes, M. Amarzguioui, O. Gron, Can a dust dominated Universe have accelerated expansion? J. Cosmol. Astropart. Phys. 01 (2007) 007, arXiv:astro-ph/0506449.
[1437] L. Ackerman, S.M. Carroll, M.B. Wise, Imprints of a primordial preferred direction on the microwave background, Phys. Rev. D 75 (2007) 083502, arXiv:astro-ph/0701357; Phys. Rev. D 80 (2009) 069901 (erratum).
[1438] R. Aurich, S. Lustig, F. Steiner, CMB anisotropy of the Poincare dodecahedron, Cl. Quant. Grav. 22 (2005) 2061–2083, arXiv:astro-ph/0412569.
[1439] COMPACT Collaboration, Y. Akrami, et al., Promise of future searches for cosmic topology, Phys. Rev. Lett. 132 (17) (2024) 171501, arXiv:2210.11426 [astro-ph.CO].
[1440] J.C. Bueno Sanchez, L. Perivolaropoulos, Topological quintessence, Phys. Rev. D 84 (2011) 123516, arXiv:1110.2587 [astro-ph.CO].
[1441] L. Perivolaropoulos, Topological quintessence: Generalizing Lambda CDM with inhomogeneous dark energy, Romanian J. Phys. 57 (2012) 950–968.
[1442] T. Koivisto, D.F. Mota, Dark energy anisotropic stress and large scale structure formation, Phys. Rev. D 73 (2006) 083502, arXiv:astro-ph/0512135.
[1443] R. Battye, A. Moss, Anisotropic dark energy and CMB anomalies, Phys. Rev. D 80 (2009) 023531, arXiv:0905.3403 [astro-ph.CO].
[1444] J.D. Barrow, Cosmological limits on slightly skew stresses, Phys. Rev. D 55 (1997) 7451–7460, arXiv:gr-qc/9701038.
[1445] J.D. Barrow, P.G. Ferreira, J. Silk, Constraints on a primordial magnetic field, Phys. Rev. Lett. 78 (1997) 3610–3613, arXiv:astro-ph/9701063.
[1446] L. Campanelli, A model of universe anisotropization, Phys. Rev. D 80 (2009) 063006, arXiv:0907.3703 [astro-ph.CO].
[1447] A. Maleknejad, M.M. Sheikh-Jabbari, J. Soda, Gauge fields and inflation, Phys. Rep. 528 (2013) 161–261, arXiv:1212.2921 [hep-th].
[1448] K. Dimopoulos, M. Karciauskas, J.M. Wagstaff, Vector curvaton with varying kinetic function, Phys. Rev. D 81 (2010) 023522, arXiv:0907.1838 [hep-ph].
[1449] M. Karciauskas, K. Dimopoulos, D.H. Lyth, Anisotropic non-Gaussianity from vector field perturbations, Phys. Rev. D 80 (2009) 023509, arXiv:0812.0264 [astro-ph]; Phys. Rev. D 85 (2012) 069905 (erratum).
[1450] C.G. Tsagas, Peculiar motions, accelerated expansion and the cosmological axis, Phys. Rev. D 84 (2011) 063503, arXiv:1107.4045 [astro-ph.CO].
[1451] T. Anton, T. Clifton, Modelling the emergence of cosmic anisotropy from non-linear structures, Cl. Quant. Grav. 40 (14) (2023) 145004, arXiv:2302.05715 [gr-qc].

[1452] E. Pastén, V.H. Cárdenas, Testing ΛCDM cosmology in a binned universe: Anomalies in the deceleration parameter, Phys. Dark Univ. 40 (2023) 101224, arXiv:2301.10740 [astro-ph.CO].

[1453] C.G. Tsagas, The peculiar Jeans length, Eur. Phys. J. C 81 (8) (2021) 753, arXiv:2103.15884 [gr-qc].

[1454] O. Roldan, A. Notari, M. Quartin, Interpreting the CMB aberration and Doppler measurements: boost or intrinsic dipole? J. Cosmol. Astropart. Phys. 06 (2016) 026, arXiv:1603.02664 [astro-ph.CO].

[1455] S. Yasini, E. Pierpaoli, Beyond the boost: measuring the intrinsic dipole of the cosmic microwave background using the spectral distortions of the monopole and quadrupole, Phys. Rev. Lett. 119 (22) (2017) 221102, arXiv:1610.00015 [astro-ph.CO].

[1456] P.d.S. Ferreira, M. Quartin, First constraints on the intrinsic CMB dipole and our velocity with doppler and aberration, Phys. Rev. Lett. 127 (10) (2021) 101301, arXiv:2011.08385 [astro-ph.CO].

[1457] M.I. Khan, R. Saha, Detection of dipole modulation in CMB temperature anisotropy maps from WMAP and planck using artificial intelligence, Astrophys. J. 947 (2) (2023) 47, arXiv:2212.04438 [astro-ph.CO].

[1458] C.E. Kester, A. Bernui, W.S. Hipólito-Ricaldi, Probing the statistical isotropy of the universe with Planck data of the cosmic microwave background, Astron. Astrophys. 683 (2024) A176, arXiv:2310.02928 [astro-ph.CO].

[1459] J.A. King, J.K. Webb, M.T. Murphy, V.V. Flambaum, R.F. Carswell, M.B. Bainbridge, M.R. Wilczynska, F.E. Koch, Spatial variation in the fine-structure constant – new results from VLT/UVES, Mon. Not. R. Astron. Soc. 422 (2012) 3370–3413, arXiv:1202.4758 [astro-ph.CO].

[1460] D.-C. Qiang, H.-K. Deng, H. Wei, Cosmic anisotropy and fast radio bursts, Cl. Quant. Grav. 37 (18) (2020) 185022, arXiv:1902.03580 [astro-ph.CO].

[1461] H.-N. Lin, Y. Sang, Probing the anisotropic distribution of baryon matter in the Universe using fast radio bursts *, Chin. Phys. C 45 (12) (2021) 125101, arXiv:2111.12934 [astro-ph.CO].

[1462] O.T. Oayda, G.F. Lewis, Testing the cosmological principle: on the time dilation of distant sources, Mon. Not. R. Astron. Soc. 523 (1) (2023) 667–675, arXiv:2305.06771 [astro-ph.CO].

[1463] V. Mittal, O.T. Oayda, G.F. Lewis, The cosmic dipole in the quaia sample of quasars: a Bayesian analysis, Mon. Not. R. Astron. Soc. 527 (3) (2024) 8497–8510, arXiv:2311.14938 [astro-ph.CO]; Mon. Not. Roy. Astron. Soc. 530 (2024) 4763–4764 (erratum).

[1464] F. Iocco, G. Mangano, G. Miele, O. Pisanti, P.D. Serpico, Primordial Nucleosynthesis: from precision cosmology to fundamental physics, Phys. Rep. 472 (2009) 1–76, arXiv:0809.0631 [astro-ph].

[1465] R.H. Cyburt, B.D. Fields, K.A. Olive, T.-H. Yeh, Big bang nucleosynthesis: 2015, Rev. Modern Phys. 88 (2016) 015004, arXiv:1505.01076 [astro-ph.CO].

[1466] I. Tanihata, H. Toki, T. Kajino (Eds.), Big bang nucleosynthesis, in: Handbook of Nuclear Physics, Springer Nature Singapore, 2023, pp. 1–21, arXiv:2301.12299 [astro-ph.CO].

[1467] Particle Data Group Collaboration, R.L. Workman, et al., Review of particle physics, PTEP 2022 (2022) 083C01.

[1468] T.-H. Yeh, K.A. Olive, B.D. Fields, The impact of new $d(p,\gamma)3$ rates on Big Bang Nucleosynthesis, J. Cosmol. Astropart. Phys. 03 (2021) 046, arXiv:2011.13874 [astro-ph.CO].

[1469] A. Coc, S. Goriely, Y. Xu, M. Saimpert, E. Vangioni, Standard Big-Bang Nucleosynthesis up to CNO with an improved extended nuclear network, Astrophys. J. 744 (2012) 158, arXiv:1107.1117 [astro-ph.CO].

[1470] R. Consiglio, P.F. de Salas, G. Mangano, G. Miele, S. Pastor, O. Pisanti, PArthENoPE reloaded, Comput. Phys. Comm. 233 (2018) 237–242, arXiv:1712.04378 [astro-ph.CO].

[1471] C. Pitrou, A. Coc, J.-P. Uzan, E. Vangioni, A new tension in the cosmological model from primordial deuterium? Mon. Not. R. Astron. Soc. 502 (2) (2021) 2474–2481, arXiv:2011.11320 [astro-ph.CO].

[1472] V. Singh, D. Bhowmick, D.N. Basu, Re-examining the Lithium abundance problem in Big-Bang nucleosynthesis, Astropart. Phys. 162 (2024) 102995, arXiv:2304.08032 [nucl-th].

[1473] S. Gariazzo, P. F. de Salas, O. Pisanti, R. Consiglio, PArthENoPE revolutions, Comput. Phys. Comm. 271 (2022) 108205, arXiv:2103.05027 [astro-ph.IM].

[1474] L. Sbordone, et al., The metal-poor end of the Spite plateau. 1: Stellar parameters, metallicities and lithium abundances, Astron. Astrophys. 522 (2010) A26, arXiv:1003.4510 [astro-ph.GA].

[1475] J.C. Howk, N. Lehner, B.D. Fields, G.J. Mathews, The detection of interstellar lithium in a low-metallicity galaxy, Nature 489 (2012) 121, arXiv:1207.3081 [astro-ph.CO].

[1476] L. Izzo, P. Molaro, G. Cescutti, E. Aydi, P. Selvelli, E. Harvey, A. Agnello, P. Bonifacio, M. Della Valle, E. Guido, M. Hernanz, Detection of ^{7}Be II in the small magellanic cloud, Mon. Not. R. Astro. Soc. 510 (4) (2022) 5302–5314, arXiv:2112.11859 [astro-ph.SR].

[1477] B.D. Fields, The primordial lithium problem, Ann. Rev. Nucl. Part. Sci. 61 (2011) 47–68, arXiv:1203.3551 [astro-ph.CO].

[1478] F. Spite, M. Spite, Abundance of lithium in unevolved halo stars and old disk stars: Interpretation and consequences, Astron. Astrophys. 115 (1982) 357–366.

[1479] R. Rebolo, P. Molaro, J.E. Beckman, Lithium abundances in metal-deficient dwarfs, Astron. Astrophys. 192 (1988) 192–205.

[1480] F. Matteucci, M. Molero, D.S. Aguado, D. Romano, The evolution of Lithium: implications of a universal Spite plateau, Mon. Not. R. Astro. Soc. 505 (1) (2021) 200–206, arXiv:2104.11504 [astro-ph.GA].

[1481] T. Makki, M.E. Eid, G. Mathews, New insight concerning primordial lithium production, 2024, arXiv:2402.17871 [astro-ph.CO].

[1482] X. Fu, A. Bressan, P. Molaro, P. Marigo, Lithium evolution in metal-poor stars: from pre-main sequence to the Spite plateau, Mon. Not. R. Astro. Soc. 452 (3) (2015) 3256–3265, arXiv:1506.05993 [astro-ph.SR].

[1483] B.D. Fields, K.A. Olive, Implications of the non-observation of ^{6}Li in halo stars for the primordial ^{7}Li problem, J. Cosmol. Astropart. Phys. 10 (2022) 078, arXiv:2204.03167 [astro-ph.GA].

[1484] V.V. Smith, D.L. Lambert, P.E. Nissen, The 6Li/7Li ratio in the metal-poor halo dwarfs HD 19445 and HD 84937, Astrophys. J. 408 (1993) 262–276.

[1485] L.M. Hobbs, J.A. Thorburn, Lithium isotope ratios in six halo stars, Astrophys. J. Lett. 428 (1994) L25.

[1486] L.M. Hobbs, J.A. Thorburn, Lithium isotope ratios in halo stars. II, Astrophys. J. 491 (2) (1997) 772–788.

[1487] V.V. Smith, D.L. Lambert, P.E. Nissen, Isotopic lithium abundances in nine halo stars, Astrophys. J. 506 (1) (1998) 405–423.

[1488] L.M. Hobbs, J.A. Thorburn, L.M. Rebull, Lithium isotope ratios in halo stars. III, Astrophys. J. 523 (2) (1999) 797–804.

[1489] R. Cayrel, M. Spite, F. Spite, E. Vangioni-Flam, M. Casse, J.A.R. Cayrel, J. Audouze, New high s/n observations of the li-6/li-7 blend in hd 84937 and two other metal-poor stars, Astron. Astrophys. 343 (1999) 923, arXiv:astro-ph/9901205.

[1490] M. Asplund, D.L. Lambert, P.E. Nissen, F. Primas, V.V. Smith, Lithium isotopic abundances in metal-poor halo stars, Astrophys. J. 644 (2006) 229–259, arXiv:astro-ph/0510636.

[1491] M. Steffen, R. Cayrel, P. Bonifacio, H.G. Ludwig, E. Caffau, 6Li in metal-poor halo stars: real or spurious? IAU Symp. 265 (2010) 23, arXiv:0910.5917 [astro-ph.SR].

[1492] A.E.G. Perez, W. Aoki, S. Inoue, S.G. Ryan, T.K. Suzuki, M. Chiba, 6Li/7Li estimates for metal-poor stars, Astron. Astrophys. 504 (2009) 213, arXiv:0909.5163 [astro-ph.SR].

[1493] K. Lind, J. Melendez, M. Asplund, R. Collet, Z. Magic, The lithium isotopic ratio in very metal-poor stars, Astron. Astrophys. 554 (2013) A96, arXiv:1305.6564 [astro-ph.SR].

[1494] E.X. Wang, T. Nordlander, M. Asplund, K. Lind, Y. Zhou, H. Reggiani, Non-detection of 6Li in Spite plateau stars with ESPRESSO, Mon. Not. R. Astron. Soc. 509 (1) (2021) 1521–1535, arXiv:2110.03822.

[1495] A. Korn, The ups and downs of inferred cosmological lithium, EPJ Web Conf. 297 (2024) 01007, arXiv:2406.09974 [astro-ph.SR].

[1496] GALAH Collaboration, X. Gao, et al., The GALAH Survey: A new constraint on cosmological lithium and Galactic lithium evolution from warm dwarf stars, Mon. Not. R. Astron. Soc. 497 (1) (2020) L30–L34, arXiv:2006.05173 [astro-ph.SR].

[1497] K.A. Olive, P. Petitjean, E. Vangioni, J. Silk, Higher D or Li: probes of physics beyond the standard model, Mon. Not. R. Astron. Soc. 426 (2012) 1427, arXiv:1203.5701 [astro-ph.CO].

[1498] A. Coc, M. Pospelov, J.-P. Uzan, E. Vangioni, Modified big bang nucleosynthesis with nonstandard neutron sources, Phys. Rev. D 90 (8) (2014) 085018, arXiv:1405.1718 [hep-ph].

[1499] K. Jedamzik, Neutralinos and Big Bang nucleosynthesis, Phys. Rev. D 70 (2004) 083510, arXiv:astro-ph/0405583.

[1500] K. Jedamzik, Did something decay, evaporate, or annihilate during Big Bang nucleosynthesis? Phys. Rev. D 70 (2004) 063524, arXiv:astro-ph/0402344.

[1501] A. Goudelis, M. Pospelov, J. Pradler, Light particle solution to the cosmic lithium problem, Phys. Rev. Lett. 116 (21) (2016) 211303, arXiv:1510.08858 [hep-ph].

[1502] S.Q. Hou, J.J. He, A. Parikh, D. Kahl, C.A. Bertulani, T. Kajino, G.J. Mathews, G. Zhao, Non-extensive statistics to the cosmological lithium problem, Astrophys. J. 834 (2) (2017) 165, arXiv:1701.04149 [astro-ph.CO].

[1503] R. Nakamura, M.-a. Hasahimoto, R. Ichimasa, K. Arai, Big-Bang nucleosynthesis: Constraints on nuclear reaction rates, neutrino degeneracy, inhomogeneous and Brans–Dicke models, Int. J. Mod. Phys. E 26 (08) (2017) 1741003, arXiv:1710.08153 [astro-ph.CO].

[1504] D.G. Yamazaki, M. Kusakabe, T. Kajino, G.J. Mathews, M.-K. Cheoun, The new hybrid BBN model with the photon cooling, X particle, and the primordial magnetic field, Int. J. Mod. Phys. E 26 (08) (2017) 1741006.

[1505] T.R. Makki, M.F. El Eid, G.J. Mathews, Impact of neutrino properties and dark matter on the primordial lithium production, Int. J. Mod. Phys. E 28 (08) (2019) 1950065, arXiv:1901.03726 [astro-ph.CO].

[1506] T.R. Makki, M.F. El Eid, G.J. Mathews, A critical analysis of the Big Bang Nucleosynthesis, Modern Phys. Lett. A 34 (24) (2019) 1950194.

[1507] A.-K. Burns, V. Keus, M. Sher, T.M.P. Tait, Constraints on variation of the weak scale from big bang nucleosynthesis, Phys. Rev. D 109 (12) (2024) 123506, arXiv:2402.08626 [hep-ph].

[1508] G.-y. Huang, W. Rodejohann, Solving the Hubble tension without spoiling Big Bang Nucleosynthesis, Phys. Rev. D 103 (2021) 123007, arXiv:2102.04280 [hep-ph].

[1509] F.F. Deppisch, L. Graf, W. Rodejohann, X.-J. Xu, Neutrino self-interactions and double beta decay, Phys. Rev. D 102 (5) (2020) 051701, arXiv:2004.11919 [hep-ph].
[1510] G.J. Mathews, A. Kedia, N. Sasankan, M. Kusakabe, Y. Luo, T. Kajino, D. Yamazaki, T. Makki, M.E. Eid, Cosmological solutions to the lithium problem, JPS Conf. Proc. 31 (2020) 011033, arXiv:1909.01245 [astro-ph.CO].
[1511] T.M. Bania, R.T. Rood, D.S. Balser, The cosmological density of baryons from observations of 3He+ in the Milky Way, Nature 415 (2002) 54–57.
[1512] E. Aver, D.A. Berg, K.A. Olive, R.W. Pogge, J.J. Salzer, E.D. Skillman, Improving helium abundance determinations with Leo P as a case study, J. Cosmol. Astropart. Phys. 03 (2021) 027, arXiv:2010.04180 [astro-ph.CO].
[1513] M. Valerdi, A. Peimbert, M. Peimbert, A. Sixtos, Determination of the primordial helium abundance based on NGC 346, an H ii region of the small magellanic cloud, Astrophys. J. 876 (2) (2019) 98, arXiv:1904.01594 [astro-ph.GA].
[1514] V. Fernández, E. Terlevich, A.I. Díaz, R. Terlevich, A Bayesian direct method implementation to fit emission line spectra: Application to the primordial He abundance determination, Mon. Not. R. Astron. Soc. 487 (3) (2019) 3221–3238, arXiv:1905.09215 [astro-ph.GA].
[1515] O.A. Kurichin, P.A. Kislitsyn, V.V. Klimenko, S.A. Balashev, A.V. Ivanchik, A new determination of the primordial helium abundance using the analyses of H II region spectra from SDSS, Mon. Not. R. Astron. Soc. 502 (2) (2021) 3045–3056, arXiv:2101.09127 [astro-ph.CO].
[1516] T. Hsyu, R.J. Cooke, J.X. Prochaska, M. Bolte, The PHLEK survey: a new determination of the primordial helium abundance, Astrophys. J. 896 (1) (2020) 77, arXiv:2005.12290 [astro-ph.GA].
[1517] M. Valerdi, A. Peimbert, M. Peimbert, Chemical abundances in seven metal-poor H II regions and a determination of the primordial helium abundance, Mon. Not. R. Astro. Soc. 505 (3) (2021) 3624–3634, arXiv:2105.12260 [astro-ph.GA].
[1518] A. Matsumoto, et al., EMPRESS. VIII. A new determination of primordial he abundance with extremely metal-poor galaxies: a suggestion of the lepton asymmetry and implications for the hubble tension, Astrophys. J. 941 (2) (2022) 167, arXiv:2203.09617 [astro-ph.CO].
[1519] T. Takahashi, S. Yamashita, Big bang nucleosynthesis and early dark energy in light of the EMPRESS Yp results and the H0 tension, Phys. Rev. D 107 (10) (2023) 103520, arXiv:2211.04087 [astro-ph.CO].
[1520] M. Escudero, A. Ibarra, V. Maura, Primordial lepton asymmetries in the precision cosmology era: Current status and future sensitivities from BBN and the CMB, Phys. Rev. D 107 (3) (2023) 035024, arXiv:2208.03201 [hep-ph].
[1521] Y.I. Izotov, T.X. Thuan, N.G. Guseva, A new determination of the primordial He abundance using the He i λ10830 Å emission line: cosmological implications, Mon. Not. R. Astron. Soc. 445 (1) (2014) 778–793, arXiv:1408.6953 [astro-ph.CO].
[1522] C. Pitrou, A. Coc, J.-P. Uzan, E. Vangioni, Resolving conclusions about the early Universe requires accurate nuclear measurements, Nat. Rev. Phys. 3 (4) (2021) 231–232, arXiv:2104.11148 [astro-ph.CO].
[1523] O. Pisanti, G. Mangano, G. Miele, P. Mazzella, Primordial Deuterium after LUNA: concordances and error budget, J. Cosmol. Astropart. Phys. 04 (2021) 020, arXiv:2011.11537 [astro-ph.CO].
[1524] E. Di Valentino, C. Gustavino, J. Lesgourgues, G. Mangano, A. Melchiorri, G. Miele, O. Pisanti, Probing nuclear rates with Planck and BICEP2, Phys. Rev. D 90 (2) (2014) 023543, arXiv:1404.7848 [astro-ph.CO].
[1525] G.E. Addison, G. Hinshaw, M. Halpern, Cosmological constraints from baryon acoustic oscillations and clustering of large-scale structure, Mon. Not. R. Astron. Soc. 436 (2013) 1674–1683, arXiv:1304.6984 [astro-ph.CO].
[1526] G.E. Addison, D.J. Watts, C.L. Bennett, M. Halpern, G. Hinshaw, J.L. Weiland, Elucidating ΛCDM: impact of baryon acoustic oscillation measurements on the hubble constant discrepancy, Astrophys. J. 853 (2) (2018) 119, arXiv:1707.06547 [astro-ph.CO].
[1527] eBOSS Collaboration, M. Blomqvist, et al., Baryon acoustic oscillations from the cross-correlation of Lyα absorption and quasars in eBOSS DR14, Astron. Astrophys. 629 (2019) A86, arXiv:1904.03430 [astro-ph.CO].
[1528] A. Cuceu, J. Farr, P. Lemos, A. Font-Ribera, Baryon acoustic oscillations and the hubble constant: past, present and future, J. Cosmol. Astropart. Phys. 10 (2019) 044, arXiv:1906.11628 [astro-ph.CO].
[1529] N. Schöneberg, L. Verde, H. Gil-Marín, S. Brieden, BAO+BBN revisited — growing the Hubble tension with a 0.7 km/s/Mpc constraint, J. Cosmol. Astropart. Phys. 11 (2022) 039, arXiv:2209.14330 [astro-ph.CO].
[1530] N. Schöneberg, L. Vacher, The mass effect — variations of the electron mass and their impact on cosmology, J. Cosmol. Astropart. Phys. 03 (2025) 004, arXiv:2407.16845 [astro-ph.CO].
[1531] B.D. Fields, K.A. Olive, T.-H. Yeh, C. Young, Big-Bang Nucleosynthesis after Planck, J. Cosmol. Astropart. Phys. 03 (2020) 010, arXiv:1912.01132 [astro-ph.CO]; JCAP 11 (2020) E02 (erratum).
[1532] M. McQuinn, The evolution of the intergalactic medium, Ann. Rev. Astron. Astrophys. 54 (2016) 313–362, arXiv:1512.00086 [astro-ph.CO].
[1533] eBOSS Collaboration, H. du Mas des Bourboux, et al., The completed SDSS-IV extended baryon oscillation spectroscopic survey: baryon acoustic oscillations with Lyα forests, Astrophys. J. 901 (2) (2020) 153, arXiv:2007.08995 [astro-ph.CO].
[1534] A. Cuceu, A. Font-Ribera, B. Joachimi, S. Nadathur, Cosmology beyond BAO from the 3D distribution of the Lyman-α forest, Mon. Not. R. Astron. Soc. 506 (4) (2021) 5439–5450, arXiv:2103.14075 [astro-ph.CO].
[1535] R. de Belsunce, O.H.E. Philcox, V. Irsic, P. McDonald, J. Guy, N. Palanque-Delabrouille, The 3D Lyman-α forest power spectrum from eBOSS DR16, Mon. Not. R. Astron. Soc. 533 (3) (2024) 3756–3770, arXiv:2403.08241 [astro-ph.CO].
[1536] DESI Collaboration, C. Ravoux, et al., The Dark Energy Spectroscopic Instrument: one-dimensional power spectrum from first Ly α forest samples with Fast Fourier Transform, Mon. Not. R. Astron. Soc. 526 (4) (2023) 5118–5140, arXiv:2306.06311 [astro-ph.CO].
[1537] N.G. Karaçaylı, et al., Optimal 1D Lyα forest power spectrum estimation – III. DESI early data, Mon. Not. R. Astron. Soc. 528 (3) (2024) 3941–3963, arXiv:2306.06316 [astro-ph.CO].
[1538] V.K. Narayanan, D.N. Spergel, R. Dave, C.-P. Ma, Constraints on the mass of warm dark matter particles and the shape of the linear power spectrum from the Lyα forest, Astrophys. J. Lett. 543 (2000) L103–L106, arXiv:astro-ph/0005095.
[1539] U. Seljak, A. Slosar, P. McDonald, Cosmological parameters from combining the Lyman-alpha forest with CMB, galaxy clustering and SN constraints, J. Cosmol. Astropart. Phys. 10 (2006) 014, arXiv:astro-ph/0604335.
[1540] M. Viel, J. Schaye, C.M. Booth, The impact of feedback from galaxy formation on the Lyman-alpha transmitted flux, Mon. Not. R. Astron. Soc. 429 (2013) 1734, arXiv:1207.6567 [astro-ph.CO].
[1541] V. Iršič, et al., The Lyman α forest power spectrum from the XQ-100 legacy survey, Mon. Not. R. Astron. Soc. 466 (4) (2017) 4332–4345, arXiv:1702.01761 [astro-ph.CO].
[1542] E. Boera, G.D. Becker, J.S. Bolton, F. Nasir, Revealing reionization with the thermal history of the intergalactic medium: new constraints from the Lyα flux power spectrum, Astrophys. J. 872 (1) (2019) 101, arXiv:1809.06980 [astro-ph.CO].
[1543] N.G. Karaçaylı, et al., Optimal 1D Ly α forest power spectrum estimation – II. KODIAQ, SQUAD, and XQ-100, Mon. Not. R. Astron. Soc. 509 (2) (2022) 2842–2855, arXiv:2108.10870 [astro-ph.CO].
[1544] B. Villasenor, B. Robertson, P. Madau, E. Schneider, New constraints on warm dark matter from the Lyman-α forest power spectrum, Phys. Rev. D 108 (2) (2023) 023502, arXiv:2209.14220 [astro-ph.CO].
[1545] E. Puchwein, et al., The Sherwood–Relics simulations: overview and impact of patchy reionization and pressure smoothing on the intergalactic medium, Mon. Not. R. Astron. Soc. 519 (4) (2023) 6162–6183, arXiv:2207.13098 [astro-ph.CO].
[1546] C.C. Doughty, J.F. Hennawi, F.B. Davies, Z. Lukić, J. Oñorbe, Convergence of small scale Ly α structure at high-z under different reionization scenarios, Mon. Not. R. Astron. Soc. 525 (3) (2023) 3790–3805, arXiv:2305.16200 [astro-ph.CO].
[1547] S. Bird, M. Fernandez, M.-F. Ho, M. Qezlou, R. Monadi, Y. Ni, N. Chen, R. Croft, T. Di Matteo, PRIYA: a new suite of Lyman-α forest simulations for cosmology, J. Cosmol. Astropart. Phys. 10 (2023) 037, arXiv:2306.05471 [astro-ph.CO].
[1548] SDSS Collaboration, P. McDonald, et al., The Linear theory power spectrum from the Lyman-alpha forest in the Sloan Digital Sky Survey, Astrophys. J. 635 (2005) 761–783, arXiv:astro-ph/0407377.
[1549] C. Pedersen, A. Font-Ribera, N.Y. Gnedin, Compressing the cosmological information in one-dimensional correlations of the Lyα forest, Astrophys. J. 944 (2) (2023) 223, arXiv:2209.09895 [astro-ph.CO].
[1550] M. Viel, J. Lesgourgues, M.G. Haehnelt, S. Matarrese, A. Riotto, Constraining warm dark matter candidates including sterile neutrinos and light gravitinos with WMAP and the Lyman-alpha forest, Phys. Rev. D 71 (2005) 063534, arXiv:astro-ph/0501562.
[1551] V. Iršič, M. Viel, M.G. Haehnelt, J.S. Bolton, G.D. Becker, First constraints on fuzzy dark matter from Lyman-α forest data and hydrodynamical simulations, Phys. Rev. Lett. 119 (3) (2017) 031302, arXiv:1703.04683 [astro-ph.CO].
[1552] E. Armengaud, N. Palanque-Delabrouille, C. Yèche, D.J.E. Marsh, J. Baur, Constraining the mass of light bosonic dark matter using SDSS Lyman-α forest, Mon. Not. R. Astron. Soc. 471 (4) (2017) 4606–4614, arXiv:1703.09126 [astro-ph.CO].
[1553] N. Palanque-Delabrouille, C. Yèche, N. Schöneberg, J. Lesgourgues, M. Walther, S. Chabanier, E. Armengaud, Hints, neutrino bounds and WDM constraints from SDSS DR14 Lyman-α and Planck full-survey data, J. Cosmol. Astropart. Phys. 04 (2020) 038, arXiv:1911.09073 [astro-ph.CO].
[1554] K.K. Rogers, H.V. Peiris, General framework for cosmological dark matter bounds using N-body simulations, Phys. Rev. D 103 (4) (2021) 043526, arXiv:2007.13751 [astro-ph.CO].
[1555] V. Iršič, et al., Unveiling dark matter free streaming at the smallest scales with the high redshift Lyman-alpha forest, Phys. Rev. D 109 (4) (2024) 043511, arXiv:2309.04533 [astro-ph.CO].
[1556] eBOSS Collaboration, S. Chabanier, et al., The one-dimensional power spectrum from the SDSS DR14 Lyα forests, J. Cosmol. Astropart. Phys. 07 (2019) 017, arXiv:1812.03554 [astro-ph.CO].

[1557] M.A. Fernandez, S. Bird, M.-F. Ho, Cosmological constraints from the eBOSS Lyman-α forest using the PRIYA simulations, J. Cosmol. Astropart. Phys. 07 (2024) 029, arXiv:2309.03943 [astro-ph.CO].

[1558] V. Iršič, et al., New Constraints on the free-streaming of warm dark matter from intermediate and small scale Lyman-α forest data, Phys. Rev. D 96 (2) (2017) 023522, arXiv:1702.01764 [astro-ph.CO].

[1559] C. Yèche, N. Palanque-Delabrouille, J. Baur, H. du Mas des Bourboux, Constraints on neutrino masses from Lyman-alpha forest power spectrum with BOSS and XQ-100, J. Cosmol. Astropart. Phys. 06 (2017) 047, arXiv:1702.03314 [astro-ph.CO].

[1560] M. Esposito, V. Iršič, M. Costanzi, S. Borgani, A. Saro, M. Viel, Weighing cosmic structures with clusters of galaxies and the intergalactic medium, Mon. Not. R. Astron. Soc. 515 (1) (2022) 857–870, arXiv:2202.00974 [astro-ph.CO].

[1561] S. Goldstein, J.C. Hill, V. Iršič, B.D. Sherwin, Canonical hubble-tension-resolving early dark energy cosmologies are inconsistent with the Lyman-α forest, Phys. Rev. Lett. 131 (20) (2023) 201001, arXiv:2303.00746 [astro-ph.CO].

[1562] K.K. Rogers, V. Poulin, 5σ tension between Planck cosmic microwave background and eBOSS Lyman-alpha forest and constraints on physics beyond ΛCDM, Phys. Rev. Res. 7 (1) (2025) L012018, arXiv:2311.16377 [astro-ph.CO].

[1563] T. Kobayashi, R. Murgia, A. De Simone, V. Iršič, M. Viel, Lyman-α constraints on ultralight scalar dark matter: Implications for the early and late universe, Phys. Rev. D 96 (12) (2017) 123514, arXiv:1708.00015 [astro-ph.CO].

[1564] J. Baur, N. Palanque-Delabrouille, C. Yeche, A. Boyarsky, O. Ruchayskiy, E. Armengaud, J. Lesgourgues, Constraints from Ly-α forests on non-thermal dark matter including resonantly-produced sterile neutrinos, J. Cosmol. Astropart. Phys. 12 (2017) 013, arXiv:1706.03118 [astro-ph.CO].

[1565] P. Gaikwad, et al., Probing the thermal state of the intergalactic medium at z > 5 with the transmission spikes in high-resolution Ly α forest spectra, Mon. Not. R. Astron. Soc. 494 (4) (2020) 5091–5109, arXiv:2001.10018 [astro-ph.CO].

[1566] P. Montero-Camacho, C.M. Hirata, P. Martini, K. Honscheid, Impact of inhomogeneous reionization on the Lyman-α forest, Mon. Not. R. Astron. Soc. 487 (1) (2019) 1047–1056, arXiv:1902.02892 [astro-ph.CO].

[1567] M. Molaro, V. Iršič, J.S. Bolton, M. Lieu, L.C. Keating, E. Puchwein, M.G. Haehnelt, M. Viel, Possible evidence for a large-scale enhancement in the Lyman-α forest power spectrum at redshift z $\geq$ 4, Mon. Not. R. Astron. Soc. 521 (1) (2023) 1489–1501, arXiv:2303.05167 [astro-ph.CO].

[1568] J. Einasto, Dark Matter and Cosmic Web Story, World Scientific Publishing Co., 2014.

[1569] M. Einasto, J. Einasto, P. Tenjes, S. Korhonen, R. Kipper, E. Tempel, L.J. Liivamägi, P. Heinämäki, Galaxy groups and clusters and their brightest galaxies within the cosmic web, Astron. Astrophys. 681 (2024) A91, arXiv:2311.01868 [astro-ph.CO].

[1570] S. Sankhyayan, J. Bagchi, E. Tempel, S. More, M. Einasto, P. Dabhade, S. Raychaudhury, R. Athreya, P. Heinämäki, Identification of superclusters and their properties in the sloan digital sky survey using the WHL cluster catalog, Astrophys. J. 958 (1) (2023) 62, arXiv:2309.06251 [astro-ph.CO].

[1571] J. Einasto, I. Suhhonenko, L.J. Liivamägi, M. Einasto, Evolution of superclusters in the cosmic web, Astron. Astrophys. 623 (2019) A97, arXiv:1901.09378 [astro-ph.CO].

[1572] M. Einasto, J. Einasto, E. Tago, G.B. Dalton, H. Andernach, The structure of the universe traced by rich clusters of galaxies, Mon. Not. R. Astro. Soc. 269 (1994) 301–322.

[1573] H. Lietzen, E. Tempel, L.J. Liivamägi, A. Montero-Dorta, M. Einasto, A. Streblyanska, C. Maraston, J.A. Rubiño Martín, E. Saar, Discovery of a massive supercluster system at z $\sim$ 0.47, Astron. Astrophys. 588 (2016) L4, arXiv:1602.08498 [astro-ph.CO].

[1574] M. Einasto, R. Kipper, P. Tenjes, H. Lietzen, E. Tempel, L.J. Liivamägi, J. Einasto, A. Tamm, P. Heinämäki, P. Nurmi, The Corona Borealis supercluster: connectivity, collapse, and evolution, Astron. Astrophys. 649 (2021) A51, arXiv:2103.02326 [astro-ph.CO].

[1575] N. Aghanim, T. Tuominen, V. Bonjean, C. Gouin, T. Bonnaire, M. Einasto, Dissecting a miniature universe: A multi-wavelength view of galaxy quenching in the Shapley supercluster, Astron. Astrophys. 689 (2024) A332, arXiv:2402.18455 [astro-ph.CO].

[1576] L.J. Liivamagi, E. Tempel, E. Saar, SDSS DR7 superclusters. The catalogues, Astron. Astrophys. 539 (2012) A80, arXiv:1012.1989 [astro-ph.CO].

[1577] R.B. Tully, H. Courtois, Y. Hoffman, D. Pomarède, The Laniakea supercluster of galaxies, Nature 513 (7516) (2014) 71, arXiv:1409.0880 [astro-ph.CO].

[1578] A. Dupuy, H.M. Courtois, Dynamic cosmography of the local Universe: Laniakea and five more watershed superclusters, Astron. Astrophys. 678 (2023) A176, arXiv:2305.02339 [astro-ph.CO].

[1579] M. Einasto, et al., The Sloan Great Wall. Morphology and galaxy content, Astrophys. J. 736 (2011) 51, arXiv:1105.1632 [astro-ph.CO].

[1580] J.M. Zúñiga, C.A. Caretta, H. Andernach, Nucleation regions in the Large-Scale Structure I: A catalogue of cores in nearby rich superclusters, Publ. Astron. Soc. Austral. 41 (2024) e078, arXiv:2405.13280 [astro-ph.CO].

[1581] S. Lim, J. Lee, An analytic formula for the supercluster mass function, Astrophys. J. 783 (2014) 39, arXiv:1201.1382 [astro-ph.CO].

[1582] S. Nadathur, S. Hotchkiss, S. Sarkar, The integrated Sachs-Wolfe imprints of cosmic superstructures: a problem for ΛCDM, J. Cosmol. Astropart. Phys. 06 (2012) 042, arXiv:1109.4126 [astro-ph.CO].

[1583] B.R. Granett, M.C. Neyrinck, I. Szapudi, An imprint of super-structures on the microwave background due to the integrated sachs-wolfe effect, Astrophys. J. Lett. 683 (2008) L99–L102, arXiv:0805.3695 [astro-ph].

[1584] I.D. Gialamas, G. Hütsi, K. Kannike, A. Racioppi, M. Raidal, M. Vasar, H. Veermäe, Interpreting DESI 2024 BAO: Late-time dynamical dark energy or a local effect? Phys. Rev. D 111 (4) (2025) 043540, arXiv:2406.07533 [astro-ph.CO].

[1585] M. Reyhani, M. Najafi, J.T. Firouzjaee, E. Di Valentino, Structure formation in various dynamical dark energy scenarios, Phys. Dark Univ. 44 (2024) 101477, arXiv:2403.15202 [astro-ph.CO].

[1586] R.K. Sachs, A.M. Wolfe, Perturbations of a cosmological model and angular variations of the microwave background, Astrophys. J. 147 (1967) 73–90.

[1587] M.J. Rees, D.W. Sciama, Large scale density inhomogeneities in the universe, Nature 217 (1968) 511–516.

[1588] S. Flender, S. Hotchkiss, S. Nadathur, The stacked ISW signal of rare superstructures in Λ CDM, J. Cosmol. Astropart. Phys. 02 (2013) 013, arXiv:1212.0776 [astro-ph.CO].

[1589] C. Hernandez-Monteagudo, R.E. Smith, On the signature of nearby superclusters and voids in the Integrated Sachs-Wolfe effect, Mon. Not. R. Astron. Soc. 435 (2013) 1094, arXiv:1212.1174 [astro-ph.CO].

[1590] S. Aiola, A. Kosowsky, B. Wang, Gaussian approximation of peak values in the integrated sachs-wolfe effect, Phys. Rev. D 91 (2015) 043510, arXiv:1410.6138 [astro-ph.CO].

[1591] A.M. Sołtan, ISW in ΛCDM or something else? Mon. Not. R. Astron. Soc. 488 (2) (2019) 2732–2742, arXiv:1812.09348 [astro-ph.CO].

[1592] Planck Collaboration, P.A.R. Ade, et al., Planck 2015 results. XXI. The integrated Sachs-Wolfe effect, Astron. Astrophys. 594 (2016) A21, arXiv:1502.01595 [astro-ph.CO].

[1593] Y.-C. Cai, M. Neyrinck, Q. Mao, J.A. Peacock, I. Szapudi, A.A. Berlind, The lensing and temperature imprints of voids on the Cosmic Microwave Background, Mon. Not. R. Astron. Soc. 466 (3) (2017) 3364–3375, arXiv:1609.00301 [astro-ph.CO].

[1594] A. Kovács, The part and the whole: voids, supervoids, and their ISW imprint, Mon. Not. R. Astron. Soc. 475 (2) (2018) 1777–1790, arXiv:1701.08583 [astro-ph.CO].

[1595] S. Nadathur, R. Crittenden, A detection of the integrated Sachs-Wolfe imprint of cosmic superstructures using a matched-filter approach, Astrophys. J. Lett. 830 (1) (2016) L19, arXiv:1608.08638 [astro-ph.CO].

[1596] DES Collaboration, A. Kovács, et al., Imprint of DES superstructures on the cosmic microwave background, Mon. Not. R. Astron. Soc. 465 (4) (2017) 4166–4179, arXiv:1610.00637 [astro-ph.CO].

[1597] DES Collaboration, A. Kovács, et al., More out of less: an excess integrated Sachs-Wolfe signal from supervoids mapped out by the Dark Energy Survey, Mon. Not. R. Astron. Soc. 484 (2019) 5267–5277, arXiv:1811.07812 [astro-ph.CO].

[1598] M. Cruz, E. Martinez-Gonzalez, P. Vielva, L. Cayon, Detection of a non-gaussian spot in wmap, Mon. Not. R. Astron. Soc. 356 (2005) 29–40, arXiv:astro-ph/0405341.

[1599] F. Finelli, J. García-Bellido, A. Kovács, F. Paci, I. Szapudi, Supervoids in the WISE–2MASS catalogue imprinting cold spots in the cosmic microwave background, Mon. Not. R. Astron. Soc. 455 (2) (2016) 1246–1256, arXiv:1405.1555 [astro-ph.CO].

[1600] A. Pataki, P. Raffai, I. Csabai, G. Rácz, I. Szapudi, Constraints on AvERA cosmologies from cosmic chronometers and type ia supernovae, 2025, arXiv:2503.21369 [astro-ph.CO].

[1601] S. Räsänen, Backreaction: directions of progress, Cl. Quant. Grav. 28 (2011) 164008, arXiv:1102.0408 [astro-ph.CO].

[1602] T. Buchert, et al., Is there proof that backreaction of inhomogeneities is irrelevant in cosmology? Cl. Quant. Grav. 32 (2015) 215021, arXiv:1505.07800 [gr-qc].

[1603] D.L. Wiltshire, Solution to the cosmological constant problem, 2024, arXiv:2404.02129 [gr-qc].

[1604] M.J. Williams, H.J. Macpherson, D.L. Wiltshire, C. Stevens, First investigation of void statistics in numerical relativity simulations, Mon. Not. R. Astron. Soc. 536 (2025) 2645–2660, arXiv:2403.15134 [astro-ph.CO].

[1605] A. Kovács, R. Beck, A. Smith, G. Rácz, I. Csabai, I. Szapudi, Evidence for a high-z ISW signal from supervoids in the distribution of eBOSS quasars, Mon. Not. R. Astron. Soc. 513 (1) (2022) 15–26, arXiv:2107.13038 [astro-ph.CO].

[1606] eBOSS Collaboration, A.D. Myers, et al., The SDSS-IV extended baryon oscillation spectroscopic survey: quasar target selection, Astrophys. J. Suppl. 221 (2) (2015) 27, arXiv:1508.04472 [astro-ph.CO].

[1607] J.R. Gott, III, M. Juric, D. Schlegel, F. Hoyle, M. Vogeley, M. Tegmark, N.A. Bahcall, J. Brinkmann, A map of the universe, Astrophys. J. 624 (2005) 463, arXiv:astro-ph/0310571.

[1608] M. Einasto, H. Lietzen, M. Gramann, E. Tempel, E. Saar, L.J. Liivamägi, P. Heinämäki, P. Nurmi, J. Einasto, Sloan Great Wall as a complex of superclusters with collapsing cores, Astron. Astrophys. 595 (2016) A70, arXiv:1608.04988 [astro-ph.CO].

[1609] M. Einasto, P. Tenjes, M. Gramann, H. Lietzen, R. Kipper, L.J. Liivamägi, E. Tempel, S. Sankhyayan, J. Einasto, The evolution of high-density cores of the BOSS Great Wall superclusters, Astron. Astrophys. 666 (2022) A52, arXiv:2204.08918 [astro-ph.CO].
[1610] J. Einasto, et al., Luminous superclusters: remnants from inflation, Astron. Astrophys. 459 (2006) L1, arXiv:astro-ph/0605393.
[1611] R.K. Sheth, A. Diaferio, How unusual are the shapley supercluster and the sloan great wall? Mon. Not. R. Astron. Soc. 417 (2011) 2938–2949, arXiv:1105.3378 [astro-ph.CO].
[1612] C. Park, Y.-Y. Choi, J. Kim, J.R. Gott III, S.S. Kim, K.-S. Kim, The challenge of the largest structures in the universe to cosmology, Astrophys. J. Lett. 759 (2012) L7, arXiv:1209.5659 [astro-ph.CO].
[1613] J. Einasto, R.H. Miller, Neighboring superclusters and their environs, in: G.O. Abell, G. Chincarini (Eds.), Early Evolution of the Universe and its Present Structure, in: IAU Symposium, vol. 104, 1983, p. 405.
[1614] P.A. Shaver, Radio surveys and large scale structure, Aust. J. Phys. 44 (6) (1991) 759.
[1615] H. Boehringer, G. Chon, J. Truemper, The Cosmic Large-Scale Structure in X-rays (CLASSIX) Cluster Survey - II. Unveiling a pancake structure with a 100 Mpc radius in the local Universe, Astron. Astrophys. 651 (2021) A15, arXiv:2105.13999 [astro-ph.CO].
[1616] P.J.E. Peebles, Flat patterns in cosmic structure, Mon. Not. R. Astron. Soc. 526 (3) (2023) 4490–4501, arXiv:2308.04245 [astro-ph.CO].
[1617] M. Einasto, E. Tago, J. Jaaniste, J. Einasto, H. Andernach, The supercluster-void network I. the supercluster catalogue and large scale distribution, Astron. Astrophys. Suppl. Ser. 123 (1997) 119, arXiv:astro-ph/9610088.
[1618] K. Dolag, J.G. Sorce, S. Pilipenko, E. Hernández-Martínez, M. Valentini, S. Gottlöber, N. Aghanim, I. Khabibullin, Simulating the LOcal Web (SLOW) - I. Anomalies in the local density field, Astron. Astrophys. 677 (2023) A169, arXiv:2302.10960 [astro-ph.CO].
[1619] P.J.E. Peebles, Improving physical cosmology: an empiricist's assessment, 2021, http://dx.doi.org/10.48550/arXiv.2106.02672, arXiv e-prints, arXiv:2106.02672 [astro-ph.CO].
[1620] O. Toomet, H. Andernach, J. Einasto, M. Einasto, E. Kasak, A.A. Starobinsky, E. Tago, The supercluster-void network v. alternative evidence for its regularity, Astron. Astrophys. 393 (2002) 1, arXiv:astro-ph/9907238.
[1621] J. Einasto, M. Einasto, S. Gottlober, V. Mller, V. Saar, A.A. Starobinsky, E. Tago, D. Tucker, H. Andernach, P. Frisch, A 120 MPC periodicity in the three-dimensional distribution of galaxy superclusters, Nature 385 (1997) 139–141, arXiv:astro-ph/9701018.
[1622] J. Einasto, M. Einasto, P. Frisch, S. Gottlober, V. Mller, V. Saar, A.A. Starobinsky, E. Tago, D. Tucker, H. Andernach, The supercluster-void network. 2. An oscillating cluster correlation function, Mon. Not. R. Astron. Soc. 289 (1997) 801–812, arXiv:astro-ph/9704127.
[1623] E. Tago, J. Einasto, M. Einasto, V. Muller, H. Andernach, Optical and x-ray clusters as tracers of the supercluster-void network. II the spatial correlation function, Astron. J. 123 (2002) 37, arXiv:astro-ph/0012537.
[1624] U. Lindner, J. Einasto, M. Einasto, W. Freudling, K. Fricke, E. Tago, The structure of supervoids - I: void hierarchy in the northern local supervoid, Astron. Astrophys. 301 (1995) 329, arXiv:astro-ph/9503044.
[1625] A. Kovács, J. García-Bellido, Cosmic troublemakers: the cold spot, the eridanus supervoid, and the great walls, Mon. Not. R. Astron. Soc. 462 (2) (2016) 1882–1893, arXiv:1511.09008 [astro-ph.CO].
[1626] M. Einasto, E. Tago, H. Lietzen, C. Park, P. Heinamaki, E. Saar, H. Song, L.J. Liivamagi, J. Einasto, Tracing a high redshift cosmic web with quasar systems, Astron. Astrophys. 568 (2014) A46, arXiv:1406.5578 [astro-ph.CO].
[1627] M. Einasto, P. Heinämäki, L.J. Liivamägi, V.J. Martinez, L. Hurtado-Gil, P. Arnalte-Mur, P. Nurmi, J. Einasto, E. Saar, Shell-like structures in our cosmic neighbourhood, Astron. Astrophys. 587 (2016) A116, arXiv:1506.05295 [astro-ph.CO].
[1628] M. Einasto, L.J. Liivamagi, E. Tago, E. Saar, E. Tempel, J. Einasto, V.J. Martinez, P. Heinamaki, SDSS DR7 superclusters. Morphology, Astron. Astrophys. 532 (2011) A5, arXiv:1105.2124 [astro-ph.CO].
[1629] R.B. Tully, C. Howlett, D. Pomarede, Ho'oleilana: an individual baryon acoustic oscillation? Astrophys. J. 954 (2) (2023) 169, arXiv:2309.00677 [astro-ph.CO].
[1630] P. Arnalte-Mur, A. Labatie, N. Clerc, V.J. Martinez, J.L. Starck, M. Lachieze-Rey, E. Saar, S. Paredes, Wavelet analysis of baryon acoustic structures in the galaxy distribution, Astron. Astrophys. 542 (2012) A34, arXiv:1101.1911 [astro-ph.CO].
[1631] M. Einasto, M. Gramann, E. Saar, L.J. Liivamagi, E. Tempel, J. Nevalainen, P. Heinamaki, C. Park, J. Einasto, Unusual A2142 supercluster with a collapsing core: distribution of light and mass, Astron. Astrophys. 580 (2015) A69, arXiv:1505.07233 [astro-ph.CO].
[1632] P. Heinämäki, P. Teerikorpi, M. Douspis, P. Nurmi, M. Einasto, M. Gramann, J. Nevalainen, E. Saar, Quasi-spherical superclusters, Astron. Astrophys. 668 (2022) A37, arXiv:2210.13294 [astro-ph.CO].
[1633] A. Vikhlinin, M. Markevitch, S.S. Murray, C. Jones, W. Forman, L. Van Speybroeck, Chandra temperature profiles for a sample of nearby relaxed galaxy clusters, Astrophys. J. 628 (2005) 655–672, arXiv:astro-ph/0412306.
[1634] E. Tempel, A. Tamm, M. Gramann, T. Tuvikene, L.J. Liivamägi, I. Suhhonenko, R. Kipper, M. Einasto, E. Saar, Flux- and volume-limited groups/clusters for the SDSS galaxies: catalogues and mass estimation, Astron. Astrophys. 566 (2014) A1, arXiv:1402.1350 [astro-ph.CO].
[1635] M.J. Rieke, D. Kelly, S. Horner, Overview of James Webb Space Telescope and NIRCam's Role, in: J.B. Heaney, L.G. Burriesci (Eds.), Cryogenic Optical Systems and Instruments XI, in: Society of Photo-Optical Instrumentation Engineers (SPIE) Conference Series, vol. 5904, 2005, pp. 1–8.
[1636] P. Santini, A. Fontana, M. Castellano, N. Leethochawalit, M. Trenti, T. Treu, D. Belfiori, S. Birrer, A. Bonchi, E. Merlin, C. Mason, T. Morishita, M. Nonino, D. Paris, G. Polenta, P. Rosati, L. Yang, K. Boyett, M. Bradac, A. Calabrò, A. Dressler, K. Glazebrook, D. Marchesini, S. Mascia, T. Nanayakkara, L. Pentericci, G. Roberts-Borsani, C. Scarlata, B. Vulcani, X. Wang, Early results from GLASS-JWST. XI. Stellar masses and mass-to-light ratio of z > 7 galaxies, Astrophys. J. Lett. 942 (2) (2023) L27, arXiv:2207.11379 [astro-ph.GA].
[1637] M. Castellano, A. Fontana, T. Treu, P. Santini, E. Merlin, N. Leethochawalit, M. Trenti, E. Vanzella, U. Mestric, A. Bonchi, D. Belfiori, M. Nonino, D. Paris, G. Polenta, G. Roberts-Borsani, K. Boyett, M.s. Bradač, A. Calabrò, K. Glazebrook, C. Grillo, S. Mascia, C. Mason, A. Mercurio, T. Morishita, T. Nanayakkara, L. Pentericci, P. Rosati, B. Vulcani, X. Wang, L. Yang, Early results from GLASS-JWST. III. Galaxy candidates at z 9-15, Astrophys. J. Lett. 938 (2) (2022) L15, arXiv:2207.09436 [astro-ph.GA].
[1638] S.L. Finkelstein, M.B. Bagley, H.C. Ferguson, S.M. Wilkins, J.S. Kartaltepe, et al., CEERS key paper. I. An early look into the first 500 Myr of galaxy formation with JWST, Astrophys. J. Lett. 946 (1) (2023) L13, arXiv:2211.05792 [astro-ph.GA].
[1639] R.P. Naidu, P.A. Oesch, P. van Dokkum, E.J. Nelson, K.A. Suess, G. Brammer, K.E. Whitaker, G. Illingworth, R. Bouwens, S. Tacchella, J. Matthee, N. Allen, R. Bezanson, C. Conroy, I. Labbe, J. Leja, E. Leonova, D. Magee, S.H. Price, D.J. Setton, V. Strait, M. Stefanon, S. Toft, J.R. Weaver, A. Weibel, Two remarkably luminous galaxy candidates at z ≈ 10-12 revealed by JWST, Astrophys. J. Lett. 940 (1) (2022) L14, arXiv:2207.09434 [astro-ph.GA].
[1640] T. Treu, et al., The glass-jwst early release science program. I. Survey design and release plans, Astrophys. J. 935 (2) (2022) 110, arXiv:2206.07978 [astro-ph.GA].
[1641] Y. Harikane, M. Ouchi, M. Oguri, Y. Ono, K. Nakajima, Y. Isobe, H. Umeda, K. Mawatari, Y. Zhang, A comprehensive study of galaxies at z ∼ 9–16 found in the early JWST data: ultraviolet luminosity functions and cosmic star formation history at the pre-reionization epoch, Astrophys. J. Suppl. 265 (1) (2023) arXiv:2208.01612 [astro-ph.GA].
[1642] P.G. Pérez-González, et al., CEERS key paper. IV. A triality in the nature of HST-dark galaxies, Astrophys. J. Lett. 946 (1) (2023) L16, arXiv:2211.00045 [astro-ph.GA].
[1643] C. Papovich, et al., CEERS key paper. V. Galaxies at 4 < z < 9 are bluer than they appear–characterizing galaxy stellar populations from rest-frame ∼1 μm imaging, Astrophys. J. Lett. 949 (2) (2023) L18, arXiv:2301.00027 [astro-ph.GA].
[1644] R.J. Bouwens, M. Stefanon, G. Brammer, P.A. Oesch, T. Herard-Demanche, G.D. Illingworth, J. Matthee, R.P. Naidu, P.G. van Dokkum, I.F. van Leeuwen, Evolution of the UV LF from z 15 to z 8 using new JWST NIRCam medium-band observations over the HUDF/XDF, Mon. Not. R. Astron. Soc. 523 (1) (2023) 1036–1055, arXiv:2211.02607 [astro-ph.GA].
[1645] N.J. Adams, C.J. Conselice, L. Ferreira, D. Austin, J.A.A. Trussler, I. Juodžbalis, S.M. Wilkins, J. Caruana, P. Dayal, A. Verma, A.P. Vijayan, Discovery and properties of ultra-high redshift galaxies (9 < z < 12) in the JWST ERO SMACS 0723 Field, Mon. Not. R. Astron. Soc. 518 (3) (2023) 4755–4766, arXiv:2207.11217 [astro-ph.GA].
[1646] R. Bouwens, G. Illingworth, P. Oesch, M. Stefanon, R. Naidu, I. van Leeuwen, D. Magee, UV luminosity density results at z > 8 from the first JWST/NIRCam fields: limitations of early data sets and the need for spectroscopy, Mon. Not. R. Astron. Soc. 523 (1) (2023) 1009–1035, arXiv:2212.06683 [astro-ph.CO].
[1647] S.L. Finkelstein, et al., The complete CEERS early universe galaxy sample: a surprisingly slow evolution of the space density of bright galaxies at z ∼ 8.5–14.5, Astrophys. J. Lett. 969 (1) (2024) L2, arXiv:2311.04279 [astro-ph.GA].
[1648] D.J. McLeod, C.T. Donnan, R.J. McLure, J.S. Dunlop, D. Magee, R. Begley, A.C. Carnall, F. Cullen, R.S. Ellis, M.L. Hamadouche, T.M. Stanton, The galaxy UV luminosity function at $z \simeq 11$ from a suite of public JWST ERS, ERO, and Cycle-1 programs, Mon. Not. R. Astron. Soc. 527 (3) (2024) 5004–5022, arXiv:2304.14469 [astro-ph.GA].
[1649] L.Y.A. Yung, R.S. Somerville, S.L. Finkelstein, S.M. Wilkins, J.P. Gardner, Are the ultra-high-redshift galaxies at z > 10 surprising in the context of standard galaxy formation models? Mon. Not. R. Astron. Soc. 527 (3) (2024) 5929–5948, arXiv:2304.04348 [astro-ph.GA].
[1650] Y.-Y. Wang, L. Lei, S.-P. Tang, G.-W. Yuan, Y.-Z. Fan, Digging into the ultraviolet luminosity functions of galaxies at high redshifts: galaxies evolution, reionization, and cosmological parameters, Astrophys. J. 975 (2) (2024) 285, arXiv:2405.09350 [astro-ph.CO].
[1651] N. Sabti, J.B. Muñoz, M. Kamionkowski, Insights from HST into ultramassive galaxies and early-universe cosmology, Phys. Rev. Lett. 132 (6) (2024) 061002, arXiv:2305.07049 [astro-ph.CO].

[1652] C.T. Donnan, D.J. McLeod, J.S. Dunlop, R.J. McLure, A.C. Carnall, R. Begley, F. Cullen, M.L. Hamadouche, R.A.A. Bowler, D. Magee, H.J. McCracken, B. Milvang-Jensen, A. Moneti, T. Targett, The evolution of the galaxy UV luminosity function at redshifts $z \simeq 8-15$ from deep JWST and ground-based near-infrared imaging, Mon. Not. R. Astron. Soc. 518 (4) (2023) 6011–6040, arXiv:2207.12356 [astro-ph.GA].

[1653] L.J. Furtak, M. Shuntov, H. Atek, A. Zitrin, J. Richard, M.D. Lehnert, J. Chevallard, Constraining the physical properties of the first lensed z 9 - 16 galaxy candidates with JWST, Mon. Not. R. Astron. Soc. 519 (2) (2023) 3064–3075, arXiv:2208.05473 [astro-ph.GA].

[1654] J.A. Zavala, et al., Dusty starbursts masquerading as ultra-high redshift galaxies in JWST CEERS observations, Astrophys. J. Lett. 943 (2) (2023) L9, arXiv:2208.01816 [astro-ph.GA].

[1655] H. Yan, Z. Ma, C. Ling, C. Cheng, J.-s. Huang, First batch of z ≈ 11–20 candidate objects revealed by the james webb space telescope early release observations on SMACS 0723-73, Astrophys. J. Lett. 942 (1) (2023) L9, arXiv:2207.11558 [astro-ph.GA].

[1656] I. Labbe, et al., A population of red candidate massive galaxies ˜600 Myr after the Big Bang, Nature 616 (7956) (2023) 266–269, arXiv:2207.12446 [astro-ph.GA].

[1657] M. Xiao, et al., Accelerated formation of ultra-massive galaxies in the first billion years, Nature 635 (8038) (2024) 311–315, arXiv:2309.02492 [astro-ph.GA].

[1658] C.M. Casey, H.B. Akins, M. Shuntov, O. Ilbert, L. Paquereau, M. Franco, C.C. Hayward, S.L. Finkelstein, M. Boylan-Kolchin, B.E. Robertson, N. Allen, M. Brinch, O.R. Cooper, X. Ding, N.E. Drakos, A.L. Faisst, S. Fujimoto, S. Gillman, S. Harish, M. Hirschmann, S. Jin, J.S. Kartaltepe, A.M. Koekemoer, V. Kokorev, D. Liu, A.S. Long, G. Magdis, C. Maraston, C.L. Martin, H.J. McCracken, J. McKinney, B. Mobasher, J. Rhodes, R.M. Rich, D.B. Sanders, J.D. Silverman, S. Toft, A.P. Vijayan, J.R. Weaver, S.M. Wilkins, L. Yang, J.A. Zavala, COSMOS-web: intrinsically luminous z $\gtrsim$ 10 galaxy candidates test early stellar mass assembly, Astrophys. J. 965 (1) (2024) 98, arXiv:2308.10932 [astro-ph.GA].

[1659] A. Weibel, P.A. Oesch, L. Barrufet, R. Gottumukkala, R.S. Ellis, P. Santini, J.R. Weaver, N. Allen, R. Bouwens, R.A.A. Bowler, G. Brammer, A.C. Carnall, F. Cullen, P. Dayal, M. Dickinson, C.T. Donnan, J.S. Dunlop, M. Giavalisco, N.A. Grogin, G.D. Illingworth, A.M. Koekemoer, I. Labbe, D. Marchesini, D.J. McLeod, R.J. McLure, R.P. Naidu, P.G. Pérez-González, M. Shuntov, M. Stefanon, S. Toft, M. Xiao, Galaxy build-up in the first 1.5 Gyr of cosmic history: insights from the stellar mass function at z 4-9 from JWST NIRCam observations, Mon. Not. R. Astron. Soc. 533 (2) (2024) 1808–1838, arXiv:2403.08872 [astro-ph.GA].

[1660] K. Chworowsky, S.L. Finkelstein, M. Boylan-Kolchin, E.J. McGrath, K.G. Iyer, C. Papovich, M. Dickinson, A.J. Taylor, L.Y.A. Yung, P. Arrabal Haro, M.B. Bagley, B.E. Backhaus, R. Bhatawdekar, Y. Cheng, N.J. Cleri, J.W. Cole, M.C. Cooper, L. Costantin, A. Dekel, M. Franco, S. Fujimoto, C.C. Hayward, B.W. Holwerda, M. Huertas-Company, M. Hirschmann, T.A. Hutchison, A.M. Koekemoer, R.L. Larson, Z. Li, A.S. Long, R.A. Lucas, N. Pirzkal, G. Rodighiero, R.S. Somerville, B.N. Vanderhoof, A. de la Vega, S.M. Wilkins, G. Yang, J.A. Zavala, Evidence for a shallow evolution in the volume densities of massive galaxies at z=4–8 from CEERS, Astron. J. 168 (3) (2024) 113, arXiv:2311.14804 [astro-ph.GA].

[1661] C.C. Lovell, I. Harrison, Y. Harikane, S. Tacchella, S.M. Wilkins, Extreme value statistics of the halo and stellar mass distributions at high redshift: are JWST results in tension with ΛCDM? Mon. Not. R. Astron. Soc. 518 (2) (2022) 2511–2520, arXiv:2208.10479 [astro-ph.GA].

[1662] M. Boylan-Kolchin, Stress testing ΛCDM with high-redshift galaxy candidates, Nat. Astron. 7 (6) (2023) 731–735, arXiv:2208.01611 [astro-ph.CO].

[1663] M. Forconi, Ruchika, A. Melchiorri, O. Mena, N. Menci, Do the early galaxies observed by JWST disagree with Planck's CMB polarization measurements? J. Cosmol. Astropart. Phys. 10 (2023) 012, arXiv:2306.07781 [astro-ph.CO].

[1664] J. Lu, L. Wang, X. Chen, D. Rubin, S. Perlmutter, D. Baade, J. Mould, J. Vinko, E. Regős, A.M. Koekemoer, Constraints on cosmological parameters with a sample of type ia supernovae from JWST, Astrophys. J. 941 (1) (2022) 71, arXiv:2210.00746 [astro-ph.CO].

[1665] J.D.R. Pierel, et al., Testing for intrinsic type ia supernova luminosity evolution at z > 2 with JWST, Astrophys. J. Lett. 981 (1) (2025) L9, arXiv:2411.11953 [astro-ph.CO].

[1666] J. Vinko, E. Regos, SN 2023adsy – a normal Type Ia Supernova at z=2.9, discovered by JWST, 2024, arXiv:2411.10427 [astro-ph.HE].

[1667] D.A. Coulter, et al., Discovery of a likely Type II SN at z=3.6 with JWST, 2025, arXiv:2501.05513 [astro-ph.HE].

[1668] T.J. Moriya, et al., Properties of high-redshift Type II supernovae discovered by the JADES transient survey, 2025, arXiv:2501.08969 [astro-ph.HE].

[1669] T.J. Moriya, Y. Harikane, A.K. Inoue, Constraint on the event rate of general relativistic instability supernovae from the early JWST deep field data, Mon. Not. R. Astron. Soc. 526 (2) (2023) 2400–2402, arXiv:2309.12049 [astro-ph.HE].

[1670] M.G. Dainotti, et al., A New Master Supernovae Ia sample and the investigation of the H_0 tension, 2025, arXiv:2501.11772 [astro-ph.CO].

[1671] P.M.M. Alonso, C. Escamilla-Rivera, R. Sandoval-Orozco, Constraining dark energy cosmologies with spatial curvature using Supernovae JWST forecasting, J. Cosmol. Astropart. Phys. 04 (2024) 084, arXiv:2309.12292 [astro-ph.CO].

[1672] C.C. Williams, S. Alberts, Z. Ji, K.N. Hainline, J. Lyu, G. Rieke, R. Endsley, K.A. Suess, F. Sun, B.D. Johnson, M. Florian, I. Shivaei, W. Rujopakarn, W.M. Baker, R. Bhatawdekar, K. Boyett, A.J. Bunker, A.J. Cameron, S. Carniani, S. Charlot, E. Curtis-Lake, C. DeCoursey, A. de Graaff, E. Egami, D.J. Eisenstein, J.L. Gibson, R. Hausen, J.M. Helton, R. Maiolino, M.V. Maseda, E.J. Nelson, P.G. Pérez-González, M.J. Rieke, B.E. Robertson, A. Saxena, S. Tacchella, C.N.A. Willmer, C.J. Willott, The galaxies missed by hubble and ALMA: the contribution of extremely red galaxies to the cosmic census at 3 < z < 8, Astrophys. J. 968 (1) (2024) 34, arXiv:2311.07483 [astro-ph.GA].

[1673] C.L. Steinhardt, V. Kokorev, V. Rusakov, E. Garcia, A. Sneppen, Templates for fitting photometry of ultra-high-redshift galaxies, Astrophys. J. Lett. 951 (2) (2023) L40, arXiv:2208.07879 [astro-ph.GA].

[1674] R. Endsley, D.P. Stark, L. Whitler, M.W. Topping, Z. Chen, A. Plat, J. Chisholm, S. Charlot, A JWST/NIRCam study of key contributors to reionization: the star-forming and ionizing properties of UV-faint z 7-8 galaxies, Mon. Not. R. Astron. Soc. 524 (2) (2023) 2312–2330, arXiv:2208.14999 [astro-ph.GA].

[1675] P. Arrabal Haro, M. Dickinson, S.L. Finkelstein, S. Fujimoto, V. Fernández, J.S. Kartaltepe, I. Jung, J.W. Cole, D. Burgarella, K. Chworowsky, T.A. Hutchison, A.M. Morales, C. Papovich, R.C. Simons, R.O. Amorín, B.E. Backhaus, M.B. Bagley, L. Bisigello, A. Calabrò, M. Castellano, N.J. Cleri, R. Davé, A. Dekel, H.C. Ferguson, A. Fontana, E. Gawiser, M. Giavalisco, S. Harish, N.P. Hathi, M. Hirschmann, B.W. Holwerda, M. Huertas-Company, A.M. Koekemoer, R.L. Larson, R.A. Lucas, B. Mobasher, P.G. Pérez-González, N. Pirzkal, C. Rose, P. Santini, J.R. Trump, A. de la Vega, X. Wang, B.J. Weiner, S.M. Wilkins, G. Yang, L.Y.A. Yung, J.A. Zavala, Spectroscopic confirmation of CEERS NIRCam-selected galaxies at $\simeq 8-10$, Astrophys. J. Lett. 951 (1) (2023) L22, arXiv:2304.05378 [astro-ph.GA].

[1676] B. Wang, S. Fujimoto, I. Labbé, L.J. Furtak, T.B. Miller, D.J. Setton, A. Zitrin, H. Atek, R. Bezanson, G. Brammer, J. Leja, P.A. Oesch, S.H. Price, I. Chemerynska, S.E. Cutler, P. Dayal, P. van Dokkum, A.D. Goulding, J.E. Greene, Y. Fudamoto, G. Khullar, V. Kokorev, D. Marchesini, R. Pan, J.R. Weaver, K.E. Whitaker, C.C. Williams, UNCOVER: illuminating the early universe-JWST/NIRSpec confirmation of z > 12 galaxies, Astrophys. J. Lett. 957 (2) (2023) L34, arXiv:2308.03745 [astro-ph.GA].

[1677] B.E. Robertson, et al., Identification and properties of intense star-forming galaxies at redshifts z > 10, Nat. Astron. 7 (5) (2023) 611–621, arXiv:2212.04480 [astro-ph.GA].

[1678] E. Curtis-Lake, S. Carniani, A. Cameron, S. Charlot, P. Jakobsen, R. Maiolino, A. Bunker, J. Witstok, R. Smit, J. Chevallard, C. Willott, P. Ferruit, S. Arribas, N. Bonaventura, M. Curti, F. D'Eugenio, M. Franx, G. Giardino, T.J. Looser, N. Lützgendorf, M.V. Maseda, T. Rawle, H.-W. Rix, B. Rodríguez del Pino, H. Übler, M. Sirianni, A. Dressler, E. Egami, D.J. Eisenstein, R. Endsley, K. Hainline, R. Hausen, B.D. Johnson, M. Rieke, B. Robertson, I. Shivaei, D.P. Stark, S. Tacchella, C.C. Williams, C.N.A. Willmer, R. Bhatawdekar, R. Bowler, K. Boyett, Z. Chen, A. de Graaff, J.M. Helton, R.E. Hviding, G.C. Jones, N. Kumari, J. Lyu, E. Nelson, M. Perna, L. Sandles, A. Saxena, K.A. Suess, F. Sun, M.W. Topping, I.E.B. Wallace, L. Whitler, Spectroscopic confirmation of four metal-poor galaxies at z= 10.3-13.2, Nat. Astron. 7 (2023) 622–632, arXiv:2212.04568 [astro-ph.GA].

[1679] S. Fujimoto, et al., CEERS spectroscopic confirmation of NIRCam-selected z $\gtrsim$ 8 galaxy candidates with JWST/NIRSpec: initial characterization of their properties, Astrophys. J. Lett. 949 (2) (2023) L25, arXiv:2301.09482 [astro-ph.GA].

[1680] S. Carniani, K. Hainline, F. D'Eugenio, D.J. Eisenstein, P. Jakobsen, J. Witstok, B.D. Johnson, J. Chevallard, R. Maiolino, J.M. Helton, C. Willott, B. Robertson, S. Alberts, S. Arribas, W.M. Baker, R. Bhatawdekar, K. Boyett, A.J. Bunker, A.J. Cameron, P.A. Cargile, S. Charlot, M. Curti, E. Curtis-Lake, E. Egami, G. Giardino, K. Isaak, Z. Ji, G.C. Jones, N. Kumari, M.V. Maseda, E. Parlanti, P.G. Pérez-González, T. Rawle, G. Rieke, M. Rieke, B.R. Del Pino, A. Saxena, J. Scholtz, R. Smit, F. Sun, S. Tacchella, H. Übler, G. Venturi, C.C. Williams, C.N.A. Willmer, Spectroscopic confirmation of two luminous galaxies at a redshift of 14, Nature 633 (8029) (2024) 318–322, arXiv:2405.18485 [astro-ph.GA].

[1681] M. Castellano, L. Napolitano, A. Fontana, G. Roberts-Borsani, T. Treu, E. Vanzella, J.A. Zavala, P. Arrabal Haro, A. Calabrò, M. Llerena, S. Mascia, E. Merlin, D. Paris, L. Pentericci, P. Santini, T.J.L.C. Bakx, P. Bergamini, G. Cupani, M. Dickinson, A.V. Filippenko, K. Glazebrook, C. Grillo, P.L. Kelly, M.A. Malkan, C.A. Mason, T. Morishita, T. Nanayakkara, P. Rosati, E. Sani, X. Wang, I. Yoon, JWST NIRSpec spectroscopy of the remarkable bright galaxy GHZ2/GLASS-z12 at redshift 12.34, Astrophys. J. 972 (2) (2024) 143, arXiv:2403.10238 [astro-ph.GA].

[1682] C. Giménez-Arteaga, et al., Spatially resolved properties of galaxies at 5 < z < 9 in the SMACS 0723 JWST ERO field, Astrophys. J. 948 (2) (2023) 126, arXiv:2212.08670 [astro-ph.GA].

[1683] A. Ferrara, Super-early JWST galaxies, outflows, and Lyα visibility in the Epoch of Reionization, Astron. Astrophys. 684 (2024) A207, arXiv:2310.12197 [astro-ph.GA].

[1684] C.A. Mason, M. Trenti, T. Treu, The brightest galaxies at cosmic dawn, Mon. Not. R. Astron. Soc. 521 (1) (2023) 497–503, arXiv:2207.14808 [astro-ph.GA].
[1685] A. Kravtsov, V. Belokurov, Stochastic star formation and the abundance of $z > 10$ UV-bright galaxies, 2024, arXiv:2405.04578 [astro-ph.GA].
[1686] S. Hegde, M.M. Wyatt, S.R. Furlanetto, A hidden population of active galactic nuclei can explain the overabundance of luminous z > 10 objects observed by JWST, J. Cosmol. Astropart. Phys. 08 (2024) 025, arXiv:2405.01629 [astro-ph.GA].
[1687] V. Gelli, C. Mason, C.C. Hayward, The impact of mass-dependent stochasticity at cosmic dawn, Astrophys. J. 975 (2) (2024) 192, arXiv:2405.13108 [astro-ph.GA].
[1688] G. Desprez, et al., ΛCDM not dead yet: massive high-z Balmer break galaxies are less common than previously reported, Mon. Not. R. Astron. Soc. 530 (3) (2024) 2935–2952, arXiv:2310.03063 [astro-ph.GA].
[1689] A. Dekel, K.C. Sarkar, Y. Birnboim, N. Mandelker, Z. Li, Efficient formation of massive galaxies at cosmic dawn by feedback-free starbursts, Mon. Not. R. Astron. Soc. 523 (3) (2023) 3201–3218, arXiv:2303.04827 [astro-ph.GA].
[1690] A. Ferrara, A. Pallottini, P. Dayal, On the stunning abundance of super-early, luminous galaxies revealed by JWST, Mon. Not. R. Astron. Soc. 522 (3) (2023) 3986–3991, arXiv:2208.00720 [astro-ph.GA].
[1691] B. Wang, J. Leja, H. Atek, I. Labbé, Y. Li, R. Bezanson, G. Brammer, S.E. Cutler, P. Dayal, L.J. Furtak, J.E. Greene, V. Kokorev, R. Pan, S.H. Price, K.A. Suess, J.R. Weaver, K.E. Whitaker, C.C. Williams, Quantifying the effects of known unknowns on inferred high-redshift galaxy properties: burstiness, IMF, and nebular physics, Astrophys. J. 963 (1) (2024) 74, arXiv:2310.06781 [astro-ph.GA].
[1692] D. Narayanan, S. Lower, P. Torrey, G. Brammer, W. Cui, R. Davé, K.G. Iyer, Q. Li, C.C. Lovell, L.V. Sales, D.P. Stark, F. Marinacci, M. Vogelsberger, Outshining by recent star formation prevents the accurate measurement of high-z galaxy stellar masses, Astrophys. J. 961 (1) (2024) 73, arXiv:2306.10118 [astro-ph.GA].
[1693] R.K. Cochrane, H. Katz, R. Begley, C.C. Hayward, P.N. Best, High-z stellar masses can be recovered robustly with JWST photometry, Astrophys. J. 978 (2) (2025) L42, arXiv:2412.02622 [astro-ph.GA].
[1694] M. Haslbauer, P. Kroupa, A.H. Zonoozi, H. Haghi, Has JWST already falsified dark-matter-driven galaxy formation? Astrophys. J. Lett. 939 (2) (2022) L31, arXiv:2210.14915 [astro-ph.GA].
[1695] E.M. Ventura, Y. Qin, S. Balu, J.S.B. Wyithe, Semi-analytic modelling of Pop. III star formation and metallicity evolution – I. Impact on the UV luminosity functions at z = 9–16, Mon. Not. R. Astron. Soc. 529 (1) (2024) 628–646, arXiv:2401.07396 [astro-ph.GA].
[1696] A. Trinca, R. Schneider, R. Valiante, L. Graziani, A. Ferrotti, K. Omukai, S. Chon, Exploring the nature of UV-bright z $\gtrsim$ 10 galaxies detected by JWST: star formation, black hole accretion, or a non-universal IMF? Mon. Not. R. Astron. Soc. 529 (4) (2024) 3563–3581, arXiv:2305.04944 [astro-ph.GA].
[1697] E.E. Salpeter, The Luminosity function and stellar evolution, Astrophys. J. 121 (1955) 161–167.
[1698] E.R. Cueto, A. Hutter, P. Dayal, S. Gottlöber, K.E. Heintz, C. Mason, M. Trebitsch, G. Yepes, ASTRAEUS - IX. Impact of an evolving stellar initial mass function on early galaxies and reionisation, Astron. Astrophys. 686 (2024) A138, arXiv:2312.12109 [astro-ph.GA].
[1699] S. Tacchella, S.L. Finkelstein, M. Bagley, M. Dickinson, H.C. Ferguson, M. Giavalisco, L. Graziani, N.A. Grogin, N. Hathi, T.A. Hutchison, I. Jung, A.M. Koekemoer, R.L. Larson, C. Papovich, N. Pirzkal, S.a. Rojas-Ruiz, M. Song, R. Schneider, R.S. Somerville, S.M. Wilkins, L.Y.A. Yung, On the stellar populations of galaxies at z=9-11: the growth of metals and stellar mass at early times, Astrophys. J. 927 (2) (2022) 170, arXiv:2111.05351 [astro-ph.GA].
[1700] L. Whitler, D.P. Stark, R. Endsley, J. Leja, S. Charlot, J. Chevallard, Star formation histories of UV-luminous galaxies at $z \simeq 6.8$: implications for stellar mass assembly at early cosmic times, Mon. Not. R. Astron. Soc. 519 (4) (2023) 5859–5881, arXiv:2206.05315 [astro-ph.GA].
[1701] F. Iocco, L. Visinelli, Compatibility of JWST results with exotic halos, Phys. Dark Univ. 44 (2024) 101496, arXiv:2403.13068 [astro-ph.CO].
[1702] A. Pallottini, A. Ferrara, Stochastic star formation in early galaxies: Implications for the James Webb Space Telescope, Astron. Astrophys. 677 (2023) L4, arXiv:2307.03219 [astro-ph.GA].
[1703] D. Ceverino, Y. Nakazato, N. Yoshida, R.S. Klessen, S.C.O. Glover, Redshift-dependent galaxy formation efficiency at z=5 - 13 in the First-Light Simulations, Astron. Astrophys. 689 (2024) A244, arXiv:2404.02537 [astro-ph.GA].
[1704] C. Turner, S. Tacchella, F. D'Eugenio, S. Carniani, M. Curti, K. Glazebrook, B.D. Johnson, S. Lim, T. Looser, R. Maiolino, T. Nanayakkara, J. Wan, Age-dating early quiescent galaxies: high star formation efficiency, but consistent with direct, higher-redshift observations, Mon. Not. R. Astron. Soc. 537 (2) (2025) 1826–1848, arXiv:2410.05377 [astro-ph.GA].
[1705] T. Harvey, C.J. Conselice, N.J. Adams, D. Austin, I. Juodžbalis, J. Trussler, Q. Li, K. Ormerod, L. Ferreira, C.C. Lovell, Q. Duan, L. Westcott, H. Harris, R. Bhatawdekar, D. Coe, S.H. Cohen, J. Caruana, C. Cheng, S.P. Driver, B. Frye, L.J. Furtak, N.A. Grogin, N.P. Hathi, B.W. Holwerda, R.A. Jansen, A.M. Koekemoer, M.A. Marshall, M. Nonino, A.P. Vijayan, S.M. Wilkins, R. Windhorst, C.N.A. Willmer, H. Yan, A. Zitrin, EPOCHS. IV. SED modeling assumptions and their impact on the stellar mass function at 6.5 $\leq$ z $\leq$ 13.5 using PEARLS and public JWST observations, Astrophys. J. 978 (1) (2025) 89, arXiv:2403.03908 [astro-ph.GA].
[1706] Y. Chen, H.J. Mo, K. Wang, Massive dark matter haloes at high redshift: implications for observations in the JWST era, Mon. Not. R. Astron. Soc. 526 (2) (2023) 2542–2559, arXiv:2304.13890 [astro-ph.GA].
[1707] J. Wang, Z. Huang, L. Huang, J. Liu, Quantifying the tension between cosmological models and JWST red candidate massive galaxies, Res. Astron. Astrophys. 24 (4) (2024) 045001, arXiv:2311.02866 [astro-ph.CO].
[1708] Y. Qin, S. Balu, J.S.B. Wyithe, Implications of z $\gtrsim$ 12 JWST galaxies for galaxy formation at high redshift, Mon. Not. R. Astron. Soc. 526 (1) (2023) 1324–1342, arXiv:2305.17959 [astro-ph.GA].
[1709] H. Atek, M. Shuntov, L.J. Furtak, J. Richard, J.-P. Kneib, G. Mahler, A. Zitrin, H.J. McCracken, S. Charlot, J. Chevallard, I. Chemerynska, Revealing galaxy candidates out to z 16 with JWST observations of the lensing cluster SMACS0723, Mon. Not. R. Astron. Soc. 519 (1) (2023) 1201–1220, arXiv:2207.12338 [astro-ph.GA].
[1710] R. Navarro-Carrera, P. Rinaldi, K.I. Caputi, E. Iani, V. Kokorev, S.E. van Mierlo, Constraints on the faint end of the galaxy stellar mass function at z $\simeq$ 4–8 from deep JWST data, Astrophys. J. 961 (2) (2024) 207, arXiv:2305.16141 [astro-ph.GA].
[1711] M. Maggiore, A. Riotto, The Halo mass function from excursion set theory. II. The diffusing barrier, Astrophys. J. 717 (2010) 515–525, arXiv:0903.1250 [astro-ph.CO].
[1712] I.E. Achitouv, P.S. Corasaniti, Primordial bispectrum and trispectrum contributions to the non-gaussian excursion set halo mass function with diffusive drifting barrier, Phys. Rev. D 86 (2012) 083011, arXiv:1207.4796 [astro-ph.CO].
[1713] D. Reed, R. Bower, C. Frenk, A. Jenkins, T. Theuns, The halo mass function from the dark ages through the present day, Mon. Not. R. Astron. Soc. 374 (2007) 2–15, arXiv:astro-ph/0607150.
[1714] S. Basilakos, M. Plionis, J.A.S. Lima, Confronting dark energy models using galaxy cluster number counts, Phys. Rev. D 82 (2010) 083517, arXiv:1006.3418 [astro-ph.CO].
[1715] S. Bhattacharya, K. Heitmann, M. White, Z. Lukic, C. Wagner, S. Habib, Mass function predictions beyond LCDM, Astrophys. J. 732 (2011) 122, arXiv:1005.2239 [astro-ph.CO].
[1716] S. Tacchella, S. Bose, C. Conroy, D.J. Eisenstein, B.D. Johnson, A redshift-independent efficiency model: star formation and stellar masses in dark matter halos at z $\gtrsim$ 4, Astrophys. J. 868 (2) (2018) 92, arXiv:1806.03299 [astro-ph.GA].
[1717] S.W. Allen, R.W. Schmidt, H. Ebeling, A.C. Fabian, L. van Speybroeck, Constraints on dark energy from Chandra observations of the largest relaxed galaxy clusters, Mon. Not. R. Astron. Soc. 353 (2004) 457, arXiv:astro-ph/0405340.
[1718] A. Vikhlinin, A. Kravtsov, W. Forman, C. Jones, M. Markevitch, S.S. Murray, L. Van Speybroeck, Chandra sample of nearby relaxed galaxy clusters: Mass, gas fraction, and mass-temperature relation, Astrophys. J. 640 (2006) 691–709, arXiv:astro-ph/0507092.
[1719] A.V. Kravtsov, D. Nagai, A.A. Vikhlinin, Effects of cooling and star formation on the baryon fractions in clusters, Astrophys. J. 625 (2005) 588–598, arXiv:astro-ph/0501227.
[1720] S. Borgani, A. Kravtsov, Cosmological simulations of galaxy clusters, Adv. Sci. Lett. 4 (2011) 204, arXiv:0906.4370 [astro-ph.CO].
[1721] A.B. Mantz, S.W. Allen, R.G. Morris, D.A. Rapetti, D.E. Applegate, P.L. Kelly, A. von der Linden, R.W. Schmidt, Cosmology and astrophysics from relaxed galaxy clusters – II. Cosmological constraints, Mon. Not. R. Astron. Soc. 440 (3) (2014) 2077–2098, arXiv:1402.6212 [astro-ph.CO].
[1722] U. Maio, M. Viel, The first billion years of a warm dark matter universe, Mon. Not. R. Astron. Soc. 446 (2015) 2760–2775, arXiv:1409.6718 [astro-ph.CO].
[1723] K. Panchal, S. Desai, Comparison of ΛCDM and $Rh = ct$ with updated galaxy cluster fgas measurements using Bayesian inference, JHEAp 43 (2024) 15–19, arXiv:2401.11138 [astro-ph.CO].
[1724] H.-L. Huang, J.-Q. Jiang, Y.-S. Piao, High-redshift JWST massive galaxies and the initial clustering of supermassive primordial black holes, Phys. Rev. D 110 (10) (2024) 103540, arXiv:2407.15781 [astro-ph.CO].
[1725] G.-W. Yuan, L. Lei, Y.-Z. Wang, B. Wang, Y.-Y. Wang, C. Chen, Z.-Q. Shen, Y.-F. Cai, Y.-Z. Fan, Rapidly growing primordial black holes as seeds of the massive high-redshift JWST Galaxies, Sci. China Phys. Mech. Astron. 67 (10) (2024) 109512, arXiv:2303.09391 [astro-ph.CO].
[1726] B. Carr, S. Clesse, J. Garcia-Bellido, M. Hawkins, F. Kuhnel, Observational evidence for primordial black holes: A positivist perspective, Phys. Rep. 1054 (2024) 1–68, arXiv:2306.03903 [astro-ph.CO].
[1727] A.D. Dolgov, Tension between HST/JWST and ΛCDM cosmology, PBH, and antimatter in the galaxy, in: 14th Frascati workshop on Multifrequency Behaviour of High Energy Cosmic Sources, 2023, arXiv:2310.00671 [astro-ph.CO].
[1728] A. Trinca, R. Schneider, R. Maiolino, R. Valiante, L. Graziani, M. Volonteri, Seeking the growth of the first black hole seeds with JWST, Mon. Not. R. Astron. Soc. 519 (3) (2023) 4753–4764, arXiv:2211.01389 [astro-ph.GA].

[1729] F. Pacucci, B. Nguyen, S. Carniani, R. Maiolino, X. Fan, JWST CEERS and JADES active galaxies at z=4–7 violate the local $M_{\odot}$–$M_{\odot}$ relation at >3σ: implications for low-mass black holes and seeding models, Astrophys. J. Lett. 957 (1) (2023) L3, arXiv:2308.12331 [astro-ph.GA].

[1730] R. Maiolino, et al., A small and vigorous black hole in the early Universe, Nature 627 (8002) (2024) 59–63, arXiv:2305.12492 [astro-ph.GA]; Nature 630 (2024) E2 (erratum).

[1731] H. Mo, Y. Chen, H. Wang, A two-phase model of galaxy formation: I. The growth of galaxies and supermassive black holes, Mon. Not. R. Astron. Soc. 532 (4) (2024) 3808–3838, arXiv:2311.05030 [astro-ph.GA].

[1732] CEERS Team Collaboration, R.L. Larson, et al., A CEERS discovery of an accreting supermassive black hole 570 Myr after the big bang: identifying a progenitor of massive z > 6 quasars, Astrophys. J. Lett. 953 (2) (2023) L29, arXiv:2303.08918 [astro-ph.GA].

[1733] A. Bogdan, et al., Evidence for heavy-seed origin of early supermassive black holes from a z≈10 X-ray quasar, Nat. Astron. 8 (1) (2024) 126–133, arXiv:2305.15458 [astro-ph.GA].

[1734] R. Schneider, R. Valiante, A. Trinca, L. Graziani, M. Volonteri, R. Maiolino, Are we surprised to find SMBHs with JWST at z ≥ 9? Mon. Not. R. Astron. Soc. 526 (3) (2023) 3250–3261, arXiv:2305.12504 [astro-ph.GA].

[1735] H.-L. Huang, Y.-T. Wang, Y.-S. Piao, Supermassive primordial black holes for the GHZ9 and UHZ1 observed by the JWST, 2024, arXiv:2410.05891 [astro-ph.GA].

[1736] A. Trinca, R. Valiante, R. Schneider, I. Juodžbalis, R. Maiolino, L. Graziani, A. Lupi, P. Natarajan, M. Volonteri, T. Zana, Episodic super-eddington accretion as a clue to overmassive black holes in the early universe, 2024, arXiv:2412.14248 [astro-ph.GA].

[1737] S. Kumar, N. Weiner, Early galaxies from rare inflationary processes and JWST observations, 2025, arXiv:2502.08701 [astro-ph.CO].

[1738] P. Parashari, R. Laha, Primordial power spectrum in light of JWST observations of high redshift galaxies, Mon. Not. R. Astron. Soc. 526 (1) (2023) L63–L69, arXiv:2305.00999 [astro-ph.CO].

[1739] S. Hirano, N. Yoshida, Early structure formation from primordial density fluctuations with a blue, tilted power spectrum: high-redshift galaxies, Astrophys. J. 963 (1) (2024) 2, arXiv:2306.11993 [astro-ph.GA].

[1740] H. Padmanabhan, A. Loeb, Alleviating the need for exponential evolution of JWST galaxies in 10^{10} $M_{\odot}$ haloes at z > 10 by a modified ΛCDM power spectrum, Astrophys. J. Lett. 953 (1) (2023) L4, arXiv:2306.04684 [astro-ph.CO].

[1741] M. Biagetti, G. Franciolini, A. Riotto, High-redshift JWST observations and primordial non-gaussianity, Astrophys. J. 944 (2) (2023) 113, arXiv:2210.04812 [astro-ph.CO].

[1742] M. De Laurentis, P. Salucci, The accurate mass distribution of M87, the giant galaxy with imaged shadow of its supermassive black hole, as a portal to new physics, Astrophys. J. 929 (1) (2022) 17, arXiv:2206.01997 [astro-ph.CO].

[1743] S.-Y. Guo, M. Khlopov, X. Liu, L. Wu, Y. Wu, B. Zhu, Footprints of axion-like particle in pulsar timing array data and James Webb Space Telescope observations, Sci. China Phys. Mech. Astron. 67 (11) (2024) 111011, arXiv:2306.17022 [hep-ph].

[1744] G. Hütsi, M. Raidal, J. Urrutia, V. Vaskonen, H. Veermäe, Did JWST observe imprints of axion miniclusters or primordial black holes? Phys. Rev. D 107 (4) (2023) 043502, arXiv:2211.02651 [astro-ph.CO].

[1745] S. Bird, C.-F. Chang, Y. Cui, D. Yang, Enhanced early galaxy formation in JWST from axion dark matter? Phys. Lett. B 858 (2024) 139062, arXiv:2307.10302 [hep-ph].

[1746] Y. Gong, B. Yue, Y. Cao, X. Chen, Fuzzy dark matter as a solution to reconcile the stellar mass density of high-z massive galaxies and reionization history, Astrophys. J. 947 (1) (2023) 28, arXiv:2209.13757 [astro-ph.CO].

[1747] A. Zhitnitsky, Structure formation paradigm and axion quark nugget dark matter model, Phys. Dark Univ. 40 (2023) 101217, arXiv:2302.00010 [hep-ph].

[1748] Q. Zhang, S. Li, X.-H. Tan, J.-Q. Xia, Constraints on primordial magnetic fields from high redshift stellar mass density, Astrophys. J. 972 (1) (2024) 117, arXiv:2408.03584 [astro-ph.CO].

[1749] H. Jiao, R. Brandenberger, A. Refregier, Early structure formation from cosmic string loops in light of early JWST observations, Phys. Rev. D 108 (4) (2023) 043510, arXiv:2304.06429 [astro-ph.CO].

[1750] H. Jiao, R. Brandenberger, A. Refregier, N-body simulation of early structure formation from cosmic string loops, Phys. Rev. D 109 (12) (2024) 123524, arXiv:2402.06235 [astro-ph.CO].

[1751] S.M. Koehler, H. Jiao, R. Kannan, Investigating cosmic strings using large-volume hydrodynamical simulations in the context of JWST's massive UV-bright galaxies, 2024, arXiv:2412.00182 [astro-ph.CO].

[1752] P. Dayal, S.K. Giri, Warm dark matter constraints from the JWST, Mon. Not. R. Astron. Soc. 528 (2) (2024) 2784–2789, arXiv:2303.14239 [astro-ph.CO].

[1753] U. Maio, M. Viel, JWST high-redshift galaxy constraints on warm and cold dark matter models, Astron. Astrophys. 672 (2023) A71, arXiv:2211.03620 [astro-ph.CO].

[1754] G. Gandolfi, A. Lapi, T. Ronconi, L. Danese, Astroparticle constraints from the cosmic star formation rate density at high redshift: current status and forecasts for JWST, Universe 8 (11) (2022) 589, arXiv:2211.02840 [astro-ph.CO].

[1755] M. Forconi, W. Giarè, O. Mena, Ruchika, E. Di Valentino, A. Melchiorri, R.C. Nunes, A double take on early and interacting dark energy from JWST, J. Cosmol. Astropart. Phys. 05 (2024) 097, arXiv:2312.11074 [astro-ph.CO].

[1756] A. Klypin, V. Poulin, F. Prada, J. Primack, M. Kamionkowski, V. Avila-Reese, A. Rodriguez-Puebla, P. Behroozi, D. Hellinger, T.L. Smith, Clustering and halo abundances in early dark energy cosmological models, Mon. Not. R. Astron. Soc. 504 (1) (2021) 769–781, arXiv:2006.14910 [astro-ph.CO].

[1757] X. Shen, M. Vogelsberger, M. Boylan-Kolchin, S. Tacchella, R.P. Naidu, Early galaxies and early dark energy: a unified solution to the hubble tension and puzzles of massive bright galaxies revealed by JWST, Mon. Not. R. Astron. Soc. 533 (4) (2024) 3923–3936, arXiv:2406.15548 [astro-ph.GA].

[1758] J.-Q. Jiang, W. Liu, H. Zhan, B. Hu, Explanation of high redshift luminous galaxies from JWST by an early dark energy model, Phys. Rev. D 111 (2) (2025) 023519, arXiv:2409.19941 [astro-ph.CO].

[1759] N. Menci, M. Castellano, P. Santini, E. Merlin, A. Fontana, F. Shankar, High-redshift galaxies from early JWST observations: constraints on dark energy models, Astrophys. J. Lett. 938 (1) (2022) L5, arXiv:2208.11471 [astro-ph.CO].

[1760] N. Menci, A.A. Sen, M. Castellano, The excess of JWST bright galaxies: a possible origin in the ground state of dynamical dark energy in the light of DESI 2024 data, Astrophys. J. 976 (2) (2024) 227, arXiv:2410.22940 [astro-ph.CO].

[1761] N. Menci, S.A. Adil, U. Mukhopadhyay, A.A. Sen, S. Vagnozzi, Negative cosmological constant in the dark energy sector: tests from JWST photometric and spectroscopic observations of high-redshift galaxies, J. Cosmol. Astropart. Phys. 07 (2024) 072, arXiv:2401.12659 [astro-ph.CO].

[1762] S.A. Adil, U. Mukhopadhyay, A.A. Sen, S. Vagnozzi, Dark energy in light of the early JWST observations: case for a negative cosmological constant? J. Cosmol. Astropart. Phys. 10 (2023) 072, arXiv:2307.12763 [astro-ph.CO].

[1763] E.A. Paraskevas, L. Perivolaropoulos, The density of virialized clusters as a probe of dark energy, Mon. Not. R. Astron. Soc. 531 (1) (2024) 1021–1033, arXiv:2308.07046 [astro-ph.CO].

[1764] P. Wang, B.-Y. Su, L. Zu, Y. Yang, L. Feng, Exploring the dark energy equation of state with JWST, Eur. Phys. J. Plus 139 (8) (2024) 711, arXiv:2307.11374 [astro-ph.CO].

[1765] M. Jõeveer, J. Einasto, E. Tago, Spatial distribution of galaxies and of clusters of galaxies in the southern galactic hemisphere, Mon. Not. R. Astro. Soc. 185 (1978) 357–370.

[1766] S.A. Gregory, L.A. Thompson, The Coma/A1367 supercluster and its environs, Astrophys. J. 222 (1978) 784–799.

[1767] R.P. Kirshner, A. Oemler Jr., P.L. Schechter, S.A. Shectman, A million cubic megaparsec void in Bootes, Astrophys. J. Lett. 248 (1981) L57–60.

[1768] V. de Lapparent, M.J. Geller, J.P. Huchra, A Slice of the universe, Astrophys. J. Lett. 302 (1986) L1–L5.

[1769] Y.B. Zeldovich, J. Einasto, S.F. Shandarin, Giant voids in the universe, Nature 300 (1982) 407–413.

[1770] P.J.E. Peebles, The void phenomenon, Astrophys. J. 557 (2001) 495–504, arXiv:astro-ph/0101127.

[1771] N. Padilla, D. Paz, M. Lares, L. Ceccarelli, D.G. Lambas, Y.-C. Cai, B. Li, Void dynamics, IAU Symp. 308 (2014) 530–537, arXiv:1410.8186 [astro-ph.CO].

[1772] A. Pisani, et al., Cosmic voids: a novel probe to shed light on our Universe, 2019, arXiv:1903.05161 [astro-ph.CO].

[1773] N. Hamaus, B.D. Wandelt, P.M. Sutter, G. Lavaux, M.S. Warren, Cosmology with void-galaxy correlations, Phys. Rev. Lett. 112 (4) (2014) 041304, arXiv:1307.2571 [astro-ph.CO].

[1774] K.C. Chan, N. Hamaus, V. Desjacques, Large-scale clustering of cosmic voids, Phys. Rev. D 90 (10) (2014) 103521, arXiv:1409.3849 [astro-ph.CO].

[1775] G. Pollina, N. Hamaus, K. Dolag, J. Weller, M. Baldi, L. Moscardini, On the linearity of tracer bias around voids, Mon. Not. R. Astron. Soc. 469 (1) (2017) 787–799, arXiv:1610.06176 [astro-ph.CO].

[1776] S. Contarini, T. Ronconi, F. Marulli, L. Moscardini, A. Veropalumbo, M. Baldi, Cosmological exploitation of the size function of cosmic voids identified in the distribution of biased tracers, Mon. Not. R. Astron. Soc. 488 (3) (2019) 3526–3540, arXiv:1904.01022 [astro-ph.CO].

[1777] J. Einasto, L.J. Liivamägi, I. Suhhonenko, M. Einasto, The biasing phenomenon, Astron. Astrophys. 630 (2019) A62, arXiv:1906.03617 [astro-ph.CO].

[1778] J.M. Colberg, et al., The aspen–amsterdam void finder comparison project, Mon. Not. R. Astron. Soc. 387 (2008) 933, arXiv:0803.0918 [astro-ph].

[1779] M.C. Neyrinck, ZOBOV: a parameter-free void-finding algorithm, Mon. Not. R. Astron. Soc. 386 (2008) 2101, arXiv:0712.3049 [astro-ph].

[1780] P.M. Sutter, G. Lavaux, N. Hamaus, A. Pisani, B.D. Wandelt, M.S. Warren, F. Villaescusa-Navarro, P. Zivick, Q. Mao, B.B. Thompson, VIDE: the void IDentification and examination toolkit, Astron. Comput. 9 (2015) 1–9, arXiv:1406.1191 [astro-ph.CO].

[1781] A. Elyiv, F. Marulli, G. Pollina, M. Baldi, E. Branchini, A. Cimatti, L. Moscardini, Cosmic voids detection without density measurements, Mon. Not. R. Astron. Soc. 448 (1) (2015) 642–653, arXiv:1410.4559 [astro-ph.CO].

[1782] D.J. Paz, C.M. Correa, S.R. Gualpa, A.N. Ruiz, C.S. Bederián, R.D. Graña, N.D. Padilla, Guess the cheese flavour by the size of its holes: a cosmological test using the abundance of popcorn voids, Mon. Not. R. Astron. Soc. 522 (2) (2023) 2553–2569, arXiv:2212.06849 [astro-ph.CO].

[1783] A.N. Ruiz, D.J. Paz, M. Lares, H.E. Luparello, L. Ceccarelli, D. Garcia Lambas, Clues on void evolution – III. Structure and dynamics in void shells, Mon. Not. R. Astron. Soc. 448 (2) (2015) 1471–1482, arXiv:1501.02120 [astro-ph.CO].

[1784] D.G. Lambas, M. Lares, L. Ceccarelli, A.N. Ruiz, D.J. Paz, V.E. Maldonado, H.E. Luparello, The sparkling Universe: the coherent motions of cosmic voids, Mon. Not. R. Astron. Soc. 455 (1) (2016) L99–L103, arXiv:1510.00712 [astro-ph.CO].

[1785] N. Schuster, N. Hamaus, K. Dolag, J. Weller, Why cosmic voids matter: mitigation of baryonic physics, J. Cosmol. Astropart. Phys. 08 (2024) 065, arXiv:2312.11241 [astro-ph.CO].

[1786] D. Paz, M. Lares, L. Ceccarelli, N. Padilla, D.G. Lambas, Clues on void evolution II: Measuring density and velocity profiles on SDSS galaxy redshift space distortions, Mon. Not. R. Astron. Soc. 436 (2013) 3480, arXiv:1306.5799 [astro-ph.CO].

[1787] N. Schuster, N. Hamaus, K. Dolag, J. Weller, Why cosmic voids matter: nonlinear structure & linear dynamics, J. Cosmol. Astropart. Phys. 05 (2023) 031, arXiv:2210.02457 [astro-ph.CO].

[1788] I. Szapudi, et al., The cold spot in the cosmic microwave background: the shadow of a supervoid, in: 49th Rencontres de Moriond on Cosmology, 2014, pp. 33–41, arXiv:1406.3622 [astro-ph.CO].

[1789] R.K. Sheth, R. van de Weygaert, A Hierarchy of voids: Much ado about nothing, Mon. Not. R. Astron. Soc. 350 (2004) 517, arXiv:astro-ph/0311260.

[1790] E. Jennings, Y. Li, W. Hu, The abundance of voids and the excursion set formalism, Mon. Not. R. Astron. Soc. 434 (2013) 2167, arXiv:1304.6087 [astro-ph.CO].

[1791] G. Verza, C. Carbone, A. Pisani, C. Porciani, S. Matarrese, The universal multiplicity function: counting haloes and voids, J. Cosmol. Astropart. Phys. 10 (2024) 079, arXiv:2401.14451 [astro-ph.CO].

[1792] G. Lavaux, B.D. Wandelt, Precision cosmography with stacked voids, Astrophys. J. 754 (2012) 109, arXiv:1110.0345 [astro-ph.CO].

[1793] N. Hamaus, A. Pisani, P.M. Sutter, G. Lavaux, S. Escoffier, B.D. Wandelt, J. Weller, Constraints on cosmology and gravity from the dynamics of voids, Phys. Rev. Lett. 117 (9) (2016) 091302, arXiv:1602.01784 [astro-ph.CO].

[1794] Y.-C. Cai, A. Taylor, J.A. Peacock, N. Padilla, Redshift-space distortions around voids, Mon. Not. R. Astron. Soc. 462 (3) (2016) 2465–2477, arXiv:1603.05184 [astro-ph.CO].

[1795] C.M. Correa, D.J. Paz, N.D. Padilla, A.N. Ruiz, R.E. Angulo, A.G. Sánchez, Non-fiducial cosmological test from geometrical and dynamical distortions around voids, Mon. Not. R. Astron. Soc. 485 (4) (2019) 5761–5772, arXiv:1811.12251 [astro-ph.CO].

[1796] C.M. Correa, D.J. Paz, A.G. Sánchez, A.N. Ruiz, N.D. Padilla, R.E. Angulo, Redshift-space effects in voids and their impact on cosmological tests. Part I: the void size function, Mon. Not. R. Astron. Soc. 500 (1) (2020) 911–925, arXiv:2007.12064 [astro-ph.CO].

[1797] C.M. Correa, D.J. Paz, N.D. Padilla, A.G. Sánchez, A.N. Ruiz, R.E. Angulo, Redshift-space effects in voids and their impact on cosmological tests – II. The void-galaxy cross-correlation function, Mon. Not. R. Astron. Soc. 509 (2) (2021) 1871–1884, arXiv:2107.01314 [astro-ph.CO].

[1798] S. Contarini, A. Pisani, N. Hamaus, F. Marulli, L. Moscardini, M. Baldi, The perspective of voids on rising cosmology tensions, Astron. Astrophys. 682 (2024) A20, arXiv:2212.07438 [astro-ph.CO].

[1799] N. Hamaus, A. Pisani, J.-A. Choi, G. Lavaux, B.D. Wandelt, J. Weller, Precision cosmology with voids in the final BOSS data, J. Cosmol. Astropart. Phys. 12 (2020) 023, arXiv:2007.07895 [astro-ph.CO].

[1800] Euclid Collaboration, N. Hamaus, et al., Euclid: Forecasts from redshift-space distortions and the Alcock–Paczynski test with cosmic voids, Astron. Astrophys. 658 (2022) A20, arXiv:2108.10347 [astro-ph.CO].

[1801] Euclid Collaboration, S. Contarini, et al., Euclid: Cosmological forecasts from the void size function, Astron. Astrophys. 667 (2022) A162, arXiv:2205.11525 [astro-ph.CO].

[1802] Euclid Collaboration, M. Bonici, et al., Euclid: Forecasts from the void-lensing cross-correlation, Astron. Astrophys. 670 (2023) A47, arXiv:2206.14211 [astro-ph.CO].

[1803] S. Raghunathan, S. Nadathur, B.D. Sherwin, N. Whitehorn, The gravitational lensing signatures of BOSS voids in the cosmic microwave background, Astrophys. J. 890 (2) (2020) 168, arXiv:1911.08475 [astro-ph.CO].

[1804] DES Collaboration, U. Demirbozan, et al., The gravitational lensing imprints of DES Y3 superstructures on the CMB: a matched filtering approach, Mon. Not. R. Astron. Soc. 534 (3) (2024) 2328–2343, arXiv:2404.18278 [astro-ph.CO].

[1805] G. Camacho-Ciurana, P. Lee, N. Arsenov, A. Kovács, I. Szapudi, I. Csabai, The cosmic microwave background lensing imprint of cosmic voids detected in the WISE-Pan-STARRS luminous red galaxy catalog, Astron. Astrophys. 689 (2024) A171, arXiv:2312.08483 [astro-ph.CO].

[1806] S. Sartori, et al., The imprint of cosmic voids from the DESI Legacy Survey DR9 LRGs in the Planck 2018 lensing map through spectroscopically calibrated mocks, 2024, arXiv:2412.02761 [astro-ph.CO].

[1807] D.R. Lorimer, M. Bailes, M.A. McLaughlin, D.J. Narkevic, F. Crawford, A bright millisecond radio burst of extragalactic origin, Science 318 (2007) 777, arXiv:0709.4301 [astro-ph].

[1808] S.P. Tendulkar, et al., The host galaxy and redshift of the repeating fast radio burst FRB 121102, Astrophys. J. Lett. 834 (2) (2017) L7, arXiv:1701.01100 [astro-ph.HE].

[1809] A. Walters, A. Weltman, B.M. Gaensler, Y.-Z. Ma, A. Witzemann, Future cosmological constraints from fast radio bursts, Astrophys. J. 856 (1) (2018) 65, arXiv:1711.11277 [astro-ph.CO].

[1810] W. Deng, B. Zhang, Cosmological implications of fast radio burst/gamma-ray burst associations, Astrophys. J. Lett. 783 (2014) L35, arXiv:1401.0059 [astro-ph.HE].

[1811] A. Walters, Y.-Z. Ma, J. Sievers, A. Weltman, Probing diffuse gas with fast radio bursts, Phys. Rev. D 100 (10) (2019) 103519, arXiv:1909.02821 [astro-ph.CO].

[1812] J.P. Macquart, et al., A census of baryons in the Universe from localized fast radio bursts, Nature 581 (7809) (2020) 391–395, arXiv:2005.13161 [astro-ph.CO].

[1813] E. Platts, A. Weltman, A. Walters, S.P. Tendulkar, J.E.B. Gordin, S. Kandhai, A living theory catalogue for fast radio bursts, Phys. Rep. 821 (2019) 1–27, arXiv:1810.05836 [astro-ph.HE].

[1814] B. Zhang, The physical mechanisms of fast radio bursts, Nature 587 (2020) 45–53, arXiv:2011.03500 [astro-ph.HE].

[1815] B. Zhang, The physics of fast radio bursts, Rev. Modern Phys. 95 (3) (2023) 035005, arXiv:2212.03972 [astro-ph.HE].

[1816] S. Kalita, A. Weltman, Continuous gravitational wave detection to understand the generation mechanism of fast radio bursts, Mon. Not. R. Astron. Soc. 520 (3) (2023) 3742–3748, arXiv:2211.00940 [astro-ph.HE].

[1817] H.E.S.S. Collaboration, J.O. Chibueze, et al., A MeerKAT, e-MERLIN, H.E.S.S., and Swift search for persistent and transient emission associated with three localized FRBs, Mon. Not. R. Astron. Soc. 515 (1) (2022) 1365–1379, arXiv:2201.00069 [astro-ph.HE].

[1818] B. Zhou, X. Li, T. Wang, Y.-Z. Fan, D.-M. Wei, Fast radio bursts as a cosmic probe? Phys. Rev. D 89 (10) (2014) 107303, arXiv:1401.2927 [astro-ph.CO].

[1819] H. Gao, Z. Li, B. Zhang, Fast radio burst/gamma-ray burst cosmography, Astrophys. J. 788 (2014) 189, arXiv:1402.2498 [astro-ph.CO].

[1820] Z. Pleunis, et al., LOFAR detection of 110–188 MHz emission and frequency-dependent activity from FRB 20180916B, Astrophys. J. Lett. 911 (1) (2021) L3, arXiv:2012.08372 [astro-ph.HE].

[1821] V. Gajjar, et al., Highest frequency detection of FRB 121102 at 4–8 GHz using the breakthrough listen digital backend at the green bank telescope, Astrophys. J. 863 (1) (2018) 2, arXiv:1804.04101 [astro-ph.HE].

[1822] L. Bonetti, J. Ellis, N.E. Mavromatos, A.S. Sakharov, E.K.G. Sarkisyan-Grinbaum, A.D.A.M. Spallicci, Photon mass limits from fast radio bursts, Phys. Lett. B 757 (2016) 548–552, arXiv:1602.09135 [astro-ph.HE].

[1823] H. Wang, X. Miao, L. Shao, Bounding the photon mass with cosmological propagation of fast radio bursts, Phys. Lett. B 820 (2021) 136596, arXiv:2103.15299 [astro-ph.HE].

[1824] H.-N. Lin, L. Tang, R. Zou, Revised constraints on the photon mass from well-localized fast radio bursts, Mon. Not. R. Astron. Soc. 520 (1) (2023) 1324–1331, arXiv:2301.12103 [gr-qc].

[1825] R. Reischke, S. Hagstotz, Consistent constraints on the equivalence principle from localized fast radio bursts, Mon. Not. R. Astron. Soc. 523 (4) (2023) 6264–6271, arXiv:2302.10072 [astro-ph.CO].

[1826] S. Kalita, Constraining fundamental constants with fast radio bursts: unveiling the role of energy scale, Mon. Not. R. Astron. Soc. 533 (1) (2024) L57–L63, arXiv:2407.01736 [gr-qc].

[1827] T. Lemos, R. Gonçalves, J. Carvalho, J. Alcaniz, A search for the fine-structure constant evolution from fast radio bursts and type Ia supernovae data, J. Cosmol. Astropart. Phys. 01 (2025) 059, arXiv:2406.11691 [astro-ph.CO].

[1828] Z.-X. Li, H. Gao, X.-H. Ding, G.-J. Wang, B. Zhang, Strongly lensed repeating fast radio bursts as precision probes of the universe, Nat. Commun. 9 (1) (2018) 3833, arXiv:1708.06357 [astro-ph.CO].

[1829] S. Hagstotz, R. Reischke, R. Lilow, A new measurement of the Hubble constant using fast radio bursts, Mon. Not. R. Astron. Soc. 511 (1) (2022) 662–667, arXiv:2104.04538 [astro-ph.CO].

[1830] Q. Wu, G.-Q. Zhang, F.-Y. Wang, An 8 per cent determination of the Hubble constant from localized fast radio bursts, Mon. Not. R. Astron. Soc. 515 (1) (2022) L1–L5, arXiv:2108.00581 [astro-ph.CO]; Mon. Not. Roy. Astron. Soc. 531 (2024) L8 (erratum).

[1831] C.W. James, et al., A measurement of hubble's constant using fast radio bursts, Mon. Not. R. Astron. Soc. 516 (4) (2022) 4862–4881, arXiv:2208.00819 [astro-ph.CO].

[1832] J. Baptista, J.X. Prochaska, A.G. Mannings, C.W. James, R.M. Shannon, S.D. Ryder, A.T. Deller, D.R. Scott, M. Glowacki, N. Tejos, Measuring the variance of the macquart relation in redshift–extragalactic dispersion measure modeling, Astrophys. J. 965 (1) (2024) 57, arXiv:2305.07022 [astro-ph.CO].

[1833] Y. Liu, H. Yu, P. Wu, Cosmological-model-independent determination of hubble constant from fast radio bursts and hubble parameter measurements, Astrophys. J. Lett. 946 (2) (2023) L49, arXiv:2210.05202 [astro-ph.CO].

[1834] J.-J. Wei, F. Melia, Investigating cosmological models and the hubble tension using localized fast radio bursts, Astrophys. J. 955 (2) (2023) 101, arXiv:2308.05918 [astro-ph.CO].

[1835] Z.-W. Zhao, J.-G. Zhang, Y. Li, J.-F. Zhang, X. Zhang, FRB dark sirens: Measuring the Hubble constant with unlocalized fast radio bursts, 2022, arXiv:2212.13433 [astro-ph.CO].
[1836] J. Gao, Z. Zhou, M. Du, R. Zou, J. Hu, L. Xu, A measurement of hubble constant using cosmographic approach from fast radio bursts and SNe Ia, 2023, arXiv:2307.08285 [astro-ph.CO].
[1837] J.A.S. Fortunato, D.J. Bacon, W.S. Hipólito-Ricaldi, D. Wands, Fast Radio Bursts and Artificial Neural Networks: a cosmological-model-independent estimation of the Hubble constant, J. Cosmol. Astropart. Phys. 01 (2025) 018, arXiv:2407.03532 [astro-ph.CO].
[1838] S. Kalita, S. Bhatporia, A. Weltman, Fast Radio Bursts as probes of the late-time universe: A new insight on the Hubble tension, Phys. Dark Univ. 48 (2025) 101926, arXiv:2410.01974 [astro-ph.CO].
[1839] E.F. Piratova-Moreno, L.A. García, C.A. Benavides-Gallego, C. Cabrera, Fast Radio Bursts as cosmological proxies: estimating the Hubble constant, 2025, arXiv:2502.08509 [astro-ph.CO].
[1840] J.B. Muñoz, E.D. Kovetz, L. Dai, M. Kamionkowski, Lensing of fast radio bursts as a probe of compact dark matter, Phys. Rev. Lett. 117 (9) (2016) 091301, arXiv:1605.00008 [astro-ph.CO].
[1841] M.W. Sammons, J.-P. Macquart, R.D. Ekers, R.M. Shannon, H. Cho, J.X. Prochaska, A.T. Deller, C.K. Day, First constraints on compact dark matter from fast radio burst microstructure, Astrophys. J. 900 (2) (2020) 122, arXiv:2002.12533 [astro-ph.CO].
[1842] R. Laha, Lensing of fast radio bursts: Future constraints on primordial black hole density with an extended mass function and a new probe of exotic compact fermion and boson stars, Phys. Rev. D 102 (2) (2020) 023016, arXiv:1812.11810 [astro-ph.CO].
[1843] K. Liao, S.B. Zhang, Z. Li, H. Gao, Constraints on compact dark matter with fast radio burst observations, Astrophys. J. 896 (1) (2020) L11, arXiv:2003.13349 [astro-ph.CO].
[1844] C. Leung, et al., Constraining primordial black holes using fast radio burst gravitational-lens interferometry with CHIME/FRB, Phys. Rev. D 106 (4) (2022) 043017, arXiv:2204.06001 [astro-ph.HE].
[1845] S. Kalita, S. Bhatporia, A. Weltman, Gravitational lensing in modified gravity: a case study for Fast Radio Bursts, J. Cosmol. Astropart. Phys. 11 (2023) 059, arXiv:2308.16604 [gr-qc].
[1846] D. Crichton, et al., Hydrogen intensity and real-time analysis experiment: 256-element array status and overview, J. Astron. Telesc. Instrum. Syst. 8 (2022) 011019, arXiv:2109.13755 [astro-ph.IM].
[1847] L. Connor, V. Ravi, Stellar prospects for FRB gravitational lensing, Mon. Not. R. Astron. Soc. 521 (3) (2023) 4024–4038, arXiv:2206.14310 [astro-ph.CO].
[1848] S.C.C. Ho, T. Hashimoto, T. Goto, Y.-W. Lin, S.J. Kim, Y. Uno, T.Y.Y. Hsiao, Future constraints on dark matter with gravitationally lensed fast radio bursts detected by BURSTT, Astrophys. J. 950 (1) (2023) 53, arXiv:2304.04990 [astro-ph.HE].
[1849] A. Weltman, et al., Fundamental physics with the square kilometre array, Publ. Astron. Soc. Austral. 37 (2020) e002, arXiv:1810.02680 [astro-ph.CO].
[1850] M.G. Hauser, E. Dwek, The cosmic infrared background: measurements and implications, Ann. Rev. Astron. Astrophys. 39 (2001) 249–307, arXiv:astro-ph/0105539.
[1851] R.C. Gilmore, P. Madau, J.R. Primack, R.S. Somerville, F. Haardt, GeV gamma-ray attenuation and the high-redshift UV background, Mon. Not. R. Astron. Soc. 399 (2009) 1694, arXiv:0905.1144 [astro-ph.CO].
[1852] N. Cappelluti, et al., The Chandra COSMOS legacy survey: Energy Spectrum of the Cosmic X-ray Background and constraints on undetected populations, Astrophys. J. 837 (1) (2017) 19, arXiv:1702.01660 [astro-ph.HE].
[1853] Fermi-LAT Collaboration, M. Ackermann, et al., Resolving the extragalactic γ-ray background above 50 GeV with the fermi large area telescope, Phys. Rev. Lett. 116 (15) (2016) 151105, arXiv:1511.00693 [astro-ph.CO].
[1854] J. Singal, et al., The second radio synchrotron background workshop: conference summary and report, Publ. Astron. Soc. Pac. 135 (1045) (2023) 036001, arXiv:2211.16547 [astro-ph.CO].
[1855] D.J. Fixsen, et al., ARCADE 2 measurement of the extra-galactic sky temperature at 3-90 GHz, Astrophys. J. 734 (2011) 5, arXiv:0901.0555 [astro-ph.CO].
[1856] J. Singal, et al., The ARCADE 2 instrument, Astrophys. J. 730 (2011) 138, arXiv:0901.0546 [astro-ph.IM].
[1857] J. Dowell, G.B. Taylor, The radio background below 100 MHz, Astrophys. J. Lett. 858 (1) (2018) L9, arXiv:1804.08581 [astro-ph.CO].
[1858] G. Jóhannesson, T.A. Porter, Signatures of recent cosmic-ray acceleration in the high-latitude gamma-ray sky, Astrophys. J. 917 (1) (2021) 30, arXiv:2104.13708 [astro-ph.HE].
[1859] C.G.T. Haslam, C.J. Salter, H. Stoffel, W.E. Wilson, A 408 MHz all-sky continuum survey. II. The atlas of contour maps, Astron. Astrophys. Suppl. Ser. 47 (1982) 1–142.
[1860] K. Maeda, H. Alvarez, J. Aparici, J. May, P. Reich, A 45-MHz continuum survey of the northern hemisphere, Astron. Astrophys. Suppl. Ser. 140 (1999) 145–154.
[1861] R.S. Roger, C.H. Costain, T.L. Landecker, C.M. Swerdlyk, The radio emission from the galaxy at 22 mhz, Astron. Astrophys. Suppl. Ser. 137 (1999) 7, arXiv:astro-ph/9902213.
[1862] J. Singal, et al., The radio synchrotron background: conference summary and report, Publ. Astron. Soc. Pac. 130 (985) (2018) 036001, arXiv:1711.09979 [astro-ph.HE].
[1863] J.J. Condon, W.D. Cotton, E.B. Fomalont, K.I. Kellermann, N. Miller, R.A. Perley, D. Scott, T. Vernstrom, J.V. Wall, Resolving the radio source background: deeper understanding through confusion, Astrophys. J. 758 (2012) 23, arXiv:1207.2439 [astro-ph.CO].
[1864] M.J. Hardcastle, T.W. Shimwell, C. Tasse, P.N. Best, A. Drabent, M.J. Jarvis, I. Prandoni, H.J.A. Röttgering, J. Sabater, D.J. Schwarz, The contribution of discrete sources to the sky temperature at 144 MHz, Astron. Astrophys. 648 (2021) A10, arXiv:2011.08294 [astro-ph.CO].
[1865] C.L. Hale, I.H. Whittam, M.J. Jarvis, P.N. Best, N.L. Thomas, I. Heywood, M. Prescott, N. Adams, J. Afonso, F. An, R.A.A. Bowler, J.D. Collier, R.H.W. Cook, R. Davé, B.S. Frank, M. Glowacki, P.W. Hatfield, S. Kolwa, C.C. Lovell, N. Maddox, L. Marchetti, L.K. Morabito, E. Murphy, I. Prandoni, Z. Randriamanakoto, A.R. Taylor, MIGHTEE: deep 1.4 GHz source counts and the sky temperature contribution of star-forming galaxies and active galactic nuclei, Mon. Not. R. Astro. Soc. 520 (2) (2023) 2668–2691, arXiv:2211.05741 [astro-ph.GA].
[1866] A. Kogut, et al., ARCADE 2 observations of galactic radio emission, Astrophys. J. 734 (2011) 4, arXiv:0901.0562 [astro-ph.GA].
[1867] J. Singal, A. Kogut, E. Jones, H. Dunlap, Axial ratio of edge-on spiral galaxies as a test for bright radio halos, Astrophys. J. Lett. 799 (1) (2015) L10, arXiv:1501.00499 [astro-ph.GA].
[1868] M.G.H. Krause, M.J. Hardcastle, Can the Local Bubble explain the radio background? Mon. Not. R. Astron. Soc. 502 (2) (2021) 2807–2814, arXiv:2101.05255 [astro-ph.HE].
[1869] A.R. Offringa, J. Singal, S. Heston, S. Horiuchi, D.M. Lucero, Measurement of the anisotropy power spectrum of the radio synchrotron background, Mon. Not. R. Astron. Soc. 509 (1) (2021) 114–121, arXiv:2110.00499 [astro-ph.CO].
[1870] F.J. Cowie, A.R. Offringa, B.K. Gehlot, J. Singal, S. Heston, S. Horiuchi, D.M. Lucero, Diffuse sources, clustering, and the excess anisotropy of the radio synchrotron background, Mon. Not. R. Astron. Soc. 523 (4) (2023) 5034–5046, arXiv:2306.00829 [astro-ph.CO].
[1871] P.P. Ponente, Y. Ascasibar, J.M. Diego, The contribution of star-forming galaxies to the cosmic radio background, Mon. Not. R. Astron. Soc. 418 (2011) 691, arXiv:1104.3012 [astro-ph.CO].
[1872] J. Singal, L. Stawarz, A. Lawrence, V. Petrosian, Sources of the radio background considered, Mon. Not. R. Astron. Soc. 409 (2010) 1172, arXiv:0909.1997 [astro-ph.CO].
[1873] E. Todarello, M. Regis, F. Bianchini, J. Singal, E. Branchini, F.J. Cowie, S. Heston, S. Horiuchi, D. Lucero, A. Offringa, Constraints on the origin of the radio synchrotron background via angular correlations, Mon. Not. R. Astron. Soc. 530 (3) (2024) 2994–3004, arXiv:2311.17641 [astro-ph.CO].
[1874] A. Fialkov, R. Barkana, Signature of excess radio background in the 21-cm global signal and power spectrum, Mon. Not. R. Astron. Soc. 486 (2) (2019) 1763–1773, arXiv:1902.02438 [astro-ph.CO].
[1875] P.L. Biermann, B.B. Nath, L.t.I. Caramete, B.C. Harms, T. Stanev, J. Becker Tjus, Cosmic backgrounds due to the formation of the first generation of supermassive black holes, Mon. Not. R. Astron. Soc. 441 (2) (2014) 1147–1156, arXiv:1403.3804 [astro-ph.CO].
[1876] K. Fang, T. Linden, Cluster mergers and the origin of the ARCADE-2 excess, J. Cosmol. Astropart. Phys. 10 (2016) 004, arXiv:1506.05807 [astro-ph.HE].
[1877] N. Fornengo, R. Lineros, M. Regis, M. Taoso, Possibility of a dark matter interpretation for the excess in isotropic radio emission reported by ARCADE, Phys. Rev. Lett. 107 (2011) 271302, arXiv:1108.0569 [hep-ph].
[1878] D. Hooper, A.V. Belikov, T.E. Jeltema, T. Linden, S. Profumo, T.R. Slatyer, The isotropic radio background and annihilating dark matter, Phys. Rev. D 86 (2012) 103003, arXiv:1203.3547 [astro-ph.CO].
[1879] K. Fang, T. Linden, Anisotropy of the extragalactic radio background from dark matter annihilation, Phys. Rev. D 91 (8) (2015) 083501, arXiv:1412.7545 [astro-ph.HE].
[1880] E.C.F.S. Fortes, O.D. Miranda, F.W. Stecker, C.A. Wuensche, Some implications of the leptonic annihilation of dark matter: possible galactic radio emission signatures and the excess radio flux of extragalactic origin, J. Cosmol. Astropart. Phys. 11 (2019) 047, arXiv:1907.13184 [hep-ph].
[1881] Y. Yang, G. Yang, X. Huang, X. Chen, T. Lu, H. Zong, Contribution of ultracompact dark matter minihalos to the isotropic radio background, Phys. Rev. D 87 (8) (2013) 083519, arXiv:1206.3750 [astro-ph.HE].
[1882] D. Spolyar, P. Bodenheimer, K. Freese, P. Gondolo, Dark stars: a new look at the first stars in the universe, Astrophys. J. 705 (2009) 1031–1042, arXiv:0903.3070 [astro-ph.CO].
[1883] T. Rindler-Daller, K. Freese, R.H.D. Townsend, L. Visinelli, Stability and pulsation of the first dark stars, Mon. Not. R. Astron. Soc. 503 (3) (2021) 3677–3691, arXiv:2011.00231 [astro-ph.CO].
[1884] K. Lawson, A.R. Zhitnitsky, Isotropic radio background from quark nugget dark matter, Phys. Lett. B 724 (2013) 17–21, arXiv:1210.2400 [astro-ph.CO].
[1885] N. Cappelluti, G. Hasinger, P. Natarajan, Exploring the high-redshift PBH-ΛCDM universe: early black hole seeding, the first stars and cosmic radiation backgrounds, Astrophys. J. 926 (2) (2022) 205, arXiv:2109.08701 [astro-ph.CO].

[1886] S. Mittal, G. Kulkarni, Background of radio photons from primordial black holes, Mon. Not. R. Astron. Soc. 510 (4) (2022) 4992–4997, arXiv:2110.11975 [astro-ph.CO].
[1887] S.K. Acharya, J. Dhandha, J. Chluba, Can accreting primordial black holes explain the excess radio background? Mon. Not. R. Astron. Soc. 517 (2) (2022) 2454–2461, arXiv:2208.03816 [astro-ph.CO].
[1888] M. Pospelov, J. Pradler, J.T. Ruderman, A. Urbano, Room for new physics in the rayleigh-jeans tail of the cosmic microwave background, Phys. Rev. Lett. 121 (3) (2018) 031103, arXiv:1803.07048 [hep-ph].
[1889] A. Caputo, H. Liu, S. Mishra-Sharma, M. Pospelov, J.T. Ruderman, Radio excess from stimulated dark matter decay, Phys. Rev. D 107 (12) (2023) 123033, arXiv:2206.07713 [hep-ph].
[1890] S.K. Acharya, J. Chluba, A closer look at dark photon explanations of the excess radio background, Mon. Not. R. Astron. Soc. 521 (3) (2023) 3939–3950, arXiv:2209.09063 [astro-ph.CO].
[1891] S.K. Acharya, B. Cyr, J. Chluba, Constraining broad photon spectrum injections from exotic and astrophysical sources, Mon. Not. R. Astron. Soc. 527 (2023) 2024, arXiv:2309.00975 [astro-ph.CO].
[1892] B. Cyr, J. Chluba, S.K. Acharya, Cosmic string solution to the radio synchrotron background, Phys. Rev. D 109 (12) (2024) L121301, arXiv:2308.03512 [astro-ph.CO].
[1893] P.S.B. Dev, P. Di Bari, I. Martínez-Soler, R. Roshan, Relic neutrino decay solution to the excess radio background, J. Cosmol. Astropart. Phys. 04 (2024) 046, arXiv:2312.03082 [hep-ph].
[1894] S.D. Bale, N. Bassett, J.O. Burns, J. Dorigo Jones, K. Goetz, C. Hellum-Bye, S. Hermann, J. Hibbard, M. Maksimovic, R. McLean, R. Monsalve, P. O'Connor, A. Parsons, M. Pulupa, R. Pund, D. Rapetti, K.M. Rotermund, B. Saliwanchik, A. Slosar, D. Sundkvist, A. Suzuki, LuSEE 'night': the lunar surface electromagnetics experiment, 2023, http://dx.doi.org/10.48550/arXiv.2301.10345, arXiv e-prints, arXiv:2301.10345 [astro-ph.IM].
[1895] E. Lee, J. Chluba, G.P. Holder, Refined modelling of the radio SZ signal: kinematic terms, relativistic temperature corrections, and anisotropies in the radio background, Mon. Not. R. Astron. Soc. 512 (4) (2022) 5153–5164, arXiv:2112.10666 [astro-ph.CO].
[1896] G. Holder, J. Chluba, The radio SZ effect as a probe of the cosmological radio background, 2021, arXiv:2110.08373 [astro-ph.CO].
[1897] R. Watkins, H.A. Feldman, M.J. Hudson, Consistently large cosmic flows on scales of 100 Mpc/h: a challenge for the standard LCDM cosmology, Mon. Not. R. Astron. Soc. 392 (2009) 743–756, arXiv:0809.4041 [astro-ph].
[1898] H.A. Feldman, R. Watkins, M.J. Hudson, Cosmic flows on 100 Mpc/h scales: standardized minimum variance bulk flow, shear and octupole moments, Mon. Not. R. Astron. Soc. 407 (2010) 2328–2338, arXiv:0911.5516 [astro-ph.CO].
[1899] J.C. Bird, K.Z. Stanek, J.L. Prieto, Using ultra long period cepheids to extend the cosmic distance ladder to 100 Mpc and beyond, Astrophys. J. 695 (2009) 874–882, arXiv:0807.4933 [astro-ph].
[1900] G. Fiorentino, R.C. Ramos, G. Clementini, M. Marconi, I. Musella, A. Aloisi, F. Annibali, A. Saha, M. Tosi, R.P. van der Marel, Multi-epoch HST observations of IZw18: characterization of variable stars at ultra-low metallicities, Astrophys. J. 711 (2010) 808–817, arXiv:1001.4044 [astro-ph.SR].
[1901] M. Marconi, I. Musella, G. Fiorentino, G. Clementini, A. Aloisi, F. Annibali, R.C. Ramos, A. Saha, M. Tosi, R.P. van der Marel, Pulsation models for ultra-low (Z=0.0004) metallicity classical cepheids, Astrophys. J. 713 (2010) 615–625, arXiv:1002.4752 [astro-ph.SR].
[1902] I. Musella, M. Marconi, R. Molinaro, G. Fiorentino, V. Ripepi, G. De Somma, M.I. Moretti, New insights into the use of Ultra Long Period Cepheids as cosmological standard candles, Mon. Not. R. Astro. Soc. 501 (1) (2021) 866–874, arXiv:2011.10533 [astro-ph.SR].
[1903] I. Musella, Ultra long period cepheids: observation and theory, Universe 8 (6) (2022) 335.
[1904] C.-C. Ngeow, C.-H. Lee, M.T.-C. Yang, C.-S. Lin, H.-Y. Hsiao, Y.-C. Cheng, Z.-Y. Lin, I.L. Lin, S.M. Kanbur, W.-H. Ip, VI-band follow-up observations of ultra-long-period cepheid candidates in M31, Astron. J. 149 (2) (2015) 66, arXiv:1501.02456 [astro-ph.SR].
[1905] I. Musella, S. Leccia, R. Molinaro, M. Marconi, F. Cusano, M. Di Criscienzo, G. Fiorentino, V. Braga, V. Ripepi, G. De Somma, M. Gatto, E. Luongo, T. Sicignano, Ultra-long-period cepheids as standard candles from gaia to rubin-LSST, Astrophys. J. Suppl. 275 (2) (2024) 26, arXiv:2410.12017 [astro-ph.GA].
[1906] DESI Collaboration, A.G. Adame, et al., The early data release of the dark energy spectroscopic instrument, Astron. J. 168 (2) (2024) 58, arXiv:2306.06308 [astro-ph.CO].
[1907] DESI Collaboration, M. Abdul Karim, et al., Data release 1 of the dark energy spectroscopic instrument, 2025, arXiv:2503.14745 [astro-ph.CO].
[1908] DESI Collaboration, W. Elbers, et al., Constraints on neutrino physics from DESI DR2 BAO and DR1 full shape, 2025, arXiv:2503.14744 [astro-ph.CO].
[1909] DES Collaboration, B. Flaugher, et al., The dark energy camera, Astron. J. 150 (2015) 150, arXiv:1504.02900 [astro-ph.IM].
[1910] Linea Science Server, DES Collaboration, T.M.C. Abbott, et al., The dark energy survey data release 2, Astrophys. J. Supp. 255 (2) (2021) 20, arXiv:2101.05765 [astro-ph.IM].
[1911] S. Miyazaki, et al., Hyper Suprime-Cam: System design and verification of image quality, Publ. Astron. Soc. Japan 70 (2018) S1.
[1912] H. Aihara, et al., First data release of the hyper suprime-cam subaru strategic program, Publ. Astron. Soc. Jap. 70 (2018) S8, arXiv:1702.08449 [astro-ph.IM].
[1913] H. Aihara, et al., Third data release of the hyper suprime-cam subaru strategic program, Publ. Astron. Soc. Jap. 74 (2) (2022) 247–272–272, arXiv:2108.13045 [astro-ph.IM].
[1914] K. Moriwaki, T. Nishimichi, N. Yoshida, Machine learning for observational cosmology, Rep. Progr. Phys. 86 (7) (2023) 076901, arXiv:2303.15794 [astro-ph.IM].
[1915] A. Lewis, Efficient sampling of fast and slow cosmological parameters, Phys. Rev. D 87 (10) (2013) 103529, arXiv:1304.4473 [astro-ph.CO].
[1916] B. Audren, J. Lesgourgues, K. Benabed, S. Prunet, Conservative Constraints on Early Cosmology: an illustration of the Monte Python cosmological parameter inference code, J. Cosmol. Astropart. Phys. 02 (2013) 001, arXiv:1210.7183 [astro-ph.CO].
[1917] T. Brinckmann, J. Lesgourgues, MontePython 3: boosted MCMC sampler and other features, Phys. Dark Univ. 24 (2019) 100260, arXiv:1804.07261 [astro-ph.CO].
[1918] J. Torrado, A. Lewis, Cobaya: Code for Bayesian Analysis of hierarchical physical models, J. Cosmol. Astropart. Phys. 05 (2021) 057, arXiv:2005.05290 [astro-ph.IM].
[1919] D. Foreman-Mackey, D.W. Hogg, D. Lang, J. Goodman, emcee: The MCMC Hammer, Publ. Astron. Soc. Pac. 125 (2013) 306–312, arXiv:1202.3665 [astro-ph.IM].
[1920] M. Karamanis, F. Beutler, J.A. Peacock, D. Nabergoj, U. Seljak, Accelerating astronomical and cosmological inference with preconditioned Monte Carlo, Mon. Not. R. Astron. Soc. 516 (2) (2022) 1644–1653, arXiv:2207.05652 [astro-ph.IM].
[1921] G. Papamakarios, E. Nalisnick, D.J. Rezende, S. Mohamed, B. Lakshminarayanan, Normalizing flows for probabilistic modeling and inference, J. Mach. Learn. Res. 22 (57) (2021) 1–64, arXiv:1912.02762 [stat.ML], http://jmlr.org/papers/v22/19-1028.html.
[1922] R.M. Neal, Slice sampling, Ann. Statist. 31 (3) (2003) 705–767.
[1923] M. Karamanis, F. Beutler, J.A. Peacock, zeus: a python implementation of ensemble slice sampling for efficient Bayesian parameter inference, Mon. Not. R. Astron. Soc. 508 (3) (2021) 3589–3603, arXiv:2105.03468 [astro-ph.IM].
[1924] M.D. Hoffman, A. Gelman, The No-U-turn sampler: adaptively setting path lengths in Hamiltonian Monte Carlo, J. Mach. Learn. Res. 15 (47) (2014) 1593–1623, arXiv:1111.4246 [stat.CO], http://jmlr.org/papers/v15/hoffman14a.html.
[1925] J. Bradbury, R. Frostig, P. Hawkins, M.J. Johnson, C. Leary, D. Maclaurin, G. Necula, A. Paszke, J. VanderPlas, S. Wanderman-Milne, Q. Zhang, JAX: composable transformations of Python+NumPy programs, 2018, http://github.com/jax-ml/jax.
[1926] J.-E. Campagne, F. Lanusse, J. Zuntz, A. Boucaud, S. Casas, M. Karamanis, D. Kirkby, D. Lanzieri, Y. Li, A. Peel, JAX-COSMO: an end-to-end differentiable and GPU accelerated cosmology library, Open J. Astrophys. 6 (2023) 1–15, arXiv:2302.05163 [astro-ph.CO].
[1927] O. Hahn, F. List, N. Porqueres, DISCO-DJ I: a differentiable Einstein-Boltzmann solver for cosmology, J. Cosmol. Astropart. Phys. 06 (2024) 063, arXiv:2311.03291 [astro-ph.CO].
[1928] L. Balkenhol, C. Trendafilova, K. Benabed, S. Galli, candl: cosmic microwave background analysis with a differentiable likelihood, Astron. Astrophys. 686 (2024) A10, arXiv:2401.13433 [astro-ph.CO].
[1929] D. Piras, A. Spurio Mancini, CosmoPower-JAX: high-dimensional Bayesian inference with differentiable cosmological emulators, 2023, http://dx.doi.org/10.21105/astro.2305.06347, arXiv:2305.06347 [astro-ph.CO].
[1930] J. Ruiz-Zapatero, D. Alonso, C. García-García, A. Nicola, A. Mootoovaloo, J.M. Sullivan, M. Bonici, P.G. Ferreira, LimberJack.jl: auto-differentiable methods for angular power spectra analyses, 2023, http://dx.doi.org/10.21105/astro.2310.08306, arXiv:2310.08306 [astro-ph.CO].
[1931] M. Bonici, F. Bianchini, J. Ruiz-Zapatero, Capse.jl: efficient and auto-differentiable CMB power spectra emulation, 2023, http://dx.doi.org/10.21105/astro.2307.14339, arXiv:2307.14339 [astro-ph.CO].
[1932] M. Bonici, G. D'Amico, J. Bel, C. Carbone, Effort: a fast and differentiable emulator for the effective field theory of the large scale structure of the universe, 2025, arXiv:2501.04639 [astro-ph.CO].
[1933] E. Bingham, J.P. Chen, M. Jankowiak, F. Obermeyer, N. Pradhan, T. Karaletsos, R. Singh, P. Szerlip, P. Horsfall, N.D. Goodman, Pyro: deep universal probabilistic programming, 2018, http://dx.doi.org/10.48550/arXiv.1810.09538, arXiv e-prints, arXiv:1810.09538 [cs.LG].
[1934] D. Piras, A. Polanska, A. Spurio Mancini, M.A. Price, J.D. McEwen, The future of cosmological likelihood-based inference: accelerated high-dimensional parameter estimation and model comparison, Open J. Astrophys. 7 (2024) arXiv:2405.12965 [astro-ph.CO].
[1935] A. Mootoovaloo, J. Ruiz-Zapatero, C. García-García, D. Alonso, Assessment of gradient-based samplers in standard cosmological likelihoods, Mon. Not. R. Astron. Soc. 534 (3) (2024) 1668–1681, arXiv:2406.04725 [astro-ph.IM].

[1936] J. Skilling, Nested sampling for general Bayesian computation, Bayesian Anal. 1 (4) (2006) 833 – 859, https://doi.org/10.1214/06-BA127.

[1937] J. Buchner, UltraNest - a robust, general purpose Bayesian inference engine, J. Open Source Softw. 6 (60) (2021) 3001, https://doi.org/10.21105/joss.03001.

[1938] W.J. Handley, M.P. Hobson, A.N. Lasenby, PolyChord: nested sampling for cosmology, Mon. Not. R. Astron. Soc. 450 (1) (2015) L61–L65, arXiv:1502.01856 [astro-ph.CO].

[1939] J.S. Speagle, dynesty: a dynamic nested sampling package for estimating Bayesian posteriors and evidences, Mon. Not. R. Astron. Soc. 493 (3) (2020) 3132–3158, arXiv:1904.02180 [astro-ph.IM].

[1940] J.U. Lange, nautilus: boosting Bayesian importance nested sampling with deep learning, Mon. Not. R. Astron. Soc. 525 (2) (2023) 3181–3194, arXiv:2306.16923 [astro-ph.IM].

[1941] I. Gómez-Vargas, J.A. Vázquez, Deep learning and genetic algorithms for cosmological Bayesian inference speed-up, Phys. Rev. D 110 (8) (2024) 083518, arXiv:2405.03293 [astro-ph.IM].

[1942] M.J. Williams, J. Veitch, C. Messenger, Importance nested sampling with normalising flows, Mach. Learn. Sci. Tech. 4 (3) (2023) 035011, arXiv:2302.08526 [astro-ph.IM].

[1943] J. Buchner, Nested sampling methods, Stat. Surv. (2021) arXiv:2101.09675 [stat.CO].

[1944] E.O. Colgáin, S. Pourojaghi, M.M. Sheikh-Jabbari, D. Sherwin, A comparison of Bayesian and frequentist confidence intervals in the presence of a late Universe degeneracy, Eur. Phys. J. C 85 (2) (2025) 124, arXiv:2307.16349 [astro-ph.CO].

[1945] J. Albert, C. Balazs, A. Fowlie, W. Handley, N. Hunt-Smith, R.R. de Austri, M. White, A comparison of Bayesian sampling algorithms for high-dimensional particle physics and cosmology applications, 2024, arXiv:2409.18464 [hep-ph].

[1946] D. Staicova, Modern Bayesian sampling methods for cosmological inference: a comparative study, Universe 11 (2) (2025) 68, arXiv:2501.06022 [astro-ph.CO].

[1947] S. Raghvendra, P. Shirzadian, K. Zhang, A new robust partial p-wasserstein-based metric for comparing distributions, 2024, http://dx.doi.org/10.48550/arXiv.2405.03664, arXiv e-prints, arXiv:2405.03664 [cs.LG].

[1948] A. Lewis, A. Challinor, A. Lasenby, Efficient computation of CMB anisotropies in closed FRW models, Astrophys. J. 538 (2000) 473–476, arXiv:astro-ph/9911177.

[1949] D. Blas, J. Lesgourgues, T. Tram, The Cosmic Linear Anisotropy Solving System (CLASS) II: Approximation schemes, J. Cosmol. Astropart. Phys. 07 (2011) 034, arXiv:1104.2933 [astro-ph.CO].

[1950] B. Moser, C.S. Lorenz, U. Schmitt, A. Refregier, J. Fluri, R. Sgier, F. Tarsitano, L. Heisenberg, Symbolic implementation of extensions of the PyCosmo Boltzmann solver, Astron. Comput. 40 (2022) 100603, arXiv:2112.08395 [astro-ph.CO].

[1951] J. Zuntz, M. Paterno, E. Jennings, D. Rudd, A. Manzotti, S. Dodelson, S. Bridle, S. Sehrish, J. Kowalkowski, CosmoSIS: modular cosmological parameter estimation, Astron. Comput. 12 (2015) 45–59, arXiv:1409.3409 [astro-ph.CO].

[1952] A. Lewis, GetDist: a Python package for analysing Monte Carlo samples, 2019, arXiv:1910.13970 [astro-ph.IM].

[1953] L. Senatore, M. Zaldarriaga, The IR-resummed effective field theory of large scale structures, J. Cosmol. Astropart. Phys. 02 (2015) 013, arXiv:1404.5954 [astro-ph.CO].

[1954] L. Senatore, Bias in the effective field theory of large scale structures, J. Cosmol. Astropart. Phys. 11 (2015) 007, arXiv:1406.7843 [astro-ph.CO].

[1955] L. Senatore, M. Zaldarriaga, Redshift space distortions in the effective field theory of large scale structures, 2014, arXiv:1409.1225 [astro-ph.CO].

[1956] P. Carrilho, C. Moretti, A. Pourtsidou, Cosmology with the EFTofLSS and BOSS: dark energy constraints and a note on priors, J. Cosmol. Astropart. Phys. 01 (2023) 028, arXiv:2207.14784 [astro-ph.CO].

[1957] T. Simon, P. Zhang, V. Poulin, T.L. Smith, Consistency of effective field theory analyses of the BOSS power spectrum, Phys. Rev. D 107 (12) (2023) 123530, arXiv:2208.05929 [astro-ph.CO].

[1958] M. Maus, S.-F. Chen, M. White, A comparison of template vs. direct model fitting for redshift-space distortions in BOSS, J. Cosmol. Astropart. Phys. 06 (2023) 005, arXiv:2302.07430 [astro-ph.CO].

[1959] E.B. Holm, L. Herold, T. Simon, E.G.M. Ferreira, S. Hannestad, V. Poulin, T. Tram, Bayesian and frequentist investigation of prior effects in EFT of LSS analyses of full-shape BOSS and eBOSS data, Phys. Rev. D 108 (12) (2023) 123514, arXiv:2309.04468 [astro-ph.CO].

[1960] J. Donald-McCann, R. Gsponer, R. Zhao, K. Koyama, F. Beutler, Analysis of unified galaxy power spectrum multipole measurements, Mon. Not. R. Astron. Soc. 526 (3) (2023) 3461–3481, arXiv:2307.07475 [astro-ph.CO].

[1961] M.M. Ivanov, A. Obuljen, C. Cuesta-Lazaro, M.W. Toomey, Full-shape analysis with simulation-based priors: Cosmological parameters and the structure growth anomaly, Phys. Rev. D 111 (6) (2025) 063548, arXiv:2409.10609 [astro-ph.CO].

[1962] A. Chudaykin, M.M. Ivanov, T. Nishimichi, On priors and scale cuts in EFT-based full-shape analyses, 2024, arXiv:2410.16358 [astro-ph.CO].

[1963] H. Zhang, M. Bonici, G. D'Amico, S. Paradiso, W.J. Percival, HOD-informed prior for EFT-based full-shape analyses of LSS, J. Cosmol. Astropart. Phys. 04 (2025) 041, arXiv:2409.12937 [astro-ph.CO].

[1964] T.L. Smith, V. Poulin, Current small-scale CMB constraints to axionlike early dark energy, Phys. Rev. D 109 (10) (2024) 103506, arXiv:2309.03265 [astro-ph.CO].

[1965] R. Murgia, G.F. Abellán, V. Poulin, Early dark energy resolution to the Hubble tension in light of weak lensing surveys and lensing anomalies, Phys. Rev. D 103 (6) (2021) 063502, arXiv:2009.10733 [astro-ph.CO].

[1966] T.L. Smith, V. Poulin, J.L. Bernal, K.K. Boddy, M. Kamionkowski, R. Murgia, Early dark energy is not excluded by current large-scale structure data, Phys. Rev. D 103 (12) (2021) 123542, arXiv:2009.10740 [astro-ph.CO].

[1967] L. Herold, E.G.M. Ferreira, E. Komatsu, New constraint on early dark energy from planck and BOSS data using the profile likelihood, Astrophys. J. Lett. 929 (1) (2022) L16, arXiv:2112.12140 [astro-ph.CO].

[1968] L. Herold, E.G.M. Ferreira, Resolving the Hubble tension with early dark energy, Phys. Rev. D 108 (4) (2023) 043513, arXiv:2210.16296 [astro-ph.CO].

[1969] A. Reeves, L. Herold, S. Vagnozzi, B.D. Sherwin, E.G.M. Ferreira, Restoring cosmological concordance with early dark energy and massive neutrinos? Mon. Not. R. Astron. Soc. 520 (3) (2023) 3688–3695, arXiv:2207.01501 [astro-ph.CO].

[1970] G. Efstathiou, E. Rosenberg, V. Poulin, Improved planck constraints on axionlike early dark energy as a resolution of the hubble tension, Phys. Rev. Lett. 132 (22) (2024) 221002, arXiv:2311.00524 [astro-ph.CO].

[1971] F. Niedermann, M.S. Sloth, Resolving the Hubble tension with new early dark energy, Phys. Rev. D 102 (6) (2020) 063527, arXiv:2006.06686 [astro-ph.CO].

[1972] J.S. Cruz, S. Hannestad, E.B. Holm, F. Niedermann, M.S. Sloth, T. Tram, Profiling cold new early dark energy, Phys. Rev. D 108 (2) (2023) 023518, arXiv:2302.07934 [astro-ph.CO].

[1973] J. Hamann, S. Hannestad, G.G. Raffelt, Y.Y.Y. Wong, Observational bounds on the cosmic radiation density, J. Cosmol. Astropart. Phys. 08 (2007) 021, arXiv:0705.0440 [astro-ph].

[1974] J. Hamann, Evidence for extra radiation? Profile likelihood versus Bayesian posterior, J. Cosmol. Astropart. Phys. 03 (2012) 021, arXiv:1110.4271 [astro-ph.CO].

[1975] S. Henrot-Versillé, F. Couchot, X. Garrido, H. Imada, T. Louis, M. Tristram, S. Vanneste, Comparison of results on $N_{\rm eff}$ from various Planck likelihoods, Astron. Astrophys. 623 (2019) A9, arXiv:1807.05003 [astro-ph.CO].

[1976] A. Gómez-Valent, Fast test to assess the impact of marginalization in Monte Carlo analyses and its application to cosmology, Phys. Rev. D 106 (6) (2022) 063506, arXiv:2203.16285 [astro-ph.CO].

[1977] E.B. Holm, L. Herold, S. Hannestad, A. Nygaard, T. Tram, Decaying dark matter with profile likelihoods, Phys. Rev. D 107 (2) (2023) L021303, arXiv:2211.01935 [astro-ph.CO].

[1978] A.R. Liddle, Information criteria for astrophysical model selection, Mon. Not. R. Astron. Soc. 377 (2007) L74–L78, arXiv:astro-ph/0701113.

[1979] H. Jeffreys, The theory of probability, in: Oxford Classic Texts in the Physical Sciences, Oxford University Press, 1939.

[1980] D.J. Spiegelhalter, N.G. Best, B.P. Carlin, A. van der Linde, Bayesian measures of model complexity and fit, J. Roy. Stat. Soc. B 64 (4) (2002) 583–639.

[1981] R. Trotta, Bayes in the sky: Bayesian inference and model selection in cosmology, Contemp. Phys. 49 (2008) 71–104, arXiv:0803.4089 [astro-ph].

[1982] P. Marshall, N. Rajguru, A.z. Slosar, Bayesian evidence as a tool for comparing datasets, Phys. Rev. D 73 (6) (2006) 067302, arXiv:astro-ph/0412535 [astro-ph].

[1983] W. Handley, P. Lemos, Quantifying tensions in cosmological parameters: Interpreting the DES evidence ratio, Phys. Rev. D 100 (4) (2019) 043504, arXiv:1902.04029 [astro-ph.CO].

[1984] M. Raveri, W. Hu, Concordance and discordance in cosmology, Phys. Rev. D 99 (2019) 043506, https://link.aps.org/doi/10.1103/PhysRevD.99.043506.

[1985] M. Raveri, G. Zacharegkas, W. Hu, Quantifying concordance of correlated cosmological data sets, Phys. Rev. D 101 (2020) 103527, https://link.aps.org/doi/10.1103/PhysRevD.101.103527.

[1986] M. Raveri, C. Doux, Non-Gaussian estimates of tensions in cosmological parameters, Phys. Rev. D 104 (2021) 043504, https://link.aps.org/doi/10.1103/PhysRevD.104.043504.

[1987] M.a. Leizerovich, S.J. Landau, C.G. Scóccola, Tensions in cosmology: A discussion of statistical tools to determine inconsistencies, Phys. Lett. B 855 (2024) 138844, arXiv:2312.08542 [astro-ph.CO].

[1988] P. Lemos, M. Raveri, A. Campos, et al., DES Collaboration, Assessing tension metrics with dark energy survey and Planck data, Mon. Not. R. Astro. Soc. 505 (4) (2021) 6179–6194, arXiv:2012.09554 [astro-ph.CO].

[1989] M. Ho, M.M. Rau, M. Ntampaka, A. Farahi, H. Trac, B. Poczos, A robust and efficient deep learning method for dynamical mass measurements of galaxy clusters, Astrophys. J. 887 (2019) 25, arXiv:1902.05950 [astro-ph.CO].

[1990] A. Peel, F. Lalande, J.-L. Starck, V. Pettorino, J. Merten, C. Giocoli, M. Meneghetti, M. Baldi, Distinguishing standard and modified gravity cosmologies with machine learning, Phys. Rev. D 100 (2) (2019) 023508, arXiv:1810.11030 [astro-ph.CO].

[1991] J.a. Caldeira, W.L.K. Wu, B. Nord, C. Avestruz, S. Trivedi, K.T. Story, DeepCMB: lensing reconstruction of the cosmic microwave background with deep neural networks, Astron. Comput. 28 (2019) 100307, arXiv:1810.01483 [astro-ph.CO].

[1992] S. He, Y. Li, Y. Feng, S. Ho, S. Ravanbakhsh, W. Chen, B. Póczos, Learning to predict the cosmological structure formation, Proc. Nat. Acad. Sci. 116 (28) (2019) 13825–13832, arXiv:1811.06533 [astro-ph.CO].

[1993] S. Ravanbakhsh, F. Lanusse, R. Mandelbaum, J. Schneider, B. Poczos, Enabling dark energy science with deep generative models of galaxy images, 2016, arXiv:1609.05796 [astro-ph.IM].

[1994] C. Escamilla-Rivera, M.A.C. Quintero, S. Capozziello, A deep learning approach to cosmological dark energy models, J. Cosmol. Astropart. Phys. 03 (2020) 008, arXiv:1910.02788 [astro-ph.CO].

[1995] ANTARES Collaboration, G. Narayan, et al., Machine learning-based brokers for real-time classification of the LSST alert stream, Astrophys. J. Suppl. 236 (1) (2018) 9, arXiv:1801.07323 [astro-ph.IM].

[1996] F. Lanusse, Q. Ma, N. Li, T.E. Collett, C.-L. Li, S. Ravanbakhsh, R. Mandelbaum, B. Poczos, CMU DeepLens: deep learning for automatic image-based galaxy–galaxy strong lens finding, Mon. Not. R. Astron. Soc. 473 (3) (2018) 3895–3906, arXiv:1703.02642 [astro-ph.IM].

[1997] G. Carleo, I. Cirac, K. Cranmer, L. Daudet, M. Schuld, N. Tishby, L. Vogt-Maranto, L. Zdeborová, Machine learning and the physical sciences, Rev. Modern Phys. 91 (4) (2019) 045002, arXiv:1903.10563 [physics.comp-ph].

[1998] P. Mehta, M. Bukov, C.-H. Wang, A.G.R. Day, C. Richardson, C.K. Fisher, D.J. Schwab, A high-bias, low-variance introduction to Machine Learning for physicists, Phys. Rep. 810 (2019) 1–124, arXiv:1803.08823 [physics.comp-ph].

[1999] C. Aggarwal, Neural Networks and Deep Learning: A Textbook, Springer International Publishing, 2018, https://books.google.com.mt/books?id=achqDwAAQBAJ.

[2000] Y.-C. Wang, Y.-B. Xie, T.-J. Zhang, H.-C. Huang, T. Zhang, K. Liu, Likelihood-free cosmological constraints with artificial neural networks: an application on hubble parameters and SNe Ia, Astrophys. J. Supp. 254 (2) (2021) 43, arXiv:2005.10628 [astro-ph.CO].

[2001] I. Gómez-Vargas, R.M. Esquivel, R. García-Salcedo, J.A. Vázquez, Neural network reconstructions for the Hubble parameter, growth rate and distance modulus, Eur. Phys. J. C 83 (4) (2023) 304, arXiv:2104.00595.

[2002] G.-J. Wang, C. Cheng, Y.-Z. Ma, J.-Q. Xia, A. Abebe, A. Beesham, CoLFI: Cosmological likelihood-free inference with neural density estimators, Astrophys. J. Suppl. 268 (1) (2023) 7, arXiv:2306.11102.

[2003] A. Manrique-Yus, E. Sellentin, Euclid-era cosmology for everyone: neural net assisted MCMC sampling for the joint 3×2 likelihood, Mon. Not. R. Astron. Soc. 491 (2) (2020) 2655–2663, arXiv:1907.05881.

[2004] A. Spurio Mancini, D. Piras, J. Alsing, B. Joachimi, M.P. Hobson, CosmoPower: emulating cosmological power spectra for accelerated Bayesian inference from next-generation surveys, Mon. Not. R. Astron. Soc. 511 (2) (2022) 1771–1788, arXiv:2106.03846.

[2005] J. Albers, C. Fidler, J. Lesgourgues, N. Schöneberg, J. Torrado, CosmicNet. Part I. Physics-driven implementation of neural networks within Einstein-Boltzmann solvers, J. Cosmol. Astropart. Phys. 09 (2019) 028, arXiv:1907.05764.

[2006] S. Günther, J. Lesgourgues, G. Samaras, N. Schöneberg, F. Stadtmann, C. Fidler, J. Torrado, CosmicNet II: emulating extended cosmologies with efficient and accurate neural networks, J. Cosmol. Astropart. Phys. 11 (2022) 035, arXiv:2207.05707.

[2007] T. Auld, M. Bridges, M.P. Hobson, S.F. Gull, Fast cosmological parameter estimation using neural networks, Mon. Not. R. Astron. Soc. 376 (2007) L11–L15, arXiv:astro-ph/0608174.

[2008] D. Grandón, E. Sellentin, Bayesian error propagation for neural-net based parameter inference, Open J. Astrophys. (2022) arXiv:2205.11587.

[2009] G.-J. Wang, S.-Y. Li, J.-Q. Xia, ECoPANN: A framework for estimating cosmological parameters using artificial neural networks, Astrophys. J. Suppl. 249 (2) (2020) 25, arXiv:2005.07089.

[2010] J. Asorey, M. Crocce, E. Gaztanaga, A. Lewis, Recovering 3D clustering information with angular correlations, Mon. Not. R. Astron. Soc. 427 (2012) 1891, arXiv:1207.6487.

[2011] C.G. Sabiu, K. Kadota, J. Asorey, I. Park, Probing ultra-light axion dark matter from 21 cm tomography using Convolutional Neural Networks, J. Cosmol. Astropart. Phys. 01 (01) (2022) 020, arXiv:2108.07972.

[2012] M. Andrés-Carcasona, M. Martinez, L.M. Mir, Fast Bayesian gravitational wave parameter estimation using convolutional neural networks, Mon. Not. R. Astron. Soc. 527 (2) (2023) 2887–2894, arXiv:2309.04303.

[2013] E. Jones, T. Do, B. Boscoe, J. Singal, Y. Wan, Z. Nguyen, Improving photometric redshift estimation for cosmology with LSST using Bayesian neural networks, Astrophys. J. 964 (2) (2024) 130, arXiv:2306.13179.

[2014] H. Aihara, et al., Second data release of the hyper suprime-cam subaru strategic program, Publ. Astron. Soc. Jap. 71 (6) (2019) 114, arXiv:1905.12221.

[2015] M. Mancarella, J. Kennedy, B. Bose, L. Lombriser, Seeking new physics in cosmology with Bayesian neural networks: Dark energy and modified gravity, Phys. Rev. D 105 (2) (2022) 023531, arXiv:2012.03992.

[2016] L. Thummel, B. Bose, A. Pourtsidou, L. Lombriser, Classifying modified gravity and dark energy theories with Bayesian neural networks: massive neutrinos, baryonic feedback, and the theoretical error, Mon. Not. R. Astron. Soc. 535 (4) (2024) 3141–3161, arXiv:2403.16949.

[2017] G.R. Dvali, G. Gabadadze, M. Porrati, 4-D gravity on a brane in 5-D Minkowski space, Phys. Lett. B 485 (2000) 208–214, arXiv:hep-th/0005016.

[2018] R. Shah, S. Saha, P. Mukherjee, U. Garain, S. Pal, LADDER: Revisiting the cosmic distance ladder with deep learning approaches and exploring its applications, Astrophys. J. Suppl. 273 (2) (2024) 27, arXiv:2401.17029.

[2019] P. Mukherjee, J. Levi Said, J. Mifsud, Neural network reconstruction of H'(z) and its application in teleparallel gravity, J. Cosmol. Astropart. Phys. 12 (2022) 029, arXiv:2209.01113.

[2020] G.-J. Wang, X.-J. Ma, S.-Y. Li, J.-Q. Xia, Reconstructing functions and estimating parameters with artificial neural networks: A test with a hubble parameter and SNe Ia, Astrophys. J. Suppl. 246 (1) (2020) 13, arXiv:1910.03636.

[2021] C. Escamilla-Rivera, M. Carvajal, C. Zamora, M. Hendry, Neural networks and standard cosmography with newly calibrated high redshift GRB observations, J. Cosmol. Astropart. Phys. 04 (04) (2022) 016, arXiv:2109.00636.

[2022] J.d.R. Olvera, I. Gómez-Vargas, J.A. Vázquez, Observational cosmology with artificial neural networks, Universe 8 (2) (2022) 120, arXiv:2112.12645.

[2023] I. Gómez-Vargas, J.B. Andrade, J.A. Vázquez, Neural networks optimized by genetic algorithms in cosmology, Phys. Rev. D 107 (4) (2023) 043509, arXiv:2209.02685.

[2024] L. Giambagli, D. Fanelli, G. Risaliti, M. Signorini, Nonparametric analysis of the Hubble diagram with neural networks, Astron. Astrophys. 678 (2023) A13, arXiv:2302.12582.

[2025] K.F. Dialektopoulos, P. Mukherjee, J. Levi Said, J. Mifsud, Neural network reconstruction of cosmology using the Pantheon compilation, Eur. Phys. J. C 83 (10) (2023) 956, arXiv:2305.15499.

[2026] K.F. Dialektopoulos, P. Mukherjee, J. Levi Said, J. Mifsud, Neural network reconstruction of scalar-tensor cosmology, Phys. Dark Univ. 43 (2024) 101383, arXiv:2305.15500.

[2027] P. Mukherjee, K.F. Dialektopoulos, J. Levi Said, J. Mifsud, A possible late-time transition of M_B inferred via neural networks, J. Cosmol. Astropart. Phys. 09 (2024) 060, arXiv:2402.10502.

[2028] B. Zhang, H. Wang, X. Nong, G. Wang, P. Wu, N. Liang, Model-independent gamma-ray bursts constraints on cosmological models using machine learning, Astrophys. Space Sci. 370 (1) (2025) 10, arXiv:2312.09440.

[2029] J.-C. Zhang, Y. Hu, K. Jiao, H.-F. Wang, Y.-B. Xie, B. Yu, L.-L. Zhao, T.-J. Zhang, A nonparametric reconstruction of the Hubble parameter H(z) based on radial basis function neural networks, Astrophys. J. Suppl. 270 (2) (2024) 23, arXiv:2311.13938.

[2030] H. Xie, X. Nong, H. Wang, B. Zhang, Z. Li, N. Liang, Constraints on cosmological models with gamma-ray bursts in cosmology-independent way, Internat. J. Modern Phys. D 34 (02) (2025) 2450073, arXiv:2307.16467.

[2031] L. Tang, X. Li, H.-N. Lin, L. Liu, Model-independently calibrating the luminosity correlations of gamma-ray bursts using deep learning, Astrophys. J. 907 (2) (2021) 121, arXiv:2011.14040.

[2032] L. Liu, L.-J. Hu, L. Tang, Y. Wu, Constraining the spatial curvature of the local universe with deep learning, Res. Astron. Astrophys. 23 (12) (2023) 125012, arXiv:2309.11334.

[2033] Pan-STARRS1 Collaboration, D.M. Scolnic, et al., The complete light-curve sample of spectroscopically confirmed SNe ia from pan-STARRS1 and cosmological constraints from the combined pantheon sample, Astrophys. J. 859 (2) (2018) 101, arXiv:1710.00845.

[2034] R. Shah, P. Mukherjee, S. Saha, U. Garain, S. Pal, Deep learning based recalibration of SDSS and DESI BAO alleviates hubble and clustering tensions, 2024, arXiv:2412.14750.

[2035] G. Papamakarios, E. Nalisnick, D. Jimenez Rezende, S. Mohamed, B. Lakshminarayanan, Normalizing flows for probabilistic modeling and inference, 2019, http://dx.doi.org/10.48550/arXiv.1912.02762, arXiv E-Prints. arXiv:1912.02762.

[2036] J. Sohl-Dickstein, E.A. Weiss, N. Maheswaranathan, S. Ganguli, Deep unsupervised learning using nonequilibrium thermodynamics, 2015, http://dx.doi.org/10.48550/arXiv.1503.03585, arXiv E-Prints. arXiv:1503.03585.

[2037] J. Song, C. Meng, S. Ermon, Denoising diffusion implicit models, 2020, http://dx.doi.org/10.48550/arXiv.2010.02502, arXiv E-Prints. arXiv:2010.02502.

[2038] H.T.J. Bevins, W.J. Handley, P. Lemos, P.H. Sims, E.d. Acedo, A. Fialkov, J. Alsing, Marginal post-processing of Bayesian inference products with normalizing flows and kernel density estimators, Mon. Not. R. Astron. Soc. 526 (3) (2023) 4613–4626, arXiv:2205.12841.

[2039] R. Friedman, S. Hassan, HIGlow: Conditional normalizing flows for high-fidelity HI map modeling, 2022, arXiv:2211.12724.

[2040] A. Mootoovaloo, C. García-García, D. Alonso, J. Ruiz-Zapatero, emuflow: normalizing flows for joint cosmological analysis, Mon. Not. R. Astron. Soc. 536 (1) (2024) 190–202, arXiv:2409.01407.

[2041] M. Raveri, C. Doux, Non-Gaussian estimates of tensions in cosmological parameters, Phys. Rev. D 104 (4) (2021) 043504, arXiv:2105.03324.

[2042] B. Dai, U. Seljak, Translation and rotation equivariant normalizing flow (TRENF) for optimal cosmological analysis, Mon. Not. R. Astron. Soc. 516 (2) (2022) 2363–2373, arXiv:2202.05282.

[2043] B. Dai, U. Seljak, Multiscale flow for robust and optimal cosmological analysis, Proc. Nat. Acad. Sci. 121 (9) (2024) e2309624121, arXiv:2306.04689.
[2044] N. Mudur, C. Cuesta-Lazaro, D.P. Finkbeiner, Cosmological field emulation and parameter inference with diffusion models, in: 37th Conference on Neural Information Processing Systems, 2023, arXiv:2312.07534.
[2045] N. Mudur, C. Cuesta-Lazaro, D.P. Finkbeiner, Diffusion-HMC: Parameter inference with diffusion-model-driven Hamiltonian Monte Carlo, Astrophys. J. 978 (1) (2025) 64, arXiv:2405.05255.
[2046] R.C. Bernardo, D. Grandón, J. Said Levi, V.H. Cárdenas, Parametric and nonparametric methods hint dark energy evolution, Phys. Dark Univ. 36 (2022) 101017, arXiv:2111.08289.
[2047] M. Wang, X. Fu, B. Xu, Y. Yang, Z. Chen, Testing the FLRW metric with Hubble and transverse BAO measurements, Phys. Rev. D 108 (10) (2023) 103506, arXiv:2305.01268.
[2048] N. Rani, D. Jain, S. Mahajan, A. Mukherjee, N. Pires, Transition Redshift: New constraints from parametric and nonparametric methods, J. Cosmol. Astropart. Phys. 12 (2015) 045, arXiv:1503.08543.
[2049] H.K. Jassal, J.S. Bagla, T. Padmanabhan, WMAP constraints on low redshift evolution of dark energy, Mon. Not. R. Astron. Soc. 356 (2005) L11–L16, arXiv:astro-ph/0404378.
[2050] B. Wang, E. Abdalla, F. Atrio-Barandela, D. Pavon, Dark matter and dark energy interactions: Theoretical challenges, cosmological implications and observational signatures, Rep. Progr. Phys. 79 (9) (2016) 096901, arXiv:1603.08299.
[2051] L. Amendola, Coupled quintessence, Phys. Rev. D 62 (2000) 043511, arXiv:astro-ph/9908023.
[2052] V.H. Cárdenas, D. Grandón, S. Lepe, Dark energy and dark matter interaction in light of the second law of thermodynamics, Eur. Phys. J. C 79 (4) (2019) 357, arXiv:1812.03540.
[2053] D. Grandón, V.H. Cárdenas, Exploring evidence of interaction between dark energy and dark matter, Gen. Relativity Gravitation 51 (3) (2019) 42, arXiv:1804.03296.
[2054] C.-Y. Sun, R.-H. Yue, New interaction between dark energy and dark matter changes sign during cosmological evolution, Phys. Rev. D 85 (2012) 043010, arXiv:1009.1214.
[2055] Y. Wang, P.M. Garnavich, Measuring time dependence of dark energy density from type Ia supernova data, Astrophys. J. 552 (2001) 445, arXiv:astro-ph/0101040.
[2056] Y. Wang, G. Lovelace, Unbiased estimate of dark energy density from type IA supernova data, Astrophys. J. Lett. 562 (2001) L115–L120, arXiv:astro-ph/0109233.
[2057] V.H. Cardenas, Exploring hints for dark energy density evolution in light of recent data, Phys. Lett. B 750 (2015) 128–134, arXiv:1405.5116.
[2058] D. Grandon, V.H. Cardenas, Studies on dark energy evolution, Cl. Quant. Grav. 38 (14) (2021) 145008, arXiv:2107.04876.
[2059] E.V. Linder, Cosmic growth history and expansion history, Phys. Rev. D 72 (2005) 043529, arXiv:astro-ph/0507263.
[2060] N.-M. Nguyen, D. Huterer, Y. Wen, Evidence for suppression of structure growth in the concordance cosmological model, Phys. Rev. Lett. 131 (11) (2023) 111001, arXiv:2302.01331.
[2061] R. Caldwell, A. Cooray, A. Melchiorri, Constraints on a new post-general relativity cosmological parameter, Phys. Rev. D 76 (2007) 023507, arXiv:astro-ph/0703375.
[2062] L. Amendola, S. Fogli, A. Guarnizo, M. Kunz, A. Vollmer, Model-independent constraints on the cosmological anisotropic stress, Phys. Rev. D 89 (6) (2014) 063538, arXiv:1311.4765.
[2063] M. Ranjbar, S. Akhshabi, M. Shadmehri, Gravitational slip parameter and gravitational waves in Einstein–Cartan theory, Eur. Phys. J. C 84 (3) (2024) 316, arXiv:2401.02129.
[2064] R.R. Caldwell, A Phantom menace? Phys. Lett. B 545 (2002) 23–29, arXiv:astro-ph/9908168.
[2065] E. Elizalde, S. Nojiri, S.D. Odintsov, Late-time cosmology in (phantom) scalar-tensor theory: Dark energy and the cosmic speed-up, Phys. Rev. D 70 (2004) 043539, arXiv:hep-th/0405034.
[2066] Y.-F. Cai, E.N. Saridakis, M.R. Setare, J.-Q. Xia, Quintom Cosmology: Theoretical implications and observations, Phys. Rep. 493 (2010) 1–60, arXiv:0909.2776.
[2067] Z.-K. Guo, Y.-S. Piao, X.-M. Zhang, Y.-Z. Zhang, Cosmological evolution of a quintom model of dark energy, Phys. Lett. B 608 (2005) 177–182, arXiv:astro-ph/0410654.
[2068] J. Tot, B. Yildirim, A. Coley, G. Leon, The dynamics of scalar-field quintom cosmological models, Phys. Dark Univ. 39 (2023) 101155, arXiv:2204.06538.
[2069] J.A. Vázquez, D. Tamayo, G. Garcia-Arroyo, I. Gómez-Vargas, I. Quiros, A.A. Sen, Coupled multiscalar field dark energy, Phys. Rev. D 109 (2) (2024) 023511, arXiv:2305.11396.
[2070] C. Armendariz-Picon, V.F. Mukhanov, P.J. Steinhardt, Essentials of k essence, Phys. Rev. D 63 (2001) 103510, arXiv:astro-ph/0006373.
[2071] G.W. Horndeski, Second-order scalar-tensor field equations in a four-dimensional space, Internat. J. Theoret. Phys. 10 (1974) 363–384.
[2072] T. Clifton, P.G. Ferreira, A. Padilla, C. Skordis, Modified gravity and cosmology, Phys. Rep. 513 (2012) 1–189, arXiv:1106.2476.
[2073] J. Gleyzes, D. Langlois, F. Piazza, F. Vernizzi, Healthy theories beyond Horndeski, Phys. Rev. Lett. 114 (21) (2015) 211101, arXiv:1404.6495.
[2074] A.A. Starobinsky, A new type of isotropic cosmological models without singularity, in: I.M. Khalatnikov, V.P. Mineev (Eds.), Phys. Lett. B 91 (1980) 99–102.
[2075] M. Leizerovich, L. Kraiselburd, S.J. Landau, C.G. Scóccola, Testing f(R) gravity models with quasar x-ray and UV fluxes, Phys. Rev. D 105 (10) (2022) 103526, arXiv:2112.01492.
[2076] Y. Pan, Y. He, J. Qi, J. Li, S. Cao, T. Liu, J. Wang, Testing f(R) gravity with the simulated data of gravitational waves from the Einstein Telescope, Astrophys. J. 911 (2) (2021) 135, arXiv:2103.05212.
[2077] P. Bode, J.P. Ostriker, N. Turok, Halo formation in warm dark matter models, Astrophys. J. 556 (2001) 93–107, arXiv:astro-ph/0010389.
[2078] B. Liu, H. Shan, J. Zhang, New galaxy UV luminosity constraints on warm dark matter from JWST, Astrophys. J. 968 (2) (2024) 79, arXiv:2404.13596.
[2079] S. Lin, et al., Can we constrain warm dark matter masses with individual galaxies? Astrophys. J. 970 (2) (2024) 170, arXiv:2401.17940.
[2080] K.A. Oman, C.S. Frenk, R.A. Crain, M.R. Lovell, J. Pfeffer, A warm dark matter cosmogony may yield more low-mass galaxy detections in 21-cm surveys than a cold dark matter one, Mon. Not. R. Astron. Soc. 533 (1) (2024) 67–78, arXiv:2401.11878.
[2081] J.C. Rose, P. Torrey, F. Villaescusa-Navarro, M. Vogelsberger, S. O'Neil, M.V. Medvedev, R. Low, R. Adhikari, D. Angles-Alcazar, Inferring warm dark matter masses with deep learning, Mon. Not. R. Astron. Soc. 527 (1) (2023) 739–755, arXiv:2304.14432.
[2082] D.N. Spergel, P.J. Steinhardt, Observational evidence for selfinteracting cold dark matter, Phys. Rev. Lett. 84 (2000) 3760–3763, arXiv:astro-ph/9909386.
[2083] DES Collaboration, D. Cross, et al., Examining the self-interaction of dark matter through central cluster galaxy offsets, Mon. Not. R. Astron. Soc. 529 (1) (2024) 52–58, arXiv:2304.10128.
[2084] D. Yang, E.O. Nadler, H.-B. Yu, Testing the parametric model for self-interacting dark matter using matched halos in cosmological simulations, Phys. Dark Univ. 47 (2025) 101807, arXiv:2406.10753.
[2085] T. Bringmann, F. Kahlhoefer, K. Schmidt-Hoberg, P. Walia, Strong constraints on self-interacting dark matter with light mediators, Phys. Rev. Lett. 118 (14) (2017) 141802, arXiv:1612.00845.
[2086] M. Visser, Jerk and the cosmological equation of state, Cl. Quant. Grav. 21 (2004) 2603–2616, arXiv:gr-qc/0309109.
[2087] M. Visser, Cosmography: Cosmology without the Einstein equations, in: D.E. McClelland, S.M. Scott (Eds.), Gen. Relativity Gravitation 37 (2005) 1541–1548, arXiv:gr-qc/0411131.
[2088] C. Cattoen, M. Visser, Cosmographic hubble fits to the supernova data, Phys. Rev. D 78 (2008) 063501, arXiv:0809.0537.
[2089] P.K.S. Dunsby, O. Luongo, On the theory and applications of modern cosmography, Int. J. Geom. Meth. Mod. Phys. 13 (03) (2016) 1630002, arXiv:1511.06532.
[2090] S. Capozziello, R. D'Agostino, O. Luongo, Extended gravity cosmography, Internat. J. Modern Phys. D 28 (10) (2019) 1930016, arXiv:1904.01427.
[2091] D. Tamayo, J.A. Vazquez, Fourier-series expansion of the dark-energy equation of state, Mon. Not. R. Astron. Soc. 487 (1) (2019) 729–736, arXiv:1901.08679.
[2092] C. Deffayet, O. Pujolas, I. Sawicki, A. Vikman, Imperfect dark energy from kinetic gravity braiding, J. Cosmol. Astropart. Phys. 10 (2010) 026, arXiv:1008.0048.
[2093] C. Gruber, O. Luongo, Cosmographic analysis of the equation of state of the universe through Padé approximations, Phys. Rev. D 89 (10) (2014) 103506, arXiv:1309.3215.
[2094] A. Aviles, A. Bravetti, S. Capozziello, O. Luongo, Precision cosmology with Padé rational approximations: Theoretical predictions versus observational limits, Phys. Rev. D 90 (4) (2014) 043531, arXiv:1405.6935.
[2095] H. Wei, X.-P. Yan, Y.-N. Zhou, Cosmological applications of Padé approximant, J. Cosmol. Astropart. Phys. 01 (2014) 045, arXiv:1312.1117.
[2096] S. Capozziello, R. D'Agostino, Reconstructing the distortion function of non-local cosmology: A model-independent approach, Phys. Dark Univ. 42 (2023) 101346, arXiv:2310.03136.
[2097] S. Capozziello, R. D'Agostino, O. Luongo, Rational approximations of $f(R)$ cosmography through Padé polynomials, J. Cosmol. Astropart. Phys. 05 (2018) 008, arXiv:1709.08407.
[2098] A. Hojjati, L. Pogosian, G.-B. Zhao, Detecting features in the dark energy equation of state: A wavelet approach, J. Cosmol. Astropart. Phys. 04 (2010) 007, arXiv:0912.4843.
[2099] J. Wagner, S. Meyer, Generalised model-independent characterisation of strong gravitational lenses V: reconstructing the lensing distance ratio by supernovae for a general friedmann universe, Mon. Not. R. Astron. Soc. 490 (2) (2019) 1913–1927, arXiv:1812.04002.
[2100] C. Mignone, M. Bartelmann, Model-independent determination of the cosmic expansion rate. I. Application to type-Ia supernovae, Astron. Astrophys. 481 (2) (2008) 295–303, arXiv:0711.0370.
[2101] C.S. Lorenz, L. Funcke, M. Löffler, E. Calabrese, Reconstruction of the neutrino mass as a function of redshift, Phys. Rev. D 104 (12) (2021) 123518, arXiv:2102.13618.

[2102] D.K. Hazra, A. Shafieloo, G.F. Smoot, Reconstruction of broad features in the primordial spectrum and inflaton potential from Planck, J. Cosmol. Astropart. Phys. 12 (2013) 035, arXiv:1310.3038.

[2103] L.A. Escamilla, J.A. Vazquez, Model selection applied to reconstructions of the dark energy, Eur. Phys. J. C 83 (3) (2023) 251, arXiv:2111.10457.

[2104] Y. Wang, L. Pogosian, G.-B. Zhao, A. Zucca, Evolution of dark energy reconstructed from the latest observations, Astrophys. J. Lett. 869 (2018) L8, arXiv:1807.03772.

[2105] G.-B. Zhao, R.G. Crittenden, L. Pogosian, X. Zhang, Examining the evidence for dynamical dark energy, Phys. Rev. Lett. 109 (2012) 171301, arXiv:1207.3804.

[2106] G.-B. Zhao, et al., Dynamical dark energy in light of the latest observations, Nat. Astron. 1 (9) (2017) 627–632, arXiv:1701.08165.

[2107] R.-G. Cai, Q. Su, On the dark sector interactions, Phys. Rev. D— Part., Fields, Gravit., Cosmol. 81 (10) (2010) 103514.

[2108] A. Moss, E. Copeland, S. Bamford, T. Clarke, A model-independent reconstruction of dark energy to very high redshift, 2021, arXiv:2109.14848.

[2109] L. Amendola, M. Kunz, D. Sapone, Measuring the dark side (with weak lensing), J. Cosmol. Astropart. Phys. 04 (2008) 013, arXiv:0704.2421.

[2110] E. Bertschinger, P. Zukin, Distinguishing modified gravity from dark energy, Phys. Rev. D 78 (2008) 024015, arXiv:0801.2431.

[2111] L. Pogosian, A. Silvestri, K. Koyama, G.-B. Zhao, How to optimally parametrize deviations from general relativity in the evolution of cosmological perturbations, Phys. Rev. D 81 (10) (2010) 104023, arXiv:1002.2382.

[2112] M. Raveri, L. Pogosian, M. Martinelli, K. Koyama, A. Silvestri, G.-B. Zhao, Principal reconstructed modes of dark energy and gravity, J. Cosmol. Astropart. Phys. 02 (2023) 061, arXiv:2107.12990.

[2113] L. Pogosian, M. Raveri, K. Koyama, M. Martinelli, A. Silvestri, G.-B. Zhao, J. Li, S. Peirone, A. Zucca, Imprints of cosmological tensions in reconstructed gravity, Nat. Astron. 6 (12) (2022) 1484–1490, arXiv:2107.12992.

[2114] S. Hee, J.A. Vázquez, W.J. Handley, M.P. Hobson, A.N. Lasenby, Constraining the dark energy equation of state using Bayes theorem and the Kullback–Leibler divergence, Mon. Not. R. Astron. Soc. 466 (1) (2017) 369–377, arXiv:1607.00270.

[2115] Z.-K. Guo, D.J. Schwarz, Y.-Z. Zhang, Reconstruction of the primordial power spectrum from CMB data, J. Cosmol. Astropart. Phys. 08 (2011) 031, arXiv:1105.5916.

[2116] A. Ravenni, L. Verde, A.J. Cuesta, Red, straight, no bends: primordial power spectrum reconstruction from CMB and large-scale structure, J. Cosmol. Astropart. Phys. 08 (2016) 028, arXiv:1605.06637.

[2117] G. Aslanyan, L.C. Price, K.N. Abazajian, R. Easther, The knotted sky I: Planck constraints on the primordial power spectrum, J. Cosmol. Astropart. Phys. 08 (2014) 052, arXiv:1403.5849.

[2118] W.J. Handley, A.N. Lasenby, H.V. Peiris, M.P. Hobson, Bayesian inflationary reconstructions from Planck 2018 data, Phys. Rev. D 100 (10) (2019) 103511, arXiv:1908.00906.

[2119] J. Alberto Vazquez, M. Bridges, M.P. Hobson, A.N. Lasenby, Reconstruction of the dark energy equation of state, J. Cosmol. Astropart. Phys. 09 (2012) 020, arXiv:1205.0847.

[2120] I. Tutusaus, B. Lamine, A. Blanchard, Model-independent cosmic acceleration and redshift-dependent intrinsic luminosity in type-Ia supernovae, Astron. Astrophys. 625 (2019) A15, arXiv:1803.06197.

[2121] F. Gerardi, M. Martinelli, A. Silvestri, Reconstruction of the dark energy equation of state from latest data: the impact of theoretical priors, J. Cosmol. Astropart. Phys. 07 (2019) 042, arXiv:1902.09423.

[2122] A. Aviles, C. Gruber, O. Luongo, H. Quevedo, Cosmography and constraints on the equation of state of the Universe in various parametrizations, Phys. Rev. D 86 (2012) 123516, arXiv:1204.2007.

[2123] K. Bamba, S. Capozziello, S. Nojiri, S.D. Odintsov, Dark energy cosmology: the equivalent description via different theoretical models and cosmography tests, Astrophys. Space Sci. 342 (2012) 155–228, arXiv:1205.3421.

[2124] S. Capozziello, R. D'Agostino, O. Luongo, Model-independent reconstruction of $f(T)$ teleparallel cosmology, Gen. Relativity Gravitation 49 (11) (2017) 141, arXiv:1706.02962.

[2125] S. Capozziello, R. D'Agostino, O. Luongo, Thermodynamic parametrization of dark energy, Phys. Dark Univ. 36 (2022) 101045, arXiv:2202.03300.

[2126] C. Cattoen, M. Visser, The Hubble series: Convergence properties and redshift variables, Cl. Quant. Grav. 24 (2007) 5985–5998, arXiv:0710.1887.

[2127] S. Capozziello, R. D'Agostino, Model-independent reconstruction of f(Q) non-metric gravity, Phys. Lett. B 832 (2022) 137229, arXiv:2204.01015.

[2128] S. Capozziello, R. D'Agostino, A cosmographic outlook on dark energy and modified gravity, in: A. Antonelli, R. Fusco Femiano, A. Morselli, G.C. Trinchero (Eds.), Frascati Phys. Ser. 74 (2022) 193–208, arXiv:2211.17194.

[2129] R. D'Agostino, R.C. Nunes, Cosmographic view on the H0 and σ8 tensions, Phys. Rev. D 108 (2) (2023) 023523, arXiv:2307.13464.

[2130] S. Capozziello, R. D'Agostino, O. Luongo, Cosmographic analysis with Chebyshev polynomials, Mon. Not. R. Astron. Soc. 476 (3) (2018) 3924–3938, arXiv:1712.04380.

[2131] S. Capozziello, R. D'Agostino, O. Luongo, Cosmographic reconstruction to discriminate between modified gravity and dark energy, Acta Phys. Pol. Supp. 13 (2020) 271.

[2132] A. Gómez-Valent, Quantifying the evidence for the current speed-up of the universe with low and intermediate-redshift data. A more model-independent approach, J. Cosmol. Astropart. Phys. 05 (2019) 026, arXiv:1810.02278.

[2133] C.E. Rasmussen, C.K. Williams, et al., Gaussian Processes for Machine Learning, 1, Springer, 2006.

[2134] C.K. Williams, Gaussian Processes for Machine Learning, MIT Press, 2005.

[2135] M. Seikel, C. Clarkson, M. Smith, Reconstruction of dark energy and expansion dynamics using Gaussian processes, J. Cosmol. Astropart. Phys. 06 (2012) 036, arXiv:1204.2832.

[2136] W. Sun, K. Jiao, T.-J. Zhang, Influence of the bounds of the hyperparameters on the reconstruction of the hubble constant with the Gaussian process, Astrophys. J. 915 (2) (2021) 123, arXiv:2105.12618.

[2137] S. Dhawan, J. Alsing, S. Vagnozzi, Non-parametric spatial curvature inference using late-universe cosmological probes, Mon. Not. R. Astron. Soc. 506 (1) (2021) L1–L5, arXiv:2104.02485.

[2138] S.-g. Hwang, B. L'Huillier, R.E. Keeley, M.J. Jee, A. Shafieloo, How to use GP: effects of the mean function and hyperparameter selection on Gaussian process regression, J. Cosmol. Astropart. Phys. 02 (2023) 014, arXiv:2206.15081.

[2139] F. Avila, A. Bernui, A. Bonilla, R.C. Nunes, Inferring $S_8(z)$ and $\gamma(z)$ with cosmic growth rate measurements using machine learning, Eur. Phys. J. C 82 (7) (2022) 594, arXiv:2201.07829.

[2140] S. Joudaki, M. Kaplinghat, R. Keeley, D. Kirkby, Model independent inference of the expansion history and implications for the growth of structure, Phys. Rev. D 97 (12) (2018) 123501, arXiv:1710.04236.

[2141] R.E. Keeley, A. Shafieloo, B. L'Huillier, E.V. Linder, Debiasing cosmic gravitational wave sirens, Mon. Not. R. Astron. Soc. 491 (3) (2020) 3983–3989, arXiv:1905.10216.

[2142] R. Calderón, B. L'Huillier, D. Polarski, A. Shafieloo, A.A. Starobinsky, Joint reconstructions of growth and expansion histories from stage-IV surveys with minimal assumptions: Dark energy beyond Λ, Phys. Rev. D 106 (8) (2022) 083513, arXiv:2206.13820.

[2143] R. Calderón, B. L'Huillier, D. Polarski, A. Shafieloo, A.A. Starobinsky, Joint reconstructions of growth and expansion histories from stage-IV surveys with minimal assumptions. II. Modified gravity and massive neutrinos, Phys. Rev. D 108 (2) (2023) 023504, arXiv:2301.00640.

[2144] M. Reyes, C. Escamilla-Rivera, On the degeneracy between $f\sigma_8$ tension and its Gaussian process forecasting, Universe 8 (8) (2022) 394, arXiv:2203.03574.

[2145] M.A. Sabogal, Ö. Akarsu, A. Bonilla, E. Di Valentino, R.C. Nunes, Exploring new physics in the late Universe's expansion through non-parametric inference, Eur. Phys. J. C 84 (7) (2024) 703, arXiv:2407.04223.

[2146] M.-J. Zhang, H. Li, Gaussian processes reconstruction of dark energy from observational data, Eur. Phys. J. C 78 (6) (2018) 460, arXiv:1806.02981.

[2147] R. Briffa, S. Capozziello, J. Levi Said, J. Mifsud, E.N. Saridakis, Constraining teleparallel gravity through Gaussian processes, Cl. Quant. Grav. 38 (5) (2020) 055007, arXiv:2009.14582.

[2148] N. Banerjee, P. Mukherjee, D. Pavón, Spatial curvature and thermodynamics, Mon. Not. R. Astron. Soc. 521 (4) (2023) 5473–5482, arXiv:2301.09823.

[2149] N. Banerjee, P. Mukherjee, D. Pavón, Checking the second law at cosmic scales, J. Cosmol. Astropart. Phys. 11 (2023) 092, arXiv:2309.12298.

[2150] P. Mukherjee, N. Banerjee, Revisiting a non-parametric reconstruction of the deceleration parameter from combined background and the growth rate data, Phys. Dark Univ. 36 (2022) 100998, arXiv:2007.15941.

[2151] A. Shafieloo, A.G. Kim, E.V. Linder, Gaussian process cosmography, Phys. Rev. D 85 (12) (2012) 123530, arXiv:1204.2272.

[2152] M.-J. Zhang, J.-Q. Xia, Test of the cosmic evolution using Gaussian processes, J. Cosmol. Astropart. Phys. 12 (2016) 005, arXiv:1606.04398.

[2153] K. Liao, A. Shafieloo, R.E. Keeley, E.V. Linder, A model-independent determination of the Hubble constant from lensed quasars and supernovae using Gaussian process regression, Astrophys. J. Lett. 886 (1) (2019) L23, arXiv:1908.04967.

[2154] P. Mukherjee, A. Mukherjee, Assessment of the cosmic distance duality relation using Gaussian process, Mon. Not. R. Astron. Soc. 504 (3) (2021) 3938–3946, arXiv:2104.06066.

[2155] F. Renzi, N.B. Hogg, W. Giarè, The resilience of the Etherington–Hubble relation, Mon. Not. R. Astron. Soc. 513 (3) (2022) 4004–4014, arXiv:2112.05701.

[2156] P. Mukherjee, N. Banerjee, Non-parametric reconstruction of the cosmological *jerk* parameter, Eur. Phys. J. C 81 (1) (2021) 36, arXiv:2007.10124.

[2157] J.F. Jesus, R. Valentim, A.A. Escobal, S.H. Pereira, D. Benndorf, Gaussian processes reconstruction of the dark energy potential, J. Cosmol. Astropart. Phys. 11 (2022) 037, arXiv:2112.09722.

[2158] D. Wang, X.-H. Meng, Improved constraints on the dark energy equation of state using Gaussian processes, Phys. Rev. D 95 (2) (2017) 023508, arXiv:1708.07750.

[2159] T. Holsclaw, U. Alam, B. Sanso, H. Lee, K. Heitmann, S. Habib, D. Higdon, Nonparametric dark energy reconstruction from supernova data, Phys. Rev. Lett. 105 (2010) 241302, arXiv:1011.3079.

[2160] M. Aljaf, D. Gregoris, M. Khurshudyan, Constraints on interacting dark energy models through cosmic chronometers and Gaussian process, Eur. Phys. J. C 81 (6) (2021) 544, arXiv:2005.01891.

[2161] A. Bonilla, S. Kumar, R.C. Nunes, S. Pan, Reconstruction of the dark sectors' interaction: A model-independent inference and forecast from GW standard sirens, Mon. Not. R. Astron. Soc. 512 (3) (2022) 4231–4238, arXiv:2102.06149.

[2162] L.A. Escamilla, O. Akarsu, E. Di Valentino, J.A. Vazquez, Model-independent reconstruction of the interacting dark energy kernel: Binned and Gaussian process, J. Cosmol. Astropart. Phys. 11 (2023) 051, arXiv:2305.16290.

[2163] P. Mukherjee, N. Banerjee, Nonparametric reconstruction of interaction in the cosmic dark sector, Phys. Rev. D 103 (12) (2021) 123530, arXiv:2105.09995.

[2164] A.M. Pinho, S. Casas, L. Amendola, Model-independent reconstruction of the linear anisotropic stress η, J. Cosmol. Astropart. Phys. 11 (2018) 027, arXiv:1805.00027.

[2165] Y. Mu, E.-K. Li, L. Xu, Model-independent reconstruction of growth index via Gaussian process, Classical Quantum Gravity 40 (22) (2023) 225003.

[2166] J.A.S. Fortunato, P.H.R.S. Moraes, J.G.d.L. Júnior, E. Brito, Search for the f(R, T) gravity functional form via gaussian processes, Eur. Phys. J. C 84 (2) (2024) 198, arXiv:2305.01325.

[2167] A.K. Singha, A. Sardar, U. Debnath, F(Q) reconstruction: In the light of various modified gravity models, Phys. Dark Universe 41 (2023) 101240.

[2168] F. Oliveira, F. Avila, A. Bernui, A. Bonilla, R.C. Nunes, Reconstructing the growth index γ with Gaussian processes, Eur. Phys. J. C 84 (6) (2024) 636, arXiv:2311.14216.

[2169] G.N. Gadbail, S. Mandal, P.K. Sahoo, Gaussian process approach for model-independent reconstruction of f(Q) gravity with direct hubble measurements, Astrophys. J. 972 (2) (2024) 174, arXiv:2404.13095.

[2170] Y. Mu, E.-K. Li, L. Xu, Data-driven and almost model-independent reconstruction of modified gravity, J. Cosmol. Astropart. Phys. 06 (2023) 022, arXiv:2302.09777.

[2171] J. Sultana, M.K. Yennapureddy, F. Melia, D. Kazanas, Constraining f(R) models with cosmic chronometers and the H ii galaxy Hubble diagram, Mon. Not. R. Astron. Soc. 514 (4) (2022) 5827–5839, arXiv:2206.10761.

[2172] E. Elizalde, M. Khurshudyan, Swampland criteria for f(r) gravity derived with a Gaussian process, Eur. Phys. J. C 82 (9) (2022) 811.

[2173] D. Wang, Pantheon+ constraints on dark energy and modified gravity: An evidence of dynamical dark energy, Phys. Rev. D 106 (6) (2022) 063515, arXiv:2207.07164.

[2174] A. Sardar, U. Debnath, Reconstruction of extended f(P) cubic gravity from other modified gravity models, Phys. Dark Universe 35 (2022) 100926.

[2175] X. Ren, S.-F. Yan, Y. Zhao, Y.-F. Cai, E.N. Saridakis, Gaussian processes and effective field theory of $f(T)$ gravity under the H_0 tension, Astrophys. J. 932 (2022) 2, arXiv:2203.01926.

[2176] Y.-F. Cai, M. Khurshudyan, E.N. Saridakis, Model-independent reconstruction of $f(T)$ gravity from Gaussian processes, Astrophys. J. 888 (2020) 62, arXiv:1907.10813.

[2177] Y. Liu, S. Cao, T. Liu, X. Li, S. Geng, Y. Lian, W. Guo, Model-independent constraints on cosmic curvature: implication from updated Hubble diagram of high-redshift standard candles, Astrophys. J. 901 (2) (2020) 129, arXiv:2008.08378.

[2178] P. Mukherjee, N. Banerjee, Constraining the curvature density parameter in cosmology, Phys. Rev. D 105 (6) (2022) 063516, arXiv:2202.07886.

[2179] Y. Pan, J. Diao, J.-Z. Qi, J. Li, S. Cao, Q.-Q. Jiang, Testing the spatial geometry of the Universe with TianQin: Prospect of using supermassive black hole binaries, Astron. Astrophys. 683 (2024) A91, arXiv:2310.14723.

[2180] J.-Z. Qi, P. Meng, J.-F. Zhang, X. Zhang, Model-independent measurement of cosmic curvature with the latest H(z) and SNe Ia data: A comprehensive investigation, Phys. Rev. D 108 (6) (2023) 063522, arXiv:2302.08889.

[2181] Y.-J. Wang, J.-Z. Qi, B. Wang, J.-F. Zhang, J.-L. Cui, X. Zhang, Cosmological model-independent measurement of cosmic curvature using distance sum rule with the help of gravitational waves, Mon. Not. R. Astron. Soc. 516 (4) (2022) 5187–5195, arXiv:2201.12553.

[2182] P.-J. Wu, J.-Z. Qi, X. Zhang, Null test for cosmic curvature using Gaussian process*, Chin. Phys. C 47 (5) (2023) 055106, arXiv:2209.08502.

[2183] Y. Yang, Y. Gong, Measurement on the cosmic curvature using the Gaussian process method, Mon. Not. R. Astron. Soc. 504 (2) (2021) 3092–3097, arXiv:2007.05714.

[2184] G.-J. Wang, X.-J. Ma, J.-Q. Xia, Machine learning the cosmic curvature in a model-independent way, Mon. Not. R. Astron. Soc. 501 (4) (2021) 5714–5722, arXiv:2004.13913.

[2185] E. Belgacem, S. Foffa, M. Maggiore, T. Yang, Gaussian processes reconstruction of modified gravitational wave propagation, Phys. Rev. D 101 (6) (2020) 063505, arXiv:1911.11497.

[2186] X. Zheng, S. Cao, Y. Liu, M. Biesiada, T. Liu, S. Geng, Y. Lian, W. Guo, Model-independent constraints on cosmic curvature: implication from the future space gravitational-wave antenna DECIGO, Eur. Phys. J. C 81 (1) (2021) 14, arXiv:2012.14607.

[2187] R. Shah, A. Bhaumik, P. Mukherjee, S. Pal, A thorough investigation of the prospects of eLISA in addressing the Hubble tension: Fisher forecast, MCMC and machine learning, J. Cosmol. Astropart. Phys. 06 (2023) 038, arXiv:2301.12708.

[2188] G. Cañas-Herrera, J. Torrado, A. Achúcarro, Bayesian reconstruction of the inflaton's speed of sound using CMB data, Phys. Rev. D 103 (2021) 123531, arXiv:2012.04640.

[2189] B.R. Dinda, N. Banerjee, Model independent bounds on type Ia supernova absolute peak magnitude, Phys. Rev. D 107 (6) (2023) 063513, arXiv:2208.14740.

[2190] A. Favale, A. Gómez-Valent, M. Migliaccio, Quantification of 2D vs 3D BAO tension using SNIa as a redshift interpolator and test of the Etherington relation, Phys. Lett. B 858 (2024) 139027, arXiv:2405.12142.

[2191] G. Rodrigues, C. Bengaly, A model-independent test of speed of light variability with cosmological observations, J. Cosmol. Astropart. Phys. 07 (07) (2022) 029, arXiv:2112.01963.

[2192] P. Mukherjee, R. Shah, A. Bhaumik, S. Pal, Reconstructing the Hubble parameter with future gravitational-wave missions using machine learning, Astrophys. J. 960 (1) (2024) 61, arXiv:2303.05169.

[2193] J.-L. Li, Y.-P. Yang, S.-X. Yi, J.-P. Hu, F.-Y. Wang, Y.-K. Qu, Constraints on the cosmological parameters with three-parameter correlation of Gamma-ray bursts, Astrophys. J. 953 (1) (2023) 58, arXiv:2306.12840.

[2194] P. Mukherjee, A.A. Sen, Model-independent cosmological inference post DESI DR1 BAO measurements, Phys. Rev. D 110 (12) (2024) 123502, arXiv:2405.19178.

[2195] M. Khurshudyan, E. Elizalde, Constraints on prospective deviations from the cold dark matter model using a Gaussian process, Galaxies 12 (4) (2024) 31, arXiv:2402.08630.

[2196] R. von Marttens, J.E. Gonzalez, J. Alcaniz, V. Marra, L. Casarini, Model-independent reconstruction of dark sector interactions, Phys. Rev. D 104 (4) (2021) 043515, arXiv:2011.10846.

[2197] P. Mukherjee, Non-Parametric Reconstruction of Some Cosmological Parameters (Ph.D. thesis), IISER, Kolkata, 2022, arXiv:2207.07857.

[2198] P. Mukherjee, G. Rodrigues, C. Bengaly, Examining the validity of the minimal varying speed of light model through cosmological observations: Relaxing the null curvature constraint, Phys. Dark Univ. 43 (2024) 101380, arXiv:2302.00867.

[2199] K. Dialektopoulos, J.L. Said, J. Mifsud, J. Sultana, K.Z. Adami, Neural network reconstruction of late-time cosmology and null tests, J. Cosmol. Astropart. Phys. 02 (02) (2022) 023, arXiv:2111.11462.

[2200] M.K. Sharma, M. Sami, Reconciling early and late time tensions with reinforcement learning, J. Cosmol. Astropart. Phys. 05 (2025) 002, arXiv:2408.04204.

[2201] A. Mitra, I. Gómez-Vargas, V. Zarikas, Dark energy reconstruction analysis with artificial neural networks: Application on simulated Supernova Ia data from Rubin Observatory, Phys. Dark Univ. 46 (2024) 101706, arXiv:2402.18124.

[2202] T.-X. Mao, J. Wang, B. Li, Y.-C. Cai, B. Falck, M. Neyrinck, A. Szalay, Baryon acoustic oscillations reconstruction using convolutional neural networks, Mon. Not. R. Astron. Soc. 501 (1) (2021) 1499–1510, arXiv:2002.10218.

[2203] G. Garcia-Arroyo, I. Gómez-Vargas, J.A. Vázquez, Reconstructing rotation curves with artificial neural networks, 2024, arXiv:2404.05833.

[2204] A. Shafieloo, U. Alam, V. Sahni, A.A. Starobinsky, Smoothing Supernova data to reconstruct the expansion history of the universe and its age, Mon. Not. R. Astron. Soc. 366 (2006) 1081–1095, arXiv:astro-ph/0505329.

[2205] A. Shafieloo, Model independent reconstruction of the expansion history of the universe and the properties of dark energy, Mon. Not. R. Astron. Soc. 380 (2007) 1573–1580, arXiv:astro-ph/0703034.

[2206] A. Shafieloo, C. Clarkson, Model independent tests of the standard cosmological model, Phys. Rev. D 81 (2010) 083537, arXiv:0911.4858.

[2207] A. Shafieloo, B. L'Huillier, A.A. Starobinsky, Falsifying ΛCDM: Model-independent tests of the concordance model with eBOSS DR14Q and Pantheon, Phys. Rev. D 98 (8) (2018) 083526, arXiv:1804.04320.

[2208] A. Shafieloo, Crossing statistic: Reconstructing the expansion history of the universe, J. Cosmol. Astropart. Phys. 08 (2012) 002, arXiv:1204.1109.

[2209] H. Koo, A. Shafieloo, R.E. Keeley, B. L'Huillier, Model selection and parameter estimation using the iterative smoothing method, J. Cosmol. Astropart. Phys. 03 (2021) 034, arXiv:2009.12045.

[2210] B. L'Huillier, A. Shafieloo, Model-independent test of the FLRW metric, the flatness of the universe, and non-local measurement of $H_0 r_d$, J. Cosmol. Astropart. Phys. 01 (2017) 015, arXiv:1606.06832.

[2211] B. L'Huillier, A. Shafieloo, H. Kim, Model-independent cosmological constraints from growth and expansion, Mon. Not. R. Astron. Soc. 476 (3) (2018) 3263–3268, arXiv:1712.04865.

[2212] B. L'Huillier, A. Mitra, A. Shafieloo, R.E. Keeley, H. Koo, Litmus tests of the flat ΛCDM model and model-independent measurement of $H_0 r_d$ with LSST and DESI, 2024, arXiv:2407.07847.

[2213] A. Montiel, R. Lazkoz, I. Sendra, C. Escamilla-Rivera, V. Salzano, Nonparametric reconstruction of the cosmic expansion with local regression smoothing and simulation extrapolation, Phys. Rev. D 89 (4) (2014) 043007, arXiv:1401.4188.

[2214] L.M. Fernández-Hernández, A. Montiel, M.A. Rodríguez-Meza, Galaxy rotation curves using a non-parametric regression method: core, cuspy and fuzzy scalar field dark matter models, Mon. Not. R. Astron. Soc. 488 (4) (2019) 5127–5144, arXiv:1809.06875.

[2215] C. Escamilla-Rivera, J. Levi Said, J. Mifsud, Performance of non-parametric reconstruction techniques in the late-time universe, J. Cosmol. Astropart. Phys. 10 (2021) 016, arXiv:2105.14332.

[2216] A. Rana, D. Jain, S. Mahajan, A. Mukherjee, Revisiting the distance duality relation using a non-parametric regression method, J. Cosmol. Astropart. Phys. 07 (2016) 026, arXiv:1511.09223.

[2217] C. Escamilla-Rivera, J.C. Fabris, Nonparametric reconstruction of the O_m diagnostic to test ΛCDM, Galaxies 4 (4) (2016) 76, arXiv:1511.07066.

[2218] G. Rudolph, Convergence analysis of canonical genetic algorithms, IEEE Trans. Neural Netw. 5 (1) (1994) 96–101.

[2219] Y. Akrami, P. Scott, J. Edsjo, J. Conrad, L. Bergstrom, A profile likelihood analysis of the constrained MSSM with genetic algorithms, JHEP 04 (2010) 057, arXiv:0910.3950.

[2220] J. Crowder, N.J. Cornish, L. Reddinger, Darwin meets Einstein: LISA data analysis using genetic algorithms, Phys. Rev. D 73 (2006) 063011, arXiv:gr-qc/0601036.

[2221] C. Bogdanos, S. Nesseris, Genetic algorithms and supernovae type Ia analysis, J. Cosmol. Astropart. Phys. 05 (2009) 006, arXiv:0903.2805.

[2222] S. Nesseris, A. Shafieloo, A model independent null test on the cosmological constant, Mon. Not. R. Astron. Soc. 408 (2010) 1879–1885, arXiv:1004.0960.

[2223] S. Nesseris, J. Garcia-Bellido, A new perspective on dark energy modeling via genetic algorithms, J. Cosmol. Astropart. Phys. 11 (2012) 033, arXiv:1205.0364.

[2224] R. Medel-Esquivel, I. Gómez-Vargas, A.A.M. Sánchez, R. García-Salcedo, J. Alberto Vázquez, Cosmological parameter estimation with genetic algorithms, Universe 10 (1) (2024) 11, arXiv:2311.05699.

[2225] A.F. Gad, Pygad: An intuitive genetic algorithm python library, Multimedia Tools Appl. (2023) 1–14.

[2226] R.C. Bernardo, J. Levi Said, Towards a model-independent reconstruction approach for late-time Hubble data, J. Cosmol. Astropart. Phys. 08 (2021) 027, arXiv:2106.08688.

[2227] M.B. Bainbridge, J.K. Webb, Artificial intelligence applied to the automatic analysis of absorption spectra. Objective measurement of the fine structure constant, Mon. Not. R. Astron. Soc. 468 (2) (2017) 1639–1670, arXiv:1606.07393.

[2228] M.B. Bainbridge, J.K. Webb, Evaluating the new automatic method for the analysis of absorption spectra using synthetic spectra, Universe 3 (2) (2017) 34, arXiv:1704.08710.

[2229] C.-C. Lee, J.K. Webb, R.F. Carswell, D. Milaković, Artificial intelligence and quasar absorption system modelling; application to fundamental constants at high redshift, Mon. Not. R. Astron. Soc. 504 (2) (2021) 1787–1800, arXiv:2008.02583.

[2230] J.K. Webb, C.-C. Lee, R.F. Carswell, D. Milaković, Getting the model right: an information criterion for spectroscopy, Mon. Not. R. Astron. Soc. 501 (2) (2021) 2268–2278, arXiv:2009.08336.

[2231] C. Escamilla-Rivera, Bayesian deep learning for dark energy, 2020, http://dx.doi.org/10.5772/intechopen.91466, arXiv:2005.06412.

[2232] C. Escamilla-Rivera, Deep learning for cosmology, in: B. Escalante, F. Carminati, G. Barnafoldi, G. Paic, L. Nellen, R. Mayo, S. Schramm, Z. Ivezic (Eds.), PoS AISIS2019 (2020) 021.

[2233] C.Z. Munõz, C. Escamilla-Rivera, Inverse Cosmography: testing the effectiveness of cosmographic polynomials using machine learning, J. Cosmol. Astropart. Phys. 12 (2020) 007, arXiv:2005.02807.

[2234] M. Gendreau, J.-Y. Potvin (Eds.), A modern introduction to memetic algorithms, in: Handbook of Metaheuristics, Springer US, Boston, MA, 2010, pp. 141–183, http://dx.doi.org/10.1007/978-1-4419-1665-5_6.

[2235] O.H.M. Ross, A review of quantum-inspired metaheuristics: Going from classical computers to real quantum computers, IEEE Access 8 (2020) 814–838.

[2236] G. Acampora, R. Schiattarella, A. Vitiello, Using quantum amplitude amplification in genetic algorithms, Expert Syst. Appl. 209 (2022) 118203.

[2237] G. Acampora, A. Vitiello, Implementing evolutionary optimization on actual quantum processors, Info. Sci. 575 (2021) 542–562.

[2238] R. Ibarrondo, G. Gatti, M. Sanz, Quantum vs classical genetic algorithms: A numerical comparison shows faster convergence, in: 2022 IEEE Symposium Series on Computational Intelligence, 2022, arXiv:2207.09251.

[2239] R. Ibarrondo, G. Gatti, M. Sanz, Quantum genetic algorithm with individuals in multiple registers, IEEE Trans. Evol. Comput. 28 (2024) 788–797, arXiv:2203.15039.

[2240] G. Sarracino, et al., A quantum genetic algorithm for cosmological functions, 2024, (in preparation).

[2241] J. Prasad, T. Souradeep, Cosmological parameter estimation using particle swarm optimization (PSO), Phys. Rev. D 85 (12) (2012) 123008, arXiv:1108.5600;
Erratum:, Phys. Rev. D 90 (2014) 109903.

[2242] A.N. Ruiz, et al., Calibration of semi-analytic models of galaxy formation using particle swarm optimization, Astrophys. J. 801 (2) (2015) 139, arXiv:1310.7034.

[2243] C. Skokos, K.E. Parsopoulos, P.A. Patsis, M.N. Vrahatis, Particle swarm optimization: An efficient method for tracing periodic orbits in 3-D Galactic potentials, Mon. Not. R. Astron. Soc. 359 (2005) 251–260, arXiv:astro-ph/0502164.

[2244] DarkMachines High Dimensional Sampling Group Collaboration, C. Balázs, et al., A comparison of optimisation algorithms for high-dimensional particle and astrophysics applications, JHEP 05 (2021) 108, arXiv:2101.04525.

[2245] T. Toni, D. Welch, N. Strelkowa, A. Ipsen, M.P.H. Stumpf, Approximate Bayesian computation scheme for parameter inference and model selection in dynamical systems, J. R. Soc. Interface 6 (31) (2010) 187–202, arXiv:0901.1925. URL https://royalsocietypublishing.org/doi/abs/10.1098/rsif.2008.0172.

[2246] T. Toni, M.P.H. Stumpf, Simulation-based model selection for dynamical systems in systems and population biology, Bioinformatics 26 (1) (2009) 104–110, arXiv:0911.1705. http://dx.doi.org/10.1093/bioinformatics/btp619.

[2247] T. Toni, M.P.H. Stumpf, Tutorial on ABC rejection and ABC SMC for parameter estimation and model selection, 2009, http://dx.doi.org/10.48550/arXiv.0910.4472, arXiv E-Prints. arXiv:0910.4472.

[2248] R.C. Bernardo, D. Grandón, J. Levi Said, V.H. Cárdenas, Dark energy by natural evolution: Constraining dark energy using approximate Bayesian computation, Phys. Dark Univ. 40 (2023) 101213, arXiv:2211.05482.

[2249] R.C. Bernardo, Y.-R. Lee, Hubble constant by natural selection: Evolution chips in the Hubble tension, Astron. Comput. 44 (2023) 100740, arXiv:2212.02203.

[2250] K.M. Sallam, S.M. Elsayed, R.K. Chakrabortty, M.J. Ryan, Improved multi-operator differential evolution algorithm for solving unconstrained problems, in: 2020 IEEE Congress on Evolutionary Computation, CEC, 2020, pp. 1–8.

[2251] E.A.T. Enriquez, R.G. Mendoza, A.C.T. Velasco, Philippine eagle optimization algorithm, 2021, arXiv E-Prints. arXiv:2112.10318.

[2252] R.C. Bernardo, R. Mendoza, E.A. Enriquez, A.C. Velasco, R. Reyes, Metaheuristic cosmological parameter estimation: The Philippine Eagle hunts down cosmic expansion, 2025, (in preparation).

[2253] K.Y. Kim, H.W. Lee, Investigating the suitability of data-driven methods for extracting physical parameters in cosmological models, Astron. Comput. 45 (2023) 100762.

[2254] K. Lodha, L. Pinol, S. Nesseris, A. Shafieloo, W. Sohn, M. Fasiello, Searching for local features in primordial power spectrum using genetic algorithms, Mon. Not. R. Astron. Soc. 530 (2) (2024) 1424–1435, arXiv:2308.04940.

[2255] A. Antony, F. Finelli, D.K. Hazra, A. Shafieloo, Discordances in cosmology and the violation of slow-roll inflationary dynamics, Phys. Rev. Lett. 130 (11) (2023) 111001, arXiv:2202.14028.

[2256] D.K. Hazra, A. Antony, A. Shafieloo, One spectrum to cure them all: signature from early Universe solves major anomalies and tensions in cosmology, J. Cosmol. Astropart. Phys. 08 (08) (2022) 063, arXiv:2201.12000.

[2257] G. Alestas, L. Kazantzidis, S. Nesseris, Machine learning constraints on deviations from general relativity from the large scale structure of the Universe, Phys. Rev. D 106 (10) (2022) 103519, arXiv:2209.12799.

[2258] EUCLID Collaboration, M. Martinelli, et al., Euclid: Forecast constraints on the cosmic distance duality relation with complementary external probes, Astron. Astrophys. 644 (2020) A80, arXiv:2007.16153.

[2259] Euclid Collaboration, M. Martinelli, et al., Euclid: Constraining dark energy coupled to electromagnetism using astrophysical and laboratory data, Astron. Astrophys. 654 (2021) A148, arXiv:2105.09746.

[2260] Euclid Collaboration, S. Nesseris, et al., Euclid: Forecast constraints on consistency tests of the ΛCDM model, Astron. Astrophys. 660 (2022) A67, arXiv:2110.11421.

[2261] M. Moresco, R. Jimenez, L. Verde, A. Cimatti, L. Pozzetti, Setting the stage for cosmic chronometers. II. Impact of stellar population synthesis models systematics and full covariance matrix, Astrophys. J. 898 (1) (2020) 82, arXiv:2003.07362.

[2262] D. Brout, et al., The pantheon+ analysis: SuperCal-fragilistic cross calibration, retrained SALT2 light-curve model, and calibration systematic uncertainty, Astrophys. J. 938 (2) (2022) 111, arXiv:2112.03864.

[2263] R.C. Bernardo, Y. Chen, Demystifying genetic algorithm for cosmological parameter estimation and such, 2024, (in preparation).

[2264] A.B. Abdessalem, N. Dervilis, D.J. Wagg, K. Worden, Automatic kernel selection for Gaussian processes regression with approximate Bayesian computation and sequential Monte Carlo, Front. Built Environ. 3 (2017) 52.

[2265] H. Zhang, Y.-C. Wang, T.-J. Zhang, T.-t. Zhang, Kernel selection for Gaussian process in cosmology: With approximate Bayesian computation rejection and nested sampling, Astrophys. J. Suppl. 266 (2) (2023) 27, arXiv:2304.03911.

[2266] V.K. Oikonomou, G. Kafanelis, Primordial cosmology of an emergent-like universe from modified gravity: Reconstruction and phenomenology optimization with a genetic algorithm, Internat. J. Modern Phys. D 33 (1) (2024) 2350114, arXiv:2312.16324.

[2267] A. Aizpuru, R. Arjona, S. Nesseris, Machine learning improved fits of the sound horizon at the baryon drag epoch, Phys. Rev. D 104 (4) (2021) 043521, arXiv:2106.00428.

[2268] R. Arjona, A. Melchiorri, S. Nesseris, Testing the ΛCDM paradigm with growth rate data and machine learning, J. Cosmol. Astropart. Phys. 05 (05) (2022) 047, arXiv:2107.04343.

[2269] M.R. Gangopadhyay, M. Sami, M.K. Sharma, Phantom dark energy as a natural selection of evolutionary processes aˆ la genetic algorithm and cosmological tensions, Phys. Rev. D 108 (10) (2023) 103526, arXiv:2303.07301.

[2270] L. Kazantzidis, L. Perivolaropoulos, Evolution of the $f\sigma_8$ tension with the Planck15/ΛCDM determination and implications for modified gravity theories, Phys. Rev. D 97 (10) (2018) 103503, arXiv:1803.01337.

[2271] V. Springel, N. Yoshida, S.D.M. White, GADGET: A code for collisionless and gasdynamical cosmological simulations, New Astron. 6 (2001) 79, arXiv:astro-ph/0003162.

[2272] V. Springel, The cosmological simulation code GADGET-2, Mon. Not. R. Astron. Soc. 364 (2005) 1105–1134, arXiv:astro-ph/0505010.

[2273] V. Springel, R. Pakmor, O. Zier, M. Reinecke, Simulating cosmic structure formation with the gadget-4 code, Mon. Not. R. Astron. Soc. 506 (2) (2021) 2871–2949, arXiv:2010.03567.

[2274] V. Springel, E pur si muove: Galilean-invariant cosmological hydrodynamical simulations on a moving mesh, Mon. Not. R. Astron. Soc. 401 (2010) 791, arXiv:0901.4107.

[2275] P.F. Hopkins, A new class of accurate, mesh-free hydrodynamic simulation methods, Mon. Not. R. Astron. Soc. 450 (1) (2015) 53–110, arXiv:1409.7395.

[2276] SWIFT Collaboration, M. Schaller, et al., Swift: a modern highly parallel gravity and smoothed particle hydrodynamics solver for astrophysical and cosmological applications, Mon. Not. R. Astron. Soc. 530 (2) (2024) 2378–2419, arXiv:2305.13380.

[2277] R. Teyssier, Cosmological hydrodynamics with adaptive mesh refinement: a new high resolution code called RAMSES, Astron. Astrophys. 385 (2002) 337–364, arXiv:astro-ph/0111367.

[2278] V. Springel, et al., Simulating the joint evolution of quasars, galaxies and their large-scale distribution, Nature 435 (2005) 629–636, arXiv:astro-ph/0504097.

[2279] J. Kim, C. Park, R. Gott III, J. Dubinski, The horizon run N-body simulation: Baryon acoustic oscillations and topology of large scale structure of the universe, Astrophys. J. 701 (2009) 1547–1559, arXiv:0812.1392.

[2280] M. Vogelsberger, S. Genel, V. Springel, P. Torrey, D. Sijacki, D. Xu, G.F. Snyder, D. Nelson, L. Hernquist, Introducing the illustris project: Simulating the coevolution of dark and visible matter in the universe, Mon. Not. R. Astron. Soc. 444 (2) (2014) 1518–1547, arXiv:1405.2921.

[2281] V. Springel, et al., First results from the IllustrisTNG simulations: matter and galaxy clustering, Mon. Not. R. Astron. Soc. 475 (1) (2018) 676–698, arXiv:1707.03397.

[2282] A. Klypin, S. Trujillo-Gomez, J. Primack, Halos and galaxies in the standard cosmological model: results from the bolshoi simulation, Astrophys. J. 740 (2011) 102, arXiv:1002.3660.

[2283] J. Schaye, et al., The EAGLE project: Simulating the evolution and assembly of galaxies and their environments, Mon. Not. R. Astron. Soc. 446 (2015) 521–554, arXiv:1407.7040.

[2284] R.A. Crain, et al., The EAGLE simulations of galaxy formation: calibration of subgrid physics and model variations, Mon. Not. R. Astron. Soc. 450 (2) (2015) 1937–1961, arXiv:1501.01311.

[2285] F. Villaescusa-Navarro, et al., The quijote simulations, Astrophys. J. Suppl. 250 (1) (2020) 2, arXiv:1909.05273.

[2286] G. Kauffmann, J.M. Colberg, A. Diaferio, S.D.M. White, Clustering of galaxies in a hierarchical universe: 1. Methods and results at z=0, Mon. Not. R. Astron. Soc. 303 (1999) 188–206, arXiv:astro-ph/9805283.

[2287] A. Mead, J. Peacock, C. Heymans, S. Joudaki, A. Heavens, An accurate halo model for fitting non-linear cosmological power spectra and baryonic feedback models, Mon. Not. R. Astron. Soc. 454 (2) (2015) 1958–1975, arXiv:1505.07833.

[2288] H.J. Hortua, Constraining cosmological parameters from N-body simulations with Bayesian neural networks, in: 35th Conference on Neural Information Processing Systems, 2021, arXiv:2112.11865.

[2289] A. Lazanu, Extracting cosmological parameters from N-body simulations using machine learning techniques, J. Cosmol. Astropart. Phys. 09 (2021) 039, arXiv:2106.11061.

[2290] C. Zhang, L. Zu, H.-Z. Chen, Y.-L.S. Tsai, Y.-Z. Fan, Weak lensing constraints on dark matter-baryon interactions with N-body simulations and machine learning, J. Cosmol. Astropart. Phys. 08 (2024) 003, arXiv:2402.18880.

[2291] M.R. Lovell, C.S. Frenk, V.R. Eke, A. Jenkins, L. Gao, T. Theuns, The properties of warm dark matter haloes, Mon. Not. R. Astron. Soc. 439 (2014) 300–317, arXiv:1308.1399.

[2292] S. Bose, W.A. Hellwing, C.S. Frenk, A. Jenkins, M.R. Lovell, J.C. Helly, B. Li, The copernicus complexio: Statistical properties of warm dark matter haloes, Mon. Not. R. Astron. Soc. 455 (1) (2016) 318–333, arXiv:1507.01998.

[2293] Y. Shtanov, V.I. Zhdanov, Discreteness effects in N-body simulations of warm dark matter, Phys. Rev. D 109 (6) (2024) 063031, arXiv:2307.07778.

[2294] F. Villaescusa-Navarro, F. Marulli, M. Viel, E. Branchini, E. Castorina, E. Sefusatti, S. Saito, Cosmology with massive neutrinos I: towards a realistic modeling of the relation between matter, haloes and galaxies, J. Cosmol. Astropart. Phys. 03 (2014) 011, arXiv:1311.0866.

[2295] J. Adamek, R. Durrer, M. Kunz, Relativistic N-body simulations with massive neutrinos, J. Cosmol. Astropart. Phys. 11 (2017) 004, arXiv:1707.06938.

[2296] J. Liu, S. Bird, J.M.Z. Matilla, J.C. Hill, Z. Haiman, M.S. Madhavacheril, A. Petri, D.N. Spergel, MassiveNuS: Cosmological massive neutrino simulations, J. Cosmol. Astropart. Phys. 03 (2018) 049, arXiv:1711.10524.

[2297] B. Li, G.-B. Zhao, R. Teyssier, K. Koyama, ECOSMOG: An efficient code for simulating modified gravity, J. Cosmol. Astropart. Phys. 01 (2012) 051, arXiv:1110.1379.

[2298] E. Puchwein, M. Baldi, V. Springel, Modified gravity-GADGET: A new code for cosmological hydrodynamical simulations of modified gravity models, Mon. Not. R. Astron. Soc. 436 (2013) 348, arXiv:1305.2418.

[2299] J. Zhang, R. An, S. Liao, W. Luo, Z. Li, B. Wang, Fully self-consistent cosmological simulation pipeline for interacting dark energy models, Phys. Rev. D 98 (10) (2018) 103530, arXiv:1811.01519.

[2300] C. Arnold, M. Leo, B. Li, Realistic simulations of galaxy formation in $f(R)$ modified gravity, Nat. Astron. 3 (10) (2019) 945–954, arXiv:1907.02977.

[2301] B.S. Wright, H.A. Winther, K. Koyama, COLA with massive neutrinos, J. Cosmol. Astropart. Phys. 10 (2017) 054, arXiv:1705.08165.

[2302] M. Baldi, F. Villaescusa-Navarro, Quijote simulations: Modified gravity, 2025, https://quijote-simulations.readthedocs.io/en/latest/mg.html. (Accessed 30 January 2025).

[2303] X.-l. Chen, S. Hannestad, R.J. Scherrer, Cosmic microwave background and large scale structure limits on the interaction between dark matter and baryons, Phys. Rev. D 65 (2002) 123515, arXiv:astro-ph/0202496.

[2304] D.V. Nguyen, D. Sarnaaik, K.K. Boddy, E.O. Nadler, V. Gluscevic, Observational constraints on dark matter scattering with electrons, Phys. Rev. D 104 (10) (2021) 103521, arXiv:2107.12380.

[2305] P. Serra, F. Zalamea, A. Cooray, G. Mangano, A. Melchiorri, Constraints on neutrino – dark matter interactions from cosmic microwave background and large scale structure data, Phys. Rev. D 81 (2010) 043507, arXiv:0911.4411.

[2306] G. Mangano, A. Melchiorri, P. Serra, A. Cooray, M. Kamionkowski, Cosmological bounds on dark matter-neutrino interactions, Phys. Rev. D 74 (2006) 043517, arXiv:astro-ph/0606190.

[2307] R.J. Wilkinson, C. Boehm, J. Lesgourgues, Constraining dark matter-neutrino interactions using the CMB and large-scale structure, J. Cosmol. Astropart. Phys. 05 (2014) 011, arXiv:1401.7597.

[2308] F.-Y. Cyr-Racine, K. Sigurdson, J. Zavala, T. Bringmann, M. Vogelsberger, C. Pfrommer, ETHOS—an effective theory of structure formation: From dark particle physics to the matter distribution of the Universe, Phys. Rev. D 93 (12) (2016) 123527, arXiv:1512.05344.

[2309] M. Vogelsberger, J. Zavala, F.-Y. Cyr-Racine, C. Pfrommer, T. Bringmann, K. Sigurdson, ETHOS – an effective theory of structure formation: dark matter physics as a possible explanation of the small-scale CDM problems, Mon. Not. R. Astron. Soc. 460 (2) (2016) 1399–1416, arXiv:1512.05349.

[2310] L. Zu, C. Zhang, H.-Z. Chen, W. Wang, Y.-L.S. Tsai, Y. Tsai, W. Luo, Y.-Z. Fan, Exploring mirror twin higgs cosmology with present and future weak lensing surveys, J. Cosmol. Astropart. Phys. 08 (2023) 023, arXiv:2304.06308.

[2311] S. Bohr, J. Zavala, F.-Y. Cyr-Racine, M. Vogelsberger, T. Bringmann, C. Pfrommer, ETHOS – an effective parametrization and classification for structure formation: the non-linear regime at z $\gtrsim$ 5, Mon. Not. R. Astron. Soc. 498 (3) (2020) 3403–3419, arXiv:2006.01842.

[2312] V. Ajani, A. Peel, V. Pettorino, J.-L. Starck, Z. Li, J. Liu, Constraining neutrino masses with weak-lensing multiscale peak counts, Phys. Rev. D 102 (10) (2020) 103531, arXiv:2001.10993.

[2313] A. Peel, V. Pettorino, C. Giocoli, J.-L. Starck, M. Baldi, Breaking degeneracies in modified gravity with higher (than 2nd) order weak-lensing statistics, Astron. Astrophys. 619 (2018) A38, arXiv:1805.05146.

[2314] V. Ajani, J.-L. Starck, V. Pettorino, Starlet ℓ_1-norm for weak lensing cosmology, Astron. Astrophys. 645 (2021) L11, arXiv:2101.01542.

[2315] J. Harnois-Déraps, N. Martinet, T. Castro, K. Dolag, B. Giblin, C. Heymans, H. Hildebrandt, Q. Xia, Cosmic shear cosmology beyond two-point statistics: a combined peak count and correlation function analysis of DES-Y1, MNRAS 506 (2) (2021) 1623–1650, arXiv:2012.02777.

[2316] J. Jasche, B.D. Wandelt, Bayesian physical reconstruction of initial conditions from large scale structure surveys, Mon. Not. R. Astron. Soc. 432 (2013) 894, arXiv:1203.3639.

[2317] J. Jasche, G. Lavaux, Physical Bayesian modelling of the non-linear matter distribution: new insights into the nearby universe, Astron. Astrophys. 625 (2019) A64, arXiv:1806.11117.

[2318] N. Porqueres, A. Heavens, D. Mortlock, G. Lavaux, Bayesian forward modelling of cosmic shear data, Mon. Not. R. Astron. Soc. 502 (2) (2021) 3035–3044, arXiv:2011.07722.

[2319] N. Porqueres, A. Heavens, D. Mortlock, G. Lavaux, Lifting weak lensing degeneracies with a field-based likelihood, Mon. Not. R. Astron. Soc. 509 (3) (2021) 3194–3202, arXiv:2108.04825.

[2320] N. Porqueres, A. Heavens, D. Mortlock, G. Lavaux, T.L. Makinen, Field-level inference of cosmic shear with intrinsic alignments and baryons, 2023, arXiv:2304.04785.

[2321] T.L. Makinen, C. Sui, B.D. Wandelt, N. Porqueres, A. Heavens, Hybrid summary statistics, 2024, arXiv:2410.07548.

[2322] DES Collaboration, N. Jeffrey, et al., Dark Energy Survey Year 3 results: likelihood-free, simulation-based wCDM inference with neural compression of weak-lensing map statistics, Mon. Not. R. Astron. Soc. 536 (2) (2025) 1303–1322, arXiv:2403.02314.

[2323] N. MacCrann, J. Zuntz, S. Bridle, B. Jain, M.R. Becker, Cosmic discordance: Are Planck CMB and CFHTLenS weak lensing measurements out of tune? Mon. Not. R. Astron. Soc. 451 (3) (2015) 2877–2888, arXiv:1408.4742.

[2324] H. Rubira, A. Mazoun, M. Garny, Full-shape BOSS constraints on dark matter interacting with dark radiation and lifting the S8 tension, J. Cosmol. Astropart. Phys. 01 (2023) 034, arXiv:2209.03974.

[2325] T. Brinckmann, J.H. Chang, P. Du, M. LoVerde, Confronting interacting dark radiation scenarios with cosmological data, Phys. Rev. D 107 (12) (2023) 123517, arXiv:2212.13264.

[2326] DES Collaboration, A. Chen, et al., Constraints on dark matter to dark radiation conversion in the late universe with DES-Y1 and external data, Phys. Rev. D 103 (12) (2021) 123528, arXiv:2011.04606.

[2327] A. He, M.M. Ivanov, R. An, V. Gluscevic, S_8 tension in the context of dark matter–baryon scattering, Astrophys. J. Lett. 954 (1) (2023) L8, arXiv:2301.08260.

[2328] E. Di Valentino, C. Bøehm, E. Hivon, F.R. Bouchet, Reducing the H_0 and σ_8 tensions with dark matter-neutrino interactions, Phys. Rev. D 97 (4) (2018) 043513, arXiv:1710.02559.

[2329] L. Zu, W. Giarè, C. Zhang, E. Di Valentino, Y.-L.S. Tsai, S. Trojanowski, Can νDM interactions solve the S_8 discrepancy?, 2025, arXiv:2501.13785.

[2330] H. Zhan, The wide-field multiband imaging and slitless spectroscopy survey to be carried out by the Survey Space Telescope of China Manned Space Program, Chin. Sci. Bull. 66 (2021) 1290–1298.

[2331] R.A.C. Croft, D.H. Weinberg, M. Bolte, S. Burles, L. Hernquist, N. Katz, D. Kirkman, D. Tytler, Towards a precise measurement of matter clustering: Lyman alpha forest data at redshifts 2-4, Astrophys. J. 581 (2002) 20–52, arXiv:astro-ph/0012324.

[2332] M. Viel, The Lyman-α forest as a probe of the coldness of dark matter, in: 19th Conference on High Energy Physics, 2008, pp. 255–260.

[2333] M. Viel, G.D. Becker, J.S. Bolton, M.G. Haehnelt, Warm dark matter as a solution to the small scale crisis: New constraints from high redshift Lyman-α forest data, Phys. Rev. D 88 (2013) 043502, arXiv:1306.2314.

[2334] M. Viel, M.G. Haehnelt, V. Springel, Inferring the dark matter power spectrum from the Lyman-alpha forest in high-resolution QSO absorption spectra, Mon. Not. R. Astron. Soc. 354 (2004) 684, arXiv:astro-ph/0404600.

[2335] A. Boyarsky, J. Lesgourgues, O. Ruchayskiy, M. Viel, Lyman-alpha constraints on warm and on warm-plus-cold dark matter models, J. Cosmol. Astropart. Phys. 05 (2009) 012, arXiv:0812.0010.

[2336] K.K. Rogers, H.V. Peiris, Strong bound on canonical ultralight axion dark matter from the lyman-alpha forest, Phys. Rev. Lett. 126 (7) (2021) 071302, arXiv:2007.12705.

[2337] M. Garny, T. Konstandin, L. Sagunski, M. Viel, Neutrino mass bounds from confronting an effective model with BOSS Lyman-α data, J. Cosmol. Astropart. Phys. 03 (2021) 049, arXiv:2011.03050.

[2338] N. Palanque-Delabrouille, et al., Neutrino masses and cosmology with Lyman-alpha forest power spectrum, J. Cosmol. Astropart. Phys. 11 (2015) 011, arXiv:1506.05976.

[2339] J.S. Bolton, A. Caputo, H. Liu, M. Viel, Comparison of low-redshift Lyman-α forest observations to hydrodynamical simulations with dark photon dark matter, Phys. Rev. Lett. 129 (21) (2022) 211102, arXiv:2206.13520.

[2340] D.C. Hooper, M. Lucca, Hints of dark matter-neutrino interactions in lyman-α data, Phys. Rev. D 105 (10) (2022) 103504, arXiv:2110.04024.

[2341] S. Furlanetto, S.P. Oh, F. Briggs, Cosmology at low frequencies: The 21 cm transition and the high-redshift universe, Phys. Rep. 433 (2006) 181–301, arXiv:astro-ph/0608032.

[2342] J.R. Pritchard, A. Loeb, 21-Cm cosmology, Rep. Progr. Phys. 75 (2012) 086901, arXiv:1109.6012.

[2343] A. Schneider, Constraining noncold dark matter models with the global 21-cm signal, Phys. Rev. D 98 (6) (2018) 063021, arXiv:1805.00021.

[2344] L. Lopez-Honorez, O. Mena, P. Villanueva-Domingo, Dark matter microphysics and 21 cm observations, Phys. Rev. D 99 (2) (2019) 023522, arXiv:1811.02716.

[2345] M. Escudero, L. Lopez-Honorez, O. Mena, S. Palomares-Ruiz, P. Villanueva-Domingo, A fresh look into the interacting dark matter scenario, J. Cosmol. Astropart. Phys. 06 (2018) 007, arXiv:1803.08427.

[2346] J.B. Muñoz, C. Dvorkin, F.-Y. Cyr-Racine, Probing the small-scale matter power spectrum with large-scale 21-cm data, Phys. Rev. D 101 (6) (2020) 063526, arXiv:1911.11144.

[2347] S. Yoshiura, K. Takahashi, T. Takahashi, Probing small scale primordial power spectrum with 21cm line global signal, Phys. Rev. D 101 (8) (2020) 083520, arXiv:1911.07442.

[2348] J.B. Muñoz, S. Bohr, F.-Y. Cyr-Racine, J. Zavala, M. Vogelsberger, ETHOS - an effective theory of structure formation: Impact of dark acoustic oscillations on cosmic dawn, Phys. Rev. D 103 (4) (2021) 043512, arXiv:2011.05333.

[2349] M.R. Lovell, J. Zavala, M. Vogelsberger, X. Shen, F.-Y. Cyr-Racine, C. Pfrommer, K. Sigurdson, M. Boylan-Kolchin, A. Pillepich, ETHOS – an effective theory of structure formation: predictions for the high-redshift Universe – abundance of galaxies and reionization, Mon. Not. R. Astron. Soc. 477 (3) (2018) 2886–2899, arXiv:1711.10497.

[2350] S. Hassan, R. Davé, K. Finlator, M.G. Santos, Simulating the 21 cm signal from reionization including non-linear ionizations and inhomogeneous recombinations, Mon. Not. R. Astron. Soc. 457 (2) (2016) 1550–1567, arXiv:1510.04280.

[2351] LOFAR Collaboration, M.P. van Haarlem, et al., LOFAR: The LOw-frequency array, Astron. Astrophys. 556 (2013) A2, arXiv:1305.3550.

[2352] D.R. DeBoer, et al., Hydrogen epoch of reionization array (HERA), Publ. Astron. Soc. Pac. 129 (974) (2017) 045001, arXiv:1606.07473.

[2353] L.V.E. Koopmans, et al., The cosmic dawn and epoch of reionization with the square kilometre array, in: T.L. Bourke, et al. (Eds.), PoS AASKA14 (2015) 001, arXiv:1505.07568.

[2354] J.S. Bullock, M. Boylan-Kolchin, Small-scale challenges to the ΛCDM paradigm, Ann. Rev. Astron. Astrophys. 55 (2017) 343–387, arXiv:1707.04256.

[2355] J.F. Navarro, C.S. Frenk, S.D.M. White, The structure of cold dark matter halos, Astrophys. J. 462 (1996) 563–575, arXiv:astro-ph/9508025.

[2356] W.J.G. de Blok, The core-cusp problem, Adv. Astron. 2010 (2010) 789293, arXiv:0910.3538.

[2357] G. Gentile, P. Salucci, U. Klein, D. Vergani, P. Kalberla, The cored distribution of dark matter in spiral galaxies, Mon. Not. R. Astron. Soc. 351 (2004) 903, arXiv:astro-ph/0403154.

[2358] J.S. Bullock, T.S. Kolatt, Y. Sigad, R.S. Somerville, A.V. Kravtsov, A.A. Klypin, J.R. Primack, A. Dekel, Profiles of dark haloes. Evolution, scatter, and environment, Mon. Not. R. Astron. Soc. 321 (2001) 559–575, arXiv:astro-ph/9908159.

[2359] K.A. Oman, et al., The unexpected diversity of dwarf galaxy rotation curves, Mon. Not. R. Astron. Soc. 452 (4) (2015) 3650–3665, arXiv:1504.01437.

[2360] A.A. Klypin, A.V. Kravtsov, O. Valenzuela, F. Prada, Where are the missing galactic satellites? Astrophys. J. 522 (1999) 82–92, arXiv:astro-ph/9901240.

[2361] B. Moore, S. Ghigna, F. Governato, G. Lake, T.R. Quinn, J. Stadel, P. Tozzi, Dark matter substructure within galactic halos, Astrophys. J. Lett. 524 (1999) L19–L22, arXiv:astro-ph/9907411.

[2362] M. Boylan-Kolchin, J.S. Bullock, M. Kaplinghat, Too big to fail? The puzzling darkness of massive Milky Way subhaloes, Mon. Not. R. Astron. Soc. 415 (2011) L40, arXiv:1103.0007.

[2363] M. Boylan-Kolchin, J.S. Bullock, M. Kaplinghat, The Milky Way's bright satellites as an apparent failure of LCDM, Mon. Not. R. Astron. Soc. 422 (2012) 1203–1218, arXiv:1111.2048.

[2364] J.F. Navarro, V.R. Eke, C.S. Frenk, The cores of dwarf galaxy halos, Mon. Not. R. Astron. Soc. 283 (1996) L72–L78, arXiv:astro-ph/9610187.

[2365] S.-H. Oh, C. Brook, F. Governato, E. Brinks, L. Mayer, W.J.G. de Blok, A. Brooks, F. Walter, The central slope of dark matter cores in dwarf galaxies: Simulations vs. THINGS, Astron. J. 142 (2011) 24, arXiv:1011.2777.

[2366] A. Zolotov, A.M. Brooks, B. Willman, F. Governato, A. Pontzen, C. Christensen, A. Dekel, T. Quinn, S. Shen, J. Wadsley, Baryons matter: Why luminous satellite galaxies have reduced central masses, Astrophys. J. 761 (2012) 71, arXiv:1207.0007.

[2367] K.S. Arraki, A. Klypin, S. More, S. Trujillo-Gomez, Effects of baryon removal on the structure of dwarf spheroidal galaxies, Mon. Not. R. Astron. Soc. 438 (2) (2014) 1466–1482, arXiv:1212.6651.

[2368] A.M. Brooks, A. Zolotov, Why baryons matter: The kinematics of dwarf spheroidal satellites, Astrophys. J. 786 (2014) 87, arXiv:1207.2468.

[2369] C.B. Brook, A. Di Cintio, Expanded haloes, abundance matching and too-big-to-fail in the local group, Mon. Not. R. Astron. Soc. 450 (4) (2015) 3920–3934, arXiv:1410.3825.

[2370] A.A. Dutton, A.V. Macciò, J. Frings, L. Wang, G.S. Stinson, C. Penzo, X. Kang, NIHAO V: too big does not fail – reconciling the conflict between ΛCDM predictions and the circular velocities of nearby field galaxies, Mon. Not. R. Astron. Soc. 457 (1) (2016) L74–L78, arXiv:1512.00453.

[2371] W. Hu, R. Barkana, A. Gruzinov, Cold and fuzzy dark matter, Phys. Rev. Lett. 85 (2000) 1158–1161, arXiv:astro-ph/0003365.

[2372] B. Moore, S. Gelato, A. Jenkins, F.R. Pearce, V. Quilis, Collisional versus collisionless dark matter, Astrophys. J. Lett. 535 (2000) L21–L24, arXiv:astro-ph/0002308.

[2373] N. Yoshida, V. Springel, S.D.M. White, G. Tormen, Collisional dark matter and the structure of dark halos, Astrophys. J. Lett. 535 (2000) L103, arXiv:astro-ph/0002362.

[2374] A. Burkert, The structure and evolution of weakly selfinteracting cold dark matter halos, Astrophys. J. Lett. 534 (2000) L143–L146, arXiv:astro-ph/0002409.

[2375] C.S. Kochanek, M.J. White, A quantitative study of interacting dark matter in halos, Astrophys. J. 543 (2000) 514, arXiv:astro-ph/0003483.

[2376] N. Yoshida, V. Springel, S.D.M. White, G. Tormen, Weakly self-interacting dark matter and the structure of dark halos, Astrophys. J. Lett. 544 (2000) L87–L90, arXiv:astro-ph/0006134.

[2377] R. Dave, D.N. Spergel, P.J. Steinhardt, B.D. Wandelt, Halo properties in cosmological simulations of selfinteracting cold dark matter, Astrophys. J. 547 (2001) 574–589, arXiv:astro-ph/0006218.

[2378] J. Miralda-Escude, A test of the collisional dark matter hypothesis from cluster lensing, Astrophys. J. 564 (2002) 60, arXiv:astro-ph/0002050.

[2379] M. Rocha, A.H.G. Peter, J.S. Bullock, M. Kaplinghat, S. Garrison-Kimmel, J. Onorbe, L.A. Moustakas, Cosmological simulations with self-interacting dark matter I: Constant density cores and substructure, Mon. Not. R. Astron. Soc. 430 (2013) 81–104, arXiv:1208.3025.

[2380] A.H.G. Peter, M. Rocha, J.S. Bullock, M. Kaplinghat, Cosmological simulations with self-interacting dark matter II: Halo shapes vs. Observations, Mon. Not. R. Astron. Soc. 430 (2013) 105, arXiv:1208.3026.

[2381] M. Vogelsberger, J. Zavala, A. Loeb, Subhaloes in self-interacting galactic dark matter haloes, Mon. Not. R. Astron. Soc. 423 (2012) 3740, arXiv:1201.5892.

[2382] O.D. Elbert, J.S. Bullock, S. Garrison-Kimmel, M. Rocha, J. Oñorbe, A.H.G. Peter, Core formation in dwarf haloes with self-interacting dark matter: no fine-tuning necessary, Mon. Not. R. Astron. Soc. 453 (1) (2015) 29–37, arXiv:1412.1477.

[2383] H.-Y. Schive, T. Chiueh, T. Broadhurst, Cosmic structure as the quantum interference of a coherent dark wave, Nat. Phys. 10 (2014) 496–499, arXiv:1406.6586.

[2384] P. Mocz, M. Vogelsberger, V.H. Robles, J. Zavala, M. Boylan-Kolchin, A. Fialkov, L. Hernquist, Galaxy formation with BECDM – I. Turbulence and relaxation of idealized haloes, Mon. Not. R. Astron. Soc. 471 (4) (2017) 4559–4570, arXiv:1705.05845.

[2385] J. Veltmaat, J.C. Niemeyer, B. Schwabe, Formation and structure of ultralight bosonic dark matter halos, Phys. Rev. D 98 (4) (2018) 043509, arXiv:1804.09647.

[2386] L. Herold, E.G.M. Ferreira, L. Heinrich, Profile likelihoods in cosmology: When, why, and how illustrated with ΛCDM, massive neutrinos, and dark energy, Phys. Rev. D 111 (8) (2025) 083504, arXiv:2408.07700.

[2387] J. Neyman, Outline of a theory of statistical estimation based on the classical theory of probability, Phil. Trans. Roy. Soc. Lond. A 236 (767) (1937) 333–380.

[2388] S.S. Wilks, The large-sample distribution of the likelihood ratio for testing composite hypotheses, Ann. Math. Stat. 9 (1) (1938) 60–62.

[2389] Y. Pawitan, In All Likelihood: Statistical Modelling and Inference Using Likelihood, Oxford Science Publications, OUP Oxford, 2001, URL https://books.google.com/books?id=M-3pSCVxV5oC.

[2390] R. Trotta, Bayesian methods in cosmology, 2017, arXiv E-Prints. arXiv:1701.01467.

[2391] G.J. Feldman, R.D. Cousins, A unified approach to the classical statistical analysis of small signals, Phys. Rev. D 57 (1998) 3873–3889, arXiv:physics/9711021.

[2392] R.D. Cousins, Why isn't every physicist a Bayesian? Am. J. Phys. 63 (1995) 398.

[2393] LiteBIRD Collaboration, P. Campeti, et al., LiteBIRD science goals and forecasts. A case study of the origin of primordial gravitational waves using large-scale CMB polarization, J. Cosmol. Astropart. Phys. 06 (2024) 008, arXiv:2312.00717.

[2394] SPIDER Collaboration, P.A.R. Ade, et al., A constraint on primordial B-modes from the first flight of the spider balloon-borne telescope, Astrophys. J. 927 (2) (2022) 174, arXiv:2103.13334.

[2395] B.A. Reid, L. Verde, R. Jimenez, O. Mena, Robust neutrino constraints by combining low redshift observations with the CMB, J. Cosmol. Astropart. Phys. 01 (2010) 003, arXiv:0910.0008.

[2396] W. Giarè, A. Gómez-Valent, E. Di Valentino, C. van de Bruck, Hints of neutrino dark matter scattering in the CMB? Constraints from the marginalized and profile distributions, Phys. Rev. D 109 (6) (2024) 063516, arXiv:2311.09116.

[2397] T. Karwal, Y. Patel, A. Bartlett, V. Poulin, T.L. Smith, D.N. Pfeffer, Procoli: Profiles of cosmological likelihoods, 2024, arXiv:2401.14225.

[2398] E.B. Holm, A. Nygaard, J. Dakin, S. Hannestad, T. Tram, PROSPECT: a profile likelihood code for frequentist cosmological parameter inference, Mon. Not. R. Astron. Soc. 535 (4) (2024) 3686–3699, arXiv:2312.02972.

[2399] F. James, M. Roos, Minuit - a system for function minimization and analysis of the parameter errors and correlations, Comput. Phys. Comm. 10 (6) (1975) 343–367, URL https://www.sciencedirect.com/science/article/pii/0010465575900399.

[2400] G. Galloni, S. Henrot-Versillé, M. Tristram, Robust constraints on tensor perturbations from cosmological data: A comparative analysis from Bayesian and frequentist perspectives, Phys. Rev. D 110 (6) (2024) 063511, arXiv:2405.04455.

[2401] C. Moretti, M. Tsedrik, P. Carrilho, A. Pourtsidou, Modified gravity and massive neutrinos: constraints from the full shape analysis of BOSS galaxies and forecasts for stage IV surveys, J. Cosmol. Astropart. Phys. 12 (2023) 025, arXiv:2306.09275.

[2402] P. Campeti, O. Özsoy, I. Obata, M. Shiraishi, New constraints on axion-gauge field dynamics during inflation from Planck and BICEP/Keck data sets, J. Cosmol. Astropart. Phys. 07 (07) (2022) 039, arXiv:2203.03401.

[2403] P. Campeti, E. Komatsu, New constraint on the tensor-to-scalar ratio from the Planck and BICEP/Keck array data using the profile likelihood, Astrophys. J. 941 (2) (2022) 110, arXiv:2205.05617.

[2404] Planck Collaboration, P.A.R. Ade, et al., Planck intermediate results. XVI. Profile likelihoods for cosmological parameters, Astron. Astrophys. 566 (2014) A54, arXiv:1311.1657.

[2405] S. Hannestad, Stochastic optimization methods for extracting cosmological parameters from cosmic microwave background radiation power spectra, Phys. Rev. D 61 (2000) 023002, arXiv:astro-ph/9911330.

[2406] S. Kirkpatrick, C.D. Gelatt, M.P. Vecchi, Optimization by simulated annealing, Science 220 (1983) 671–680.

[2407] S. Henrot-Versillé, O. Perdereau, S. Plaszczynski, B.R. d'Orfeuil, M. Spinelli, M. Tristram, Agnostic cosmology in the CAMEL framework, 2016, arXiv:1607.02964.

[2408] A. Nygaard, E.B. Holm, S. Hannestad, T. Tram, CONNECT: a neural network based framework for emulating cosmological observables and cosmological parameter inference, J. Cosmol. Astropart. Phys. 05 (2023) 025, arXiv:2205.15726.

[2409] A. Nygaard, E.B. Holm, S. Hannestad, T. Tram, Fast and effortless computation of profile likelihoods using CONNECT, J. Cosmol. Astropart. Phys. 11 (2023) 064, arXiv:2308.06379.

[2410] T. Bringmann, F. Kahlhoefer, K. Schmidt-Hoberg, P. Walia, Converting non-relativistic dark matter to radiation, Phys. Rev. D 98 (2) (2018) 023543, arXiv:1803.03644.

[2411] F. Couchot, S. Henrot-Versillé, O. Perdereau, S. Plaszczynski, B. Rouillé d'Orfeuil, M. Spinelli, M. Tristram, Cosmological constraints on the neutrino mass including systematic uncertainties, Astron. Astrophys. 606 (2017) A104, arXiv:1703.10829.

[2412] A.X. Gonzalez-Morales, R. Poltis, B.D. Sherwin, L. Verde, Are priors responsible for cosmology favoring additional neutrino species?, 2011, arXiv:1106.5052.

[2413] L. Herold, M. Kamionkowski, Revisiting the impact of neutrino mass hierarchies on neutrino mass constraints in light of recent DESI data, Phys. Rev. D 111 (8) (2025) 083518, arXiv:2412.03546.

[2414] S. Henrot-Versille, et al., Improved constraint on the primordial gravitational-wave density using recent cosmological data and its impact on cosmic string models, Cl. Quant. Grav. 32 (4) (2015) 045003, arXiv:1408.5299.

[2415] A.J.S. Capistrano, R.C. Nunes, L.A. Cabral, Lower tensor-to-scalar ratio as possible signature of modified gravity, Phys. Rev. D 109 (12) (2024) 123517, arXiv:2403.13860.

[2416] B. Hu, J. Torrado, Searching for primordial localized features with CMB and LSS spectra, Phys. Rev. D 91 (6) (2015) 064039, arXiv:1410.4804.

[2417] A. Avilez, C. Skordis, Cosmological constraints on Brans-Dicke theory, Phys. Rev. Lett. 113 (1) (2014) 011101, arXiv:1303.4330.

[2418] J. de Cruz Pérez, J. Solà Peracaula, Brans–Dicke cosmology mimicking running vacuum, Modern Phys. Lett. A 33 (38) (2018) 1850228, arXiv:1809.03329.

[2419] J. Solà Peracaula, A. Gomez-Valent, J. de Cruz Pérez, C. Moreno-Pulido, Brans–Dicke gravity with a cosmological constant smoothes out ΛCDM tensions, Astrophys. J. Lett. 886 (1) (2019) L6, arXiv:1909.02554.

[2420] J. Solà Peracaula, A. Gómez-Valent, J. de Cruz Pérez, C. Moreno-Pulido, Brans–Dicke cosmology with a Λ-term: a possible solution to ΛCDM tensions, Cl. Quant. Grav. 37 (24) (2020) 245003, arXiv:2006.04273.

[2421] S. Joudaki, P.G. Ferreira, N.A. Lima, H.A. Winther, Testing gravity on cosmic scales: A case study of Jordan-Brans-Dicke theory, Phys. Rev. D 105 (4) (2022) 043522, arXiv:2010.15278.

[2422] C. Wetterich, The cosmon model for an asymptotically vanishing time dependent cosmological 'constant', Astron. Astrophys. 301 (1995) 321–328, arXiv:hep-th/9408025.

[2423] V. Pettorino, L. Amendola, C. Baccigalupi, C. Quercellini, Constraints on coupled dark energy using CMB data from WMAP and SPT, Phys. Rev. D 86 (2012) 103507, arXiv:1207.3293.

[2424] V. Pettorino, Testing modified gravity with Planck: the case of coupled dark energy, Phys. Rev. D 88 (2013) 063519, arXiv:1305.7457.

[2425] Planck Collaboration, P.A.R. Ade, et al., Planck 2015 results. XIV. Dark energy and modified gravity, Astron. Astrophys. 594 (2016) A14, arXiv:1502.01590.

[2426] B.J. Barros, L. Amendola, T. Barreiro, N.J. Nunes, Coupled quintessence with a ΛCDM background: removing the σ_8 tension, J. Cosmol. Astropart. Phys. 01 (2019) 007, arXiv:1802.09216.

[2427] A. Gómez-Valent, V. Pettorino, L. Amendola, Update on coupled dark energy and the H_0 tension, Phys. Rev. D 101 (12) (2020) 123513, arXiv:2004.00610.

[2428] A. Gómez-Valent, Z. Zheng, L. Amendola, C. Wetterich, V. Pettorino, Coupled and uncoupled early dark energy, massive neutrinos, and the cosmological tensions, Phys. Rev. D 106 (10) (2022) 103522, arXiv:2207.14487.

[2429] L.W.K. Goh, A. Gómez-Valent, V. Pettorino, M. Kilbinger, Constraining constant and tomographic coupled dark energy with low-redshift and high-redshift probes, Phys. Rev. D 107 (8) (2023) 083503, arXiv:2211.13588.

[2430] P.J.E. Peebles, B. Ratra, Cosmology with a time variable cosmological constant, Astrophys. J. Lett. 325 (1988) L17.

[2431] P. Brax, C. van de Bruck, E. Di Valentino, W. Giarè, S. Trojanowski, New insights on ν–DM interactions, Mon. Not. R. Astron. Soc. 527 (1) (2023) L122–L126, arXiv:2303.16895.

[2432] P. Brax, C. van de Bruck, E. Di Valentino, W. Giarè, S. Trojanowski, Extended analysis of neutrino-dark matter interactions with small-scale CMB experiments, Phys. Dark Univ. 42 (2023) 101321, arXiv:2305.01383.

[2433] BOSS Collaboration, L. Anderson, et al., The clustering of galaxies in the SDSS-III baryon oscillation spectroscopic survey: Baryon acoustic oscillations in the data release 9 spectroscopic galaxy sample, Mon. Not. R. Astron. Soc. 427 (4) (2013) 3435–3467, arXiv:1203.6594.

[2434] eBOSS Collaboration, M. Ata, et al., The clustering of the SDSS-IV extended baryon oscillation spectroscopic survey DR14 quasar sample: first measurement of baryon acoustic oscillations between redshift 0.8 and 2.2, Mon. Not. R. Astron. Soc. 473 (4) (2018) 4773–4794, arXiv:1705.06373.

[2435] DES Collaboration, T.M.C. Abbott, et al., Dark energy survey year 1 results: Measurement of the baryon acoustic oscillation scale in the distribution of galaxies to redshift 1, Mon. Not. R. Astron. Soc. 483 (4) (2019) 4866–4883, arXiv:1712.06209.

[2436] DES Collaboration, K.C. Chan, et al., BAO from angular clustering: Optimization and mitigation of theoretical systematics, Mon. Not. R. Astron. Soc. 480 (3) (2018) 3031–3051, arXiv:1801.04390.

[2437] R. Ruggeri, C. Blake, How accurately can we measure the baryon acoustic oscillation feature? Mon. Not. R. Astron. Soc. 498 (3) (2020) 3744–3757, arXiv:1909.13011.

[2438] A. Cuceu, A. Font-Ribera, B. Joachimi, Bayesian methods for fitting baryon acoustic oscillations in the Lyman-α forest, J. Cosmol. Astropart. Phys. 07 (2020) 035, arXiv:2004.02761.

[2439] A.G. Sanchez, Arguments against using h^{-1}Mpc units in observational cosmology, Phys. Rev. D 102 (12) (2020) 123511, arXiv:2002.07829.

[2440] L.F. Secco, T. Karwal, W. Hu, E. Krause, Role of the Hubble scale in the weak lensing versus CMB tension, Phys. Rev. D 107 (8) (2023) 083532, arXiv:2209.12997.

[2441] M. Forconi, A. Favale, A. Gómez-Valent, Illustrating the consequences of a misuse of σ_8 in cosmology, 2025, arXiv:2501.11571.

[2442] V. Poulin, T.L. Smith, R. Calderón, T. Simon, Implications of the cosmic calibration tension beyond H0 and the synergy between early- and late-time new physics, Phys. Rev. D 111 (8) (2025) 083552, arXiv:2407.18292.

[2443] D. Pedrotti, J.-Q. Jiang, L.A. Escamilla, S.S. da Costa, S. Vagnozzi, Multidimensionality of the Hubble tension: The roles of Ωm and ωc, Phys. Rev. D 111 (2) (2025) 023506, arXiv:2408.04530.

[2444] M. Kamionkowski, A.G. Riess, The Hubble tension and early dark energy, Ann. Rev. Nucl. Part. Sci. 73 (2023) 153–180, arXiv:2211.04492.

[2445] V. Poulin, T.L. Smith, T. Karwal, The ups and downs of early dark energy solutions to the Hubble tension: A review of models, hints and constraints circa 2023, Phys. Dark Univ. 42 (2023) 101348, arXiv:2302.09032.

[2446] E. McDonough, J.C. Hill, M.M. Ivanov, A. La Posta, M.W. Toomey, Observational constraints on early dark energy, Internat. J. Modern Phys. D 33 (11) (2024) 2430003, arXiv:2310.19899.

[2447] A. Albrecht, C. Skordis, Phenomenology of a realistic accelerating universe using only Planck scale physics, Phys. Rev. Lett. 84 (2000) 2076–2079, arXiv:astro-ph/9908085.

[2448] M. Doran, M.J. Lilley, J. Schwindt, C. Wetterich, Quintessence and the separation of CMB peaks, Astrophys. J. 559 (2001) 501–506, arXiv:astro-ph/0012139.

[2449] C. Wetterich, Phenomenological parameterization of quintessence, Phys. Lett. B 594 (2004) 17–22, arXiv:astro-ph/0403289.

[2450] M. Doran, G. Robbers, Early dark energy cosmologies, J. Cosmol. Astropart. Phys. 06 (2006) 026, arXiv:astro-ph/0601544.

[2451] M. Kamionkowski, J. Pradler, D.G.E. Walker, Dark energy from the string axiverse, Phys. Rev. Lett. 113 (25) (2014) 251302, arXiv:1409.0549.

[2452] T. Karwal, M. Kamionkowski, Dark energy at early times, the Hubble parameter, and the string axiverse, Phys. Rev. D 94 (10) (2016) 103523, arXiv:1608.01309.

[2453] V. Poulin, T.L. Smith, D. Grin, T. Karwal, M. Kamionkowski, Cosmological implications of ultralight axionlike fields, Phys. Rev. D 98 (8) (2018) 083525, arXiv:1806.10608.

[2454] V. Poulin, T.L. Smith, T. Karwal, M. Kamionkowski, Early dark energy can resolve the Hubble tension, Phys. Rev. Lett. 122 (22) (2019) 221301, arXiv:1811.04083.

[2455] T.L. Smith, V. Poulin, M.A. Amin, Oscillating scalar fields and the Hubble tension: a resolution with novel signatures, Phys. Rev. D 101 (6) (2020) 063523, arXiv:1908.06995.

[2456] A.R. Khalife, M.B. Zanjani, S. Galli, S. Günther, J. Lesgourgues, K. Benabed, Review of Hubble tension solutions with new SH0ES and SPT-3G data, J. Cosmol. Astropart. Phys. 04 (2024) 059, arXiv:2312.09814.

[2457] J.C. Hill, E. McDonough, M.W. Toomey, S. Alexander, Early dark energy does not restore cosmological concordance, Phys. Rev. D 102 (4) (2020) 043507, arXiv:2003.07355.

[2458] V. Poulin, T.L. Smith, A. Bartlett, Dark energy at early times and ACT data: A larger Hubble constant without late-time priors, Phys. Rev. D 104 (12) (2021) 123550, arXiv:2109.06229.

[2459] E. McDonough, M.-X. Lin, J.C. Hill, W. Hu, S. Zhou, Early dark sector, the Hubble tension, and the swampland, Phys. Rev. D 106 (4) (2022) 043525, arXiv:2112.09128.

[2460] S. Alexander, E. McDonough, Axion-dilaton destabilization and the Hubble tension, Phys. Lett. B 797 (2019) 134830, arXiv:1904.08912.

[2461] M. Cicoli, M. Licheri, R. Mahanta, E. McDonough, F.G. Pedro, M. Scalisi, Early dark energy in type IIB string theory, JHEP 06 (2023) 052, arXiv:2303.03414.

[2462] E. McDonough, M. Scalisi, Towards early dark energy in string theory, JHEP 10 (2023) 118, arXiv:2209.00011.

[2463] R. Kappl, H.P. Nilles, M.W. Winkler, Modulated natural inflation, Phys. Lett. B 753 (2016) 653–659, arXiv:1511.05560.

[2464] L. Yin, Reducing the H_0 tension with exponential acoustic dark energy, Eur. Phys. J. C 82 (1) (2022) 78, arXiv:2012.13917.

[2465] G. Ye, Y.-S. Piao, Is the Hubble tension a hint of AdS phase around recombination? Phys. Rev. D 101 (8) (2020) 083507, arXiv:2001.02451.

[2466] A. Adil, A. Albrecht, L. Knox, Quintessential cosmological tensions, Phys. Rev. D 107 (6) (2023) 063521, arXiv:2207.10235.

[2467] P. Agrawal, F.-Y. Cyr-Racine, D. Pinner, L. Randall, Rock 'n' roll solutions to the Hubble tension, Phys. Dark Univ. 42 (2023) 101347, arXiv:1904.01016.

[2468] M.-X. Lin, G. Benevento, W. Hu, M. Raveri, Acoustic dark energy: Potential conversion of the hubble tension, Phys. Rev. D 100 (6) (2019) 063542, arXiv:1905.12618.

[2469] R. Jackiw, S.Y. Pi, Chern-Simons modification of general relativity, Phys. Rev. D 68 (2003) 104012, arXiv:gr-qc/0308071.

[2470] M.J. Duncan, N. Kaloper, K.A. Olive, Axion hair and dynamical torsion from anomalies, Nuclear Phys. B 387 (1992) 215–235.

[2471] S. Basilakos, N.E. Mavromatos, J. Solà Peracaula, Gravitational and chiral anomalies in the running vacuum universe and matter-antimatter asymmetry, Phys. Rev. D 101 (4) (2020) 045001, arXiv:1907.04890.

[2472] S. Basilakos, N.E. Mavromatos, J. Solà Peracaula, Quantum anomalies in string-inspired running vacuum universe: Inflation and axion dark matter, Phys. Lett. B 803 (2020) 135342, arXiv:2001.03465.

[2473] N.E. Mavromatos, J. Solà Peracaula, Stringy-running-vacuum-model inflation: from primordial gravitational waves and stiff axion matter to dynamical dark energy, Eur. Phys. J. ST 230 (9) (2021) 2077–2110, arXiv:2012.07971.

[2474] E. Guendelman, R. Herrera, D. Benisty, Unifying inflation with early and late dark energy with multiple fields: Spontaneously broken scale invariant two measures theory, Phys. Rev. D 105 (12) (2022) 124035, arXiv:2201.06470.

[2475] E.L.D. Perico, J.A.S. Lima, S. Basilakos, J. Sola, Complete cosmic history with a dynamical $\Lambda = \Lambda(H)$ term, Phys. Rev. D 88 (2013) 063531, arXiv:1306.0591.

[2476] J.A.S. Lima, S. Basilakos, J. Sola, Expansion history with decaying vacuum: A complete cosmological scenario, Mon. Not. R. Astron. Soc. 431 (2013) 923–929, arXiv:1209.2802.

[2477] J. Solà, A. Gómez-Valent, The $\bar{\Lambda}$CDM cosmology: From inflation to dark energy through running Λ, Internat. J. Modern Phys. D 24 (2015) 1541003, arXiv:1501.03832.

[2478] J. Solà Peracaula, H. Yu, Particle and entropy production in the running vacuum universe, Gen. Relativity Gravitation 52 (2) (2020) 17, arXiv:1910.01638.

[2479] N.E. Mavromatos, J. Solà Peracaula, Inflationary physics and trans-Planckian conjecture in the stringy running vacuum model: from the phantom vacuum to the true vacuum, Eur. Phys. J. Plus 136 (11) (2021) 1152, arXiv:2105.02659.

[2480] P. Svrcek, E. Witten, Axions in string theory, JHEP 06 (2006) 051, arXiv:hep-th/0605206.

[2481] P. Dorlis, N.E. Mavromatos, S.-N. Vlachos, Condensate-induced inflation from primordial gravitational waves in string-inspired Chern-Simons gravity, Phys. Rev. D 110 (6) (2024) 063512, arXiv:2403.09005.

[2482] N.E. Mavromatos, P. Dorlis, S.-N. Vlachos, Torsion-induced axions in string theory, quantum gravity and the cosmological tensions, in: Workshop on the Standard Model and beyond, 2024, arXiv:2404.18741.

[2483] L. McAllister, E. Silverstein, A. Westphal, Gravity waves and linear inflation from axion monodromy, Phys. Rev. D 82 (2010) 046003, arXiv:0808.0706.

[2484] A. Gómez-Valent, N.E. Mavromatos, J. Solà Peracaula, Stringy running vacuum model and current tensions in cosmology, Cl. Quant. Grav. 41 (1) (2024) 015026, arXiv:2305.15774.

[2485] A. Gomez-Valent, J. Solà Peracaula, Phantom matter: A challenging solution to the cosmological tensions, Astrophys. J. 975 (1) (2024) 64, arXiv:2404.18845.

[2486] R. Kallosh, A. Linde, Universality class in conformal inflation, J. Cosmol. Astropart. Phys. 07 (2013) 002, arXiv:1306.5220.

[2487] R. Kallosh, A. Linde, D. Roest, Superconformal inflationary α-attractors, JHEP 11 (2013) 198, arXiv:1311.0472.

[2488] M. Galante, R. Kallosh, A. Linde, D. Roest, Unity of cosmological inflation attractors, Phys. Rev. Lett. 114 (14) (2015) 141302, arXiv:1412.3797.

[2489] M. Braglia, W.T. Emond, F. Finelli, A.E. Gumrukcuoglu, K. Koyama, Unified framework for early dark energy from α-attractors, Phys. Rev. D 102 (8) (2020) 083513, arXiv:2005.14053.

[2490] L. Brissenden, K. Dimopoulos, S. Sánchez López, Non-oscillating early dark energy and quintessence from α-attractors, Astropart. Phys. 157 (2024) 102925, arXiv:2301.03572.

[2491] D. Chowdhury, G. Tasinato, I. Zavala, Dark energy, D-branes and pulsar timing arrays, J. Cosmol. Astropart. Phys. 11 (2023) 090, arXiv:2307.01188.

[2492] O.F. Ramadan, T. Karwal, J. Sakstein, Attractive proposal for resolving the Hubble tension: Dynamical attractors that unify early and late dark energy, Phys. Rev. D 109 (6) (2024) 063525, arXiv:2309.08082.

[2493] E.J. Copeland, A.R. Liddle, D. Wands, Exponential potentials and cosmological scaling solutions, Phys. Rev. D 57 (1998) 4686–4690, arXiv:gr-qc/9711068.

[2494] T. Barreiro, E.J. Copeland, N.J. Nunes, Quintessence arising from exponential potentials, Phys. Rev. D 61 (2000) 127301, arXiv:astro-ph/9910214.

[2495] A. Gómez-Valent, Z. Zheng, L. Amendola, V. Pettorino, C. Wetterich, Early dark energy in the pre- and postrecombination epochs, Phys. Rev. D 104 (8) (2021) 083536, arXiv:2107.11065.

[2496] V. Pettorino, L. Amendola, C. Wetterich, How early is early dark energy? Phys. Rev. D 87 (2013) 083009, arXiv:1301.5279.

[2497] E.J. Copeland, A. Moss, S. Sevillano Muñoz, J.M.M. White, Scaling solutions as early dark energy resolutions to the Hubble tension, J. Cosmol. Astropart. Phys. 05 (2024) 078, arXiv:2309.15295.

[2498] T. Karwal, M. Raveri, B. Jain, J. Khoury, M. Trodden, Chameleon early dark energy and the Hubble tension, Phys. Rev. D 105 (6) (2022) 063535, arXiv:2106.13290.

[2499] M.-X. Lin, E. McDonough, J.C. Hill, W. Hu, Dark matter trigger for early dark energy coincidence, Phys. Rev. D 107 (10) (2023) 103523, arXiv:2212.08098.

[2500] G. Liu, Z. Zhou, Y. Mu, L. Xu, Alleviating cosmological tensions with a coupled scalar fields model, Phys. Rev. D 108 (8) (2023) 083523, arXiv:2307.07228.

[2501] G. Garcia-Arroyo, L.A. Ureña-López, J.A. Vázquez, Interacting scalar fields: Dark matter and early dark energy, Phys. Rev. D 110 (2) (2024) 023529, arXiv:2402.08815.

[2502] A. Talebian, Early dark energy and dark photon dark matter from waterfall symmetry breaking, Phys. Rev. D 109 (12) (2024) 123526, arXiv:2312.08254.

[2503] K.V. Berghaus, T. Karwal, Thermal friction as a solution to the hubble tension, Phys. Rev. D 101 (8) (2020) 083537, arXiv:1911.06281.

[2504] J. Sakstein, M. Trodden, Early dark energy from massive neutrinos as a natural resolution of the hubble tension, Phys. Rev. Lett. 124 (16) (2020) 161301, arXiv:1911.11760.

[2505] M. Carrillo González, Q. Liang, J. Sakstein, M. Trodden, Neutrino-assisted early dark energy: Theory and cosmology, J. Cosmol. Astropart. Phys. 04 (2021) 063, arXiv:2011.09895.

[2506] D.H.F. de Souza, R. Rosenfeld, Can neutrino-assisted early dark energy models ameliorate the H0 tension in a natural way? Phys. Rev. D 108 (8) (2023) 083512, arXiv:2302.04644.

[2507] M. Carrillo González, Q. Liang, J. Sakstein, M. Trodden, Neutrino-assisted early dark energy is a natural resolution of the hubble tension, 2023, arXiv:2302.09091.

[2508] X. Li, A. Shafieloo, A simple phenomenological emergent dark energy model can resolve the hubble tension, Astrophys. J. Lett. 883 (1) (2019) L3, arXiv:1906.08275.

[2509] L.Á. García, L. Castañeda, J.M. Tejeiro, A novel early dark energy model, New Astron. 84 (2021) 101503, arXiv:2009.07357.

[2510] H.B. Benaoum, L.Á. García, L. Castañeda, Early dark energy induced by non-linear electrodynamics, 2023, arXiv:2307.05917.

[2511] X. Li, A. Shafieloo, Evidence for emergent dark energy, Astrophys. J. 902 (1) (2020) 58, arXiv:2001.05103.

[2512] S. Nojiri, S.D. Odintsov, D. Saez-Chillon Gomez, G.S. Sharov, Modeling and testing the equation of state for (Early) dark energy, Phys. Dark Univ. 32 (2021) 100837, arXiv:2103.05304.

[2513] V.I. Sabla, R.R. Caldwell, Microphysics of early dark energy, Phys. Rev. D 106 (6) (2022) 063526, arXiv:2202.08291.

[2514] H. Moshafi, H. Firouzjahi, A. Talebian, Multiple transitions in vacuum dark energy and H_0 tension, Astrophys. J. 940 (2) (2022) 121, arXiv:2208.05583.

[2515] A.J. Ross, L. Samushia, C. Howlett, W.J. Percival, A. Burden, M. Manera, The clustering of the SDSS DR7 main galaxy sample – I. A 4 per cent distance measure at $z = 0.15$, Mon. Not. R. Astron. Soc. 449 (1) (2015) 835–847, arXiv:1409.3242.

[2516] E.-M. Mueller, W. Percival, E. Linder, S. Alam, G.-B. Zhao, A.G. Sánchez, F. Beutler, J. Brinkmann, The clustering of galaxies in the completed SDSS-III Baryon Oscillation Spectroscopic Survey: constraining modified gravity, Mon. Not. R. Astron. Soc. 475 (2) (2018) 2122–2131, arXiv:1612.00812.

[2517] A.G. Riess, et al., Milky way cepheid standards for measuring cosmic distances and application to gaia DR2: Implications for the hubble constant, Astrophys. J. 861 (2) (2018) 126, arXiv:1804.10655.

[2518] S. Vagnozzi, Consistency tests of ΛCDM from the early integrated Sachs-Wolfe effect: Implications for early-time new physics and the Hubble tension, Phys. Rev. D 104 (6) (2021) 063524, arXiv:2105.10425.

[2519] G. Ye, B. Hu, Y.-S. Piao, Implication of the Hubble tension for the primordial universe in light of recent cosmological data, Phys. Rev. D 104 (6) (2021) 063510, arXiv:2103.09729.

[2520] I.d.O.C. Pedreira, M. Benetti, E.G.M. Ferreira, L.L. Graef, L. Herold, Visual tool for assessing tension-resolving models in the H0-σ8 plane, Phys. Rev. D 109 (10) (2024) 103525, arXiv:2311.04977.

[2521] BOSS Collaboration, H. Gil-Marín, et al., The clustering of galaxies in the SDSS-III Baryon Oscillation Spectroscopic Survey: RSD measurement from the LOS-dependent power spectrum of DR12 BOSS galaxies, Mon. Not. R. Astron. Soc. 460 (4) (2016) 4188–4209, arXiv:1509.06386.

[2522] BOSS Collaboration, H. Gil-Marín, et al., The clustering of galaxies in the SDSS-III Baryon Oscillation Spectroscopic Survey: BAO measurement from the LOS-dependent power spectrum of DR12 BOSS galaxies, Mon. Not. R. Astron. Soc. 460 (4) (2016) 4210–4219, arXiv:1509.06373.

[2523] eBOSS Collaboration, V. de Sainte Agathe, et al., Baryon acoustic oscillations at z=2.34 from the correlations of lyα absorption in eBOSS DR14, Astron. Astrophys. 629 (2019) A85, arXiv:1904.03400.

[2524] M.M. Ivanov, E. McDonough, J.C. Hill, M. Simonović, M.W. Toomey, S. Alexander, M. Zaldarriaga, Constraining early dark energy with large-scale structure, Phys. Rev. D 102 (10) (2020) 103502, arXiv:2006.11235.

[2525] G. D'Amico, L. Senatore, P. Zhang, H. Zheng, The hubble tension in light of the full-shape analysis of large-scale structure data, J. Cosmol. Astropart. Phys. 05 (2021) 072, arXiv:2006.12420.

[2526] F. Beutler, P. McDonald, Unified galaxy power spectrum measurements from 6dFGS, BOSS, and eBOSS, J. Cosmol. Astropart. Phys. 11 (2021) 031, arXiv:2106.06324.

[2527] D. Piras, L. Herold, L. Lucie-Smith, E. Komatsu, ΛCDM and early dark energy in latent space: A data-driven parametrization of the CMB temperature power spectrum, Phys. Rev. D 111 (8) (2025) 083537, arXiv:2502.09810.

[2528] J.C. Hill, et al., Atacama Cosmology Telescope: Constraints on prerecombination early dark energy, Phys. Rev. D 105 (12) (2022) 123536, arXiv:2109.04451.

[2529] A. La Posta, T. Louis, X. Garrido, J.C. Hill, Constraints on prerecombination early dark energy from SPT-3G public data, Phys. Rev. D 105 (8) (2022) 083519, arXiv:2112.10754.

[2530] T.L. Smith, M. Lucca, V. Poulin, G.F. Abellan, L. Balkenhol, K. Benabed, S. Galli, R. Murgia, Hints of early dark energy in Planck, SPT, and ACT data: New physics or systematics? Phys. Rev. D 106 (4) (2022) 043526, arXiv:2202.09379.

[2531] J.-Q. Jiang, Y.-S. Piao, Toward early dark energy and ns=1 with Planck, ACT, and SPT observations, Phys. Rev. D 105 (10) (2022) 103514, arXiv:2202.13379.

[2532] G. Benevento, W. Hu, M. Raveri, Can late dark energy transitions raise the hubble constant? Phys. Rev. D 101 (10) (2020) 103517, arXiv:2002.11707.

[2533] D. Camarena, V. Marra, On the use of the local prior on the absolute magnitude of type Ia supernovae in cosmological inference, Mon. Not. R. Astron. Soc. 504 (2021) 5164–5171, arXiv:2101.08641.

[2534] G. Efstathiou, To H0 or not to H0? Mon. Not. R. Astron. Soc. 505 (3) (2021) 3866–3872, arXiv:2103.08723.

[2535] G. Efstathiou, S. Gratton, A detailed description of the CamSpec likelihood pipeline and a reanalysis of the Planck high frequency maps, 2019, arXiv:1910.00483.

[2536] Planck Collaboration, Y. Akrami, et al., Planck intermediate results. VII. Joint Planck LFI and HFI data processing, Astron. Astrophys. 643 (2020) A42, arXiv:2007.04997.

[2537] J.-Q. Jiang, G. Ye, Y.-S. Piao, Impact of the Hubble tension on the r- n_s contour, Phys. Lett. B 851 (2024) 138588, arXiv:2303.12345.

[2538] W. Liu, H. Zhan, Y. Gong, X. Wang, Can early dark energy be probed by the high-redshift galaxy abundance? Mon. Not. R. Astron. Soc. 533 (1) (2024) 860–871, arXiv:2402.14339.

[2539] M. Boylan-Kolchin, D.R. Weisz, Uncertain times: the redshift–time relation from cosmology and stars, Mon. Not. R. Astron. Soc. 505 (2) (2021) 2764–2783, arXiv:2103.15825.

[2540] P. Diego-Palazuelos, et al., Cosmic birefringence from Planck public release 4, in: 56th Rencontres de Moriond on Cosmology, 2022, arXiv:2203.04830.

[2541] K. Murai, F. Naokawa, T. Namikawa, E. Komatsu, Isotropic cosmic birefringence from early dark energy, Phys. Rev. D 107 (4) (2023) L041302, arXiv:2209.07804.

[2542] J.R. Eskilt, L. Herold, E. Komatsu, K. Murai, T. Namikawa, F. Naokawa, Constraints on early dark energy from isotropic cosmic birefringence, Phys. Rev. Lett. 131 (12) (2023) 121001, arXiv:2303.15369.

[2543] L. Yin, J. Kochappan, T. Ghosh, B.-H. Lee, Is cosmic birefringence model-dependent? J. Cosmol. Astropart. Phys. 10 (2023) 007, arXiv:2305.07937.

[2544] L. Hart, J. Chluba, Using the cosmological recombination radiation to probe early dark energy and fundamental constant variations, Mon. Not. R. Astron. Soc. 519 (3) (2023) 3664–3680, arXiv:2209.12290.

[2545] T. Rudelius, Constraints on early dark energy from the axion weak gravity conjecture, J. Cosmol. Astropart. Phys. 01 (2023) 014, arXiv:2203.05575.

[2546] A. Hebecker, P. Mangat, S. Theisen, L.T. Witkowski, Can gravitational instantons really constrain axion inflation? JHEP 02 (2017) 097, arXiv:1607.06814.

[2547] B. Heidenreich, M. Reece, T. Rudelius, Sharpening the weak gravity conjecture with dimensional reduction, JHEP 02 (2016) 140, arXiv:1509.06374.

[2548] J.-Q. Jiang, G. Ye, Y.-S. Piao, Return of Harrison–Zeldovich spectrum in light of recent cosmological tensions, Mon. Not. R. Astron. Soc. 527 (1) (2023) L54–L59, arXiv:2210.06125.

[2549] Z.-Y. Peng, Y.-S. Piao, Testing the ns-H0 scaling relation with Planck-independent CMB data, Phys. Rev. D 109 (2) (2024) 023519, arXiv:2308.01012.

[2550] H. Wang, G. Ye, J.-Q. Jiang, Y.-S. Piao, Towards primordial gravitational waves and $n_s = 1$ in light of BICEP/Keck, DESI BAO and Hubble tension, 2024, arXiv:2409.17879.

[2551] R. Kallosh, A. Linde, Hybrid cosmological attractors, Phys. Rev. D 106 (2) (2022) 023522, arXiv:2204.02425.

[2552] G. Ye, J.-Q. Jiang, Y.-S. Piao, Toward inflation with ns=1 in light of the Hubble tension and implications for primordial gravitational waves, Phys. Rev. D 106 (10) (2022) 103528, arXiv:2205.02478.

[2553] F. Niedermann, M.S. Sloth, New early dark energy as a solution to the H_0 and S_8 tensions, 2023, arXiv:2307.03481.

[2554] F. Niedermann, M.S. Sloth, New early dark energy, Phys. Rev. D 103 (4) (2021) L041303, arXiv:1910.10739.

[2555] K. Freese, M.W. Winkler, Chain early dark energy: A proposal for solving the Hubble tension and explaining today's dark energy, Phys. Rev. D 104 (8) (2021) 083533, arXiv:2102.13655.

[2556] J.S. Cruz, F. Niedermann, M.S. Sloth, Cold new early dark energy pulls the trigger on the H $_0$ and S $_8$ tensions: a simultaneous solution to both tensions without new ingredients, J. Cosmol. Astropart. Phys. 11 (2023) 033, arXiv:2305.08895.

[2557] F. Niedermann, M.S. Sloth, New early dark energy is compatible with current LSS data, Phys. Rev. D 103 (10) (2021) 103537, arXiv:2009.00006.

[2558] B.S. Haridasu, H. Khoraminezhad, M. Viel, Scrutinizing early dark energy models through CMB lensing, 2022, arXiv:2212.09136.

[2559] J.S. Cruz, F. Niedermann, M.S. Sloth, A grounded perspective on new early dark energy using ACT, SPT, and BICEP/Keck, J. Cosmol. Astropart. Phys. 02 (2023) 041, arXiv:2209.02708.

[2560] I.J. Allali, M.P. Hertzberg, F. Rompineve, Dark sector to restore cosmological concordance, Phys. Rev. D 104 (8) (2021) L081303, arXiv:2104.12798.

[2561] D. Aloni, A. Berlin, M. Joseph, M. Schmaltz, N. Weiner, A step in understanding the Hubble tension, Phys. Rev. D 105 (12) (2022) 123516, arXiv:2111.00014.

[2562] F. Niedermann, M.S. Sloth, Hot new early dark energy, Phys. Rev. D 105 (6) (2022) 063509, arXiv:2112.00770.

[2563] F. Niedermann, M.S. Sloth, Hot new early dark energy: Towards a unified dark sector of neutrinos, dark energy and dark matter, Phys. Lett. B 835 (2022) 137555, arXiv:2112.00759.

[2564] M. Garny, F. Niedermann, H. Rubira, M.S. Sloth, Hot new early dark energy bridging cosmic gaps: Supercooled phase transition reconciles stepped dark radiation solutions to the Hubble tension with BBN, Phys. Rev. D 110 (2) (2024) 023531, arXiv:2404.07256.

[2565] N. Schöneberg, G. Franco Abellán, A step in the right direction? Analyzing the Wess Zumino Dark Radiation solution to the Hubble tension, J. Cosmol. Astropart. Phys. 12 (2022) 001, arXiv:2206.11276.

[2566] A. Berlin, N. Blinov, Thermal dark matter below an MeV, Phys. Rev. Lett. 120 (2) (2018) 021801, arXiv:1706.07046.

[2567] M. Berbig, S. Jana, A. Trautner, The Hubble tension and a renormalizable model of gauged neutrino self-interactions, Phys. Rev. D 102 (11) (2020) 115008, arXiv:2004.13039.

[2568] M. Escudero, T. Schwetz, J. Terol-Calvo, A seesaw model for large neutrino masses in concordance with cosmology, JHEP 02 (2023) 142, arXiv:2211.01729;
Addendum:, JHEP 06 (2024) 119.

[2569] D. Aloni, M. Joseph, M. Schmaltz, N. Weiner, Dark radiation from neutrino mixing after big bang nucleosynthesis, Phys. Rev. Lett. 131 (22) (2023) 221001, arXiv:2301.10792.

[2570] W. Fischler, J. Meyers, Dark radiation emerging after big bang nucleosynthesis? Phys. Rev. D 83 (2011) 063520, arXiv:1011.3501.

[2571] D. Hooper, F.S. Queiroz, N.Y. Gnedin, Non-thermal dark matter mimicking an additional neutrino species in the early universe, Phys. Rev. D 85 (2012) 063513, arXiv:1111.6599.

[2572] O.E. Bjaelde, S. Das, A. Moss, Origin of delta N_eff as a result of an interaction between dark radiation and dark matter, J. Cosmol. Astropart. Phys. 10 (2012) 017, arXiv:1205.0553.

[2573] K. Choi, K.-Y. Choi, C.S. Shin, Dark radiation and small-scale structure problems with decaying particles, Phys. Rev. D 86 (2012) 083529, arXiv:1208.2496.

[2574] A. Nygaard, E.B. Holm, T. Tram, S. Hannestad, Decaying dark matter and the hubble tension, 2023, arXiv:2307.00418.

[2575] S. Gariazzo, O. Mena, On the dark radiation role in the Hubble constant tension, 2023, arXiv:2306.15067.

[2576] G. Steigman, D.N. Schramm, J.E. Gunn, Cosmological limits to the number of massive leptons, Phys. Lett. B 66 (1977) 202–204.

[2577] M. Archidiacono, E. Giusarma, S. Hannestad, O. Mena, Cosmic dark radiation and neutrinos, Adv. High Energy Phys. 2013 (2013) 191047, arXiv:1307.0637.

[2578] M. Archidiacono, S. Gariazzo, Two sides of the same coin: Sterile neutrinos and dark radiation, status and perspectives, Universe 8 (3) (2022) 175, arXiv:2201.10319.

[2579] K. Akita, M. Yamaguchi, A precision calculation of relic neutrino decoupling, J. Cosmol. Astropart. Phys. 08 (2020) 012, arXiv:2005.07047.

[2580] J. Froustey, C. Pitrou, M.C. Volpe, Neutrino decoupling including flavour oscillations and primordial nucleosynthesis, J. Cosmol. Astropart. Phys. 12 (2020) 015, arXiv:2008.01074.

[2581] J.J. Bennett, G. Buldgen, P.F. De Salas, M. Drewes, S. Gariazzo, S. Pastor, Y.Y.Y. Wong, Towards a precision calculation of $N_{\rm eff}$ in the standard model II: Neutrino decoupling in the presence of flavour oscillations and finite-temperature QED, J. Cosmol. Astropart. Phys. 04 (2021) 073, arXiv:2012.02726.

[2582] M. Drewes, Y. Georis, M. Klasen, L.P. Wiggering, Y.Y.Y. Wong, Towards a precision calculation of N $_{eff}$ in the standard model. Part III. Improved estimate of NLO contributions to the collision integral, J. Cosmol. Astropart. Phys. 06 (2024) 032, arXiv:2402.18481.

[2583] L. García, J. Tejeiro, L. Castañeda, Primordial nucleosynthesis in the presence of sterile neutrinos, in: A. Bracco, E. Nappi (Eds.), Proc. Int. Sch. Phys. Fermi 178 (2011) 309–316.

[2584] L.A. Anchordoqui, H. Goldberg, Neutrino cosmology after WMAP 7-year data and LHC first Z' bounds, Phys. Rev. Lett. 108 (2012) 081805, arXiv:1111.7264.

[2585] L.A. Anchordoqui, H. Goldberg, G. Steigman, Right-handed neutrinos as the dark radiation: Status and forecasts for the LHC, Phys. Lett. B 718 (2013) 1162–1165, arXiv:1211.0186.

[2586] T.D. Jacques, L.M. Krauss, C. Lunardini, Additional light sterile neutrinos and cosmology, Phys. Rev. D 87 (8) (2013) 083515, arXiv:1301.3119;
Erratum:, Phys. Rev. D 88 (2013) 109901.

[2587] S. Roy Choudhury, S. Choubey, Constraining light sterile neutrino mass with the BICEP2/Keck array 2014 B-mode polarization data, Eur. Phys. J. C 79 (7) (2019) 557, arXiv:1807.10294.

[2588] S. Weinberg, Goldstone Bosons as fractional cosmic neutrinos, Phys. Rev. Lett. 110 (24) (2013) 241301, arXiv:1305.1971.

[2589] W. Lin, L. Visinelli, D. Xu, T.T. Yanagida, Neutrino astronomy as a probe of physics beyond the standard model: Decay of sub-MeV B-L gauge boson dark matter, Phys. Rev. D 106 (7) (2022) 075011, arXiv:2202.04496.

[2590] P. Arias, D. Cadamuro, M. Goodsell, J. Jaeckel, J. Redondo, A. Ringwald, WISPy cold dark matter, J. Cosmol. Astropart. Phys. 06 (2012) 013, arXiv:1201.5902.

[2591] D.J.E. Marsh, Axion cosmology, Phys. Rep. 643 (2016) 1–79, arXiv:1510.07633.

[2592] D. Baumann, D. Green, B. Wallisch, New target for cosmic axion searches, Phys. Rev. Lett. 117 (17) (2016) 171301, arXiv:1604.08614.

[2593] F. D'Eramo, R.Z. Ferreira, A. Notari, J.L. Bernal, Hot axions and the H_0 tension, J. Cosmol. Astropart. Phys. 11 (2018) 014, arXiv:1808.07430.

[2594] E.G.M. Ferreira, Ultra-light dark matter, Astron. Astrophys. Rev. 29 (1) (2021) 7, arXiv:2005.03254.

[2595] Y.K. Semertzidis, S. Youn, Axion dark matter: How to see it? Sci. Adv. 8 (8) (2022) abm9928, arXiv:2104.14831.

[2596] F. Chadha-Day, J. Ellis, D.J.E. Marsh, Axion dark matter: What is it and why now? Sci. Adv. 8 (8) (2022) abj3618, arXiv:2105.01406.

[2597] D. Green, Y. Guo, B. Wallisch, Cosmological implications of axion-matter couplings, J. Cosmol. Astropart. Phys. 02 (02) (2022) 019, arXiv:2109.12088.

[2598] C.A.J. O'Hare, Cosmology of axion dark matter, PoS COSMICWISPers (2024) 040, arXiv:2403.17697.

[2599] L. Caloni, M. Gerbino, M. Lattanzi, L. Visinelli, Novel cosmological bounds on thermally-produced axion-like particles, J. Cosmol. Astropart. Phys. 09 (2022) 021, arXiv:2205.01637.

[2600] F. D'Eramo, E. Di Valentino, W. Giarè, F. Hajkarim, A. Melchiorri, O. Mena, F. Renzi, S. Yun, Cosmological bound on the QCD axion mass, redux, J. Cosmol. Astropart. Phys. 09 (2022) 022, arXiv:2205.07849.

[2601] J.M. Cline, Z. Liu, W. Xue, Millicharged atomic dark matter, Phys. Rev. D 85 (2012) 101302, arXiv:1201.4858.

[2602] J. Fan, A. Katz, L. Randall, M. Reece, Double-disk dark matter, Phys. Dark Univ. 2 (2013) 139–156, arXiv:1303.1521.

[2603] H. Vogel, J. Redondo, Dark radiation constraints on minicharged particles in models with a hidden photon, J. Cosmol. Astropart. Phys. 02 (2014) 029, arXiv:1311.2600.

[2604] K. Petraki, L. Pearce, A. Kusenko, Self-interacting asymmetric dark matter coupled to a light massive dark photon, J. Cosmol. Astropart. Phys. 07 (2014) 039, arXiv:1403.1077.

[2605] R. Foot, S. Vagnozzi, Dissipative hidden sector dark matter, Phys. Rev. D 91 (2015) 023512, arXiv:1409.7174.

[2606] R. Foot, S. Vagnozzi, Diurnal modulation signal from dissipative hidden sector dark matter, Phys. Lett. B 748 (2015) 61–66, arXiv:1412.0762.

[2607] R. Foot, S. Vagnozzi, Solving the small-scale structure puzzles with dissipative dark matter, J. Cosmol. Astropart. Phys. 07 (2016) 013, arXiv:1602.02467.

[2608] V.V. Flambaum, I.B. Samsonov, Ultralight dark photon as a model for early universe dark matter, Phys. Rev. D 100 (6) (2019) 063541, arXiv:1908.09432.

[2609] L.A. Anchordoqui, S.E. Perez Bergliaffa, Hot thermal universe endowed with massive dark vector fields and the hubble tension, Phys. Rev. D 100 (12) (2019) 123525, arXiv:1910.05860.

[2610] G. Steigman, Equivalent neutrinos, light WIMPs, and the chimera of dark radiation, Phys. Rev. D 87 (10) (2013) 103517, arXiv:1303.0049.

[2611] C. Brust, D.E. Kaplan, M.T. Walters, New light species and the CMB, JHEP 12 (2013) 058, arXiv:1303.5379.

[2612] R.C. Nunes, A. Bonilla, Probing the properties of relic neutrinos using the cosmic microwave background, the Hubble Space Telescope and galaxy clusters, Mon. Not. R. Astron. Soc. 473 (4) (2018) 4404–4409, arXiv:1710.10264.

[2613] A. Bonilla, R.C. Nunes, E.M.C. Abreu, Forecast on lepton asymmetry from future CMB experiments, Mon. Not. R. Astron. Soc. 485 (2) (2019) 2486–2491, arXiv:1810.06356.

[2614] NANOGrav Collaboration, Z. Arzoumanian, et al., The NANOGrav 12.5 yr data set: Search for an isotropic stochastic gravitational-wave background, Astrophys. J. Lett. 905 (2) (2020) L34, arXiv:2009.04496.

[2615] B. Goncharov, et al., On the evidence for a common-spectrum process in the search for the nanohertz gravitational-wave background with the parkes pulsar timing array, Astrophys. J. Lett. 917 (2) (2021) L19, arXiv:2107.12112.

[2616] EPTA Collaboration, S. Chen, et al., Common-red-signal analysis with 24-yr high-precision timing of the European Pulsar Timing Array: inferences in the stochastic gravitational-wave background search, Mon. Not. R. Astron. Soc. 508 (4) (2021) 4970–4993, arXiv:2110.13184.

[2617] J. Antoniadis, et al., The International Pulsar Timing Array second data release: Search for an isotropic gravitational wave background, Mon. Not. R. Astron. Soc. 510 (4) (2022) 4873–4887, arXiv:2201.03980.

[2618] B. Allen, J.D. Romano, Detecting a stochastic background of gravitational radiation: Signal processing strategies and sensitivities, Phys. Rev. D 59 (1999) 102001, arXiv:gr-qc/9710117.

[2619] T.L. Smith, E. Pierpaoli, M. Kamionkowski, A new cosmic microwave background constraint to primordial gravitational waves, Phys. Rev. Lett. 97 (2006) 021301, arXiv:astro-ph/0603144.

[2620] L.A. Boyle, A. Buonanno, Relating gravitational wave constraints from primordial nucleosynthesis, pulsar timing, laser interferometers, and the CMB: Implications for the early Universe, Phys. Rev. D 78 (2008) 043531, arXiv:0708.2279.

[2621] S. Kuroyanagi, T. Takahashi, S. Yokoyama, Blue-tilted tensor spectrum and thermal history of the universe, J. Cosmol. Astropart. Phys. 02 (2015) 003, arXiv:1407.4785.

[2622] G. Cabass, L. Pagano, L. Salvati, M. Gerbino, E. Giusarma, A. Melchiorri, Updated constraints and forecasts on primordial tensor modes, Phys. Rev. D 93 (6) (2016) 063508, arXiv:1511.05146.

[2623] I. Ben-Dayan, B. Keating, D. Leon, I. Wolfson, Constraints on scalar and tensor spectra from N_{eff}, J. Cosmol. Astropart. Phys. 06 (2019) 007, arXiv:1903.11843.

[2624] M. Aich, Y.-Z. Ma, W.-M. Dai, J.-Q. Xia, How much primordial tensor mode is allowed? Phys. Rev. D 101 (6) (2020) 063536, arXiv:1912.00995.

[2625] W. Giarè, M. Forconi, E. Di Valentino, A. Melchiorri, Towards a reliable calculation of relic radiation from primordial gravitational waves, Mon. Not. R. Astron. Soc. 520 (2023) 2, arXiv:2210.14159.

[2626] NANOGrav Collaboration, A. Afzal, et al., The NANOGrav 15 yr data set: Search for signals from new physics, Astrophys. J. Lett. 951 (1) (2023) L11, arXiv:2306.16219;
Erratum:, Astrophys. J. Lett. 971 (2024) L27;
Erratum:, Astrophys. J. 971 (2024) L27.

[2627] M. Benetti, L.L. Graef, S. Vagnozzi, Primordial gravitational waves from NANOGrav: A broken power-law approach, Phys. Rev. D 105 (4) (2022) 043520, arXiv:2111.04758.

[2628] S. Vagnozzi, Inflationary interpretation of the stochastic gravitational wave background signal detected by pulsar timing array experiments, JHEAp 39 (2023) 81–98, arXiv:2306.16912.

[2629] M. Kawasaki, K. Kohri, N. Sugiyama, Cosmological constraints on late time entropy production, Phys. Rev. Lett. 82 (1999) 4168, arXiv:astro-ph/9811437.

[2630] G. Gelmini, S. Palomares-Ruiz, S. Pascoli, Low reheating temperature and the visible sterile neutrino, Phys. Rev. Lett. 93 (2004) 081302, arXiv:astro-ph/0403323.

[2631] P.F. de Salas, M. Lattanzi, G. Mangano, G. Miele, S. Pastor, O. Pisanti, Bounds on very low reheating scenarios after Planck, Phys. Rev. D 92 (12) (2015) 123534, arXiv:1511.00672.

[2632] M. Gerbino, K. Freese, S. Vagnozzi, M. Lattanzi, O. Mena, E. Giusarma, S. Ho, Impact of neutrino properties on the estimation of inflationary parameters from current and future observations, Phys. Rev. D 95 (4) (2017) 043512, arXiv:1610.08830.

[2633] Z. Hou, R. Keisler, L. Knox, M. Millea, C. Reichardt, How massless neutrinos affect the cosmic microwave background damping tail, Phys. Rev. D 87 (2013) 083008, arXiv:1104.2333.

[2634] D. Baumann, Primordial cosmology, PoS TASI2017 (2018) 009, arXiv:1807.03098.

[2635] S. Vagnozzi, Cosmological searches for the neutrino mass scale and mass ordering, 2019, arXiv:1907.08010.

[2636] E. Di Valentino, A. Melchiorri, J. Silk, Reconciling Planck with the local value of H_0 in extended parameter space, Phys. Lett. B 761 (2016) 242–246, arXiv:1606.00634.

[2637] S. Vagnozzi, New physics in light of the H_0 tension: An alternative view, Phys. Rev. D 102 (2) (2020) 023518, arXiv:1907.07569.

[2638] S. Bashinsky, U. Seljak, Neutrino perturbations in CMB anisotropy and matter clustering, Phys. Rev. D 69 (2004) 083002, arXiv:astro-ph/0310198.

[2639] B. Follin, L. Knox, M. Millea, Z. Pan, First detection of the acoustic oscillation phase shift expected from the cosmic neutrino background, Phys. Rev. Lett. 115 (9) (2015) 091301, arXiv:1503.07863.

[2640] E. Di Valentino, A. Melchiorri, J. Silk, Cosmological constraints in extended parameter space from the Planck 2018 Legacy release, J. Cosmol. Astropart. Phys. 01 (2020) 013, arXiv:1908.01391.

[2641] O. Seto, Y. Toda, Comparing early dark energy and extra radiation solutions to the hubble tension with BBN, Phys. Rev. D 103 (12) (2021) 123501, arXiv:2101.03740.

[2642] S. Hagstotz, P.F. de Salas, S. Gariazzo, M. Gerbino, M. Lattanzi, S. Vagnozzi, K. Freese, S. Pastor, Bounds on light sterile neutrino mass and mixing from cosmology and laboratory searches, Phys. Rev. D 104 (12) (2021) 123524, arXiv:2003.02289.

[2643] G. Barenboim, W.H. Kinney, W.-I. Park, Flavor versus mass eigenstates in neutrino asymmetries: implications for cosmology, Eur. Phys. J. C 77 (9) (2017) 590, arXiv:1609.03200.

[2644] O. Seto, Y. Toda, Hubble tension in lepton asymmetric cosmology with an extra radiation, Phys. Rev. D 104 (6) (2021) 063019, arXiv:2104.04381.

[2645] D. Baumann, D. Green, J. Meyers, B. Wallisch, Phases of new physics in the CMB, J. Cosmol. Astropart. Phys. 01 (2016) 007, arXiv:1508.06342.

[2646] N. Blinov, G. Marques-Tavares, Interacting radiation after Planck and its implications for the hubble tension, J. Cosmol. Astropart. Phys. 09 (2020) 029, arXiv:2003.08387.

[2647] D.E. Kaplan, G.Z. Krnjaic, K.R. Rehermann, C.M. Wells, Atomic dark matter, J. Cosmol. Astropart. Phys. 05 (2010) 021, arXiv:0909.0753.

[2648] F.-Y. Cyr-Racine, K. Sigurdson, Cosmology of atomic dark matter, Phys. Rev. D 87 (10) (2013) 103515, arXiv:1209.5752.

[2649] S. Bansal, J. Barron, D. Curtin, Y. Tsai, Precision cosmological constraints on atomic dark matter, JHEP 10 (2023) 095, arXiv:2212.02487.

[2650] Z. Chacko, D. Curtin, M. Geller, Y. Tsai, Cosmological signatures of a mirror twin higgs, JHEP 09 (2018) 163, arXiv:1803.03263.

[2651] F.-Y. Cyr-Racine, K. Sigurdson, Limits on neutrino-neutrino scattering in the early universe, Phys. Rev. D 90 (12) (2014) 123533, arXiv:1306.1536.

[2652] M. Archidiacono, S. Hannestad, Updated constraints on non-standard neutrino interactions from Planck, J. Cosmol. Astropart. Phys. 07 (2014) 046, arXiv:1311.3873.

[2653] L. Lancaster, F.-Y. Cyr-Racine, L. Knox, Z. Pan, A tale of two modes: Neutrino free-streaming in the early universe, J. Cosmol. Astropart. Phys. 07 (2017) 033, arXiv:1704.06657.

[2654] I.M. Oldengott, T. Tram, C. Rampf, Y.Y.Y. Wong, Interacting neutrinos in cosmology: exact description and constraints, J. Cosmol. Astropart. Phys. 11 (2017) 027, arXiv:1706.02123.

[2655] G. Barenboim, P.B. Denton, I.M. Oldengott, Constraints on inflation with an extended neutrino sector, Phys. Rev. D 99 (8) (2019) 083515, arXiv:1903.02036.

[2656] A. Das, S. Ghosh, Flavor-specific interaction favors strong neutrino self-coupling in the early universe, J. Cosmol. Astropart. Phys. 07 (2021) 038, arXiv:2011.12315.

[2657] S. Roy Choudhury, S. Hannestad, T. Tram, Updated constraints on massive neutrino self-interactions from cosmology in light of the H_0 tension, J. Cosmol. Astropart. Phys. 03 (2021) 084, arXiv:2012.07519.

[2658] T. Brinckmann, J.H. Chang, M. LoVerde, Self-interacting neutrinos, the Hubble parameter tension, and the cosmic microwave background, Phys. Rev. D 104 (6) (2021) 063523, arXiv:2012.11830.

[2659] S. Roy Choudhury, S. Hannestad, T. Tram, Massive neutrino self-interactions and inflation, J. Cosmol. Astropart. Phys. 10 (2022) 018, arXiv:2207.07142.

[2660] A. Das, S. Ghosh, The magnificent ACT of flavor-specific neutrino self-interaction, J. Cosmol. Astropart. Phys. 09 (2023) 042, arXiv:2303.08843.

[2661] D. Camarena, F.-Y. Cyr-Racine, J. Houghteling, Confronting self-interacting neutrinos with the full shape of the galaxy power spectrum, Phys. Rev. D 108 (10) (2023) 103535, arXiv:2309.03941.

[2662] A. He, R. An, M.M. Ivanov, V. Gluscevic, Self-interacting neutrinos in light of large-scale structure data, Phys. Rev. D 109 (10) (2024) 103527, arXiv:2309.03956.

[2663] N. Bostan, S. Roy Choudhury, First constraints on non-minimally coupled Natural and Coleman-Weinberg inflation and massive neutrino self-interactions with Planck+BICEP/Keck, J. Cosmol. Astropart. Phys. 07 (2024) 032, arXiv:2310.01491.

[2664] N. Blinov, K.J. Kelly, G.Z. Krnjaic, S.D. McDermott, Constraining the self-interacting neutrino interpretation of the hubble tension, Phys. Rev. Lett. 123 (19) (2019) 191102, arXiv:1905.02727.

[2665] S.S. da Costa, D.R. da Silva, Á.S. de Jesus, N. Pinto-Neto, F.S. Queiroz, The H_0 trouble: confronting non-thermal dark matter and phantom cosmology with the CMB, BAO, and type Ia supernovae data, J. Cosmol. Astropart. Phys. 04 (2024) 035, arXiv:2311.07420.

[2666] M. Escudero, S.J. Witte, A CMB search for the neutrino mass mechanism and its relation to the Hubble tension, Eur. Phys. J. C 80 (4) (2020) 294, arXiv:1909.04044.

[2667] G. Barenboim, U. Nierste, Modified majoron model for cosmological anomalies, Phys. Rev. D 104 (2) (2021) 023013, arXiv:2005.13280.

[2668] M. Escudero, S.J. Witte, The hubble tension as a hint of leptogenesis and neutrino mass generation, Eur. Phys. J. C 81 (6) (2021) 515, arXiv:2103.03249.

[2669] M. Archidiacono, S. Hannestad, R.S. Hansen, T. Tram, Cosmology with self-interacting sterile neutrinos and dark matter - A pseudoscalar model, Phys. Rev. D 91 (6) (2015) 065021, arXiv:1404.5915.

[2670] F. Forastieri, M. Lattanzi, G. Mangano, A. Mirizzi, P. Natoli, N. Saviano, Cosmic microwave background constraints on secret interactions among sterile neutrinos, J. Cosmol. Astropart. Phys. 07 (2017) 038, arXiv:1704.00626.

[2671] M. Archidiacono, S. Gariazzo, C. Giunti, S. Hannestad, T. Tram, Sterile neutrino self-interactions: H_0 tension and short-baseline anomalies, J. Cosmol. Astropart. Phys. 12 (2020) 029, arXiv:2006.12885.

[2672] M.A. Corona, R. Murgia, M. Cadeddu, M. Archidiacono, S. Gariazzo, C. Giunti, S. Hannestad, Pseudoscalar sterile neutrino self-interactions in light of Planck, SPT and ACT data, J. Cosmol. Astropart. Phys. 06 (06) (2022) 010, arXiv:2112.00037.

[2673] M. Joseph, D. Aloni, M. Schmaltz, E.N. Sivarajan, N. Weiner, A step in understanding the S8 tension, Phys. Rev. D 108 (2) (2023) 023520, arXiv:2207.03500.

[2674] H. Bagherian, M. Joseph, M. Schmaltz, E.N. Sivarajan, Confronting interacting radiation models for the Hubble tension with Lyman-α data, Phys. Rev. D 111 (4) (2025) 043513, arXiv:2405.17554.

[2675] W. Cho, K.-Y. Choi, S. Mahapatra, Reconciling cosmological tensions with inelastic dark matter and dark radiation in a U(1)D framework, J. Cosmol. Astropart. Phys. 09 (2024) 065, arXiv:2408.03004.

[2676] W. Yang, E. Di Valentino, S. Pan, Y. Wu, J. Lu, Dynamical dark energy after Planck CMB final release and H_0 tension, Mon. Not. R. Astron. Soc. 501 (4) (2021) 5845–5858, arXiv:2101.02168.

[2677] F. Dong, C. Park, S.E. Hong, J. Kim, H. Seong Hwang, H. Park, S. Appleby, Tomographic Alcock–Paczyński test with Redshift-space correlation function: Evidence for the dark energy equation-of-state parameter w > −1, Astrophys. J. 953 (1) (2023) 98, arXiv:2305.00206.

[2678] M. Najafi, S. Pan, E. Di Valentino, J.T. Firouzjaee, Dynamical dark energy confronted with multiple CMB missions, Phys. Dark Univ. 45 (2024) 101539, arXiv:2407.14939.

[2679] S. Vagnozzi, L. Visinelli, O. Mena, D.F. Mota, Do we have any hope of detecting scattering between dark energy and baryons through cosmology? Mon. Not. R. Astron. Soc. 493 (1) (2020) 1139–1152, arXiv:1911.12374.

[2680] G. Alestas, L. Kazantzidis, L. Perivolaropoulos, $w - M$ phantom transition at z_t <0.1 as a resolution of the Hubble tension, Phys. Rev. D 103 (8) (2021) 083517, arXiv:2012.13932.

[2681] W. Yang, S. Pan, E. Di Valentino, E.N. Saridakis, S. Chakraborty, Observational constraints on one-parameter dynamical dark-energy parametrizations and the H_0 tension, Phys. Rev. D 99 (4) (2019) 043543, arXiv:1810.05141.

[2682] V. Marra, L. Perivolaropoulos, Rapid transition of Geff at zt≃0.01 as a possible solution of the Hubble and growth tensions, Phys. Rev. D 104 (2) (2021) L021303, arXiv:2102.06012.

[2683] G. Alestas, D. Camarena, E. Di Valentino, L. Kazantzidis, V. Marra, S. Nesseris, L. Perivolaropoulos, Late-transition versus smooth $H(z)$-deformation models for the resolution of the Hubble crisis, Phys. Rev. D 105 (6) (2022) 063538, arXiv:2110.04336.

[2684] G. Alestas, L. Perivolaropoulos, Late-time approaches to the Hubble tension deforming H(z), worsen the growth tension, Mon. Not. R. Astron. Soc. 504 (3) (2021) 3956–3962, arXiv:2103.04045.

[2685] L. Heisenberg, H. Villarrubia-Rojo, J. Zosso, Can late-time extensions solve the H0 and σ8 tensions? Phys. Rev. D 106 (4) (2022) 043503, arXiv:2202.01202.

[2686] E. Frion, D. Camarena, L. Giani, T. Miranda, D. Bertacca, V. Marra, O.F. Piattella, Bayesian analysis of a Unified Dark Matter model with transition: can it alleviate the H_0 tension? Open J. Astrophys. 7 (2024) arXiv:2307.06320.

[2687] S. Kumar, R.C. Nunes, S. Pan, P. Yadav, New late-time constraints on f(R) gravity, Phys. Dark Univ. 42 (2023) 101281, arXiv:2301.07897.

[2688] S. Capozziello, G. Sarracino, G. De Somma, A critical discussion on the H_0 tension, Universe 10 (3) (2024) 140, arXiv:2403.12796.

[2689] D. Bousis, L. Perivolaropoulos, Hubble tension tomography: BAO vs SN Ia distance tension, Phys. Rev. D 110 (10) (2024) 103546, arXiv:2405.07039.

[2690] G. Alestas, L. Kazantzidis, L. Perivolaropoulos, H_0 tension, phantom dark energy, and cosmological parameter degeneracies, Phys. Rev. D 101 (12) (2020) 123516, arXiv:2004.08363.

[2691] R. Briffa, C. Escamilla-Rivera, J. Said Levi, J. Mifsud, N.L. Pullicino, Impact of H_0 priors on $f(T)$ late time cosmology, Eur. Phys. J. Plus 137 (5) (2022) 532, arXiv:2108.03853.

[2692] J. Levi Said, J. Mifsud, J. Sultana, K.Z. Adami, Reconstructing teleparallel gravity with cosmic structure growth and expansion rate data, J. Cosmol. Astropart. Phys. 06 (2021) 015, arXiv:2103.05021.

[2693] A. Theodoropoulos, L. Perivolaropoulos, The Hubble tension, the M crisis of late time H(z) deformation models and the reconstruction of quintessence Lagrangians, Universe 7 (8) (2021) 300, arXiv:2109.06256.

[2694] G. Alestas, L. Perivolaropoulos, K. Tanidis, Constraining a late time transition of G_{eff} using low-z galaxy survey data, Phys. Rev. D 106 (2) (2022) 023526, arXiv:2201.05846.

[2695] L. Perivolaropoulos, F. Skara, Gravitational transitions via the explicitly broken symmetron screening mechanism, Phys. Rev. D 106 (4) (2022) 043528, arXiv:2203.10374.

[2696] E.A. Paraskevas, A. Cam, L. Perivolaropoulos, O. Akarsu, Transition dynamics in the ΛsCDM model: Implications for bound cosmic structures, Phys. Rev. D 109 (10) (2024) 103522, arXiv:2402.05908.

[2697] E.A. Paraskevas, L. Perivolaropoulos, Effects of a late gravitational transition on gravitational waves and anticipated constraints, Universe 9 (7) (2023) 317, arXiv:2307.00298.

[2698] L. Perivolaropoulos, F. Skara, A reanalysis of the latest SH0ES data for H_0: Effects of new degrees of freedom on the Hubble tension, Universe 8 (10) (2022) 502, arXiv:2208.11169.

[2699] L. Perivolaropoulos, Is the Hubble crisis connected with the extinction of dinosaurs? Universe 8 (5) (2022) 263, arXiv:2201.08997.

[2700] Ö. Akarsu, J.D. Barrow, L.A. Escamilla, J.A. Vazquez, Graduated dark energy: Observational hints of a spontaneous sign switch in the cosmological constant, Phys. Rev. D 101 (6) (2020) 063528, arXiv:1912.08751.

[2701] L.A. Anchordoqui, I. Antoniadis, D. Lust, N.T. Noble, J.F. Soriano, From infinite to infinitesimal: Using the Universe as a dataset to probe Casimir corrections to the vacuum energy from fields inhabiting the dark dimension, Phys. Dark Univ. 46 (2024) 101715, arXiv:2404.17334.

[2702] A. De Felice, S. Kumar, S. Mukohyama, R.C. Nunes, Observational bounds on extended minimal theories of massive gravity: new limits on the graviton mass, J. Cosmol. Astropart. Phys. 04 (2024) 013, arXiv:2311.10530.

[2703] G. 't Hooft, Dimensional reduction in quantum gravity, Conf. Proc. C 930308 (1993) 284–296, arXiv:gr-qc/9310026.

[2704] L. Susskind, The world as a hologram, J. Math. Phys. 36 (1995) 6377–6396, arXiv:hep-th/9409089.

[2705] R. Bousso, A covariant entropy conjecture, JHEP 07 (1999) 004, arXiv:hep-th/9905177.

[2706] A.G. Cohen, D.B. Kaplan, A.E. Nelson, Effective field theory, black holes, and the cosmological constant, Phys. Rev. Lett. 82 (1999) 4971–4974, arXiv:hep-th/9803132.

[2707] S. Wang, Y. Wang, M. Li, Holographic dark energy, Phys. Rep. 696 (2017) 1–57, arXiv:1612.00345.

[2708] S. Nojiri, S.D. Odintsov, T. Paul, Different faces of generalized holographic dark energy, Symmetry 13 (6) (2021) 928, arXiv:2105.08438.

[2709] S. Nojiri, S.D. Odintsov, V.K. Oikonomou, T. Paul, Unifying holographic inflation with holographic dark energy: a covariant approach, Phys. Rev. D 102 (2) (2020) 023540, arXiv:2007.06829.

[2710] O. Trivedi, M. Khlopov, A.V. Timoshkin, Tsallis holographic dark energy with power law Ansatz approach, Symmetry 16 (4) (2024) 446, arXiv:2402.05784.

[2711] M. Tavayef, A. Sheykhi, K. Bamba, H. Moradpour, Tsallis holographic dark energy, Phys. Lett. B 781 (2018) 195–200, arXiv:1804.02983.

[2712] E.N. Saridakis, Barrow holographic dark energy, Phys. Rev. D 102 (12) (2020) 123525, arXiv:2005.04115.

[2713] H. Moradpour, S.A. Moosavi, I.P. Lobo, J.P. Morais Graça, A. Jawad, I.G. Salako, Thermodynamic approach to holographic dark energy and the Rényi entropy, Eur. Phys. J. C 78 (10) (2018) 829, arXiv:1803.02195.

[2714] N. Drepanou, A. Lymperis, E.N. Saridakis, K. Yesmakhanova, Kaniadakis holographic dark energy and cosmology, Eur. Phys. J. C 82 (5) (2022) 449, arXiv:2109.09181.

[2715] L.N. Granda, A. Oliveros, Infrared cut-off proposal for the Holographic density, Phys. Lett. B 669 (2008) 275–277, arXiv:0810.3149.

[2716] P. Mukherjee, A. Mukherjee, H.K. Jassal, A. Dasgupta, N. Banerjee, Holographic dark energy: constraints on the interaction from diverse observational data sets, Eur. Phys. J. Plus 134 (4) (2019) 147, arXiv:1710.02417.

[2717] P. Adhikary, S. Das, S. Basilakos, E.N. Saridakis, Barrow holographic dark energy in a nonflat universe, Phys. Rev. D 104 (12) (2021) 123519, arXiv:2104.13118.

[2718] H. Moradpour, A.H. Ziaie, M. Kord Zangeneh, Generalized entropies and corresponding holographic dark energy models, Eur. Phys. J. C 80 (8) (2020) 732, arXiv:2005.06271.

[2719] A. Sayahian Jahromi, S.A. Moosavi, H. Moradpour, J.P. Morais Graça, I.P. Lobo, I.G. Salako, A. Jawad, Generalized entropy formalism and a new holographic dark energy model, Phys. Lett. B 780 (2018) 21–24, arXiv:1802.07722.

[2720] O. Trivedi, A. Bidlan, P. Moniz, Fractional holographic dark energy, Phys. Lett. B 858 (2024) 139074, arXiv:2407.16685.

[2721] H. Moradpour, S. Jalalzadeh, U.K. Sharma, On the thermodynamics of reconciling quantum and gravity, Eur. Phys. J. Plus 139 (2) (2024) 170, arXiv:2304.06494.

[2722] R.-Y. Guo, J.-F. Zhang, X. Zhang, Can the H_0 tension be resolved in extensions to ΛCDM cosmology? J. Cosmol. Astropart. Phys. 02 (2019) 054, arXiv:1809.02340.

[2723] T. Jacobson, Thermodynamics of space-time: The Einstein equation of state, Phys. Rev. Lett. 75 (1995) 1260–1263, arXiv:gr-qc/9504004.

[2724] E.P. Verlinde, On the origin of gravity and the laws of Newton, JHEP 04 (2011) 029, arXiv:1001.0785.

[2725] T. Padmanabhan, Gravitational entropy of static space-times and microscopic density of states, Cl. Quant. Grav. 21 (2004) 4485–4494, arXiv:gr-qc/0308070.

[2726] R.-G. Cai, S.P. Kim, First law of thermodynamics and Friedmann equations of Friedmann-Robertson-Walker universe, JHEP 02 (2005) 050, arXiv:hep-th/0501055.

[2727] J.D. Bekenstein, Black holes and entropy, Phys. Rev. D 7 (1973) 2333–2346.

[2728] S.W. Hawking, Black hole explosions, Nature 248 (1974) 30–31.

[2729] G.W. Gibbons, S.W. Hawking, Cosmological event horizons, thermodynamics, and particle creation, Phys. Rev. D 15 (1977) 2738–2751.
[2730] D.A. Easson, P.H. Frampton, G.F. Smoot, Entropic accelerating universe, Phys. Lett. B 696 (2011) 273–277, arXiv:1002.4278.
[2731] H. Gohar, V. Salzano, Generalized mass-to-horizon relation: A new global approach to entropic cosmologies and its connection to ΛCDM, Phys. Rev. D 109 (8) (2024) 084075, arXiv:2307.06239.
[2732] N. Komatsu, S. Kimura, Entropic cosmology for a generalized black-hole entropy, Phys. Rev. D 88 (2013) 083534, arXiv:1307.5949.
[2733] R.C. Nunes, E.M. Barboza Jr., E.M.C. Abreu, J.A. Neto, Probing the cosmological viability of non-gaussian statistics, J. Cosmol. Astropart. Phys. 08 (2016) 051, arXiv:1509.05059.
[2734] H. Moradpour, R.C. Nunes, E.M.C. Abreu, J.A. Neto, A note on the relations between thermodynamics, energy definitions and Friedmann equations, Modern Phys. Lett. A 32 (13) (2017) 1750078, arXiv:1603.01465.
[2735] E.M.C. Abreu, J.A. Neto, E.M. Barboza, R.C. Nunes, Tsallis and Kaniadakis statistics from the viewpoint of entropic gravity formalism, Internat. J. Modern Phys. A 32 (05) (2017) 1750028, arXiv:1701.06898.
[2736] C. Tsallis, L.J.L. Cirto, Black hole thermodynamical entropy, Eur. Phys. J. C 73 (2013) 2487, arXiv:1202.2154.
[2737] J.D. Barrow, The area of a rough black hole, Phys. Lett. B 808 (2020) 135643, arXiv:2004.09444.
[2738] I. Cimidiker, M.P. Dabrowski, H. Gohar, Generalized uncertainty principle impact on nonextensive black hole thermodynamics, Cl. Quant. Grav. 40 (14) (2023) 145001, arXiv:2301.00609.
[2739] J.D. Bekenstein, Universal upper bound on the entropy-to-energy ratio for bounded systems, Phys. Rev. D 23 (2) (1981) 287–298.
[2740] M.H.P.M. van Putten, On the hubble expansion in a big bang quantum cosmology, JHEAp 45 (2025) 194–199, arXiv:2403.10865.
[2741] D. Camarena, V. Marra, Local determination of the hubble constant and the deceleration parameter, Phys. Rev. Res. 2 (1) (2020) 013028, arXiv:1906.11814.
[2742] B. De Simone, M.H.P.M. van Putten, M.G. Dainotti, G. Lambiase, A doublet of cosmological models to challenge the H0 tension in the Pantheon Supernovae Ia catalog, JHEAp 45 (2025) 290–298, arXiv:2411.05744.
[2743] S. Basilakos, A. Lymperis, M. Petronikolou, E.N. Saridakis, Alleviating both H_0 and σ_8 tensions in Tsallis cosmology, Eur. Phys. J. C 84 (3) (2024) 297, arXiv:2308.01200.
[2744] M. Asghari, A. Sheykhi, Observational constraints on Tsallis modified gravity, Mon. Not. R. Astron. Soc. 508 (2) (2021) 2855–2861, arXiv:2106.15551.
[2745] H. Gohar, V. Salzano, Cosmological constraints on entropic cosmology with matter creation, Eur. Phys. J. C 81 (4) (2021) 338, arXiv:2008.09635.
[2746] W.J.C. da Silva, R. Silva, Cosmological perturbations in the Tsallis holographic dark energy scenarios, Eur. Phys. J. Plus 136 (5) (2021) 543, arXiv:2011.09520.
[2747] A. Melchiorri, L. Mersini-Houghton, C.J. Odman, M. Trodden, The state of the dark energy equation of state, Phys. Rev. D 68 (2003) 043509, arXiv:astro-ph/0211522.
[2748] A. Melchiorri, L. Mersini-Houghton, Does the low CMB quadrupole provide a new cosmic coincidence problem?, 2004, arXiv:hep-ph/0403222.
[2749] P.J. Steinhardt, L.-M. Wang, I. Zlatev, Cosmological tracking solutions, Phys. Rev. D 59 (1999) 123504, arXiv:astro-ph/9812313.
[2750] N. Roy, A.X. Gonzalez-Morales, L.A. Urena-Lopez, New general parametrization of quintessence fields and its observational constraints, Phys. Rev. D 98 (6) (2018) 063530, arXiv:1803.09204.
[2751] F.X. Linares Cedeño, N. Roy, L.A. Ureña-López, Tracker phantom field and a cosmological constant: Dynamics of a composite dark energy model, Phys. Rev. D 104 (12) (2021) 123502, arXiv:2105.07103.
[2752] N. Roy, S. Goswami, S. Das, Quintessence or phantom: Study of scalar field dark energy models through a general parametrization of the Hubble parameter, Phys. Dark Univ. 36 (2022) 101037, arXiv:2201.09306.
[2753] J.A. Nájera, C. Escamilla-Rivera, Phantom scalar field cosmologies constrained by early cosmic measurements, Universe 10 (6) (2024) 232, arXiv:2403.16562.
[2754] WMAP Collaboration, G. Hinshaw, et al., Nine-year Wilkinson microwave anisotropy probe (WMAP) observations: Cosmological parameter results, Astrophys. J. Suppl. 208 (2013) 19, arXiv:1212.5226.
[2755] B. Feng, X.-L. Wang, X.-M. Zhang, Dark energy constraints from the cosmic age and supernova, Phys. Lett. B 607 (2005) 35–41, arXiv:astro-ph/0404224.
[2756] T. Qiu, Theoretical aspects of quintom models, in: K. Bamba, C.-Q. Geng (Eds.), Modern Phys. Lett. A 25 (2010) 909–921, arXiv:1002.3971.
[2757] M.-J. Zhang, H. Li, Observational constraint on the dark energy scalar field, Chin. Phys. C 45 (4) (2021) 045103, arXiv:1809.08936.
[2758] G. Leon, A. Paliathanasis, J.L. Morales-Martínez, The past and future dynamics of quintom dark energy models, Eur. Phys. J. C 78 (9) (2018) 753, arXiv:1808.05634.
[2759] S. Panpanich, P. Burikham, S. Ponglertsakul, L. Tannukij, Resolving Hubble tension with quintom dark energy model, Chin. Phys. C 45 (1) (2021) 015108, arXiv:1908.03324.
[2760] D. Wang, W. Zhang, X.-H. Meng, Searching for the evidence of dynamical dark energy, Eur. Phys. J. C 79 (3) (2019) 211, arXiv:1903.08913.
[2761] L.A. Escamilla, S. Pan, E. Di Valentino, A. Paliathanasis, J.A. Vázquez, W. Yang, Testing an oscillatory behavior of dark energy, Phys. Rev. D 111 (2) (2025) 023531, arXiv:2404.00181.
[2762] J.A. Vázquez, D. Tamayo, A.A. Sen, I. Quiros, Bayesian model selection on scalar ϵ-field dark energy, Phys. Rev. D 103 (4) (2021) 043506, arXiv:2009.01904.
[2763] J.-Q. Xia, H. Li, X. Zhang, Dark energy constraints after Planck, Phys. Rev. D 88 (2013) 063501, arXiv:1308.0188.
[2764] L. Fu, L. Chen, M. Yang, J. Wang, M.-J. Zhang, A better reconciliation of hubble tension in the dark energy scalar field, Res. Astron. Astrophys. 23 (3) (2023) 035004.
[2765] N. Roy, L.A. Ureña-López, Tracker behaviour of quintom dark energy and the Hubble tension, 2023, arXiv:2312.04003.
[2766] M. Cicoli, G. Dibitetto, F.G. Pedro, New accelerating solutions in late-time cosmology, Phys. Rev. D 101 (10) (2020) 103524, arXiv:2002.02695.
[2767] M. Cicoli, G. Dibitetto, F.G. Pedro, Out of the swampland with multifield quintessence? JHEP 10 (2020) 035, arXiv:2007.11011.
[2768] Y. Akrami, M. Sasaki, A.R. Solomon, V. Vardanyan, Multi-field dark energy: Cosmic acceleration on a steep potential, Phys. Lett. B 819 (2021) 136427, arXiv:2008.13660.
[2769] J.R. Eskilt, Y. Akrami, A.R. Solomon, V. Vardanyan, Cosmological dynamics of multifield dark energy, Phys. Rev. D 106 (2) (2022) 023512, arXiv:2201.08841.
[2770] L. Anguelova, J. Dumancic, R. Gass, L.C.R. Wijewardhana, Dark energy from inspiraling in field space, J. Cosmol. Astropart. Phys. 03 (03) (2022) 018, arXiv:2111.12136.
[2771] L. Anguelova, J. Dumancic, R. Gass, L.C.R. Wijewardhana, Dynamics of inspiraling dark energy, Eur. Phys. J. C 84 (4) (2024) 365, arXiv:2311.07839.
[2772] C. Armendariz-Picon, T. Damour, V.F. Mukhanov, k - inflation, Phys. Lett. B 458 (1999) 209–218, arXiv:hep-th/9904075.
[2773] J. Garriga, V.F. Mukhanov, Perturbations in k-inflation, Phys. Lett. B 458 (1999) 219–225, arXiv:hep-th/9904176.
[2774] R.C. Batista, A short review on clustering dark energy, Universe 8 (1) (2021) 22, arXiv:2204.12341.
[2775] J. Dakin, S. Hannestad, T. Tram, M. Knabenhans, J. Stadel, Dark energy perturbations in N-body simulations, J. Cosmol. Astropart. Phys. 08 (2019) 013, arXiv:1904.05210.
[2776] F. Hassani, J. Adamek, M. Kunz, F. Vernizzi, k-Evolution: a relativistic N-body code for clustering dark energy, J. Cosmol. Astropart. Phys. 12 (2019) 011, arXiv:1910.01104.
[2777] L. Blot, P.S. Corasaniti, F. Schmidt, Non-linear Eulerian hydrodynamics of dark energy: Riemann problem and finite volume schemes, J. Cosmol. Astropart. Phys. 05 (2023) 001, arXiv:2210.04800.
[2778] R.C. Batista, H.P. de Oliveira, L.R.W. Abramo, Spherical collapse of non-top-hat profiles in the presence of dark energy with arbitrary sound speed, J. Cosmol. Astropart. Phys. 02 (2023) 037, arXiv:2210.14769.
[2779] I. Ben-Dayan, U. Kumar, Theoretical priors and the dark energy equation of state, Eur. Phys. J. C 84 (2) (2024) 167, arXiv:2310.03092.
[2780] B.R. Dinda, N. Banerjee, Constraints on the speed of sound in the k-essence model of dark energy, Eur. Phys. J. C 84 (2) (2024) 177, arXiv:2309.10538.
[2781] M. Bastero-Gil, P.H. Frampton, L. Mersini-Houghton, Modified dispersion relations from closed strings in toroidal cosmology, Phys. Rev. D 65 (2002) 106002, arXiv:hep-th/0110167.
[2782] L. Mersini-Houghton, M. Bastero-Gil, P. Kanti, Relic dark energy from transPlanckian regime, Phys. Rev. D 64 (2001) 043508, arXiv:hep-ph/0101210.
[2783] L. Mersini-Houghton, M. Bastero-Gil, Dark energy may probe string theory, in: 3rd International Sakharov Conference on Physics, 2002, arXiv:hep-th/0212153.
[2784] M. Bastero-Gil, L. Mersini-Houghton, SN1A data and the CMB of modified curvature at short and long distances, Phys. Rev. D 65 (2002) 023502, arXiv:astro-ph/0107256.
[2785] M. Bastero-Gil, L. Mersini-Houghton, Equation of state of the transPlanckian dark energy and the coincidence problem, Phys. Rev. D 67 (2003) 103519, arXiv:hep-th/0205271.
[2786] M. Bastero-Gil, K. Freese, L. Mersini-Houghton, What can WMAP tell us about the very early universe? New physics as an explanation of suppressed large scale power and running spectral index, Phys. Rev. D 68 (2003) 123514, arXiv:hep-ph/0306289.
[2787] I.L. Shapiro, J. Sola, Scaling behavior of the cosmological constant: Interface between quantum field theory and cosmology, JHEP 02 (2002) 006, arXiv:hep-th/0012227.
[2788] J. Sola, Dark energy: A quantum fossil from the inflationary Universe? in: M. Bordag, V.M. Mostepanenko (Eds.), J. Phys. A 41 (2008) 164066, arXiv:0710.4151.
[2789] I.L. Shapiro, J. Sola, On the possible running of the cosmological 'constant', Phys. Lett. B 682 (2009) 105–113, arXiv:0910.4925.
[2790] C. Moreno-Pulido, J. Sola, Running vacuum in quantum field theory in curved spacetime: renormalizing ρ_{vac} without $\sim m^4$ terms, Eur. Phys. J. C 80 (8) (2020) 692, arXiv:2005.03164.

[2791] C. Moreno-Pulido, J. Sola Peracaula, Renormalizing the vacuum energy in cosmological spacetime: implications for the cosmological constant problem, Eur. Phys. J. C 82 (6) (2022) 551, arXiv:2201.05827.

[2792] C. Moreno-Pulido, J. Sola Peracaula, S. Cheraghchi, Running vacuum in QFT in FLRW spacetime: the dynamics of $\rho_{\rm vac}(H)$ from the quantized matter fields, Eur. Phys. J. C 83 (7) (2023) 637, arXiv:2301.05205.

[2793] J. Sola, Cosmological constant and vacuum energy: old and new ideas, in: T. Papakostas, D.A. Pliakis (Eds.), J. Phys. Conf. Ser. 453 (2013) 012015, arXiv:1306.1527.

[2794] J. Sola Peracaula, The cosmological constant problem and running vacuum in the expanding universe, Phil. Trans. Roy. Soc. Lond. A 380 (2022) 20210182, arXiv:2203.13757.

[2795] S. Basilakos, J.A.S. Lima, J. Sola, From inflation to dark energy through a dynamical Lambda: an attempt at alleviating fundamental cosmic puzzles, Internat. J. Modern Phys. D 22 (2013) 1342008, arXiv:1307.6251.

[2796] S. Basilakos, N.E. Mavromatos, J. Solà Peracaula, Scalar field theory description of the running vacuum model: the vacuumon, J. Cosmol. Astropart. Phys. 12 (2019) 025, arXiv:1901.06638.

[2797] H. Fritzsch, J. Sola, Matter non-conservation in the universe and dynamical dark energy, Cl. Quant. Grav. 29 (2012) 215002, arXiv:1202.5097.

[2798] A. Gomez-Valent, J. Sola, Vacuum models with a linear and a quadratic term in H: structure formation and number counts analysis, Mon. Not. R. Astron. Soc. 448 (2015) 2810–2821, arXiv:1412.3785.

[2799] A. Gomez-Valent, E. Karimkhani, J. Sola, Background history and cosmic perturbations for a general system of self-conserved dynamical dark energy and matter, J. Cosmol. Astropart. Phys. 12 (2015) 048, arXiv:1509.03298.

[2800] H. Fritzsch, J. Sola, Fundamental constants and cosmic vacuum: the micro and macro connection, Modern Phys. Lett. A 30 (22) (2015) 1540034, arXiv:1502.01411.

[2801] H. Fritzsch, J. Solà, R.C. Nunes, Running vacuum in the universe and the time variation of the fundamental constants of nature, Eur. Phys. J. C 77 (3) (2017) 193, arXiv:1605.06104.

[2802] J. Solà Peracaula, The dynamics of vacuum, gravity and matter: Implications on the fundamental constants, Internat. J. Modern Phys. A 39 (09n10) (2024) 2441016, arXiv:2308.13349.

[2803] J. Sola, A. Gomez-Valent, J. de Cruz Pérez, Hints of dynamical vacuum energy in the expanding universe, Astrophys. J. Lett. 811 (2015) L14, arXiv:1506.05793.

[2804] J. Solà, A. Gómez-Valent, J. de Cruz Pérez, First evidence of running cosmic vacuum: challenging the concordance model, Astrophys. J. 836 (1) (2017) 43, arXiv:1602.02103.

[2805] J. Solà Peracaula, J. de Cruz Pérez, A. Gómez-Valent, Dynamical dark energy vs. Λ=const in light of observations, EPL 121 (3) (2018) 39001, arXiv:1606.00450.

[2806] J. Solà Peracaula, J. de Cruz Pérez, A. Gomez-Valent, Possible signals of vacuum dynamics in the Universe, Mon. Not. R. Astron. Soc. 478 (4) (2018) 4357–4373, arXiv:1703.08218.

[2807] J. Solà, A. Gómez-Valent, J. de Cruz Pérez, The H_0 tension in light of vacuum dynamics in the Universe, Phys. Lett. B 774 (2017) 317–324, arXiv:1705.06723.

[2808] A. Gomez-Valent, J. Sola, Relaxing the σ_8-tension through running vacuum in the universe, EPL 120 (3) (2017) 39001, arXiv:1711.00692.

[2809] A. Gómez-Valent, J. Solà Peracaula, Density perturbations for running vacuum: a successful approach to structure formation and to the σ_8-tension, Mon. Not. R. Astron. Soc. 478 (1) (2018) 126–145, arXiv:1801.08501.

[2810] A. Gómez-Valent, J. Solà, S. Basilakos, Dynamical vacuum energy in the expanding universe confronted with observations: a dedicated study, J. Cosmol. Astropart. Phys. 01 (2015) 004, arXiv:1409.7048.

[2811] C.-Q. Geng, C.-C. Lee, L. Yin, Constraints on running vacuum model with $H(z)$ and $f\sigma_8$, J. Cosmol. Astropart. Phys. 08 (2017) 032, arXiv:1704.02136.

[2812] P. Tsiapi, S. Basilakos, Testing dynamical vacuum models with CMB power spectrum from Planck, Mon. Not. R. Astron. Soc. 485 (2) (2019) 2505–2510, arXiv:1810.12902.

[2813] P. Asimakis, S. Basilakos, N.E. Mavromatos, E.N. Saridakis, Big bang nucleosynthesis constraints on higher-order modified gravities, Phys. Rev. D 105 (8) (2022) 084010, arXiv:2112.10863.

[2814] J. Solà Peracaula, A. Gómez-Valent, J. de Cruz Perez, C. Moreno-Pulido, Running vacuum against the H_0 and σ_8 tensions, EPL 134 (1) (2021) 19001, arXiv:2102.12758.

[2815] J. Sola Peracaula, A. Gomez-Valent, J. de Cruz Perez, C. Moreno-Pulido, Running vacuum in the universe: Phenomenological status in light of the latest observations, and its impact on the σ_8 and H_0 tensions, Universe 9 (6) (2023) 262, arXiv:2304.11157.

[2816] J. de Cruz Perez, J. Sola Peracaula, Running vacuum in Brans & Dicke theory: A possible cure for the σ8 and H0 tensions, Phys. Dark Univ. 43 (2024) 101406, arXiv:2302.04807.

[2817] N.E. Mavromatos, Geometrical origins of the universe dark sector: string-inspired torsion and anomalies as seeds for inflation and dark matter, Phil. Trans. A. Math. Phys. Eng. Sci. 380 (2222) (2022) 20210188, arXiv:2108.02152.

[2818] N.E. Mavromatos, Lorentz symmetry violation in string-inspired effective modified gravity theories, Lect. Notes Phys. 1017 (2023) 3–48, arXiv:2205.07044.

[2819] J. Alexandre, N. Houston, N.E. Mavromatos, Starobinsky-type inflation in dynamical supergravity breaking scenarios, Phys. Rev. D 89 (2) (2014) 027703, arXiv:1312.5197.

[2820] W. Yang, E. Di Valentino, S. Pan, A. Shafieloo, X. Li, Generalized emergent dark energy model and the Hubble constant tension, Phys. Rev. D 104 (6) (2021) 063521, arXiv:2103.03815.

[2821] A. Banihashemi, N. Khosravi, A.H. Shirazi, Phase transition in the dark sector as a proposal to lessen cosmological tensions, Phys. Rev. D 101 (12) (2020) 123521, arXiv:1808.02472.

[2822] A. Banihashemi, N. Khosravi, A.H. Shirazi, Ginzburg-Landau theory of dark energy: A framework to study both temporal and spatial cosmological tensions simultaneously, Phys. Rev. D 99 (8) (2019) 083509, arXiv:1810.11007.

[2823] A. Banihashemi, N. Khosravi, A. Shafieloo, Dark energy as a critical phenomenon: a hint from Hubble tension, J. Cosmol. Astropart. Phys. 06 (2021) 003, arXiv:2012.01407.

[2824] V.L. Ginzburg, L.D. Landau, On the theory of superconductivity, in: D. ter Haar (Ed.), Zh. Eksp. Teor. Fiz. 20 (1950) 1064–1082.

[2825] A. Banihashemi, N. Khosravi, Fluctuations in the Ginzburg–Landau theory of dark energy: Internal (in)consistencies in the Planck data set, Astrophys. J. 931 (2) (2022) 148, arXiv:2201.04119.

[2826] M. Rezaei, T. Naderi, M. Malekjani, A. Mehrabi, A Bayesian comparison between ΛCDM and phenomenologically emergent dark energy models, Eur. Phys. J. C 80 (5) (2020) 374, arXiv:2004.08168.

[2827] S. Pan, W. Yang, E. Di Valentino, A. Shafieloo, S. Chakraborty, Reconciling H_0 tension in a six parameter space? J. Cosmol. Astropart. Phys. 06 (06) (2020) 062, arXiv:1907.12551.

[2828] R. Shah, P. Mukherjee, S. Pal, Reconciling S8: insights from interacting dark sectors, Mon. Not. R. Astron. Soc. 536 (3) (2024) 2404–2420, arXiv:2404.06396.

[2829] A. Hernández-Almada, G. Leon, J. Magaña, M.A. García-Aspeitia, V. Motta, Generalized emergent dark energy: observational hubble data constraints and stability analysis, Mon. Not. R. Astron. Soc. 497 (2) (2020) 1590–1602, arXiv:2002.12881.

[2830] W. Yang, E. Di Valentino, S. Pan, O. Mena, Emergent dark energy, neutrinos and cosmological tensions, Phys. Dark Univ. 31 (2021) 100762, arXiv:2007.02927.

[2831] Z. Liu, H. Miao, Update constraints on neutrino mass and mass hierarchy in light of dark energy models, Internat. J. Modern Phys. D 29 (13) (2020) 2050088, arXiv:2002.05563.

[2832] E. Di Valentino, S. Gariazzo, C. Giunti, O. Mena, S. Pan, W. Yang, Minimal dark energy: Key to sterile neutrino and Hubble constant tensions? Phys. Rev. D 105 (10) (2022) 103511, arXiv:2110.03990.

[2833] M.A. García-Aspeitia, G. Fernandez-Anaya, A. Hernández-Almada, G. Leon, J. Magaña, Cosmology under the fractional calculus approach, Mon. Not. R. Astron. Soc. 517 (4) (2022) 4813–4826, arXiv:2207.00878.

[2834] L. Pizzuti, I.D. Saltas, L. Amendola, Mg-mamposst: a code to test modifications of gravity with internal kinematics and lensing analyses of galaxy clusters, Mon. Not. R. Astron. Soc. 506 (1) (2021) 595–612, arXiv:2011.15089.

[2835] H.B. Benaoum, W. Yang, S. Pan, E. Di Valentino, Modified emergent dark energy and its astronomical constraints, Internat. J. Modern Phys. D 31 (03) (2022) 2250015, arXiv:2008.09098.

[2836] L. Parker, A. Raval, New quantum aspects of a vacuum dominated universe, Phys. Rev. D 62 (2000) 083503, arXiv:gr-qc/0003103;
Erratum:, Phys. Rev. D 67 (2003) 029903.

[2837] L. Parker, D.A.T. Vanzella, Acceleration of the universe, vacuum metamorphosis, and the large time asymptotic form of the heat kernel, Phys. Rev. D 69 (2004) 104009, arXiv:gr-qc/0312108.

[2838] R.R. Caldwell, W. Komp, L. Parker, D.A.T. Vanzella, A sudden gravitational transition, Phys. Rev. D 73 (2006) 023513, arXiv:astro-ph/0507622.

[2839] E. Di Valentino, E.V. Linder, A. Melchiorri, H_0 ex machina: Vacuum metamorphosis and beyond H_0, Phys. Dark Univ. 30 (2020) 100733, arXiv:2006.16291.

[2840] G. Lambiase, S. Mohanty, A. Narang, P. Parashari, Testing dark energy models in the light of σ_8 tension, Eur. Phys. J. C 79 (2) (2019) 141, arXiv:1804.07154.

[2841] R.A. Battye, A. Moss, Evidence for massive neutrinos from cosmic microwave background and lensing observations, Phys. Rev. Lett. 112 (5) (2014) 051303, arXiv:1308.5870.

[2842] Y. Wang, K. Freese, P. Gondolo, M. Lewis, Future type IA supernova data as tests of dark energy from modified Friedmann equations, Astrophys. J. 594 (2003) 25–32, arXiv:astro-ph/0302064.

[2843] R. Lazkoz, V. Salzano, L. Fernandez-Jambrina, M. Bouhmadi-López, Ripped ΛCDM: An observational contender to the consensus cosmological model, Phys. Dark Univ. 45 (2024) 101511, arXiv:2311.10526.

[2844] L. Huang, S.-J. Wang, W.-W. Yu, No-go guide for the Hubble tension: Late-time or local-scale new physics, Sci. China Phys. Mech. Astron. 68 (2) (2025) 220413, arXiv:2401.14170.

[2845] N. Kitazawa, Late-time data require smaller sound horizon at recombination, 2023, arXiv:2310.10017.

[2846] Ruchika, 2D BAO vs 3D BAO: Hints for new physics?, 2024, arXiv:2406.05453.
[2847] R.E. Keeley, A. Shafieloo, Ruling out new physics at low redshift as a solution to the H0 tension, Phys. Rev. Lett. 131 (11) (2023) 111002, arXiv:2206.08440.
[2848] M.W. Hossain, A. Maqsood, Comparison between axionlike and power law potentials in a cosmological background, Phys. Rev. D 109 (10) (2024) 103512, arXiv:2311.17825.
[2849] C.G. Boiza, M. Bouhmadi-López, Speeding up the Universe with a generalised axion-like potential, 2024, arXiv:2409.18184.
[2850] C.G. Boiza, M. Bouhmadi-López, Cosmological perturbations in a generalised axion-like dark energy model, Phys. Dark Univ. 48 (2025) 101845, arXiv:2410.22467.
[2851] M.W. Hossain, A. Maqsood, Cosmological implications of tracker scalar fields as dynamical dark energy, 2025, arXiv:2502.19274.
[2852] H.-W. Chiang, C.G. Boiza, M. Bouhmadi-López, Observational constraints on generalised axion-like potentials for the late universe, 2025, arXiv:2503.04898.
[2853] H. Benaoum, Accelerated universe from modified Chaplygin gas and tachyonic fluid, Universe 8 (7) (2022) 340, arXiv:hep-th/0205140.
[2854] H. Stefancic, Expansion around the vacuum equation of state - Sudden future singularities and asymptotic behavior, Phys. Rev. D 71 (2005) 084024, arXiv:astro-ph/0411630.
[2855] M. Bouhmadi-López, M. Brilenkov, R. Brilenkov, J. Morais, A. Zhuk, Scalar perturbations in the late Universe: viability of the Chaplygin gas models, J. Cosmol. Astropart. Phys. 12 (2015) 037, arXiv:1509.06963.
[2856] W. Yang, S. Pan, S. Vagnozzi, E. Di Valentino, D.F. Mota, S. Capozziello, Dawn of the dark: unified dark sectors and the EDGES Cosmic Dawn 21-cm signal, J. Cosmol. Astropart. Phys. 11 (2019) 044, arXiv:1907.05344.
[2857] I. Albarran, M. Bouhmadi-López, J. Morais, Cosmological perturbations in an effective and genuinely phantom dark energy Universe, Phys. Dark Univ. 16 (2017) 94–108, arXiv:1611.00392.
[2858] K.R. Dienes, L. Heurtier, F. Huang, D. Kim, T.M.P. Tait, B. Thomas, Stasis in an expanding universe: A recipe for stable mixed-component cosmological eras, Phys. Rev. D 105 (2) (2022) 023530, arXiv:2111.04753.
[2859] K.R. Dienes, L. Heurtier, F. Huang, T.M.P. Tait, B. Thomas, Stasis, stasis, triple stasis, Phys. Rev. D 109 (8) (2024) 083508, arXiv:2309.10345.
[2860] K.R. Dienes, L. Heurtier, F. Huang, T.M.P. Tait, B. Thomas, Cosmological stasis from dynamical scalars: Tracking solutions and the possibility of a stasis-induced inflation, Phys. Rev. D 110 (12) (2024) 123514, arXiv:2406.06830.
[2861] L.R.W. Abramo, R.H. Brandenberger, V.F. Mukhanov, The energy - momentum tensor for cosmological perturbations, Phys. Rev. D 56 (1997) 3248–3257, arXiv:gr-qc/9704037.
[2862] R.H. Brandenberger, Back reaction of cosmological perturbations, in: 3rd International Conference on Particle Physics and the Early Universe, 2000, pp. 198–206, arXiv:hep-th/0004016.
[2863] M.A.C. Alvarez, L. Graef, R. Brandenberger, Back-reaction of super-hubble fluctuations, late time tracking and recent observational results, 2025, arXiv:2502.17395.
[2864] L.A. Escamilla, E. Özülker, Ö. Akarsu, E. Di Valentino, J.A. Vázquez, Do we need wavelets in the late universe?, 2024, arXiv:2408.12516.
[2865] Ö. Akarsu, A. Çam, E.A. Paraskevas, L. Perivolaropoulos, Linear matter density perturbations in the Λ_sCDM model: Examining growth dynamics and addressing the S_8 tension, 2025, arXiv:2502.20384.
[2866] M. Biagetti, G. Franciolini, A. Riotto, Enhancing massive galaxy formation at high redshift in non-standard cosmologies, Astrophys. J. 944 (2) (2023) 113, arXiv:2210.04812.
[2867] D. Wang, Y. Liu, JWST high redshift galaxy observations have a strong tension with Planck CMB measurements, 2022, arXiv:2301.00347.
[2868] K. Dutta, Ruchika, A. Roy, A.A. Sen, M.M. Sheikh-Jabbari, Beyond ΛCDM with low and high redshift data: implications for dark energy, Gen. Relativity Gravitation 52 (2) (2020) 15, arXiv:1808.06623.
[2869] G. Acquaviva, Ö. Akarsu, N. Katirci, J.A. Vazquez, Simple-graduated dark energy and spatial curvature, Phys. Rev. D 104 (2) (2021) 023505, arXiv:2104.02623.
[2870] Ö. Akarsu, L. Perivolaropoulos, A. Tsikoundoura, A.E. Yükselci, A. Zhuk, Dynamical dark energy with AdS-to-dS and dS-to-dS transitions: Implications for the H_0 tension, 2025, arXiv:2502.14667.
[2871] E. Ozulker, Is the dark energy equation of state parameter singular? Phys. Rev. D 106 (6) (2022) 063509, arXiv:2203.04167.
[2872] O. Akarsu, A. De Felice, E. Di Valentino, S. Kumar, R.C. Nunes, E. Ozulker, J.A. Vazquez, A. Yadav, Λ_sCDM cosmology from a type-II minimally modified gravity, 2024, arXiv:2402.07716.
[2873] D. Green, J. Meyers, Cosmological preference for a negative neutrino mass, Phys. Rev. D 111 (8) (2025) 083507, arXiv:2407.07878.
[2874] W. Elbers, C.S. Frenk, A. Jenkins, B. Li, S. Pascoli, Negative neutrino masses as a mirage of dark energy, Phys. Rev. D 111 (6) (2025) 063534, arXiv:2407.10965.
[2875] S.-F. Ge, L. Tan, Identifying neutrino mass ordering with cosmic gravitational focusing, Phys. Rev. D 111 (8) (2025) 083539, arXiv:2409.11115.
[2876] J.D. Barrow, Sudden future singularities, Cl. Quant. Grav. 21 (2004) L79–L82, arXiv:gr-qc/0403084.
[2877] A. De Felice, A. Doll, S. Mukohyama, A theory of type-II minimally modified gravity, J. Cosmol. Astropart. Phys. 09 (2020) 034, arXiv:2004.12549.
[2878] A. De Felice, S. Mukohyama, M.C. Pookkillath, Addressing H_0 tension by means of VCDM, Phys. Lett. B 816 (2021) 136201, arXiv:2009.08718; Erratum:, Phys. Lett. B 818 (2021) 136364.
[2879] J.A. Vazquez, S. Hee, M.P. Hobson, A.N. Lasenby, M. Ibison, M. Bridges, Observational constraints on conformal time symmetry, missing matter and double dark energy, J. Cosmol. Astropart. Phys. 07 (2018) 062, arXiv:1208.2542.
[2880] BOSS Collaboration, T. Delubac, et al., Baryon acoustic oscillations in the Lyα forest of BOSS DR11 quasars, Astron. Astrophys. 574 (2015) A59, arXiv:1404.1801.
[2881] V. Sahni, Y. Shtanov, Brane world models of dark energy, J. Cosmol. Astropart. Phys. 11 (2003) 014, arXiv:astro-ph/0202346.
[2882] S. Bag, V. Sahni, A. Shafieloo, Y. Shtanov, Phantom braneworld and the Hubble tension, Astrophys. J. 923 (2) (2021) 212, arXiv:2107.03271.
[2883] E. Di Valentino, E.V. Linder, A. Melchiorri, Vacuum phase transition solves the H_0 tension, Phys. Rev. D 97 (4) (2018) 043528, arXiv:1710.02153.
[2884] E. Mörtsell, S. Dhawan, Does the hubble constant tension call for new physics? J. Cosmol. Astropart. Phys. 09 (2018) 025, arXiv:1801.07260.
[2885] V. Poulin, K.K. Boddy, S. Bird, M. Kamionkowski, Implications of an extended dark energy cosmology with massive neutrinos for cosmological tensions, Phys. Rev. D 97 (12) (2018) 123504, arXiv:1803.02474.
[2886] S. Capozziello, Ruchika, A.A. Sen, Model independent constraints on dark energy evolution from low-redshift observations, Mon. Not. R. Astron. Soc. 484 (2019) 4484, arXiv:1806.03943.
[2887] Ö. Akarsu, J.D. Barrow, C.V.R. Board, N.M. Uzun, J.A. Vazquez, Screening Λ in a new modified gravity model, Eur. Phys. J. C 79 (10) (2019) 846, arXiv:1903.11519.
[2888] L. Visinelli, S. Vagnozzi, U. Danielsson, Revisiting a negative cosmological constant from low-redshift data, Symmetry 11 (8) (2019) 1035, arXiv:1907.07953.
[2889] A. Perez, D. Sudarsky, E. Wilson-Ewing, Resolving the H_0 tension with diffusion, Gen. Relativity Gravitation 53 (1) (2021) 7, arXiv:2001.07536.
[2890] Ö. Akarsu, N. Katırcı, S. Kumar, R.C. Nunes, B. Öztürk, S. Sharma, Rastall gravity extension of the standard ΛCDM model: theoretical features and observational constraints, Eur. Phys. J. C 80 (11) (2020) 1050, arXiv:2004.04074.
[2891] R. Calderón, R. Gannouji, B. L'Huillier, D. Polarski, Negative cosmological constant in the dark sector? Phys. Rev. D 103 (2) (2021) 023526, arXiv:2008.10237.
[2892] G. Ye, Y.-S. Piao, T_0 censorship of early dark energy and AdS vacua, Phys. Rev. D 102 (8) (2020) 083523, arXiv:2008.10832.
[2893] A. Paliathanasis, G. Leon, Dynamics of a two scalar field cosmological model with phantom terms, Cl. Quant. Grav. 38 (7) (2021) 075013, arXiv:2009.12874.
[2894] O. Akarsu, E.O. Colgain, E. Özulker, S. Thakur, L. Yin, Inevitable manifestation of wiggles in the expansion of the late universe, Phys. Rev. D 107 (12) (2023) 123526, arXiv:2207.10609.
[2895] S. Di Gennaro, Y.C. Ong, Sign switching dark energy from a running barrow entropy, Universe 8 (10) (2022) 541, arXiv:2205.09311.
[2896] Y.C. Ong, An effective sign switching dark energy: Lotka–Volterra model of two interacting fluids, Universe 9 (10) (2023) 437, arXiv:2212.04429.
[2897] B. Alexandre, S. Gielen, J. Magueijo, Overall signature of the metric and the cosmological constant, J. Cosmol. Astropart. Phys. 02 (2024) 036, arXiv:2306.11502.
[2898] Y. Tiwari, B. Ghosh, R.K. Jain, Towards a possible solution to the Hubble tension with Horndeski gravity, Eur. Phys. J. C 84 (3) (2024) 220, arXiv:2301.09382.
[2899] L.A. Anchordoqui, I. Antoniadis, D. Lust, Anti-de Sitter $\rightarrow$ de Sitter transition driven by Casimir forces and mitigating tensions in cosmological parameters, Phys. Lett. B 855 (2024) 138775, arXiv:2312.12352.
[2900] L.A. Anchordoqui, I. Antoniadis, D. Bielli, A. Chatrabhuti, H. Isono, Thin-wall vacuum decay in the presence of a compact dimension meets the H_0 and S_8 tensions, 2024, arXiv:2410.18649.
[2901] H. Wang, Z.-Y. Peng, Y.-S. Piao, Can recent DESI BAO measurements accommodate a negative cosmological constant? Phys. Rev. D 111 (6) (2025) L061306, arXiv:2406.03395.
[2902] Y. Toda, W. Giarè, E. Özülker, E. Di Valentino, S. Vagnozzi, Combining pre- and post-recombination new physics to address cosmological tensions: Case study with varying electron mass and sign-switching cosmological constant, Phys. Dark Univ. 46 (2024) 101676, arXiv:2407.01173.
[2903] O. Akarsu, B. Bulduk, A. De Felice, N. Katırcı, N.M. Uzun, Unexplored regions in teleparallel $f(T)$ gravity: Sign-changing dark energy density, 2024, arXiv:2410.23068.
[2904] M.S. Souza, A.M. Barcelos, R.C. Nunes, Ö. Akarsu, S. Kumar, Mapping the Λ_sCDM scenario to f(T) modified gravity: Effects on structure growth rate, Universe 11 (1) (2025) 2, arXiv:2501.18031.
[2905] P. Mukherjee, D. Kumar, A.A. Sen, Quintessential implications of the presence of AdS in the dark energy sector, 2025, arXiv:2501.18335.

[2906] U.K. Tyagi, S. Haridasu, S. Basak, Holographic and gravity-thermodynamic approaches in entropic cosmology: Bayesian assessment using late-time data, Phys. Rev. D 110 (6) (2024) 063503, arXiv:2406.07446.
[2907] M.T. Manoharan, Insights on Granda–Oliveros holographic dark energy: possibility of negative dark energy at $z \gtrsim 2$, Eur. Phys. J. C 84 (5) (2024) 552.
[2908] A. Gómez-Valent, J. Solà Peracaula, Composite dark energy and the cosmological tensions, Phys. Lett. B 864 (2025) 139391, arXiv:2412.15124.
[2909] S. Dwivedi, M. Högås, 2D BAO vs. 3D BAO: Solving the Hubble tension with bimetric cosmology, Universe 10 (11) (2024) 406, arXiv:2407.04322.
[2910] R.E. Keeley, K.N. Abazajian, M. Kaplinghat, A. Shafieloo, The preference for evolving dark energy from cosmological distance measurements and possible signatures in the growth rate of perturbations, 2025, arXiv:2502.12667.
[2911] E. Di Valentino, A. Mukherjee, A.A. Sen, Dark energy with phantom crossing and the H_0 tension, Entropy 23 (4) (2021) 404, arXiv:2005.12587.
[2912] S. Kumar, R.C. Nunes, Echo of interactions in the dark sector, Phys. Rev. D 96 (10) (2017) 103511, arXiv:1702.02143.
[2913] E. Di Valentino, A. Melchiorri, O. Mena, Can interacting dark energy solve the H_0 tension? Phys. Rev. D 96 (4) (2017) 043503, arXiv:1704.08342.
[2914] W. Yang, A. Mukherjee, E. Di Valentino, S. Pan, Interacting dark energy with time varying equation of state and the H_0 tension, Phys. Rev. D 98 (12) (2018) 123527, arXiv:1809.06883.
[2915] S. Pan, W. Yang, E. Di Valentino, E.N. Saridakis, S. Chakraborty, Interacting scenarios with dynamical dark energy: Observational constraints and alleviation of the H_0 tension, Phys. Rev. D 100 (10) (2019) 103520, arXiv:1907.07540.
[2916] S. Kumar, R.C. Nunes, S.K. Yadav, Dark sector interaction: a remedy of the tensions between CMB and LSS data, Eur. Phys. J. C 79 (7) (2019) 576, arXiv:1903.04865.
[2917] E. Di Valentino, A. Melchiorri, O. Mena, S. Vagnozzi, Nonminimal dark sector physics and cosmological tensions, Phys. Rev. D 101 (6) (2020) 063502, arXiv:1910.09853.
[2918] E. Di Valentino, A. Melchiorri, O. Mena, S. Vagnozzi, Interacting dark energy in the early 2020s: A promising solution to the H_0 and cosmic shear tensions, Phys. Dark Univ. 30 (2020) 100666, arXiv:1908.04281.
[2919] M. Lucca, D.C. Hooper, Shedding light on dark matter-dark energy interactions, Phys. Rev. D 102 (12) (2020) 123502, arXiv:2002.06127.
[2920] S. Kumar, Remedy of some cosmological tensions via effective phantom-like behavior of interacting vacuum energy, Phys. Dark Univ. 33 (2021) 100862, arXiv:2102.12902.
[2921] R.C. Nunes, S. Vagnozzi, S. Kumar, E. Di Valentino, O. Mena, New tests of dark sector interactions from the full-shape galaxy power spectrum, Phys. Rev. D 105 (12) (2022) 123506, arXiv:2203.08093.
[2922] M.A. Sabogal, E. Silva, R.C. Nunes, S. Kumar, E. Di Valentino, Sign switching in dark sector coupling interactions as a candidate for resolving cosmological tensions, Phys. Rev. D 111 (4) (2025) 043531, arXiv:2501.10323.
[2923] M. Montero, C. Vafa, I. Valenzuela, The dark dimension and the Swampland, JHEP 02 (2023) 022, arXiv:2205.12293.
[2924] L.A. Anchordoqui, I. Antoniadis, Large extra dimensions from higher-dimensional inflation, Phys. Rev. D 109 (10) (2024) 103508, arXiv:2310.20282.
[2925] N. Arkani-Hamed, S. Dubovsky, A. Nicolis, G. Villadoro, Quantum horizons of the standard model landscape, JHEP 06 (2007) 078, arXiv:hep-th/0703067.
[2926] J.F. Soriano, S. Wohlberg, L.A. Anchordoqui, New insights on a sign-switching Λ, Phys. Dark Univ. 48 (2025) 101911, arXiv:2502.19239.
[2927] A. Awad, W. El Hanafy, G.G.L. Nashed, E.N. Saridakis, Phase portraits of general f(T) cosmology, J. Cosmol. Astropart. Phys. 02 (2018) 052, arXiv:1710.10194.
[2928] M. Hashim, W. El Hanafy, A. Golovnev, A.A. El-Zant, Toward a concordance teleparallel cosmology. Part I. Background dynamics, J. Cosmol. Astropart. Phys. 07 (2021) 052, arXiv:2010.14964.
[2929] M. Hashim, A.A. El-Zant, W. El Hanafy, A. Golovnev, Toward a concordance teleparallel cosmology. Part II. Linear perturbation, J. Cosmol. Astropart. Phys. 07 (2021) 053, arXiv:2104.08311.
[2930] M. Cicoli, S. De Alwis, A. Maharana, F. Muia, F. Quevedo, De Sitter vs Quintessence in string theory, Fortsch. Phys. 67 (1–2) (2019) 1800079, arXiv:1808.08967.
[2931] Ruchika, S.A. Adil, K. Dutta, A. Mukherjee, A.A. Sen, Observational constraints on axion(s) dark energy with a cosmological constant, Phys. Dark Univ. 40 (2023) 101199, arXiv:2005.08813.
[2932] J. Grande, J. Solà, H. Stefancic, LXCDM: A cosmon model solution to the cosmological coincidence problem? J. Cosmol. Astropart. Phys. 08 (2006) 011, arXiv:gr-qc/0604057.
[2933] A.A. Sen, Deviation from LambdaCDM: Pressure parametrization, Phys. Rev. D 77 (2008) 043508, arXiv:0708.1072.
[2934] S. Kumar, A. Nautiyal, A.A. Sen, Deviation from ΛCDM with cosmic strings networks, Eur. Phys. J. C 73 (9) (2013) 2562, arXiv:1207.4024.
[2935] R.Y. Wen, L.T. Hergt, N. Afshordi, D. Scott, A cosmic glitch in gravity, J. Cosmol. Astropart. Phys. 03 (2024) 045, arXiv:2311.03028.
[2936] J.M. Maldacena, The Large N limit of superconformal field theories and supergravity, Adv. Theor. Math. Phys. 2 (1998) 231–252, arXiv:hep-th/9711200.
[2937] R. Bousso, J. Polchinski, Quantization of four form fluxes and dynamical neutralization of the cosmological constant, JHEP 06 (2000) 006, arXiv:hep-th/0004134.
[2938] M. Demirtas, M. Kim, L. McAllister, J. Moritz, A. Rios-Tascon, Exponentially small cosmological constant in string theory, Phys. Rev. Lett. 128 (1) (2022) 011602, arXiv:2107.09065.
[2939] A.A. Sen, S.A. Adil, S. Sen, Do cosmological observations allow a negative Λ? Mon. Not. R. Astron. Soc. 518 (1) (2022) 1098–1105, arXiv:2112.10641.
[2940] C.B.V. Dash, T.G. Sarkar, A.A. Sen, Post-reionization H i 21-cm signal: a probe of negative cosmological constant, M Mon. Not. R. Astron. Soc. 527 (4) (2023) 11694–11706, arXiv:2309.01623.
[2941] C. Andrei, A. Ijjas, P.J. Steinhardt, Rapidly descending dark energy and the end of cosmic expansion, Proc. Nat. Acad. Sci. 119 (15) (2022) e2200539119, arXiv:2201.07704.
[2942] S. Vagnozzi, Seven hints that early-time new physics alone is not sufficient to solve the hubble tension, Universe 9 (9) (2023) 393, arXiv:2308.16628.
[2943] Y.L. Bolotin, A. Kostenko, O.A. Lemets, D.A. Yerokhin, Cosmological evolution with interaction between dark energy and dark matter, Internat. J. Modern Phys. D 24 (03) (2014) 1530007, arXiv:1310.0085.
[2944] B. Wang, E. Abdalla, F. Atrio-Barandela, D. Pavón, Further understanding the interaction between dark energy and dark matter: current status and future directions, Rep. Progr. Phys. 87 (3) (2024) 036901, arXiv:2402.00819.
[2945] M.A. van der Westhuizen, A. Abebe, Interacting dark energy: clarifying the cosmological implications and viability conditions, J. Cosmol. Astropart. Phys. 01 (2024) 048, arXiv:2302.11949.
[2946] J.S. Alcaniz, J.A.S. Lima, Interpreting cosmological vacuum decay, Phys. Rev. D 72 (2005) 063516, arXiv:astro-ph/0507372.
[2947] D. Pavon, B. Wang, Le Chatelier-Braun principle in cosmological physics, Gen. Relativity Gravitation 41 (2009) 1–5, arXiv:0712.0565.
[2948] V. da Fonseca, T. Barreiro, N.J. Nunes, A simple parametrisation for coupled dark energy, Phys. Dark Univ. 35 (2022) 100940, arXiv:2104.14889.
[2949] M. Carrillo González, M. Trodden, Field theories and fluids for an interacting dark sector, Phys. Rev. D 97 (4) (2018) 043508, arXiv:1705.04737; Erratum:, Phys. Rev. D 101 (2020) 089901.
[2950] M. Zumalacarregui, T.S. Koivisto, D.F. Mota, P. Ruiz-Lapuente, Disformal scalar fields and the dark sector of the universe, J. Cosmol. Astropart. Phys. 05 (2010) 038, arXiv:1004.2684.
[2951] C. van de Bruck, J. Morrice, Disformal couplings and the dark sector of the universe, J. Cosmol. Astropart. Phys. 04 (2015) 036, arXiv:1501.03073.
[2952] E.M. Teixeira, A. Nunes, N.J. Nunes, Disformally coupled quintessence, Phys. Rev. D 101 (8) (2020) 083506, arXiv:1912.13348.
[2953] C. van de Bruck, E.M. Teixeira, Dark D-Brane Cosmology: from background evolution to cosmological perturbations, Phys. Rev. D 102 (10) (2020) 103503, arXiv:2007.15414.
[2954] C. Van De Bruck, J. Mifsud, Searching for dark matter - dark energy interactions: going beyond the conformal case, Phys. Rev. D 97 (2) (2018) 023506, arXiv:1709.04882.
[2955] J. Valiviita, E. Majerotto, R. Maartens, Instability in interacting dark energy and dark matter fluids, J. Cosmol. Astropart. Phys. 07 (2008) 020, arXiv:0804.0232.
[2956] M.B. Gavela, D. Hernandez, L. Lopez Honorez, O. Mena, S. Rigolin, Dark coupling, J. Cosmol. Astropart. Phys. 07 (2009) 034, arXiv:0901.1611; Erratum:, JCAP 05 (2010) E01.
[2957] Y. Zhai, W. Giarè, C. van de Bruck, E. Di Valentino, O. Mena, R.C. Nunes, A consistent view of interacting dark energy from multiple CMB probes, J. Cosmol. Astropart. Phys. 07 (2023) 032, arXiv:2303.08201.
[2958] W. Giarè, Y. Zhai, S. Pan, E. Di Valentino, R.C. Nunes, C. van de Bruck, Tightening the reins on nonminimal dark sector physics: Interacting dark energy with dynamical and nondynamical equation of state, Phys. Rev. D 110 (6) (2024) 063527, arXiv:2404.02110.
[2959] A. Paliathanasis, S. Pan, W. Yang, Dynamics of nonlinear interacting dark energy models, Internat. J. Modern Phys. D 28 (12) (2019) 1950161, arXiv:1903.02370.
[2960] J. De-Santiago, I.E. Sánchez G., D. Tamayo, Non-linear coupling in the dark sector as a running vacuum model, Gen. Relativity Gravitation 50 (8) (2018) 101, arXiv:1612.02836.
[2961] F. Arevalo, A.P.R. Bacalhau, W. Zimdahl, Cosmological dynamics with non-linear interactions, Cl. Quant. Grav. 29 (2012) 235001, arXiv:1112.5095.
[2962] E. Ebrahimi, H. Golchin, A. Mehrabi, S.M.S. Movahed, Consistency of nonlinear interacting ghost dark energy with recent observations, Internat. J. Modern Phys. D 26 (11) (2017) 1750124, arXiv:1611.06551.
[2963] M. Khurshudyan, A. Khurshudyan, On cosmology of interacting varying polytropic dark fluids, Modern Phys. Lett. A 34 (17) (2019) 1950133, arXiv:1707.04116.
[2964] G. Cheng, Y.-Z. Ma, F. Wu, J. Zhang, X. Chen, Testing interacting dark matter and dark energy model with cosmological data, Phys. Rev. D 102 (4) (2020) 043517, arXiv:1911.04520.

[2965] W. Yang, S. Pan, A. Paliathanasis, Cosmological constraints on an exponential interaction in the dark sector, Mon. Not. R. Astron. Soc. 482 (1) (2019) 1007–1016, arXiv:1804.08558.

[2966] M. Khurshudyan, A. Khurshudyan, Some interacting dark energy models, Symmetry 10 (11) (2018) 577, arXiv:1708.02293.

[2967] S. Pan, W. Yang, A. Paliathanasis, Non-linear interacting cosmological models after Planck 2018 legacy release and the H_0 tension, Mon. Not. R. Astron. Soc. 493 (3) (2020) 3114–3131, arXiv:2002.03408.

[2968] Z. Haba, A. Stachowski, M. Szydłowski, Dynamics of the diffusive DM-DE interaction – dynamical system approach, J. Cosmol. Astropart. Phys. 07 (2016) 024, arXiv:1603.07620.

[2969] G. Koutsoumbas, K. Ntrekis, E. Papantonopoulos, E.N. Saridakis, Unification of dark matter - dark energy in generalized Galileon theories, J. Cosmol. Astropart. Phys. 02 (2018) 003, arXiv:1704.08640.

[2970] S. Calogero, H. Velten, Cosmology with matter diffusion, J. Cosmol. Astropart. Phys. 11 (2013) 025, arXiv:1308.3393.

[2971] E.F. Piratova Moreno, L.Á. García, Late accelerated expansion of the universe in diffusive scenarios, Rev. Mex. Astron. Astrofis. 59 (2) (2023) 389–399.

[2972] T. Josset, A. Perez, D. Sudarsky, Dark energy from violation of energy conservation, Phys. Rev. Lett. 118 (2) (2017) 021102, arXiv:1604.04183.

[2973] A. Perez, D. Sudarsky, Dark energy from quantum gravity discreteness, Phys. Rev. Lett. 122 (22) (2019) 221302, arXiv:1711.05183.

[2974] A. Perez, D. Sudarsky, Black holes, Planckian granularity, and the changing cosmological 'constant', Gen. Relativity Gravitation 53 (4) (2021) 40, arXiv:1911.06059.

[2975] C. Corral, N. Cruz, E. González, Diffusion in unimodular gravity: Analytical solutions, late-time acceleration, and cosmological constraints, Phys. Rev. D 102 (2) (2020) 023508, arXiv:2005.06052.

[2976] F.X. Linares Cedeño, U. Nucamendi, Revisiting cosmological diffusion models in unimodular gravity and the H_0 tension, Phys. Dark Univ. 32 (2021) 100807, arXiv:2009.10268.

[2977] S.J. Landau, M. Benetti, A. Perez, D. Sudarsky, Cosmological constraints on unimodular gravity models with diffusion, Phys. Rev. D 108 (4) (2023) 043524, arXiv:2211.07424.

[2978] D. Wands, J. De-Santiago, Y. Wang, Inhomogeneous vacuum energy, Cl. Quant. Grav. 29 (2012) 145017, arXiv:1203.6776.

[2979] M. Sebastianutti, N.B. Hogg, M. Bruni, The interacting vacuum and tensions: A comparison of theoretical models, Phys. Dark Univ. 46 (2024) 101546, arXiv:2312.14123.

[2980] S. Weinberg, The cosmological constant problem, in: J.-P. Hsu, D. Fine (Eds.), Rev. Modern Phys. 61 (1989) 1–23.

[2981] G.F.R. Ellis, H. van Elst, J. Murugan, J.-P. Uzan, On the trace-free Einstein equations as a viable alternative to general relativity, Cl. Quant. Grav. 28 (2011) 225007, arXiv:1008.1196.

[2982] M. de Cesare, E. Wilson-Ewing, Interacting dark sector from the trace-free Einstein equations: Cosmological perturbations with no instability, Phys. Rev. D 106 (2) (2022) 023527, arXiv:2112.12701.

[2983] A. Shafieloo, D.K. Hazra, V. Sahni, A.A. Starobinsky, Metastable dark energy with radioactive-like decay, Mon. Not. R. Astron. Soc. 473 (2) (2018) 2760–2770, arXiv:1610.05192.

[2984] J.S.T. de Souza, G. S. Vicente, L.L. Graef, Constraints on metastable dark energy decaying into dark matter, Universe 10 (9) (2024) 371, arXiv:2403.04970.

[2985] X. Li, A. Shafieloo, V. Sahni, A.A. Starobinsky, Revisiting metastable dark energy and tensions in the estimation of cosmological parameters, Astrophys. J. 887 (2019) 153, arXiv:1904.03790.

[2986] W. Yang, E. Di Valentino, S. Pan, S. Basilakos, A. Paliathanasis, Metastable dark energy models in light of *Planck* 2018 data: Alleviating the H_0 tension, Phys. Rev. D 102 (6) (2020) 063503, arXiv:2001.04307.

[2987] K. Urbanowski, Cosmological "constant" in a universe born in the metastable false vacuum state, Eur. Phys. J. C 82 (3) (2022) 242, arXiv:2110.11957.

[2988] K. Urbanowski, A universe born in a metastable false vacuum state needs not die, Eur. Phys. J. C 83 (1) (2023) 55, arXiv:2207.10965.

[2989] E. Abdalla, L.L. Graef, B. Wang, A model for dark energy decay, Phys. Lett. B 726 (2013) 786–790, arXiv:1202.0499.

[2990] R.G. Landim, E. Abdalla, Metastable dark energy, Phys. Lett. B 764 (2017) 271–276, arXiv:1611.00428.

[2991] R.G. Landim, R.J.F. Marcondes, F.F. Bernardi, E. Abdalla, Interacting dark energy in the dark $SU(2)_R$ model, Braz. J. Phys. 48 (4) (2018) 364–369, arXiv:1711.07282.

[2992] D. Stojkovic, G.D. Starkman, R. Matsuo, Dark energy, the colored anti-de Sitter vacuum, and LHC phenomenology, Phys. Rev. D 77 (2008) 063006, arXiv:hep-ph/0703246.

[2993] E. Greenwood, E. Halstead, R. Poltis, D. Stojkovic, Dark energy, the electroweak vacua and collider phenomenology, Phys. Rev. D 79 (2009) 103003, arXiv:0810.5343.

[2994] F. Simpson, Scattering of dark matter and dark energy, Phys. Rev. D 82 (2010) 083505, arXiv:1007.1034.

[2995] A. Pourtsidou, C. Skordis, E.J. Copeland, Models of dark matter coupled to dark energy, Phys. Rev. D 88 (8) (2013) 083505, arXiv:1307.0458.

[2996] M. Asghari, J. Beltrán Jiménez, S. Khosravi, D.F. Mota, On structure formation from a small-scales-interacting dark sector, J. Cosmol. Astropart. Phys. 04 (2019) 042, arXiv:1902.05532.

[2997] D. Figueruelo, et al., J-PAS: Forecasts for dark matter - dark energy elastic couplings, J. Cosmol. Astropart. Phys. 07 (2021) 022, arXiv:2103.01571.

[2998] J. Beltrán Jiménez, D. Bettoni, D. Figueruelo, F.A. Teppa Pannia, S. Tsujikawa, Probing elastic interactions in the dark sector and the role of S8, Phys. Rev. D 104 (10) (2021) 103503, arXiv:2106.11222.

[2999] V. Poulin, J.L. Bernal, E.D. Kovetz, M. Kamionkowski, Sigma-8 tension is a drag, Phys. Rev. D 107 (12) (2023) 123538, arXiv:2209.06217.

[3000] J.B. Jiménez, D. Bettoni, D. Figueruelo, F.A. Teppa Pannia, On evidence for elastic interactions in the dark sector, Phys. Dark Univ. 47 (2025) 101761, arXiv:2410.18645.

[3001] J. Beltrán Jiménez, E. Di Dio, D. Figueruelo, A smoking gun from the power spectrum dipole for elastic interactions in the dark sector, J. Cosmol. Astropart. Phys. 11 (2023) 088, arXiv:2212.08617 [astro-ph.CO].

[3002] J. Beltrán Jiménez, D. Figueruelo, F.A. Teppa Pannia, Nondegeneracy of massive neutrinos and elastic interactions in the dark sector, Phys. Rev. D 110 (2) (2024) 023527, arXiv:2403.03216 [astro-ph.CO].

[3003] M. Baldi, F. Simpson, Structure formation simulations with momentum exchange: alleviating tensions between high-redshift and low-redshift cosmological probes, Mon. Not. R. Astron. Soc. 465 (1) (2017) 653–666, arXiv:1605.05623 [astro-ph.CO].

[3004] A. Pourtsidou, T. Tram, Reconciling CMB and structure growth measurements with dark energy interactions, Phys. Rev. D 94 (4) (2016) 043518, arXiv:1604.04222 [astro-ph.CO].

[3005] P. Agrawal, G. Obied, P.J. Steinhardt, C. Vafa, On the cosmological implications of the String Swampland, Phys. Lett. B 784 (2018) 271–276, arXiv:1806.09718 [hep-th].

[3006] W.H. Kinney, S. Vagnozzi, L. Visinelli, The zoo plot meets the swampland: mutual (in)consistency of single-field inflation, string conjectures, and cosmological data, Cl. Quant. Grav. 36 (11) (2019) 117001, arXiv:1808.06424 [astro-ph.CO].

[3007] P. Agrawal, G. Obied, C. Vafa, H_0 tension, swampland conjectures, and the epoch of fading dark matter, Phys. Rev. D 103 (4) (2021) 043523, arXiv:1906.08261 [astro-ph.CO].

[3008] A. Salam, E. Sezgin, Chiral compactification on Minkowski x S**2 of N=2 Einstein–Maxwell supergravity in six-dimensions, Phys. Lett. B 147 (1984) 47.

[3009] M. Cvetic, G.W. Gibbons, C.N. Pope, A string and M theory origin for the Salam–Sezgin model, Nuclear Phys. B 677 (2004) 164–180, arXiv:hep-th/0308026.

[3010] L.A. Anchordoqui, I. Antoniadis, D. Lüst, J.F. Soriano, T.R. Taylor, H_0 tension and the String Swampland, Phys. Rev. D 101 (2020) 083532, arXiv:1912.00242 [hep-th].

[3011] L.A. Anchordoqui, I. Antoniadis, D. Lüst, J.F. Soriano, Dark energy, Ricci-nonflat spaces, and the Swampland, Phys. Lett. B 816 (2021) 136199, arXiv:2005.10075 [hep-th].

[3012] D. Benisty, S. Pan, D. Staicova, E. Di Valentino, R.C. Nunes, Late-time constraints on interacting dark energy: Analysis independent of H0, rd, and MB, Astron. Astrophys. 688 (2024) A156, arXiv:2403.00056 [astro-ph.CO].

[3013] G.A. Hoerning, R.G. Landim, L.O. Ponte, R.P. Rolim, F.B. Abdalla, E. Abdalla, Constraints on interacting dark energy revisited: implications for the hubble tension, 2023, arXiv:2308.05807 [astro-ph.CO].

[3014] S. Pan, W. Yang, On the interacting dark energy scenarios – the case for Hubble constant tension, 2023, arXiv:2310.07260 [astro-ph.CO].

[3015] W. Yang, S. Pan, E. Di Valentino, R.C. Nunes, S. Vagnozzi, D.F. Mota, Tale of stable interacting dark energy, observational signatures, and the H_0 tension, J. Cosmol. Astropart. Phys. 09 (2018) 019, arXiv:1805.08252 [astro-ph.CO].

[3016] A. Bhattacharyya, U. Alam, K.L. Pandey, S. Das, S. Pal, Are H_0 and σ_8 tensions generic to present cosmological data? Astrophys. J. 876 (2) (2019) 143, arXiv:1805.04716 [astro-ph.CO].

[3017] E. Di Valentino, R.Z. Ferreira, L. Visinelli, U. Danielsson, Late time transitions in the quintessence field and the H_0 tension, Phys. Dark Univ. 26 (2019) 100385, arXiv:1906.11255 [astro-ph.CO].

[3018] Y.-H. Yao, X.-H. Meng, Can interacting dark energy with dynamical coupling resolve the Hubble tension, 2022, arXiv:2207.05955 [astro-ph.CO].

[3019] S. Gariazzo, E. Di Valentino, O. Mena, R.C. Nunes, Late-time interacting cosmologies and the Hubble constant tension, Phys. Rev. D 106 (2) (2022) 023530, arXiv:2111.03152 [astro-ph.CO].

[3020] R.-Y. Guo, L. Feng, T.-Y. Yao, X.-Y. Chen, Exploration of interacting dynamical dark energy model with interaction term including the equation-of-state parameter: alleviation of the H_0 tension, J. Cosmol. Astropart. Phys. 12 (12) (2021) 036, arXiv:2110.02536 [gr-qc].

[3021] R.C. Nunes, E. Di Valentino, Dark sector interaction and the supernova absolute magnitude tension, Phys. Rev. D 104 (6) (2021) 063529, arXiv:2107.09151 [astro-ph.CO].

[3022] Y. Zhao, Y. Liu, S. Liao, J. Zhang, X. Liu, W. Du, Constraining interacting dark energy models with the halo concentration–mass relation, Mon. Not. R. Astron. Soc. 523 (4) (2023) 5962–5971, arXiv:2212.02050 [astro-ph.CO].

[3023] L.-Y. Gao, Z.-W. Zhao, S.-S. Xue, X. Zhang, Relieving the H 0 tension with a new interacting dark energy model, J. Cosmol. Astropart. Phys. 07 (2021) 005, arXiv:2101.10714 [astro-ph.CO].

[3024] H. Amirhashchi, A.K. Yadav, N. Ahmad, V. Yadav, Interacting dark sectors in anisotropic universe: Observational constraints and H0 tension, Phys. Dark Univ. 36 (2022) 101043, arXiv:2001.03775 [astro-ph.CO].

[3025] S. Pan, W. Yang, C. Singha, E.N. Saridakis, Observational constraints on sign-changeable interaction models and alleviation of the H_0 tension, Phys. Rev. D 100 (8) (2019) 083539, arXiv:1903.10969 [astro-ph.CO].

[3026] L.-Y. Gao, S.-S. Xue, X. Zhang, Dark energy and matter interacting scenario to relieve H_0 and S_8 tensions*, Chin. Phys. C 48 (5) (2024) 051001, arXiv:2212.13146 [astro-ph.CO].

[3027] W. Yang, S. Pan, E. Di Valentino, O. Mena, A. Melchiorri, 2021-H0 odyssey: closed, phantom and interacting dark energy cosmologies, J. Cosmol. Astropart. Phys. 10 (2021) 008, arXiv:2101.03129 [astro-ph.CO].

[3028] W. Yang, S. Pan, R.C. Nunes, D.F. Mota, Dark calling Dark: Interaction in the dark sector in presence of neutrino properties after Planck CMB final release, J. Cosmol. Astropart. Phys. 04 (2020) 008, arXiv:1910.08821 [astro-ph.CO].

[3029] M. Lucca, Dark energy–dark matter interactions as a solution to the S8 tension, Phys. Dark Univ. 34 (2021) 100899, arXiv:2105.09249 [astro-ph.CO].

[3030] R. An, C. Feng, B. Wang, Relieving the tension between weak lensing and cosmic microwave background with interacting dark matter and dark energy models, J. Cosmol. Astropart. Phys. 02 (2018) 038, arXiv:1711.06799 [astro-ph.CO].

[3031] S. Sinha, N. Banerjee, Density perturbation in an interacting holographic dark energy model, Eur. Phys. J. Plus 135 (10) (2020) 779, arXiv:1911.06520 [gr-qc].

[3032] S. Sinha, Differentiating dark interactions with perturbation, Phys. Rev. D 103 (12) (2021) 123547, arXiv:2101.08959 [astro-ph.CO].

[3033] S. Sinha, M. Banerjee, S. Das, Perturbation in an interacting dark universe, Phys. Dark Univ. 42 (2023) 101273, arXiv:2204.05174 [gr-qc].

[3034] B.J. Barros, D. Castelão, V. da Fonseca, T. Barreiro, N.J. Nunes, I. Tereno, Is there evidence for CIDER in the Universe? J. Cosmol. Astropart. Phys. 01 (2023) 013, arXiv:2209.04468 [astro-ph.CO].

[3035] O. Trivedi, Recent advances in cosmological singularities, Symmetry 16 (3) (2024) 298, arXiv:2309.08954 [gr-qc].

[3036] J. de Haro, S. Nojiri, S.D. Odintsov, V.K. Oikonomou, S. Pan, Finite-time cosmological singularities and the possible fate of the universe, Phys. Rep. 1034 (2023) 1–114, arXiv:2309.07465 [gr-qc].

[3037] S. Nojiri, S.D. Odintsov, S. Tsujikawa, Properties of singularities in (phantom) dark energy universe, Phys. Rev. D 71 (2005) 063004, arXiv:hep-th/0501025.

[3038] S. Nojiri, S.D. Odintsov, V.K. Oikonomou, Modified gravity theories on a Nutshell: Inflation, bounce and late-time evolution, Phys. Rep. 692 (2017) 1–104, arXiv:1705.11098 [gr-qc].

[3039] S. Nojiri, S.D. Odintsov, Inhomogeneous equation of state of the universe: Phantom era, future singularity and crossing the phantom barrier, Phys. Rev. D 72 (2005) 023003, arXiv:hep-th/0505215.

[3040] K. Bamba, S. Nojiri, S.D. Odintsov, The Universe future in modified gravity theories: Approaching the finite-time future singularity, J. Cosmol. Astropart. Phys. 10 (2008) 045, arXiv:0807.2575 [hep-th].

[3041] S. Nojiri, S.D. Odintsov, Quantum escape of sudden future singularity, Phys. Lett. B 595 (2004) 1–8, arXiv:hep-th/0405078.

[3042] S. Castello, N. Grimm, C. Bonvin, Rescuing constraints on modified gravity using gravitational redshift in large-scale structure, Phys. Rev. D 106 (8) (2022) 083511, arXiv:2204.11507 [astro-ph.CO].

[3043] S. Castello, M. Mancarella, N. Grimm, D. Sobral-Blanco, I. Tutusaus, C. Bonvin, Gravitational redshift constraints on the effective theory of interacting dark energy, J. Cosmol. Astropart. Phys. 05 (2024) 003, arXiv:2311.14425 [astro-ph.CO].

[3044] C. Bonvin, L.E. Pogosian, Can cosmology distinguish a dark force from a modification of gravity? Nat. Astron. 7 (9) (2023) 1023–1024.

[3045] S. Castello, Z. Wang, L. Dam, C. Bonvin, L. Pogosian, Disentangling modified gravity from a dark force with gravitational redshift, Phys. Rev. D 110 (10) (2024) 103523, arXiv:2404.09379 [astro-ph.CO].

[3046] D. Sobral-Blanco, C. Bonvin, Measuring anisotropic stress with relativistic effects, Phys. Rev. D 104 (6) (2021) 063516, arXiv:2102.05086 [astro-ph.CO].

[3047] D. Sobral-Blanco, C. Bonvin, Measuring the distortion of time with relativistic effects in large-scale structure, Mon. Not. R. Astron. Soc. 519 (1) (2022) L39–L44, arXiv:2205.02567 [astro-ph.CO].

[3048] Y.-H. Li, J.-F. Zhang, X. Zhang, Testing models of vacuum energy interacting with cold dark matter, Phys. Rev. D 93 (2) (2016) 023002, arXiv:1506.06349 [astro-ph.CO].

[3049] L. Feng, H.-L. Li, J.-F. Zhang, X. Zhang, Exploring neutrino mass and mass hierarchy in interacting dark energy models, Sci. China Phys. Mech. Astron. 63 (2) (2020) 220401, arXiv:1903.08848 [astro-ph.CO].

[3050] Y.-H. Li, X. Zhang, Large-scale stable interacting dark energy model: cosmological perturbations and observational constraints, Phys. Rev. D 89 (8) (2014) 083009, arXiv:1312.6328 [astro-ph.CO].

[3051] L. Feng, X. Zhang, Revisit of the interacting holographic dark energy model after Planck 2015, J. Cosmol. Astropart. Phys. 08 (2016) 072, arXiv:1607.05567 [astro-ph.CO].

[3052] M.-M. Zhao, D.-Z. He, J.-F. Zhang, X. Zhang, Search for sterile neutrinos in holographic dark energy cosmology: Reconciling Planck observation with the local measurement of the Hubble constant, Phys. Rev. D 96 (4) (2017) 043520, arXiv:1703.08456 [astro-ph.CO].

[3053] Y.-H. Li, J.-F. Zhang, X. Zhang, Exploring the full parameter space for an interacting dark energy model with recent observations including redshift-space distortions: Application of the parametrized post-Friedmann approach, Phys. Rev. D 90 (12) (2014) 123007, arXiv:1409.7205 [astro-ph.CO].

[3054] Y.-H. Li, J.-F. Zhang, X. Zhang, Parametrized post-Friedmann framework for interacting dark energy, Phys. Rev. D 90 (6) (2014) 063005, arXiv:1404.5220 [astro-ph.CO].

[3055] R.-Y. Guo, Y.-H. Li, J.-F. Zhang, X. Zhang, Weighing neutrinos in the scenario of vacuum energy interacting with cold dark matter: application of the parameterized post-Friedmann approach, J. Cosmol. Astropart. Phys. 05 (2017) 040, arXiv:1702.04189 [astro-ph.CO].

[3056] X. Zhang, Probing the interaction between dark energy and dark matter with the parametrized post-Friedmann approach, Sci. China Phys. Mech. Astron. 60 (5) (2017) 050431, arXiv:1702.04564 [astro-ph.CO].

[3057] L. Feng, Y.-H. Li, F. Yu, J.-F. Zhang, X. Zhang, Exploring interacting holographic dark energy in a perturbed universe with parameterized post-Friedmann approach, Eur. Phys. J. C 78 (10) (2018) 865, arXiv:1807.03022 [astro-ph.CO].

[3058] Y.-H. Li, X. Zhang, IDECAMB: an implementation of interacting dark energy cosmology in CAMB, J. Cosmol. Astropart. Phys. 09 (2023) 046, arXiv:2306.01593 [astro-ph.CO].

[3059] J.-J. Guo, J.-F. Zhang, Y.-H. Li, D.-Z. He, X. Zhang, Probing the sign-changeable interaction between dark energy and dark matter with current observations, Sci. China Phys. Mech. Astron. 61 (3) (2018) 030011, arXiv:1710.03068 [astro-ph.CO].

[3060] H.-L. Li, J.-F. Zhang, L. Feng, X. Zhang, Reexploration of interacting holographic dark energy model: Cases of interaction term excluding the Hubble parameter, Eur. Phys. J. C 77 (12) (2017) 907, arXiv:1711.06159 [astro-ph.CO].

[3061] L. Feng, D.-Z. He, H.-L. Li, J.-F. Zhang, X. Zhang, Constraints on active and sterile neutrinos in an interacting dark energy cosmology, Sci. China Phys. Mech. Astron. 63 (9) (2020) 290404, arXiv:1910.03872 [astro-ph.CO].

[3062] M. Zhang, B. Wang, P.-J. Wu, J.-Z. Qi, Y. Xu, J.-F. Zhang, X. Zhang, Prospects for constraining interacting dark energy models with 21 cm intensity mapping experiments, Astrophys. J. 918 (2) (2021) 56, arXiv:2102.03979 [astro-ph.CO].

[3063] T.-N. Li, P.-J. Wu, G.-H. Du, S.-J. Jin, H.-L. Li, J.-F. Zhang, X. Zhang, Constraints on interacting dark energy models from the desi baryon acoustic oscillation and des supernovae data, Astrophys. J. 976 (1) (2024) 1, arXiv:2407.14934 [astro-ph.CO].

[3064] J. Gleyzes, D. Langlois, M. Mancarella, F. Vernizzi, Effective theory of interacting dark energy, J. Cosmol. Astropart. Phys. 08 (2015) 054, arXiv:1504.05481 [astro-ph.CO].

[3065] J. Gleyzes, D. Langlois, M. Mancarella, F. Vernizzi, Effective theory of dark energy at redshift survey scales, J. Cosmol. Astropart. Phys. 02 (2016) 056, arXiv:1509.02191 [astro-ph.CO].

[3066] C.M. Will, The confrontation between general relativity and experiment, Living Rev. Rel. 17 (2014) 4, arXiv:1403.7377 [gr-qc].

[3067] A. Addazi, et al., Quantum gravity phenomenology at the dawn of the multi-messenger era—A review, Prog. Part. Nucl. Phys. 125 (2022) 103948, arXiv:2111.05659 [hep-ph].

[3068] R. Alves Batista, et al., White paper and roadmap for quantum gravity phenomenology in the multi-messenger era, Cl. Quant. Grav. 42 (3) (2025) 032001, arXiv:2312.00409 [gr-qc].

[3069] M.H. Goroff, A. Sagnotti, The ultraviolet behavior of einstein gravity, Nuclear Phys. B 266 (1986) 709–736.

[3070] L. Barack, et al., Black holes, gravitational waves and fundamental physics: a roadmap, Cl. Quant. Grav. 36 (14) (2019) 143001, arXiv:1806.05195 [gr-qc].

[3071] S.M. Carroll, The cosmological constant, Living Rev. Rel. 4 (2001) 1, arXiv:astro-ph/0004075.

[3072] Supernova Search Team Collaboration, A.G. Riess, et al., Observational evidence from supernovae for an accelerating universe and a cosmological constant, Astron. J. 116 (1998) 1009–1038, arXiv:astro-ph/9805201.

[3073] Supernova Cosmology Project Collaboration, S. Perlmutter, et al., Measurements of Ω and Λ from 42 high redshift supernovae, Astrophys. J. 517 (1999) 565–586, arXiv:astro-ph/9812133.

[3074] M. Davis, G. Efstathiou, C.S. Frenk, S.D.M. White, The evolution of large scale structure in a universe dominated by cold dark matter, Astrophys. J. 292 (1985) 371–394.

[3075] G. Bertone, D. Hooper, History of dark matter, Rev. Modern Phys. 90 (4) (2018) 045002, arXiv:1605.04909 [astro-ph.CO].

[3076] E. Aprile, T. Doke, Liquid xenon detectors for particle physics and astrophysics, Rev. Modern Phys. 82 (2010) 2053–2097, arXiv:0910.4956 [physics.ins-det].

[3077] M. Misiaszek, N. Rossi, Direct detection of dark matter: A critical review, Symmetry 16 (2) (2024) 201, arXiv:2310.20472 [hep-ph].

[3078] F. Bajardi, S. Capozziello, Noether Symmetries in Theories of Gravity, in: Cambridge Monographs on Mathematical Physics, Cambridge University Press, 2022.

[3079] CANTATA Collaboration (Eds.), E.N. Saridakis, R. Lazkoz, V. Salzano, P. Vargas Moniz, S. Capozziello, J. Beltrán Jiménez, M. De Laurentis, G.J. Olmo (Eds.), Modified Gravity and Cosmology. An Update by the CANTATA Network, Springer, 2021, arXiv:2105.12582 [gr-qc].

[3080] K.S. Stelle, Renormalization of higher derivative quantum gravity, Phys. Rev. D 16 (1977) 953–969.

[3081] F. Bajardi, S. Capozziello, D. Vernieri, Non-local curvature and Gauss–Bonnet cosmologies by Noether symmetries, Eur. Phys. J. Plus 135 (12) (2020) 942, arXiv:2011.01317 [gr-qc].

[3082] F. Bajardi, D. Vernieri, S. Capozziello, Exact solutions in higher-dimensional Lovelock and AdS_5 Chern–Simons gravity, J. Cosmol. Astropart. Phys. 11 (11) (2021) 057, arXiv:2106.07396 [gr-qc].

[3083] J.J. Halliwell, Scalar fields in cosmology with an exponential potential, Phys. Lett. B 185 (1987) 341.

[3084] J.-P. Uzan, Cosmological scaling solutions of nonminimally coupled scalar fields, Phys. Rev. D 59 (1999) 123510, arXiv:gr-qc/9903004.

[3085] Z. Urban, F. Bajardi, S. Capozziello, The Noether–Bessel-Hagen symmetry approach for dynamical systems, Int. J. Geom. Meth. Mod. Phys. 17 (14) (2020) 2050215, arXiv:2003.13756 [gr-qc].

[3086] M. Krssak, R.J. van den Hoogen, J.G. Pereira, C.G. Böhmer, A.A. Coley, Teleparallel theories of gravity: illuminating a fully invariant approach, Cl. Quant. Grav. 36 (18) (2019) 183001, arXiv:1810.12932 [gr-qc].

[3087] S. Bahamonde, K.F. Dialektopoulos, C. Escamilla-Rivera, G. Farrugia, V. Gakis, M. Hendry, M. Hohmann, J. Levi Said, J. Mifsud, E. Di Valentino, Teleparallel gravity: from theory to cosmology, Rep. Progr. Phys. 86 (2) (2023) 026901, arXiv:2106.13793 [gr-qc].

[3088] A. Jiménez Cano, Metric-Affine Gauge Theories of Gravity. Foundations and New Insights (Ph.D. thesis), Granada U., Theor. Phys. Astrophys., 2021, arXiv:2201.12847 [gr-qc].

[3089] I. Ayuso, R. Lazkoz, V. Salzano, Observational constraints on cosmological solutions of $f(Q)$ theories, Phys. Rev. D 103 (6) (2021) 063505, arXiv:2012.00046 [astro-ph.CO].

[3090] M. Hohmann, C. Pfeifer, N. Voicu, Mathematical foundations for field theories on Finsler spacetimes, J. Math. Phys. 63 (3) (2022) 032503, arXiv:2106.14965 [math-ph].

[3091] C. Pfeifer, Finsler spacetime geometry in Physics, Int. J. Geom. Meth. Mod. Phys. 16 (supp02) (2019) 1941004, arXiv:1903.10185 [gr-qc].

[3092] J.D. Barrow, S. Cotsakis, Inflation and the conformal structure of higher order gravity theories, Phys. Lett. B 214 (1988) 515–518.

[3093] T.P. Sotiriou, V. Faraoni, f(R) theories of gravity, Rev. Modern Phys. 82 (2010) 451–497, arXiv:0805.1726 [gr-qc].

[3094] A. De Felice, S. Tsujikawa, f(R) theories, Living Rev. Rel. 13 (2010) 3, arXiv:1002.4928 [gr-qc].

[3095] S. Capozziello, M. De Laurentis, Extended theories of gravity, Phys. Rep. 509 (2011) 167–321, arXiv:1108.6266 [gr-qc].

[3096] A.A. Starobinsky, Disappearing cosmological constant in f(R) gravity, JETP Lett. 86 (2007) 157–163, arXiv:0706.2041 [astro-ph].

[3097] A. Paliathanasis, M. Tsamparlis, S. Basilakos, Constraints and analytical solutions of $f(R)$ theories of gravity using Noether symmetries, Phys. Rev. D 84 (2011) 123514, arXiv:1111.4547 [astro-ph.CO].

[3098] S. Nojiri, S.D. Odintsov, Modified f(R) gravity consistent with realistic cosmology: From matter dominated epoch to dark energy universe, Phys. Rev. D 74 (2006) 086005, arXiv:hep-th/0608008.

[3099] G. Papagiannopoulos, S. Basilakos, J.D. Barrow, A. Paliathanasis, New integrable models and analytical solutions in $f(R)$ cosmology with an ideal gas, Phys. Rev. D 97 (2) (2018) 024026, arXiv:1801.01274 [gr-qc].

[3100] F. Bajardi, R. D'Agostino, M. Benetti, V. De Falco, S. Capozziello, Early and late time cosmology: the f(R) gravity perspective, Eur. Phys. J. Plus 137 (11) (2022) 1239, arXiv:2211.06268 [gr-qc].

[3101] S. Nojiri, S.D. Odintsov, Unified cosmic history in modified gravity: from F(R) theory to Lorentz non-invariant models, Phys. Rep. 505 (2011) 59–144, arXiv:1011.0544 [gr-qc].

[3102] S. Capozziello, et al., Constraining Theories of Gravity by GINGER experiment, Eur. Phys. J. Plus 136 (4) (2021) 394, arXiv:2103.15135 [gr-qc]; Eur. Phys. J. Plus 136 (2021) 563, Erratum.

[3103] T. Schiavone, G. Montani, F. Bombacigno, f(R) gravity in the Jordan frame as a paradigm for the Hubble tension, Mon. Not. R. Astron. Soc. 522 (1) (2023) L72–L77, arXiv:2211.16737 [gr-qc].

[3104] G. Montani, M. De Angelis, F. Bombacigno, N. Carlevaro, Metric f(R) gravity with dynamical dark energy as a scenario for the Hubble tension, Mon. Not. R. Astron. Soc. 527 (1) (2023) L156–L161, arXiv:2306.11101 [gr-qc].

[3105] G. Montani, N. Carlevaro, M. De Angelis, Modified gravity in the presence of matter creation: Scenario for the late universe, Entropy 26 (8) (2024) 662, arXiv:2407.12409 [gr-qc].

[3106] G. Montani, N. Carlevaro, M.G. Dainotti, Running Hubble constant: Evolutionary dark energy, Phys. Dark Univ. 48 (2025) 101847, arXiv:2411.07060 [gr-qc].

[3107] G. Montani, N. Carlevaro, M.G. Dainotti, Slow-rolling scalar dynamics as solution for the Hubble tension, Phys. Dark Univ. 44 (2024) 101486, arXiv:2311.04822 [gr-qc].

[3108] G. Montani, N. Carlevaro, L.A. Escamilla, E. Di Valentino, Kinetic model for dark energy—dark matter interaction: Scenario for the Hubble tension, Phys. Dark Univ. 48 (2025) 101848, arXiv:2404.15977 [gr-qc].

[3109] M. Barroso Varela, O. Bertolami, Is cosmological data suggesting a nonminimal coupling between matter and gravity? Phys. Dark Univ. 48 (2025) 101861, arXiv:2412.09348 [astro-ph.CO].

[3110] M.G. Dainotti, B. De Simone, T. Schiavone, G. Montani, E. Rinaldi, G. Lambiase, On the Hubble constant tension in the SNe Ia Pantheon sample, Astrophys. J. 912 (2) (2021) 150, arXiv:2103.02117 [astro-ph.CO].

[3111] S. Nojiri, S.D. Odintsov, V.K. Oikonomou, Integral F(R) gravity and saddle point condition as a remedy for the H0-tension, Nuclear Phys. B 980 (2022) 115850, arXiv:2205.11681 [gr-qc].

[3112] I. Ayuso, J.A.R. Cembranos, Nonminimal scalar-tensor theories, Phys. Rev. D 101 (4) (2020) 044007, arXiv:1411.1653 [gr-qc].

[3113] J.D. Barrow, Slow roll inflation in scalar - tensor theories, Phys. Rev. D 51 (1995) 2729–2732.

[3114] Y. Shtanov, J.H. Traschen, R.H. Brandenberger, Universe reheating after inflation, Phys. Rev. D 51 (1995) 5438–5455, arXiv:hep-ph/9407247.

[3115] R. Allahverdi, R. Brandenberger, F.-Y. Cyr-Racine, A. Mazumdar, Reheating in inflationary cosmology: theory and applications, Ann. Rev. Nucl. Part. Sci. 60 (2010) 27–51, arXiv:1001.2600 [hep-th].

[3116] P.B. Greene, Inflationary reheating and fermions, AIP Conf. Proc. 478 (1) (1999) 72–74, arXiv:hep-ph/9905256.

[3117] T. Kobayashi, Horndeski theory and beyond: a review, Rep. Progr. Phys. 82 (8) (2019) 086901, arXiv:1901.07183 [gr-qc].

[3118] C. Deffayet, X. Gao, D.A. Steer, G. Zahariade, From k-essence to generalised Galileons, Phys. Rev. D 84 (2011) 064039, arXiv:1103.3260 [hep-th].

[3119] R. Kase, S. Tsujikawa, Dark energy in Horndeski theories after GW170817: A review, Internat. J. Modern Phys. D 28 (05) (2019) 1942005, arXiv:1809.08735 [gr-qc].

[3120] R. D'Agostino, R.C. Nunes, Probing observational bounds on scalar-tensor theories from standard sirens, Phys. Rev. D 100 (4) (2019) 044041, arXiv:1907.05516 [gr-qc].

[3121] J.M. Ezquiaga, M. Zumalacárregui, Dark energy after GW170817: Dead ends and the road ahead, Phys. Rev. Lett. 119 (25) (2017) 251304, arXiv:1710.05901 [astro-ph.CO].

[3122] A. Bonilla, R. D'Agostino, R.C. Nunes, J.C.N. de Araujo, Forecasts on the speed of gravitational waves at high z, J. Cosmol. Astropart. Phys. 03 (2020) 015, arXiv:1910.05631 [gr-qc].

[3123] I.D. Saltas, J. Christensen-Dalsgaard, Searching for dark energy with the Sun, Astron. Astrophys. 667 (2022) A115, arXiv:2205.14134 [astro-ph.SR].

[3124] E. Babichev, C. Charmousis, B. Muntz, A. Padilla, I.D. Saltas, Horndeski speed tests with scalar-photon couplings, J. Cosmol. Astropart. Phys. 01 (2025) 041, arXiv:2407.20339 [gr-qc].

[3125] C. de Rham, S. Melville, Gravitational rainbows: LIGO and dark energy at its cutoff, Phys. Rev. Lett. 121 (22) (2018) 221101, arXiv:1806.09417 [hep-th].

[3126] M. Ballardini, M. Braglia, F. Finelli, D. Paoletti, A.A. Starobinsky, C. Umiltà, Scalar-tensor theories of gravity, neutrino physics, and the H_0 tension, J. Cosmol. Astropart. Phys. 10 (2020) 044, arXiv:2004.14349 [astro-ph.CO].

[3127] M. Petronikolou, S. Basilakos, E.N. Saridakis, Alleviating H0 tension in Horndeski gravity, Phys. Rev. D 106 (12) (2022) 124051, arXiv:2110.01338 [gr-qc].

[3128] M. Petronikolou, E.N. Saridakis, Alleviating the H_0 tension in Scalar–Tensor and Bi-Scalar–Tensor theories, Universe 9 (9) (2023) 397, arXiv:2308.16044 [gr-qc].

[3129] M. Ballardini, A.G. Ferrari, F. Finelli, Phantom scalar-tensor models and cosmological tensions, J. Cosmol. Astropart. Phys. 04 (2023) 029, arXiv:2302.05291 [astro-ph.CO].

[3130] A.G. Ferrari, M. Ballardini, F. Finelli, D. Paoletti, N. Mauri, Cosmological effects of the Galileon term in scalar-tensor theories, Phys. Rev. D 108 (6) (2023) 063520, arXiv:2307.02987 [astro-ph.CO].

[3131] A.G. Ferrari, M. Ballardini, F. Finelli, D. Paoletti, Scalar-tensor gravity and DESI 2024 BAO data, Phys. Rev. D 111 (8) (2025) 083523, arXiv:2501.15298 [astro-ph.CO].

[3132] S. Peirone, G. Benevento, N. Frusciante, S. Tsujikawa, Cosmological data favor Galileon ghost condensate over ΛCDM, Phys. Rev. D 100 (6) (2019) 063540, arXiv:1905.05166 [astro-ph.CO].

[3133] N. Frusciante, S. Peirone, L. Atayde, A. De Felice, Phenomenology of the generalized cubic covariant Galileon model and cosmological bounds, Phys. Rev. D 101 (6) (2020) 064001, arXiv:1912.07586 [astro-ph.CO].

[3134] S. Banerjee, M. Petronikolou, E.N. Saridakis, Alleviating the H0 tension with new gravitational scalar tensor theories, Phys. Rev. D 108 (2) (2023) 024012, arXiv:2209.02426 [gr-qc].

[3135] C. Brans, R.H. Dicke, Mach's principle and a relativistic theory of gravitation, Phys. Rev. 124 (1961) 925–935.

[3136] R.H. Dicke, Mach's principle and invariance under transformation of units, Phys. Rev. 125 (1962) 2163–2167.

[3137] I. Ayuso, J.P. Mimoso, N.J. Nunes, What if Newton's gravitational constant was negative? Galaxies 7 (1) (2019) 38, arXiv:1903.07604 [gr-qc].

[3138] O. Akarsu, N. Katırcı, N. Özdemir, J.A. Vázquez, Anisotropic massive Brans–Dicke gravity extension of the standard ΛCDM model, Eur. Phys. J. C 80 (1) (2020) 32, arXiv:1903.06679 [gr-qc].

[3139] A. Gómez-Valent, P. Hassan Puttasiddappa, Difficulties in reconciling non-negligible differences between the local and cosmological values of the gravitational coupling in extended Brans–Dicke theories, J. Cosmol. Astropart. Phys. 09 (2021) 040, arXiv:2105.14819 [astro-ph.CO].

[3140] J.D. Barrow, S. Cotsakis, Chaotic behavior in higher order gravity theories, Phys. Lett. B 232 (1989) 172–176.

[3141] S. Cotsakis, G. Flessas, Stability of FRW cosmology in higher order gravity, Phys. Rev. D 48 (1993) 3577–3584.

[3142] S. Cotsakis, J. Demaret, Y.D. Rop, L. Querella, Mixmaster universe in fourth-order gravity theories, Phys. Rev. D 48 (10) (1993) 4595.

[3143] S. Carloni, J.a.L. Rosa, J.P.S. Lemos, Cosmology of $f(R,\Box R)$ gravity, Phys. Rev. D 99 (10) (2019) 104001, arXiv:1808.07316 [gr-qc].

[3144] L. Amendola, A. Battaglia Mayer, S. Capozziello, F. Occhionero, S. Gottlober, V. Muller, H.J. Schmidt, Generalized sixth order gravity and inflation, Cl. Quant. Grav. 10 (1993) L43–L47.

[3145] R.R. Cuzinatto, C.A.M. de Melo, L.G. Medeiros, P.J. Pompeia, $f(R,\nabla_{\mu_1}R,....,\nabla_{\mu_1}...\nabla_{\mu_n}R)$ theories of gravity in Einstein frame: a higher order modified Starobinsky inflation model in the Palatini approach, Phys. Rev. D 99 (8) (2019) 084053, arXiv:1806.08850 [gr-qc].

[3146] S. Gottlober, H.J. Schmidt, A.A. Starobinsky, Sixth order gravity and conformal transformations, Cl. Quant. Grav. 7 (1990) 893.

[3147] A. Paliathanasis, $f(R,\Box R)$-gravity and equivalency with the modified GUP Scalar field models, Eur. Phys. J. C 84 (4) (2024) 422, arXiv:2404.04519 [gr-qc].

[3148] D. Wands, Extended gravity theories and the Einstein–Hilbert action, Cl. Quant. Grav. 11 (1994) 269–280, arXiv:gr-qc/9307034.

[3149] A.L. Berkin, K.-i. Maeda, Effects of R**3 and R box R terms on R**2 inflation, Phys. Lett. B 245 (1990) 348–354.

[3150] F. Bajardi, R. D'Agostino, Corrections to general relativity with higher-order invariants and cosmological applications, Int. J. Geom. Meth. Mod. Phys. 21 (10) (2024) 2440006.

[3151] B.M.N. Carter, I.P. Neupane, Towards inflation and dark energy cosmologies from modified Gauss–Bonnet theory, J. Cosmol. Astropart. Phys. 06 (2006) 004, arXiv:hep-th/0512262.

[3152] F. Bajardi, S. Capozziello, Equivalence of nonminimally coupled cosmologies by Noether symmetries, Internat. J. Modern Phys. D 29 (14) (2020) 2030015, arXiv:2010.07914 [gr-qc].

[3153] A.D. Millano, G. Leon, A. Paliathanasis, Phase-space analysis of an Einstein–Gauss–Bonnet scalar field cosmology, Mathematics 11 (6) (2023) 1408, arXiv:2302.09371 [gr-qc].

[3154] A.D. Millano, G. Leon, A. Paliathanasis, Global dynamics in Einstein–Gauss–Bonnet scalar field cosmology with matter, Phys. Rev. D 108 (2) (2023) 023519, arXiv:2304.08659 [gr-qc].

[3155] S. Santos Da Costa, F.V. Roig, J.S. Alcaniz, S. Capozziello, M. De Laurentis, M. Benetti, Dynamical analysis on $f(R,\mathcal{G})$ cosmology, Cl. Quant. Grav. 35 (7) (2018) 075013, arXiv:1802.02572 [gr-qc].

[3156] B. Li, J.D. Barrow, D.F. Mota, The cosmology of modified Gauss–Bonnet gravity, Phys. Rev. D 76 (2007) 044027, arXiv:0705.3795 [gr-qc].

[3157] G. Cognola, E. Elizalde, S. Nojiri, S.D. Odintsov, S. Zerbini, Dark energy in modified Gauss–Bonnet gravity: Late-time acceleration and the hierarchy problem, Phys. Rev. D 73 (2006) 084007, arXiv:hep-th/0601008.

[3158] S. Nojiri, S.D. Odintsov, Modified Gauss–Bonnet theory as gravitational alternative for dark energy, Phys. Lett. B 631 (2005) 1–6, arXiv:hep-th/0508049.

[3159] S. Nojiri, S.D. Odintsov, M. Sasaki, Gauss–Bonnet dark energy, Phys. Rev. D 71 (2005) 123509, arXiv:hep-th/0504052.

[3160] D. Wang, D. Mota, 4D Gauss–Bonnet gravity: Cosmological constraints, H_0 tension and large scale structure, Phys. Dark Univ. 32 (2021) 100813, arXiv:2103.12358 [astro-ph.CO].

[3161] M. Benetti, S. Santos da Costa, S. Capozziello, J.S. Alcaniz, M. De Laurentis, Observational constraints on Gauss–Bonnet cosmology, Internat. J. Modern Phys. D 27 (08) (2018) 1850084, arXiv:1803.00895 [gr-qc].

[3162] S.F. Hassan, R.A. Rosen, Bimetric gravity from ghost-free massive gravity, JHEP 02 (2012) 126, arXiv:1109.3515 [hep-th].

[3163] M. Högås, E. Mörtsell, Constraints on bimetric gravity. Part I. Analytical constraints, J. Cosmol. Astropart. Phys. 05 (2021) 001, arXiv:2101.08794 [gr-qc].

[3164] M. Högås, E. Mörtsell, Constraints on bimetric gravity. Part II. Observational constraints, J. Cosmol. Astropart. Phys. 05 (2021) 002, arXiv:2101.08795 [gr-qc].

[3165] M. Högås, Was Einstein Wrong? : Theoretical and Observational Constraints on Massive Gravity (Ph.D. thesis), Stockholm University, Faculty of Science, Department of Physics, 2022.

[3166] P. Ntelis, A. Morris, Functors of actions, Found. Phys. 53 (1) (2023) 29, arXiv:2010.06707 [physics.gen-ph].

[3167] P. Ntelis, New avenues and observational constraints on functors of actions theories, PoS EPS-HEP2023 (2024) 104.

[3168] J. Beltrán Jiménez, L. Heisenberg, T.S. Koivisto, The geometrical trinity of gravity, Universe 5 (7) (2019) 173, arXiv:1903.06830 [hep-th].

[3169] S. Capozziello, V. De Falco, C. Ferrara, Comparing equivalent gravities: common features and differences, Eur. Phys. J. C 82 (10) (2022) 865, arXiv:2208.03011 [gr-qc].

[3170] M. Hohmann, L. Järv, M. Krššák, C. Pfeifer, Teleparallel theories of gravity as analogue of nonlinear electrodynamics, Phys. Rev. D 97 (10) (2018) 104042, arXiv:1711.09930 [gr-qc].

[3171] J.W. Maluf, The teleparallel equivalent of general relativity, Ann. Phys. 525 (2013) 339–357, arXiv:1303.3897 [gr-qc].

[3172] C. Xu, E.N. Saridakis, G. Leon, Phase-space analysis of teleparallel dark energy, J. Cosmol. Astropart. Phys. 07 (2012) 005, arXiv:1202.3781 [gr-qc].

[3173] Y.N. Obukhov, J.G. Pereira, Metric affine approach to teleparallel gravity, Phys. Rev. D 67 (2003) 044016, arXiv:gr-qc/0212080.

[3174] C.-Q. Geng, C.-C. Lee, E.N. Saridakis, Observational constraints on teleparallel dark energy, J. Cosmol. Astropart. Phys. 01 (2012) 002, arXiv:1110.0913 [astro-ph.CO].

[3175] F. Bajardi, S. Capozziello, Noether symmetries and quantum cosmology in extended teleparallel gravity, Int. J. Geom. Meth. Mod. Phys. 18 (supp01) (2021) 2140002, arXiv:2101.00432 [gr-qc].

[3176] K. Hayashi, T. Shirafuji, New general relativity, Phys. Rev. D 19 (1979) 3524–3553; Phys. Rev. D 24 (1982) 3312–3314, Addendum.

[3177] S. Bahamonde, C.G. Böhmer, M. Krˇ sšák, New classes of modified teleparallel gravity models, Phys. Lett. B 775 (2017) 37–43, arXiv:1706.04920 [gr-qc].

[3178] L. Järv, M. Rünkla, M. Saal, O. Vilson, Nonmetricity formulation of general relativity and its scalar-tensor extension, Phys. Rev. D 97 (12) (2018) 124025, arXiv:1802.00492 [gr-qc].

[3179] M. Hohmann, C. Pfeifer, Teleparallel axions and cosmology, Eur. Phys. J. C 81 (4) (2021) 376, arXiv:2012.14423 [gr-qc].

[3180] Y.-F. Cai, S. Capozziello, M. De Laurentis, E.N. Saridakis, f(T) teleparallel gravity and cosmology, Rep. Progr. Phys. 79 (10) (2016) 106901, arXiv:1511.07586 [gr-qc].

[3181] B. Li, T.P. Sotiriou, J.D. Barrow, $f(T)$ gravity and local Lorentz invariance, Phys. Rev. D 83 (2011) 064035, arXiv:1010.1041 [gr-qc].

[3182] R. Ferraro, F. Fiorini, Modified teleparallel gravity: Inflation without inflaton, Phys. Rev. D 75 (2007) 084031, arXiv:gr-qc/0610067.

[3183] E.V. Linder, Einstein's other gravity and the acceleration of the universe, Phys. Rev. D 81 (2010) 127301, arXiv:1005.3039 [astro-ph.CO]; Phys. Rev. D 82 (2010) 109902, Erratum.

[3184] S.-H. Chen, J.B. Dent, S. Dutta, E.N. Saridakis, Cosmological perturbations in f(T) gravity, Phys. Rev. D 83 (2011) 023508, arXiv:1008.1250 [astro-ph.CO].

[3185] K. Bamba, C.-Q. Geng, C.-C. Lee, L.-W. Luo, Equation of state for dark energy in $f(T)$ gravity, J. Cosmol. Astropart. Phys. 01 (2011) 021, arXiv:1011.0508 [astro-ph.CO].

[3186] G. Kofinas, E.N. Saridakis, Teleparallel equivalent of Gauss–Bonnet gravity and its modifications, Phys. Rev. D 90 (2014) 084044, arXiv:1404.2249 [gr-qc].

[3187] A. Paliathanasis, J.D. Barrow, P.G.L. Leach, Cosmological solutions of $f(T)$ gravity, Phys. Rev. D 94 (2) (2016) 023525, arXiv:1606.00659 [gr-qc].

[3188] A. Finch, J.L. Said, Galactic rotation dynamics in f(T) gravity, Eur. Phys. J. C 78 (7) (2018) 560, arXiv:1806.09677 [astro-ph.GA].

[3189] G. Farrugia, J. Levi Said, V. Gakis, E.N. Saridakis, Gravitational waves in modified teleparallel theories, Phys. Rev. D 97 (12) (2018) 124064, arXiv:1804.07365 [gr-qc].

[3190] I. Soudi, G. Farrugia, V. Gakis, J. Levi Said, E.N. Saridakis, Polarization of gravitational waves in symmetric teleparallel theories of gravity and their modifications, Phys. Rev. D 100 (4) (2019) 044008, arXiv:1810.08220 [gr-qc].

[3191] G. Farrugia, J. Levi Said, A. Finch, Gravitoelectromagnetism, solar system tests, and weak-field solutions in $f(T,B)$ gravity with observational constraints, Universe 6 (2) (2020) 34, arXiv:2002.08183 [gr-qc].

[3192] N. Dimakis, A. Paliathanasis, T. Christodoulakis, Exploring quantum cosmology within the framework of teleparallel f(T) gravity, Phys. Rev. D 109 (2) (2024) 024031, arXiv:2308.08759 [gr-qc].

[3193] I.S. Albuquerque, N. Frusciante, A designer approach to f(Q) gravity and cosmological implications, Phys. Dark Univ. 35 (2022) 100980, arXiv:2202.04637 [astro-ph.CO].

[3194] F.K. Anagnostopoulos, V. Gakis, E.N. Saridakis, S. Basilakos, New models and big bang nucleosynthesis constraints in f(Q) gravity, Eur. Phys. J. C 83 (1) (2023) 58, arXiv:2205.11445 [gr-qc].

[3195] S. Capozziello, M. Shokri, Slow-roll inflation in f(Q) non-metric gravity, Phys. Dark Univ. 37 (2022) 101113, arXiv:2209.06670 [gr-qc].

[3196] F. Bajardi, D. Vernieri, S. Capozziello, Bouncing cosmology in f(Q) symmetric teleparallel gravity, Eur. Phys. J. Plus 135 (11) (2020) 912, arXiv:2011.01248 [gr-qc].

[3197] A. Banerjee, A. Pradhan, T. Tangphati, F. Rahaman, Wormhole geometries in $f(Q)$ gravity and the energy conditions, Eur. Phys. J. C 81 (11) (2021) 1031, arXiv:2109.15105 [gr-qc].

[3198] R. D'Agostino, R.C. Nunes, Forecasting constraints on deviations from general relativity in f(Q) gravity with standard sirens, Phys. Rev. D 106 (12) (2022) 124053, arXiv:2210.11935 [gr-qc].

[3199] M. Hohmann, C. Pfeifer, Gravitational wave birefringence in spatially curved teleparallel cosmology, Phys. Lett. B 834 (2022) 137437, arXiv:2203.01856 [gr-qc].

[3200] W. Khyllep, A. Paliathanasis, J. Dutta, Cosmological solutions and growth index of matter perturbations in $f(Q)$ gravity, Phys. Rev. D 103 (10) (2021) 103521, arXiv:2103.08372 [gr-qc].

[3201] S. Capozziello, M. Caruana, G. Farrugia, J. Levi Said, J. Sultana, Cosmic growth in f(T) teleparallel gravity, Gen. Relativity Gravitation 56 (2) (2024) 27, arXiv:2308.15995 [gr-qc].

[3202] A. Paliathanasis, Dynamical analysis of fQ-cosmology, Phys. Dark Univ. 41 (2023) 101255, arXiv:2304.04219 [gr-qc].

[3203] A. Paliathanasis, f(T) cosmology with nonzero curvature, Modern Phys. Lett. A 36 (38) (2021) 2150261, arXiv:2107.00620 [gr-qc].

[3204] Y. Yang, X. Ren, Q. Wang, Z. Lu, D. Zhang, Y.-F. Cai, E.N. Saridakis, Quintom cosmology and modified gravity after DESI 2024, Sci. Bull. 69 (2024) 2698–2704, arXiv:2404.19437 [astro-ph.CO].

[3205] A. Paliathanasis, Attractors in fQ,B-gravity, Phys. Dark Univ. 45 (2024) 101519.

[3206] C. Wu, X. Ren, Y. Yang, Y.-M. Hu, E.N. Saridakis, Background-dependent and classical correspondences between $f(Q)$ and $f(T)$ gravity, 2024, arXiv:2412.01104 [gr-qc].

[3207] F. Cotton, A generalization of the Einstein–Maxwell equations, in: APS April Meeting Abstracts, in: APS Meeting Abstracts, vol. 2016, 2016, p. L1.049.

[3208] M. Aljaf, E. Elizalde, M. Khurshudyan, K. Myrzakulov, A. Zhadyranova, Solving the H_0 tension in f(T) gravity through Bayesian machine learning, Eur. Phys. J. C 82 (12) (2022) 1130, arXiv:2205.06252 [astro-ph.CO].

[3209] S.-F. Yan, P. Zhang, J.-W. Chen, X.-Z. Zhang, Y.-F. Cai, E.N. Saridakis, Interpreting cosmological tensions from the effective field theory of torsional gravity, Phys. Rev. D 101 (12) (2020) 121301, arXiv:1909.06388 [astro-ph.CO].

[3210] X. Ren, T.H.T. Wong, Y.-F. Cai, E.N. Saridakis, Data-driven reconstruction of the late-time cosmic acceleration with f(T) gravity, Phys. Dark Univ. 32 (2021) 100812, arXiv:2103.01260 [astro-ph.CO].

[3211] R.C. Nunes, Structure formation in $f(T)$ gravity and a solution for H_0 tension, J. Cosmol. Astropart. Phys. 05 (2018) 052, arXiv:1802.02281 [gr-qc].

[3212] R. D'Agostino, R.C. Nunes, Measurements of H_0 in modified gravity theories: The role of lensed quasars in the late-time Universe, Phys. Rev. D 101 (10) (2020) 103505, arXiv:2002.06381 [astro-ph.CO].

[3213] C. de Rham, S. Garcia-Saenz, L. Heisenberg, V. Pozsgay, Cosmology of extended Proca–Nuevo, J. Cosmol. Astropart. Phys. 03 (2022) 053, arXiv:2110.14327 [hep-th].

[3214] B.J. Barros, T. Barreiro, T. Koivisto, N.J. Nunes, Testing $F(Q)$ gravity with redshift space distortions, Phys. Dark Univ. 30 (2020) 100616, arXiv:2004.07867 [gr-qc].

[3215] Q. Wang, X. Ren, Y.-F. Cai, W. Luo, E.N. Saridakis, Observational test of f(Q) gravity with weak gravitational lensing, Astrophys. J. 974 (1) (2024) 7, arXiv:2406.00242 [astro-ph.CO].

[3216] Z. Sakr, L. Schey, Investigating the Hubble tension and σ_8 discrepancy in f(Q) cosmology, J. Cosmol. Astropart. Phys. 10 (2024) 052, arXiv:2405.03627 [astro-ph.CO].

[3217] C. Pfeifer, M.N.R. Wohlfarth, Finsler geometric extension of Einstein gravity, Phys. Rev. D 85 (2012) 064009, arXiv:1112.5641 [gr-qc].

[3218] S. Basilakos, P. Stavrinos, Cosmological equivalence between the Finsler–Randers space-time and the DGP gravity model, Phys. Rev. D 87 (4) (2013) 043506, arXiv:1301.4327 [gr-qc].

[3219] S. Basilakos, A.P. Kouretsis, E.N. Saridakis, P. Stavrinos, Resembling dark energy and modified gravity with Finsler–Randers cosmology, Phys. Rev. D 88 (2013) 123510, arXiv:1311.5915 [gr-qc].

[3220] G. Papagiannopoulos, S. Basilakos, A. Paliathanasis, S. Savvidou, P.C. Stavrinos, Finsler–Randers cosmology: dynamical analysis and growth of matter perturbations, Cl. Quant. Grav. 34 (22) (2017) 225008, arXiv:1709.03748 [gr-qc].

[3221] G. Papagiannopoulos, S. Basilakos, A. Paliathanasis, S. Pan, P. Stavrinos, Dynamics in varying vacuum Finsler–Randers cosmology, Eur. Phys. J. C 80 (9) (2020) 816, arXiv:2005.06231 [gr-qc].

[3222] M. Hohmann, C. Pfeifer, N. Voicu, The kinetic gas universe, Eur. Phys. J. C 80 (9) (2020) 809, arXiv:2005.13561 [gr-qc].

[3223] M. Hohmann, C. Pfeifer, N. Voicu, Relativistic kinetic gases as direct sources of gravity, Phys. Rev. D 101 (2) (2020) 024062, arXiv:1910.14044 [gr-qc].

[3224] S. Heefer, C. Pfeifer, A. Reggio, A. Fuster, A Cosmological unicorn solution to Finsler gravity, Phys. Rev. D 108 (6) (2023) 064051, arXiv:2306.00722 [gr-qc].

[3225] A.F. Zakharov, P. Jovanovic, D. Borka, V.B. Jovanovic, Constraining the range of Yukawa gravity interaction from S2 star orbits II: Bounds on graviton mass, J. Cosmol. Astropart. Phys. 05 (2016) 045, arXiv:1605.00913 [gr-qc].

[3226] P. Jovanović, V.B. Jovanović, D. Borka, A.F. Zakharov, Constraints on yukawa gravity parameters from observations of bright stars, J. Cosmol. Astropart. Phys. 03 (2023) 056, arXiv:2211.12951 [astro-ph.GA].

[3227] P. Jovanović, V.B. Jovanović, D.s. Borka, A.F. Zakharov, Improvement of graviton mass constraints using GRAVITY's detection of Schwarzschild precession in the orbit of S2 star around the Galactic Center, Phys. Rev. D 109 (6) (2024) 064046, arXiv:2305.13448 [astro-ph.GA].

[3228] T. Harko, F.S.N. Lobo, f(R,L_m) gravity, Eur. Phys. J. C 70 (2010) 373–379, arXiv:1008.4193 [gr-qc].

[3229] T. Harko, F.S.N. Lobo, S. Nojiri, S.D. Odintsov, $f(R,T)$ gravity, Phys. Rev. D 84 (2011) 024020, arXiv:1104.2669 [gr-qc].

[3230] N. Katırcı, M. Kavuk, $f(R,T_{\mu\nu}T^{\mu\nu})$ gravity and Cardassian-like expansion as one of its consequences, Eur. Phys. J. Plus 129 (2014) 163, arXiv:1302.4300 [gr-qc].

[3231] M. Roshan, F. Shojai, Energy-momentum squared gravity, Phys. Rev. D 94 (4) (2016) 044002, arXiv:1607.06049 [gr-qc].

[3232] O. Akarsu, N. Katırcı, S. Kumar, Cosmic acceleration in a dust only universe via energy-momentum powered gravity, Phys. Rev. D 97 (2) (2018) 024011, arXiv:1709.02367 [gr-qc].

[3233] C.V.R. Board, J.D. Barrow, Cosmological models in energy-momentum-squared gravity, Phys. Rev. D 96 (12) (2017) 123517, arXiv:1709.09501 [gr-qc]; Phys. Rev. D 98 (2018) 129902, Erratum.

[3234] Z. Haghani, T. Harko, F.S.N. Lobo, H.R. Sepangi, S. Shahidi, Further matters in space-time geometry: f(R,T,R$\mu\nu$T$\mu\nu$) gravity, Phys. Rev. D 88 (4) (2013) 044023, arXiv:1304.5957 [gr-qc].

[3235] I. Ayuso, J. Beltran Jimenez, A. de la Cruz-Dombriz, Consistency of universally nonminimally coupled $f(R,T,R_{\mu\nu}T^{\mu\nu})$ theories, Phys. Rev. D 91 (10) (2015) 104003, arXiv:1411.1636 [hep-th]; Phys. Rev. D 93 (2016) 089901, Addendum.

[3236] T. Harko, F.S.N. Lobo, G. Otalora, E.N. Saridakis, Nonminimal torsion-matter coupling extension of f(T) gravity, Phys. Rev. D 89 (2014) 124036, arXiv:1404.6212 [gr-qc].

[3237] S. Carloni, F.S.N. Lobo, G. Otalora, E.N. Saridakis, Dynamical system analysis for a nonminimal torsion-matter coupled gravity, Phys. Rev. D 93 (2016) 024034, arXiv:1512.06996 [gr-qc].

[3238] T. Harko, F.S.N. Lobo, G. Otalora, E.N. Saridakis, $f(T,\mathcal{T})$ gravity and cosmology, J. Cosmol. Astropart. Phys. 12 (2014) 021, arXiv:1405.0519 [gr-qc].

[3239] O. Akarsu, M. Bouhmadi-López, N. Katırcı, E. Nazari, M. Roshan, N.M. Uzun, Equivalence of matter-type modified gravity theories to general relativity with nonminimal matter interaction, Phys. Rev. D 109 (10) (2024) 104055, arXiv:2306.11717 [gr-qc].

[3240] F.G. Alvarenga, A. de la Cruz-Dombriz, M.J.S. Houndjo, M.E. Rodrigues, D. Sáez-Gómez, Dynamics of scalar perturbations in $f(R,T)$ gravity, Phys. Rev. D 87 (10) (2013) 103526, arXiv:1302.1866 [gr-qc]; Phys. Rev. D 87 (2013) 129905, Erratum.

[3241] M. Asghari, A. Sheykhi, Growth of cosmic perturbations in the modified f(R,T) gravity, Phys. Dark Univ. 46 (2024) 101695, arXiv:2405.11840 [gr-qc].

[3242] S. Anand, P. Chaubal, A. Mazumdar, S. Mohanty, P. Parashari, Bounds on neutrino mass in viscous cosmology, J. Cosmol. Astropart. Phys. 05 (2018) 031, arXiv:1712.01254 [astro-ph.CO].

[3243] S. Anand, P. Chaubal, A. Mazumdar, S. Mohanty, Cosmic viscosity as a remedy for tension between PLANCK and LSS data, J. Cosmol. Astropart. Phys. 11 (2017) 005, arXiv:1708.07030 [astro-ph.CO].

[3244] P. Parashari, S. Anand, P. Chaubal, G. Lambiase, S. Mohanty, A. Mazumdar, A. Narang, Status of σ_8 tension in different cosmological models, Springer Proc. Phys. 261 (2021) 907–912.

[3245] S. Mohanty, S. Anand, P. Chaubal, A. Mazumdar, P. Parashari, σ_8 discrepancy and its solutions, J. Astrophys. Astron. 39 (4) (2018) 46.

[3246] J. Khoury, A. Weltman, Chameleon fields: Awaiting surprises for tests of gravity in space, Phys. Rev. Lett. 93 (2004) 171104, arXiv:astro-ph/0309300.

[3247] J. Khoury, A. Weltman, Chameleon cosmology, Phys. Rev. D 69 (2004) 044026, arXiv:astro-ph/0309411.

[3248] B. Li, J.D. Barrow, N-body simulations for coupled scalar field cosmology, Phys. Rev. D 83 (2011) 024007, arXiv:1005.4231 [astro-ph.CO].

[3249] A. Paliathanasis, Dynamical analysis in chameleon dark energy, Fortsch. Phys. 71 (8-9) (2023) 2300088, arXiv:2306.03880 [gr-qc].

[3250] H. Farajollahi, A. Salehi, F. Tayebi, A. Ravanpak, Stability analysis in tachyonic potential Chameleon cosmology, J. Cosmol. Astropart. Phys. 05 (2011) 017, arXiv:1105.4045 [gr-qc].

[3251] A. Paliathanasis, Dynamics in interacting scalar-torsion cosmology, Universe 7 (7) (2021) 244, arXiv:2107.05880 [gr-qc].

[3252] A. Paliathanasis, Chameleon mechanism in scalar nonmetricity cosmology, Ann. Phys. 468 (2024) 169724, arXiv:2407.05042 [gr-qc].

[3253] A. Paliathanasis, 4D Einstein–Gauss–Bonnet cosmology with Chameleon mechanism, Gen. Relativity Gravitation 56 (7) (2024) 84.

[3254] A. Paliathanasis, G. Leon, J.D. Barrow, Einstein-aether theory in Weyl integrable geometry, Eur. Phys. J. C 80 (12) (2020) 1099, arXiv:2007.06435 [gr-qc].

[3255] V.G. Gurzadyan, A. Stepanian, H_0 tension: clue to common nature of dark sector? Eur. Phys. J. C 79 (7) (2019) 568, arXiv:1905.03442 [astro-ph.CO].

[3256] V.G. Gurzadyan, A. Stepanian, Hubble tension vs two flows, Eur. Phys. J. Plus 136 (2) (2021) 235, arXiv:2102.10100 [gr-qc].

[3257] V.G. Gurzadyan, A. Stepanian, Hubble tension and absolute constraints on the local Hubble parameter, Astron. Astrophys. 653 (2021) A145, arXiv:2108.07407 [astro-ph.CO].

[3258] V.G. Gurzadyan, N.N. Fimin, V.M. Chechetkin, Cosmic voids and the kinetic analysis - II. Link to Hubble tension, Astron. Astrophys. 672 (2023) A95, arXiv:2303.03194 [astro-ph.CO].

[3259] V.G. Gurzadyan, N.N. Fimin, V.M. Chechetkin, Cosmic voids and the kinetic analysis - III. Hubble tension and structure formation in the late Universe, Astron. Astrophys. 677 (2023) A161, arXiv:2309.11734 [astro-ph.CO].

[3260] V.G. Gurzadyan, N.N. Fimin, V.M. Chechetkin, Cosmic voids and the kinetic analysis - IV. Hubble tension and the cosmological constant, Astron. Astrophys. 694 (2025) A252, arXiv:2501.09598 [gr-qc].

[3261] V.G. Gurzadyan, Structure formation in the local Universe and the cosmological constant, 2025, arXiv:2502.02864 [gr-qc].

[3262] R. Erdem, Gravitational particle production and the Hubble tension, Universe 10 (9) (2024) 338, arXiv:2402.16791 [gr-qc].

[3263] A. Borowiec, M. Postolak, Is it possible to separate baryonic from dark matter within the Λ-CDM formalism? Phys. Lett. B 860 (2025) 139176, arXiv:2309.10364 [gr-qc].

[3264] S. Vagnozzi, L. Visinelli, P. Brax, A.-C. Davis, J. Sakstein, Direct detection of dark energy: The XENON1T excess and future prospects, Phys. Rev. D 104 (6) (2021) 063023, arXiv:2103.15834 [hep-ph].

[3265] T. O'Shea, A.-C. Davis, M. Giannotti, S. Vagnozzi, L. Visinelli, J.K. Vogel, Solar chameleons: Novel channels, Phys. Rev. D 110 (6) (2024) 063027, arXiv:2406.01691 [hep-ph].

[3266] K. Hinterbichler, J. Khoury, Symmetron fields: screening long-range forces through local symmetry restoration, Phys. Rev. Lett. 104 (2010) 231301, arXiv:1001.4525 [hep-th].

[3267] M. Högås, E. Mörtsell, Impact of symmetron screening on the Hubble tension: New constraints using cosmic distance ladder data, Phys. Rev. D 108 (2) (2023) 024007, arXiv:2303.12827 [astro-ph.CO].

[3268] E. Babichev, C. Deffayet, An introduction to the vainshtein mechanism, Cl. Quant. Grav. 30 (2013) 184001, arXiv:1304.7240 [gr-qc].

[3269] H. Akaike, A new look at the statistical model identification, IEEE Trans. Autom. Control 19 (6) (1974) 716–723.

[3270] G. Schwarz, Estimating the dimension of a model, Ann. Stat. 6 (1978) 461–464.

[3271] E. Belgacem, Y. Dirian, S. Foffa, M. Maggiore, Nonlocal gravity. conceptual aspects and cosmological predictions, J. Cosmol. Astropart. Phys. 03 (2018) 002, arXiv:1712.07066 [hep-th].

[3272] E. Di Valentino, E. Saridakis, A. Riess, Cosmological tensions in the birthplace of the heliocentric model, Nat. Astron. 6 (2022) 1353, arXiv:2211.05248 [astro-ph.CO].

[3273] M. Braglia, M. Ballardini, F. Finelli, K. Koyama, Early modified gravity in light of the H_0 tension and LSS data, Phys. Rev. D 103 (4) (2021) 043528, arXiv:2011.12934 [astro-ph.CO].

[3274] G. Benevento, J.A. Kable, G.E. Addison, C.L. Bennett, An exploration of an early gravity transition in light of cosmological tensions, Astrophys. J. 935 (2) (2022) 156, arXiv:2202.09356 [astro-ph.CO].

[3275] S.H.-S. Alexander, M.E. Peskin, M.M. Sheikh-Jabbari, Leptogenesis from gravity waves in models of inflation, Phys. Rev. Lett. 96 (2006) 081301, arXiv:hep-th/0403069.

[3276] D.H. Lyth, C. Quimbay, Y. Rodriguez, Leptogenesis and tensor polarisation from a gravitational Chern–Simons term, JHEP 03 (2005) 016, arXiv:hep-th/0501153.

[3277] J. Alexandre, N. Houston, N.E. Mavromatos, Dynamical supergravity breaking via the Super–Higgs effect revisited, Phys. Rev. D 88 (2013) 125017, arXiv:1310.4122 [hep-th].

[3278] J. Alexandre, N. Houston, N.E. Mavromatos, Inflation via gravitino condensation in dynamically broken supergravity, Internat. J. Modern Phys. D 24 (04) (2015) 1541004, arXiv:1409.3183 [gr-qc].

[3279] O. Bertolami, C. Gomes, Nonminimally coupled Boltzmann equation: Foundations, Phys. Rev. D 102 (8) (2020) 084051, arXiv:2002.08184 [gr-qc].

[3280] M.P.L.P. Ramos, J. Páramos, Baryogenesis in nonminimally coupled $f(R)$ theories, Phys. Rev. D 96 (10) (2017) 104024, arXiv:1709.04442 [gr-qc].

[3281] T. Złośnik, F. Urban, L. Marzola, T. Koivisto, Spacetime and dark matter from spontaneous breaking of Lorentz symmetry, Cl. Quant. Grav. 35 (23) (2018) 235003, arXiv:1807.01100 [gr-qc].

[3282] M. Nikjoo, T. Zlosnik, Hamiltonian formulation of gravity as a spontaneously-broken gauge theory of the Lorentz group, Cl. Quant. Grav. 41 (4) (2024) 045005, arXiv:2308.01108 [gr-qc].

[3283] P. Gallagher, T.S. Koivisto, L. Marzola, L. Varrin, T. Zlosnik, Consistent first-order action functional for gauge theories, Phys. Rev. D 109 (6) (2024) L061503, arXiv:2311.07464 [hep-th].

[3284] P. Gallagher, T. Koivisto, The Λ and the CDM as integration constants, Symmetry 13 (11) (2021) 2076, arXiv:2103.05435 [gr-qc].

[3285] T. Koivisto, Cosmology in the Lorentz gauge theory, Int. J. Geom. Meth. Mod. Phys. 20 (Supp01) (2023) 2450040, arXiv:2306.00963 [gr-qc].

[3286] N.J. Popławski, Non-particle dark matter from Hubble parameter, Eur. Phys. J. C 79 (9) (2019) 734, arXiv:1906.03947 [physics.gen-ph].

[3287] F. Izaurieta, S. Lepe, O. Valdivia, The spin tensor of dark matter and the Hubble parameter tension, Phys. Dark Univ. 30 (2020) 100662, arXiv:2004.13163 [gr-qc].

[3288] S. Akhshabi, S. Zamani, Cosmological distances and hubble tension in Einstein–Cartan theory, Gen. Relativity Gravitation 55 (9) (2023) 102, arXiv:2305.00415 [gr-qc].

[3289] T.S. Koivisto, T. Zlosnik, Paths to gravitation via the gauging of parametrized field theories, Phys. Rev. D 107 (12) (2023) 124013, arXiv:2212.04562 [gr-qc].

[3290] D. Iosifidis, E. Jensko, T.S. Koivisto, Relativistic interacting fluids in cosmology, J. Cosmol. Astropart. Phys. 11 (2024) 043, arXiv:2406.01412 [gr-qc].

[3291] D. Benisty, E.I. Guendelman, D. Vasak, J. Struckmeier, H. Stoecker, Quadratic curvature theories formulated as Covariant Canonical Gauge theories of Gravity, Phys. Rev. D 98 (10) (2018) 106021, arXiv:1809.10447 [gr-qc].

[3292] R. Ferraro, F. Fiorini, On Born–Infeld gravity in Weitzenbock spacetime, Phys. Rev. D 78 (2008) 124019, arXiv:0812.1981 [gr-qc].

[3293] F. Fiorini, R. Ferraro, A Type of Born-Infeld regular gravity and its cosmological consequences, Internat. J. Modern Phys. A 24 (2009) 1686–1689, arXiv:0904.1767 [gr-qc].

[3294] S. Jana, Cosmology in a reduced Born-Infeld $f(T)$ theory of gravity, Phys. Rev. D 90 (2014) 124007, arXiv:1410.7117 [gr-qc].

[3295] S. Nesseris, L. Perivolaropoulos, A comparison of cosmological models using recent supernova data, Phys. Rev. D 70 (2004) 043531, arXiv:astro-ph/0401556.

[3296] F. Fiorini, Nonsingular promises from Born–Infeld gravity, Phys. Rev. Lett. 111 (2013) 041104, arXiv:1306.4392 [gr-qc].

[3297] M. Bouhmadi-Lopez, C.-Y. Chen, P. Chen, Cosmological singularities in born-infeld determinantal gravity, Phys. Rev. D 90 (2014) 123518, arXiv:1407.5114 [gr-qc].

[3298] F. Fiorini, Primordial brusque bounce in Born-Infeld determinantal gravity, Phys. Rev. D 94 (2) (2016) 024030, arXiv:1511.03227 [gr-qc].

[3299] E. Wilson-Ewing, The matter bounce scenario in loop quantum cosmology, J. Cosmol. Astropart. Phys. 03 (2013) 026, arXiv:1211.6269 [gr-qc].

[3300] Y.-F. Cai, S.-H. Chen, J.B. Dent, S. Dutta, E.N. Saridakis, Matter bounce cosmology with the f(T) gravity, Cl. Quant. Grav. 28 (2011) 215011, arXiv:1104.4349 [astro-ph.CO].

[3301] K. Bamba, J. de Haro, S.D. Odintsov, Future singularities and teleparallelism in loop quantum cosmology, J. Cosmol. Astropart. Phys. 02 (2013) 008, arXiv:1211.2968 [gr-qc].

[3302] J. Amorós, J. de Haro, S.D. Odintsov, Bouncing loop quantum cosmology from $F(T)$ gravity, Phys. Rev. D 87 (2013) 104037, arXiv:1305.2344 [gr-qc].

[3303] A. Casalino, B. Sanna, L. Sebastiani, S. Zerbini, Bounce Models within Teleparallel modified gravity, Phys. Rev. D 103 (2) (2021) 023514, arXiv:2010.07609 [gr-qc].

[3304] J. Haro, J. Amoros, Viability of the matter bounce scenario in $F(T)$ gravity and Loop Quantum Cosmology for general potentials, J. Cosmol. Astropart. Phys. 12 (2014) 031, arXiv:1406.0369 [gr-qc].

[3305] J. de Haro, J. Amorós, Viability of the matter bounce scenario, J. Phys. Conf. Ser. 600 (1) (2015) 012024, arXiv:1411.7611 [gr-qc].

[3306] J. Haro, J. Amorós, Matter bounce scenario in $F(T)$ gravity, PoS FFP14 (2016) 163, arXiv:1501.06270 [gr-qc].

[3307] J. de Haro, Y.-F. Cai, An Extended Matter Bounce Scenario: current status and challenges, Gen. Relativity Gravitation 47 (8) (2015) 95, arXiv:1502.03230 [gr-qc].

[3308] S. Raatikainen, S. Rasanen, Higgs inflation and teleparallel gravity, J. Cosmol. Astropart. Phys. 12 (2019) 021, arXiv:1910.03488 [gr-qc].

[3309] A. Ashtekar, M. Bojowald, J. Lewandowski, Mathematical structure of loop quantum cosmology, Adv. Theor. Math. Phys. 7 (2) (2003) 233–268, arXiv:gr-qc/0304074.

[3310] A. Ashtekar, T. Pawlowski, P. Singh, Quantum nature of the big bang, Phys. Rev. Lett. 96 (2006) 141301, arXiv:gr-qc/0602086.

[3311] A. Ashtekar, T. Pawlowski, P. Singh, Quantum nature of the big bang: improved dynamics, Phys. Rev. D 74 (2006) 084003, arXiv:gr-qc/0607039.

[3312] A. Ashtekar, A. Corichi, P. Singh, Robustness of key features of loop quantum cosmology, Phys. Rev. D 77 (2008) 024046, arXiv:0710.3565 [gr-qc].

[3313] V. Taveras, Corrections to the Friedmann equations from LQG for a Universe with a free scalar field, Phys. Rev. D 78 (2008) 064072, arXiv:0807.3325 [gr-qc].

[3314] P. Diener, B. Gupt, M. Megevand, P. Singh, Numerical evolution of squeezed and non-Gaussian states in loop quantum cosmology, Cl. Quant. Grav. 31 (2014) 165006, arXiv:1406.1486 [gr-qc].

[3315] J. Yang, Y. Ding, Y. Ma, Alternative quantization of the Hamiltonian in loop quantum cosmology II: Including the Lorentz term, Phys. Lett. B 682 (2009) 1–7, arXiv:0904.4379 [gr-qc].

[3316] A. Dapor, K. Liegener, Cosmological effective Hamiltonian from full loop quantum gravity dynamics, Phys. Lett. B 785 (2018) 506–510, arXiv:1706.09833 [gr-qc].

[3317] B.-F. Li, P. Singh, A. Wang, Towards cosmological dynamics from loop quantum gravity, Phys. Rev. D 97 (8) (2018) 084029, arXiv:1801.07313 [gr-qc].

[3318] B.-F. Li, P. Singh, A. Wang, Qualitative dynamics and inflationary attractors in loop cosmology, Phys. Rev. D 98 (6) (2018) 066016, arXiv:1807.05236 [gr-qc].

[3319] M. Assanioussi, A. Dapor, K. Liegener, T. Pawłowski, Emergent de Sitter epoch of the Loop Quantum Cosmos: a detailed analysis, Phys. Rev. D 100 (8) (2019) 084003, arXiv:1906.05315 [gr-qc].

[3320] A. Delhom, G.J. Olmo, P. Singh, A diffeomorphism invariant family of metric-affine actions for loop cosmologies, J. Cosmol. Astropart. Phys. 06 (2023) 059, arXiv:2302.04285 [gr-qc].

[3321] G.J. Olmo, Palatini approach to modified gravity: f(r) theories and beyond, Internat. J. Modern Phys. D 20 (2011) 413–462, arXiv:1101.3864 [gr-qc].

[3322] G.J. Olmo, P. Singh, Effective action for loop quantum cosmology a la Palatini, J. Cosmol. Astropart. Phys. 01 (2009) 030, arXiv:0806.2783 [gr-qc].

[3323] F. Bombacigno, F. Cianfrani, G. Montani, Big-Bounce cosmology in the presence of Immirzi field, Phys. Rev. D 94 (6) (2016) 064021, arXiv:1607.00910 [gr-qc].

[3324] F. Bombacigno, G. Montani, Big bounce cosmology for Palatini R^2 gravity with a Nieh–Yan term, Eur. Phys. J. C 79 (5) (2019) 405, arXiv:1809.07563 [gr-qc].

[3325] F. Bombacigno, S. Boudet, G.J. Olmo, G. Montani, Big bounce and future time singularity resolution in Bianchi I cosmologies: The projective invariant Nieh-Yan case, Phys. Rev. D 103 (12) (2021) 124031, arXiv:2105.06870 [gr-qc].

[3326] S. Boudet, F. Bombacigno, F. Moretti, G.J. Olmo, Torsional birefringence in metric-affine Chern–Simons gravity: gravitational waves in late-time cosmology, J. Cosmol. Astropart. Phys. 01 (2023) 026, arXiv:2209.14394 [gr-qc].

[3327] S. Boudet, F. Bombacigno, G.J. Olmo, P.J. Porfirio, Quasinormal modes of Schwarzschild black holes in projective invariant Chern-Simons modified gravity, J. Cosmol. Astropart. Phys. 05 (05) (2022) 032, arXiv:2203.04000 [gr-qc].

[3328] F. Bombacigno, F. Moretti, S. Boudet, G.J. Olmo, Landau damping for gravitational waves in parity-violating theories, J. Cosmol. Astropart. Phys. 02 (2023) 009, arXiv:2210.07673 [gr-qc].

[3329] K. Choi, String or M theory axion as a quintessence, Phys. Rev. D 62 (2000) 043509, arXiv:hep-ph/9902292.

[3330] J.E. Kim, H.P. Nilles, A Quintessential axion, Phys. Lett. B 553 (2003) 1–6, arXiv:hep-ph/0210402.

[3331] A. Arvanitaki, S. Dimopoulos, S. Dubovsky, N. Kaloper, J. March-Russell, String axiverse, Phys. Rev. D 81 (2010) 123530, arXiv:0905.4720 [hep-th].

[3332] S. Chakraborty, E. González, G. Leon, B. Wang, Time-averaging axion-like interacting scalar fields models, Eur. Phys. J. C 81 (11) (2021) 1039, arXiv:2107.04651 [gr-qc].

[3333] J.E. Kim, H.P. Nilles, Axionic dark energy and a composite QCD axion, J. Cosmol. Astropart. Phys. 05 (2009) 010, arXiv:0902.3610 [hep-th].

[3334] A. Chatzistavrakidis, E. Erfani, H.P. Nilles, I. Zavala, Axiology, J. Cosmol. Astropart. Phys. 09 (2012) 006, arXiv:1207.1128 [hep-ph].

[3335] A. Chatzistavrakidis, G. Karagiannis, P. Schupp, Torsion-induced gravitational θ term and gravitoelectromagnetism, Eur. Phys. J. C 80 (11) (2020) 1034, arXiv:2007.06632 [gr-qc].

[3336] F. Zhang, J.-X. Feng, X. Gao, Scalar induced gravitational waves in symmetric teleparallel gravity with a parity-violating term, Phys. Rev. D 108 (6) (2023) 063513, arXiv:2307.00330 [gr-qc].

[3337] M. Lattanzi, S. Mercuri, A solution of the strong CP problem via the Peccei–Quinn mechanism through the Nieh–Yan modified gravity and cosmological implications, Phys. Rev. D 81 (2010) 125015, arXiv:0911.2698 [gr-qc].

[3338] M. Li, H. Rao, D. Zhao, A simple parity violating gravity model without ghost instability, J. Cosmol. Astropart. Phys. 11 (2020) 023, arXiv:2007.08038 [gr-qc].

[3339] A. Chatzistavrakidis, G. Karagiannis, G. Manolakos, P. Schupp, Axion gravitodynamics, Lense–Thirring effect, and gravitational waves, Phys. Rev. D 105 (10) (2022) 104029, arXiv:2111.04388 [gr-qc].

[3340] M. Lagos, L. Jenks, M. Isi, K. Hotokezaka, B.D. Metzger, E. Burns, W.M. Farr, S. Perkins, K.W.K. Wong, N. Yunes, Birefringence tests of gravity with multimessenger binaries, Phys. Rev. D 109 (12) (2024) 124003, arXiv:2402.05316 [gr-qc].

[3341] J. Su, T. Harko, S.-D. Liang, Irreversible thermodynamic description of dark matter and radiation creation during inflationary reheating, Adv. High Energy Phys. 2017 (2017) 7650238, arXiv:1708.08004 [gr-qc].

[3342] T. Harko, H. Sheikhahmadi, Warm inflation with non-comoving scalar field and radiation fluid, Eur. Phys. J. C 81 (2) (2021) 165, arXiv:2102.04728 [gr-qc].

[3343] T. Matei, T. Harko, G. Mocanu, Dark matter and radiation production during warm inflation in a curved universe-an irreversible thermodynamic approach, 2023, arXiv:2303.02464 [gr-qc].

[3344] I. Prigogine, J. Geheniau, E. Gunzig, P. Nardone, Thermodynamics of cosmological matter creation, Proc. Nat. Acad. Sci. 85 (20) (1988) 7428.

[3345] I. Prigogine, J. Geheniau, E. Gunzig, P. Nardone, Thermodynamics and cosmology, Gen. Relativity Gravitation 21 (1989) 767–776.

[3346] T. Harko, Thermodynamic interpretation of the generalized gravity models with geometry - matter coupling, Phys. Rev. D 90 (4) (2014) 044067, arXiv:1408.3465 [gr-qc].

[3347] T. Harko, F.S.N. Lobo, J.P. Mimoso, D. Pavón, Gravitational induced particle production through a nonminimal curvature–matter coupling, Eur. Phys. J. C 75 (2015) 386, arXiv:1508.02511 [gr-qc].

[3348] M.A.S. Pinto, T. Harko, F.S.N. Lobo, Gravitationally induced particle production in scalar-tensor f(R,T) gravity, Phys. Rev. D 106 (4) (2022) 044043, arXiv:2205.12545 [gr-qc].

[3349] R.A.C. Cipriano, T. Harko, F.S.N. Lobo, M.A.S. Pinto, J.a.L. Rosa, Gravitationally induced matter creation in scalar–tensor f(R,T$_{\mu\nu}$T$_{\mu\nu}$) gravity, Phys. Dark Univ. 44 (2024) 101463, arXiv:2310.15018 [gr-qc].

[3350] M.A.S. Pinto, T. Harko, F.S.N. Lobo, Irreversible geometrothermodynamics of open systems in modified gravity, Entropy 25 (6) (2023) 944, arXiv:2306.13912 [gr-qc].

[3351] S. Basilakos, S. Das, E.C. Vagenas, Quantum gravity corrections and entropy at the Planck time, J. Cosmol. Astropart. Phys. 09 (2010) 027, arXiv:1009.0365 [hep-th].

[3352] S. Das, M. Fridman, G. Lambiase, E.C. Vagenas, Baryon asymmetry and minimum length, in: 16th Marcel Grossmann Meeting on Recent Developments in Theoretical and Experimental General Relativity, Astrophysics and Relativistic Field Theories, 2021, arXiv:2111.01278 [gr-qc].

[3353] S. Das, M. Fridman, G. Lambiase, E.C. Vagenas, Baryon asymmetry from the generalized uncertainty principle, Phys. Lett. B 824 (2022) 136841, arXiv:2107.02077 [gr-qc].

[3354] L.A. Escamilla, D. Fiorucci, G. Montani, E. Di Valentino, Exploring the Hubble tension with a late time Modified Gravity scenario, Phys. Dark Univ. 46 (2024) 101652, arXiv:2408.04354 [astro-ph.CO].

[3355] M.V. Battisti, G. Montani, The Big bang singularity in the framework of a generalized uncertainty principle, Phys. Lett. B 656 (2007) 96–101, arXiv:gr-qc/0703025.

[3356] S. Kouwn, Implications of minimum and maximum length scales in cosmology, Phys. Dark Univ. 21 (2018) 76–81, arXiv:1805.07278 [astro-ph.CO].

[3357] F. Fragomeno, D.M. Gingrich, S. Hergott, S. Rastgoo, E. Vienneau, A generalized uncertainty-inspired quantum black hole, Phys. Rev. D 111 (2) (2025) 024048, arXiv:2406.03909 [gr-qc].

[3358] M. Reuter, Nonperturbative evolution equation for quantum gravity, Phys. Rev. D 57 (1998) 971–985, arXiv:hep-th/9605030.

[3359] M. Reuter, F. Saueressig, From big bang to asymptotic de Sitter: Complete cosmologies in a quantum gravity framework, J. Cosmol. Astropart. Phys. 09 (2005) 012, arXiv:hep-th/0507167.

[3360] A. Bonanno, M. Reuter, Entropy signature of the running cosmological constant, J. Cosmol. Astropart. Phys. 08 (2007) 024, arXiv:0706.0174 [hep-th].

[3361] S. Weinberg, Asymptotically safe inflation, Phys. Rev. D 81 (2010) 083535, arXiv:0911.3165 [hep-th].

[3362] A. Bonanno, A. Platania, Asymptotically safe inflation from quadratic gravity, Phys. Lett. B 750 (2015) 638–642, arXiv:1507.03375 [gr-qc].

[3363] IceCube Collaboration, M.G. Aartsen, et al., Evidence for astrophysical muon neutrinos from the Northern Sky with IceCube, Phys. Rev. Lett. 115 (8) (2015) 081102, arXiv:1507.04005 [astro-ph.HE].

[3364] IceCube Collaboration, M.G. Aartsen, et al., Determining neutrino oscillation parameters from atmospheric muon neutrino disappearance with three years of IceCube DeepCore data, Phys. Rev. D 91 (7) (2015) 072004, arXiv:1410.7227 [hep-ex].

[3365] M. Chianese, A. Merle, A consistent theory of decaying dark matter connecting IceCube to the sesame street, J. Cosmol. Astropart. Phys. 04 (2017) 017, arXiv:1607.05283 [hep-ph].

[3366] G. Lambiase, S. Mohanty, A. Stabile, PeV IceCube signals and Dark Matter relic abundance in modified cosmologies, Eur. Phys. J. C 78 (4) (2018) 350, arXiv:1804.07369 [astro-ph.CO].

[3367] P. Jizba, G. Lambiase, Tsallis cosmology and its applications in dark matter physics with focus on IceCube high-energy neutrino data, Eur. Phys. J. C 82 (12) (2022) 1123, arXiv:2206.12910 [hep-th].

[3368] P. Jizba, G. Lambiase, Constraints on tsallis cosmology from big bang nucleosynthesis and the relic abundance of cold dark matter particles, Entropy 25 (11) (2023) 1495, arXiv:2310.19045 [gr-qc].

[3369] K. Lundmark, Über die Bestimmung der Entfernungen, Dimensionen, Massen und Dichtigkeit fur die nächstgelegenen anagalacktischen Sternsysteme, Medd. Fran Lunds Astron. Obs. Ser. I 125 (1930) 1–13.

[3370] F. Zwicky, Die Rotverschiebung von extragalaktischen Nebeln, Helv. Phys. Acta 6 (1933) 110–127.

[3371] F. Zwicky, On the masses of Nebulae and of clusters of Nebulae, Astrophys. J. 86 (1937) 217–246.

[3372] V.C. Rubin, W.K. Ford Jr., Rotation of the Andromeda Nebula from a spectroscopic survey of emission regions, Astrophys. J. 159 (1970) 379–403.

[3373] K.C. Freeman, On the disks of spiral and SO Galaxies, Astrophys. J. 160 (1970) 811.

[3374] J. de Swart, G. Bertone, J. van Dongen, How dark matter came to matter, Nat. Astron. 1 (2017) 0059, arXiv:1703.00013 [astro-ph.CO].

[3375] G. Jungman, M. Kamionkowski, K. Griest, Supersymmetric dark matter, Phys. Rep. 267 (1996) 195–373, arXiv:hep-ph/9506380.

[3376] G. Bertone, D. Hooper, J. Silk, Particle dark matter: Evidence, candidates and constraints, Phys. Rep. 405 (2005) 279–390, arXiv:hep-ph/0404175.
[3377] F. Iocco, M. Pato, G. Bertone, Evidence for dark matter in the inner Milky Way, Nat. Phys. 11 (2015) 245–248, arXiv:1502.03821 [astro-ph.GA].
[3378] I. de Martino, S.S. Chakrabarty, V. Cesare, A. Gallo, L. Ostorero, A. Diaferio, Dark matters on the scale of galaxies, Universe 6 (8) (2020) 107, arXiv:2007.15539 [astro-ph.CO].
[3379] M. Cirelli, A. Strumia, J. Zupan, Dark matter, 2024, arXiv:2406.01705 [hep-ph].
[3380] M. Vogelsberger, F. Marinacci, P. Torrey, E. Puchwein, Cosmological simulations of Galaxy formation, Nat. Rev. Phys. 2 (1) (2020) 42–66, arXiv:1909.07976 [astro-ph.GA].
[3381] R. Davé, D. Anglés-Alcázar, D. Narayanan, Q. Li, M.H. Rafieferantsoa, S. Appleby, Simba: cosmological simulations with black hole growth and feedback, Mon. Not. R. Astron. Soc. 486 (2) (2019) 2827–2849, arXiv:1901.10203 [astro-ph.GA].
[3382] L. Roszkowski, Particle dark matter: A Theorist's perspective, Pramana 62 (2004) 389–401, arXiv:hep-ph/0404052.
[3383] J.E. Kim, G. Carosi, Axions and the strong CP problem, Rev. Modern Phys. 82 (2010) 557–602, arXiv:0807.3125 [hep-ph]; Rev. Mod. Phys. 91 (2019) 049902, Erratum.
[3384] H. Baer, K.-Y. Choi, J.E. Kim, L. Roszkowski, Dark matter production in the early Universe: beyond the thermal WIMP paradigm, Phys. Rep. 555 (2015) 1–60, arXiv:1407.0017 [hep-ph].
[3385] B. Paczynski, Gravitational microlensing by the galactic halo, Astrophys. J. 304 (1986) 1–5.
[3386] K. Griest, Galactic microlensing as a method of detecting massive compact halo objects, Astrophys. J. 366 (1991) 412–421.
[3387] MACHO Collaboration, C. Alcock, et al., The MACHO project: Microlensing results from 5.7 years of LMC observations, Astrophys. J. 542 (2000) 281–307, arXiv:astro-ph/0001272.
[3388] EROS-2 Collaboration, P. Tisserand, et al., Limits on the Macho content of the galactic Halo from the EROS-2 survey of the magellanic clouds, Astron. Astrophys. 469 (2007) 387–404, arXiv:astro-ph/0607207.
[3389] L. Wyrzykowski, et al., The OGLE View of Microlensing towards the Magellanic Clouds. III. Ruling out sub-solar MACHOs with the OGLE-III LMC data, Mon. Not. R. Astron. Soc. 413 (2011) 493, arXiv:1012.1154 [astro-ph.GA].
[3390] H. Niikura, et al., Microlensing constraints on primordial black holes with Subaru/HSC Andromeda observations, Nat. Astron. 3 (6) (2019) 524–534, arXiv:1701.02151 [astro-ph.CO].
[3391] D.N. Page, Particle emission rates from a black hole: massless particles from an uncharged, nonrotating hole, Phys. Rev. D 13 (1976) 198–206.
[3392] M. Ricotti, J.P. Ostriker, K.J. Mack, Effect of primordial black holes on the cosmic microwave background and cosmological parameter estimates, Astrophys. J. 680 (2008) 829, arXiv:0709.0524 [astro-ph].
[3393] D. Gaggero, G. Bertone, F. Calore, R.M.T. Connors, M. Lovell, S. Markoff, E. Storm, Searching for primordial black holes in the radio and X-ray sky, Phys. Rev. Lett. 118 (24) (2017) 241101, arXiv:1612.00457 [astro-ph.HE].
[3394] S.K. Acharya, R. Khatri, CMB and BBN constraints on evaporating primordial black holes revisited, J. Cosmol. Astropart. Phys. 06 (2020) 018, arXiv:2002.00898 [astro-ph.CO].
[3395] M. Korwar, S. Profumo, Updated constraints on primordial black hole evaporation, J. Cosmol. Astropart. Phys. 05 (2023) 054, arXiv:2302.04408 [hep-ph].
[3396] N. Becker, D.C. Hooper, F. Kahlhoefer, J. Lesgourgues, N. Schöneberg, Cosmological constraints on multi-interacting dark matter, J. Cosmol. Astropart. Phys. 02 (2021) 019, arXiv:2010.04074 [astro-ph.CO].
[3397] S. Tremaine, J.E. Gunn, Dynamical role of light neutral Leptons in cosmology, Phys. Rev. Lett. 42 (1979) 407–410.
[3398] J. Alvey, N. Sabti, V. Tiki, D. Blas, K. Bondarenko, A. Boyarsky, M. Escudero, M. Fairbairn, M. Orkney, J.I. Read, New constraints on the mass of fermionic dark matter from dwarf spheroidal galaxies, Mon. Not. R. Astron. Soc. 501 (1) (2021) 1188–1201, arXiv:2010.03572 [hep-ph].
[3399] G. Chauhan, P.S.B. Dev, I. Dubovyk, B. Dziewit, W. Flieger, K. Grzanka, J. Gluza, B. Karmakar, S. Zięba, Phenomenology of lepton masses and mixing with discrete flavor symmetries, Prog. Part. Nucl. Phys. 138 (2024) 104126, arXiv:2310.20681 [hep-ph].
[3400] V. Keus, S.F. King, S. Moretti, Three-Higgs-doublet models: symmetries, potentials and Higgs boson masses, JHEP 01 (2014) 052, arXiv:1310.8253 [hep-ph].
[3401] S. Centelles Chuliá, E. Ma, R. Srivastava, J.W.F. Valle, Dirac neutrinos and dark matter stability from Lepton quarticity, Phys. Lett. B 767 (2017) 209–213, arXiv:1606.04543 [hep-ph].
[3402] S. Weinberg, Baryon and Lepton nonconserving processes, Phys. Rev. Lett. 43 (1979) 1566–1570.
[3403] F. Wilczek, A. Zee, Operator analysis of nucleon decay, Phys. Rev. Lett. 43 (1979) 1571–1573.
[3404] S. Weinberg, Varieties of Baryon and Lepton nonconservation, Phys. Rev. D 22 (1980) 1694.
[3405] H.A. Weldon, A. Zee, Operator analysis of new physics, Nuclear Phys. B 173 (1980) 269–290.
[3406] J.R. Ellis, J.S. Hagelin, D.V. Nanopoulos, K.A. Olive, M. Srednicki, Supersymmetric relics from the big bang, Nuclear Phys. B 238 (1984) 453–476.
[3407] M. Drees, M.M. Nojiri, The Neutralino relic density in minimal $N = 1$ supergravity, Phys. Rev. D 47 (1993) 376–408, arXiv:hep-ph/9207234.
[3408] H. Baer, M. Brhlik, Cosmological relic density from minimal supergravity with implications for collider physics, Phys. Rev. D 53 (1996) 597–605, arXiv:hep-ph/9508321.
[3409] V.D. Barger, C. Kao, Relic density of neutralino dark matter in supergravity models, Phys. Rev. D 57 (1998) 3131–3139, arXiv:hep-ph/9704403.
[3410] A.B. Lahanas, D.V. Nanopoulos, V.C. Spanos, Neutralino relic density in a universe with nonvanishing cosmological constant, Phys. Rev. D 62 (2000) 023515, arXiv:hep-ph/9909497.
[3411] R.H. Cyburt, J. Ellis, B.D. Fields, F. Luo, K.A. Olive, V.C. Spanos, Nucleosynthesis constraints on a massive gravitino in neutralino dark matter scenarios, J. Cosmol. Astropart. Phys. 10 (2009) 021, arXiv:0907.5003 [astro-ph.CO].
[3412] T. Han, Z. Liu, S. Su, Light neutralino dark matter: Direct/indirect detection and collider searches, JHEP 08 (2014) 093, arXiv:1406.1181 [hep-ph].
[3413] L. Roszkowski, E.M. Sessolo, S. Trojanowski, WIMP dark matter candidates and searches—current status and future prospects, Rep. Progr. Phys. 81 (6) (2018) 066201, arXiv:1707.06277 [hep-ph].
[3414] T. Falk, K.A. Olive, M. Srednicki, Heavy sneutrinos as dark matter, Phys. Lett. B 339 (1994) 248–251, arXiv:hep-ph/9409270.
[3415] C. Arina, N. Fornengo, Sneutrino cold dark matter, a new analysis: Relic abundance and detection rates, JHEP 11 (2007) 029, arXiv:0709.4477 [hep-ph].
[3416] S. Weinberg, Cosmological constraints on the scale of supersymmetry breaking, Phys. Rev. Lett. 48 (1982) 1303.
[3417] M.Y. Khlopov, A.D. Linde, Is it easy to save the gravitino? Phys. Lett. B 138 (1984) 265–268.
[3418] J.R. Ellis, J.E. Kim, D.V. Nanopoulos, Cosmological gravitino regeneration and decay, Phys. Lett. B 145 (1984) 181–186.
[3419] M. Bolz, A. Brandenburg, W. Buchmuller, Thermal production of gravitinos, Nuclear Phys. B 606 (2001) 518–544, arXiv:hep-ph/0012052; Nucl. Phys. B 790 (2008) 336–337, Erratum.
[3420] M. Kawasaki, K. Kohri, T. Moroi, A. Yotsuyanagi, Big-bang nucleosynthesis and gravitino, Phys. Rev. D 78 (2008) 065011, arXiv:0804.3745 [hep-ph].
[3421] J. Pradler, F.D. Steffen, Thermal gravitino production and collider tests of leptogenesis, Phys. Rev. D 75 (2007) 023509, arXiv:hep-ph/0608344.
[3422] V.S. Rychkov, A. Strumia, Thermal production of gravitinos, Phys. Rev. D 75 (2007) 075011, arXiv:hep-ph/0701104.
[3423] J. Ellis, M.A.G. Garcia, D.V. Nanopoulos, K.A. Olive, M. Peloso, Post-inflationary gravitino production revisited, J. Cosmol. Astropart. Phys. 03 (2016) 008, arXiv:1512.05701 [astro-ph.CO].
[3424] E. Dudas, Y. Mambrini, K. Olive, Case for an EeV gravitino, Phys. Rev. Lett. 119 (5) (2017) 051801, arXiv:1704.03008 [hep-ph].
[3425] K. Kaneta, Y. Mambrini, K.A. Olive, Radiative production of nonthermal dark matter, Phys. Rev. D 99 (6) (2019) 063508, arXiv:1901.04449 [hep-ph].
[3426] H. Eberl, I.D. Gialamas, V.C. Spanos, Gravitino thermal production revisited, Phys. Rev. D 103 (7) (2021) 075025, arXiv:2010.14621 [hep-ph].
[3427] L. Covi, J.E. Kim, L. Roszkowski, Axinos as cold dark matter, Phys. Rev. Lett. 82 (1999) 4180–4183, arXiv:hep-ph/9905212.
[3428] L. Covi, H.-B. Kim, J.E. Kim, L. Roszkowski, Axinos as dark matter, JHEP 05 (2001) 033, arXiv:hep-ph/0101009.
[3429] K. Aoki, K.-i. Maeda, Dark matter in ghost-free bigravity theory: from a galaxy scale to the universe, Phys. Rev. D 90 (2014) 124089, arXiv:1409.0202 [gr-qc].
[3430] K. Aoki, S. Mukohyama, Massive gravitons as dark matter and gravitational waves, Phys. Rev. D 94 (2) (2016) 024001, arXiv:1604.06704 [hep-th].
[3431] E. Babichev, L. Marzola, M. Raidal, A. Schmidt-May, F. Urban, H. Veermäe, M. von Strauss, Bigravitational origin of dark matter, Phys. Rev. D 94 (8) (2016) 084055, arXiv:1604.08564 [hep-ph].
[3432] E. Babichev, L. Marzola, M. Raidal, A. Schmidt-May, F. Urban, H. Veermäe, M. von Strauss, Heavy spin-2 dark matter, J. Cosmol. Astropart. Phys. 09 (2016) 016, arXiv:1607.03497 [hep-th].
[3433] E.W. Kolb, S. Ling, A.J. Long, R.A. Rosen, Cosmological gravitational particle production of massive spin-2 particles, JHEP 05 (2023) 181, arXiv:2302.04390 [astro-ph.CO].
[3434] H.-C. Cheng, J.L. Feng, K.T. Matchev, Kaluza–Klein dark matter, Phys. Rev. Lett. 89 (2002) 211301, arXiv:hep-ph/0207125.
[3435] G. Servant, T.M.P. Tait, Is the lightest Kaluza–Klein particle a viable dark matter candidate? Nuclear Phys. B 650 (2003) 391–419, arXiv:hep-ph/0206071.
[3436] D. Hooper, S. Profumo, Dark matter and collider phenomenology of universal extra dimensions, Phys. Rep. 453 (2007) 29–115, arXiv:hep-ph/0701197.
[3437] A. Cordero-Cid, J. Hernández-Sánchez, V. Keus, S.F. King, S. Moretti, D. Rojas, D. Sokołowska, CP violating scalar Dark Matter, JHEP 12 (2016) 014, arXiv:1608.01673 [hep-ph].
[3438] J. Hernandez-Sanchez, V. Keus, S. Moretti, D. Rojas-Ciofalo, D. Sokolowska, Complementary probes of two-component dark matter, 2020, arXiv:2012.11621 [hep-ph].

[3439] T. Alanne, M. Heikinheimo, V. Keus, N. Koivunen, K. Tuominen, Direct and indirect probes of Goldstone dark matter, Phys. Rev. D 99 (7) (2019) 075028, arXiv:1812.05996 [hep-ph].

[3440] V. Keus, Dark CP-violation through the Z-portal, Phys. Rev. D 101 (7) (2020) 073007, arXiv:1909.09234 [hep-ph].

[3441] K. Griest, D. Seckel, Three exceptions in the calculation of relic abundances, Phys. Rev. D 43 (1991) 3191–3203.

[3442] J. Edsjo, P. Gondolo, Neutralino relic density including coannihilations, Phys. Rev. D 56 (1997) 1879–1894, arXiv:hep-ph/9704361.

[3443] P. Gondolo, G. Gelmini, Cosmic abundances of stable particles: Improved analysis, Nuclear Phys. B 360 (1991) 145–179.

[3444] J. Hisano, S. Matsumoto, M.M. Nojiri, O. Saito, Direct detection of the wino and higgsino-like neutralino dark matters at one-loop level, Phys. Rev. D 71 (2005) 015007, arXiv:hep-ph/0407168.

[3445] N. Arkani-Hamed, D.P. Finkbeiner, T.R. Slatyer, N. Weiner, A theory of dark matter, Phys. Rev. D 79 (2009) 015014, arXiv:0810.0713 [hep-ph].

[3446] C. Boehm, P. Fayet, Scalar dark matter candidates, Nuclear Phys. B 683 (2004) 219–263, arXiv:hep-ph/0305261.

[3447] M. Pospelov, A. Ritz, M.B. Voloshin, Secluded WIMP Dark Matter, Phys. Lett. B 662 (2008) 53–61, arXiv:0711.4866 [hep-ph].

[3448] J.L. Feng, J. Kumar, The WIMPless miracle: dark-matter particles without weak-scale masses or weak interactions, Phys. Rev. Lett. 101 (2008) 231301, arXiv:0803.4196 [hep-ph].

[3449] K.M. Zurek, Dark matter candidates of a very low mass, Ann. Rev. Nucl. Part. Sci. 74 (2024) 287–319, arXiv:2401.03025 [hep-ph].

[3450] R. Essig, et al., Snowmass2021 Cosmic Frontier: The landscape of low-threshold dark matter direct detection in the next decade, in: Snowmass 2021, 2022, arXiv:2203.08297 [hep-ph].

[3451] G. Krnjaic, et al., A snowmass whitepaper: dark matter production at intensity-frontier experiments, 2022, arXiv:2207.00597 [hep-ph].

[3452] T. Yanagida, Horizontal symmetry and mass of the top quark, Phys. Rev. D 20 (1979) 2986.

[3453] T. Yanagida, Horizontal symmetry and masses of neutrinos, Progr. Theoret. Phys. 64 (1980) 1103.

[3454] R.N. Mohapatra, G. Senjanovic, Neutrino mass and spontaneous parity nonconservation, Phys. Rev. Lett. 44 (1980) 912.

[3455] J. Schechter, J.W.F. Valle, Neutrino masses in SU(2) x U(1) theories, Phys. Rev. D 22 (1980) 2227.

[3456] M. Fukugita, T. Yanagida, Baryogenesis without grand unification, Phys. Lett. B 174 (1986) 45–47.

[3457] P.B. Pal, L. Wolfenstein, Radiative decays of massive neutrinos, Phys. Rev. D 25 (1982) 766.

[3458] S. Dodelson, L.M. Widrow, Sterile-neutrinos as dark matter, Phys. Rev. Lett. 72 (1994) 17–20, arXiv:hep-ph/9303287.

[3459] X.-D. Shi, G.M. Fuller, A New dark matter candidate: Nonthermal sterile neutrinos, Phys. Rev. Lett. 82 (1999) 2832–2835, arXiv:astro-ph/9810076.

[3460] R.S.L. Hansen, S. Vogl, Thermalizing sterile neutrino dark matter, Phys. Rev. Lett. 119 (25) (2017) 251305, arXiv:1706.02707 [hep-ph].

[3461] A. De Gouvêa, M. Sen, W. Tangarife, Y. Zhang, Dodelson–Widrow mechanism in the presence of self-interacting neutrinos, Phys. Rev. Lett. 124 (8) (2020) 081802, arXiv:1910.04901 [hep-ph].

[3462] T. Bringmann, P.F. Depta, M. Hufnagel, J. Kersten, J.T. Ruderman, K. Schmidt-Hoberg, Minimal sterile neutrino dark matter, Phys. Rev. D 107 (7) (2023) L071702, arXiv:2206.10630 [hep-ph].

[3463] F. Wilczek, Problem of strong P and T invariance in the presence of instantons, Phys. Rev. Lett. 40 (1978) 279–282.

[3464] S. Weinberg, A new light boson? Phys. Rev. Lett. 40 (1978) 223–226.

[3465] R.D. Peccei, H.R. Quinn, CP conservation in the presence of instantons, Phys. Rev. Lett. 38 (1977) 1440–1443.

[3466] J.E. Kim, Weak interaction singlet and strong CP invariance, Phys. Rev. Lett. 43 (1979) 103.

[3467] M.A. Shifman, A.I. Vainshtein, V.I. Zakharov, Can confinement ensure natural CP invariance of strong interactions? Nuclear Phys. B 166 (1980) 493–506.

[3468] A.R. Zhitnitsky, On possible suppression of the axion hadron interactions, Sov. J. Nucl. Phys. 31 (1980) 260 (in Russian).

[3469] M. Dine, W. Fischler, M. Srednicki, A simple solution to the strong cp problem with a harmless axion, Phys. Lett. B 104 (1981) 199–202.

[3470] J. Preskill, M.B. Wise, F. Wilczek, Cosmology of the invisible axion, Phys. Lett. B 120 (1983) 127–132.

[3471] L.F. Abbott, P. Sikivie, A cosmological bound on the invisible axion, Phys. Lett. B 120 (1983) 133–136.

[3472] M. Dine, W. Fischler, The not so harmless axion, Phys. Lett. B 120 (1983) 137–141.

[3473] A.D. Linde, Axions in inflationary cosmology, Phys. Lett. B 259 (1991) 38–47.

[3474] M.P. Hertzberg, M. Tegmark, F. Wilczek, Axion cosmology and the energy scale of inflation, Phys. Rev. D 78 (2008) 083507, arXiv:0807.1726 [astro-ph].

[3475] L. Visinelli, P. Gondolo, Dark matter axions revisited, Phys. Rev. D 80 (2009) 035024, arXiv:0903.4377 [astro-ph.CO].

[3476] G. Lazarides, R.K. Schaefer, D. Seckel, Q. Shafi, Dilution of cosmological axions by entropy production, Nuclear Phys. B 346 (1990) 193–212.

[3477] L. Visinelli, P. Gondolo, Axion cold dark matter in non-standard cosmologies, Phys. Rev. D 81 (2010) 063508, arXiv:0912.0015 [astro-ph.CO].

[3478] L. Di Luzio, F. Mescia, E. Nardi, Redefining the axion window, Phys. Rev. Lett. 118 (3) (2017) 031801, arXiv:1610.07593 [hep-ph].

[3479] L. Di Luzio, F. Mescia, E. Nardi, Window for preferred axion models, Phys. Rev. D 96 (7) (2017) 075003, arXiv:1705.05370 [hep-ph].

[3480] S.M. Barr, D. Seckel, Planck scale corrections to axion models, Phys. Rev. D 46 (1992) 539–549.

[3481] L. Di Luzio, M. Giannotti, E. Nardi, L. Visinelli, The landscape of QCD axion models, Phys. Rep. 870 (2020) 1–117, arXiv:2003.01100 [hep-ph].

[3482] I.G. Irastorza, J. Redondo, New experimental approaches in the search for axion-like particles, Prog. Part. Nucl. Phys. 102 (2018) 89–159, arXiv:1801.08127 [hep-ph].

[3483] L. Amendola, R. Barbieri, Dark matter from an ultra-light pseudo-Goldsone-boson, Phys. Lett. B 642 (2006) 192–196, arXiv:hep-ph/0509257.

[3484] D.J.E. Marsh, J. Silk, A model for halo formation with axion mixed dark matter, Mon. Not. R. Astron. Soc. 437 (3) (2014) 2652–2663, arXiv:1307.1705 [astro-ph.CO].

[3485] D.J.E. Marsh, D. Grin, R. Hlozek, P.G. Ferreira, Axiverse cosmology and the energy scale of inflation, Phys. Rev. D 87 (2013) 121701, arXiv:1303.3008 [astro-ph.CO].

[3486] L. Hui, J.P. Ostriker, S. Tremaine, E. Witten, Ultralight scalars as cosmological dark matter, Phys. Rev. D 95 (4) (2017) 043541, arXiv:1610.08297 [astro-ph.CO].

[3487] L. Visinelli, Light axion-like dark matter must be present during inflation, Phys. Rev. D 96 (2) (2017) 023013, arXiv:1703.08798 [astro-ph.CO].

[3488] L. Visinelli, S. Vagnozzi, Cosmological window onto the string axiverse and the supersymmetry breaking scale, Phys. Rev. D 99 (6) (2019) 063517, arXiv:1809.06382 [hep-ph].

[3489] H.-Y. Schive, M.-H. Liao, T.-P. Woo, S.-K. Wong, T. Chiueh, T. Broadhurst, W.Y.P. Hwang, Understanding the core-halo relation of quantum wave dark matter from 3D simulations, Phys. Rev. Lett. 113 (26) (2014) 261302, arXiv:1407.7762 [astro-ph.GA].

[3490] M. Nori, M. Baldi, AX-GADGET: a new code for cosmological simulations of Fuzzy Dark Matter and Axion models, Mon. Not. R. Astron. Soc. 478 (3) (2018) 3935–3951, arXiv:1801.08144 [astro-ph.CO].

[3491] P. Mocz, et al., First star-forming structures in fuzzy cosmic filaments, Phys. Rev. Lett. 123 (14) (2019) 141301, arXiv:1910.01653 [astro-ph.GA].

[3492] J. Veltmaat, B. Schwabe, J.C. Niemeyer, Baryon-driven growth of solitonic cores in fuzzy dark matter halos, Phys. Rev. D 101 (8) (2020) 083518, arXiv:1911.09614 [astro-ph.CO].

[3493] S. May, V. Springel, The halo mass function and filaments in full cosmological simulations with fuzzy dark matter, Mon. Not. R. Astron. Soc. 524 (3) (2023) 4256–4274, arXiv:2209.14886 [astro-ph.CO].

[3494] T. Zimmermann, J. Alvey, D.J.E. Marsh, M. Fairbairn, J.I. Read, Dwarf galaxies imply dark matter is heavier than 2.2 × 10-21 eV, Phys. Rev. Lett. 134 (15) (2025) 151001, arXiv:2405.20374 [astro-ph.CO].

[3495] L. Teodori, A. Caputo, K. Blum, Ultra-light dark matter simulations and stellar dynamics: tension in dwarf galaxies for $m < 5 \times 10^{-21}$ eV, 2025, arXiv:2501.07631 [astro-ph.GA].

[3496] I. De Martino, T. Broadhurst, S.H. Henry Tye, T. Chiueh, H.-Y. Schive, R. Lazkoz, Recognizing axionic dark matter by compton and de broglie scale modulation of pulsar timing, Phys. Rev. Lett. 119 (22) (2017) 221103, arXiv:1705.04367 [astro-ph.CO].

[3497] R. Hlozek, D.J.E. Marsh, D. Grin, Using the full power of the cosmic microwave background to probe axion dark matter, Mon. Not. R. Astron. Soc. 476 (3) (2018) 3063–3085, arXiv:1708.05681 [astro-ph.CO].

[3498] N. Bar, D. Blas, K. Blum, S. Sibiryakov, Galactic rotation curves versus ultralight dark matter: implications of the soliton-host halo relation, Phys. Rev. D 98 (8) (2018) 083027, arXiv:1805.00122 [astro-ph.CO].

[3499] N. Bar, K. Blum, J. Eby, R. Sato, Ultralight dark matter in disk galaxies, Phys. Rev. D 99 (10) (2019) 103020, arXiv:1903.03402 [astro-ph.CO].

[3500] A. Pozo, T. Broadhurst, I. De Martino, H.N. Luu, G.F. Smoot, J. Lim, M. Neyrinck, Wave dark matter and ultra-diffuse galaxies, Mon. Not. R. Astron. Soc. 504 (2) (2021) 2868–2876, arXiv:2003.08313 [astro-ph.GA].

[3501] J.H.H. Chan, H.-Y. Schive, S.-K. Wong, T. Chiueh, T. Broadhurst, Multiple images and flux ratio anomaly of fuzzy gravitational lenses, Phys. Rev. Lett. 125 (11) (2020) 111102, arXiv:2002.10473 [astro-ph.GA].

[3502] N. Dalal, A. Kravtsov, Excluding fuzzy dark matter with sizes and stellar kinematics of ultrafaint dwarf galaxies, Phys. Rev. D 106 (6) (2022) 063517, arXiv:2203.05750 [astro-ph.CO].

[3503] I. De Martino, Constraining ultralight bosons in dwarf spheroidal galaxies with a radially varying anisotropy, Phys. Rev. D 108 (12) (2023) 123044, arXiv:2312.07217 [astro-ph.GA].

[3504] R. Della Monica, I. de Martino, Bounding the mass of ultralight bosonic dark matter particles with the motion of the S2 star around Sgr A*, Phys. Rev. D 108 (10) (2023) L101303, arXiv:2305.10242 [gr-qc].

[3505] A. Burkert, Fuzzy dark matter and dark matter halo cores, Astrophys. J. 904 (2) (2020) 161, arXiv:2006.11111 [astro-ph.GA].

[3506] A. Aboubrahim, P. Nath, Interacting ultralight dark matter and dark energy and fits to cosmological data in a field theory approach, J. Cosmol. Astropart. Phys. 09 (2024) 076, arXiv:2406.19284 [astro-ph.CO].

[3507] P. Ullio, M. Kamionkowski, P. Vogel, Spin dependent WIMPs in DAMA? JHEP 07 (2001) 044, arXiv:hep-ph/0010036.

[3508] XENON Collaboration, E. Aprile, et al., First dark matter search with nuclear recoils from the XENONnT experiment, Phys. Rev. Lett. 131 (4) (2023) 041003, arXiv:2303.14729 [hep-ex].

[3509] LZ Collaboration, J. Aalbers, et al., First dark matter search results from the LUX-ZEPLIN (LZ) experiment, Phys. Rev. Lett. 131 (4) (2023) 041002, arXiv:2207.03764 [hep-ex].

[3510] PandaX Collaboration, Z. Huang, et al., Constraints on the axial-vector and pseudo-scalar mediated WIMP-nucleus interactions from PandaX-4T experiment, Phys. Lett. B 834 (2022) 137487, arXiv:2208.03626 [hep-ex].

[3511] DarkSide-50 Collaboration, P. Agnes, et al., Search for low-mass dark matter WIMPs with 12 ton-day exposure of DarkSide-50, Phys. Rev. D 107 (6) (2023) 063001, arXiv:2207.11966 [hep-ex].

[3512] DarkSide-20k Collaboration, C.E. Aalseth, et al., DarkSide-20k: A 20 tonne two-phase LAr TPC for direct dark matter detection at LNGS, Eur. Phys. J. Plus 133 (2018) 131, arXiv:1707.08145 [physics.ins-det].

[3513] ArDM Collaboration, J. Calvo, et al., Commissioning of the ArDM experiment at the Canfranc underground laboratory: first steps towards a tonne-scale liquid argon time projection chamber for Dark Matter searches, J. Cosmol. Astropart. Phys. 03 (2017) 003, arXiv:1612.06375 [physics.ins-det].

[3514] P. Sikivie, Experimental tests of the invisible axion, Phys. Rev. Lett. 51 (1983) 1415–1417; Phys. Rev. Lett. 52 (1984) 695, Erratum.

[3515] P. Sikivie, Detection rates for 'invisible' axion searches, Phys. Rev. D 32 (1985) 2988; Phys. Rev. D 36 (1987) 974, Erratum.

[3516] OSQAR Collaboration, P. Pugnat, et al., First results from the OSQAR photon regeneration experiment: No light shining through a wall, Phys. Rev. D 78 (2008) 092003, arXiv:0712.3362 [hep-ex].

[3517] ALPS Collaboration, K. Ehret, et al., Resonant laser power build-up in ALPS: A 'Light-shining-through-walls' experiment, Nucl. Instrum. Meth. A 612 (2009) 83–96, arXiv:0905.4159 [physics.ins-det].

[3518] R. Bähre, et al., Any light particle search II —Technical Design Report, J. Instrum. 8 (2013) T09001, arXiv:1302.5647 [physics.ins-det].

[3519] OSQAR Collaboration, R. Ballou, et al., New exclusion limits on scalar and pseudoscalar axionlike particles from light shining through a wall, Phys. Rev. D 92 (9) (2015) 092002, arXiv:1506.08082 [hep-ex].

[3520] D. Horns, J. Jaeckel, A. Lindner, A. Lobanov, J. Redondo, A. Ringwald, Searching for WISPy cold dark matter with a dish antenna, J. Cosmol. Astropart. Phys. 04 (2013) 016, arXiv:1212.2970 [hep-ph].

[3521] P. Sikivie, N. Sullivan, D.B. Tanner, Proposal for axion dark matter detection using an LC circuit, Phys. Rev. Lett. 112 (13) (2014) 131301, arXiv:1310.8545 [hep-ph].

[3522] ADMX Collaboration, S.J. Asztalos, et al., Large scale microwave cavity search for dark matter axions, Phys. Rev. D 64 (2001) 092003.

[3523] B.M. Brubaker, et al., First results from a microwave cavity axion search at 24 μeV, Phys. Rev. Lett. 118 (6) (2017) 061302, arXiv:1610.02580 [astro-ph.CO].

[3524] R. Barbieri, C. Braggio, G. Carugno, C.S. Gallo, A. Lombardi, A. Ortolan, R. Pengo, G. Ruoso, C.C. Speake, Searching for galactic axions through magnetized media: the QUAX proposal, Phys. Dark Univ. 15 (2017) 135–141, arXiv:1606.02201 [hep-ph].

[3525] D. Alesini, et al., Search for invisible axion dark matter of mass $m_a = 43$ μeV with the QUAX–$a\gamma$ experiment, Phys. Rev. D 103 (10) (2021) 102004, arXiv:2012.09498 [hep-ex].

[3526] C.M. Adair, et al., Search for dark matter axions with CAST-CAPP, Nat. Commun. 13 (1) (2022) 6180, arXiv:2211.02902 [hep-ex].

[3527] D. Alesini, et al., The future search for low-frequency axions and new physics with the FLASH resonant cavity experiment at Frascati National Laboratories, Phys. Dark Univ. 42 (2023) 101370, arXiv:2309.00351 [physics.ins-det].

[3528] S. Arguedas Cuendis, et al., The 3 cavity prototypes of RADES: An axion detector using microwave filters at CAST, Springer Proc. Phys. 245 (2020) 45–51, arXiv:1903.04323 [physics.ins-det].

[3529] J.L. Ouellet, et al., First results from ABRACADABRA-10 cm: A search for Sub-μeV axion dark matter, Phys. Rev. Lett. 122 (12) (2019) 121802, arXiv:1810.12257 [hep-ex].

[3530] M.A. Fedderke, P.W. Graham, D.F.J. Kimball, S. Kalia, Earth as a transducer for dark-photon dark-matter detection, Phys. Rev. D 104 (7) (2021) 075023, arXiv:2106.00022 [hep-ph].

[3531] CAST Collaboration, V. Anastassopoulos, et al., New CAST limit on the axion-photon interaction, Nat. Phys. 13 (2017) 584–590, arXiv:1705.02290 [hep-ex].

[3532] E. Armengaud, et al., Conceptual design of the International Axion Observatory (IAXO), J. Instrum. 9 (2014) T05002, arXiv:1401.3233 [physics.ins-det].

[3533] J.E. Gunn, B.W. Lee, I. Lerche, D.N. Schramm, G. Steigman, Some astrophysical consequences of the existence of a heavy stable neutral Lepton, Astrophys. J. 223 (1978) 1015–1031.

[3534] F.W. Stecker, The cosmic gamma-ray background from the annihilation of primordial stable neutral heavy Leptons, Astrophys. J. 223 (1978) 1032–1036.

[3535] L.M. Krauss, K. Freese, W. Press, D. Spergel, Cold dark matter candidates and the solar neutrino problem, Astrophys. J. 299 (1985) 1001.

[3536] K. Freese, Can scalar neutrinos or massive dirac neutrinos be the missing mass? Phys. Lett. B 167 (1986) 295–300.

[3537] T.K. Gaisser, G. Steigman, S. Tilav, Limits on cold dark matter candidates from deep underground detectors, Phys. Rev. D 34 (1986) 2206.

[3538] J. Silk, M. Srednicki, Cosmic ray anti-protons as a probe of a photino dominated universe, Phys. Rev. Lett. 53 (1984) 624.

[3539] F.W. Stecker, S. Rudaz, T.F. Walsh, Galactic anti-protons from photinos, Phys. Rev. Lett. 55 (1985) 2622–2625.

[3540] J.R. Ellis, R.A. Flores, K. Freese, S. Ritz, D. Seckel, J. Silk, Cosmic ray constraints on the annihilations of relic particles in the galactic halo, Phys. Lett. B 214 (1988) 403–412.

[3541] M. Cirelli, G. Corcella, A. Hektor, G. Hutsi, M. Kadastik, P. Panci, M. Raidal, F. Sala, A. Strumia, PPPC 4 DM ID: A poor particle physicist cookbook for dark matter indirect detection, J. Cosmol. Astropart. Phys. 03 (2011) 051, arXiv:1012.4515 [hep-ph]; J. Cosmol. Astropart. Phys. 10 (2012) E01, Erratum.

[3542] L. Pieri, J. Lavalle, G. Bertone, E. Branchini, Implications of high-resolution simulations on indirect dark matter searches, Phys. Rev. D 83 (2011) 023518, arXiv:0908.0195 [astro-ph.HE].

[3543] M. Ackermann, et al., Constraints on dark matter annihilation in clusters of galaxies with the fermi large area telescope, J. Cosmol. Astropart. Phys. 05 (2010) 025, arXiv:1002.2239 [astro-ph.CO].

[3544] Fermi-LAT Collaboration, M. Ackermann, et al., Searching for dark matter annihilation from milky way dwarf spheroidal galaxies with six years of fermi large area telescope data, Phys. Rev. Lett. 115 (23) (2015) 231301, arXiv:1503.02641 [astro-ph.HE].

[3545] M. Ajello, et al., The origin of the extragalactic gamma-ray background and implications for dark-matter annihilation, Astrophys. J. Lett. 800 (2) (2015) L27, arXiv:1501.05301 [astro-ph.HE].

[3546] HAWC Collaboration, R. Alfaro, et al., Searching for TeV dark matter in irregular dwarf galaxies with HAWC observatory, Astrophys. J. 945 (1) (2023) 25, arXiv:2302.07929 [astro-ph.HE].

[3547] IceCube Collaboration, R. Abbasi, et al., Search for GeV-scale dark matter annihilation in the Sun with IceCube DeepCore, Phys. Rev. D 105 (6) (2022) 062004, arXiv:2111.09970 [astro-ph.HE].

[3548] IceCube Collaboration, R. Abbasi, et al., Search for neutrino lines from dark matter annihilation and decay with icecube, Phys. Rev. D 108 (10) (2023) 102004, arXiv:2303.13663 [astro-ph.HE].

[3549] AMS Collaboration, M. Aguilar, et al., First result from the alpha magnetic spectrometer on the international space station: precision measurement of the positron fraction in primary cosmic rays of 0.5–350 GeV, Phys. Rev. Lett. 110 (2013) 141102.

[3550] Fermi-LAT Collaboration, M. Ackermann, et al., The fermi galactic center GeV excess and implications for dark matter, Astrophys. J. 840 (1) (2017) 43, arXiv:1704.03910 [astro-ph.HE].

[3551] CTA Consortium Collaboration, M. Doro, et al., Dark matter and fundamental physics with the cherenkov telescope array, Astropart. Phys. 43 (2013) 189–214, arXiv:1208.5356 [astro-ph.IM].

[3552] CTA Collaboration, J. Carr, et al., Prospects for indirect dark matter searches with the Cherenkov Telescope Array (CTA), PoS ICRC2015 (2016) 1203, arXiv:1508.06128 [astro-ph.HE].

[3553] CTA Consortium Collaboration, B.S. Acharya, et al., Science with the Cherenkov Telescope Array, WSP, 2018, arXiv:1709.07997 [astro-ph.IM].

[3554] CTA Consortium Collaboration, A. Morselli, Search for dark matter with IACTs and the Cherenkov Telescope Array, J. Phys. Conf. Ser. 2429 (1) (2023) 012019, arXiv:2302.11318 [astro-ph.HE].

[3555] CTAO Collaboration, S. Abe, et al., Dark matter line searches with the Cherenkov Telescope Array, J. Cosmol. Astropart. Phys. 07 (2024) 047, arXiv:2403.04857 [hep-ph].

[3556] D. Walsh, R.F. Carswell, R.J. Weymann, 0957 + 561 A, B - Twin quasistellar objects or gravitational lens, Nature 279 (1979) 381–384.

[3557] M.V. Gorenstein, I.I. Shapiro, N.L. Cohen, B.E. Corey, E.E. Falco, J.M. Marcaide, A.E.E. Rogers, A.R. Whitney, R.W. Porcas, R.A. Preston, A. Rius, Detection of a compact radio source near the center of a gravitational lens: Quasar image or galactic core? Science 219 (4580) (1983) 54–56.

[3558] A. Galan, G. Vernardos, Q. Minor, D. Sluse, L. Van de Vyvere, M. Gomer, Exploiting the diversity of modeling methods to probe systematic biases in strong lensing analyses, Astron. Astrophys. 692 (2024) A87, arXiv:2406.08484 [astro-ph.CO].

[3559] M. Meneghetti, et al., The Frontier Fields lens modelling comparison project, Mon. Not. R. Astron. Soc. 472 (3) (2017) 3177–3216, arXiv:1606.04548 [astro-ph.CO].

[3560] M. Meneghetti, R. Argazzi, F. Pace, L. Moscardini, K. Dolag, M. Bartelmann, G. Li, M. Oguri, Arc sensitivity to cluster ellipticity, asymmetries and substructures, Astron. Astrophys. 461 (2007) 25–38, arXiv:astro-ph/0606006.

[3561] J. Wagner, A model-independent characterisation of strong gravitational lensing by observables, Universe 5 (2019) 177, arXiv:1906.05285 [astro-ph.CO].

[3562] R.E. Griffiths, M. Rudisel, J. Wagner, T. Hamilton, P.-C. Huang, C. Villforth, Hamilton's Object – a clumpy galaxy straddling the gravitational caustic of a galaxy cluster: constraints on dark matter clumping, Mon. Not. R. Astron. Soc. 506 (2) (2021) 1595–1608, arXiv:2105.04562 [astro-ph.CO].
[3563] J. Lin, J. Wagner, R.E. Griffiths, Generalized model-independent characterization of strong gravitational lenses VIII. Automated multiband feature detection to constrain local lens properties, Mon. Not. R. Astron. Soc. 517 (2) (2022) 1821–1836, arXiv:2207.01630 [astro-ph.CO].
[3564] M. Meneghetti, et al., A persistent excess of galaxy-galaxy strong lensing observed in galaxy clusters, Astron. Astrophys. 678 (2023) L2, arXiv:2309.05799 [astro-ph.CO].
[3565] S. Vegetti, et al., Strong gravitational lensing as a probe of dark matter, Space Sci. Rev. 220 (5) (2024) 58, arXiv:2306.11781 [astro-ph.CO].
[3566] M. Castellano, et al., Constraints on photoionization feedback from number counts of ultra-faint high-redshift galaxies in the Frontier Fields, Astrophys. J. Lett. 823 (2) (2016) L40, arXiv:1605.01524 [astro-ph.GA].
[3567] B. Yue, et al., On the faint-end of the galaxy luminosity function in the Epoch of Reionization: updated constraints from the HST Frontier Fields, Astrophys. J. 868 (2) (2018) 115, arXiv:1711.05130 [astro-ph.GA].
[3568] P. Dayal, A. Mesinger, F. Pacucci, Early galaxy formation in warm dark matter cosmologies, Astrophys. J. 806 (1) (2015) 67, arXiv:1408.1102 [astro-ph.GA].
[3569] N. Menci, A. Grazian, A. Lamastra, F. Calura, M. Castellano, P. Santini, Galaxy formation in sterile neutrino dark matter models, Astrophys. J. 854 (1) (2018) 1, arXiv:1801.03697 [astro-ph.CO].
[3570] N. Menci, A. Grazian, M. Castellano, N.G. Sanchez, A stringent limit on the warm dark matter particle masses from the abundance of z=6 galaxies in the hubble frontier fields, Astrophys. J. Lett. 825 (1) (2016) L1, arXiv:1606.02530 [astro-ph.CO].
[3571] R.J. Bouwens, et al., UV luminosity functions at redshifts $z \sim 4$ to $z \sim 10$: 10000 galaxies from HST legacy fields, Astrophys. J. 803 (1) (2015) 34, arXiv:1403.4295 [astro-ph.CO].
[3572] R.J. Bouwens, G.D. Illingworth, P.A. Oesch, J. Caruana, B. Holwerda, R. Smit, S. Wilkins, Reionization after planck: The derived growth of the cosmic ionizing emissivity now matches the growth of the Galaxy UV luminosity density, Astrophys. J. 811 (2) (2015) 140, arXiv:1503.08228 [astro-ph.CO].
[3573] B.E. Robertson, R.S. Ellis, S.R. Furlanetto, J.S. Dunlop, Cosmic reionization and early star-forming galaxies: a joint analysis of new constraints from planck and the Hubble space telescope, Astrophys. J. Lett. 802 (2) (2015) L19, arXiv:1502.02024 [astro-ph.CO].
[3574] S.L. Finkelstein, A. D'Aloisio, J.-P. Paardekooper, R. Ryan, P. Behroozi, K. Finlator, R. Livermore, P.R.U. Sanderbeck, C.D. Vecchia, S. Khochfar, Conditions for reionizing the Universe with A low galaxy ionizing photon escape fraction, Astrophys. J. 879 (1) (2019) 36, arXiv:1902.02792 [astro-ph.CO].
[3575] I.P. Carucci, P.-S. Corasaniti, Cosmic reionization history and dark matter scenarios, Phys. Rev. D 99 (2) (2019) 023518, arXiv:1811.07904 [astro-ph.CO].
[3576] M. Romanello, N. Menci, M. Castellano, The epoch of reionization in warm dark matter scenarios, Universe 7 (10) (2021) 365, arXiv:2110.05262 [astro-ph.CO].
[3577] P.S. Corasaniti, S. Agarwal, D.J.E. Marsh, S. Das, Constraints on dark matter scenarios from measurements of the galaxy luminosity function at high redshifts, Phys. Rev. D 95 (8) (2017) 083512, arXiv:1611.05892 [astro-ph.CO].
[3578] A. Rudakovskyi, A. Mesinger, D. Savchenko, N. Gillet, Constraints on warm dark matter from UV luminosity functions of high-z galaxies with Bayesian model comparison, Mon. Not. R. Astron. Soc. 507 (2) (2021) 3046–3056, arXiv:2104.04481 [astro-ph.CO].
[3579] A. Lapi, T. Ronconi, L. Boco, F. Shankar, N. Krachmalnicoff, C. Baccigalupi, L. Danese, Astroparticle constraints from cosmic reionization and primordial galaxy formation, Universe 8 (9) (2022) 476, arXiv:2205.09474 [astro-ph.CO].
[3580] A. Lapi, L. Danese, Cold or warm? Constraining dark matter with primeval galaxies and cosmic reionization after planck, J. Cosmol. Astropart. Phys. 09 (2015) 003, arXiv:1508.02147 [astro-ph.CO].
[3581] A. Garzilli, A. Magalich, O. Ruchayskiy, A. Boyarsky, How to constrain warm dark matter with the Lyman-α forest, Mon. Not. R. Astron. Soc. 502 (2) (2021) 2356–2363, arXiv:1912.09397 [astro-ph.CO].
[3582] M. Drewes, et al., A white paper on keV sterile neutrino dark matter, J. Cosmol. Astropart. Phys. 01 (2017) 025, arXiv:1602.04816 [hep-ph].
[3583] B. Dasgupta, J. Kopp, Sterile neutrinos, Phys. Rep. 928 (2021) 1–63, arXiv:2106.05913 [hep-ph].
[3584] K.N. Abazajian, Sterile neutrinos in cosmology, Phys. Rep. 711-712 (2017) 1–28, arXiv:1705.01837 [hep-ph].
[3585] K.J. Kelly, M. Sen, W. Tangarife, Y. Zhang, Origin of sterile neutrino dark matter via secret neutrino interactions with vector bosons, Phys. Rev. D 101 (11) (2020) 115031, arXiv:2005.03681 [hep-ph].
[3586] M.D. Astros, S. Vogl, Boosting the production of sterile neutrino dark matter with self-interactions, JHEP 03 (2024) 032, arXiv:2307.15565 [hep-ph].
[3587] M. Shaposhnikov, I. Tkachev, The nuMSM, inflation, and dark matter, Phys. Lett. B 639 (2006) 414–417, arXiv:hep-ph/0604236.
[3588] A. Kusenko, Sterile neutrinos, dark matter, and the pulsar velocities in models with a Higgs singlet, Phys. Rev. Lett. 97 (2006) 241301, arXiv:hep-ph/0609081.
[3589] K. Petraki, A. Kusenko, Dark-matter sterile neutrinos in models with a gauge singlet in the Higgs sector, Phys. Rev. D 77 (2008) 065014, arXiv:0711.4646 [hep-ph].
[3590] F. Bezrukov, H. Hettmansperger, M. Lindner, keV sterile neutrino Dark Matter in gauge extensions of the Standard Model, Phys. Rev. D 81 (2010) 085032, arXiv:0912.4415 [hep-ph].
[3591] A. Kusenko, F. Takahashi, T.T. Yanagida, Dark matter from split seesaw, Phys. Lett. B 693 (2010) 144–148, arXiv:1006.1731 [hep-ph].
[3592] J.A. Dror, D. Dunsky, L.J. Hall, K. Harigaya, Sterile neutrino dark matter in left-right theories, JHEP 07 (2020) 168, arXiv:2004.09511 [hep-ph].
[3593] M. Heikinheimo, K. Huitu, V. Keus, N. Koivunen, Cosmological constraints on light flavons, JHEP 06 (2019) 065, arXiv:1812.10963 [hep-ph].
[3594] S. May, V. Springel, Structure formation in large-volume cosmological simulations of fuzzy dark matter: impact of the non-linear dynamics, Mon. Not. R. Astron. Soc. 506 (2) (2021) 2603–2618, arXiv:2101.01828 [astro-ph.CO].
[3595] A. Gough, C. Uhlemann, When to interfere with dark matter? The impact of wave dynamics on statistics, Open J. Astrophys. 7 (2024) 2024, arXiv:2405.15852 [astro-ph.CO].
[3596] K.K. Rogers, R. Hložek, A. Laguë, M.M. Ivanov, O.H.E. Philcox, G. Cabass, K. Akitsu, D.J.E. Marsh, Ultra-light axions and the S_8 tension: joint constraints from the cosmic microwave background and galaxy clustering, J. Cosmol. Astropart. Phys. 06 (2023) 023, arXiv:2301.08361 [astro-ph.CO].
[3597] R.C. Pantig, A. Övgün, Black hole in quantum wave dark matter, Fortsch. Phys. 71 (1) (2023) 2200164, arXiv:2210.00523 [gr-qc].
[3598] V. Cardoso, T. Ikeda, R. Vicente, M. Zilhão, Parasitic black holes: The swallowing of a fuzzy dark matter soliton, Phys. Rev. D 106 (12) (2022) L121302, arXiv:2207.09469 [gr-qc].
[3599] G. Mustafa, S.K. Maurya, S. Ray, F. Javed, Construction of thin-shell around new wormhole solutions via solitonic quantum wave dark matter, Ann. Phys. 460 (2024) 169551.
[3600] K.K. Boddy, V. Gluscevic, V. Poulin, E.D. Kovetz, M. Kamionkowski, R. Barkana, Critical assessment of CMB limits on dark matter-baryon scattering: New treatment of the relative bulk velocity, Phys. Rev. D 98 (12) (2018) 123506, arXiv:1808.00001 [astro-ph.CO].
[3601] Z. Li, et al., The Atacama Cosmology Telescope: limits on dark matter-baryon interactions from DR4 power spectra, J. Cosmol. Astropart. Phys. 02 (2023) 046, arXiv:2208.08985 [astro-ph.CO].
[3602] R. Barkana, Possible interaction between baryons and dark-matter particles revealed by the first stars, Nature 555 (7694) (2018) 71–74, arXiv:1803.06698 [astro-ph.CO].
[3603] V. Gluscevic, K.K. Boddy, Constraints on scattering of keV–TeV dark matter with protons in the early universe, Phys. Rev. Lett. 121 (8) (2018) 081301, arXiv:1712.07133 [astro-ph.CO].
[3604] M. Postolak, Did the Big Bang and cosmic inflation really happen? (A tale of alternative cosmological models), 2024, arXiv:2404.18503 [physics.pop-ph].
[3605] J. Sakstein, H. Desmond, B. Jain, Screened fifth forces mediated by dark matter–Baryon interactions: theory and astrophysical probes, Phys. Rev. D 100 (10) (2019) 104035, arXiv:1907.03775 [astro-ph.CO].
[3606] M.A. Buen-Abad, R. Essig, D. McKeen, Y.-M. Zhong, Cosmological constraints on dark matter interactions with ordinary matter, Phys. Rep. 961 (2022) 1–35, arXiv:2107.12377 [astro-ph.CO].
[3607] C. Dvorkin, K. Blum, M. Kamionkowski, Constraining dark matter-Baryon scattering with linear cosmology, Phys. Rev. D 89 (2) (2014) 023519, arXiv:1311.2937 [astro-ph.CO].
[3608] B. Moore, Evidence against dissipationless dark matter from observations of galaxy haloes, Nature 370 (1994) 629.
[3609] S.-H. Oh, W.J.G. de Blok, F. Walter, E. Brinks, R.C. Kennicutt Jr., High-resolution dark matter density profiles of things dwarf galaxies: correcting for non-circular motions, Astron. J. 136 (2008) 2761, arXiv:0810.2119 [astro-ph].
[3610] J. Kormendy, K.C. Freeman, Scaling laws for dark matter halos in late-type and dwarf spheroidal galaxies, IAU Symp. 220 (2004) 377, arXiv:astro-ph/0407321.
[3611] F. Donato, P. Salucci, Cores of dark matter halos correlate with disk scale lengths, Mon. Not. R. Astron. Soc. 353 (2004) L17–L22, arXiv:astro-ph/0403206.
[3612] F. Donato, G. Gentile, P. Salucci, C.F. Martins, M.I. Wilkinson, G. Gilmore, E.K. Grebel, A. Koch, R. Wyse, A constant dark matter halo surface density in galaxies, Mon. Not. R. Astron. Soc. 397 (2009) 1169–1176, arXiv:0904.4054 [astro-ph.CO].
[3613] G. Gentile, B. Famaey, H. Zhao, P. Salucci, Universality of galactic surface densities within one dark halo scale-length, Nature 461 (2009) 627, arXiv:0909.5203 [astro-ph.CO].
[3614] C. Di Paolo, P. Salucci, A. Erkurt, The universal rotation curve of low surface brightness galaxies – IV. The interrelation between dark and luminous matter, Mon. Not. R. Astron. Soc. 490 (4) (2019) 5451–5477, arXiv:1805.07165.
[3615] G. Sharma, P. Salucci, G. van de Ven, Observational evidence of evolving dark matter profiles at $z \leq 1$, Astron. Astrophys. 659 (2022) A40, arXiv:2109.14224 [astro-ph.GA].
[3616] P. Salucci, N. Turini, C. Di Paolo, Paradigms and scenarios for the dark matter phenomenon, Universe 6 (8) (2020) 118, arXiv:2008.04052 [astro-ph.CO].

[3617] Y. Shoji, E. Kuflik, Y. Birnboim, N.C. Stone, Heating galaxy clusters with interacting dark matter, Mon. Not. R. Astron. Soc. 528 (3) (2024) 4082–4091, arXiv:2306.08679 [astro-ph.CO].

[3618] G. Choi, T.T. Yanagida, N. Yokozaki, A model of interacting dark matter and dark radiation for H_0 and σ_8 tensions, JHEP 01 (2021) 127, arXiv:2010.06892 [hep-ph].

[3619] M.G. Yengejeh, S. Fakhry, J.T. Firouzjaee, H. Fathi, The integrated Sachs–Wolfe effect in interacting dark matter–dark energy models, Phys. Dark Univ. 39 (2023) 101144, arXiv:2206.01030 [astro-ph.CO].

[3620] Y. Wu, S. Baum, K. Freese, L. Visinelli, H.-B. Yu, Dark stars powered by self-interacting dark matter, Phys. Rev. D 106 (4) (2022) 043028, arXiv:2205.10904 [hep-ph].

[3621] N.F. Bell, G. Busoni, M.E. Ramirez-Quezada, S. Robles, M. Virgato, Improved treatment of dark matter capture in white dwarfs, J. Cosmol. Astropart. Phys. 10 (2021) 083, arXiv:2104.14367 [hep-ph].

[3622] K.-L. Leung, M.-c. Chu, L.-M. Lin, Tidal deformability of dark matter admixed neutron stars, Phys. Rev. D 105 (12) (2022) 123010, arXiv:2207.02433 [astro-ph.HE].

[3623] O. Akarsu, N. Katirci, S. Kumar, R.C. Nunes, M. Sami, Cosmological implications of scale-independent energy-momentum squared gravity: Pseudo nonminimal interactions in dark matter and relativistic relics, Phys. Rev. D 98 (6) (2018) 063522, arXiv:1807.01588 [gr-qc].

[3624] Z. Zhou, G. Liu, Y. Mu, L. Xu, Limit on the dark matter mass from its interaction with photons, Phys. Rev. D 105 (10) (2022) 103509, arXiv:2205.08070 [astro-ph.CO].

[3625] J. Stadler, C. Bœhm, Constraints on γ-CDM interactions matching the Planck data precision, J. Cosmol. Astropart. Phys. 10 (2018) 009, arXiv:1802.06589 [astro-ph.CO].

[3626] Y. Ali-Haïmoud, Testing dark matter interactions with CMB spectral distortions, Phys. Rev. D 103 (4) (2021) 043541, arXiv:2101.04070 [astro-ph.CO].

[3627] Z. Xu, X. Hou, X. Gong, J. Wang, Black hole space-time in dark matter halo, J. Cosmol. Astropart. Phys. 09 (2018) 038, arXiv:1803.00767 [gr-qc].

[3628] R.A. Konoplya, A. Zhidenko, Solutions of the Einstein equations for a black hole surrounded by a galactic halo, Astrophys. J. 933 (2) (2022) 166, arXiv:2202.02205 [gr-qc].

[3629] X. Hou, Z. Xu, J. Wang, Rotating black hole shadow in perfect fluid dark matter, J. Cosmol. Astropart. Phys. 12 (2018) 040, arXiv:1810.06381 [gr-qc].

[3630] X. Hou, Z. Xu, M. Zhou, J. Wang, Black hole shadow of Sgr A* in dark matter halo, J. Cosmol. Astropart. Phys. 07 (2018) 015, arXiv:1804.08110 [gr-qc].

[3631] S. Haroon, M. Jamil, K. Jusufi, K. Lin, R.B. Mann, Shadow and deflection angle of rotating black holes in perfect fluid dark matter with a cosmological constant, Phys. Rev. D 99 (4) (2019) 044015, arXiv:1810.04103 [gr-qc].

[3632] Z. Xu, X. Gong, S.-N. Zhang, Black hole immersed dark matter halo, Phys. Rev. D 101 (2) (2020) 024029.

[3633] K. Jusufi, M. Jamil, T. Zhu, Shadows of Sgr A* black hole surrounded by superfluid dark matter halo, Eur. Phys. J. C 80 (5) (2020) 354, arXiv:2005.05299 [gr-qc].

[3634] Z. Xu, J. Wang, M. Tang, Deformed black hole immersed in dark matter spike, J. Cosmol. Astropart. Phys. 09 (2021) 007, arXiv:2104.13158 [gr-qc].

[3635] S. Nampalliwar, S. Kumar, K. Jusufi, Q. Wu, M. Jamil, P. Salucci, Modeling the Sgr A* black hole immersed in a dark matter spike, Astrophys. J. 916 (2) (2021) 116, arXiv:2103.12439 [astro-ph.HE].

[3636] K. Jusufi, Saurabh, Black hole shadows in Verlinde's emergent gravity, Mon. Not. R. Astron. Soc. 503 (1) (2021) 1310–1318, arXiv:2010.15870 [gr-qc].

[3637] R.A. Konoplya, Black holes in galactic centers: Quasinormal ringing, greybody factors and Unruh temperature, Phys. Lett. B 823 (2021) 136734, arXiv:2109.01640 [gr-qc].

[3638] K. Saurabh, K. Jusufi, Imprints of dark matter on black hole shadows using spherical accretions, Eur. Phys. J. C 81 (6) (2021) 490, arXiv:2009.10599 [gr-qc].

[3639] R.C. Pantig, A. Övgün, Dark matter effect on the weak deflection angle by black holes at the center of Milky Way and M87 galaxies, Eur. Phys. J. C 82 (5) (2022) 391, arXiv:2201.03365 [gr-qc].

[3640] R.C. Pantig, A. Övgün, Dehnen halo effect on a black hole in an ultra-faint dwarf galaxy, J. Cosmol. Astropart. Phys. 08 (08) (2022) 056, arXiv:2202.07404 [astro-ph.GA].

[3641] F. Atamurotov, U. Papnoi, K. Jusufi, Shadow and deflection angle of charged rotating black hole surrounded by perfect fluid dark matter, Cl. Quant. Grav. 39 (2) (2022) 025014, arXiv:2104.14898 [gr-qc].

[3642] K. Jusufi, Black holes surrounded by Einstein clusters as models of dark matter fluid, Eur. Phys. J. C 83 (2) (2023) 103, arXiv:2202.00010 [gr-qc].

[3643] R.C. Pantig, P.K. Yu, E.T. Rodulfo, A. Övgün, Shadow and weak deflection angle of extended uncertainty principle black hole surrounded with dark matter, Ann. Phys. 436 (2022) 168722, arXiv:2104.04304 [gr-qc].

[3644] D. Liu, Y. Yang, A. Övgün, Z.-W. Long, Z. Xu, Gravitational ringing and superradiant instabilities of the Kerr-like black holes in a dark matter halo, Eur. Phys. J. C 83 (7) (2023) 565, arXiv:2204.11563 [gr-qc].

[3645] A. Anjum, M. Afrin, S.G. Ghosh, Investigating effects of dark matter on photon orbits and black hole shadows, Phys. Dark Univ. 40 (2023) 101195, arXiv:2301.06373 [gr-qc].

[3646] A. Övgün, L.J.F. Sese, R.C. Pantig, Constraints via the event horizon telescope for black hole solutions with dark matter under the generalized uncertainty principle minimal length scale effect, Ann. Phys. 536 (4) (2024) 2300390, arXiv:2309.07442 [gr-qc].

[3647] A. Errehymy, S.K. Maurya, G. Mustafa, S. Hansraj, H.I. Alrebdi, A.-H. Abdel-Aty, Black hole solutions with dark matter halos in the four-dimensional einstein-gauss-bonnet gravity, Fortsch. Phys. 71 (10-11) (2023) 2300052.

[3648] C.-K. Qiao, M. Zhou, Gravitational lensing of Schwarzschild and charged black holes immersed in perfect fluid dark matter halo, J. Cosmol. Astropart. Phys. 12 (2023) 005, arXiv:2212.13311 [gr-qc].

[3649] X. Zhou, Y. Xue, B. Mu, J. Tao, Temporal and spatial chaos of RN-AdS black holes immersed in perfect fluid dark matter, Phys. Dark Univ. 39 (2023) 101168, arXiv:2209.03612 [gr-qc].

[3650] S. Capozziello, S. Zare, D.F. Mota, H. Hassanabadi, Dark matter spike around bumblebee black holes, J. Cosmol. Astropart. Phys. 2023 (2305) (2023) 027, arXiv:2303.13554 [gr-qc].

[3651] S. Capozziello, S. Zare, H. Hassanabadi, Testing bumblebee gravity with global monopoles in a dark matter spike by eht observations from M87 and Sgr A, 2023, arXiv:2311.12896 [gr-qc].

[3652] Y.-G. Liu, C.-K. Qiao, J. Tao, Gravitational lensing of spherically symmetric black holes in dark matter halos, J. Cosmol. Astropart. Phys. 10 (2024) 075, arXiv:2312.15760 [gr-qc].

[3653] Y. Yang, D. Liu, A. Övgün, G. Lambiase, Z.-W. Long, Black hole surrounded by the pseudo-isothermal dark matter halo, Eur. Phys. J. C 84 (1) (2024) 63, arXiv:2308.05544 [gr-qc].

[3654] G. Gómez, P. Valageas, Constraining self-interacting scalar field dark matter from the black hole shadow of the Event Horizon Telescope, Phys. Rev. D 109 (10) (2024) 103038, arXiv:2403.08988 [astro-ph.CO].

[3655] C.-K. Qiao, P. Su, Time delay of light in the gravitational lensing of supermassive black holes in dark matter halos, Eur. Phys. J. C 84 (10) (2024) 1032, arXiv:2403.05682 [gr-qc].

[3656] C.F.B. Macedo, J.L. Rosa, D. Rubiera-Garcia, Optical appearance of black holes surrounded by a dark matter halo, J. Cosmol. Astropart. Phys. 07 (2024) 046, arXiv:2402.13047 [gr-qc].

[3657] S.R. Wu, B.Q. Wang, Z.W. Long, H. Chen, Rotating black holes surrounded by a dark matter halo in the galactic center of M87 and Sgr A∗, Phys. Dark Univ. 44 (2024) 101455.

[3658] R.C. Pantig, Apparent and emergent dark matter around a Schwarzschild black hole, Phys. Dark Univ. 45 (2024) 101550, arXiv:2405.07531 [gr-qc].

[3659] R.A. Konoplya, Shadow of a black hole surrounded by dark matter, Phys. Lett. B 795 (2019) 1–6, arXiv:1905.00064 [gr-qc].

[3660] M.A. Buen-Abad, G. Marques-Tavares, M. Schmaltz, Non-Abelian dark matter and dark radiation, Phys. Rev. D 92 (2) (2015) 023531, arXiv:1505.03542 [hep-ph].

[3661] J. Lesgourgues, G. Marques-Tavares, M. Schmaltz, Evidence for dark matter interactions in cosmological precision data? J. Cosmol. Astropart. Phys. 02 (2016) 037, arXiv:1507.04351 [astro-ph.CO].

[3662] Z. Chacko, Y. Cui, S. Hong, T. Okui, Y. Tsai, Partially acoustic dark matter, interacting dark radiation, and large scale structure, JHEP 12 (2016) 108, arXiv:1609.03569 [astro-ph.CO].

[3663] M.A. Buen-Abad, M. Schmaltz, J. Lesgourgues, T. Brinckmann, Interacting dark sector and precision cosmology, J. Cosmol. Astropart. Phys. 01 (2018) 008, arXiv:1708.09406 [astro-ph.CO].

[3664] M.A. Buen-Abad, R. Emami, M. Schmaltz, Cannibal dark matter and large scale structure, Phys. Rev. D 98 (8) (2018) 083517, arXiv:1803.08062 [hep-ph].

[3665] M.A. Buen-Abad, Z. Chacko, C. Kilic, G. Marques-Tavares, T. Youn, Stepped partially acoustic dark matter, large scale structure, and the hubble tension, JHEP 06 (2023) 012, arXiv:2208.05984 [hep-ph].

[3666] N. Schöneberg, G. Franco Abellán, T. Simon, A. Bartlett, Y. Patel, T.L. Smith, Comparative analysis of interacting stepped dark radiation, Phys. Rev. D 108 (12) (2023) 123513, arXiv:2306.12469 [astro-ph.CO].

[3667] M.A. Buen-Abad, Z. Chacko, C. Kilic, G. Marques-Tavares, T. Youn, Stepped partially acoustic dark matter: likelihood analysis and cosmological tensions, J. Cosmol. Astropart. Phys. 11 (2023) 005, arXiv:2306.01844 [astro-ph.CO].

[3668] L.G. van den Aarssen, T. Bringmann, C. Pfrommer, Is dark matter with long-range interactions a solution to all small-scale problems of ΛCDM cosmology? Phys. Rev. Lett. 109 (2012) 231301, arXiv:1205.5809 [astro-ph.CO].

[3669] T. Bringmann, J. Hasenkamp, J. Kersten, Tight bonds between sterile neutrinos and dark matter, J. Cosmol. Astropart. Phys. 07 (2014) 042, arXiv:1312.4947 [hep-ph].

[3670] T. Bringmann, H.T. Ihle, J. Kersten, P. Walia, Suppressing structure formation at dwarf galaxy scales and below: late kinetic decoupling as a compelling alternative to warm dark matter, Phys. Rev. D 94 (10) (2016) 103529, arXiv:1603.04884 [hep-ph].

[3671] G. Poulot, E.M. Teixeira, C. van de Bruck, N.J. Nunes, Scalar field dark matter with time-varying equation of state, 2024, arXiv:2404.10524 [astro-ph.CO].

[3672] C. van de Bruck, G. Poulot, E.M. Teixeira, Scalar field dark matter and dark energy: a hybrid model for the dark sector, J. Cosmol. Astropart. Phys. 07 (2023) 019, arXiv:2211.13653 [hep-th].

[3673] E.M. Teixeira, G. Poulot, C. van de Bruck, E. Di Valentino, V. Poulin, Alleviating cosmological tensions with a hybrid dark sector, 2024, arXiv:2412.14139 [astro-ph.CO].

[3674] BOSS Collaboration, C.P. Ahn, et al., The ninth data release of the Sloan digital sky survey: first spectroscopic data from the SDSS-III Baryon oscillation spectroscopic survey, Astrophys. J. Suppl. 203 (2012) 21, arXiv:1207.7137 [astro-ph.IM].

[3675] C. Howlett, A. Ross, L. Samushia, W. Percival, M. Manera, The clustering of the SDSS main galaxy sample – II. Mock galaxy catalogues and a measurement of the growth of structure from redshift space distortions at $z = 0.15$, Mon. Not. R. Astron. Soc. 449 (1) (2015) 848–866, arXiv:1409.3238 [astro-ph.CO].

[3676] J.L. Menestrina, R.J. Scherrer, Dark radiation from particle decays during big bang nucleosynthesis, Phys. Rev. D 85 (2012) 047301, arXiv:1111.0605 [astro-ph.CO].

[3677] M.C. Gonzalez-Garcia, V. Niro, J. Salvado, Dark radiation and decaying matter, JHEP 04 (2013) 052, arXiv:1212.1472 [hep-ph].

[3678] Z. Berezhiani, A.D. Dolgov, I.I. Tkachev, Reconciling planck results with low redshift astronomical measurements, Phys. Rev. D 92 (6) (2015) 061303, arXiv:1505.03644 [astro-ph.CO].

[3679] K. Vattis, S.M. Koushiappas, A. Loeb, Dark matter decaying in the late Universe can relieve the H0 tension, Phys. Rev. D 99 (12) (2019) 121302, arXiv:1903.06220 [astro-ph.CO].

[3680] K. Enqvist, S. Nadathur, T. Sekiguchi, T. Takahashi, Decaying dark matter and the tension in σ_8, J. Cosmol. Astropart. Phys. 09 (2015) 067, arXiv:1505.05511 [astro-ph.CO].

[3681] G. Franco Abellán, R. Murgia, V. Poulin, J. Lavalle, Implications of the S_8 tension for decaying dark matter with warm decay products, Phys. Rev. D 105 (6) (2022) 063525, arXiv:2008.09615 [astro-ph.CO].

[3682] G. Franco Abellán, R. Murgia, V. Poulin, Linear cosmological constraints on two-body decaying dark matter scenarios and the S8 tension, Phys. Rev. D 104 (12) (2021) 123533, arXiv:2102.12498 [astro-ph.CO].

[3683] W. Liu, L.A. Anchordoqui, E. Di Valentino, S. Pan, Y. Wu, W. Yang, Constraints from high-precision measurements of the cosmic microwave background: the case of disintegrating dark matter with Λ or dynamical dark energy, J. Cosmol. Astropart. Phys. 02 (02) (2022) 012, arXiv:2108.04188 [astro-ph.CO].

[3684] L.A. Anchordoqui, V. Barger, H. Goldberg, X. Huang, D. Marfatia, L.H.M. da Silva, T.J. Weiler, IceCube neutrinos, decaying dark matter, and the Hubble constant, Phys. Rev. D 92 (6) (2015) 061301, arXiv:1506.08788 [hep-ph]; Phys. Rev. D 94 (2016) 069901, Erratum.

[3685] L.A. Anchordoqui, V. Barger, D. Marfatia, M.H. Reno, T.J. Weiler, Oscillations of sterile neutrinos from dark matter decay eliminates the IceCube-Fermi tension, Phys. Rev. D 103 (7) (2021) 075022, arXiv:2101.09559 [astro-ph.HE].

[3686] A. Chudaykin, D. Gorbunov, I. Tkachev, Dark matter component decaying after recombination: Lensing constraints with Planck data, Phys. Rev. D 94 (2016) 023528, arXiv:1602.08121 [astro-ph.CO].

[3687] V. Poulin, P.D. Serpico, J. Lesgourgues, A fresh look at linear cosmological constraints on a decaying dark matter component, J. Cosmol. Astropart. Phys. 08 (2016) 036, arXiv:1606.02073 [astro-ph.CO].

[3688] S.J. Clark, K. Vattis, S.M. Koushiappas, Cosmological constraints on late-universe decaying dark matter as a solution to the H_0 tension, Phys. Rev. D 103 (4) (2021) 043014, arXiv:2006.03678 [astro-ph.CO].

[3689] A. Chudaykin, D. Gorbunov, I. Tkachev, Dark matter component decaying after recombination: Sensitivity to baryon acoustic oscillation and redshift space distortion probes, Phys. Rev. D 97 (8) (2018) 083508, arXiv:1711.06738 [astro-ph.CO].

[3690] A. Nygaard, T. Tram, S. Hannestad, Updated constraints on decaying cold dark matter, J. Cosmol. Astropart. Phys. 05 (2021) 017, arXiv:2011.01632 [astro-ph.CO].

[3691] L.A. Anchordoqui, Decaying dark matter, the H_0 tension, and the lithium problem, Phys. Rev. D 103 (3) (2021) 035025, arXiv:2010.09715 [hep-ph].

[3692] Z. Davari, N. Khosravi, Can decaying dark matter scenarios alleviate both H0 and σ8 tensions? Mon. Not. R. Astron. Soc. 516 (3) (2022) 4373–4382, arXiv:2203.09439 [astro-ph.CO].

[3693] T. Simon, G. Franco Abellán, P. Du, V. Poulin, Y. Tsai, Constraining decaying dark matter with BOSS data and the effective field theory of large-scale structures, Phys. Rev. D 106 (2) (2022) 023516, arXiv:2203.07440 [astro-ph.CO].

[3694] J. Bucko, S.K. Giri, F.H. Peters, A. Schneider, Probing the two-body decaying dark matter scenario with weak lensing and the cosmic microwave background, Astron. Astrophys. 683 (2024) A152, arXiv:2307.03222 [astro-ph.CO].

[3695] K. Sigurdson, M. Kamionkowski, Charged - particle decay and suppression of small - scale power, Phys. Rev. Lett. 92 (2004) 171302, arXiv:astro-ph/0311486.

[3696] J.A.R. Cembranos, J.L. Feng, A. Rajaraman, F. Takayama, SuperWIMP solutions to small scale structure problems, Phys. Rev. Lett. 95 (2005) 181301, arXiv:hep-ph/0507150.

[3697] M. Kaplinghat, Dark matter from early decays, Phys. Rev. D 72 (2005) 063510, arXiv:astro-ph/0507300.

[3698] L.E. Strigari, M. Kaplinghat, J.S. Bullock, Dark matter halos with cores from hierarchical structure formation, Phys. Rev. D 75 (2007) 061303, arXiv:astro-ph/0606281.

[3699] J.A.R. Cembranos, J.L. Feng, L.E. Strigari, Resolving cosmic gamma ray anomalies with dark matter decaying now, Phys. Rev. Lett. 99 (2007) 191301, arXiv:0704.1658 [astro-ph].

[3700] K.R. Dienes, B. Thomas, Dynamical dark matter: I. Theoretical overview, Phys. Rev. D 85 (2012) 083523, arXiv:1106.4546 [hep-ph].

[3701] K.R. Dienes, B. Thomas, Dynamical dark matter: II. An explicit model, Phys. Rev. D 85 (2012) 083524, arXiv:1107.0721 [hep-ph].

[3702] K.R. Dienes, F. Huang, J. Kost, S. Su, B. Thomas, Deciphering the archaeological record: cosmological imprints of nonminimal dark sectors, Phys. Rev. D 101 (12) (2020) 123511, arXiv:2001.02193 [astro-ph.CO].

[3703] L.A. Anchordoqui, I. Antoniadis, D. Lust, Aspects of the dark dimension in cosmology, Phys. Rev. D 107 (8) (2023) 083530, arXiv:2212.08527 [hep-ph].

[3704] G. Obied, C. Dvorkin, E. Gonzalo, C. Vafa, Dark dimension and decaying dark matter gravitons, Phys. Rev. D 109 (6) (2024) 063540, arXiv:2311.05318 [astro-ph.CO].

[3705] C. Vafa, The string landscape and the swampland, 2005, arXiv:hep-th/0509212.

[3706] E. Gonzalo, M. Montero, G. Obied, C. Vafa, Dark dimension gravitons as dark matter, JHEP 11 (2023) 109, arXiv:2209.09249 [hep-ph].

[3707] A. Desai, K.R. Dienes, B. Thomas, Constraining dark-matter ensembles with supernova data, Phys. Rev. D 101 (3) (2020) 035031, arXiv:1909.07981 [astro-ph.CO].

[3708] E.N. Saridakis, Do we need soft cosmology? Phys. Lett. B 822 (2021) 136649, arXiv:2105.08646 [astro-ph.CO].

[3709] E.N. Saridakis, W. Yang, S. Pan, F.K. Anagnostopoulos, S. Basilakos, Observational constraints on soft dark energy and soft dark matter: Challenging ΛCDM cosmology, Nuclear Phys. B 986 (2023) 116042, arXiv:2112.08330 [astro-ph.CO].

[3710] L.M.C. Sagis, Dynamic properties of interfaces in soft matter: experiments and theory, Rev. Modern Phys. 83 (4) (2011) 1367–1403.

[3711] Z. Davari, A. Ashoorioon, K. Rezazadeh, Spherical collapse approach for non-standard dark matter models and enhanced early galaxy formation in JWST, Mon. Not. R. Astron. Soc. 534 (3) (2024) 2848–2857, arXiv:2311.15083 [astro-ph.CO].

[3712] V. Poulin, J. Lesgourgues, P.D. Serpico, Cosmological constraints on exotic injection of electromagnetic energy, J. Cosmol. Astropart. Phys. 03 (2017) 043, arXiv:1610.10051 [astro-ph.CO].

[3713] T.R. Slatyer, C.-L. Wu, General constraints on dark matter decay from the cosmic microwave background, Phys. Rev. D 95 (2) (2017) 023010, arXiv:1610.06933 [astro-ph.CO].

[3714] S. Colafrancesco, M. Regis, P. Marchegiani, G. Beck, R. Beck, H. Zechlin, A. Lobanov, D. Horns, Probing the nature of Dark Matter with the SKA, PoS AASKA14 (2015) 100, arXiv:1502.03738 [astro-ph.HE].

[3715] K. Dutta, A. Ghosh, A. Kar, B. Mukhopadhyaya, A general study of decaying scalar dark matter: existing limits and projected radio signals at the SKA, J. Cosmol. Astropart. Phys. 09 (2022) 005, arXiv:2204.06024 [hep-ph].

[3716] S.F. King, R. Roshan, X. Wang, G. White, M. Yamazaki, Quantum gravity effects on dark matter and gravitational waves, Phys. Rev. D 109 (2) (2024) 024057, arXiv:2308.03724 [hep-ph].

[3717] S.F. King, R. Roshan, X. Wang, G. White, M. Yamazaki, Quantum gravity effects on fermionic dark matter and gravitational waves, J. Cosmol. Astropart. Phys. 05 (2024) 071, arXiv:2311.12487 [hep-ph].

[3718] T. Asaka, M. Shaposhnikov, The νMSM, dark matter and baryon asymmetry of the universe, Phys. Lett. B 620 (2005) 17–26, arXiv:hep-ph/0505013.

[3719] A. Datta, R. Roshan, A. Sil, Imprint of the Seesaw mechanism on feebly interacting dark matter and the baryon asymmetry, Phys. Rev. Lett. 127 (23) (2021) 231801, arXiv:2104.02030 [hep-ph].

[3720] I.H. Redmount, Dynamics of a void-dominated universe: cell-lattice models, Mon. Not. R. Astro. Soc. 235 (1988) 1301–1312.

[3721] E. Yusofi, M. Khanpour, B. Khanpour, M.A. Ramzanpour, M. Mohsenzadeh, Surface tension of cosmic voids as a possible source for dark energy, Mon. Not. R. Astron. Soc. 511 (1) (2022) L82–L86, arXiv:1907.12418 [astro-ph.CO].

[3722] S. Mohammadi, E. Yusofi, M. Mohsenzadeh, M.K. Salem, A possible role for the merger of clusters/voids in the cosmological expansion, Mon. Not. R. Astron. Soc. 525 (3) (2023) 3274–3280, arXiv:2309.07826 [astro-ph.CO].

[3723] H. Moshafi, A. Talebian, E. Yusofi, E. Di Valentino, Observational constraints on the dark energy with a quadratic equation of state, Phys. Dark Univ. 45 (2024) 101524, arXiv:2403.02000 [astro-ph.CO].

[3724] S. Ahmadi, E. Yusofi, M.A. Ramzanpour, Incorporating the cosmological constant in a modified uncertainty principle, Modern Phys. Lett. A 39 (27n28) (2024) 2450125, arXiv:2401.16126 [gr-qc].

[3725] A. Shahriar, M. Abbasiyan-Motlaq, M. Mohsenzadeh, E. Yusofi, Hubble expansion and entropy rates in a cosmological model with merging clusters and voids, 2024, arXiv:2412.05917 [astro-ph.CO].

[3726] R. van de Weygaert, E. Platen, Cosmic Voids: structure, dynamics and galaxies, Int. J. Mod. Phys. Conf. Ser. 01 (2011) 41–66, arXiv:0912.2997 [astro-ph.CO].

[3727] H.-Y. Wu, D. Huterer, Sample variance in the local measurements of the Hubble constant, Mon. Not. R. Astron. Soc. 471 (4) (2017) 4946–4955, arXiv:1706.09723 [astro-ph.CO].

[3728] D. Camarena, V. Marra, Impact of the cosmic variance on H_0 on cosmological analyses, Phys. Rev. D 98 (2) (2018) 023537, arXiv:1805.09900 [astro-ph.CO].

[3729] R.C. Keenan, A.J. Barger, L.L. Cowie, Evidence for a ∼300 megaparsec scale under-density in the local galaxy distribution, Astrophys. J. 775 (2013) 62, arXiv:1304.2884 [astro-ph.CO].

[3730] H. Böhringer, G. Chon, M. Bristow, C.A. Collins, The extended ROSAT-ESO Flux-Limited X-ray Galaxy Cluster Survey (REFLEX II): v. exploring a local underdensity in the southern sky, Astron. Astrophys. 574 (2015) A26, arXiv:1410.2172 [astro-ph.CO].

[3731] H. Böhringer, G. Chon, C.A. Collins, Observational evidence for a local underdensity in the Universe and its effect on the measurement of the Hubble Constant, Astron. Astrophys. 633 (2020) A19, arXiv:1907.12402 [astro-ph.CO].

[3732] S.J. Maddox, G. Efstathiou, W.J. Sutherland, J. Loveday, Galaxy correlations on large scales., Mon. Not. R. Astro. Soc. 242 (1990) 43.

[3733] T. Shanks, Galaxy count models and the extragalactic background light, in: S. Bowyer, C. Leinert (Eds.), The Galactic and Extragalactic Background Radiation, in: IAU Symposium, vol. 139, 1990, p. 269.

[3734] J.S. Huang, L.L. Cowie, J.P. Gardner, E.M. Hu, A. Songaila, R.J. Wainscoat, The hawaii k-band galaxy survey. 2. Bright k-band imaging, Astrophys. J. 476 (1997) 12, arXiv:astro-ph/9610084.

[3735] G.S. Busswell, T. Shanks, P.J. Outram, W.J. Frith, N. Metcalfe, R. Fong, The local hole in the galaxy distribution: New optical evidence, Mon. Not. R. Astron. Soc. 354 (2004) 991, arXiv:astro-ph/0302330.

[3736] W.J. Frith, G.S. Busswell, R. Fong, N. Metcalfe, T. Shanks, The local hole in the galaxy distribution: Evidence from 2MASS, Mon. Not. R. Astron. Soc. 345 (2003) 1049, arXiv:astro-ph/0302331.

[3737] W.J. Frith, T. Shanks, P.J. Outram, 2MASS constraints on the local large-scale structure: A Challenge to lambda-CDM? Mon. Not. R. Astron. Soc. 361 (2005) 701–709, arXiv:astro-ph/0411204.

[3738] W.J. Frith, N. Metcalfe, T. Shanks, New h-band galaxy number counts: a large local hole in the galaxy distribution? Mon. Not. R. Astron. Soc. 371 (2006) 1601–1609, arXiv:astro-ph/0509875.

[3739] J.R. Whitbourn, T. Shanks, The Local Hole revealed by galaxy counts and redshifts, Mon. Not. R. Astron. Soc. 437 (2014) 2146–2162, arXiv:1307.4405 [astro-ph.CO].

[3740] Extragalactic Astronomy Group, Durham University Collaboration, J.R. Whitbourn, T. Shanks, The galaxy luminosity function and the Local Hole, Mon. Not. R. Astron. Soc. 459 (1) (2016) 496–507, arXiv:1603.02322 [astro-ph.CO].

[3741] J.H.W. Wong, T. Shanks, N. Metcalfe, J.R. Whitbourn, The local hole: a galaxy underdensity covering 90 per cent of sky to ≈200 Mpc, Mon. Not. R. Astron. Soc. 511 (4) (2022) 5742–5755, arXiv:2107.08505 [astro-ph.CO].

[3742] M. Rubart, D. Bacon, D.J. Schwarz, Impact of local structure on the cosmic radio dipole, Astron. Astrophys. 565 (2014) A111, arXiv:1402.0376 [astro-ph.CO].

[3743] R.E. Angulo, V. Springel, S.D.M. White, A. Jenkins, C.M. Baugh, C.S. Frenk, Scaling relations for galaxy clusters in the Millennium-XXL simulation, Mon. Not. R. Astron. Soc. 426 (2012) 2046, arXiv:1203.3216 [astro-ph.CO].

[3744] M. Haslbauer, I. Banik, P. Kroupa, The KBC void and Hubble tension contradict ΛCDM on a Gpc scale – Milgromian dynamics as a possible solution, Mon. Not. R. Astron. Soc. 499 (2) (2020) 2845–2883, arXiv:2009.11292 [astro-ph.CO].

[3745] R.C. Keenan, A.J. Barger, L.L. Cowie, Local large-scale structure and the assumption of homogeneity, IAU Symp. 308 (2014) 295–298, arXiv:1409.8458 [astro-ph.CO].

[3746] T. Shanks, L. Hogarth, N. Metcalfe, Gaia Cepheid parallaxes and 'Local Hole' relieve H_0 tension, Mon. Not. R. Astron. Soc. 484 (1) (2019) L64–L68, arXiv:1810.02595 [astro-ph.CO].

[3747] T. Shanks, L.M. Hogarth, N. Metcalfe, J. Whitbourn, Local Hole revisited: evidence for bulk motions and self-consistent outflow, Mon. Not. R. Astron. Soc. 490 (4) (2019) 4715–4720, arXiv:1909.01878 [astro-ph.CO].

[3748] Q. Ding, T. Nakama, Y. Wang, A gigaparsec-scale local void and the Hubble tension, Sci. China Phys. Mech. Astron. 63 (9) (2020) 290403, arXiv:1912.12600 [astro-ph.CO].

[3749] M.S. Martín, C. Rubio, Hubble tension and matter inhomogeneities: A theoretical perspective, Ann. Phys. 458 (2023) 169444, arXiv:2107.14377 [astro-ph.CO].

[3750] N. Kaiser, Clustering in real space and in redshift space, Mon. Not. R. Astron. Soc. 227 (1987) 1–27.

[3751] S. Mazurenko, I. Banik, P. Kroupa, M. Haslbauer, A simultaneous solution to the Hubble tension and observed bulk flow within 250 h−1 Mpc, Mon. Not. R. Astron. Soc. 527 (3) (2024) 4388–4396, arXiv:2311.17988 [astro-ph.CO].

[3752] H. Alnes, M. Amarzguioui, CMB anisotropies seen by an off-center observer in a spherically symmetric inhomogeneous Universe, Phys. Rev. D 74 (2006) 103520, arXiv:astro-ph/0607334.

[3753] V. Nistane, G. Cusin, M. Kunz, CMB sky for an off-center observer in a local void. Part I. Framework for forecasts, J. Cosmol. Astropart. Phys. 12 (2019) 038, arXiv:1908.05484 [astro-ph.CO].

[3754] A. Cimatti, M. Moresco, Revisiting the oldest stars as cosmological probes: new constraints on the Hubble constant, Astrophys. J. 953 (2) (2023) 149, arXiv:2302.07899 [astro-ph.CO].

[3755] M. Xiang, H.-W. Rix, H. Yang, J. Liu, Y. Huang, N. Frankel, The formation and survival of the Milky Way's oldest stellar disk, Nat. Astron. 9 (1) (2025) 101–110, arXiv:2410.09705 [astro-ph.GA].

[3756] L. Perivolaropoulos, Hubble tension or distance ladder crisis? Phys. Rev. D 110 (12) (2024) 123518, arXiv:2408.11031 [astro-ph.CO].

[3757] C. Krishnan, E.O. Colgáin, Ruchika, A.A. Sen, M.M. Sheikh-Jabbari, T. Yang, Is there an early Universe solution to Hubble tension? Phys. Rev. D 102 (10) (2020) 103525, arXiv:2002.06044 [astro-ph.CO].

[3758] C. Krishnan, E.O. Colgáin, M.M. Sheikh-Jabbari, T. Yang, Running Hubble tension and a H0 diagnostic, Phys. Rev. D 103 (10) (2021) 103509, arXiv:2011.02858 [astro-ph.CO].

[3759] X.D. Jia, J.P. Hu, F.Y. Wang, Evidence of a decreasing trend for the Hubble constant, Astron. Astrophys. 674 (2023) A45, arXiv:2212.00238 [astro-ph.CO].

[3760] X.D. Jia, J.P. Hu, S.X. Yi, F.Y. Wang, Uncorrelated estimations of H_0 redshift evolution from DESI baryon acoustic oscillation observations, Astrophys. J. Lett. 979 (2) (2025) L34, arXiv:2406.02019 [astro-ph.CO].

[3761] S. Mazurenko, I. Banik, P. Kroupa, The redshift dependence of the inferred H_0 in a local void solution to the Hubble tension, Mon. Not. R. Astro. Soc. 536 (4) (2025) 3232–3241, arXiv:2412.12245 [astro-ph.CO].

[3762] I. Banik, V. Kalaitzidis, Testing the local void solution to the Hubble tension using baryon acoustic oscillation measurements over the last twenty years, 2025, arXiv:2501.17934 [astro-ph.CO].

[3763] K. Rezazadeh, A. Ashoorioon, D. Grin, Cascading dark energy, Astrophys. J. 975 (1) (2024) 137, arXiv:2208.07631 [astro-ph.CO].

[3764] M. Khanpour, E. Yusofi, B. Khanpour, Gravitational merging as a possible source for the cosmological accelerating, 2017, arXiv:1709.08612 [astro-ph.CO].

[3765] W.D. Kenworthy, D. Scolnic, A. Riess, The local perspective on the hubble tension: local structure does not impact measurement of the Hubble constant, Astrophys. J. 875 (2) (2019) 145, arXiv:1901.08681 [astro-ph.CO].

[3766] M.M. Phillips, The absolute magnitudes of Type IA supernovae, Astrophys. J. Lett. 413 (1993) L105–L108.

[3767] A. Friedman, On the Curvature of space, Z. Phys. 10 (1922) 377–386.

[3768] A. Friedmann, Über die Möglichkeit einer Welt mit konstanter negativer Krümmung des Raumes, Zeitschrift Phys. 21 (1) (1924) 326–332.

[3769] M.C. March, R. Trotta, P. Berkes, G.D. Starkman, P.M. Vaudrevange, Improved constraints on cosmological parameters from SNIa data, Mon. Not. R. Astron. Soc. 418 (2011) 2308–2329, arXiv:1102.3237 [astro-ph.CO].

[3770] SDSS Collaboration, J. Marriner, J.P. Bernstein, R. Kessler, H. Lampeitl, R. Miquel, J. Mosher, R.C. Nichol, M. Sako, M. Smith, A more general model for the intrinsic scatter in Type Ia Supernova distance moduli, Astrophys. J. 740 (2011) 72, arXiv:1107.4631 [astro-ph.CO].

[3771] R. Kessler, D. Scolnic, Correcting Type Ia Supernova distances for selection biases and contamination in photometrically identified samples, Astrophys. J. 836 (1) (2017) 56, arXiv:1610.04677 [astro-ph.CO].

[3772] S. Castello, M. Högås, E. Mörtsell, A cosmological underdensity does not solve the Hubble tension, J. Cosmol. Astropart. Phys. 07 (2022) 003, arXiv:2110.04226 [astro-ph.CO]; J. Cosmol. Astropart. Phys. 09 (2022) E01, Erratum.

[3773] D. Camarena, V. Marra, Z. Sakr, C. Clarkson, The Copernican principle in light of the latest cosmological data, Mon. Not. R. Astron. Soc. 509 (1) (2021) 1291–1302, arXiv:2107.02296 [astro-ph.CO].

[3774] D. Camarena, V. Marra, Z. Sakr, C. Clarkson, A void in the Hubble tension? The end of the line for the Hubble bubble, Cl. Quant. Grav. 39 (18) (2022) 184001, arXiv:2205.05422 [astro-ph.CO].

[3775] Z.G. Lane, A. Seifert, R. Ridden-Harper, D.L. Wiltshire, Cosmological foundations revisited with Pantheon+, Mon. Not. R. Astron. Soc. 536 (2) (2025) 1752–1777, arXiv:2311.01438 [astro-ph.CO].

[3776] A. Seifert, Z.G. Lane, M. Galoppo, R. Ridden-Harper, D.L. Wiltshire, Supernovae evidence for foundational change to cosmological models, Mon. Not. R. Astron. Soc. 537 (1) (2025) L55–L60, arXiv:2412.15143 [astro-ph.CO].

[3777] DES Collaboration, P. Wiseman, et al., Rates and delay times of Type Ia supernovae in the Dark Energy Survey, Mon. Not. R. Astron. Soc. 506 (3) (2021) 3330–3348, arXiv:2105.11954 [astro-ph.GA].

[3778] N. Nicolas, M. Rigault, Y. Copin, R. Graziani, G. Aldering, M. Briday, Y.L. Kim, J. Nordin, S. Perlmutter, M. Smith, Redshift evolution of the underlying Type Ia supernova stretch distribution, Astron. Astrophys. 649 (2021) A74, arXiv:2005.09441 [astro-ph.CO].

[3779] P. Wiseman, M. Sullivan, M. Smith, B. Popovic, Further evidence that galaxy age drives observed Type Ia supernova luminosity differences, Mon. Not. R. Astron. Soc. 520 (4) (2023) 6214–6222, arXiv:2302.05341 [astro-ph.GA].

[3780] R.E. Keeley, A. Shafieloo, B. L'Huillier, An analysis of variance of the pantheon+ dataset: Systematics in the covariance matrix? Universe 10 (12) (2024) 439, arXiv:2212.07917 [astro-ph.CO].

[3781] K.S. Mandel, D. Scolnic, H. Shariff, R.J. Foley, R.P. Kirshner, The Type Ia supernova color–magnitude relation and host galaxy dust: A simple hierarchical bayesian model, Astrophys. J. 842 (2) (2017) 93, arXiv:1609.04470 [astro-ph.CO].

[3782] V.V. Luković, B.S. Haridasu, N. Vittorio, Exploring the evidence for a large local void with supernovae Ia data, Mon. Not. R. Astron. Soc. 491 (2) (2020) 2075–2087, arXiv:1907.11219 [astro-ph.CO].
[3783] E. Asencio, I. Banik, P. Kroupa, A massive blow for ΛCDM – the high redshift, mass, and collision velocity of the interacting galaxy cluster El Gordo contradicts concordance cosmology, Mon. Not. R. Astron. Soc. 500 (4) (2020) 5249–5267, arXiv:2012.03950 [astro-ph.CO].
[3784] E. Asencio, I. Banik, P. Kroupa, The El Gordo galaxy cluster challenges ΛCDM for any plausible collision velocity, Astrophys. J. 954 (2) (2023) 162, arXiv:2308.00744 [astro-ph.CO].
[3785] J.P. Hu, X.D. Jia, J. Hu, F.Y. Wang, Hints of new physics for the Hubble tension: Violation of cosmological principle, Astrophys. J. Lett. 975 (2) (2024) L36, arXiv:2410.06450 [astro-ph.CO].
[3786] A. Sah, M. Rameez, S. Sarkar, C. Tsagas, Anisotropy in Pantheon+ supernovae, 2024, arXiv:2411.10838 [astro-ph.CO].
[3787] R. Durrer, A. Neronov, Cosmological magnetic fields: Their generation, evolution and observation, Astron. Astrophys. Rev. 21 (2013) 62, arXiv:1303.7121 [astro-ph.CO].
[3788] K. Subramanian, The origin, evolution and signatures of primordial magnetic fields, Rep. Progr. Phys. 79 (7) (2016) 076901, arXiv:1504.02311 [astro-ph.CO].
[3789] T. Vachaspati, Progress on cosmological magnetic fields, Rep. Progr. Phys. 84 (7) (2021) 074901, arXiv:2010.10525 [astro-ph.CO].
[3790] A. Elyiv, A. Neronov, D.V. Semikoz, Gamma-ray induced cascades and magnetic fields in intergalactic medium, Phys. Rev. D 80 (2009) 023010, arXiv:0903.3649 [astro-ph.CO].
[3791] A. Neronov, I. Vovk, Evidence for strong extragalactic magnetic fields from Fermi observations of TeV blazars, Science 328 (2010) 73–75, arXiv:1006.3504 [astro-ph.HE].
[3792] F. Tavecchio, G. Ghisellini, L. Foschini, G. Bonnoli, G. Ghirlanda, P. Coppi, The intergalactic magnetic field constrained by Fermi/LAT observations of the TeV blazar 1ES 0229+200, Mon. Not. R. Astron. Soc. 406 (2010) L70–L74, arXiv:1004.1329 [astro-ph.CO].
[3793] F. Tavecchio, G. Ghisellini, G. Bonnoli, L. Foschini, Extreme TeV blazars and the intergalactic magnetic field, Mon. Not. R. Astron. Soc. 414 (2011) 3566, arXiv:1009.1048 [astro-ph.HE].
[3794] A.M. Taylor, I. Vovk, A. Neronov, Extragalactic magnetic fields constraints from simultaneous GeV-TeV observations of blazars, Astron. Astrophys. 529 (2011) A144, arXiv:1101.0932 [astro-ph.HE].
[3795] I. Vovk, A.M. Taylor, D. Semikoz, A. Neronov, Fermi/LAT observations of 1ES 0229+200: implications for extragalactic magnetic fields and background light, Astrophys. J. Lett. 747 (2012) L14, arXiv:1112.2534 [astro-ph.CO].
[3796] K. Dolag, M. Kachelriess, S. Ostapchenko, R. Tomas, Lower limit on the strength and filling factor of extragalactic magnetic fields, Astrophys. J. Lett. 727 (2011) L4, arXiv:1009.1782 [astro-ph.HE].
[3797] K. Subramanian, J.D. Barrow, Microwave background signals from tangled magnetic fields, Phys. Rev. Lett. 81 (1998) 3575–3578, arXiv:astro-ph/9803261.
[3798] K. Jedamzik, V. Katalinic, A.V. Olinto, A Limit on primordial small scale magnetic fields from CMB distortions, Phys. Rev. Lett. 85 (2000) 700–703, arXiv:astro-ph/9911100.
[3799] R. Durrer, P.G. Ferreira, T. Kahniashvili, Tensor microwave anisotropies from a stochastic magnetic field, Phys. Rev. D 61 (2000) 043001, arXiv:astro-ph/9911040.
[3800] T.R. Seshadri, K. Subramanian, CMBR polarization signals from tangled magnetic fields, Phys. Rev. Lett. 87 (2001) 101301, arXiv:astro-ph/0012056.
[3801] A. Mack, T. Kahniashvili, A. Kosowsky, Microwave background signatures of a primordial stochastic magnetic field, Phys. Rev. D 65 (2002) 123004, arXiv:astro-ph/0105504.
[3802] K. Subramanian, J.D. Barrow, Small-scale microwave background anisotropies due to tangled primordial magnetic fields, Mon. Not. R. Astron. Soc. 335 (2002) L57, arXiv:astro-ph/0205312.
[3803] K. Subramanian, T.R. Seshadri, J.D. Barrow, Small - scale CMB polarization anisotropies due to tangled primordial magnetic fields, Mon. Not. R. Astron. Soc. 344 (2003) L31, arXiv:astro-ph/0303014.
[3804] S. Mollerach, D. Harari, S. Matarrese, CMB polarization from secondary vector and tensor modes, Phys. Rev. D 69 (2004) 063002, arXiv:astro-ph/0310711.
[3805] A. Lewis, Observable primordial vector modes, Phys. Rev. D 70 (2004) 043518, arXiv:astro-ph/0403583.
[3806] C. Scoccola, D. Harari, S. Mollerach, B polarization of the CMB from Faraday rotation, Phys. Rev. D 70 (2004) 063003, arXiv:astro-ph/0405396.
[3807] K. Sethi, Primordial magnetic fields in the post-recombination era and early reionization, Mon. Not. R. Astron. Soc. 356 (2005) 778–788, arXiv:astro-ph/0405413.
[3808] A. Kosowsky, T. Kahniashvili, G. Lavrelashvili, B. Ratra, Faraday rotation of the Cosmic Microwave Background polarization by a stochastic magnetic field, Phys. Rev. D 71 (2005) 043006, arXiv:astro-ph/0409767.
[3809] T. Kahniashvili, B. Ratra, Effects of cosmological magnetic helicity on the cosmic microwave background, Phys. Rev. D 71 (2005) 103006, arXiv:astro-ph/0503709.
[3810] I. Brown, R. Crittenden, Non-Gaussianity from cosmic magnetic fields, Phys. Rev. D 72 (2005) 063002, arXiv:astro-ph/0506570.
[3811] A. Zizzo, C. Burigana, On the effect of cyclotron emission on the spectral distortions of the cosmic microwave background, New Astron. 11 (2005) 1–16, arXiv:astro-ph/0505259.
[3812] G. Chen, P. Mukherjee, T. Kahniashvili, B. Ratra, Y. Wang, Looking for cosmological Alfven waves in WMAP data, Astrophys. J. 611 (2004) 655–659, arXiv:astro-ph/0403695.
[3813] A. Lewis, CMB anisotropies from primordial inhomogeneous magnetic fields, Phys. Rev. D 70 (2004) 043011, arXiv:astro-ph/0406096.
[3814] H. Tashiro, N. Sugiyama, R. Banerjee, Nonlinear evolution of cosmic magnetic fields and cosmic microwave background anisotropies, Phys. Rev. D 73 (2006) 023002, arXiv:astro-ph/0509220.
[3815] D. Yamazaki, K. Ichiki, T. Kajino, G.J. Mathews, Constraints on the evolution of the primordial magnetic field from the small scale cmb angular anisotropy, Astrophys. J. 646 (2006) 719–729, arXiv:astro-ph/0602224.
[3816] T. Kahniashvili, B. Ratra, CMB anisotropies due to cosmological magnetosonic waves, Phys. Rev. D 75 (2007) 023002, arXiv:astro-ph/0611247.
[3817] M. Giovannini, K.E. Kunze, Magnetized CMB observables: A Dedicated numerical approach, Phys. Rev. D 77 (2008) 063003, arXiv:0712.3483 [astro-ph].
[3818] T.R. Seshadri, K. Subramanian, CMB bispectrum from primordial magnetic fields on large angular scales, Phys. Rev. Lett. 103 (2009) 081303, arXiv:0902.4066 [astro-ph.CO].
[3819] C. Caprini, F. Finelli, D. Paoletti, A. Riotto, The cosmic microwave background temperature bispectrum from scalar perturbations induced by primordial magnetic fields, J. Cosmol. Astropart. Phys. 06 (2009) 021, arXiv:0903.1420 [astro-ph.CO].
[3820] R.-G. Cai, B. Hu, H.-B. Zhang, Acoustic signatures in the Cosmic Microwave Background bispectrum from primordial magnetic fields, J. Cosmol. Astropart. Phys. 08 (2010) 025, arXiv:1006.2985 [astro-ph.CO].
[3821] P. Trivedi, K. Subramanian, T.R. Seshadri, Primordial magnetic field limits from cosmic microwave background bispectrum of magnetic passive scalar modes, Phys. Rev. D 82 (2010) 123006, arXiv:1009.2724 [astro-ph.CO].
[3822] I.A. Brown, Intrinsic bispectra of cosmic magnetic fields, Astrophys. J. 733 (2011) 83, arXiv:1012.2892 [astro-ph.CO].
[3823] M. Shiraishi, D. Nitta, S. Yokoyama, K. Ichiki, K. Takahashi, Cosmic microwave background bispectrum of vector modes induced from primordial magnetic fields, Phys. Rev. D 82 (2010) 121302, arXiv:1009.3632 [astro-ph.CO]; Phys. Rev. D 83 (2011) 029901, Erratum.
[3824] M. Shiraishi, D. Nitta, S. Yokoyama, K. Ichiki, K. Takahashi, Cosmic microwave background bispectrum of tensor passive modes induced from primordial magnetic fields, Phys. Rev. D 83 (2011) 123003, arXiv:1103.4103 [astro-ph.CO].
[3825] P. Trivedi, T.R. Seshadri, K. Subramanian, Cosmic microwave background trispectrum and primordial magnetic field limits, Phys. Rev. Lett. 108 (2012) 231301, arXiv:1111.0744 [astro-ph.CO].
[3826] D.G. Yamazaki, K. Ichiki, T. Kajino, G.J. Mathews, New constraints on the primordial magnetic field, Phys. Rev. D 81 (2010) 023008, arXiv:1001.2012 [astro-ph.CO].
[3827] D. Paoletti, F. Finelli, CMB constraints on a stochastic background of primordial magnetic fields, Phys. Rev. D 83 (2011) 123533, arXiv:1005.0148 [astro-ph.CO].
[3828] J.R. Shaw, A. Lewis, Constraining primordial magnetism, Phys. Rev. D 86 (2012) 043510, arXiv:1006.4242 [astro-ph.CO].
[3829] K.E. Kunze, CMB anisotropies in the presence of a stochastic magnetic field, Phys. Rev. D 83 (2011) 023006, arXiv:1007.3163 [astro-ph.CO].
[3830] L. Pogosian, T. Vachaspati, A. Yadav, Primordial magnetism in CMB B-modes, Can. J. Phys. 91 (2013) 451–454, arXiv:1210.0308 [astro-ph.CO].
[3831] D. Paoletti, F. Finelli, Constraints on a stochastic background of primordial magnetic fields with WMAP and south pole telescope data, Phys. Lett. B 726 (2013) 45–49, arXiv:1208.2625 [astro-ph.CO].
[3832] K.E. Kunze, E. Komatsu, Constraining primordial magnetic fields with distortions of the black-body spectrum of the cosmic microwave background: pre- and post-decoupling contributions, J. Cosmol. Astropart. Phys. 01 (2014) 009, arXiv:1309.7994 [astro-ph.CO].
[3833] M. Shiraishi, T. Sekiguchi, First observational constraints on tensor non-Gaussianity sourced by primordial magnetic fields from cosmic microwave background, Phys. Rev. D 90 (10) (2014) 103002, arXiv:1304.7277 [astro-ph.CO].
[3834] P. Trivedi, K. Subramanian, T.R. Seshadri, Primordial magnetic field limits from the CMB trispectrum: Scalar modes and Planck constraints, Phys. Rev. D 89 (4) (2014) 043523, arXiv:1312.5308 [astro-ph.CO].
[3835] M. Ballardini, F. Finelli, D. Paoletti, CMB anisotropies generated by a stochastic background of primordial magnetic fields with non-zero helicity, J. Cosmol. Astropart. Phys. 10 (2015) 031, arXiv:1412.1836 [astro-ph.CO].
[3836] T. Kahniashvili, Y. Maravin, G. Lavrelashvili, A. Kosowsky, Primordial magnetic helicity constraints from WMAP nine-year data, Phys. Rev. D 90 (8) (2014) 083004, arXiv:1408.0351 [astro-ph.CO].

[3837] K.E. Kunze, E. Komatsu, Constraints on primordial magnetic fields from the optical depth of the cosmic microwave background, J. Cosmol. Astropart. Phys. 06 (2015) 027, arXiv:1501.00142 [astro-ph.CO].

[3838] Planck Collaboration, P.A.R. Ade, et al., Planck 2015 results. XIX. Constraints on primordial magnetic fields, Astron. Astrophys. 594 (2016) A19, arXiv:1502.01594 [astro-ph.CO].

[3839] J. Ganc, M.S. Sloth, Probing correlations of early magnetic fields using mu-distortion, J. Cosmol. Astropart. Phys. 08 (2014) 018, arXiv:1404.5957 [astro-ph.CO].

[3840] J. Chluba, D. Paoletti, F. Finelli, J.-A. Rubiño Martín, Effect of primordial magnetic fields on the ionization history, Mon. Not. R. Astron. Soc. 451 (2) (2015) 2244–2250, arXiv:1503.04827 [astro-ph.CO].

[3841] A. Zucca, Y. Li, L. Pogosian, Constraints on Primordial Magnetic Fields from Planck combined with the South Pole Telescope CMB B-mode polarization measurements, Phys. Rev. D 95 (6) (2017) 063506, arXiv:1611.00757 [astro-ph.CO].

[3842] D.R. Sutton, C. Feng, C.L. Reichardt, Current and future constraints on primordial magnetic fields, Astrophys. J. 846 (2) (2017) 164, arXiv:1702.01871 [astro-ph.CO].

[3843] T. Minoda, K. Ichiki, H. Tashiro, Small-scale CMB anisotropies induced by the primordial magnetic fields, J. Cosmol. Astropart. Phys. 03 (2021) 093, arXiv:2012.12542 [astro-ph.CO].

[3844] R. Banerjee, K. Jedamzik, Are cluster magnetic fields primordial?, Phys. Rev. Lett. 91 (2003) 251301, arXiv:astro-ph/0306211; Phys. Rev. Lett. 93 (2004) 179901, Erratum;

[3845] K. Jedamzik, T. Abel, Weak primordial magnetic fields and anisotropies in the cosmic microwave background radiation 2011, arXiv:1108.2517 [astro-ph.CO].

[3846] K. Jedamzik, T. Abel, Small-scale primordial magnetic fields and anisotropies in the cosmic microwave background radiation J. Cosmol. Astropart. Phys. 10 (2013) 050.

[3847] K. Jedamzik, A. Saveliev, Stringent limit on primordial magnetic fields from the cosmic microwave background radiation Phys. Rev. Lett. 123 (2) (2019) 021301, arXiv:1804.06115 [astro-ph.CO].

[3848] K. Jedamzik, L. Pogosian, Relieving the Hubble tension with primordial magnetic fields Phys. Rev. Lett. 125 (18) (2020) 181302, arXiv:2004.09487 [astro-ph.CO].

[3849] L. Thiele, Y. Guan, J.C. Hill, A. Kosowsky, D.N. Spergel, Can small-scale baryon inhomogeneities resolve the Hubble tension? An investigation with ACT DR4 Phys. Rev. D 104 (6) (2021) 063535, arXiv:2105.03003 [astro-ph.CO].

[3850] M. Rashkovetskyi, J.B. Muñoz, D.J. Eisenstein, C. Dvorkin, Small-scale clumping at recombination and the Hubble tension Phys. Rev. D 104 (10) (2021) 103517, arXiv:2108.02747 [astro-ph.CO].

[3851] S. Galli, L. Pogosian, K. Jedamzik, L. Balkenhol, Consistency of Planck, ACT, and SPT constraints on magnetically assisted recombination and forecasts for future experiments Phys. Rev. D 105 (2) (2022) 023513, arXiv:2109.03816 [astro-ph.CO].

[3852] K. Jedamzik, T. Abel, Y. Ali-Haimoud, Cosmic recombination in the presence of primordial magnetic fields J. Cosmol. Astropart. Phys. 03 (2025) 012, arXiv:2312.11448 [astro-ph.CO].

[3853] A. Korochkin, O. Kalashev, A. Neronov, D. Semikoz, Sensitivity reach of gamma-ray measurements for strong cosmological magnetic fields Astrophys. J. 906 (2) (2021) 116, arXiv:2007.14331 [astro-ph.CO].

[3854] A.H. Guth, The inflationary universe: A possible solution to the horizon and flatness problems Phys. Rev. D 23 (1981) 347–356.

[3855] A.R. Liddle, D.H. Lyth, The end for extended inflation? Ann. N. Y. Acad. Sci. 688 (1993) 653, arXiv:astro-ph/9302010.

[3856] A.D. Linde, Fast roll inflation JHEP 11 (2001) 052, arXiv:hep-th/0110195.

[3857] H. Motohashi, A.A. Starobinsky, J. Yokoyama, Inflation with a constant rate of roll J. Cosmol. Astropart. Phys. 09 (2015) 018, arXiv:1411.5021 [astro-ph.CO].

[3858] M. Guerrero, D. Rubiera-Garcia, D. Saez-Chillon Gomez, Constant roll inflation in multifield models Phys. Rev. D 102 (2020) 123528, arXiv:2008.07260 [gr-qc].

[3859] T. Bjorkmo, R.Z. Ferreira, M.C.D. Marsh, Mild non-gaussianities under perturbative control from rapid-turn inflation models J. Cosmol. Astropart. Phys. 12 (2019) 036, arXiv:1908.11316 [hep-th].

[3860] L. Anguelova, C.I. Lazaroiu, Dynamical consistency conditions for rapid turn inflation J. Cosmol. Astropart. Phys. 05 (2023) 020, arXiv:2210.00031 [hep-th].

[3861] C. Gomes, J.G. Rosa, O. Bertolami, Inflation in non-minimal matter-curvature coupling theories J. Cosmol. Astropart. Phys. 06 (2017) 021, arXiv:1611.02124 [gr-qc].

[3862] İ.İ. Çimdiker, Starobinsky inflation in emergent gravity Phys. Dark Univ. 30 (2020) 100736.

[3863] N. Bostan, C. Karahan, O. Sargın, Inflation in symmergent metric-palatini gravity J. Cosmol. Astropart. Phys. 02 (2024) 028, arXiv:2308.04507 [astro-ph.CO].

[3864] A. Maleknejad, M.M. Sheikh-Jabbari, Non-Abelian gauge field inflation Phys. Rev. D 84 (2011) 043515, arXiv:1102.1932 [hep-ph].

[3865] P. Adshead, M. Wyman, Chromo-Natural Inflation: Natural inflation on a steep potential with classical non-Abelian gauge fields Phys. Rev. Lett. 108 (2012) 261302, arXiv:1202.2366 [hep-th].

[3866] W.D. Garretson, G.B. Field, S.M. Carroll, Primordial magnetic fields from pseudoGoldstone bosons Phys. Rev. D 46 (1992) 5346–5351, arXiv:hep-ph/9209238.

[3867] M.M. Anber, L. Sorbo, N-flationary magnetic fields J. Cosmol. Astropart. Phys. 10 (2006) 018, arXiv:astro-ph/0606534.

[3868] N. Barnaby, M. Peloso, Large nongaussianity in axion inflation Phys. Rev. Lett. 106 (2011) 181301, arXiv:1011.1500 [hep-ph].

[3869] J.L. Cook, L. Sorbo, Particle production during inflation and gravitational waves detectable by ground-based interferometers Phys. Rev. D 85 (2012) 023534, arXiv:1109.0022 [astro-ph.CO]; Phys. Rev. D 86 (2012) 069901, Erratum.

[3870] L. Sorbo, Parity violation in the Cosmic Microwave Background from a pseudoscalar inflaton J. Cosmol. Astropart. Phys. 06 (2011) 003, arXiv:1101.1525 [astro-ph.CO].

[3871] M.M. Anber, L. Sorbo, Non-gaussianities and chiral gravitational waves in natural steep inflation Phys. Rev. D 85 (2012) 123537, arXiv:1203.5849 [astro-ph.CO].

[3872] E. Dimastrogiovanni, M. Peloso, Stability analysis of chromo-natural inflation and possible evasion of Lyth's bound Phys. Rev. D 87 (10) (2013) 103501, arXiv:1212.5184 [astro-ph.CO].

[3873] P. Adshead, E. Martinec, E.I. Sfakianakis, M. Wyman, Higgsed chromo-natural inflation JHEP 12 (2016) 137, arXiv:1609.04025 [hep-th].

[3874] E. Dimastrogiovanni, M. Fasiello, T. Fujita, Primordial gravitational waves from axion-gauge fields dynamics J. Cosmol. Astropart. Phys. 01 (2017) 019, arXiv:1608.04216 [astro-ph.CO].

[3875] A. Agrawal, T. Fujita, E. Komatsu, Large tensor non-gaussianity from axion-gauge field dynamics Phys. Rev. D 97 (10) (2018) 103526, arXiv:1707.03023 [astro-ph.CO].

[3876] R.R. Caldwell, C. Devulder, Axion gauge field inflation and gravitational leptogenesis: A lower bound on B modes from the matter-antimatter asymmetry of the universe Phys. Rev. D 97 (2) (2018) 023532, arXiv:1706.03765 [astro-ph.CO].

[3877] B. Thorne, T. Fujita, M. Hazumi, N. Katayama, E. Komatsu, M. Shiraishi, Finding the chiral gravitational wave background of an axion-SU(2) inflationary model using CMB observations and laser interferometers Phys. Rev. D 97 (4) (2018) 043506, arXiv:1707.03240 [astro-ph.CO].

[3878] E. Dimastrogiovanni, M. Fasiello, R.J. Hardwick, H. Assadullahi, K. Koyama, D. Wands, Non-gaussianity from axion-gauge fields interactions during inflation J. Cosmol. Astropart. Phys. 11 (2018) 029, arXiv:1806.05474 [astro-ph.CO].

[3879] T. Fujita, R. Namba, I. Obata, Mixed non-gaussianity from axion-gauge field dynamics J. Cosmol. Astropart. Phys. 04 (2019) 044, arXiv:1811.12371 [astro-ph.CO].

[3880] V. Domcke, B. Mares, F. Muia, M. Pieroni, Emerging chromo-natural inflation J. Cosmol. Astropart. Phys. 04 (2019) 034, arXiv:1807.03358 [hep-ph].

[3881] K.D. Lozanov, A. Maleknejad, E. Komatsu, Schwinger effect by an $SU(2)$ gauge field during inflation JHEP 02 (2019) 041, arXiv:1805.09318 [hep-th].

[3882] Y. Watanabe, E. Komatsu, Gravitational wave from Axion-SU(2) gauge fields: Effective field theory for kinetically driven inflation 2020, arXiv:2004.04350 [hep-th].

[3883] J. Holland, I. Zavala, G. Tasinato, On chromonatural inflation in string theory J. Cosmol. Astropart. Phys. 12 (2020) 026, arXiv:2009.00653 [hep-th].

[3884] V. Domcke, V. Guidetti, Y. Welling, A. Westphal, Resonant backreaction in axion inflation J. Cosmol. Astropart. Phys. 09 (2020) 009, arXiv:2002.02952 [astro-ph.CO].

[3885] O. Iarygina, E.I. Sfakianakis, R. Sharma, A. Brandenburg, Backreaction of axion-SU(2) dynamics during inflation J. Cosmol. Astropart. Phys. 04 (2024) 018, arXiv:2311.07557 [astro-ph.CO].

[3886] K. Ishiwata, E. Komatsu, I. Obata, Axion-gauge field dynamics with backreaction J. Cosmol. Astropart. Phys. 03 (03) (2022) 010, arXiv:2111.14429 [hep-ph].

[3887] R. Durrer, R. von Eckardstein, D. Garg, K. Schmitz, O. Sobol, S. Vilchinskii, Scalar perturbations from inflation in the presence of gauge fields Phys. Rev. D 110 (4) (2024) 043533, arXiv:2404.19694 [astro-ph.CO].

[3888] E. Dimastrogiovanni, M. Fasiello, A. Papageorgiou, Novel primordial black hole production mechanism from non-Abelian gauge fields during inflation Phys. Rev. D 110 (10) (2024) 103542, arXiv:2403.13581 [astro-ph.CO].

[3889] E. Gaztañaga, K.S. Kumar, Finding origins of CMB anomalies in the inflationary quantum fluctuations J. Cosmol. Astropart. Phys. 06 (2024) 001, arXiv:2401.08288 [astro-ph.CO].

[3890] L.A. Anchordoqui, V. Barger, H. Goldberg, X. Huang, D. Marfatia, S-dual Inflation: BICEP2 data without unlikeliness Phys. Lett. B 734 (2014) 134–136, arXiv:1403.4578 [hep-ph].

[3891] L.A. Anchordoqui, I. Antoniadis, D. Lüst, J.F. Soriano, S-dual inflation and the string swampland Phys. Rev. D 103 (12) (2021) 123537, arXiv:2103.07982 [hep-th].

[3892] A. Övgün, Inflation and acceleration of the universe by nonlinear magnetic monopole fields Eur. Phys. J. C 77 (2) (2017) 105, arXiv:1604.01837 [gr-qc].

[3893] H.B. Benaoum, G. Leon, A. Ovgun, H. Quevedo, Inflation driven by non-linear electrodynamics Eur. Phys. J. C 83 (5) (2023) 367, arXiv:2206.13157 [gr-qc].

[3894] G. Otalora, A. Övgün, J. Saavedra, N. Videla, Inflation from a nonlinear magnetic monopole field nonminimally coupled to curvature J. Cosmol. Astropart. Phys. 06 (2018) 003, arXiv:1803.11358 [gr-qc].
[3895] A. Övgün, G. Leon, J. Magaña, K. Jusufi, Falsifying cosmological models based on a non-linear electrodynamics Eur. Phys. J. C 78 (6) (2018) 462, arXiv:1709.09794 [gr-qc].
[3896] S.I. Kruglov, Universe acceleration and nonlinear electrodynamics Phys. Rev. D 92 (12) (2015) 123523, arXiv:1601.06309 [gr-qc].
[3897] V.A. De Lorenci, R. Klippert, M. Novello, J.M. Salim, Nonlinear electrodynamics and FRW cosmology Phys. Rev. D 65 (2002) 063501.
[3898] M. Novello, S.E. Perez Bergliaffa, J. Salim, Non-linear electrodynamics and the acceleration of the universe Phys. Rev. D 69 (2004) 127301, arXiv:astro-ph/0312093.
[3899] M. Novello, E. Goulart, J.M. Salim, S.E. Perez Bergliaffa, Cosmological effects of nonlinear electrodynamics Cl. Quant. Grav. 24 (2007) 3021–3036, arXiv:gr-qc/0610043.
[3900] D.N. Vollick, Homogeneous and isotropic cosmologies with nonlinear electromagnetic radiation Phys. Rev. D 78 (2008) 063524, arXiv:0807.0448 [gr-qc].
[3901] M. LoVerde, A. Miller, S. Shandera, L. Verde, Effects of scale-dependent non-Gaussianity on cosmological structures J. Cosmol. Astropart. Phys. 04 (2008) 014, arXiv:0711.4126 [astro-ph].
[3902] C. Stahl, B. Famaey, R. Ibata, O. Hahn, N. Martinet, T. Montandon, Scale-dependent local primordial non-Gaussianity as a solution to the S8 tension Phys. Rev. D 110 (6) (2024) 063501, arXiv:2404.03244 [astro-ph.CO].
[3903] F.L. Bezrukov, M. Shaposhnikov, The Standard Model Higgs boson as the inflaton Phys. Lett. B 659 (2008) 703–706, arXiv:0710.3755 [hep-th].
[3904] J. Rubio, Higgs inflation Front. Astron. Space Sci. 5 (2019) 50, arXiv:1807.02376 [hep-ph].
[3905] F. Bezrukov, D. Gorbunov, M. Shaposhnikov, On initial conditions for the Hot Big Bang J. Cosmol. Astropart. Phys. 06 (2009) 029, arXiv:0812.3622 [hep-ph].
[3906] J. Garcia-Bellido, D.G. Figueroa, J. Rubio, Preheating in the Standard Model with the Higgs-Inflaton coupled to gravity Phys. Rev. D 79 (2009) 063531, arXiv:0812.4624 [hep-ph].
[3907] J. Repond, J. Rubio, Combined Preheating on the lattice with applications to Higgs inflation J. Cosmol. Astropart. Phys. 07 (2016) 043, arXiv:1604.08238 [astro-ph.CO].
[3908] F. Bezrukov, J. Rubio, M. Shaposhnikov, Living beyond the edge: Higgs inflation and vacuum metastability Phys. Rev. D 92 (8) (2015) 083512, arXiv:1412.3811 [hep-ph].
[3909] F. Bezrukov, M. Pauly, J. Rubio, On the robustness of the primordial power spectrum in renormalized Higgs inflation J. Cosmol. Astropart. Phys. 02 (2018) 040, arXiv:1706.05007 [hep-ph].
[3910] J.G. Rodrigues, M. Benetti, J.S. Alcaniz, Possible discrepancies between cosmological and electroweak observables in Higgs Inflation JHEP 11 (2021) 091, arXiv:2105.07009 [hep-ph].
[3911] J.G. Rodrigues, M. Benetti, R. de Souza, J. Alcaniz, Higgs inflation: Constraining the top quark mass and breaking the H0-σ8 correlation Phys. Lett. B 852 (2024) 138607, arXiv:2301.11788 [astro-ph.CO].
[3912] M. Shaposhnikov, D. Zenhausern, Scale invariance, unimodular gravity and dark energy Phys. Lett. B 671 (2009) 187–192, arXiv:0809.3395 [hep-th].
[3913] J. Garcia-Bellido, J. Rubio, M. Shaposhnikov, D. Zenhausern, Higgs-dilaton cosmology: From the early to the late universe Phys. Rev. D 84 (2011) 123504, arXiv:1107.2163 [hep-ph].
[3914] C. Germani, A. Kehagias, New model of inflation with non-minimal derivative coupling of standard model Higgs Boson to gravity Phys. Rev. Lett. 105 (2010) 011302, arXiv:1003.2635 [hep-ph].
[3915] F. Bauer, D.A. Demir, Higgs–Palatini inflation and unitarity Phys. Lett. B 698 (2011) 425–429, arXiv:1012.2900 [hep-ph].
[3916] S. Rasanen, Higgs inflation in the Palatini formulation with kinetic terms for the metric Open J. Astrophys. 2 (1) (2019) 1, arXiv:1811.09514 [gr-qc].
[3917] J. Rubio, E.S. Tomberg, Preheating in Palatini Higgs inflation J. Cosmol. Astropart. Phys. 04 (2019) 021, arXiv:1902.10148 [hep-ph].
[3918] M. Shaposhnikov, A. Shkerin, I. Timiryasov, S. Zell, Higgs inflation in Einstein–Cartan gravity J. Cosmol. Astropart. Phys. 02 (2021) 008, arXiv:2007.14978 [hep-ph]; J. Cosmol. Astropart. Phys. 10 (2021) E01, Erratum.
[3919] M. Piani, J. Rubio, Higgs–Dilaton inflation in Einstein–Cartan gravity J. Cosmol. Astropart. Phys. 05 (05) (2022) 009, arXiv:2202.04665 [gr-qc].
[3920] S. Casas, M. Pauly, J. Rubio, Higgs-dilaton cosmology: An inflation–dark-energy connection and forecasts for future galaxy surveys Phys. Rev. D 97 (4) (2018) 043520, arXiv:1712.04956 [astro-ph.CO].
[3921] M. Trashorras, S. Nesseris, J. Garcia-Bellido, Cosmological Constraints on Higgs–Dilaton Inflation Phys. Rev. D 94 (6) (2016) 063511, arXiv:1604.06760 [astro-ph.CO].
[3922] S. Casas, G.K. Karananas, M. Pauly, J. Rubio, Scale-invariant alternatives to general relativity. III. The inflation-dark energy connection Phys. Rev. D 99 (6) (2019) 063512, arXiv:1811.05984 [astro-ph.CO].
[3923] Planck Collaboration, Y. Akrami, et al., Planck 2018 results. X. Constraints on inflation Astron. Astrophys. 641 (2020) A10, arXiv:1807.06211 [astro-ph.CO].
[3924] BICEP, Keck Collaboration, P.A.R. Ade, et al., Improved constraints on primordial gravitational waves using Planck, WMAP, and BICEP/Keck observations through the 2018 observing season Phys. Rev. Lett. 127 (15) (2021) 151301, arXiv:2110.00483 [astro-ph.CO].
[3925] W. Giarè, Inflation, the Hubble tension, and early dark energy: An alternative overview Phys. Rev. D 109 (12) (2024) 123545, arXiv:2404.12779 [astro-ph.CO].
[3926] E. Silverstein, D. Tong, Scalar speed limits and cosmology: Acceleration from D-cceleration Phys. Rev. D 70 (2004) 103505, arXiv:hep-th/0310221.
[3927] M. Alishahiha, E. Silverstein, D. Tong, DBI in the sky Phys. Rev. D 70 (2004) 123505, arXiv:hep-th/0404084.
[3928] X. Chen, Inflation from warped space JHEP 08 (2005) 045, arXiv:hep-th/0501184.
[3929] X. Chen, Running non-Gaussianities in DBI inflation Phys. Rev. D 72 (2005) 123518, arXiv:astro-ph/0507053.
[3930] H.V. Peiris, D. Baumann, B. Friedman, A. Cooray, Phenomenology of D-Brane inflation with general speed of sound Phys. Rev. D 76 (2007) 103517, arXiv:0706.1240 [astro-ph].
[3931] A. Ashoorioon, H. Firouzjahi, M.M. Sheikh-Jabbari, M-flation: inflation from matrix valued scalar fields J. Cosmol. Astropart. Phys. 06 (2009) 018, arXiv:0903.1481 [hep-th].
[3932] D.D. Dimitrijevic, N. Bilić, G.S. Djordjevic, M. Milosevic, M. Stojanovic, Tachyon scalar field in a braneworld cosmology Internat. J. Modern Phys. A 33 (34) (2018) 1845017.
[3933] N. Bilic, S. Domazet, G.S. Djordjevic, Particle creation and reheating in a braneworld inflationary scenario Phys. Rev. D 96 (8) (2017) 083518, arXiv:1707.06023 [hep-th].
[3934] N. Bilic, D. Dimitrijevic, G. Djordjevic, M. Milosevic, Tachyon inflation in an ads braneworld with backreaction Internat. J. Modern Phys. A 32 (05) (2017) 1750039, arXiv:1607.04524 [gr-qc].
[3935] C.-M. Lin, D-term inflation in braneworld models: Consistency with cosmic-string bounds and early-time Hubble tension resolving models Phys. Rev. D 106 (10) (2022) 103511, arXiv:2204.10475 [hep-th].
[3936] L. Lombriser, On the cosmological constant problem Phys. Lett. B 797 (2019) 134804, arXiv:1901.08588 [gr-qc].
[3937] J. Frieman, M. Turner, D. Huterer, Dark energy and the accelerating universe Ann. Rev. Astron. Astrophys. 46 (2008) 385–432, arXiv:0803.0982 [astro-ph].
[3938] M. Park, M. Raveri, B. Jain, Reconstructing quintessence Phys. Rev. D 103 (10) (2021) 103530, arXiv:2101.04666 [astro-ph.CO].
[3939] S. Goldstein, M. Park, M. Raveri, B. Jain, L. Samushia, Beyond dark energy Fisher forecasts: How the Dark Energy Spectroscopic Instrument will constrain LCDM and quintessence models Phys. Rev. D 107 (6) (2023) 063530, arXiv:2207.01612 [astro-ph.CO].
[3940] L.A. Anchordoqui, I. Antoniadis, D. Lust, S-dual Quintessence, the Swampland, and the DESI DR2 Results 2025, arXiv:2503.19428 [hep-th].
[3941] P.J.E. Peebles, A. Vilenkin, Quintessential inflation Phys. Rev. D 59 (1999) 063505, arXiv:astro-ph/9810509.
[3942] M. Wali Hossain, R. Myrzakulov, M. Sami, E.N. Saridakis, Unification of inflation and dark energy à la quintessential inflation Internat. J. Modern Phys. D 24 (05) (2015) 1530014, arXiv:1410.6100 [gr-qc].
[3943] J. de Haro, J. Amorós, S. Pan, Simple inflationary quintessential model Phys. Rev. D 93 (8) (2016) 084018, arXiv:1601.08175 [gr-qc].
[3944] J. de Haro, J. Amorós, S. Pan, Simple inflationary quintessential model II: Power law potentials Phys. Rev. D 94 (6) (2016) 064060, arXiv:1607.06726 [gr-qc].
[3945] J. Haro, W. Yang, S. Pan, Reheating in quintessential inflation via gravitational production of heavy massive particles: A detailed analysis J. Cosmol. Astropart. Phys. 01 (2019) 023, arXiv:1811.07371 [gr-qc].
[3946] J. Haro, J. Amorós, S. Pan, The Peebles – Vilenkin quintessential inflation model revisited Eur. Phys. J. C 79 (6) (2019) 505, arXiv:1901.00167 [gr-qc].
[3947] J. Haro, J. Amorós, S. Pan, Scaling solutions in quintessential inflation Eur. Phys. J. C 80 (5) (2020) 404, arXiv:1908.01516 [gr-qc].
[3948] K. Dimopoulos, J.W.F. Valle, Modeling quintessential inflation Astropart. Phys. 18 (2002) 287–306, arXiv:astro-ph/0111417.
[3949] C.-Q. Geng, M.W. Hossain, R. Myrzakulov, M. Sami, E.N. Saridakis, Quintessential inflation with canonical and noncanonical scalar fields and Planck 2015 results Phys. Rev. D 92 (2) (2015) 023522, arXiv:1502.03597 [gr-qc].
[3950] K. Dimopoulos, C. Owen, Quintessential inflation with α-attractors J. Cosmol. Astropart. Phys. 06 (2017) 027, arXiv:1703.00305 [gr-qc].
[3951] C.-Q. Geng, C.-C. Lee, M. Sami, E.N. Saridakis, A.A. Starobinsky, Observational constraints on successful model of quintessential inflation J. Cosmol. Astropart. Phys. 06 (2017) 011, arXiv:1705.01329 [gr-qc].
[3952] M.W. Hossain, R. Myrzakulov, M. Sami, E.N. Saridakis, Variable gravity: A suitable framework for quintessential inflation Phys. Rev. D 90 (2) (2014) 023512, arXiv:1402.6661 [gr-qc].
[3953] M.W. Hossain, R. Myrzakulov, M. Sami, E.N. Saridakis, Class of quintessential inflation models with parameter space consistent with BICEP2 Phys. Rev. D 89 (12) (2014) 123513, arXiv:1404.1445 [gr-qc].
[3954] J. Rubio, C. Wetterich, Emergent scale symmetry: connecting inflation and dark energy Phys. Rev. D 96 (6) (2017) 063509, arXiv:1705.00552 [gr-qc].

[3955] D. Bettoni, J. Rubio, Quintessential inflation: A tale of emergent and broken symmetries Galaxies 10 (1) (2022) 22, arXiv:2112.11948 [astro-ph.CO].

[3956] Y. Akrami, S. Casas, S. Deng, V. Vardanyan, Quintessential α-attractor inflation: forecasts for Stage IV galaxy surveys J. Cosmol. Astropart. Phys. 04 (2021) 006, arXiv:2010.15822 [astro-ph.CO].

[3957] W. Giarè, E. Di Valentino, E.V. Linder, E. Specogna, Testing α-attractor quintessential inflation against CMB and low-redshift data Phys. Dark Univ. 46 (2024) 101713, arXiv:2402.01560 [astro-ph.CO].

[3958] D. Benisty, E.I. Guendelman, Lorentzian quintessential inflation Internat. J. Modern Phys. D 29 (14) (2020) 2042002, arXiv:2004.00339 [astro-ph.CO].

[3959] D. Benisty, E.I. Guendelman, Quintessential inflation from lorentzian slow roll Eur. Phys. J. C 80 (6) (2020) 577, arXiv:2006.04129 [astro-ph.CO].

[3960] L. Aresté Saló, D. Benisty, E.I. Guendelman, J.d. Haro, Quintessential inflation and cosmological seesaw mechanism: reheating and observational constraints J. Cosmol. Astropart. Phys. 07 (2021) 007, arXiv:2102.09514 [astro-ph.CO].

[3961] L. Aresté Saló, D. Benisty, E.I. Guendelman, J. de Haro, α-Attractors in quintessential inflation motivated by supergravity Phys. Rev. D 103 (12) (2021) 123535, arXiv:2103.07892 [astro-ph.CO].

[3962] A.D. Rendall, Dynamics of k-essence Cl. Quant. Grav. 23 (2006) 1557–1570, arXiv:gr-qc/0511158.

[3963] D. Langlois, S. Renaux-Petel, Perturbations in generalized multi-field inflation J. Cosmol. Astropart. Phys. 04 (2008) 017, arXiv:0801.1085 [hep-th].

[3964] A.E. Romano, S.A. Vallejo-Peña, K. Turzyński, Model-independent approach to effective sound speed in multi-field inflation Eur. Phys. J. C 82 (8) (2022) 767, arXiv:2006.00969 [gr-qc].

[3965] S.A. Hosseini Mansoori, H. Moshafi, Alleviating H_0 and s_8 tensions simultaneously in K-essence cosmology Astrophys. J. 975 (2) (2024) 275, arXiv:2405.05843 [astro-ph.CO].

[3966] S.X. Tian, Z.-H. Zhu, Early dark energy in k-essence Phys. Rev. D 103 (4) (2021) 043518, arXiv:2102.06399 [gr-qc].

[3967] A. Jawad, S. Rani, A.M. Sultan, K. Embreen, k-Essence inflation evading swampland conjectures and inflationary parameters Universe 8 (10) (2022) 532.

[3968] S. Hussain, S. Nelleri, K. Bhattacharya, Comprehensive study of k-essence model: dynamical system analysis and observational constraints from latest Type Ia supernova and BAO observations J. Cosmol. Astropart. Phys. 03 (2025) 025, arXiv:2406.07179 [astro-ph.CO].

[3969] W. Giarè, M. De Angelis, C. van de Bruck, E. Di Valentino, Tracking the multifield dynamics with cosmological data: a Monte Carlo approach J. Cosmol. Astropart. Phys. 12 (2023) 014, arXiv:2306.12414 [astro-ph.CO].

[3970] D. Staicova, Special cases of the multi-measure model – Understanding the prolonged inflation JHEAp 36 (2022) 120–127, arXiv:2011.02967 [gr-qc].

[3971] D. Staicova, M. Stoilov, Electromagnetic waves in cosmological Space-Time II. Luminosity distance Universe 11 (2025) 50, arXiv:2502.11634 [gr-qc].

[3972] I. Antoniadis, J. Cunat, A. Guillen, Cosmological perturbations from five-dimensional inflation JHEP 05 (2024) 290, arXiv:2311.17680 [hep-ph].

[3973] C. Petretti, M. Braglia, X. Chen, D.K. Hazra, S. Paban, Investigating the origin of CMB large-scale features using LiteBIRD and CMB-S4 2024, arXiv:2411.03459 [astro-ph.CO].

[3974] L.A. Anchordoqui, I. Antoniadis, Primordial power spectrum of five dimensional uniform inflation 2024, arXiv:2412.19213 [astro-ph.CO].

[3975] T. Hirose, Analysis of inflationary models in higher-dimensional uniform inflation JHEP 04 (2025) 077, arXiv:2501.13581 [hep-ph].

[3976] C. Moreno-Pulido, J. Sola Peracaula, Equation of state of the running vacuum Eur. Phys. J. C 82 (12) (2022) 1137, arXiv:2207.07111 [gr-qc].

[3977] J.A.S. Lima, S. Basilakos, J. Solà, Thermodynamical aspects of running vacuum models Eur. Phys. J. C 76 (4) (2016) 228, arXiv:1509.00163 [gr-qc].

[3978] M.B. Green, J.H. Schwarz, E. Witten, Superstring Theory Vol. 1: 25th Anniversary Edition, in: Cambridge Monographs on Mathematical Physics, Cambridge University Press, 2012.

[3979] M.B. Green, J.H. Schwarz, Anomaly cancellation in supersymmetric D=10 gauge theory and superstring theory Phys. Lett. B 149 (1984) 117–122.

[3980] S. Basilakos, N.E. Mavromatos, J. Solà, Starobinsky-like inflation and running vacuum in the context of supergravity Universe 2 (3) (2016) 14, arXiv:1505.04434 [gr-qc].

[3981] R. Brandenberger, L.L. Graef, G. Marozzi, G.P. Vacca, Backreaction of super-Hubble cosmological perturbations beyond perturbation theory Phys. Rev. D 98 (10) (2018) 103523, arXiv:1807.07494 [hep-th].

[3982] V. Comeau, R. Brandenberger, Back-reaction of long-wavelength cosmological fluctuations as measured by a clock field Eur. Phys. J. C 84 (3) (2024) 272, arXiv:2302.05873 [gr-qc].

[3983] D.W. Hogg, D.J. Eisenstein, M.R. Blanton, N.A. Bahcall, J. Brinkmann, J.E. Gunn, D.P. Schneider, Cosmic homogeneity demonstrated with luminous red galaxies Astrophys. J. 624 (2005) 54–58, arXiv:astro-ph/0411197.

[3984] J. Yadav, S. Bharadwaj, B. Pandey, T.R. Seshadri, Testing homogeneity on large scales in the Sloan Digital Sky Survey Data Release One Mon. Not. R. Astron. Soc. 364 (2005) 601–606, arXiv:astro-ph/0504315.

[3985] M. Scrimgeour, et al., The WiggleZ Dark Energy Survey: the transition to large-scale cosmic homogeneity Mon. Not. R. Astron. Soc. 425 (2012) 116–134, arXiv:1205.6812 [astro-ph.CO].

[3986] J.K. Yadav, J.S. Bagla, N. Khandai, Fractal Dimension as a measure of the scale of Homogeneity Mon. Not. R. Astron. Soc. 405 (2010) 2009, arXiv:1001.0617 [astro-ph.CO].

[3987] I. Horvath, J. Hakkila, Z. Bagoly, Possible structure in the GRB sky distribution at redshift two Astron. Astrophys. 561 (2014) L12, arXiv:1401.0533 [astro-ph.CO].

[3988] L.G. Balazs, Z. Bagoly, J.E. Hakkila, I. Horvath, J. Kobori, I. Racz, L.V. Toth, A giant ring-like structure at $0.78 < z < 0.86$ displayed by GRBs Mon. Not. R. Astron. Soc. 452 (3) (2015) 2236–2246, arXiv:1507.00675 [astro-ph.CO].

[3989] A.M. Lopez, R.G. Clowes, G.M. Williger, A giant arc on the sky Mon. Not. R. Astron. Soc. 516 (2) (2022) 1557–1572, arXiv:2201.06875 [astro-ph.CO].

[3990] A.M. Lopez, R.G. Clowes, G.M. Williger, A Big Ring on the sky J. Cosmol. Astropart. Phys. 07 (2024) 055, arXiv:2402.07591 [astro-ph.CO].

[3991] S. Nadathur, Seeing patterns in noise: gigaparsec-scale 'structures' that do not violate homogeneity Mon. Not. R. Astron. Soc. 434 (2013) 398–406, arXiv:1306.1700 [astro-ph.CO].

[3992] T.N. Ukwatta, P.R. Wozniak, Investigation of redshift- and duration-dependent clustering of gamma-ray bursts Mon. Not. R. Astron. Soc. 455 (1) (2016) 703–711, arXiv:1507.07117 [astro-ph.HE].

[3993] T. Sawala, M. Teeriaho, C.S. Frenk, J. Helly, A. Jenkins, G. Racz, M. Schaller, J. Schaye, The emperor's new arc: gigaparsec patterns abound in a ΛCDM universe 2025, arXiv e-prints, arXiv:2502.03515 [astro-ph.CO].

[3994] M.L. McClure, C.C. Dyer, Anisotropy in the Hubble constant as observed in the HST extragalactic distance scale key project results New Astron. 12 (2007) 533–543, arXiv:astro-ph/0703556.

[3995] K. Migkas, F. Pacaud, G. Schellenberger, J. Erler, N.T. Nguyen-Dang, T.H. Reiprich, M.E. Ramos-Ceja, L. Lovisari, Cosmological implications of the anisotropy of ten galaxy cluster scaling relations Astron. Astrophys. 649 (2021) A151, arXiv:2103.13904 [astro-ph.CO].

[3996] H. Bondi, T. Gold, The steady-state theory of the expanding universe Mon. Not. R. Astron. Soc. 108 (1948) 252.

[3997] F. Hoyle, A new model for the expanding universe Mon. Not. R. Astron. Soc. 108 (1948) 372–382.

[3998] D. Benisty, E.I. Guendelman, Cosmological principle in Newtonian dynamics Modern Phys. Lett. A 35 (16) (2020) 2050131, arXiv:1902.06511 [gr-qc].

[3999] E.I. Guendelman, E. Zamlung, D. Benisty, Noether symmetry in Newtonian dynamics and cosmology Gen. Relativity Gravitation 53 (11) (2021) 99, arXiv:2010.06448 [gr-qc].

[4000] K. Migkas, G. Schellenberger, T.H. Reiprich, F. Pacaud, M.E. Ramos-Ceja, L. Lovisari, Probing cosmic isotropy with a new X-ray galaxy cluster sample through the $L_X - T$ scaling relation Astron. Astrophys. 636 (2020) A15, arXiv:2004.03305 [astro-ph.CO].

[4001] A. Pandya, K. Migkas, T.H. Reiprich, A. Stanford, F. Pacaud, G. Schellenberger, L. Lovisari, M.E. Ramos-Ceja, N.T. Nguyen-Dang, S. Park, Examining the local universe isotropy with galaxy cluster velocity dispersion scaling relations Astron. Astrophys. 691 (2024) A355, arXiv:2408.00726 [astro-ph.CO].

[4002] Z. Zhai, W.J. Percival, Sample variance for supernovae distance measurements and the Hubble tension Phys. Rev. D 106 (10) (2022) 103527, arXiv:2207.02373 [astro-ph.CO].

[4003] R. Cooke, D. Lynden-Bell, Does the universe accelerate equally in all directions? Mon. Not. R. Astron. Soc. 401 (2010) 1409–1414, arXiv:0909.3861 [astro-ph.CO].

[4004] F. Sorrenti, R. Durrer, M. Kunz, The low multipoles in the Pantheon+SH0ES data J. Cosmol. Astropart. Phys. 04 (2025) 013, arXiv:2403.17741 [astro-ph.CO].

[4005] F. Sorrenti, R. Durrer, M. Kunz, A local infall from a cosmographic analysis of Pantheon+ J. Cosmol. Astropart. Phys. 12 (2024) 003, arXiv:2407.07002 [astro-ph.CO].

[4006] P. Boubel, M. Colless, K. Said, L. Staveley-Smith, Testing anisotropic Hubble expansion 2024, arXiv e-prints, arXiv:2412.14607 [astro-ph.CO].

[4007] V. Yadav, Measuring Hubble constant in an anisotropic extension of ΛCDM model Phys. Dark Univ. 42 (2023) 101365, arXiv:2306.16135 [astro-ph.CO].

[4008] Planck Collaboration, P.A.R. Ade, et al., Planck intermediate results. XIII. Constraints on peculiar velocities Astron. Astrophys. 561 (2014) A97, arXiv:1303.5090 [astro-ph.CO].

[4009] A. Kashlinsky, F. Atrio-Barandela, D. Kocevski, H. Ebeling, A measurement of large-scale peculiar velocities of clusters of galaxies: technical details Astrophys. J. 691 (2009) 1479–1493, arXiv:0809.3733 [astro-ph].

[4010] T. Westmeier, N. Deg, K. Spekkens, T.N. Reynolds, A.X. Shen, S. Gaudet, S. Goliath, M.T. Huynh, P. Venkataraman, X. Lin, T. O'Beirne, B. Catinella, L. Cortese, H. Dénes, A. Elagali, B.Q. For, G.I.G. Józsa, C. Howlett, J.M. van der Hulst, R.J. Jurek, P. Kamphuis, V.A. Kilborn, D. Kleiner, B.S. Koribalski, K. Lee-Waddell, C. Murugeshan, J. Rhee, P. Serra, L. Shao, L. Staveley-Smith, J. Wang, O.I. Wong, M.A. Zwaan, J.R. Allison, C.S. Anderson, L. Ball, D.C.J. Bock, D. Brodrick, J.D. Bunton, F.R. Cooray, N. Gupta, D.B. Hayman, E.K. Mahony,

V.A. Moss, A. Ng, S.E. Pearce, W. Raja, D.N. Roxby, M.A. Voronkov, K.A. Warhurst, H.M. Courtois, K. Said, WALLABY pilot survey: Public release of H I data for almost 600 galaxies from phase 1 of ASKAP pilot observations Publ. Astron. Soc. Aust. 39 (2022) e058, arXiv:2211.07094 [astro-ph.GA].

[4011] C. Murugeshan, N. Deg, T. Westmeier, A.X. Shen, B.Q. For, K. Spekkens, O.I. Wong, L. Staveley-Smith, B. Catinella, K. Lee-Waddell, H. Dénes, J. Rhee, L. Cortese, S. Goliath, R. Halloran, J.M. van der Hulst, P. Kamphuis, B.S. Koribalski, R.C. Kraan-Korteweg, F. Lelli, P. Venkataraman, L. Verdes-Montenegro, N. Yu, WALLABY Pilot Survey: Public data release of ∼ 1800 H I sources and high-resolution cut-outs from Pilot Survey Phase 2 Publ. Astron. Soc. Aust. 41 (2024) e088, arXiv:2409.13130 [astro-ph.GA].

[4012] H.M. Courtois, J. Mould, A.M. Hollinger, A. Dupuy, C.-P. Zhang, In search for the Local Universe dynamical homogeneity scale with CF4++ peculiar velocities 2025, arXiv:2502.01308 [astro-ph.CO].

[4013] M. Rameez, Concerns about the reliability of publicly available SNe Ia data 2019, arXiv:1905.00221 [astro-ph.CO].

[4014] M. Rameez, S. Sarkar, Is there really a Hubble tension? Cl. Quant. Grav. 38 (15) (2021) 154005, arXiv:1911.06456 [astro-ph.CO].

[4015] C.A.P. Bengaly, R. Maartens, M.G. Santos, Probing the Cosmological Principle in the counts of radio galaxies at different frequencies J. Cosmol. Astropart. Phys. 04 (2018) 031, arXiv:1710.08804 [astro-ph.CO].

[4016] A.K. Singal, Discordance of dipole asymmetries seen in recent large radio surveys with the cosmological principle Mon. Not. R. Astron. Soc. 524 (3) (2023) 3636–3646, arXiv:2303.05141 [astro-ph.CO].

[4017] J. Darling, The universe is brighter in the direction of our motion: galaxy counts and fluxes are consistent with the CMB dipole Astrophys. J. Lett. 931 (2) (2022) L14, arXiv:2205.06880 [astro-ph.CO].

[4018] J.D. Wagenveld, et al., The MeerKAT Absorption Line Survey Data Release 2: Wideband continuum catalogues and a measurement of the cosmic radio dipole Astron. Astrophys. 690 (2024) A163, arXiv:2408.16619 [astro-ph.CO].

[4019] P. Tiwari, A. Nusser, Revisiting the NVSS number count dipole J. Cosmol. Astropart. Phys. 03 (2016) 062, arXiv:1509.02532 [astro-ph.CO].

[4020] C. Dalang, C. Bonvin, On the kinematic cosmic dipole tension Mon. Not. R. Astron. Soc. 512 (3) (2022) 3895–3905, arXiv:2111.03616 [astro-ph.CO].

[4021] S. von Hausegger, The expected kinematic matter dipole is robust against source evolution Mon. Not. R. Astron. Soc. 535 (1) (2024) L49–L53, arXiv:2404.07929 [astro-ph.CO].

[4022] L. Giani, C. Howlett, K. Said, T. Davis, S. Vagnozzi, An effective description of Laniakea: impact on cosmology and the local determination of the Hubble constant J. Cosmol. Astropart. Phys. 01 (2024) 071, arXiv:2311.00215 [astro-ph.CO].

[4023] H. Boehringer, G. Chon, J. Truemper, R.C. Kraan-Korteweg, N. Schartel, Unveiling the largest structures in the nearby Universe: Discovery of the Quipu superstructure 2025, arXiv e-prints, arXiv:2501.19236 [astro-ph.CO].

[4024] B. Javanmardi, C. Porciani, P. Kroupa, J. Pflamm-Altenburg, Probing the isotropy of cosmic acceleration traced by Type Ia supernovae Astrophys. J. 810 (1) (2015) 47, arXiv:1507.07560 [astro-ph.CO].

[4025] J. Hu, J. Hu, X. Jia, B. Gao, F. Wang, Testing cosmic anisotropy with Pade approximation and Pantheon+ sample Astron. Astrophys. 689 (2024) A215, arXiv:2406.14827 [astro-ph.CO].

[4026] Planck Collaboration, N. Aghanim, et al., Planck 2013 results. XXVII. Doppler boosting of the CMB: Eppur si muove Astron. Astrophys. 571 (2014) A27, arXiv:1303.5087 [astro-ph.CO].

[4027] P.d.S. Ferreira, M. Quartin, Disentangling Doppler modulation, aberration and the temperature dipole in the CMB Phys. Rev. D 104 (6) (2021) 063503, arXiv:2107.10846 [astro-ph.CO].

[4028] S. Saha, S. Shaikh, S. Mukherjee, T. Souradeep, B.D. Wandelt, Bayesian estimation of our local motion from the Planck-2018 CMB temperature map J. Cosmol. Astropart. Phys. 10 (2021) 072, arXiv:2106.07666 [astro-ph.CO].

[4029] T.R. Jaffe, A.J. Banday, H.K. Eriksen, K.M. Gorski, F.K. Hansen, Evidence of vorticity and shear at large angular scales in the WMAP data: A Violation of cosmological isotropy? Astrophys. J. Lett. 629 (2005) L1–L4, arXiv:astro-ph/0503213.

[4030] T.R. Jaffe, S. Hervik, A.J. Banday, K.M. Gorski, On the viability of Bianchi type viih models with dark energy Astrophys. J. 644 (2006) 701–708, arXiv:astro-ph/0512433.

[4031] M. Bridges, J.D. McEwen, A.N. Lasenby, M.P. Hobson, Markov chain Monte Carlo analysis of Bianchi VII(h) models Mon. Not. R. Astron. Soc. 377 (2007) 1473–1480, arXiv:astro-ph/0605325.

[4032] Planck Collaboration, P.A.R. Ade, et al., Planck 2013 results. XXVI. Background geometry and topology of the Universe Astron. Astrophys. 571 (2014) A26, arXiv:1303.5086 [astro-ph.CO].

[4033] L. Bianchi, Sugli spazi a tre dimensioni che ammettono un gruppo continuo di movimenti Soc. Ital. Sci. Mem. Mat. 11 (1898) 267–352.

[4034] L. Bianchi, On the three-dimensional spaces which admit a continuous group of motions Gen. Relativity Gravitation 33 (2001) 2171–2253.

[4035] O. Akarsu, S. Kumar, S. Sharma, L. Tedesco, Constraints on a Bianchi type I spacetime extension of the standard ΛCDM model Phys. Rev. D 100 (2) (2019) 023532, arXiv:1905.06949 [astro-ph.CO].

[4036] H. Stephani, D. Kramer, M.A.H. MacCallum, C. Hoenselaers, E. Herlt, Exact solutions of Einstein's field equations, in: Cambridge Monographs on Mathematical Physics, Cambridge Univ. Press, Cambridge, 2003.

[4037] A. Pontzen, A. Challinor, Bianchi model CMB polarization and its implications for CMB anomalies Mon. Not. R. Astron. Soc. 380 (2007) 1387–1398, arXiv:0706.2075 [astro-ph].

[4038] E. Russell, C.B. Kılınç, O.K. Pashaev, Bianchi I model: an alternative way to model the present-day Universe Mon. Not. R. Astron. Soc. 442 (3) (2014) 2331–2341, arXiv:1312.3502 [astro-ph.CO].

[4039] G. Lemaitre, The expanding universe Ann. Soc. Sci. Brux. A 53 (1933) 51–85.

[4040] R.C. Tolman, Effect of imhomogeneity on cosmological models Proc. Nat. Acad. Sci. 20 (1934) 169–176.

[4041] H. Bondi, Spherically symmetrical models in general relativity Mon. Not. R. Astron. Soc. 107 (1947) 410–425.

[4042] V. Marra, T. Castro, D. Camarena, S. Borgani, A. Ragagnin, The BEHOMO project: Λ Lemaître-Tolman-Bondi N-body simulations Astron. Astrophys. 664 (2022) A179, arXiv:2203.04009 [astro-ph.CO].

[4043] M. Barriola, A. Vilenkin, Gravitational field of a global monopole Phys. Rev. Lett. 63 (1989) 341.

[4044] L. Perivolaropoulos, Six puzzles for LCDM cosmology 2008, arXiv:0811.4684 [astro-ph].

[4045] J.C.B. Sanchez, L. Perivolaropoulos, Evolution of dark energy perturbations in scalar-tensor cosmologies Phys. Rev. D 81 (2010) 103505, arXiv:1002.2042 [astro-ph.CO].

[4046] L. Perivolaropoulos, Large scale cosmological anomalies and inhomogeneous dark energy Galaxies 2 (2014) 22–61, arXiv:1401.5044 [astro-ph.CO].

[4047] G.F.R. Ellis, The Bianchi models: Then and now Gen. Relativity Gravitation 38 (2006) 1003–1015.

[4048] T. Schucker, A. Tilquin, G. Valent, Bianchi I meets the Hubble diagram Mon. Not. R. Astron. Soc. 444 (3) (2014) 2820–2836, arXiv:1405.6523 [astro-ph.CO].

[4049] G. Valent, Bianchi type II,III and V diagonal Einstein metrics re-visited Gen. Relativity Gravitation 41 (2009) 2433–2459, arXiv:1002.1454 [math-ph].

[4050] D.H. King, Gravity wave insights to Bianchi type IX universes Phys. Rev. D 44 (1991) 2356–2368.

[4051] H. Ringstrom, The Bianchi IX attractor Ann. Henri Poincare 2 (2001) 405–500, arXiv:gr-qc/0006035.

[4052] A. Ashtekar, J. Samuel, Bianchi cosmologies: The Role of spatial topology Cl. Quant. Grav. 8 (2011) 2191.

[4053] G.F.R. Ellis, M.A.H. MacCallum, A Class of homogeneous cosmological models Comm. Math. Phys. 12 (1969) 108–141.

[4054] P. Cea, The ellipsoidal universe in the planck satellite era Mon. Not. R. Astron. Soc. 441 (2) (2014) 1646–1661, arXiv:1401.5627 [astro-ph.CO].

[4055] T. Koivisto, D.F. Mota, Accelerating cosmologies with an anisotropic equation of state Astrophys. J. 679 (2008) 1–5, arXiv:0707.0279 [astro-ph].

[4056] G.C. McVittie, The mass-particle in an expanding universe Mon. Not. R. Astron. Soc. 93 (1933) 325–339.

[4057] N. Kaloper, M. Kleban, D. Martin, McVittie's Legacy: Black holes in an expanding universe Phys. Rev. D 81 (2010) 104044, arXiv:1003.4777 [hep-th].

[4058] M. Sereno, P. Jetzer, Evolution of gravitational orbits in the expanding universe Phys. Rev. D 75 (2007) 064031, arXiv:astro-ph/0703121.

[4059] V. Faraoni, A. Jacques, Cosmological expansion and local physics Phys. Rev. D 76 (2007) 063510, arXiv:0707.1350 [gr-qc].

[4060] R. Nandra, A.N. Lasenby, M.P. Hobson, The effect of a massive object on an expanding universe Mon. Not. R. Astron. Soc. 422 (2012) 2931–2944, arXiv:1104.4447 [gr-qc].

[4061] D. Benisty, M.M. Chaichian, A. Tureanu, Galaxy groups in the presence of cosmological constant: Increasing the masses of groups Phys. Lett. B 858 (2024) 139033, arXiv:2405.14944 [astro-ph.GA].

[4062] S. Peirani, J.A. de Freitas Pacheco, Mass determination of groups of galaxies: effects of the cosmological constant New Astron. 11 (2006) 325–330, arXiv:astro-ph/0508614.

[4063] S. Peirani, J.A.D.F. Pacheco, Dynamics of nearby groups of galaxies: the role of the cosmological constant Astron. Astrophys. 488 (2008) 845–851, arXiv:0806.4245 [astro-ph].

[4064] I.D. Karachentsev, O.G. Kashibadze, D.I. Makarov, R.B. Tully, The Hubble flow around the local group Mon. Not. R. Astron. Soc. 393 (2009) 1265, arXiv:0811.4610 [astro-ph].

[4065] J. Peñarrubia, Y.-Z. Ma, M.G. Walker, A. McConnachie, A dynamical model of the local cosmic expansion Mon. Not. R. Astron. Soc. 443 (3) (2014) 2204–2222, arXiv:1405.0306 [astro-ph.GA].

[4066] P. Teerikorpi, A.D. Chernin, The Hubble diagram for a system within dark energy: the location of the zero-gravity radius and the global Hubble rate Astron. Astrophys. 516 (2010) A93, arXiv:1006.0066 [astro-ph.CO].

[4067] A. Del Popolo, M. Deliyergiyev, M.H. Chan, Improved Lemaitre–Tolman model and the mass and turn-around radius in group of galaxies Phys. Dark Univ. 31 (2021) 100780, arXiv:2103.12714 [astro-ph.CO].

[4068] A. Del Popolo, M.H. Chan, Improved Lemaitre–Tolman model and the mass and turn-around radius in group of galaxies. II. The role of dark energy Astrophys. J. 926 (2) (2022) 156, arXiv:2210.10397 [astro-ph.CO].

[4069] P. Szekeres, Quasispherical gravitational collapse Phys. Rev. D 12 (1975) 2941.
[4070] M.-N. Célérier, Precision cosmology with exact inhomogeneous solutions of general relativity: the szekeres models 2024, arXiv e-prints, arXiv:2407.04452 [gr-qc].
[4071] J. Kristian, R.K. Sachs, Observations in cosmology Astrophys. J. 143 (1966) 379–399.
[4072] C.A. Clarkson, On the Observational Characteristics of Inhomogeneous Cosmologies: Undermining the Cosmological Principle or Have Cosmologists Put All Their EGS in One Basket? Glasgow U., 1999, arXiv:astro-ph/0008089.
[4073] T. Nadolny, R. Durrer, M. Kunz, H. Padmanabhan, A new way to test the Cosmological Principle: measuring our peculiar velocity and the large-scale anisotropy independently J. Cosmol. Astropart. Phys. 11 (2021) 009, arXiv:2106.05284 [astro-ph.CO].
[4074] D.L. Wiltshire, Cosmic clocks, cosmic variance and cosmic averages New J. Phys. 9 (2007) 377, arXiv:gr-qc/0702082.
[4075] D.L. Wiltshire, Average observational quantities in the timescape cosmology Phys. Rev. D 80 (2009) 123512, arXiv:0909.0749 [astro-ph.CO].
[4076] J.A.G. Duley, M.A. Nazer, D.L. Wiltshire, Timescape cosmology with radiation fluid Cl. Quant. Grav. 30 (2013) 175006, arXiv:1306.3208 [astro-ph.CO].
[4077] D.L. Wiltshire, Cosmic structure, averaging and dark energy in: Cosmology and Gravitation: XVth Brazilian School of Cosmology and Gravitation, Cambridge Scientific Publishers, 2014, arXiv:1311.3787 [astro-ph.CO].
[4078] T. Buchert, On average properties of inhomogeneous fluids in general relativity. 1. Dust cosmologies Gen. Relativity Gravitation 32 (2000) 105–125, arXiv:gr-qc/9906015.
[4079] T. Buchert, On average properties of inhomogeneous fluids in general relativity: Perfect fluid cosmologies Gen. Relativity Gravitation 33 (2001) 1381–1405, arXiv:gr-qc/0102049.
[4080] T. Buchert, P. Mourier, X. Roy, On average properties of inhomogeneous fluids in general relativity III: general fluid cosmologies Gen. Relativity Gravitation 52 (3) (2020) 27, arXiv:1912.04213 [gr-qc].
[4081] A. Ishibashi, R.M. Wald, Can the acceleration of our universe be explained by the effects of inhomogeneities? Cl. Quant. Grav. 23 (2006) 235–250, arXiv:gr-qc/0509108.
[4082] D.L. Wiltshire, Cosmological equivalence principle and the weak-field limit Phys. Rev. D 78 (2008) 084032, arXiv:0809.1183 [gr-qc].
[4083] K. Bolejko, M.A. Nazer, D.L. Wiltshire, Differential cosmic expansion and the Hubble flow anisotropy J. Cosmol. Astropart. Phys. 06 (2016) 035, arXiv:1512.07364 [astro-ph.CO].
[4084] D. Sapone, E. Majerotto, S. Nesseris, Curvature versus distances: Testing the FLRW cosmology Phys. Rev. D 90 (2) (2014) 023012, arXiv:1402.2236 [astro-ph.CO].
[4085] C. Clarkson, B. Bassett, T.H.-C. Lu, A general test of the Copernican Principle Phys. Rev. Lett. 101 (2008) 011301, arXiv:0712.3457 [astro-ph].
[4086] DES Collaboration, R. Camilleri, et al., The dark energy survey supernova program: investigating beyond-ΛCDM Mon. Not. R. Astron. Soc. 533 (3) (2024) 2615–2639, arXiv:2406.05048 [astro-ph.CO].
[4087] A. Heinesen, C. Blake, Y.-Z. Li, D.L. Wiltshire, Baryon acoustic oscillation methods for generic curvature: application to the SDSS-III Baryon Oscillation Spectroscopic Survey J. Cosmol. Astropart. Phys. 03 (2019) 003, arXiv:1811.11963 [astro-ph.CO].
[4088] A.S. Eddington, On the instability of Einstein's spherical world Mon. Not. R. Astro. Soc. 90 (1930) 668–678.
[4089] V.M. Slipher, Spectrographic observations of nebulae Popul. Astron. 23 (1915) 21–24.
[4090] H.S. Leavitt, 1777 variables in the magellanic clouds Harv. Obs. Ann. 60 (1908) 87–108.
[4091] G. Lemaitre, A homogeneous universe of constant mass and growing radius accounting for the radial velocity of extragalactic nebulae Ann. Soc. Sci. Brux. A 47 (1927) 49–59.
[4092] E. Hubble, A relation between distance and radial velocity among extra-galactic nebulae Proc. Nat. Acad. Sci. 15 (1929) 168–173.
[4093] D.J. Schwarz, D. Bacon, S. Chen, C. Clarkson, D. Huterer, M. Kunz, R. Maartens, A. Raccanelli, M. Rubart, J.-L. Starck, Testing foundations of modern cosmology with SKA all-sky surveys PoS AASKA14 (2015) 032, arXiv:1501.03820 [astro-ph.CO].
[4094] P. Horava, Quantum gravity at a Lifshitz point Phys. Rev. D 79 (2009) 084008, arXiv:0901.3775 [hep-th].
[4095] P. Horava, Spectral dimension of the universe in quantum gravity at a Lifshitz point Phys. Rev. Lett. 102 (2009) 161301, arXiv:0902.3657 [hep-th].
[4096] H. Lu, J. Mei, C.N. Pope, Solutions to Horava gravity Phys. Rev. Lett. 103 (2009) 091301, arXiv:0904.1595 [hep-th].
[4097] G. Calcagni, Cosmology of the Lifshitz universe JHEP 09 (2009) 112, arXiv:0904.0829 [hep-th].
[4098] C. Charmousis, G. Niz, A. Padilla, P.M. Saffin, Strong coupling in Horava gravity JHEP 08 (2009) 070, arXiv:0905.2579 [hep-th].
[4099] R. Brandenberger, Matter bounce in horava–lifshitz cosmology Phys. Rev. D 80 (2009) 043516, arXiv:0904.2835 [hep-th].
[4100] T.P. Sotiriou, M. Visser, S. Weinfurtner, Quantum gravity without Lorentz invariance JHEP 10 (2009) 033, arXiv:0905.2798 [hep-th].
[4101] R.-G. Cai, L.-M. Cao, N. Ohta, Topological black holes in Horava–Lifshitz gravity Phys. Rev. D 80 (2009) 024003, arXiv:0904.3670 [hep-th].
[4102] G. Panotopoulos, D. Vernieri, I. Lopes, Quark stars with isotropic matter in Hořava gravity and Einstein–æther theory Eur. Phys. J. C 80 (6) (2020) 537, arXiv:2006.07652 [gr-qc].
[4103] D. Vernieri, Anisotropic fluid spheres in Hořava gravity and Einstein-æther theory with a nonstatic æther Phys. Rev. D 100 (10) (2019) 104021, arXiv:1906.07738 [gr-qc].
[4104] T.P. Sotiriou, I. Vega, D. Vernieri, Rotating black holes in three-dimensional Hořava gravity Phys. Rev. D 90 (4) (2014) 044046, arXiv:1405.3715 [gr-qc].
[4105] G. Leon, A. Paliathanasis, Extended phase-space analysis of the Hořava–Lifshitz cosmology Eur. Phys. J. C 79 (9) (2019) 746, arXiv:1902.09961 [gr-qc].
[4106] E. Di Valentino, N.A. Nilsson, M.-I. Park, A new test of dynamical dark energy models and cosmic tensions in Hořava gravity Mon. Not. R. Astron. Soc. 519 (4) (2023) 5043–5058, arXiv:2212.07683 [astro-ph.CO].
[4107] N.A. Nilsson, Preferred-frame effects, the H_0 tension, and probes of Hořava–Lifshitz gravity Eur. Phys. J. Plus 135 (4) (2020) 361, arXiv:1910.14414 [gr-qc].
[4108] S.M. Carroll, E.A. Lim, Lorentz-violating vector fields slow the universe down Phys. Rev. D 70 (2004) 123525, arXiv:hep-th/0407149.
[4109] R. Alves Batista, et al., EuCAPT white paper: Opportunities and challenges for theoretical astroparticle physics in the next decade 2021, arXiv:2110.10074 [astro-ph.HE].
[4110] D. Amati, M. Ciafaloni, G. Veneziano, Can space-time be probed below the string size? Phys. Lett. B 216 (1989) 41–47.
[4111] M. Maggiore, A generalized uncertainty principle in quantum gravity Phys. Lett. B 304 (1993) 65–69, arXiv:hep-th/9301067.
[4112] C. Quesne, V.M. Tkachuk, Lorentz-covariant deformed algebra with minimal length Czech. J. Phys. 56 (2006) 1269–1274, arXiv:quant-ph/0612093.
[4113] C. Quesne, V.M. Tkachuk, Lorentz-covariant deformed algebra with minimal length and application to the 1+1-dimensional Dirac oscillator J. Phys. A 39 (2006) 10909–10922, arXiv:quant-ph/0604118.
[4114] G. Lambiase, F. Scardigli, Lorentz violation and generalized uncertainty principle Phys. Rev. D 97 (7) (2018) 075003, arXiv:1709.00637 [hep-th].
[4115] Q.G. Bailey, V.A. Kostelecky, Signals for Lorentz violation in post-Newtonian gravity Phys. Rev. D 74 (2006) 045001, arXiv:gr-qc/0603030.
[4116] S. Capozziello, M. Benetti, A.D.A.M. Spallicci, Addressing the cosmological H_0 tension by the heisenberg uncertainty Found. Phys. 50 (9) (2020) 893–899, arXiv:2007.00462 [gr-qc].
[4117] H. Moradpour, S. Aghababaei, C. Corda, N. Sadeghnezhad, H_0 tension and uncertainty principles Phys. Scr. 97 (5) (2022) 055008.
[4118] K.N. Abazajian, et al., Inflation physics from the cosmic microwave background and large scale structure Astropart. Phys. 63 (2015) 55–65, arXiv:1309.5381 [astro-ph.CO].
[4119] A. Kaya, The imprint of primordial gravitational waves on the CMB intensity profile Phys. Lett. B 817 (2021) 136353, arXiv:2105.02236 [astro-ph.CO].
[4120] S.M.M. Rasouli, P. Vargas Moniz, Noncommutative minisuperspace, gravity-driven acceleration, and kinetic inflation Phys. Rev. D 90 (8) (2014) 083533, arXiv:1411.1346 [gr-qc].
[4121] F.G. Alvarenga, J.C. Fabris, N.A. Lemos, G.A. Monerat, Quantum cosmological perfect fluid models Gen. Relativity Gravitation 34 (2002) 651–663, arXiv:gr-qc/0106051.
[4122] A. Kempf, G. Mangano, R.B. Mann, Hilbert space representation of the minimal length uncertainty relation Phys. Rev. D 52 (1995) 1108–1118, arXiv:hep-th/9412167.
[4123] S. Das, E.C. Vagenas, Universality of quantum gravity corrections Phys. Rev. Lett. 101 (2008) 221301, arXiv:0810.5333 [hep-th].
[4124] A.F. Ali, S. Das, E.C. Vagenas, Discreteness of space from the generalized uncertainty principle Phys. Lett. B 678 (2009) 497–499, arXiv:0906.5396 [hep-th].
[4125] A. Das, S. Das, E.C. Vagenas, Discreteness of space from GUP in strong gravitational fields Phys. Lett. B 809 (2020) 135772, arXiv:2006.05781 [gr-qc].
[4126] S. Aghababaei, H. Moradpour, E.C. Vagenas, Hubble tension bounds the GUP and EUP parameters Eur. Phys. J. Plus 136 (10) (2021) 997, arXiv:2109.14826 [gr-qc].
[4127] T. Jacobson, S. Liberati, D. Mattingly, Lorentz violation at high energy: Concepts, phenomena and astrophysical constraints Ann. Phys. 321 (2006) 150–196, arXiv:astro-ph/0505267.
[4128] G. Amelino-Camelia, Quantum-spacetime phenomenology Living Rev. Rel. 16 (2013) 5, arXiv:0806.0339 [gr-qc].
[4129] M. Arzano, G. Gubitosi, J.J. Relancio, Deformed relativistic symmetry principles Lect. Notes Phys. 1017 (2023) 49–103, arXiv:2211.11684 [hep-th].
[4130] G. Amelino-Camelia, J.R. Ellis, N.E. Mavromatos, D.V. Nanopoulos, S. Sarkar, Tests of quantum gravity from observations of gamma-ray bursts Nature 393 (1998) 763–765, arXiv:astro-ph/9712103.
[4131] J.R. Ellis, K. Farakos, N.E. Mavromatos, V.A. Mitsou, D.V. Nanopoulos, Astrophysical probes of the constancy of the velocity of light Astrophys. J. 535 (2000) 139–151, arXiv:astro-ph/9907340.

[4132] J.R. Ellis, N.E. Mavromatos, D.V. Nanopoulos, A.S. Sakharov, Quantum-gravity analysis of gamma-ray bursts using wavelets Astron. Astrophys. 402 (2003) 409–424, arXiv:astro-ph/0210124.

[4133] MAGIC, Other Contributors Collaboration, J. Albert, et al., Probing Quantum Gravity using Photons from a flare of the active galactic nucleus Markarian 501 Observed by the MAGIC telescope Phys. Lett. B 668 (2008) 253–257, arXiv:0708.2889 [astro-ph].

[4134] C. Pfeifer, Redshift and lateshift from homogeneous and isotropic modified dispersion relations Phys. Lett. B 780 (2018) 246–250, arXiv:1802.00058 [gr-qc].

[4135] J.R. Ellis, N.E. Mavromatos, D.V. Nanopoulos, Quantum gravitational diffusion and stochastic fluctuations in the velocity of light Gen. Relativity Gravitation 32 (2000) 127–144, arXiv:gr-qc/9904068.

[4136] J.R. Ellis, N.E. Mavromatos, D.V. Nanopoulos, Derivation of a vacuum refractive index in a stringy space-time foam model Phys. Lett. B 665 (2008) 412–417, arXiv:0804.3566 [hep-th].

[4137] J. Ellis, N.E. Mavromatos, D.V. Nanopoulos, D-Foam phenomenology: dark energy, the velocity of light and a possible D-Void Internat. J. Modern Phys. A 26 (2011) 2243–2262, arXiv:0912.3428 [astro-ph.CO].

[4138] U. Jacob, T. Piran, Lorentz-violation-induced arrival delays of cosmological particles J. Cosmol. Astropart. Phys. 01 (2008) 031, arXiv:0712.2170 [astro-ph].

[4139] L. Barcaroli, L.K. Brunkhorst, G. Gubitosi, N. Loret, C. Pfeifer, Planck-scale-modified dispersion relations in homogeneous and isotropic spacetimes Phys. Rev. D 95 (2) (2017) 024036, arXiv:1612.01390 [gr-qc].

[4140] G. Amelino-Camelia, D. Frattulillo, G. Gubitosi, G. Rosati, S. Bedić, Phenomenology of DSR-relativistic in-vacuo dispersion in FLRW spacetime J. Cosmol. Astropart. Phys. 01 (2024) 070, arXiv:2307.05428 [gr-qc].

[4141] N.E. Mavromatos, V.A. Mitsou, S. Sarkar, A. Vergou, Implications of a stochastic microscopic Finsler cosmology Eur. Phys. J. C 72 (2012) 1956, arXiv:1012.4094 [hep-ph].

[4142] N.E. Mavromatos, V.A. Mitsou, Observational evidence for negative-energy dust in late-times cosmology Astropart. Phys. 29 (2008) 442–452, arXiv:0707.4671 [astro-ph].

[4143] S. Basilakos, N.E. Mavromatos, V.A. Mitsou, M. Plionis, Dynamics and constraints of the dissipative liouville cosmology Astropart. Phys. 36 (2012) 7–17, arXiv:1107.3532 [astro-ph.CO].

[4144] R.J. Protheroe, H. Meyer, An Infrared background TeV gamma-ray crisis? Phys. Lett. B 493 (2000) 1–6, arXiv:astro-ph/0005349.

[4145] G. Amelino-Camelia, T. Piran, Cosmic rays and TeV photons as probes of quantum properties of space-time Phys. Lett. B 497 (2001) 265–270, arXiv:hep-ph/0006210.

[4146] J.-P. Uzan, The fundamental constants and their variation: Observational status and theoretical motivations Rev. Modern Phys. 75 (2003) 403, arXiv:hep-ph/0205340.

[4147] J.-P. Uzan, Varying constants, gravitation and cosmology Living Rev. Rel. 14 (2011) 2, arXiv:1009.5514 [astro-ph.CO].

[4148] C.J.A.P. Martins, The status of varying constants: a review of the physics, searches and implications 2017, arXiv:1709.02923 [astro-ph.CO].

[4149] J.D. Bekenstein, Fine structure constant: Is it really a constant? Phys. Rev. D 25 (1982) 1527–1539.

[4150] C.J.A.P. Martins, P.E. Vielzeuf, M. Martinelli, E. Calabrese, S. Pandolfi, Evolution of the fine-structure constant in runaway dilaton models Phys. Lett. B 743 (2015) 377–382, arXiv:1503.05068 [astro-ph.CO].

[4151] J. Rich, Which fundamental constants for cosmic microwave background and baryon-acoustic oscillation? Astron. Astrophys. 584 (2015) A69, arXiv:1503.06012 [astro-ph.CO].

[4152] S. Galli, C.J.A.P. Martins, A. Melchiorri, E. Menegoni, Testing the variation of fundamental constants with the CMB Astrophys. Space Sci. Proc. (2011) 59–67.

[4153] B. Lamine, Y. Ozdalkiran, L. Mirouze, F. Erdogan, S. Ilic, I. Tutusaus, R. Kou, A. Blanchard, Cosmological measurement of the gravitational constant G using the CMB, the BAO and the BBN 2024, arXiv e-prints. arXiv:2407.15553 [astro-ph.CO].

[4154] M.H. van Putten, Entropic constraint on cosmic variation of Planck mass and the Boltzmann constant Results Phys. 57 (2024) 107425, https://www.sciencedirect.com/science/article/pii/S2211379724001074.

[4155] I. Banik, H. Desmond, N. Samaras, Strong constraints on a sharp change in G as a solution to the Hubble tension Mon. Not. R. Astro. Soc. (2025) arXiv:2411.15301 [astro-ph.CO].

[4156] M. Kaplinghat, R.J. Scherrer, M.S. Turner, Constraining variations in the fine structure constant with the cosmic microwave background Phys. Rev. D 60 (1999) 023516, arXiv:astro-ph/9810133.

[4157] P.P. Avelino, C.J.A.P. Martins, G. Rocha, P.T.P. Viana, Looking for a varying alpha in the cosmic microwave background Phys. Rev. D 62 (2000) 123508, arXiv:astro-ph/0008446.

[4158] R.A. Battye, R. Crittenden, J. Weller, Cosmic concordance and the fine structure constant Phys. Rev. D 63 (2001) 043505, arXiv:astro-ph/0008265.

[4159] P.P. Avelino, S. Esposito, G. Mangano, C.J.A.P. Martins, A. Melchiorri, G. Miele, O. Pisanti, G. Rocha, P.T.P. Viana, Early universe constraints on a time varying fine structure constant Phys. Rev. D 64 (2001) 103505, arXiv:astro-ph/0102144.

[4160] G. Rocha, R. Trotta, C.J.A.P. Martins, A. Melchiorri, P.P. Avelino, R. Bean, P.T.P. Viana, Measuring alpha in the early universe: cmb polarization, reionization and the fisher matrix analysis Mon. Not. R. Astron. Soc. 352 (2004) 20, arXiv:astro-ph/0309211.

[4161] C.J.A.P. Martins, A. Melchiorri, G. Rocha, R. Trotta, P.P. Avelino, P.T.P. Viana, Wmap constraints on varying alpha and the promise of reionization Phys. Lett. B 585 (2004) 29–34, arXiv:astro-ph/0302295.

[4162] C.G. Scoccola, S.J. Landau, H. Vucetich, WMAP 5-year constraints on α and m_e Mem. Soc. Ast. It. 80 (4) (2009) 814–819, arXiv:0910.1083 [astro-ph.CO].

[4163] E. Menegoni, M. Archidiacono, E. Calabrese, S. Galli, C.J.A.P. Martins, A. Melchiorri, The fine structure constant and the CMB damping scale Phys. Rev. D 85 (2012) 107301, arXiv:1202.1476 [astro-ph.CO].

[4164] L. Hart, J. Chluba, New constraints on time-dependent variations of fundamental constants using Planck data Mon. Not. R. Astron. Soc. 474 (2) (2018) 1850–1861, arXiv:1705.03925 [astro-ph.CO].

[4165] J. Chluba, R.M. Thomas, Towards a complete treatment of the cosmological recombination problem Mon. Not. R. Astron. Soc. 412 (2011) 748, arXiv:1010.3631 [astro-ph.CO].

[4166] L. Hart, J. Chluba, Updated fundamental constant constraints from Planck 2018 data and possible relations to the Hubble tension Mon. Not. R. Astron. Soc. 493 (3) (2020) 3255–3263, arXiv:1912.03986 [astro-ph.CO].

[4167] J. Chluba, L. Hart, Varying fundamental constants meet Hubble 2023, arXiv:2309.12083 [astro-ph.CO].

[4168] Planck Collaboration, P.A.R. Ade, et al., Planck intermediate results - XXIV. Constraints on variations in fundamental constants Astron. Astrophys. 580 (2015) A22, arXiv:1406.7482 [astro-ph.CO].

[4169] S. Bize, et al., Testing the stability of fundamental constants with the Hg-199+ single-ion optical clock Phys. Rev. Lett. 90 (2003) 150802, arXiv:physics/0212109.

[4170] T. Rosenband, et al., Frequency ratio of Al+ and Hg+ single-ion optical clocks; metrology at the 17th decimal place Science 319 (5871) (2008) 1154622.

[4171] P. Bonifacio, et al., Fundamental constants and high resolution spectroscopy Astron. Nachr. 335 (2014) 83, arXiv:1310.6280 [astro-ph.CO].

[4172] S.M. Kotuš, M.T. Murphy, R.F. Carswell, High-precision limit on variation in the fine-structure constant from a single quasar absorption system Mon. Not. R. Astron. Soc. 464 (3) (2017) 3679–3703, arXiv:1609.03860 [astro-ph.CO].

[4173] O. Seto, Y. Toda, Big bang nucleosynthesis constraints on varying electron mass solution to the Hubble tension Phys. Rev. D 107 (8) (2023) 083512, arXiv:2206.13209 [astro-ph.CO].

[4174] T.L. Smith, D. Grin, D. Robinson, D. Qi, Probing spatial variation of the fine-structure constant using the CMB Phys. Rev. D 99 (4) (2019) 043531, arXiv:1808.07486 [astro-ph.CO].

[4175] M. Lucca, J. Chluba, A. Rotti, CRRfast: an emulator for the cosmological recombination radiation with effects from inhomogeneous recombination Mon. Not. R. Astron. Soc. 530 (1) (2024) 668–683, arXiv:2306.08085 [astro-ph.CO].

[4176] T. Sekiguchi, T. Takahashi, Early recombination as a solution to the H_0 tension Phys. Rev. D 103 (8) (2021) 083507, arXiv:2007.03381 [astro-ph.CO].

[4177] L. Hart, J. Chluba, Varying fundamental constants principal component analysis: additional hints about the Hubble tension Mon. Not. R. Astron. Soc. 510 (2) (2022) 2206–2227, arXiv:2107.12465 [astro-ph.CO].

[4178] N. Lee, Y. Ali-Haïmoud, N. Schöneberg, V. Poulin, What it takes to solve the hubble tension through modifications of cosmological recombination Phys. Rev. Lett. 130 (16) (2023) 161003, arXiv:2212.04494 [astro-ph.CO].

[4179] K. Hoshiya, Y. Toda, Electron mass variation from dark sector interactions and compatibility with cosmological observations Phys. Rev. D 107 (4) (2023) 043505, arXiv:2202.07714 [astro-ph.CO].

[4180] T. Damour, A.M. Polyakov, The String dilaton and a least coupling principle Nuclear Phys. B 423 (1994) 532–558, arXiv:hep-th/9401069.

[4181] T. Chiba, T. Kobayashi, M. Yamaguchi, J. Yokoyama, Time variation of proton-electron mass ratio and fine structure constant with runaway dilaton Phys. Rev. D 75 (2007) 043516, arXiv:hep-ph/0610027.

[4182] V. da Fonseca, et al., Fundamental physics with ESPRESSO: Constraining a simple parametrisation for varying α Astron. Astrophys. 666 (2022) A57, arXiv:2204.02930 [astro-ph.CO].

[4183] B.J. Barros, V. da Fonseca, Coupling quintessence kinetics to electromagnetism J. Cosmol. Astropart. Phys. 06 (2023) 048, arXiv:2209.12189 [astro-ph.CO].

[4184] L. Vacher, J.a.F. Dias, N. Schöneberg, C.J.A.P. Martins, S. Vinzl, S. Nesseris, G. Cañas Herrera, M. Martinelli, Constraints on extended Bekenstein models from cosmological, astrophysical, and local data Phys. Rev. D 106 (8) (2022) 083522, arXiv:2207.03258 [astro-ph.CO].

[4185] H.M. Tohfa, J. Crump, E. Baker, L. Hart, D. Grin, M. Brosius, J. Chluba, Cosmic microwave background search for fine-structure constant evolution Phys. Rev. D 109 (10) (2024) 103529, arXiv:2307.06768 [astro-ph.CO].

[4186] L. Vacher, N. Schöneberg, J.D.F. Dias, C.J.A.P. Martins, F. Pimenta, Runaway dilaton models: improved constraints from the full cosmological evolution Phys. Rev. D 107 (10) (2023) 104002, arXiv:2301.13500 [astro-ph.CO].
[4187] L. Vacher, N. Schöneberg, Incompatibility of fine-structure constant variations at recombination with local observations Phys. Rev. D 109 (10) (2024) 103520, arXiv:2403.02256 [astro-ph.CO].
[4188] G.P. Lynch, L. Knox, J. Chluba, Reconstructing the recombination history by combining early and late cosmological probes Phys. Rev. D 110 (6) (2024) 063518, arXiv:2404.05715 [astro-ph.CO].
[4189] O. Seto, Y. Toda, DESI constraints on the varying electron mass model and axionlike early dark energy Phys. Rev. D 110 (8) (2024) 083501, arXiv:2405.11869 [astro-ph.CO].
[4190] G.P. Lynch, L. Knox, J. Chluba, DESI observations and the Hubble tension in light of modified recombination Phys. Rev. D 110 (8) (2024) 083538, arXiv:2406.10202 [astro-ph.CO].
[4191] R.A. Sunyaev, Y.B. Zeldovich, Small scale entropy and adiabatic density perturbations? Antimatter in the Universe Astrophys. Space Sci. 9 (3) (1970) 368–382.
[4192] W. Hu, N. Sugiyama, Anisotropies in the cosmic microwave background: An Analytic approach Astrophys. J. 444 (1995) 489–506, arXiv:astro-ph/9407093.
[4193] W. Hu, D. Scott, N. Sugiyama, M.J. White, The Effect of physical assumptions on the calculation of microwave background anisotropies Phys. Rev. D 52 (1995) 5498–5515, arXiv:astro-ph/9505043.
[4194] J. Chluba, R.A. Sunyaev, Induced two-photon decay of the 2s level and the rate of cosmological hydrogen recombination Astron. Astrophys. 446 (2006) 39–42, arXiv:astro-ph/0508144.
[4195] A. Lewis, J. Weller, R. Battye, The cosmic microwave background and the ionization history of the universe Mon. Not. R. Astron. Soc. 373 (2006) 561–570, arXiv:astro-ph/0606552.
[4196] J.R. Shaw, J. Chluba, Precise cosmological parameter estimation using CosmoRec Mon. Not. R. Astron. Soc. 415 (2011) 1343, arXiv:1102.3683 [astro-ph.CO].
[4197] J. Chluba, R.A. Sunyaev, Is there need and another way to measure the Cosmic Microwave Background temperature more accurately? Astron. Astrophys. 478 (2008) L27, arXiv:0707.0188 [astro-ph].
[4198] R.A. Sunyaev, J. Chluba, Signals from the epoch of cosmological recombination Astron. Nachr. 330 (2009) 657–674, arXiv:0908.0435 [astro-ph.CO].
[4199] L. Hart, A. Rotti, J. Chluba, Sensitivity forecasts for the cosmological recombination radiation in the presence of foregrounds Mon. Not. R. Astron. Soc. 497 (4) (2020) 4535–4548, arXiv:2006.04826 [astro-ph.CO].
[4200] J. Chluba, et al., New horizons in cosmology with spectral distortions of the cosmic microwave background Exper. Astron. 51 (3) (2021) 1515–1554, arXiv:1909.01593 [astro-ph.CO].
[4201] H. Desmond, B. Jain, J. Sakstein, Local resolution of the Hubble tension: The impact of screened fifth forces on the cosmic distance ladder Phys. Rev. D 100 (4) (2019) 043537, arXiv:1907.03778 [astro-ph.CO]; Phys.Rev.D 101 (2020) 069904, Erratum; Phys. Rev. D 101 (2020) 129901, Erratum.
[4202] C. Burrage, J. Sakstein, A compendium of chameleon constraints J. Cosmol. Astropart. Phys. 11 (2016) 045, arXiv:1609.01192 [astro-ph.CO].
[4203] C. Burrage, J. Sakstein, Tests of chameleon gravity Living Rev. Rel. 21 (1) (2018) 1, arXiv:1709.09071 [astro-ph.CO].
[4204] T. Baker, et al., Novel Probes Project: Tests of gravity on astrophysical scales Rev. Modern Phys. 93 (1) (2021) 015003, arXiv:1908.03430 [astro-ph.CO].
[4205] J. Sakstein, Astrophysical tests of screened modified gravity Internat. J. Modern Phys. D 27 (15) (2018) 1848008, arXiv:2002.04194 [astro-ph.CO].
[4206] P. Brax, S. Casas, H. Desmond, B. Elder, Testing screened modified gravity Universe 8 (1) (2021) 11, arXiv:2201.10817 [gr-qc].
[4207] L. Berezhiani, J. Khoury, J. Wang, Universe without dark energy: Cosmic acceleration from dark matter-baryon interactions Phys. Rev. D 95 (12) (2017) 123530, arXiv:1612.00453 [hep-th].
[4208] R. Wojtak, J. Hjorth, Intrinsic tension in the supernova sector of the local Hubble constant measurement and its implications Mon. Not. R. Astron. Soc. 515 (2) (2022) 2790–2799, arXiv:2206.08160 [astro-ph.CO].
[4209] H. Desmond, J. Sakstein, Screened fifth forces lower the TRGB-calibrated Hubble constant too Phys. Rev. D 102 (2) (2020) 023007, arXiv:2003.12876 [astro-ph.CO].
[4210] M. Högås, E. Mörtsell, Hubble tension and fifth forces Phys. Rev. D 108 (12) (2023) 124050, arXiv:2309.01744 [astro-ph.CO].
[4211] Ruchika, H. Rathore, S. Roy Choudhury, V. Rentala, A gravitational constant transition within cepheids as supernovae calibrators can solve the Hubble tension J. Cosmol. Astropart. Phys. 06 (2024) 056, arXiv:2306.05450 [astro-ph.CO].
[4212] L. Amendola, P.S. Corasaniti, F. Occhionero, Time variability of the gravitational constant and type Ia supernovae 1999, arXiv:astro-ph/9907222.
[4213] E. Garcia-Berro, E. Gaztanaga, J. Isern, O. Benvenuto, L. Althaus, On the evolution of cosmological type ia supernovae and the gravitational constant 1999, arXiv:astro-ph/9907440.
[4214] E. Gaztanaga, E. Garcia-Berro, J. Isern, E. Bravo, I. Dominguez, Bounds on the possible evolution of the gravitational constant from cosmological type Ia supernovae Phys. Rev. D 65 (2002) 023506, arXiv:astro-ph/0109299.
[4215] B.S. Wright, B. Li, Type Ia supernovae, standardizable candles, and gravity Phys. Rev. D 97 (8) (2018) 083505, arXiv:1710.07018 [astro-ph.CO].
[4216] W. Zhao, B.S. Wright, B. Li, Constraining the time variation of Newton's constant G with gravitational-wave standard sirens and supernovae J. Cosmol. Astropart. Phys. 10 (2018) 052, arXiv:1804.03066 [astro-ph.CO].
[4217] I. Goldman, Neutron Stars constraints on a late G transition Phys. Lett. B 858 (2024) 139084, arXiv:2402.09859 [astro-ph.CO].
[4218] R.P. Gupta, Constraining co-varying coupling constants from globular cluster age Universe 9 (2) (2023) 70, arXiv:2302.00552 [astro-ph.CO].
[4219] R.P. Gupta, Constraining coupling constants' Variation with Supernovae, Quasars, and GRBs Symmetry 15 (2) (2023) 259, arXiv:2301.09795 [astro-ph.CO].
[4220] R.P. Gupta, Effect of evolving physical constants on type Ia supernova luminosity Mon. Not. R. Astron. Soc. 511 (3) (2022) 4238–4250, arXiv:2112.10654 [gr-qc].
[4221] J.W. Moffat, Scalar-tensor-vector gravity theory J. Cosmol. Astropart. Phys. 03 (2006) 004, arXiv:gr-qc/0506021.
[4222] J.D. Barrow, J. Magueijo, Varying alpha theories and solutions to the cosmological problems Phys. Lett. B 443 (1998) 104–110, arXiv:astro-ph/9811072.
[4223] A.J. Anderson, P. Barry, A.N. Bender, B.A. Benson, L.E. Bleem, J.E. Carlstrom, T.W. Cecil, C.L. Chang, T.M. Crawford, K.R. Dibert, M.A. Dobbs, K. Fichman, N.W. Halverson, W.L. Holzapfel, A. Hryciuk, K.S. Karkare, J. Li, M. Lisovenko, D. Marrone, J. McMahon, J. Montgomery, T. Natoli, Z. Pan, S. Raghunathan, C.L. Reichardt, M. Rouble, E. Shirokoff, G. Smecher, A.A. Stark, J.D. Vieira, M.R. Young, SPT-3G+: mapping the high-frequency cosmic microwave background using kinetic inductance detectors in: J. Zmuidzinas, J.-R. Gao (Eds.), Millimeter, Submillimeter, and Far-Infrared Detectors and Instrumentation for Astronomy XI, in: Society of Photo-Optical Instrumentation Engineers (SPIE) Conference Series, vol. 12190, 2022, p. 1219003, arXiv:2208.08559 [astro-ph.IM].
[4224] ACT Collaboration, W. Coulton, et al., Atacama Cosmology Telescope: High-resolution component-separated maps across one third of the sky Phys. Rev. D 109 (6) (2024) 063530, arXiv:2307.01258 [astro-ph.CO].
[4225] POLARBEAR Collaboration, A. Suzuki, et al., The POLARBEAR-2 and the Simons Array Experiment J. Low Temp. Phys. 184 (3-4) (2016) 805–810, arXiv:1512.07299 [astro-ph.IM].
[4226] H. Li, et al., Probing primordial gravitational waves: Ali CMB polarization telescope Natl. Sci. Rev. 6 (1) (2019) 145–154, arXiv:1710.03047 [astro-ph.CO].
[4227] QUBIC Collaboration, J.C. Hamilton, et al., QUBIC I: Overview and science program J. Cosmol. Astropart. Phys. 04 (04) (2022) 034, arXiv:2011.02213 [astro-ph.IM].
[4228] CLASS Collaboration, R. Datta, et al., Cosmology Large Angular Scale Surveyor (CLASS): 90 GHz Telescope pointing, beam profile, window function, and polarization performance Astrophys. J. Suppl. 273 (2) (2024) 26, arXiv:2308.13309 [astro-ph.IM].
[4229] GroundBIRD Collaboration, K. Lee, et al., GroundBIRD: A CMB polarization experiment with MKID Arrays J. Low Temp. Phys. 200 (5-6) (2020) 384–391, arXiv:2011.07705 [astro-ph.IM].
[4230] H. Hui, et al., BICEP Array: a multi-frequency degree-scale CMB polarimeter Proc. SPIE Int. Soc. Opt. Eng. 10708 (2018) 1070807, arXiv:1808.00568 [astro-ph.IM].
[4231] LiteBIRD Collaboration, T. Namikawa, et al., LiteBIRD science goals and forecasts: improving sensitivity to inflationary gravitational waves with multi-tracer delensing J. Cosmol. Astropart. Phys. 06 (2024) 010, arXiv:2312.05194 [astro-ph.CO].
[4232] LiteBIRD Collaboration, D. Paoletti, et al., LiteBIRD science goals and forecasts: primordial magnetic fields J. Cosmol. Astropart. Phys. 07 (2024) 086, arXiv:2403.16763 [astro-ph.CO].
[4233] LiteBIRD Collaboration, M. Remazeilles, et al., LiteBIRD science goals and forecasts. Mapping the hot gas in the Universe J. Cosmol. Astropart. Phys. 12 (2024) 026, arXiv:2407.17555 [astro-ph.CO].
[4234] LiteBIRD Collaboration, E. de la Hoz, et al., LiteBIRD Science Goals and Forecasts: constraining isotropic cosmic birefringence 2025, arXiv:2503.22322 [astro-ph.CO].
[4235] N. Sehgal, et al., CMB-HD: An ultra-deep, high-resolution millimeter-wave survey over half the sky 2019, arXiv:1906.10134 [astro-ph.CO].
[4236] CMB-HD Collaboration, S. Aiola, et al., Snowmass2021 CMB-HD White Paper 2022, arXiv:2203.05728 [astro-ph.CO].
[4237] S. Hanany, et al., PICO: Probe of inflation and cosmic origins 2019, arXiv e-prints, arXiv:1902.10541 [astro-ph.IM].
[4238] PRISM Collaboration, P. André, et al., PRISM (Polarized Radiation Imaging and Spectroscopy Mission): An extended white paper J. Cosmol. Astropart. Phys. 02 (2014) 006, arXiv:1310.1554 [astro-ph.CO].
[4239] CHIME Collaboration, M. Amiri, et al., An overview of CHIME, the Canadian Hydrogen Intensity Mapping Experiment Astrophys. J. Supp. 261 (2) (2022) 29, arXiv:2201.07869 [astro-ph.IM].

[4240] E. Abdalla, et al., The BINGO project - I. Baryon acoustic oscillations from integrated neutral gas observations Astron. Astrophys. 664 (2022) A14, arXiv:2107.01633 [astro-ph.CO].

[4241] L. Amendola, et al., Cosmology and fundamental physics with the euclid satellite Living Rev. Rel. 21 (1) (2018) 2, arXiv:1606.00180 [astro-ph.CO].

[4242] M. Takada, R.S. Ellis, M. Chiba, J.E. Greene, H. Aihara, N. Arimoto, K. Bundy, J. Cohen, O. Doré, G. Graves, J.E. Gunn, T. Heckman, C.M. Hirata, P. Ho, J.-P. Kneib, O. Le Fèvre, L. Lin, S. More, H. Murayama, T. Nagao, M. Ouchi, M. Seiffert, J.D. Silverman, L. Sodré, D.N. Spergel, M.A. Strauss, H. Sugai, Y. Suto, H. Takami, R. Wyse, Extragalactic science, cosmology, and galactic archaeology with the subaru prime focus spectrograph Publ. Astron. Soc. Jpn. 66 (1) (2014) R1, arXiv:1206.0737 [astro-ph.CO].

[4243] N. Tamura, et al., Prime Focus Spectrograph (PFS) for the Subaru Telescope: Overview, recent progress, and future perspectives Proc. SPIE Int. Soc. Opt. Eng. 9908 (2016) 99081M, arXiv:1608.01075 [astro-ph.IM].

[4244] B. Blum, et al., Snowmass2021 cosmic frontier white paper: Rubin observatory after LSST in: Snowmass 2021, 2022, arXiv:2203.07220 [astro-ph.CO].

[4245] R. Braun, T.L. Bourke, J.A. Green, E. Keane, J. Wagg, Advancing astrophysics with the square kilometre array PoS AASKA14 (2015) 174.

[4246] DESI Collaboration, D.J. Schlegel, et al., A spectroscopic road map for cosmic frontier: DESI, DESI-II, Stage-5 2022, arXiv:2209.03585 [astro-ph.CO].

[4247] R.S. de Jong, et al., 4MOST: 4-metre multi-object spectroscopic telescope in: I.S. McLean, S.K. Ramsay, H. Takami (Eds.), Ground-based and Airborne Instrumentation for Astronomy IV, in: Society of Photo-Optical Instrumentation Engineers (SPIE) Conference Series, vol. 8446, 2012, p. 84460T, arXiv:1206.6885 [astro-ph.IM].

[4248] SPHEREx Collaboration, O. Doré, et al., Cosmology with the SPHEREX all-sky spectral survey 2014, arXiv:1412.4872 [astro-ph.CO].

[4249] K.A. Cleary, et al., COMAP early science: I. Overview 2021, arXiv:2111.05927 [astro-ph.CO].

[4250] PUMA Collaboration, A. Slosar, et al., Packed Ultra-wideband Mapping Array (PUMA): A radio telescope for cosmology and transients Bull. Am. Astron. Soc. 51 (2019) 53, arXiv:1907.12559 [astro-ph.IM].

[4251] DES Collaboration, T. Abbott, et al., The Dark Energy Survey: more than dark energy – an overview Mon. Not. R. Astron. Soc. 460 (2) (2016) 1270–1299, arXiv:1601.00329 [astro-ph.CO].

[4252] L.J. Romualdez, et al., Overview, design, and flight results from SuperBIT: a high-resolution, wide-field, visible-to-near-UV balloon-borne astronomical telescope in: C.J. Evans, L. Simard, H. Takami (Eds.), Ground-based and Airborne Instrumentation for Astronomy VII, in: Society of Photo-Optical Instrumentation Engineers (SPIE) Conference Series, vol. 10702, 2018, p. 107020R, arXiv:1807.02887 [astro-ph.IM].

[4253] B. Sathyaprakash, et al., Scientific objectives of einstein telescope Cl. Quant. Grav. 29 (2012) 124013, arXiv:1206.0331 [gr-qc]; Class. Quant. Grav. 30 (2013) 079501, Erratum.

[4254] A. Abac, et al., The science of the Einstein telescope 2025, arXiv:2503.12263 [gr-qc].

[4255] M. Punturo, et al., The Einstein Telescope: A third-generation gravitational wave observatory Cl. Quant. Grav. 27 (2010) 194002.

[4256] A. Utina, et al., ETpathfinder: a cryogenic testbed for interferometric gravitational-wave detectors Cl. Quant. Grav. 39 (21) (2022) 215008, arXiv:2206.04905 [astro-ph.IM].

[4257] S. Borhanian, B.S. Sathyaprakash, Listening to the Universe with next generation ground-based gravitational-wave detectors Phys. Rev. D 110 (8) (2024) 083040, arXiv:2202.11048 [gr-qc].

[4258] I. Gupta, et al., Characterizing gravitational wave detector networks: from A$^\sharp$ to cosmic explorer Cl. Quant. Grav. 41 (24) (2024) 245001, arXiv:2307.10421 [gr-qc].

[4259] TianQin Collaboration, J. Mei, et al., The TianQin project: current progress on science and technology PTEP 2021 (5) (2021) 05A107, arXiv:2008.10332 [gr-qc].

[4260] J. Luo, et al., Fundamental physics and cosmology with TianQin 2025, arXiv:2502.20138 [gr-qc].

[4261] Z. Ren, T. Zhao, Z. Cao, Z.-K. Guo, W.-B. Han, H.-B. Jin, Y.-L. Wu, Taiji data challenge for exploring gravitational wave universe Front. Phys. (Beijing) 18 (6) (2023) 64302, arXiv:2301.02967 [gr-qc].

[4262] S. Kawamura, et al., Current status of space gravitational wave antenna DECIGO and B-DECIGO PTEP 2021 (5) (2021) 05A105, arXiv:2006.13545 [gr-qc].

[4263] NANOGrav Collaboration, G. Agazie, et al., The NANOGrav 15 yr Data Set: Evidence for a gravitational-wave background Astrophys. J. Lett. 951 (1) (2023) L8, arXiv:2306.16213 [astro-ph.HE].

[4264] R.N. Manchester, G. Hobbs, M. Bailes, W.A. Coles, W. van Straten, M.J. Keith, R.M. Shannon, N.D.R. Bhat, A. Brown, S.G. Burke-Spolaor, D.J. Champion, A. Chaudhary, R.T. Edwards, G. Hampson, A.W. Hotan, A. Jameson, F.A. Jenet, M.J. Kesteven, J. Khoo, J. Kocz, K. Maciesiak, S. Oslowski, V. Ravi, J.R. Reynolds, J.M. Sarkissian, J.P.W. Verbiest, Z.L. Wen, W.E. Wilson, D. Yardley, W.M. Yan, X.P. You, The parkes pulsar timing array project Publ. Astron. Soc. Aust. 30 (2013) e017, arXiv:1210.6130 [astro-ph.IM].

[4265] R.N. Manchester, IPTA, The international pulsar timing array Classical Quantum Gravity 30 (22) (2013) 224010, arXiv:1309.7392 [astro-ph.IM].

[4266] A.P. Beardsley, et al., Science with the Murchison Widefield Array: Phase I results and Phase II opportunities Publ. Astron. Soc. Aust. 36 (2019) e050, arXiv:1910.02895 [astro-ph.IM].

[4267] J. Cumner, et al., Radio antenna design for sky-averaged 21cm cosmology experiments: The REACH case J. Astron. Inst. 11 (01) (2022) 2250001, arXiv:2109.10098 [astro-ph.IM].

[4268] H.T. Intema, P. Jagannathan, K.P. Mooley, D.A. Frail, The GMRT 150 MHz All-sky Radio Survey: First alternative data release TGSS ADR1 Astron. Astrophys. 598 (2017) A78, arXiv:1603.04368 [astro-ph.CO].

[4269] R. Nan, D. Li, C. Jin, Q. Wang, L. Zhu, W. Zhu, H. Zhang, Y. Yue, L. Qian, The Five-Hundred Aperture Spherical Radio Telescope (fast) Project Internat. J. Modern Phys. D 20 (6) (2011) 989–1024, arXiv:1105.3794 [astro-ph.IM].

[4270] M.J. Graham, et al., The Zwicky transient facility: Science objectives Publ. Astron. Soc. Pac. 131 (1001) (2019) 078001, arXiv:1902.01945 [astro-ph.IM].

[4271] W.M. Wood-Vasey, et al., The nearby supernova factory New Astron. Rev. 48 (2004) 637–640, arXiv:astro-ph/0401513.

[4272] Y. Wang, et al., ATLAS Probe: Breakthrough science of galaxy evolution, cosmology, milky way, and the solar system 2019, arXiv:1909.00070 [astro-ph.IM].

[4273] I. Hook, The science case for the European ELT in: A. Moorwood (Ed.), Science with the VLT in the ELT Era, in: Astrophysics and Space Science Proceedings, vol. 9, 2009, p. 225.

[4274] M. Colless, Key early science with MANIFEST on GMT 2018, arXiv e-prints, arXiv:1809.05804 [astro-ph.IM].

[4275] TMT International Science Development Teams & TMT Science Advisory Committee Collaboration, W. Skidmore, et al., Thirty meter telescope detailed science case: 2015 Res. Astron. Astrophys. 15 (12) (2015) 1945–2140, arXiv:1505.01195 [astro-ph.IM].

[4276] ESO Very Large Telescope, The VLT White Book, European Organisation for Astronomical Research in the Southern Hemisphere, 1988, https://www.eso.org/public/products/books/book_0004/.

[4277] R. Bustos, M. Rubio, A. Otárola, N. Nagar, Parque astronómico de atacama: An ideal site for millimeter, submillimeter, and mid-infrared astronomy Publ. Astron. Soc. Aust. 126 (946) (2014) 1126, arXiv:1410.2451 [astro-ph.IM].

[4278] M. Davis, et al., Science objectives and early results of the DEEP2 redshift survey Proc. SPIE Int. Soc. Opt. Eng. 4834 (2003) 161–172, arXiv:astro-ph/0209419.

[4279] S. Johnston, J. Wall, Science with ASKAP - the Australian Square Kilometre Array Pathfinder Exper. Astron. 22 (2008) 151, arXiv:0810.5187 [astro-ph].

[4280] M. Bailes, A. Jameson, C. Flynn, T. Bateman, E.D. Barr, S. Bhandari, J.D. Bunton, M. Caleb, D. Campbell-Wilson, W. Farah, B. Gaensler, A.J. Green, R.W. Hunstead, F. Jankowski, E.F. Keane, V.V. Krishnan, T. Murphy, M. O'Neill, S. Osłowski, A. Parthasarathy, V. Ravi, P. Rosado, D. Temby, The UTMOST: A hybrid digital signal processor transforms the Molonglo observatory synthesis telescope Publ. Astron. Soc. Aust. 34 (2017) e045, arXiv:1708.09619 [astro-ph.IM].

[4281] J. Jonas, MeerKAT Team, The meerkat radio telescope in: MeerKAT Science: On the Pathway to the SKA, 2016, p. 1.

[4282] C.J. Law, et al., Deep synoptic array science: First FRB and host galaxy catalog Astrophys. J. 967 (1) (2024) 29, arXiv:2307.03344 [astro-ph.HE].

[4283] T. Clarke, W. Peters, W. Brisken, S. Giacintucci, N. Kassim, E. Polisensky, J. Helmboldt, E.E. Richards, A. Erickson, P.S. Ray, M.T. Kerr, J. Deneva, W. Coburn, R. Huber, J. Long, The VLA Low-band Ionosphere and Transient Experiment (VLITE) in: American Astronomical Society Meeting Abstracts #231, in: American Astronomical Society Meeting Abstracts, vol. 231, 2018, p. 354.11.

[4284] G. Hallinan, DSA-2000 collaboration, The dsa-2000: the future of radio survey science in: American Astronomical Society Meeting Abstracts, in: American Astronomical Society Meeting Abstracts, vol. 241, 2023, p. 239.07.

[4285] B. Adebahr, et al., Apercal-The Apertif calibration pipeline Astron. Comput. 38 (2022) 100514, arXiv:2112.03722 [astro-ph.IM].

[4286] K. Vanderlinde, A. Liu, B. Gaensler, D. Bond, G. Hinshaw, C. Ng, C. Chiang, I. Stairs, J.-A. Brown, J. Sievers, J. Mena, K. Smith, K. Bandura, K. Masui, K. Spekkens, L. Belostotski, M. Dobbs, N. Turok, P. Boyle, M. Rupen, T. Landecker, U.-L. Pen, V. Kaspi, The Canadian Hydrogen Observatory and Radio-transient Detector (CHORD) in: Canadian Long Range Plan for Astronomy and Astrophysics White Papers, vol. 2020, 2019, p. 28, arXiv:1911.01777 [astro-ph.IM].

[4287] G.J. Hill, et al., The Hobby-Eberly Telescope Dark Energy Experiment (HETDEX): Description and early pilot survey results ASP Conf. Ser. 399 (2008) 115–118, arXiv:0806.0183 [astro-ph].

[4288] A. Fasano, et al., CONCERTO: Instrument and status EPJ Web Conf. 293 (2024) 00018, arXiv:2311.04704 [astro-ph.IM].

[4289] V.L. Butler, et al., TIME: the Tomographic Ionized-carbon Mapping Experiment: an update on design, characterization, and data from the 2022 commissioning observations in: J. Zmuidzinas, J.-R. Gao (Eds.), Millimeter, Submillimeter, and Far-Infrared Detectors and Instrumentation for Astronomy XII, in: Society of Photo-Optical Instrumentation Engineers (SPIE) Conference Series, vol. 13102, 2024, p. 131022G.

[4290] A. Cooray, T.-C. Chang, S. Unwin, M. Zemcov, A. Coffey, P. Morrissey, N. Raouf, S. Lipscy, M. Shannon, G. Wu, R. Cen, R.R. Chary, O. Doré, X. Fan, G.G. Fazio, S.L. Finkelstein, C. Heneka, B. Lee, P. Linden, H. Nayyeri, J. Rhodes, R. Sadoun, M.B. Silva, H. Trac, H.-Y. Wu, Z. Zheng, Cosmic dawn intensity mapper in: Bulletin of the American Astronomical Society, vol. 51, 2019, p. 23, arXiv:1903.03144 [astro-ph.GA].

[4291] G.J. Stacey, et al., CCAT-prime: Science with an ultra-widefield submillimeter observatory at cerro chajnantor in: Ground-based and Airborne Telescopes VII, 2018, arXiv:1807.04354 [astro-ph.GA].

[4292] W. Sutherland, J. Emerson, G. Dalton, E. Atad-Ettedgui, S. Beard, R. Bennett, N. Bezawada, A. Born, M. Caldwell, P. Clark, S. Craig, D. Henry, P. Jeffers, B. Little, A. McPherson, J. Murray, M. Stewart, B. Stobie, D. Terrett, K. Ward, M. Whalley, G. Woodhouse, The Visible and Infrared Survey Telescope for Astronomy (VISTA): Design, technical overview, and performance Astron. Astrophys. 575 (2015) A25, arXiv:1409.4780 [astro-ph.IM].

[4293] J. Silk, The limits of cosmology: role of the Moon Phil. Trans. A. Math. Phys. Eng. Sci. 379 (2021) 20190561, arXiv:2011.04671 [astro-ph.CO].